Soil-Structure Interaction Analyses and Results for the US-APWR Standard Plant

Non-Proprietary Version

November 2012

Revision History

Revision	Page	Description
0	All	Original Issue
1	2, 4 thru 15, 17, 18, 19, 21, 26, 28, 33, 34, 36, 37, 41, 49, 50, 59 A-15, C-1 thru C-36, D-1 thru D-33, E-1 thru E-74, F-8, F-9, F-10, F-11, H-10, H-11	Section 3.6.2 was changed to provide clarification of how PS/B loads were developed Section 3.7 was changed to provide revised lateral pressure loads for underground exterior walls Raised the R/B maximum frequency of SSI analysis to 50 Hz for soil cases 900-100 and 900-200 Revised ISRS for PCCV, CIS, R/B + FH/A and SDOF Updated seismic design shear and axial forces for IC18, IC08, IC05, IC15, IC04, IC14, IC03, IC02 and IC01. Updated PS/B Gas Turbine Generator ISRS in vertical direction. Updated soil profile 270-500 (Table 3-3A) and 560-100 (Table 3-3E) Updated Dynamic Lateral Earth Pressure (Table 4-12) Corrected shear and axial force values in Table 4-14 Figure 3-8 is added to provide distribution of total lateral pressure loads for design of underground exterior walls Corrected Titles for Appendix H, Figures 10 & 11
2	All	R/B Complex is full finite element model. Updated analyses and results to reflect new input soil profiles and time histories. Revision 2 completely supersedes Revision 1.
3	All	General Revision. MUAP-10001 Revision 4 is merged with Revision 2 of this report and revised to reflect the common basemat configuration, addition of the Essential Service Water Pipe Chase, and analysis methodology.

Mitsubishi Heavy Industries, Ltd.

16-5, Konan 2-chome, Minato-ku

Tokyo 108-8215 Japan

ABSTRACT

The purpose of this Technical Report (TeR) is to present the seismic Soil-Structure Interaction (SSI) and Structure-Soil-Structure Interaction (SSSI) analyses and results of the US-APWR Standard Plant Reactor Building (R/B) complex. These include the Pre-stressed Concrete Containment Vessel (PCCV), Containment Internal Structure (CIS), R/B including the Fuel Handling Area (FH/A), Auxiliary Building (A/B), the East and West Power Source Buildings (East PS/B & West PS/B), and the Essential Service Water Pipe Chase (ESWPC) resting on a common reinforced concrete basemat, referred to as the R/B complex. These site-independent SSI and SSSI analyses are carried out using the ACS SASSI computer program for six generic soil profiles to obtain the response of the standard design to the types of soil conditions expected throughout the Central and Eastern United States (CEUS). The analyses for the R/B complex consider the common basemat to be embedded in a saturated subgrade at approximately 42 ft below the plant nominal ground surface elevation. A set of three statistically independent acceleration time histories representing the input ground motion for the three orthogonal directions are converted to in-column time histories and input at the nominal bottom elevation of the foundation. These acceleration time histories are compatible with the US-APWR Certified Seismic Design Response Spectra (CSDRS).

The Dynamic Finite Element (FE) Model of the R/B complex is used to represent the dynamic properties of R/B complex structures. In general, in order to address the effects of concrete cracking, two sets of stiffness and damping properties are assigned to the models to simulate two bounding conditions. Full stiffness with Operating Basis Earthquake (OBE) damping is used to represent uncracked concrete and reduced stiffness with Safe Shutdown Earthquake (SSE) damping is used to represent cracked concrete. For the CIS, there are structural components which are exceptions for the reduced stiffness conditions (e.g., CIS primary shield walls). The full and reduced stiffness conditions of the R/B complex model are further discussed in Part 2 Section 02.4.2.

The seismic responses obtained from the site-independent SSI and SSSI analyses presented in this report form the basis for standard seismic design of R/B complex. The analyses consider the two bounding stiffness and damping properties for the structures, the embedded foundation, and effects due to the Turbine Building (T/B) but do not consider the effects of the water table elevation. TeR MUAP-11007 presents the evaluation of the significance of the water table on the standard plant seismic design. The results of SSI analyses include: relative displacements for evaluation of adequacy of gaps between structures and design of umbilicals, damped In-Structure Response Spectra (ISRS) for the seismic design basis of the category I Structures, Systems, and Components (SSCs), maximum nodal accelerations to develop seismic loads which are used for the design of structural members, and nodal acceleration time histories which serve as input to sliding and other stability evaluations of the R/B complex.

The report is divided into the following three parts:

Part 1: Describes the development of the design basis time histories and design basis soil profiles.

Part 2: Describes the development and validation of the design basis Dynamic FE model of the R/B complex.

Part 3: Presents the methodologies and results for the SSI and SSSI analyses.

TABLE OF CONTENTS

PART 1 - TIME HISTORY AND SOIL PROFILE SEISMIC DESIGN BASES FOR THE US-APWR STANDARD PLANT

01.1.0 INTRODUCTION
01.2.0 PURPOSE
01.3.0 OBJECTIVES
01.4.0 APPROACH / METHODOLOGY
01.5.0 RESULTS
01.6.0 REFERENCES

PART 2 - DEVELOPMENT AND VALIDATION OF THE DESIGN BASIS FINITE ELEMENT MODEL FOR SEISMIC ANALYSIS OF THE US-APWR STANDARD PLANT

02.1.0 INTRODUCTION
02.2.0 PURPOSE
02.3.0 OBJECTIVES
02.4.0 APPROACH / METHODOLOGY
02.5.0 RESULTS
02.6.0 REFERENCES

PART 3 - SSI & SSSI ANALYSES AND RESULTS FOR THE US-APWR STANDARD PLANT

03.1.0 INTRODUCTION
03.2.0 DESCRIPTION OF US-APWR STANDARD PLANT STRUCTURES
03.3.0 US-APWR SEISMIC DESIGN BASIS
03.4.0 ANALYSIS RESULTS
03.5.0 CONCLUSION
03.6.0 REFERENCES

APPENDICES

Appendix 1-A Statistical Justification of RVT Methodology: 30 vs. 60 Realizations
Appendix 2-A Reduced Stiffness for Cracked Pre-Stressed Concrete Containment Vessel (PCCV)
Appendix 3-A R/B Complex Node Numbering and Grouping for ISRS Plots
Appendix 3-B ISRS Plots for the R/B Complex
Appendix 3-C Transfer Function Plots
Appendix 3-D Parametric Study of Soil Model Depth

LIST OF ACRONYMS AND ABBREVIATIONS

The following list defines the acronyms used in this document.

1-D	One-Dimensional
3-D	Three-Dimensional
A/B	Auxiliary Building
AI	Arias Intensity
AISC	American Institute of Steel Construction
ARS	Acceleration Response Spectra
ASCE	American Society of Civil Engineers
ASME	American Society of Mechanical Engineers
ATF	Acceleration Transfer Function
CEUS	Central and Eastern United States
CIS	Containment Internal Structure
CSDRS	Certified Seismic Design Response Spectra
CW	Clockwise
DM	Direct Method
DOE	Department of Energy
EFWP	Emergency Feed Water Pit
EPRI	Electric Power Research Institute
ESWPC	Essential Service Water Pipe Chase
EW	East-West
FCO	Full Column Outcrop
FE	Finite Element
FFT	Fast Fourier Transformation
FH/A	Fuel Handling Area
GTG	Gas Turbine Generator
ISRS	In-Structure Response Spectra
MCP	Main Coolant Piping
MSM	Modified Subtraction Method
NEI	Nuclear Engineering Institute
NFSP	New Fuel Storage Pit
NRC	Nuclear Regulatory Commission
NS	North-South
NSSS	Nuclear Steam Supply System
OBE	Operating-Basis Earthquake
PCCV	Pre-stressed Concrete Containment Vessel
PEER	Pacific Earthquake Engineering Research
PGA	Peak Ground Acceleration
PI	Plasticity Index
PS/B	Power Source Building
PSD	Power Spectral Density
P-SV	Primary-Secondary Vertical
PZR	Pressurizer
R/B	Reactor Building

RC	Reinforced Concrete
RCL	Reactor Coolant Loop
RCP	Reactor Coolant Pump
RG	Regulatory Guide
RV	Reactor Vessel
RVT	Random Vibration Theory
RWSP	Refueling Water Storage Pit
SC	Steel-Concrete
SCP	Strain Compatible Properties
SFP	Spent Fuel Pit
SG	Steam Generator
SM	Subtraction Method
SRP	Standard Review Plan
SRSS	Square Root of the Sum of the Squares
SSC	Structures, Systems, and Component
SSE	Safe-Shutdown Earthquake
SSI	Soil-Structure Interaction
SSSI	Structure Soil Structure Interaction
T/B	Turbine Building
TeR	Technical Report
V	Vertical
V/H	Vertical divided by Horizontal
V_p	Compression Wave Velocity
V_s	Shear Wave Velocity
WUS	Western United States
ZPA	Zero Period Acceleration

Soil-Structure Interaction Analyses and Results for the US-APWR Standard Plant

PART 1 of 3

Time History and Soil Profile Seismic Design Bases for the US-APWR Standard Plant

PART 1 TABLE OF CONTENTS

Section Title Page No.

LIST OF FIGURES 01-iii

LIST OF TABLES 01-v

01.1.0 INTRODUCTION 01.1-1

01.2.0 PURPOSE 01.2-1

01.3.0 OBJECTIVES 01.3-1
01.3.1 Design Basis Time Histories 01.3-1
01.3.2 Generic Layered Soil Profiles and Strain Compatible Properties 01.3-1

01.4.0 APPROACH / METHODOLOGY 01.4-1
01.4.1 Design Basis Time Histories 01.4-1
01.4.1.1 Target Response Spectra – The CSDRS 01.4-1
01.4.1.2 Power Spectral Densities Compatible with CSDRS 01.4-1
01.4.1.3 Development of Design Basis Time Histories in Accordance with SRP 3.7.1 Option 1, Approach 1 ..... 01.4-4
01.4.2 Development of Soil Profiles and Strain Compatible Properties 01.4-6
01.4.2.1 Selection of Profiles 01.4-8
01.4.2.2 Development of US-APWR CSDRS Strain Compatible Properties 01.4-8

01.5.0 RESULTS 01.5-1
01.5.1 Target PSDs and Design Basis Time Histories 01.5-1
01.5.1.1 Target PSDs Compatible with CSDRS 01.5-1
01.5.1.2 Design Basis Time Histories 01.5-2
01.5.2 Development of Soil Profiles 01.5-3
01.5.2.1 Site Response Analysis 01.5-4
01.5.2.2 Strain Compatible Properties 01.5-5

01.6.0 REFERENCES 01.6-1

APPENDIX 1-A Statistical Justification of RVT Methodology: 30 vs. 60 Realizations 1-A-i

LIST OF FIGURES

Figure **Title** **Page No.**

Figure 01.4.1.1-1 US-APWR Horizontal CSDRS 01.4-14

Figure 01.4.1.1-2 US-APWR Vertical CSDRS..... 01.4-15

Figure 01.4.1.2.1-1 Time-Envelope Function to Develop US-APWR Target PSDs 01.4-16

Figure 01.4.1.2.1-2 Work Flow to Develop a Target PSD Compatible with the CSDRS . 01.4-17

Figure 01.4.1.2.2-1 Time-Envelope Function Used in NUREG/CR-5347 Appendix B 01.4-18

Figure 01.4.1.2.2-2 Procedure to Verify the Appropriate Equation to Calculate PSD from a Time History to Envelop the Target PSD up to 50 Hz..... 01.4-19

Figure 01.4.2-1 Top 500 ft of the Candidate Shear Wave Velocity Profiles and Associated $\overline{V_S}(30m)$ Velocities 01.4-20

Figure 01.4.2-2 (TR-102293, Reference 01-8) Cohesionless Soil Modulus Reduction and Hysteretic Damping Curves 01.4-21

Figure 01.4.2.1-1 Six Generic Soil Profiles, Shear Wave Velocity V(s) 01.4-22

Figure 01.4.2.1-2 Six Generic Soil Profiles, Compression Wave Velocity (Vp)..... 01.4-23

Figure 01.4.2.1-3 Six Generic Soil Profiles, Shear Wave Velocity Damping (%) 01.4-24

Figure 01.5.1.1-1 US-APWR Initial Horizontal Target PSD..... 01.5-22

Figure 01.5.1.1.2-1 Horizontal Pseudo-Velocity Response Spectra (PSV) at 2% Damping of 30 Artificial Horizontal Time Histories 01.5-23

Figure 01.5.1.1.2-2 Vertical Pseudo-Velocity Response Spectra (PSV) at 2% Damping of 30 Artificial Vertical Time Histories 01.5-24

Figure 01.5.1.1.2-3 US-APWR Final Horizontal and Vertical Target PSDs..... 01.5-25

Figure 01.5.1.1-4 Scenario I PSDs vs. SRP 3.7.1 Target PSD 01.5-26

Figure 01.5.1.1-5 Scenario II PSDs vs. SRP 3.7.1 Target PSD 01.5-27

Figure 01.5.1.1-6 Scenario III PSDs vs. SRP 3.7.1 Target PSD 01.5-28

Figure 01.5.1.2-1 Acceleration, Velocity, and Displacement Time History for Component H1 (180)..... 01.5-29

Figure 01.5.1.2-2 Acceleration, Velocity, and Displacement Time History for Component H2 (090)..... 01.5-30

Figure 01.5.1.2-3 Acceleration, Velocity, and Displacement Time History for Component V (UP)..... 01.5-31

Figure 01.5.1.2-4a Damped Response Spectra Plots for Northridge Mount Baldy Component H1 (180)..... 01.5-32

Figure 01.5.1.2-4b Damped Response Spectra Plots for Northridge Mount Baldy Component H1 (180)..... 01.5-33

Figure 01.5.1.2-5a Damped Response Spectra Plots for Northridge Mount Baldy Component H2 (090)..... 01.5-34

Figure 01.5.1.2-5b Damped Response Spectra Plots for Northridge Mount Baldy Component H2 (090) 01.5-35

Figure 01.5.1.2-6a Damped Response Spectra Plots for Mount Baldy Component V (UP) 01.5-36

Figure 01.5.1.2-6b Damped Response Spectra Plots for Mount Baldy Component V (UP) 01.5-37

Figure 01.5.1.2-7 Smoothed Power Spectral Density Plots for Component H1 (180) 01.5-38

Figure 01.5.1.2-8 Smoothed Power Spectral Density Plots for Component H2 (090) 01.5-38

Figure 01.5.1.2-9 Smoothed Power Spectral Density Plots for Component V (UP) 01.5-39

Figure 01.5.1.2-10 Arias Intensities of the Northridge – Mount Baldy Artificial Time History Components Showing 5%-75% Duration 01.5-39

Figure 01.5.2-1 Foundation Level Base-Case Shear and Compression Wave Velocity Profiles 01.5-40

Figure 01.5.2-2 Small Strain Shear Wave Velocity Damping 01.5-42

Figure 01.5.2.1-1 Median Spectra (5% damped) Compared to CSDRS Horizontal Components 01.5-43

Figure 01.5.2.1-2 Median Spectra (5% damped) Compared to CSDRS Vertical Components 01.5-44

Figure 01.5.2.1-3 Median Spectra (5% damped) Compared to CSDRS Vertical Components Using RG 1.60 V/H Ratios 01.5-45

Figure 01.5.2.2-1 Strain Compatible Properties Computed for Profile 270-200 ..... 01.5-46

Figure 01.5.2.2-2 Strain Compatible Properties Computed for Profile 270-500 ..... 01.5-49

Figure 01.5.2.2-3 Strain Compatible Properties Computed for Profile 560-500 ..... 01.5-52

Figure 01.5.2.2-4 Strain Compatible Properties Computed for Profile 900-100 ..... 01.5-55

Figure 01.5.2.2-5 Strain Compatible Properties Computed for Profile 900-200 ..... 01.5-58

Figure 01.5.2.2-6 Strain Compatible Properties Computed for Profile 2032-100 ..... 01.5-61

LIST OF TABLES

Table **Title** **Page No.**

Table 01.4.1.1-1 Target Control Points for US-APWR CSDRS 01.4-10

Table 01.4.1.2.1-1 Time Envelope Function to Develop US-APWR Target PSDs..... 01.4-11

Table 01.4.1.2.2-1 Time-Envelope Function Used in NUREG/CR-5347..... 01.4-11

Table 01.4.2-1 Initial Profile Categories 01.4-12

Table 01.4.2.1-1 Final Profile Categories..... 01.4-13

Table 01.5.1.2-1 Summary of SRP 3.7.1 Option 1, Approach 1 Requirements Compliance..... 01.5-8

Table 01.5.1.2-2 Magnitudes and Distance Bins and Strong Motion Duration Criteria 01.5-8

Table 01.5.1.2-3 CEUS V/A & AD/V^2 Mean Ratios ± One Standard Deviation..... 01.5-9

Table 01.5.2.1-1 Magnitudes, Distances, and Median Peak Accelerations 01.5-9

Table 01.5.2.2-1 Strain Compatible Properties for Profile 270-200..... 01.5-10

Table 01.5.2.2-2 Strain Compatible Properties for Profile 270-500..... 01.5-13

Table 01.5.2.2-3 Strain Compatible Properties for Profile 560-500..... 01.5-16

Table 01.5.2.2-4 Strain Compatible Properties for Profile 900-100..... 01.5-19

Table 01.5.2.2-5 Strain Compatible Properties for Profile 900-200..... 01.5-20

Table 01.5.2.2-6 Strain Compatible Properties for Profile 2032-100..... 01.5-21

01.1.0 INTRODUCTION

The design of the US-APWR standard plant structures is based on the analyses of the seismic responses determined by dynamic models, considering the effects of Soil-Structure Interaction (SSI) and Structure-Soil-Structure Interaction (SSSI). Consistent with Nuclear Regulatory Commission (NRC) Standard Review Plan (SRP) 3.7.1 (Reference 01-1), the seismic response analyses incorporates the following considerations which are presented in this part of the Technical Report (TeR):

- development of suitable acceleration time histories, compatible with the US-APWR Certified Seismic Design Response Spectra (CSDRS) used as input ground motion in the SSI and SSSI analyses;
- development of multiple generic soil profiles that provide realistic representation of various soil conditions at potential sites within the Central and Eastern United States (CEUS).

The CSDRS compatible ground motion time histories and the generic layered profiles presented in Part 1 of this TeR are used to develop the inputs to the site-independent SSI and SSSI analyses of the Reactor Building (R/B) complex. This Part of the TeR documents the development of time histories of the three ground motion components compatible with the CSDRS. The time histories are generated using seed ground motion recordings that comply with the criteria of SRP 3.7.1 (Reference 01-1), Subsection 3.7.1.II.1B using Option 1, Approach 1. The R/B complex foundation is an embedded foundation with an embedment depth of approximately 42 ft from plant grade. In SSI and SSSI analyses, the structure is analyzed as an embedded structure using ACS SASSI. The input time histories needed for the analyses are within (in-layer) motions corresponding to each of the soil profiles considered. The CSDRS is identified as an outcrop motion in the free field at the foundation bottom level of the structure. Therefore, the CSDRS compatible time histories presented in this TeR are converted to within motions in Part 3 of this TeR through full soil column analysis for each soil profile considered, and the within motions are used as input to the analyses.

In addition, the seismic design is based on a set of SSI analyses that addresses the effect of the soil layering as well as the elevation of the ground water table at one foot below plant grade. The effects of groundwater level on the SSI analyses are addressed in MUAP-11007 (Reference 01-2). These SSI analyses consider generic profiles representing layered soil properties. The development of Strain Compatible Properties (SCP) of the generic layered soil profiles consistent with the CSDRS and its applied elevation is documented in this Part of the TeR. The near field backfill materials surrounding the basemat of the R/B complex are modeled together with the structure in SSI and SSSI analyses and are discussed and documented in Part 3 of this TeR.

01.2.0 PURPOSE

The purpose of Part 1 of this TeR is to present the technical approach for the development of the time histories and soil profile design bases for the seismic response analyses of the US-APWR standard plant R/B complex. This TeR outlines the general methodology used for the development of the CSDRS compatible ground motion time histories and the soil profiles used for the standard design.

01.3.0 OBJECTIVES

01.3.1 Design Basis Time Histories

SRP 3.7.1 (Reference 01-1), Subsection 3.7.1.II SRP Acceptance Criteria 1B, Option 1 Approach 1 provides methodology used to generate a design basis time history with three components compatible with the CSDRS from seed recorded earthquake ground motions. The earthquake seed used to develop the design basis time history is a segment of the January 17, 1994 Northridge earthquake recorded at the Mt. Baldy Station. The seed time history is modified to envelope the CSDRS at damping values representative of structures, systems, and components.

For an artificial time history developed using SRP 3.7.1 Option 1, Approach 1, a minimum Power Spectral Density (PSD) requirement must be satisfied in order to prevent insufficient energy for certain frequencies in the artificial time history. When Regulatory Guide (RG) 1.60 (Reference 01-3) response spectra are used as design response spectra, the criteria for a compatible target PSD are contained in SRP 3.7.1 Appendix A. For design response spectra other than the RG 1.60 response spectra, a target PSD is generated in accordance with SRP 3.7.1 to be compatible with the design response spectra. This TeR describes how the target PSDs are developed.

The final design basis time history components are developed to match with the CSDRS and the target PSDs, in accordance with SRP 3.7.1 Subsection 3.7.1.II.1B. They are used to develop the input ground motion for the SSI and SSSI analyses described in Part 3 of this TeR.

01.3.2 Generic Layered Soil Profiles and Strain Compatible Properties

The goal of the soil profile selection process is to provide a suite of soil profiles which together with the CSDRS will result in a seismically qualified design that can be constructed at a variety of CEUS potential sites. The objective of the generic layered soil profiles and SCP is to provide a set of input soil properties that result in a range of SSI. A set of generic layered soil profiles is developed and used as input for the site-independent SSI and SSSI analyses of the US-APWR. These soil profiles represent dynamic soil properties that are compatible with the strains generated by the seismic ground motions whose spectra, as full column outcrop spectra at the R/B complex foundation bottom, are enveloped by the US-APWR CSDRS (refer to Section 01.4.2.2). These soil properties are developed from a database of Western United States (WUS) as well as CEUS measured soil velocities. The representative generic profiles are developed by averaging the shear wave velocities of suites of profiles reflecting similar surficial geology in the two regions. The generic layered profiles, for which SCP, shear and compression wave velocities and corresponding hysteretic damping values are developed, provide dynamic soil/rock properties that capture a range of SSI responses expected at potential sites across the CEUS, including the effects of the layering of the subgrade and the elevation of the water table. Part 3 of this TeR demonstrates, using SSI first peak frequencies, that there is a range of frequencies represented in the site independent analysis.

01.4.0 APPROACH / METHODOLOGY

01.4.1 Design Basis Time Histories

The design basis time histories, used as input motions for the seismic response analyses, were developed in compliance with SRP 3.7.1.II.1B Option 1, Approach 1. One criterion of the SRP is that the PSDs of the components of the time history must bound 80% of a target PSD. The SRP provides a target PSD for use with time histories that are developed to be compatible only with the RG 1.60 spectra. Thus a PSD must be developed to use with the CSDRS. Since the CSDRS contains frequency content that is higher than that of the RG 1.60 spectra, the method of computing the PSD from a time history required refinement.

This methodology section presents the site independent target response spectra, which is used as the basis for seismic design (Section 01.4.1.1), the development of the target power spectral densities (Section 01.4.1.2) and the development of the design basis time histories (Section 01.4.1.3).

01.4.1.1 Target Response Spectra – The CSDRS

The CSDRS for US-APWR are derived from RG 1.60 spectra by scaling the spectra contained in RG 1.60 from 1.0 g to 0.3 g Peak Ground Acceleration (PGA) values, and by modifying the RG 1.60 control points to broaden the spectra in the higher frequency range. The RG 1.60 spectral values are based on recorded seismic events for WUS earthquakes. NUREG/CR-6728 (Reference 01-4) indicates that earthquakes in the CEUS have more energy content in the higher frequency range than earthquakes in the WUS. Thus, the RG 1.60 spectra control points have been modified by shifting the control points at 9 Hz and 33 Hz to 12 Hz and 50 Hz, respectively, for both the horizontal and the vertical spectra.

Control points for target spectral accelerations are shown in Table 01.4.1.1-1. The CSDRS are developed from 0.25 Hz to 100 Hz following RG 1.60 spectra. The accelerations between 0.25 Hz and 0.10 Hz are computed to maintain constant displacement for the E control points similar to the accelerations of the D control points of RG 1.60. There are two target response spectra components: one for horizontal components and one for the vertical component of ground motions. Figure 01.4.1.1-1 and Figure 01.4.1.1-2 show the horizontal and vertical CSDRS at different damping values, respectively.

01.4.1.2 Power Spectral Densities Compatible with CSDRS

The target PSD provided in SRP 3.7.1 Appendix A is only applicable to a RG 1.60 horizontal response spectrum. The CSDRS is broadened from the RG 1.60 spectra by increasing the spectral responses for high frequencies up to 50 Hz. SRP 3.7.1 Option 1, Approach 1 requires a minimum PSD to be satisfied for the each component of the time histories. Therefore, it is necessary to develop US-APWR target PSDs for both horizontal and vertical time history.

Furthermore, the upper frequency limit of the PSD envelope criteria needs to be increased beyond 24 Hz as stipulated in SRP 3.7.1, Appendix A, in order to be compatible with the CSDRS broadened to 50 Hz from RG 1.60 spectrum. As demonstrated in Section 01.4.1.2.2, the PSD calculation equation needs to be refined to achieve an appropriate envelope to the target PSD at frequencies higher than 24 Hz.

01.4.1.2.1 Development of US-APWR Target PSD

This section presents the methodology which is utilized to develop both the horizontal and vertical target PSDs which are compatible with the CSDRS. These target PSDs are subsequently used in the development of design basis time histories from a recorded seed described in Section 01.4.1.3 below.

NUREG/CR-5347 Appendix B (Reference 01-5) provides a methodology to develop a target PSD compatible with a target response spectrum using random process simulation. The methodology starts with an initial trial target PSD as input, and then iterates the process several times by adjusting the input trial PSD, until the convergence criteria is met (Step 4 as listed below).

The procedure to develop the target PSDs is as follows:

1. Select a reasonable horizontal trial PSD;
2. Generate 30 artificial time histories from a deterministic time envelope function and 30 sets of randomly selected phase relationships, using the trial PSD and Equations 01.4.1.2.1-1 through 01.4.1.2.1-3 (Equations 7 through 9 in NUREG/CR-5347, Appendix B (Reference 01-5)). The time envelope function *g(t)*, as shown in Table 01.4.1.2.1-1 and Figure 01.4.1.2.1-1, similar to "Function B" in NUREG/CR-5347 Appendix B, is selected to simulate real earthquake time histories. Total duration of the time histories is set to be 20.24 seconds to satisfy the SRP 3.7.1 guidance requirements on minimum time history duration of 20 seconds.

   Given a trial PSD function, $S_O(\omega)$, and a time envelope function, *g(t)*, an artificial acceleration time history, $\ddot{z}_0(t)$, is generated from:

$$\ddot{z}_0(t) = g(t)\ddot{\zeta}_O(t) \qquad \text{Equation 01.4.1.2.1-1}$$

$$\ddot{\zeta}_O(t) = \sqrt{2}\sum_{k=1}^{N}\sqrt{S_O(\omega_k)\Delta\omega}\ \cos(\omega_k t + \phi_k) \qquad \text{Equation 01.4.1.2.1-2}$$

   with

$$\omega_k = k\Delta\omega \qquad \Delta\omega = \frac{\omega_u}{N} \qquad \text{Equation 01.4.1.2.1-3}$$

   and ϕ_k is a sequence of independent realizations, i.e., random numbers, uniformly distributed between 0 and 2π. N is the total number of frequencies used to create the artificial time history, and ω_u in Equation 01.4.1.2.1-3 is the highest angular frequency desired for the frequency content of the artificial time history. In the calculation described here, the maximum frequency desired f_u ($f_u = \omega_u / 2\pi$) is 100 Hz, and the desired incremental frequency Δf ($\Delta f = \Delta\omega / 2\pi$) is 0.01 Hz. Therefore, N is 10,000.
3. Calculate the 2% damped pseudo-velocity response spectra from the acceleration CSDRS and compare the average velocity response spectra of the 30 time histories with the 2% damped CSDRS pseudo-velocity response spectra.
4. Modify the trial PSD and repeat the process from Steps 2 and 3 until the average pseudo-velocity response spectra lies "*close to, but generally below*" (Reference 01-5) the CSDRS pseudo-velocity response spectra.

5. Once the average response spectrum of the 30 artificial time histories lies "*close to, but generally below*" the CSDRS, the trial PSD is the target PSD compatible with the CSDRS.

The same process is used to generate the vertical target PSD compatible with the vertical US-APWR CSDRS.

Figure 01.4.1.2.1-2 shows the flowchart to develop the target PSDs.

01.4.1.2.2 PSD Calculation Methodology from Time Histories

This section presents a refinement to the methodology used to compute a PSD from a time history. The refinement is necessary because the PSD is expected to be reliably computed to frequencies well beyond the 24 Hz as defined in Appendix A to SRP 3.7.1. The limit for reliable PSD computation for the design basis time history described here is established to conservatively equal the frequency at which the CSDRS returns to the PGA which is 50 Hz. The methodology described uses a known target response spectrum together with a known target PSD, both shown in SRP 3.7.1, Appendix A. Once the refined methodology is developed, it is subsequently used in the development of the artificial time histories from a recorded seed described in the Section 01.4.1.3 below.

Required Frequency Range for Target PSD

SRP 3.7.1 Appendix A indicates that the PSD match is unnecessary for frequencies beyond 24 Hz, since the power beyond 24 Hz for the target PSD is so low as to be inconsequential. Further, SRP 3.7.1 Appendix B specifies that "for Central and Eastern US Rock Sites checks above 50 Hz are unnecessary." Therefore, the upper bound frequency limit for the PSD evaluation is conservatively compared beyond 24 Hz out to 50 Hz. The lower bound frequency limit is the same of specified in SRP 3.7.1 Appendix A, which is 0.3 Hz.

Appropriate PSD Calculation Equations up to 50 Hz

SRP 3.7.1 Appendix A provides an equation to calculate PSD from a time history, also shown here in Equation 01.4.1.2.2-1. As indicated in SRP 3.7.1 Appendix A, the upper frequency limit was set to 24 Hz for the RG 1.60 compatible target PSD. However, as discussed above, the minimum PSD requirement for US-APWR applies to a frequency range from 0.3 Hz to 50 Hz, due to the broadened CSDRS. Therefore, verification that the PSD calculation equation provided in SRP 3.7.1 Appendix A (Equation 01.4.1.2.2-1) can produce appropriate PSD results between 0.3 Hz and 50 Hz from a time history is necessary. The following procedure is employed for the verification process. Choosing the SRP 3.7.1, Appendix A target PSD as input, 30 artificial time histories were generated using the algorithm provided in NUREG/CR-5347, Appendix B (Reference 01-5), also shown in Equations 01.4.1.2.1-1, 01.4.1.2.1-2, and 01.4.1.2.1-3. The PSDs of the artificial time histories were then calculated using three different equations (scenarios). The equation that produces results that match the input target PSD closely up to 50 Hz is the one that will be used to calculate PSDs from time histories. The detailed procedure is explained as follows.

1. Generate 30 artificial time histories using the SRP 3.7.1, Appendix A target PSD, 30 sets of random phase angles uniformly distributed between 0 and 2π, and an envelope function shown in Figure 01.4.1.2.2-1 and Table 01.4.1.2.2-1, which is the same function as used in the NUREG/CR-5347 Appendix B.
2. Calculate the PSDs of the 30 time histories using Equation 01.4.1.2.2-1,

$$S_0(f) = \frac{2|F(f)|^2}{2\pi T_D}$$ Equation 01.4.1.2.2-1

where $S_o(f)$ = PSD at frequency f;

$|F(f)|$ = Fourier Amplitudes at frequency f;

for the following three scenarios:

i. Compute 1-sided Fourier amplitudes $|F(f)|$ over the total time history duration with T_D equal to the total duration.

ii. Compute 1-sided Fourier amplitudes $|F(f)|$ over the strong motion duration with T_D equal to the strong motion duration, calculated as shown in Equation 01.4.1.2.2-2,

$$T_D = T_{AI=75\%} - T_{AI=5\%}$$ Equation 01.4.1.2.2-2

The strong motion duration is defined as the time between 5% and 75% of the normalized cumulative Arias Intensity (AI). The normalized cumulative AI is based in the total cumulative energy. The total cumulative energy is calculated using Equation 01.4.1.2.2-3.

$$E = \frac{\pi}{2g}\int_0^T a(\tau)^2 d\tau$$ Equation 01.4.1.2.2-3

where T is total duration of the time history; and a(τ) is the acceleration time history

The normalized cumulative AI is computed using Equation below.

$$AI(t) = \frac{\pi}{2gE}\int_0^t a(\tau)^2 d\tau$$ Equation 01.4.1.2.2-4

iii. Compute Fourier amplitudes $|F(f)|$ over the total time history duration with T_D equal to an "equivalent stationary phase strong motion duration," computed as shown in Equation 01.4.1.2.2-5,

$$T_D = \frac{T_{AI=75\%} - T_{AI=5\%}}{75\% - 5\%} = \frac{T_{AI=75\%} - T_{AI=5\%}}{0.7}$$ Equation 01.4.1.2.2-5

T_D calculated in this way corresponds to the time between AI = 0% and AI = 100% calculated considering a straight line with a slope calculated from AI = 5% to AI = 75%, i.e., slope between AI pairs [t(AI =5%), AI = 5%] and [t(AI =75%), AI = 75%].

3. Finally, smooth the PSDs within ±20% frequency range at the frequencies of interest. Compute the average of the smoothed PSDs of the 30 time histories, and then compare it with the SRP 3.7.1 Appendix A target PSD.

Figure 01.4.1.2.2-2 shows the flowchart to verify the PSD calculation equations from time histories.

01.4.1.3 Development of Design Basis Time Histories in Accordance with SRP 3.7.1 Option 1, Approach 1

A segment including the strong motion portion of the BAL (Mount Baldy, CA) recordings, i.e., the three components of the earthquake, of the January 17th, 1994, Magnitude 6.7 Northridge

Earthquake, obtained from the Pacific Earthquake Engineering Research (PEER) Center's digital ground motion library (Reference 01-6) are chosen as the seed ground motions for generating the seismic design basis time histories. The BAL recordings of the Northridge earthquake are selected because they have the required durations and correlations (statistical independence among the three components) and because their spectral shapes, when scaled, are a reasonably good match to the CSDRS in the 2-20 Hz range for all three orthogonal components. The recorded time histories contain 4,000 digitized data points using a 0.01 second time step. The strong motion portion of the recorded time histories between t=11.0 to t=33.08 seconds, i.e., duration of 22.08 seconds, are extracted as the seeds which are developed to be compatible with the CSDRS. The digitized acceleration values are linearly interpolated to obtain accelerations at every 0.005 seconds to enable the modified time histories to account for higher frequency content after adjustment such that their Nyquist frequency is 100 Hz.

The goal of the development process is to produce modified time histories whose response spectra envelop the CSDRS for the US-APWR. In order to achieve this goal, the Fourier amplitudes of the seed acceleration time histories are modified to generate three new acceleration time histories. This Fourier amplitude modification process is iterated until the response spectra calculated from the modified Northridge time histories envelop the target response spectra at damping ratios of 2%, 3%, 5%, 7%, and 10%. Once the response spectra of the time histories envelop the CSDRS, the PSD envelope requirements are assessed. At frequencies with PSD lower than 80% of the target PSD, the Fourier amplitudes of the time histories are adjusted to satisfy the PSD requirements. Then a baseline correction is applied to the time histories. Next, the resulting time histories are verified for their compliance with the SRP 3.7.1, Option 1, Approach 1 Acceptance Criteria. When necessary, the baseline corrected time histories are scaled to comply with the enveloping criteria for the spectra at the 2%, 3%, 5%, 7%, and 10% damping ratios, and the envelope requirements for the target power spectral density functions. Finally, the modified Northridge time histories are checked for the requirements of strong motion duration, correlation coefficients, and V/A and AD/V^2 ratios, where A is the maximum ground acceleration, V is the maximum ground velocity, and D is the maximum ground displacement. The final modified Northridge time histories are the design basis time histories used as input ground motions for the SSI and SSSI analyses.

01.4.2 Development of Soil Profiles and Strain Compatible Properties

A suite of soil profiles and depths to basement material (to be subsequently referred to as "baserock") is considered. The soil profiles are selected from a database of initial small-strain site properties that represent a range of generic site conditions from deep soft soil to firm rock that may exist across the continental US. These profiles are then adjusted to make them appropriate for potential sites across much of the CEUS.

The suite of baseline profiles is based on averaging measured shear wave velocities for profiles with similar velocities at sites located in WUS, and the CEUS. Measurements of site profiles typically do not extend to the same depths for all profiles averaged within groups of similar surficial geology or velocities. The number of available profiles generally decreases rapidly with depth as noted in "Surface Geology Based Strong Motion Amplification Factors for the San Francisco Bay and Los Angeles Areas" (Reference 01-7). Therefore, these profiles were extended to become the generic profiles at deeper depths.

These initial small-strain profiles reflect realistic generic site conditions with continuously increasing stiffness of the soil with depth that are developed by averaging shear and compression wave velocities of multiple profiles. The increase in small strain shear wave velocity is due to confining pressure increase for the softer profiles (e.g., sands, gravels, loess, till, etc.) and a decrease in weathering with increasing depth for the stiffer profiles (e.g., saprolite).

The profile selection process is described below:

1. 100 feet is as shallow a soil depth that is reasonable. Any sites with soil depths less than 100 feet will likely have all soil removed to rock;
2. Except for the Mississippi Embayment, the Gulf Coastal Plain and the Atlantic Coastal Plain, 500 feet is approximated as the deepest site that will be encountered in the CEUS. It is recognized that for soil sites with same nominal shear-wave velocity $\overline{V_S}$ (30m) and a deeper overburden depth, more energy dissipation from the radiation damping mechanism will occur. The SSI effects will tend to reduce seismic structural response for deeper soil depths. Therefore, the 500 ft overburden depth is selected as the upper limit of overburden depth for the soil profile categories. Furthermore, 500 ft overburden depth is about the deepest depth for the sites with soft overburden materials (soils) that will be encountered in much of the CEUS;
3. Selected an intermediate depth of 200 feet;
4. Select profiles ranging from firm soils (270 m/s), to stiff soil to soft rock (560 m/s), and a range in firm rock (900 m/s) and (2032m/s);
5. To make the suite of profiles regionally appropriate for CEUS sites, the baserock conditions are set to that of hard rock, approximately 9,300 ft/s (2,830 m/s, EPRI Technical Report TR-102293, Reference 01-8). This value is consistent with the hard rock site conditions defined in EPRI TR-1009684 (Reference 01-9) Ground Motion Prediction Equations;
6. Adjusted the soft soil (270 m/s) for foundation conditions. The minimum shear wave velocity for the top 30 meters must be greater than 1000 fps (305 m/s). The soft shallow materials would be either removed or improved for appropriate foundation conditions;
7. Added sedimentary rock between the soils (270 m/s and 560 m/s) and the baserock which is present in the CEUS.

The generic profiles are classified using a nominal shear-wave velocity $\overline{V_S}$ (30m) representing the average shear wave velocity over the top 30 meters. This classification is consistent with current practice for building codes and is a convenient metric with which to distinguish the initial profiles, prior to soil removal or improvement.

The initial suite of nine small strain baseline candidate profiles is illustrated in Figure 01.4.2-1 to depths of 500 feet and ranges in nominal shear wave velocity $\overline{V_S}$ (30m) from soft soil at 190 m/s to firm rock at 2,830 m/s.

To accommodate the possible range in profiles for CEUS, a suite of profile depths to rock conditions is developed ranging from 25 ft to 2,000 ft. The suite of nine profile depth bins is listed on Table 01.4.2-1 along with the $\overline{V_S}$ (30m) values for each category. A layer of sedimentary type of rock with gradually increasing stiffness is inserted above the hard baserock ($\overline{V_S}$ = 2.83 km/s, Table 01.4.2-1) to accommodate the presence of sedimentary rocks (sandstones, shales, claystones) beneath the shallow softer soil profiles with nominal shear wave velocity of 560 m/s below and nominal top soil thickness of 500 ft and less. The occurrence of sedimentary rock or weathered basement overlying hard basement rock is common across much of the CEUS. The soft rock layers are assumed to exhibit linear behavior under the moderate loading levels of the site response analyses (Section 01.5.2.1) with the shear and compression wave damping fixed at 0.5% ($Q_{S,P}$ = 100). Also, listed in Table 01.4.2-1 for reference, is the hard rock crustal model, the top layer of which defines the CEUS baserock conditions (EPRI TR-102293 (Reference 01-8) and TR-1009684 (Reference 01-9)).

The strain-dependent soil profiles are obtained from a set of Random Vibration Theory (RVT) approach based site response analyses that use the point-source model to generate both the input horizontal and vertical motions. The RVT equivalent-linear approach, as referred to RG 1.208 (Reference 01-10), and the point-source model is a commonly used method for generation of site specific design spectra and has been validated in References 01-4, 01-8, 01-11, and 01-12. Magnitude **M**7.5 is used as its broad spectral shape and reflects the appropriate loading level for a single earthquake and a single soil profile while maintaining consistency with the CSDRS. A smaller magnitude would result in higher short period motions and higher strains. Distances to the **M**7.5 control earthquake are adjusted such that the median spectrum computed for each profile approaches, but does not exceed, the horizontal and vertical CSDRS at foundation bottom level. The SCP are generated for the seismic loadings whose median spectra as Full Column Outcrop (FCO) spectra at R/B complex foundation bottom level are enveloped by the CSDRS.

Site response analyses, which use modulus reduction and hysteretic damping curves from EPRI TR-102293 (Reference 01-8) to account for non-linear properties of the soil/rock as a function of the earthquake induced strains, are also performed. The curves are appropriate for generic soils comprised of gravels, sands, and low Plasticity Index (PI) clays (refer to Reference 01-8) and are shown in Figure 01.4.2-2. These curves also provide realistic SCP for the generic rock materials when subjected to low intensity strains generated by ground motions which spectra, as full column response spectra, at foundation bottom are enveloped by the CSDRS. The input control motions used for the site response analyses reflect contributions of multiple site conditions and earthquakes of varying sizes that define the CSDRS as broadband design spectra. The use of input control motions that represent a single earthquake ensures that the site response analyses provide appropriate SCP of the generic soil profiles reflecting realistic strains in the soil columns.

01.4.2.1 Selection of Profiles

The small strain profiles selected for the development of SCP include soft and hard soil profiles (nominal shear wave velocity of 270 m/s and 560 m/s respectively) and soft and firm rock profiles (nominal shear wave velocity of 900 m/s and 2,032 m/s, respectively).

The development of softer soil SCP considers additional soil removal if necessary to maintain a minimum (-1σ) strain compatible shear wave velocity of at least 800 ft/s near the plant grade surface. There are two 270 m/s profiles where the top 68 ft of soil is replaced. Although the profile name remains 270 the $\overline{V_S}$ (30m) has increased to 425 m/s. These two profiles of softer 270 m/s soil representing layers of dense cohesionless soil and/or over-consolidated stiff clay are considered with depths of 200 ft and 500 ft above rock foundations consisting of sedimentary or weathered rock section overlying Precambrian basement material.

The third soil profile considered is a 500 ft thick layer of stiff 560 m/s soil representative of glacial till sites consisting of highly consolidated mixtures of fine and course grained soils over 1000 ft deep strata of sedimentary or weather rock resting on the rock basement.

Two soft rock profiles (900 m/s) are considered with depths of 100 ft and 200 ft.

The sixth profile is a firm rock profile with a nominal shear wave velocity of 2,032 m/s and depth of 100 ft is selected to represent a residual soil (saprolite) over weathered rock and underlain by hard rock. This profile is intended to reflect hard rock foundation depths after removal of the soft surficial residual soils.

The saturated soil small strain Compression Wave Velocity (V_p) is developed from the combined compression wave velocities from the database by increasing V_p up to a minimum of 5000 fps, maintaining the gradient that is similar to the unsaturated soil profile developed from the database and smoothing the resulting V_p profile. This gradient smoothing adjustment approach resulted in more realistic representation of saturated site conditions than simply setting a V_p value of 5,000 ft/sec to reflect the properties of saturated soil.

These types of selected generic profiles are appropriate for the CEUS. The final soil profile categories are summarized in Table 01.4.2-1. The small strain Shear Wave Velocity (V_s) and V_p are plotted in Figure 01.4.2.1-1 and Figure 01.4.2.1-2. The shear strain damping is plotted in Figure 01.4.2.1-3. The nomenclature for the final soil profiles gives both the shear wave velocity and the depth to bedrock. For example, soil profile 560-500 designates the soil with shear wave velocity of 560 m/s with a depth of 500 ft.

The development of generic profiles assumed a water table located at the plant grade elevation by setting the value of compression wave velocity at or above 5,000 ft/s which is the compression wave velocity of water. The Civil Structural Design Criteria (Reference 01-13) specifies a water table depth of one foot below the plant grade which, for the development of vertical motions, is equivalent to the surface. Due to the absence of fluids over the top one foot, the lower compression-wave velocity has a very minor impact on vertical motions for the softer profiles. In order to study the water table fluctuation effect on the seismic response of the structures, a set of unsaturated soil profiles are developed for SSI analysis and are presented in Technical Report MUAP-11007 (Reference 01-2).

01.4.2.2 Development of US-APWR CSDRS Strain Compatible Properties

Thirty realizations are generated for each soil profile in order to characterize, in a fully probabilistic manner, the range and variation in SCP of the top soil. Thirty realizations provide a very stable estimate of the mean strain compatible soil properties that are used as input for the SSI analyses, the statistic of importance as the median spectrum defines the loading level

for each soil and rock. For the standard deviation, 30 realizations are sufficient to estimate sigma within 20 percent at the 90 percent confidence level from standard statistical tables and 60 realizations marginally improves the stability to only 15 percent. To substantially improve the stability to five percent requires over 500 realizations. The interest in the standard deviation is only to provide additional clarity in the process of developing the suite of generic SCP by showing reasonable range between -1 sigma and +1 sigma properties. Therefore, a suite of 30 realizations is considered sufficient for the purpose of developing generic profiles as the mean of the strain compatible soil properties. More detailed explanation of the statistical importance of 30 versus 60 realizations is provided in Appendix 1-A.

Each base-case profile is randomized in velocity as well as nonlinear dynamic material properties represented by degradation curves defining the stiffness reduction and the damping as functions of strain for each realization.

RVT equivalent-linear site response analyses are performed on each random profile for horizontal motions while linear analyses are used for vertical motions (refer to EPRI TR-102293 (Reference 01-8) and NCEER 97-0010 (Reference 01-14). Modulus reduction and hysteretic damping curves from EPRI TR-102293 are used for the horizontal component site response analyses. The curves are appropriate for generic soils comprised of gravels, sands, and low PI clays (refer to Reference 01-8) and are shown in Figure 01.4.2-1. These curves also provide realistic SCP for the generic rock materials when subjected to low intensity strains generated by ground motions that are consistent with the CSDRS.

The CSDRS is adopted from the RG 1.60 spectral shape which reflects a median plus one-sigma analysis of several earthquakes and a range of site conditions. Since the RG 1.60 and the CSDRS were based on a plus one-sigma analysis of earthquakes ranging in magnitude from approximately **M**5.4 to **M**7.7, the overall shape is consistent with a median magnitude of approximately **M**7.5. In order to maintain consistency with the spectral shape of the CSDRS, control motions are used as input for the site response analyses that reflect a representative magnitude of **M**7.5 for CEUS earthquake. A point-source model is used to develop control motions (refer to References 01-4 and 01-8). Source distances (loading levels) are adjusted such that the median 5% damped response spectrum developed for each profile and depth to baserock approaches, but does not exceed, the CSDRS.

For site response analyses, the use of realistic control motions, reflecting a magnitude consistent with the shape of the CSDRS, results in reasonable levels of cyclic shear strains for each soil/rock column and avoids the condition of overdriving the soil/rock columns if excited by a broad band CSDRS defined input motion. The broad band nature of the CSDRS can be taken to reflect the envelope of motions from a single earthquake and a range in site conditions. With this approach, shear strain levels and associated SCP reflect realistic loading conditions for CEUS sites and are appropriate for use as input in the site-independent SSI analyses. On the other hand, the use of a broad band CSDRS excitation would result in unrealistically high values for the strain compatible soil damping that will overestimate the dissipation of energy in the SSI system due to soil material damping. The resulting SCP are developed as median and $\pm 1\sigma$ estimates from the analyses of the random profile realizations. Since a single CSDRS reflects design motions representing a suite of profiles, its use to characterize input motions for SSI analyses with any single profile results in conservative motions within the structure over a wide frequency range.

Table 01.4.1.1-1 Target Control Points for US-APWR CSDRS

Horizontal Control Points			Vertical Control Points		
	Frequency (Hz)	Acceleration (g)		Frequency (Hz)	Acceleration (g)
2% Damping			2% Damping		
A	(50)	0.3	A	(50)	0.3
B	(12)	1.06	B	(12)	1.06
C	(2.5)	1.28	C	(3.5)	1.22
D	(0.25)	0.17	D	(0.25)	0.12
E	(0.1)	0.028	E	(0.1)	0.018
3% Damping			3% Damping		
A	(50)	0.3	A	(50)	0.3
B	(12)	0.92	B	(12)	0.92
C	(2.5)	1.10	C	(3.5)	1.05
D	(0.25)	0.154	D	(0.25)	0.106
E	(0.1)	0.0251	E	(0.1)	0.0164
5% Damping			5% Damping		
A	(50)	0.3	A	(50)	0.3
B	(12)	0.78	B	(12)	0.78
C	(2.5)	0.94	C	(3.5)	0.89
D	(0.25)	0.140	D	(0.25)	0.094
E	(0.1)	0.0226	E	(0.1)	0.015
7% Damping			7% Damping		
A	(50)	0.3	A	(50)	0.3
B	(12)	0.68	B	(12)	0.68
C	(2.5)	0.82	C	(3.5)	0.78
D	(0.25)	0.13	D	(0.25)	0.086
E	(0.1)	0.021	E	(0.1)	0.014
10% Damping			10% Damping		
A	(50)	0.3	A	(50)	0.3
B	(12)	0.57	B	(12)	0.57
C	(2.5)	0.68	C	(3.5)	0.65
D	(0.25)	0.12	D	(0.25)	0.078
E	(0.1)	0.019	E	(0.1)	0.012

Notes:
1. 0.3 g PGA
2. Based on RG 1.60, Revision 1 amplification factors
3. For Control Point D & E, acceleration is computed as follows:
   Acceleration = $(\varpi^2 D / 386.4\ \text{in/sec}^2)(F_A)(0.3)$
   ϖ = 2π(frequency) [rad/sec]
   D = Displacement [in]
   F_A = Amplification Factor from RG 1.60

Table 01.4.1.2.1-1 Time Envelope Function to Develop US-APWR Target PSDs

Time	Envelope Function (sec)
t_r	2.00
t_m	10.24
t_d	8.00

t_r = rise time
t_m = strong motion duration
t_d = decay time

Table 01.4.1.2.2-1 Time-Envelope Function Used in NUREG/CR-5347

(Reference 01-5)

Time	Envelope Function (sec)
t_r	1.40
t_m	10.24
t_d	7.00

t_r = rise time
t_m = strong motion duration
t_d = decay time

Table 01.4.2-1 Initial Profile Categories

Categories $\overline{V_S}$ (30m) (m/s)
190
270
400
560
760
900
1,364
2,032
2830
Depth to Rock (ft) for each Category
25 ± 10
50 ± 20
100 ± 40
200 ± 80
500 ± 200
1,000 ± 400
2,000 ± 800

Hard rock crustal model (References 01-8 and 01-9)			
Depth (km)	**V_s (km/s)**	**V_p (km/s)**	**ρ (cgs)**
1	2.83	4.9	2.52
11	3.52	6.1	2.71
28	3.75	6.5	2.78
INFINITE	4.62	8.0	3.35

Notes: V_s =Shear wave velocity
V_p = Compression wave velocity
ρ(cgs) = Density (grams per cubic centimeter)

Table 01.4.2.1-1 Final Profile Categories

Category (initial $\overline{V_S}$ [30m]) (m/s)	Depth to Rock* (ft)
270	200
	500
560	500
900	100
	200
2,032	100

* For soft and hard soil profiles 270 m/s and 560 m/s, underlying baserock conditions reflect soft rock with a shear wave velocity of 1 km/s. For soft and firm rock profiles 900 m/s and 2,032 m/s, underlying baserock conditions reflect hard rock with a shear wave velocity of 2.83 km/s (Table 01.4.2-1).

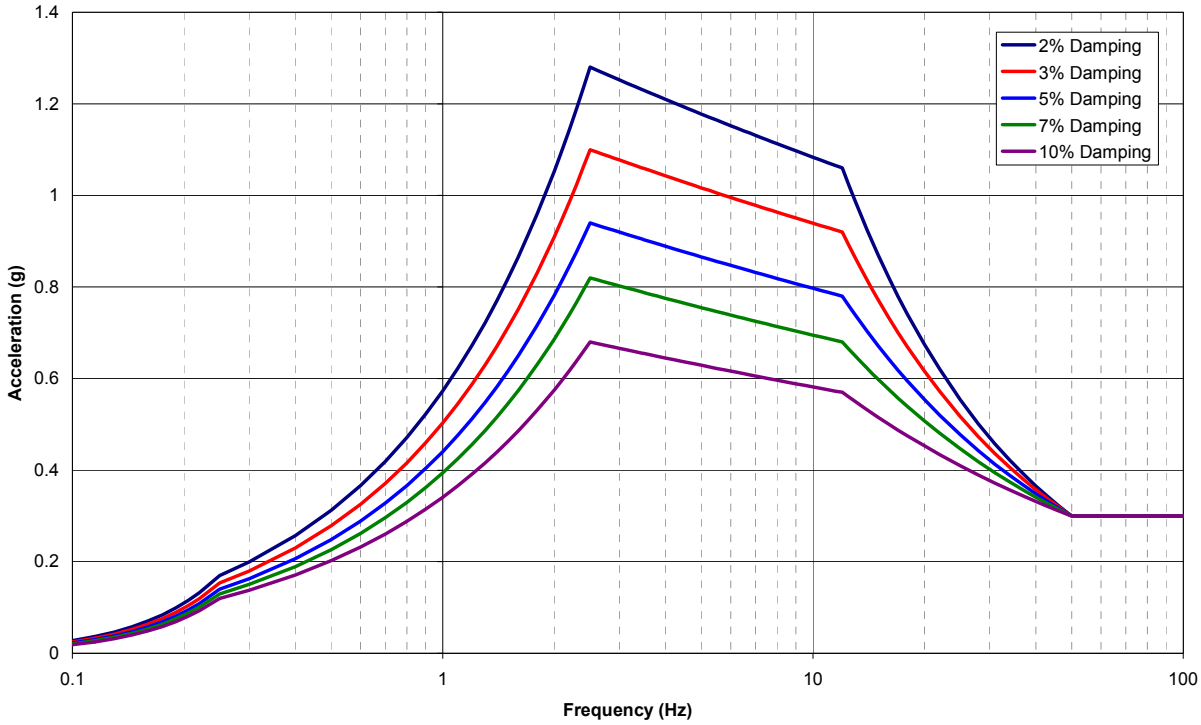

Figure 01.4.1.1-1 US-APWR Horizontal CSDRS

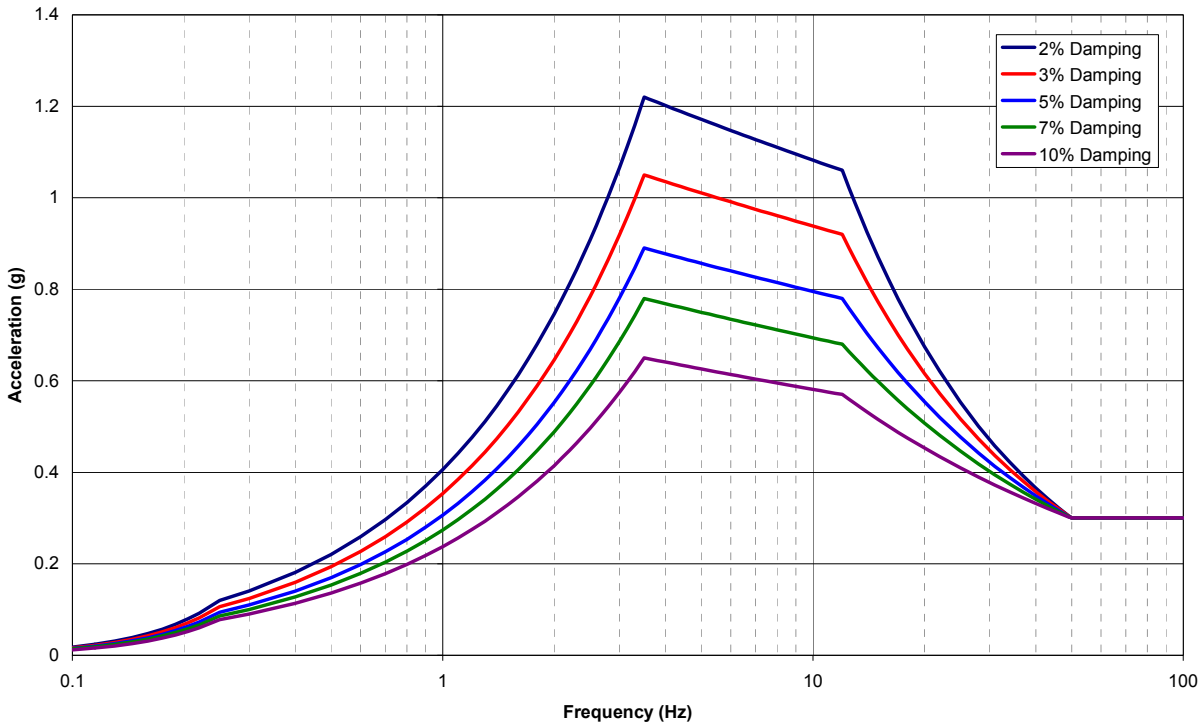

Figure 01.4.1.1-2 US-APWR Vertical CSDRS

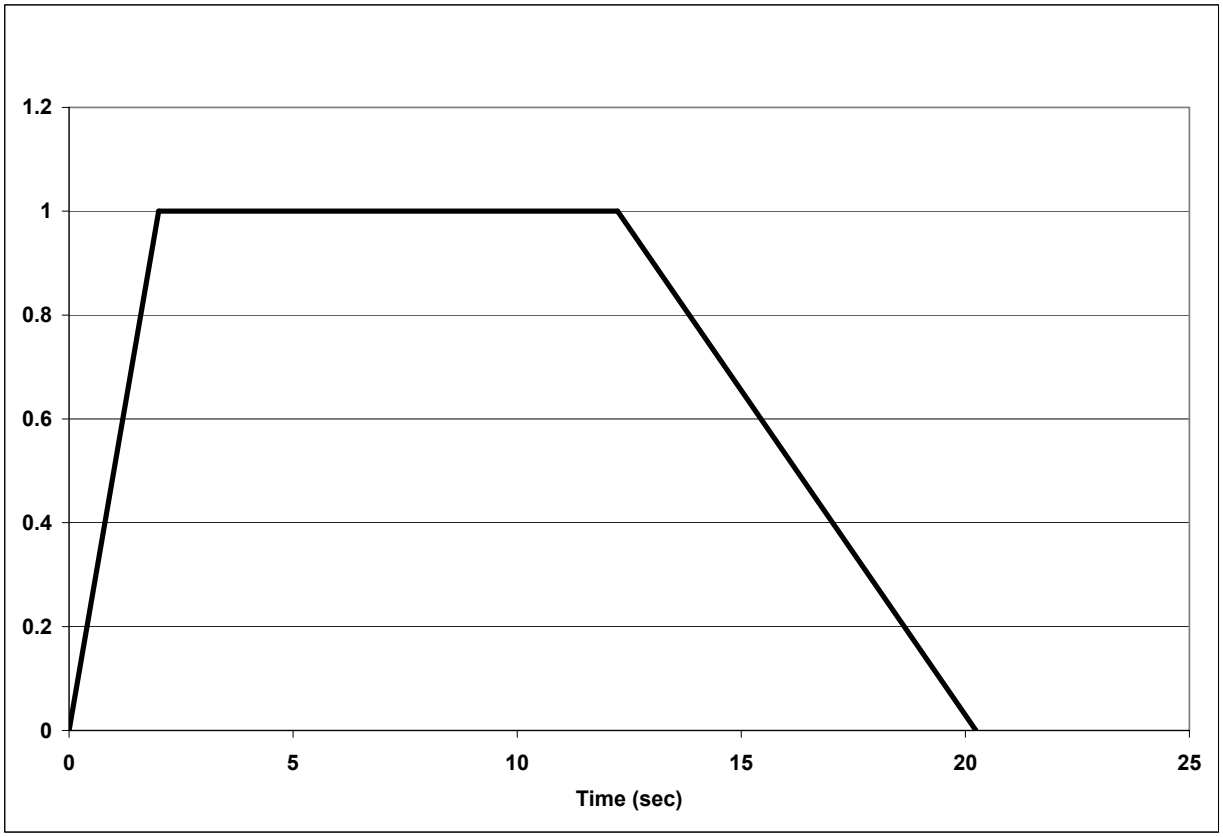

Figure 01.4.1.2.1-1 Time-Envelope Function to Develop US-APWR Target PSDs

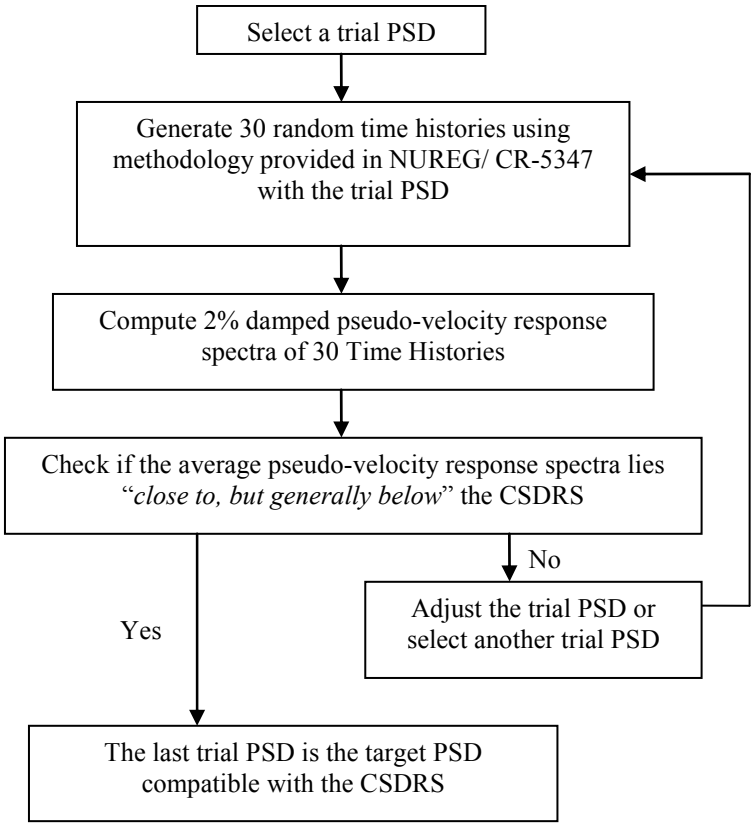

Figure 01.4.1.2.1-2 Work Flow to Develop a Target PSD Compatible with the CSDRS

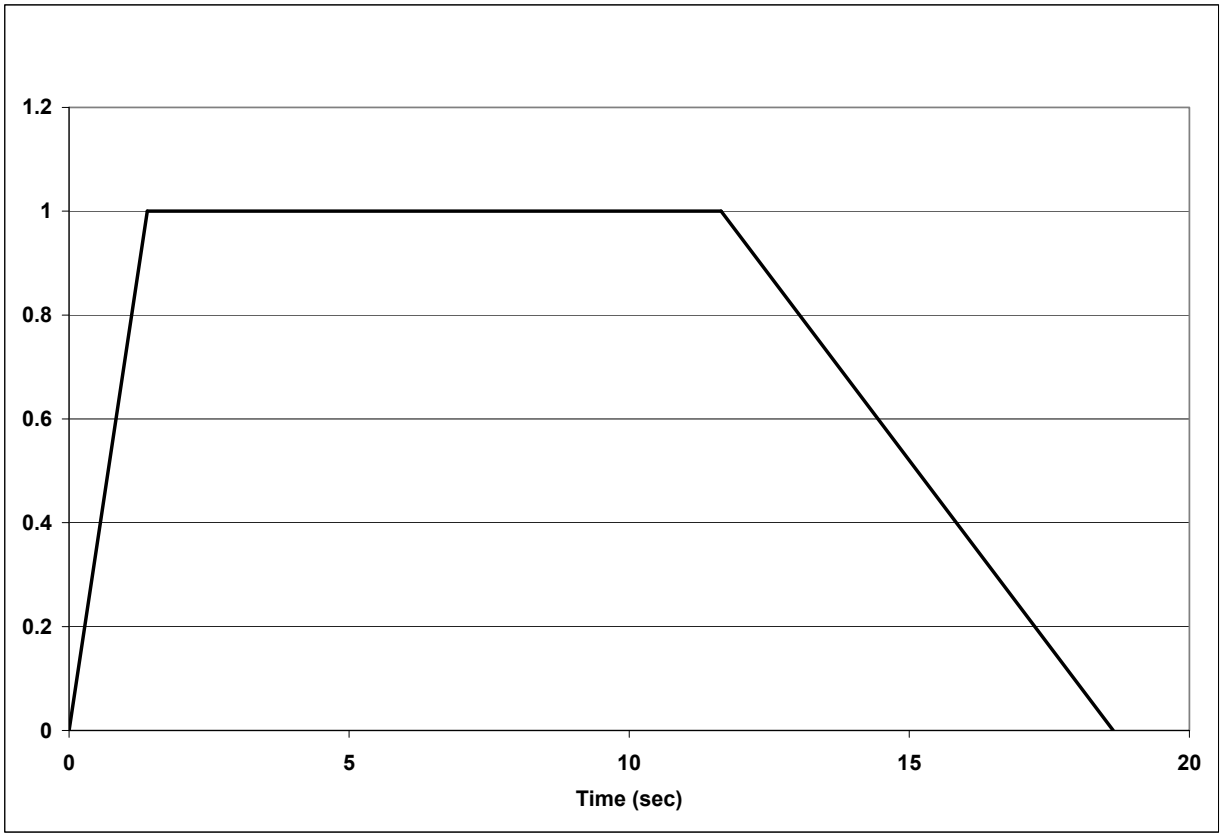

Figure 01.4.1.2.2-1 Time-Envelope Function Used in NUREG/CR-5347 Appendix B

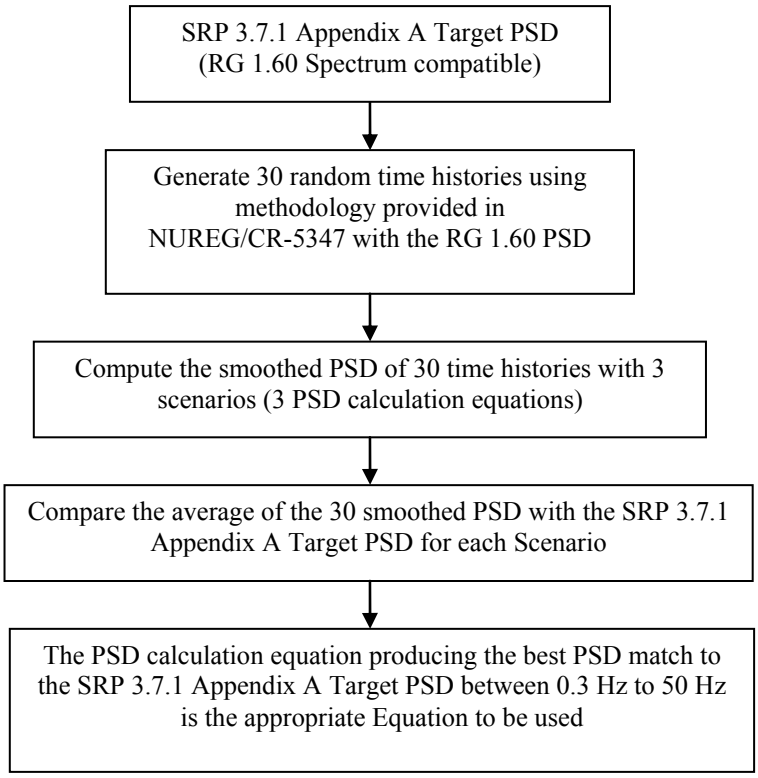

Figure 01.4.1.2.2-2 Procedure to Verify the Appropriate Equation to Calculate PSD from a Time History to Envelop the Target PSD up to 50 Hz

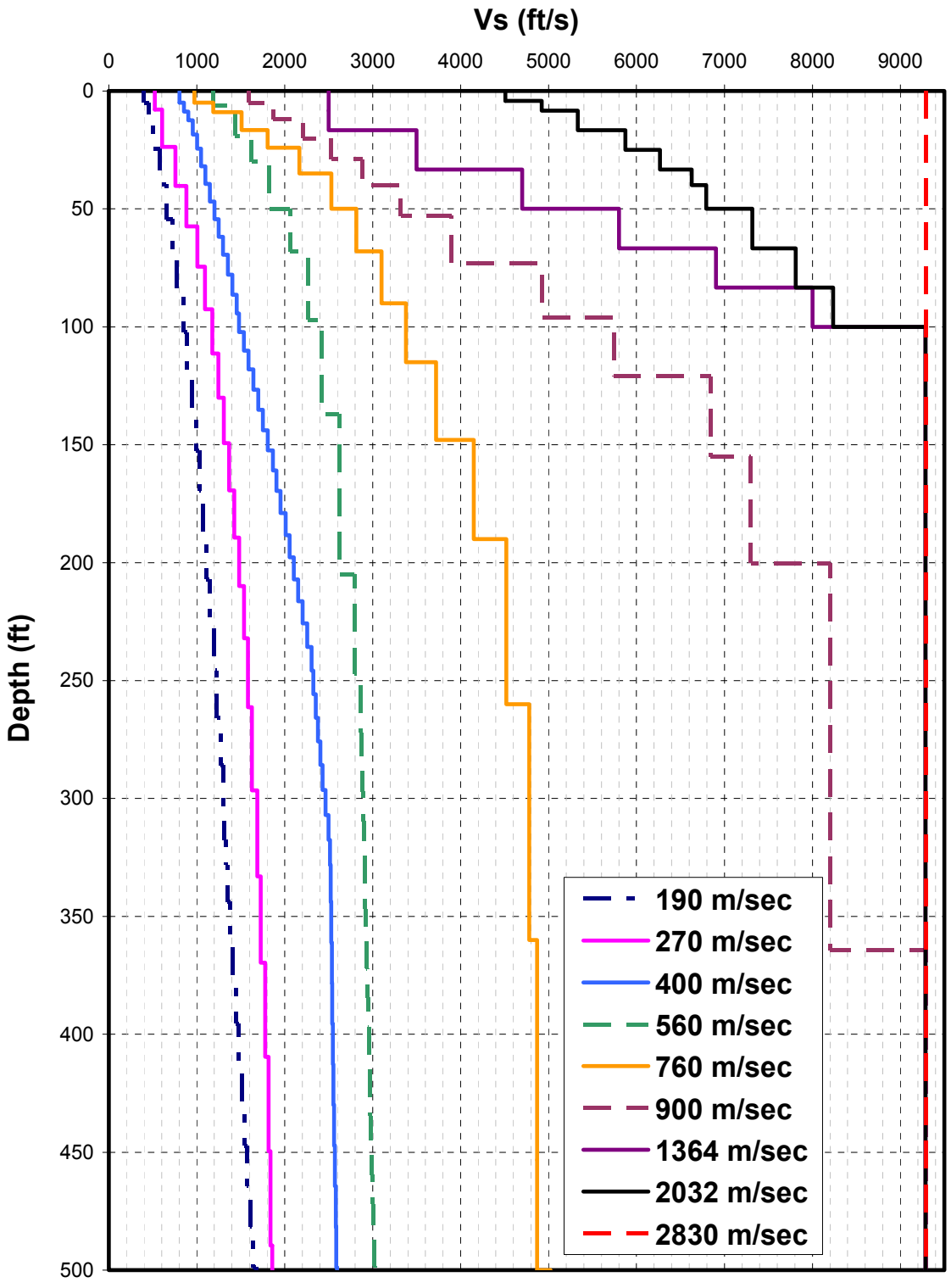

Figure 01.4.2-1 Top 500 ft of the Candidate Shear Wave Velocity Profiles and Associated $\overline{V_S}(30m)$ Velocities

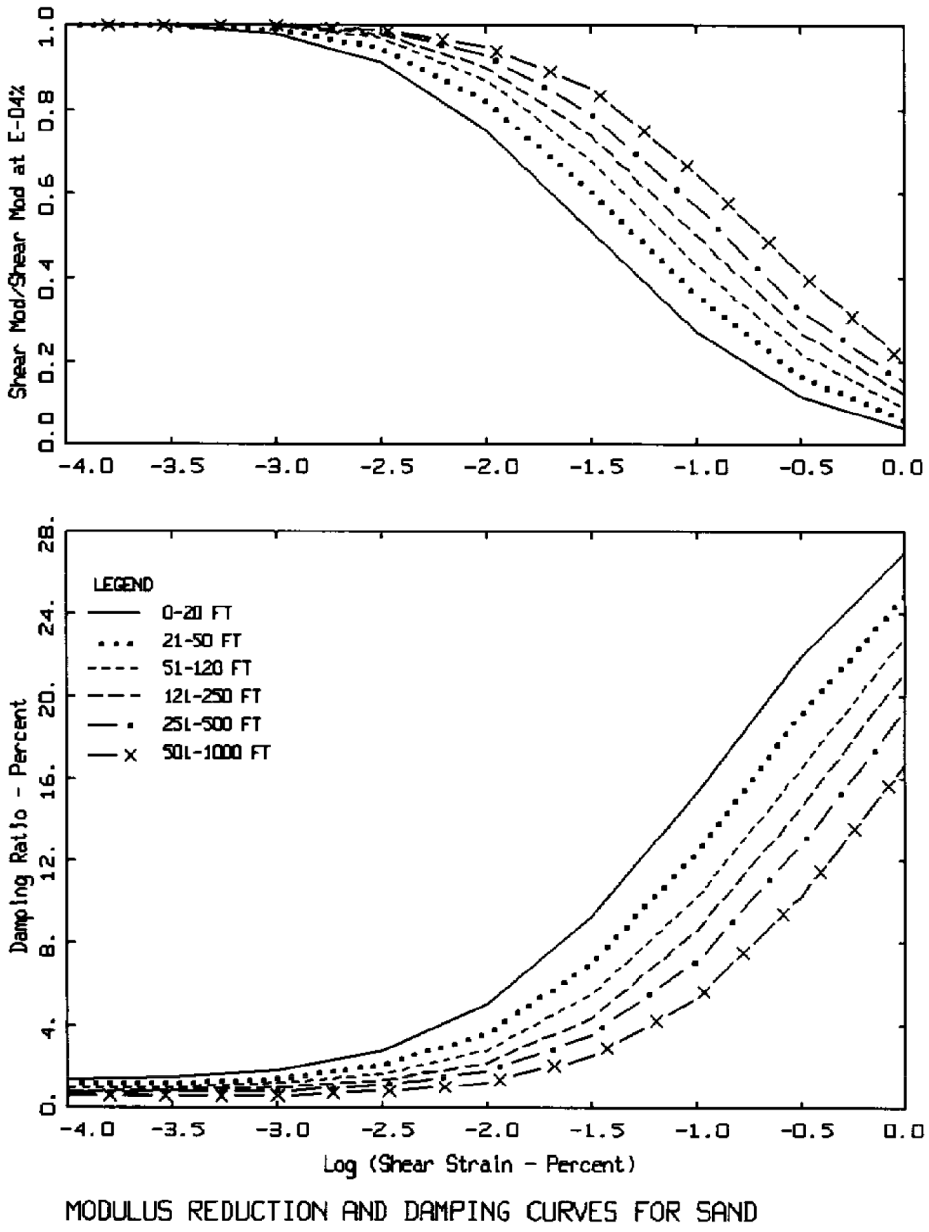

Figure 01.4.2-2 (TR-102293, Reference 01-8) Cohesionless Soil Modulus Reduction and Hysteretic Damping Curves

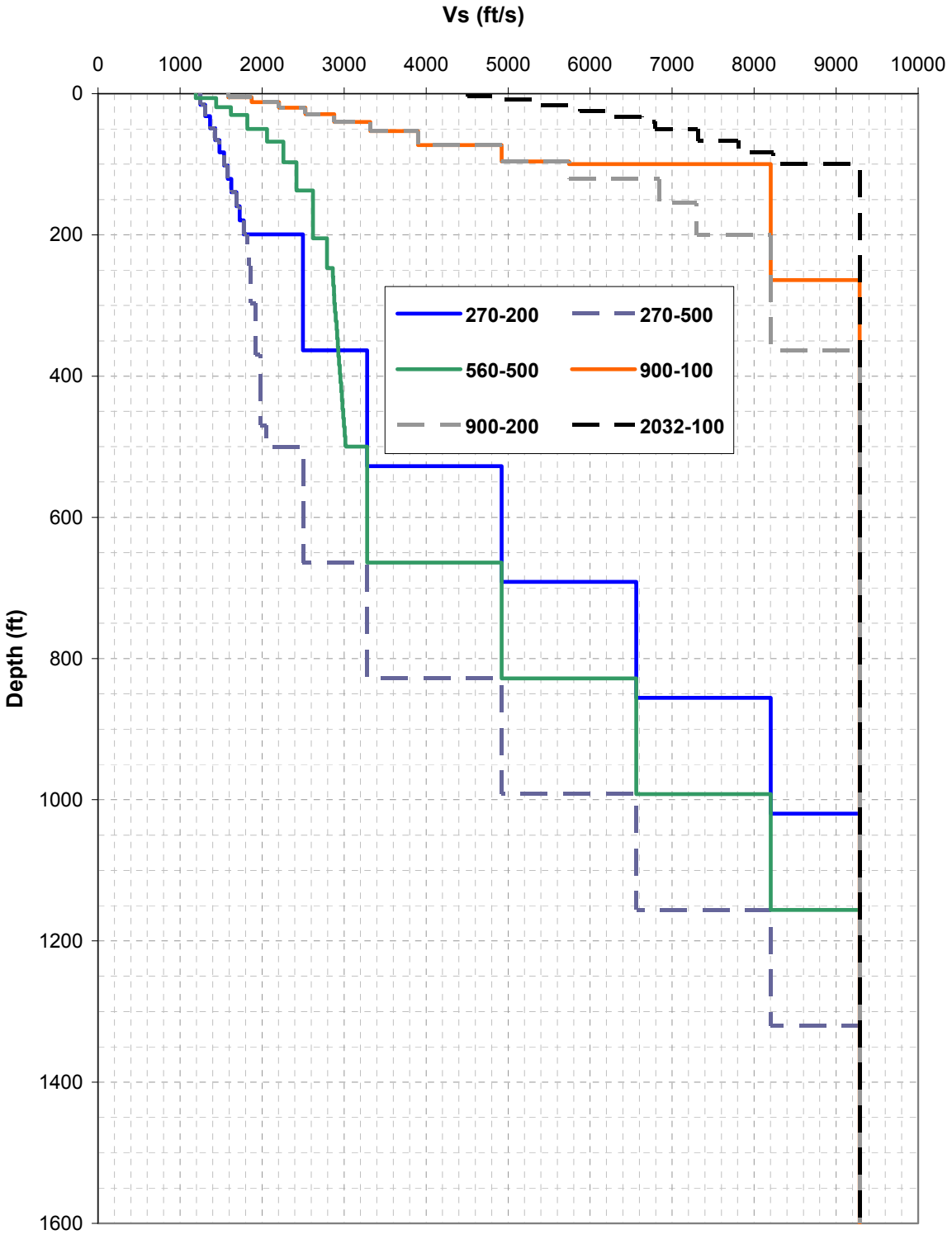

Figure 01.4.2.1-1 Six Generic Soil Profiles, Shear Wave Velocity V(s)

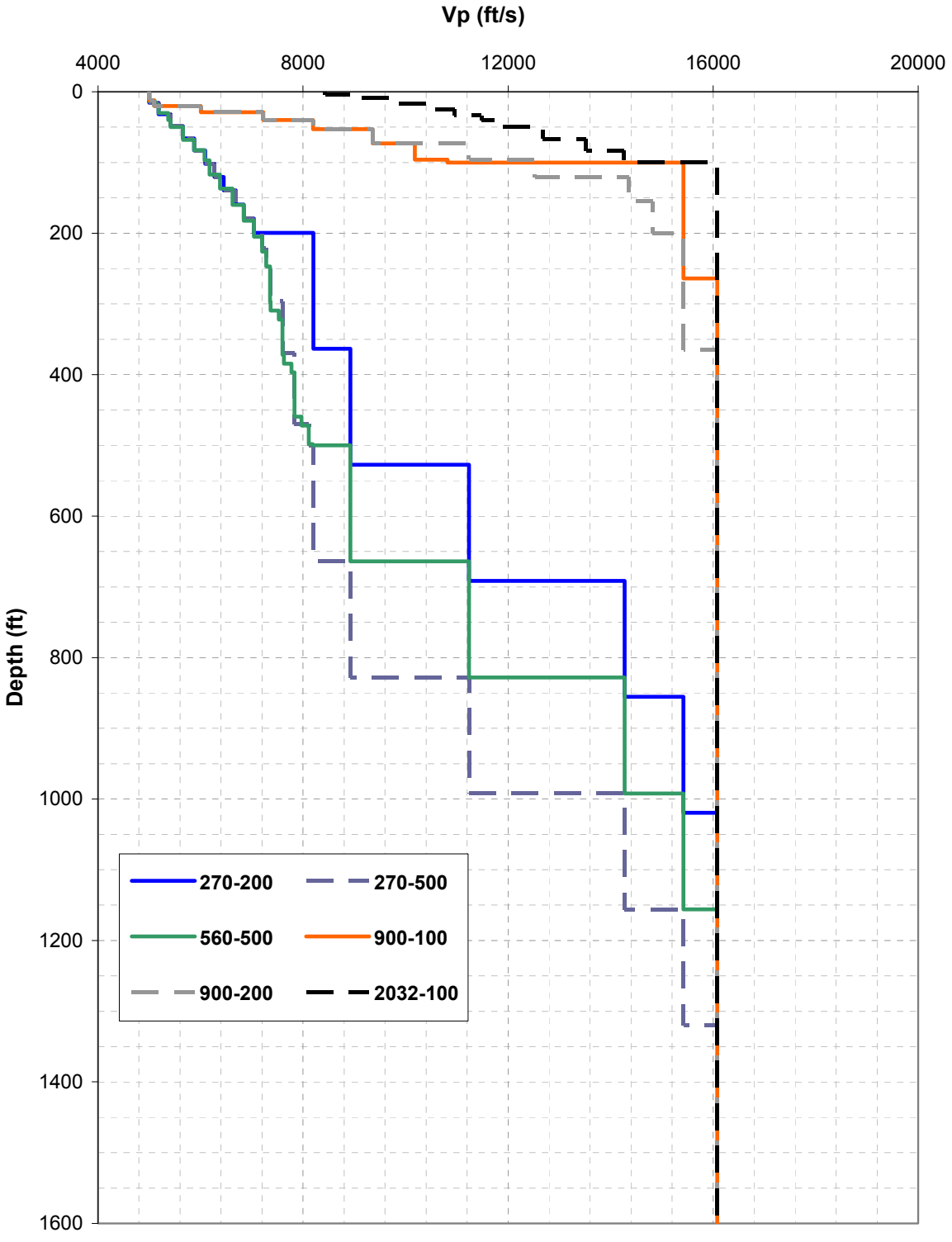

Figure 01.4.2.1-2 Six Generic Soil Profiles, Compression Wave Velocity (Vp)

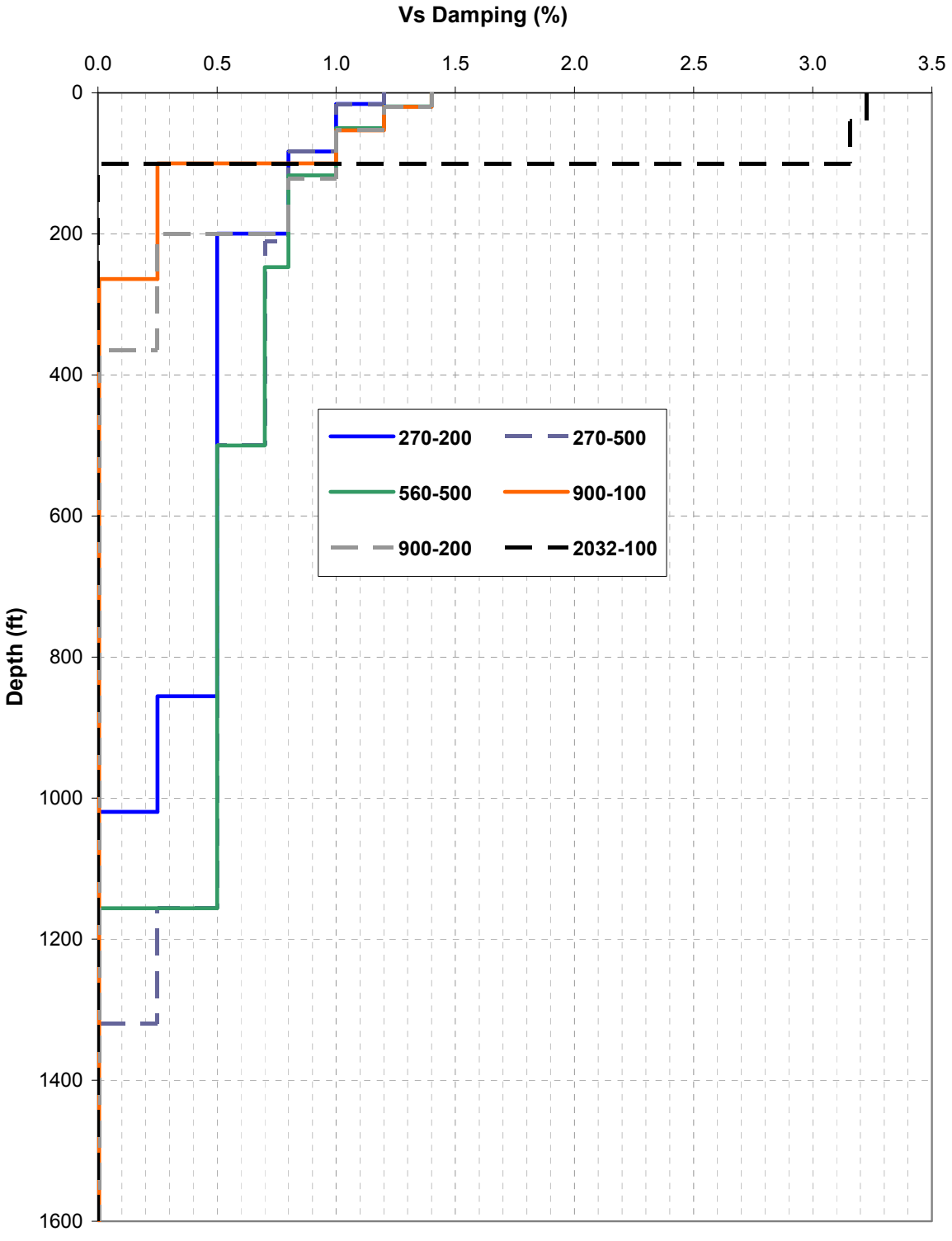

Figure 01.4.2.1-3 Six Generic Soil Profiles, Shear Wave Velocity Damping (%)

01.5.0 RESULTS

01.5.1 Target PSDs and Design Basis Time Histories

01.5.1.1 Target PSDs Compatible with CSDRS

The process described below follows the work flow outlined in Figure 01.4.1.2.1-2 and described in Section 01.4.1.2.1.

01.5.1.1.1 Selection of Initial Trial Target PSD

An initial trial horizontal target PSD is developed to envelop the "Modified SRP Target PSD" using a straight line for each PSD frequency segment. The "Modified SRP Target PSD" is defined as:

(Modified SRP Target PSD)

= (SRP Target PSD) * [(US-APWR CSDRS)/(RG 1.60 Spectra)]^2

Where the SRP Target PSD is from SRP 3.7.1 Appendix A.

This Modified SRP Target PSD is a series of curved lines. The initial trial horizontal target PSD is developed using equations of the same form as those presented in SRP 3.7.1 Appendix A. These equations are developed so that straight line segments (on a log-log plot) bound the curved lines of the Modified SRP Target PSD computed above. The equations that define the initial trial horizontal target PSD are shown below:

$$S_{0H1}(f) = \begin{cases} 650(f/2.5)^{0.2} & \text{for } f < 2.5\text{Hz} \\ 650(2.5/f)^{1.65} & \text{for } 2.5\text{Hz} \le f < 12\text{Hz} \\ 48.85(12.0/f)^{3} & \text{for } 12\text{Hz} \le f < 16\text{Hz} \\ 20.61(16/f)^{8} & \text{for } 16\text{Hz} \le f \end{cases} \quad (\text{in}^2/\text{sec}^3) \quad \text{Equation 01.5.1.1.1-1}$$

These equations are plotted in Figure 01.5.1.1-1.

Similarly, the equations that define the initial trial vertical target PSD are:

$$S_{0V}(f) = \begin{cases} 380(f/3.5)^{0.2} & \text{for } f < 3.5\text{Hz} \\ 380(3.5/f)^{1.6} & \text{for } 3.5\text{Hz} \le f < 12\text{Hz} \\ 48.85(12.0/f)^{3} & \text{for } 12\text{Hz} \le f < 16\text{Hz} \\ 20.61(18/f)^{7} & \text{for } 16\text{Hz} \le f \end{cases} \quad (\text{in}^2/\text{sec}^3) \quad \text{Equation 01.5.1.1.1-2}$$

The initial trial vertical target PSD is almost identical to the initial trial horizontal target PSD except that the first leg ends at 3.5 Hz, which is consistent with the control point of the vertical CSDRS.

01.5.1.1.2 Development of US-APWR Target PSD

Using the methodology described in Section 01.4.1.2.1, the final target PSDs were developed after several iterations. Figure 01.5.1.1.2-1 and Figure 01.5.1.1.2-2 show that the pseudo-velocity response spectra of the 30 artificial time histories closely match the CSDRS (velocity), which demonstrates that the target PSDs (Equations 01.5.1.1.2-1 and 01.5.1.1.2-2) are compatible with the CSDRS.

The final horizontal target PSD anchored to 1.0g is as follows:

$$S_{0H}(f)=\begin{cases}650(f/2.5)^{0.2} & \text{for } f<2.5\text{Hz}\\ 650(2.5/f)^{1.6} & \text{for } 2.5\text{Hz}\le f<12\text{Hz}\\ 52.9(12.0/f)^{3} & \text{for } 12\text{Hz}\le f<18\text{Hz}\\ 15.7(18/f)^{7} & \text{for } 18\text{Hz}\le f\end{cases} \quad (\text{in}^2/\text{sec}^3) \qquad \text{Equation 01.5.1.1.2-1}$$

The final vertical target PSD anchored to 1.0g is as follows:

$$S_{0V}(f)=\begin{cases}380(f/3.5)^{0.2} & \text{for } f<3.5\text{Hz}\\ 380(3.5/f)^{1.6} & \text{for } 3.5\text{Hz}\le f<12\text{Hz}\\ 52.9(12.0/f)^{3} & \text{for } 12\text{Hz}\le f<18\text{Hz}\\ 15.7(18/f)^{7} & \text{for } 18\text{Hz}\le f\end{cases} \quad (\text{in}^2/\text{sec}^3) \qquad \text{Equation 01.5.1.1.2-2}$$

As shown in Equations 01.5.1.1.2-1 and 01.5.1.1.2-2, and Figure 01.5.1.1.2-3, the control point at 9 Hz is extended to 12 Hz, and the control point at 16 Hz is extended to 18 Hz from the SRP 3.7.1 target PSD. All of these changes increase the power requirements of the design basis time histories at frequencies above 2.5 Hz relative to time histories compatible with RG 1.60.

These target PSDs are then used in the development of the design basis time histories as described in Section 01.5.1.2 below.

01.5.1.1.3 PSD Calculation Methodology from Time Histories

As described in Section 01.4.1.2.2, three scenarios of PSD calculation were performed using three different equations. The PSDs of 30 generated artificial time histories were then compared with the input PSD provided in SRP 3.7.1 Appendix A (Reference 01-1). Theoretically, if an infinite number of artificial time histories were generated, the average of the smoothed PSD curves, computed using the appropriate PSD calculation equation, should match the input PSD exactly. Since the sample size (30 time histories) is not infinite, and there will always be numerical rounding during the process, an exact match would never occur. However, even with a limited sample size, the appropriate PSD calculation equation can easily be identified. As shown in Figure 01.5.1.1-4, the average of the smoothed PSDs produced in "Scenario I" lies below the target PSD for most of the frequencies below 20 Hz, while average of the smoothed PSDs shown in Figure 01.5.1.1-5, computed in "Scenario II," is much higher than the target PSD beyond 20 Hz. "Scenario III" produced the best match between 0.3 Hz and 50 Hz as shown in Figure 01.5.1.1-6.

In summary, the PSD calculation follows the steps below:

- The Fourier amplitudes are computed over the total time history duration.
- The "equivalent stationary phase strong motion duration" is used to calculate the PSD of the time history as shown in Equation 01.4.1.2.2-5.

This refined methodology for computing PSDs from time histories is used in the development of the design basis time histories as described in Section 01.5.1.2 below.

01.5.1.2 Design Basis Time Histories

The design basis time histories (three components) are developed by modifying the Northridge seed time histories as shown in Figure 01.5.1.2-1, Figure 01.5.1.2-2, and Figure 01.5.1.2-3.

The corresponding velocity and displacement time histories have also been computed and are plotted in the same set of Figures. Each of these component time histories meets the criteria of SRP 3.7.1 Option 1, Approach 1. Compliance to these is summarized in Table 01.5.1.2-1.

Figure 01.5.1.2-4 through Figure 01.5.1.2-6 graphically demonstrate that the response spectra derived from the design basis time histories are developed in accordance with SRP 3.7.1 Option 1, Approach 1, for time history components 180 (H1 or X or NS), 090 (H2 or Y or EW), and Vertical (UP), respectively. The response spectra of each component envelopes the CSDRS at 2%, 3%, 5%, 7%, and 10% damping values.

Figure 01.5.1.2-7 through Figure 01.5.1.2-9 show that the smoothed PSDs of the design basis time histories are greater than 80% of the horizontal and 80% of the vertical target PSDs presented in Equations 01.5.1.1.2-1 and 01.5.1.1.2-2 at all frequencies between 0.3 Hz and 50 Hz, for time history components 180 H1, 090 H2, and Vertical (UP), respectively.

Table 01.5.1.2-1 also provides statistical independence values of the three components of the design basis time histories, which satisfies the criterion that the absolute value of correlation coefficients between the components must be less than 0.16.

As demonstrated in Table 01.5.1.2-1, the total durations of the design basis time histories meet the SRP guidance criteria that the durations exceed 20 seconds. The table also shows the rise time, strong motion duration, and decay time of each component. These values are computed based on the definition of strong motion duration in SRP 3.7.1, using the normalized AI. Figure 01.5.1.2-10 shows the normalized AI plots of cumulative energy for each component. The time history components show an initial time interval of gradual energy buildup, followed by a ramp of rapid energy accumulation, and then followed by a gradual tapering of energy accumulation. The strong motion duration should be at least six seconds according to SRP 3.7.1 and in compliance with duration criteria for earthquake magnitude and distance bins listed in Table 01.5.1.2-2. The strong motion durations of the design basis time history satisfy both duration criteria.

Table 01.5.1.2-1 also shows the V/A and AD/V^2 values for mean ratios ± one standard deviation for the earthquakes of magnitude bins of **M**6.5+ with distance bins from 10 to 100 km, using data provided in Table 3-6 of NUREG/CR-6728 (Reference 01-4). The V/A and AD/V^2 ratios of the design basis time histories are within the limits in Table 01.5.1.2-1.

Adequate representation of the Fourier components at low frequency is achieved by ensuring the artificial time history matches the CSDRS at all damping values and meets the PSD targets. As demonstrated above, the time histories developed from the Northridge Mt. Baldy seeds satisfy all the requirements described in the Option 1, Approach 1 of SRP 3.7.1 (Reference 01-1).

01.5.2 Development of Soil Profiles

Following the approach discussed in Section 01.4.2.2, SCPs are developed for the $\overline{V_S}$ (30m) profile categories of 270 m/s, 560 m/s, 900 m/s, and 2,032 m/s. The selected small strain (base case) shear and compression wave profiles are shown in Figure 01.5.2-1 to their maximum depths. Figure 01.5.2-2 presents the small-strain shear wave damping from all soil profiles from the top of plant grade to baserock, respectively.

Since the water table was taken at the plant finished grade for the purposes of the SSI analyses, the minimum compression wave velocity was set at 5,000 ft/s for the soil profiles, as discussed in Section 01.4.2.1. The effects of ground water table level on the soil material properties and on the seismic responses of the R/B complex are addressed in MHI TeR

MUAP-11007 (Reference 01-2). The uncertainty introduced in the standard design by the effects of groundwater level on the seismic response are within the general level of variation present in the seismic response analyses (refer to Reference 01-2). Therefore, it is unnecessary to directly address the effects that the water table may have on the seismic response of the standard design.

01.5.2.1 Site Response Analysis

Site response analyses using the equivalent linear RVT approach described in Section 01.4.2 are performed to develop the CSDRS strain-compatible soil properties used as input for the SSI analyses. The site response analyses to develop the SCP are with the same point-source model used to generate both the horizontal and vertical motions. Magnitude **M**7.5 is used as its broad spectral shape is consistent with that of the CSDRS. Distances are adjusted such that the median spectrum as full column outcrop spectrum at foundation level computed for each profile approaches, but does not exceed the horizontal and vertical CSDRS. The distances and median estimates of the horizontal and vertical peak accelerations are listed in Table 01.5.2.1-1 and the median spectrum computed for each profile is compared to the CSDRS spectrum in Figure 01.5.2.1-1 for horizontal components. Due to the shape of the US-APWR CSDRS, nearly all the profile spectra approach the design spectrum at high frequencies (approximately 25 Hz to 50 Hz). This frequency range then becomes the effective control for non-exceedance and associated distance adjustment for most of the profiles. The exceptions are reflected by the fundamental low-frequency resonance of the softest (270 m/s and 560 m/s) and deepest (500 ft) profiles.

For the vertical motions, Figure 01.5.2.1-2 compares the median spectra computed for the profiles with the vertical component CSDRS. In this case, the vertical motions are modeled assuming incident inclined Primary-Secondary Vertical (P-SV) wave propagation and linear elastic soil/rock properties (References 01-4, 01-8, and 01-11). Linear analyses for vertical motions with incident inclined P-SV waves has been shown to be appropriate for loading levels up to approximately 0.5g (Reference 01-4) and consistent with empirical Ground Motion Prediction Equations from “Empirical Response Spectral Attenuation Relations for Shallow Crustal Earthquakes” (Reference 01-15). Use of linear analyses is also consistent with observations of spectral shapes for vertical motions at soil sites being independent of loading level (Reference 01-14). For applications to sites with a water table at or very near the surface, linearity of the constrained modulus is also a realistic assumption as compression waves control the high-frequencies in vertical motions (Reference 01-16), where nonlinearity has its largest effect. For saturated conditions where fluids control the compression wave velocity (i.e., $V_P \approx 5{,}000$ ft/s), little nonlinearity is expected in the constrained modulus due to the presence of fluids. For depths where the skeleton controls the compression wave velocity ($V_P \geq 5{,}000$ ft/s), little nonlinearity is also expected due to the small dilatational strains, even at high loading levels.

As Figure 01.5.2.1-2 shows, most of the vertical spectra fall below the vertical CSDRS design spectrum. This trend is consistent with vertical spectra recorded at both soil and rock sites in WUS and is a result of the large source distances (Reference 01-8) (e.g., > 50 km, Table 01.5.2.1-1). Empirical (Refer to Reference 01-17) as well as simulated (References 01-4 and 01-14) Vertical divided by Horizontal (V/H) ratios decrease with increasing distance in both WUS and CEUS and are less than one at distances exceeding 50 km.

The vertical CSDRS that is developed using V/H ratios from RG 1.60 (Reference 01-3), which are independent of distance, represents vertical motions that are elevated as shown in Figure

01.5.2.1-3. With the RG 1.60 V/H ratios, there are some exceedances near 0.5 Hz and 1.0 Hz for the softest profile (270 m/s) and largest depths to soft rock material (500 ft).

01.5.2.2 Strain Compatible Properties

For the selected profile categories and depths to hard or soft rock material (Table 01.4.2-1), generic profiles of SCP are developed reflecting median or best estimate over the 30 realizations of profiles and G/Gmax and hysteretic damping curves (Section 01.4.2.2). Upper and lower range estimates are also developed in order to show that the range between -1 sigma and +1 sigma properties are reasonable. The SCP are summarized in Table 01.5.2.2-1 to Table 01.5.2.2-6, with Figure 01.5.2.2-1 to Figure 01.5.2.2-6 showing the median and ±1σ estimates for the shear and compression wave velocities and associated damping.

The distribution of modulus reduction and hysteretic damping curves with depth assumes confining pressure of the original (full) column. In addition, the SCP of all six saturated FCO soil profiles: shear wave velocity, compression wave velocity, and shear wave damping ratios are presented in Figure 01.5.2.2-1 through Figure 01.5.2.2-6 per soil case. In these figures, the solid orange line represents median values; the dash blue line represents lower bound value (-Sigma); and the dash red line represents upper bound value (+Sigma). The horizontal dashed green line represents the bottom of the R/B complex foundation at approximately 42 ft. In each figure below, sheet 1 of 3 presents shear wave velocity diagrams, sheet 2 of 3 presents compression wave velocity diagrams, and sheet 3 of 3 presents shear wave damping ratio diagrams.

The resulting strain compatible shear wave velocity and damping profiles reflect the distribution in cyclic shear-strains generated by the vertical propagation of shear waves from baserock to the surface. The effects of variation in nonlinear dynamic material properties and the reflection of the waves through the soil column are superimposed resulting in cyclic shear-strain concentrations that can occur not only at interfaces between the softer and stiffer material. The generic profiles represent a realistic non-monotonic change in strain compatible shear-wave velocity and damping with depth reflecting the complex response of the soil shear columns. The non uniformity of the strain compatible soil profiles increases the reflection of the waves propagating through the site and decreases the radial damping of the SSI system. This results in amplified peak SSI response of the structures in particular when the structural frequencies are resonant with the soil column frequencies.

The following properties are taken from the results of the site response analyses listed in Table 01.5.2.2-1 through Table 01.5.2.2-6 and used as input for site independent SSI analyses:

- Unit weight
- Median values of strain compatible shear wave velocities (V_s)
- Median values of strain compatible compression wave velocities (V_p)
- Median values of strain compatible shear wave damping (D_s)

The site profiles used for the site independent SSI analyses use the median values of shear wave damping for both shear and compression wave damping in order to account, in a more realistic manner, for the dissipation of energy in the soil under the wave propagation pattern present in the SSI model. The SCP developed from the site response analyses are adjusted as described in Section 03.3.1 to match the structural model mesh and ensure the passage of short waves with high frequency (short wavelengths).

Due to the simplified assumption in wave propagation in SSI analyses as vertically propagating compression waves, strain iterated shear wave damping is typically assumed for compression wave damping to avoid unrealistic vertical motions at high frequencies. Also, seismic SSI analysis is usually performed separately for horizontal and vertical seismic input motions. In these analyses, the horizontal and vertical input motions are assumed caused by different horizontal and vertical seismic wave field excitations even though the seismic input environment is always Three-Dimensional (3-D) consisting of simultaneous 3-component seismic input motions.

The site independent SSI analyses that are performed separately for each of the three directional earthquake excitations use the same generic profiles representing the total unit weight and strain compatible shear wave velocity, compression wave velocity and hysteretic damping ratio for the soil layer media. The strain compatible damping values assigned to these six generic profiles are well below the 15% limit recommended by SRP 3.7.1 (Reference 01-1) on shear wave damping and 10% limit on compression wave damping recommended by the correlation studies in Reference 01-18.

The same median values of shear wave damping are used for both shear and compression wave damping in order to account, in a more realistic manner, for the dissipation of energy in the soil under the wave propagation pattern present in the SSI model. The seismic SSI analyses for horizontal and vertical seismic input motions assume that the input motions are caused by different horizontal and vertical seismic wave field excitations even though the seismic input environment is always 3-D consisting of simultaneous 3-component seismic input motions. Due to the simplified wave propagation assumption made in the SSI vertical motion analyses where the motion is applied as vertically propagating compression waves, strain iterated shear wave damping is assumed for compression wave damping to avoid unrealistic vertical motions at high frequencies.

Correlation studies of the vertical site response motions recorded in actual earthquakes with the vertical motions predicted from vertical One-Dimensional (1-D) wave propagation site response analyses have been made (Reference 01-1). These studies conclude that, using the strain compatible soil damping values derived from the horizontal site response analyses as the damping values for vertical site response analysis, but limiting their values to no more than 10%, produces reasonably good correlation between the predicted and recorded vertical site response motions. Consistent with this conclusion, the soil damping values used for the horizontal and vertical SSI analyses are the shear strain compatible soil damping values derived from the horizontal free field site response analyses. The horizontal SSI response analyses are performed assuming vertically propagating plane shear wave field excitations. The vertical SSI response analysis is performed assuming vertically propagating plane compression wave field excitation, the shear strain compatible damping values derived from the horizontal site response analyses are used but with their values limited to no more than 10%, as recommended by the correlation studies reported in Reference 01-18.

The site response analyses use very low values for the material damping of hard baserock in order to model the low dissipation of energy in the deep hard rock strata. In order to improve the numerical stability of SSI results, the damping of the baserock material when included in the site profile is set to a low nominal value of 0.1%. This modification does not affect the SSI response because, unlike in the site response analyses, the thickness of the modeled hardrock strata in the SSI site model has a finite thickness so the use of higher damping values realistically projects the actual dissipation of energy in the baserock.

In order to obtain a general description of the range of subgrade properties considered in the site independent SSI analyses, the shear column frequencies of the selected median soil profiles are calculated as follows:

$$f_{sc} = \frac{Vs_{ave}}{4 \cdot H}$$ Equation 01.5.2.2-1

where: H is the depth of the soil column taken as the nominal depth of the top soil strata, and Vs_{ave} is the average shear wave velocity of the top soil layers calculated as follows using the equivalent arrival time method:

$$Vs_{ave} = \frac{H}{\sum_i d_i / Vs_i}$$ Equation 01.5.2.2-2

where: d_i and Vs_i are the thickness and shear wave velocity of each layer of top soil, respectively.

The shear wave column frequencies for each of the selected profiles are presented in Figure 03.4.1.1-4 of this report and shows that the majority of sites in the CEUS are embodied in the selection of the generic layered profiles.

Table 01.5.1.2-1 Summary of SRP 3.7.1 Option 1, Approach 1 Requirements Compliance

Requirement		H2 (90)	H1 (180)	V (UP)
Time Histories Requirements				
Total duration in seconds (if ≥ 20 seconds OK)		22.08	22.08	22.08
Rise time in seconds: Arias intensity 5% (if 1 second or longer OK)		2.815	3.031	1.337
Strong motion duration in seconds: Arias intensity between 5% and 75% (minimum 6 seconds and satisfying NUREG/CR-6728 criteria)(1)		9.543	7.868	10.35
Decay time in seconds: Arias intensity between 75% and 100% (if 5 seconds or longer OK)		9.722	11.181	10.393
Statistical independence (if absolute value ≤ 0.16 OK)		-0.0179	-0.0179	
		-0.0552		-0.0552
			-0.0696	-0.0696
V/A (if 7.51 ≤ V/A ≤ 66.40 OK)(2)		53.179	66.355	42.661
AD/V^2 (if 1.86 ≤ AD/V^2 ≤ 16.79 OK)(2)		4.306	2.997	5.766
Response Spectra Requirements				
SRP 3.7.1 Option 1, Approach 1				
Number of points with acceleration ratio < 1 (if ≤ 5 OK)	2%	2	5	5
	3%	0	0	1
	5%	0	0	0
	7%	0	0	0
	10%	4	0	2
Number of points with acceleration ratio < 0.9 (if 0 OK)	All	0	0	0
Power Spectral Density Function Requirements				
Number of points below 80% of target between 0.3 and 50 hz (if 0 OK)		0	0	0

(1) Refer to Table 01.5.1.2-2.
(2) Refer to Table 01.5.1.2-3.

Table 01.5.1.2-2 Magnitudes and Distance Bins and Strong Motion Duration Criteria

(NUREG/CR-6728, Table 3-2, Reference 01-4)

M	***R* (km)**	**Durations (sec)**	
		Rock	**Soil**
6.5 (6 - 7)	10 – 50	**3.1** – 7.0	3.6 – 8.2
	50 – 100	5.1 – 11.6	5.7 – 12.8
	100 -200	8.1 – 18.3	8.7 – 19.5
7.5 (7+)	10 – 50	6.6 – 14.0	7.2 – 16.1
	50 – 100	8.7 – 19.5	12.2 – 27.5
	100 -200	11.7 – 26.3	16.2 – **36.5**

Table 01.5.1.2-3 CEUS V/A & AD/V^2 Mean Ratios ± One Standard Deviation

Distance Bin	M	V / A (cm/sec/g), σ_{ln} (1)	AD / V^2, σ_{ln} (1)	V/A / $e^{(\sigma_{ln})}$ (in/sec/g) (2)	V/A * $e^{(\sigma_{ln})}$ (in/sec/g) (2)	AD/V^2 / $e^{(\sigma_{ln})}$	AD/V^2 * $e^{(\sigma_{ln})}$
10 - 50, Rock	6.32	31.75, 0.51	6.58, 0.70	**7.51**	20.82	3.27	13.25
10 - 50 Soil	6.41	51.74, 0.35	3.49, 0.47	14.35	28.91	2.18	5.58
50 - 100, Rock	6.38	32.59, 0.33	4.66, 0.52	9.22	17.85	2.77	7.84
50 - 100, Soil	6.57	56.04, 0.36	3.01, 0.48	15.39	31.62	**1.86**	4.86
10 - 50, Rock	7.38	58.24, 0.72	7.78, 0.63	11.16	47.11	4.14	14.61
10 - 50 Soil	7.47	128.74, 0.27	3.57, 0.35	38.69	**66.4**	2.52	5.07
50 - 100, Rock	7.49	50.29, 0.56	10.60,0.46	11.31	34.66	6.69	**16.79**

(1) See NUREG/CR-6728, Table 3-6, Reference 01-4.
(2) Units are changed to facilitate comparison to time history results

Table 01.5.2.1-1 Magnitudes, Distances, and Median Peak Accelerations

Profile	Magnitude	Distance (km)	PGA H(g)	PGA V(g)
270-200	7.5	68.0	0.268	0.117
270-500	7.5	62.0	0.232	0.124
560-500	7.5	59.5	0.259	0.130
900-100	7.5	68.0	0.198	0.078
900-200	7.5	65.0	0.204	0.087
2032-100	7.5	52.0	0.193	0.089

Table 01.5.2.2-1 Strain Compatible Properties for Profile 270-200 (Sheet 1 of 3)

Layer	Thickness	Top-Depth	Unit Weight	V_s	V_p	V_s Damp.	V_p Damp.	Poisson's Ratio
	ft	ft	kcf	ft/s	ft/s	%	%	
Median								
1	7.92	0.00	0.1250	1296	5284	1.5155	1.1972	0.468
2	7.91	7.92	0.1250	1289	5420	2.1967	1.1972	0.470
3	7.92	15.83	0.1250	1224	5153	2.3708	1.0045	0.470
4	7.91	23.75	0.1250	1196	5127	2.7042	1.0045	0.471
5	8.58	31.66	0.1250	1234	5328	2.8632	1.0045	0.471
6	1.76	40.24	0.1250	1208	5265	3.0446	1.0045	0.472
7	6.82	42.00	0.1250	1188	5213	3.1959	1.0045	0.472
8	8.58	48.82	0.1250	1204	5318	3.2979	1.0045	0.473
9	8.58	57.40	0.1250	1262	5555	3.2877	1.0045	0.473
10	8.58	65.98	0.1250	1281	5653	3.3797	1.0045	0.473
11	8.58	74.56	0.1250	1315	5808	3.4046	1.0045	0.473
12	9.38	83.14	0.1250	1308	5788	2.6319	0.7992	0.473
13	9.37	92.52	0.1250	1382	6093	2.5810	0.7992	0.473
14	9.38	101.89	0.1250	1394	6159	2.6245	0.7992	0.473
15	9.37	111.27	0.1250	1441	6343	2.5950	0.7992	0.473
16	9.38	120.64	0.1250	1389	6160	2.7607	0.7992	0.473
17	9.37	130.02	0.1250	1449	6406	2.6956	0.7992	0.473
18	10.00	139.39	0.1313	1481	6533	2.6090	0.7992	0.473
19	10.00	149.39	0.1313	1496	6617	2.6265	0.7992	0.473
20	10.00	159.39	0.1313	1519	6729	2.6256	0.7992	0.473
21	10.00	169.39	0.1313	1547	6843	2.6305	0.7992	0.473
22	10.00	179.39	0.1313	1535	6809	2.6978	0.7992	0.473
23	10.00	189.39	0.1313	1576	6988	2.6668	0.7992	0.473
24	0.60	199.39	0.1313	1572	6976	2.6945	0.7992	0.473
25	164.05	200.00	0.1313	2509	8230	0.5000	0.5000	0.449
26	164.05	364.05	0.1344	3281	8924	0.5000	0.5000	0.422
27	164.05	528.10	0.1400	4921	11240	0.5000	0.5000	0.381
28	164.05	692.15	0.1438	6562	14270	0.5000	0.5000	0.366
29	164.05	856.20	0.1500	8203	15420	0.2500	0.2500	0.303
30	3281.00	1020.20	0.1575	9285	16080	0.0005	0.0005	0.250

Table 01.5.2.2-1 Strain Compatible Properties for Profile 270-200 (Sheet 2 of 3)

Layer	Thickness	Top-Depth	Unit Weight	V_s	V_p	V_s Damp.	V_p Damp.	Poisson's Ratio
	ft	ft	kcf	ft/s	ft/s	%	%	
-1 Sigma								
1	7.92	0.00	0.1250	1042	4289	1.0898	1.1713	0.467
2	7.91	7.92	0.1250	1021	4377	1.4996	1.1713	0.468
3	7.92	15.83	0.1250	965	4175	1.6772	0.9829	0.467
4	7.91	23.75	0.1250	946	4208	1.8879	0.9829	0.468
5	8.58	31.66	0.1250	962	4340	1.9700	0.9829	0.468
6	1.76	40.24	0.1250	937	4281	2.0994	0.9829	0.468
7	6.82	42.00	0.1250	919	4231	2.1788	0.9829	0.469
8	8.58	48.82	0.1250	937	4398	2.3915	0.9829	0.469
9	8.58	57.40	0.1250	1030	4750	2.3703	0.9829	0.469
10	8.58	65.98	0.1250	1070	4931	2.4375	0.9829	0.469
11	8.58	74.56	0.1250	1120	5179	2.5019	0.9829	0.469
12	9.38	83.14	0.1250	1103	5098	1.9576	0.7836	0.470
13	9.37	92.52	0.1250	1142	5243	1.8952	0.7836	0.469
14	9.38	101.89	0.1250	1149	5266	1.9198	0.7836	0.470
15	9.37	111.27	0.1250	1239	5525	1.8892	0.7836	0.470
16	9.38	120.64	0.1250	1202	5376	2.0301	0.7836	0.470
17	9.37	130.02	0.1250	1261	5631	1.9113	0.7836	0.470
18	10.00	139.39	0.1313	1261	5688	1.8754	0.7836	0.470
19	10.00	149.39	0.1313	1239	5661	1.8175	0.7836	0.470
20	10.00	159.39	0.1313	1231	5678	1.7966	0.7836	0.469
21	10.00	169.39	0.1313	1290	5901	1.8322	0.7836	0.470
22	10.00	179.39	0.1313	1300	5960	1.9176	0.7836	0.470
23	10.00	189.39	0.1313	1326	6112	1.9657	0.7836	0.470
24	0.60	199.39	0.1313	1321	6096	1.9672	0.7836	0.470
25	164.05	200.00	0.1313	1945	6380	0.5000	0.5000	0.449
26	164.05	364.05	0.1344	3281	8924	0.5000	0.5000	0.422
27	164.05	528.10	0.1400	4921	11240	0.5000	0.5000	0.381
28	164.05	692.15	0.1438	6562	14270	0.5000	0.5000	0.366
29	164.05	856.20	0.1500	8203	15420	0.2500	0.2500	0.303
30	3281.00	1020.20	0.1575	9285	16080	0.0005	0.0005	0.250

Table 01.5.2.2-1 Strain Compatible Properties for Profile 270-200 (Sheet 3 of 3)

Layer	Thickness	Top-Depth	Unit Weight	V_s	V_p	V_s Damp.	V_p Damp.	Poisson's Ratio
	ft	ft	kcf	ft/s	ft/s	%	%	
+1 Sigma								
1	7.92	0.00	0.1250	1611	6511	2.1075	1.2237	0.469
2	7.91	7.92	0.1250	1628	6712	3.2181	1.2237	0.472
3	7.92	15.83	0.1250	1552	6361	3.3513	1.0265	0.473
4	7.91	23.75	0.1250	1512	6248	3.8735	1.0265	0.474
5	8.58	31.66	0.1250	1583	6542	4.1613	1.0265	0.475
6	1.76	40.24	0.1250	1559	6475	4.4153	1.0265	0.476
7	6.82	42.00	0.1250	1538	6424	4.6878	1.0265	0.476
8	8.58	48.82	0.1250	1548	6431	4.5478	1.0265	0.477
9	8.58	57.40	0.1250	1546	6498	4.5603	1.0265	0.476
10	8.58	65.98	0.1250	1532	6481	4.6860	1.0265	0.476
11	8.58	74.56	0.1250	1543	6513	4.6330	1.0265	0.476
12	9.38	83.14	0.1250	1550	6573	3.5385	0.8150	0.476
13	9.37	92.52	0.1250	1671	7082	3.5149	0.8150	0.476
14	9.38	101.89	0.1250	1691	7204	3.5878	0.8150	0.476
15	9.37	111.27	0.1250	1677	7282	3.5645	0.8150	0.475
16	9.38	120.64	0.1250	1605	7059	3.7544	0.8150	0.476
17	9.37	130.02	0.1250	1664	7288	3.8018	0.8150	0.476
18	10.00	139.39	0.1313	1739	7505	3.6298	0.8150	0.476
19	10.00	149.39	0.1313	1807	7734	3.7956	0.8150	0.476
20	10.00	159.39	0.1313	1876	7974	3.8370	0.8150	0.476
21	10.00	169.39	0.1313	1855	7936	3.7765	0.8150	0.476
22	10.00	179.39	0.1313	1812	7778	3.7954	0.8150	0.476
23	10.00	189.39	0.1313	1874	7989	3.6179	0.8150	0.476
24	0.60	199.39	0.1313	1869	7982	3.6908	0.8150	0.476
25	164.05	200.00	0.1313	3236	10617	0.5000	0.5000	0.449
26	164.05	364.05	0.1344	3281	8924	0.5000	0.5000	0.422
27	164.05	528.10	0.1400	4921	11240	0.5000	0.5000	0.381
28	164.05	692.15	0.1438	6562	14270	0.5000	0.5000	0.366
29	164.05	856.20	0.1500	8203	15420	0.2500	0.2500	0.303
30	3281.00	1020.20	0.1575	9285	16080	0.0005	0.0005	0.250

Table 01.5.2.2-2 Strain Compatible Properties for Profile 270-500 (Sheet 1 of 3)

Layer	Thickness	Top-Depth	Unit Weight	V_s	V_p	V_s Damp.	V_p Damp.	Poisson's Ratio
	ft	ft	kcf	ft/s	ft/s	%	%	
Median								
1	7.92	0.00	0.1250	1178	5106	1.6503	1.1975	0.472
2	7.91	7.92	0.1250	1173	5266	2.4173	1.1975	0.474
3	7.92	15.83	0.1250	1180	5115	2.4924	1.0042	0.472
4	7.91	23.75	0.1250	1167	5142	2.8266	1.0042	0.473
5	8.58	31.66	0.1250	1228	5298	2.9364	1.0045	0.471
6	1.76	40.24	0.1250	1242	5382	3.0409	1.0045	0.472
7	6.82	42.00	0.1250	1256	5457	3.0991	1.0045	0.472
8	8.58	48.82	0.1250	1301	5658	3.1433	1.0045	0.472
9	8.58	57.40	0.1250	1277	5618	3.3644	1.0045	0.472
10	8.58	65.98	0.1250	1271	5625	3.5185	1.0045	0.473
11	8.58	74.56	0.1250	1327	5872	3.4768	1.0045	0.473
12	9.38	83.14	0.1250	1309	5806	2.7050	0.7992	0.473
13	9.37	92.52	0.1250	1352	5992	2.6959	0.7992	0.473
14	9.38	101.89	0.1250	1350	6001	2.7597	0.7992	0.473
15	9.37	111.27	0.1250	1332	5956	2.8628	0.7992	0.473
16	9.38	120.64	0.1250	1419	6309	2.7569	0.7992	0.473
17	9.37	130.02	0.1250	1448	6427	2.7579	0.7992	0.473
18	10.00	139.39	0.1313	1504	6632	2.6348	0.7992	0.473
19	10.00	149.39	0.1313	1541	6790	2.6176	0.7992	0.473
20	10.00	159.39	0.1313	1578	6956	2.6024	0.7992	0.473
21	10.00	169.39	0.1313	1575	6958	2.6456	0.7992	0.473
22	10.00	179.39	0.1313	1589	7029	2.6633	0.7992	0.473
23	10.00	189.39	0.1313	1592	7052	2.7018	0.7992	0.473
24	10.60	199.39	0.1313	1616	7160	2.6988	0.7992	0.473
25	10.60	209.99	0.1313	1710	7317	2.3014	0.7033	0.471
26	11.50	220.59	0.1313	1771	7563	2.2571	0.7033	0.471
27	11.50	232.09	0.1313	1684	7245	2.4179	0.7033	0.471
28	17.67	243.59	0.1313	1691	7291	2.4399	0.7033	0.471
29	17.67	261.26	0.1313	1705	7358	2.4727	0.7033	0.471
30	17.67	278.93	0.1313	1759	7574	2.4306	0.7033	0.471
31	18.25	296.59	0.1313	1795	7723	2.4210	0.7033	0.471
32	18.25	314.84	0.1313	1776	7665	2.4980	0.7033	0.471
33	18.25	333.09	0.1313	1752	7591	2.5717	0.7033	0.472
34	18.25	351.34	0.1313	1749	7585	2.6153	0.7033	0.472
35	20.00	369.59	0.1313	1768	7659	2.6208	0.7033	0.472
36	20.00	389.59	0.1313	1747	7600	2.6857	0.7033	0.472
37	20.00	409.59	0.1313	1788	7767	2.6602	0.7033	0.472
38	20.00	429.59	0.1313	1791	7791	2.6901	0.7033	0.472
39	20.00	449.59	0.1313	1817	7903	2.6761	0.7033	0.472
40	20.00	469.60	0.1313	1780	7770	2.7660	0.7033	0.472
41	10.40	489.60	0.1313	1783	7791	2.7846	0.7033	0.472
42	164.05	500.00	0.1313	2376	7795	0.5000	0.5000	0.449
43	164.05	664.05	0.1344	3281	8924	0.5000	0.5000	0.422
44	164.05	828.10	0.1400	4922	11240	0.5000	0.5000	0.381
45	164.05	992.15	0.1438	6562	14270	0.5000	0.5000	0.366
46	164.05	1156.20	0.1500	8203	15420	0.2500	0.2500	0.303
47	3281.00	1320.30	0.1575	9285	16080	0.0005	0.0005	0.250

Table 01.5.2.2-2 Strain Compatible Properties for Profile 270-500 (Sheet 2 of 3)

Layer	Thickness	Top-Depth	Unit Weight	V_s	V_p	V_s Damp.	V_p Damp.	Poisson's Ratio
	ft	ft	kcf	ft/s	ft/s	%	%	
-1 Sigma								
1	7.92	0.00	0.1250	869	3836	1.1125	1.1743	0.470
2	7.91	7.92	0.1250	898	4147	1.5884	1.1743	0.472
3	7.92	15.83	0.1250	904	4015	1.7752	0.9838	0.469
4	7.91	23.75	0.1250	891	4042	2.0023	0.9838	0.470
5	8.58	31.66	0.1250	981	4333	2.0158	0.9829	0.469
6	1.76	40.24	0.1250	987	4391	2.0732	0.9829	0.469
7	6.82	42.00	0.1250	1003	4482	2.1247	0.9829	0.469
8	8.58	48.82	0.1250	1057	4711	2.1696	0.9829	0.469
9	8.58	57.40	0.1250	1033	4713	2.4061	0.9829	0.469
10	8.58	65.98	0.1250	1045	4794	2.4803	0.9829	0.469
11	8.58	74.56	0.1250	1077	4972	2.4577	0.9829	0.469
12	9.38	83.14	0.1250	1068	4878	1.9703	0.7836	0.470
13	9.37	92.52	0.1250	1128	5164	2.0141	0.7836	0.470
14	9.38	101.89	0.1250	1130	5179	2.0532	0.7836	0.470
15	9.37	111.27	0.1250	1098	5089	2.0959	0.7836	0.470
16	9.38	120.64	0.1250	1160	5334	2.0052	0.7836	0.470
17	9.37	130.02	0.1250	1213	5517	2.1205	0.7836	0.470
18	10.00	139.39	0.1313	1288	5751	1.9921	0.7836	0.470
19	10.00	149.39	0.1313	1311	5882	2.0177	0.7836	0.470
20	10.00	159.39	0.1313	1310	5899	1.8902	0.7836	0.470
21	10.00	169.39	0.1313	1341	6048	1.9062	0.7836	0.470
22	10.00	179.39	0.1313	1330	6035	1.8928	0.7836	0.470
23	10.00	189.39	0.1313	1340	6060	1.9384	0.7836	0.470
24	10.60	199.39	0.1313	1371	6190	1.9629	0.7836	0.470
25	10.60	209.99	0.1313	1464	6445	1.5845	0.6859	0.468
26	11.50	220.59	0.1313	1490	6571	1.5342	0.6859	0.468
27	11.50	232.09	0.1313	1418	6296	1.6116	0.6859	0.468
28	17.67	243.59	0.1313	1413	6326	1.6627	0.6859	0.468
29	17.67	261.26	0.1313	1448	6469	1.6908	0.6859	0.468
30	17.67	278.93	0.1313	1480	6579	1.6760	0.6859	0.468
31	18.25	296.59	0.1313	1542	6824	1.7063	0.6859	0.469
32	18.25	314.84	0.1313	1554	6884	1.8094	0.6859	0.469
33	18.25	333.09	0.1313	1520	6788	1.8890	0.6859	0.469
34	18.25	351.34	0.1313	1523	6797	1.9708	0.6859	0.469
35	20.00	369.59	0.1313	1551	6788	1.9815	0.6859	0.469
36	20.00	389.59	0.1313	1512	6737	2.0543	0.6859	0.469
37	20.00	409.59	0.1313	1563	6949	2.0095	0.6859	0.469
38	20.00	429.59	0.1313	1582	7052	2.0189	0.6859	0.469
39	20.00	449.59	0.1313	1575	7047	1.9524	0.6859	0.469
40	20.00	469.60	0.1313	1557	6974	2.0757	0.6859	0.469
41	10.40	489.60	0.1313	1584	7099	2.0916	0.6859	0.469
42	164.05	500.00	0.1313	2067	6781	0.5000	0.5000	0.449
43	164.05	664.05	0.1344	3281	8924	0.5000	0.5000	0.422
44	164.05	828.10	0.1400	4922	11240	0.5000	0.5000	0.381
45	164.05	992.15	0.1438	6562	14270	0.5000	0.5000	0.366
46	164.05	1156.20	0.1500	8203	15420	0.2500	0.2500	0.303
47	3281.00	1320.30	0.1575	9285	16080	0.0005	0.0005	0.250

Table 01.5.2.2-2 Strain Compatible Properties for Profile 270-500 (Sheet 3 of 3)

Layer	Thickness	Top-Depth	Unit Weight	V_s	V_p	V_s Damp.	V_p Damp.	Poisson's Ratio
	ft	ft	kcf	ft/s	ft/s	%	%	
+1 Sigma								
1	7.92	0.00	0.1250	1596	6798	2.4480	1.2212	0.473
2	7.91	7.92	0.1250	1532	6686	3.6790	1.2212	0.476
3	7.92	15.83	0.1250	1541	6515	3.4994	1.0251	0.474
4	7.91	23.75	0.1250	1527	6542	3.9902	1.0251	0.476
5	8.58	31.66	0.1250	1538	6478	4.2774	1.0265	0.474
6	1.76	40.24	0.1250	1563	6597	4.4602	1.0265	0.475
7	6.82	42.00	0.1250	1571	6643	4.5205	1.0265	0.475
8	8.58	48.82	0.1250	1600	6795	4.5540	1.0265	0.475
9	8.58	57.40	0.1250	1578	6697	4.7044	1.0265	0.476
10	8.58	65.98	0.1250	1546	6601	4.9913	1.0265	0.476
11	8.58	74.56	0.1250	1635	6934	4.9184	1.0265	0.477
12	9.38	83.14	0.1250	1604	6909	3.7137	0.8150	0.476
13	9.37	92.52	0.1250	1620	6952	3.6085	0.8150	0.476
14	9.38	101.89	0.1250	1613	6955	3.7092	0.8150	0.476
15	9.37	111.27	0.1250	1616	6971	3.9103	0.8150	0.477
16	9.38	120.64	0.1250	1736	7462	3.7902	0.8150	0.476
17	9.37	130.02	0.1250	1728	7488	3.5870	0.8150	0.476
18	10.00	139.39	0.1313	1755	7647	3.4848	0.8150	0.475
19	10.00	149.39	0.1313	1811	7839	3.3958	0.8150	0.476
20	10.00	159.39	0.1313	1902	8204	3.5830	0.8150	0.476
21	10.00	169.39	0.1313	1851	8005	3.6718	0.8150	0.476
22	10.00	179.39	0.1313	1898	8188	3.7476	0.8150	0.476
23	10.00	189.39	0.1313	1892	8206	3.7660	0.8150	0.476
24	10.60	199.39	0.1313	1905	8281	3.7106	0.8150	0.476
25	10.60	209.99	0.1313	1998	8308	3.3424	0.7211	0.474
26	11.50	220.59	0.1313	2105	8705	3.3205	0.7211	0.474
27	11.50	232.09	0.1313	1999	8338	3.6275	0.7211	0.474
28	17.67	243.59	0.1313	2023	8403	3.5803	0.7211	0.474
29	17.67	261.26	0.1313	2008	8370	3.6164	0.7211	0.474
30	17.67	278.93	0.1313	2091	8719	3.5251	0.7211	0.474
31	18.25	296.59	0.1313	2089	8741	3.4350	0.7211	0.474
32	18.25	314.84	0.1313	2030	8536	3.4485	0.7211	0.474
33	18.25	333.09	0.1313	2021	8489	3.5013	0.7211	0.475
34	18.25	351.34	0.1313	2007	8465	3.4707	0.7211	0.475
35	20.00	369.59	0.1313	2016	8642	3.4662	0.7211	0.474
36	20.00	389.59	0.1313	2018	8573	3.5112	0.7211	0.475
37	20.00	409.59	0.1313	2045	8681	3.5217	0.7211	0.475
38	20.00	429.59	0.1313	2028	8607	3.5844	0.7211	0.475
39	20.00	449.59	0.1313	2097	8864	3.6682	0.7211	0.475
40	20.00	469.60	0.1313	2034	8657	3.6858	0.7211	0.475
41	10.40	489.60	0.1313	2007	8551	3.7072	0.7211	0.475
42	164.05	500.00	0.1313	2731	8960	0.5000	0.5000	0.449
43	164.05	664.05	0.1344	3281	8924	0.5000	0.5000	0.422
44	164.05	828.10	0.1400	4922	11240	0.5000	0.5000	0.381
45	164.05	992.15	0.1438	6562	14270	0.5000	0.5000	0.366
46	164.05	1156.20	0.1500	8203	15420	0.2500	0.2500	0.303
47	3281.00	1320.30	0.1575	9285	16080	0.0005	0.0005	0.250

Table 01.5.2.2-3 Strain Compatible Properties for Profile 560-500 (Sheet 1 of 3)

Layer	Thickness	Top-Depth	Unit Weight	V_s	V_p	V_s Damp.	V_p Damp.	Poisson's Ratio
	ft	ft	kcf	ft/s	ft/s	%	%	
Median								
1	6.00	0.00	0.1250	1066	4647	2.1584	1.4005	0.472
2	6.50	6.00	0.1250	1412	5192	2.6111	1.4006	0.460
3	6.50	12.50	0.1250	1369	5300	3.2096	1.4006	0.464
4	11.00	19.00	0.1250	1440	4946	2.6191	1.1954	0.453
5	10.00	30.00	0.1313	1649	5192	2.5520	1.1944	0.444
6	2.00	40.00	0.1313	1636	5240	2.7055	1.1946	0.446
7	8.00	42.00	0.1313	1627	5240	2.8134	1.1946	0.446
8	18.00	50.00	0.1313	1906	5515	2.2508	1.0088	0.432
9	14.50	68.00	0.1313	2262	6146	2.0787	1.0097	0.421
10	14.50	82.50	0.1313	2249	6357	2.1940	1.0091	0.428
11	20.00	97.00	0.1313	2230	6010	2.2981	1.0100	0.420
12	20.00	117.00	0.1313	2218	6206	1.7958	0.7977	0.426
13	22.67	137.01	0.1313	2452	6557	1.7184	0.7974	0.418
14	22.67	159.67	0.1313	2440	6774	1.7836	0.7976	0.425
15	22.67	182.34	0.1313	2430	6970	1.8396	0.7978	0.430
16	21.00	205.00	0.1313	2747	7485	1.7122	0.7976	0.422
17	21.00	226.00	0.1313	2739	7567	1.7506	0.7976	0.424
18	12.50	247.00	0.1313	2798	7457	1.5493	0.7071	0.418
19	12.50	259.50	0.1313	2795	7444	1.5653	0.7071	0.418
20	12.50	272.00	0.1313	2793	7422	1.5804	0.7071	0.417
21	12.50	284.50	0.1313	2790	7409	1.5948	0.7072	0.417
22	12.50	297.00	0.1313	2787	7393	1.6085	0.7072	0.417
23	12.50	309.50	0.1313	2785	7535	1.6217	0.7070	0.421
24	12.50	322.01	0.1313	2783	7574	1.6341	0.7069	0.422
25	12.50	334.51	0.1313	2781	7561	1.6461	0.7069	0.422
26	12.50	347.01	0.1313	2779	7539	1.6576	0.7069	0.421
27	12.50	359.51	0.1313	2777	7518	1.6689	0.7070	0.421
28	12.50	372.01	0.1313	2775	7525	1.6813	0.7070	0.421
29	12.50	384.51	0.1313	2773	7650	1.6937	0.7068	0.424
30	12.50	397.01	0.1313	2771	7688	1.7061	0.7067	0.425
31	12.50	409.51	0.1313	2769	7666	1.7184	0.7068	0.425
32	12.50	422.01	0.1313	2767	7645	1.7305	0.7068	0.424
33	12.50	434.51	0.1313	2766	7624	1.7422	0.7068	0.424
34	12.50	447.02	0.1313	2764	7602	1.7534	0.7068	0.424
35	12.50	459.52	0.1313	2762	7714	1.7646	0.7067	0.426
36	13.12	472.02	0.1313	2760	7826	1.7763	0.7065	0.429
37	13.12	485.14	0.1313	2759	7804	1.7886	0.7065	0.428
38	1.73	498.27	0.1313	2758	7853	1.7950	0.7065	0.429
39	164.05	500.00	0.1344	3461	9415	0.5000	0.5000	0.422
40	164.05	664.05	0.1400	4921	11240	0.5000	0.5000	0.381
41	164.05	828.10	0.1438	6562	14270	0.5000	0.5000	0.366
42	164.05	992.15	0.1500	8203	15420	0.2500	0.2500	0.303
43	3281.00	1156.20	0.1575	9285	16080	0.0050	0.0050	0.250

Table 01.5.2.2-3 Strain Compatible Properties for Profile 560-500 (Sheet 2 of 3)

Layer	Thickness	Top-Depth	Unit Weight	V_s	V_p	V_s Damp.	V_p Damp.	Poisson's Ratio
	ft	ft	kcf	ft/s	ft/s	%	%	
-1 Sigma								
1	6.00	0.00	0.1250	800	3586	1.5162	1.3690	0.470
2	6.50	6.00	0.1250	1039	3953	1.7540	1.3550	0.457
3	6.50	12.50	0.1250	994	4035	2.1223	1.3567	0.460
4	11.00	19.00	0.1250	1102	3938	1.8955	1.1551	0.448
5	10.00	30.00	0.1313	1373	4429	1.7639	1.1475	0.438
6	2.00	40.00	0.1313	1360	4470	1.8623	1.1485	0.440
7	8.00	42.00	0.1313	1351	4470	1.9331	1.1485	0.441
8	18.00	50.00	0.1313	1569	4636	1.6372	0.9645	0.426
9	14.50	68.00	0.1313	1883	5256	1.5221	0.9604	0.414
10	14.50	82.50	0.1313	1869	5436	1.6007	0.9630	0.421
11	20.00	97.00	0.1313	1833	5029	1.6558	0.9590	0.413
12	20.00	117.00	0.1313	1820	5194	1.3062	0.7629	0.420
13	22.67	137.01	0.1313	2064	5659	1.3003	0.7597	0.412
14	22.67	159.67	0.1313	2052	5846	1.3492	0.7622	0.419
15	22.67	182.34	0.1313	2042	6016	1.3909	0.7644	0.424
16	21.00	205.00	0.1313	2447	6785	1.3317	0.7613	0.417
17	21.00	226.00	0.1313	2439	6859	1.3623	0.7622	0.419
18	12.50	247.00	0.1313	2514	6759	1.1543	0.6665	0.413
19	12.50	259.50	0.1313	2511	6747	1.1664	0.6664	0.413
20	12.50	272.00	0.1313	2508	6728	1.1777	0.6662	0.412
21	12.50	284.50	0.1313	2506	6716	1.1886	0.6660	0.412
22	12.50	297.00	0.1313	2503	6702	1.1988	0.6659	0.412
23	12.50	309.50	0.1313	2501	6830	1.2087	0.6672	0.416
24	12.50	322.01	0.1313	2498	6866	1.2180	0.6675	0.417
25	12.50	334.51	0.1313	2496	6854	1.2270	0.6674	0.416
26	12.50	347.01	0.1313	2494	6834	1.2357	0.6672	0.416
27	12.50	359.51	0.1313	2492	6815	1.2443	0.6670	0.415
28	12.50	372.01	0.1313	2490	6821	1.2533	0.6671	0.416
29	12.50	384.51	0.1313	2487	6935	1.2618	0.6681	0.419
30	12.50	397.01	0.1313	2485	6969	1.2700	0.6685	0.420
31	12.50	409.51	0.1313	2483	6949	1.2782	0.6683	0.419
32	12.50	422.01	0.1313	2481	6930	1.2865	0.6681	0.419
33	12.50	434.51	0.1313	2479	6910	1.2945	0.6679	0.419
34	12.50	447.02	0.1313	2476	6891	1.3022	0.6677	0.418
35	12.50	459.52	0.1313	2474	6993	1.3098	0.6687	0.421
36	13.12	472.02	0.1313	2472	7094	1.3180	0.6696	0.424
37	13.12	485.14	0.1313	2470	7074	1.3269	0.6694	0.423
38	1.73	498.27	0.1313	2469	7119	1.3316	0.6698	0.424
39	164.05	500.00	0.1344	3101	8434	0.5000	0.5000	0.422
40	164.05	664.05	0.1400	4921	11240	0.5000	0.5000	0.381
41	164.05	828.10	0.1438	6562	14270	0.5000	0.5000	0.366
42	164.05	992.15	0.1500	8203	15420	0.2500	0.2500	0.303
43	3281.00	1156.20	0.1575	9285	16080	0.0050	0.0050	0.250

Table 01.5.2.2-3 Strain Compatible Properties for Profile 560-500 (Sheet 3 of 3)

Layer	Thickness	Top-Depth	Unit Weight	V_s	V_p	V_s Damp.	V_p Damp.	Poisson's Ratio
	ft	ft	kcf	ft/s	ft/s	%	%	
+1 Sigma								
1	6.00	0.00	0.1250	1419	6022	3.0727	1.4327	0.474
2	6.50	6.00	0.1250	1917	6819	3.8870	1.4479	0.463
3	6.50	12.50	0.1250	1887	6961	4.8541	1.4460	0.468
4	11.00	19.00	0.1250	1881	6213	3.6189	1.2371	0.459
5	10.00	30.00	0.1313	1981	6086	3.6923	1.2433	0.449
6	2.00	40.00	0.1313	1969	6143	3.9305	1.2426	0.451
7	8.00	42.00	0.1313	1961	6143	4.0948	1.2426	0.452
8	18.00	50.00	0.1313	2316	6562	3.0943	1.0551	0.438
9	14.50	68.00	0.1313	2718	7186	2.8389	1.0614	0.428
10	14.50	82.50	0.1313	2707	7433	3.0072	1.0575	0.435
11	20.00	97.00	0.1313	2715	7181	3.1896	1.0638	0.427
12	20.00	117.00	0.1313	2703	7416	2.4689	0.8340	0.433
13	22.67	137.01	0.1313	2912	7598	2.2708	0.8370	0.425
14	22.67	159.67	0.1313	2901	7850	2.3580	0.8347	0.432
15	22.67	182.34	0.1313	2892	8077	2.4331	0.8327	0.437
16	21.00	205.00	0.1313	3082	8258	2.2014	0.8355	0.427
17	21.00	226.00	0.1313	3075	8348	2.2495	0.8348	0.430
18	12.50	247.00	0.1313	3114	8226	2.0793	0.7502	0.423
19	12.50	259.50	0.1313	3111	8212	2.1006	0.7503	0.423
20	12.50	272.00	0.1313	3109	8188	2.1206	0.7506	0.422
21	12.50	284.50	0.1313	3107	8174	2.1399	0.7508	0.422
22	12.50	297.00	0.1313	3104	8156	2.1582	0.7510	0.422
23	12.50	309.50	0.1313	3102	8312	2.1757	0.7491	0.426
24	12.50	322.01	0.1313	3100	8356	2.1923	0.7486	0.427
25	12.50	334.51	0.1313	3098	8341	2.2082	0.7488	0.427
26	12.50	347.01	0.1313	3096	8318	2.2235	0.7491	0.426
27	12.50	359.51	0.1313	3095	8294	2.2383	0.7493	0.426
28	12.50	372.01	0.1313	3093	8302	2.2554	0.7492	0.426
29	12.50	384.51	0.1313	3092	8440	2.2736	0.7476	0.429
30	12.50	397.01	0.1313	3090	8481	2.2919	0.7472	0.430
31	12.50	409.51	0.1313	3089	8457	2.3102	0.7475	0.430
32	12.50	422.01	0.1313	3087	8434	2.3276	0.7477	0.430
33	12.50	434.51	0.1313	3086	8410	2.3447	0.7480	0.429
34	12.50	447.02	0.1313	3085	8387	2.3610	0.7482	0.429
35	12.50	459.52	0.1313	3083	8510	2.3773	0.7468	0.432
36	13.12	472.02	0.1313	3082	8634	2.3939	0.7455	0.434
37	13.12	485.14	0.1313	3081	8609	2.4109	0.7458	0.434
38	1.73	498.27	0.1313	3080	8664	2.4198	0.7452	0.435
39	164.05	500.00	0.1344	3864	10510	0.5000	0.5000	0.422
40	164.05	664.05	0.1400	4921	11240	0.5000	0.5000	0.381
41	164.05	828.10	0.1438	6562	14270	0.5000	0.5000	0.366
42	164.05	992.15	0.1500	8203	15420	0.2500	0.2500	0.303
43	3281.00	1156.20	0.1575	9285	16080	0.0050	0.0050	0.250

Table 01.5.2.2-4 Strain Compatible Properties for Profile 900-100

Layer	Thickness	Top-Depth	Unit Weight	V_s	V_p	V_s Damp.	V_p Damp.	Poisson's Ratio
	ft	ft	kcf	ft/s	ft/s	%	%	
Median								
1	5.00	0.00	0.1250	1477	4703	1.6561	1.4006	0.445
2	7.00	5.00	0.1313	1925	5272	1.8957	1.4002	0.423
3	8.00	12.00	0.1313	2101	5026	2.1232	1.3993	0.394
4	9.00	20.00	0.1313	2694	6506	1.5027	1.1906	0.396
5	11.00	29.00	0.1313	3001	7655	1.5006	1.1919	0.409
6	2.00	40.00	0.1344	3210	8053	1.4750	1.1915	0.405
7	11.00	42.00	0.1344	3249	8160	1.5082	1.1915	0.406
8	20.00	53.00	0.1344	4103	9920	1.2820	1.0111	0.397
9	23.00	73.00	0.1400	5315	12172	1.1762	1.0122	0.382
10	4.00	96.00	0.1425	5634	12325	1.1654	1.0131	0.368
11	164.05	100.00	0.1500	8623	16210	0.2500	0.2500	0.303
12	3281.00	264.05	0.1575	9285	16080	0.0050	0.0050	0.250
-1 Sigma								
1	5.00	0.00	0.1250	1046	3369	1.2114	1.3452	0.443
2	7.00	5.00	0.1313	1401	3898	1.4643	1.3251	0.419
3	8.00	12.00	0.1313	1493	3664	1.5893	1.3005	0.386
4	9.00	20.00	0.1313	2052	4999	1.0529	1.1194	0.393
5	11.00	29.00	0.1313	2328	6004	1.0889	1.1277	0.406
6	2.00	40.00	0.1344	2535	6446	1.0580	1.1252	0.401
7	11.00	42.00	0.1344	2587	6580	1.0732	1.1252	0.402
8	20.00	53.00	0.1344	3167	7718	0.9605	0.9537	0.394
9	23.00	73.00	0.1400	4526	10379	0.9068	0.9488	0.381
10	4.00	96.00	0.1425	4897	10726	0.9043	0.9440	0.366
11	164.05	100.00	0.1500	6533	12282	0.2500	0.2500	0.303
12	3281.00	264.05	0.1575	9285	16080	0.0050	0.0050	0.250
+1 Sigma								
1	5.00	0.00	0.1250	2087	6563	2.2641	1.4581	0.447
2	7.00	5.00	0.1313	2646	7131	2.4542	1.4796	0.427
3	8.00	12.00	0.1313	2957	6895	2.8365	1.5056	0.401
4	9.00	20.00	0.1313	3537	8467	2.1448	1.2663	0.400
5	11.00	29.00	0.1313	3868	9761	2.0678	1.2597	0.413
6	2.00	40.00	0.1344	4064	10061	2.0565	1.2617	0.410
7	11.00	42.00	0.1344	4080	10118	2.1195	1.2617	0.410
8	20.00	53.00	0.1344	5314	12752	1.7111	1.0719	0.400
9	23.00	73.00	0.1400	6242	14274	1.5256	1.0797	0.384
10	4.00	96.00	0.1425	6481	14163	1.5018	1.0873	0.370
11	164.05	100.00	0.1500	11380	21394	0.2500	0.2500	0.303
12	3281.00	264.05	0.1575	9285	16080	0.0050	0.0050	0.250

Table 01.5.2.2-5 Strain Compatible Properties for Profile 900-200

Layer	Thickness	Top-Depth	Unit Weight	V_s	V_p	V_s Damp.	V_p Damp.	Poisson's Ratio
	ft	ft	kcf	ft/s	ft/s	%	%	
Median								
1	5.00	0.00	0.1250	1521	4859	1.6802	1.4006	0.446
2	7.00	5.00	0.1313	2003	5478	1.8486	1.4002	0.423
3	8.00	12.00	0.1313	2196	5239	2.0639	1.3993	0.393
4	9.00	20.00	0.1313	2606	6327	1.5526	1.1906	0.398
5	11.00	29.00	0.1313	2954	7556	1.5364	1.1919	0.410
6	2.00	40.00	0.1344	3186	8010	1.5151	1.1915	0.406
7	11.00	42.00	0.1344	3431	8608	1.4775	1.1915	0.405
8	20.00	53.00	0.1344	3749	9101	1.3504	1.0111	0.398
9	23.00	73.00	0.1400	4731	10856	1.2525	1.0122	0.383
10	25.00	96.00	0.1425	5660	12397	1.1986	1.0131	0.368
11	34.00	121.00	0.1438	6589	13884	0.9323	0.7957	0.355
12	45.00	155.00	0.1469	6576	13407	0.9452	0.7952	0.342
13	164.05	200.00	0.1500	7958	14961	0.2500	0.2500	0.303
14	3281.00	364.05	0.1575	9285	16080	0.0050	0.0050	0.250
-1 Sigma								
1	5.00	0.00	0.1250	1014	3306	1.1961	1.3452	0.443
2	7.00	5.00	0.1313	1531	4264	1.3289	1.3251	0.419
3	8.00	12.00	0.1313	1688	4120	1.4403	1.3005	0.387
4	9.00	20.00	0.1313	1939	4792	1.0713	1.1194	0.392
5	11.00	29.00	0.1313	2286	5930	1.1030	1.1277	0.405
6	2.00	40.00	0.1344	2439	6224	1.1011	1.1252	0.402
7	11.00	42.00	0.1344	2810	7144	1.0991	1.1252	0.402
8	20.00	53.00	0.1344	3027	7462	1.0445	0.9537	0.393
9	23.00	73.00	0.1400	4025	9258	0.9739	0.9488	0.381
10	25.00	96.00	0.1425	4679	10273	0.9537	0.9440	0.366
11	34.00	121.00	0.1438	5748	12125	0.7329	0.7415	0.353
12	45.00	155.00	0.1469	5782	11802	0.7372	0.7374	0.340
13	164.05	200.00	0.1500	6912	12994	0.2500	0.2500	0.303
14	3281.00	364.05	0.1575	9285	16080	0.0050	0.0050	0.250
+1 Sigma								
1	5.00	0.00	0.1250	2283	7142	2.3603	1.4581	0.448
2	7.00	5.00	0.1313	2621	7038	2.5715	1.4796	0.426
3	8.00	12.00	0.1313	2856	6661	2.9575	1.5056	0.400
4	9.00	20.00	0.1313	3503	8355	2.2502	1.2663	0.403
5	11.00	29.00	0.1313	3818	9627	2.1401	1.2597	0.414
6	2.00	40.00	0.1344	4162	10309	2.0849	1.2617	0.410
7	11.00	42.00	0.1344	4189	10372	1.9863	1.2617	0.409
8	20.00	53.00	0.1344	4644	11099	1.7458	1.0719	0.402
9	23.00	73.00	0.1400	5561	12730	1.6108	1.0797	0.385
10	25.00	96.00	0.1425	6848	14960	1.5065	1.0873	0.370
11	34.00	121.00	0.1438	7553	15898	1.1858	0.8538	0.356
12	45.00	155.00	0.1469	7478	15231	1.2120	0.8575	0.343
13	164.05	200.00	0.1500	9163	17226	0.2500	0.2500	0.303
14	3281.00	364.05	0.1575	9285	16080	0.0050	0.0050	0.250

Table 01.5.2.2-6 Strain Compatible Properties for Profile 2032-100

Layer	Thickness	Top-Depth	Unit Weight	V_s	V_p	V_s Damp.	V_p Damp.	Poisson's Ratio
	ft	ft	kcf	ft/s	ft/s	%	%	
Median								
1	4.17	0.00	0.1400	5168	9669	2.8114	3.1230	0.300
2	4.17	4.17	0.1400	5302	9838	2.8265	3.1208	0.295
3	8.33	8.33	0.1400	5794	10554	2.8356	3.1157	0.284
4	8.33	16.67	0.1400	5889	10461	2.8509	3.1082	0.268
5	8.33	25.00	0.1400	6090	10652	2.8643	3.1033	0.257
6	6.66	33.34	0.1400	6558	11359	2.8681	3.1002	0.250
7	2.01	40.00	0.1400	6556	11355	2.9735	3.1008	0.250
8	8.00	42.00	0.1400	6968	12069	2.9765	3.1008	0.250
9	16.67	50.00	0.1400	7258	12572	2.9805	3.1008	0.250
10	16.67	66.67	0.1400	7571	13113	2.9806	3.1008	0.250
11	16.66	83.34	0.1400	8017	13886	2.9803	3.1008	0.250
12	3281.00	100.00	0.1575	8890	15397	0.000001	0.000001	0.250
-1 Sigma								
1	4.17	0.00	0.1400	3956	7401	1.8636	2.7248	0.300
2	4.17	4.17	0.1400	4131	7665	1.8889	2.7165	0.295
3	8.33	8.33	0.1400	4688	8540	1.9064	2.6973	0.284
4	8.33	16.67	0.1400	4851	8619	1.9345	2.6696	0.268
5	8.33	25.00	0.1400	5068	8863	1.9574	2.6516	0.257
6	6.66	33.34	0.1400	5389	9335	1.9609	2.6406	0.250
7	2.01	40.00	0.1400	5314	9203	2.2123	2.7293	0.250
8	8.00	42.00	0.1400	5647	9781	2.2132	2.7293	0.250
9	16.67	50.00	0.1400	6110	10583	2.2160	2.7293	0.250
10	16.67	66.67	0.1400	6531	11310	2.2201	2.7293	0.250
11	16.66	83.34	0.1400	6856	11875	2.2174	2.7293	0.250
12	3281.00	100.00	0.1575	6551	11347	0.000001	0.000001	0.250
+1 Sigma								
1	4.17	0.00	0.1400	6752	12631	4.2412	3.5793	0.300
2	4.17	4.17	0.1400	6806	12628	4.2295	3.5853	0.295
3	8.33	8.33	0.1400	7160	13043	4.2175	3.5991	0.285
4	8.33	16.67	0.1400	7148	12696	4.2016	3.6188	0.268
5	8.33	25.00	0.1400	7320	12801	4.1913	3.6319	0.257
6	6.66	33.34	0.1400	7980	13821	4.1951	3.6399	0.250
7	2.01	40.00	0.1400	8089	14010	3.9967	3.5228	0.250
8	8.00	42.00	0.1400	8599	14893	4.0032	3.5228	0.250
9	16.67	50.00	0.1400	8622	14934	4.0088	3.5228	0.250
10	16.67	66.67	0.1400	8778	15203	4.0017	3.5228	0.250
11	16.66	83.34	0.1400	9375	16237	4.0057	3.5228	0.250
12	3281.00	100.00	0.1575	12063	20893	0.000001	0.000001	0.250

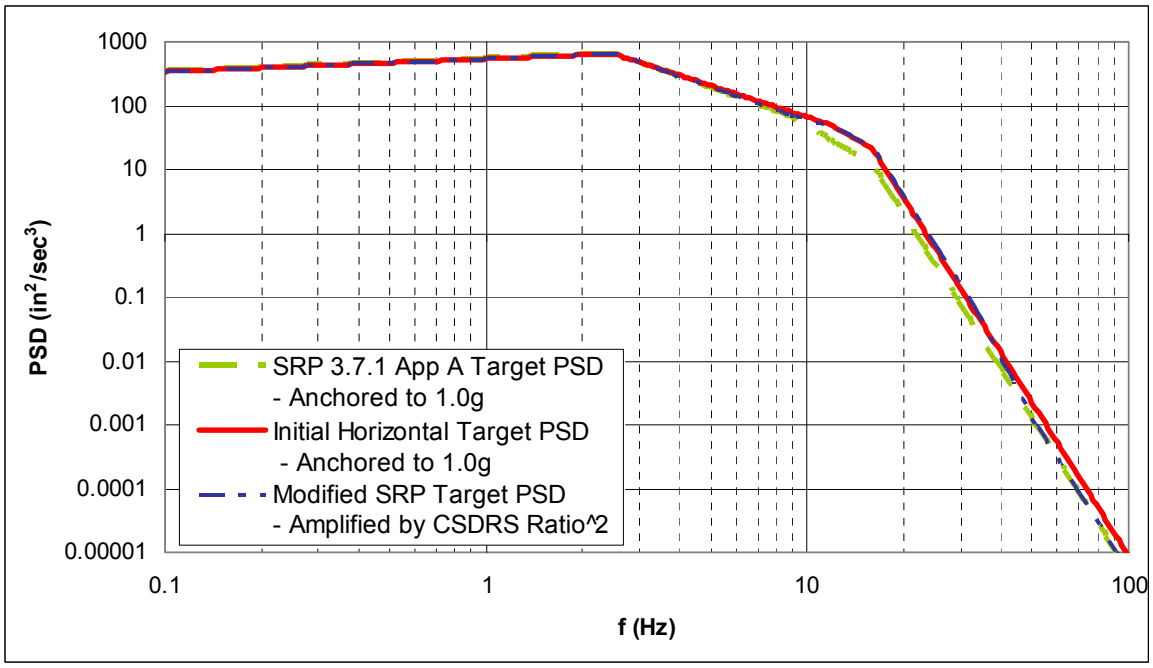

(a)

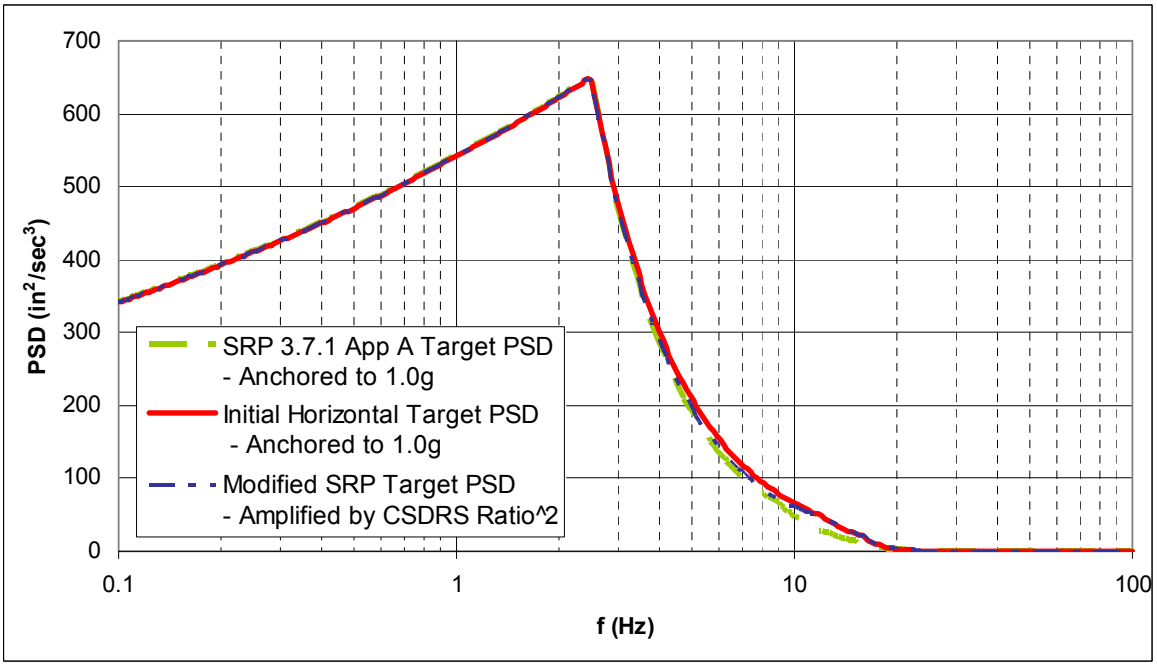

(b)

Figure 01.5.1.1-1 US-APWR Initial Horizontal Target PSD

(a) Log-Log Scale; (b) Semi-Log Scale

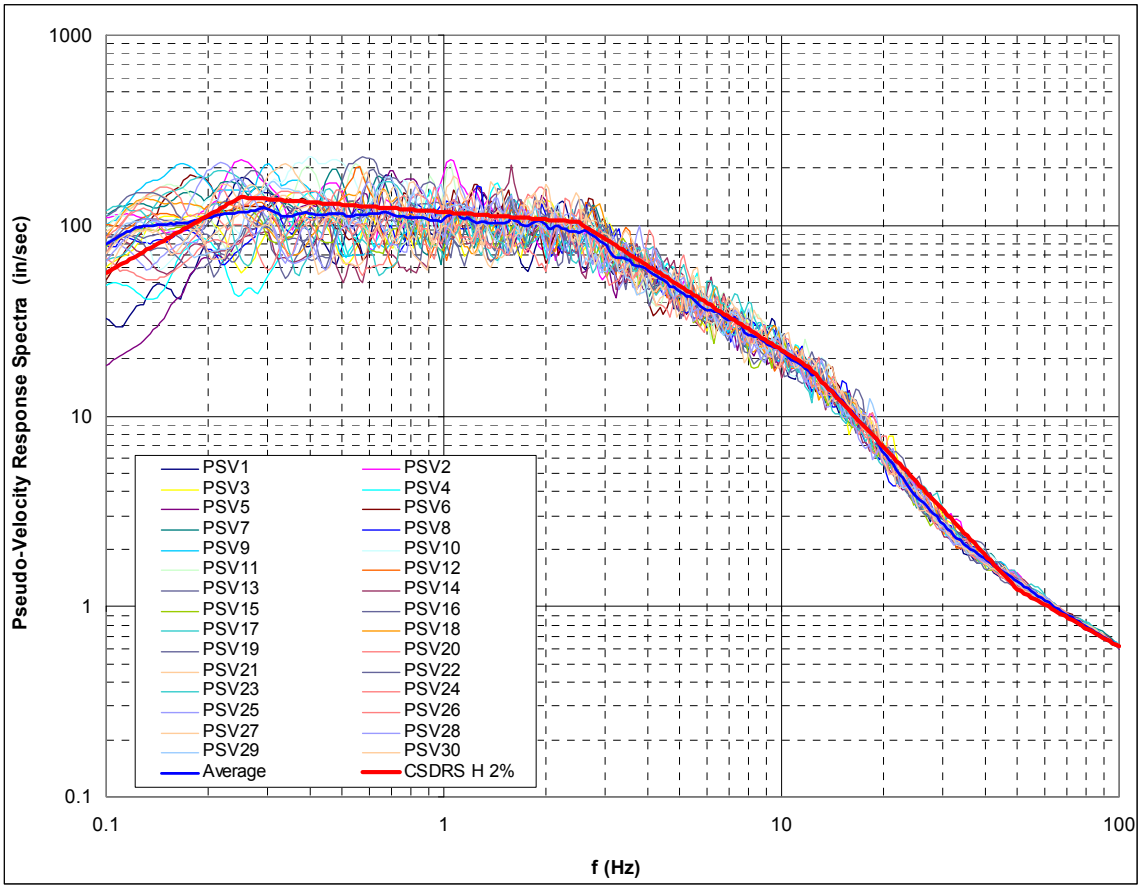

Figure 01.5.1.1.2-1 Horizontal Pseudo-Velocity Response Spectra (PSV) at 2% Damping of 30 Artificial Horizontal Time Histories

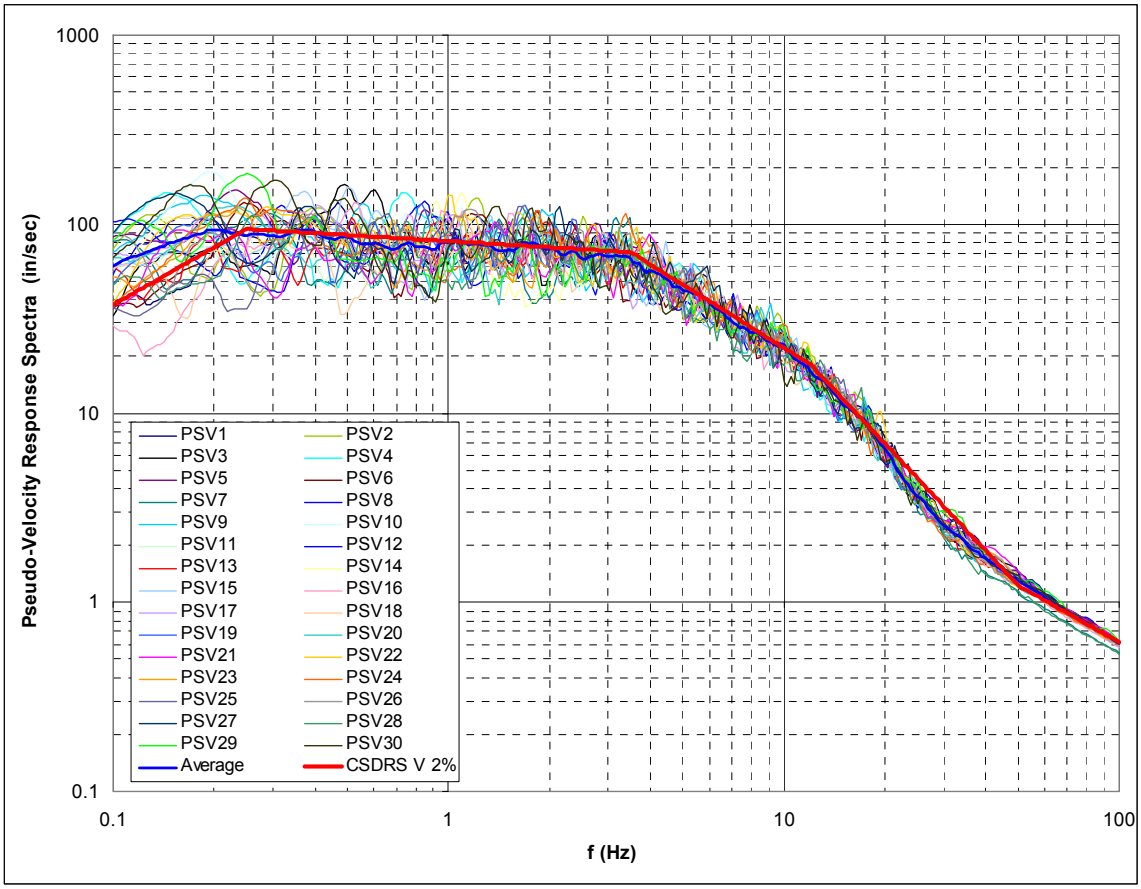

Figure 01.5.1.1.2-2 Vertical Pseudo-Velocity Response Spectra (PSV) at 2% Damping of 30 Artificial Vertical Time Histories

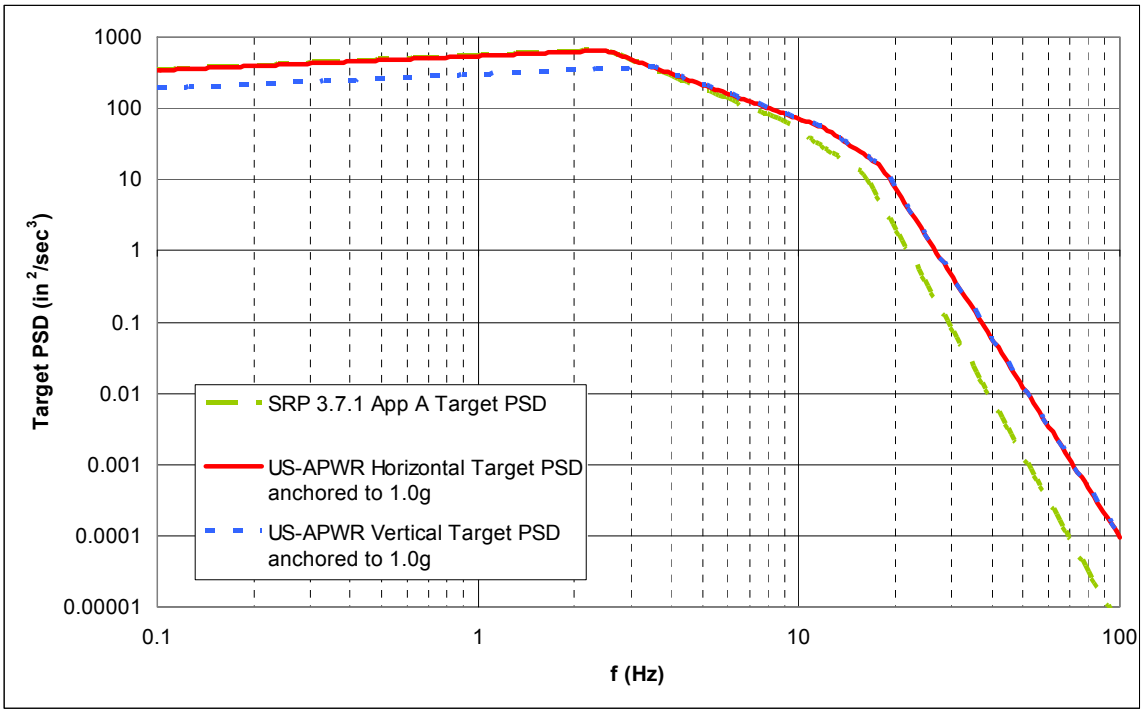

Figure 01.5.1.1.2-3 US-APWR Final Horizontal and Vertical Target PSDs

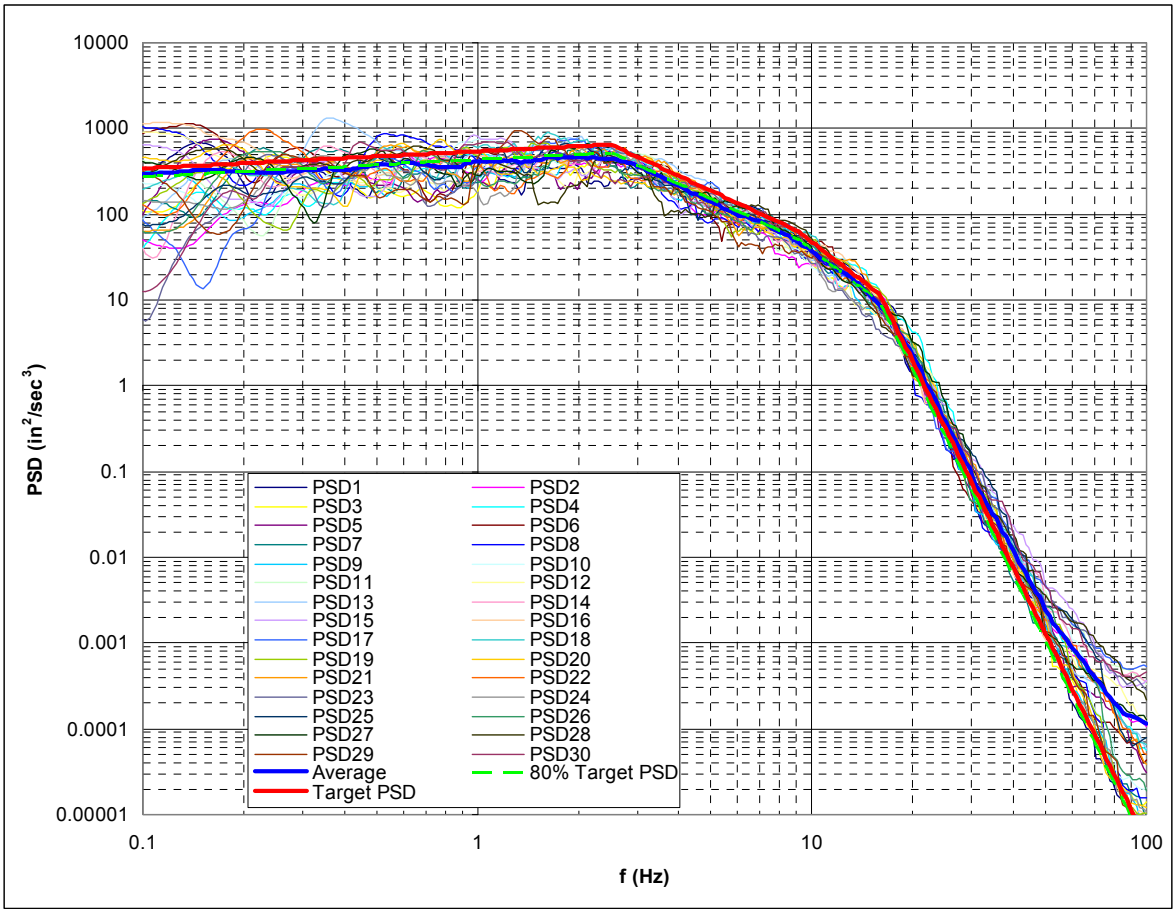

Figure 01.5.1.1-4 Scenario I PSDs vs. SRP 3.7.1 Target PSD

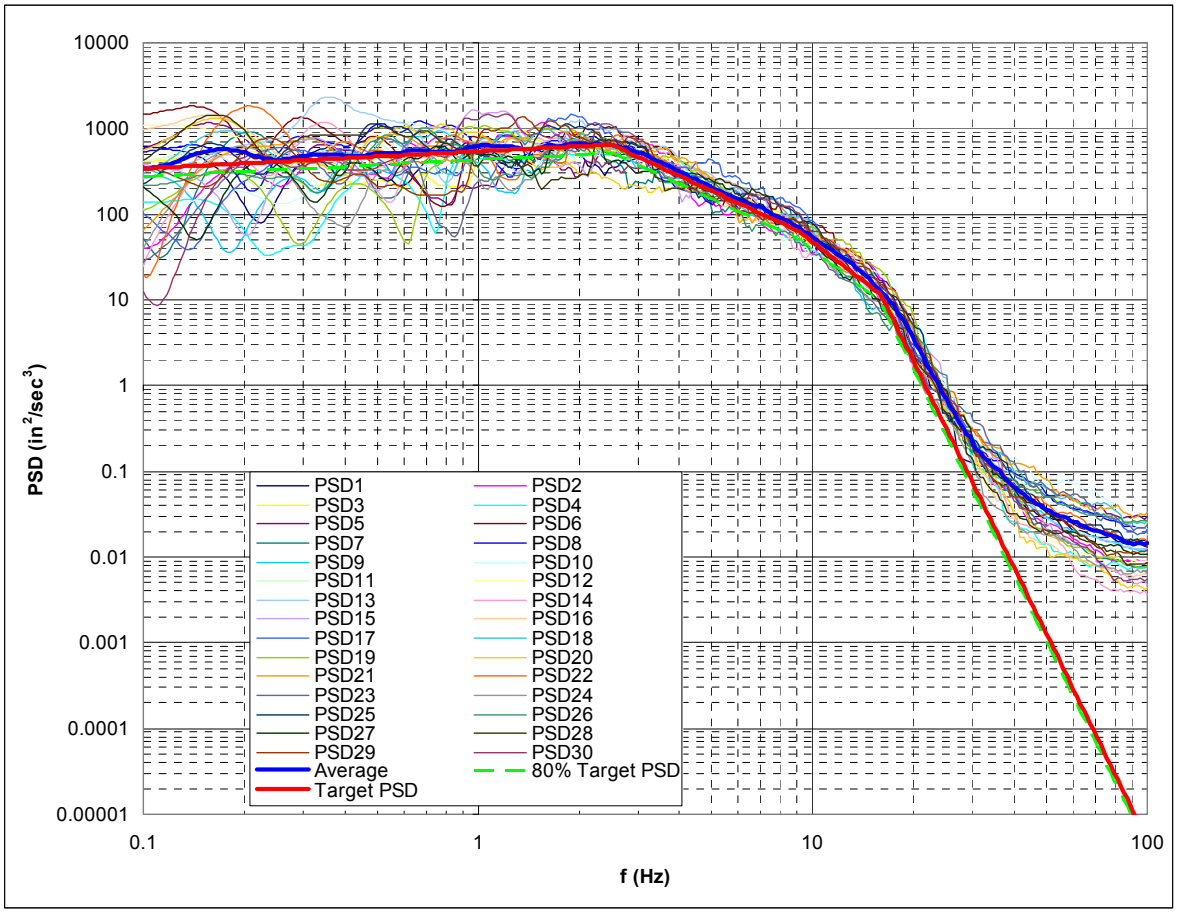

Figure 01.5.1.1-5 Scenario II PSDs vs. SRP 3.7.1 Target PSD

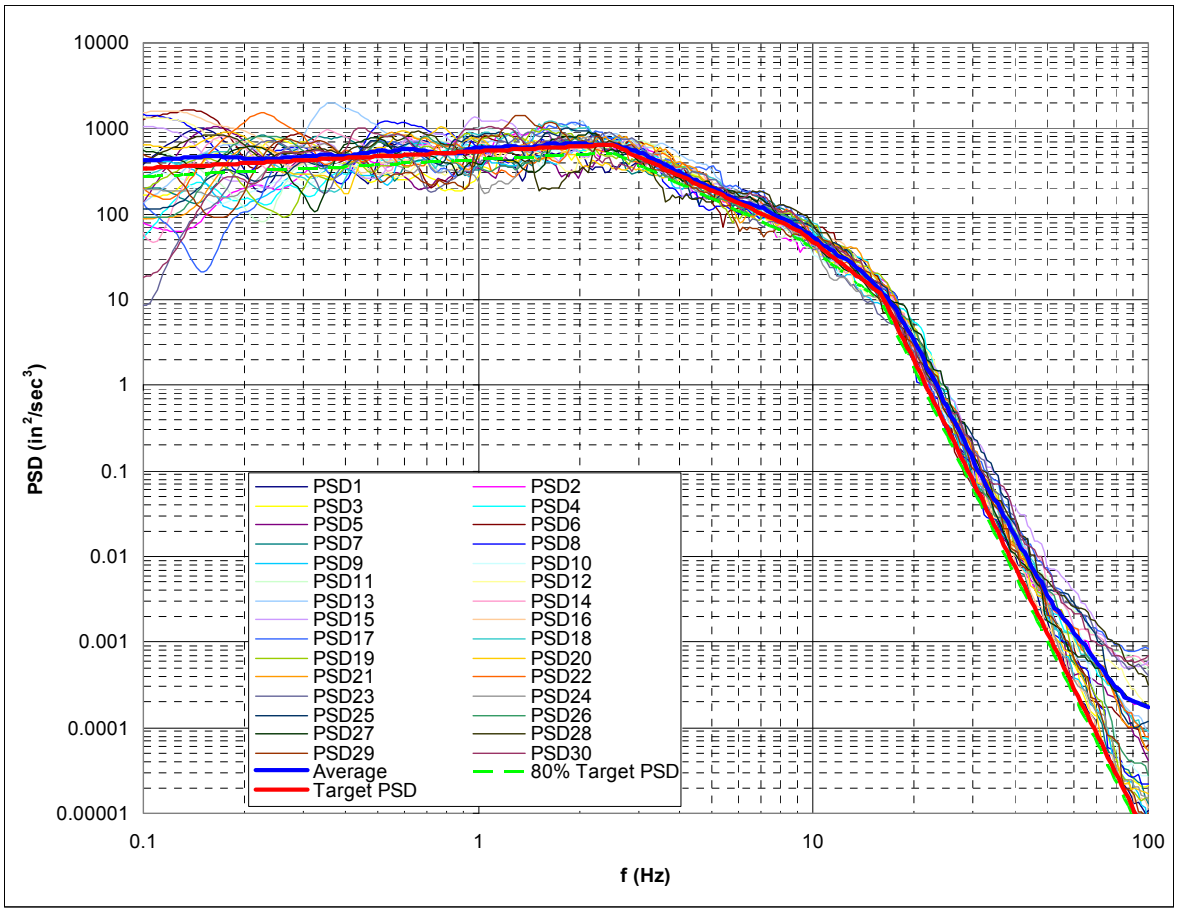

Figure 01.5.1.1-6 Scenario III PSDs vs. SRP 3.7.1 Target PSD

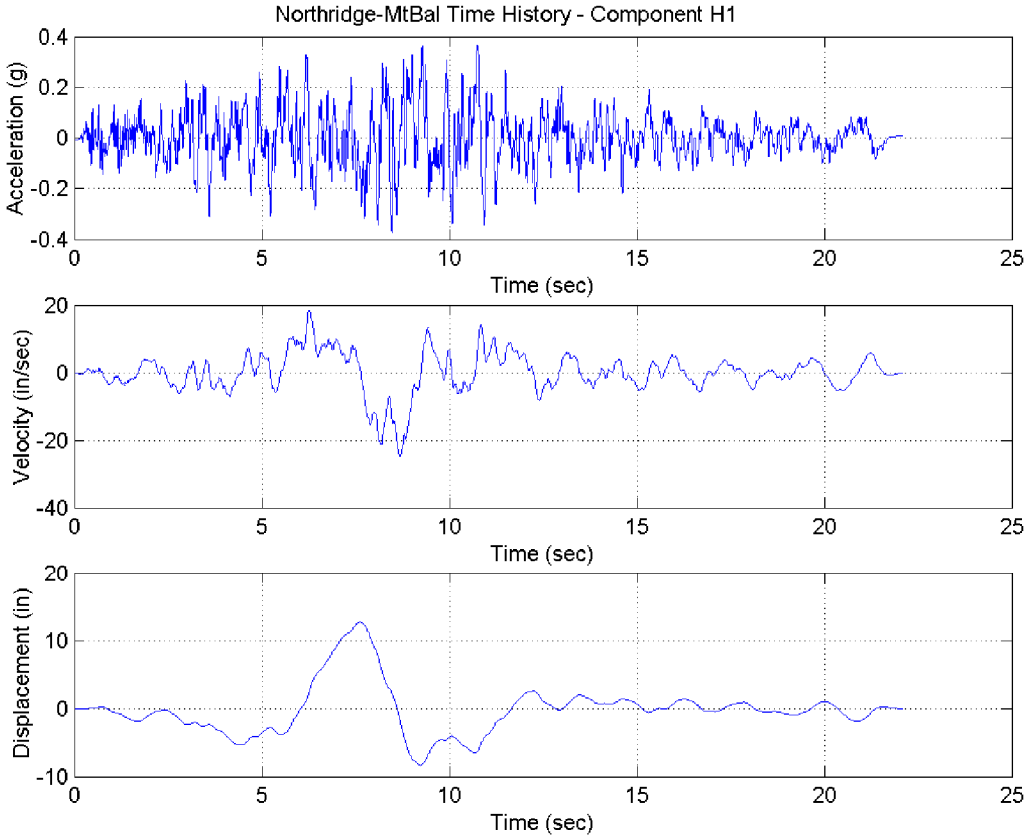

Figure 01.5.1.2-1 Acceleration, Velocity, and Displacement Time History for Component H1 (180)

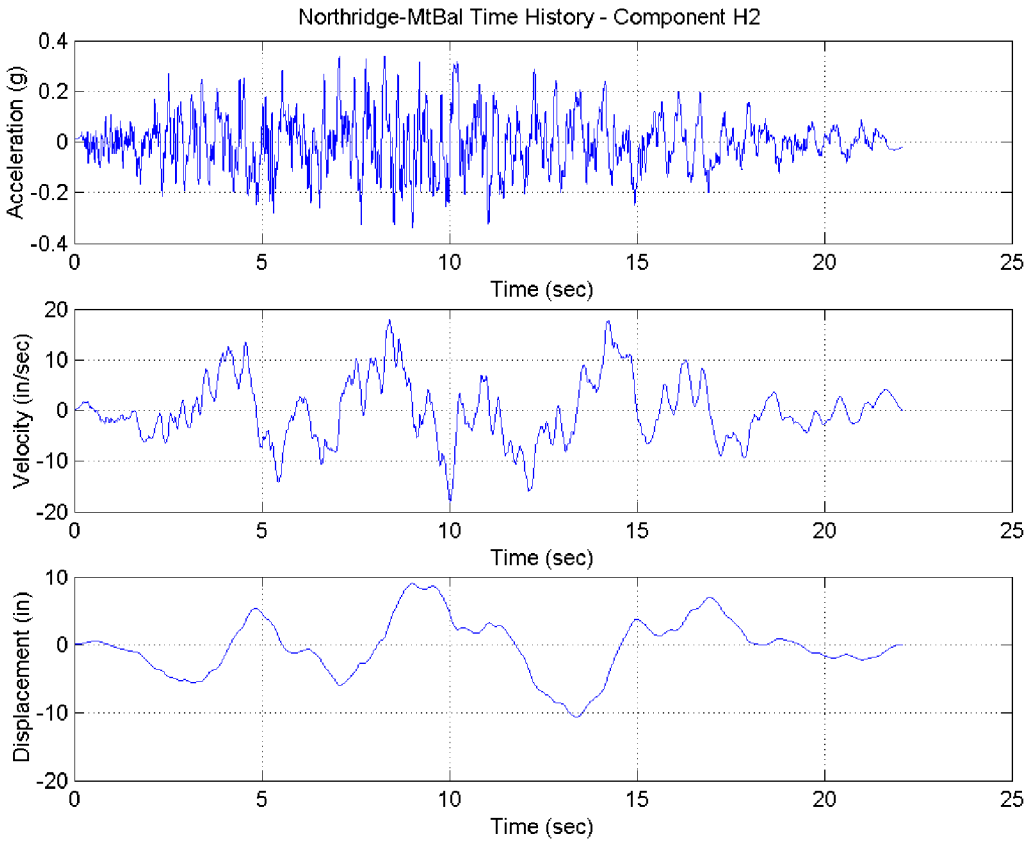

Figure 01.5.1.2-2 Acceleration, Velocity, and Displacement Time History for Component H2 (090)

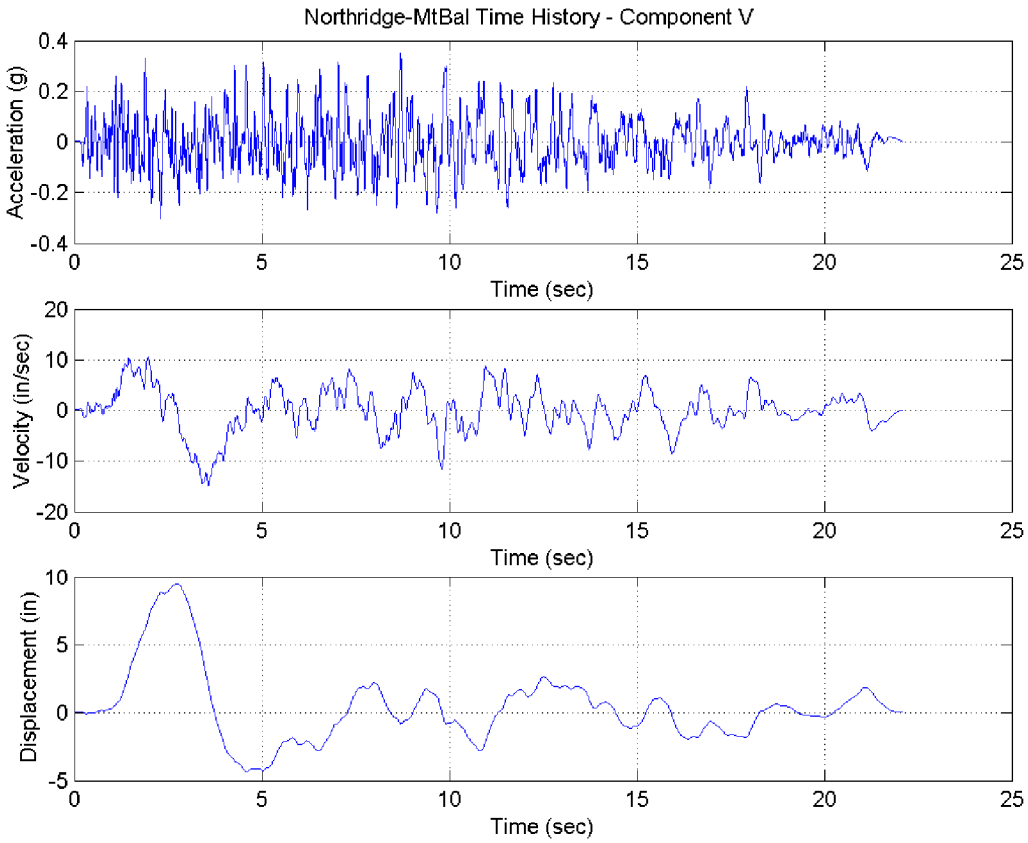

Figure 01.5.1.2-3 Acceleration, Velocity, and Displacement Time History for Component V (UP)

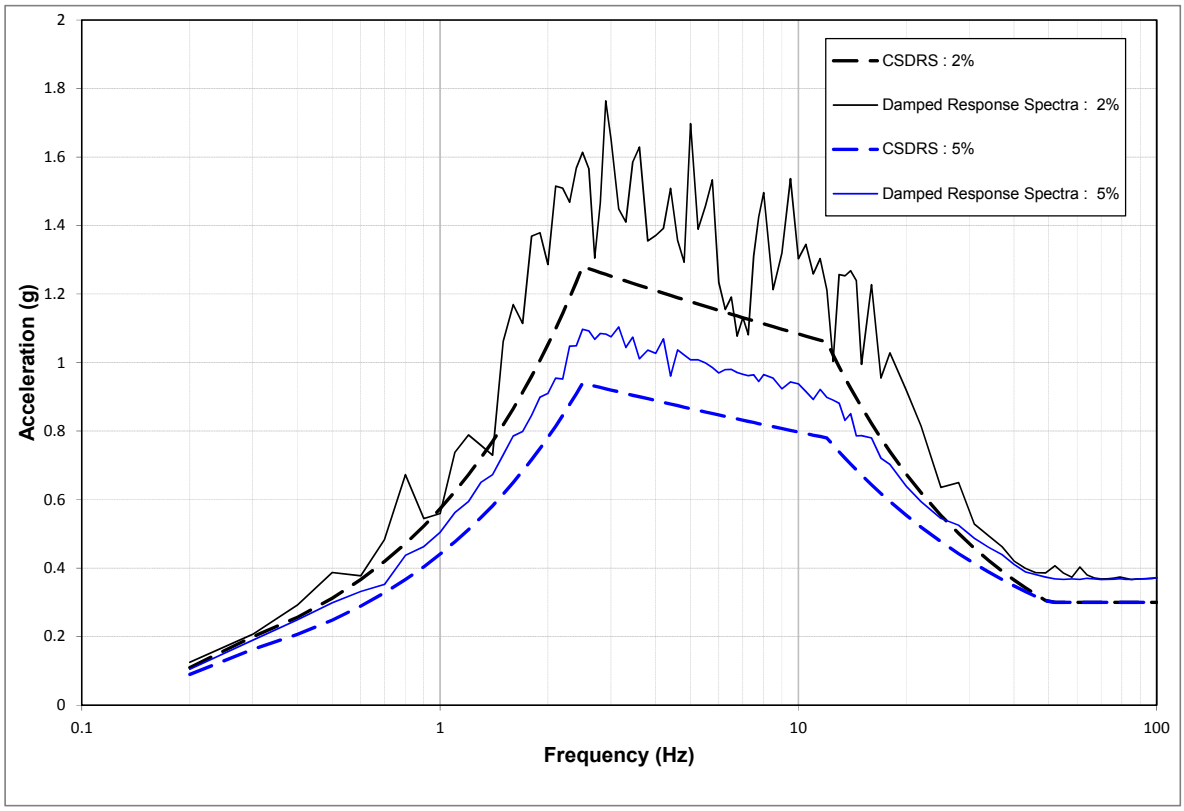

Figure 01.5.1.2-4a Damped Response Spectra Plots for Northridge Mount Baldy Component H1 (180)

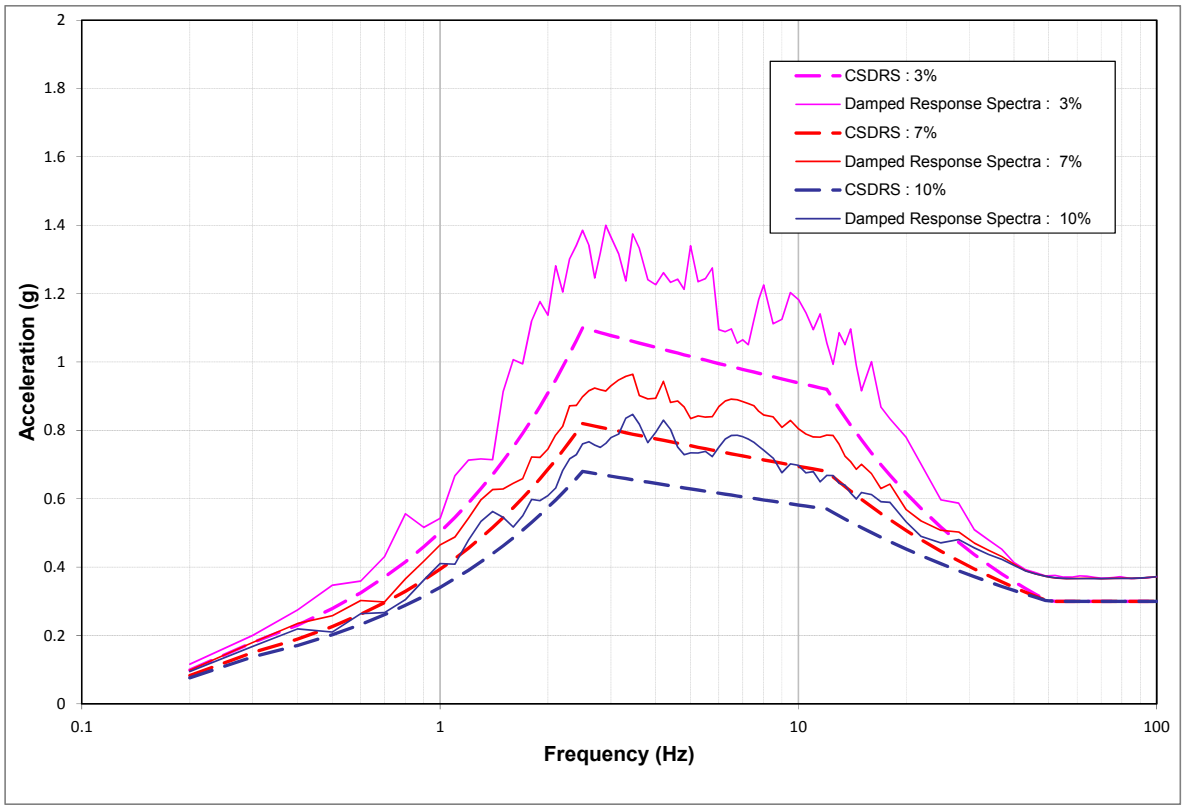

Figure 01.5.1.2-4b Damped Response Spectra Plots for Northridge Mount Baldy Component H1 (180)

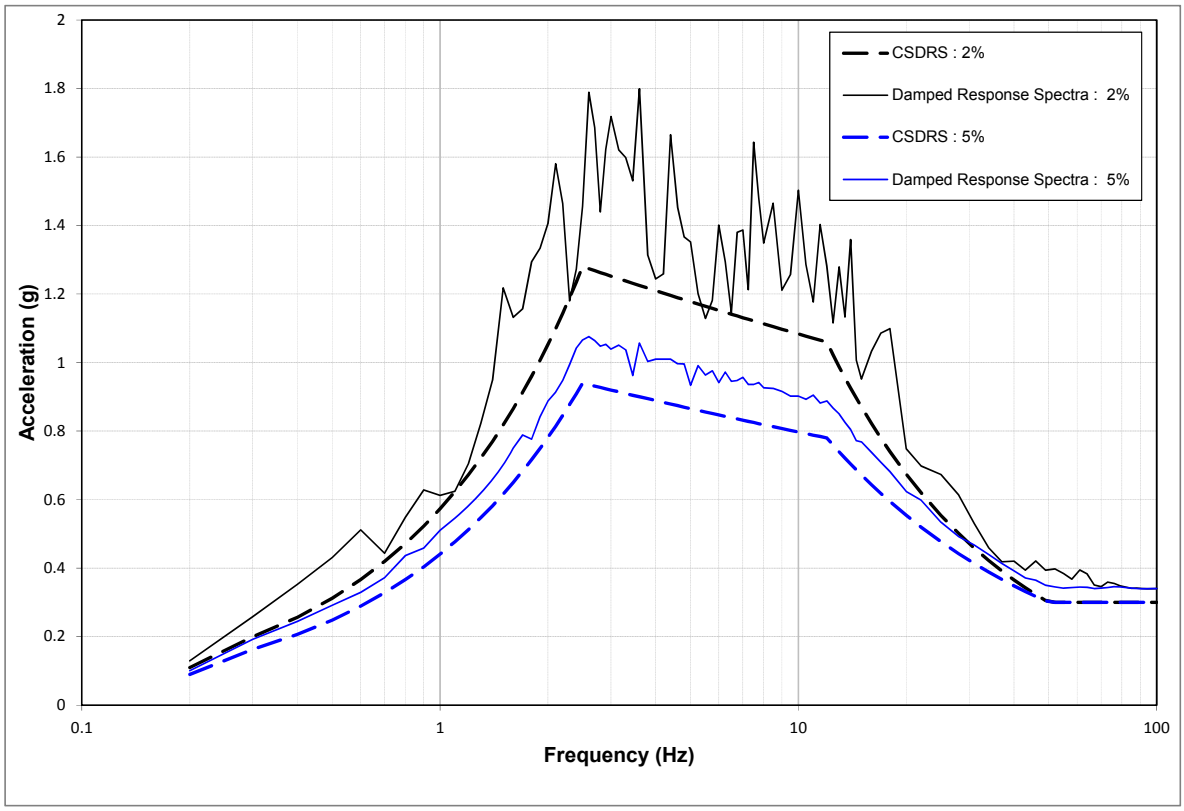

Figure 01.5.1.2-5a Damped Response Spectra Plots for Northridge Mount Baldy Component H2 (090)

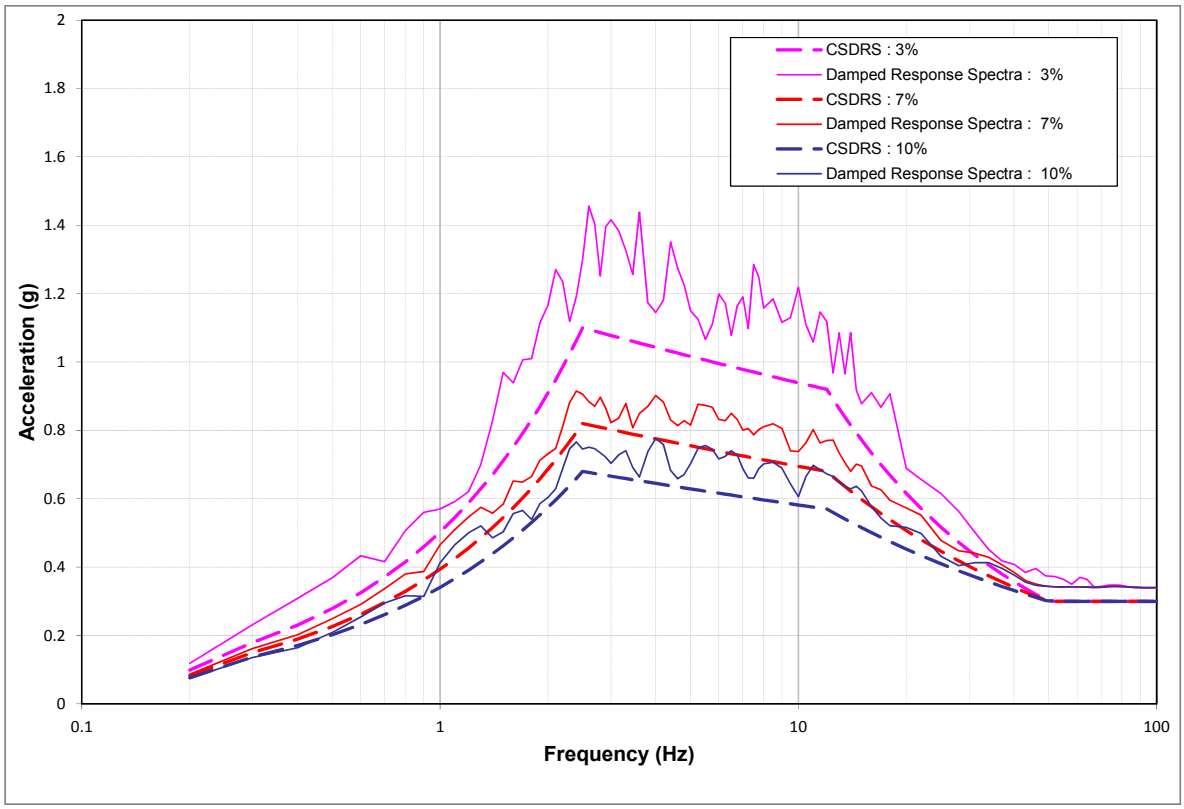

Figure 01.5.1.2-5b Damped Response Spectra Plots for Northridge Mount Baldy Component H2 (090)

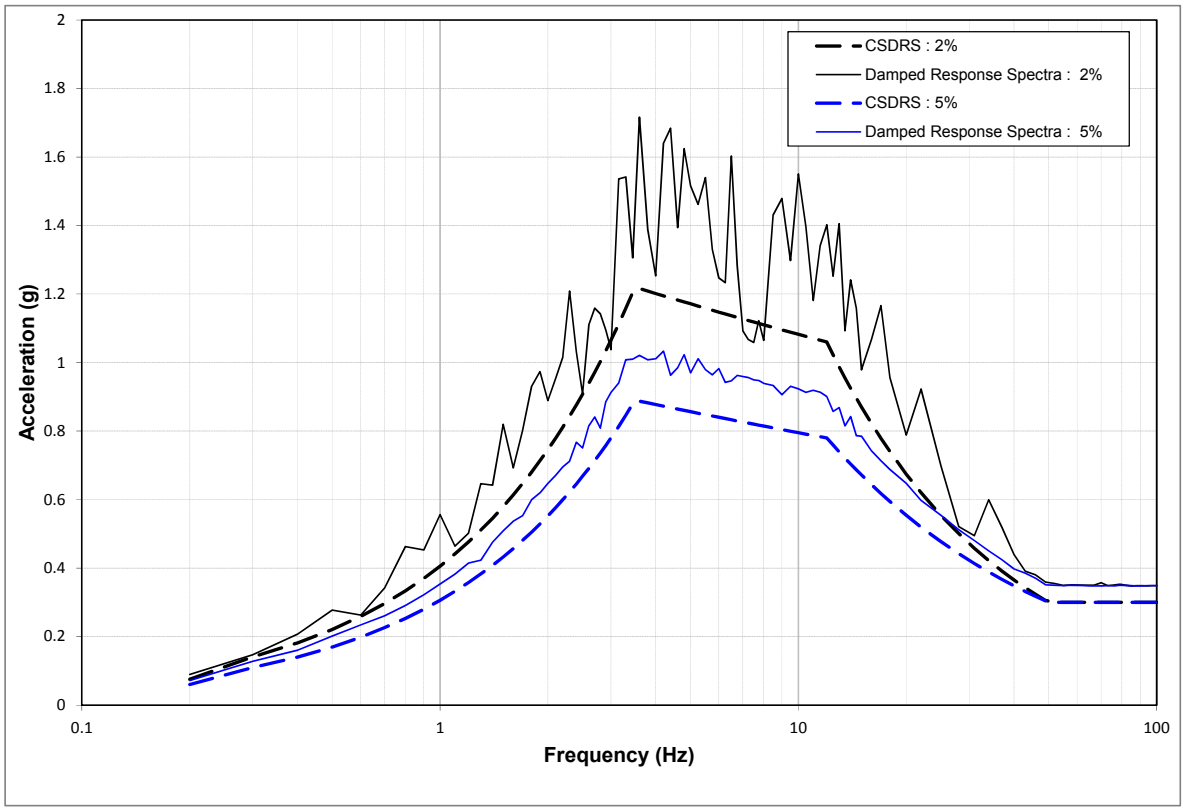

Figure 01.5.1.2-6a Damped Response Spectra Plots for Mount Baldy Component V (UP)

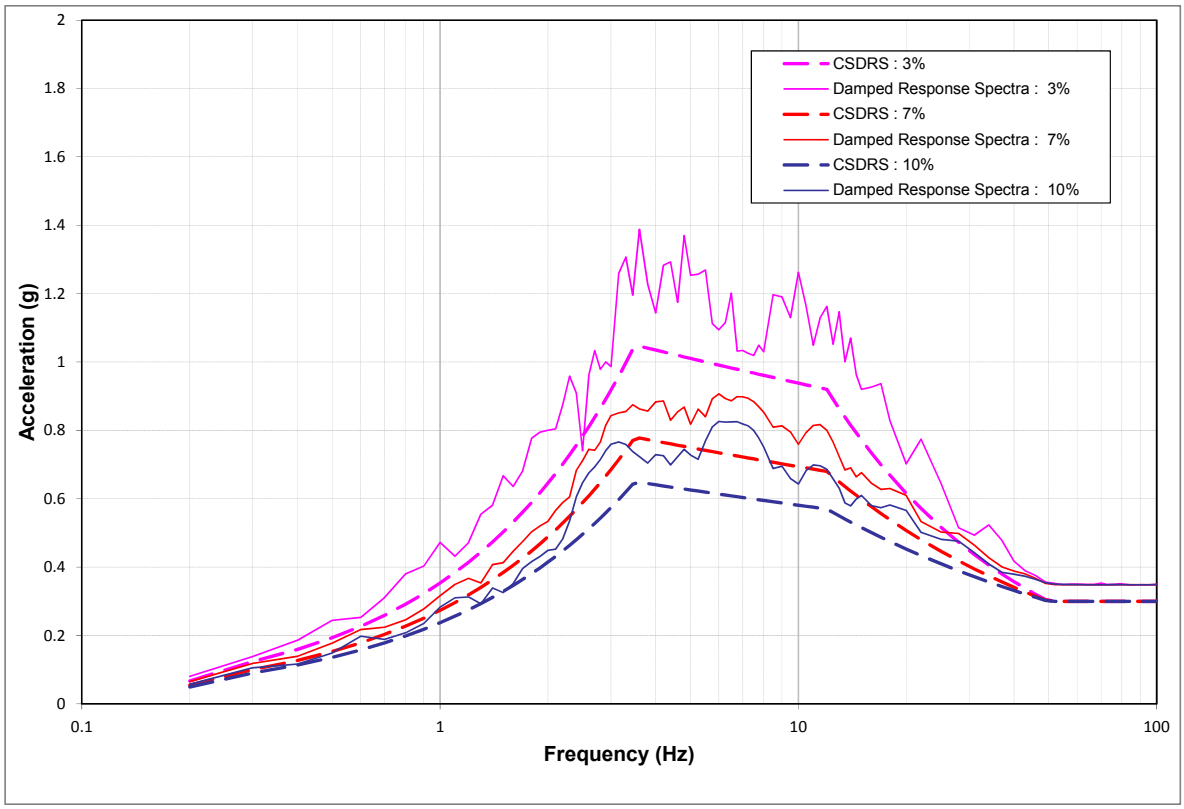

Figure 01.5.1.2-6b Damped Response Spectra Plots for Mount Baldy Component V (UP)

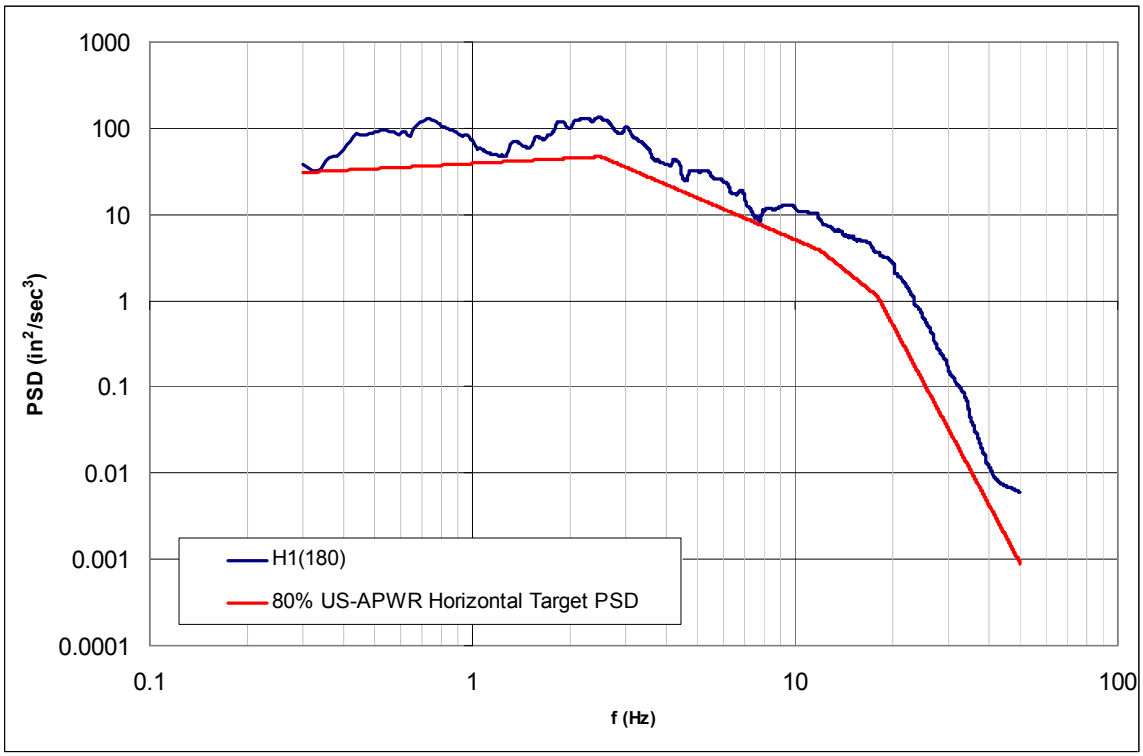

Figure 01.5.1.2-7 Smoothed Power Spectral Density Plots for Component H1 (180)

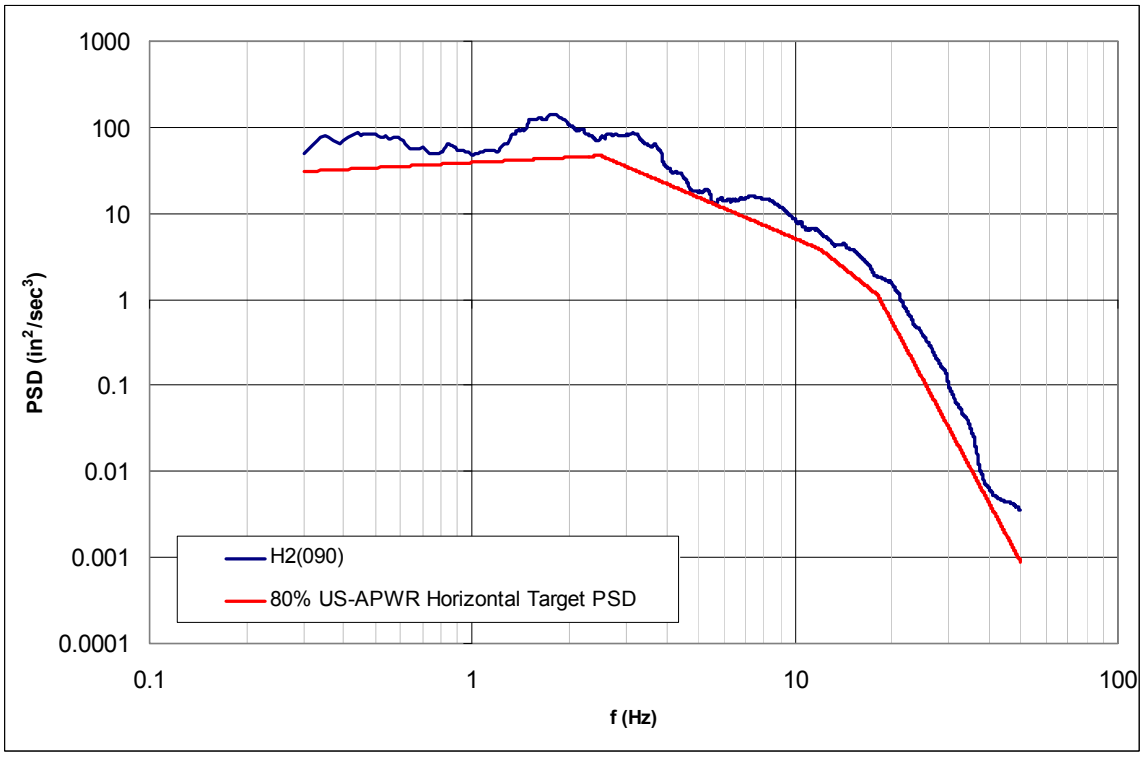

Figure 01.5.1.2-8 Smoothed Power Spectral Density Plots for Component H2 (090)

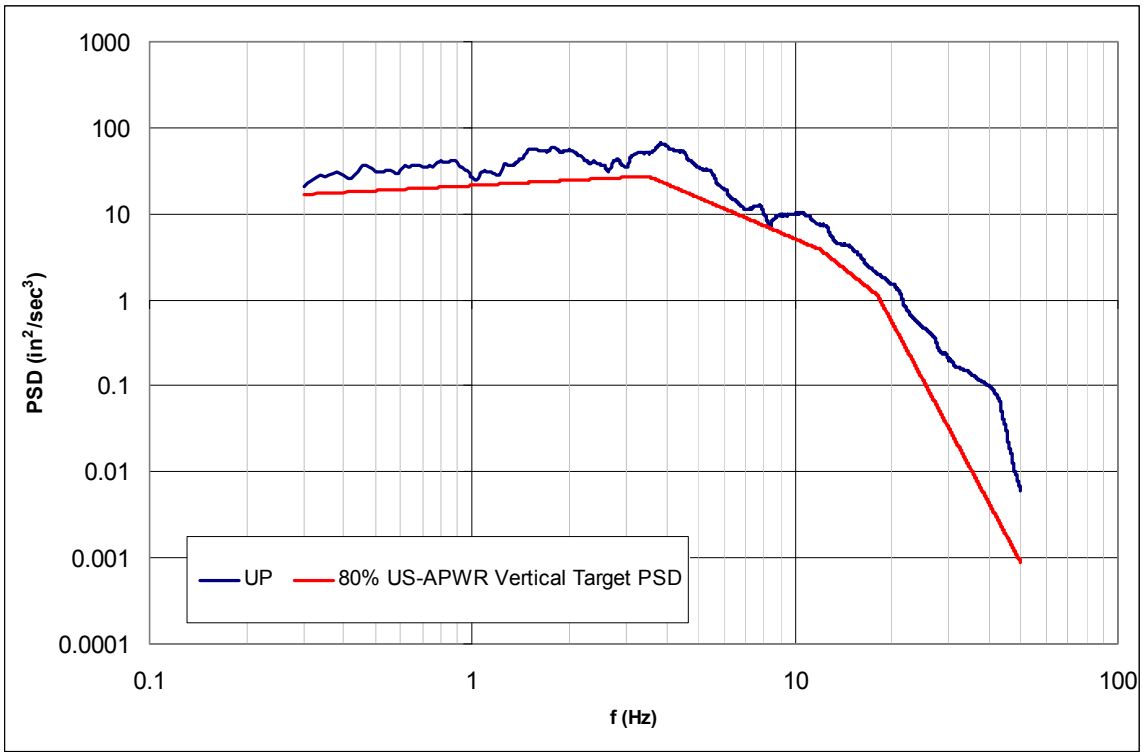

Figure 01.5.1.2-9 Smoothed Power Spectral Density Plots for Component V (UP)

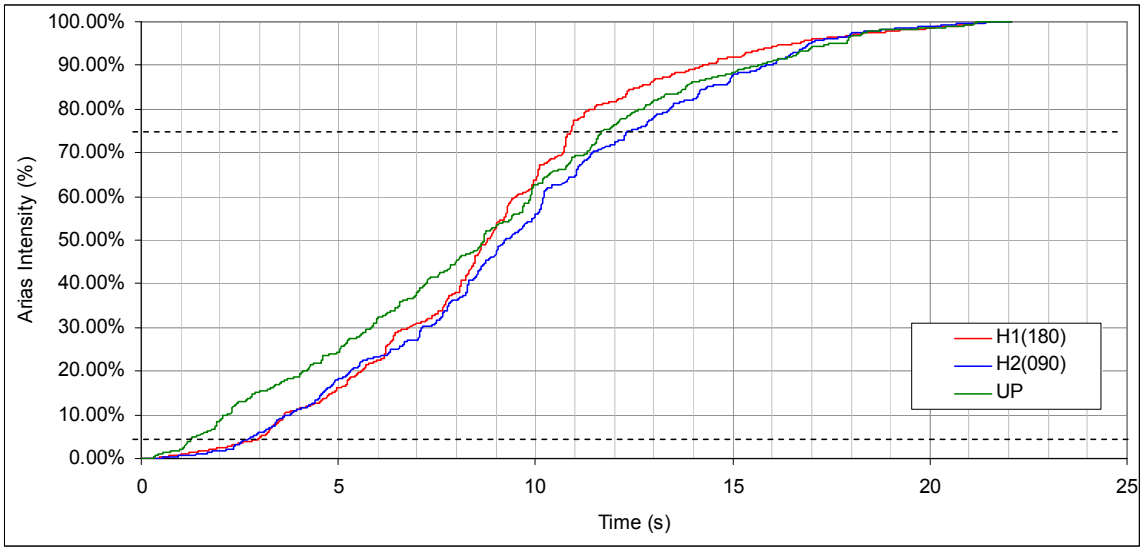

Figure 01.5.1.2-10 Arias Intensities of the Northridge – Mount Baldy Artificial Time History Components Showing 5%-75% Duration

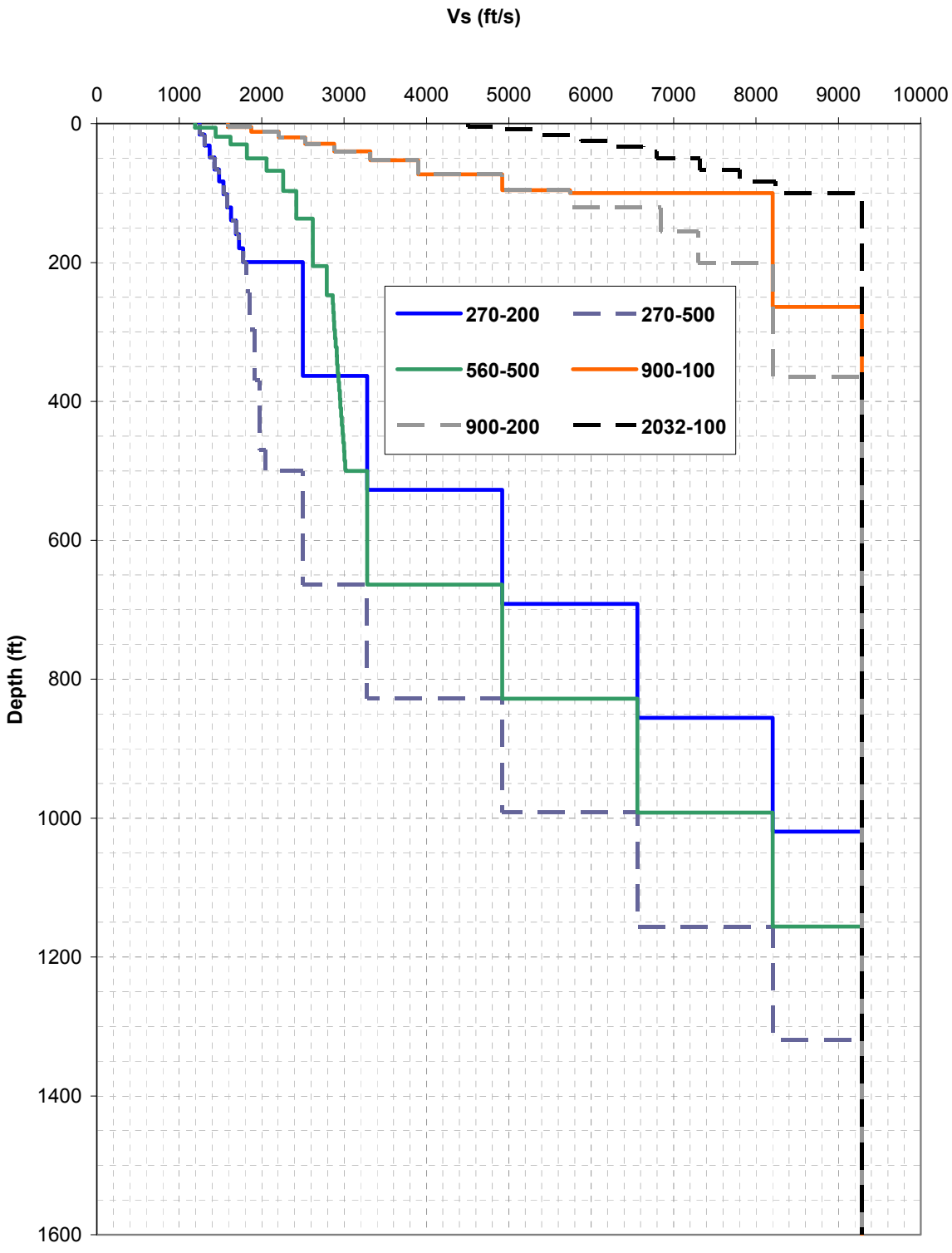

Figure 01.5.2-1 Foundation Level Base-Case Shear and Compression Wave Velocity Profiles (Sheet 1 of 2)

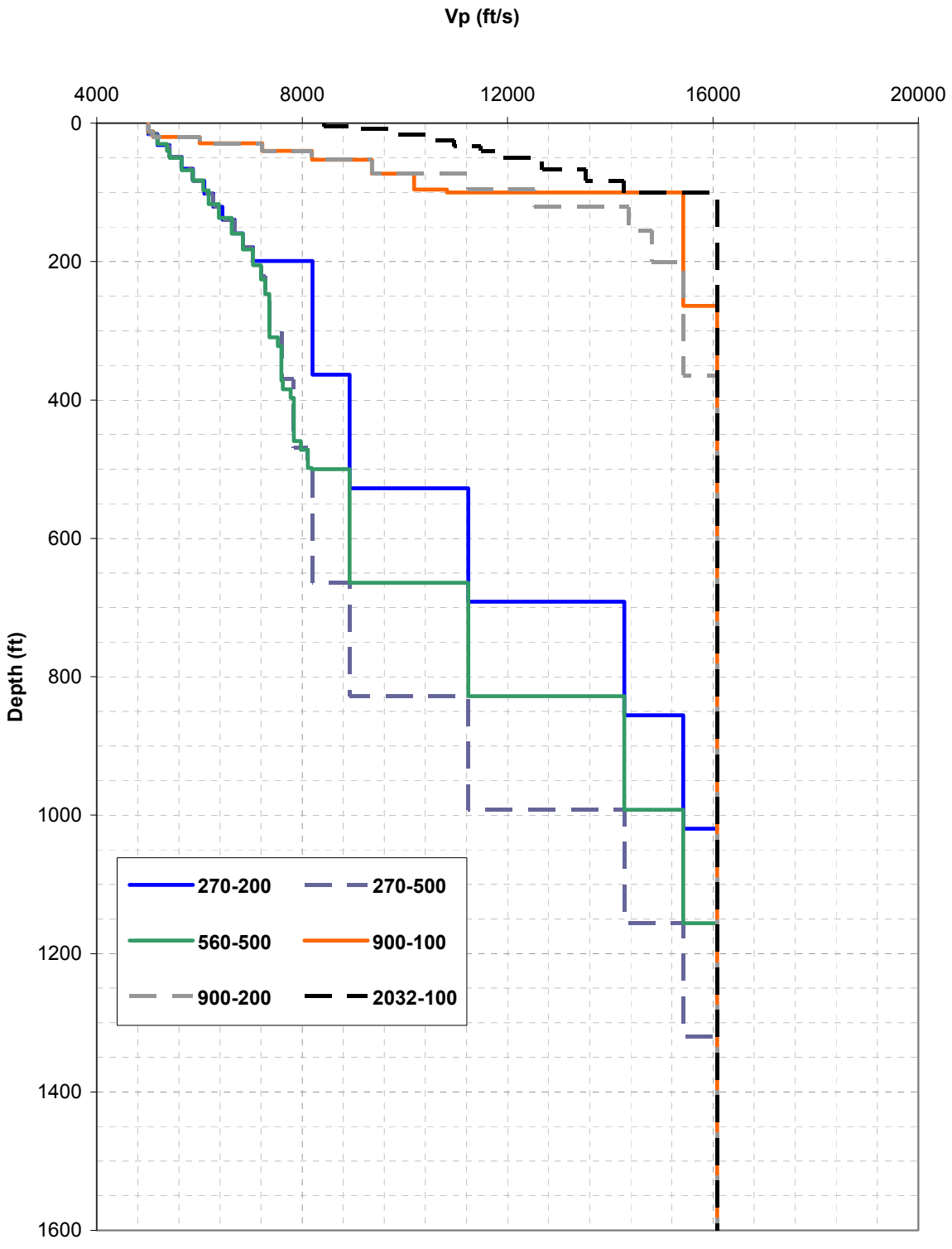

Figure 01.5.2-1 Foundation Level Base-Case Shear and Compression Wave Velocity Profiles (Sheet 2 of 2)

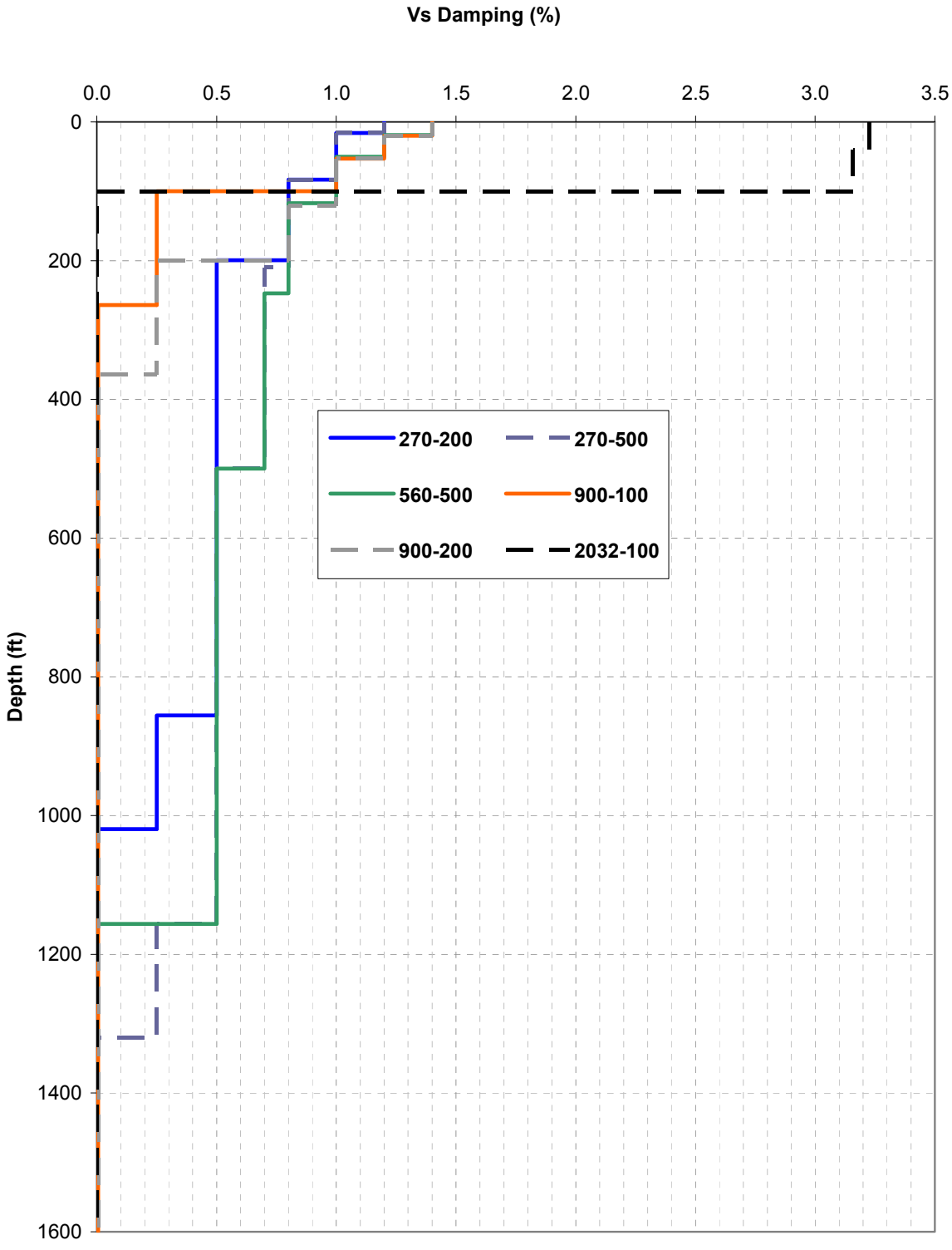

Figure 01.5.2-2 Small Strain Shear Wave Velocity Damping

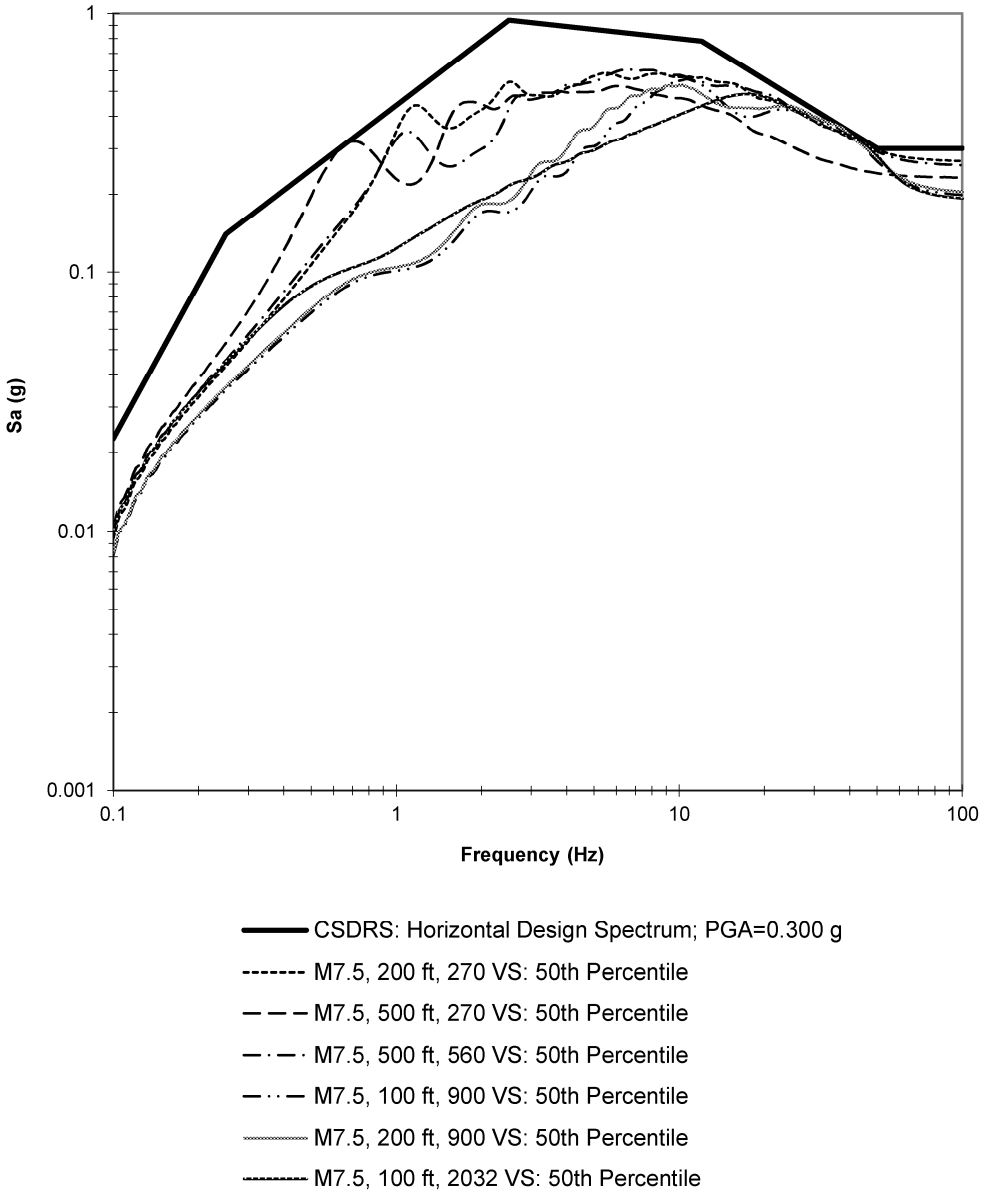

Figure 01.5.2.1-1 Median Spectra (5% damped) Compared to CSDRS Horizontal Components

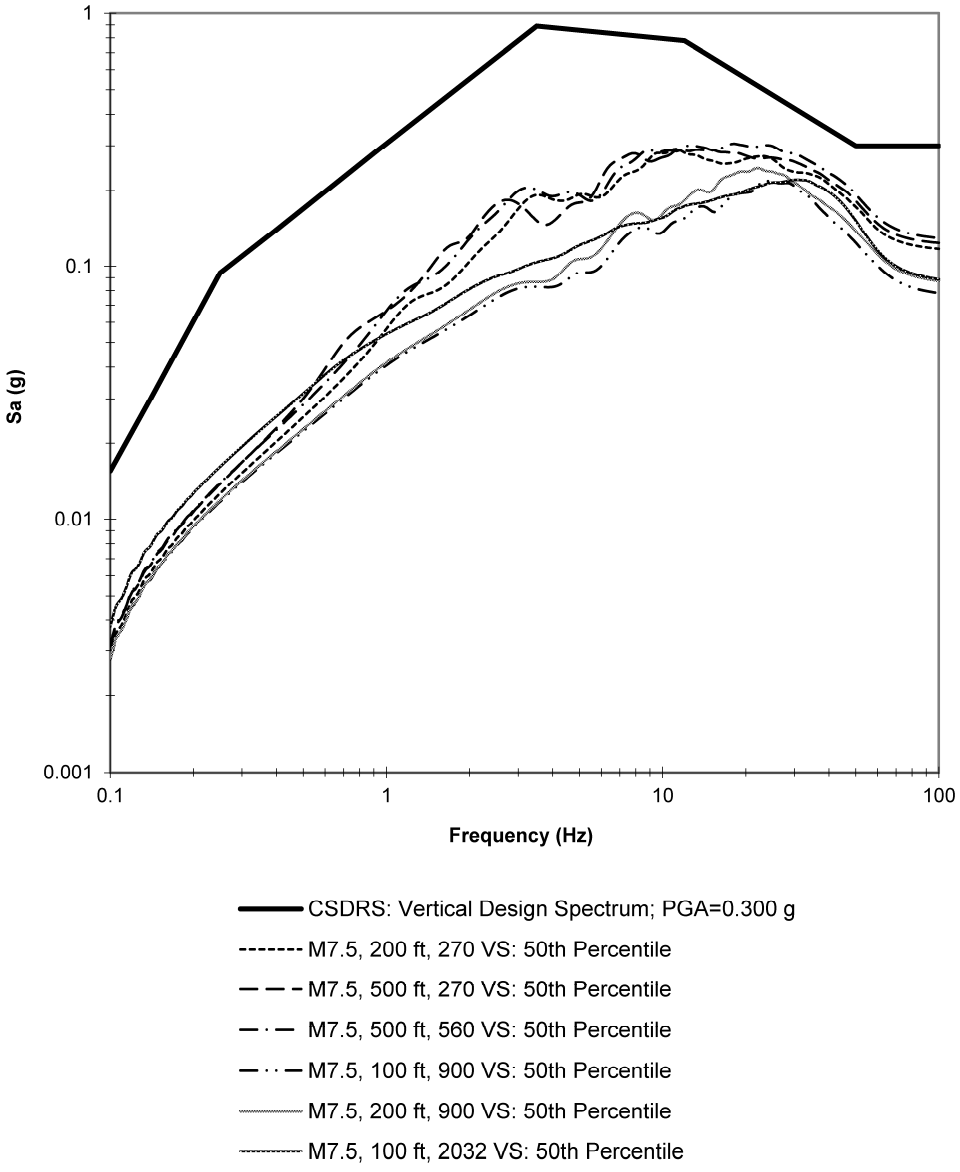

Figure 01.5.2.1-2 Median Spectra (5% damped) Compared to CSDRS Vertical Components

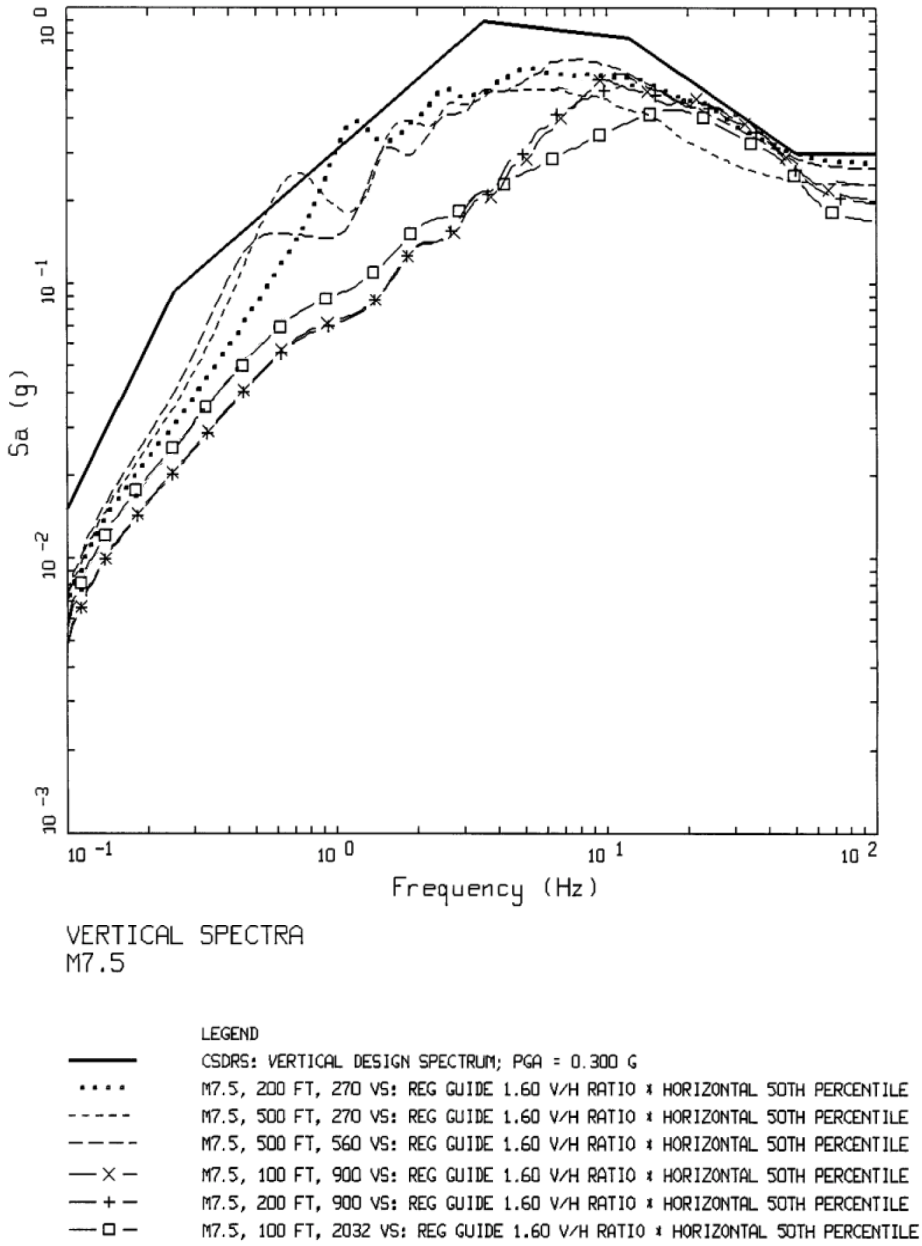

Figure 01.5.2.1-3 Median Spectra (5% damped) Compared to CSDRS Vertical Components Using RG 1.60 V/H Ratios

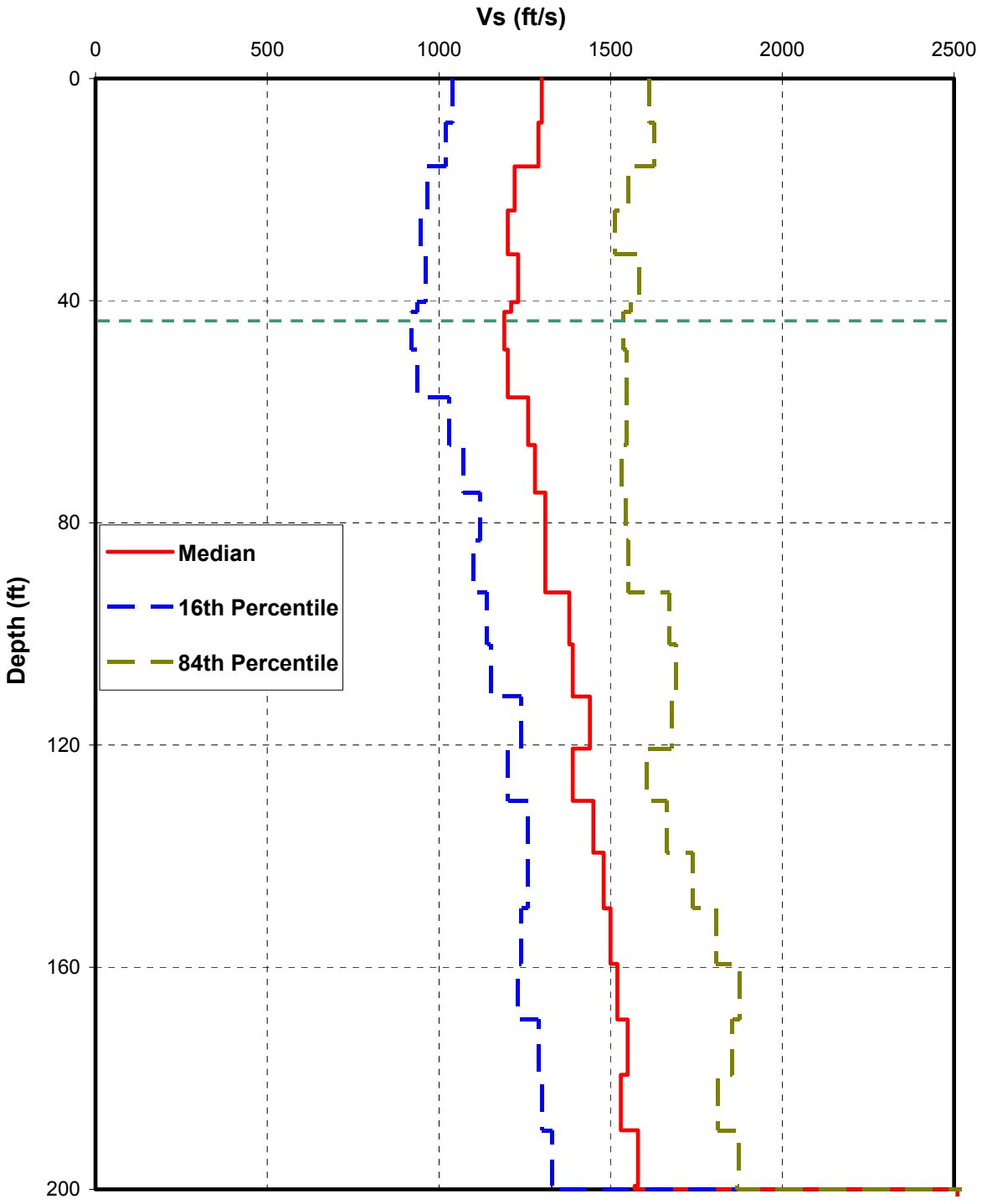

Figure 01.5.2.2-1 Strain Compatible Properties Computed for Profile 270-200 (Sheet 1 of 3)

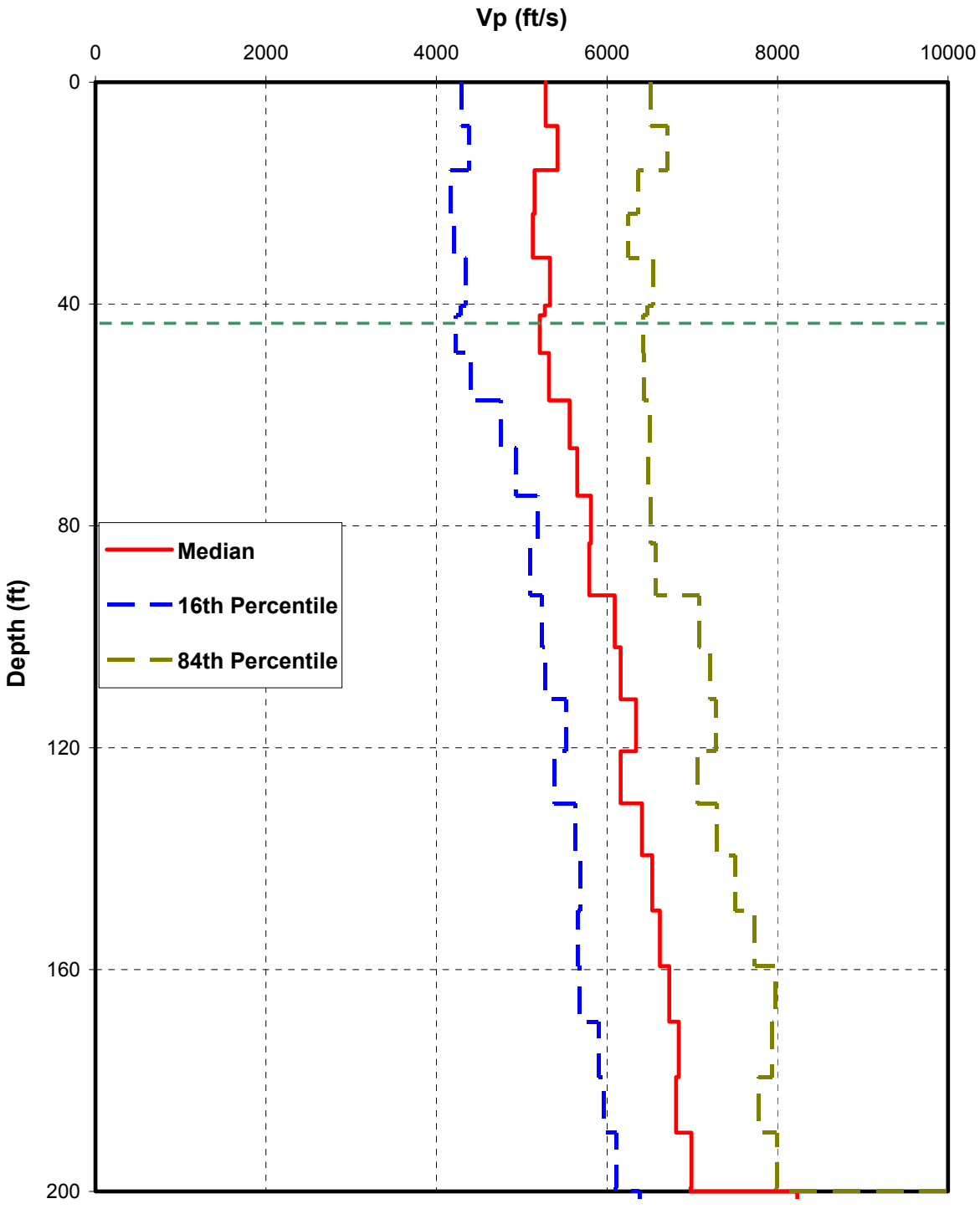

Figure 01.5.2.2-1 Strain Compatible Properties Computed for Profile 270-200 (Sheet 2 of 3)

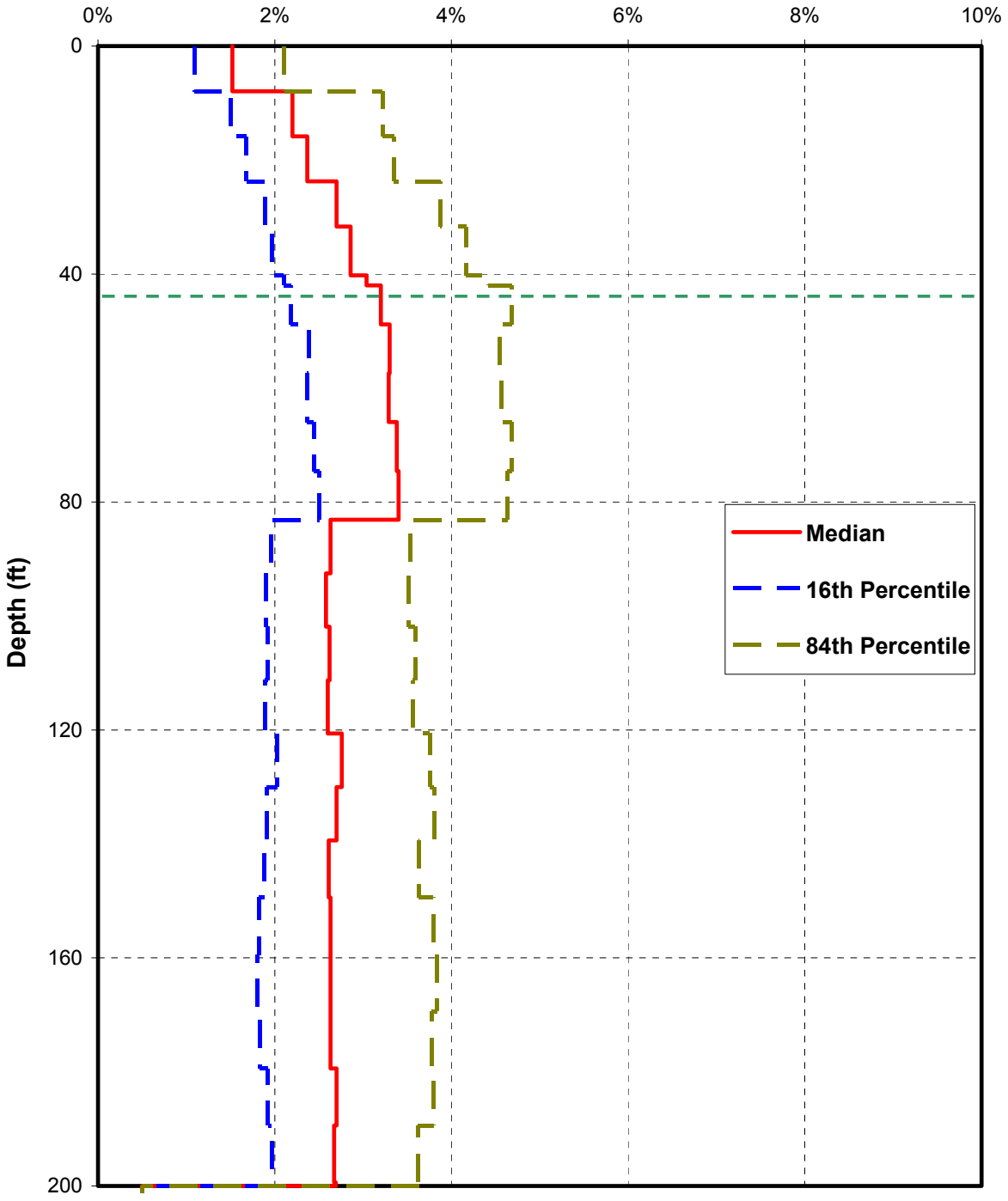

Figure 01.5.2.2-1 Strain Compatible Properties Computed for Profile 270-200 (Sheet 3 of 3)

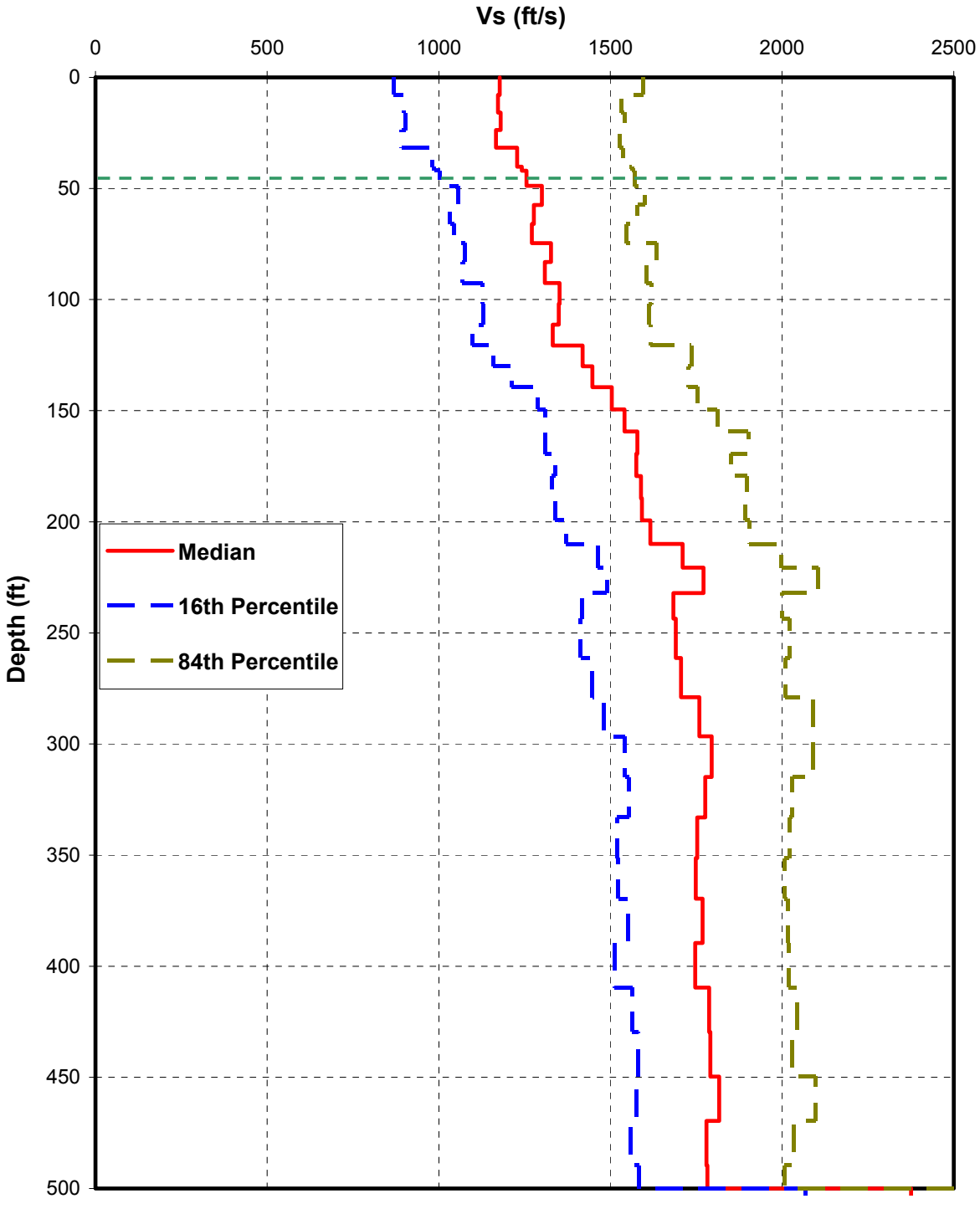

Figure 01.5.2.2-2 Strain Compatible Properties Computed for Profile 270-500 (Sheet 1 of 3)

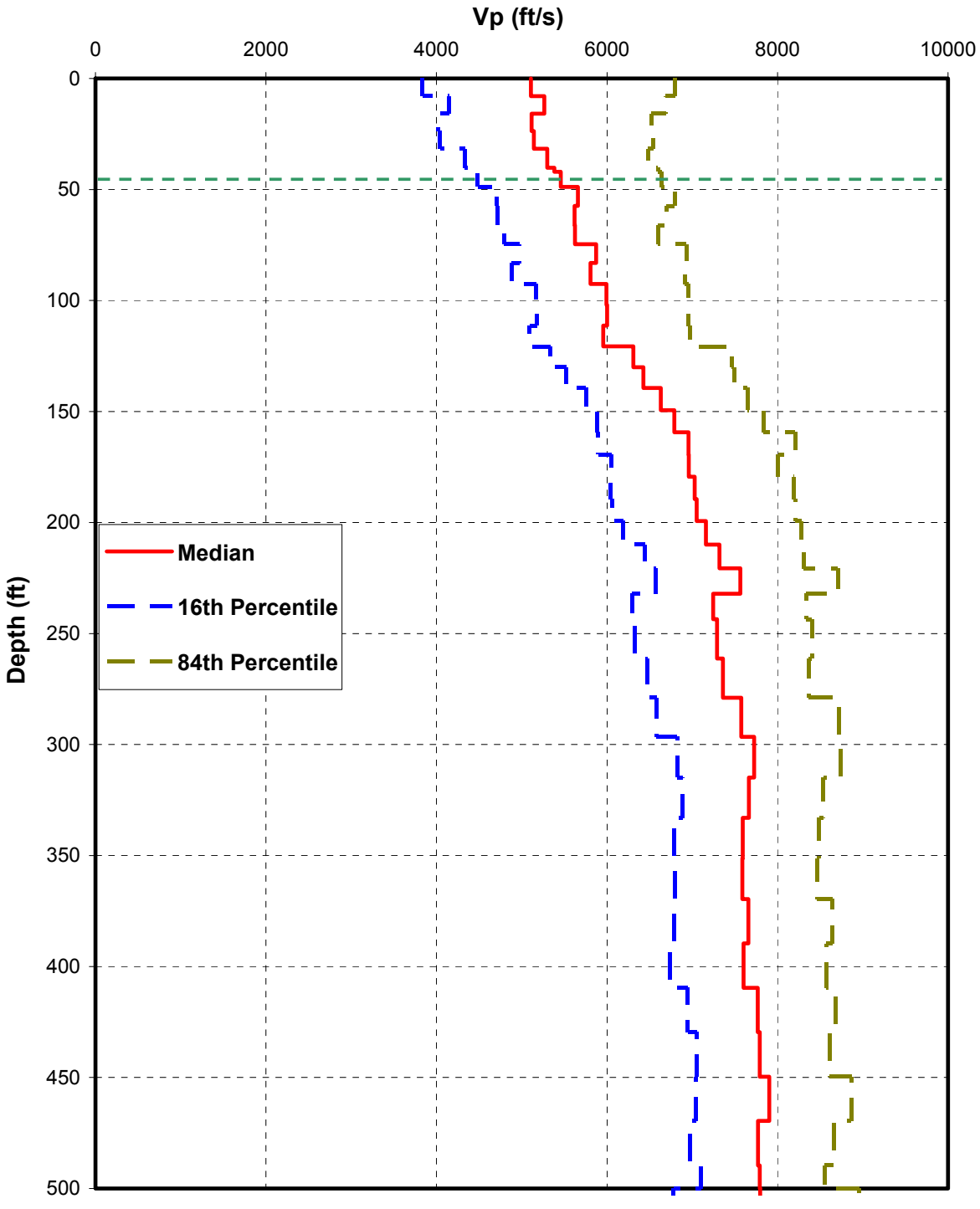

Figure 01.5.2.2-2 Strain Compatible Properties Computed for Profile 270-500 (Sheet 2 of 3)

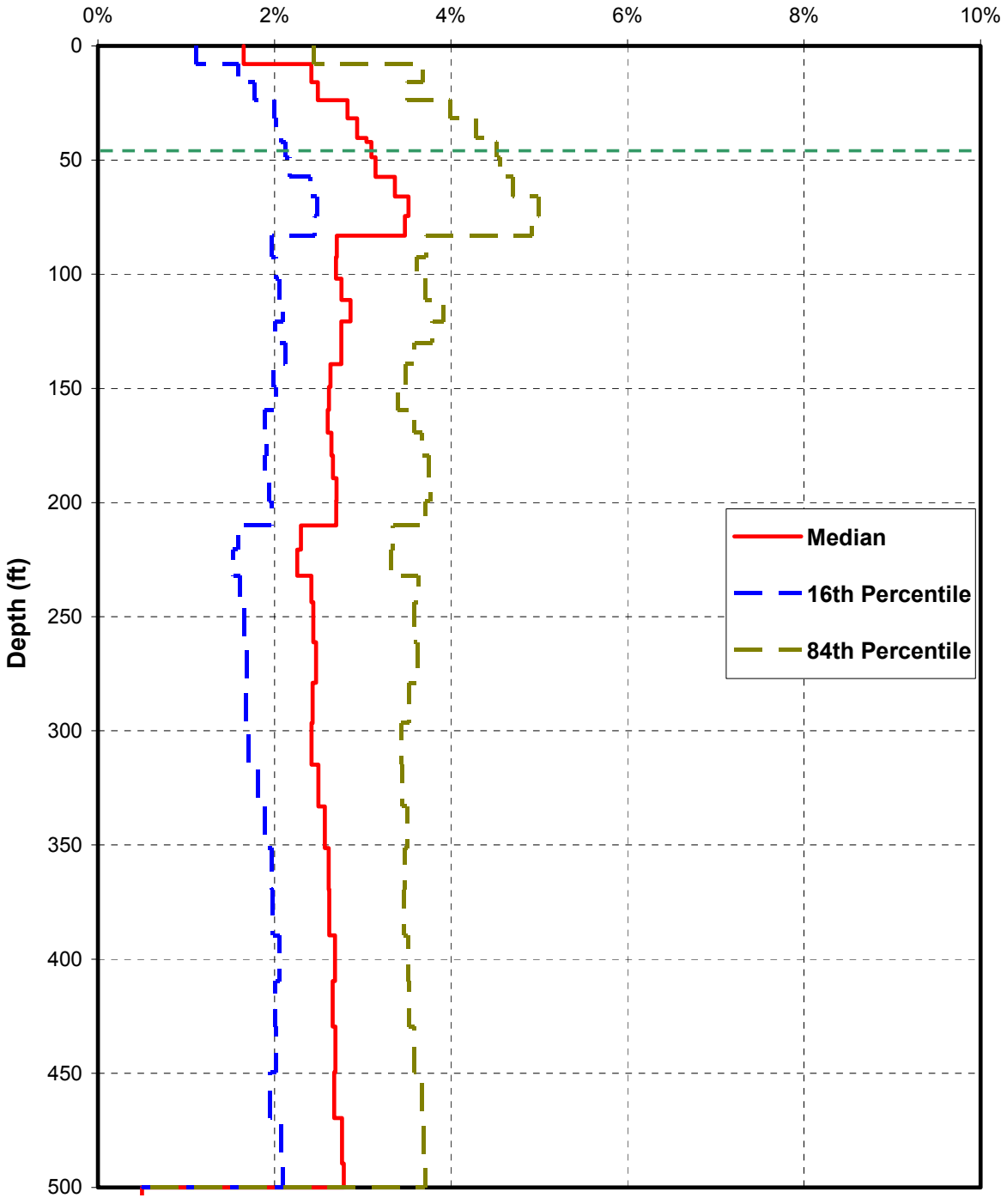

Figure 01.5.2.2-2 Strain Compatible Properties Computed for Profile 270-500 (Sheet 3 of 3)

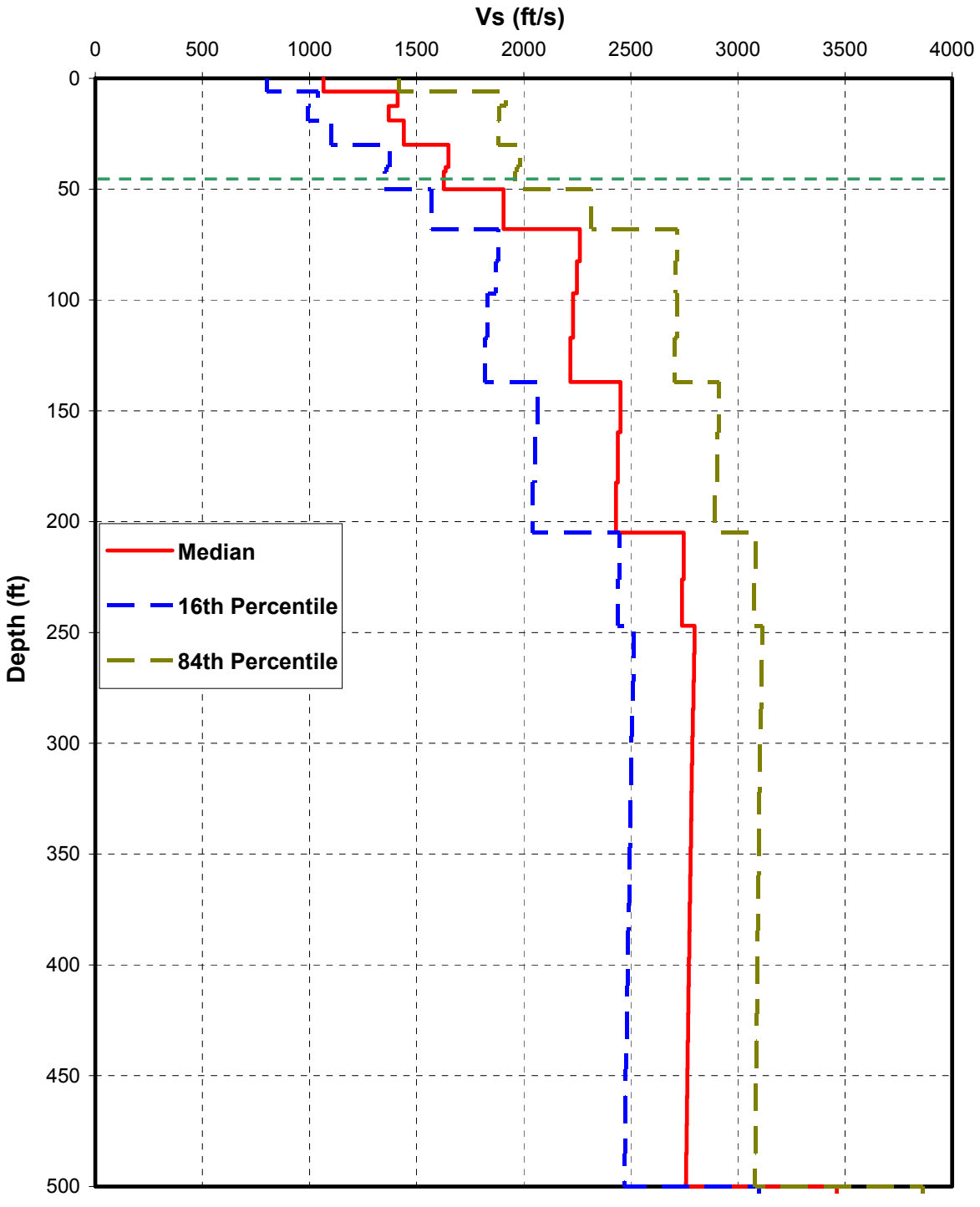

Figure 01.5.2.2-3 Strain Compatible Properties Computed for Profile 560-500 (Sheet 1 of 3)

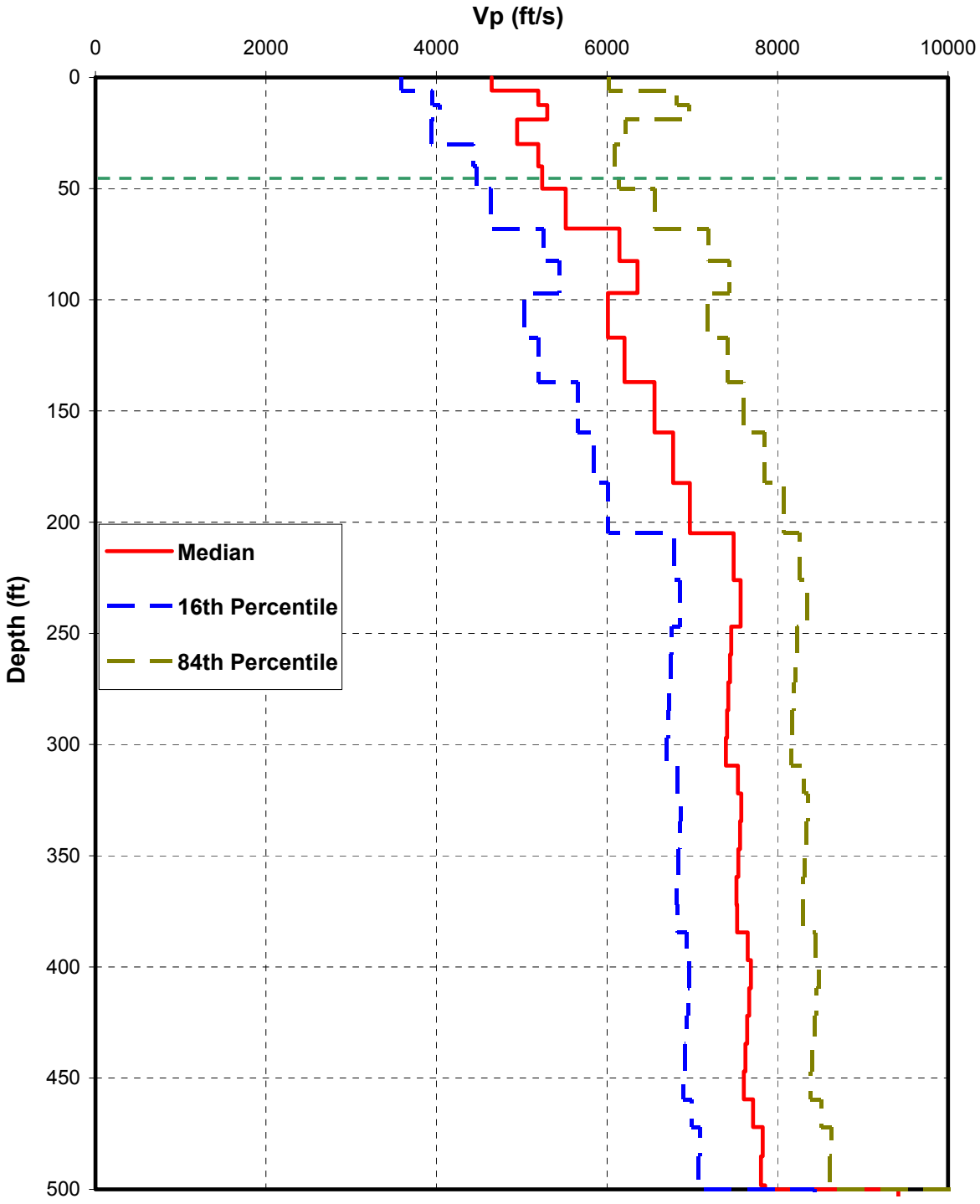

Figure 01.5.2.2-3 Strain Compatible Properties Computed for Profile 560-500 (Sheet 2 of 3)

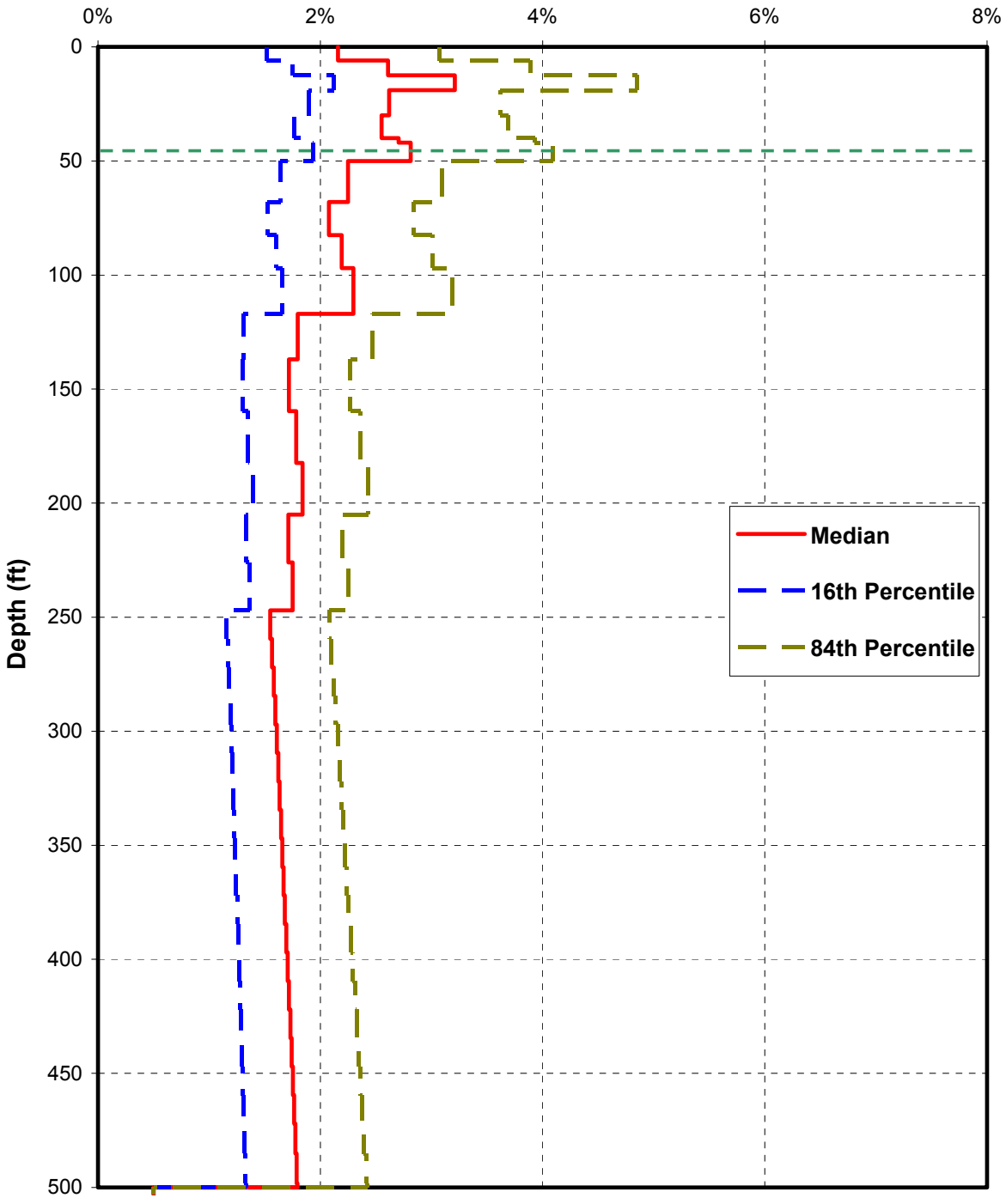

Figure 01.5.2.2-3 Strain Compatible Properties Computed for Profile 560-500 (Sheet 3 of 3)

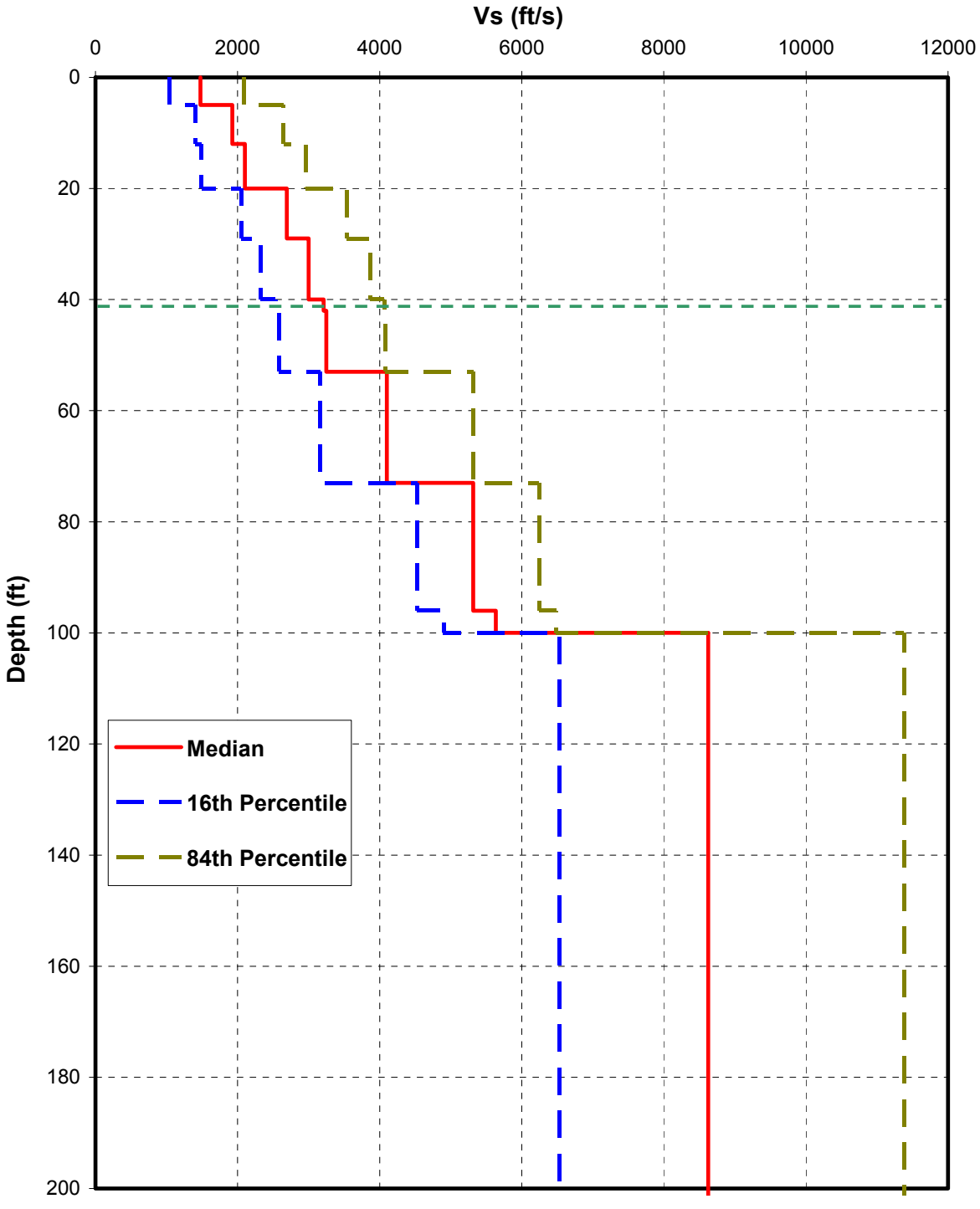

Figure 01.5.2.2-4 Strain Compatible Properties Computed for Profile 900-100 (Sheet 1 of 3)

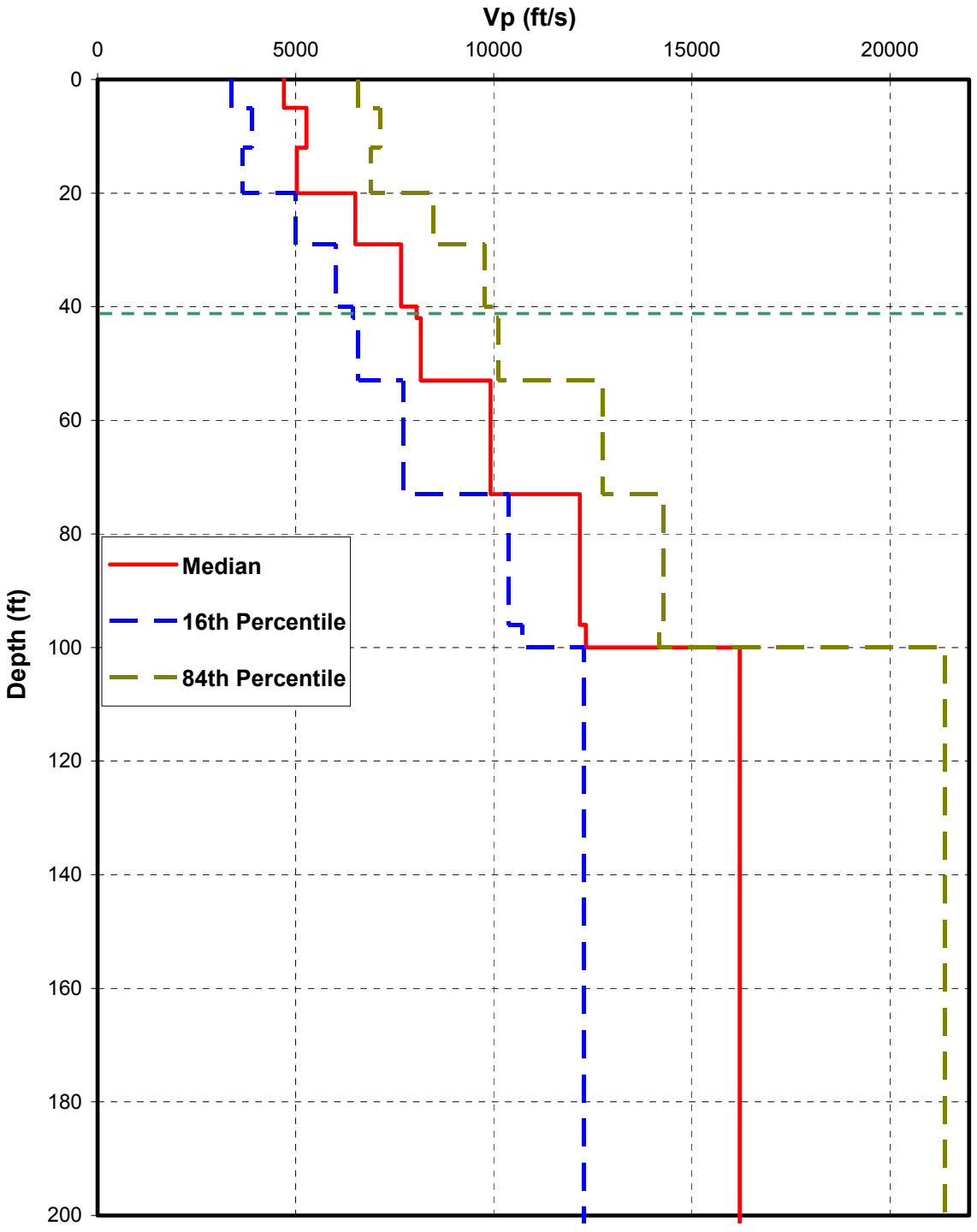

Figure 01.5.2.2-4 Strain Compatible Properties Computed for Profile 900-100 (Sheet 2 of 3)

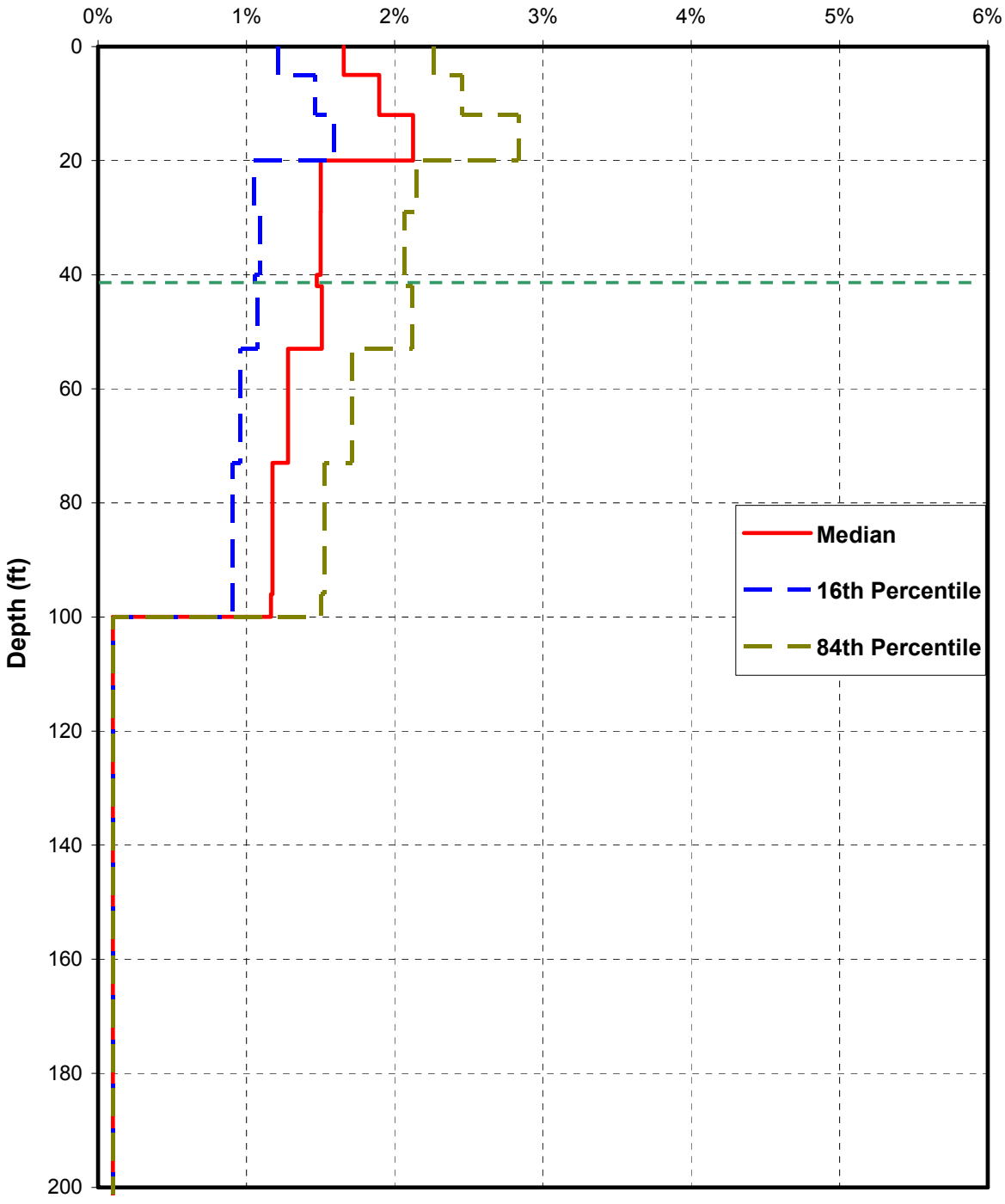

Figure 01.5.2.2-4 Strain Compatible Properties Computed for Profile 900-100 (Sheet 3 of 3)

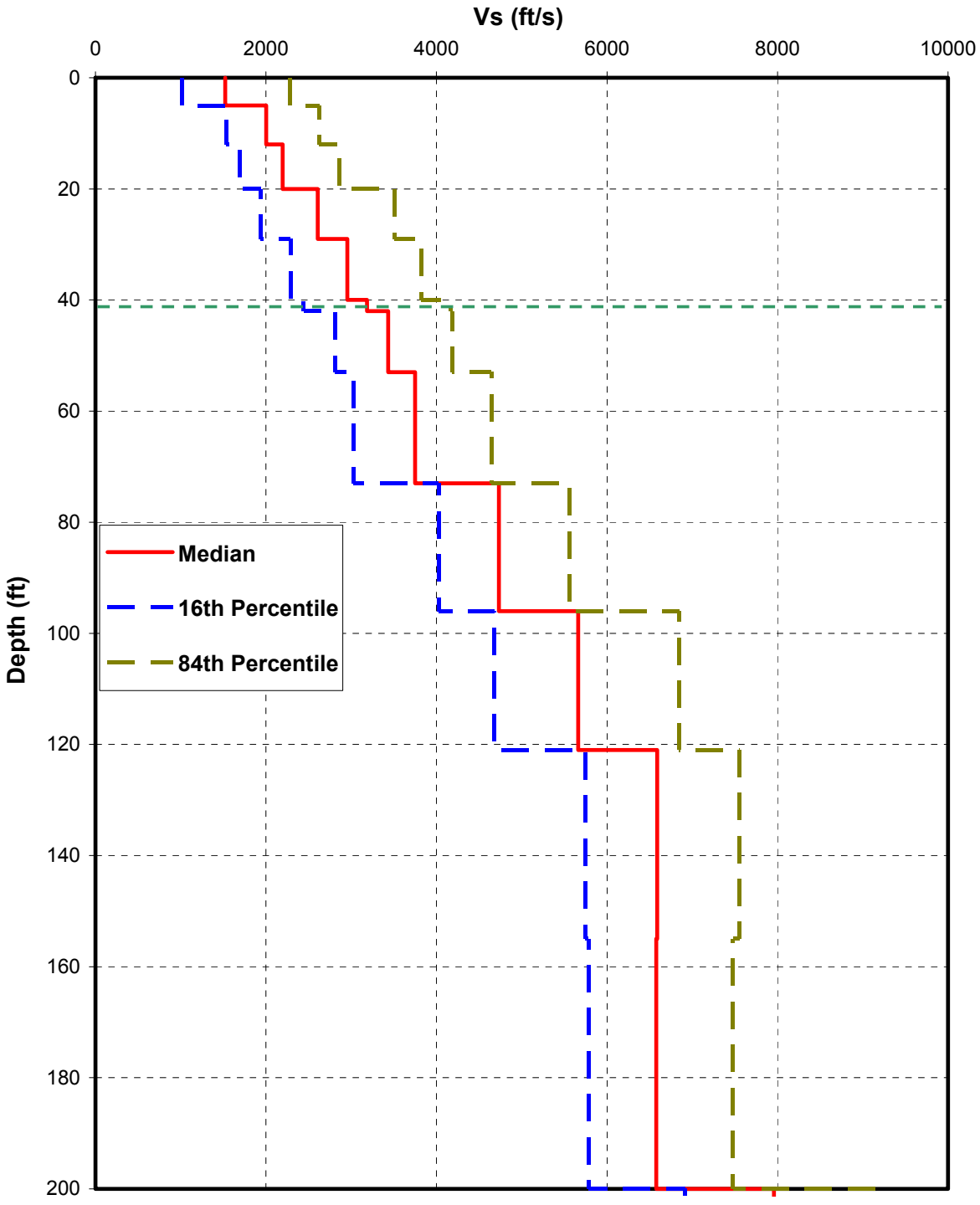

Figure 01.5.2.2-5 Strain Compatible Properties Computed for Profile 900-200 (Sheet 1 of 3)

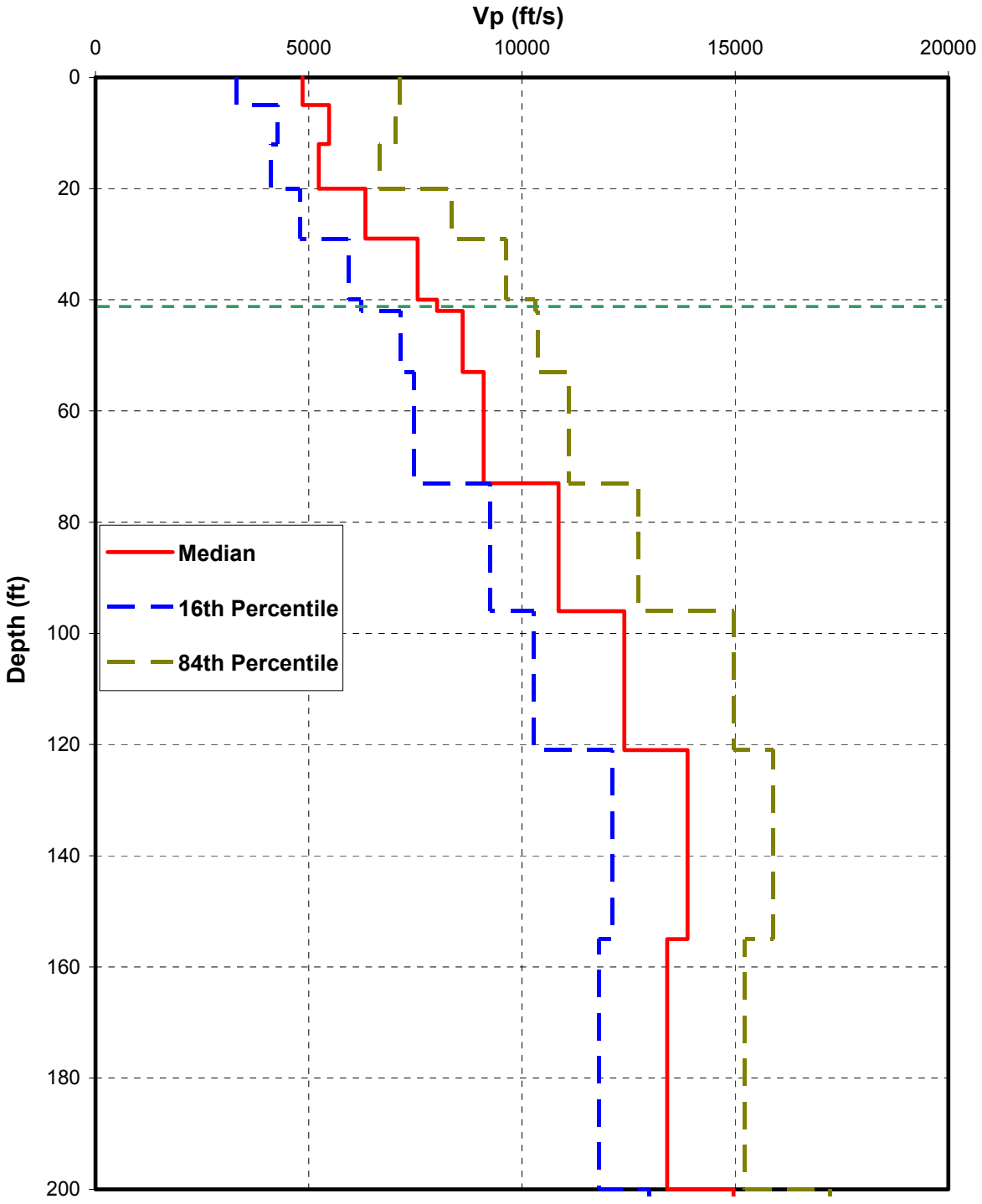

Figure 01.5.2.2-5 Strain Compatible Properties Computed for Profile 900-200 (Sheet 2 of 3)

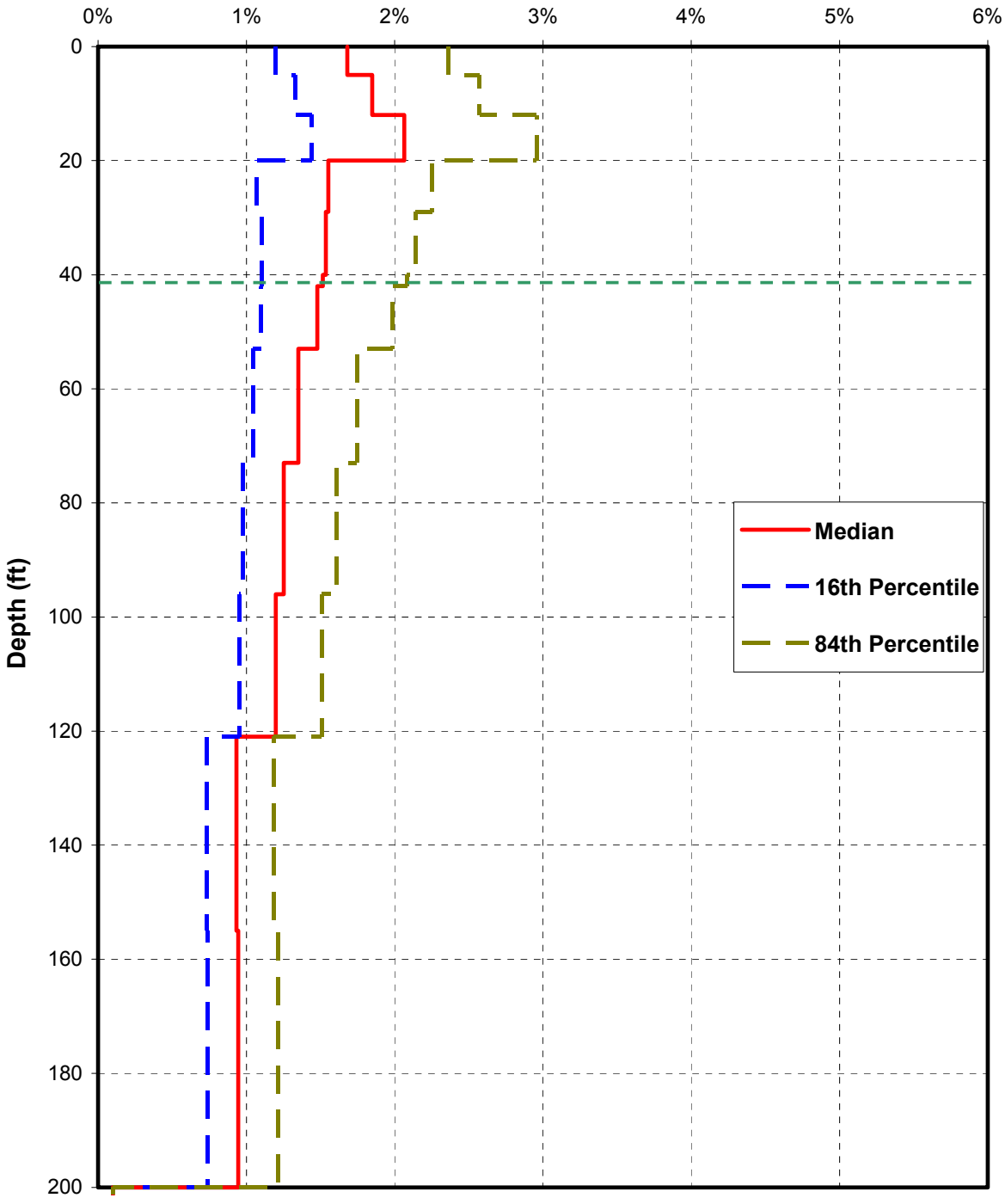

Figure 01.5.2.2-5 Strain Compatible Properties Computed for Profile 900-200 (Sheet 3 of 3)

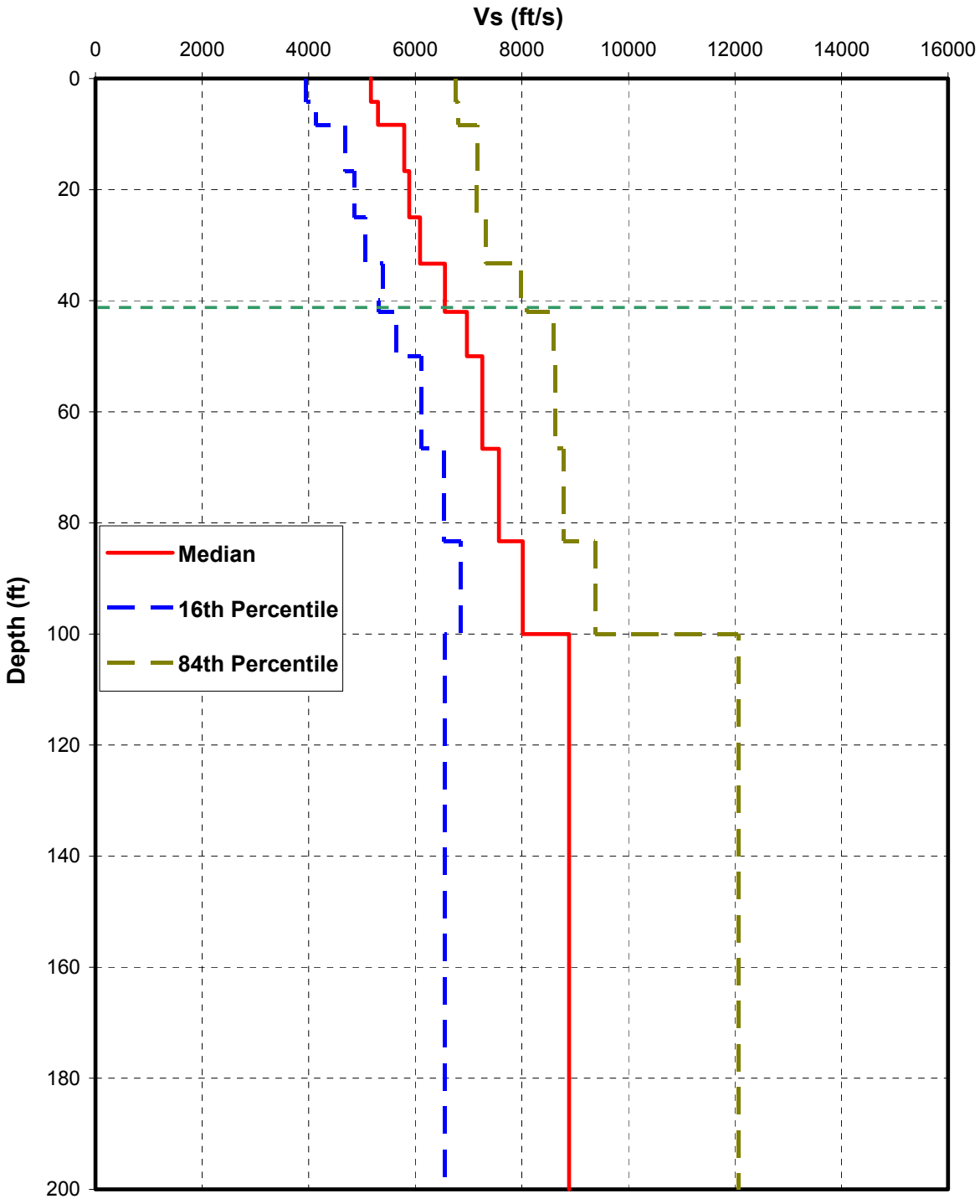

Figure 01.5.2.2-6 Strain Compatible Properties Computed for Profile 2032-100 (Sheet 1 of 3)

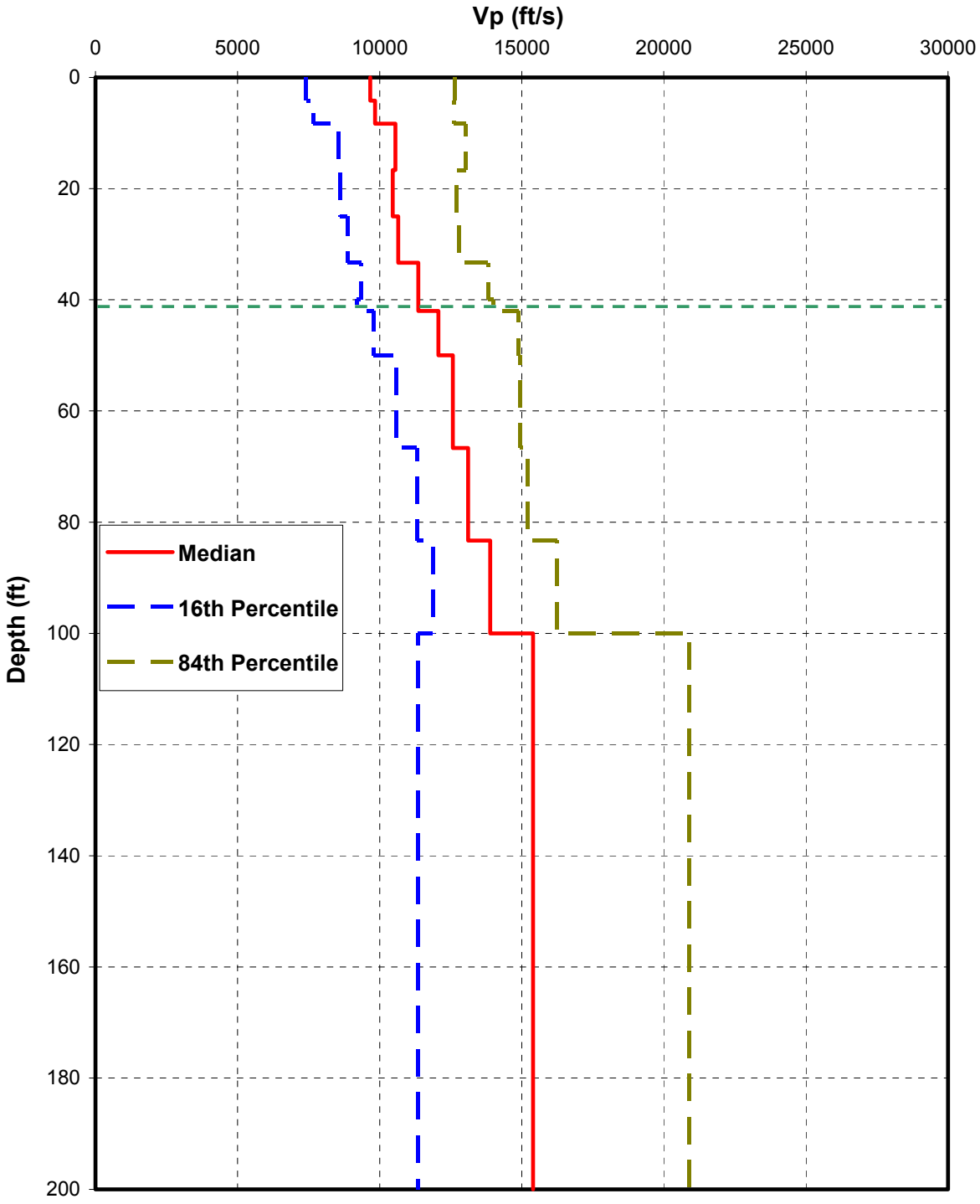

Figure 01.5.2.2-6 Strain Compatible Properties Computed for Profile 2032-100 (Sheet 2 of 3)

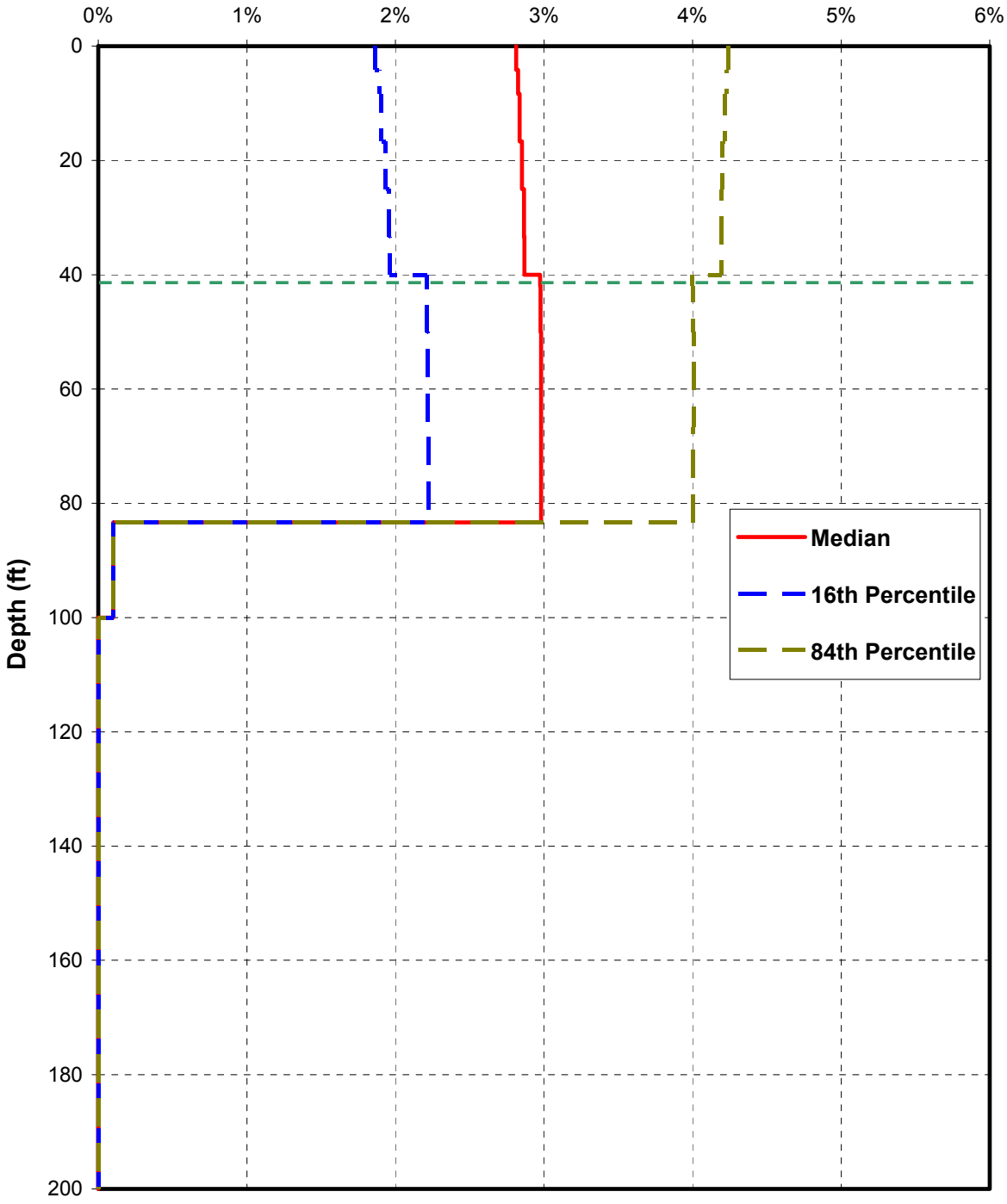

Figure 01.5.2.2-6 Strain Compatible Properties Computed for Profile 2032-100 (Sheet 3 of 3)

01.6.0 REFERENCES

01-1. Seismic Design Parameters, NUREG-0800 Section 3.7.1, Revision 3, U.S. Nuclear Regulatory Commission, Washington, DC, March 2007.

01-2. Ground Water Effects on SSI, Mitsubishi Heavy Industries, Technical Report MUAP-11007, Revision 2, November, 2012

01-3. Design Response Spectra for Seismic Design of Nuclear Power Plants, RG 1.60, Revision 1, U. S. Nuclear Regulatory Commission, December 1973.

01-4. Technical Basis for Revision of Regulatory Guidance on Design Ground Motions: Hazard- and Risk-Consistent Ground Motions Spectra Guidelines, NUREG/CR-6728, Prepared for Division of Engineering Technology, Washington, D.C., 2001.

01-5. Recommendations for Resolution of Public Comments on USI A-40 "Seismic Design Criteria," NUREG/CR-5347, U.S. Nuclear Regulatory Commission, Washington, D.C., May, 1989.

01-6. PEER NGA Strong Motion Database, Pacific Earthquake Engineering Research Center, http://peer.berkeley.edu/nga/, University of California, Berkeley, CA, 2006.

01-7. Surface Geology Based Strong Motion Amplification Factors for the San Francisco Bay and Los Angeles Areas, A PEARL report to PG&E/CEC/Caltrans, Award No. SA2120-59652. Silva, W. J.S. Li, B. Darragh, and N. Gregor, 1999.

01-8. Guidelines for Determining Design Basis Ground Motions, Volumes 1-5, TR-102293, Electric Power Research Institute, Palo Alto, CA, 1993.

Vol.1: Methodology and Guidelines for Estimating Earthquake Ground Motion in Eastern North America.

Vol.2: Appendices for Ground Motion Estimation.

Vol.3: Appendices for Field Investigations.

Vol.4: Appendices for Laboratory Investigations.

Vol.5: Quantification of Seismic Source Effects.

01-9. CEUS Ground Motion Project, Final Report, Technical Report TR-1009684, Electric Power Research Institute, Palo Alto, CA, 2004.

01-10. A Performance-Based Approach to Define the Site-Specific Earthquake Ground Motion, RG 1.208, Revision 0, U. S. Nuclear Regulatory Commission, March 2007.

01-11. Technical Basis for Revision of Regulatory Guidance on Design Ground Motions: Development of Hazard- and Risk-Consistent Seismic Spectra for Two Sites, NUREG/CR-6769, U.S. Nuclear Regulatory Commission, Office of Nuclear Regulatory Research, Washington, DC, April, 2002.

01-12. Description and Validation of the Stochastic Ground Motion Model, Report Submitted to Brookhaven National Laboratory, Silva, W. J., Abrahamson N., Toro G., and C. Constantino, Associated Universities, Inc., 1996.

01-13. US-APWR Standard Design Civil Structural Design Criteria, Mitsubishi Heavy Industries, N0-CF00003, Revision 4, August, 2012.

01-14. Characteristics of Vertical Strong Ground Motions for Applications to Engineering Design, NCEER-97-0010, Proceedings of the FHWA/NCEER Workshop on the

National Representation of Seismic Ground Motion for New and Existing Highway Facilities, I.M. Friedland, M.S Power and R. L. Mayes eds., Silva, W.J., 1997.

01-15. Empirical Response Spectral Attenuation Relations for Shallow Crustal Earthquakes, Seismological Research Letter, 68(1), pages 94-127, Abrahamson, N.A. and Silva, W.J., 1997.

01-16. Properties of Vertical Ground Motions, Bulletin of the Seismological Society of America, 92(2), pages 3152-3164, Beresnev, I.A, Nightengale, A.M. Silva, W.J., 2002.

01-17. Updated Near-Source Ground-Motion (Attenuation) Relations for the Horizontal and Vertical Components of Peak Ground Acceleration and Acceleration Response Spectra, Bulletin of the Seismic Society of America, 93(1), pages 314-331, Campbell, K. W. and Y. Bozorgnia, 2003.

01-18. Site Response Analyses of Vertical Excitation, Proceedings of the Third Specialty Conference on Geotechnical Earthquake Engineering and Soil Dynamics, Mok, Chin Man, Chang, C.-Y., and Lagapsi, Dante E., Seattle, Washington, Geotechnical Special Publication No. 75, ASCE, August 3 - 6, 1998.

Appendix 1-A

Statistical Justification of RVT Methodology 30 vs. 60 Realizations

APPENDIX 1-A TABLE OF CONTENTS

Section	Title	Page No.
1-A.1.0	**JUSTIFICATION OF RVT METHODOLOGY: 30 VS. 60 REALIZATIONS**	**1-A.1**

LIST OF FIGURES

Figure	Title	Page No.
Figure 1-A.1.0-1	Comparison of Median Estimates for Strain Compatible Properties Developed for 60 and 30 Realizations for 500 ft Deep Profile 560-500 – Shear Wave Velocity	1-A.2
Figure 1-A.1.0-2	Comparison of Median Estimates for Strain Compatible Properties Developed for 60 and 30 Realizations for 500 ft Deep Profile 560-500 – Compression Wave Velocity	1-A.3
Figure 1-A.1.0-3	Comparison of Median Estimates for Strain Compatible Properties Developed for 60 and 30 Realizations for 500 ft Deep Profile 560-500 – Shear Wave Damping	1-A.4
Figure 1-A.1.0-4	Comparison of Median Estimates for Strain Compatible Properties Developed for 60 and 30 Realizations for 500 ft Deep Profile 560-500 – Compression Wave Damping	1-A.5
Figure 1-A.1.0-5	Comparison of Standard Deviation for Median Estimates for Strain Compatible Properties Developed for 60 and 30 Realizations for 500 ft Deep Profile 560-500 – Shear Wave Velocity	1-A.6
Figure 1-A.1.0-6	Comparison of Standard Deviation for Median Estimates for Strain Compatible Properties Developed for 60 and 30 Realizations for 500 ft Deep Profile 560-500 – Compression Wave Velocity	1-A.7
Figure 1-A.1.0-7	Comparison of Standard Deviation for Median Estimates for Strain Compatible Properties Developed for 60 and 30 Realizations for 500 ft Deep Profile 560-500 – Shear Wave Damping	1-A.8
Figure 1-A.1.0-8	Comparison of Standard Deviation for Median Estimates for Strain Compatible Properties Developed for 60 and 30 Realizations for 500 ft Deep Profile 560-500 – Compression Wave Damping	1-A.9

1-A.1.0 JUSTIFICATION OF RVT METHODOLOGY: 30 VS. 60 REALIZATIONS

Thirty realizations are generated for each base profile in order to characterize, in a fully probabilistic manner, the range and variation in SCP of the top soil. Thirty realizations provide a stable estimate of the mean strain compatible soil properties that are used as input for the SSI analyses, the statistic of importance as the median spectrum defines the loading level for each soil and rock. For the standard deviation determination, 30 realizations are sufficient to estimate sigma within 20 percent at the 90 percent confidence level from standard statistical tables and 60 realizations marginally improves the stability to only 15 percent. To substantially improve the stability to five percent requires over 500 realizations. The interest in the standard deviation is only to provide additional clarity in the process of developing the suite of generic SCP by showing reasonable range between -1 sigma and +1 sigma properties. Therefore, a suite of 30 realizations is considered sufficient for the purpose of developing generic profiles as the mean of the strain compatible soil properties.

In order to illustrate the numerical stability in SCP between 30 and 60 realizations, Figure 1-A.1.0-1 through Figure 1-A.1.0-4 compare median strain compatible property estimates computed for the two sample sizes for the deep (500 ft) profile 560 - 500. The maximum difference is about 5% and occurs over shallow and narrow depth ranges. Over the deeper portion of the profile, beyond a depth of about 150 ft, the difference is approximately 2% in shear wave and compression wave velocity and about 4% in shear-wave damping.

A similar stability of 30 verses 60 realizations is provided for the standard deviation. Figure 1-A.1.0-5 through Figure 1-A.1.0-8 are plots, corresponding to Figure 1-A.1.0-1 through Figure 1-A.1.0-4, for the standard deviations (sigmas) of the SCP. In all figures, the solid blue line represents 60 realizations while the dashed pink line represents 30 realizations. The horizontal dashed green line represents approximately the location of the bottom of the R/B complex basemat. The percent difference between 30 verses 60 realizations is slightly larger for sigma compared to the mean, as expected from standard statistical tables. These results support the conclusion, based on standard statistical tables, that the difference in estimates of means and standard deviations is not significant between sample sizes of 30 and 60. The guidance in RG 1.208 (Reference 01-10) for 60 realizations refers to the standard deviation of the simulated response spectra, which is not used in developing the SCP. The demonstration of stability of the SCP, median and sigma estimates with respect to sample sizes of 30 verses 60 is offered to provide additional clarity in the process of developing the SCP. As illustrated in the Figure 1-A.1.0-1 through Figure 1-A.1.0-8, there are marginal differences in shear wave velocity and damping values by increasing the sample size from 30 to 60. Therefore using 30 realizations is utilized to provide adequate generic profiles of the mean SCP to be used as input for the site-independent SSI analyses.

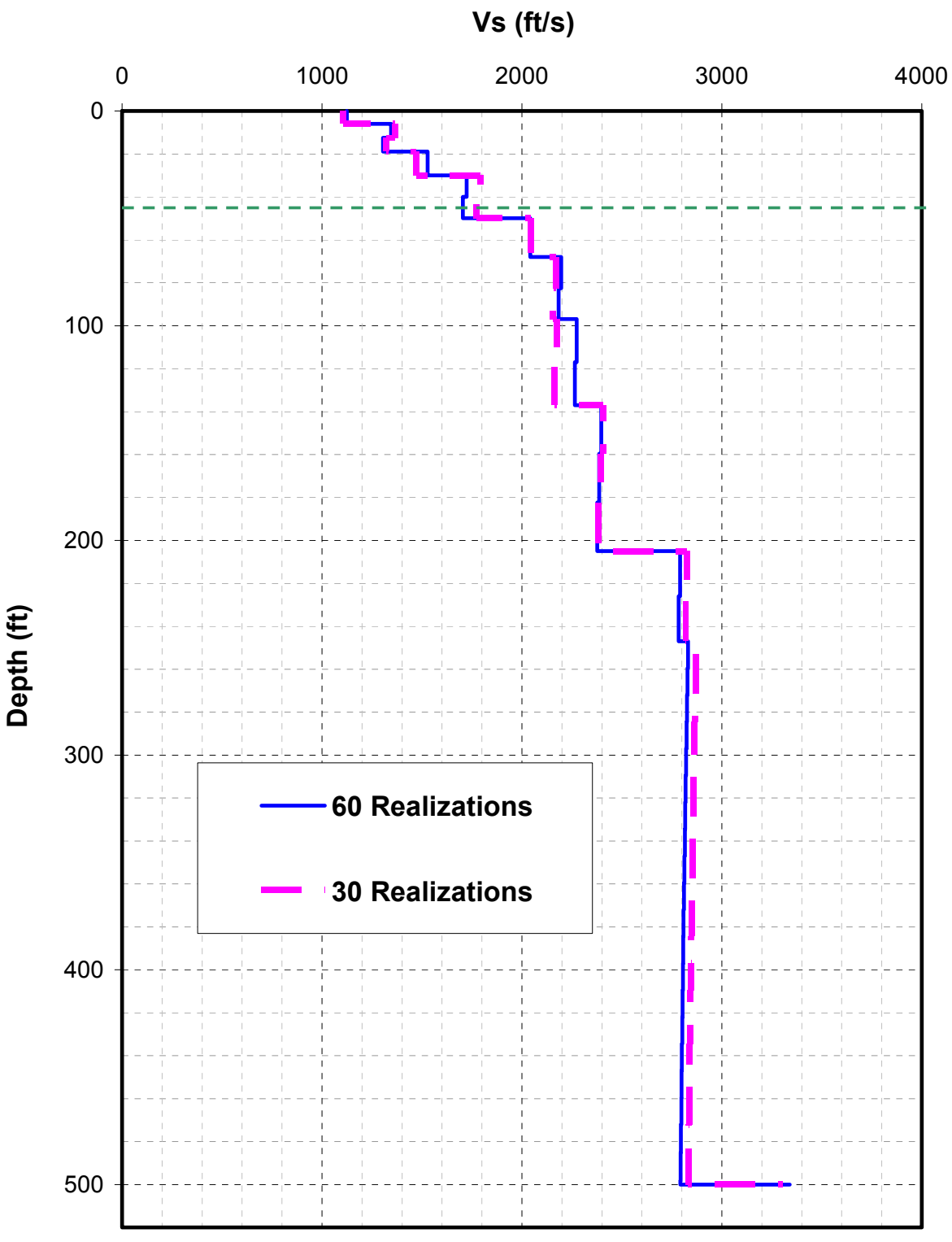

Figure 1-A.1.0-1 Comparison of Median Estimates for Strain Compatible Properties Developed for 60 and 30 Realizations for 500 ft Deep Profile 560-500 – Shear Wave Velocity

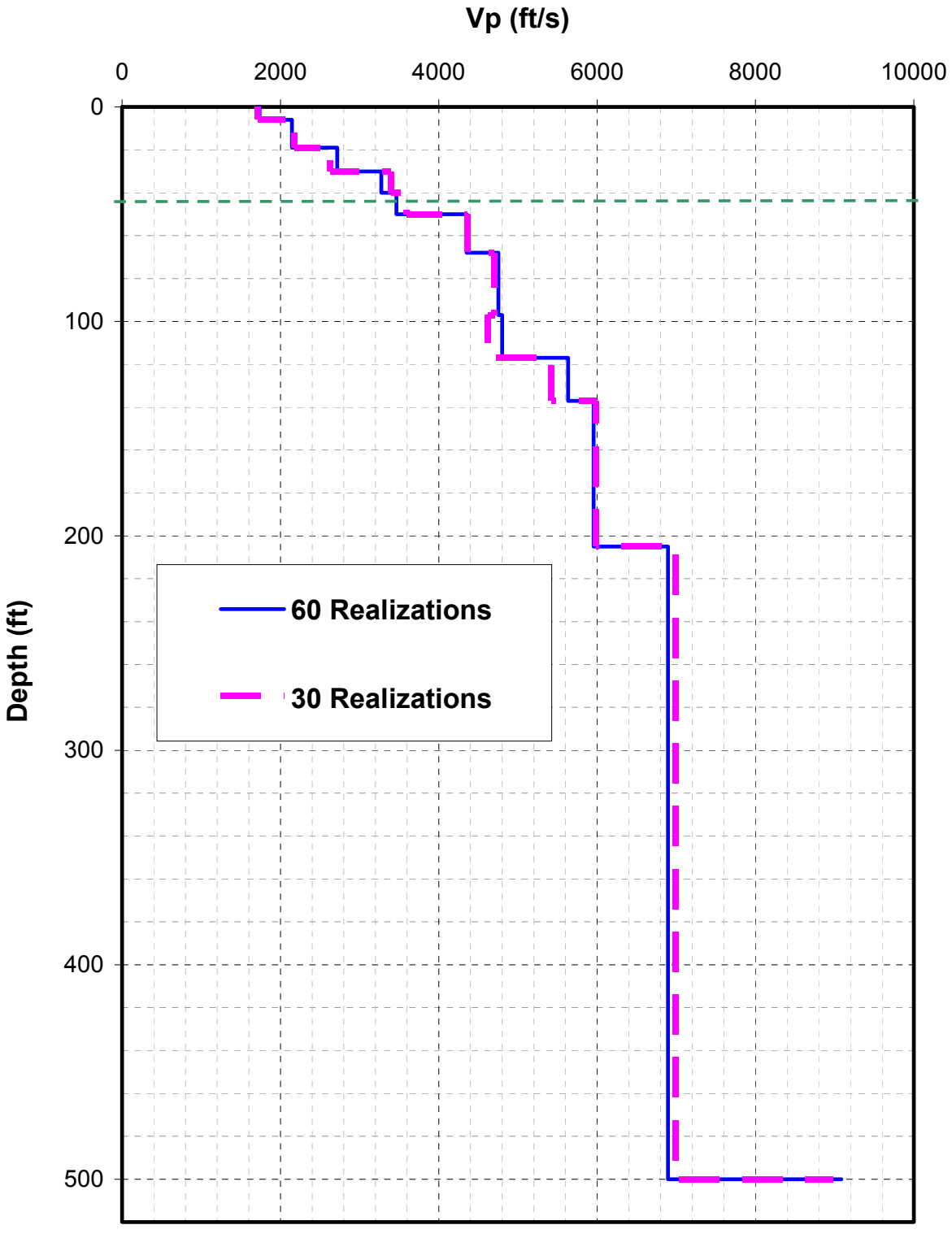

Figure 1-A.1.0-2 Comparison of Median Estimates for Strain Compatible Properties Developed for 60 and 30 Realizations for 500 ft Deep Profile 560-500 – Compression Wave Velocity

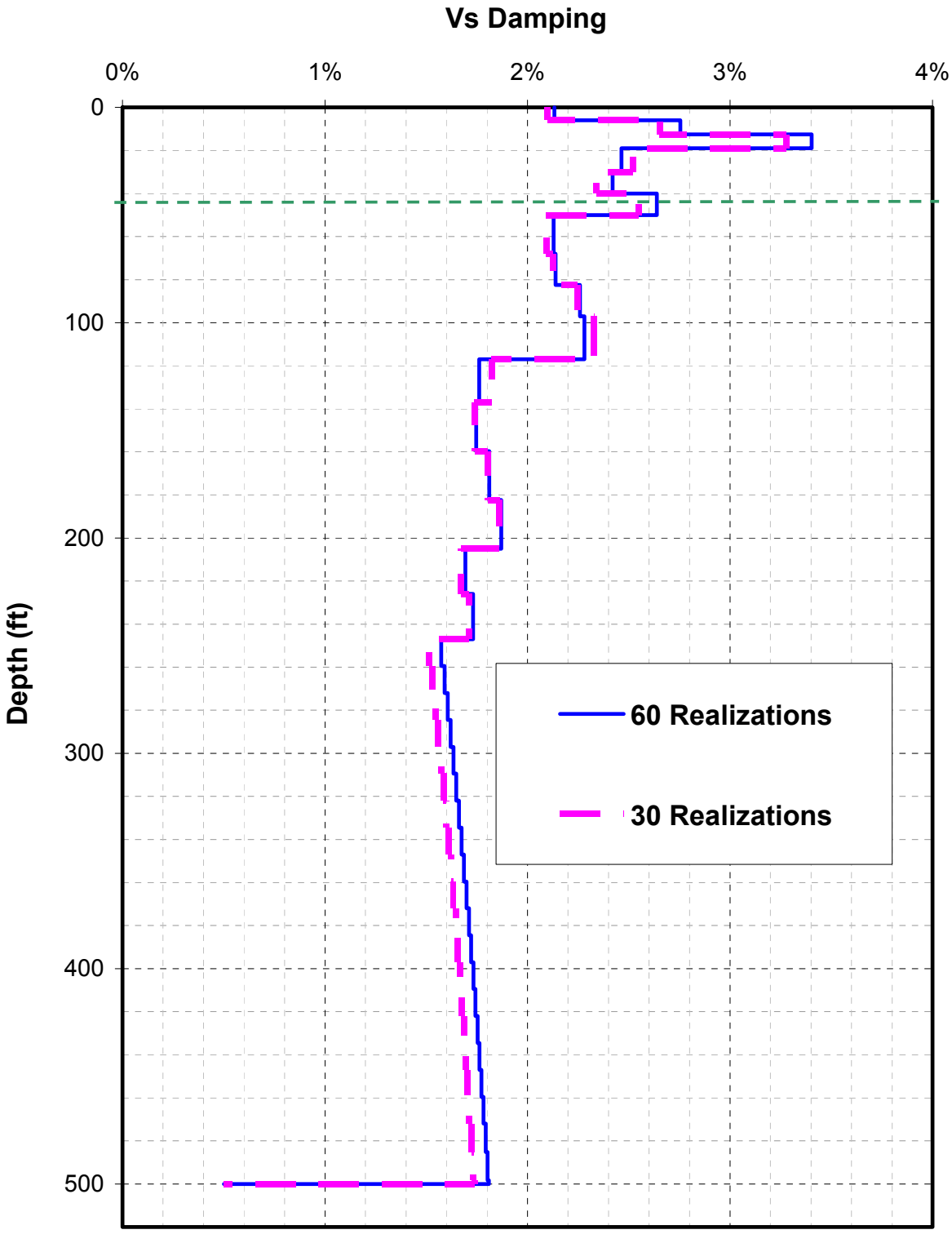

Figure 1-A.1.0-3 Comparison of Median Estimates for Strain Compatible Properties Developed for 60 and 30 Realizations for 500 ft Deep Profile 560-500 – Shear Wave Damping

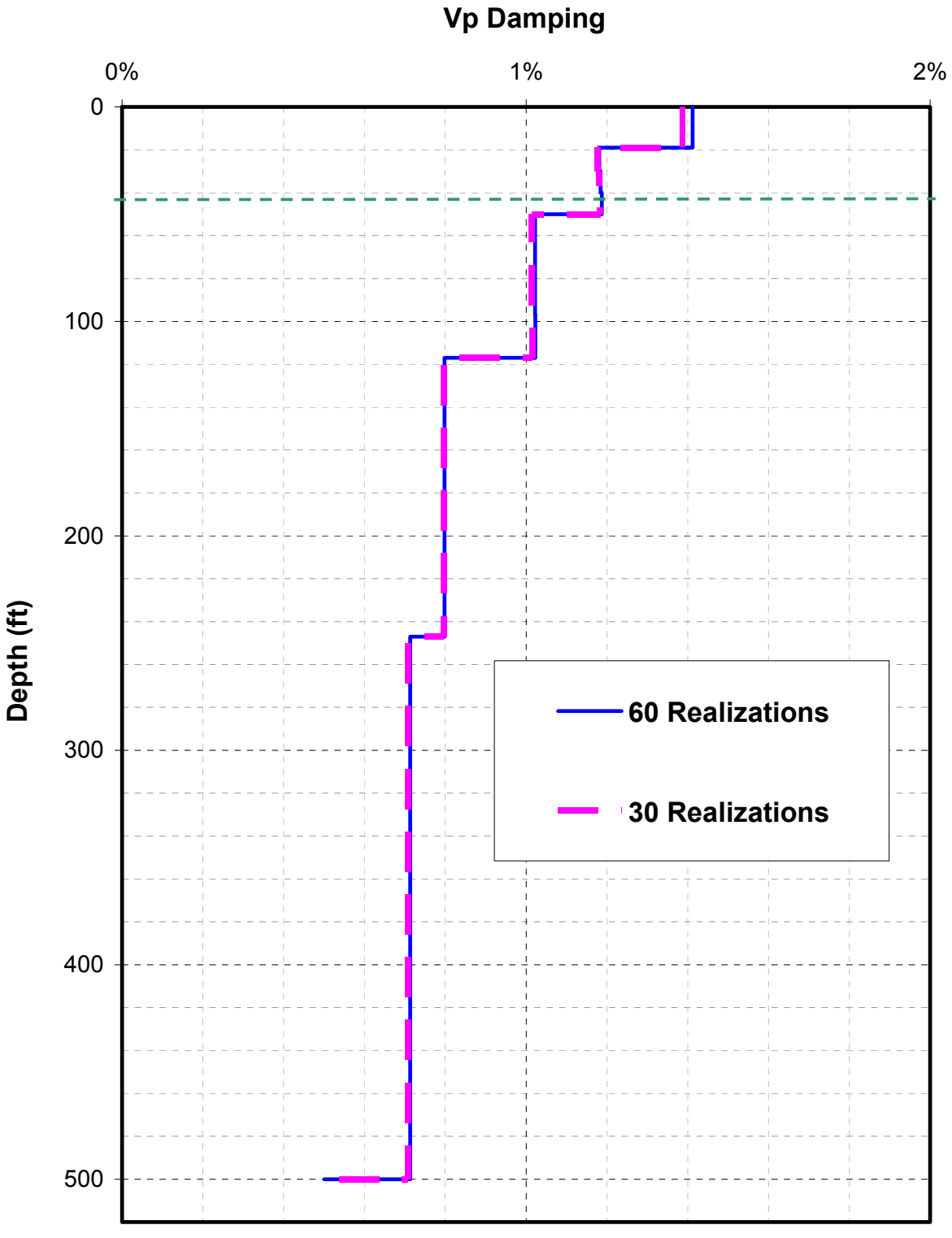

Figure 1-A.1.0-4 Comparison of Median Estimates for Strain Compatible Properties Developed for 60 and 30 Realizations for 500 ft Deep Profile 560-500 – Compression Wave Damping

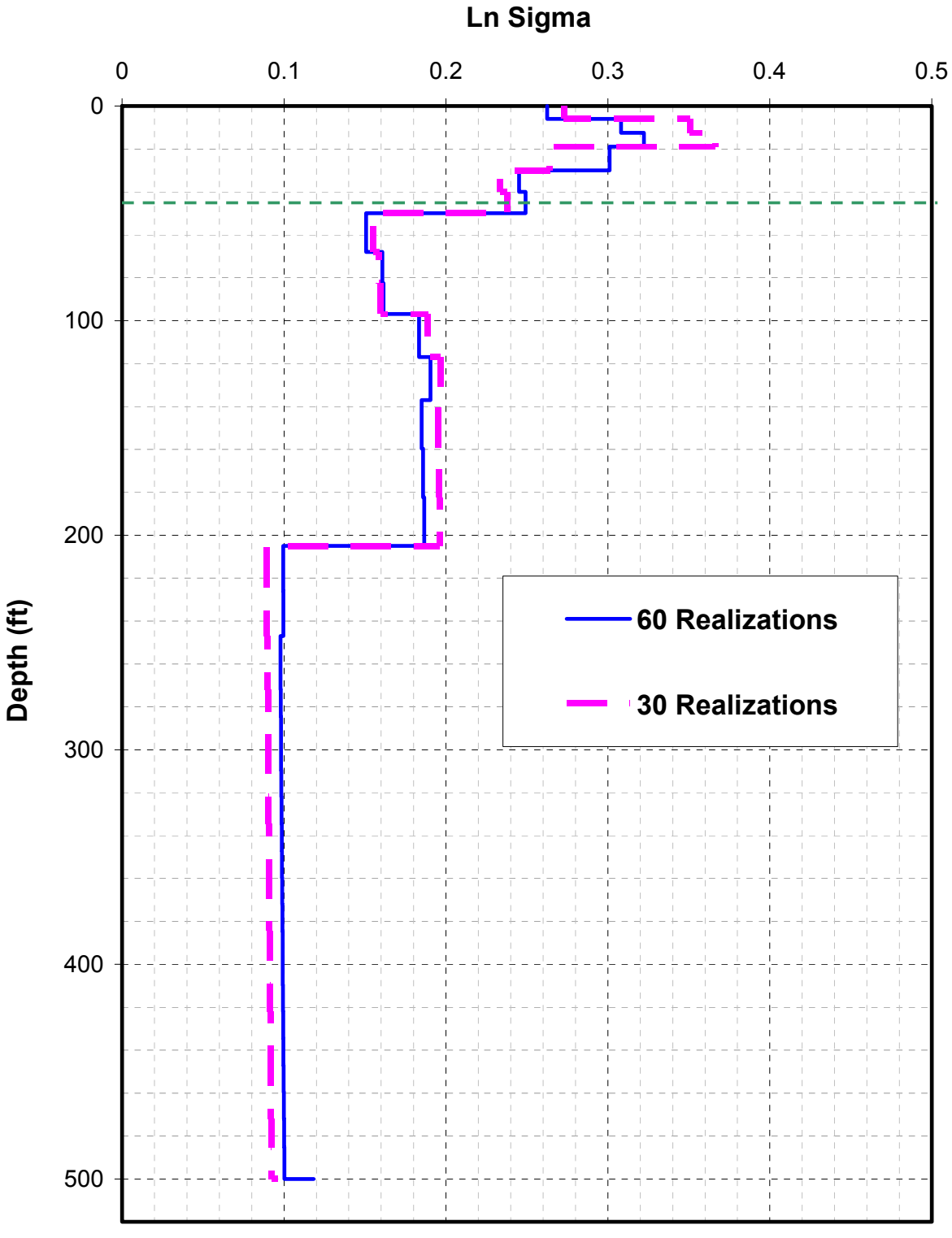

Figure 1-A.1.0-5 Comparison of Standard Deviation for Median Estimates for Strain Compatible Properties Developed for 60 and 30 Realizations for 500 ft Deep Profile 560-500 – Shear Wave Velocity

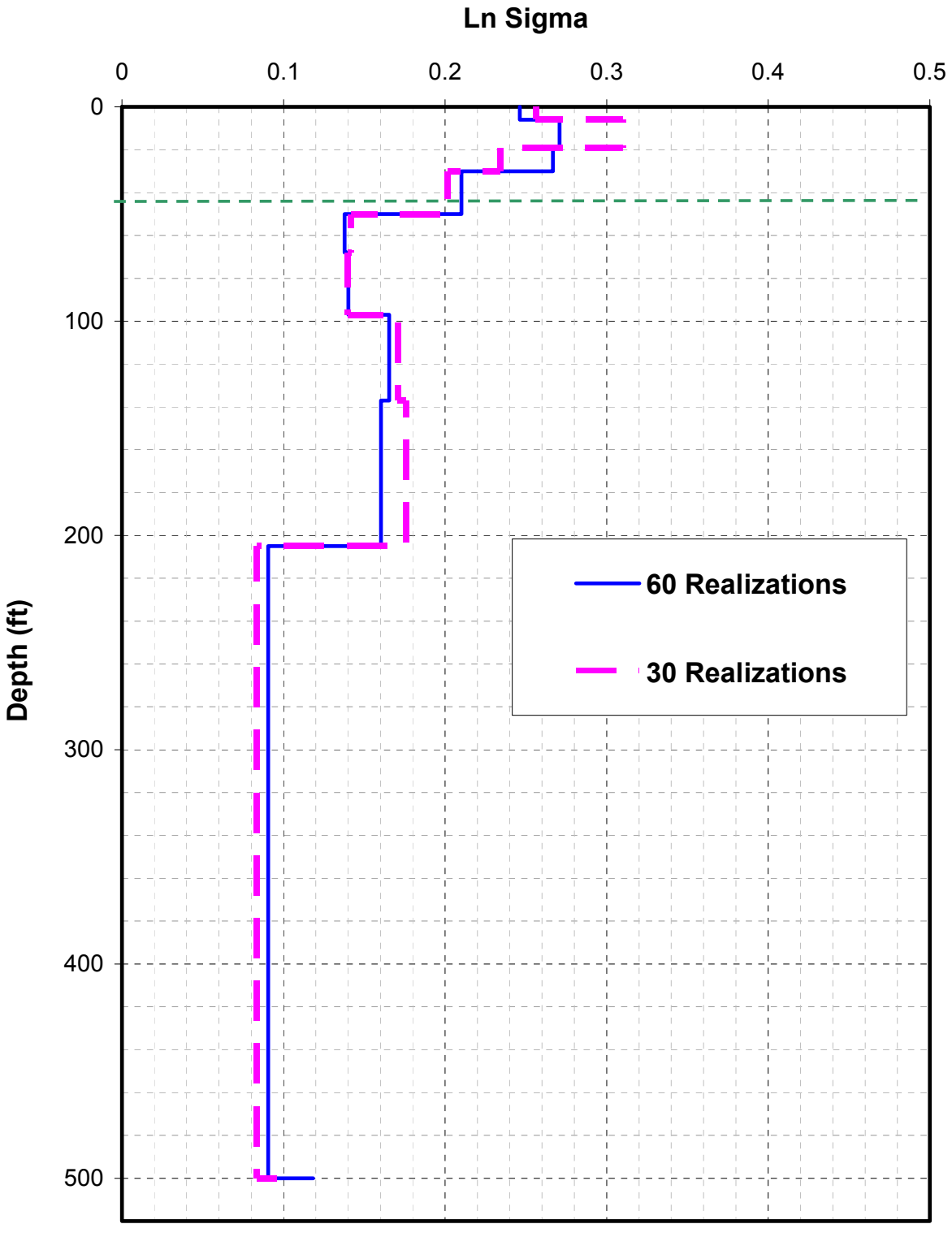

Figure 1-A.1.0-6 Comparison of Standard Deviation for Median Estimates for Strain Compatible Properties Developed for 60 and 30 Realizations for 500 ft Deep Profile 560-500 – Compression Wave Velocity

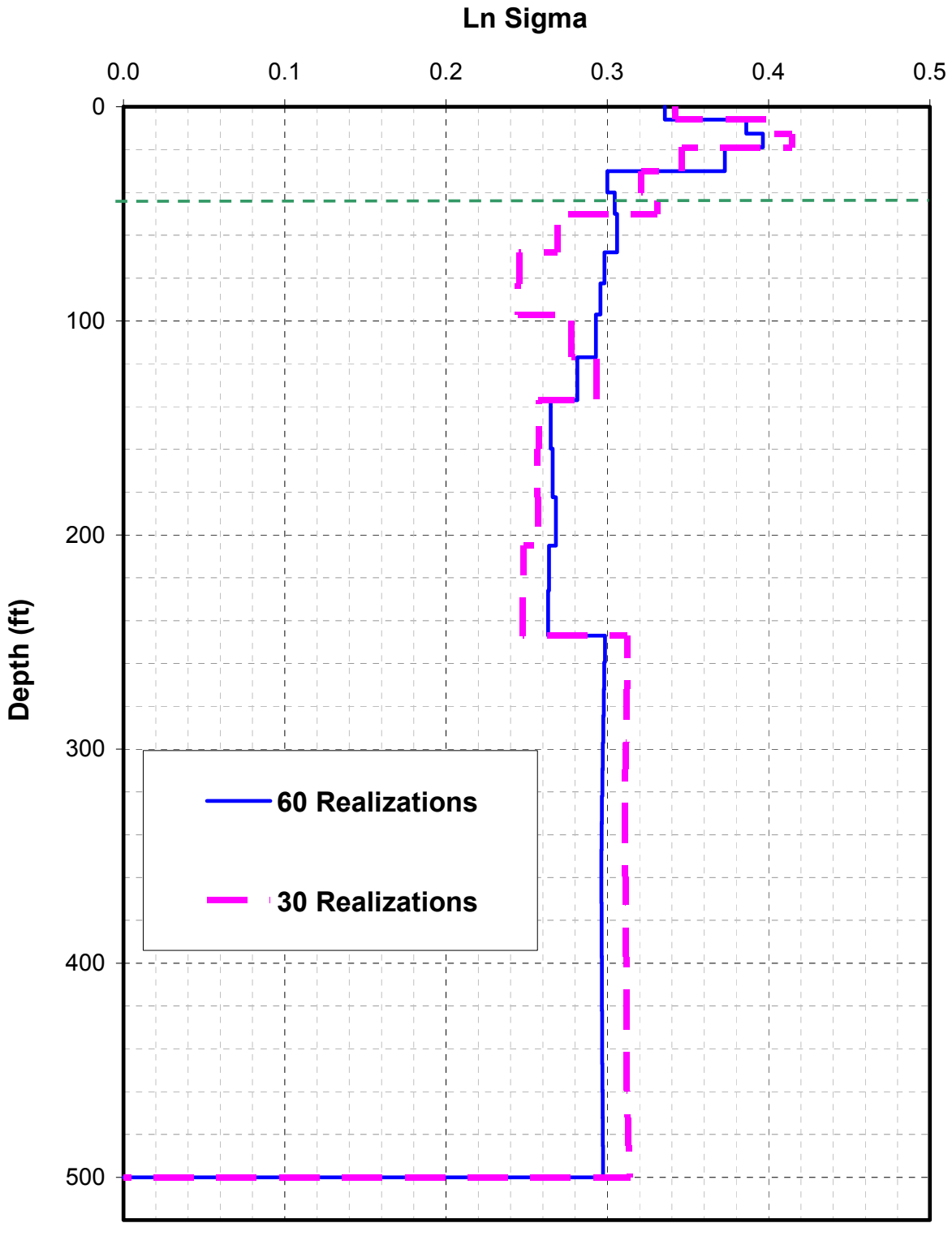

Figure 1-A.1.0-7 Comparison of Standard Deviation for Median Estimates for Strain Compatible Properties Developed for 60 and 30 Realizations for 500 ft Deep Profile 560-500 – Shear Wave Damping

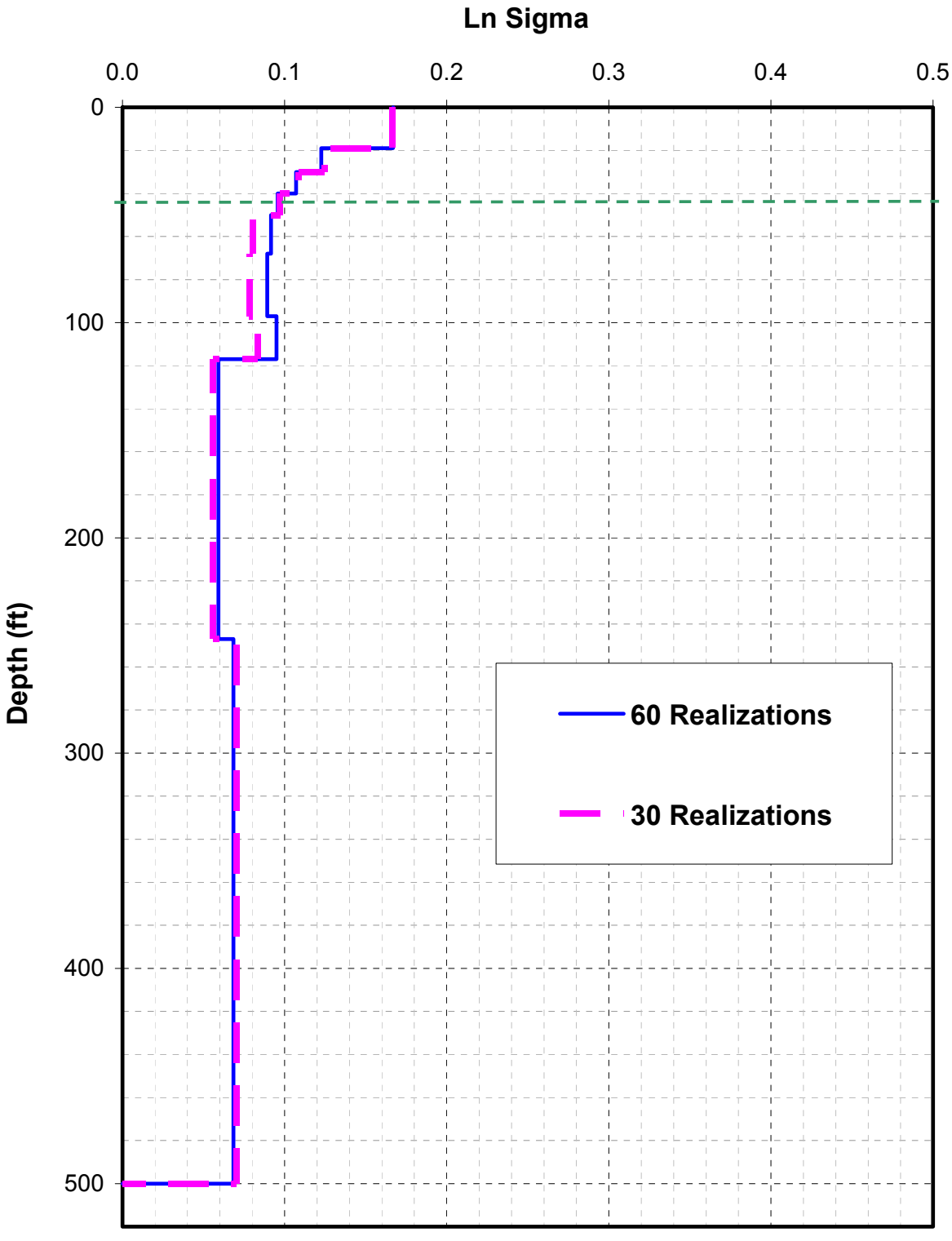

Figure 1-A.1.0-8 Comparison of Standard Deviation for Median Estimates for Strain Compatible Properties Developed for 60 and 30 Realizations for 500 ft Deep Profile 560-500 – Compression Wave Damping

Soil-Structure Interaction Analyses and Results for the US-APWR Standard Plant

PART 2 of 3

Development and Validation of the Design Basis Finite Element Model for Seismic Analysis of the US-APWR Standard Plant

PART 2 TABLE OF CONTENTS

Section Title Page No.

LIST OF FIGURES iii

LIST OF TABLES xvii

02.1.0 INTRODUCTION 02.1-1

02.2.0 PURPOSE 02.2-1

02.3.0 OBJECTIVES 02.3-1
02.3.1 Description of the R/B Complex Structures 02.3-1
02.3.1.1 R/B 02.3-1
02.3.1.2 PCCV 02.3-2
02.3.1.3 CIS 02.3-2
02.3.1.4 East PS/B and West PS/B 02.3-2
02.3.1.5 A/B 02.3-3
02.3.1.6 ESWPC 02.3-3
02.3.2 Dynamic Finite Element Model of the R/B Complex 02.3-3
02.3.3 Consideration of Concrete Cracking in Dynamic Analyses 02.3-4

02.4.0 APPROACH / METHODOLOGY 02.4-1
02.4.1 SASSI Dynamic Finite Element Model of the R/B Complex 02.4-1
02.4.1.1 Development of the R/B Complex Dynamic FE Model 02.4-1
02.4.1.2 Validation of the Dynamic Model 02.4-9
02.4.2 Consideration of Concrete Cracking in Seismic Analysis 02.4-10
02.4.2.1 Effects of Concrete Cracking on Reinforced Concrete Shear Wall Structures 02.4-11
02.4.2.2 Effects of Concrete Cracking on the CIS 02.4-12
02.4.2.3 Effects of Concrete Cracking on the PCCV 02.4-12
02.4.3 Conversion of the R/B Complex Dynamic FE Model from ANSYS to SASSI Format 02.4-12

02.5.0 RESULTS 02.5-1
02.5.1 Dynamic Model of the Reactor Building Complex 02.5-1
02.5.1.1 Development of the Reactor Building Complex Dynamic FE Model 02.5-1
02.5.1.2 Reactor Coolant Loop (RCL) Model 02.5-2
02.5.1.3 Validation of the Reactor Building Complex Dynamic FE Model 02.5-3
02.5.1.4 Summary of the R/B Complex Dynamic FE Model 02.5-12
02.5.1.5 Validation of the Dynamic Model Translation into SASSI Format 02.5-13

02.6.0 REFERENCES 02.6-1

APPENDIX 2-A Reduced Stiffness for Cracked Pre-stressed Concrete Containment Vessel (PCCV) 2-A-i

LIST OF FIGURES

Figure **Title** **Page No.**

Figure 02.3.1-1 Plan View of R/B Complex at EL 3'-7" 02.3-7

Figure 02.3.1-2 North-South Cross-Section of R/B Complex (Column Line of 13R (Figure 02.3.1-1) looking East)....02.3-8

Figure 02.3.1-3 North-South Cross-Section of R/B Complex (Column Line of 4R (Figure 02.3.1-1) looking East)....02.3-9

Figure 02.3.1-4 East-West Cross-Section of R/B Complex (Column Line of FR (Figure 02.3.1-1) looking North) 02.3-10

Figure 02.3.1-5 East-West Cross-Section of R/B Complex (Column Line of K2R (Figure 02.3.1-1) looking North) 02.3-11

Figure 02.4.1.1.1-1 Integrated R/B Complex Dynamic FE Model 02.4-18

Figure 02.4.1.1.1-2 Integrated R/B Complex Detailed FE Model 02.4-19

Figure 02.4.1.1.1-3 PCCV Detailed Model 02.4-20

Figure 02.4.1.1.1-4 CIS Detailed Model **(includes the CIS and the RCL models)** 02.4-21

Figure 02.4.1.1.1-5 Connection of Shell to Solid Elements 02.4-22

Figure 02.4.1.1.1-6 Transitional Shell Elements between SC Walls and Reactor Cavity 02.4-23

Figure 02.4.1.1.1-7 Connection of Beam to Solid Elements....02.4-24

Figure 02.4.1.1.1-8 Connection of Beam to Shell Elements....02.4-25

Figure 02.4.1.1.4-1 Example of Hydrodynamic Masses (Example shown for SFP)....02.4-26

Figure 02.4.1.1.5-1A FE Models to Calculate Wall Stiffness Reduction Factors – Model A 02.4-27

Figure 02.4.1.1.5-1B FE Models to Calculate Wall Stiffness Reduction Factors – Model B 02.4-27

Figure 02.4.1.1.8-1 Extracted Detailed FE Model of Floor Slabs 02.4-28

Figure 02.4.1.1.8-2 Floor Slab Model Boundary Conditions....02.4-28

Figure 02.5.1.1-1 Dynamic R/B Complex FE Model....02.5-36

Figure 02.5.1.1-2 Section View of Dynamic R/B Complex FE Model Looking East 02.5-37

Figure 02.5.1.1-3 Section View of Dynamic R/B Complex FE Model Looking North 02.5-38

Figure 02.5.1.1-4 PCCV Dynamic Model....02.5-39

Figure 02.5.1.1-5 CIS Dynamic Model – Shell Elements (Excluding RCL) 02.5-40

Figure 02.5.1.1-6 CIS Dynamic Model – Solid Elements....02.5-41

Figure 02.5.1.1-7 CIS Dynamic Model – Beam Elements (Excluding RCL)....02.5-42

Figure 02.5.1.1-8 East PS/B Dynamic Model 02.5-43

Figure 02.5.1.1-9 West PS/B Dynamic Model 02.5-44

Figure 02.5.1.1-10 A/B Dynamic Model....02.5-45

Figure 02.5.1.2.1-1 US-APWR Reactor Coolant Loop (RCL).....02.5-46
Figure 02.5.1.2.1-2 Dynamic Model of RCL.....02.5-47
Figure 02.5.1.2.2-1 Reactor Vessel Support.....02.5-48
Figure 02.5.1.2.2-2 Reactor Vessel Support FE Model Connection.....02.5-49
Figure 02.5.1.2.2-3 Steam Generator Lower Lateral Support.....02.5-50
Figure 02.5.1.2.2-4 Reactor Coolant Pump (RCP) Tie Rod Support.....02.5-51
Figure 02.5.1.2.2-5 Steam Generator Supports FE Model Connections.....02.5-52
Figure 02.5.1.3.1.1-1 Displacement Locations on R/B Exterior Walls.....02.5-53
Figure 02.5.1.3.1.1-2 R/B 1g Static Analysis – NS Direction (X) at Location C.....02.5-54
Figure 02.5.1.3.1.1-3 R/B 1g Static Analysis – EW Direction (Y) at Location C.....02.5-55
Figure 02.5.1.3.1.1-4 R/B 1g Static Analysis – Vertical Direction (Z) at Location C.....02.5-56
Figure 02.5.1.3.1.1-5 R/B 1g Static Analysis – NS Direction (X) at Location H.....02.5-57
Figure 02.5.1.3.1.1-6 R/B 1g Static Analysis – EW Direction (Y) at Location H.....02.5-58
Figure 02.5.1.3.1.1-7 R/B 1g Static Analysis – Vertical Direction (Z) at Location H.....02.5-59
Figure 02.5.1.3.1.2-1 R/B Modal Analysis – Cumulative Mass in the NS Direction (X).....02.5-60
Figure 02.5.1.3.1.2-2 R/B Modal Analysis – Cumulative Mass in the EW Direction (Y).....02.5-61
Figure 02.5.1.3.1.2-3 R/B Modal Analysis – Cumulative Mass in the Vertical Direction (Z).....02.5-62
Figure 02.5.1.3.1.2-4 R/B Detailed Mode Shape – Mode 1 at Frequency 4.601 Hz- NS Direction (X).....02.5-63
Figure 02.5.1.3.1.2-5 R/B Dynamic Mode Shape – Mode 1 at Frequency 4.739 Hz - NS Direction (X).....02.5-63
Figure 02.5.1.3.1.2-6 R/B Detailed Mode Shape – Mode 4at Frequency 5.996 Hz- NS Direction (X).....02.5-64
Figure 02.5.1.3.1.2-7 R/B Dynamic Mode Shape – Mode 4 at Frequency 5.943 Hz- NS Direction (X).....02.5-64
Figure 02.5.1.3.1.2-8 R/B Detailed Mode Shape – Mode 5 at Frequency 6.711 Hz - NS Direction (X).....02.5-65
Figure 02.5.1.3.1.2-9 R/B Dynamic Mode Shape – Mode 5 at Frequency 6.775 Hz - NS Direction (X).....02.5-65
Figure 02.5.1.3.1.2-10 R/B Detailed Mode Shape – Mode 2 at Frequency 5.506 Hz - EW Direction (Y).....02.5-66
Figure 02.5.1.3.1.2-11 R/B Dynamic Mode Shape – Mode 2 at Frequency 5.543 Hz - EW Direction (Y).....02.5-66
Figure 02.5.1.3.1.2-12 R/B Detailed Mode Shape – Mode 3 at Frequency 5.827 Hz- EW Direction (Y).....02.5-67

Figure 02.5.1.3.1.2-13 R/B Dynamic Mode Shape – Mode 3 at Frequency 5.894 Hz- EW Direction (Y) 02.5-67

Figure 02.5.1.3.1.2-14 R/B Detailed Mode Shape – Mode 21 at Frequency 12.435 Hz - Vertical Direction (Z) 02.5-68

Figure 02.5.1.3.1.2-15 R/B Detailed Mode Shape – Mode 22 at Frequency 12.529 Hz - Vertical Direction (Z) 02.5-68

Figure 02.5.1.3.1.2-16 R/B Dynamic Mode Shape – Mode 22 at Frequency 12.569 Hz - Vertical Direction (Z) 02.5-69

Figure 02.5.1.3.1.2-17 R/B Detailed Mode Shape – Mode 23 at Frequency 12.665 Hz - Vertical Direction (Z) 02.5-69

Figure 02.5.1.3.1.2-18 R/B Dynamic Mode Shape – Mode 24 at Frequency 13.226 Hz - Vertical Direction (Z) 02.5-70

Figure 02.5.1.3.1.3-1 R/B Harmonic Response Analysis – NS Direction (X) at Plan Location B-Elevation at Fourth Floor 02.5-71

Figure 02.5.1.3.1.3-2 R/B Harmonic Response Analysis – EW Direction (Y) at Plan Location B-Elevation at Fourth Floor 02.5-72

Figure 02.5.1.3.1.3-3 R/B Harmonic Response Analysis – Vertical Direction (Z) at Plan Location B-Elevation at Fourth Floor 02.5-73

Figure 02.5.1.3.2.1-1 Displacement Locations on PCCV 02.5-74

Figure 02.5.1.3.2.1-2 PCCV 1g Static Analysis – NS Direction (X) at North Face of Structure 02.5-75

Figure 02.5.1.3.2.1-3 PCCV 1g Static Analysis – EW direction (Y) at North Face of Structure 02.5-75

Figure 02.5.1.3.2.1-4 PCCV 1g Static Analysis – Vertical direction (Z) at North Face of Structure 02.5-76

Figure 02.5.1.3.2.2-1 PCCV Modal Analysis – Cumulative Mass in the NS Direction (X) 02.5-76

Figure 02.5.1.3.2.2-2 PCCV Modal Analysis – Cumulative Mass in the EW Direction (Y) 02.5-77

Figure 02.5.1.3.2.2-3 PCCV Modal Analysis – Cumulative Mass in the Vertical Direction (Z) 02.5-78

Figure 02.5.1.3.2.2-4 PCCV Detailed Mode Shape – Mode 2 at Frequency 4.46 Hz- NS Direction (X) 02.5-79

Figure 02.5.1.3.2.2-5 PCCV Dynamic Mode Shape – Mode 2 at Frequency 4.48 Hz - NS Direction (X) 02.5-79

Figure 02.5.1.3.2.2-6 PCCV Detailed Mode Shape – Mode 20 at Frequency 12.92 Hz- NS Direction (X) 02.5-80

Figure 02.5.1.3.2.2-7 PCCV Dynamic Mode Shape – Mode 22 at Frequency 12.91 Hz- NS Direction (X) 02.5-80

Figure 02.5.1.3.2.2-8 PCCV Detailed Mode Shape – Mode 21 at Frequency 13.05 Hz - NS Direction (X) 02.5-81

Figure 02.5.1.3.2.2-9 PCCV Dynamic Mode Shape – Mode 23 at Frequency 12.94 Hz- NS Direction (X) 02.5-81

Figure 02.5.1.3.2.2-10 PCCV Detailed Mode Shape – Mode 1 at Frequency 4.32 Hz- EW Direction (Y) 02.5-82

Figure 02.5.1.3.2.2-11 PCCV Dynamic Mode Shape – Mode 1 at Frequency 4.31 Hz - EW Direction (Y) 02.5-82

Figure 02.5.1.3.2.2-12 PCCV Detailed Mode Shape – Mode 3 at Frequency 4.68 Hz- EW Direction (Y) 02.5-83

Figure 02.5.1.3.2.2-13 PCCV Dynamic Mode Shape – Mode 3 at Frequency 4.66 Hz - EW Direction (Y) 02.5-83

Figure 02.5.1.3.2.2-14 PCCV Detailed Mode Shape – Mode 21 at Frequency 13.05 Hz - EW Direction (Y) 02.5-84

Figure 02.5.1.3.2.2-15 PCCV Dynamic Mode Shape – Mode 21 at Frequency 12.8 Hz - EW Direction (Y) 02.5-84

Figure 02.5.1.3.2.2-16 PCCV Detailed Mode Shape – Mode 19 at Frequency 12.575 Hz - Vertical Direction (Z) 02.5-85

Figure 02.5.1.3.2.2-17 PCCV Dynamic Mode Shape – Mode 19 at Frequency 12.575 Hz - Vertical Direction (Z) 02.5-85

Figure 02.5.1.3.2.3-1 PCCV Harmonic Response Analysis – NS Direction (X) at North Face of Structure - Main Equipment Hatch Elevation 02.5-86

Figure 02.5.1.3.2.3-2 PCCV Harmonic Response Analysis – EW Direction (Y) at North Face of Structure - Main Equipment Hatch Elevation 02.5-87

Figure 02.5.1.3.2.3-3 PCCV Harmonic Response Analysis – Vertical Direction (Z) at North Face of Structure - Main Equipment Hatch Elevation 02.5-88

Figure 02.5.1.3.3.1-1 Displacement Locations on the CIS 02.5-89

Figure 02.5.1.3.3.1-2 CIS 1g Static Analysis – NS Direction (X) at North Face of Structure (Uncracked Analyses) 02.5-90

Figure 02.5.1.3.3.1-3 CIS 1g Static Analysis – EW Direction (Y) at North Face of Structure (Uncracked Analyses) 02.5-91

Figure 02.5.1.3.3.1-4 CIS 1g Static Analysis – Vertical Direction (Z) at North Face of Structure (Uncracked Analyses) 02.5-92

Figure 02.5.1.3.3.1-5 CIS 1g Static Analysis – NS Direction (X) at RV (Uncracked Analyses) 02.5-93

Figure 02.5.1.3.3.1-6 CIS 1g Static Analysis – EW Direction (Y) at RV (Uncracked Analyses) 02.5-94

Figure 02.5.1.3.3.1-7 CIS 1g Static Analysis – NS Direction (X) at D-SG (Uncracked Analyses) 02.5-95

Figure 02.5.1.3.3.1-8 CIS 1g Static Analysis – EW Direction (Y) at D-SG (Uncracked Analyses) 02.5-96

Figure 02.5.1.3.3.1-9 CIS 1g Static Analysis – NS Direction (X) at B-RCP (Uncracked Analyses) 02.5-97

Figure 02.5.1.3.3.1-10 CIS 1g Static Analysis – EW Direction (Y) at B-RCP (Uncracked Analyses) 02.5-98

Figure 02.5.1.3.3.1-11 CIS 1g Static Analysis – NS Direction (X) at North Face of Structure (Cracked Analyses)....02.5-99

Figure 02.5.1.3.3.1-12 CIS 1g Static Analysis – EW Direction (Y) at North Face of Structure (Cracked Analyses)....02.5-100

Figure 02.5.1.3.3.1-13 CIS 1g Static Analysis – Vertical Direction (Z) at North Face of Structure (Cracked Analyses)....02.5-101

Figure 02.5.1.3.3.1-14 CIS 1g Static Analysis – NS Direction (X) at RV (Cracked Analyses)....02.5-102

Figure 02.5.1.3.3.1-15 CIS 1g Static Analysis – EW Direction (Y) at RV (Cracked Analyses)....02.5-103

Figure 02.5.1.3.3.1-16 CIS 1g Static Analysis – NS Direction (X) at D-SG (Cracked Analyses) 02.5-104

Figure 02.5.1.3.3.1-17 CIS 1g Static Analysis – EW Direction (Y) at D-SG (Cracked Analyses) 02.5-105

Figure 02.5.1.3.3.1-18 CIS 1g Static Analysis – NS Direction (X) at B-RCP (Cracked Analyses) 02.5-106

Figure 02.5.1.3.3.1-19 CIS 1g Static Analysis – EW Direction (Y) at B-RCP (Cracked Analyses) 02.5-107

Figure 02.5.1.3.3.2-1 CIS Modal Analysis – Cumulative Mass in the NS Direction (X) (Uncracked Analyses) 02.5-108

Figure 02.5.1.3.3.2-2 CIS Modal Analysis – Cumulative Mass in the EW Direction (Y) (Uncracked Analyses) 02.5-109

Figure 02.5.1.3.3.2-3 CIS Modal Analysis – Cumulative Mass in the Vertical Direction (Z) (Uncracked Analyses) 02.5-110

Figure 02.5.1.3.3.2-4 CIS Detailed Mode Shape – Mode 1 at Frequency 4.47 Hz - NS Direction (X) 02.5-111

Figure 02.5.1.3.3.2-5 CIS Dynamic Mode Shape – Mode 1 at Frequency 4.52 Hz - NS Direction (X) 02.5-111

Figure 02.5.1.3.3.2-6 CIS Detailed Mode Shape – Mode 5 at Frequency 6.57 Hz - NS Direction (X) 02.5-112

Figure 02.5.1.3.3.2-7 CIS Dynamic Mode Shape – Mode 5 at Frequency 6.74 Hz - NS Direction (X) 02.5-112

Figure 02.5.1.3.3.2-8 CIS Detailed Mode Shape – Mode 2 at Frequency 4.79 Hz - EW Direction (Y)....02.5-113

Figure 02.5.1.3.3.2-9 CIS Dynamic Mode Shape – Mode 2 at Frequency 4.9 Hz - EW Direction (Y)....02.5-113

Figure 02.5.1.3.3.2-10 CIS Detailed Mode Shape – Mode 3 at Frequency 5.74 Hz - EW Direction (Y)....02.5-114

Figure 02.5.1.3.3.2-11 CIS Dynamic Mode Shape – Mode 3 at Frequency 5.92 Hz- EW Direction (Y) 02.5-114

Figure 02.5.1.3.3.2-12 CIS Detailed Mode Shape – Mode 36 at Frequency 14.18 Hz - Vertical Direction (Z) 02.5-115

Figure 02.5.1.3.3.2-13 CIS Dynamic Mode Shape – Mode 36 at Frequency 14.25 Hz - Vertical Direction (Z) 02.5-115

Figure 02.5.1.3.3.2-14 CIS Detailed Mode Shape – Mode 43 at Frequency 15.2 Hz - Vertical Direction (Z) 02.5-116

Figure 02.5.1.3.3.2-15 CIS Dynamic Mode Shape – Mode 44 at Frequency 15.39 Hz - Vertical Direction (Z) 02.5-116

Figure 02.5.1.3.3.2-16 CIS Detailed Mode Shape – Mode 46 at Frequency 15.36 Hz - Vertical Direction (Z) 02.5-117

Figure 02.5.1.3.3.2-17 CIS Dynamic Mode Shape – Mode 45 at Frequency 15.41 Hz - Vertical Direction (Z) 02.5-117

Figure 02.5.1.3.3.2-18 CIS Detailed Mode Shape – Mode 48 at Frequency 15.63 Hz - Vertical Direction (Z) 02.5-118

Figure 02.5.1.3.3.2-19 CIS Dynamic Mode Shape – Mode 49 at Frequency 16.34 Hz - Vertical Direction (Z) 02.5-118

Figure 02.5.1.3.3.2-20 CIS Detailed Mode Shape – Mode 50 at Frequency 15.99 Hz - Vertical Direction (Z) 02.5-119

Figure 02.5.1.3.3.2-21 CIS Dynamic Mode Shape – Mode 50 at Frequency 16.38 Hz - Vertical Direction (Z) 02.5-119

Figure 02.5.1.3.3.2-22 CIS Detailed Mode Shape – Mode 53 at Frequency 16.45 Hz - Vertical Direction (Z) 02.5-120

Figure 02.5.1.3.3.2-23 CIS Dynamic Mode Shape – Mode 55 at Frequency 16.88 Hz - Vertical Direction (Z) 02.5-120

Figure 02.5.1.3.3.2-24 CIS Detailed Mode Shape – Mode 56 at Frequency 16.69 Hz - Vertical Direction (Z) 02.5-121

Figure 02.5.1.3.3.2-25 CIS Dynamic Mode Shape – Mode 56 at Frequency 17.00 Hz - Vertical Direction (Z) 02.5-121

Figure 02.5.1.3.3.2-26 CIS Modal Analysis – Cumulative Mass in the NS Direction (X) (Cracked Analyses) 02.5-122

Figure 02.5.1.3.3.2-27 CIS Modal Analysis – Cumulative Mass in the EW Direction (Y) (Cracked Analyses) 02.5-123

Figure 02.5.1.3.3.2-28 CIS Modal Analysis – Cumulative Mass in the Vertical Direction (Z) (Cracked Analyses) 02.5-124

Figure 02.5.1.3.3.3-1 CIS Harmonic Response Analysis – RV Nozzle NS Direction (X) (Uncracked Analyses) 02.5-125

Figure 02.5.1.3.3.3-2 CIS Harmonic Response Analysis – RV Nozzle EW Direction (Y) (Uncracked Analyses) 02.5-126

Figure 02.5.1.3.3.3-3 CIS Harmonic Response Analysis – RV Nozzle Vertical Direction (Z) (Uncracked Analyses) 02.5-127

Figure 02.5.1.3.3.3-4 CIS Harmonic Response Analysis – RV Nozzle NS Direction (X) (Cracked Analyses) 02.5-128

Figure 02.5.1.3.3.3-5 CIS Harmonic Response Analysis – RV Nozzle EW Direction (Y) (Cracked Analyses) 02.5-129

Figure 02.5.1.3.3.3-6 CIS Harmonic Response Analysis – RV Nozzle Vertical Direction (Z) (Cracked Analyses) 02.5-130

Figure 02.5.1.3.4.1-1 Displacement Locations on East PS/B Exterior Walls 02.5-131

Figure 02.5.1.3.4.1-2 East PS/B NS Direction (X) 1g Static Analysis – Southeast Corner 02.5-132

Figure 02.5.1.3.4.1-3 East PS/B EW Direction (Y) 1g Static Analysis – Southeast Corner 02.5-133

Figure 02.5.1.3.4.1-4 East PS/B Vertical Direction (Z) 1g Static Analysis – Southeast Corner 02.5-134

Figure 02.5.1.3.4.2-1 East PS/B Modal Analysis – Cumulative Mass in the NS Direction (X) 02.5-135

Figure 02.5.1.3.4.2-2 East PS/B Modal Analysis – Cumulative Mass in the EW Direction (Y) 02.5-136

Figure 02.5.1.3.4.2-3 East PS/B Modal Analysis – Cumulative Mass in the Vertical Direction (Z) 02.5-137

Figure 02.5.1.3.4.2-4 East PS/B Detailed Mode Shape – Mode 2 at Frequency 11.71 Hz - NS Direction (X) 02.5-138

Figure 02.5.1.3.4.2-5 East PS/B Dynamic Mode Shape – Mode 2 at Frequency 11.8 Hz - NS Direction (X) 02.5-138

Figure 02.5.1.3.4.2-6 East PS/B Detailed Mode Shape – Mode 1 at Frequency 9.71 Hz - EW Direction (Y) 02.5-139

Figure 02.5.1.3.4.2-7 East PS/B Dynamic Mode Shape – Mode 1 at Frequency 9.9 Hz - EW Direction (Y) 02.5-139

Figure 02.5.1.3.4.2-8 East PS/B Detailed Mode Shape – Mode 13 at Frequency 20.5 Hz - Vertical Direction (Z) 02.5-140

Figure 02.5.1.3.4.2-9 East PS/B Dynamic Mode Shape – Mode 14 at Frequency 21.94 Hz - Vertical Direction (Z) 02.5-140

Figure 02.5.1.3.4.2-10 East PS/B Detailed Mode Shape – Mode 16 at Frequency 22 Hz- Vertical Direction (Z) 02.5-141

Figure 02.5.1.3.4.2-11 East PS/B Dynamic Mode Shape – Mode 15 at Frequency 22.18 Hz - Vertical Direction (Z) 02.5-141

Figure 02.5.1.3.4.2-12 East PS/B Detailed Mode Shape – Mode 37 at Frequency 28.4 Hz - Vertical Direction (Z) 02.5-142

Figure 02.5.1.3.4.2-13 East PS/B Dynamic Mode Shape – Mode 34 at Frequency 27.83 Hz - Vertical Direction (Z) 02.5-142

Figure 02.5.1.3.4.2-14 East PS/B Detailed Mode Shape – Mode 53 at Frequency 32.9 Hz - Vertical Direction (Z) 02.5-143

Figure 02.5.1.3.4.2-15 East PS/B Dynamic Mode Shape – Mode 57 at Frequency 34 Hz - Vertical Direction (Z) 02.5-143

Figure 02.5.1.3.4.3-1 East PS/B Harmonic Response Analysis – NW Corner– Elev. 48'-6" - NS Direction (X) 02.5-144

Figure 02.5.1.3.4.3-2 East PS/B Harmonic Response Analysis – NW Corner– Elev. 48'-6" - EW Direction (Y) 02.5-145

Figure 02.5.1.3.4.3-3 East PS/B Harmonic Response Analysis – NW Corner– Elev. 48'-6" - Vertical Direction (Z) 02.5-146

Figure 02.5.1.3.5.1-1 Displacement Locations on West PS/B Exterior Walls 02.5-147

Figure 02.5.1.3.5.1-2 West PS/B NS Direction (X) 1g Static Analysis – Southwest Corner 02.5-148

Figure 02.5.1.3.5.1-3 West PS/B EW Direction (Y) 1g Static Analysis – Southwest Corner 02.5-149

Figure 02.5.1.3.5.1-4 West PS/B Vertical Direction (Z) 1g Static Analysis – Southwest Corner....02.5-150

Figure 02.5.1.3.5.2-1 West PS/B Modal Analysis – Cumulative Mass in the NS Direction (X) 02.5-151

Figure 02.5.1.3.5.2-2 West PS/B Modal Analysis – Cumulative Mass in the EW Direction (Y) 02.5-152

Figure 02.5.1.3.5.2-3 West PS/B Modal Analysis – Cumulative Mass in the Vertical Direction (Z)....02.5-153

Figure 02.5.1.3.5.2-4 West PS/B Detailed Mode Shape – Mode 1 at Frequency 8.28 Hz - NS Direction (X)....02.5-154

Figure 02.5.1.3.5.2-5 West PS/B Dynamic Mode Shape – Mode 1 at Frequency 8.59 Hz - NS Direction (X)....02.5-154

Figure 02.5.1.3.5.2-6 West PS/B Detailed Mode Shape – Mode 10 at Frequency 19.67 Hz - NS Direction (X)....02.5-155

Figure 02.5.1.3.5.2-7 West PS/B Dynamic Mode Shape – Mode 9 at Frequency 20.13 Hz - NS Direction (X)....02.5-155

Figure 02.5.1.3.5.2-8 West PS/B Detailed Mode Shape – Mode 2 at Frequency 11.89 Hz - EW Direction (Y) 02.5-156

Figure 02.5.1.3.5.2-9 West PS/B Dynamic Mode Shape – Mode 2 at Frequency 12.15 Hz - EW Direction (Y) 02.5-156

Figure 02.5.1.3.5.2-10 West PS/B Detailed Mode Shape – Mode 8 at Frequency 19.7 Hz - Vertical Direction (Z) 02.5-157

Figure 02.5.1.3.5.2-11 West PS/B Dynamic Mode Shape – Mode 9 at Frequency 19.1 Hz - Vertical Direction (Z) 02.5-157

Figure 02.5.1.3.5.2-12 West PS/B Detailed Mode Shape – Mode 36 at Frequency 29.8 Hz - Vertical Direction (Z) 02.5-158

Figure 02.5.1.3.5.2-13 West PS/B Dynamic Mode Shape – Mode 36 at Frequency 29.2 Hz - Vertical Direction (Z) 02.5-158

Figure 02.5.1.3.5.3-1 West PS/B Harmonic Response Analysis – SW Corner– Elev. 48'-6" - NS Direction (X)....02.5-159

Figure 02.5.1.3.5.3-2 West PS/B Harmonic Response Analysis – SW Corner– Elev. 48'-6" - EW Direction (Y) 02.5-160

Figure 02.5.1.3.5.3-3 West PS/B Harmonic Response Analysis – SW Corner– Elev. 48'-6" - Vertical Direction (Z) 02.5-161

Figure 02.5.1.3.6.1-1 Displacement Locations on A/B Exterior Walls 02.5-162

Figure 02.5.1.3.6.1-2 A/B NS Direction (X) 1g Static Analysis – Southwest Corner 02.5-163

Figure 02.5.1.3.6.1-3 A/B EW Direction (Y) 1g Static Analysis – Southwest Corner 02.5-164

Figure 02.5.1.3.6.1-4 A/B Vertical Direction (Z) 1g Static Analysis – Southwest Corner 02.5-165

Figure 02.5.1.3.6.2-1 A/B Modal Analysis – Cumulative Mass in the NS Direction (X)....02.5-166

Figure 02.5.1.3.6.2-2 A/B Modal Analysis – Cumulative Mass in the EW Direction (Y)....02.5-167

Figure 02.5.1.3.6.2-3 A/B Modal Analysis – Cumulative Mass in the Vertical Direction (Z)....02.5-168

Figure 02.5.1.3.6.2-4 A/B Detailed Mode Shape – Mode 2 at Frequency 8.31 Hz - NS Direction (X) 02.5-169

Figure 02.5.1.3.6.2-5 A/B Dynamic Mode Shape – Mode 2 at Frequency 8.39 Hz - NS Direction (X) 02.5-169

Figure 02.5.1.3.6.2-6 A/B Detailed Mode Shape – Mode 1 at Frequency 6.82 Hz - EW Direction (Y)....02.5-170

Figure 02.5.1.3.6.2-7 A/B Dynamic Mode Shape – Mode 1 at Frequency 6.96 Hz - EW Direction (Y)....02.5-170

Figure 02.5.1.3.6.2-8 A/B Detailed Mode Shape – Mode 14 at Frequency 14.5 Hz - Vertical Direction (Z) 02.5-171

Figure 02.5.1.3.6.2-9 A/B Dynamic Mode Shape – Mode 15 at Frequency 15.87 Hz - Vertical Direction (Z)....02.5-171

Figure 02.5.1.3.6.2-10 A/B Detailed Mode Shape – Mode 31 at Frequency 18.39 Hz - Vertical Direction (Z)....02.5-172

Figure 02.5.1.3.6.2-11 A/B Dynamic Mode Shape – Mode 27 at Frequency 17.94 Hz - Vertical Direction (Z)....02.5-172

Figure 02.5.1.3.6.2-12 A/B Detailed Mode Shape – Mode 44 at Frequency 19.95 Hz - Vertical Direction (Z)....02.5-173

Figure 02.5.1.3.6.2-13 A/B Dynamic Mode Shape – Mode 48 at Frequency 20.48 Hz - Vertical Direction (Z)....02.5-173

Figure 02.5.1.3.7.1-1 R/B Complex Comparison Locations - Plan View 02.5-174

Figure 02.5.1.3.7.1-2 R/B Complex NS Direction (X) 1g Static Analysis – Comparison Point A 02.5-175

Figure 02.5.1.3.7.1-3 R/B Complex EW Direction (Y) 1g Static Analysis – Comparison Point A 02.5-176

Figure 02.5.1.3.7.1-4 R/B Complex Vertical Direction (Z) 1g Static Analysis – Comparison Point A 02.5-177

Figure 02.5.1.3.7.1-5 R/B Complex NS Direction (X) 1g Static Analysis – Comparison Point H 02.5-178

Figure 02.5.1.3.7.1-6 R/B Complex EW Direction (Y) 1g Static Analysis – Comparison Point H 02.5-179

Figure 02.5.1.3.7.1-7 R/B Complex Vertical Direction (Z) 1g Static Analysis – Comparison Point H 02.5-180

Figure 02.5.1.3.7.1-8 R/B Complex NS Direction (X) 1g Static Analysis – Comparison Point M 02.5-181

Figure 02.5.1.3.7.1-9 R/B Complex EW Direction (Y) 1g Static Analysis – Comparison Point M 02.5-182

Figure 02.5.1.3.7.1-10 R/B Complex Vertical Direction (Z) 1g Static Analysis – Comparison Point M 02.5-183

Figure 02.5.1.3.7.2-1 R/B Complex Modal Analysis – Cumulative Mass in the NS Direction (X) 02.5-184

Figure 02.5.1.3.7.2-2 R/B Complex Modal Analysis – Cumulative Mass in the EW Direction (Y) 02.5-185

Figure 02.5.1.3.7.2-3 R/B Complex Modal Analysis – Cumulative Mass in the Vertical Direction (Z) 02.5-186

Figure 02.5.1.3.7.2-4 R/B Complex Detailed Mode Shape – Mode 5 at Frequency 4.22 Hz - NS Direction (X) 02.5-187

Figure 02.5.1.3.7.2-5 R/B Complex Dynamic Mode Shape – Mode 2 at Frequency 4.27 Hz - NS Direction (X) 02.5-187

Figure 02.5.1.3.7.2-6 R/B Complex Detailed Mode Shape – Mode 7 at Frequency 4.3 Hz - NS Direction (X) 02.5-188

Figure 02.5.1.3.7.2-7 R/B Complex Dynamic Mode Shape – Mode 4 at Frequency 4.87 Hz - NS Direction (X) 02.5-188

Figure 02.5.1.3.7.2-8 R/B Complex Detailed Mode Shape – Mode 15 at Frequency 6.39 Hz - NS Direction (X) 02.5-189

Figure 02.5.1.3.7.2-9 R/B Complex Dynamic Mode Shape – Mode 12 at Frequency 6.41 Hz - NS Direction (X) 02.5-189

Figure 02.5.1.3.7.2-10 R/B Complex Detailed Mode Shape – Mode 52 at Frequency 10.73 Hz - NS Direction (X) 02.5-190

Figure 02.5.1.3.7.2-11 R/B Complex Dynamic Mode Shape – Mode 44 at Frequency 10.93 Hz - NS Direction (X) 02.5-190

Figure 02.5.1.3.7.2-12 R/B Complex Detailed Mode Shape – Mode 4 at Frequency 4.18 Hz - EW Direction (Y) 02.5-191

Figure 02.5.1.3.7.2-13 R/B Complex Dynamic Mode Shape – Mode 1 at Frequency 4.18 Hz - EW Direction (Y) 02.5-191

Figure 02.5.1.3.7.2-14 R/B Complex Detailed Mode Shape – Mode 12 at Frequency 6.12 Hz - EW Direction (Y) 02.5-192

Figure 02.5.1.3.7.2-15 R/B Complex Dynamic Mode Shape – Mode 8 at Frequency 6.12 Hz - EW Direction (Y) 02.5-192

Figure 02.5.1.3.7.2-16 R/B Complex Detailed Mode Shape – Mode 15 at Frequency 6.39 Hz - EW Direction (Y) 02.5-193

Figure 02.5.1.3.7.2-17 R/B Complex Dynamic Mode Shape – Mode 12 at Frequency 6.41 Hz - EW Direction (Y) 02.5-193

Figure 02.5.1.3.7.2-18 R/B Complex Detailed Mode Shape – Mode 17 at Frequency 6.92 Hz - EW Direction (Y) 02.5-194

Figure 02.5.1.3.7.2-19 R/B Complex Dynamic Mode Shape – Mode 15 at Frequency 7.04 Hz - EW Direction (Y) 02.5-194

Figure 02.5.1.3.7.2-20 R/B Complex Detailed Mode Shape – Mode 19 at Frequency 7.03 Hz - EW Direction (Y) 02.5-195

Figure 02.5.1.3.7.2-21 R/B Complex Dynamic Mode Shape – Mode 16 at Frequency 7.12 Hz - EW Direction (Y) 02.5-195

Figure 02.5.1.3.7.2-22 R/B Complex Detailed Mode Shape – Mode 71 at Frequency 12.10 Hz - Vertical Direction (Z) 02.5-196

Figure 02.5.1.3.7.2-23 R/B Complex Dynamic Mode Shape – Mode 62 at Frequency 12.15 Hz - Vertical Direction (Z) 02.5-196

Figure 02.5.1.3.7.2-24 R/B Complex Detailed Mode Shape – Mode 79 at Frequency 12.68 Hz - Vertical Direction (Z) 02.5-197

Figure 02.5.1.3.7.2-25 R/B Complex Dynamic Mode Shape – Mode 70 at Frequency 12.74 Hz - Vertical Direction (Z) 02.5-197

Figure 02.5.1.3.7.2-26 R/B Complex Detailed Mode Shape – Mode 80 at Frequency 12.70 Hz - Vertical Direction (Z) 02.5-198

Figure 02.5.1.3.7.2-27 R/B Complex Dynamic Mode Shape – Mode 76 at Frequency 13.16 Hz - Vertical Direction (Z) 02.5-198

Figure 02.5.1.3.7.2-28 R/B Complex Detailed Mode Shape – Mode 83 at Frequency 12.85 Hz - Vertical Direction (Z) 02.5-199

Figure 02.5.1.3.7.2-29 R/B Complex Dynamic Mode Shape – Mode 78 at Frequency 13.28 Hz - Vertical Direction (Z) 02.5-199

Figure 02.5.1.3.7.2-30 R/B Complex Detailed Mode Shape – Mode 87 at Frequency 13.05 Hz - Vertical Direction (Z) 02.5-200

Figure 02.5.1.4-1 Integrated R/B Complex Dynamic FE Model (ANSYS).....02.5-201

Figure 02.5.1.4-2 Section View of R/B Complex Dynamic FE Model Looking East (Column Line 13R) 02.5-202

Figure 02.5.1.4-3 Section View of R/B Complex Dynamic FE Model Looking East (Column Line 4R) 02.5-203

Figure 02.5.1.4-4 Section View of R/B Complex Dynamic FE Model Looking North (Column Line FR) 02.5-204

Figure 02.5.1.4-5 Section View of R/B Complex Dynamic FE Model Looking North (Column Line K2R) 02.5-205

Figure 02.5.1.4-6 Integrated R/B Complex Dynamic FE Model (SASSI) 02.5-206
Figure 02.5.1.5-1 Integrated R/B Complex Dynamic FE Model – ATF Locations 02.5-207
Figure 02.5.1.5-2 Nodes on PCCV.....02.5-208
Figure 02.5.1.5-3 Nodes on the Floor of the CIS.....02.5-208
Figure 02.5.1.5.1-1 R/B-FH/A – NS Direction (X) – First Dominant Mode 02.5-209
Figure 02.5.1.5.1-2 R/B-FH/A – EW Direction (Y) – First Dominant Mode.....02.5-210
Figure 02.5.1.5.1-3 R/B-FH/A – Vertical Direction (Z) – First Dominant Mode.....02.5-211
Figure 02.5.1.5.1-4 R/B-FH/A ATF Results – NS Direction (X) Transfer Function at NE Corner 02.5-212
Figure 02.5.1.5.1-5 R/B-FH/A ATF Results – NS Direction (X) Transfer Function at NW Corner 02.5-213
Figure 02.5.1.5.1-6 R/B-FH/A ATF Results – NS Direction (X) Transfer Function at SE Corner 02.5-214
Figure 02.5.1.5.1-7 R/B-FH/A ATF Results – NS Direction (X) Transfer Function at SW Corner 02.5-215
Figure 02.5.1.5.1-8 R/B-FH/A ATF Results – EW Direction (Y) Transfer Function at NE Corner 02.5-216
Figure 02.5.1.5.1-9 R/B-FH/A ATF Results – EW Direction (Y) Transfer Function at NW Corner 02.5-217
Figure 02.5.1.5.1-10 R/B-FH/A ATF Results – EW Direction (Y) Transfer Function at SE Corner 02.5-218
Figure 02.5.1.5.1-11 R/B-FH/A ATF Results – EW Direction (Y) Transfer Function at SW Corner 02.5-219
Figure 02.5.1.5.1-12 R/B-FH/A ATF Results – Vertical Direction (Z) Transfer Function at NE Corner 02.5-220
Figure 02.5.1.5.1-13 R/B-FH/A ATF Results – Vertical Direction (Z) Transfer Function at NW Corner 02.5-221
Figure 02.5.1.5.1-14 R/B-FH/A ATF Results – Vertical Direction (Z) Transfer Function at SE Corner.....02.5-222
Figure 02.5.1.5.1-15 R/B-FH/A ATF Results – Vertical Direction (Z) Transfer Function at SW Corner.....02.5-223
Figure 02.5.1.5.2-1 PCCV – NS Direction (X) – First Dominant Mode.....02.5-224
Figure 02.5.1.5.2-2 PCCV – EW Direction (Y) – First Dominant Mode 02.5-225
Figure 02.5.1.5.2-3 PCCV – Vertical Direction (Z) – First Dominant Mode 02.5-226
Figure 02.5.1.5.2-4 PCCV ATF Results – NS Direction (X) Transfer Function at Top of Dome 02.5-227
Figure 02.5.1.5.2-5 PCCV ATF Results – EW Direction (Y) Transfer Function at Top of Dome 02.5-228
Figure 02.5.1.5.2-6 PCCV ATF Results – Vertical Direction (Z) Transfer Function at Top of Dome 02.5-229

Figure 02.5.1.5.3-1 CIS – NS Direction (X) – First Dominant Mode 02.5-230
Figure 02.5.1.5.3-2 CIS – EW Direction (Y) – First Dominant Mode 02.5-231
Figure 02.5.1.5.3-3 CIS – Vertical Direction (Z) – First Dominant Mode 02.5-232
Figure 02.5.1.5.3-4 CIS SG Compartment ATF Results – NS Direction (X) Transfer Function 02.5-233
Figure 02.5.1.5.3-5 CIS SG Compartment ATF Results – EW Direction (Y) Transfer Function 02.5-234
Figure 02.5.1.5.3-6 CIS SG Compartment ATF Results – Vertical Direction (Z) Transfer Function 02.5-235
Figure 02.5.1.5.3-7 CIS PZR Compartment ATF Results – NS Direction (X) Transfer Function 02.5-236
Figure 02.5.1.5.3-8 CIS PZR Compartment ATF Results – EW Direction (Y) Transfer Function 02.5-237
Figure 02.5.1.5.3-9 CIS PZR Compartment ATF Results – Vertical Direction (Z) Transfer Function 02.5-238
Figure 02.5.1.5.3-10 CIS D-SG ATF Results – NS Direction (X) Transfer Function 02.5-239
Figure 02.5.1.5.3-11 CIS D-SG ATF Results – EW Direction (Y) Transfer Function 02.5-240
Figure 02.5.1.5.3-12 CIS D-SG ATF Results – Vertical Direction (Z) Transfer Function 02.5-241
Figure 02.5.1.5.4-1 East PS/B – NS Direction (X) – First Dominant Mode 02.5-242
Figure 02.5.1.5.4-2 East PS/B – EW Direction (Y) – First Dominant Mode 02.5-243
Figure 02.5.1.5.4-3 East PS/B – Vertical Direction (Z) – First Dominant Mode 02.5-244
Figure 02.5.1.5.4-4 East PS/B ATF Results – NS Direction (X) Transfer Function at Center of Building 02.5-245
Figure 02.5.1.5.4-5 East PS/B ATF Results – EW Direction (Y) Transfer Function at Center of Building 02.5-246
Figure 02.5.1.5.4-6 East PS/B ATF Results – Vertical Direction (Z) Transfer Function at Center of Building 02.5-247
Figure 02.5.1.5.5-1 West PS/B – NS Direction (X) – First Dominant Mode 02.5-248
Figure 02.5.1.5.5-2 West PS/B – EW Direction (Y) – First Dominant Mode 02.5-249
Figure 02.5.1.5.5-3 West PS/B – Vertical Direction (Z) – First Dominant Mode 02.5-250
Figure 02.5.1.5.5-4 West PS/B ATF Results – NS Direction (X) Transfer Function at Center of Building 02.5-251
Figure 02.5.1.5.5-5 West PS/B ATF Results – EW Direction (Y) Transfer Function at Center of Building 02.5-252
Figure 02.5.1.5.5-6 West PS/B ATF Results – Vertical Direction (Z) Transfer Function at Center of Building 02.5-253
Figure 02.5.1.5.6-1 A/B – NS Direction (X) – First Dominant Mode 02.5-254
Figure 02.5.1.5.6-2 A/B – EW Direction (Y) – First Dominant Mode 02.5-255

Figure 02.5.1.5.6-3 A/B – Vertical Direction (Z) – First Dominant Mode 02.5-256
Figure 02.5.1.5.6-4 A/B ATF Results – NS Direction (X) Transfer Function at Center of Building 02.5-257
Figure 02.5.1.5.6-5 A/B ATF Results – EW Direction (Y) Transfer Function at Center of Building 02.5-258
Figure 02.5.1.5.6-6 A/B ATF Results – Vertical Direction (Z) Transfer Function at Center of Building 02.5-259

LIST OF TABLES

Table **Title** **Page No.**

Table 02.3.1-1 Main Dimensions of the R/B Complex 02.3-5
Table 02.3.1.4-1 Main Dimensions of the East PS/B 02.3-5
Table 02.3.1.4-2 Main Dimensions of the West PS/B 02.3-5
Table 02.3.1.5-1 Main Dimensions of the A/B 02.3-6
Table 02.3.1.6-1 Main Dimensions of the ESWPC 02.3-6
Table 02.4.1.1.1-1 Summary of Element Types 02.4-14
Table 02.4.1.1.1-2 Input Material Properties 02.4-15
Table 02.4.1.1.3-1 Assigned Stiffness and Damping Properties 02.4-16
Table 02.4.1.1.3-2 Summary of SC Module Stiffness and Damping Values 02.4-17
Table 02.5.1.3-1 Typical 1g Analysis Result Observations 02.5-16
Table 02.5.1.3-2 Typical Comparison of Fundamental Frequencies 02.5-16
Table 02.5.1.3-3 Typical Comparison of ATF 02.5-16
Table 02.5.1.3-4 Mass Comparison of the Detailed and Dynamic Models 02.5-17
Table 02.5.1.3.1.1-1 R/B Floor Mass Comparison 02.5-18
Table 02.5.1.3.1.1-2 R/B 1g Static Analysis – Roof Displacement Comparison 02.5-18
Table 02.5.1.3.1.2-1 R/B Modal Analysis Detailed Model – NS Direction (X) 02.5-18
Table 02.5.1.3.1.2-2 R/B Modal Analysis Dynamic Model – NS Direction (X) 02.5-19
Table 02.5.1.3.1.2-3 R/B Modal Analysis Detailed Model – EW Direction (Y) 02.5-19
Table 02.5.1.3.1.2-4 R/B Modal Analysis Dynamic Model – EW Direction (Y) 02.5-19
Table 02.5.1.3.1.2-5 R/B Modal Analysis Detailed Model – Vertical Direction (Z) 02.5-19
Table 02.5.1.3.1.2-6 R/B Modal Analysis Dynamic Model – Vertical Direction (Z) 02.5-20
Table 02.5.1.3.2.1-1 PCCV 1g Static Analysis – Displacement Comparison 02.5-20
Table 02.5.1.3.2.2-1 PCCV Modal Analysis Detailed Model – NS Direction (X) 02.5-20
Table 02.5.1.3.2.2-2 PCCV Modal Analysis Dynamic Model – NS Direction (X) 02.5-20
Table 02.5.1.3.2.2-3 PCCV Modal Analysis Detailed Model – EW Direction (Y) 02.5-21
Table 02.5.1.3.2.2-4 PCCV Modal Analysis Dynamic Model – EW Direction (Y) 02.5-21
Table 02.5.1.3.2.2-5 PCCV Modal Analysis Detailed Model – Vertical Direction (Z) 02.5-21
Table 02.5.1.3.2.2-6 PCCV Modal Analysis Dynamic Model – Vertical Direction (Z) 02.5-21
Table 02.5.1.3.3.1-1 CIS 1g Static Analysis – Displacement Comparison – Uncracked Model 02.5-22
Table 02.5.1.3.3.1-2 CIS 1g Static Analysis – Displacement Comparison – Cracked Model 02.5-22
Table 02.5.1.3.3.2-1 CIS Modal Analysis – Detailed Model – NS Direction (X) 02.5-23

Table 02.5.1.3.3.2-2 CIS Modal Analysis – Dynamic Model – NS Direction (X) 02.5-23
Table 02.5.1.3.3.2-3 CIS Modal Analysis – Detailed Model – EW Direction (Y) 02.5-23
Table 02.5.1.3.3.2-4 CIS Modal Analysis – Dynamic Model – EW Direction (Y) 02.5-23
Table 02.5.1.3.3.2-5 CIS Modal Analysis – Detailed Model – Vertical Direction (Z) 02.5-24
Table 02.5.1.3.3.2-6 CIS Modal Analysis – Dynamic Model – Vertical Direction (Z) 02.5-24
Table 02.5.1.3.4.1-1 East PS/B 1g Static Analysis – Roof Displacement Comparison 02.5-25
Table 02.5.1.3.4.2-1 East PS/B Modal Analysis – Detailed Model – NS Direction (X).....02.5-25
Table 02.5.1.3.4.2-2 East PS/B Modal Analysis – Dynamic Model – NS Direction (X).....02.5-25
Table 02.5.1.3.4.2-3 East PS/B Modal Analysis – Detailed Model – EW Direction (Y).....02.5-25
Table 02.5.1.3.4.2-4 East PS/B Modal Analysis – Dynamic Model – EW Direction (Y).....02.5-25
Table 02.5.1.3.4.2-5 East PS/B Modal Analysis – Detailed Model – Vertical Direction (Z).....02.5-26
Table 02.5.1.3.4.2-6 East PS/B Modal Analysis – Dynamic Model – Vertical Direction (Z).....02.5-26
Table 02.5.1.3.5.1-1 West PS/B 1g Static Analysis – Roof Displacement Comparison 02.5-26
Table 02.5.1.3.5.2-1 West PS/B Modal Analysis – Detailed Model – NS Direction (X) 02.5-26
Table 02.5.1.3.5.2-2 West PS/B Modal Analysis – Dynamic Model – NS Direction (X) 02.5-27
Table 02.5.1.3.5.2-3 West PS/B Modal Analysis – Detailed Model – EW Direction (Y) 02.5-27
Table 02.5.1.3.5.2-4 West PS/B Modal Analysis – Dynamic Model – EW Direction (Y) 02.5-27
Table 02.5.1.3.5.2-5 West PS/B Modal Analysis – Detailed Model – Vertical Direction (Z).....02.5-27
Table 02.5.1.3.5.2-6 West PS/B Modal Analysis – Dynamic Model – Vertical Direction (Z).....02.5-27
Table 02.5.1.3.6.1-1 A/B 1g Static Analysis – Roof Displacement Comparison 02.5-28
Table 02.5.1.3.6.2-1 A/B Modal Analysis – Detailed Model – NS Direction (X) 02.5-28
Table 02.5.1.3.6.2-2 A/B Modal Analysis – Dynamic Model – NS Direction (X) 02.5-28
Table 02.5.1.3.6.2-3 A/B Modal Analysis – Detailed Model – EW Direction (Y) 02.5-28
Table 02.5.1.3.6.2-4 A/B Modal Analysis – Dynamic Model – EW Direction (Y).....02.5-28
Table 02.5.1.3.6.2-5 A/B Modal Analysis – Detailed Model – Vertical Direction (Z) 02.5-29

Table 02.5.1.3.6.2-6 A/B Modal Analysis – Dynamic Model – Vertical Direction (Z).....02.5-29

Table 02.5.1.3.7.1-1 R/B Complex 1g Static Analysis – Roof Displacement Comparison 02.5-29

Table 02.5.1.3.7.2-1 R/B Complex Modal Analysis – Detailed Model – NS Direction (X).....02.5-30

Table 02.5.1.3.7.2-2 R/B Complex Modal Analysis – Dynamic Model – NS Direction (X).....02.5-30

Table 02.5.1.3.7.2-3 R/B Complex Modal Analysis – Detailed Model – EW Direction (Y).....02.5-30

Table 02.5.1.3.7.2-4 R/B Complex Modal Analysis – Dynamic Model – EW Direction (Y).....02.5-31

Table 02.5.1.3.7.2-5 R/B Complex Modal Analysis – Detailed Model – Vertical Direction (Z).....02.5-31

Table 02.5.1.3.7.2-6 R/B Complex Modal Analysis – Dynamic Model – Vertical Direction (Z).....02.5-31

Table 02.5.1.5-1 Nodes Coordinates List.....02.5-32

Table 02.5.1.5-2 Nodes Equation Numbers.....02.5-32

Table 02.5.1.5-3 Structural Stiffness on the Nodes.....02.5-32

Table 02.5.1.5.1-1 R/B-FH/A Dominant Mode Contributions 02.5-33

Table 02.5.1.5.2-1 PCCV Dominant Mode Contributions.....02.5-33

Table 02.5.1.5.3-1 CIS Dominant Mode Contributions.....02.5-34

Table 02.5.1.5.4-1 East PS/B Dominant Mode Contributions 02.5-34

Table 02.5.1.5.5-1 West PS/B Dominant Mode Contributions 02.5-34

Table 02.5.1.5.6-1 A/B Dominant Mode Contributions.....02.5-35

02.1.0 INTRODUCTION

The design of the US-APWR R/B complex is based on the analyses of the seismic responses of a dynamic model, considering the effects of Soil-Structure Interaction (SSI) and Structure Soil Structure Interaction (SSSI). The R/B complex consists of the Reactor Building (R/B), the Pre-stressed Concrete Containment Vessel (PCCV), the Containment Internal Structure (CIS) including the Reactor Coolant Loop (RCL), the East Power Source Building (East PS/B), the West Power Source Building (West PS/B), the Auxiliary Building (A/B), and the Essential Service Water Pipe Chase (ESWPC), all on a common foundation basemat. All structures on the basemat are seismic category I structures with the exception of the A/B which is a seismic category II structure. The SSSI analysis is for the seismic response of the R/B complex considering its potential interaction with the Turbine Building (T/B). The T/B is a seismic category II structure. Consistent with Nuclear Regulatory Commission (NRC) Standard Review Plan (SRP) 3.7.2 (Reference 02-5), the seismic response analyses incorporates each of the following issues:

- ability of the model to adequately represent the dynamic properties of the structures, and to address the effects of concrete cracking on the seismic response.
- ability of the model to develop design basis In-Structure Response Spectra (ISRS) for seismic qualification of the equipment.
- ability of the model to accurately predict seismic displacements and internal forces

A Dynamic Finite Element (FE) model is developed representing the dynamic properties of the R/B complex consisting of the R/B, PCCV, CIS, East PS/B, West PS/B, A/B, ESWPC, and the common foundation basemat. To account for the effects of dynamic coupling of the CIS with equipment and pipe, the model also includes the RCL representing the stiffness and mass inertia properties of the major equipment and pipe supported by the CIS. Section 02.4.1 in this Technical Report (TeR) presents the methodology used for development of the Dynamic FE model for SASSI analyses of the R/B complex. The results of the validation analyses of the model are described in Section 02.5.1.3.

Two different levels of stiffness and damping properties are assigned to the Dynamic FE model in order to capture variations of the material properties of the structural members due to cracking. The first level represents the full stiffness (uncracked concrete) of the structures corresponding to low stress levels, and the second level represents the reduced stiffness (cracked concrete) of the structures corresponding to high stress levels. Operating-Basis Earthquake (OBE) damping values are assigned to the model with full stiffness (uncracked concrete) in order to represent the lower level of dissipation of energy in the structure when subjected to lower stresses. Safe-Shutdown Earthquake (SSE) damping values are assigned to the model with reduced (cracked) concrete properties in order to represent the higher dissipation of energy in the structure when subjected to high stresses. Within the CIS, there are structural components which are exceptions for the reduced stiffness conditions (e.g., CIS primary shield walls). Two SSI analyses of the R/B complex are performed for each soil profile corresponding to each of the two bounding levels of stiffness and damping. The responses obtained from the two SSI analyses for each soil profile, i.e., twelve analyses in all, are enveloped in order to address the possible range of effects of concrete cracking on the seismic response of the building.

Further, the Dynamic FE model is combined with the T/B to develop the SSSI model. This model is analyzed for soil profiles where SSSI is possible. ISRS are then developed for the R/B complex and these are enveloped with the enveloped ISRS developed for the SSI model described above.

The Dynamic model described in this report is the analysis model for the R/B complex for the SSI and SSSI analyses. Each of the structures that comprise the Dynamic model are validated separately and then the whole Dynamic model is validated. The validations of the Dynamic models of the R/B, PCCV, CIS, A/B, East PS/B and West PS/B, the whole Dynamic model, and subsequent translation from ANSYS to SASSI are performed following the methodology described in Section 02.4.1.2 and Section 02.4.3.

02.2.0 PURPOSE

The purpose of Part 2 of this TeR is to outline the technical approach for development of the seismic response analyses model of the R/B complex.

02.3.0 OBJECTIVES

The objective of the Part 2 of this TeR is to describe the development and validation of the R/B complex Three Dimensional (3-D) Dynamic FE model for SSI and SSSI analyses using SASSI (Reference 02-1). The model is first developed using the ANSYS finite element software and is validated using ANSYS. The completed model is then translated into SASSI format and re-validated in SASSI.

02.3.1 Description of the R/B Complex Structures

The US-APWR R/B complex consists of the R/B and Fuel Handling Area (FH/A), PCCV, CIS, A/B, East PS/B, West PS/B, and ESWPC supported on a common reinforced concrete basemat. The R/B, East PS/B, West PS/B, and A/B are combined structures that share structural shear walls. The PCCV and CIS are independent structures that share the common basemat with the other structures. The ESWPC located at the south side of the R/B complex shares the common southern exterior wall with R/B, East PS/B and West PS/B. Figure 02.3.1-1 through Figure 02.3.1-5 show the layout of the various structures of the R/B complex.

The entire R/B complex is represented by the Dynamic model. The R/B complex is approximately 336 ft–4 in. in the North-South (NS) direction and 409ft–8in. in the East-West (EW) direction,The total footprint area is 127,016 ft^2. The model weighs approximately 1,218,900 kips in total, with an average contact pressure beneath the foundation of approximately 9.6 ksf. The major features that define the geometry of the Dynamic model in Section 02.3.2 are presented in the following sections for each structure within the R/B complex. Table 02.3.1-1 presents the major dimensions of the R/B complex.

02.3.1.1 R/B

The R/B is a rectangular reinforced concrete structure consisting of vertical shear and bearing walls and horizontal slabs/roofs with five major floors that make up the following four functional areas:

- Safety system pumps and heat exchanger area;
- Fuel handling area;
- Main steam and feed water area;
- Safety related electrical area.

The FH/A is located on the northern side of the R/B. The operating floor of the FH/A is at the same elevation as the PCCV operating floor (Elevation 76ft-5in.) and is located adjacent to the main equipment hatch of the PCCV. The FH/A houses the following equipment and facilities:

- Fuel handling crane;
- Fuel transfer system, including the refueling canal;
- Cask wash-down pit;
- Cask pit;
- Fuel inspection pit;
- New fuel storage pit and storage racks;
- Spent fuel pit and storage racks;
- Hatchway providing access to truck bay area on ground floor.

The fuel handling crane is a bridge crane located to span the spent fuel pit, refueling canal, and cask loading pit. The crane is supported on a steel frame structure located above the FH/A operating floor. The steel frame structure resides inside the reinforced concrete walls of the FH/A area of the R/B .

02.3.1.2 PCCV

The PCCV has two concrete buttresses set diametrically opposite to each other at azimuths 90° and 270° (East and West sides). Its cylindrical shell has several openings allowing for transfer of equipment, personnel, and penetration of steam and feed water pipes into and/or from the PCCV. The dome and cylindrical shell concrete are specified to have a compressive strength (f'_c) of 7,000 psi.

The PCCV also supports a polar crane supported on a steel runway girder and corbel system located at elevation 145ft-7in.

02.3.1.3 CIS

The CIS includes the structures above the mat foundation that are internal to, but not supported by, the PCCV. (The CIS is approximately 140 ft in diameter with reinforced concrete floors at elevations 25ft-3in., 50ft-2in., and 76ft-5in. The top of the Steam Generator (SG) compartments reach an elevation of 112ft-0in. and the top of the pressurizer compartment is at elevation 139ft-6in). The structure supports the Pressurizer (PZR), Reactor Vessel (RV), and the RCL components. The RCL components consist of the SG, Reactor Coolant Pumps (RCP) and associated reactor coolant pipe. The CIS also provides storage and containment of the refueling water. The main structural elements of the CIS are Steel-Concrete Structures. These modules are comprised of steel face plates bonded to a thick concrete core with headed studs and are tied to each other by transverse plates.

02.3.1.4 East PS/B and West PS/B

The East PS/B and West PS/B each contain three identical gas turbine generators which are separated by physical barriers and located at the ground floor elevation (El. 3ft-7in.). Safety related chillers, electrical equipment, I&C and heating ventilating and air conditioning equipment are also located in these buildings. The buildings consist of reinforced concrete shear/bearing walls, columns, roof, and floor slabs. The major dimensions that define the geometries of the East PS/B and West PS/B and the characteristics in each structure are presented in Table 02.3.1.4-1 and Table 02.3.1.4-2, respectively.

02.3.1.5 A/B

The A/B consists of reinforced concrete shear/bearing walls, columns, roof, and floor slabs. Steel beams are used to provide additional support to part of the roof slab and third floor slab. The reinforced concrete walls and columns carry the vertical and lateral seismic loads from the roof and floor slabs and transfer them to the basemat. The lateral seismic loads are resisted primarily by the reinforced concrete shear walls. The major dimensions that define the geometry of the A/B and the characteristics in the structure are presented in Table 02.3.1.5-1.

02.3.1.6 ESWPC

The ESWPC consists of reinforced concrete shear/bearing walls and floor slabs. The major dimensions that define the geometry of the ESWPC and the characteristics in the structure are presented in Table 02.3.1.6-1.

02.3.2 Dynamic Finite Element Model of the R/B Complex

The Dynamic FE model of the R/B complex is developed using ANSYS (Reference 02-2) and then is translated to SASSI. The purpose of the SASSI structural model is to adequately represent the dynamic (stiffness and mass) properties of the R/B complex structures, and to capture or address the following effects:

- Coupling of the structure with the major Nuclear Steam Supply System (NSSS) equipment and piping;
- Flexibility of the common basemat foundation;
- Variation of stiffness and damping due to concrete cracking;
- Local out-of-plane modes of vibration for slabs with frequencies up to 50 Hz;

The resulting Dynamic FE model is used for the SASSI analyses of the R/B complex structures documented in Part 3 of this TeR to provide input design parameters that appropriately address the frequency dependence of the SSI impedance, layering of the subgrade, elevation of the water table, and dissipation of energy due to material damping.

A Detailed FE model is also developed using ANSYS to serve as a benchmark for the development of the Dynamic model. This Detailed model is a much more refined representation of the R/B complex than the Dynamic model. The Detailed model is highly consistent with the design drawings as far as wall and slab locations and contains a much finer mesh than the Dynamic FE model. The Dynamic model does have walls and floors moved slightly from the design drawing locations in order to achieve a mesh that is acceptable to SASSI.

A set of static and dynamic analyses are performed on the combined Detailed and Dynamic FE models to validate the dynamic properties of the combined Dynamic FE model before it is translated into SASSI. Once translated to SASSI, validation SSI analyses are performed with the newly translated R/B complex structure dynamic model resting on the surface of a uniform half-space with very high stiffness (hard rock) to simulate fixed base conditions. Acceleration Transfer Functions (ATFs) are obtained from the SASSI validation analyses at selected nodes which are then compared to the results obtained from harmonic analyses of the ANSYS Dynamic FE model.

02.3.3 Consideration of Concrete Cracking in Dynamic Analyses

The cracking of concrete affects the dynamic characteristics of structures that are constructed of reinforced concrete, pre-stressed concrete and SC modules, altering their responses when subjected to seismic excitation. An important objective of the dynamic structural models is to appropriately address the variations of the dynamic properties of these structures reflecting the extent of cracking that can occur under different loading conditions.

Two levels of stiffness and damping properties are developed and assigned to the structural models used for seismic response analyses in order to capture the variations of structural stiffness and damping due to concrete cracking: (1) full (uncracked concrete) stiffness corresponding to low stress levels; and (2) reduced (cracked concrete) stiffness corresponding to high stress levels. In accordance with the associated stress level and recommendations of RG 1.61 (Reference 02-3), lower OBE values for structural damping are assigned in conjunction with the full (uncracked concrete) stiffness properties, and higher SSE damping values are assigned in conjunction with the reduced (cracked concrete) stiffness properties. In order to ensure that the design of the R/B complex properly addresses the effects of concrete cracking, the envelope of the results obtained from the seismic response analyses of Dynamic FE models with full and reduced stiffness are used to develop the seismic design.

Section 02.4.2 describes the structural modeling approach used to include the variation of stiffness and damping properties due to concrete cracking. Provisions of the current NRC and standard industry practices are reviewed for consideration of the effects of concrete cracking when modeling the effective stiffness of reinforced concrete members for dynamic analyses. The reduction of stiffness of the reinforced concrete members that crack under the most critical load combination are adjusted based on the provisions and recommendations of standard industry practices. Appendix 2-A of this TeR provide the technical basis for the selection of the stiffness reduction levels for the PCCV.

Table 02.3.1-1 Main Dimensions of the R/B Complex

Table 02.3.1.4-1 Main Dimensions of the East PS/B

Table 02.3.1.4-2 Main Dimensions of the West PS/B

Table 02.3.1.5-1 Main Dimensions of the A/B

Table 02.3.1.6-1 Main Dimensions of the ESWPC

Security-Related Information – Withheld Under 10 CFR 2.390

Figure 02.3.1-1 Plan View of R/B Complex at EL 3'-7"

Security-Related Information – Withheld Under 10 CFR 2.390

Figure 02.3.1-2 North-South Cross-Section of R/B Complex (Column Line of 13R (Figure 02.3.1-1) looking East)

Security-Related Information – Withheld Under 10 CFR 2.390

Figure 02.3.1-3 North-South Cross-Section of R/B Complex (Column Line of 4R (Figure 02.3.1-1) looking East)

Security-Related Information – Withheld Under 10 CFR 2.390

Figure 02.3.1-4 East-West Cross-Section of R/B Complex (Column Line of FR (Figure 02.3.1-1) looking North)

Security-Related Information – Withheld Under 10 CFR 2.390

Figure 02.3.1-5 East-West Cross-Section of R/B Complex (Column Line of K2R (Figure 02.3.1-1) looking North)

02.4.0 APPROACH / METHODOLOGY

02.4.1 SASSI Dynamic Finite Element Model of the R/B Complex

The Dynamic FE model of the R/B complex is developed and validated using ANSYS (Reference 02-2) and then translated into SASSI (Reference 02-1) format. The dynamic model is a simplified, coarsely meshed model that is validated against a more refined, detailed model. The translation process is described in the following steps:

Step 1: Develop the R/B Complex Dynamic FE Model

ANSYS Workbench and ANSYS parametric design language are used to develop an integrated 3-D FE model that includes the R/B, PCCV, CIS, A/B, East and West PS/Bs, and ESWPC coupled with the lumped mass stick model representing the dynamic properties of the RCL. The numbering of the nodes is adjusted following the guidelines of the SASSI manual in order to optimize the computational effort.

Step 2: Validate the R/B Complex Dynamic FE Model to ensure that the model adequately captures the dynamic behavior of the structures

The Dynamic FE model is separated into six parts for the purpose of validation: R/B-FH/A, PCCV, CIS (with RCL), A/B, East PS/B, and West PS/B. The ESWPC is split and included in the R/B-FH/A, East PS/B, and West PS/B models. Static, modal, harmonic response and stiffness analyses using ANSYS solvers are performed on each of the six parts of the Dynamic FE model by establishing fixed boundary conditions at the base of each structure. An identical set of fixed base analyses are also performed on Detailed FE models of each structure. The results obtained from the Dynamic FE models and Detailed FE models are compared to demonstrate the ability of the less refined Dynamic FE model to adequately capture the dynamic behavior of the corresponding Detailed FE models.

After all six parts are validated independently; the same process is used to validate the combined Dynamic FE model.

Step 3: Translate the Dynamic FE Model into SASSI format and verify the accuracy of the translation

The translator built into the SASSI code serves as the platform for the translation of the Dynamic FE model from ANSYS to SASSI house module format. In order to validate the translation of the model, a validation SSI analysis is performed on the SASSI Dynamic FE model resting on a very stiff elastic half space. The dynamic properties of the model revealed by the resulting ATFs at selected locations are compared to the fixed base dynamic properties and responses obtained from ANSYS modal analyses to ensure the translation is completed correctly.

02.4.1.1 Development of the R/B Complex Dynamic FE Model

02.4.1.1.1 Finite Element Modeling

The R/B complex Dynamic FE model consists of beam, shell, solid, and spring elements. The use of finite elements provides an accurate representation of the dynamic properties of the structures and the foundation that enables an accurate modeling of dynamic interaction with the flexible foundation and the surrounding soil. Shell elements are used to model the

reinforced concrete shear walls and slabs. 3-D beam elements model the reinforced concrete or steel columns and beams. Solid elements are used to model the basemat foundation and the massive structural members of the CIS. Spring and beam elements are used to model the supports and connection of the RCL model with the CIS FE mesh. The ANSYS finite element types used in the model are compatible with the SASSI built in converter.

The Dynamic FE model is presented in Figure 02.4.1.1.1-1. This model has a total of 33,564 nodes, 47,580 elements and has an average mesh size of approximately 9 ft. The Dynamic FE model is based on the Detailed FE model presented in Figure 02.4.1.1.1-2. The Detailed FE model has a total of 62,252 nodes, 74,961 elements, with an average mesh size of approximately 5 ft. Figure 02.4.1.1.1-3 and Figure 02.4.1.1.1-4 present the detailed PCCV and CIS FE models, respectively. Table 02.4.1.1.1-1 provides the different element types that are used in the Dynamic FE model. Table 02.4.1.1.1-2 provides the input material properties.

The development of the model ensures that the connection between two different element types is such that an adequate transfer of forces and/or moments from one structural component to the other is enabled. The nodes of the solid elements have only three translational degrees of freedom and can therefore not transfer the moments from shell or beam elements. In order to enable the transfer of bending moments from the walls modeled by shell elements to the basemat and massive concrete sections of the CIS modeled by solid elements, the shell elements are extended into or overlaid on the solid elements as shown in Figure 02.4.1.1.1-5. A special layer of transitional rigid shell elements is created between the CIS reactor cavity top flange solid elements and the adjacent surrounding SC walls as shown in Figure 02.4.1.1.1-6.

In addition, each node of the SASSI shell elements has five degrees of freedom that enable beam elements to transfer forces and bending moments to shell elements but not torsional moments. Therefore, massless beam elements are generated on the surface of the shell or solid elements as shown in Figure 02.4.1.1.1-7 and Figure 02.4.1.1.1-8 in order to provide adequate transfer of moments from beams in all three rotational degrees of freedom. For beams or columns connecting to slabs or walls in the R/B model, the effect of adding torsional stiffness to the slab and wall shell elements (Allman in-plane rotational stiffness in ANSYS SHELL63 element) is evaluated and the impact on the results is found to be negligible.

02.4.1.1.2 Discretization Considerations: Mesh Size

The R/B complex Dynamic FE model has an adequate number of discrete mass degrees of freedom to capture the global and local translational, rocking, and torsional responses of the structures. The element size is selected such that the structural response is not significantly affected by further refinement of the element size. The mesh also ensures that the discretized structures with full (uncracked concrete) stiffness properties are able to capture the local responses and responses of significant modes of vibration with frequencies equal to or below 70 Hz which guarantees the objective of calculating the mode and mode shapes up to a frequency of 50 Hz.

For consideration of wave passage in the structure only, in order to transmit shear waves with frequencies up to 70 Hz, the maximum element size cannot be greater than one fifth of the wavelength to be transmitted (Reference 02-1). The maximum structural element size is determined as follows:

Given: Concrete Compressive Strength f_c'=5,000 psi, Poisson's Ratio υ =0.17
and Unit Weight γ = 0.15 kcf

The Young's Modulus (E_c) and Shear Modulus (G_s) of normal weight concrete are (Reference 02-4):

$$E_c = 57\sqrt{f_c'} = 57 \cdot \sqrt{5000} = 4031\,\text{ksi} = 580393\,\text{ksf}$$

$$G_c = \frac{E_c}{2(1+\nu)} = \frac{580393}{2(1+0.17)} = 248031\,\text{ksf} \qquad \text{Equation 02.4.1.1.2-1}$$

The shear wave velocity of the concrete is:

$$Vs_c = \sqrt{\frac{G_c \cdot g}{\gamma}} = \sqrt{\frac{248031 \cdot 32.2}{0.15}} = 7297\text{ft/sec} \qquad \text{Equation 02.4.1.1.2-2}$$

Wavelength of the wave with frequency of 70 Hz:

$$\lambda_c = TVs_c = \frac{Vs_c}{f_{\max}} = \frac{7297}{70} = 104.2\,\text{ft} \qquad \text{Equation 02.4.1.1.2-3}$$

The maximum size of an element determined by wave passage in the structure alone:

$$d_{FE} = \frac{\lambda_c}{5} = \frac{104.2\,\text{ft}}{5} \approx 21\,\text{ft} \qquad \text{Equation 02.4.1.1.2-4}$$

Therefore, the mesh size of the model should be equal to or less than 21 ft in order to be able to transfer shear waves with frequencies of up to 70 Hz. The average mesh size in the Dynamic FE model of 9 ft satisfies this requirement.

02.4.1.1.3 Modeling of Stiffness and Damping

The SASSI house module introduces the stiffness and damping properties of the structure into SSI analysis in the form of a frequency independent complex stiffness matrix (Refer to the SASSI Theoretical Manual, Reference 02-1). Complex moduli are used to represent the stiffness and damping properties of the different structural materials. This leads to stiffness and damping ratios which can be different for different materials assigned to the finite elements.

While maintaining geometry, mass and FE meshing, two different levels of stiffness are assigned to the model in order to address the effect of uncracked and cracked concrete on the seismic response. The responses obtained from the analyses of the models with two different stiffness properties are enveloped to develop design seismic loads and ISRS used for the seismic design of pipe and equipment.

Table 02.4.1.1.3-1 provides the stiffness and damping properties assigned to the SASSI Dynamic FE model. Section 02.4.2 provides the background information for the values in this Table.

Two sets of stiffness and damping values are developed to capture the potential range of stresse and associated cracking levels in each of the different concrete structure types (or categories) in the CIS, including various Reinforced Concrete (RC) structural elements, the SC primary and secondary shielding walls, and the massive concrete portions of the structure. There is also structural steel with non-structural concrete infill in some portions of the CIS. For these sections, no concrete stiffness or damping is applied. The first set of values represents limited concrete cracking and higher stiffness anticipated for seismic loading during normal plant operations (referred to as Loading Condition A), and the second set of values represents

a significant reduction in stiffness associated with extensive concrete cracking under seismic loading coupled with accident thermal conditions (referred to as Loading Condition B). The two sets of category-specific stiffness and damping values are listed in Table 02.4.1.1.3-2. When the CIS is combined with other buildings in the R/B complex, Loading Condition A is considered as the Full Stiffness condition and Loading Condition B as the Reduced Stiffness condition. Stiffness and damping of the steel framing and massive concrete in the CIS are assigned according to Table 02.4.1.1.3-1.

02.4.1.1.4 Modeling of Mass

The mass included in the R/B complex Dynamic FE model includes contributions from the structural mass in addition to that of equipment, dead loads, and live loads.

Generally, the structural mass is assigned as a density to the finite elements based on the material properties of the components of the structures. The density is then increased to account for equipment, live, snow and other applicable loads. A mass equivalent to 25% of floor design live load and 75% of roof design snow load is included in the model in accordance with SRP 3.7.2 Acceptance Criteria II.1.D (Reference 02-5). Each load is applied over a particular area and the density of the elements in that area is increased such that the total increase in mass matches the mass of the applied loads.

Equipment load also includes a 50 psf dead load to account for miscellaneous pipe, minor equipment, and raceway loads applied on slabs in the R/B complex model, with the exception of a few locations where a heavier pipe load is used instead (e.g., main steam and feedwater pipe).

The above process is not applicable for the NSSS and major pipe that constitutes the RCL. The RCL dynamic mass is included directly in the RCL model.

The mass is applied to the Dynamic FE model in two steps. First, a mass density equal to the sum of the structural self-weight and pipe load is calculated and assigned to each of the shell elements modeling the R/B complex slabs. Where mass is carried by grating not explicitly modeled, the total mass supported is evenly distributed on the supporting walls and slabs.

The remaining loads are applied as either additional mass densities on slab shell elements or concentrated lumped masses on wall and slab key points.

The density and thickness of the elements are further modified to account for stiffness reductions due to minor openings and cracking, but it is done in such a way as to not change the mass of the elements. Refer to Section 02.4.1.1.5 for further discussion.

The PCCV Polar Crane and Fuel Handling cranes are modeled in their respective parked locations with trolley masses and lifted load masses (Spent fuel cask, RV head, etc.) included.

The mass used for the New Fuel Storage Pit (NFSP) and Spent Fuel Pit (SFP) includes the mass of the fuel and the fuel storage racks contained within the pits. This is accomplished as described above by adding the masses as lumped masses to the concrete slabs of the pits (pools). The dynamic characteristics of the racks are not modeled or coupled with the structure. Liquid masses contained in the SFP, Emergency Feed Water Pits (EFWP), and Refueling Water Storage Pit (RWSP) are modeled as directional masses using mass elements attached to walls and slabs. In accordance with Reference 02-6, the hydrodynamic responses of the water in the SFP and the EFWPs are evaluated, and the hydrodynamic masses are separated into the lower impulsive and the upper convective parts. Figure 02.4.1.1.4-1 shows a representative dynamic model for the SFP when it is subject to seismic motion in the NS direction. The impulsive mass is rigidly fastened to the walls as it moves with the walls

responding to the seismic excitation. Depending on the ratio of the water depth to the pit width, the lower portion of the impulsive part can be considered as fully constrained which responds as a rigid body. The impulsive pressure is evenly and uniformly divided into a pressure force on the wall accelerating into the fluid, and a suction force on the opposite wall accelerating away from the fluid. The convective mass is also included in the Dynamic FE model and is fastened to the walls by springs that produce the period of vibration corresponding to the period of fluid sloshing which is usually several seconds. The stiffness's of these connecting springs are calculated based on the sloshing period and are usually small enough such that the effective forces transferred to the walls are negligible.

02.4.1.1.5 Adjustment of Stiffness and Mass Properties

The mesh of the Dynamic FE model does not always permit an accurate modeling of the openings in the walls. The elastic modulus and thickness of shell elements are adjusted to accurately model the reduction of shear stiffness of the wall due to openings.

The density of shell elements is also adjusted to accurately represent the mass of the wall accounting for openings and the adjusted wall thickness.

Finite element analyses are performed using ANSYS to obtain the stiffness reduction factors needed to adjust the material properties and account for the reduced stiffness due to the shear wall openings. The correction factors are obtained by comparing the results from the static analyses of two detailed solid FE models shown in Figure 02.4.1.1.5-1A and B. Model A represents the actual geometry of the wall with openings, and model B represents the wall without openings. Unit displacements are applied at the top of each model in both the in-plane and the out-of-plane directions, to generate the reactions at the bottom, which are then used to calculate the in-plane and out-of-plane wall stiffness. The ratio between the reactions obtained from model A and model B is used to determine out-of-plane stiffness reduction factors (m) and the in-plane stiffness reduction factor (n) that are then used to determine the adjusted elastic modulus (E_o), thickness (t_o), and density (γ_o) of the wall as described in Section 02.4.1.1.7.

02.4.1.1.6 Stiffness of Composite Steel-Concrete Beams and Columns

In the FH/A, the crane supporting steel columns and girts are continuously anchored to the exterior concrete walls with headed steel studs. The steel roof beams are also continuously anchored to the concrete roof slabs. The concrete/steel composite moment of inertia is based on the effective width of concrete and the degree of compositeness provided by the studs. The shear force that can be transferred between steel and concrete depends on the capacity of the studs, the yield strength of the steel section and the ultimate compressive strength of the effective concrete.

Based on AISC 360-05 Commentary (Reference 02-7), 75% of the composite transformed moment of inertia is used in calculating the effective moment of inertia of the composite section (I_{eff}):

$$I_{eff} = 0.75 \cdot I_{tr}$$ for a fully composite member Equation 02.4.1.1.6-1

$$I_{eff} = I_x + \sqrt{Q_n / C_f} \cdot (I_{tr} - I_x)$$ for a partially composite member, with $Q_n/C_f \geq 0.25$

Equation 02.4.1.1.6-2

Where: Q_n = shear capacity of the studs between the points of inflection (zero moment)
C_f = smaller of steel yield force or concrete ultimate compressive force
I_x = moment of inertia of the steel column or beam
I_{tr} = composite transformed moment of inertia, calculated as follows:

$$I_{tr} = I_X + \left(t_c + t_d + \frac{d}{2} - y_{bar} \right)^2 \cdot A_s + \frac{b_{eff} \cdot t_c^3}{12} + \left(y_{bar} - \frac{t_c}{2} \right)^2 \cdot b_{eff} \cdot t_c \qquad \text{Equation 02.4.1.1.6-3}$$

Where: t_c = slab or wall thickness
t_d = steel deck thickness, if any
d = depth of the steel member
y_{bar} = centroidal distance of the transformed section, measured from the top of concrete:

$$y_{bar} = \frac{0.5 \cdot b_{eff} \cdot t_c^2 + A_s \left(t_c + t_d + 0.5 \cdot d \right)}{b_{eff} \cdot t_c + A_s} \qquad \text{Equation 02.4.1.1.6-4}$$

A_s = area of the steel member
b_{eff} = effective width of concrete, after transforming to steel = b_e/n
b_e = effective width of concrete, before transforming to steel
n = modular ratio = E_s/E_c
E_s = Young's Modulus for steel
E_c = Young's Modulus for concrete

In order to incorporate the composite stiffness of the steel beams and the reinforced concrete slabs the moments of inertia of the beams are increased. This modeling approach provides an accurate representation of the actual out-of-plane bending stiffness of the composite concrete-steel cross-sections which is validated through comparison of responses obtained from the detailed and dynamic models.

In the above, the effective width of concrete (before transformation to steel section) is based on AISC 360-05, Section I3 as shown below.

In the Dynamic FE model, beam and shell elements are used to represent the individual members. The locations of the centerlines of the beam and shell elements are coincident so the effective bending stiffness of the section (*EI*) in the Dynamic FE model is the sum of the individual moments of inertia:

$$EI = \frac{t_c^{\,3} \cdot b_e}{12} \cdot E_c + I_X \cdot E_s \qquad \text{Equation 02.4.1.1.6-5}$$

Therefore, the moment of inertia of the beam element that results in bending stiffness of the section (*EI*) that is equivalent to the stiffness of the actual composite section is calculated as follows:

$$I_S = I_X \cdot \alpha = I_{eff} - \frac{t_c^{\,3} \cdot b_e}{12} \cdot \frac{E_c}{E_s} \qquad \text{Equation 02.4.1.1.6-6}$$

Where $\alpha = I_S / I_X$ is a factor used to adjust the bending moment of inertia of the beam element in the FE model in order to simulate the actual composite stiffness of the reinforced concrete-steel beam cross section.

In the CIS, the RC floors at elevations 50'-2" and 76'-5" are supported from below by steel beams in both radial and circumferential directions. The radial beams are significant and thus

explicitly modeled, while the majority of the less substantial circumferential beams are not directly modeled. However, their stiffness contributions are included by adjusting the RC floor stiffness using the correction factors obtained from modeling a representative section between two adjacent radial beams at both elevations.

02.4.1.1.7 Implementation of Stiffness Reduction in the Dynamic FE Model

The R/B complex Dynamic FE model only uses finite elements with isotropic material properties to represent the stiffness and mass properties of reinforced concrete members. The cracking of the concrete can affect different aspect of the stiffness of the members depending on the cracking pattern developed under different loading conditions. For example, high loads applied on slabs will generate cracks in the concrete that affect mainly the out-of plane stiffness and have a small effect on the in-plane stiffness of the slab. Modeling procedures are described for the reduction of stiffness properties of beam and shell elements in order to simulate different cracking effects.

The stiffness matrix of beam elements is defined by material properties (modulus of elasticity and Poisson's ratio) and the beam section properties (moment inertia, shear area, etc). The most convenient way to reduce the stiffness of those reinforced members modeled using beam elements is through assigning reduced section properties while maintaining the same modulus of elasticity and Poisson's ratio. For example, if the flexural stiffness is required to be reduced, then the bending moment inertia of the beam is reduced.

Four shell element input parameters including the modulus of elasticity (E_0), Poisson's ratio (ν), shell thickness (t_0) and unit weight (γ_0) define the properties of the modeled reinforced concrete member. The following procedures are used to reduce stiffness of the reinforced concrete member shell elements by adjusting the shell modulus of elasticity to value (E_c), the shell thickness to value (t_c) and the shell unit weight to value (γ_c):

Case 1: If the concrete cracking reduces both the in-plane and out-of-plane stiffness of the member by 1/n reduction factor, the adjusted properties of shell elements are:

$$E_c = \frac{1}{n} E_o \qquad \text{Equation 02.4.1.1.7-1}$$

$$t_c = t_0 \qquad \text{Equation 02.4.1.1.7-2}$$

$$\gamma_c = \gamma_o \qquad \text{Equation 02.4.1.1.7-3}$$

Case 2: If the concrete cracking reduces out-of-plane stiffness of the member by 1/n reduction factor and the in-plane stiffness remains the same, the adjusted properties of shell element are:

$$E_c = \sqrt{n} E_o \qquad \text{Equation 02.4.1.1.7-4}$$

$$t_c = \sqrt{\frac{1}{n}} t_0 \qquad \text{Equation 02.4.1.1.7-5}$$

$$\gamma_c = \sqrt{n} \gamma_o \qquad \text{Equation 02.4.1.1.7-6}$$

Case 3: If the concrete cracking reduces in-plane stiffness of the member by 1/n reduction factor and the out-of-plane stiffness remains the same, the adjusted properties of shell element are:

$$E_c = \frac{\sqrt{n}}{n^2} E_o \qquad \text{Equation 02.4.1.1.7-7}$$

$$t_c = \sqrt{n} t_0 \qquad \text{Equation 02.4.1.1.7-8}$$

$$\gamma_c = \frac{1}{\sqrt{n}} \gamma_o \qquad \text{Equation 02.4.1.1.7-9}$$

Changes in thickness and modulus of the elasticity provided above affect both the in-plane axial and shear stiffness of the shell element. Since the axial stiffness of the wall unlikely controls the response of slab and shear wall structures to the seismic loading, the changes of axial stiffness are justified. The reduced stiffness (cracked) Dynamic FE model is developed using Case 1, assuming in-plane and out-of-plane stiffness reduction.

02.4.1.1.8 Adjustment of Out-of-Plane Dynamic Properties of Slabs

The development of the Dynamic FE model requires simplifications of the model geometry in order to produce a regular mesh and to minimize the size of the model to be suitable for SSI analyses using SASSI. These simplifications in modeling the building geometry affect the spans of some of the floor slabs in the Dynamic R/B model and their local out-of-plane response. The stiffness and mass properties of these flexible slabs are adjusted to model the actual mass and stiffness properties of the slab.

The dynamic stiffness properties of the slabs at each of the major floor elevations are obtained by isolating each elevation. Figure 02.4.1.1.8-1 shows an FE model of the R/B floor slabs that is extracted from the Detailed FE model. Boundary conditions are established as shown in Figure 02.4.1.1.8-2 at the upper and lower border of the model to restrain horizontal displacements of the walls and accurately model the bending stiffness at the wall/slab interfaces. Figure 02.4.1.1.8-2 is meant to show representative boundary conditions, not the exact support conditions of all the individual slabs, which may be supported on three or four sides with walls. The horizontal and vertical displacements of the slab at the junctions of the slab with the supporting walls are also restrained in order to eliminate the effects of the axial stiffness of the walls on the modal analyses results and to ignore the slab horizontal modes as well. Where the slab is supported by columns, the vertical displacement is constrained.

Modal analysis using ANSYS is performed on the isolated elevations of Detailed FE model and Dynamic FE model to obtain the dynamic properties. If the frequency of the first dominant mode of the slab obtained from Detailed FE model with full (uncracked concrete) stiffness properties is greater than 70 Hz, the slab is considered rigid. There is no need to adjust the stiffness of the shell elements modeling rigid slabs.

For the flexible slabs with frequency below 70 Hz, the stiffness is adjusted as needed by tuning the modulus of elasticity of the slab shell elements in the Dynamic FE model to match the frequency obtained from the Detailed FE model. The difference in first dominant frequency of vibration of the slabs obtained from the modal analyses of the two FE models is minimized through an iterative process. This process is iterated until the difference in dominant frequencies for slabs at a given elevation are at a minimum. The largest difference in slab frequency after the completion of the above process is 6%.

02.4.1.2 Validation of the Dynamic Model

The development of the R/B complex Dynamic FE model is based on a number of adjustments in geometry and load configurations in order to minimize the size of the model and make it suitable for SSI analysis using SASSI. The validation ensures that these modeling adjustments do not affect the ability of the Dynamic FE model to accurately represent the dynamic response of the R/B complex structures as described in SRP Sections 3.7.2.II.1 and 3.7.2.II.3 (Reference 02-5) and by ISG-01, Section 3.1 (Reference 02-8).

As previously described, the R/B complex Dynamic FE model is divided into six parts: R/B-FH/A-ESWPC, CIS coupled with RCL, PCCV, East PS/B, West PS/B, and A/B. The integrated model is divided into the individual components such that each structure is independent of the others. Common walls in the integrated model are included in each individual model for the purpose of validation. A series of fixed base analyses are performed on the six separate models using ANSYS and the results are compared to the ones obtained from corresponding analyses on the Detailed FE models of the R/B-FH/A-ESWPC, CIS, PCCV, East PS/B, West PS/B, and A/B structures. Once validation of the individual models is complete, a confirmatory validation analyses on the integrated R/B complex model are performed.

The validation of the Dynamic FE Model of the R/B complex, with the exception of the CIS, that are carried out on models with full (uncracked concrete) stiffness are also valid for the models with reduced (cracked concrete) stiffness. The result of the global stiffness reduction is manifested by a shift of the response of the structure to lower frequencies. Hence, a 50% stiffness reduction corresponds to a shift of frequencies by $\sqrt{2} = 1.4$ times. Therefore, the dynamic validation analyses consider responses for frequencies of $1.4 \times 50 = 70$ Hz and higher in order to ensure that the model with reduced (cracked concrete) stiffness properties can also meet the requirement of ISG-1, Section 3.1 (Reference 02-8) to accurately capture responses with frequencies up to 50 Hz.

Due to the complexity of the CIS, different stiffness and damping values are assigned to different types of structural components for the two bounding stiffness and damping conditions. As shown in Table 02.4.1.1.3-2, the reduction of stiffness applied to the CIS to account for cracking of the concrete of SC modules, reinforced concrete slabs and massive concrete portions is not uniform. Therefore, unlike the other structures, two sets of validation analyses are performed for the CIS to ensure the adequacy of the CIS Dynamic FE model with full (uncracked concrete) stiffness and reduced (cracked concrete) stiffness.

The FE analysis computer program ANSYS (Reference 02-2) serves as the platform for three different types of analyses performed to validate the dynamic properties of the R/B complex Dynamic FE model.

Sets of static analyses are performed on both the Dynamic FE Models and Detailed FE Models by applying 1g quasi-static acceleration on the models with fixed boundary conditions established at the bottom of the model to calculate nodal displacements and reaction forces. The reaction force results are compared to ensure that the mass assigned to the Dynamic FE Model and Detailed FE Model are similar. For the R/B, the masses assigned to each major floor elevation are also compared in order to check the correlation of the mass distribution in the two models. The global distribution of mass and stiffness of the structure is checked further by comparison of the deflection results from the 1g static analyses of the two FE models.

The comparison of the results for deflection along the corners of the structures under 1g quasi-static acceleration in the two horizontal and the vertical directions, respectively, are

used to determine if the number of discrete mass degrees of freedom are sufficient to capture accurately the dynamic response of the structures. The check is performed to ensure that the deflection shapes calculated from the analyses of the Dynamic FE Model correlate well with those obtained from the analyses of the Detailed FE Models. The Dynamic FE Model is considered to adequately represent the stiffness and mass distribution if the differences in the displacements results obtained from 1g static analyses of the Dynamic FE Model and Detailed FE Model are small.

Modal analyses are performed using ANSYS on the Dynamic FE Models and the Detailed FE Models of R/B, CIS, PCCV, East and West PS/Bs, and A/B with fixed conditions at the bottom of the models. The analyses provide the fixed base dynamic properties of the models, such as the natural frequencies, mode shapes, modal mass participation and the total effective mass (mobilized mass) of all of the extracted natural modes of vibration of the structures.

In order to depict the global dynamic response of the structures and determine the dominant frequencies of vibration, the results of the modal analyses of the Dynamic FE Model and Detailed FE Model, the cumulative mass versus frequency are plotted together and compared. The Dynamic FE Model is considered to have sufficient accuracy if the cumulative mass versus frequency plots are consistent with those obtained from the Detailed FE Model. Additionally, the individual models are analyzed for frequencies and mode shapes up to 100 Hz and the modal data for each direction are extracted. A comparative analysis of the modes between individual buildings of the Detailed FE Model dynamics and the Dynamic FE Model dynamics is performed. Parameters and discussion are provided that demonstrate that the models are dynamically equivalent.

After the models are developed the mass statistics are extracted and presented in Table 02.5.1.3-4. The mode shapes were normalized to mass. Thus there was no direction given to force the maximum displacement of a shape to be positive. Consequently, some of the plots will show that a mode shape of the Detailed FE Model will appear as a mirror image, i.e., reversal of sign, of the Dynamic FE Model. There is no impact on the results since the signs of the participation factors will also be reversed.

In addition to the 1g static and modal analyses performed above which only provide a global comparison between the Dynamic FE Model and the Detailed FE Model, a series of full harmonic analyses are performed in ANSYS on the Dynamic FE Models and the Detailed FE Models of R/B, CIS, PCCV, East and West PS/Bs, and A/B with fixed condition at the bottom of the models. The harmonic analysis calculates the response of the structure to cyclic loads over a frequency range. To model the fundamental concept of ATF in SASSI which directly relates the input motion to the structural response, a 1g ground (global) acceleration is applied in each of the three orthogonal directions, respectively, from which the ATFs at selected locations are derived based on the displacement response at the specified range of frequencies. A constant damping ratio of 5% is applied in all the harmonic analyses.

02.4.2 Consideration of Concrete Cracking in Seismic Analysis

In order to capture the variations of dynamic properties of R/B complex due to concrete cracking, the site-independent SSI analyses consider two levels of stiffness and damping properties:

1. Full (uncracked concrete) stiffness and lower material damping; and;
2. Reduced (cracked concrete) stiffness and higher material damping

The bounding case of a full stiffness level represents the case when the stresses in the reinforced concrete, pre-stressed concrete and steel-concrete modular structures are of low intensity such that the concrete remains essentially uncracked. A reduced stiffness level considers the case when the structures are subjected to higher stress levels that result in cracking of the concrete.

This section describes the approach used to include the effect of the concrete cracking on the stiffness and damping properties in the dynamic structural models of concrete shear wall structures (Section 02.4.2.1), CIS (Section 02.4.2.2), and PCCV (Sections 02.4.2.3).

02.4.2.1 Effects of Concrete Cracking on Reinforced Concrete Shear Wall Structures

In accordance with ASCE 4-98 (Reference 02-9), Section 3.1.3, and ASCE/SEI 43-05 (Reference 02-10), Section 3.4.1, traditional reinforced concrete members and elements are to be modeled as either cracked or uncracked sections. For the uncracked sections/elements, the stiffness is directly obtained from the concrete linear elastic properties and the section or element geometric dimensions. For the cracked concrete, a reduction to the uncracked concrete stiffness included. The reduction factors shown in Table 3-1 of ASCE/SEI 43-05 are used in linear elastic analysis to address the effects of concrete cracking on the seismic response.

The design of the reinforced concrete shear wall structures is based on the ultimate capacity of the reinforced concrete sections. Therefore, the design of reinforced concrete members addresses code stress limits corresponding to reduced cracked concrete stiffness properties and higher SSE material damping levels as discussed in Section 1.2 of RG 1.61 (Reference 02-3). However, there is a possibility that the response of the structure under lower stress levels at certain frequency ranges will be higher than the response corresponding to the higher stress state under cracked conditions. In order to ensure that the structural integrity and functionality of the components and the equipment is not compromised under seismic loading conditions, the development of ISRS in Part 3 of this TeR also considers the responses of the reinforced concrete structure with full (uncracked concrete) stiffness properties and lower OBE damping levels.

The seismic response analyses of reinforced concrete shear wall type of structures consider two stiffness and damping values in order to address the possible variations in the extent of concrete cracking:

1. Full stiffness representing low stress levels corresponding to uncracked concrete properties where the stiffness of the members are represent by gross cross sectional properties.
2. Reduced stiffness representing higher stress levels resulting in cracking of the concrete where the stiffness of the members are reduced in accordance with guidelines provided in Table 3-1 of ASCE/SEI 43-05. The stiffness of the composite members made of reinforced concrete and steel beams, such as the walls and the roof of FH/A are also reduced accordingly to represent 50% reduction in stiffness in the reinforced concrete part of the composite sections.

The structural material damping values used for these two different stress levels are OBE damping of (4%) for the full (uncracked concrete) stiffness condition and SSE damping of (7%) for the reduced (cracked concrete) stiffness condition, as shown in Table 02.4.1.1.3-1.

02.4.2.2 Effects of Concrete Cracking on the CIS

The CIS is comprised of different types of structural members including composite SC walls, massive reinforced concrete sections, and reinforced concrete slabs. The members can experience varying levels of stress resulting in different patterns of concrete cracking under the different loading conditions that can occur. Depending on the plant conditions, the CIS members can be subjected to design seismic loads in combination with normal operating or design basis accidental thermal loads resulting in different levels of stiffness reduction due to concrete cracking. Table 02.4.1.1.3-2 shows the summary of CIS stiffness and damping. The CIS members are classified in six categories, two stiffness levels corresponding to:

1. Loading Condition A: (SSE Seismic, plus operating temperatures): conditions characterized with insignificant reduction of stiffness and concrete cracking; and;
2. Loading Condition B: (SSE Seismic, plus accident temperatures): conditions characterized with significant reduction of stiffness due to cracking of the concrete under high design basis accidental thermal loads and SSE seismic.

Different material damping values are assigned to the different members depending on the level of stresses and corresponding concrete cracking.

02.4.2.3 Effects of Concrete Cracking on the PCCV

Similar to the CIS, the level of stress in the PCCV during a seismic design event depends on the plant conditions. The design of the PCCV structure is based on the premise that during normal operating conditions the pre-stressed concrete cross sections remain in compression. During the normal operating conditions, the earthquake design loads can cause only limited cracking having insignificant effect on the overall stiffness of the PCCV. Accordingly, the dissipation of energy due to material damping of the PCCV structure under normal operating conditions is low. The accident loading conditions include high temperatures and pressure loads in the reactor containment that can generate high stresses in the pre-stressed concrete accompanied with cracking that can result in a reduction of the global stiffness of the PCCV structure and higher dissipation of energy due to the material damping. The stress evaluations provided in Appendix 2-A, indicate that the reduction of the overall stiffness of PCCV structure under seismic design loads in combination with accident loads can be up to (50%).

Two stiffness levels are considered for the seismic response analyses of PCCV:

1. Normal operating conditions corresponding to insignificant concrete cracking and full (uncracked concrete) stiffness of the pre-stressed concrete structure, using 3% damping, and;
2. Accident conditions when the high thermal and pressure loads generate high stresses that can result in significant cracking of the pre-stressed concrete and a 50% reduction of the stiffness, using 5% damping.

The structural material damping values used for these two different stiffness and stress levels are also provided in Table 02.4.1.1.3-1.

02.4.3 Conversion of the R/B Complex Dynamic FE Model from ANSYS to SASSI Format

The translator built into the SASSI code serves as the platform for the translation of the R/B complex Dynamic FE model from ANSYS to SASSI house module format. Prior to the translation, the nodes of the model are renumbered according to the guidelines provided in the

SASSI manual (Reference 02-1) in order to minimize the bandwidth of the complex stiffness matrix and thus, reduce the computational effort.

The translation of the model from ANSYS into SASSI format is validated by performing validation SSI analyses of the translated SASSI Dynamic FE model in which fixed base conditions are simulated by placing the model on a very stiff elastic half space. The results of the validation of the SSI analyses for ATFs at selected locations are compared with the results of the ANSYS fixed base dynamic analyses. The peaks in the ATFs indicate that the dominant natural frequencies of the structure are compared to the results of the fixed base modal analyses.

Table 02.4.1.1.1-1 Summary of Element Types

Table 02.4.1.1.1-2 Input Material Properties

Table 02.4.1.1.3-1 Assigned Stiffness and Damping Properties

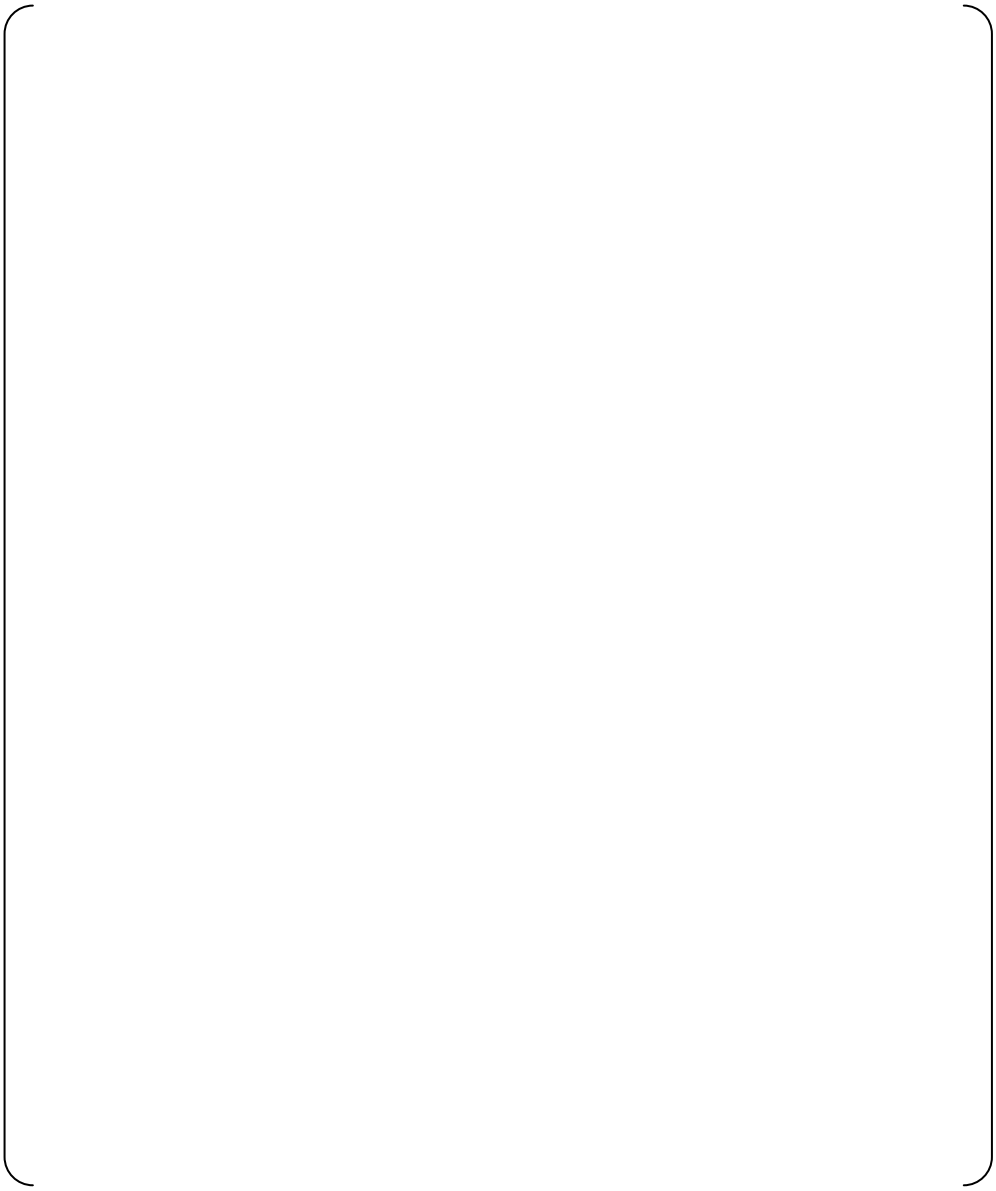

Table 02.4.1.1.3-2 Summary of SC Module Stiffness and Damping Values

(see Table 7-1 of MUAP-11018, Reference 02-11)

Figure 02.4.1.1.1-1 Integrated R/B Complex Dynamic FE Model

Figure 02.4.1.1.1-2 Integrated R/B Complex Detailed FE Model

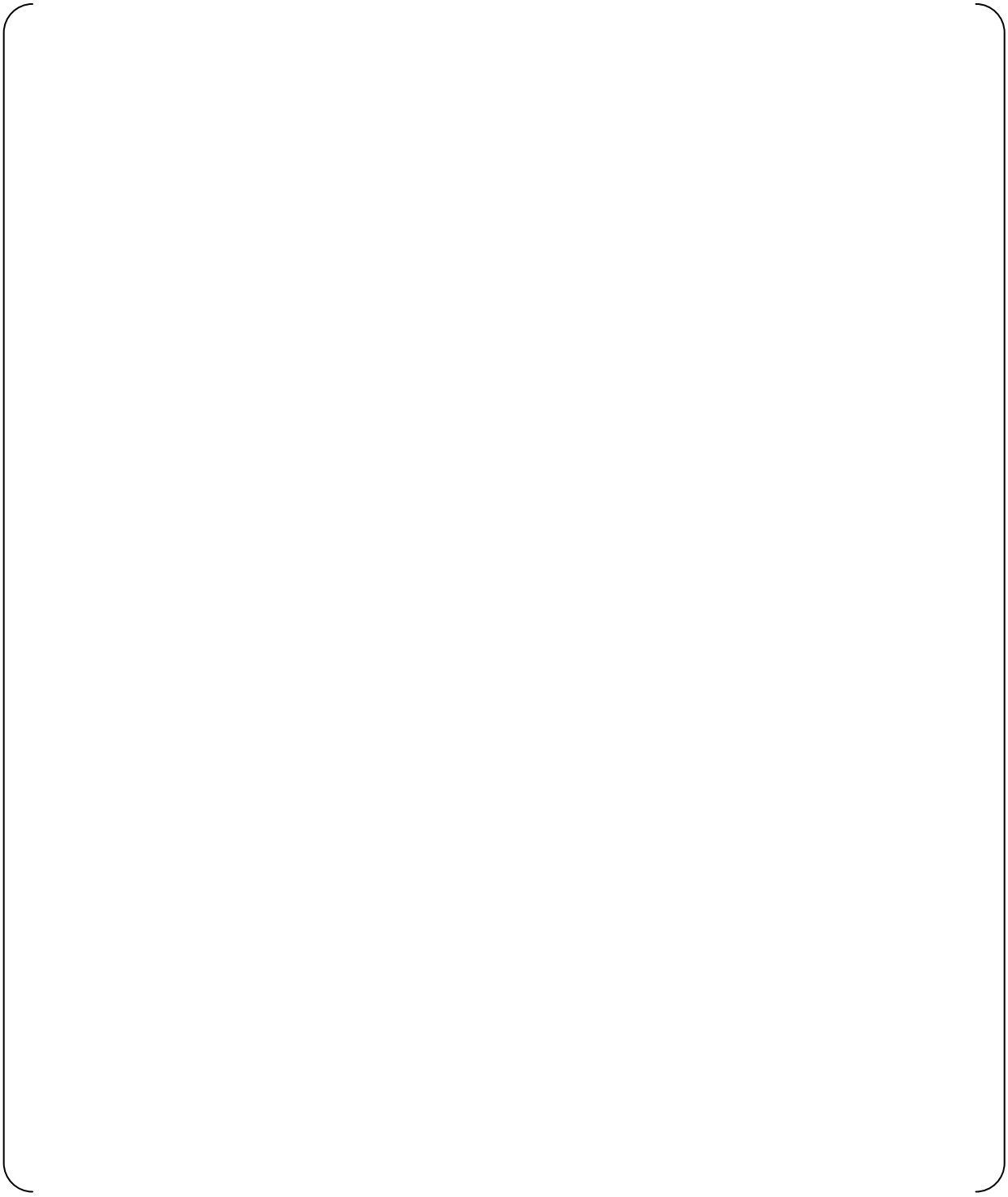

Figure 02.4.1.1.1-3 PCCV Detailed Model

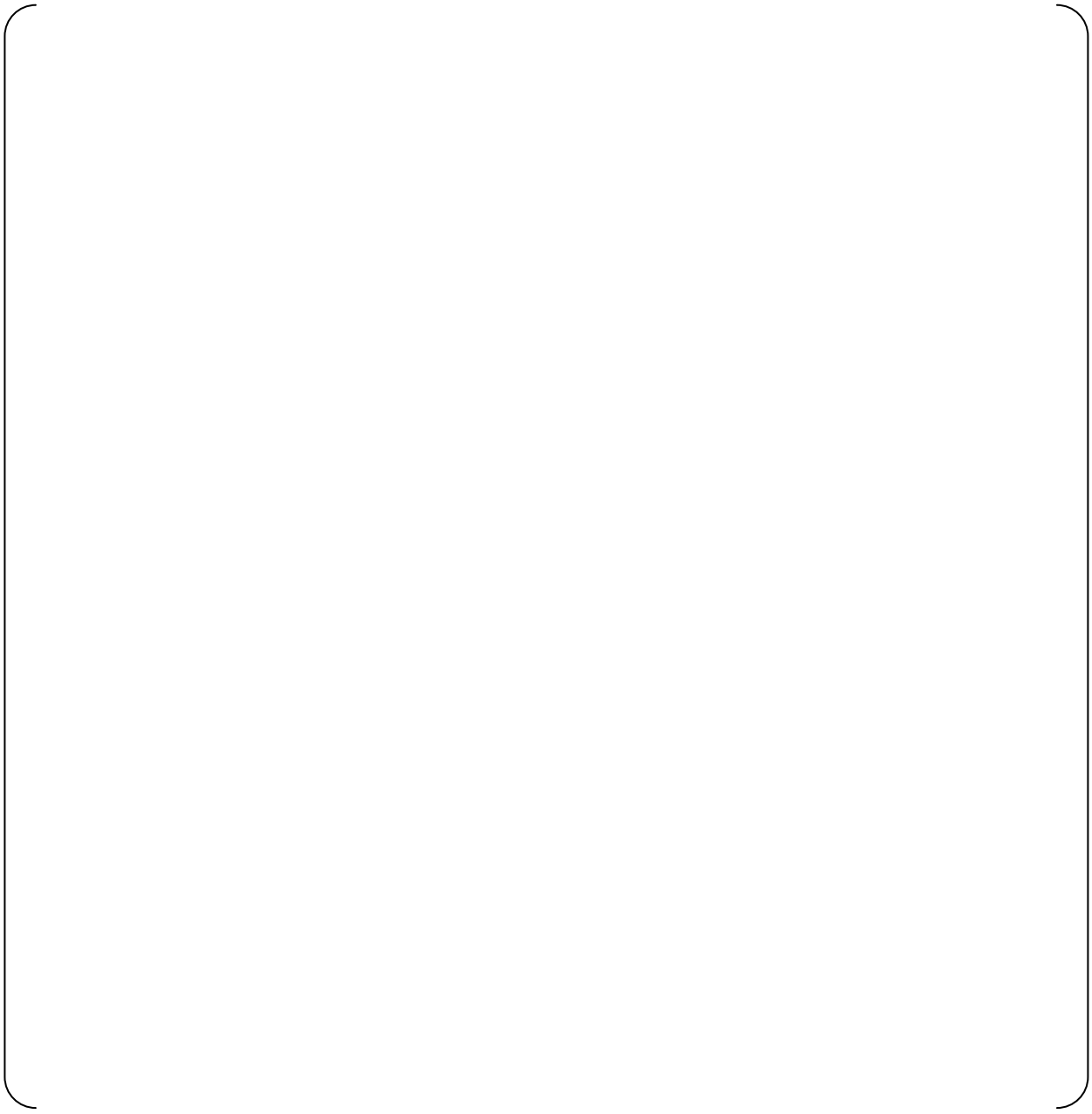

Figure 02.4.1.1.1-4 CIS Detailed Model
(includes the CIS and the RCL models)

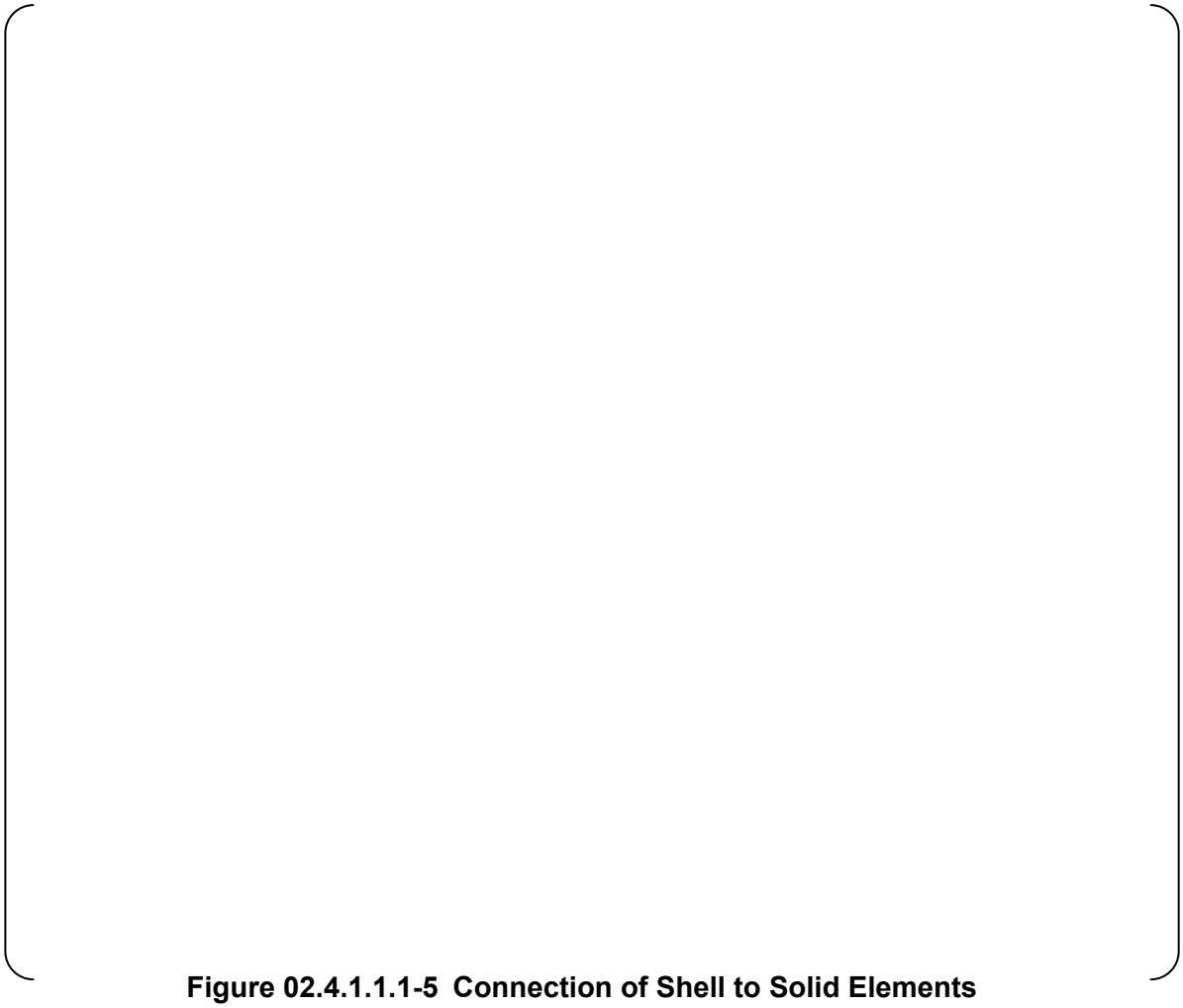

Figure 02.4.1.1.1-5 Connection of Shell to Solid Elements

Figure 02.4.1.1.1-6 Transitional Shell Elements between SC Walls and Reactor Cavity

Figure 02.4.1.1.1-7 Connection of Beam to Solid Elements

Figure 02.4.1.1.1-8 Connection of Beam to Shell Elements

Figure 02.4.1.1.4-1 Example of Hydrodynamic Masses

(Example shown for SFP)

Figure 02.4.1.1.5-1A FE Models to Calculate Wall Stiffness Reduction Factors – Model A

Figure 02.4.1.1.5-1B FE Models to Calculate Wall Stiffness Reduction Factors – Model B

Figure 02.4.1.1.8-1 Extracted Detailed FE Model of Floor Slabs

Figure 02.4.1.1.8-2 Floor Slab Model Boundary Conditions

02.5.0 RESULTS

02.5.1 Dynamic Model of the Reactor Building Complex

02.5.1.1 Development of the Reactor Building Complex Dynamic FE Model

Developed using the ANSYS preprocessor, the R/B complex Dynamic FE model is an integrated 3-D model of the R/B-FH/A, PCCV, CIS, East and West PS/B, A/B, and ESWPC structures sharing common shear walls and resting on top of a common 13'-4" to 43'-3" thick basemat. Typical element size in the basemat and the slabs is approximately 9 ft, while the element size for the walls in the vertical direction is approximately 1.5 times larger (Section 02.4.1.1.1 and Table 02.4.1.1.1-1 show the element type used to simulate the R/B complex structure). The total number of nodes in the model is 33,564 and the total number of elements is 47,580. Figure 02.5.1.1-1 shows an overview of the R/B complex model, while Figure 02.5.1.1-2 and Figure 02.5.1.1-3 reveal the interior structures with section views. Figure 02.5.1.1-4 through Figure 02.5.1.1-10 show the PCCV, CIS shell elements (excluding the RCL), CIS solid elements, CIS beam elements (excluding RCL), East PS/B, West PS/B, and A/B as individual structures, respectively. The global origin is located at the center of the PCCV and top of the basement with the X axis pointing North, Y axis pointing West, and Z axis pointing upward. Once the model is translated into SASSI format, the global coordinate system is rotated 180 degrees about the Z axis so that the X axis is pointing South and the Y axis pointing East. The element mesh used in the dynamic model is selected to provide sufficient modeling to capture the dynamic properties of the structure. The validations performed in Section 02.5.1.3 show that no further refinement of the Dynamic FE model is necessary.

The R/B complex Dynamic FE model is developed incrementally using ANSYS in the following seven steps:

Step 1. R/B complex structures geometry is created in a manner that allows control of the model FE mesh.

Step 2. Attributes are assigned and additional masses are applied on each of the structures.

Step 3. Mesh controls are set and the model, excluding the RCL, is meshed.

Step 4. Modifications are implemented as needed to make the model more consistent with the Detailed FE model.

Step 5. The nodes are renumbered sequentially in the order of their X, Y, and Z coordinates as recommended by the SASSI Manual in order to enhance computational efficiency.

Step 6. The model used for ANSYS analyses of RCL is translated into a format that can be translated into SASSI.

Step 7. RCL structure is added to the FE model of R/B complex structures and proper connections are implemented to represent the physical supports attached to the CIS.

For simplicity without compromising accuracy, slab elevations in the Dynamic FE model are slightly shifted upward or downward such that the middle planes of nearby upper or lower slabs fall into a major common horizontal plane. Also, only large openings in slabs and walls are included in the model. Wall properties are adjusted to account for the presence of small openings not included in the model as described in Section 02.4.1.1.5.

Special attention is given in the Dynamic FE model as to how wall and slab shell elements are connected to the basement/mat solid elements. Wall shell elements are extended into the

basemat solid elements to ensure a proper transfer of bending moment between them. Likewise, slab shell elements joining the basement walls are extended one element to overlay the basement top surface. These connecting elements are also assigned a zero density not to increase the overall mass of the basemat. See Figure 02.4.1.1.1-5 for an example of this type of connection.

Also for simplicity, only the main steel frame in the Fuel Handling crane support system, including a simplified rail truss girder, and the main steel framing in the CIS are modeled in the Dynamic FE model. The steel sections are modeled as beam elements to share nodes with the concrete shell elements representing the Fuel Handling exterior walls and slab. Thus, the composite behavior of the crane support system would not be fully represented in the FE model without further adjustment. The adjustment made is that all steel sections are assigned an increased moment of inertia in their strong axis to account for their composite behavior. An adjusted moment of inertia is also assigned to the embedded sections of the crane support steel columns between elevation 65'-0" and 76'-5", encased in 7'-8" by 4'-0" concrete columns.

The thickness of the PCCV is also simplified for ease of modeling. For the Dynamic FE model, only the large equipment hatch is modeled and the elements modeling the buttresses on the East and West sides of the structure are not offset with respect to adjacent elements. Also, the personnel airlocks as well as the Main Steam and Feed Water penetrations are not modeled in the Dynamic FE model. The stiffness and weight of the Dynamic PCCV model are not adjusted to account for the openings since they were found to have a negligible impact on the overall response of the structure. Figure 02.5.1.1-4 shows the Dynamic PCCV model.

The PCCV polar crane (crane self-weight supported by the polar crane girder) is modeled into the PCCV directly and attached to the crane rail girder supported by the corbels located at the 0^0 and 180^0 azimuths. This is a generic crane design intended solely to be used for seismic analyses. Therefore, the polar crane is modeled to approximate the design weight.

The CIS portion of the Dynamic FE model (excluding the RCL) contains approximately 4,631 elements and 3,876 nodes with nominal mesh size of 7.2 ft in the vertical direction and 9 ft in the horizontal direction. It consists of a combination of shell, solid and beam elements. The solid elements shown in Figure 02.5.1.1-6 make up the CIS base which starts at elevation 2'-7" and the reactor support which extends up to elevation 35'-10.87". The shell elements make up the remaining walls and slabs of the structure and begin at the same elevation as the CIS solid elements, but extend to the top of the pressurizer compartment at elevation 139'-6". The beam elements shown in Figure 02.5.1.1-7 represent the steel frames and the supports for the RCL components. Connection details and explanations for the interface between the various element types are presented in Section 02.4.1.1.1.

02.5.1.2 Reactor Coolant Loop (RCL) Model

02.5.1.2.1 Description of RCL Model

The US-APWR is a four loop nuclear power plant. Each of the four RCLs that are connected to the RV includes a SG, RCP, and the Main Coolant Piping (MCP) system as shown in the schematic sketch in Figure 02.5.1.2.1-1. The MCP is separated in three legs: (1) a hot leg pipe transferring coolant flow from the RV to SG, (2) a crossover leg pipe transferring coolant from SG to RCP; and (3) a cold leg pipe transferring coolant from the RCP back to the RV. The PZR is also modeled supported in the pressurizer compartment and connected to the RV.

The model used for dynamic analyses of the RCL includes several parts representing the dynamic properties of the NSSS components and MCP. Spring elements model the stiffness

of the supports of the components and piping. Figure 02.5.1.2.1-2 presents the model used for dynamic analyses of RCL.

The model of the RCL and major pipe components used for seismic analyses of NSSS are translated into elements acceptable to SASSI format and then coupled with the Dynamic CIS model. The translation included changes of ANSYS modeling features such as pipe element types, rigid links and constraint equations that can be supported by the SASSI translator. The pipe elements are replaced by 3-D beam elements with stiffness values equivalent to those of the straight and curved pipe sections. The rigid links and constraint equations are replaced by rigid beams. The coupling of the RCL to the CIS is accomplished such that there are no local effects from the CIS imparted upon the RCL. The validation of the model in Section 02.5.1.3 demonstrates that these modifications do not affect the overall stiffness of the model and thus the dynamic response of the RCL components.

02.5.1.2.2 Coupling of RCL Model

The system supporting the RV consists of eight steel support pads which are integrated with the inlet and outlet nozzle forgings. The support pads are placed on brackets, which are supported by a steel structure embedded in the primary shield wall. The supports allow radial thermal growth of the RV and reactor coolant system. Figure 02.5.1.2.2-1 shows the configuration of the RV support. Details of the modeling of the connection of the RV with the Dynamic FE model of the CIS are is presented in Figure 02.5.1.2.2-2.

The SG support system consists of an upper shell support structure, an intermediate shell support structure, and a lower support structure as shown in Figure 02.5.1.2.2-3. The upper and intermediate shell supports are lateral restraints (snubbers) attached to structural steel brackets. The lower support structure provides both vertical and lateral support to the SG and is constructed entirely of structural steel. It consists of four pinned-end columns of the lower support that transfer the vertical loads from the SG to the CIS structure and lateral supports that transfer lateral loads to the CIS only when they are in contact with the SG. This design solution allows for the thermal expansion of the SG and attached pipe but introduces geometric non-linearity in the dynamic system because the springs modeling the lower lateral support are engaged only when they are in compression. The RCL model used for the analyses mentioned in this TeR represents the contact condition which reflects the worst stress condition in the system through geometric nonlinear analysis. Figure 02.5.1.2.2-4 shows the RCP tie rod support. Figure 02.5.1.2.2-5 presents modeling of the connections between the model of SG and Dynamic FE model.

02.5.1.3 Validation of the Reactor Building Complex Dynamic FE Model

Validation of the R/B complex Dynamic FE model is carried out in accordance with the methodology described in Section 02.4.1.2. Three sets of analysis using ANSYS are performed for the validation. They are:

- 1g analysis to check and validate element connectivity, mass and stiffness distributions represented by displacement distribution at various locations
- Modal analysis to validate global dynamic properties of the model represented by the fundamental frequencies and associated mode shapes and modal masses
- Harmonic analysis to obtain ATF at various locations to validate the global and local dynamic properties of the model.

The R/B complex Dynamic model is divided into six sub-models that represent the portions of R/B, PCCV, CIS, East PS/B, West PS/B, and A/B. The sub-models are developed by selecting the elements and associated properties within each building footprint area, including the common walls, from the completed R/B complex dynamic model. The ESWPC is divided into three sections and they are included in the sub-models of the East PS/B, R/B, and West PS/B accordingly. The three sets of validation analyses are performed on each of the sub-models. As a confirmatory validation, the completed R/B complex dynamic model is also validated by performing 1g static analysis and modal analysis. The PCCV and CIS are free standing structures. Their dynamic properties represented by the corresponding sub-models are similar to their dynamic properties that are represented in the R/B complex model. The four sub-models, R/B, East PS/B, West PS/B and A/B, are more flexible than their corresponding portions within the R/B complex dynamic model when they are integrated. Therefore, validating the sub-models up to a certain frequency results in that the R/B complex model is capable of capturing the response for the frequencies up to that frequency and even higher.

The six sub-models and the completed R/B complex Dynamic model are checked and validated against the corresponding detailed models. The dynamic models have nominal mesh size of 9 ft and the detailed models have nominal mesh sizes of 4 to 6 ft, 6 ft for the PCCV, 5 ft for the R/B and 4 ft for the remainder of the buildings. The wall and floor slab thickness of the R/B complex structure are generally about 3 to 5 ft. The 4 to 6 ft mesh size is the reasonable lower limit for finite element simulations to capture the dynamic properties of the R/B complex structures. Comparison of the dynamic properties of the dynamic models with the detailed models therefore is considered as a "convergence study" of the dynamic properties in terms of mesh size selection as required by SRP 3.7.2, stated as "the element size should be selected on the basis that further refinement has only a negligible effect on the solution results."

The validation results conclude that the dynamic model and detailed model represent approximately the same mass and stiffness distribution, the same dynamic properties in terms of the fundamental frequencies and associated mode shapes and modal masses, and comparable ATFs at various locations. Therefore the R/B complex dynamic model adequately represents the building mass stiffness and dynamic properties for SSI analysis.

As a typical case, Table 02.5.1.3-1 presents a summary of a 1g static analysis validation observations and results. The last column lists the maximum displacement difference at the four corners of the buildings. The displacement difference was calculated for the corners of each building as follows: for a given location (building corner),

$$\text{Displacement difference} = \sqrt{\frac{\sum_{i=1}^{n}(D_i - d_i)^2}{\sum_{i=1}^{n} D_i^2}} \qquad \text{Equation 02.5.1.3-1}$$

where D_i is the nodal displacement obtained from the detailed model at its Node i , d_i is the corresponding displacement at same location but predicted by linear interpolation of nodal displacements obtained from the dynamic model, and n is the total number of nodes at the selected corner.

As shown in Table 02.5.1.3-1, the maximum displacement difference is 1.54% to 7.39%, and also as expected the coarse mesh models are stiffer than the refined model. The results of the dynamic models are approximately same as that obtained from the detailed models.

Table 02.5.1.3-2 presents comparison of the fundamental frequencies obtained from the dynamic model and the corresponding detailed model. For each dominant mode of the dynamic model presented in the table, a close match to the same mode is found in the

detailed model. This is one of the indications of dynamic equivalency of the detailed and the dynamic model.

Table 02.5.1.3-3 presents observations on the comparison of ATF obtained from the Harmonic analyses of detailed and dynamic models. Generally, the ATFs are comparable and differences in peak frequencies and amplitude are insignificant. Differences of ATF amplitude at peak frequency at some locations are observed but are justified as shown on Table 3 for the vertical ATF for one of the nodes at the RV nozzles.

The mass of the individual models as well as the completed R/B complex model are extracted from the ANSYS analyses for both the Dynamic FE and the Detailed FE models. This data is presented in Table 02.5.1.3-4 shows that the all the models have mass that are within 2% of each other with the exception of the R/B models which are within 3%. The subsequent subsections present detailed validation results and discussion on the sub-models and the completed R/B complex model for each of the three analyses described in Section 02.4.1.2.

02.5.1.3.1 Validation of the R/B-FH/A

02.5.1.3.1.1 1g Static Analysis

Partial static analyses under 1g vertical load are performed using ANSYS to determine the accuracy of the mass used in the Dynamic model at each floor. Table 02.5.1.3.1.1-1 presents the comparison of the major floor masses for the North and South halves of the R/B obtained from the analyses of the two FE models; the Dynamic FE model and the Detailed FE model. The mass of each floor section is taken as the mass of the floor plus that of the walls between the current floor and the floor at the immediate lower elevation. The results in Table 02.5.1.3.1.1-1 indicate that the total mass of the two models are comparable with a difference of 1.32%. The mass differences for each floor section are also acceptable, ranging from 0.31% to 8.42%.

In addition, displacement results from the 1g static analyses are used to compare the distributions of mass and horizontal stiffness of the two models. Displacement in all three orthogonal directions (X, Y, and Z) along the height at various exterior wall locations C and H (Shown in Figure 02.5.1.3.1.1-1) of both models are plotted in Figure 02.5.1.3.1.1-2 though Figure 02.5.1.3.1.1-7. These Figures demonstrate that the Dynamic model lateral stiffness is comparable to that of the detailed model (structure behavior follows the same trend for both models). Table 02.5.1.3.1.1-2 indicates that the maximum roof level lateral displacement difference between the two models at the various locations identified in Figure 02.5.1.3.1.1-1 varies from 0.17% to 4.03% in the NS (X) direction, from 0.13% to 2.09% in the EW (Y) direction, and from 0.26% to 5.63% in the vertical (Z) direction.

02.5.1.3.1.2 Modal Analysis

Fixed base modal analyses using ANSYS are performed on both the Detailed and the Dynamic FE models of the R/B. Plots of Cumulative Mass versus Frequency are shown in Figure 02.5.1.3.1.2-1 through Figure 02.5.1.3.1.2-3.

The data for the R/B model comparison is shown in Table 02.5.1.3.1.2-1 through Table 02.5.1.3.1.2-6. All modes with modal mass greater than 10% of the net modal mass computed, which is up to 100 Hz are presented. In some cases, data for modes with less than 10% modal mass is presented if it is thought to add some clarity.

The data for the X direction (Table 02.5.1.3.1.2-1 and Table 02.5.1.3.1.2-2) show that the dominate modes of the detailed dynamic model and the dynamic model are all very close to

one another in frequency, modal mass and shape. (The data in Figure 02.5.1.3.1.2-6 and Figure 02.5.1.3.1.1-7 is an example of the sign reversal of the mode shape previously described.) The data plotted in Figure 02.5.1.3.1.2-4 through Figure 02.5.1.3.1.2-9, show that the shapes of the modes between the detailed and dynamic models are very similar to each other. The data for the Y direction (Table 02.5.1.3.1.2-3 and Table 02.5.1.3.1.2-4) also show that the dominate modes are all very close to one another in frequency, modal mass and shape. The mode shapes presented in Figure 02.5.1.3.1.2-10 through Figure 02.5.1.3.1.2-13, show that the mode shapes are very close to each other.

The data for the Z direction (Table 02.5.1.3.1.2-5 and Table 02.5.1.3.1.2-6) show that a one to one comparison of modes is not possible. Thus an examination of the mode shapes is necessary. With respect to the Detailed model mode shapes, Figure 02.5.1.3.1.2-14 and Figure 02.5.1.3.1.2-15, the lower frequency mode (mode 21, f = 12.435 Hz) only involves the FH/A to the north (+X) direction and small amount of the remainder of the building. The next mode (mode 22, f = 12.529 Hz) involves both the FH/A to the north and the superstructure to the south and little else. The modal mass of this mode is below the 10% threshold. The sum of the modal masses of these two modes is (2740.6+1158.6) 3899.2 or 23.3% of the total. An examination of mode 22 of the dynamic model (f = 12.569 Hz), Figure 02.5.1.3.1.2-16 indicates that this mode involves both the FH/A and the superstructure to the south and has a mass of 25% of the total. Thus, the sum of the two modes from the Detailed model is equivalent to the single mode (22) of the Dynamic model. This will often occur since the Detailed model has a higher fidelity than the Dynamic model.

However, the ability of the detailed model to develop mode shapes with a refined capability does not mean that the dynamic model does not have the ability to properly capture the dynamic responses. As long as the mode shapes of the dynamic model are of a reasonable shape, i.e., no sharp changes in the slopes of eigenvector shape, sometimes referred to as “kinks” and the modes have the modal mass comparable to the modal mass of the equivalent mode shape from the detailed model, then the model will be able to capture the dynamic responses appropriately. This comparative analysis is especially clear for the modes that describe horizontal response. The vertical responses are somewhat less clear to see, especially for the smaller structures where the floor spans between the detailed and dynamic models are not the same. Though the spans were calibrated to reflect frequency and mass appropriately, the comparative analyses are not always as clear as for the R/B. In these cases, however, as the mass distributions over several closely spaced modes are presented and shown to be comparable. The results of the modal analysis indicate that the Dynamic model adequately captures the dynamic properties of the Detailed model.

02.5.1.3.1.3 Harmonic Response Analysis

A harmonic response analysis using ANSYS is performed on both the Detailed and the Dynamic R/B models. This analysis captures the structural response at numerous frequencies (acceleration vs. frequency) for each model. The locations of the response points are the same as those demonstrated in Figure 02.5.1.3.1.1-1 for the static analyses. The harmonic analysis results demonstrate that the Dynamic R/B model’s dynamic properties are adequate to capture structural responses and are shown in Figure 02.5.1.3.1.3-1 through Figure 02.5.1.3.1.3-3.

02.5.1.3.2 Validation of the PCCV

02.5.1.3.2.1 1g Static Analysis

A 1g static analysis in the vertical (Z) direction with full constraint at the bottom is performed on both PCCV models to verify their overall static weight. The total weight of the PCCV Dynamic model is 79,494 kips while the total weight of the PCCV Detailed model is 78,163 kips. This represents a difference of 1.70% between the total weights of both models.

A 1g Static Analysis in all three orthogonal directions with full constraint at the bottom of the containment structure is also performed on both models. The displacement results from both static analyses are used to compare the structure stiffness of the two models in all directions. Figure 02.5.1.3.2.1-1 shows the locations on the PCCV in which displacements are compared. The displacement distributions along the height of the vessel are plotted for the North face in Figure 02.5.1.3.2.1-2 through Figure 02.5.1.3.2.1-4 below, and indicate that the Dynamic PCCV model stiffness is comparable to that of the Detailed model (structure behavior follows the same trend for both models). Table 02.5.1.3.2.1-1 indicates that the maximum lateral displacement difference at the top of the dome between the two models is 0.21% in the NS (X) direction, 1.46% in the EW (Y) direction, and 0.68% in the vertical (Z) direction.

02.5.1.3.2.2 Modal Analysis

Fixed base modal analyses using ANSYS are performed on both the Detailed FE model and the Dynamic FE model of the PCCV. Plots of Cumulative Mass versus Frequency are shown in Figure 02.5.1.3.2.2-1 through Figure 02.5.1.3.2.2-3 below and provide the comparison of the modal analyses results. Dynamic data for the PCCV is presented in Table 02.5.1.3.2.2-1 through Table 02.5.1.3.2.2-6. The PCCV is a relatively simple structure as it relates to dynamic response, and the tables and plots show a single dominate mode in the X direction, see Figure 02.5.1.3.2.2-4 and Figure 02.5.1.3.2.2-5 and two modes in the Y direction, see Figure 02.5.1.3.2.2-10 through Figure 02.5.1.3.2.2-13 and one dominate mode in the Z direction Figure 02.5.1.3.2.2-16 and Figure 02.5.1.3.2.2-17. The detailed dynamic and the dynamic models provide comparable results for frequency and modal mass. The results of the modal analysis indicate that the Dynamic FE model adequately captures the dynamic properties of the Detailed FE model.

02.5.1.3.2.3 Harmonic Response Analysis

A harmonic response analysis using ANSYS is performed on both the Detailed and the Dynamic PCCV models. This analysis captures the structural response at numerous frequencies (acceleration vs. frequency) for each model. The locations of the response points are the same as those demonstrated in Figure 02.5.1.3.2.1-1 for the static analyses. The harmonic analysis results demonstrate that the Dynamic PCCV model's dynamic properties are adequate to capture structural responses and are shown in Figure 02.5.1.3.2.3-1 through Figure 02.5.1.3.2.3-3.

02.5.1.3.3 Validation of the CIS

Due to the complexity of the CIS, different stiffness and damping values are assigned to different types of structural components for the two bounding stiffness and damping conditions as described in Table 02.4.1.1.3-2. Hence, a non-uniform reduction of stiffness is applied for the different types of components in order to account for cracking of the concrete in SC modules, reinforced concrete slabs and massive concrete portions of the CIS. Therefore,

unlike the other Category I structures, two sets of validation analyses are performed for the CIS to ensure the adequacy of the CIS Dynamic FE model with full (uncracked concrete) stiffness and reduced (cracked concrete) stiffness.

02.5.1.3.3.1 1g Static Analysis

A 1g static analysis in the vertical (Z) direction with full constraint at the bottom is performed on both the uncracked (full stiffness) and cracked (reduced stiffness) versions of the detailed and dynamic CIS models to verify their overall weight. The total weight of the uncracked dynamic CIS model is found to be 105,510 kips while the total weight of the uncracked detailed CIS model is found to be 105,460 kips. This results in a 0.05% difference between the total weights of both models. The total weights of the cracked dynamic and detailed models are the same as the uncracked models.

A 1g Static Analysis in all three orthogonal (X, Y, and Z) directions with full constraint at the bottom of the CIS is also performed on both the uncracked and cracked versions of the dynamic and detailed models. The displacement results from the static analyses are used to compare the structure stiffness of each model in the lateral directions. The displacement distributions at representative locations (see Figure 02.5.1.3.3.1-1) along the height of the uncracked CIS models are plotted in Figure 02.5.1.3.3.1-2 through Figure 02.5.1.3.3.1-10 and indicate that distribution of mass and stiffness of the Dynamic FE model with full stiffness is comparable to that of the detailed FE model. Table 02.5.1.3.3.1-1 provides a summary of the maximum displacements for the uncracked model at the represented locations. The displacement distributions at several locations along the height of the cracked CIS models are plotted in Figure 02.5.1.3.3.1-11 through Figure 02.5.1.3.3.1-19 and indicate that distribution of mass and stiffness of the Dynamic FE model with reduced stiffness is comparable to that of the detailed FE model. Table 02.5.1.3.3.1-2 provides a summary of the maximum displacements for the cracked model at the represented locations.

02.5.1.3.3.2 Modal Analysis

A modal analysis using ANSYS is performed on both the uncracked and cracked versions of the Detailed and Dynamic FE models. Plots of Cumulative Mass versus Frequency for the uncracked CIS models are shown in Figure 02.5.1.3.3.2-1 through Figure 02.5.1.3.3.2-3. Plots of the Cumulative mass versus Frequency for the cracked CIS models are shown in Figure 02.5.1.3.3.2-26 through Figure 02.5.1.3.3.2-28. Dynamic data for the CIS is presented in Table 02.5.1.3.3.2-1 through Table 02.5.1.3.3.2-6. In the horizontal directions, the modal frequencies and mode shapes presented are comparable mode for mode, see Table 02.5.1.3.3.2-1 through Table 02.5.1.3.3.2-4, and Figure 02.5.1.3.3.2-4 through Figure 02.5.1.3.3.2-11. A one to one, mode by mode comparison between the detailed dynamic and the dynamic models cannot be provided. An examination of the mode shapes, Figure 02.5.1.3.3.2-12 through Figure 02.5.1.3.3.2-25 show that the largest values of the shape occur at the periphery of the floor located in the upper portions of the structure. The bulk of the mass, however, is located in the lower portions, owing to the mass of concrete supporting the RV and the SG enclosures. Thus since the modal mass is a function of the eigenvector and the mass matrix, small changes in the eigenvector can result in large changes in model mass, all other variables held constant. Thus when the largest values on a shape are associated with the smaller masses, the modal mass terms between the detailed dynamic model and the dynamic model may not be equivalent even though the frequencies of the mode shapes are very close to one another. However, as the eigenvalue extraction and modal mass computation progress through the higher frequencies, the net modal masses over closely spaced modes have to become equal if

the models are dynamically equivalent. This is demonstrated in Table 02.5.1.3.3.2-5 through Table 02.5.1.3.3.2-6. The cumulative mass fractions begin to converge to each other at mode 48 (38.8) of the detailed dynamic model and mode 49 (37.4) of the dynamic model. Further, they remain very close together from these points on to modes 56 for both models. The results of the modal analyses indicate that the Dynamic FE models adequately capture the dynamic properties of the Detailed FE models.

02.5.1.3.3.3 Harmonic Response Analysis

A harmonic response analysis using ANSYS is performed on both uncracked and cracked versions of the Detailed and the Dynamic CIS models. This analysis captures the structural response at numerous frequencies (acceleration vs. frequency) for each model at several locations throughout the CIS. The harmonic analysis results demonstrate that the Dynamic CIS model's dynamic properties are adequate to capture structural responses. Responses for the uncracked model and are shown in Figure 02.5.1.3.3.3-1 through Figure 02.5.1.3.3.3-3. Responses for the cracked model and are shown in Figure 02.5.1.3.3.3-4 through Figure 02.5.1.3.3.3-6.

02.5.1.3.4 Validation of the East PS/B

02.5.1.3.4.1 1g Static Analysis

Displacement results from the 1g static analyses are used to compare the distributions of mass and horizontal stiffness of the Dynamic and Detailed East PS/B models. The total weight of the Detailed FE model is 64,736 kip while the Dynamic FE model is 64,401 kip, yielding a 0.52% difference. Displacement in all three orthogonal directions (X, Y, and Z) along the height at various exterior wall locations (Shown in Figure 02.5.1.3.4.1-1) of both models are plotted in Figure 02.5.1.3.4.1-2 though Figure 02.5.1.3.4.1-4. They demonstrate that the Dynamic model lateral stiffness is comparable to that of the detailed model (structure behavior follows the same trend for both models). Table 02.5.1.3.4.1-1 indicates that the maximum roof level lateral displacement difference between the two models at the various locations identified in Figure 02.5.1.3.4.1-1 varies from 1.35% to 7.94% in the NS (X) direction, from 2.66% to 8.57% in the EW (Y) direction, and from 0.06% to 3.39% in the vertical (Z) direction.

02.5.1.3.4.2 Modal Analysis

Fixed base modal analyses using ANSYS are performed on both the Detailed and the Dynamic FE models of the East PS/B. Plots of Cumulative Mass versus Frequency are shown in Figure 02.5.1.3.4.2-1 through Figure 02.5.1.3.4.2-3. The dynamic data for the East PS/B is presented in Table 02.5.1.3.4.2-1 through Table 02.5.1.3.4.2-6. In the horizontal directions, the modal frequencies and mode shapes presented are comparable mode for mode, see Table 02.5.1.3.4.2-1 through Table 02.5.1.3.4.2-4, and Figure 02.5.1.3.4.2-4 through Figure 02.5.1.3.4.2-7. The East PS/B is a small and relative simple structure, thus its horizontal response is dominated by one mode in each direction. In the vertical direction, the structure is more complex. However, recognizing the arguments presented above for complex mode shape, it is evident from the tables and the plots that the combination of modes from 1 through 13 to 16 from the detailed FE model are equivalent to modes 1 through 14 to 15 of the dynamic model. And from mode 17 through 37 to 53 of the detailed FE model are equivalent to modes 16 through 34 to 57 of the Dynamic FE model. Only the modes with reportable mass are provided in the tables and plots. The results of the modal analysis indicate that the Dynamic FE model adequately captures the dynamic properties of the Detailed FE model.

02.5.1.3.4.3 Harmonic Response Analysis

A harmonic response analysis using ANSYS is performed on both the Detailed and the Dynamic East PS/B models. This analysis captures the structural response at numerous frequencies (acceleration vs. frequency) for each model. The locations of the response points are the same as those demonstrated in Figure 02.5.1.3.4.1-1 for the static analyses. The harmonic analysis results demonstrate that the Dynamic East PS/B model's dynamic properties are adequate to capture structural responses and are shown in Figure 02.5.1.3.4.3-1 through Figure 02.5.1.3.4.3-3.

02.5.1.3.5 Validation of the West PS/B

02.5.1.3.5.1 1g Static Analysis

Displacement results from the 1g static analyses are used to compare the distributions of mass and horizontal stiffness of the Dynamic and Detailed West PS/B models. The total weight of the Detailed FE model is 63,901 kip while the Dynamic FE model is 63,347 kip, yielding a 0.87% difference. Displacement in all three orthogonal directions (X, Y, and Z) along the height at various exterior wall locations (Shown in Figure 02.5.1.3.5.1-1) of both models are plotted in Figure 02.5.1.3.5.1-2 though Figure 02.5.1.3.5.1-4. They demonstrate that the Dynamic model lateral stiffness is comparable to that of the detailed model (structure behavior follows the same trend for both models). Table 02.5.1.3.5.1-1 indicates that the maximum roof level lateral displacement difference between the two models at the various locations identified in Figure 02.5.1.3.5.1-1 varies from 4.53% to 7.87% in the NS (X) direction, from 3.02% to 4.15% in the EW (Y) direction, and from 1.42% to 4.15% in the vertical (Z) direction.

02.5.1.3.5.2 Modal Analysis

Fixed base modal analyses using ANSYS are performed on both the Detailed and the Dynamic FE models of the West PS/B. Plots of Cumulative Mass versus Frequency are shown in Figure 02.5.1.3.5.2-1 through Figure 02.5.1.3.5.2-3. The dynamic data for the West PS/B is presented in Table 02.5.1.3.5.2-1 through Table 02.5.1.3.5.2-6. In the horizontal directions, the modal frequencies and mode shapes presented are comparable mode for mode, see Table 02.5.1.3.5.2-1 through Table 02.5.1.3.5.2-4, and Figure 02.5.1.3.5.2-4 through Figure 02.5.1.3.5.2-9. The West PS/B is a small and relative simple structure, thus its horizontal response is dominated by two modes in the X direction and one mode in the Y direction. In the vertical direction, the structure is more complex. However, recognizing the arguments presented above for complex mode shape, it is evident from the tables and the plots that the combination of modes from 1 to 8 from the detailed FE model are equivalent to modes 1 to 9 of the Dynamic FE model. And from mode 9 to 36 of the detailed FE model are equivalent to modes 10 to 36 of the Dynamic FE model. Fewer mode plots are presented here than for the East PS/B however a similar number of modes are evident. The results of the modal analysis indicate that the Dynamic FE model adequately captures the dynamic properties of the Detailed FE model.

02.5.1.3.5.3 Harmonic Response Analysis

A harmonic response analysis using ANSYS is performed on both the Detailed and the Dynamic West PS/B models. This analysis captures the structural response at numerous frequencies (acceleration vs. frequency) for each model. The locations of the response points

are the same as those demonstrated in Figure 02.5.1.3.5.1-1 for the static analyses. The harmonic analysis results demonstrate that the Dynamic West PS/B model's dynamic properties are adequate to capture structural responses and are shown in Figure 02.5.1.3.5.3-1 through Figure 02.5.1.3.5.3-3.

02.5.1.3.6 Validation of the A/B

02.5.1.3.6.1 1g Static Analysis

Displacement results from the 1g static analyses are used to compare the distributions of mass and horizontal stiffness of the Dynamic and Detailed A/B models. The total weight of the Detailed FE model is 268,219 kip while the Dynamic FE model is 268,294 kip, yielding a 0.03% difference. Displacement in all three orthogonal directions (X, Y, and Z) along the height at various exterior wall locations (Shown in Figure 02.5.1.3.6.1-1) of both models are plotted in Figure 02.5.1.3.6.1-2 though Figure 02.5.1.3.6.1-4. They demonstrate that the Dynamic model lateral stiffness is comparable to that of the detailed model (structure behavior follows the same trend for both models). Table 02.5.1.3.6.1-1 indicates that the maximum roof level lateral displacement difference between the two models at the various locations identified in Figure 02.5.1.3.6.1-1 varies from 0.60% to 3.38% in the NS (X) direction, from 2.46% to 9.07% in the EW (Y) direction, and from 0.34% to 15.05% in the vertical (Z) direction.

02.5.1.3.6.2 Modal Analysis

Fixed base modal analyses using ANSYS are performed on both the Detailed and the Dynamic FE models of the A/B. Plots of Cumulative Mass versus Frequency are shown in Figure 02.5.1.3.6.2-1 through Figure 02.5.1.3.6.2-3. The dynamic data for the A/B is presented in Table 02.5.1.3.6.2-1 through Table 02.5.1.3.6.2-6. In the horizontal directions, the modal frequencies and mode shapes presented are comparable mode for mode, see Table 02.5.1.3.6.2-1 through Table 02.5.1.3.6.2-4, and Figure 02.5.1.3.6.2-4 through Figure 02.5.1.3.6.2-7. Horizontal response is dominated by only one mode in each direction. Vertically the modes are not comparable one to one for the reasons cited above. However the data shows that between the narrow span of approximately 14 to 20 Hz the cumulative mass fractions are comparable. The results of the modal analysis indicate that the Dynamic FE model adequately captures the dynamic properties of the Detailed FE model.

02.5.1.3.6.3 Harmonic Response Analysis

The A/B is a Seismic Category II structure and therefore does not require a harmonic response analysis.

02.5.1.3.7 Validation of the Combined R/B Complex

Validation of the combined R/B complex Dynamic FE model is carried out in accordance with the methodology described in Section 02.4.1.2. A summary of these results for the combined R/B complex model is presented hereafter.

02.5.1.3.7.1 1g Static Analysis

Displacement results from the 1g static analyses are used to compare the distributions of mass and horizontal stiffness of the two models. Displacement in all three orthogonal

directions (X, Y, and Z) along the height at exterior wall location H (Shown in Figure 02.5.1.3.7.1-1) of both models are plotted in Figure 02.5.1.3.7.1-2 though Figure 02.5.1.3.7.1-10. They demonstrate that the Dynamic model lateral stiffness is comparable to that of the Detailed model (structure behavior follows the same trend for both models). Table 02.5.1.3.7.1-1 indicates that the maximum roof level lateral displacement difference between the two models at the various locations identified in Figure 02.5.1.3.7.1-1 varies from 0.02% to 10.74% in the NS (X) direction, from 0.15% to 6.75% in the EW (Y) direction, and from 0.00% to 11.27% in the vertical (Z) direction.

02.5.1.3.7.2 Modal Analysis

Fixed base modal analyses using ANSYS are performed on both the Detailed and the Dynamic FE models of the R/B complex. Plots of Cumulative Mass versus Frequency are shown in Figure 02.5.1.3.7.2-1 through Figure 02.5.1.3.7.2-3. The data for the R/B complex model comparison is shown in Table 02.5.1.3.7.2-1 and Table 02.5.1.3.7.2-2 for the X direction modes, Table 02.5.1.3.7.2-3 and Table 02.5.1.3.7.2-4 for the Y direction modes, and Table 02.5.1.3.7.2-5 and Table 02.5.1.3.7.2-6 for the Z direction modes. All modes with modal mass greater than 5% of the net modal mass computed, which is up to 100 Hz are presented. In some cases, data for modes with less than 5% modal mass is presented if it is thought to add some clarity. The criterion for the plots has been reduced since this model is much larger than the any of the individual models previously described.

The total dynamic mass appears in the Tables to be a lower fraction of the total than previously reported for the individual buildings, except the R/B model. This is because the foundation is included in the total mass reported. The mass of the foundation is 11608 for the detailed FE model and 11640 for the dynamic model. This is 29.6% of the total for the detailed FE dynamic model and 30.2% of the total for the dynamic model. Thus when the mode fraction up to 100 Hz reported in the Tables exceeds 70.4% (100.0-29.6) for the detailed FE model and 69.8% (100.0-30.2) for the Dynamic FE model, some of the mass of the foundation is participating in the modes that are extracted. Examining the mass fractions in the tables shows that for all three directions all the superstructure mass is captured in the modes up to 100 Hz.

The data in Table 02.5.1.3.7.2-1 through Table 02.5.1.3.7.2-4 and their accompanying figures show that the detailed FE model and the Dynamic FE model are equivalent mode for mode. In the vertical direction, owing to the argument previously presented regarding the cumulative mass over closely spaced modes, the data presented in Table 02.5.1.3.7.2-5 and Table 02.5.1.3.7.2-6, and accompanying figures, the models are dynamically equivalent. The results of the modal analysis indicate that the Dynamic FE model adequately captures the dynamic properties of the Detailed FE model.

02.5.1.4 Summary of the R/B Complex Dynamic FE Model

Validation of the Dynamic FE model is carried out in accordance with the methodology described in Section 02.4.1.2 to ensure that the integrated 3-D Dynamic FE model truly represents the dynamic properties of the R/B complex structures. Validation procedures and results are summarized in Section 02.5.1.3. Figure 02.5.1.4-1 shows an overview of the integrated 3-D Dynamic FE model while Figure 02.5.1.4-2 through Figure 02.5.1.4-5 reveal the interior structures with section views. Figure 02.5.1.4-6 presents the integrated 3-D Dynamic FE model after being translated into SASSI format.

02.5.1.5 Validation of the Dynamic Model Translation into SASSI Format

After the individual Dynamic FE models are validated against the Detailed FE models, the combined R/B complex Dynamic FE model is translated into SASSI (Reference 02-1) using the built in file converter. To confirm that the translation is accurate, a SASSI analysis is performed on the R/B complex model sitting on hard rock to simulate a fixed base condition. ATF are produced at prescribed locations presented in Figure 02.5.1.5-1 and compared with modal analysis results obtained from ANSYS to ensure that the structural response is accurate. The following Sections demonstrate that the integrated 3-D Dynamic SASSI model accurately represents the structural response of the combined Dynamic FE model developed in ANSYS.

Since the ANSYS FE formulation implementation is not identical with the SASSI FE formulation implementation, a few modifications were applied to the SASSI FE model to improve its numerical conditioning for the SASSI analysis. These FE model modifications were related to the introduction of appropriate boundary condition constraints for the node rotational degree of freedoms of the SOLID and SHELL elements, to avoid potential stiffness matrix singularities due to zero rotational terms.

The SASSI software includes a 3-D four-node Plate/Shell element with three translational and three rotational degrees of freedom per node. The shell elements are similar to the SAP IV thin Kirchhoff shell/plate elements. There is no stiffness corresponding to the in-plane rotational (drilling) degree of freedom in the element coordinate system for this shell/plate element. In the analysis of flat plates the stiffness associated with the rotation normal to the shell surface is not defined; therefore, the rotation normal degree of freedom must not to be included in the analysis. In cases where the curvature is very small or for flat plates, the in-plane rotational degree of freedom should be restrained by the addition of a "Spring/Boundary element" with a small rotational stiffness to prevent a numerical instability. In the SAP IV User Manual, Bathe and Wilson (Reference 02-12) suggested the normal rotational stiffness should be less or about 10% of the element bending stiffness, so that there is no influence on the system behavior.

in order to improve the numerical conditioning for the stiffness matrix, for the shell/plate elements that are oblique to global coordinate axes, small rotational stiffnesses around the normal axis to the shell elements were added to avoid the in-plane rotation singularity. The added rotational stiffnesses were equal to 10 that is 0.0001- 0.000001 times the shell element out-of-plane bending stiffnesses. In the cases of shell elements that are all in the same plane that is parallel to one of the global coordinate axes (with no other element type with rotational stiffness around the normal of the shell common plane), then, the in-plane rotations were fixed for those elements.

Three nodes are selected for the R/B complex FE model for illustration; two nodes are on the PCCV shell at different elevations and one node is on the top floor of the CIS, as shown in Figure 02.5.1.5-2 and Figure 02.5.1.5-3. Their coordinates are listed in the Table 02.5.1.5-1. The nodes and corresponding equation numbers are listed in Table 02.5.1.5-2. The diagonal stiffness matrix elements for the selected finite elements are listed in Table 02.5.1.5-3. Compare the shell element bending values, kr_{xx}, kr_{yy} and kr_{zz} that have values of hundreds of thousands, or millions, with the spring rotational stiffnesses introduced to improve the system numerical conditioning that are slightly less than 10. Thus, the added numerical rotational stiffnesses are negligible in comparison with the shell stiffnesses.

All rotations for the nodes that belong to only solid elements were also fixed.

02.5.1.5.1 R/B-FH/A SASSI Validation

The dominant mode contributions were found for the R/B-FH/A using the ANSYS Integrated 3-D Dynamic FE model. These are tabulated in Table 02.5.1.5.1-1. Figure 02.5.1.5.1-1 through Figure 02.5.1.5.1-3 show the contour plots of the first dominant mode shapes. The SASSI transfer functions are plotted along with the corresponding dominant modes for the NS(X), EW(Y), and Vertical (Z) direction in Figure 02.5.1.5.1-4 through Figure 02.5.1.5.1-15. The transfer function peaks occur close to the R/B-FH/A dominant modes for all three directions. This indicates proper translation from ANSYS to SASSI.

02.5.1.5.2 PCCV SASSI Validation

The dominant mode contributions were found for the PCCV using the ANSYS Integrated 3-D Dynamic FE model. These are tabulated in Table 02.5.1.5.2-1. Figure 02.5.1.5.2-1 through Figure 02.5.1.5.2-3 show the contour plots of the first dominant mode shapes. The SASSI transfer functions are plotted along with the corresponding dominant modes for the NS(X), EW(Y), and Vertical (Z) direction in Figure 02.5.1.5.2-4 through Figure 02.5.1.5.2-6. The transfer function peaks occur close to the PCCV dominant modes for all three directions. This indicates proper translation from ANSYS to SASSI.

02.5.1.5.3 CIS SASSI Validation

The dominant mode contributions were found for the CIS using the ANSYS Integrated 3-D Dynamic FE model. These are tabulated in Table 02.5.1.5.3-1. Figure 02.5.1.5.3-1 through Figure 02.5.1.5.3-3 show the contour plots of the first dominant mode shapes. The SASSI transfer functions are plotted along with the corresponding dominant modes for the NS(X), EW(Y), and Vertical (Z) direction in Figure 02.5.1.5.3-4 through Figure 02.5.1.5.3-12. The transfer function peaks occur close to the CIS dominant modes for all three directions. This indicates proper translation from ANSYS to SASSI.

02.5.1.5.4 East PS/B SASSI Validation

The dominant mode contributions were found for the East PS/B using the ANSYS Integrated 3-D Dynamic FE model, These are tabulated in Table 02.5.1.5.4-1. Figure 02.5.1.5.4-1 through Figure 02.5.1.5.4-3 show the contour plots of the first dominant mode shapes. The SASSI transfer functions are plotted along with the corresponding dominant modes for the NS(X), EW(Y), and Vertical (Z) direction in Figure 02.5.1.5.4-4 through Figure 02.5.1.5.4-6. The transfer function peaks occur close to the East PS/B dominant modes for all three directions. This indicates proper translation from ANSYS to SASSI.

02.5.1.5.5 West PS/B SASSI Validation

The dominant mode contributions were found for the West PS/B using the ANSYS Integrated 3-D Dynamic FE model. These are tabulated in Table 02.5.1.5.5-1. Figure 02.5.1.5.5-1 through Figure 02.5.1.5.5-3 show the contour plots of the first dominant mode shapes. The SASSI transfer functions are plotted along with the corresponding dominant modes for the NS(X), EW(Y), and Vertical (Z) direction in Figure 02.5.1.5.5-4 through Figure 02.5.1.5.5-6. The transfer function peaks occur close to the West PS/B dominant modes for all three directions. This indicates proper translation from ANSYS to SASSI.

02.5.1.5.6 A/B SASSI Validation

The dominant mode contributions were found for the A/B using the ANSYS Integrated 3-D Dynamic FE model, These are tabulated in Table 02.5.1.5.6-1. Figure 02.5.1.5.6-1 through Figure 02.5.1.5.6-3 show the contour plots of the first dominant mode shapes. The SASSI transfer functions are plotted along with the corresponding dominant modes for the NS(X), EW(Y), and Vertical (Z) direction in Figure 02.5.1.5.6-4 through Figure 02.5.1.5.6-6. The transfer function peaks occur close to the A/B dominant modes for all three directions. This indicates proper translation from ANSYS to SASSI.

Table 02.5.1.3-1 Typical 1g Analysis Result Observations

Model	Nominal Mesh Size (ft)		Observations - 1g NS Direction Results		
	Dynamic	Detailed	Typical Figure	Qualitative Observations	Max Error (%)
R/B	9	5	Figure 02.5.1.3.1.1-2	Dynamic Model Stiffer	4.94
PCCV	9	6	Figure 02.5.1.3.2.1-2	Results are close	1.54
CIS	9	4	Figure 02.5.1.3.3.1-2	Dynamic Model Stiffer	7.00
East PS/B	9	4	Figure 02.5.1.3.4.1-2	Dynamic Model Stiffer	4.79
West PS/B	9	4	Figure 02.5.1.3.5.1-2	Dynamic Model Stiffer	7.39
A/B	9	4	Figure 02.5.1.3.6.1-2	Dynamic Model Stiffer	3.36

Table 02.5.1.3-2 Typical Comparison of Fundamental Frequencies

Building	Detailed Model		Dynamic Model		Dynamic vs Detailed	Figure
	Mode #	Frequency (Hz)	Mode #	Frequency (Hz)	Frequency --	
R/B	1	4.60	1	4.74	2.91%	Figure 02.5.1.3.1.2-1
	4	5.96	4	5.94	-0.29%	
	5	6.71	5	6.78	0.94%	
	29	13.60	27	13.78	1.28%	
PCCV	2	4.46	2	4.48	0.52%	Figure 02.5.1.3.2.2-1
	20	12.92	23	12.94	0.19%	
	21	13.05	22	12.91	-1.06%	
	23	13.25	24	13.37	0.83%	
CIS	1	6.00	1	6.08	1.20%	Figure 02.5.1.3.3.2-1
	5	8.46	5	8.63	2.04%	
	23	12.08	23	12.33	2.04%	
	44	16.27	43	16.35	0.50%	

Table 02.5.1.3-3 Typical Comparison of ATF

Model	Observations - Harmonic Analysis Results Dynamic vs detailed		
	Typical Figure	Location	Qualitative Observations and Justification*
R/B	Figure 02.5.1.3.1.3-1	The Fourth Floor Horizontal ATF	PF match. Amp difference within 10%
PCCV	Figure 02.5.1.3.2.3-1	Main Equipment Hatch Horizontal ATF	PF match. Amp difference within 10%
CIS	Figure 02.5.1.3.3.1-2	RV Nozzle Horizontal ATF	PF generally match. Amp difference within 10%. One PF shifted (16.5 Hz vs. 19 Hz). This will be covered by 15% broadening in ISRS.
	Figure 02.5.1.3.3.1-3	RC Nozzle Vertical ATF	PF and Amp generally match. One PF shifted (38 Hz vs. 40Hz, 5% shift). Difference Amp at the first PF (16 Hz) is observed. There are close modes at PF of 18 Hz and 22 Hz. Figure 02.5.1.3.3.2-3 shows 10% of mass mobilized at PF of 16 Hz, 20% at PF of 18 Hz, and 65% at PF of 22 Hz. The modes at 18 Hz and 22 Hz have much more significant contributions on the response than the mode at PF of 16.
*PF=Peak Frequency; Amp=Amplitude			

Table 02.5.1.3-4 Mass Comparison of the Detailed and Dynamic Models

Building	Masses (k-ft/s2)						Ratio of Total Dyn/Det
	Superstructure		Foundation		Total		
	Detailed	Dynamic	Detailed	Dynamic	Detailed	Dynamic	
R/B	13103	12434	7929	7961	21032	20395	0.97
PCCV	2417	2458	0	0	2417	2458	1.02
CIS	3373	3374	0	0	3373	3374	1
East PS/B	1264	1253	748	748	2012	2002	1
West PS/B	1178	1160	808	808	1986	1969	0.99
A/B	6214	6216	2122	2123	8337	8338	1
Complex	27548	26896	11608	11640	39156	38536	0.98

Table 02.5.1.3.1.1-1 R/B Floor Mass Comparison

R/B Floor Mass Comparison (kip*sec^2/ft)				
Elev. Start	**Elev. End**	**Detailed Model**	**Dynamic Model**	**Diff. (%)**
-39'-8"	2'-7"	10,694	10,479	-2.01%
South Half				
2'-7"	48'-6"	1,082	1,094	1.02%
25'-3"	63'-4"	1,104	1,099	-0.48%
48'-6"	74'-10"	536	529	-1.33%
63'-4"	130'-6"	780	778	-0.31%
74'-10"	130'-6"	912	902	-1.05%
99'-9"	130'-6"	636	643	1.16%
North Half				
2'-7"	48'-6"	1,419	1,440	1.47%
25'-3"	74'-10"	1,105	1,081	-2.23%
48'-6"	113'-10"	1,328	1,333	0.38%
74'-10"	156'-0"	689	676	-1.88%
113'-10"	156'-0"	431	395	-8.42%
74'-10"	156'-0"	1,120	1,071	-4.40%
----------	----------	20,721	20,447	-1.32%

Note: Elevations shown are for the Dynamic Model.

Table 02.5.1.3.1.1-2 R/B 1g Static Analysis – Roof Displacement Comparison

Location	NS Direction			EW Direction			Vertical Direction		
	Displacement (ft)		Difference	Displacement (ft)		Difference	Displacement (ft)		Difference
	Detailed Model	Dynamic Model		Detailed Model	Dynamic Model		Detailed Model	Dynamic Model	
A	0.027	0.026	4.03%	0.028	0.029	1.70%	0.028	0.029	1.70%
B	0.024	0.024	0.17%	0.039	0.038	2.09%	0.003	0.003	4.97%
C	0.028	0.028	2.31%	0.030	0.030	1.81%	0.005	0.005	3.10%
D	0.038	0.038	1.72%	0.031	0.031	1.13%	0.006	0.006	1.18%
E	0.029	0.029	0.87%	0.031	0.030	1.70%	0.005	0.005	2.81%
F	0.025	0.024	2.32%	0.043	0.042	2.04%	0.004	0.004	4.27%
G	0.056	0.055	1.59%	0.039	0.039	0.13%	0.008	0.008	0.26%
H	0.071	0.069	2.88%	0.039	0.039	0.13%	0.008	0.007	5.63%

Table 02.5.1.3.1.2-1 R/B Modal Analysis Detailed Model – NS Direction (X)

Modal Mass for Modes up to 100 Hz = 17,161 k-ft/s2 = 82% of total				
Mode	Frequency (Hz)	Modal Mass	Mass Fraction (%)	Figure
1	4.601	2827.1	16.4	02.5.1.3.1.2-4
4	5.996	3242.8	18.9	02.5.1.3.1.2-6
5	6.711	1917.3	11.2	02.5.1.3.1.2-8
Sum		7987.2	46.5	

Table 02.5.1.3.1.2-2 R/B Modal Analysis Dynamic Model – NS Direction (X)

Modal Mass for Modes up to 100 Hz = 16,840 k-ft/s2 = 83% of total				
Mode	Frequency (Hz)	Modal Mass	Mass Fraction (%)	Figure
1	4.739	2759.7	16.5	02.5.1.3.1.2-5
4	5.943	2803.3	16.7	02.5.1.3.1.2-7
5	6.775	2238.8	13.3	02.5.1.3.1.2-9
Sum		7801.8	46.3	

Table 02.5.1.3.1.2-3 R/B Modal Analysis Detailed Model – EW Direction (Y)

Modal Mass for Modes up to 100 Hz = 17,303 k-ft/s2 = 82% of total				
Mode	Frequency (Hz)	Modal Mass	Mass Fraction (%)	Figure
2	5.506	7246.7	41.9	02.5.1.3.1.2-10
3	5.827	1142.5	6.6	02.5.1.3.1.2-12
Sum		8389.2	48.5	

Table 02.5.1.3.1.2-4 R/B Modal Analysis Dynamic Model – EW Direction (Y)

Modal Mass for Modes up to 100 Hz = 16,908 k-ft/s2 = 83% of total				
Mode	Frequency (Hz)	Modal Mass	Mass Fraction (%)	Figure
2	5.543	7153.8	42.3	02.5.1.3.1.2-11
3	5.894	1173.7	6.9	02.5.1.3.1.2-13
Sum		8327.5	49.3	

Table 02.5.1.3.1.2-5 R/B Modal Analysis Detailed Model – Vertical Direction (Z)

Modal Mass for Modes up to 100 Hz = 16,698 k-ft/s2 = 79% of total				
Mode	Frequency (Hz)	Modal Mass	Mass Fraction (%)	Figure
21	12.435	2740.6	16.4	02.5.1.3.1.2-14
22	12.529	1158.6	6.9	02.5.1.3.1.2-15
23	12.665	2491.5	14.9	02.5.1.3.1.2-17
Sum		6390.7	38.3	

Table 02.5.1.3.1.2-6 R/B Modal Analysis Dynamic Model – Vertical Direction (Z)

Modal Mass for Modes up to 100 Hz = 16,616 k-ft/s2 = 81% of total				
Mode	Frequency (Hz)	Modal Mass	Mass Fraction (%)	Figure
22	12.569	4156.5	25	02.5.1.3.1.2-16
24	13.226	1843.1	11.1	02.5.1.3.1.2-18
Sum		5999.6	36.1	

Table 02.5.1.3.2.1-1 PCCV 1g Static Analysis – Displacement Comparison

NS Direction			EW Direction			Vertical Direction		
Displacement (ft)		Difference	Displacement (ft)		Difference	Displacement (ft)		Difference
Detailed Model	Dynamic Model		Detailed Model	Dynamic Model		Detailed Model	Dynamic Model	
0.0556	0.0555	0.21%	0.0539	0.0547	1.46%	0.0077	0.0076	0.68%

Table 02.5.1.3.2.2-1 PCCV Modal Analysis Detailed Model – NS Direction (X)

Modal Mass for Modes up to 100 Hz = 2339.9 k-ft/s2 = 97% of total				
Mode	Frequency (Hz)	Modal Mass	Mass Fraction (%)	Figure
2	4.46	1673.3	71.5	02.5.1.3.2.2-4
20	12.92	181.2	7.7	02.5.1.3.2.2-6
21	13.05	136.8	5.9	02.5.1.3.2.2-8
Sum		1991.3	85.1	

Table 02.5.1.3.2.2-2 PCCV Modal Analysis Dynamic Model – NS Direction (X)

Modal Mass for Modes up to 100 Hz = 2374.2 k-ft/s2 = 97% of total				
Mode	Frequency (Hz)	Modal Mass	Mass Fraction (%)	Figure
2	4.48	1682.1	70.9	02.5.1.3.2.2-5
22	12.91	153.4	6.5	02.5.1.3.2.2-7
23	12.94	224.1	9.4	02.5.1.3.2.2-9
Sum		2059.6	86.7	

Table 02.5.1.3.2.2-3 PCCV Modal Analysis Detailed Model – EW Direction (Y)

Modal Mass for Modes up to 100 Hz = 2340.4 k-ft/s2 = 97% of total				
Mode	Frequency (Hz)	Modal Mass	Mass Fraction (%)	Figure
1	4.32	746.8	31.9	02.5.1.3.2.2-10
3	4.68	956.7	40.9	02.5.1.3.2.2-12
21	13.05	231.8	9.9	02.5.1.3.2.2-14
Sum		1935.3	82.7	

Table 02.5.1.3.2.2-4 PCCV Modal Analysis Dynamic Model – EW Direction (Y)

Modal Mass for Modes up to 100 Hz = 2372.8 k-ft/s2 = 97% of total				
Mode	Frequency (Hz)	Modal Mass	Mass Fraction (%)	Figure
1	4.31	724.9	30.6	02.5.1.3.2.2-11
3	4.66	1002.9	42.3	02.5.1.3.2.2-13
21	12.8	240.1	10.1	02.5.1.3.2.2-15
Sum		1967.9	82.9	

Table 02.5.1.3.2.2-5 PCCV Modal Analysis Detailed Model – Vertical Direction (Z)

Modal Mass for Modes up to 100 Hz = 2305.8 k-ft/s2 = 95% of total				
Mode	Frequency (Hz)	Modal Mass	Mass Fraction (%)	Figure
19	12.575	1576.2	68.4	02.5.1.3.2.2-16
Sum		1576.2	68.4	

Table 02.5.1.3.2.2-6 PCCV Modal Analysis Dynamic Model – Vertical Direction (Z)

Modal Mass for Modes up to 100 Hz = 2343.2 k-ft/s2 = 95% of total				
Mode	Frequency (Hz)	Modal Mass	Mass Fraction (%)	Figure
19	12.575	1429.9	61	02.5.1.3.2.2-17
Sum		1429.9	61	

Table 02.5.1.3.3.1-1 CIS 1g Static Analysis – Displacement Comparison – Uncracked Model

Location	NS Direction			EW Direction			Vertical Direction		
	Displacement (ft)		Difference	Displacement (ft)		Difference	Displacement (ft)		Difference
	Detailed Model	Dynamic Model		Detailed Model	Dynamic Model		Detailed Model	Dynamic Model	
Top of CIS									
North	0.00907	0.00857	5.51%	0.01093	0.01054	3.54%	0.00128	0.00130	1.72%
South	0.04576	0.04420	3.40%	0.03628	0.03491	3.78%	0.00262	0.00250	4.43%
East	0.01762	0.01645	6.62%	0.02481	0.02312	6.82%	0.00245	0.00231	5.44%
West	0.01766	0.01645	6.85%	0.02459	0.02287	7.01%	0.00249	0.00232	6.73%
Top of Reactor Vessel									
Top of Reactor	0.00750	0.00681	9.16%	0.00704	0.00641	8.97%	0.00208	0.00178	14.32%
Top of Steam Generators									
Northeast	0.02531	0.02429	4.02%	0.03383	0.03208	5.15%	0.00395	0.00395	0.13%
Northwest	0.02617	0.02531	3.30%	0.03438	0.03260	5.20%	0.00395	0.00396	0.08%
Southeast	0.02636	0.02534	3.86%	0.03290	0.03135	4.74%	0.00394	0.00395	0.25%
Southwest	0.02565	0.02449	4.53%	0.03336	0.03181	4.67%	0.00394	0.00395	0.30%
Top of Reactor Coolant Pumps									
Northeast	0.01791	0.01739	2.90%	0.01677	0.01629	2.87%	0.00106	0.00106	0.33%
Northwest	0.01850	0.01800	2.71%	0.01755	0.01720	1.98%	0.00107	0.00107	0.06%
Southeast	0.01957	0.01851	5.43%	0.01884	0.01854	1.57%	0.00112	0.00112	0.17%
Southwest	0.01919	0.01808	5.76%	0.01831	0.01788	2.34%	0.00111	0.00112	0.85%

Table 02.5.1.3.3.1-2 CIS 1g Static Analysis – Displacement Comparison – Cracked Model

Location	NS Direction			EW Direction			Vertical Direction		
	Displacement (ft)		Difference	Displacement (ft)		Difference	Displacement (ft)		Difference
	Detailed Model	Dynamic Model		Detailed Model	Dynamic Model		Detailed Model	Dynamic Model	
Top of CIS									
North	0.01630	0.01558	4.43%	0.02200	0.02101	4.49%	0.00182	0.00185	1.71%
South	0.08191	0.07955	2.88%	0.06991	0.06704	4.11%	0.00491	0.00468	4.61%
East	0.03276	0.03067	6.37%	0.04605	0.04289	6.85%	0.00523	0.00496	5.11%
West	0.03237	0.03022	6.63%	0.04584	0.04265	6.97%	0.00536	0.00499	7.00%
Top of Reactor Vessel									
Top of Reactor	0.00900	0.00823	8.49%	0.00923	0.00843	8.67%	0.00220	0.00188	14.82%
Top of Steam Generators									
Northeast	0.03994	0.03818	4.40%	0.05471	0.05182	5.28%	0.00397	0.00397	0.10%
Northwest	0.04028	0.03868	3.97%	0.05502	0.05208	5.34%	0.00397	0.00398	0.04%
Southeast	0.04109	0.03932	4.31%	0.05364	0.05102	4.87%	0.00395	0.00396	0.13%
Southwest	0.04005	0.03803	5.04%	0.05379	0.05121	4.79%	0.00396	0.00397	0.17%
Top of Reactor Coolant Pumps									
Northeast	0.01978	0.01915	3.20%	0.01754	0.01660	5.37%	0.00106	0.00105	0.57%
Northwest	0.02036	0.01970	3.26%	0.02055	0.02005	2.45%	0.00107	0.00107	0.19%
Southeast	0.02153	0.02020	6.18%	0.02012	0.01950	3.06%	0.00110	0.00110	0.02%
Southwest	0.02121	0.01980	6.65%	0.01978	0.01897	4.10%	0.00110	0.00110	0.66%

Table 02.5.1.3.3.2-1 CIS Modal Analysis – Detailed Model – NS Direction (X)

Modal Mass for Modes up to 100 Hz = 3018 k-ft/s2 = 89% of total				
Mode	Frequency (Hz)	Modal Mass	Mass Fraction (%)	Figure
1	4.47	359.3	11.9	02.5.1.3.3.2-4
5	6.57	857.1	28.4	02.5.1.3.3.2-6
Sum		1216.4	40.3	

Table 02.5.1.3.3.2-2 CIS Modal Analysis – Dynamic Model – NS Direction (X)

Modal Mass for Modes up to 100 Hz = 3014.1 k-ft/s2 = 89% of total				
Mode	Frequency (Hz)	Modal Mass	Mass Fraction (%)	Figure
1	4.52	334.5	10	02.5.1.3.3.2-5
5	6.74	885	29.4	02.5.1.3.3.2-7
Sum		1219.5	40.4	

Table 02.5.1.3.3.2-3 CIS Modal Analysis – Detailed Model – EW Direction (Y)

Modal Mass for Modes up to 100 Hz = 3044.5 k-ft/s2 = 90% of total				
Mode	Frequency (Hz)	Modal Mass	Mass Fraction (%)	Figure
2	4.79	865.5	28.4	02.5.1.3.3.2-8
3	5.74	320.3	10.5	02.5.1.3.3.2-10
Sum		1185.8	38.9	

Table 02.5.1.3.3.2-4 CIS Modal Analysis – Dynamic Model – EW Direction (Y)

Modal Mass for Modes up to 100 Hz = 3023.9 k-ft/s2 = 90% of total				
Mode	Frequency (Hz)	Modal Mass	Mass Fraction (%)	Figure
2	4.9	824	27.2	02.5.1.3.3.2-9
3	5.92	370.1	12.3	02.5.1.3.3.2-11
Sum		1194.1	39.5	

Table 02.5.1.3.3.2-5 CIS Modal Analysis – Detailed Model – Vertical Direction (Z)

Modal Mass for Modes up to 100 Hz = 2619.9.5 k-ft/s2 = 77% of total					
Mode	Frequency (Hz)	Modal Mass	Mass Fraction (%)	Cumm. Mass Fraction (%)	Figure
36	14.18	187	7.14	16.2	02.5.1.3.3.2-12
43	15.2	76.4	2.92	22.9	02.5.1.3.3.2-14
46	15.36	213.9	8.16	31.1	02.5.1.3.3.2-16
48	15.63	197.4	7.53	38.8	02.5.1.3.3.2-18
50	15.99	111.3	4.25	44.1	02.5.1.3.3.2-20
53	16.45	242.9	9.27	53.4	02.5.1.3.3.2-22
56	16.69	140.4	5.36	60.6	02.5.1.3.3.2-24

Table 02.5.1.3.3.2-6 CIS Modal Analysis – Dynamic Model – Vertical Direction (Z)

Modal Mass for Modes up to 100 Hz = 2613.6 k-ft/s2 = 77% of total					
Mode	Frequency (Hz)	Modal Mass	Mass Fraction (%)	Cumm. Mass Fraction (%)	Figure
36	14.25	86.7	3.32	12	02.5.1.3.3.2-13
44	15.39	136	5.2	22.5	02.5.1.3.3.2-15
45	15.41	135.9	5.2	27.7	02.5.1.3.3.2-17
49	16.34	123.6	4.73	37.4	02.5.1.3.3.2-19
50	16.38	176.1	6.74	44.1	02.5.1.3.3.2-21
55	16.88	121.6	4.65	53.5	02.5.1.3.3.2-23
56	17	112.2	4.49	57.8	02.5.1.3.3.2-25

Table 02.5.1.3.4.1-1 East PS/B 1g Static Analysis – Roof Displacement Comparison

Location	NS Direction			EW Direction			Vertical Direction		
	Displacement (ft)		Difference	Displacement (ft)		Difference	Displacement (ft)		Difference
	Detailed Model	Dynamic Model		Detailed Model	Dynamic Model		Detailed Model	Dynamic Model	
Northeast	0.0074	0.0073	1.75%	0.0104	0.0102	2.66%	0.0010	0.0010	1.23%
Northwest	0.0076	0.0075	1.35%	0.0131	0.0120	8.57%	0.0014	0.0014	3.39%
Southeast	0.0079	0.0086	7.94%	0.0097	0.0094	2.96%	0.0012	0.0012	0.06%
Southwest	0.0067	0.0066	2.16%	0.0086	0.0084	2.81%	0.0010	0.0010	1.17%

Table 02.5.1.3.4.2-1 East PS/B Modal Analysis – Detailed Model – NS Direction (X)

Modal Mass for Modes up to 100 Hz = 1323.7 k-ft/s2 = 66% of total				
Mode	Frequency (Hz)	Modal Mass	Mass Fraction (%)	Figure
2	11.71	956.2	72.2	02.5.1.3.4.2-4
Sum		956.2	72.2	

Table 02.5.1.3.4.2-2 East PS/B Modal Analysis – Dynamic Model – NS Direction (X)

Modal Mass for Modes up to 100 Hz = 1307.9 k-ft/s2 = 65% of total				
Mode	Frequency (Hz)	Modal Mass	Mass Fraction (%)	Figure
2	11.8	909.9	69.6	02.5.1.3.4.2-5
Sum		909.9	69.6	

Table 02.5.1.3.4.2-3 East PS/B Modal Analysis – Detailed Model – EW Direction (Y)

Modal Mass for Modes up to 100 Hz = 1365.5 k-ft/s2 = 68% of total				
Mode	Frequency (Hz)	Modal Mass	Mass Fraction (%)	Figure
1	9.71	843.4	61.8	02.5.1.3.4.2-6
Sum		843.4	61.8	

Table 02.5.1.3.4.2-4 East PS/B Modal Analysis – Dynamic Model – EW Direction (Y)

Modal Mass for Modes up to 100 Hz = 1351.9 k-ft/s2 = 68% of total				
Mode	Frequency (Hz)	Modal Mass	Mass Fraction (%)	Figure
1	9.9	833.2	61.6	02.5.1.3.4.2-7
Sum		833.2	61.6	

Table 02.5.1.3.4.2-5 East PS/B Modal Analysis – Detailed Model – Vertical Direction (Z)

Modal Mass for Modes up to 100 Hz = 1365.5 k-ft/s2 69% of total					
Mode	Frequency (Hz)	Modal Mass	Mass Fraction (%)	Cumm. Mass Fraction (%)	Figure
13	20.5	41.3	3.02	13.2	02.5.1.3.4.2-8
16	22	90.6	6.63	23.2	02.5.1.3.4.2-10
37	28.4	94.8	6.94	48.37	02.5.1.3.4.2-12
53	32.9	61.5	4.5	71.4	02.5.1.3.4.2-14

Table 02.5.1.3.4.2-6 East PS/B Modal Analysis – Dynamic Model – Vertical Direction (Z)

Modal Mass for Modes up to 100 Hz = 1245.7 k-ft/s2 = 63% of total					
Mode	Frequency (Hz)	Modal Mass	Mass Fraction (%)	Cumm. Mass Fraction (%)	Figure
14	21.94	60.7	4.87	12.6	02.5.1.3.4.2-9
15	22.18	100.2	8.04	20.7	02.5.1.3.4.2-11
34	27.83	44.9	3.6	46.1	02.5.1.3.4.2-13
57	34	78.2	6.28	73.1	02.5.1.3.4.2-15

Table 02.5.1.3.5.1-1 West PS/B 1g Static Analysis – Roof Displacement Comparison

Location	NS Direction			EW Direction			Vertical Direction		
	Displacement (ft)		Difference	Displacement (ft)		Difference	Displacement (ft)		Difference
	Detailed Model	Dynamic Model		Detailed Model	Dynamic Model		Detailed Model	Dynamic Model	
Northeast	0.0142	0.0132	7.25%	0.0070	0.0067	3.12%	0.0013	0.0013	1.42%
Northwest	0.0124	0.0116	6.02%	0.0070	0.0068	3.02%	0.0012	0.0011	4.15%
Southeast	0.0130	0.0120	7.87%	0.0061	0.0059	3.12%	0.0012	0.0011	3.18%
Southwest	0.0122	0.0116	4.53%	0.0069	0.0066	4.15%	0.0011	0.0011	2.62%

Table 02.5.1.3.5.2-1 West PS/B Modal Analysis – Detailed Model – NS Direction (X)

Modal Mass for Modes up to 100 Hz = 1257 k-ft/s2 = 63% of total				
Mode	Frequency (Hz)	Modal Mass	Mass Fraction (%)	Figure
1	8.28	707.4	56.3	02.5.1.3.5.2-4
10	19.67	221.1	17.6	02.5.1.3.5.2-6
Sum		928.5	73.9	

Table 02.5.1.3.5.2-2 West PS/B Modal Analysis – Dynamic Model – NS Direction (X)

Modal Mass for Modes up to 100 Hz = 1248.5 k-ft/s2 = 63% of total				
Mode	Frequency (Hz)	Modal Mass	Mass Fraction (%)	Figure
1	8.59	703.8	56.4	02.5.1.3.5.2-5
9	20.13	246.4	21.4	02.5.1.3.5.2-7
Sum		950.2	76.1	

Table 02.5.1.3.5.2-3 West PS/B Modal Analysis – Detailed Model – EW Direction (Y)

Modal Mass for Modes up to 100 Hz = 1262.8 k-ft/s2 = 64% of total				
Mode	Frequency (Hz)	Modal Mass	Mass Fraction (%)	Figure
2	11.89	792.8	62.8	02.5.1.3.5.2-8
Sum		792.8	62.8	

Table 02.5.1.3.5.2-4 West PS/B Modal Analysis – Dynamic Model – EW Direction (Y)

Modal Mass for Modes up to 100 Hz = 1237.5 k-ft/s2 = 63% of total				
Mode	Frequency (Hz)	Modal Mass	Mass Fraction (%)	Figure
2	12.15	798.7	64.5	02.5.1.3.5.2-9
Sum		798.7	64.5	

Table 02.5.1.3.5.2-5 West PS/B Modal Analysis – Detailed Model – Vertical Direction (Z)

Modal Mass for Modes up to 100 Hz = 1170.4 k-ft/s2 59% of total					
Mode	Frequency (Hz)	Modal Mass	Mass Fraction (%)	Cumm. Mass Fraction (%)	Figure
8	19.7	178.8	15.61	22.23	02.5.1.3.5.2-10
36	29.8	85.4	7.45	55.3	02.5.1.3.5.2-12

Table 02.5.1.3.5.2-6 West PS/B Modal Analysis – Dynamic Model – Vertical Direction (Z)

Modal Mass for Modes up to 100 Hz = 1145.7 k-ft/s2 = 58% of total					
Mode	Frequency (Hz)	Modal Mass	Mass Fraction (%)	Cumm. Mass Fraction (%)	Figure
9	19.1	172.3	14.72	23	02.5.1.3.5.2-11
36	29.2	53.2	4.55	52.2	02.5.1.3.5.2-13

Table 02.5.1.3.6.1-1 A/B 1g Static Analysis – Roof Displacement Comparison

Location	NS Direction			EW Direction			Vertical Direction		
	Displacement (ft)		Difference	Displacement (ft)		Difference	Displacement (ft)		Difference
	Detailed Model	Dynamic Model		Detailed Model	Dynamic Model		Detailed Model	Dynamic Model	
Northeast	0.0174	0.0170	2.49%	0.0242	0.0229	5.36%	0.0029	0.0029	0.81%
Northwest	0.0139	0.0135	3.38%	0.0181	0.0165	9.07%	0.0025	0.0021	15.05%
Southeast	0.0176	0.0175	0.60%	0.0259	0.0251	3.11%	0.0032	0.0034	4.99%
Southwest	0.0134	0.0132	1.08%	0.0204	0.0199	2.46%	0.0019	0.0019	0.34%

Table 02.5.1.3.6.2-1 A/B Modal Analysis – Detailed Model – NS Direction (X)

Modal Mass for Modes up to 100 Hz = 6509.2 k-ft/s2 = 78% of total				
Mode	Frequency (Hz)	Modal Mass	Mass Fraction (%)	Figure
2	8.31	4148.1	64.4	02.5.1.3.6.2-4
Sum		4148.1	64.4	

Table 02.5.1.3.6.2-2 A/B Modal Analysis – Dynamic Model – NS Direction (X)

Modal Mass for Modes up to 100 Hz = 6505.9 k-ft/s2 = 78% of total				
Mode	Frequency (Hz)	Modal Mass	Mass Fraction (%)	Figure
2	8.39	4168.3	64.1	02.5.1.3.6.2-5
Sum		4168.3	64.1	

Table 02.5.1.3.6.2-3 A/B Modal Analysis – Detailed Model – EW Direction (Y)

Modal Mass for Modes up to 100 Hz = 6556.6 k-ft/s2 = 79% of total				
Mode	Frequency (Hz)	Modal Mass	Mass Fraction (%)	Figure
1	6.82	4024.3	61.4	02.5.1.3.6.2-6
Sum		4024.3	61.4	

Table 02.5.1.3.6.2-4 A/B Modal Analysis – Dynamic Model – EW Direction (Y)

Modal Mass for Modes up to 100 Hz = 6583.2 k-ft/s2 = 79% of total				
Mode	Frequency (Hz)	Modal Mass	Mass Fraction (%)	Figure
1	6.96	3946.9	60	02.5.1.3.6.2-7
Sum		3946.9	60	

Table 02.5.1.3.6.2-5 A/B Modal Analysis – Detailed Model – Vertical Direction (Z)

Modal Mass for Modes up to 100 Hz = 6008.4 k-ft/s2 72% of total					
Mode	Frequency (Hz)	Modal Mass	Mass Fraction (%)	Cumm. Mass Fraction (%)	Figure
14	14.5	607.8	10.12	19.4	02.5.1.3.6.2-8
31	18.39	222.4	3.7	38.7	02.5.1.3.6.2-10
44	19.95	248	4.13	58.7	02.5.1.3.6.2-12

Table 02.5.1.3.6.2-6 A/B Modal Analysis – Dynamic Model – Vertical Direction (Z)

Modal Mass for Modes up to 100 Hz = 6005.0 k-ft/s2 = 72% of total					
Mode	Frequency (Hz)	Modal Mass	Mass Fraction (%)	Cumm. Mass Fraction (%)	Figure
15	15.87	634	10.56	23.1	02.5.1.3.6.2-9
27	17.94	359.6	5.99	42.9	02.5.1.3.6.2-11
48	20.48	150	2.5	59	02.5.1.3.6.2-13

Table 02.5.1.3.7.1-1 R/B Complex 1g Static Analysis – Roof Displacement Comparison

Location	NS Direction			EW Direction			Vertical Direction		
	Displacement (ft)		Difference	Displacement (ft)		Difference	Displacement (ft)		Difference
	Detailed Model	Dynamic Model		Detailed Model	Dynamic Model		Detailed Model	Dynamic Model	
A	0.06914	0.06794	1.74%	0.03328	0.03323	0.15%	0.00770	0.00731	5.04%
B	0.03740	0.03689	1.38%	0.02302	0.02289	0.53%	0.00574	0.00570	0.78%
C	0.02477	0.02425	2.09%	0.03597	0.03547	1.40%	0.00364	0.00352	3.51%
D	0.02277	0.02283	0.28%	0.02552	0.02485	2.59%	0.00375	0.00390	4.06%
E	0.05502	0.05433	1.24%	0.03410	0.03401	0.27%	0.00765	0.00768	0.41%
F	0.02664	0.02599	2.43%	0.01987	0.01984	0.16%	0.00431	0.00427	0.97%
G	0.02791	0.02776	0.53%	0.02281	0.02251	1.32%	0.00451	0.00442	1.95%
H	0.02797	0.02757	1.42%	0.02217	0.02188	1.32%	0.00452	0.00444	1.84%
I	0.01449	0.01419	2.06%	0.01733	0.01616	6.75%	0.00245	0.00217	11.27%
J	0.02486	0.02466	0.82%	0.02105	0.02083	1.04%	0.00443	0.00440	0.72%
K	0.01295	0.01292	0.27%	0.01692	0.01668	1.40%	0.00181	0.00187	3.27%
L	0.01031	0.01031	0.02%	0.01045	0.01006	3.70%	0.00094	0.00103	9.94%
M	0.01134	0.01256	10.74%	0.01054	0.01031	2.14%	0.00118	0.00119	1.10%
N	0.01009	0.01014	0.49%	0.01012	0.00989	2.33%	0.00108	0.00108	0.00%

Table 02.5.1.3.7.2-1 R/B Complex Modal Analysis – Detailed Model – NS Direction (X)

Modal Mass for Modes up to 100 Hz = 27,689.6 k-ft/s2 = 72% of total					
Mode	Frequency (Hz)	Modal Mass	Mass Fraction (%)	Cumm. Mass Fraction (%)	Figure
5	4.22	1927.8	7	7	02.5.1.3.7.2-4
7	4.3	2922.7	10.6	17.6	02.5.1.3.7.2-6
15	6.39	3675.3	13.3	36.5	02.5.1.3.7.2-8
52	10.73	1600.9	5.8	59.3	02.5.1.3.7.2-10
Sum		10126.7	36.5		

Table 02.5.1.3.7.2-2 R/B Complex Modal Analysis – Dynamic Model – NS Direction (X)

Modal Mass for Modes up to 100 Hz = 30878.5 k-ft/s2 = 82% of total					
Mode	Frequency (Hz)	Modal Mass	Mass Fraction (%)	Cumm. Mass Fraction (%)	Figure
2	4.27	2040.7	6.6	6.7	02.5.1.3.7.2-5
4	4.87	2996.5	9.7	16.4	02.5.1.3.7.2-7
12	6.41	3636.2	11.8	34.5	02.5.1.3.7.2-9
44	10.93	1477.7	4.8	57.9	02.5.1.3.7.2-11
Sum		10151.1	32.9		

Table 02.5.1.3.7.2-3 R/B Complex Modal Analysis – Detailed Model – EW Direction (Y)

Modal Mass for Modes up to 100 Hz = 27856.2 = 73% of total					
Mode	Frequency (Hz)	Modal Mass	Mass Fraction (%)	Cumm. Mass Fraction (%)	Figure
4	4.18	1515.5	5.4	5.5	02.5.1.3.7.2-12
12	6.12	4484.8	16.1	23.2	02.5.1.3.7.2-14
15	6.39	1779.7	6.4	30.5	02.5.1.3.7.2-16
17	6.92	1697.8	6.1	36.6	02.5.1.3.7.2-18
19	7.03	2295.6	8.2	46.3	02.5.1.3.7.2-20
Sum		11773.4	42.2		

Table 02.5.1.3.7.2-4 R/B Complex Modal Analysis – Dynamic Model – EW Direction (Y)

Modal Mass for Modes up to 100 Hz = 30970.2 k-ft/s2 = 82% of total					
Mode	Frequency (Hz)	Modal Mass	Mass Fraction (%)	Cumm. Mass Fraction (%)	Figure
1	4.18	1534.7	5	5	02.5.1.3.7.2-13
8	6.12	4070.2	13.1	20	02.5.1.3.7.2-15
12	6.41	2168.6	7	31.3	02.5.1.3.7.2-17
15	7.04	3059.7	9.9	42.3	02.5.1.3.7.2-19
16	7.12	1549.2	5	47.3	02.5.1.3.7.2-21
Sum		12382.4	40		

Table 02.5.1.3.7.2-5 R/B Complex Modal Analysis – Detailed Model – Vertical Direction (Z)

Modal Mass for Modes up to 100 Hz = 26725.7 k-ft/s2 = 70% of total					
Mode	Frequency (Hz)	Modal Mass	Mass Fraction (%)	Cumm. Mass Fraction (%)	Figure
71	12.1	2766	10.4	13.8	02.5.1.3.7.2-22
79	12.68	1120.2	4.2	23.9	02.5.1.3.7.2-24
80	12.7	1433.4	5.4	29.3	02.5.1.3.7.2-26
83	12.85	977.9	3.7	33.7	02.5.1.3.7.2-28
87	13.05	496.2	1.9	35.6	02.5.1.3.7.2-30
Sum		6793.7	25.4		

Table 02.5.1.3.7.2-6 R/B Complex Modal Analysis – Dynamic Model – Vertical Direction (Z)

Modal Mass for Modes up to 100 Hz = 29866.1 k-ft/s2 = 79% of total					
Mode	Frequency (Hz)	Modal Mass	Mass Fraction (%)	Cumm. Mass Fraction (%)	Figure
62	12.15	2766	9.3	13.8	02.5.1.3.7.2-23
70	12.74	3645.2	12.2	26.1	02.5.1.3.7.2-25
76	13.16	878.1	2.9	29.7	02.5.1.3.7.2-27
78	13.28	942.7	3.2	33.1	02.5.1.3.7.2-29
Sum		8232	27.6		

Table 02.5.1.5-1 Nodes Coordinates List

Node ID	Constraint ID						X	Y	Z	Location
43505	0	0	0	0	0	0	76.75	0	17.363	Containtment Wall – Low Elevation
56612	0	0	0	0	0	0	56.583	-6.75	75.417	Internal Structure Floor – High Elevation
61858	0	0	0	0	0	0	76.143	0	165	Containtment Wall – High Elevation

Table 02.5.1.5-2 Nodes Equation Numbers

Node Number	Equation Number for All Six DOFs (X, Y, Z, XX, YY, ZZ)					
43505	148925	148926	148927	148928	148929	148930
56612	212197	212198	212199	212200	212201	212202
61858	235425	235426	235427	235428	235429	235430

Table 02.5.1.5-3 Structural Stiffness on the Nodes

	Diagonal Stiffness Matrix Elements (Compare with Rotational Spring Stiffness of less than 10)					
Node ID	k_{xx}	k_{yy}	k_{zz}	kr_{xx}	kr_{yy}	kr_{zz}
43505	8379546	10309727.4	5983420	119052.4	57198349	92811478
56612	3935851.3	2981937.5	1895002	6095676	4413599	1945899
61858	3876490.3	7042790.5	4745087	875550.8	25236092	41467446

Table 02.5.1.5.1-1 R/B-FH/A Dominant Mode Contributions

Building	Direction	MODE	FREQUENCY (Hz)	PERIOD (s)	EFFECTIVE MASS (kips*s^2/ft)
R/B	X	4	4.87347	0.20519	2996.49
		7	5.9644	0.16766	600.066
		29	9.5148	0.1051	661.707
		44	10.9252	0.091531	1477.69
		86	13.7576	0.072687	718.645
	Y	8	6.12187	0.16335	4070.2
		17	7.46886	0.13389	176.463
		38	10.3641	0.096487	718.569
		122	15.634	0.063963	135.646
	Z	48	11.2864	0.088602	445.024
		62	12.1534	0.082281	2796.83
		76	13.1631	0.07597	878.126
		138	16.491	0.060639	134.676
		186	18.8581	0.053027	147.052

Table 02.5.1.5.2-1 PCCV Dominant Mode Contributions

Building	Direction	MODE	FREQUENCY (Hz)	PERIOD (s)	EFFECTIVE MASS (kips*s^2/ft)
PCCV	X	2	4.26536	0.23445	2042.39
		66	12.5722	0.07954	233.417
	Y	1	4.18314	0.23905	1534.65
		64	12.4063	0.080604	423.864
	Z	62	12.1534	0.082281	2796.83
		233	20.3642	0.049106	258.677

Table 02.5.1.5.3-1 CIS Dominant Mode Contributions

Building	Direction	MODE	FREQUENCY (Hz)	PERIOD (s)	EFFECTIVE MASS (kips*s^2/ft)
CIS	X	23	8.28912	0.12064	570.763
		61	11.9893	0.083408	338.592
		219	19.99	0.050025	132.482
		18	7.59861	0.1316	80.3722
	Y	11	6.32335	0.15814	1344.05
		64	12.4063	0.080604	423.864
		400	24.8037	0.040317	171.142
	Z	62	12.1534	0.082281	2796.83
		117	15.4544	0.064707	186.996
		254	20.992	0.047637	144.287

Table 02.5.1.5.4-1 East PS/B Dominant Mode Contributions

Building	Direction	MODE	FREQUENCY (Hz)	PERIOD (s)	EFFECTIVE MASS (kips*s^2/ft)
East PS/B	X	12	6.40603	0.1561	3636.19
		44	10.9252	0.091531	1477.69
		78	13.2831	0.075283	174.22
	Y	16	7.11635	0.14052	1549.15
		96	14.3577	0.069649	460.71
		122	15.634	0.063963	135.646
	Z	70	12.7434	0.078472	3645.2
		138	16.491	0.060639	134.676
		254	20.992	0.047637	144.287

Table 02.5.1.5.5-1 West PS/B Dominant Mode Contributions

Building	Direction	MODE	FREQUENCY (Hz)	PERIOD (s)	EFFECTIVE MASS (kips*s^2/ft)
West PS/B	X	25	8.84034	0.11312	302.736
		44	10.9252	0.091531	1477.69
		181	18.6967	0.053485	112.357
	Y	16	7.11635	0.14052	1549.15
		76	13.1631	0.07597	128.925
	Z	70	12.7434	0.078472	3645.2
		107	15.056	0.066419	123.737
		241	20.6378	0.048455	153.926

Table 02.5.1.5.6-1 A/B Dominant Mode Contributions

Building	Direction	MODE	FREQUENCY (Hz)	PERIOD (s)	EFFECTIVE MASS (kips*s^2/ft)
A/B	X	8	6.12187	0.16335	1276.76
		44	10.9252	0.091531	1477.69
		68	12.6206	0.079236	194.548
	Y	15	7.03958	0.14205	3059.65
		27	9.23838	0.10824	827.042
		38	10.3641	0.096487	718.569
	Z	136	16.408	0.060946	215.07
		241	20.6378	0.048455	153.926

Figure 02.5.1.1-1 Dynamic R/B Complex FE Model

Figure 02.5.1.1-2 Section View of Dynamic R/B Complex FE Model Looking East

Figure 02.5.1.1-3 Section View of Dynamic R/B Complex FE Model Looking North

Figure 02.5.1.1-4 PCCV Dynamic Model

Figure 02.5.1.1-5 CIS Dynamic Model – Shell Elements (Excluding RCL)

Figure 02.5.1.1-6 CIS Dynamic Model – Solid Elements

Figure 02.5.1.1-7 CIS Dynamic Model – Beam Elements (Excluding RCL)

Figure 02.5.1.1-8 East PS/B Dynamic Model

Figure 02.5.1.1-9 West PS/B Dynamic Model

Figure 02.5.1.1-10 A/B Dynamic Model

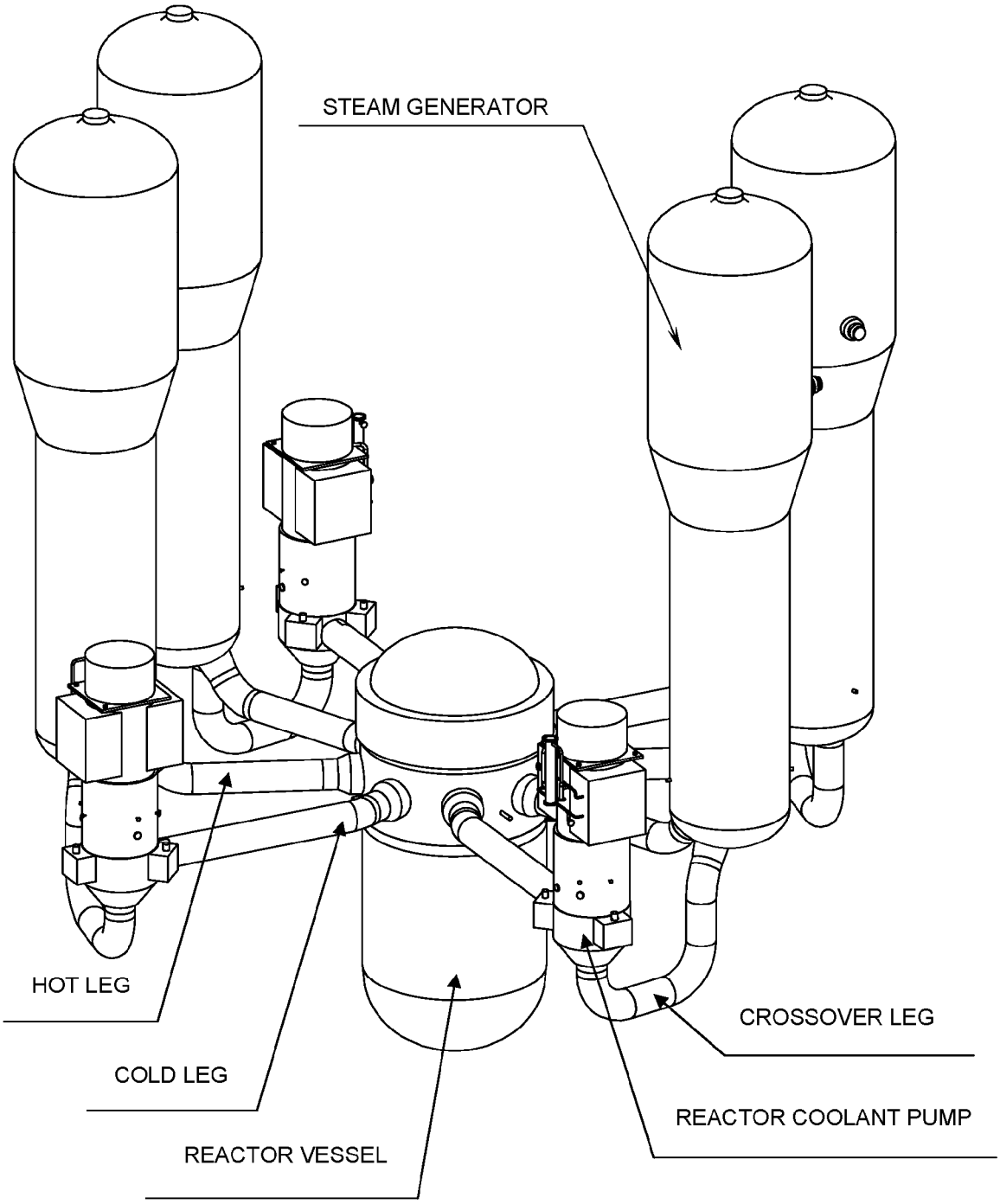

Figure 02.5.1.2.1-1 US-APWR Reactor Coolant Loop (RCL)

Figure 02.5.1.2.1-2 Dynamic Model of RCL

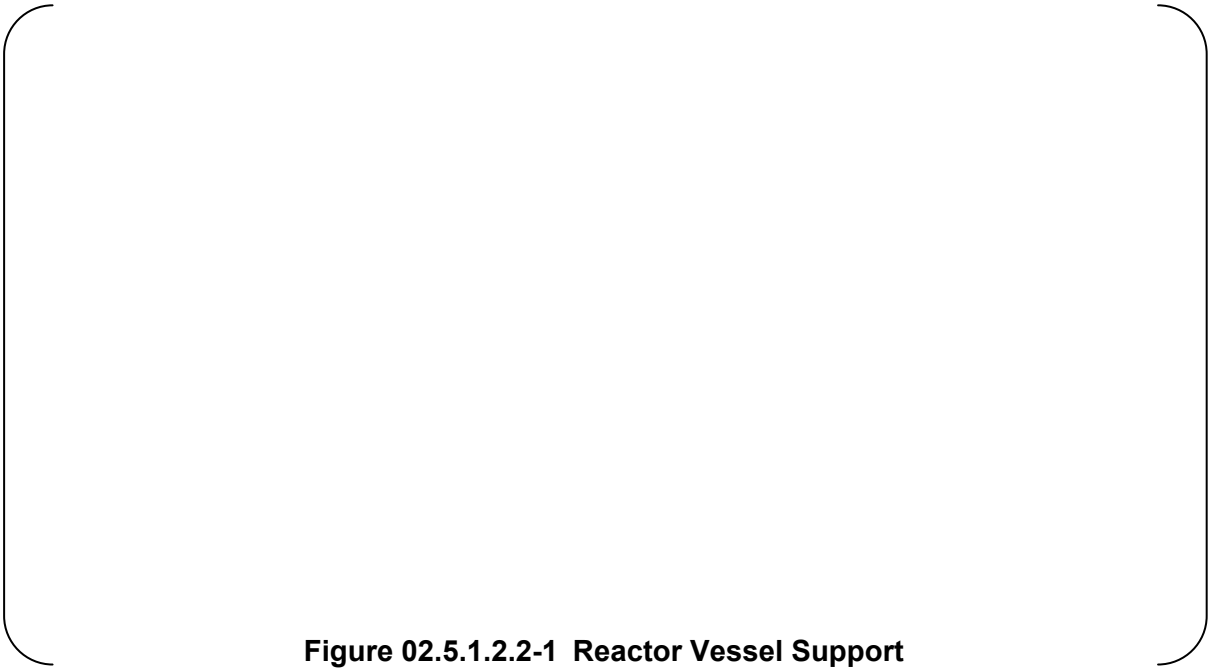

Figure 02.5.1.2.2-1 Reactor Vessel Support

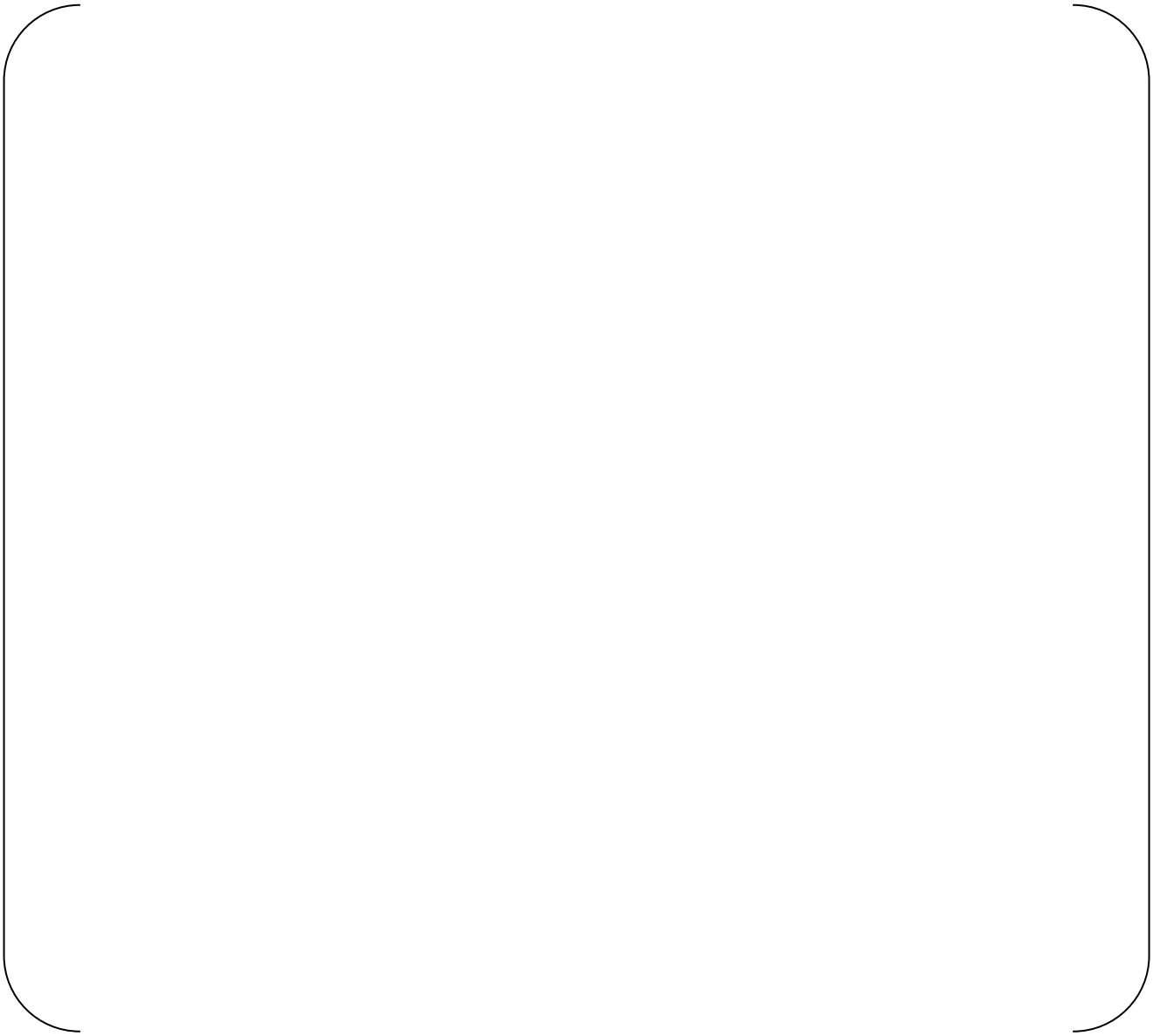

Figure 02.5.1.2.2-2 Reactor Vessel Support FE Model Connection

Figure 02.5.1.2.2-3 Steam Generator Lower Lateral Support

Figure 02.5.1.2.2-4 Reactor Coolant Pump (RCP) Tie Rod Support

Figure 02.5.1.2.2-5 Steam Generator Supports FE Model Connections

Figure 02.5.1.3.1.1-1 Displacement Locations on R/B Exterior Walls

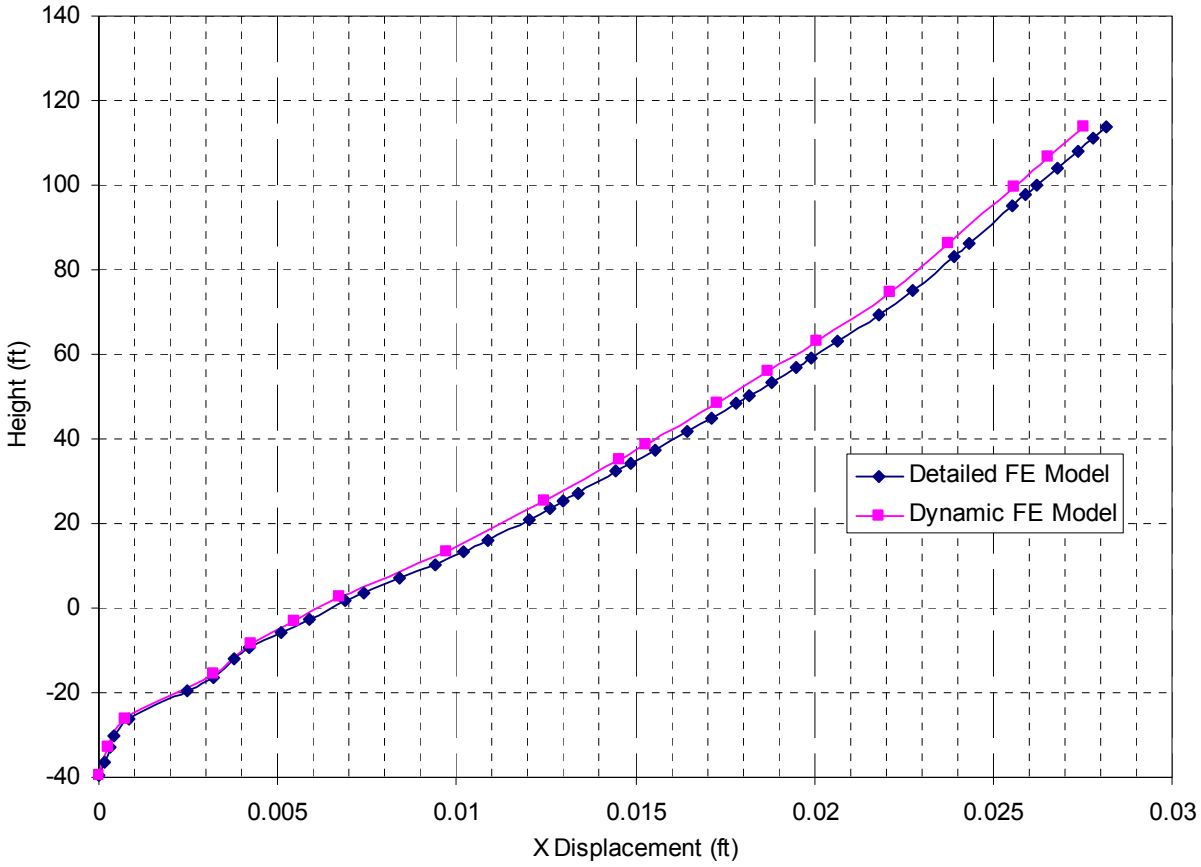

Figure 02.5.1.3.1.1-2 R/B 1g Static Analysis – NS Direction (X) at Location C

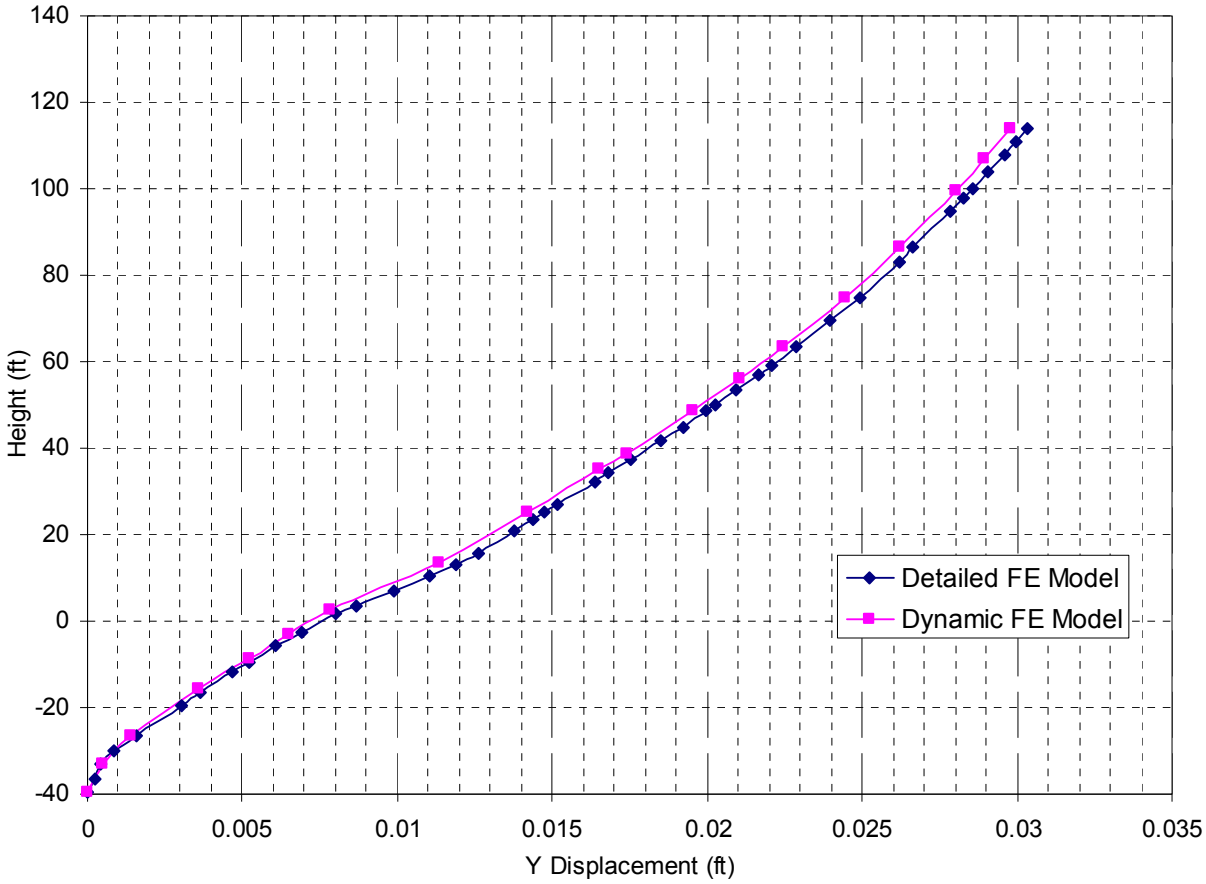

Figure 02.5.1.3.1.1-3 R/B 1g Static Analysis – EW Direction (Y) at Location C

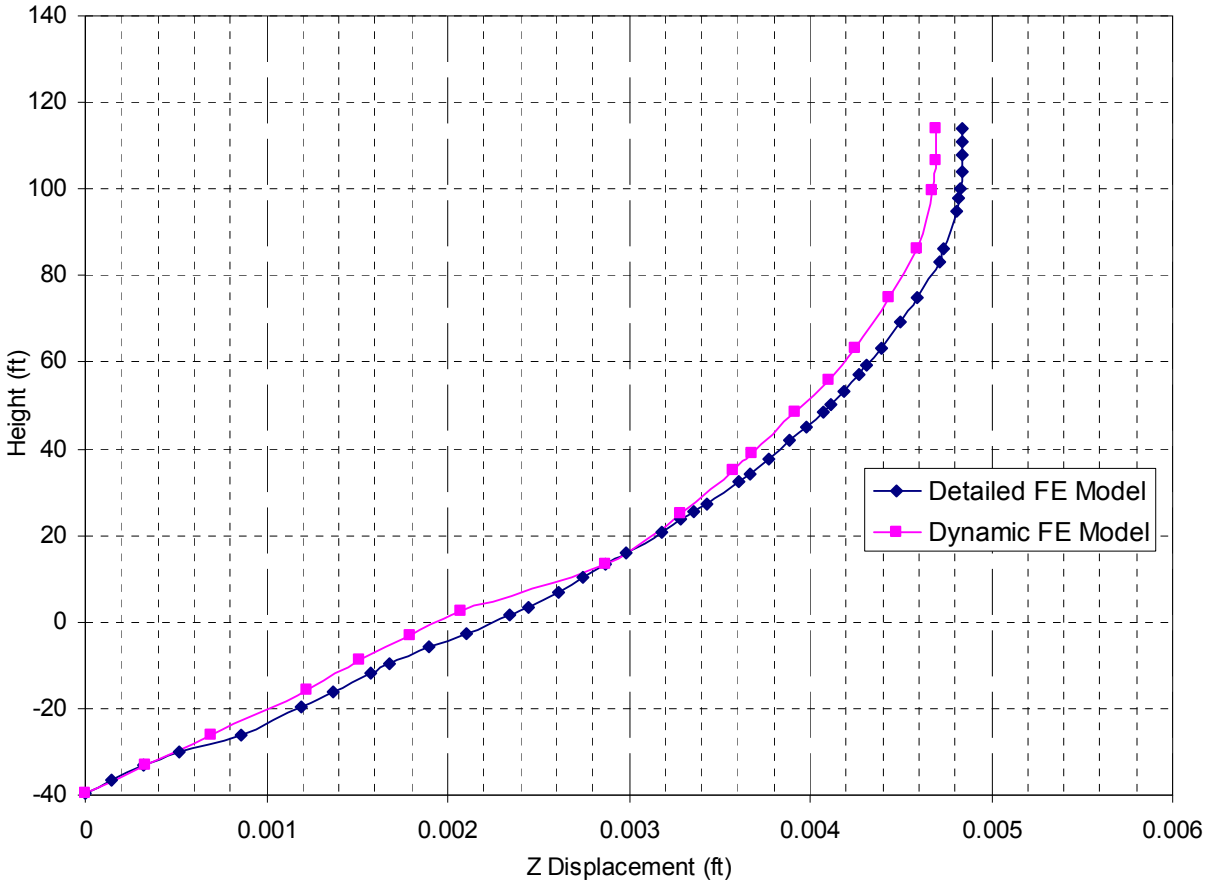

Figure 02.5.1.3.1.1-4 R/B 1g Static Analysis – Vertical Direction (Z) at Location C

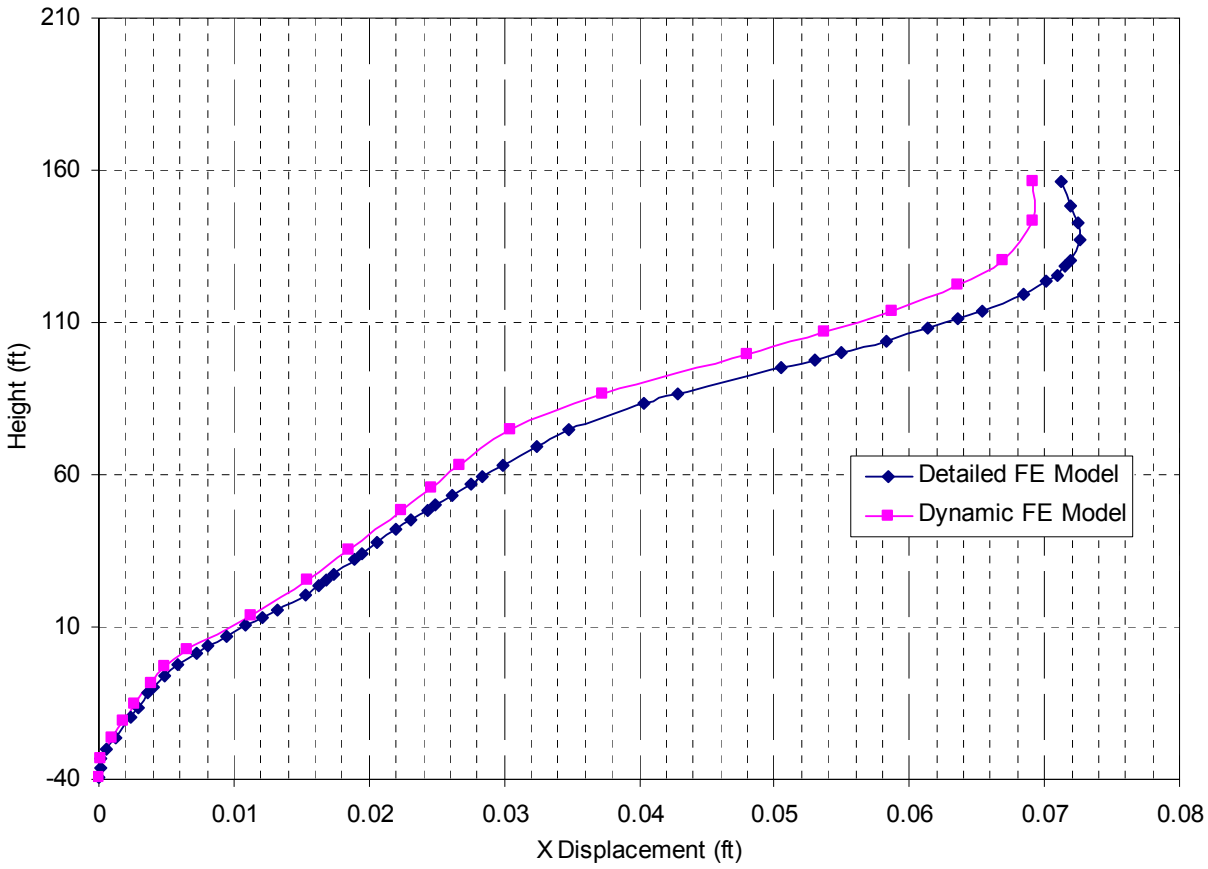

Note: The curves shown for this location on the R/B are due to the stiffness of the FH/A in the NS direction being greater than the EW direction. The Northern wall of the FH/A is flexible in comparison to the Eastern and Western walls combined with the roof diaphragm. Therefore, the Northern wall has a greater deflection at midheight than at the roof diaphragm.

Figure 02.5.1.3.1.1-5 R/B 1g Static Analysis – NS Direction (X) at Location H

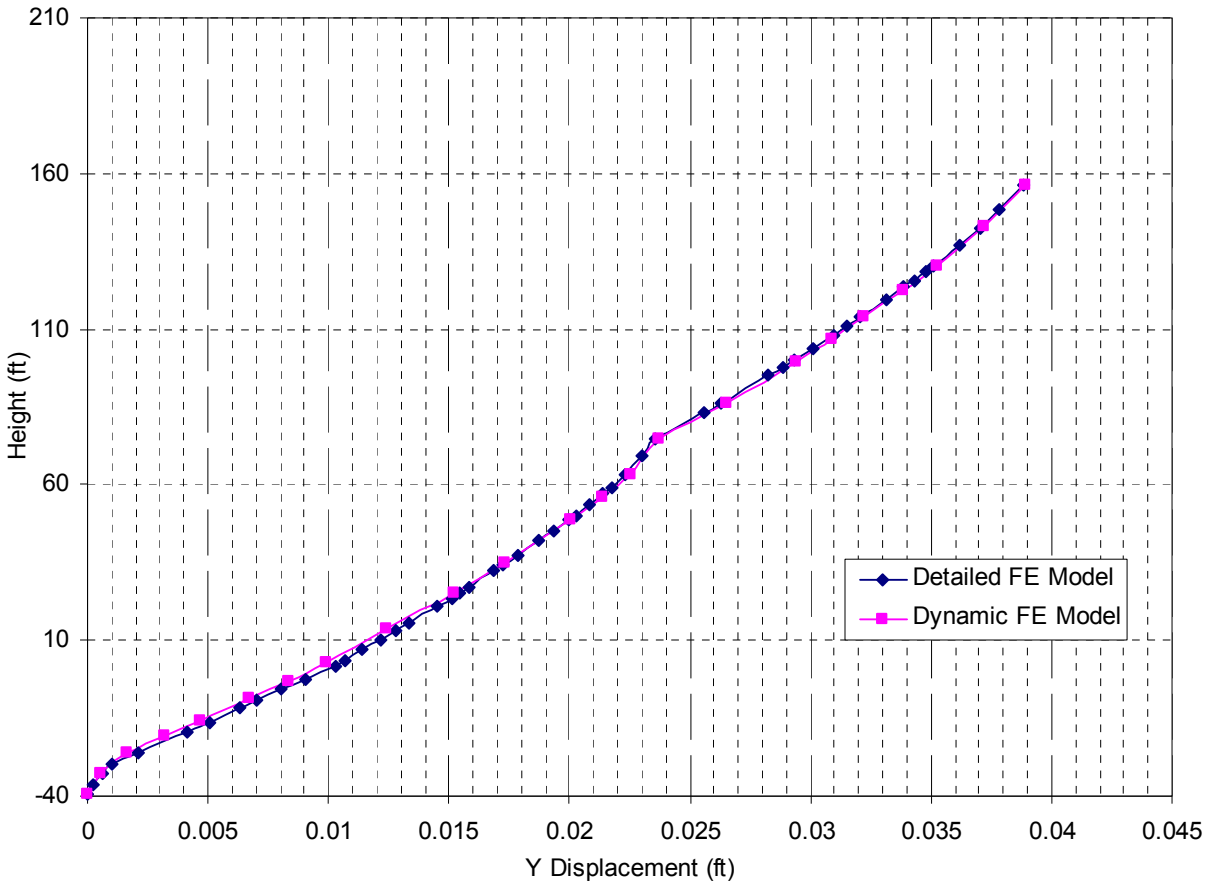

Figure 02.5.1.3.1.1-6 R/B 1g Static Analysis – EW Direction (Y) at Location H

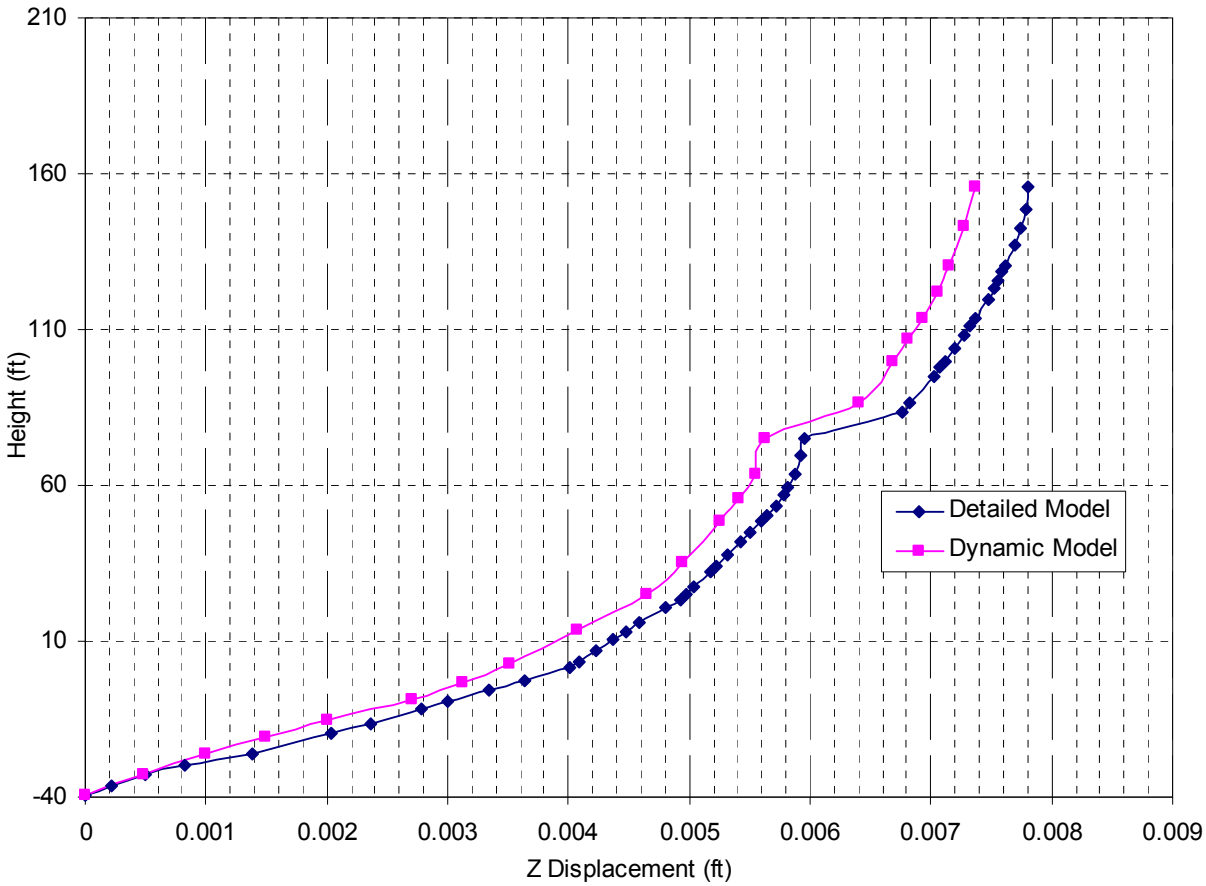

Figure 02.5.1.3.1.1-7 R/B 1g Static Analysis – Vertical Direction (Z) at Location H

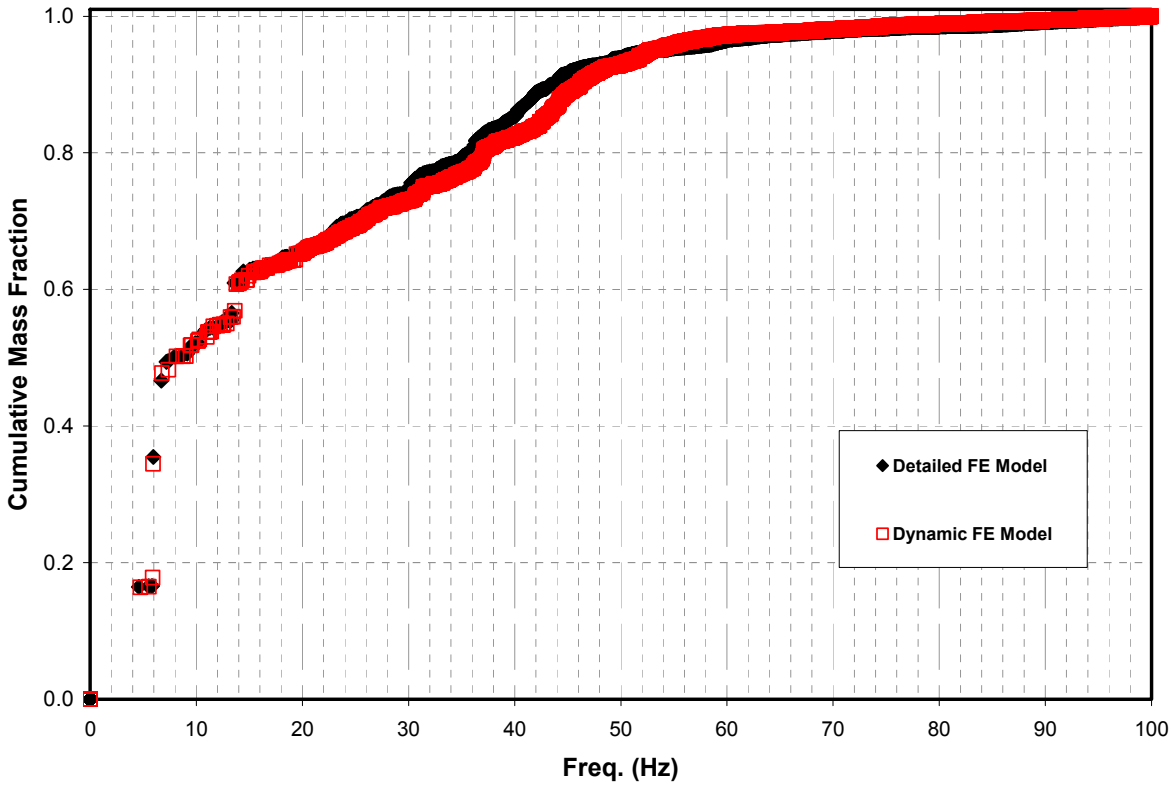

Figure 02.5.1.3.1.2-1 R/B Modal Analysis – Cumulative Mass in the NS Direction (X)

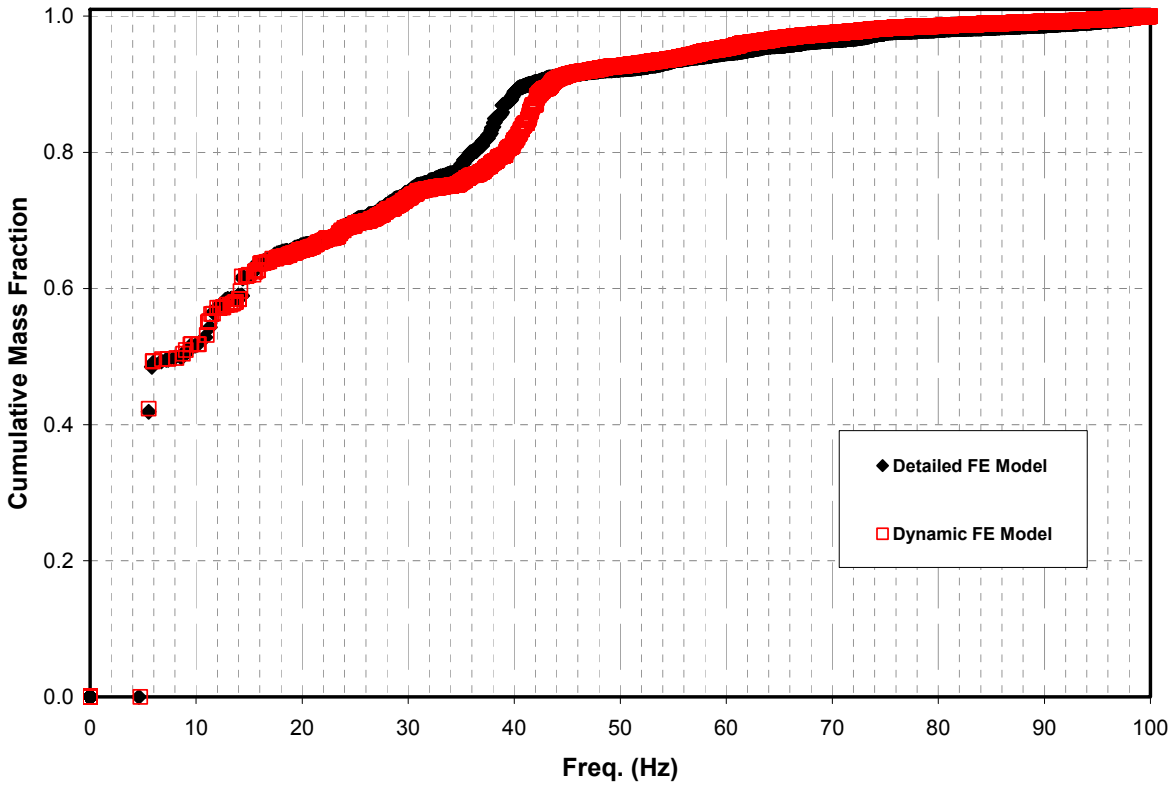

Figure 02.5.1.3.1.2-2 R/B Modal Analysis – Cumulative Mass in the EW Direction (Y)

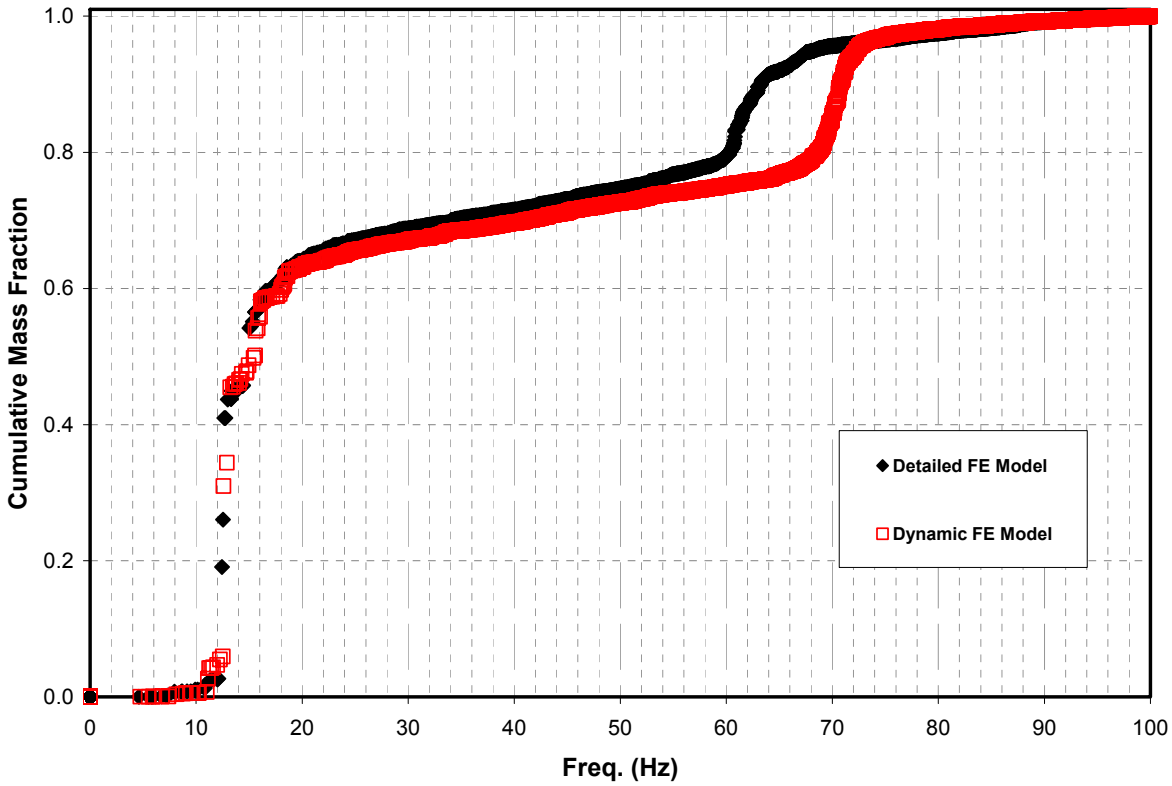

Figure 02.5.1.3.1.2-3 R/B Modal Analysis – Cumulative Mass in the Vertical Direction (Z)

Figure 02.5.1.3.1.2-4 R/B Detailed Mode Shape – Mode 1 at Frequency 4.601 Hz- NS Direction (X)

Figure 02.5.1.3.1.2-5 R/B Dynamic Mode Shape – Mode 1 at Frequency 4.739 Hz - NS Direction (X)

Figure 02.5.1.3.1.2-6 R/B Detailed Mode Shape – Mode 4at Frequency 5.996 Hz- NS Direction (X)

Figure 02.5.1.3.1.2-7 R/B Dynamic Mode Shape – Mode 4 at Frequency 5.943 Hz- NS Direction (X)

Figure 02.5.1.3.1.2-8 R/B Detailed Mode Shape – Mode 5 at Frequency 6.711 Hz - NS Direction (X)

Figure 02.5.1.3.1.2-9 R/B Dynamic Mode Shape – Mode 5 at Frequency 6.775 Hz - NS Direction (X)

Figure 02.5.1.3.1.2-10 R/B Detailed Mode Shape – Mode 2 at Frequency 5.506 Hz - EW Direction (Y)

Figure 02.5.1.3.1.2-11 R/B Dynamic Mode Shape – Mode 2 at Frequency 5.543 Hz - EW Direction (Y)

Figure 02.5.1.3.1.2-12 R/B Detailed Mode Shape – Mode 3 at Frequency 5.827 Hz- EW Direction (Y)

Figure 02.5.1.3.1.2-13 R/B Dynamic Mode Shape – Mode 3 at Frequency 5.894 Hz- EW Direction (Y)

Figure 02.5.1.3.1.2-14 R/B Detailed Mode Shape – Mode 21 at Frequency 12.435 Hz - Vertical Direction (Z)

Figure 02.5.1.3.1.2-15 R/B Detailed Mode Shape – Mode 22 at Frequency 12.529 Hz - Vertical Direction (Z)

Figure 02.5.1.3.1.2-16 R/B Dynamic Mode Shape – Mode 22 at Frequency 12.569 Hz - Vertical Direction (Z)

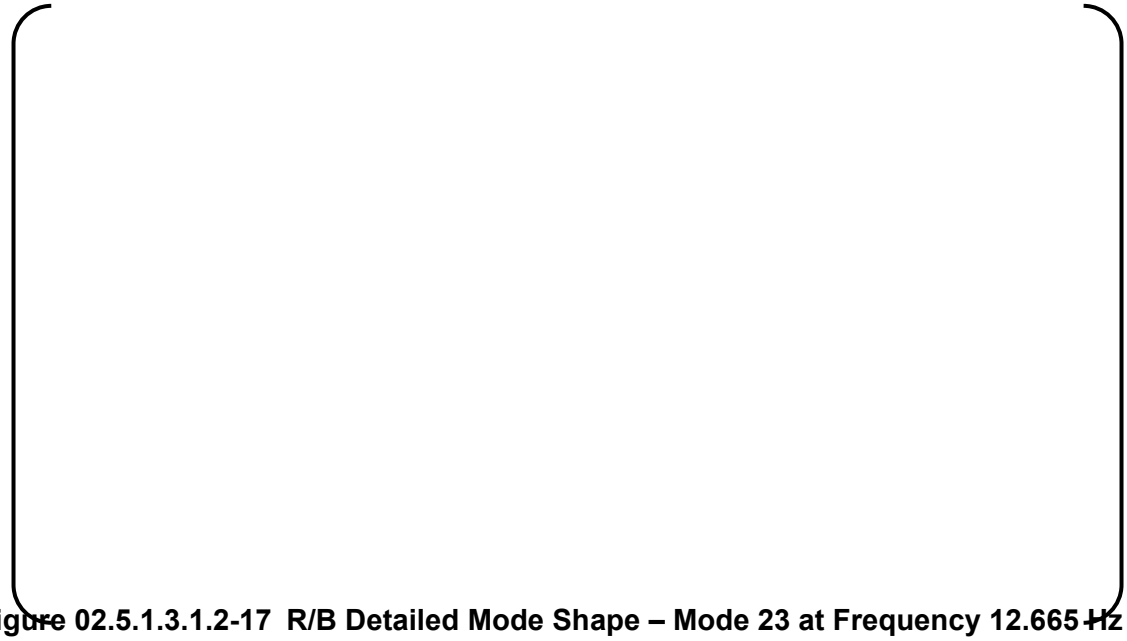

Figure 02.5.1.3.1.2-17 R/B Detailed Mode Shape – Mode 23 at Frequency 12.665 Hz - Vertical Direction (Z)

Figure 02.5.1.3.1.2-18 R/B Dynamic Mode Shape – Mode 24 at Frequency 13.226 Hz - Vertical Direction (Z)

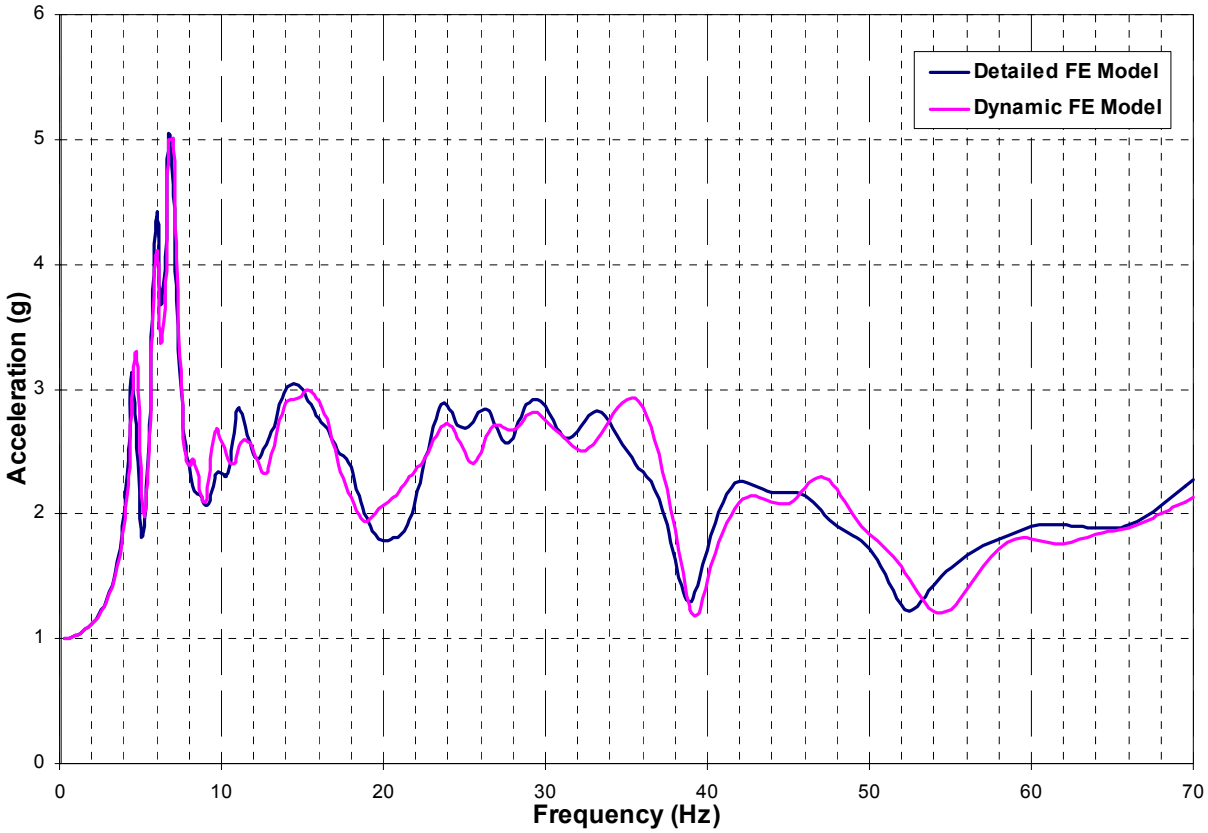

Figure 02.5.1.3.1.3-1 R/B Harmonic Response Analysis – NS Direction (X) at Plan Location B-Elevation at Fourth Floor

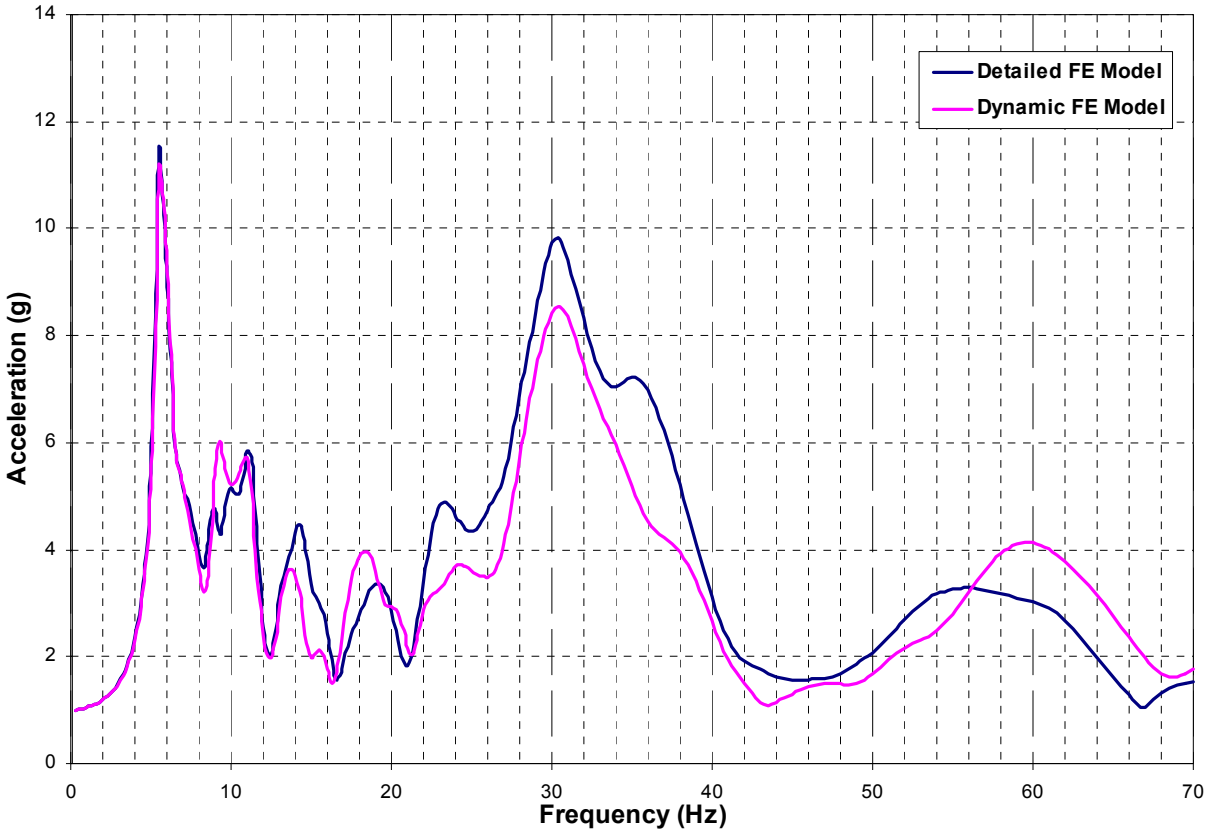

Figure 02.5.1.3.1.3-2 R/B Harmonic Response Analysis – EW Direction (Y) at Plan Location B-Elevation at Fourth Floor

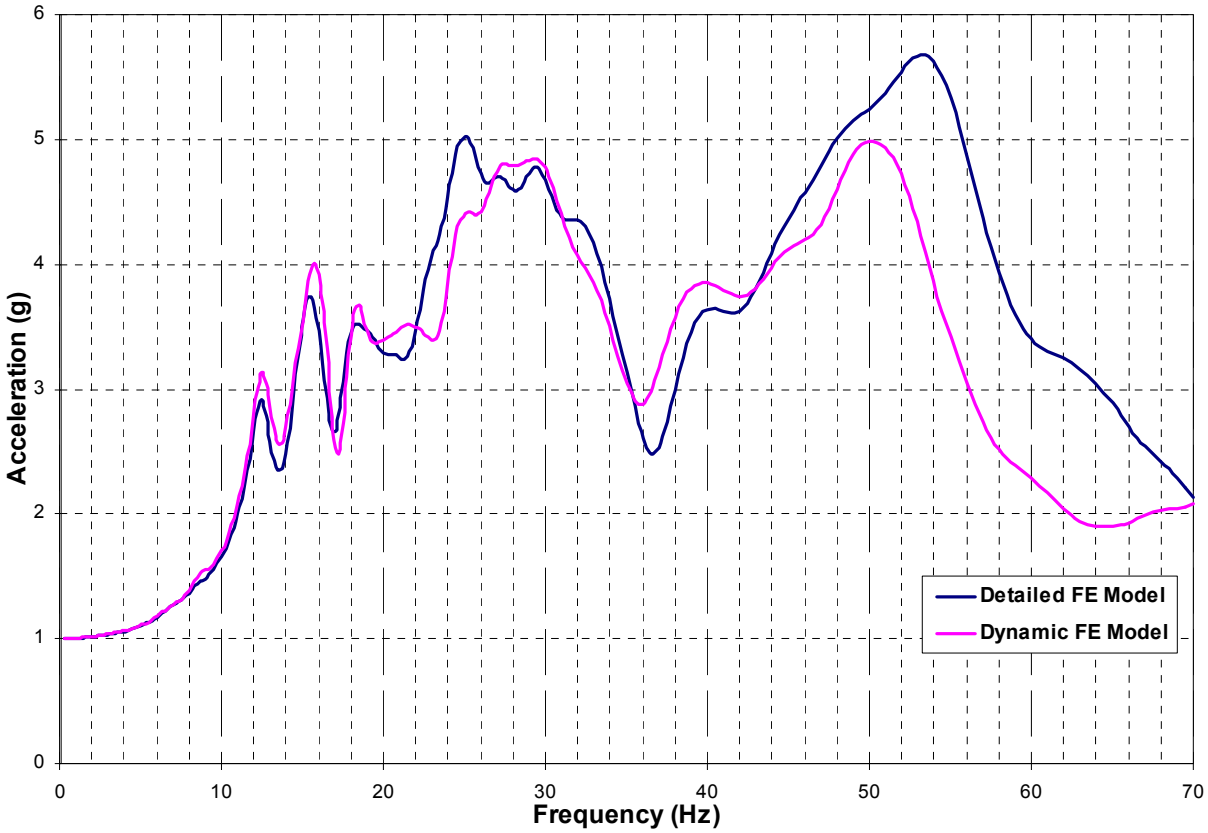

Figure 02.5.1.3.1.3-3 R/B Harmonic Response Analysis – Vertical Direction (Z) at Plan Location B-Elevation at Fourth Floor

Figure 02.5.1.3.2.1-1 Displacement Locations on PCCV

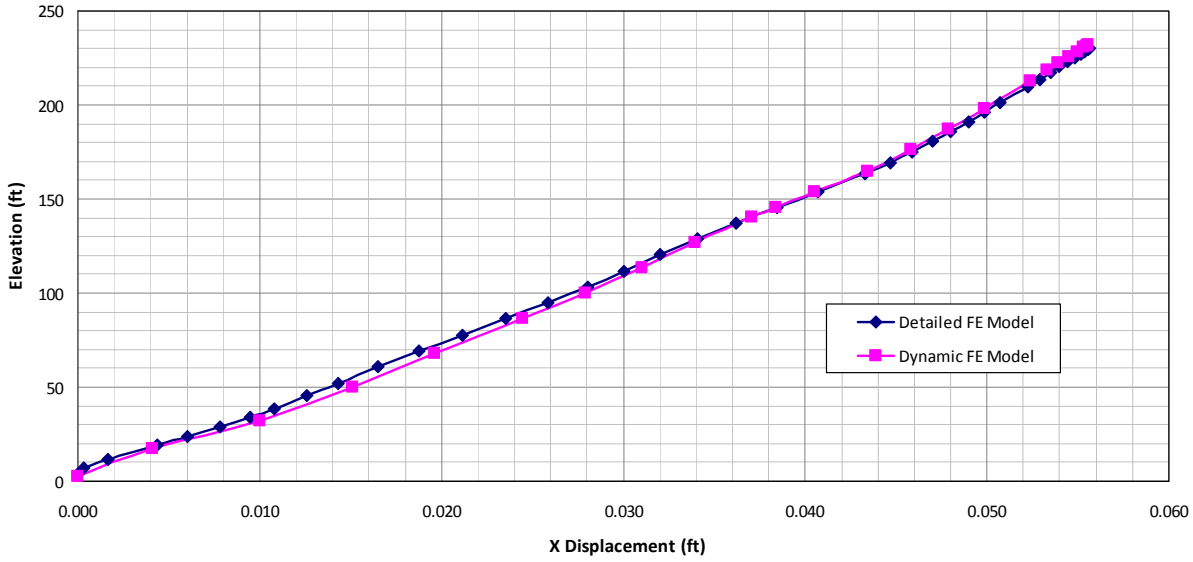

Figure 02.5.1.3.2.1-2 PCCV 1g Static Analysis – NS Direction (X) at North Face of Structure

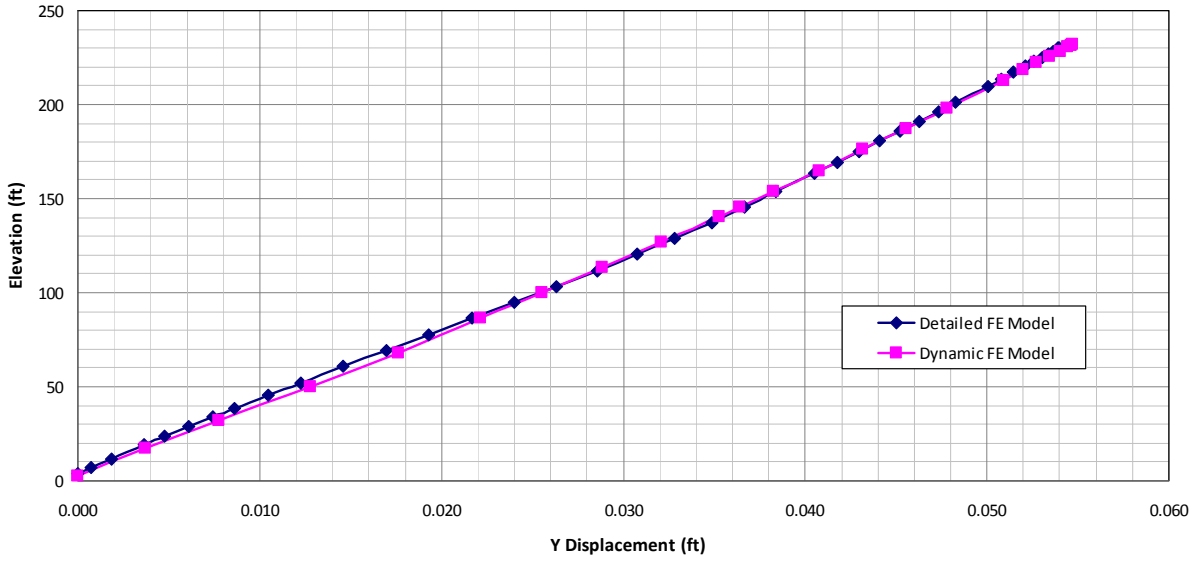

Figure 02.5.1.3.2.1-3 PCCV 1g Static Analysis – EW direction (Y) at North Face of Structure

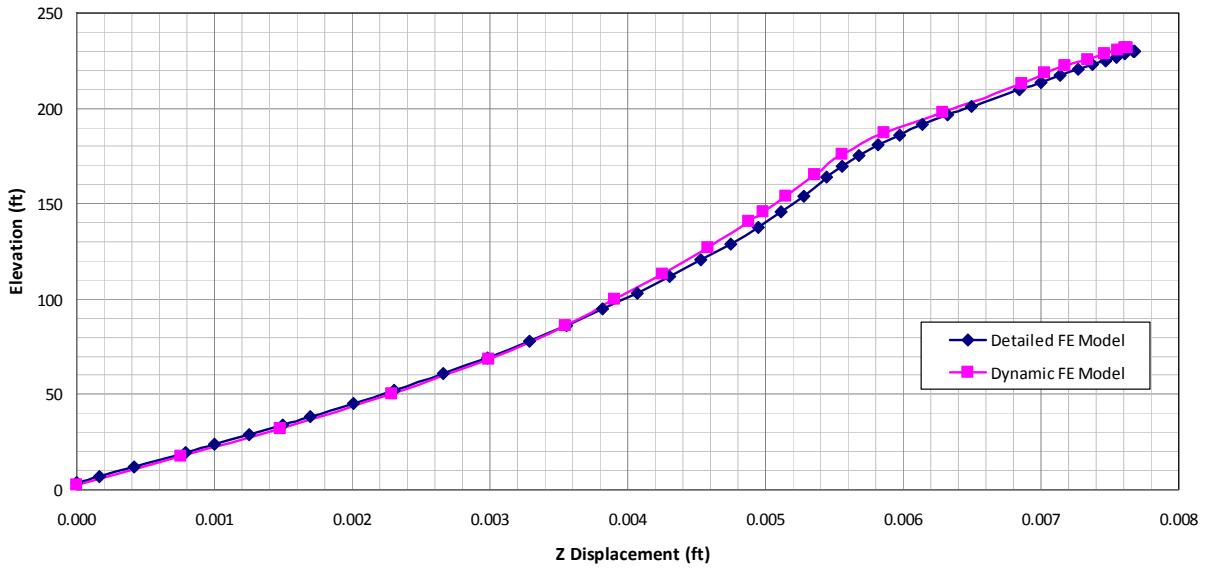

Figure 02.5.1.3.2.1-4 PCCV 1g Static Analysis – Vertical direction (Z) at North Face of Structure

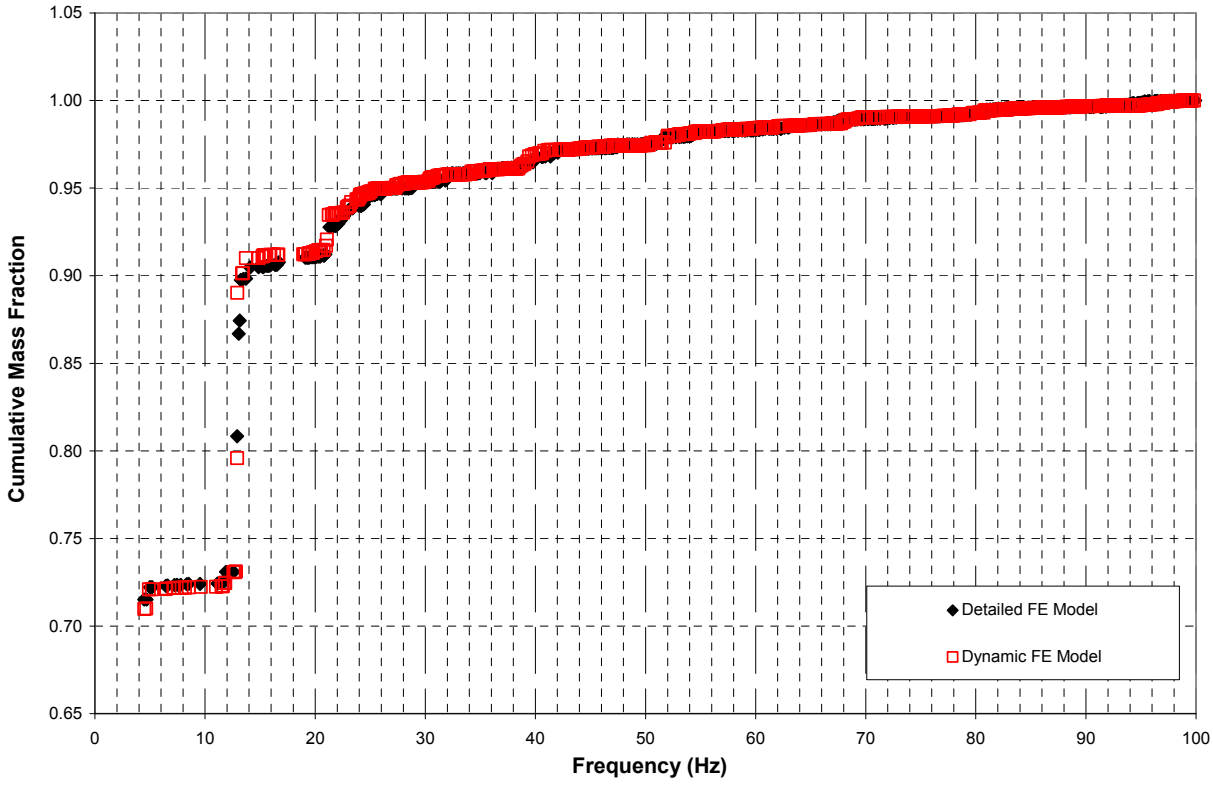

Figure 02.5.1.3.2.2-1 PCCV Modal Analysis – Cumulative Mass in the NS Direction (X)

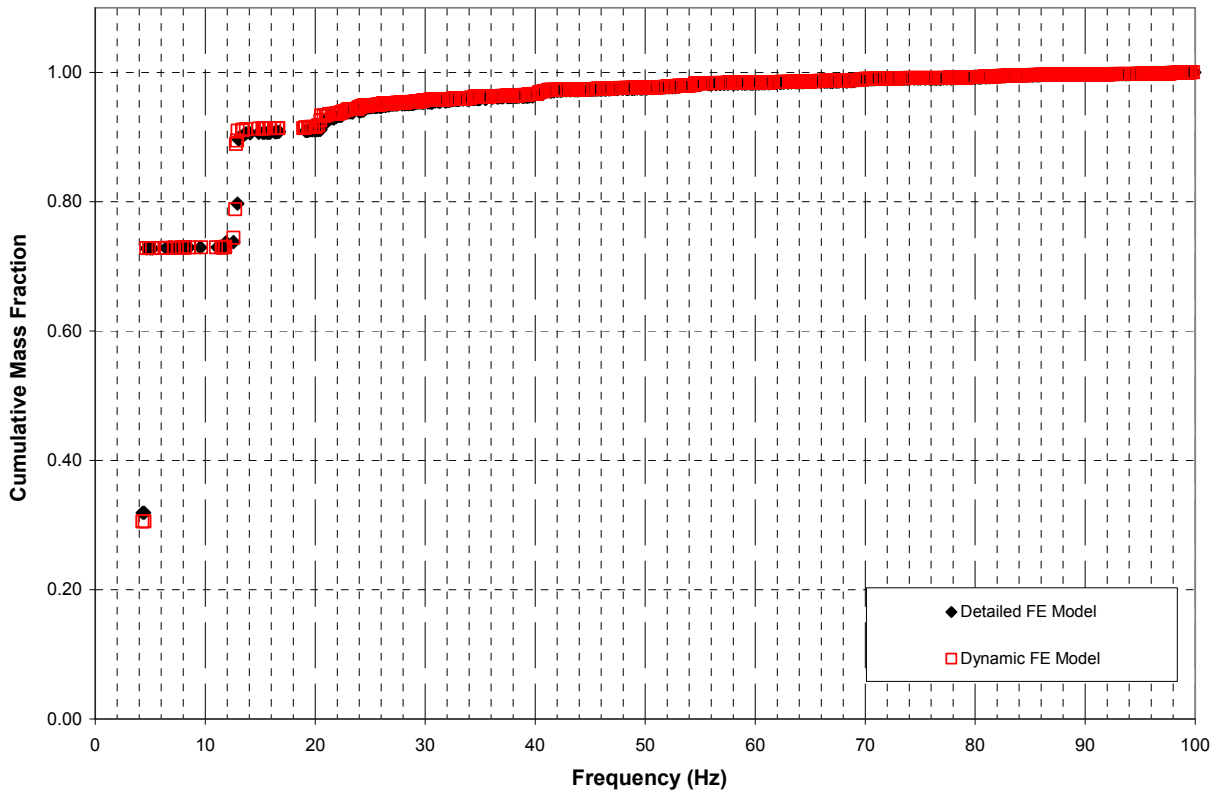

Figure 02.5.1.3.2.2-2 PCCV Modal Analysis – Cumulative Mass in the EW Direction (Y)

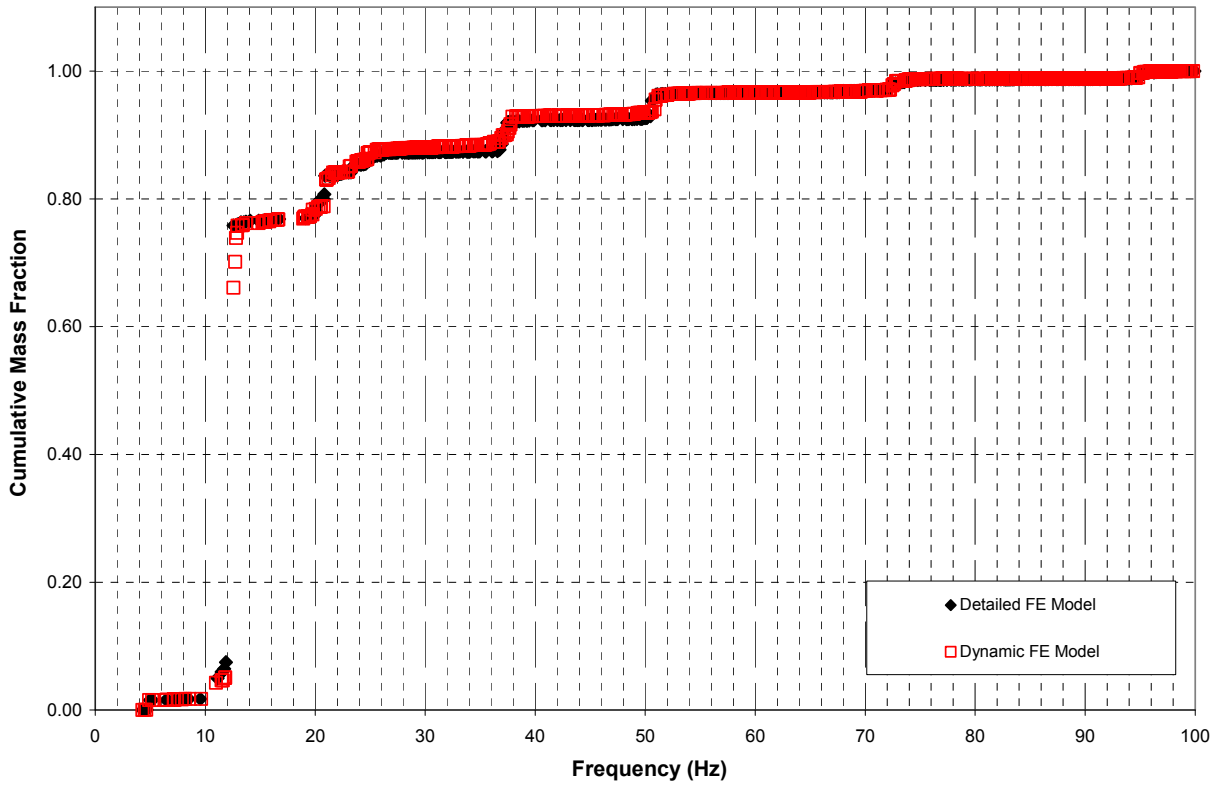

Figure 02.5.1.3.2.2-3 PCCV Modal Analysis – Cumulative Mass in the Vertical Direction (Z)

Figure 02.5.1.3.2.2-4 PCCV Detailed Mode Shape – Mode 2 at Frequency 4.46 Hz- NS Direction (X)

Figure 02.5.1.3.2.2-5 PCCV Dynamic Mode Shape – Mode 2 at Frequency 4.48 Hz - NS Direction (X)

Figure 02.5.1.3.2.2-6 PCCV Detailed Mode Shape – Mode 20 at Frequency 12.92 Hz- NS Direction (X)

Figure 02.5.1.3.2.2-7 PCCV Dynamic Mode Shape – Mode 22 at Frequency 12.91 Hz- NS Direction (X)

Figure 02.5.1.3.2.2-8 PCCV Detailed Mode Shape – Mode 21 at Frequency 13.05 Hz - NS Direction (X)

Figure 02.5.1.3.2.2-9 PCCV Dynamic Mode Shape – Mode 23 at Frequency 12.94 Hz- NS Direction (X)

Figure 02.5.1.3.2.2-10 PCCV Detailed Mode Shape – Mode 1 at Frequency 4.32 Hz- EW Direction (Y)

Figure 02.5.1.3.2.2-11 PCCV Dynamic Mode Shape – Mode 1 at Frequency 4.31 Hz - EW Direction (Y)

Figure 02.5.1.3.2.2-12 PCCV Detailed Mode Shape – Mode 3 at Frequency 4.68 Hz- EW Direction (Y)

Figure 02.5.1.3.2.2-13 PCCV Dynamic Mode Shape – Mode 3 at Frequency 4.66 Hz - EW Direction (Y)

Figure 02.5.1.3.2.2-14 PCCV Detailed Mode Shape – Mode 21 at Frequency 13.05 Hz - EW Direction (Y)

Figure 02.5.1.3.2.2-15 PCCV Dynamic Mode Shape – Mode 21 at Frequency 12.8 Hz - EW Direction (Y)

Figure 02.5.1.3.2.2-16 PCCV Detailed Mode Shape – Mode 19 at Frequency 12.575 Hz - Vertical Direction (Z)

Figure 02.5.1.3.2.2-17 PCCV Dynamic Mode Shape – Mode 19 at Frequency 12.575 Hz - Vertical Direction (Z)

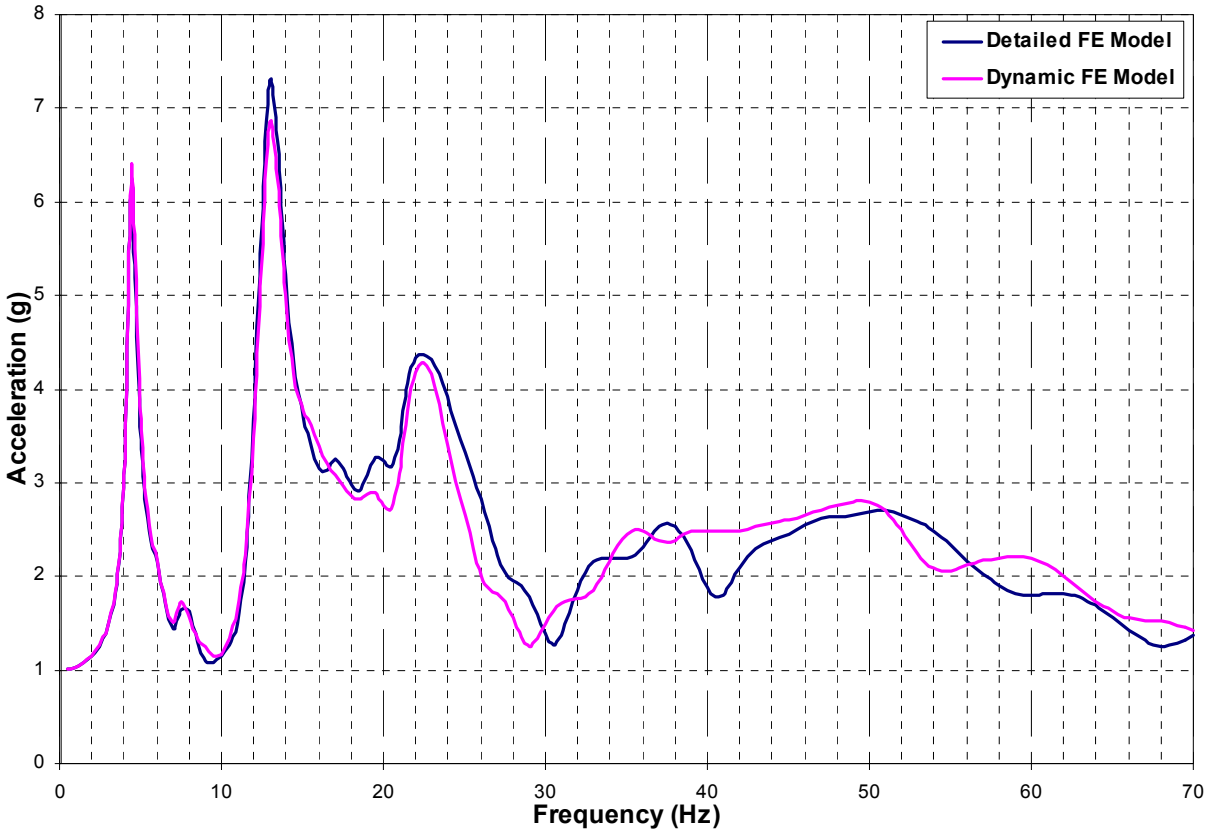

Figure 02.5.1.3.2.3-1 PCCV Harmonic Response Analysis – NS Direction (X) at North Face of Structure - Main Equipment Hatch Elevation

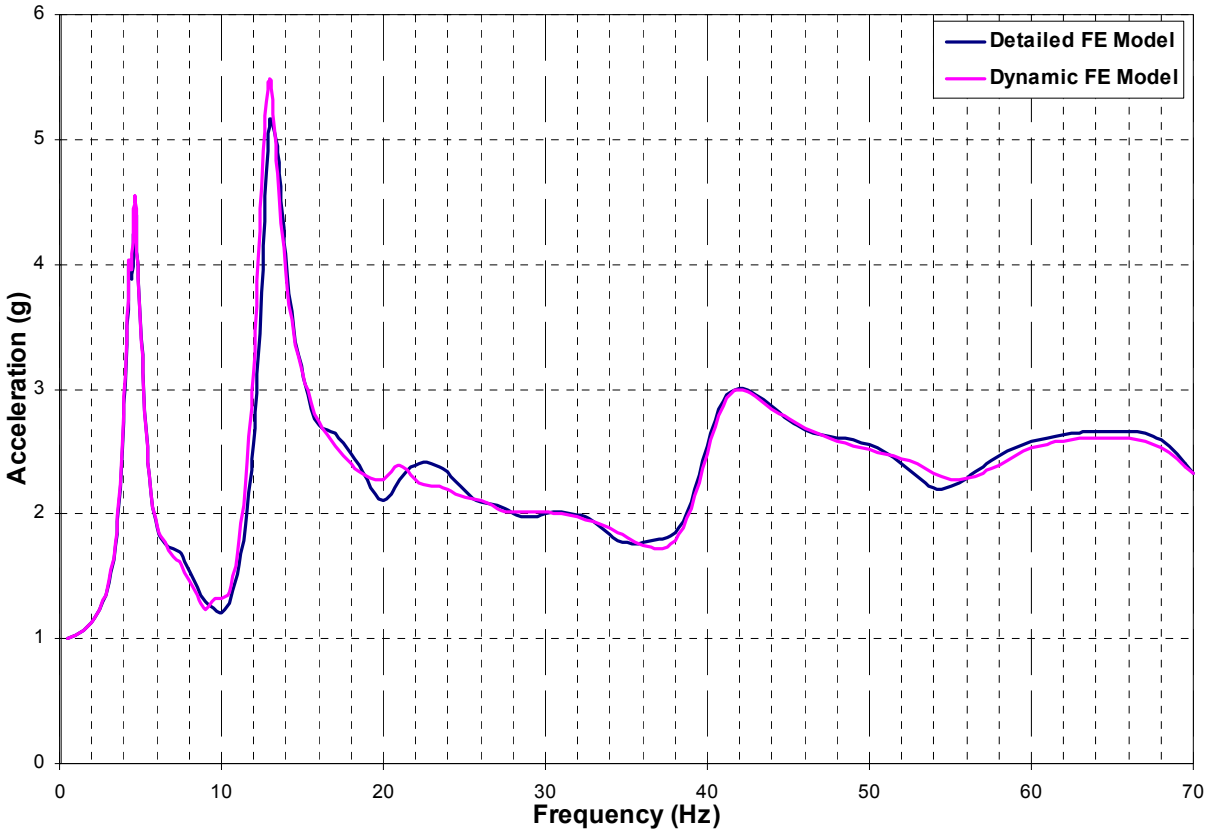

Figure 02.5.1.3.2.3-2 PCCV Harmonic Response Analysis – EW Direction (Y) at North Face of Structure - Main Equipment Hatch Elevation

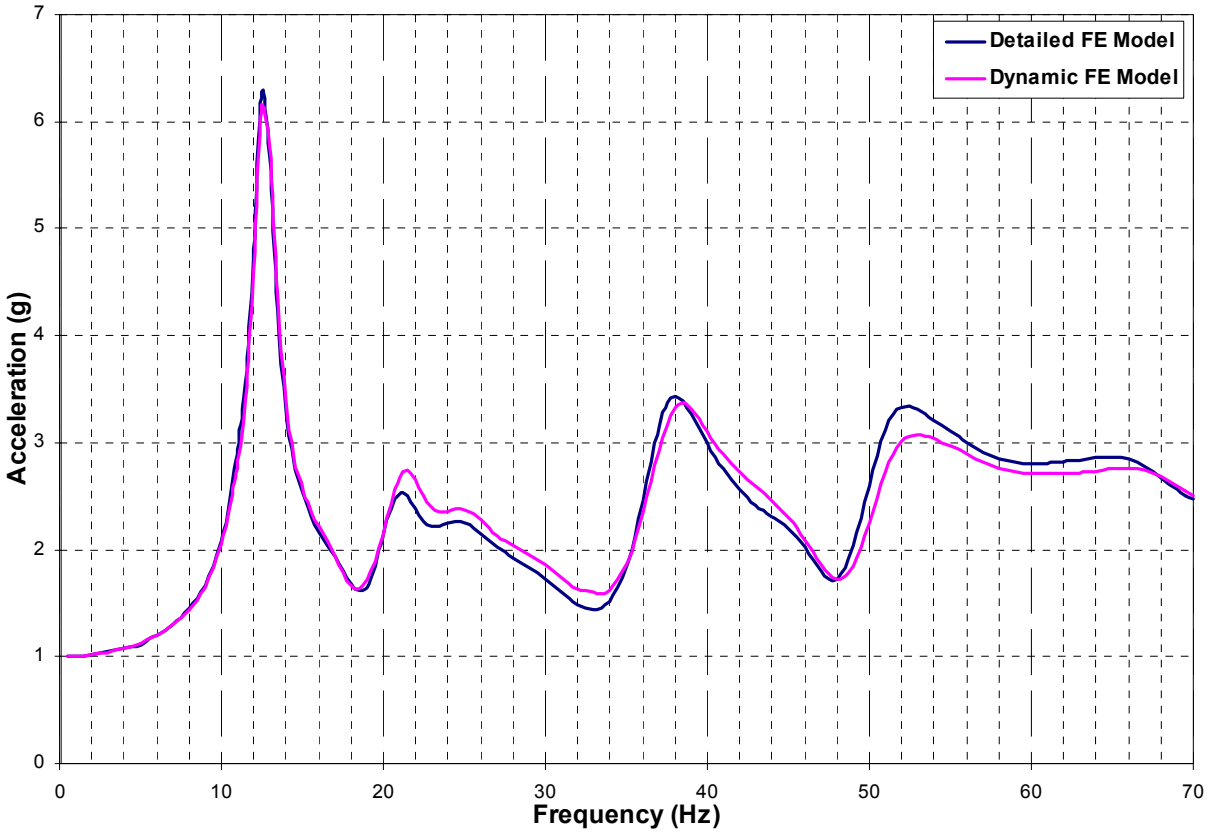

Figure 02.5.1.3.2.3-3 PCCV Harmonic Response Analysis – Vertical Direction (Z) at North Face of Structure - Main Equipment Hatch Elevation

Figure 02.5.1.3.3.1-1 Displacement Locations on the CIS

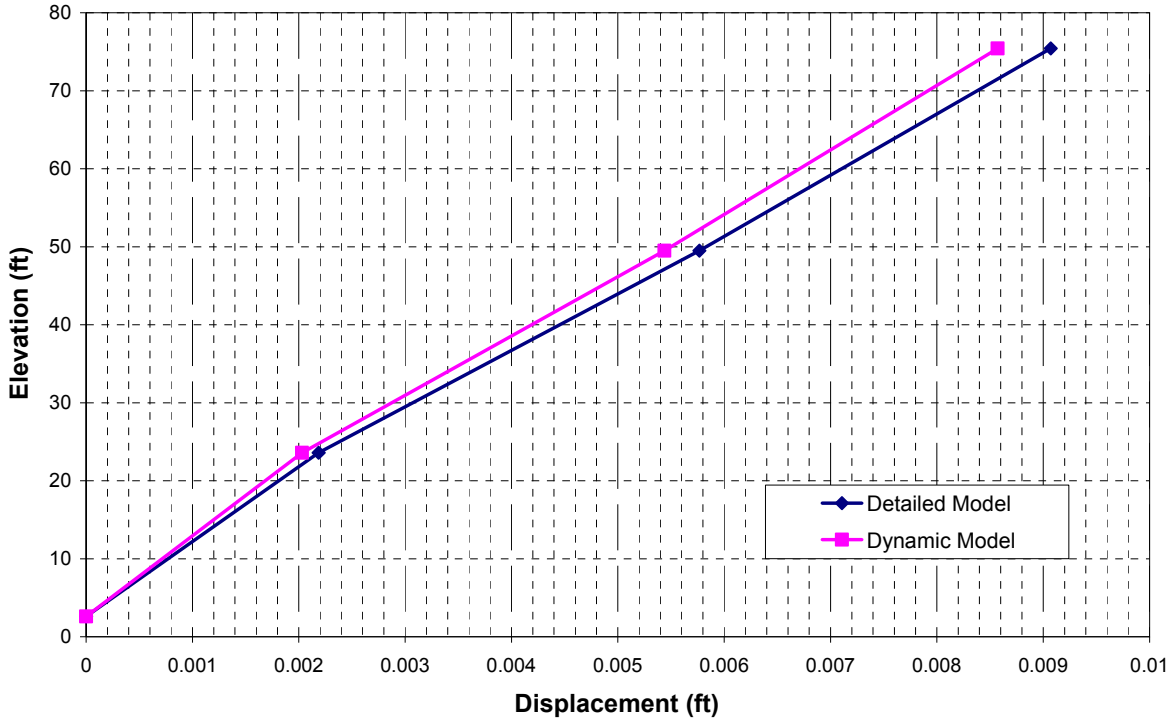

Figure 02.5.1.3.3.1-2 CIS 1g Static Analysis – NS Direction (X) at North Face of Structure (Uncracked Analyses)

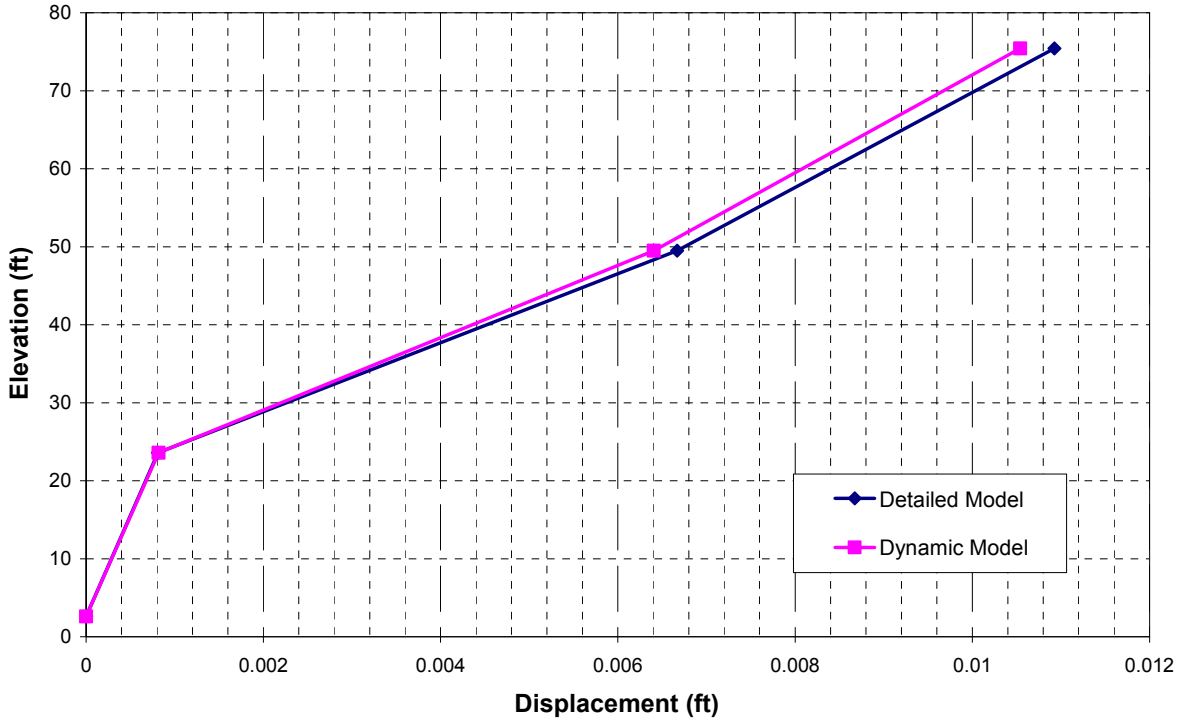

Figure 02.5.1.3.3.1-3 CIS 1g Static Analysis – EW Direction (Y) at North Face of Structure (Uncracked Analyses)

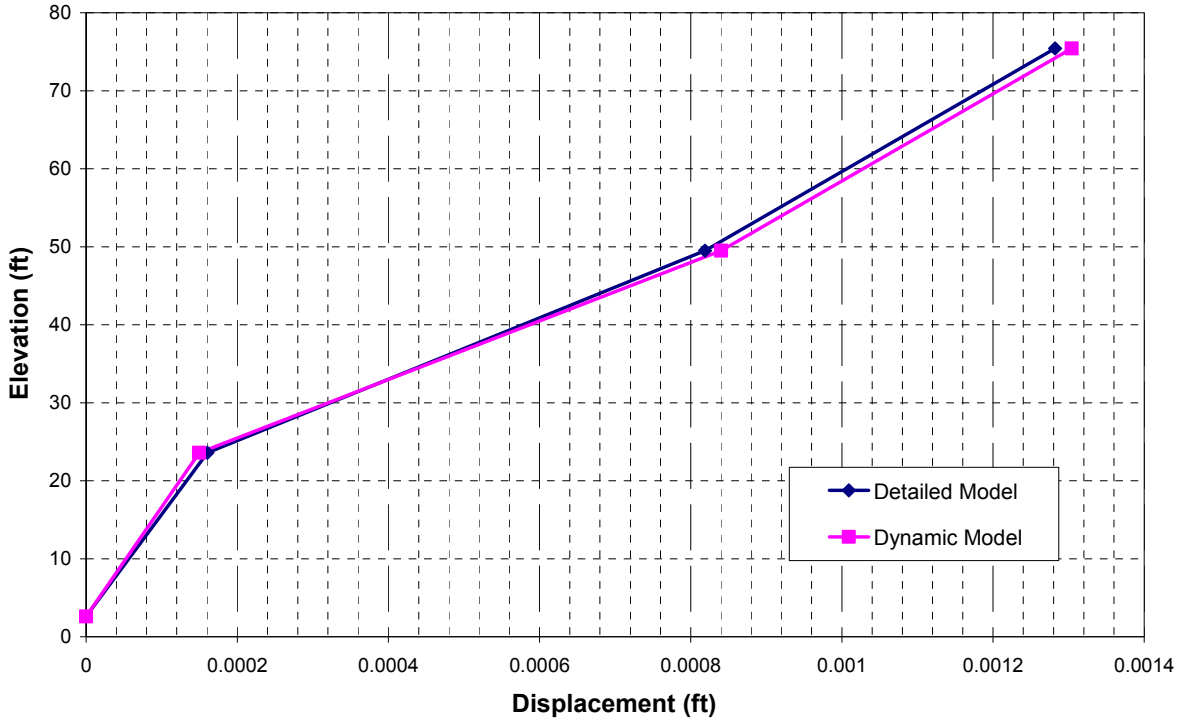

Figure 02.5.1.3.3.1-4 CIS 1g Static Analysis – Vertical Direction (Z) at North Face of Structure (Uncracked Analyses)

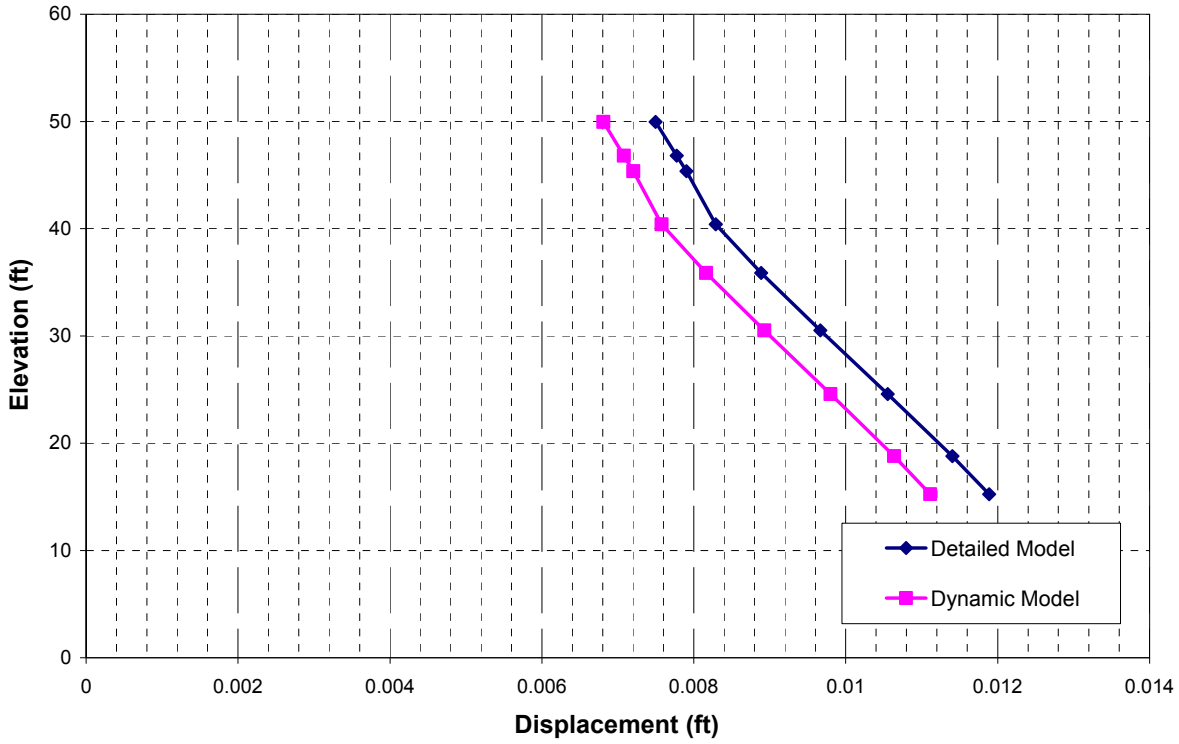

Note: The RV is supported from support points located at EL. 40ft-0in., therefore the deflection curves have a negative slope.

Figure 02.5.1.3.3.1-5 CIS 1g Static Analysis – NS Direction (X) at RV (Uncracked Analyses)

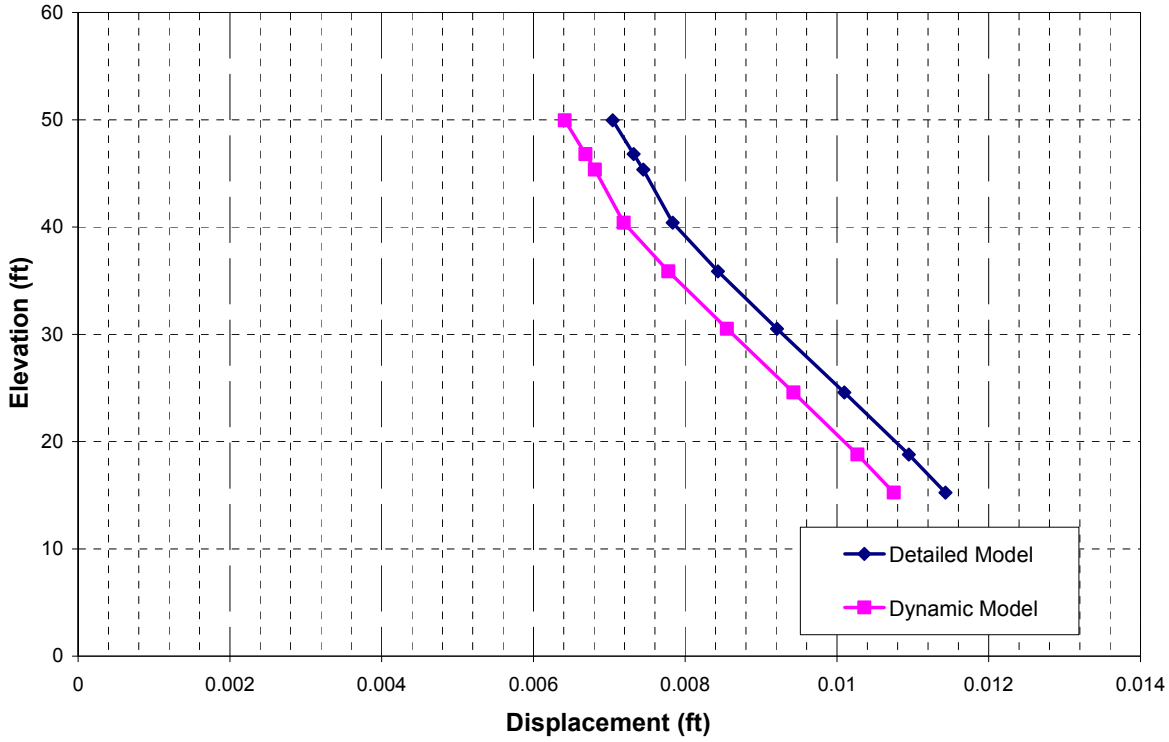

Note: The RV is supported from support points located at EL. 40ft-0in., therefore the deflection curves have a negative slope.

Figure 02.5.1.3.3.1-6 CIS 1g Static Analysis – EW Direction (Y) at RV (Uncracked Analyses)

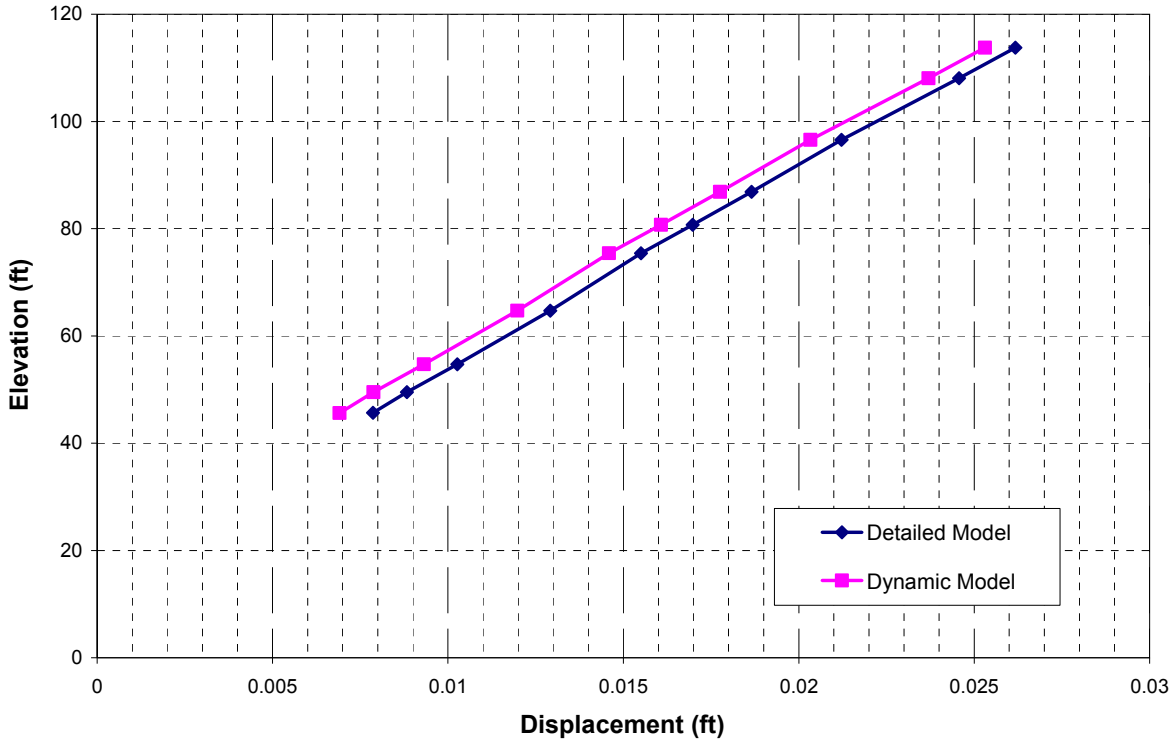

Figure 02.5.1.3.3.1-7 CIS 1g Static Analysis – NS Direction (X) at D-SG (Uncracked Analyses)

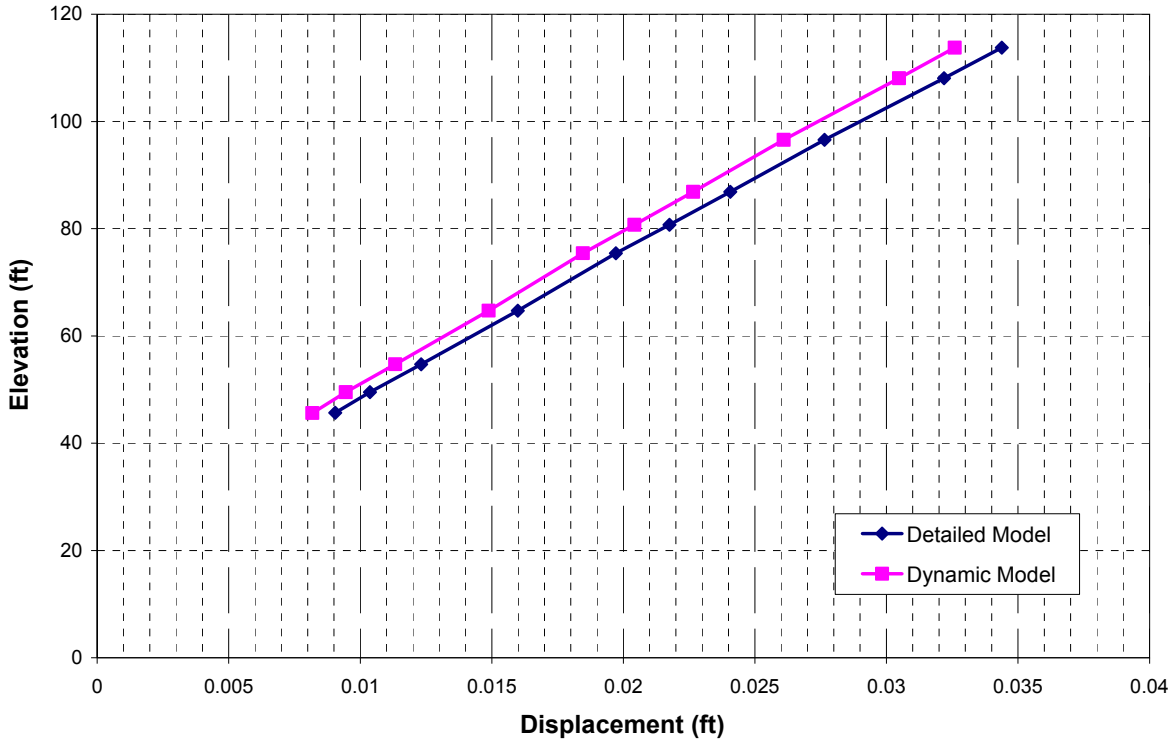

Figure 02.5.1.3.3.1-8 CIS 1g Static Analysis – EW Direction (Y) at D-SG (Uncracked Analyses)

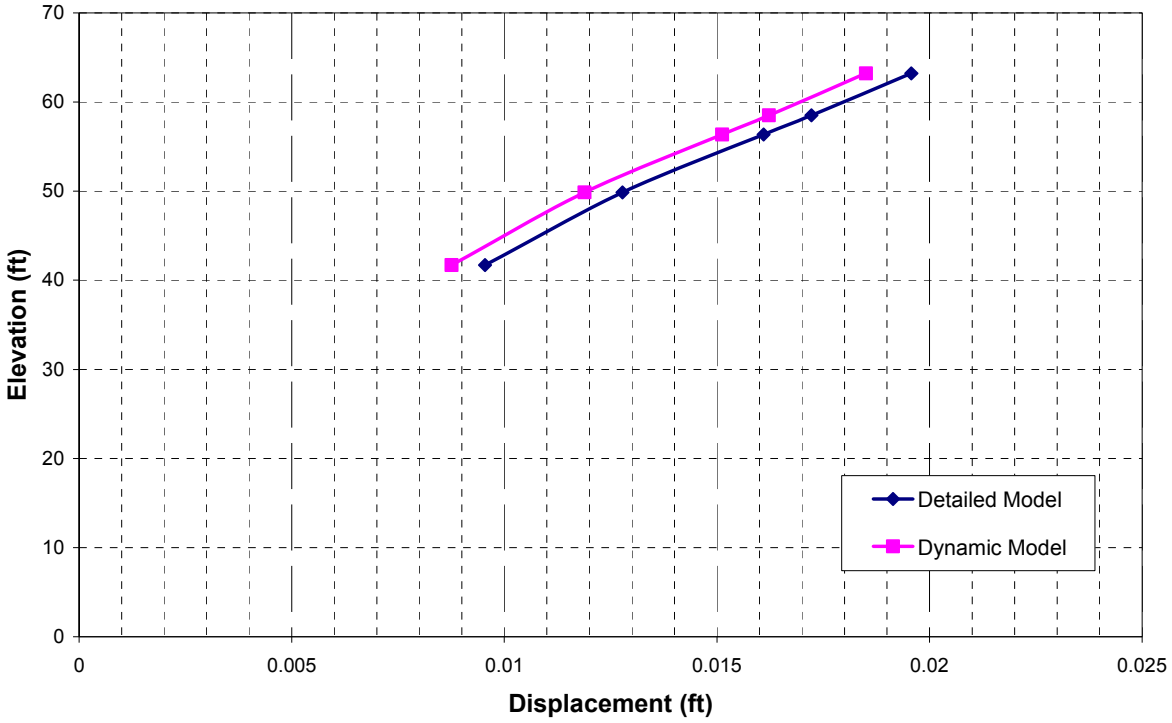

Figure 02.5.1.3.3.1-9 CIS 1g Static Analysis – NS Direction (X) at B-RCP (Uncracked Analyses)

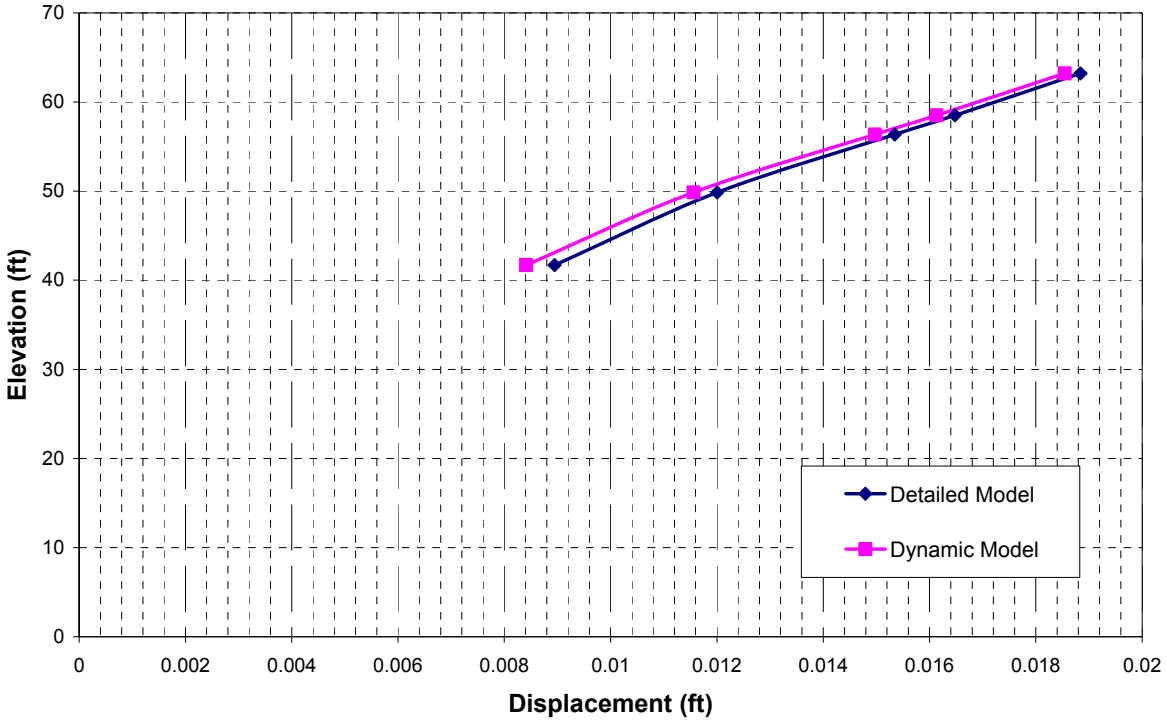

Figure 02.5.1.3.3.1-10 CIS 1g Static Analysis – EW Direction (Y) at B-RCP (Uncracked Analyses)

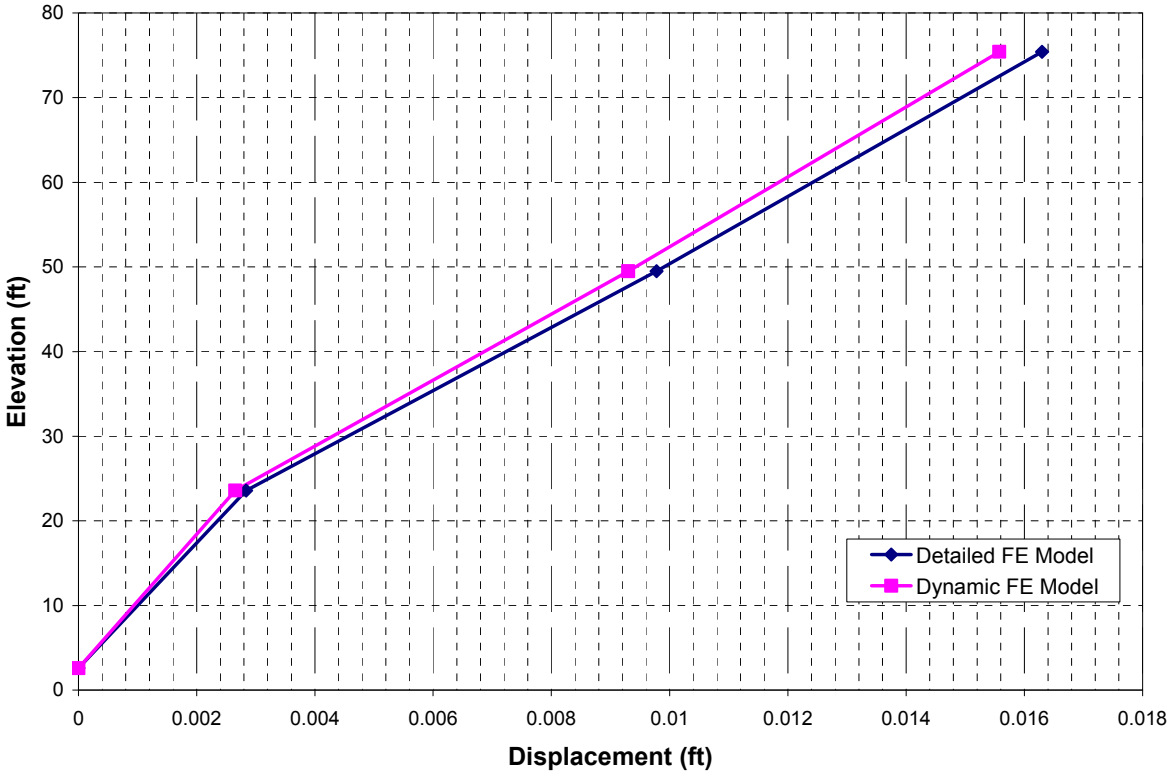

Figure 02.5.1.3.3.1-11 CIS 1g Static Analysis – NS Direction (X) at North Face of Structure (Cracked Analyses)

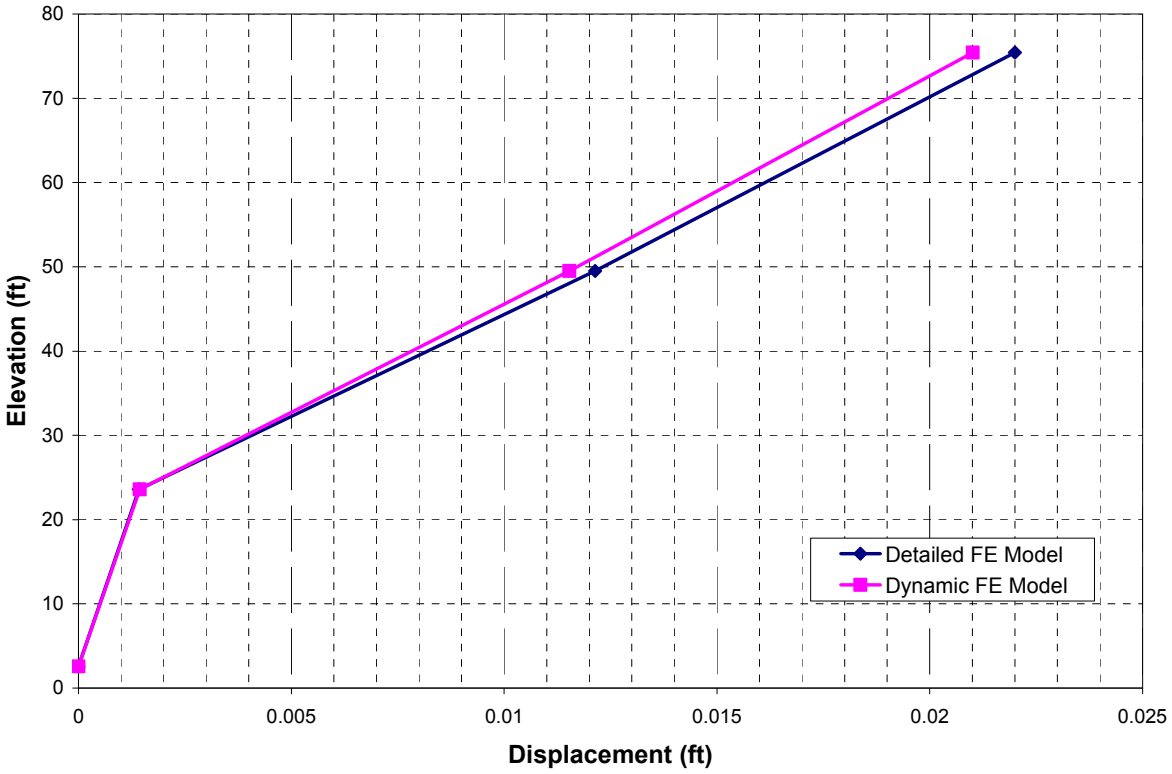

Figure 02.5.1.3.3.1-12 CIS 1g Static Analysis – EW Direction (Y) at North Face of Structure (Cracked Analyses)

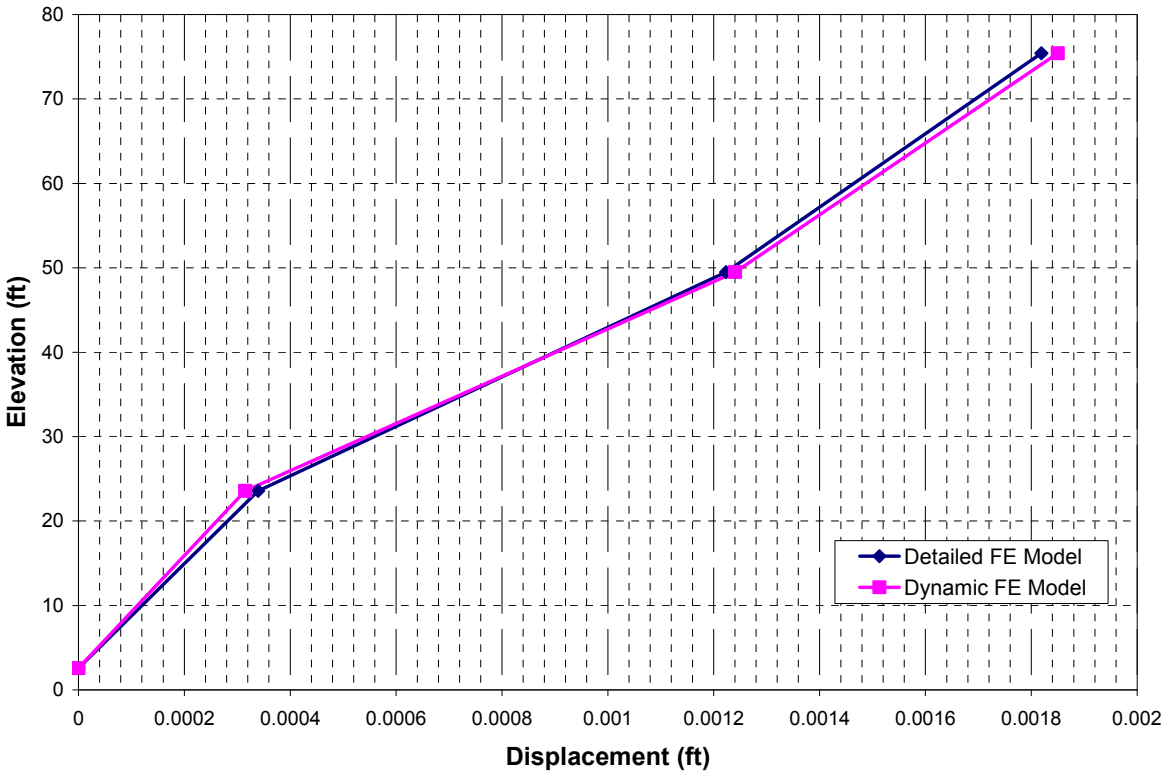

Figure 02.5.1.3.3.1-13 CIS 1g Static Analysis – Vertical Direction (Z) at North Face of Structure (Cracked Analyses)

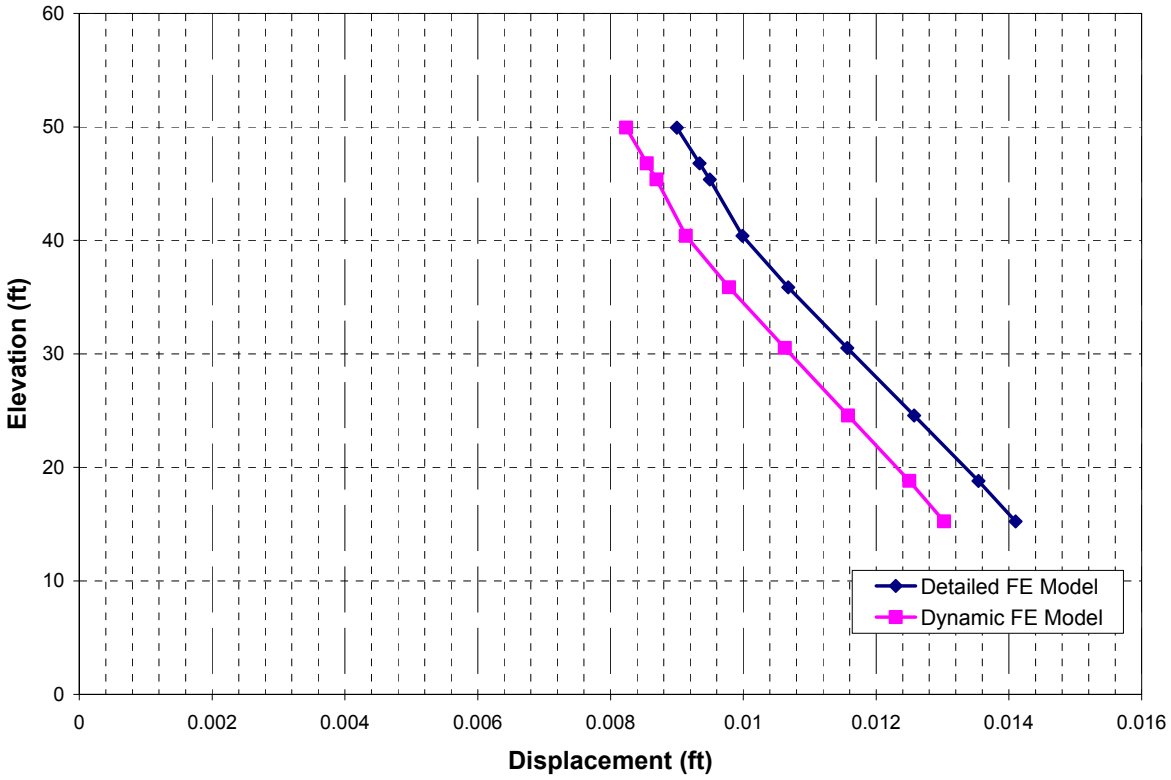

Note: The RV is supported from support points located at EL. 40ft-0in., therefore the deflection curves have a negative slope.

Figure 02.5.1.3.3.1-14 CIS 1g Static Analysis – NS Direction (X) at RV (Cracked Analyses)

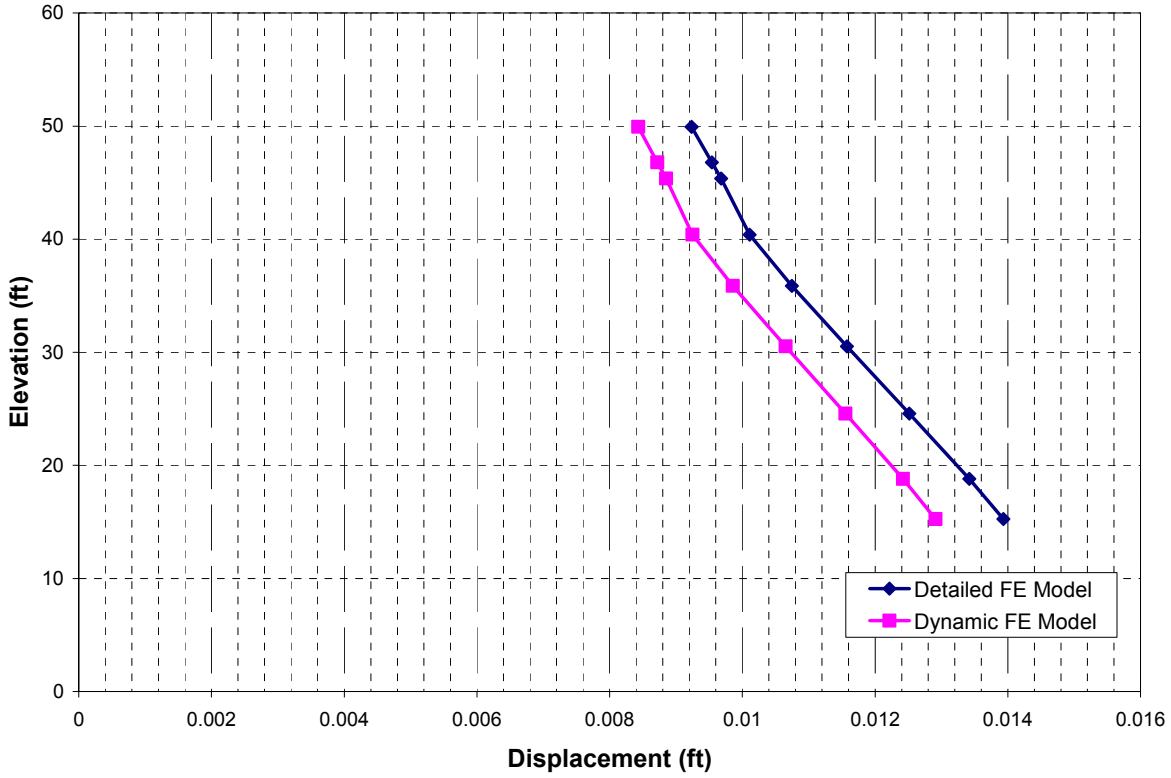

Note: The RV is supported from support points located at EL. 40ft-0in., therefore the deflection curves have a negative slope.

Figure 02.5.1.3.3.1-15 CIS 1g Static Analysis – EW Direction (Y) at RV (Cracked Analyses)

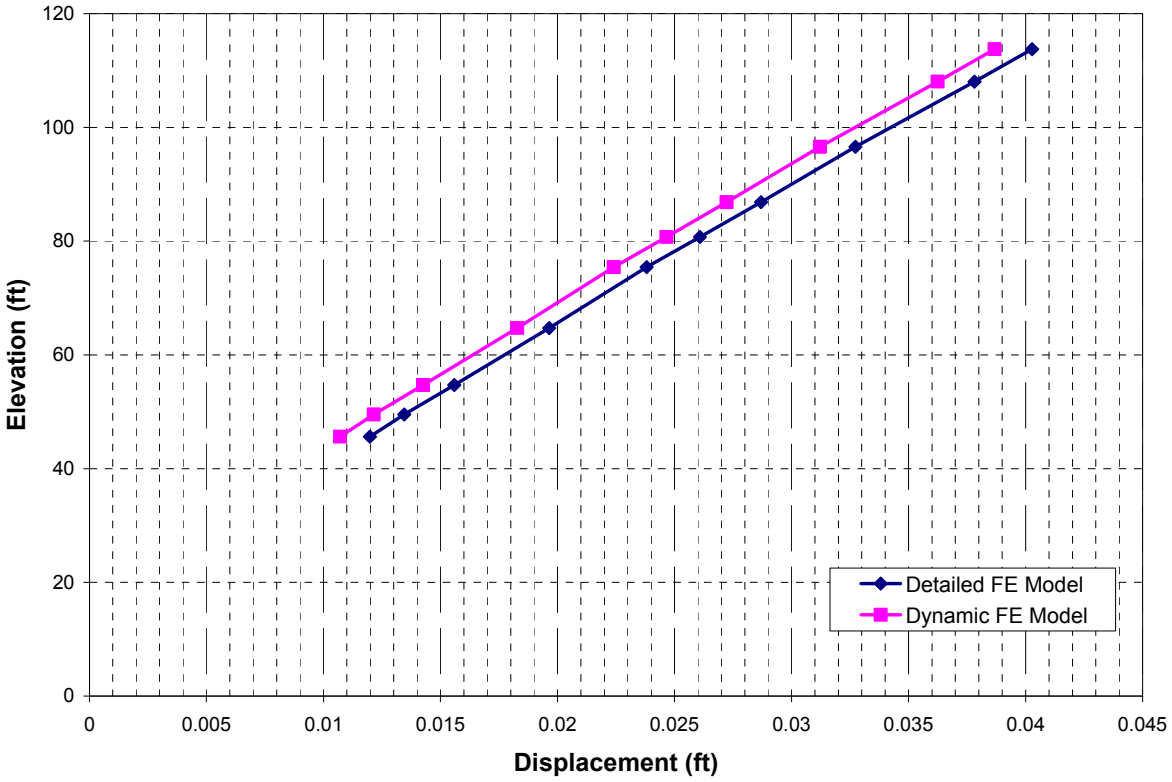

Figure 02.5.1.3.3.1-16 CIS 1g Static Analysis – NS Direction (X) at D-SG (Cracked Analyses)

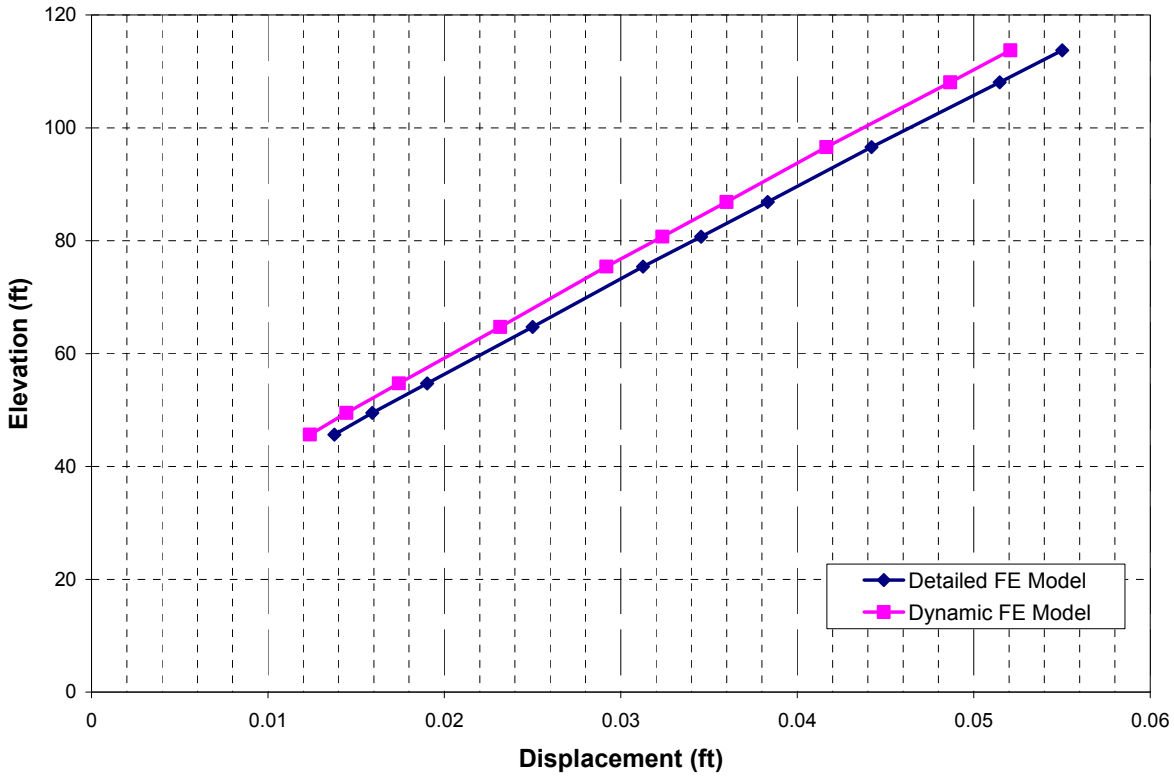

Figure 02.5.1.3.3.1-17 CIS 1g Static Analysis – EW Direction (Y) at D-SG (Cracked Analyses)

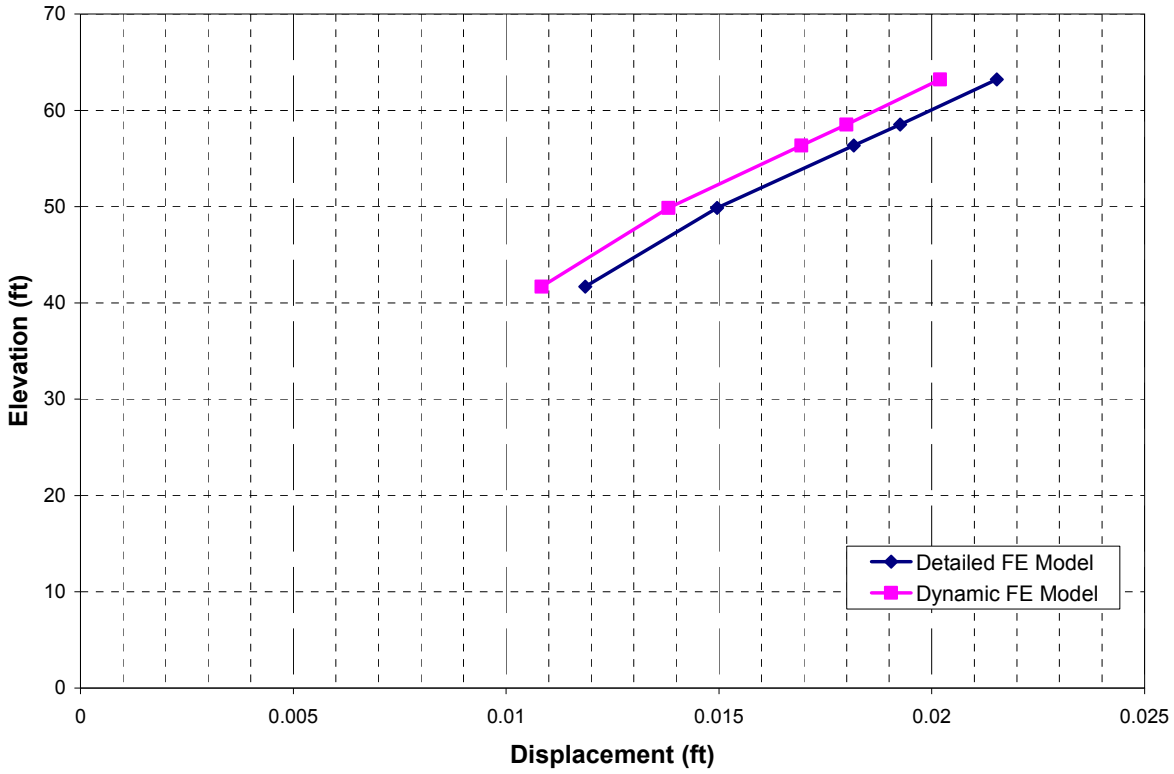

Figure 02.5.1.3.3.1-18 CIS 1g Static Analysis – NS Direction (X) at B-RCP (Cracked Analyses)

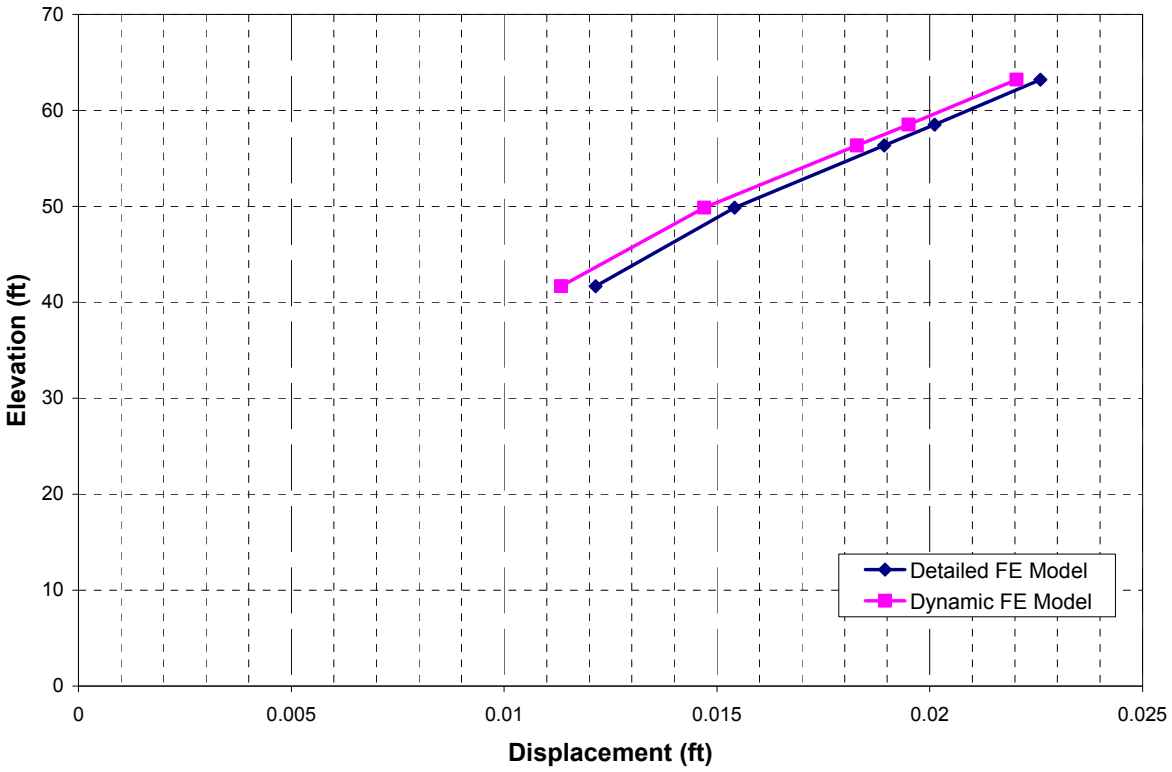

Figure 02.5.1.3.3.1-19 CIS 1g Static Analysis – EW Direction (Y) at B-RCP (Cracked Analyses)

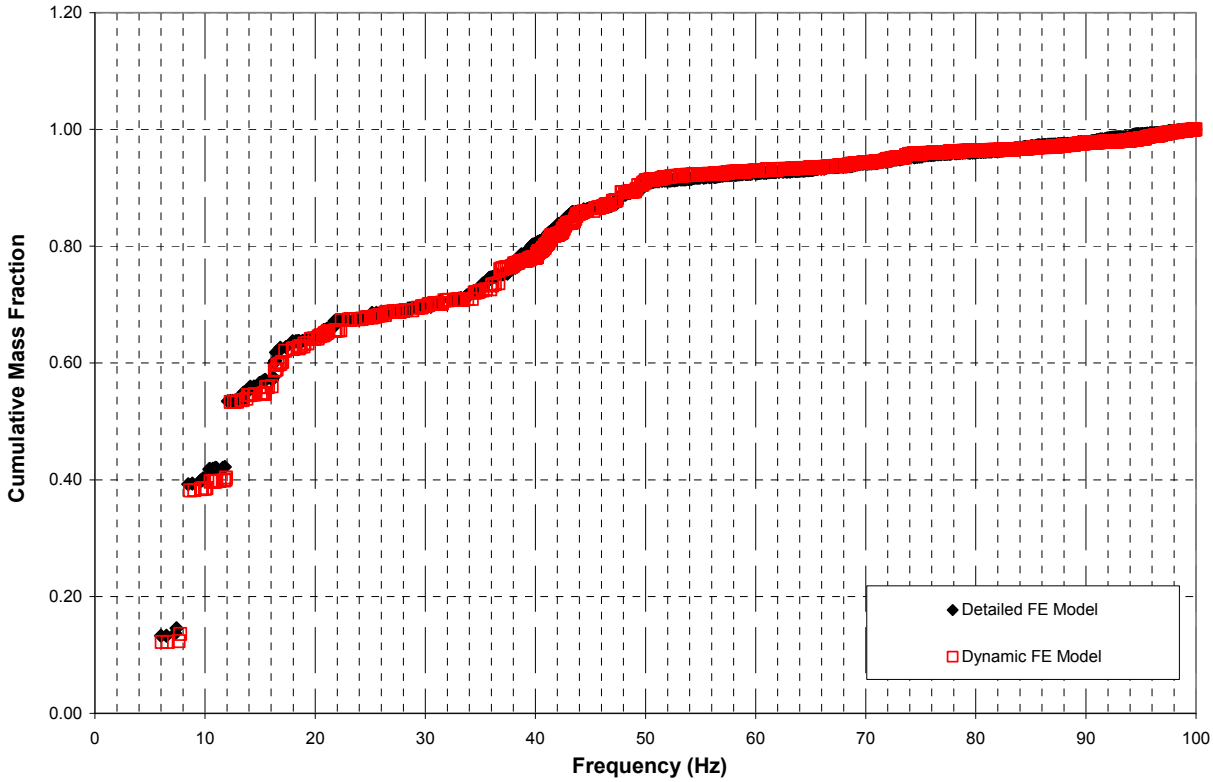

Figure 02.5.1.3.3.2-1 CIS Modal Analysis – Cumulative Mass in the NS Direction (X) (Uncracked Analyses)

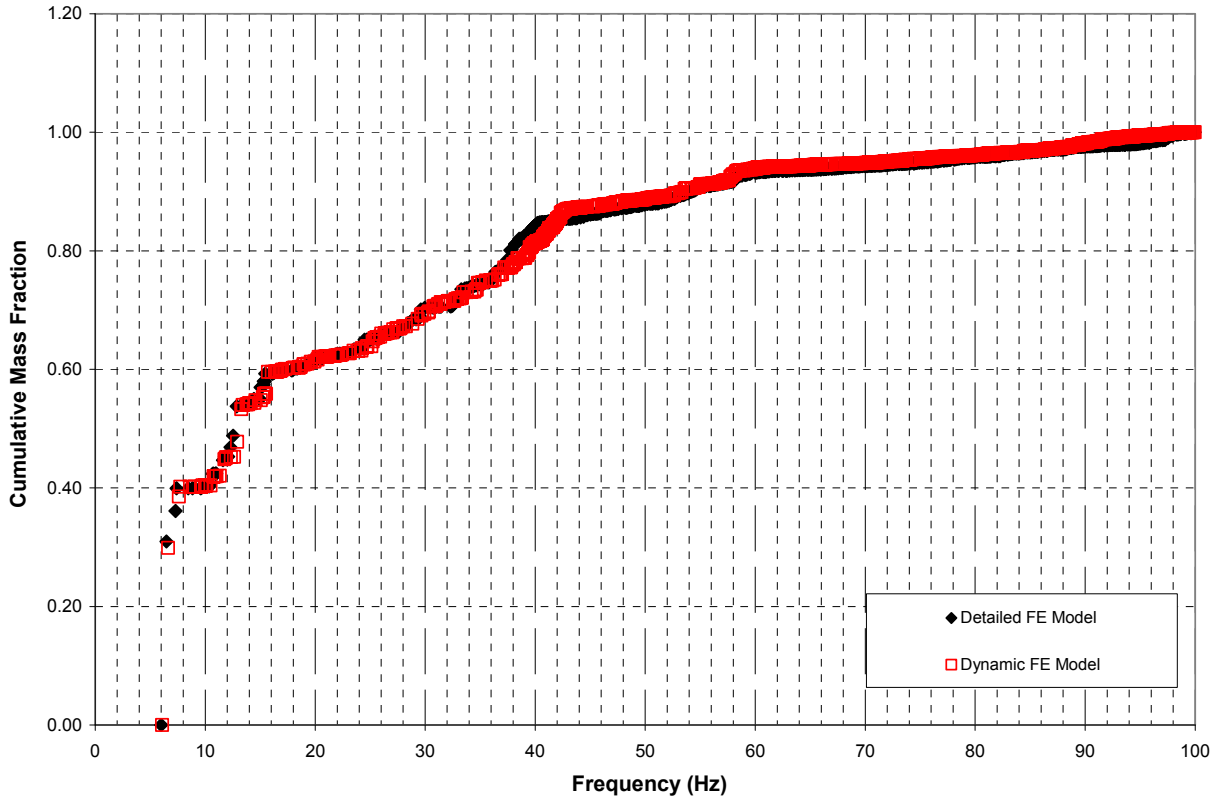

Figure 02.5.1.3.3.2-2 CIS Modal Analysis – Cumulative Mass in the EW Direction (Y) (Uncracked Analyses)

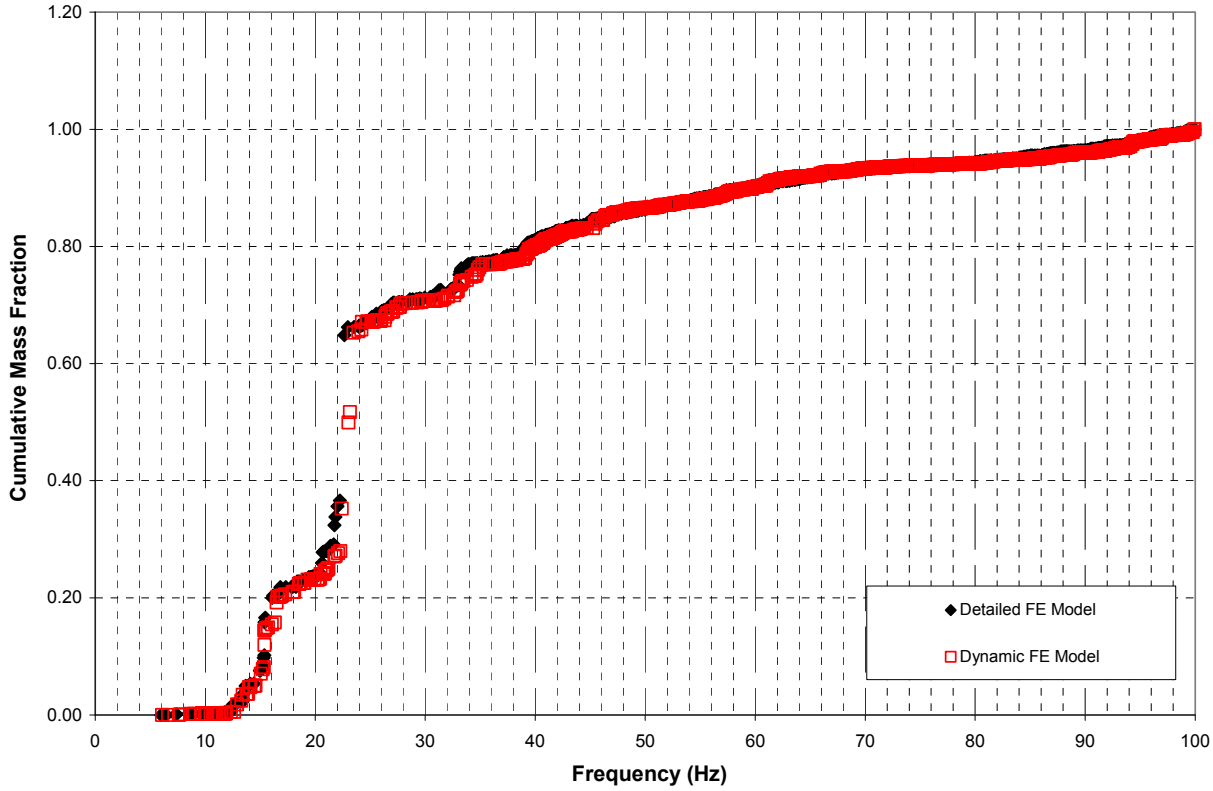

Figure 02.5.1.3.3.2-3 CIS Modal Analysis – Cumulative Mass in the Vertical Direction (Z) (Uncracked Analyses)

Figure 02.5.1.3.3.2-4 CIS Detailed Mode Shape – Mode 1 at Frequency 4.47 Hz - NS Direction (X)

Figure 02.5.1.3.3.2-5 CIS Dynamic Mode Shape – Mode 1 at Frequency 4.52 Hz - NS Direction (X)

Figure 02.5.1.3.3.2-6 CIS Detailed Mode Shape – Mode 5 at Frequency 6.57 Hz - NS Direction (X)

Figure 02.5.1.3.3.2-7 CIS Dynamic Mode Shape – Mode 5 at Frequency 6.74 Hz - NS Direction (X)

Figure 02.5.1.3.3.2-8 CIS Detailed Mode Shape – Mode 2 at Frequency 4.79 Hz - EW Direction (Y)

Figure 02.5.1.3.3.2-9 CIS Dynamic Mode Shape – Mode 2 at Frequency 4.9 Hz - EW Direction (Y)

Figure 02.5.1.3.3.2-10 CIS Detailed Mode Shape – Mode 3 at Frequency 5.74 Hz - EW Direction (Y)

Figure 02.5.1.3.3.2-11 CIS Dynamic Mode Shape – Mode 3 at Frequency 5.92 Hz- EW Direction (Y)

Figure 02.5.1.3.3.2-12 CIS Detailed Mode Shape – Mode 36 at Frequency 14.18 Hz - Vertical Direction (Z)

Figure 02.5.1.3.3.2-13 CIS Dynamic Mode Shape – Mode 36 at Frequency 14.25 Hz - Vertical Direction (Z)

Figure 02.5.1.3.3.2-14 CIS Detailed Mode Shape – Mode 43 at Frequency 15.2 Hz - Vertical Direction (Z)

Figure 02.5.1.3.3.2-15 CIS Dynamic Mode Shape – Mode 44 at Frequency 15.39 Hz - Vertical Direction (Z)

Figure 02.5.1.3.3.2-16 CIS Detailed Mode Shape – Mode 46 at Frequency 15.36 Hz - Vertical Direction (Z)

Figure 02.5.1.3.3.2-17 CIS Dynamic Mode Shape – Mode 45 at Frequency 15.41 Hz - Vertical Direction (Z)

Figure 02.5.1.3.3.2-18 CIS Detailed Mode Shape – Mode 48 at Frequency 15.63 Hz - Vertical Direction (Z)

Figure 02.5.1.3.3.2-19 CIS Dynamic Mode Shape – Mode 49 at Frequency 16.34 Hz - Vertical Direction (Z)

Figure 02.5.1.3.3.2-20 CIS Detailed Mode Shape – Mode 50 at Frequency 15.99 Hz - Vertical Direction (Z)

Figure 02.5.1.3.3.2-21 CIS Dynamic Mode Shape – Mode 50 at Frequency 16.38 Hz - Vertical Direction (Z)

Figure 02.5.1.3.3.2-22 CIS Detailed Mode Shape – Mode 53 at Frequency 16.45 Hz - Vertical Direction (Z)

Figure 02.5.1.3.3.2-23 CIS Dynamic Mode Shape – Mode 55 at Frequency 16.88 Hz - Vertical Direction (Z)

Figure 02.5.1.3.3.2-24 CIS Detailed Mode Shape – Mode 56 at Frequency 16.69 Hz - Vertical Direction (Z)

Figure 02.5.1.3.3.2-25 CIS Dynamic Mode Shape – Mode 56 at Frequency 17.00 Hz - Vertical Direction (Z)

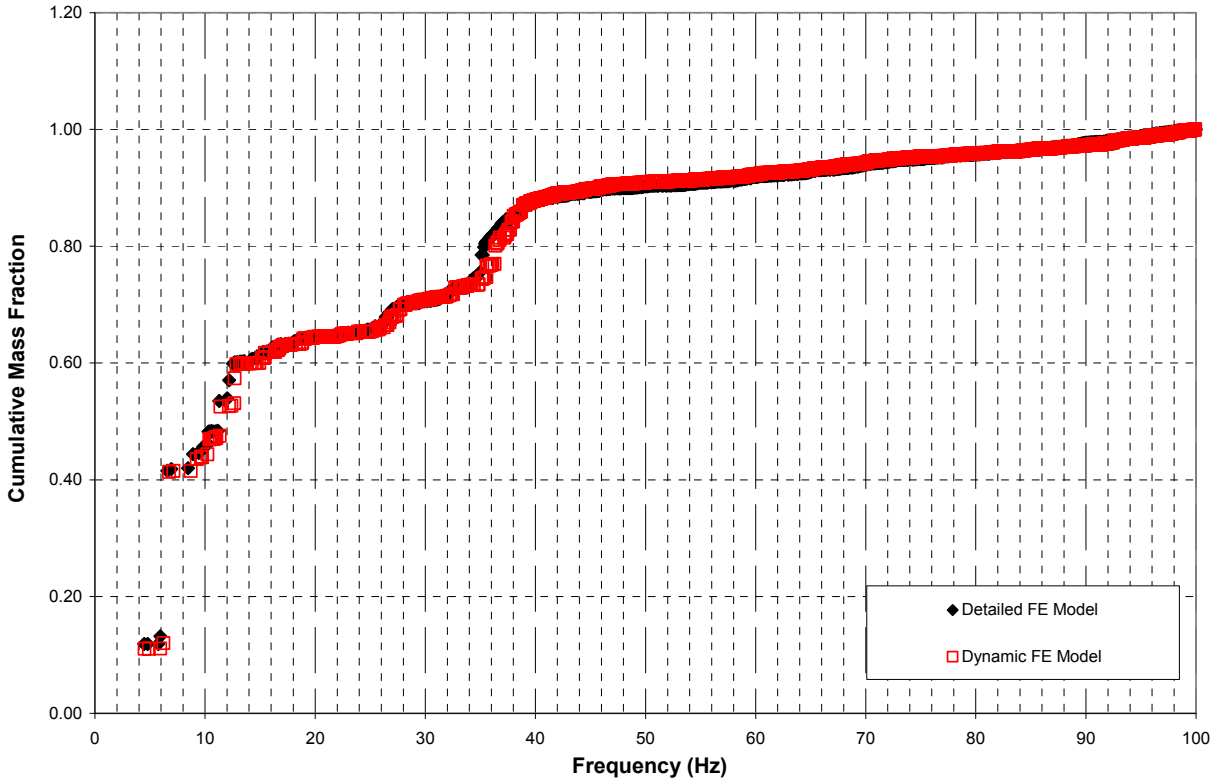

Figure 02.5.1.3.3.2-26 CIS Modal Analysis – Cumulative Mass in the NS Direction (X) (Cracked Analyses)

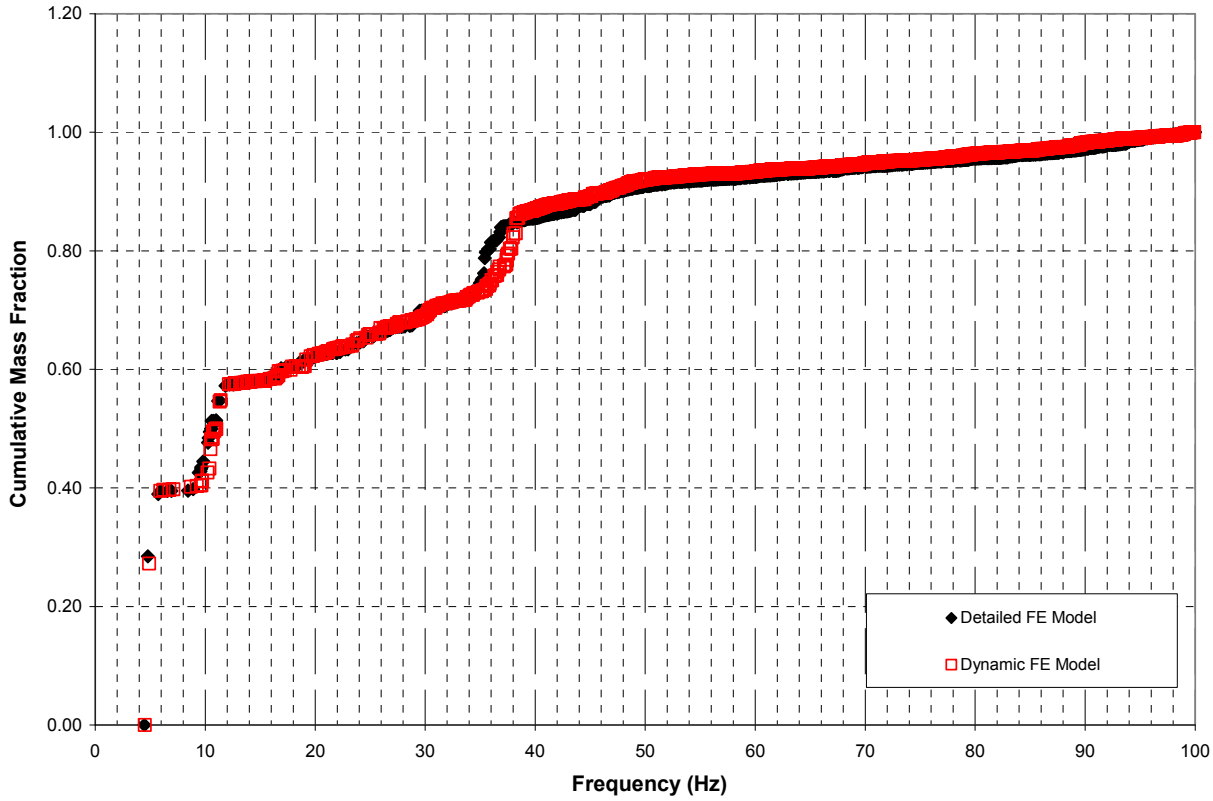

Figure 02.5.1.3.3.2-27 CIS Modal Analysis – Cumulative Mass in the EW Direction (Y) (Cracked Analyses)

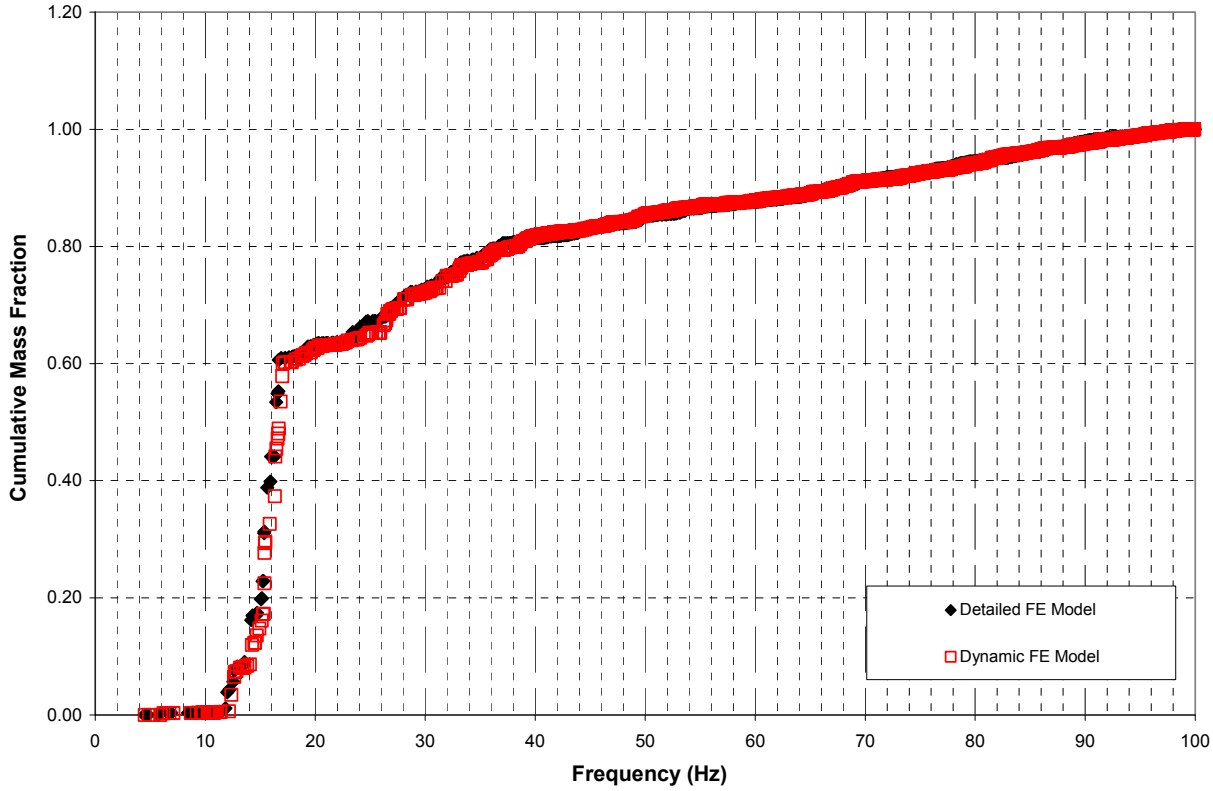

Figure 02.5.1.3.3.2-28 CIS Modal Analysis – Cumulative Mass in the Vertical Direction (Z) (Cracked Analyses)

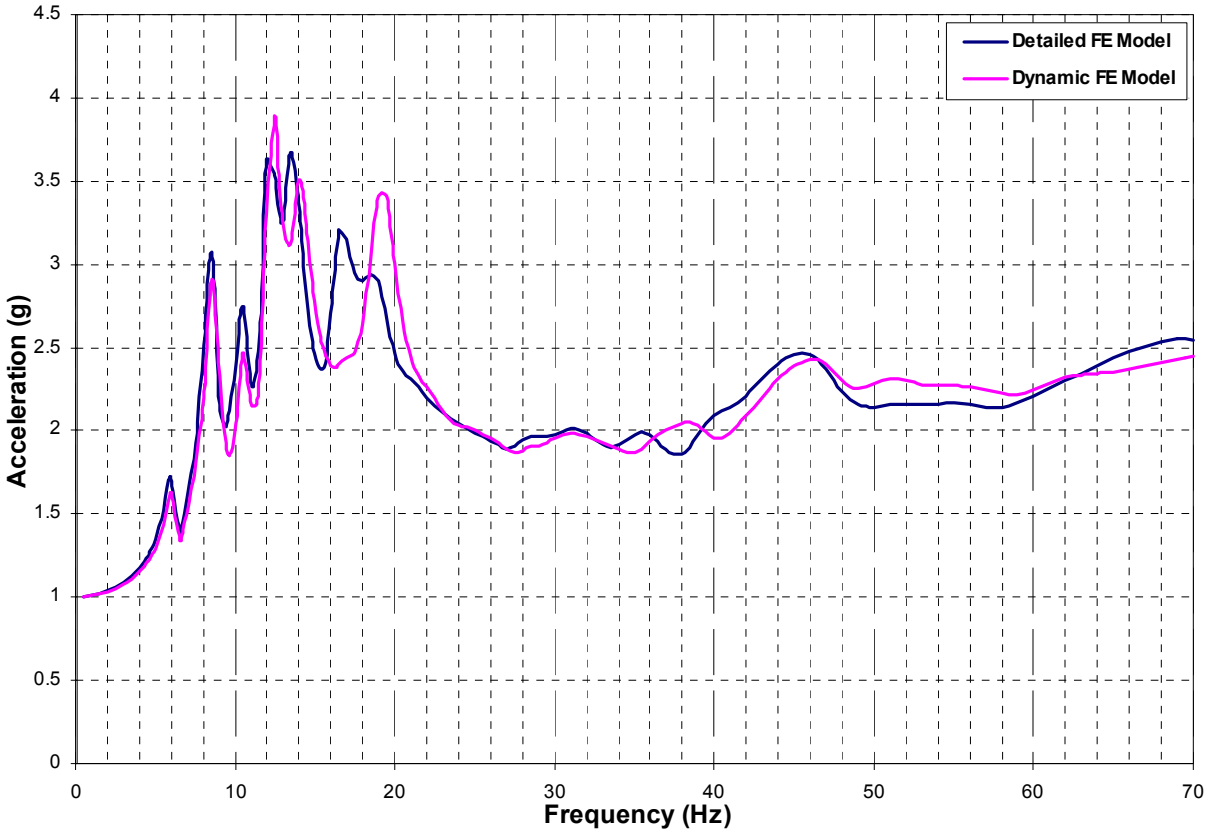

Figure 02.5.1.3.3.3-1 CIS Harmonic Response Analysis – RV Nozzle NS Direction (X) (Uncracked Analyses)

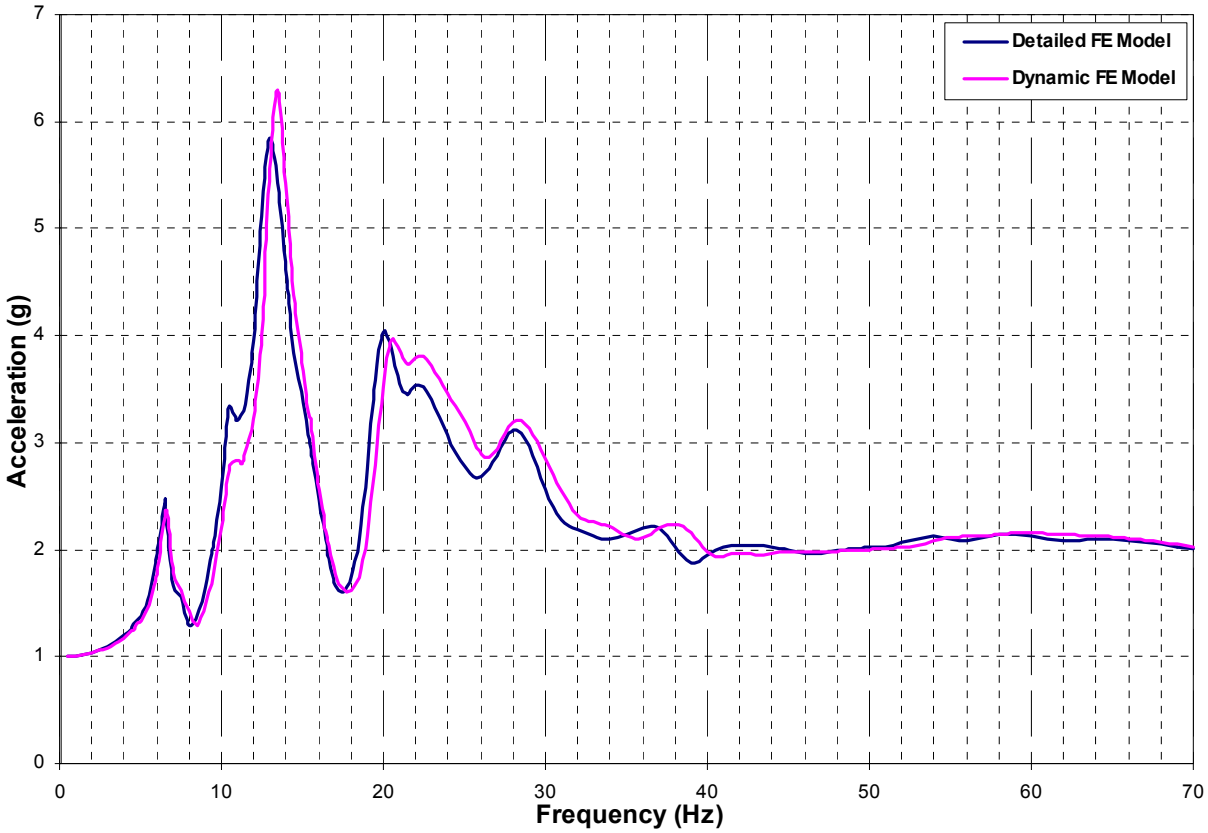

Figure 02.5.1.3.3.3-2 CIS Harmonic Response Analysis – RV Nozzle EW Direction (Y) (Uncracked Analyses)

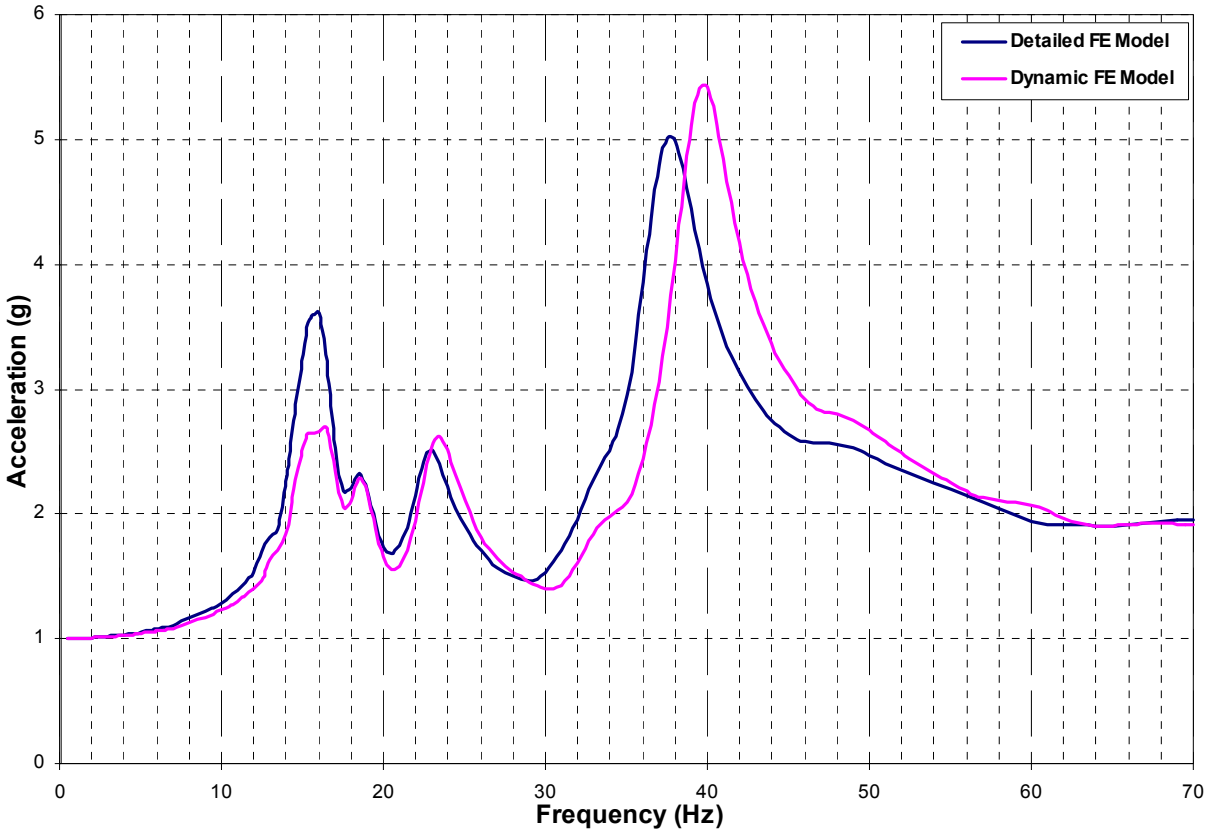

Figure 02.5.1.3.3.3-3 CIS Harmonic Response Analysis – RV Nozzle Vertical Direction (Z) (Uncracked Analyses)

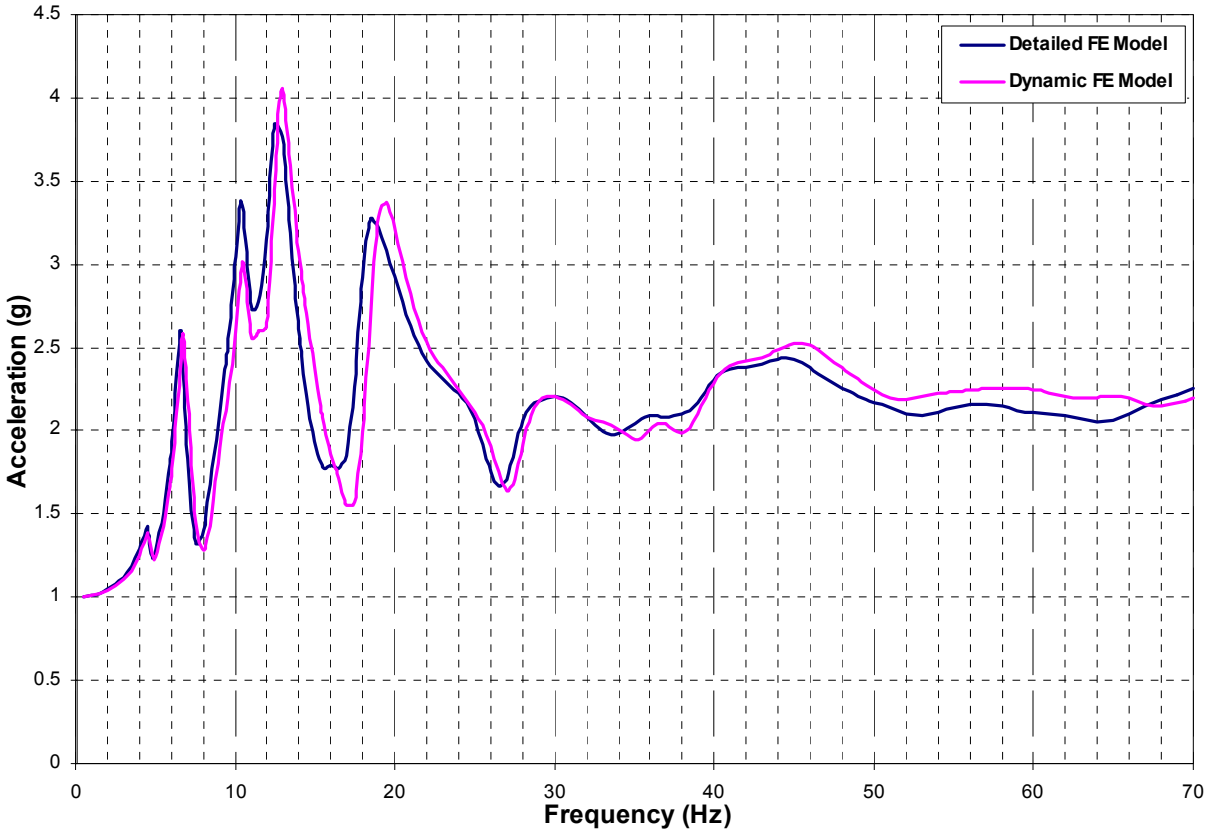

Figure 02.5.1.3.3.3-4 CIS Harmonic Response Analysis – RV Nozzle NS Direction (X) (Cracked Analyses)

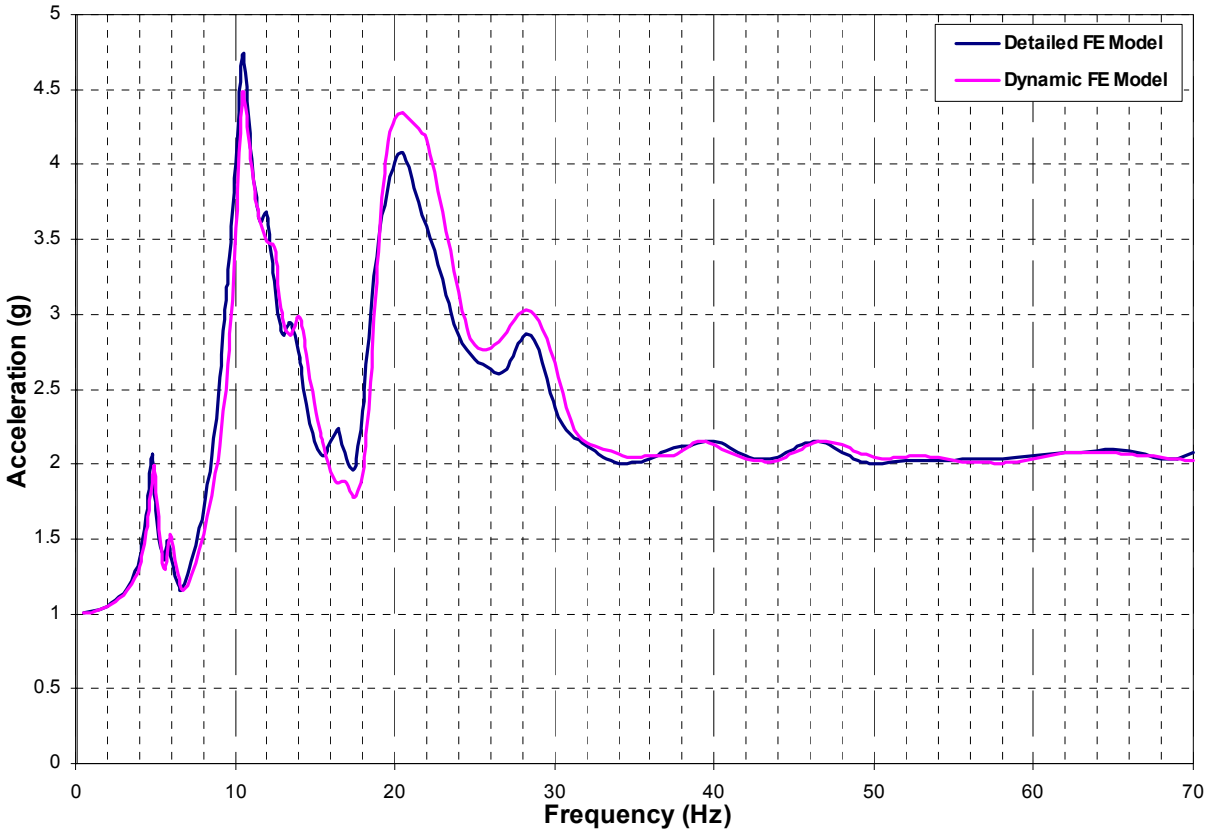

Figure 02.5.1.3.3.3-5 CIS Harmonic Response Analysis – RV Nozzle EW Direction (Y) (Cracked Analyses)

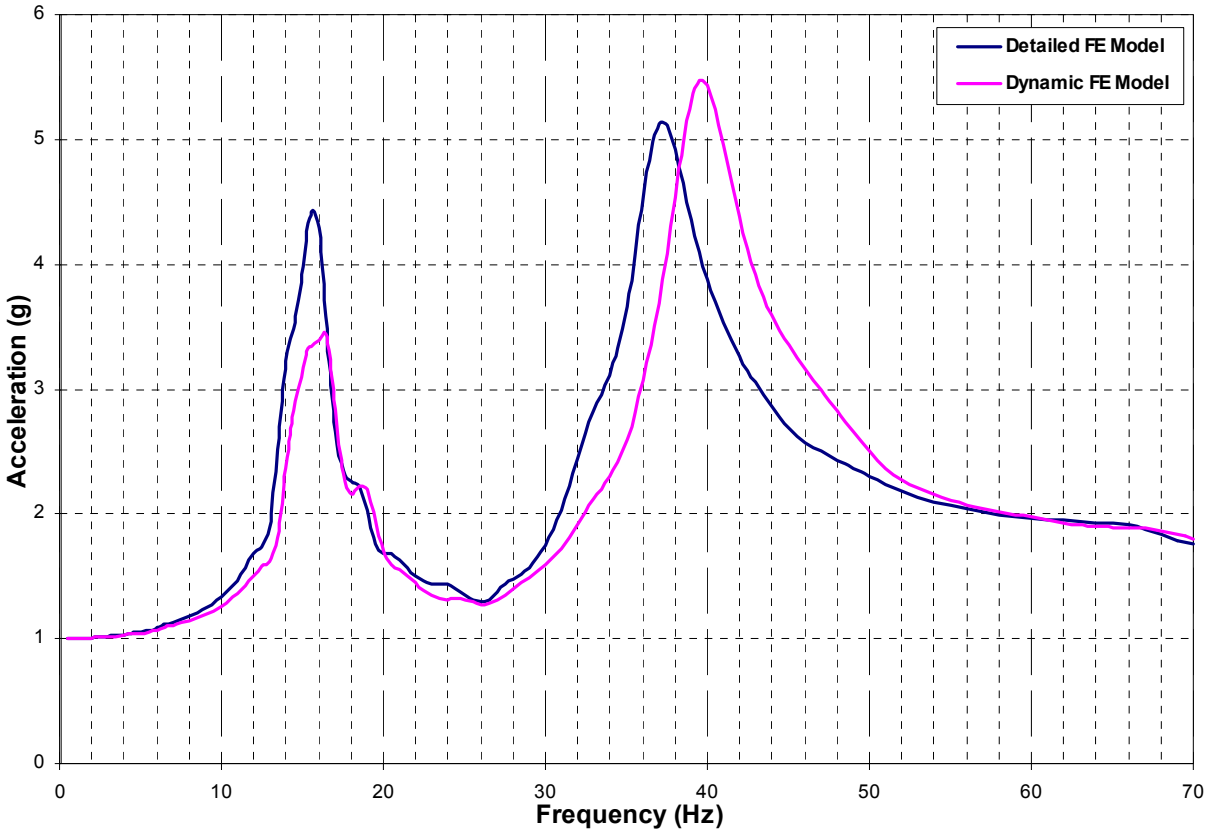

Figure 02.5.1.3.3.3-6 CIS Harmonic Response Analysis – RV Nozzle Vertical Direction (Z) (Cracked Analyses)

Figure 02.5.1.3.4.1-1 Displacement Locations on East PS/B Exterior Walls

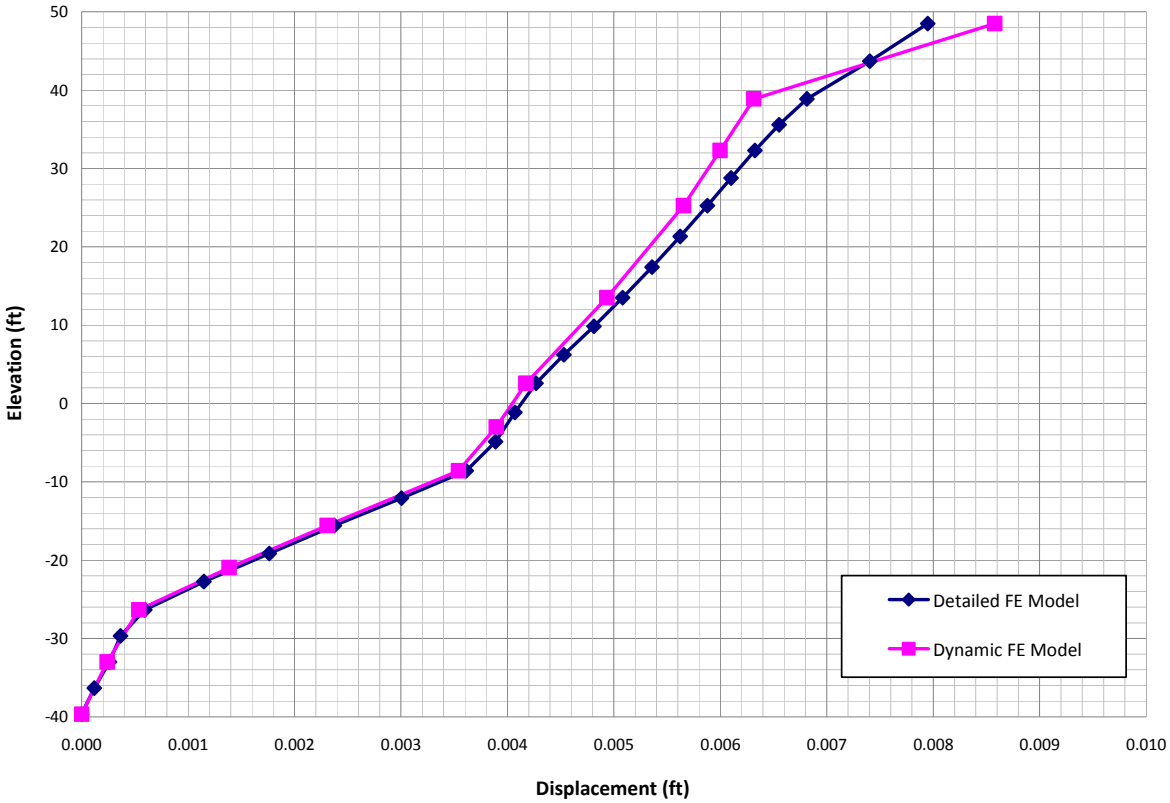

Figure 02.5.1.3.4.1-2 East PS/B NS Direction (X) 1g Static Analysis – Southeast Corner

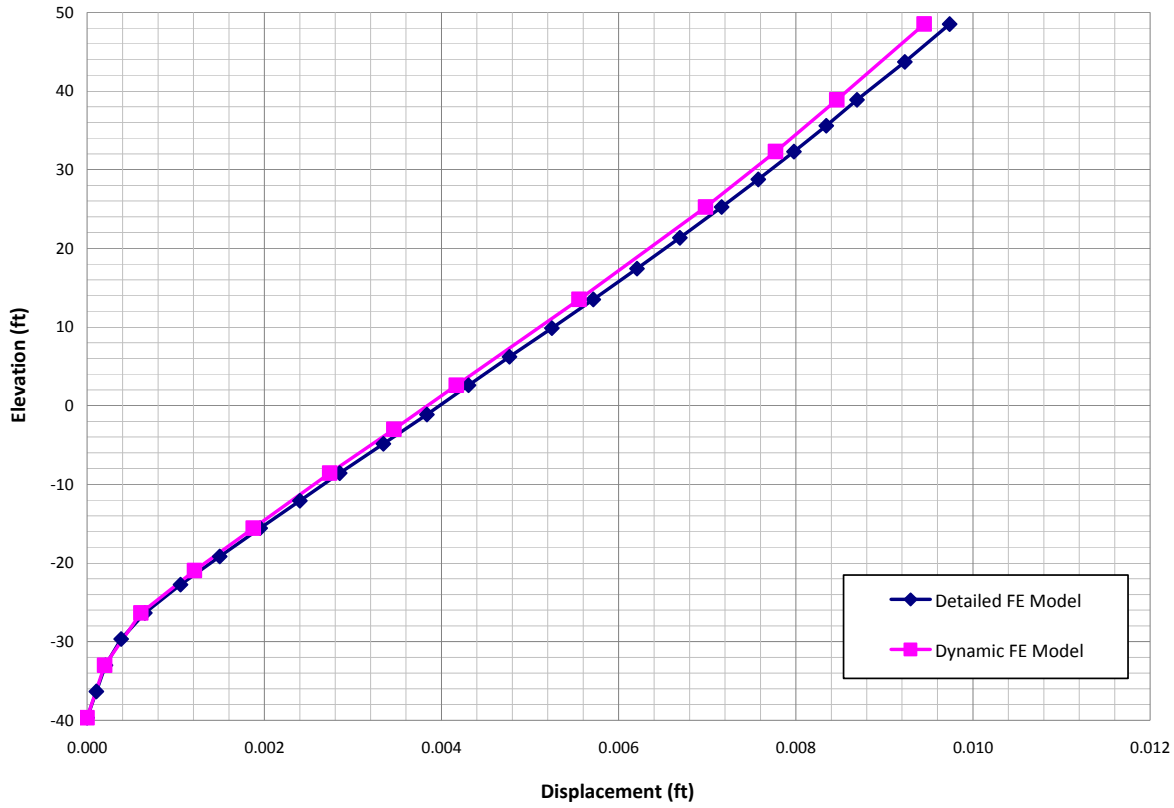

Figure 02.5.1.3.4.1-3 East PS/B EW Direction (Y) 1g Static Analysis – Southeast Corner

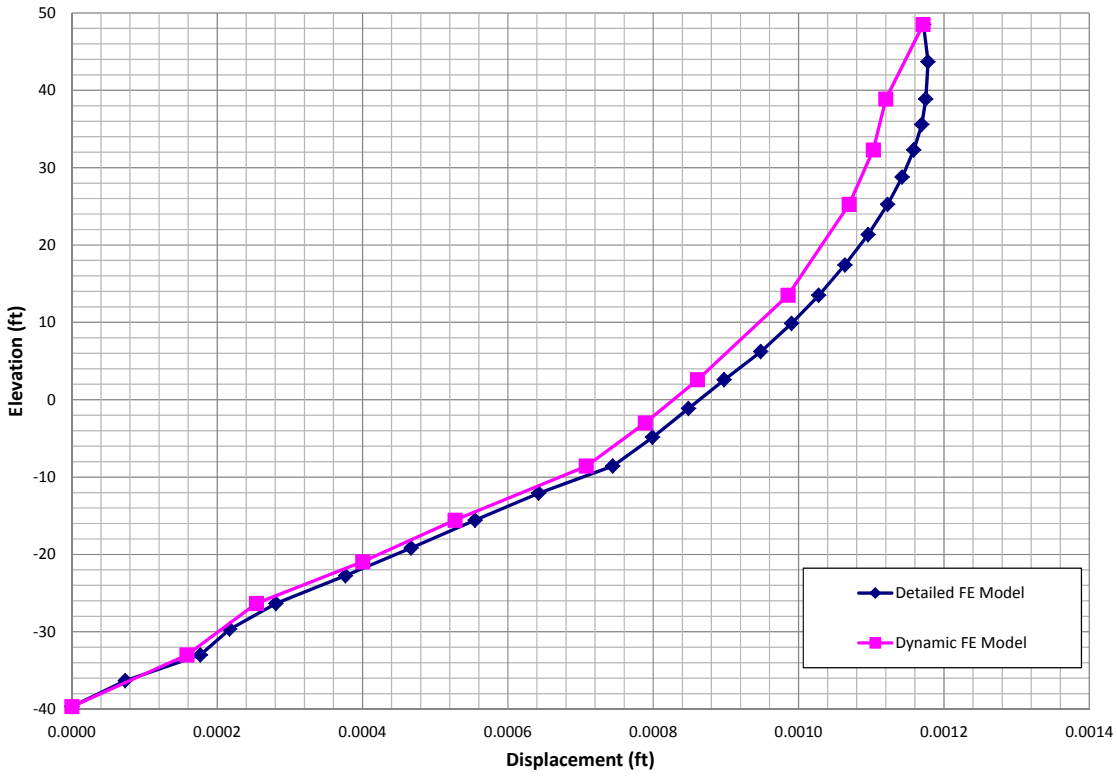

Figure 02.5.1.3.4.1-4 East PS/B Vertical Direction (Z) 1g Static Analysis – Southeast Corner

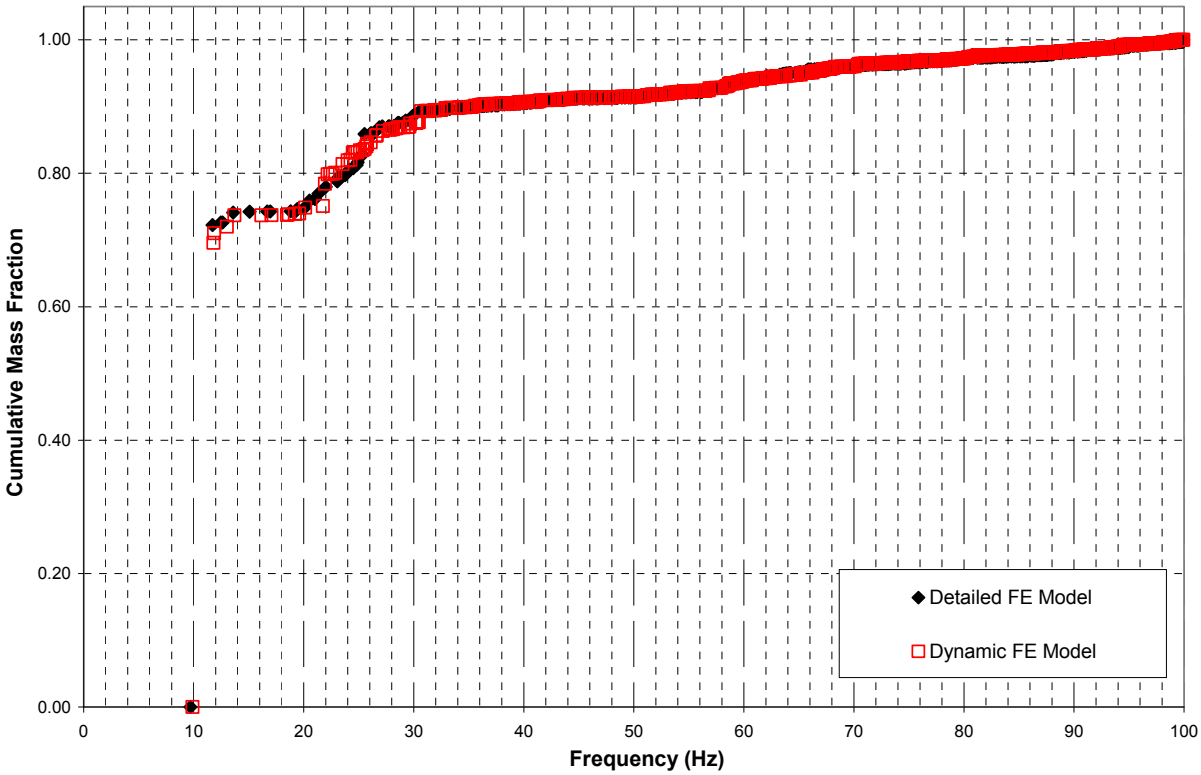

Figure 02.5.1.3.4.2-1 East PS/B Modal Analysis – Cumulative Mass in the NS Direction (X)

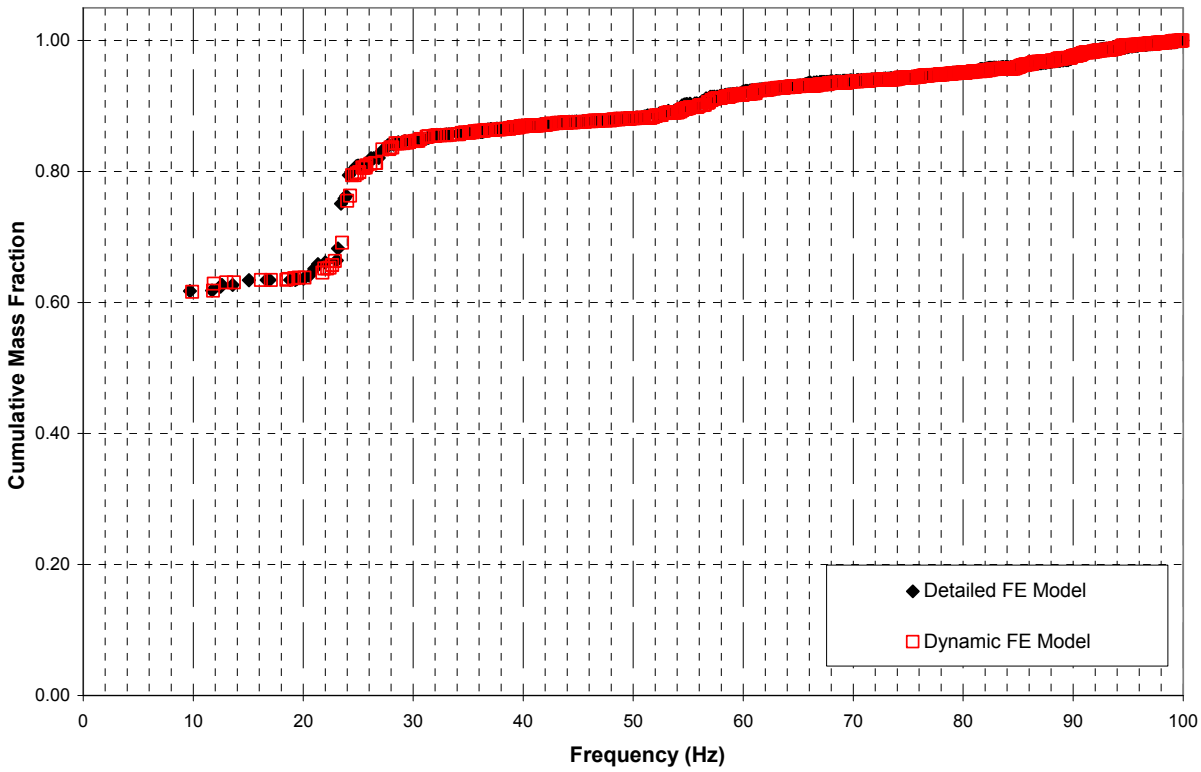

Figure 02.5.1.3.4.2-2 East PS/B Modal Analysis – Cumulative Mass in the EW Direction (Y)

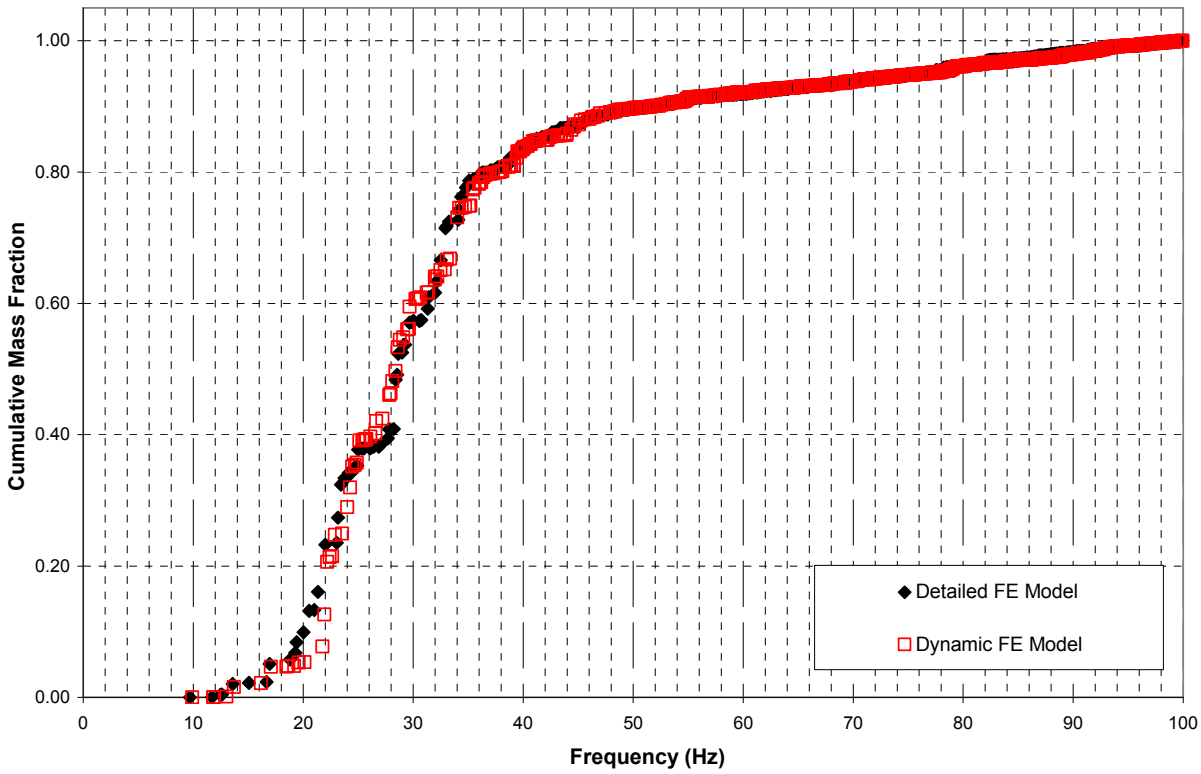

Figure 02.5.1.3.4.2-3 East PS/B Modal Analysis – Cumulative Mass in the Vertical Direction (Z)

Figure 02.5.1.3.4.2-4 East PS/B Detailed Mode Shape – Mode 2 at Frequency 11.71 Hz - NS Direction (X)

Figure 02.5.1.3.4.2-5 East PS/B Dynamic Mode Shape – Mode 2 at Frequency 11.8 Hz - NS Direction (X)

Figure 02.5.1.3.4.2-6 East PS/B Detailed Mode Shape – Mode 1 at Frequency 9.71 Hz - EW Direction (Y)

Figure 02.5.1.3.4.2-7 East PS/B Dynamic Mode Shape – Mode 1 at Frequency 9.9 Hz - EW Direction (Y)

Figure 02.5.1.3.4.2-8 East PS/B Detailed Mode Shape – Mode 13 at Frequency 20.5 Hz - Vertical Direction (Z)

Figure 02.5.1.3.4.2-9 East PS/B Dynamic Mode Shape – Mode 14 at Frequency 21.94 Hz - Vertical Direction (Z)

Figure 02.5.1.3.4.2-10 East PS/B Detailed Mode Shape – Mode 16 at Frequency 22 Hz- Vertical Direction (Z)

Figure 02.5.1.3.4.2-11 East PS/B Dynamic Mode Shape – Mode 15 at Frequency 22.18 Hz - Vertical Direction (Z)

Figure 02.5.1.3.4.2-12 East PS/B Detailed Mode Shape – Mode 37 at Frequency 28.4 Hz - Vertical Direction (Z)

Figure 02.5.1.3.4.2-13 East PS/B Dynamic Mode Shape – Mode 34 at Frequency 27.83 Hz - Vertical Direction (Z)

Figure 02.5.1.3.4.2-14 East PS/B Detailed Mode Shape – Mode 53 at Frequency 32.9 Hz - Vertical Direction (Z)

Figure 02.5.1.3.4.2-15 East PS/B Dynamic Mode Shape – Mode 57 at Frequency 34 Hz - Vertical Direction (Z)

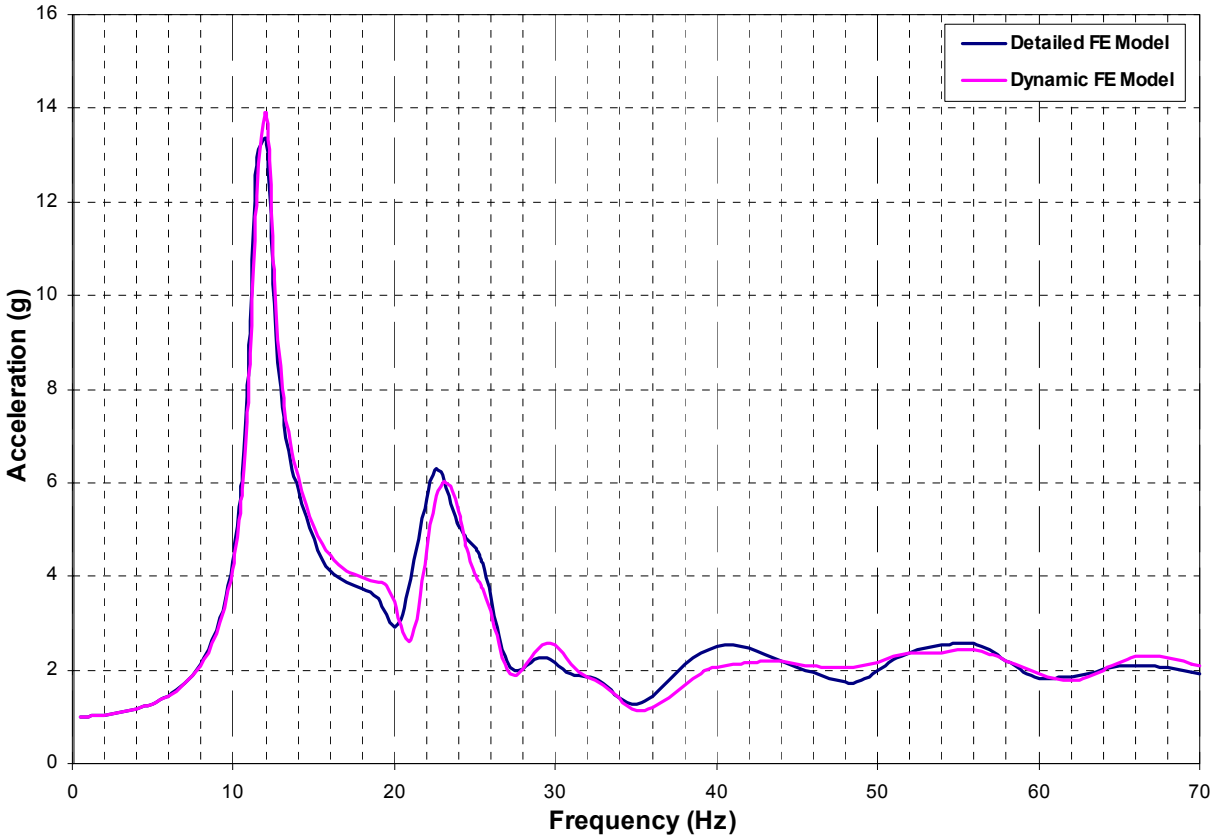

Figure 02.5.1.3.4.3-1 East PS/B Harmonic Response Analysis – NW Corner– Elev. 48'-6" - NS Direction (X)

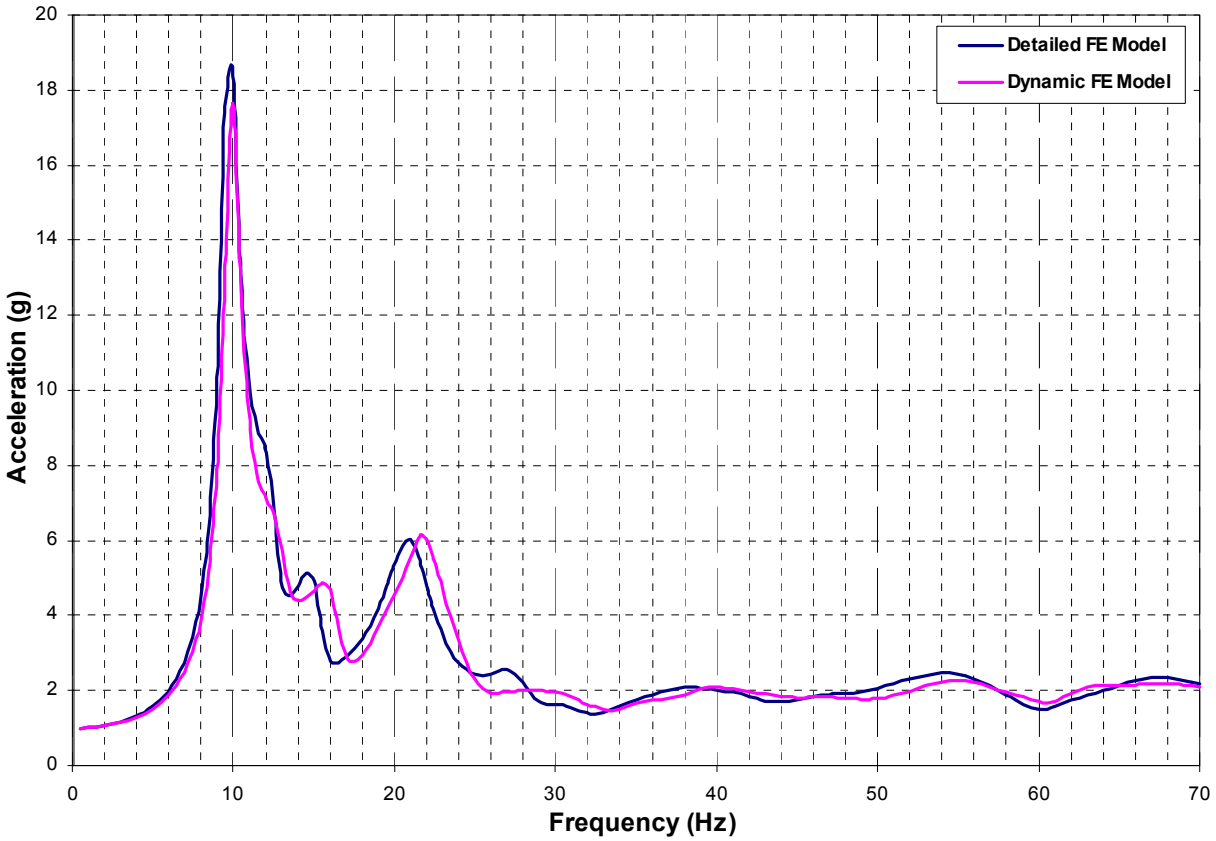

Figure 02.5.1.3.4.3-2 East PS/B Harmonic Response Analysis – NW Corner– Elev. 48'-6" - EW Direction (Y)

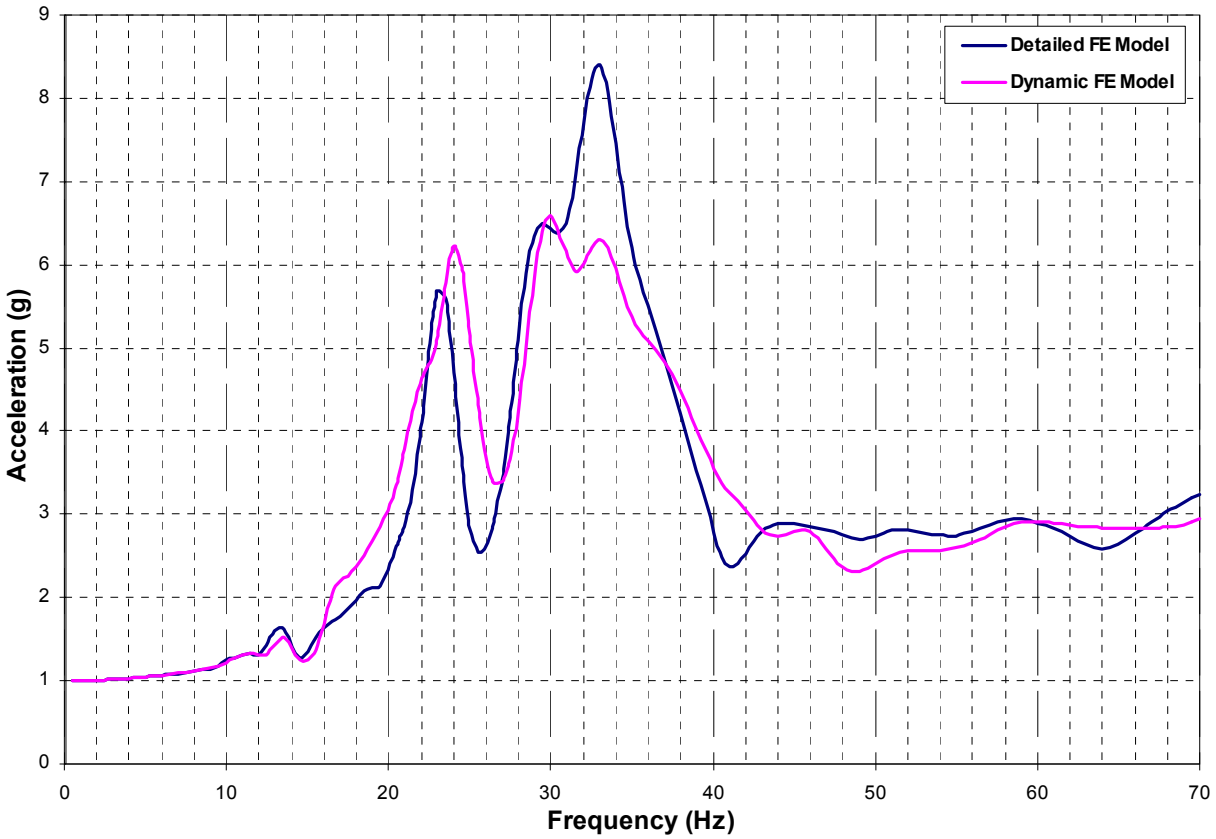

Figure 02.5.1.3.4.3-3 East PS/B Harmonic Response Analysis – NW Corner– Elev. 48'-6" - Vertical Direction (Z)

Figure 02.5.1.3.5.1-1 Displacement Locations on West PS/B Exterior Walls

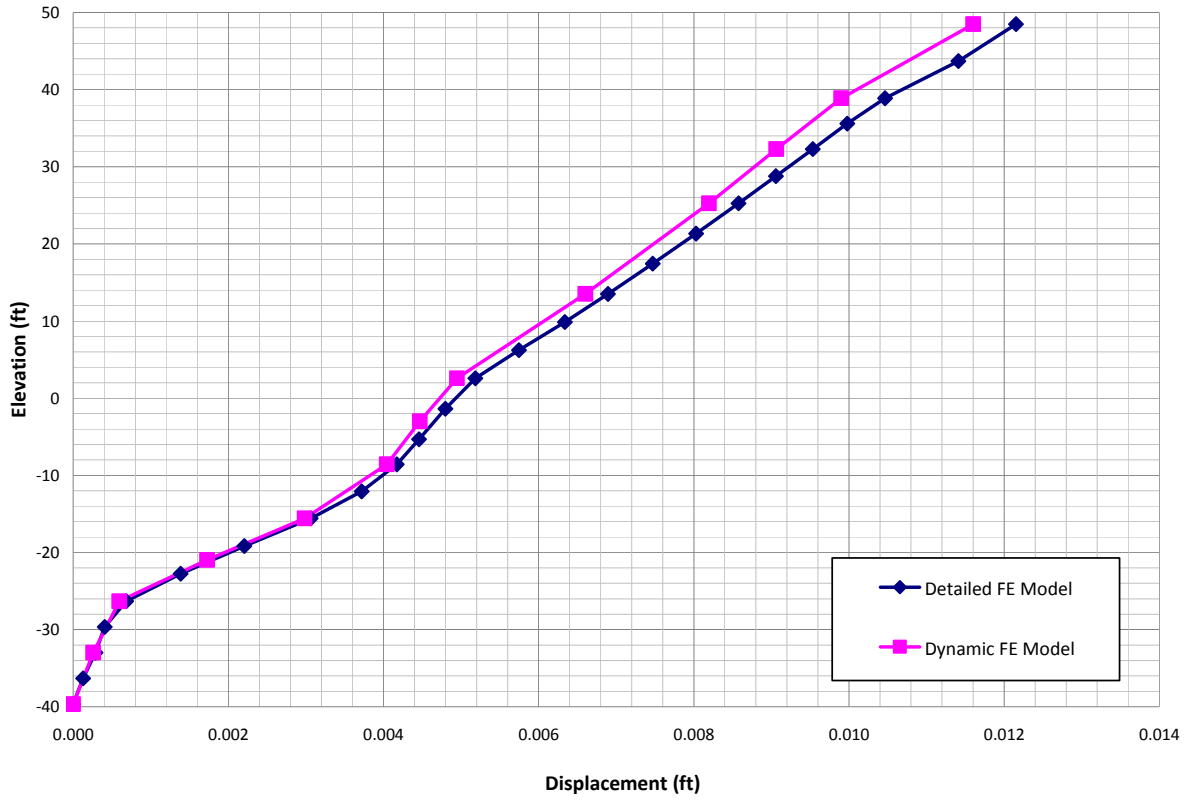

Figure 02.5.1.3.5.1-2 West PS/B NS Direction (X) 1g Static Analysis – Southwest Corner

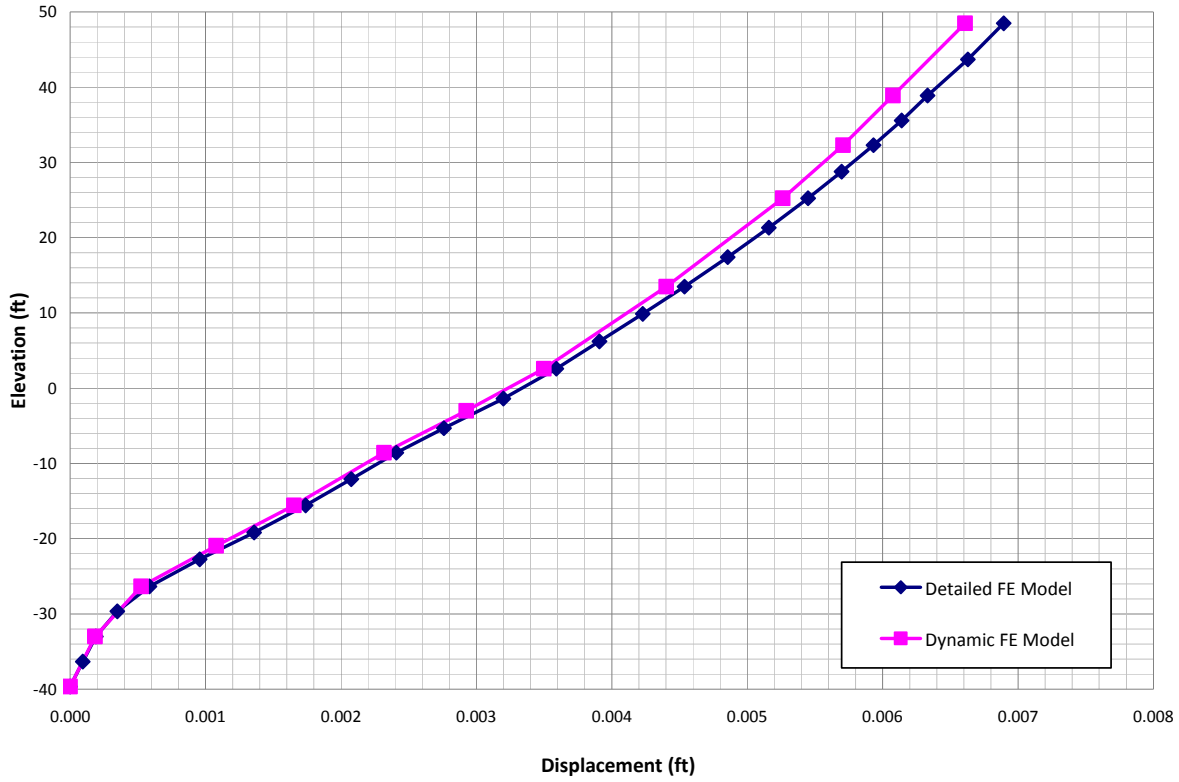

Figure 02.5.1.3.5.1-3 West PS/B EW Direction (Y) 1g Static Analysis – Southwest Corner

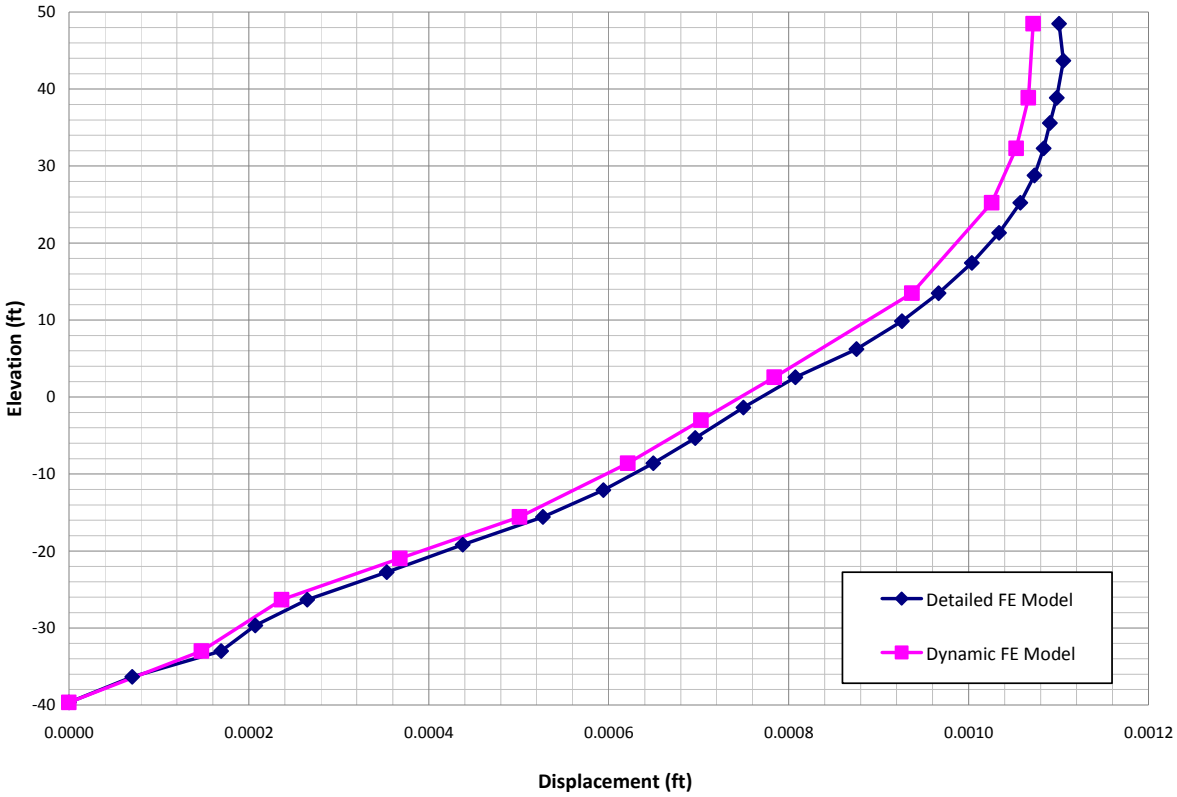

Figure 02.5.1.3.5.1-4 West PS/B Vertical Direction (Z) 1g Static Analysis – Southwest Corner

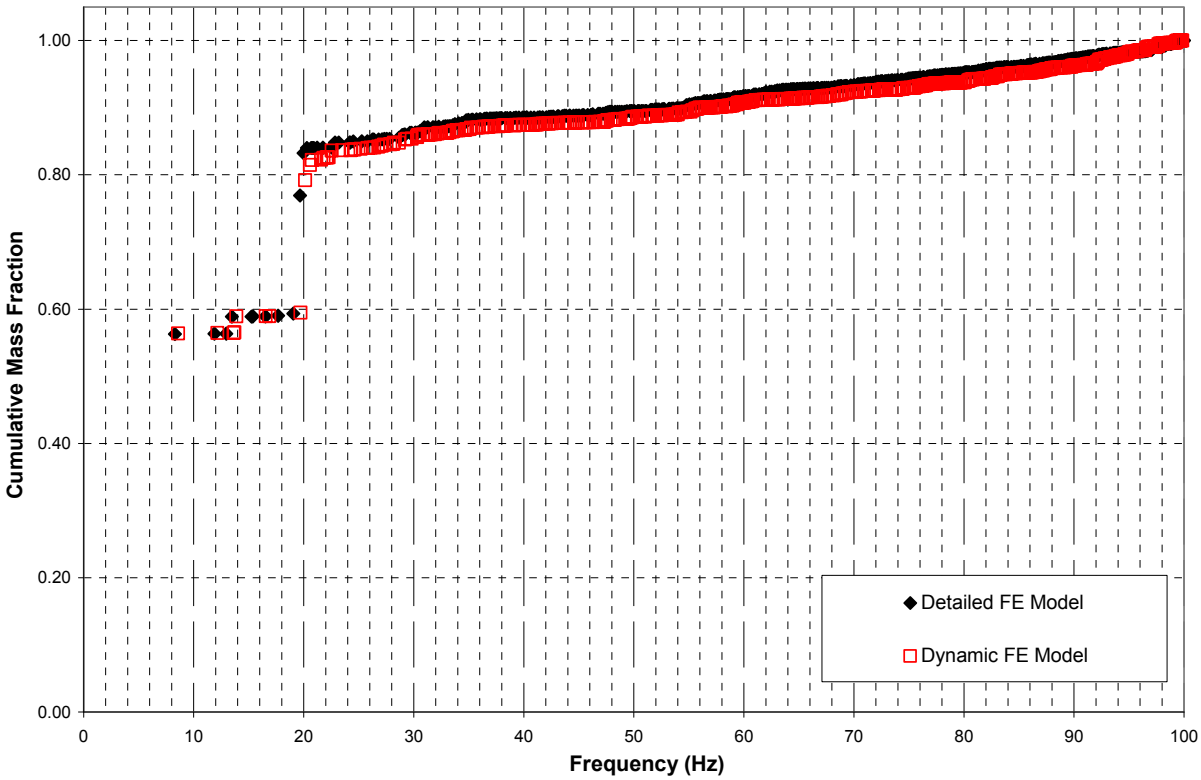

Figure 02.5.1.3.5.2-1 West PS/B Modal Analysis – Cumulative Mass in the NS Direction (X)

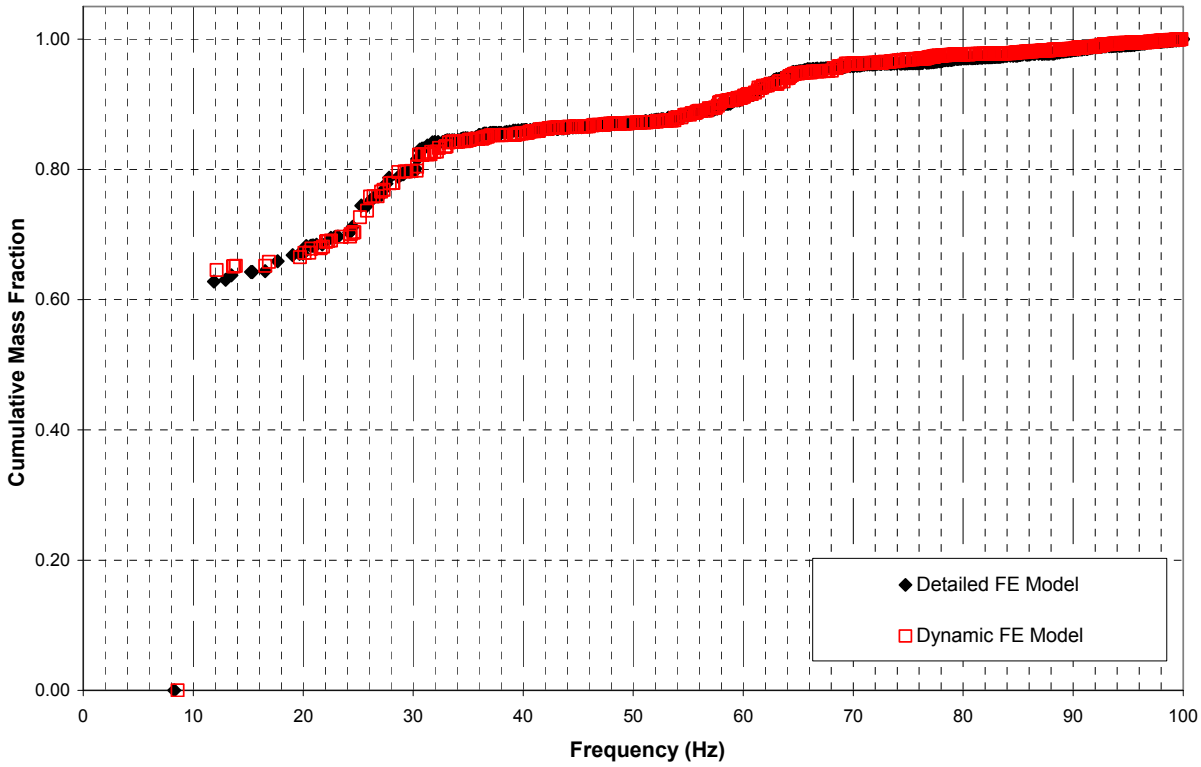

Figure 02.5.1.3.5.2-2 West PS/B Modal Analysis – Cumulative Mass in the EW Direction (Y)

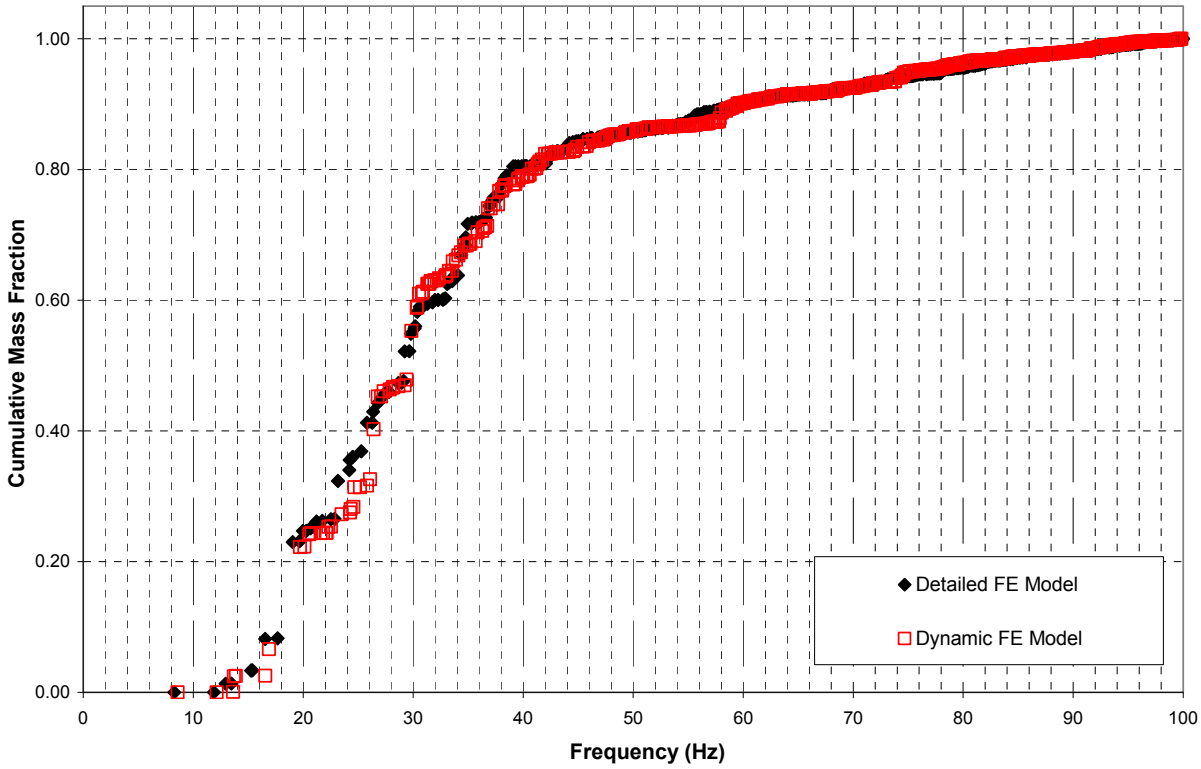

Figure 02.5.1.3.5.2-3 West PS/B Modal Analysis – Cumulative Mass in the Vertical Direction (Z)

Figure 02.5.1.3.5.2-4 West PS/B Detailed Mode Shape – Mode 1 at Frequency 8.28 Hz - NS Direction (X)

Figure 02.5.1.3.5.2-5 West PS/B Dynamic Mode Shape – Mode 1 at Frequency 8.59 Hz - NS Direction (X)

Figure 02.5.1.3.5.2-6 West PS/B Detailed Mode Shape – Mode 10 at Frequency 19.67 Hz - NS Direction (X)

Figure 02.5.1.3.5.2-7 West PS/B Dynamic Mode Shape – Mode 9 at Frequency 20.13 Hz - NS Direction (X)

Figure 02.5.1.3.5.2-8 West PS/B Detailed Mode Shape – Mode 2 at Frequency 11.89 Hz - EW Direction (Y)

Figure 02.5.1.3.5.2-9 West PS/B Dynamic Mode Shape – Mode 2 at Frequency 12.15 Hz - EW Direction (Y)

Figure 02.5.1.3.5.2-10 West PS/B Detailed Mode Shape – Mode 8 at Frequency 19.7 Hz - Vertical Direction (Z)

Figure 02.5.1.3.5.2-11 West PS/B Dynamic Mode Shape – Mode 9 at Frequency 19.1 Hz - Vertical Direction (Z)

Figure 02.5.1.3.5.2-12 West PS/B Detailed Mode Shape – Mode 36 at Frequency 29.8 Hz - Vertical Direction (Z)

Figure 02.5.1.3.5.2-13 West PS/B Dynamic Mode Shape – Mode 36 at Frequency 29.2 Hz - Vertical Direction (Z)

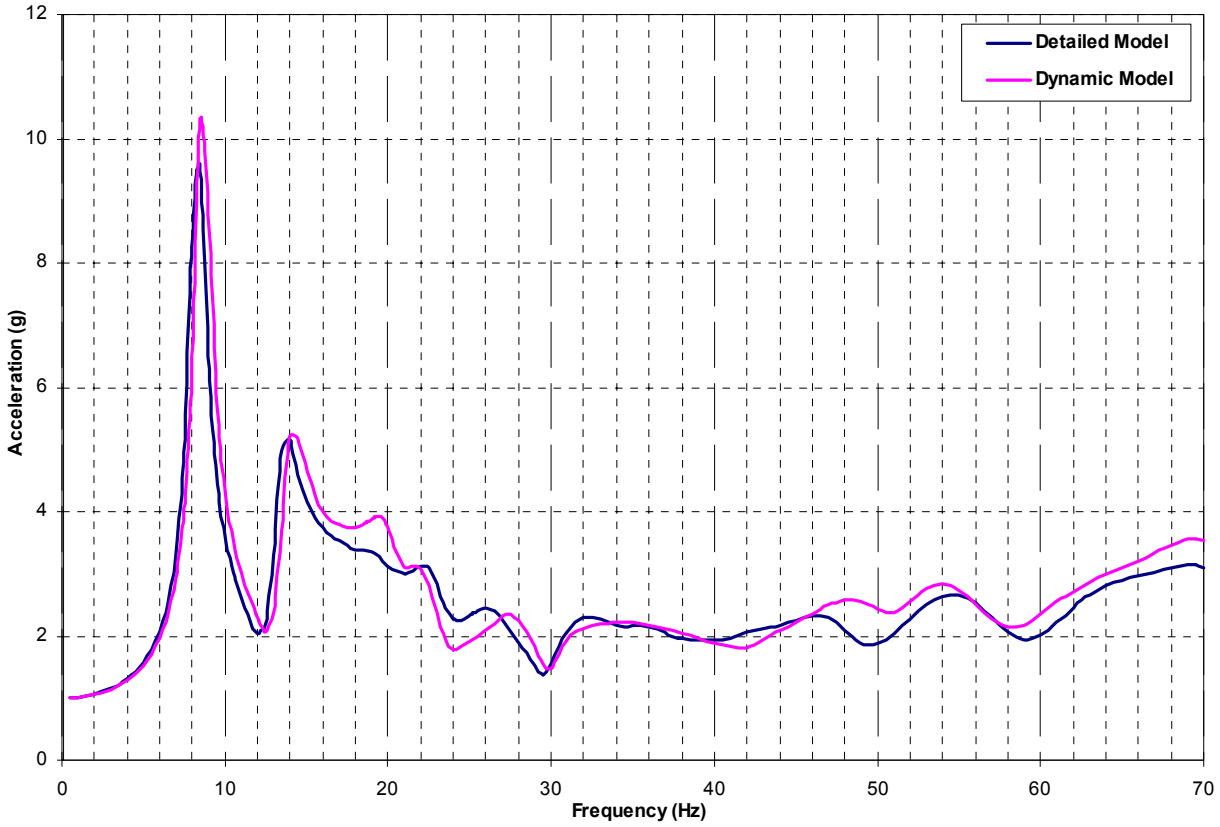

Figure 02.5.1.3.5.3-1 West PS/B Harmonic Response Analysis – SW Corner– Elev. 48'-6" - NS Direction (X)

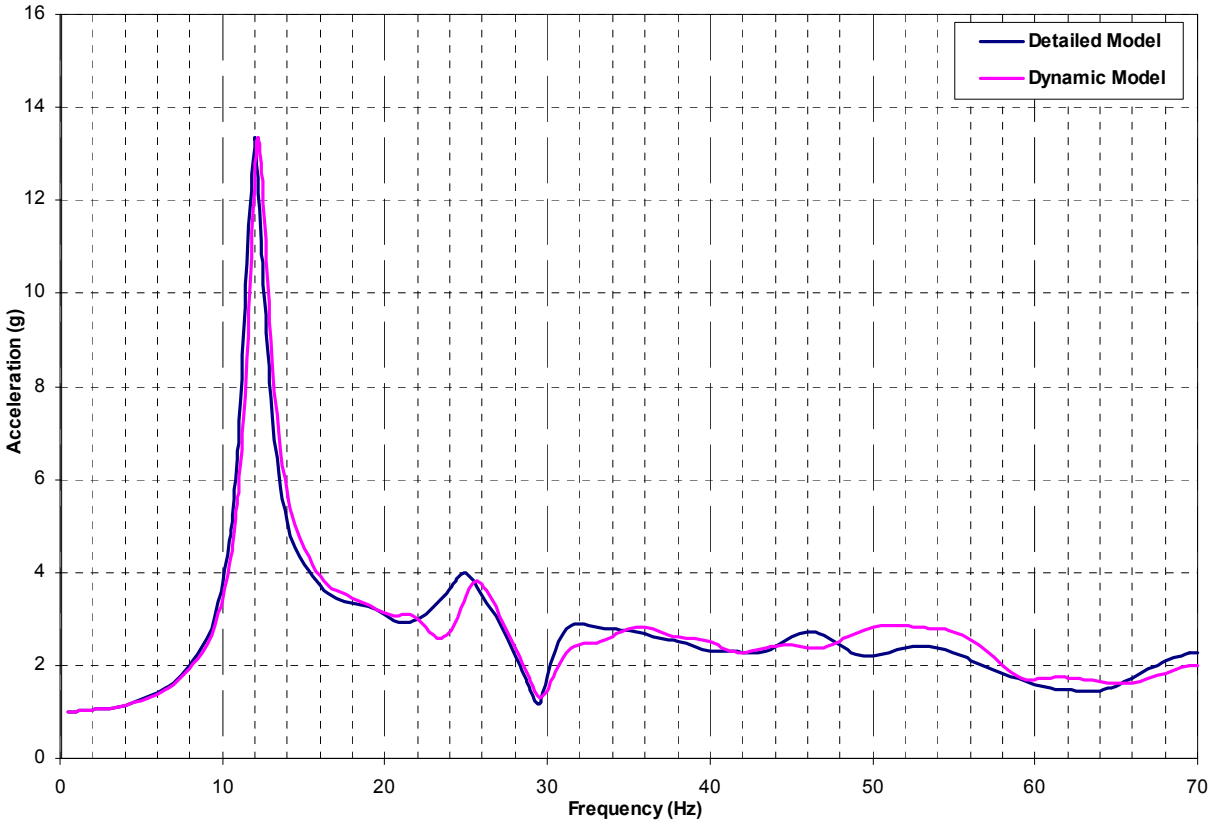

Figure 02.5.1.3.5.3-2 West PS/B Harmonic Response Analysis – SW Corner– Elev. 48'-6" - EW Direction (Y)

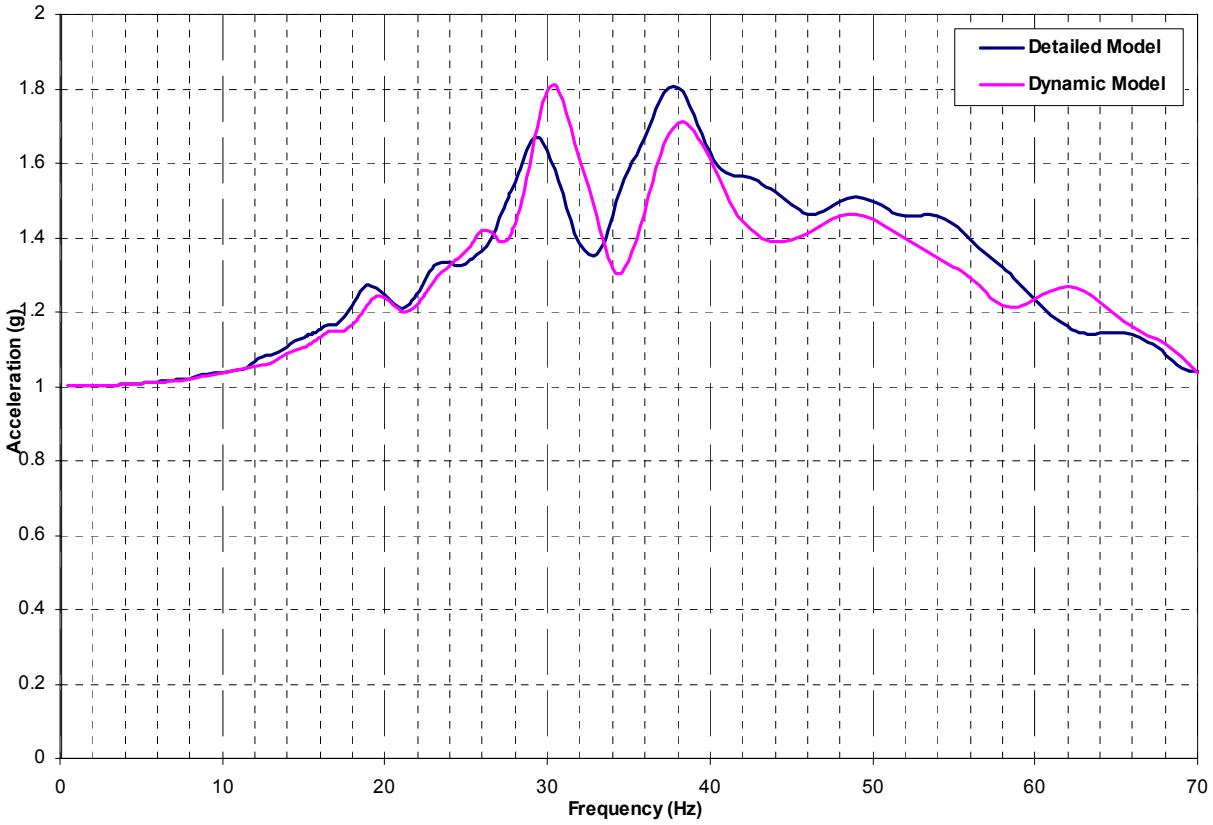

Figure 02.5.1.3.5.3-3 West PS/B Harmonic Response Analysis – SW Corner– Elev. 48'-6" - Vertical Direction (Z)

Figure 02.5.1.3.6.1-1 Displacement Locations on A/B Exterior Walls

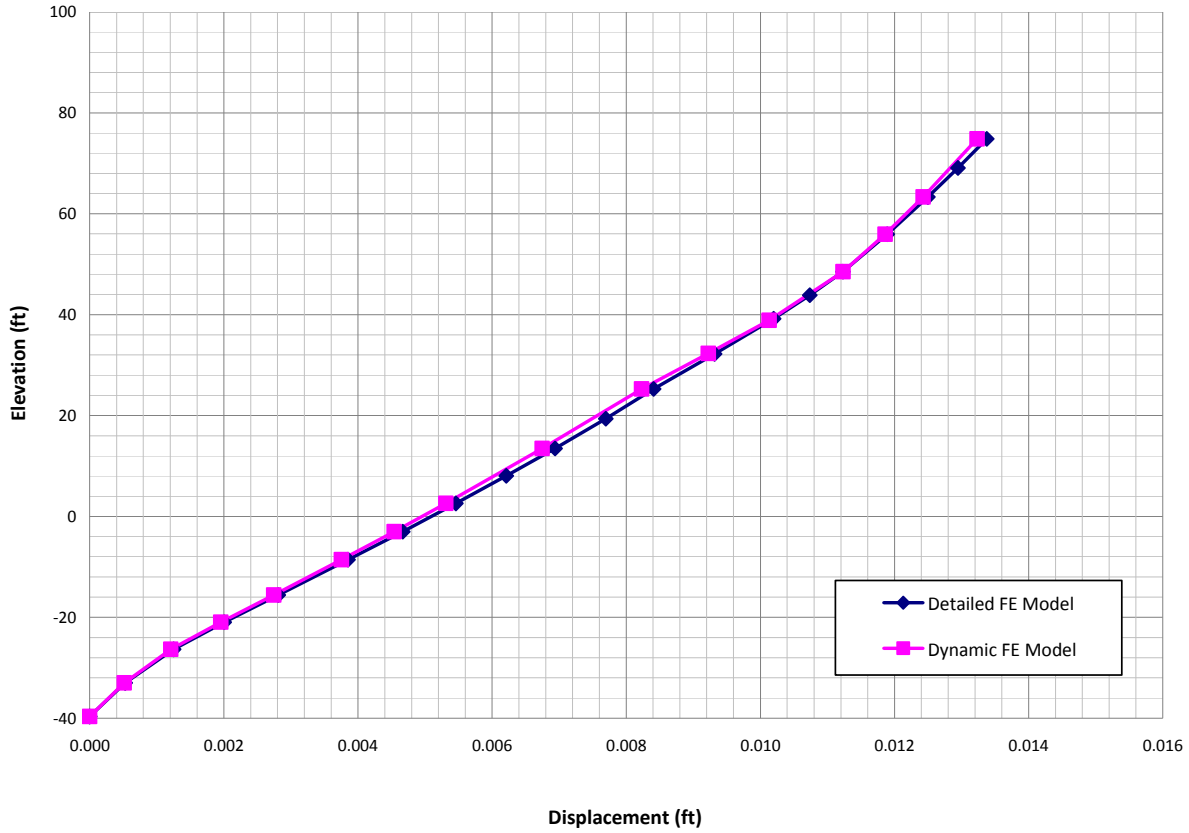

Figure 02.5.1.3.6.1-2 A/B NS Direction (X) 1g Static Analysis – Southwest Corner

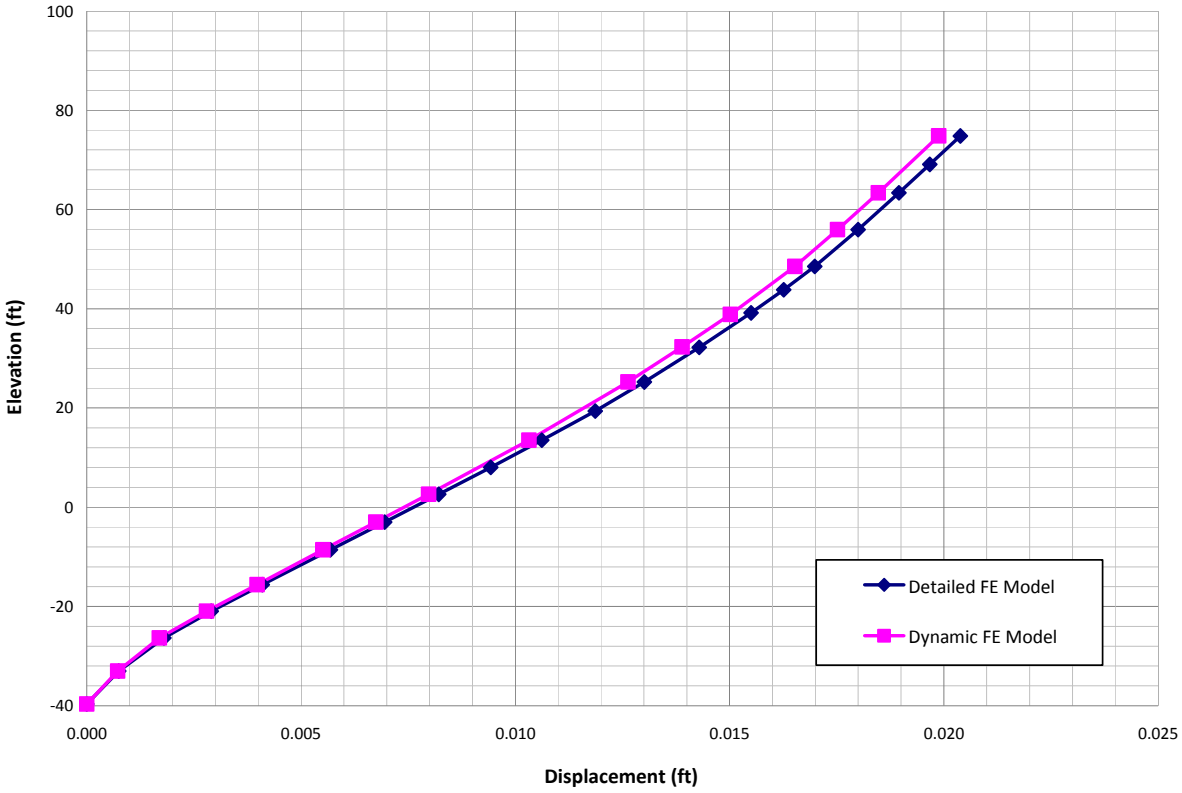

Figure 02.5.1.3.6.1-3 A/B EW Direction (Y) 1g Static Analysis – Southwest Corner

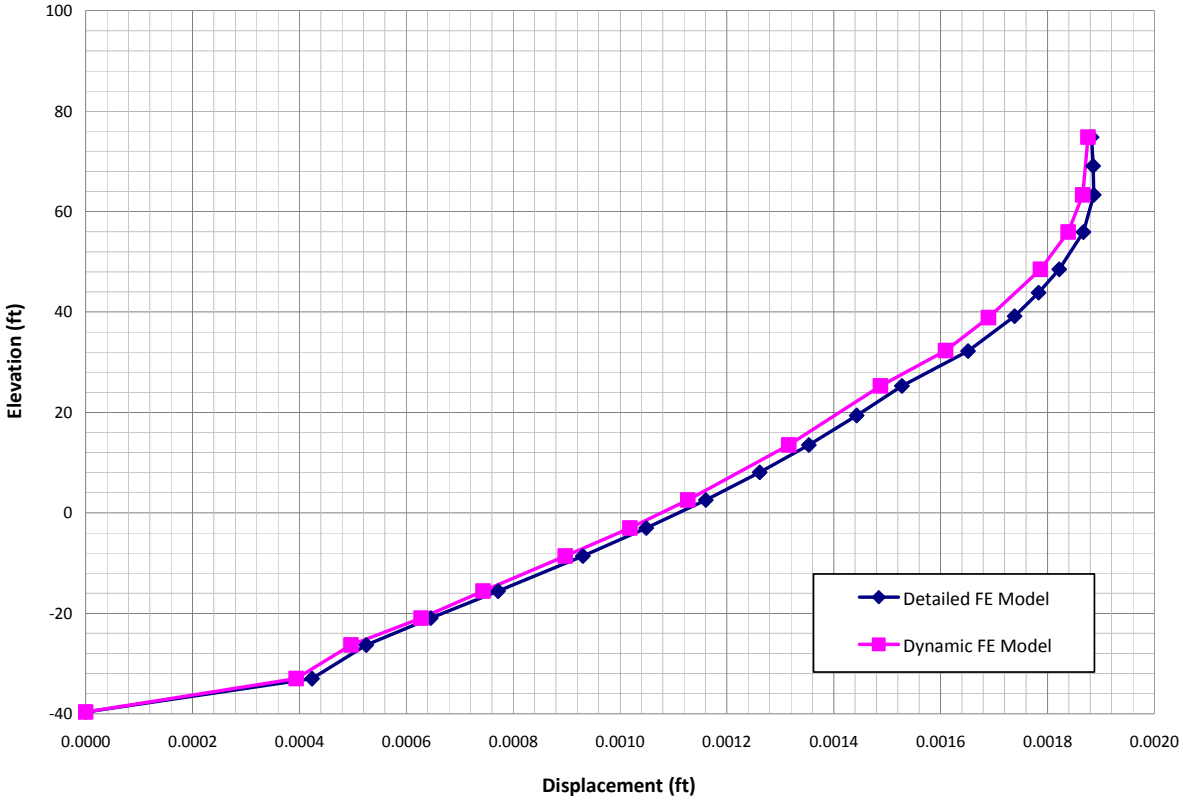

Figure 02.5.1.3.6.1-4 A/B Vertical Direction (Z) 1g Static Analysis – Southwest Corner

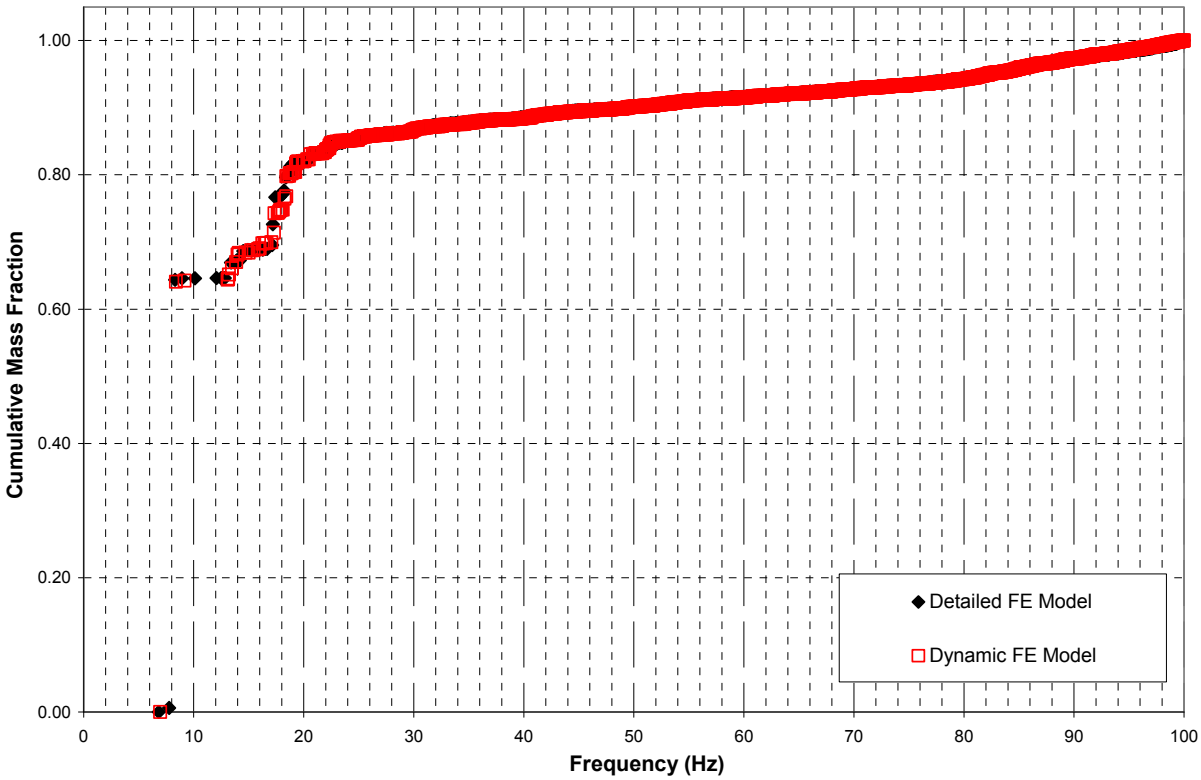

Figure 02.5.1.3.6.2-1 A/B Modal Analysis – Cumulative Mass in the NS Direction (X)

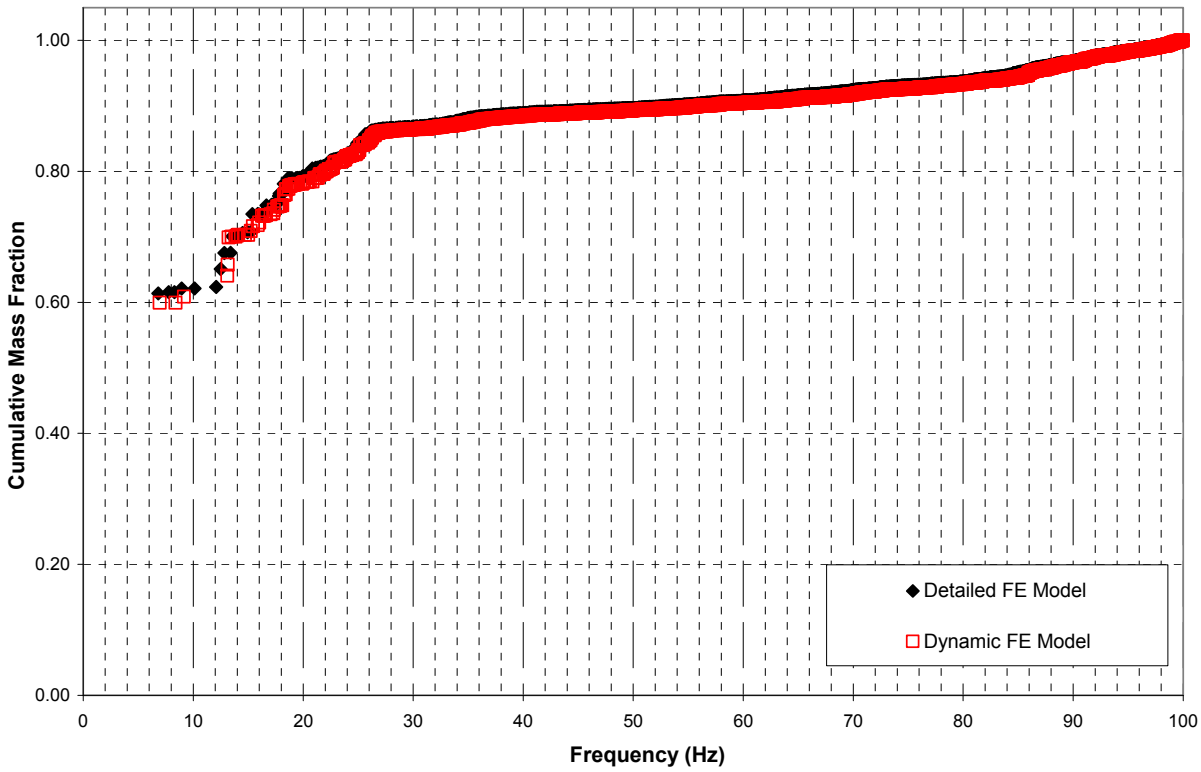

Figure 02.5.1.3.6.2-2 A/B Modal Analysis – Cumulative Mass in the EW Direction (Y)

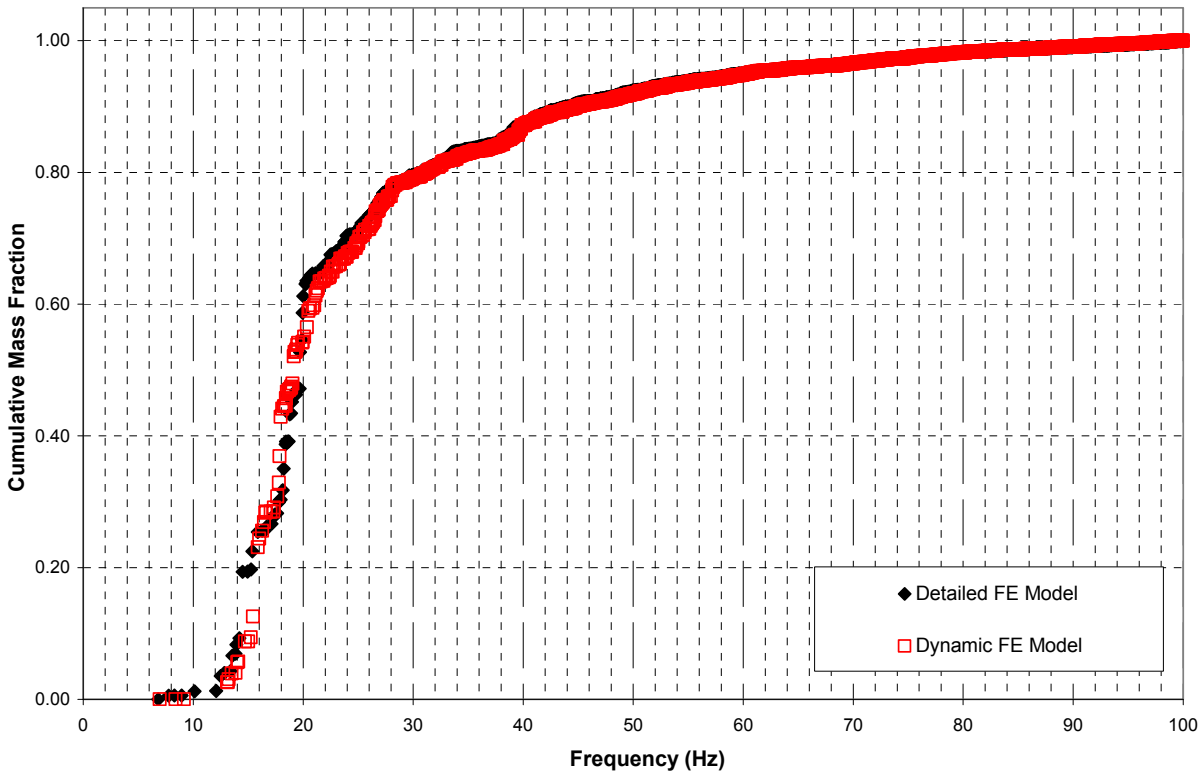

Figure 02.5.1.3.6.2-3 A/B Modal Analysis – Cumulative Mass in the Vertical Direction (Z)

Figure 02.5.1.3.6.2-4 A/B Detailed Mode Shape – Mode 2 at Frequency 8.31 Hz - NS Direction (X)

Figure 02.5.1.3.6.2-5 A/B Dynamic Mode Shape – Mode 2 at Frequency 8.39 Hz - NS Direction (X)

Figure 02.5.1.3.6.2-6 A/B Detailed Mode Shape – Mode 1 at Frequency 6.82 Hz - EW Direction (Y)

Figure 02.5.1.3.6.2-7 A/B Dynamic Mode Shape – Mode 1 at Frequency 6.96 Hz - EW Direction (Y)

Figure 02.5.1.3.6.2-8 A/B Detailed Mode Shape – Mode 14 at Frequency 14.5 Hz - Vertical Direction (Z)

Figure 02.5.1.3.6.2-9 A/B Dynamic Mode Shape – Mode 15 at Frequency 15.87 Hz - Vertical Direction (Z)

Figure 02.5.1.3.6.2-10 A/B Detailed Mode Shape – Mode 31 at Frequency 18.39 Hz - Vertical Direction (Z)

Figure 02.5.1.3.6.2-11 A/B Dynamic Mode Shape – Mode 27 at Frequency 17.94 Hz - Vertical Direction (Z)

Figure 02.5.1.3.6.2-12 A/B Detailed Mode Shape – Mode 44 at Frequency 19.95 Hz - Vertical Direction (Z)

Figure 02.5.1.3.6.2-13 A/B Dynamic Mode Shape – Mode 48 at Frequency 20.48 Hz - Vertical Direction (Z)

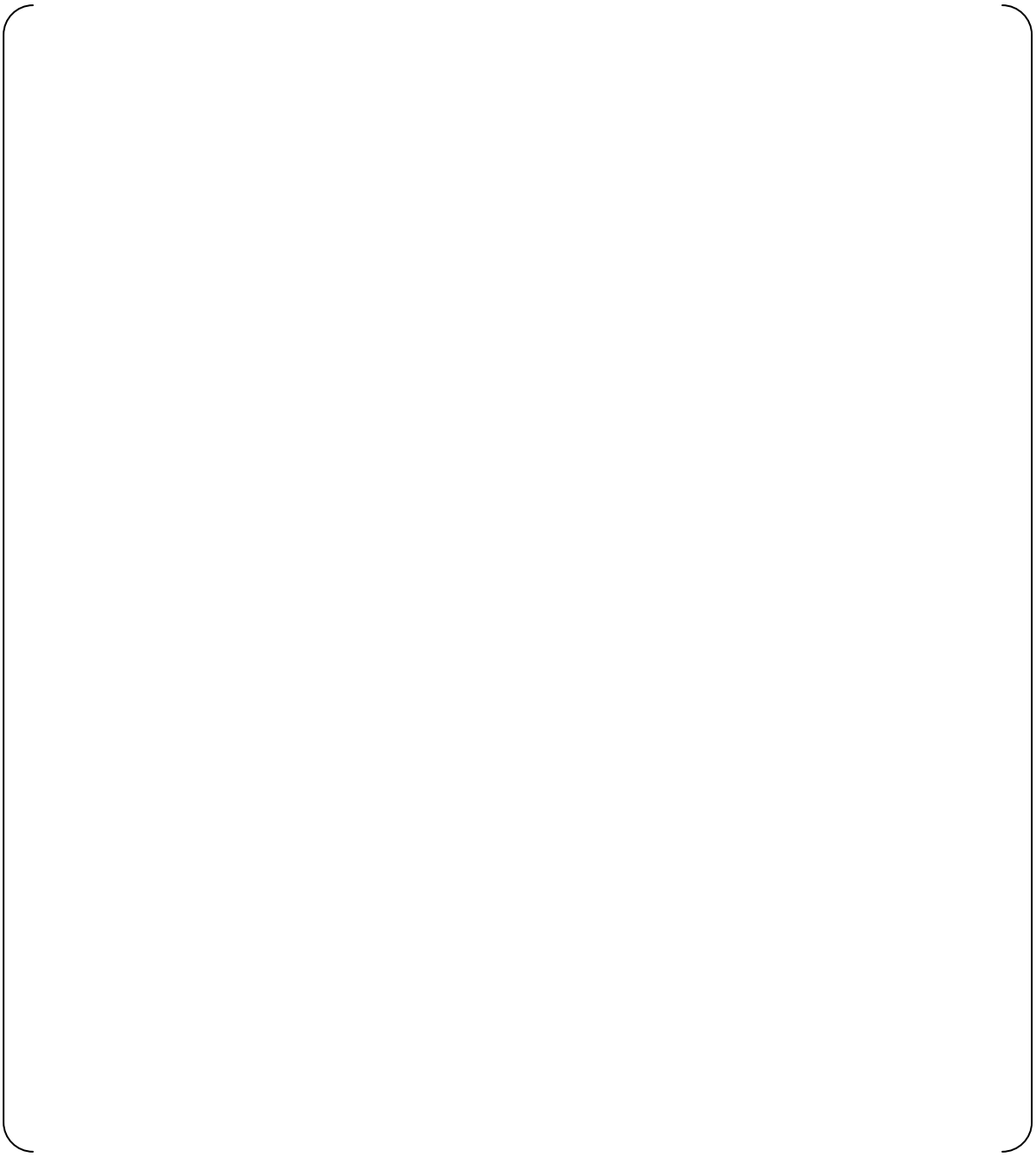

Figure 02.5.1.3.7.1-1 R/B Complex Comparison Locations - Plan View

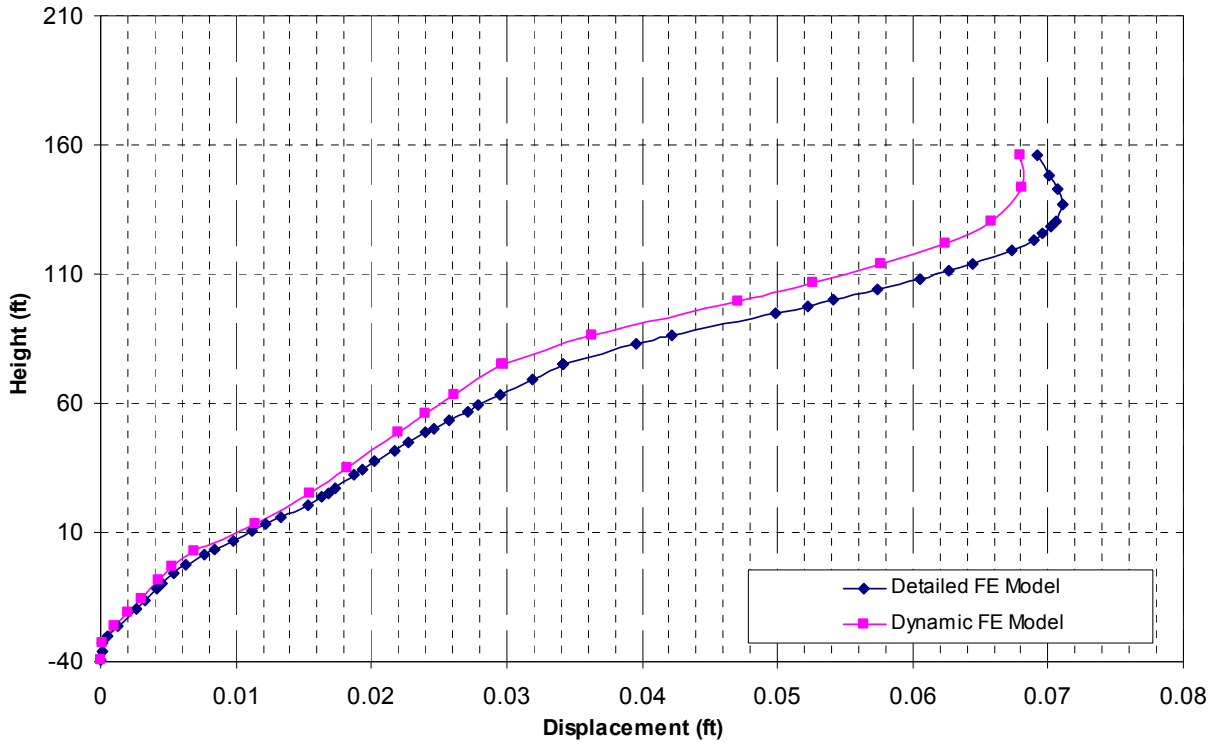

Note: The curves shown for this location on the R/B are due to the stiffness of the FH/A in the NS direction being greater than the EW direction. The Northern wall of the FH/A is flexible in comparison to the Eastern and Western walls combined with the roof diaphragm. Therefore, the Northern wall has a greater deflection at midheight than at the roof diaphragm

Figure 02.5.1.3.7.1-2 R/B Complex NS Direction (X) 1g Static Analysis – Comparison Point A

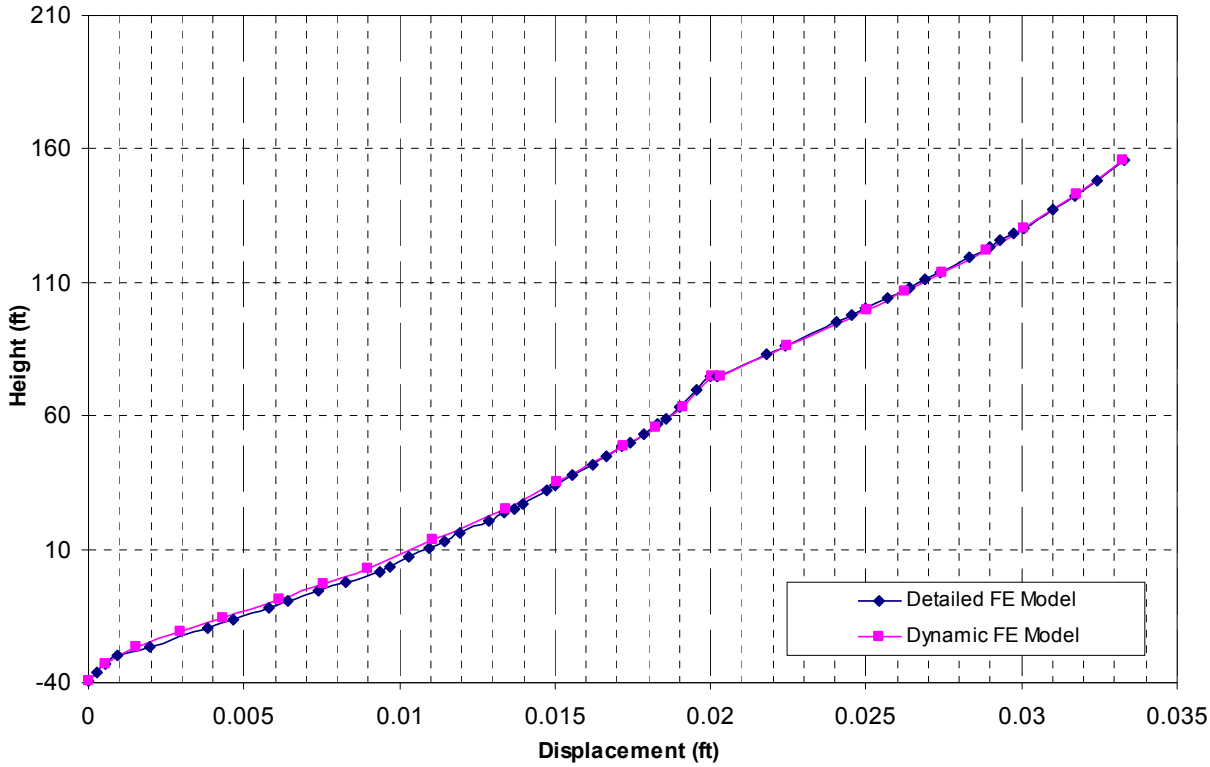

Figure 02.5.1.3.7.1-3 R/B Complex EW Direction (Y) 1g Static Analysis – Comparison Point A

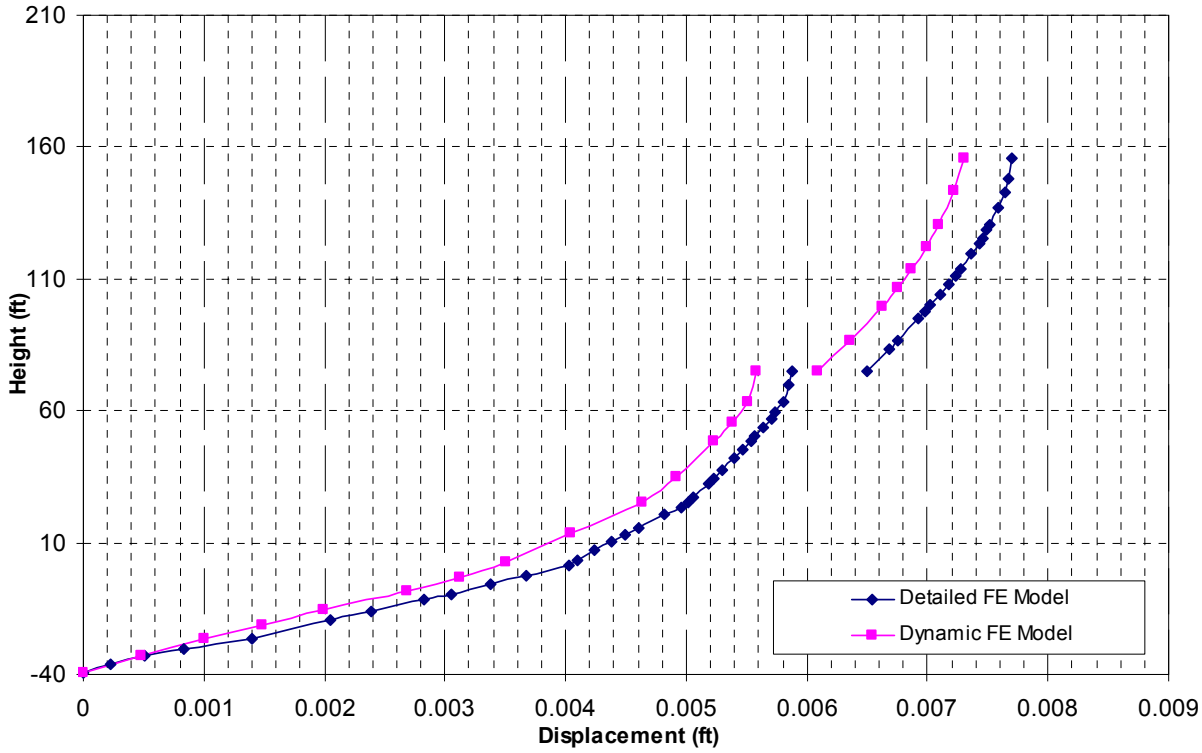

Figure 02.5.1.3.7.1-4 R/B Complex Vertical Direction (Z) 1g Static Analysis – Comparison Point A

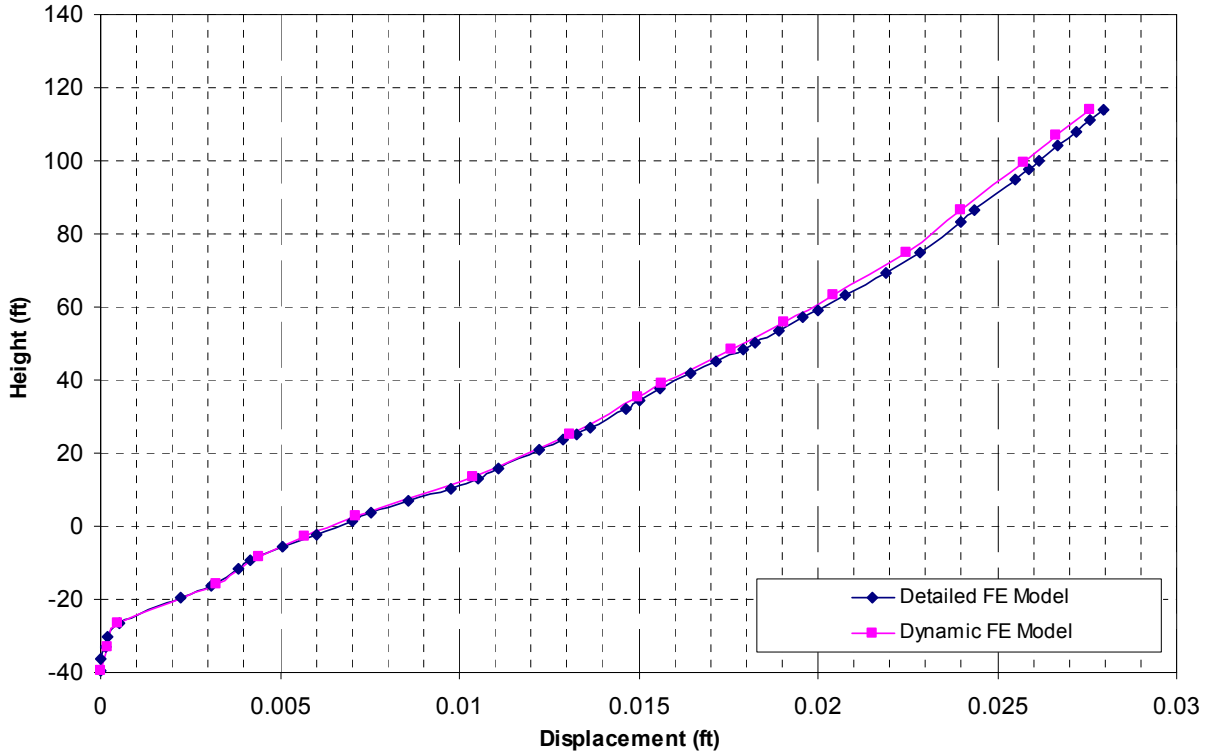

Figure 02.5.1.3.7.1-5 R/B Complex NS Direction (X) 1g Static Analysis – Comparison Point H

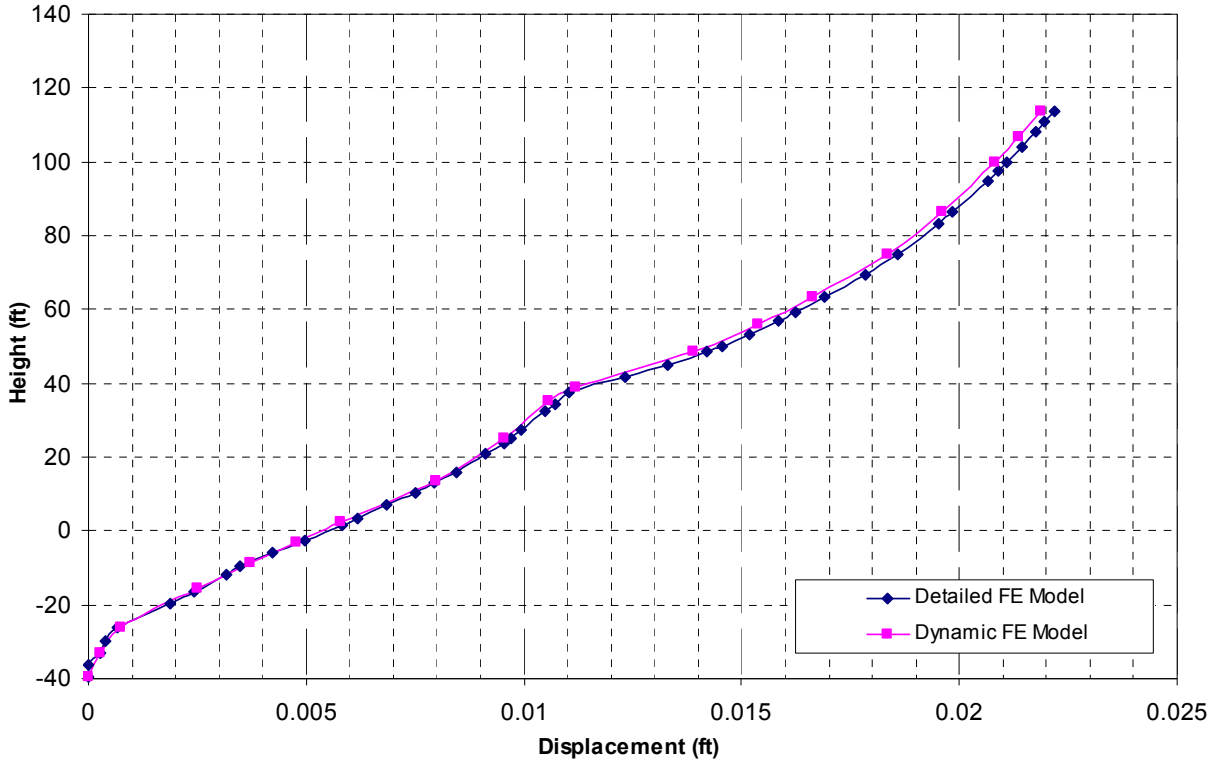

Figure 02.5.1.3.7.1-6 R/B Complex EW Direction (Y) 1g Static Analysis – Comparison Point H

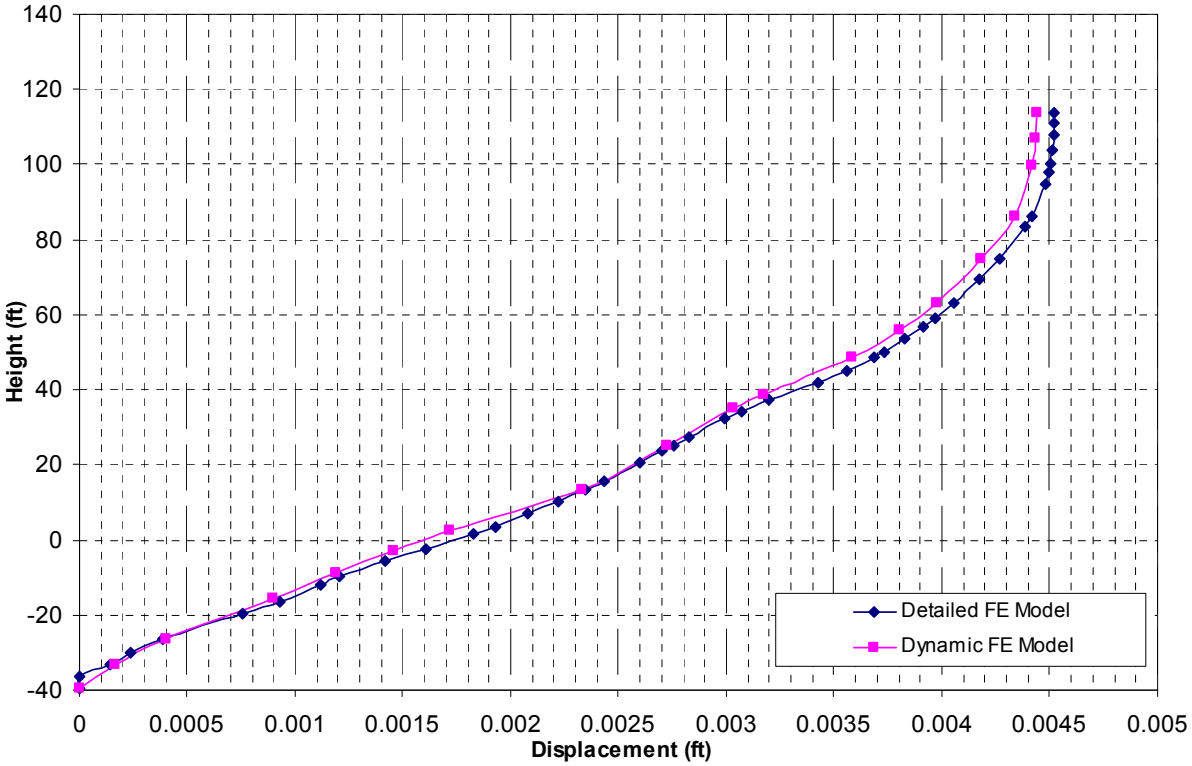

Figure 02.5.1.3.7.1-7 R/B Complex Vertical Direction (Z) 1g Static Analysis – Comparison Point H

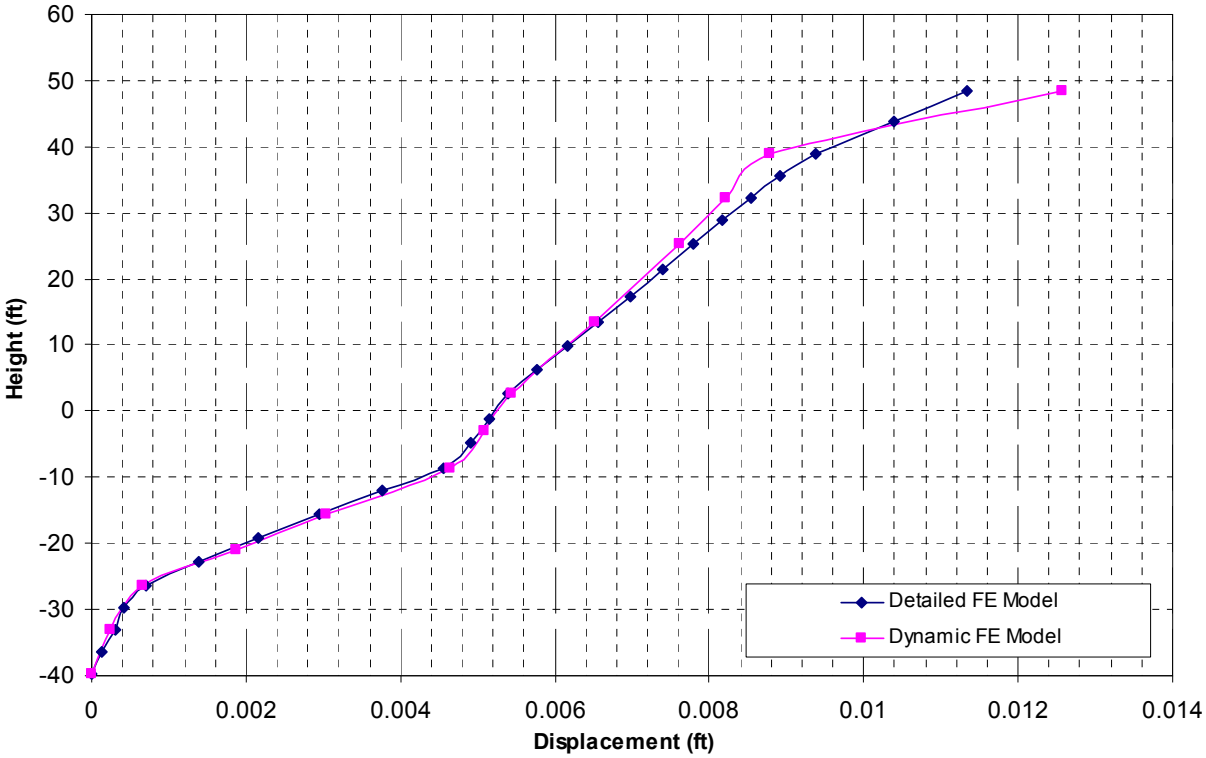

Figure 02.5.1.3.7.1-8 R/B Complex NS Direction (X) 1g Static Analysis – Comparison Point M

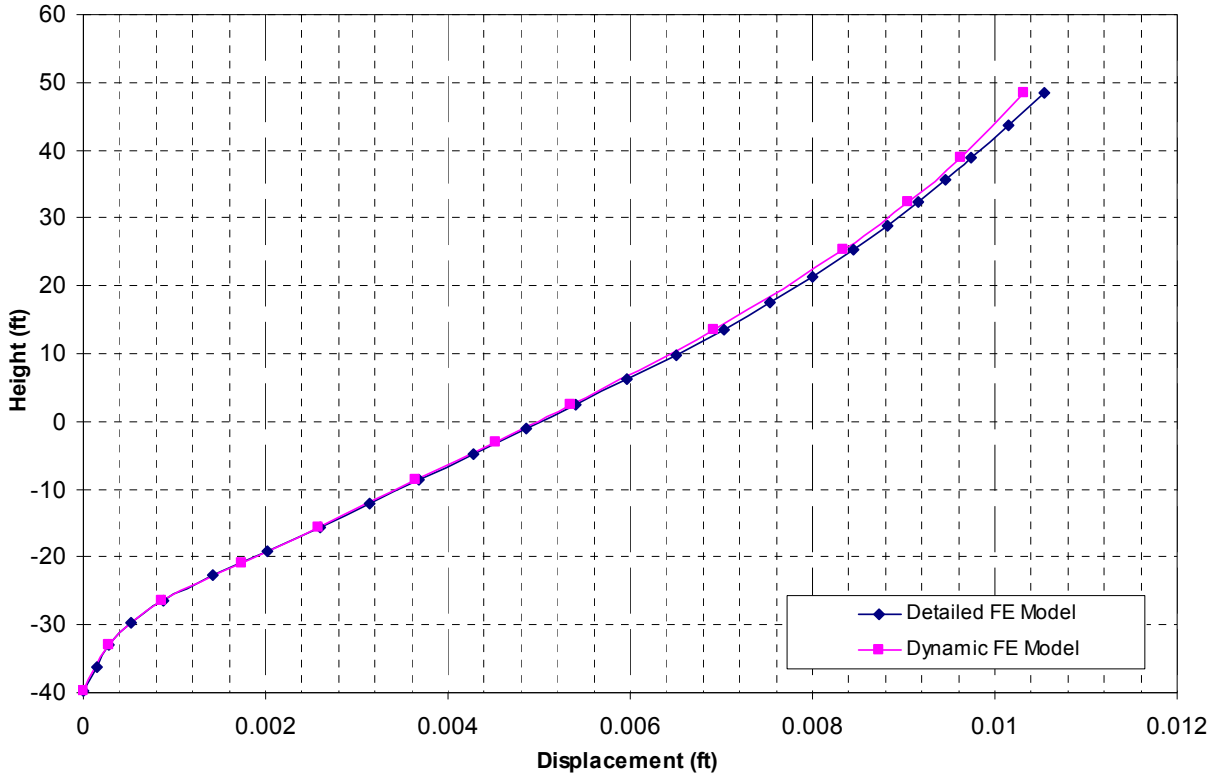

Figure 02.5.1.3.7.1-9 R/B Complex EW Direction (Y) 1g Static Analysis – Comparison Point M

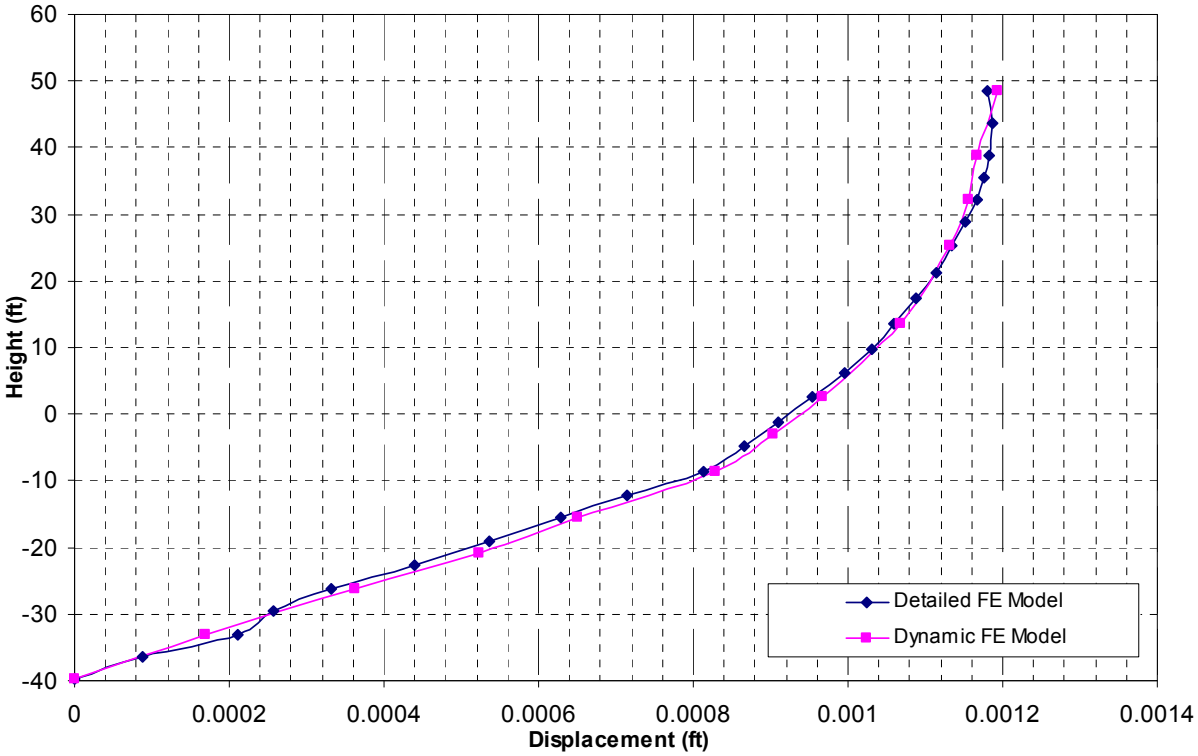

Figure 02.5.1.3.7.1-10 R/B Complex Vertical Direction (Z) 1g Static Analysis – Comparison Point M

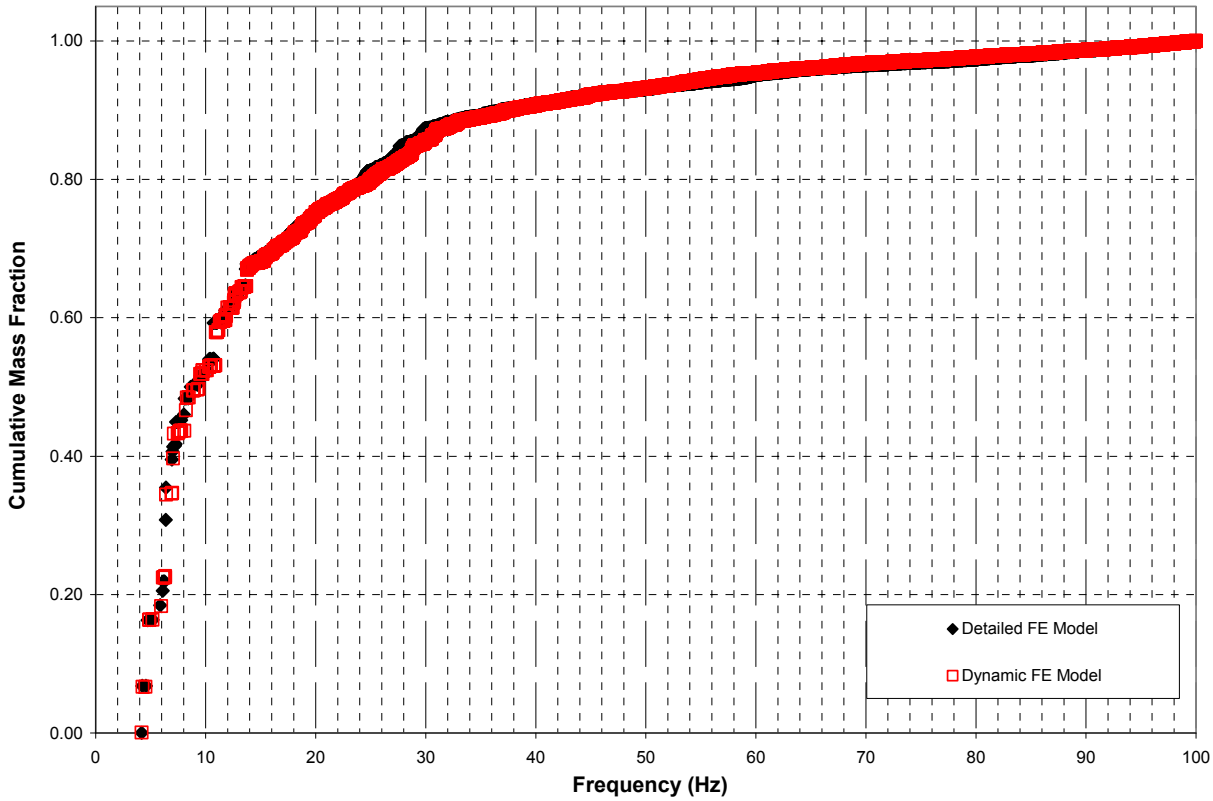

Figure 02.5.1.3.7.2-1 R/B Complex Modal Analysis – Cumulative Mass in the NS Direction (X)

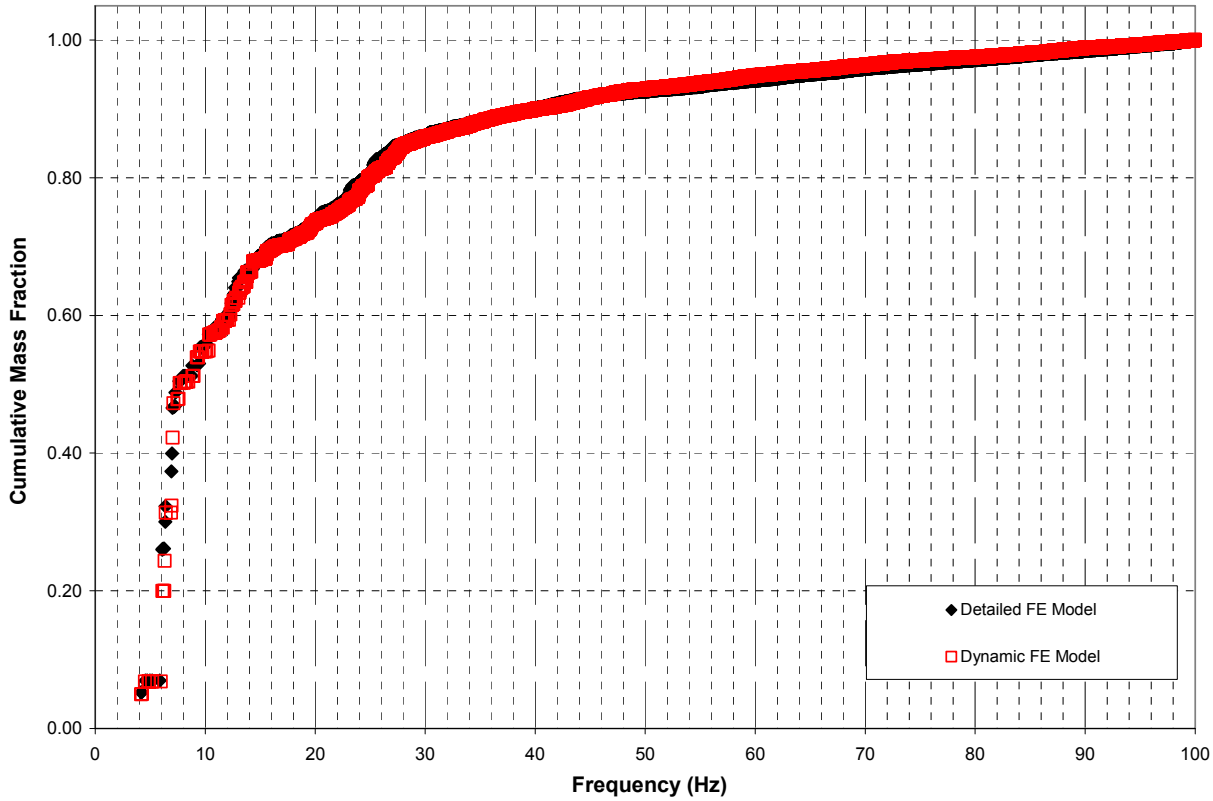

Figure 02.5.1.3.7.2-2 R/B Complex Modal Analysis – Cumulative Mass in the EW Direction (Y)

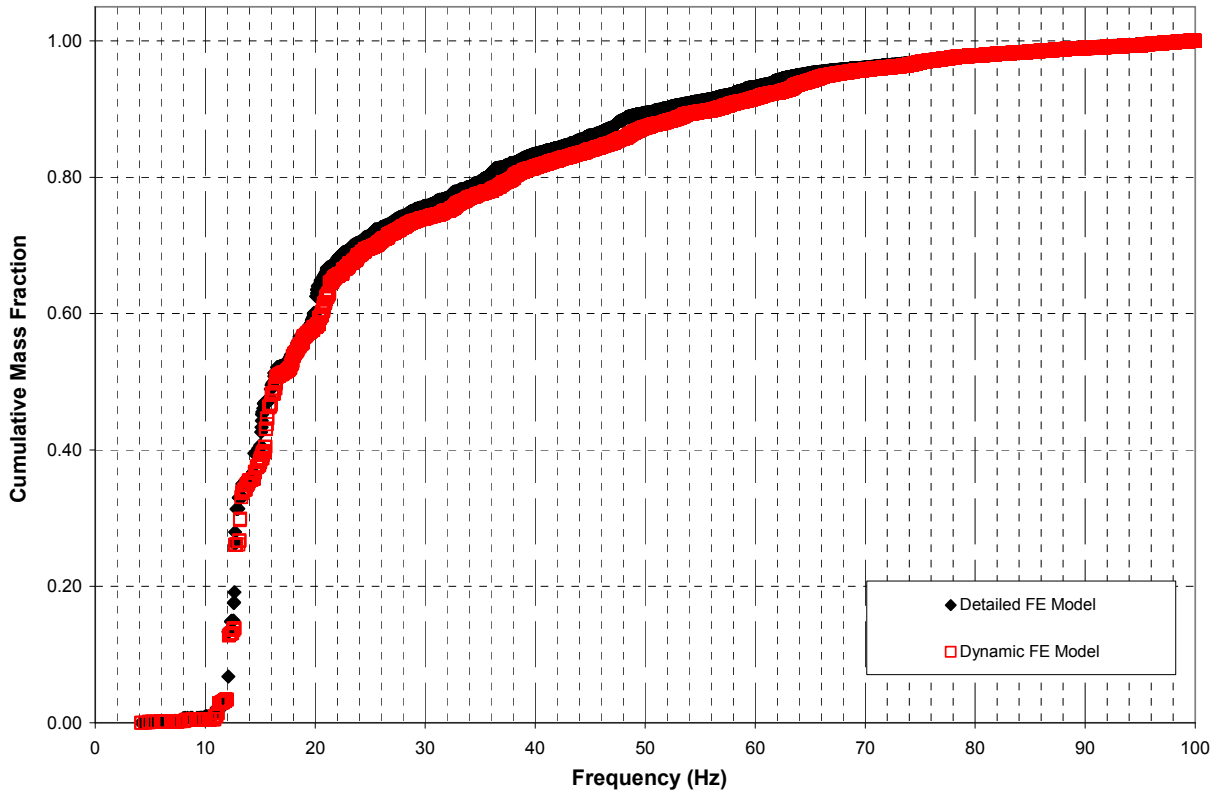

Figure 02.5.1.3.7.2-3 R/B Complex Modal Analysis – Cumulative Mass in the Vertical Direction (Z)

Figure 02.5.1.3.7.2-4 R/B Complex Detailed Mode Shape – Mode 5 at Frequency 4.22 Hz - NS Direction (X)

Figure 02.5.1.3.7.2-5 R/B Complex Dynamic Mode Shape – Mode 2 at Frequency 4.27 Hz - NS Direction (X)

Figure 02.5.1.3.7.2-6 R/B Complex Detailed Mode Shape – Mode 7 at Frequency 4.3 Hz - NS Direction (X)

Figure 02.5.1.3.7.2-7 R/B Complex Dynamic Mode Shape – Mode 4 at Frequency 4.87 Hz - NS Direction (X)

Figure 02.5.1.3.7.2-8 R/B Complex Detailed Mode Shape – Mode 15 at Frequency 6.39 Hz - NS Direction (X)

Figure 02.5.1.3.7.2-9 R/B Complex Dynamic Mode Shape – Mode 12 at Frequency 6.41 Hz - NS Direction (X)

Figure 02.5.1.3.7.2-10 R/B Complex Detailed Mode Shape – Mode 52 at Frequency 10.73 Hz - NS Direction (X)

Figure 02.5.1.3.7.2-11 R/B Complex Dynamic Mode Shape – Mode 44 at Frequency 10.93 Hz - NS Direction (X)

Figure 02.5.1.3.7.2-12 R/B Complex Detailed Mode Shape – Mode 4 at Frequency 4.18 Hz - EW Direction (Y)

Figure 02.5.1.3.7.2-13 R/B Complex Dynamic Mode Shape – Mode 1 at Frequency 4.18 Hz - EW Direction (Y)

Figure 02.5.1.3.7.2-14 R/B Complex Detailed Mode Shape – Mode 12 at Frequency 6.12 Hz - EW Direction (Y)

Figure 02.5.1.3.7.2-15 R/B Complex Dynamic Mode Shape – Mode 8 at Frequency 6.12 Hz - EW Direction (Y)

Figure 02.5.1.3.7.2-16 R/B Complex Detailed Mode Shape – Mode 15 at Frequency 6.39 Hz - EW Direction (Y)

Figure 02.5.1.3.7.2-17 R/B Complex Dynamic Mode Shape – Mode 12 at Frequency 6.41 Hz - EW Direction (Y)

Figure 02.5.1.3.7.2-18 R/B Complex Detailed Mode Shape – Mode 17 at Frequency 6.92 Hz - EW Direction (Y)

Figure 02.5.1.3.7.2-19 R/B Complex Dynamic Mode Shape – Mode 15 at Frequency 7.04 Hz - EW Direction (Y)

Figure 02.5.1.3.7.2-20 R/B Complex Detailed Mode Shape – Mode 19 at Frequency 7.03 Hz - EW Direction (Y)

Figure 02.5.1.3.7.2-21 R/B Complex Dynamic Mode Shape – Mode 16 at Frequency 7.12 Hz - EW Direction (Y)

Figure 02.5.1.3.7.2-22 R/B Complex Detailed Mode Shape – Mode 71 at Frequency 12.10 Hz - Vertical Direction (Z)

Figure 02.5.1.3.7.2-23 R/B Complex Dynamic Mode Shape – Mode 62 at Frequency 12.15 Hz - Vertical Direction (Z)

Figure 02.5.1.3.7.2-24 R/B Complex Detailed Mode Shape – Mode 79 at Frequency 12.68 Hz - Vertical Direction (Z)

Figure 02.5.1.3.7.2-25 R/B Complex Dynamic Mode Shape – Mode 70 at Frequency 12.74 Hz - Vertical Direction (Z)

Figure 02.5.1.3.7.2-26 R/B Complex Detailed Mode Shape – Mode 80 at Frequency 12.70 Hz - Vertical Direction (Z)

Figure 02.5.1.3.7.2-27 R/B Complex Dynamic Mode Shape – Mode 76 at Frequency 13.16 Hz - Vertical Direction (Z)

Figure 02.5.1.3.7.2-28 R/B Complex Detailed Mode Shape – Mode 83 at Frequency 12.85 Hz - Vertical Direction (Z)

Figure 02.5.1.3.7.2-29 R/B Complex Dynamic Mode Shape – Mode 78 at Frequency 13.28 Hz - Vertical Direction (Z)

Figure 02.5.1.3.7.2-30 R/B Complex Detailed Mode Shape – Mode 87 at Frequency 13.05 Hz - Vertical Direction (Z)

Figure 02.5.1.4-1 Integrated R/B Complex Dynamic FE Model (ANSYS)

Figure 02.5.1.4-2 Section View of R/B Complex Dynamic FE Model Looking East (Column Line 13R)

Figure 02.5.1.4-3 Section View of R/B Complex Dynamic FE Model Looking East (Column Line 4R)

Figure 02.5.1.4-4 Section View of R/B Complex Dynamic FE Model Looking North (Column Line FR)

Figure 02.5.1.4-5 Section View of R/B Complex Dynamic FE Model Looking North (Column Line K2R)

Figure 02.5.1.4-6 Integrated R/B Complex Dynamic FE Model (SASSI)

Figure 02.5.1.5-1 Integrated R/B Complex Dynamic FE Model – ATF Locations

Figure 02.5.1.5-2 Nodes on PCCV

Figure 02.5.1.5-3 Nodes on the Floor of the CIS

Figure 02.5.1.5.1-1 R/B-FH/A – NS Direction (X) – First Dominant Mode

Figure 02.5.1.5.1-2 R/B-FH/A – EW Direction (Y) – First Dominant Mode

Figure 02.5.1.5.1-3 R/B-FH/A – Vertical Direction (Z) – First Dominant Mode

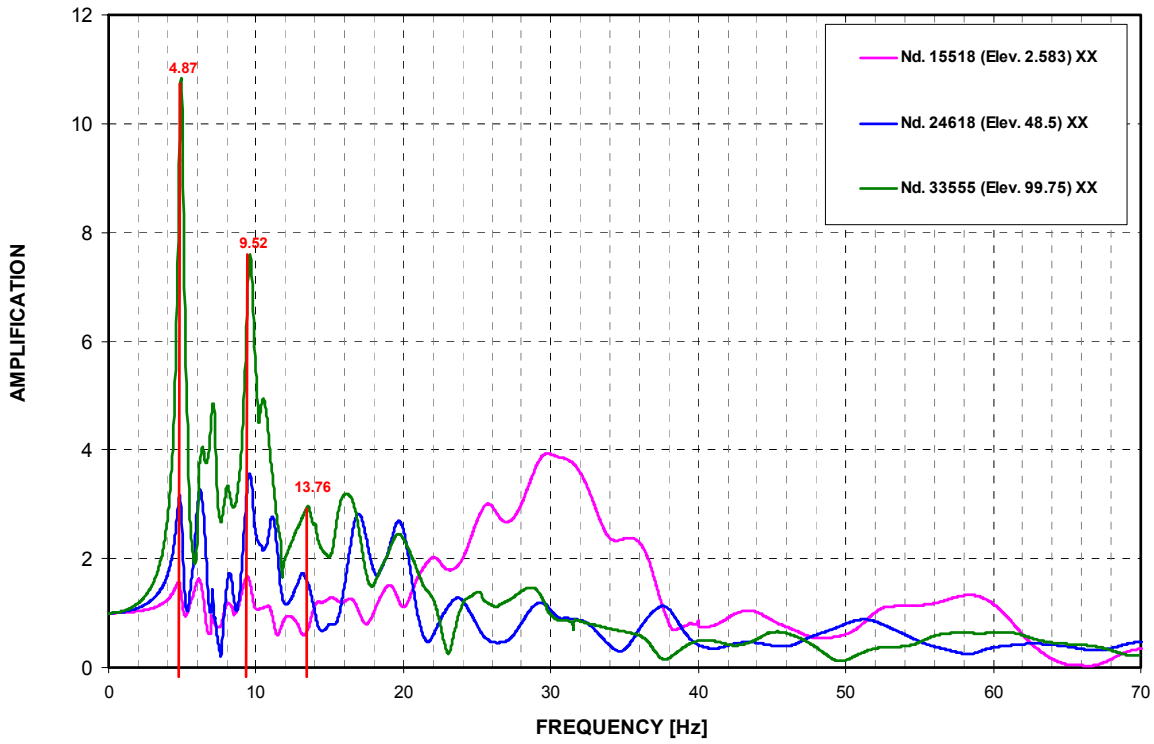

Figure 02.5.1.5.1-4 R/B-FH/A ATF Results – NS Direction (X) Transfer Function at NE Corner

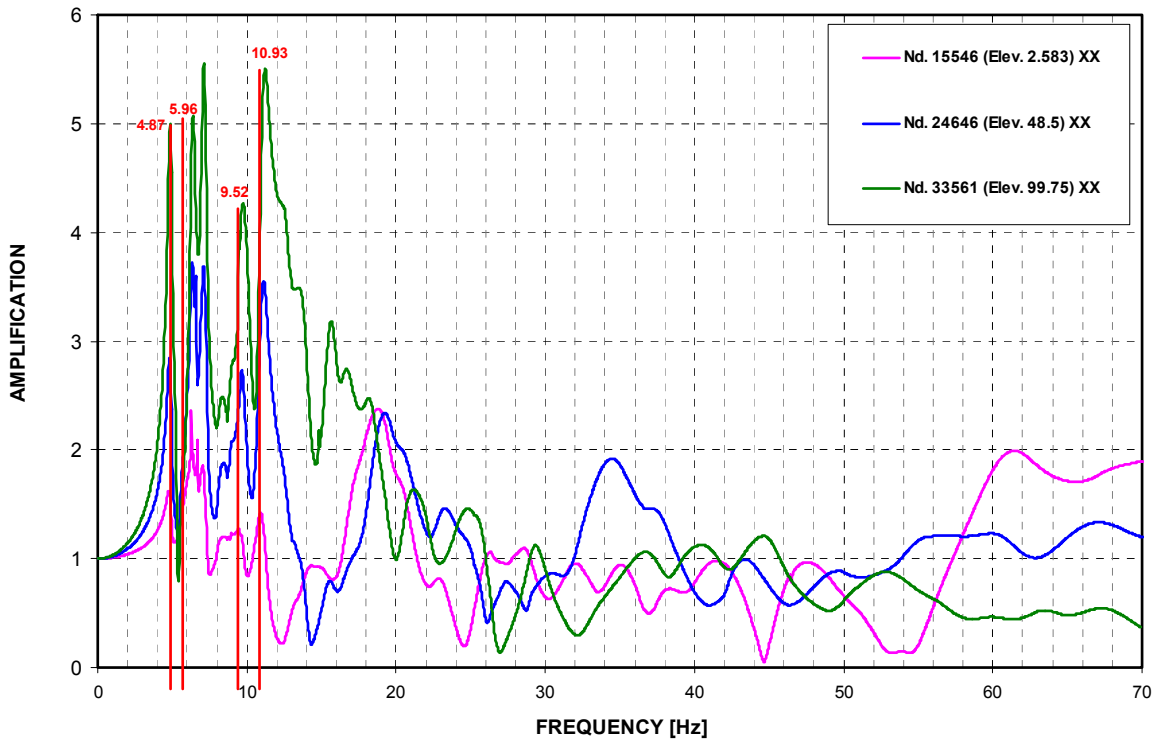

Figure 02.5.1.5.1-5 R/B-FH/A ATF Results – NS Direction (X) Transfer Function at NW Corner

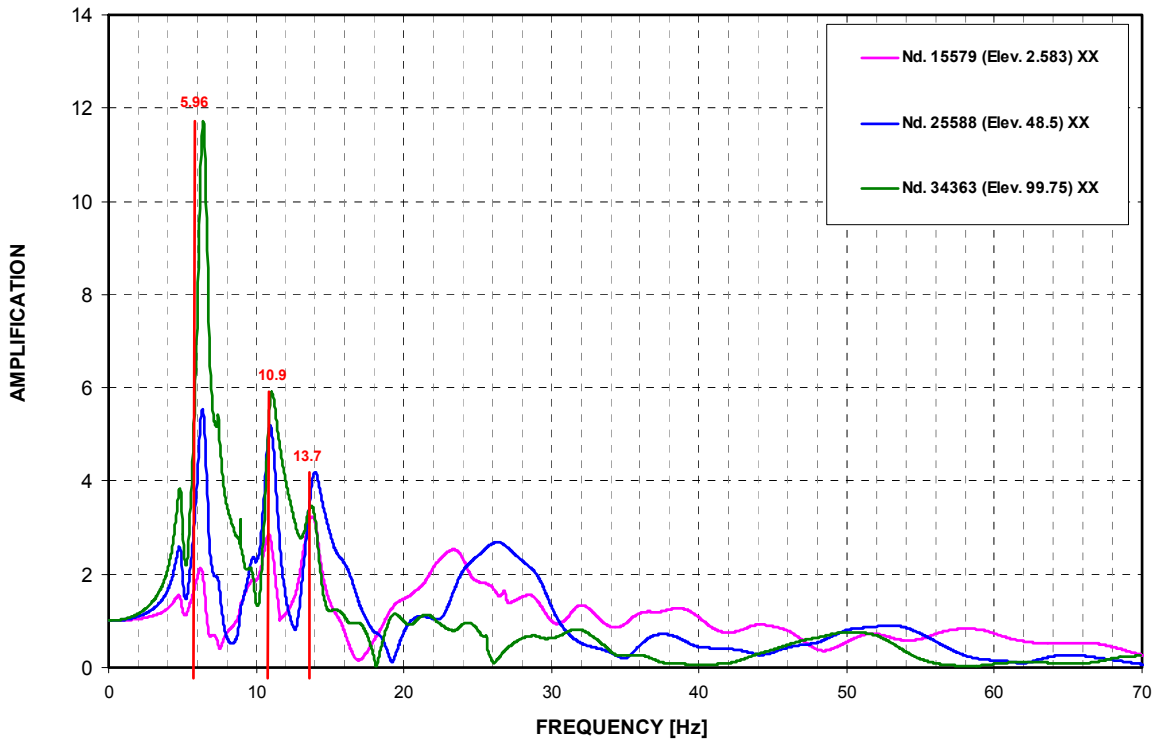

Figure 02.5.1.5.1-6 R/B-FH/A ATF Results – NS Direction (X) Transfer Function at SE Corner

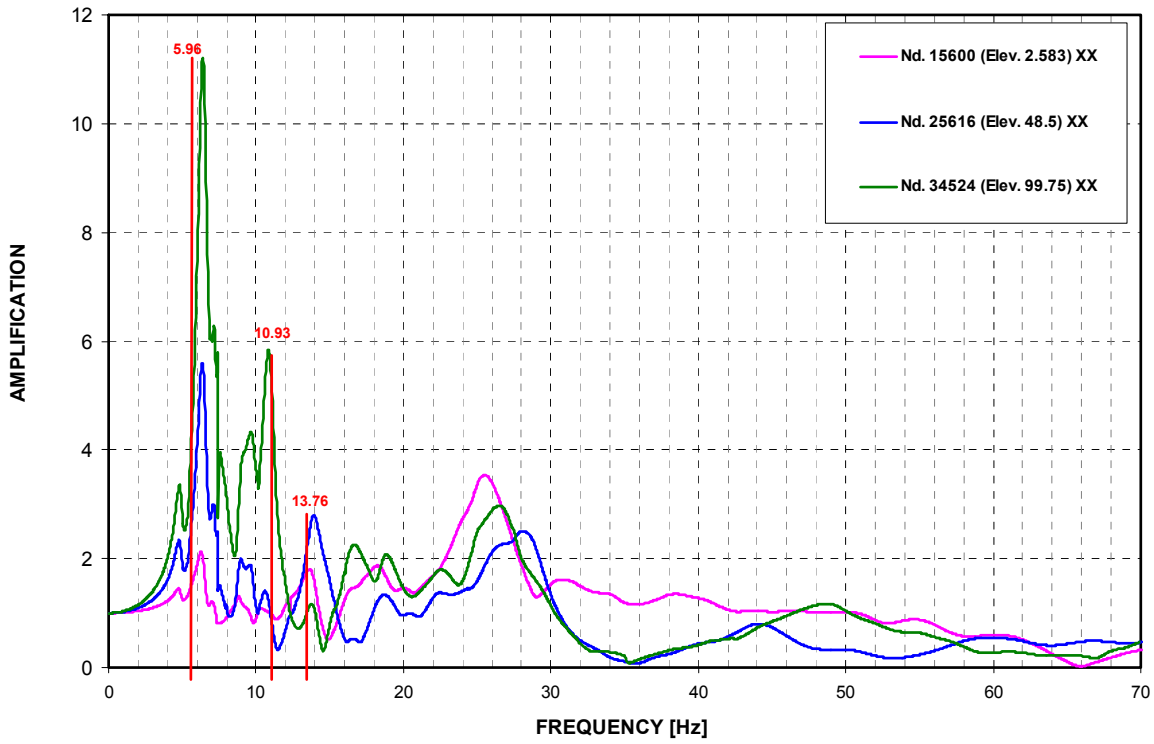

Figure 02.5.1.5.1-7 R/B-FH/A ATF Results – NS Direction (X) Transfer Function at SW Corner

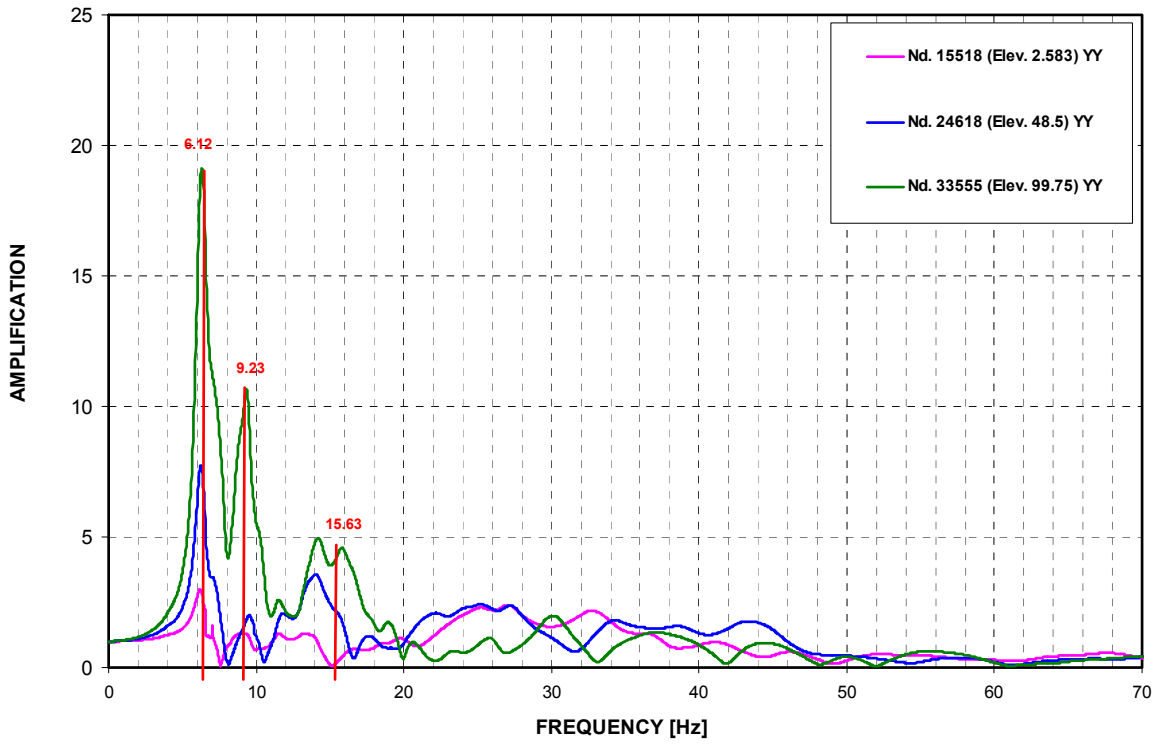

Figure 02.5.1.5.1-8 R/B-FH/A ATF Results – EW Direction (Y) Transfer Function at NE Corner

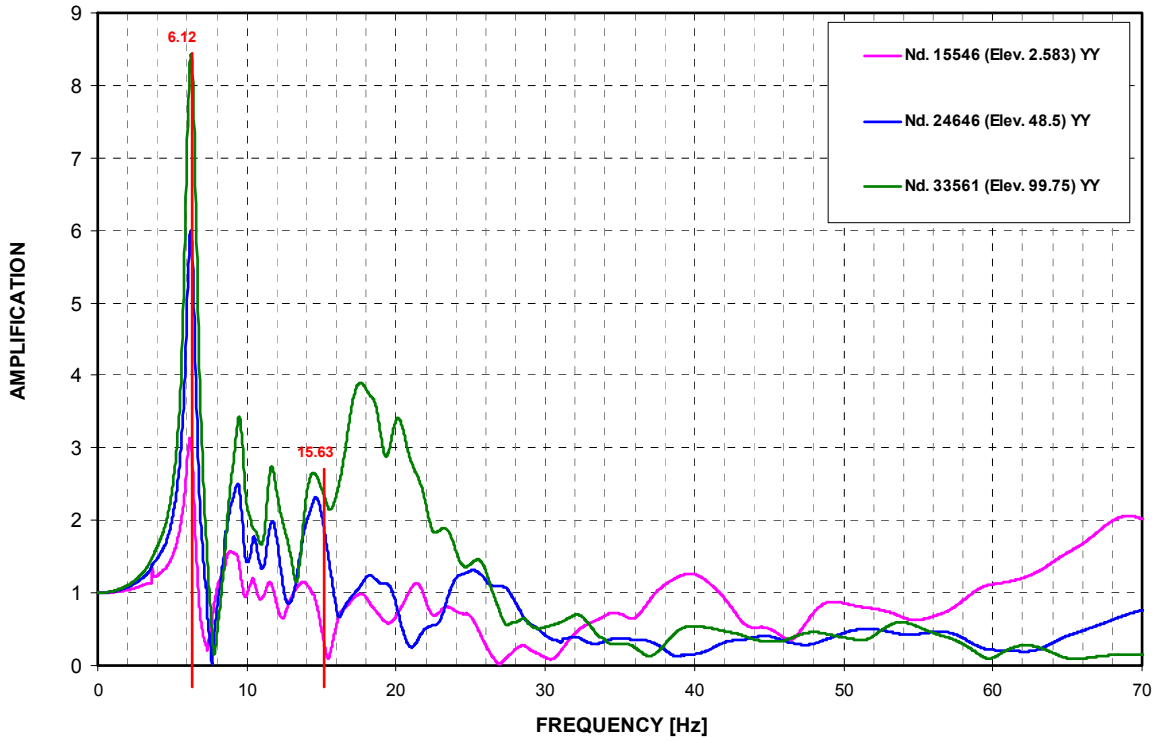

Figure 02.5.1.5.1-9 R/B-FH/A ATF Results – EW Direction (Y) Transfer Function at NW Corner

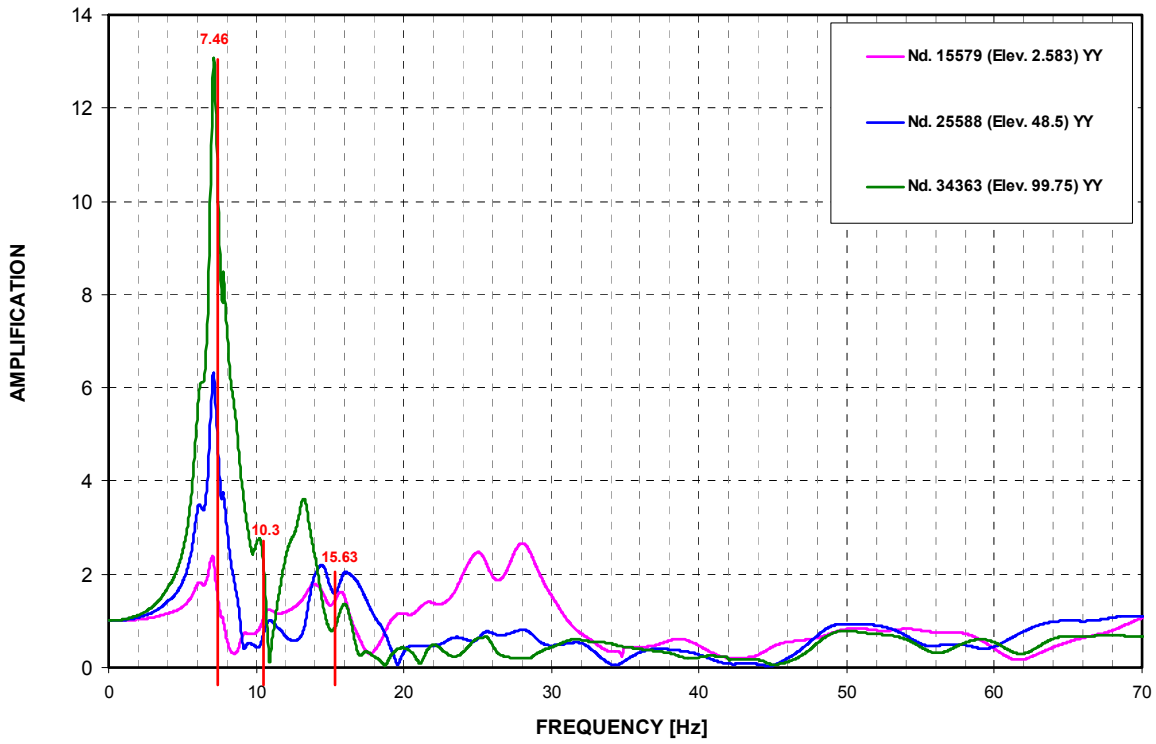

Figure 02.5.1.5.1-10 R/B-FH/A ATF Results – EW Direction (Y) Transfer Function at SE Corner

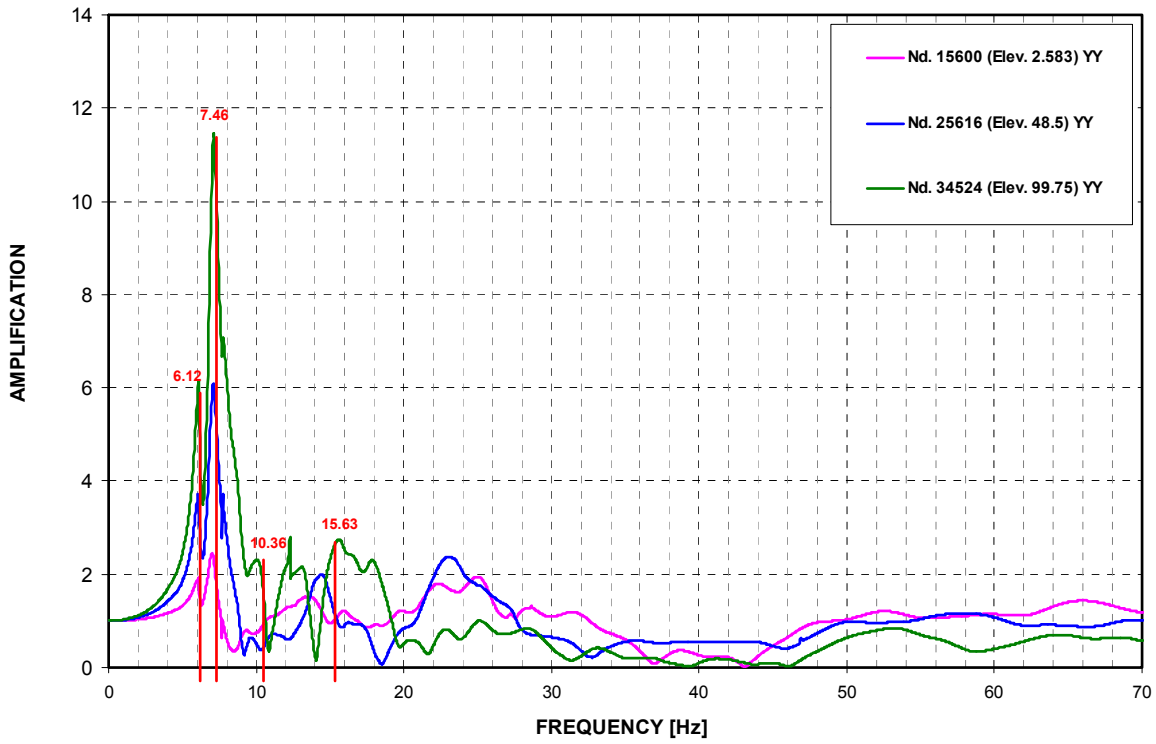

Figure 02.5.1.5.1-11 R/B-FH/A ATF Results – EW Direction (Y) Transfer Function at SW Corner

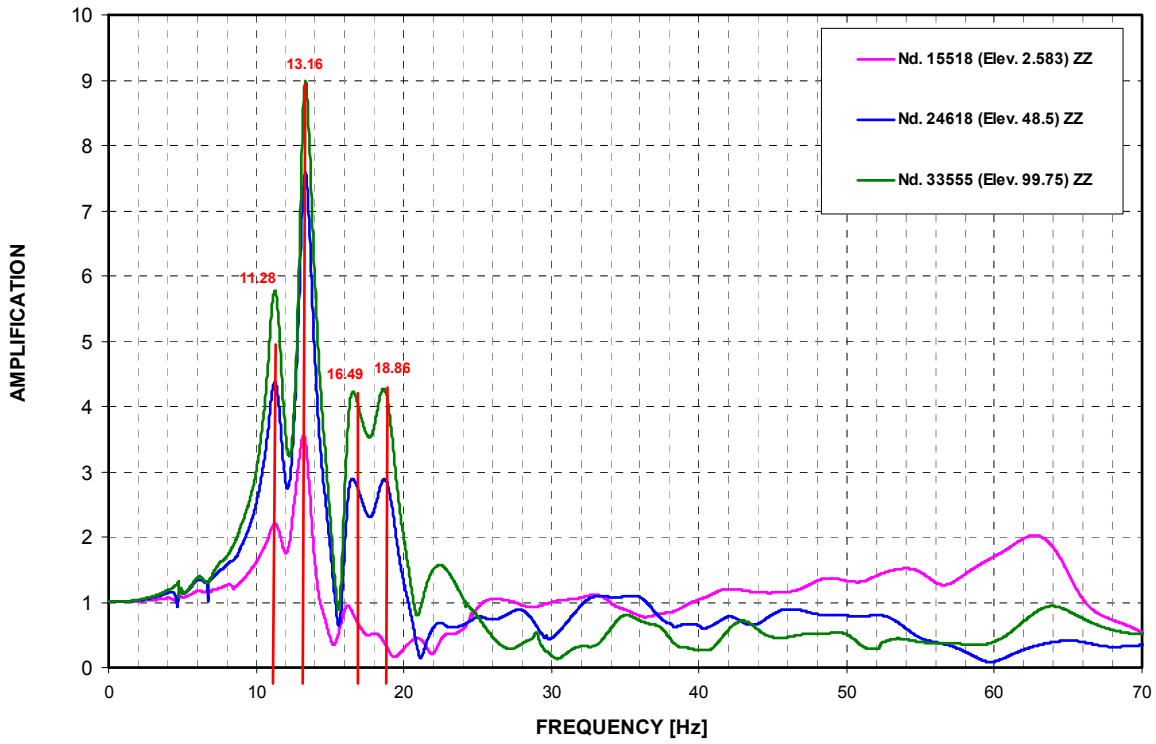

Figure 02.5.1.5.1-12 R/B-FH/A ATF Results – Vertical Direction (Z) Transfer Function at NE Corner

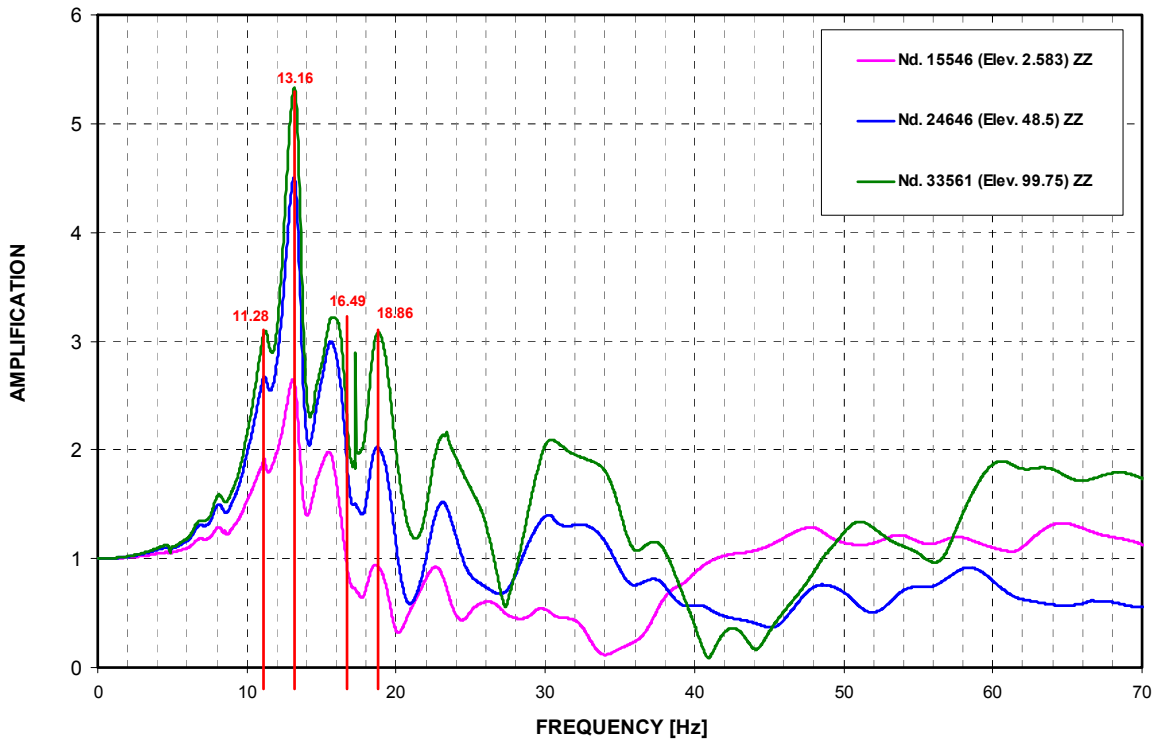

Figure 02.5.1.5.1-13 R/B-FH/A ATF Results – Vertical Direction (Z) Transfer Function at NW Corner

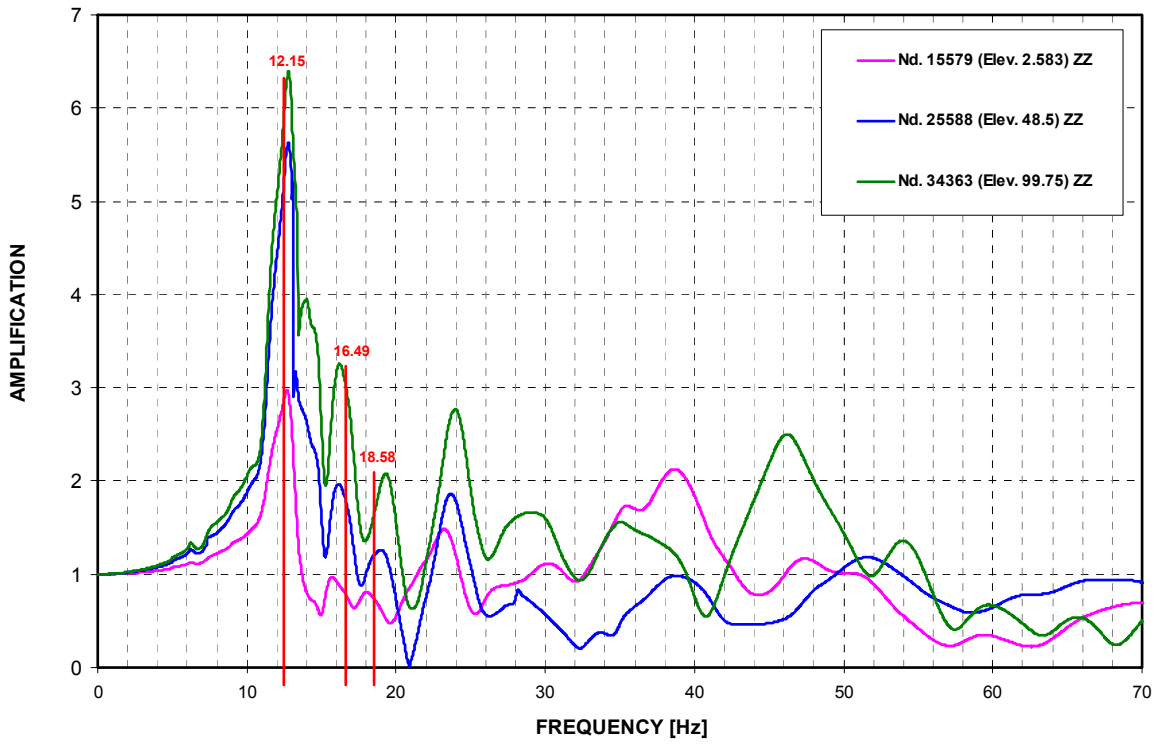

Figure 02.5.1.5.1-14 R/B-FH/A ATF Results – Vertical Direction (Z) Transfer Function at SE Corner

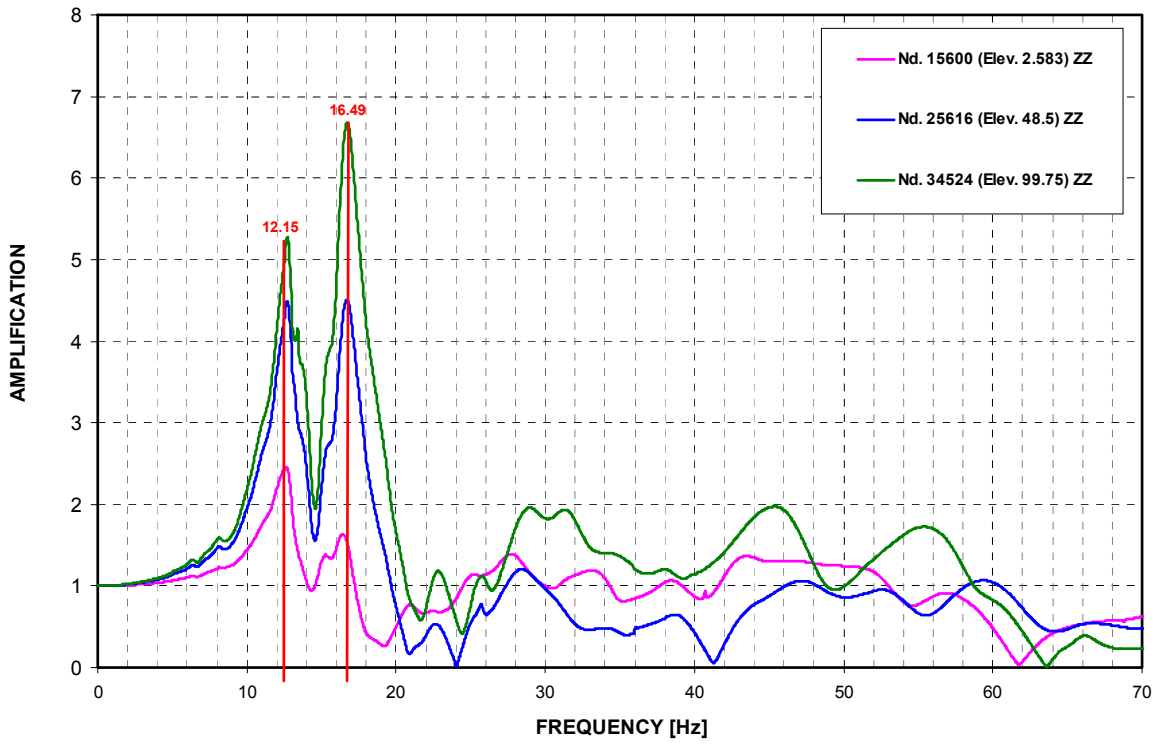

Figure 02.5.1.5.1-15 R/B-FH/A ATF Results – Vertical Direction (Z) Transfer Function at SW Corner

Figure 02.5.1.5.2-1 PCCV – NS Direction (X) – First Dominant Mode

Figure 02.5.1.5.2-2 PCCV – EW Direction (Y) – First Dominant Mode

Figure 02.5.1.5.2-3 PCCV – Vertical Direction (Z) – First Dominant Mode

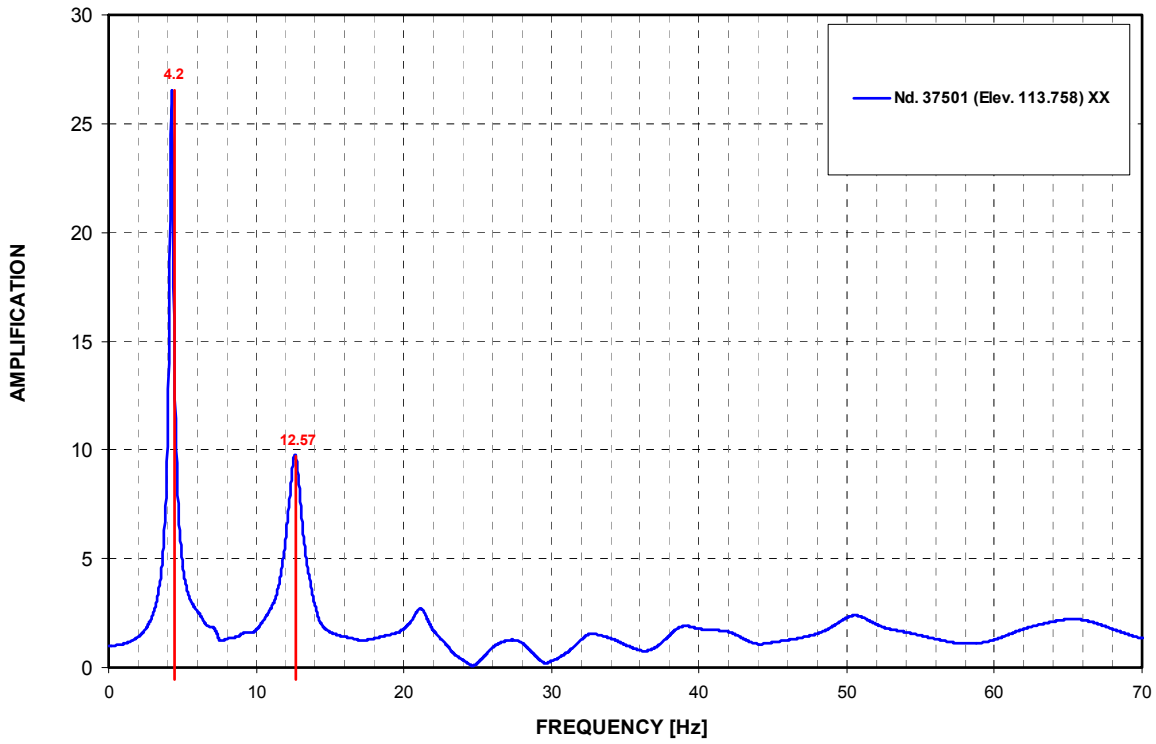

Figure 02.5.1.5.2-4 PCCV ATF Results – NS Direction (X) Transfer Function at Top of Dome

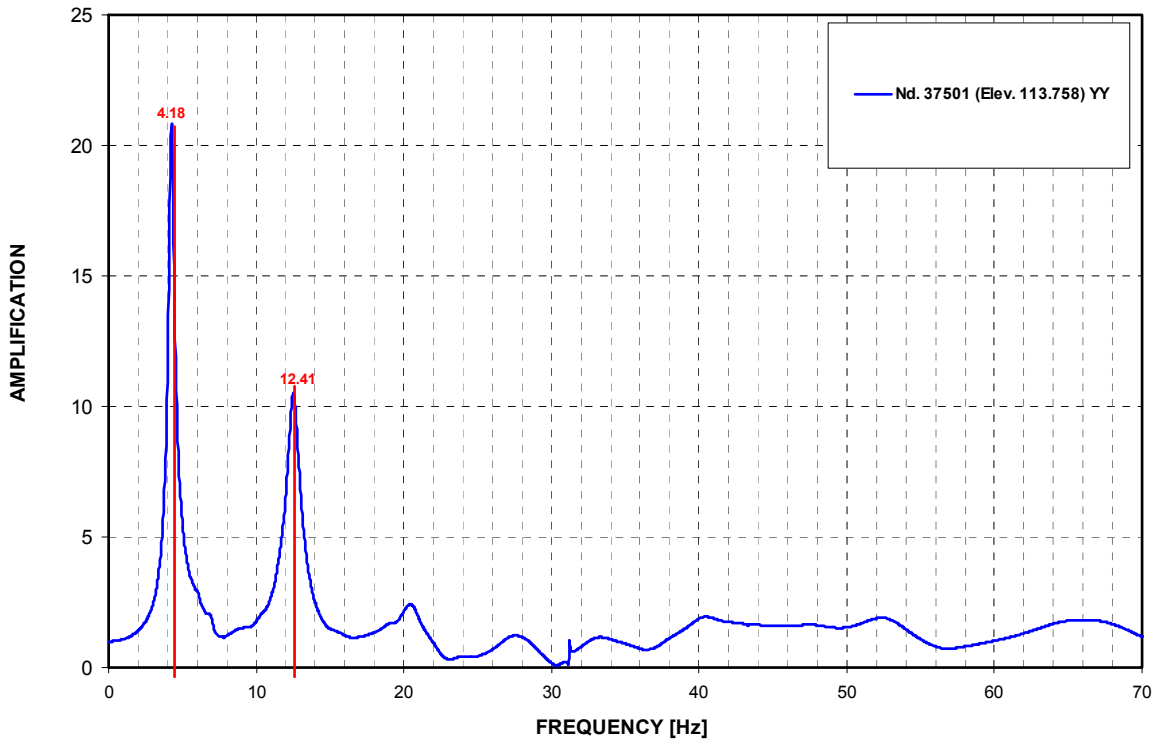

Figure 02.5.1.5.2-5 PCCV ATF Results – EW Direction (Y) Transfer Function at Top of Dome

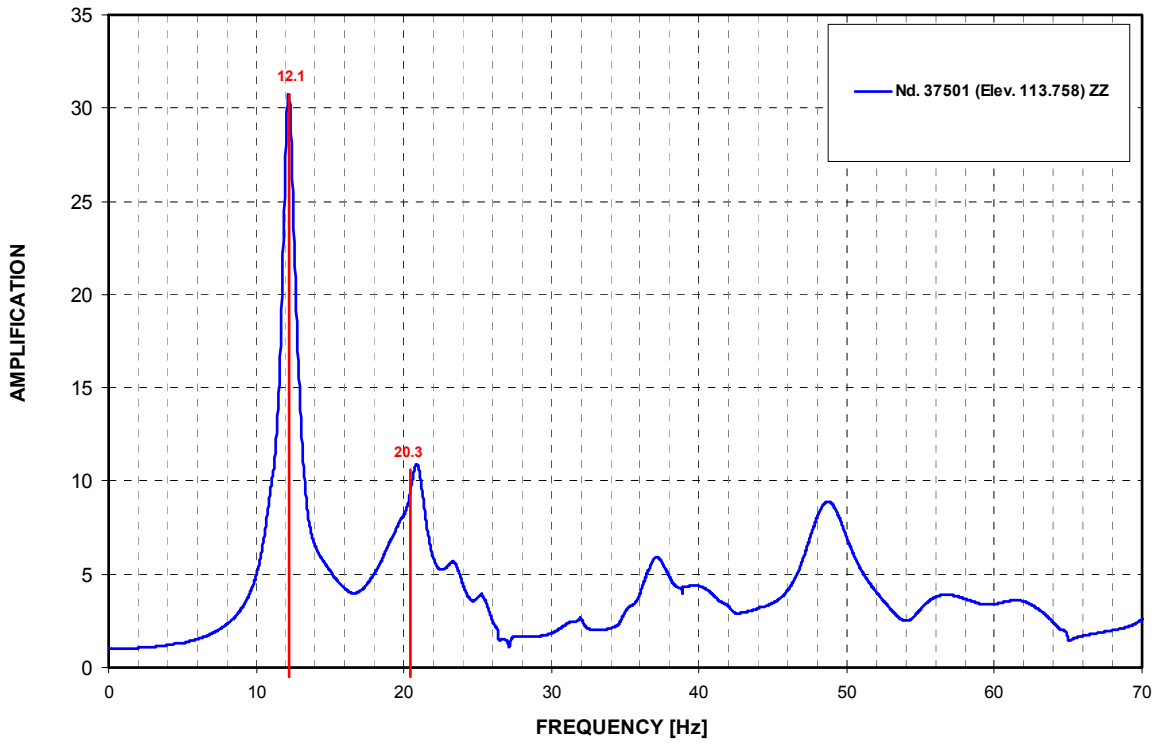

Figure 02.5.1.5.2-6 PCCV ATF Results – Vertical Direction (Z) Transfer Function at Top of Dome

Figure 02.5.1.5.3-1 CIS – NS Direction (X) – First Dominant Mode

Figure 02.5.1.5.3-2 CIS – EW Direction (Y) – First Dominant Mode

Figure 02.5.1.5.3-3 CIS – Vertical Direction (Z) – First Dominant Mode

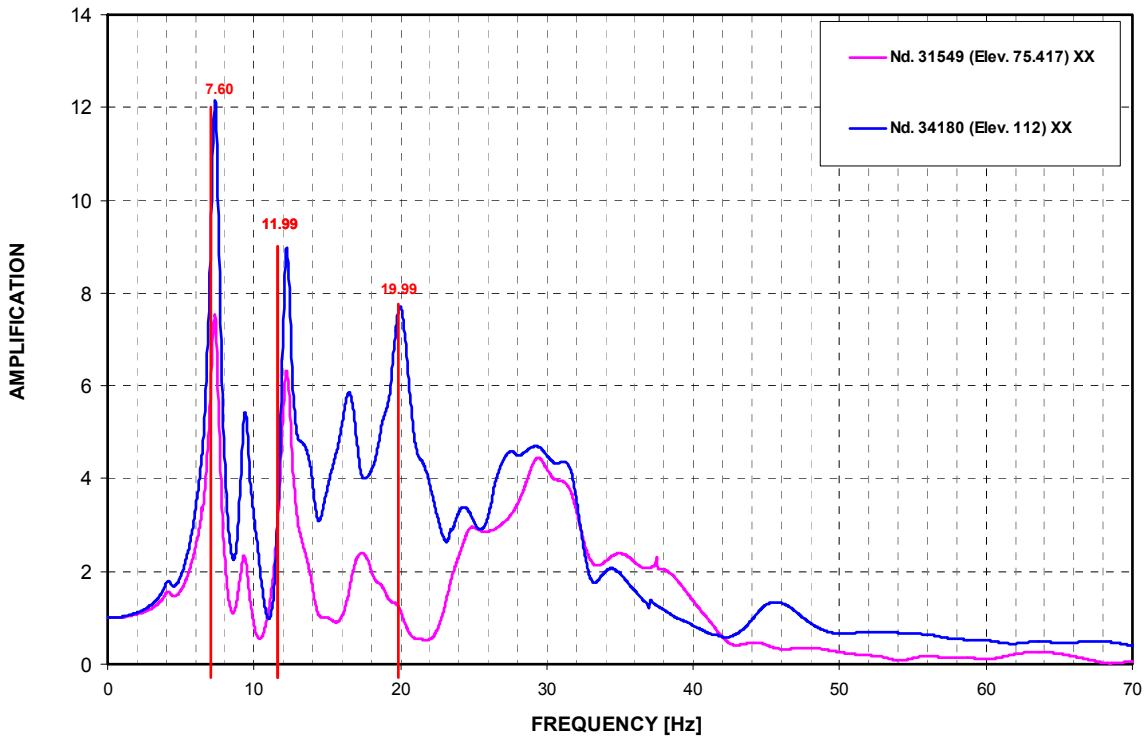

Figure 02.5.1.5.3-4 CIS SG Compartment ATF Results – NS Direction (X) Transfer Function

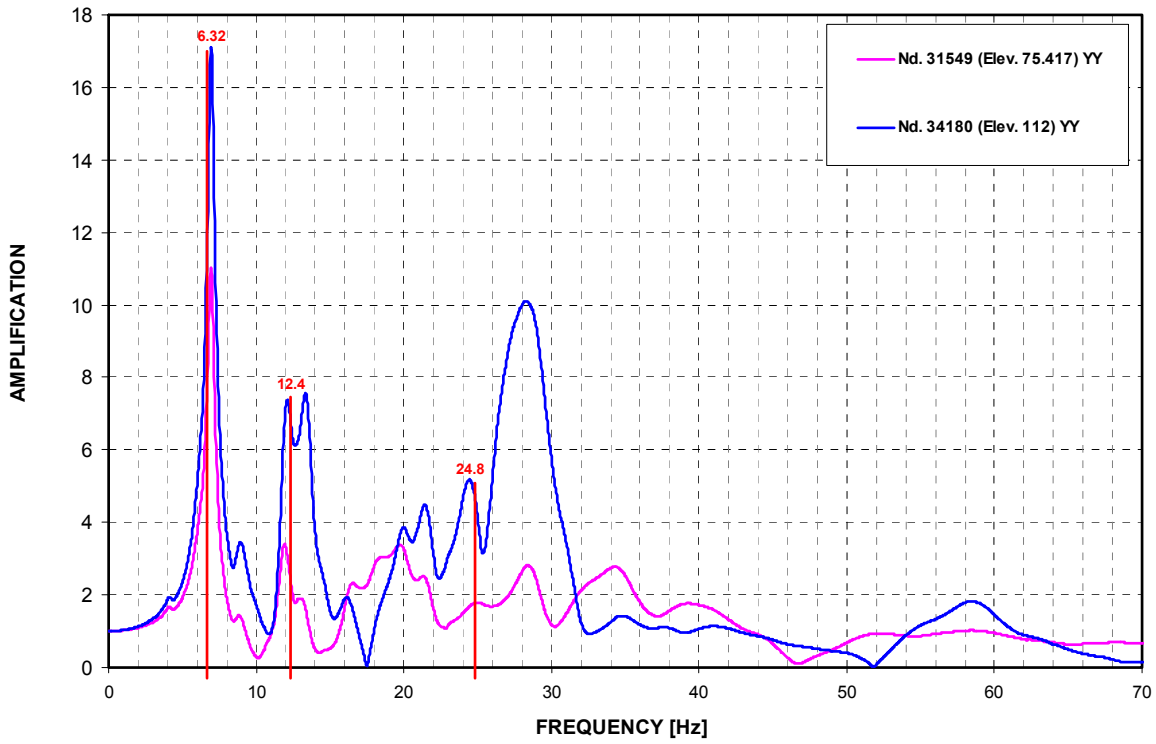

Figure 02.5.1.5.3-5 CIS SG Compartment ATF Results – EW Direction (Y) Transfer Function

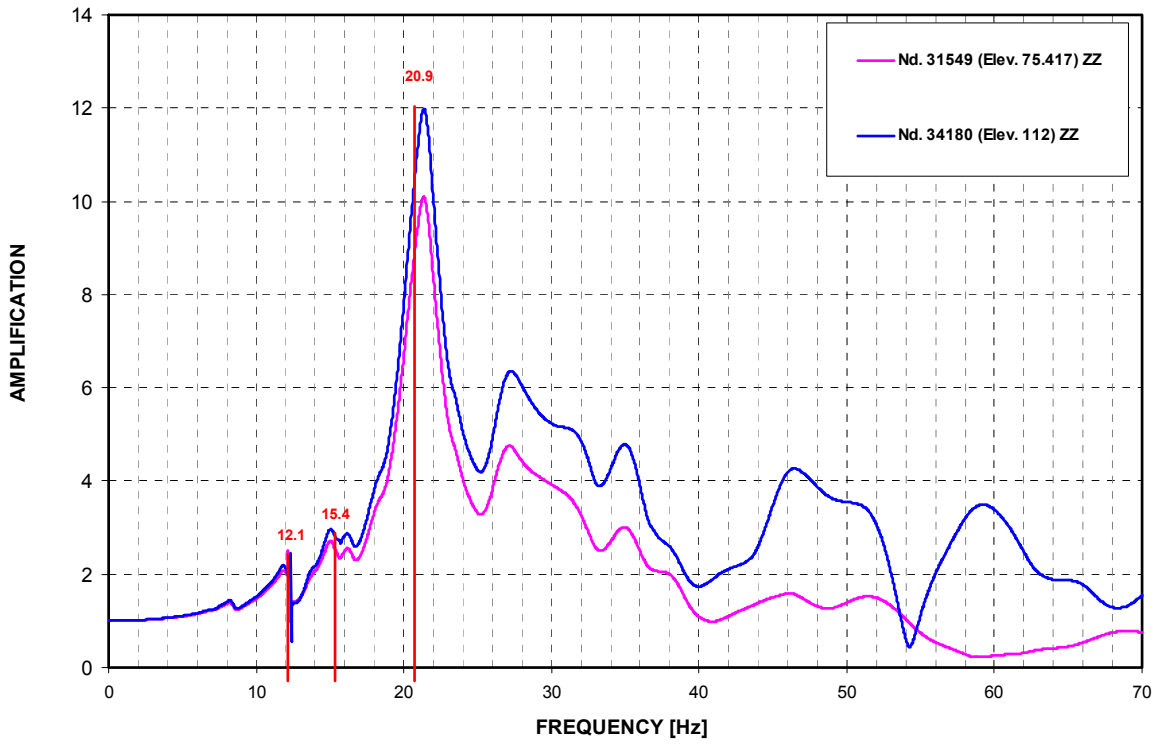

Figure 02.5.1.5.3-6 CIS SG Compartment ATF Results – Vertical Direction (Z) Transfer Function

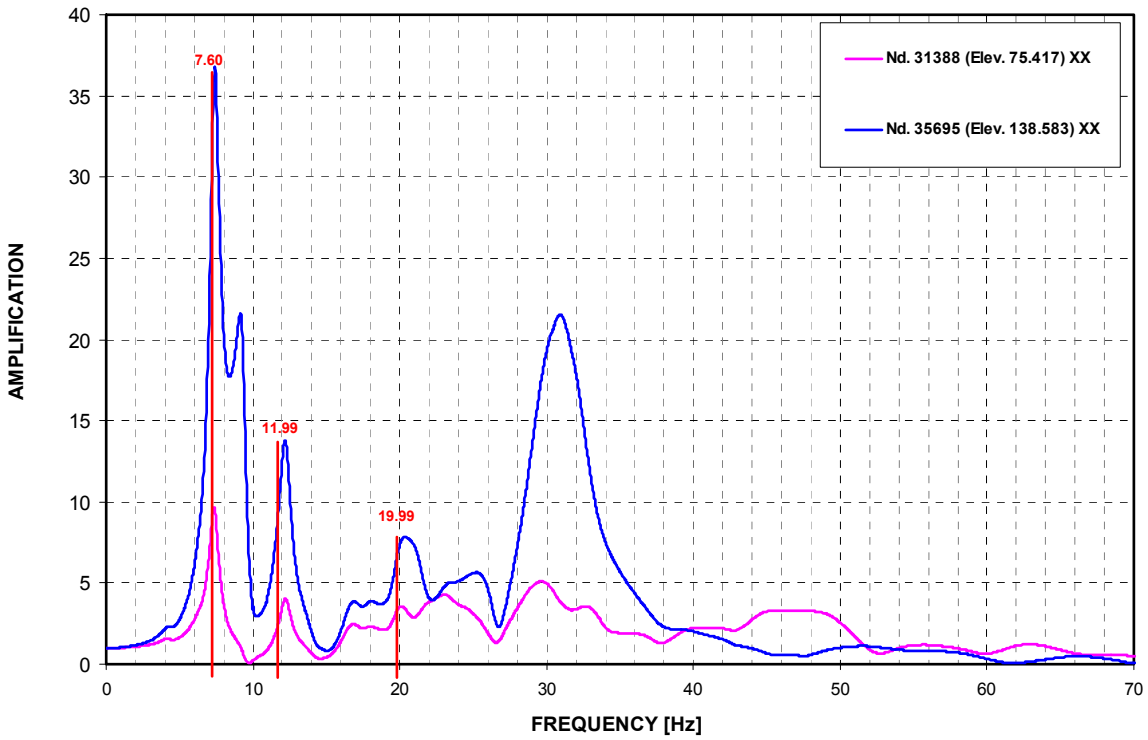

Figure 02.5.1.5.3-7 CIS PZR Compartment ATF Results – NS Direction (X) Transfer Function

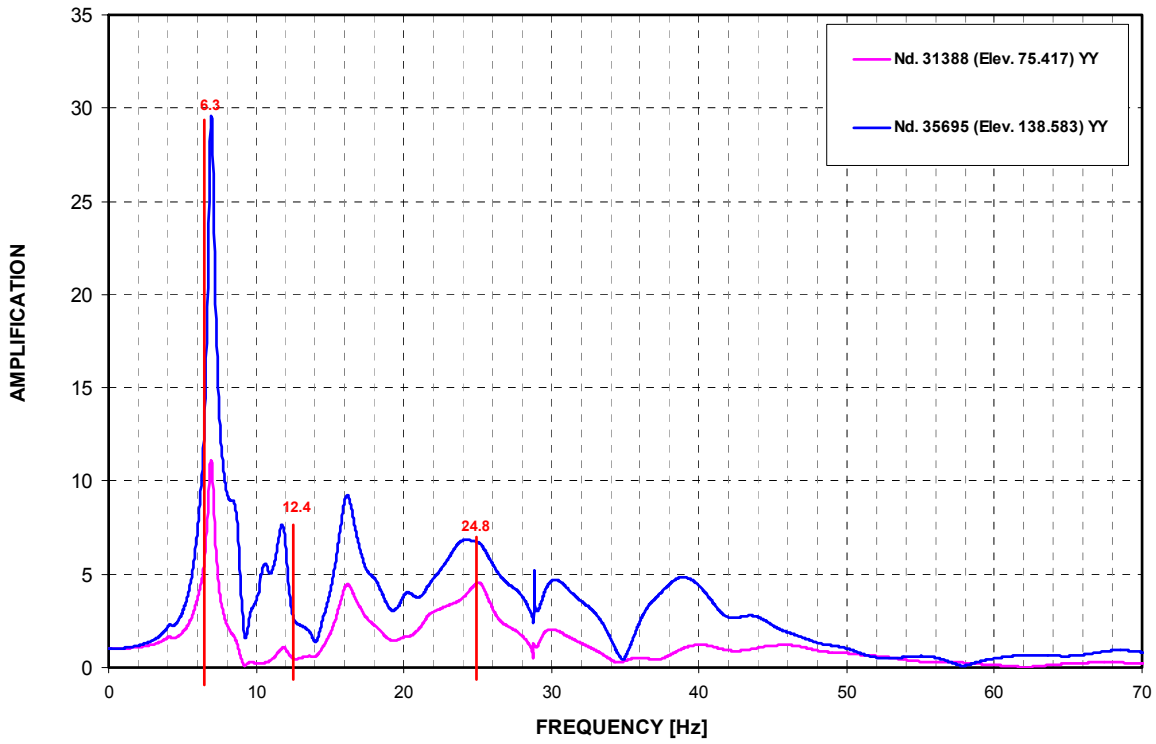

Figure 02.5.1.5.3-8 CIS PZR Compartment ATF Results – EW Direction (Y) Transfer Function

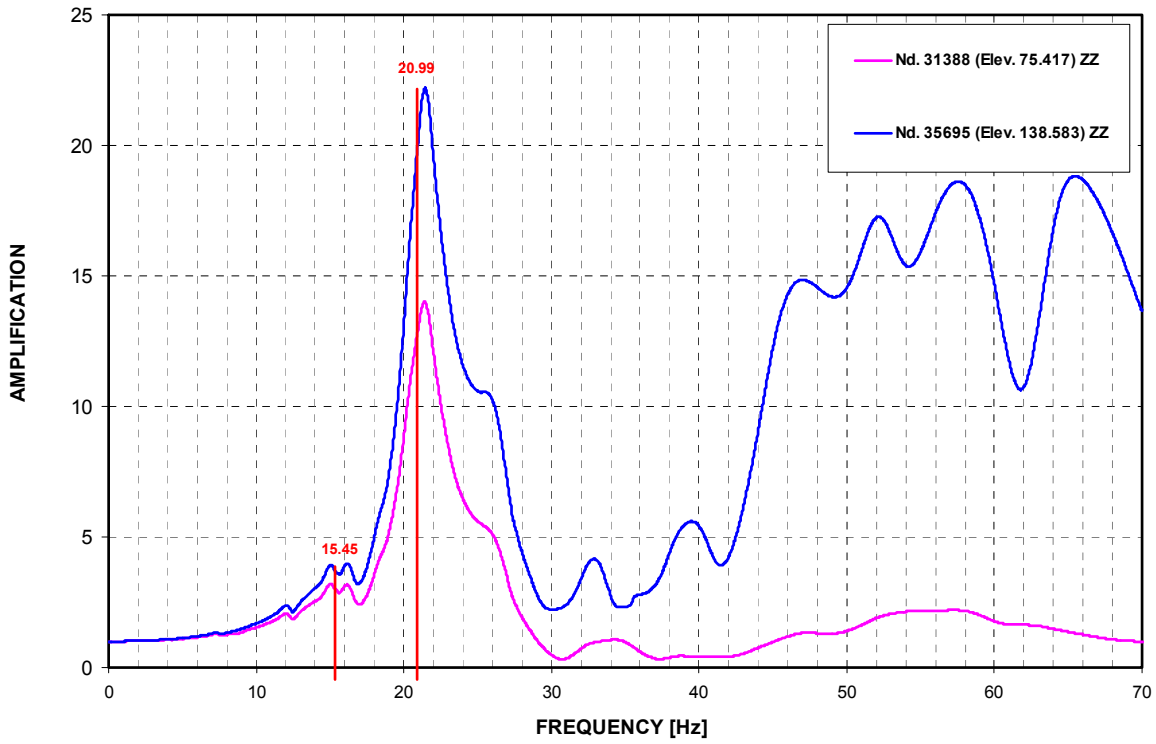

Figure 02.5.1.5.3-9 CIS PZR Compartment ATF Results – Vertical Direction (Z) Transfer Function

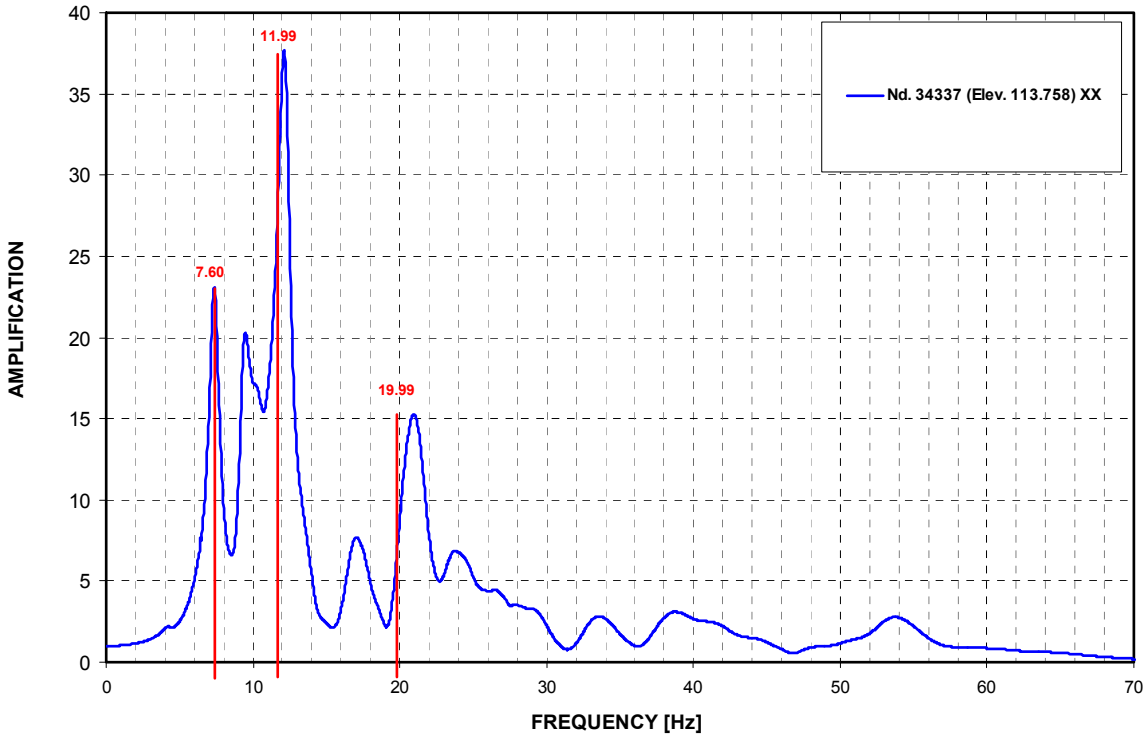

Figure 02.5.1.5.3-10 CIS D-SG ATF Results – NS Direction (X) Transfer Function

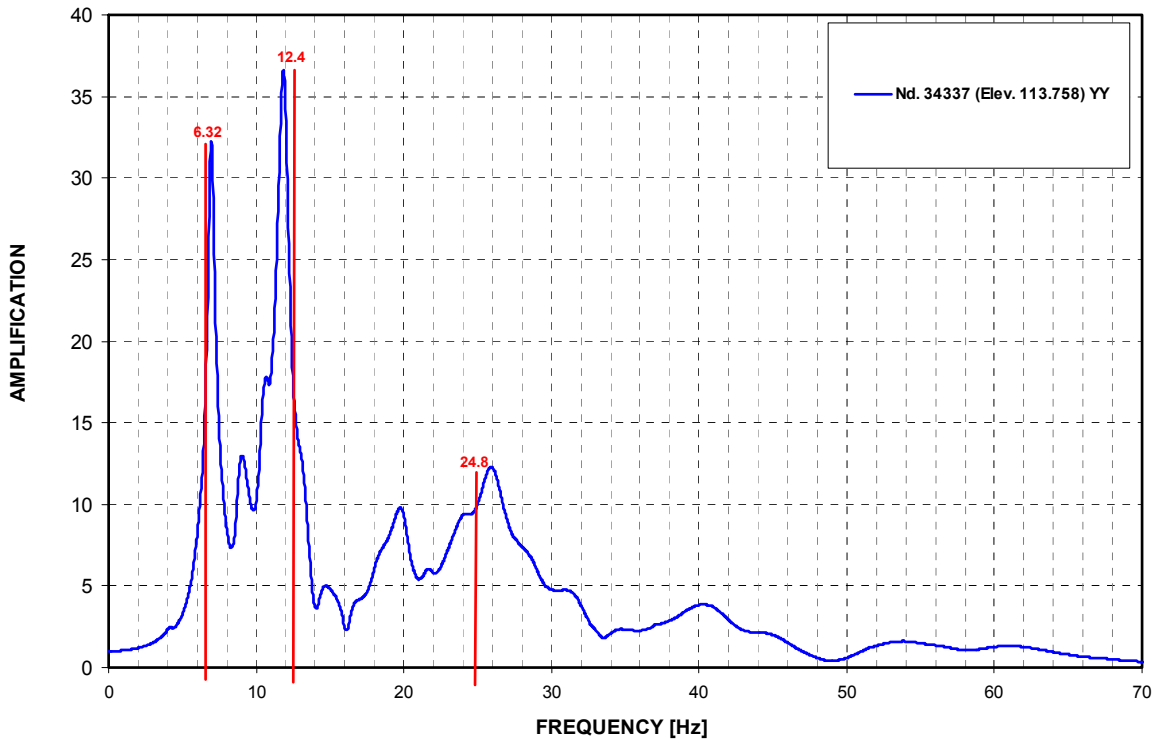

Figure 02.5.1.5.3-11 CIS D-SG ATF Results – EW Direction (Y) Transfer Function

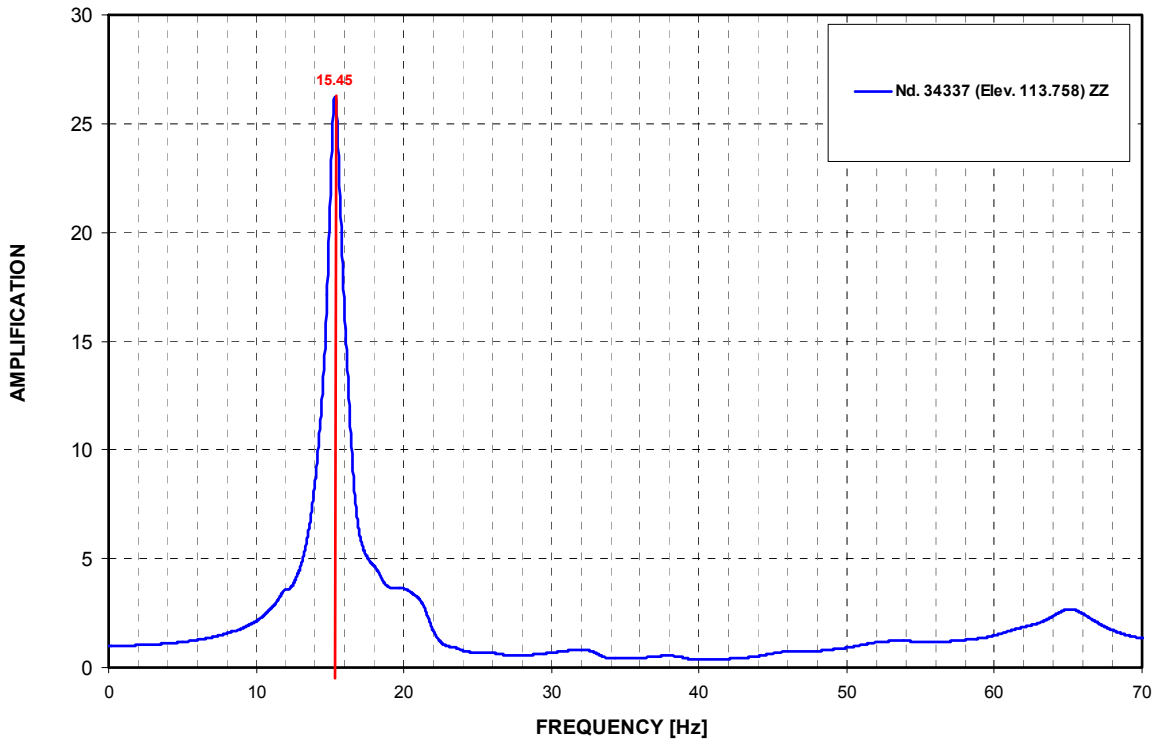

Figure 02.5.1.5.3-12 CIS D-SG ATF Results – Vertical Direction (Z) Transfer Function

Figure 02.5.1.5.4-1 East PS/B – NS Direction (X) – First Dominant Mode

Figure 02.5.1.5.4-2 East PS/B – EW Direction (Y) – First Dominant Mode

Figure 02.5.1.5.4-3 East PS/B – Vertical Direction (Z) – First Dominant Mode

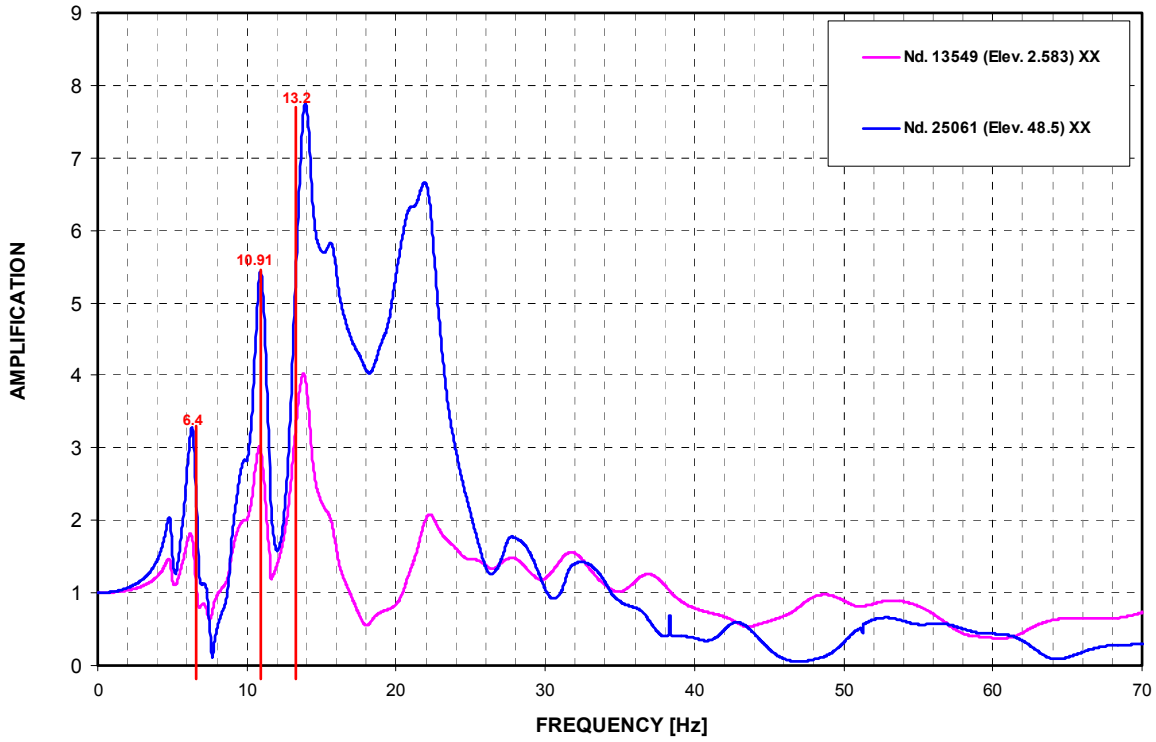

Figure 02.5.1.5.4-4 East PS/B ATF Results – NS Direction (X) Transfer Function at Center of Building

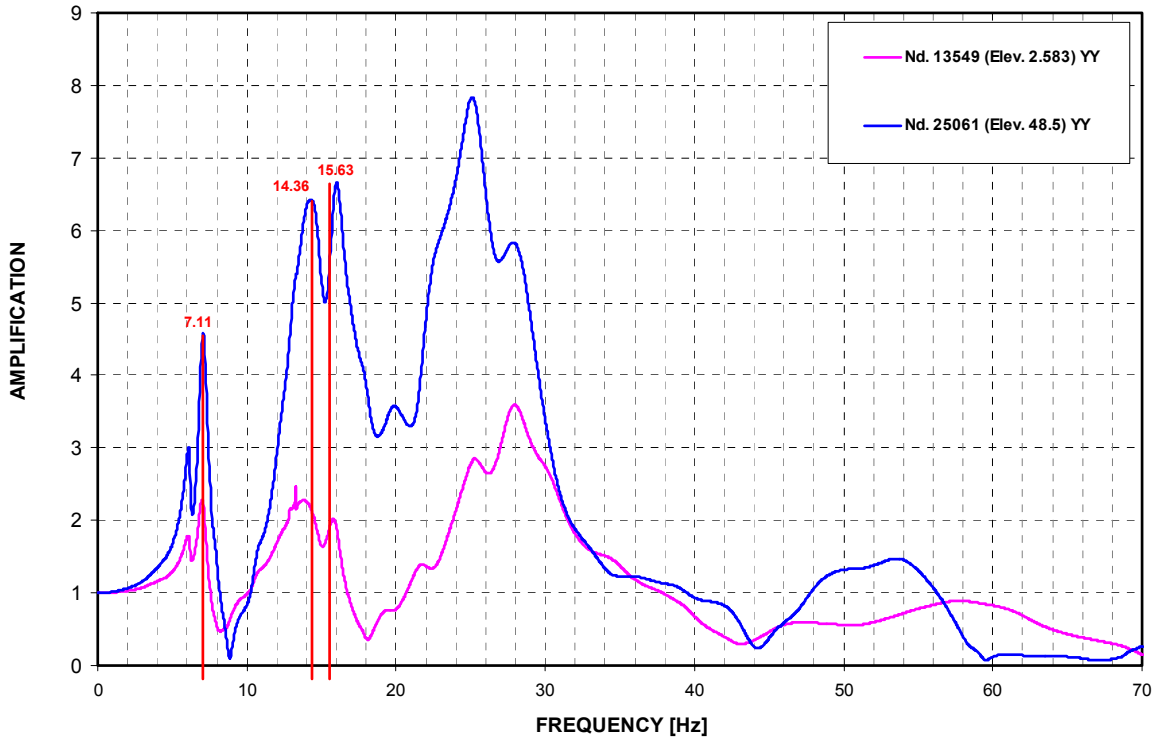

Figure 02.5.1.5.4-5 East PS/B ATF Results – EW Direction (Y) Transfer Function at Center of Building

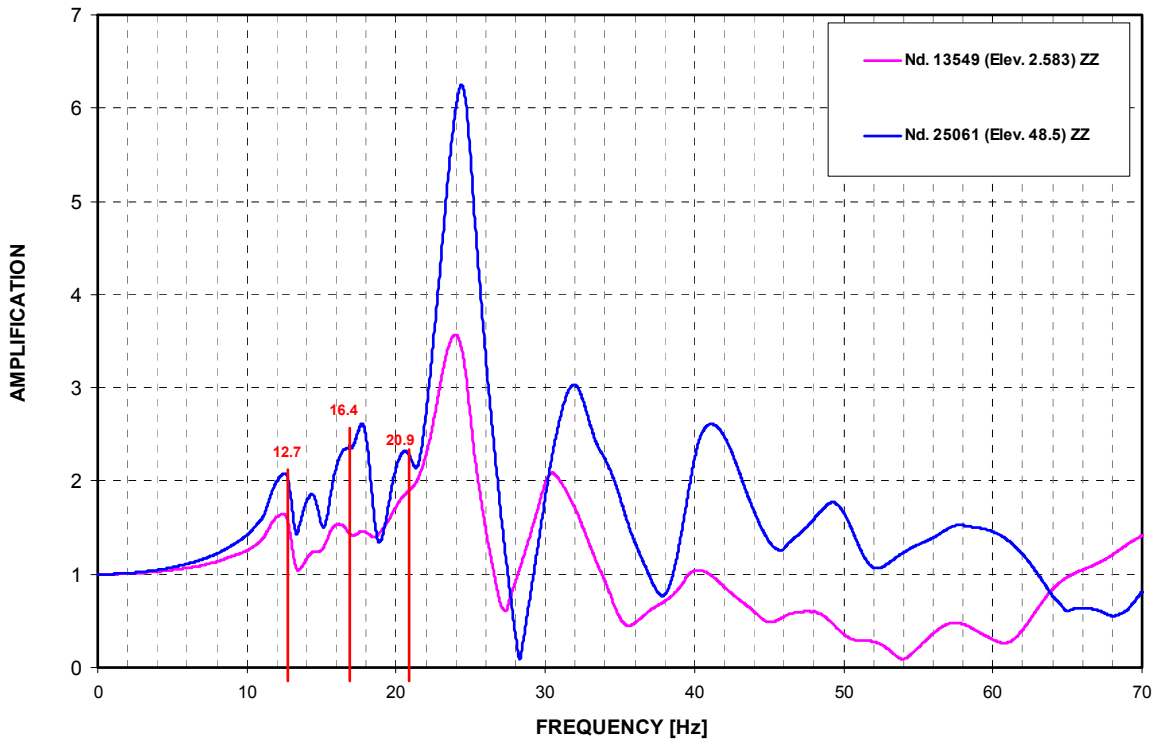

Figure 02.5.1.5.4-6 East PS/B ATF Results – Vertical Direction (Z) Transfer Function at Center of Building

Figure 02.5.1.5.5-1 West PS/B – NS Direction (X) – First Dominant Mode

Figure 02.5.1.5.5-2 West PS/B – EW Direction (Y) – First Dominant Mode

Figure 02.5.1.5.5-3 West PS/B – Vertical Direction (Z) – First Dominant Mode

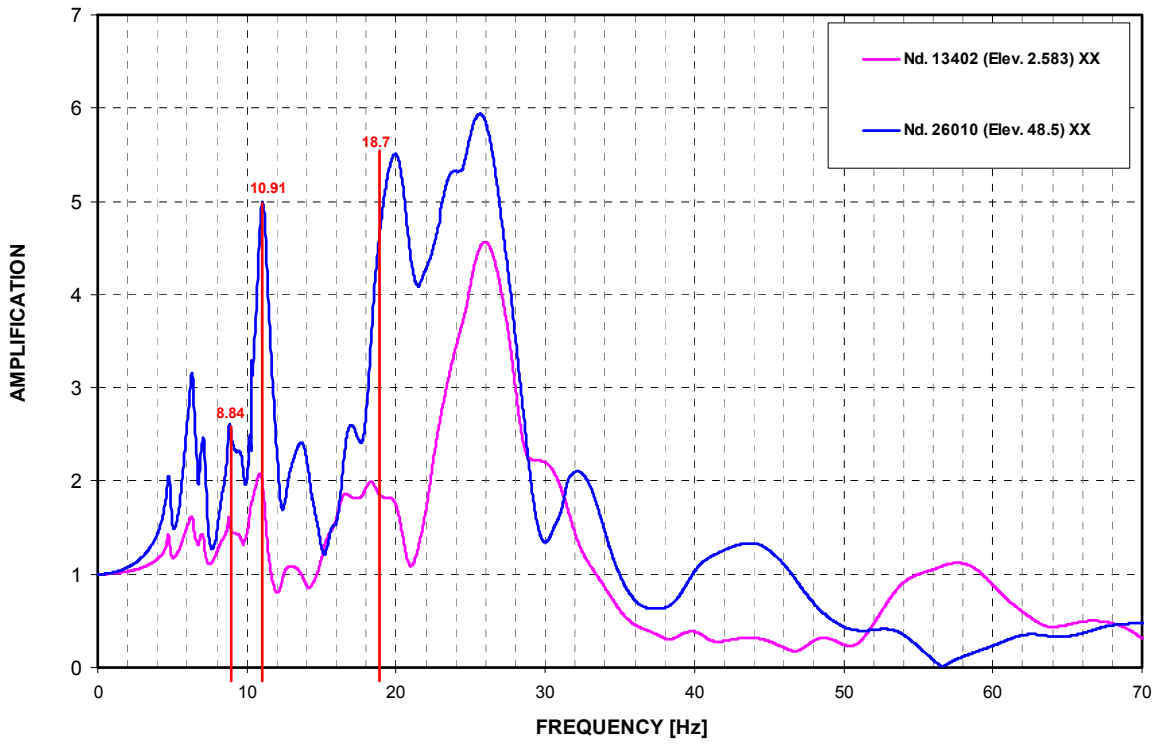

Figure 02.5.1.5.5-4 West PS/B ATF Results – NS Direction (X) Transfer Function at Center of Building

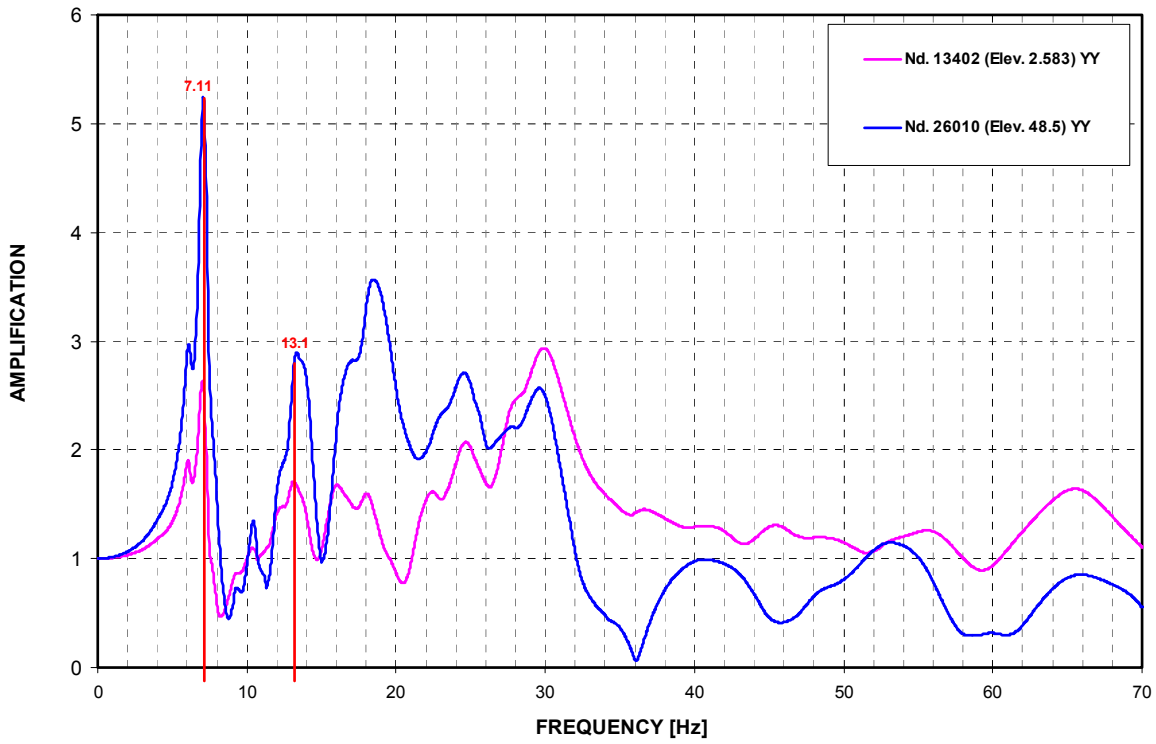

Figure 02.5.1.5.5-5 West PS/B ATF Results – EW Direction (Y) Transfer Function at Center of Building

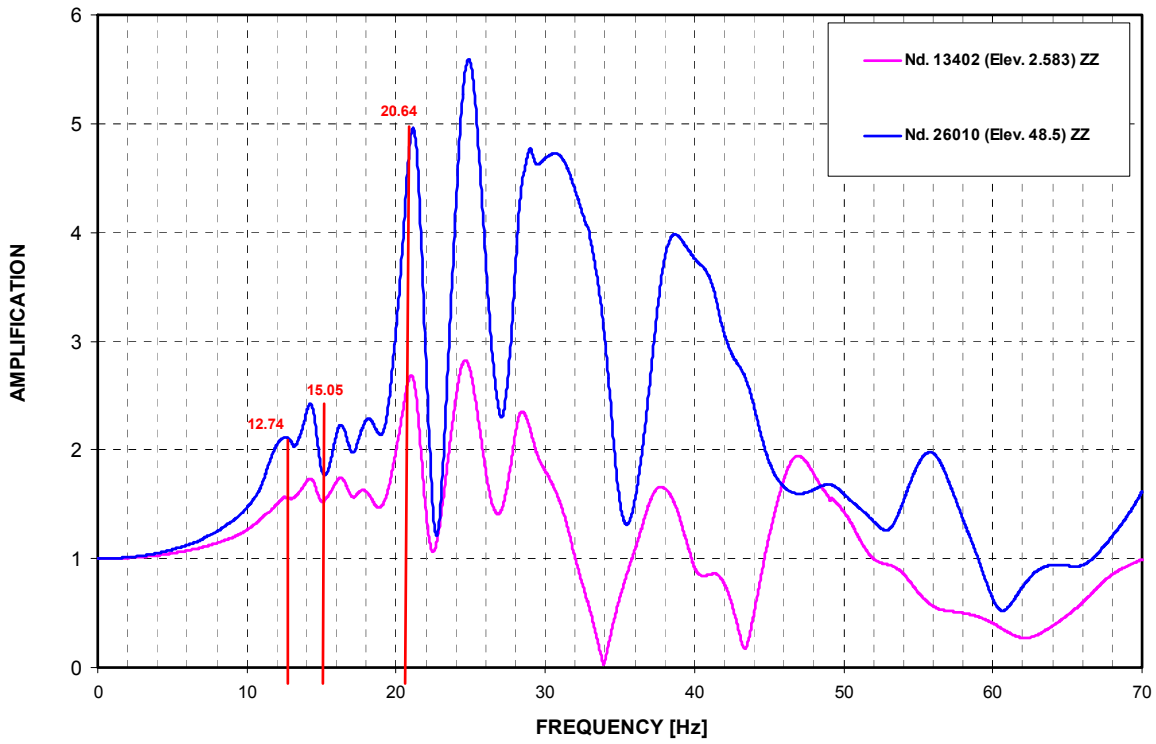

Figure 02.5.1.5.5-6 West PS/B ATF Results – Vertical Direction (Z) Transfer Function at Center of Building

Figure 02.5.1.5.6-1 A/B – NS Direction (X) – First Dominant Mode

Figure 02.5.1.5.6-2 A/B – EW Direction (Y) – First Dominant Mode

Figure 02.5.1.5.6-3 A/B – Vertical Direction (Z) – First Dominant Mode

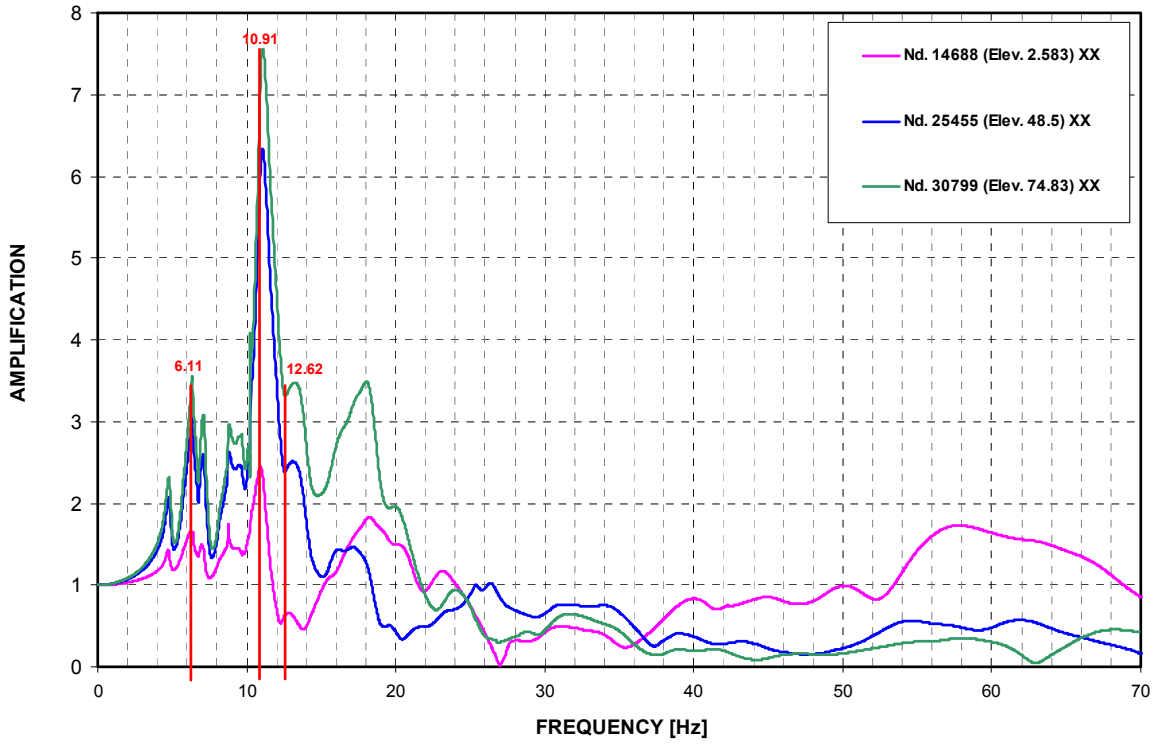

Figure 02.5.1.5.6-4 A/B ATF Results – NS Direction (X) Transfer Function at Center of Building

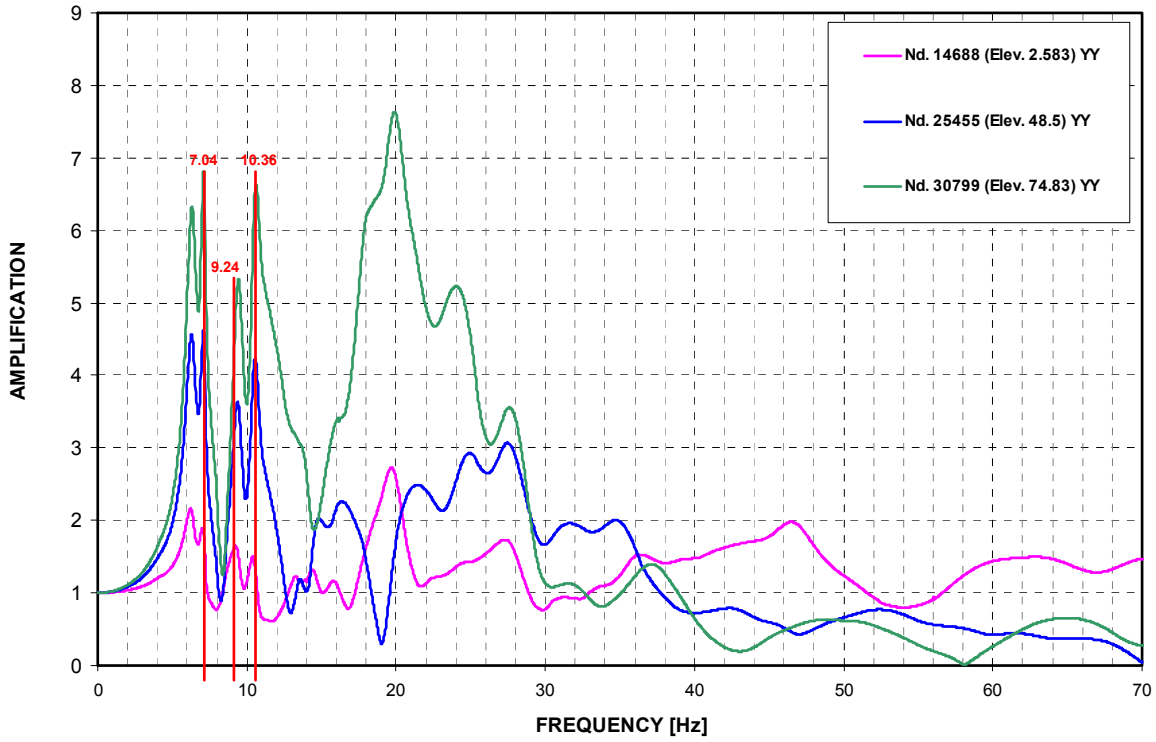

Figure 02.5.1.5.6-5 A/B ATF Results – EW Direction (Y) Transfer Function at Center of Building

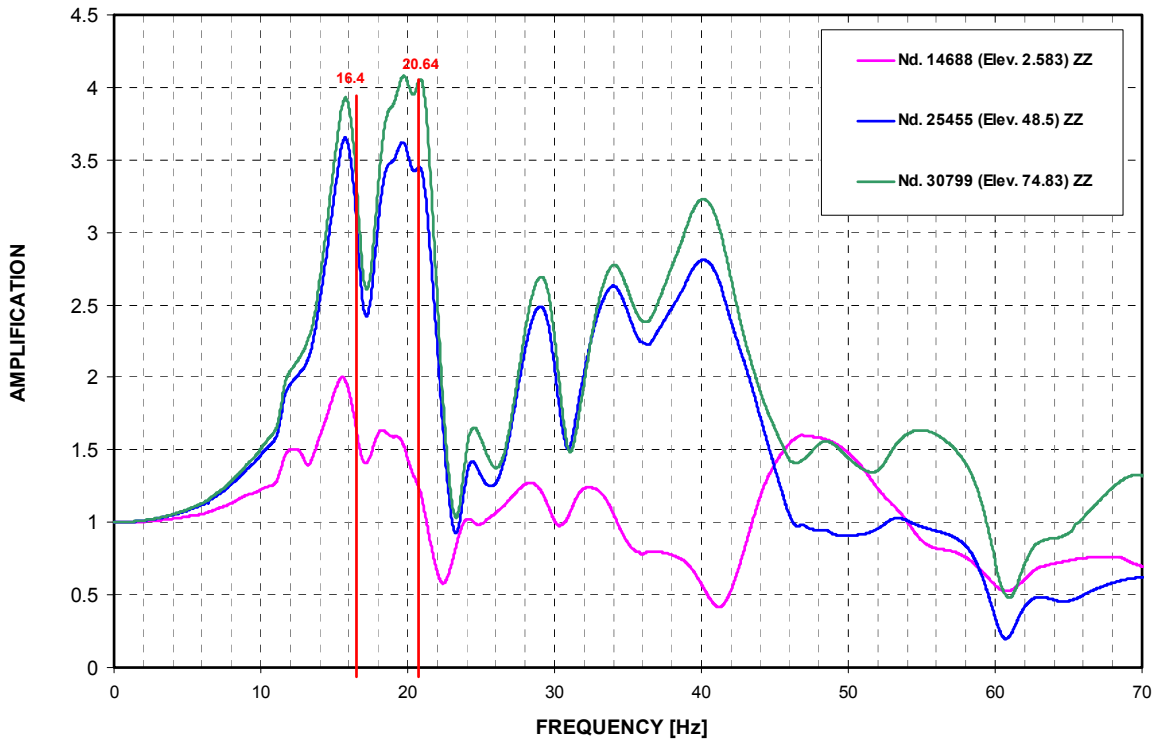

Figure 02.5.1.5.6-6 A/B ATF Results – Vertical Direction (Z) Transfer Function at Center of Building

02.6.0 REFERENCES

02-1. SASSI, Version 2.3.0 including “Option A” & NQA “Option FS”, “An Advanced Computational Software for 3-D Dynamic Analysis Including Soil Structure Interaction,” User Manuals Revision 7.0, Ghiocel Predictive Technologies, Inc., September 26, 2012.

02-2. ANSYS, Release 13.0, SAS IP, Inc., 2010.

02-3. Damping Values for Seismic Design of Nuclear Power Plants, Regulatory Guide 1.61, Revision 1, U. S. Nuclear Regulatory Commission, March 2007.

02-4. Code Requirements for Nuclear Safety Related Concrete Structures, ACI 349-06, American Concrete Institute, 2007.

02-5. Seismic System Analysis, NUREG-0800 Standard Review Plan, SRP Section 3.7.2, Revision 3, U.S. Nuclear Regulatory Commission, Washington, DC, March 2007.

02-6. Nuclear Reactors and Earthquakes, Chapter 6, TID-7024, United States Atomic Energy Commission, Division of Reactor Development, Washington, D.C., 1963.

02-7. Specification for Structural Steel Buildings, AISC 360-05, American Institute of Steel Construction, Inc., Chicago, IL 2005.

02-8. Interim Staff Guidance on Seismic Issues Associated with High Frequency Ground Motion in Design Certification and Combined License Applications, DC/COL-ISG-1, Nuclear Regulatory Commission, May 2008.

02-9. Seismic Analysis of Safety-Related Nuclear Structures and Commentary, ASCE 4-98, American Society of Civil Engineers, 1998.

02-10. Seismic Design Criteria for Structures, Systems, and Components in Nuclear Facilities, ASCE/SEI 43-05, American Society of Civil Engineers, 2005.

02-11. Containment Internal Structure: Stiffness and Damping for Analysis for the US-APWR Standard Plant, MUAP-11018, Revision 1, Mitsubishi Heavy Industries, Ltd., December, 2012.

02-12. SAP IV A Structural Analysis Program for Static and Dynamic Response of Linear Systems, Klaus-Jurgen Bathe, Edward L. Wilson, Fred E. Peterson, University of California, 1974.

02-13. ASME Boiler and Pressure Vessel Code, Section III, Division 2, ASME B&PVC, America Society of Mechanical Engineers, 2001 through 2003 Winter Addenda, New York, N.Y.

02-14. Evaluation of the Seismic Design Criteria in ASCE/SEI Standard 43-05 for Application to Nuclear Power Plants, NUREG/CR-6926, U.S. Nuclear Regulatory Commission, Office of Nuclear Regulatory Research, Washington, DC 20555-0001, 2007.

02-15. Prestandard and Commentary for the Seismic Rehabilitation of Buildings, FEMA 356, prepared by American Society of Civil Engineers (ASCE) for Federal Emergency Management Agency, Washington, D.C., November, 2000.

02-16. Seismic Proving Test of a Prestressed Concrete Containment Vessel Shaking Test and Analytical Results, ICONE-7405, Y. Sasaki, S. Tsurumaki, K. Satoh, H. Fuyama, T. Kitani, H. Eto, K. Tsuda, K. Takiguchi, and H. Akiyama, April, 1999.

Appendix 2-A

Reduced Stiffness for Cracked Pre-Stressed Concrete Containment Vessel (PCCV)

APPENDIX 2-A TABLE OF CONTENTS

Section	Title	Page No.
2-A.1.0	**BACKGROUND**	**2-A.1**
2-A.1.1	Upper Bound Analyses	2-A.1
2-A.1.2	Lower Bound Analyses	2-A.2

2-A.1.0 BACKGROUND

The design evaluation of the PCCV structure is to be performed for both Service and Factored load conditions in accordance with American Society of Mechanical Engineers (ASME) Section III, Division 2 load combinations (Reference 02-13). The load conditions consist of: 1) Primary loads only, and 2) Primary plus Secondary (thermal), for the various ASME load combinations. Tension induced concrete cracking is expected to occur in the area near the basemat and at the transition area between the dome and the cylindrical shell for primary load combinations that include pressure and pressure plus seismic loads. For the load combinations that include primary plus secondary thermal conditions, it is expected that the design evaluation found varying degrees of concrete cracking would be expected to occur in generally all areas from the base mat to the dome apex.

Concrete cracking affects the stiffness of the PCCV structure and therefore affects the seismic structural response. Given that the PCCV structure is predicted to crack under primary load conditions excluding thermal, it is reasonable to use a reduced stiffness in the evaluation of the PCCV seismic response. In absence of industry guidance specific to post tensioned containment structures, the recommended reduced stiffness values consistent with standard industry practices for RC structures are used and are considered conservative for the PCCV post tensioned concrete structure.

In order to envelope the seismic response of the PCCV, two sets of seismic analyses (upper bound and lower bound) are performed, considering the PCCV to be completely uncracked, and considering that the PCCV is cracked for various load combinations as noted above. Each set of PCCV seismic analyses will use the same finite element analytical model changing the stiffness and damping values as follows.

References 02-14, 02-9, 02-10, 02-15, and 02-16 are also used in the development of the upper and lower bound analyses presented.

2-A.1.1 Upper Bound Analyses

The upper bound analyses will use full stiffness properties representing the uncracked PCCV as follows:

Flexural Rigidity: $1.0E_cI_g$

Shear Rigidity: $1.0G_cA_w$

Axial Rigidity: $1.0E_cA_g$

For the upper bound case the load combination stress levels are taken to be less than 80% of the applicable code stress limits, thereby an OBE damping value of 3% critical damping are used.

E_c = Concrete compressive modulus = $57{,}000(f'_c)^{½}$

I_g = Gross moment of inertia

G_c = Concrete shear modulus = $0.4E_c$

A_w = Web (shear) area

A_g = Gross area of concrete section

2-A.1.2 Lower Bound Analyses

The lower bound analyses will use reduced stiffness properties representing the cracked concrete PCCV as follows:

Flexural Rigidity: $0.5E_cI_g$

Shear Rigidity: $0.5G_cA_w$

Axial Rigidity: $0.5E_cA_g$

For the lower bound condition the load combination stress levels are taken to be more than 80% of code stress limits, thereby a SSE damping value of 5% critical damping are used.

Soil-Structure Interaction Analyses and Results for the US-APWR Standard Plant

PART 3 of 3

Soil-Structure Interaction & Structure-Soil-Structure Interaction Analyses and Results for the US-APWR Standard Plant

PART 3 TABLE OF CONTENTS

Section	Title	Page No.
LIST OF FIGURES		**03-iv**
LIST OF TABLES		**03-vii**
03.1.0	**INTRODUCTION**	**03.1-1**
03.2.0	**DESCRIPTION OF US-APWR STANDARD PLANT STRUCTURES**	**03.2-1**
03.2.1	R/B Complex	03.2-1
03.2.2	T/B for SSSI Analyses	03.2-1
03.3.0	**US-APWR SEISMIC DESIGN BASIS**	**03.3-1**
03.3.1	Input Dynamic Soil Properties	03.3-1
03.3.2	Input Motions- Within Motions	03.3-3
03.3.3	SSI & SSSI Analyses Approach	03.3-4
03.3.3.1	Number of Points in FFT	03.3-4
03.3.3.2	Adequacy of Frequency Analyzed and Accuracy of the ATF	03.3-4
03.3.3.3	Three Directional Seismic Excitations	03.3-5
03.3.3.4	Modified Subtraction Method	03.3-5
03.3.3.5	Cut-off Frequency of the Analyses	03.3-6
03.3.4	SSI and SSSI Analyses – ACS SASSI Model Description	03.3-6
03.3.4.1	R/B Complex Embedded Model (SSI Model)	03.3-7
03.3.4.2	R/B Complex –T/B Embedded Model (SSSI Model)	03.3-8
03.3.5	Analysis Matrix	03.3-8
03.3.6	Computation of In-Structure Response Spectra (ISRS)	03.3-9
03.3.7	Computation of Equivalent-Static Seismic Loads	03.3-10
03.3.8	Computation of Maximum Displacement	03.3-11
03.4.0	**ANALYSIS RESULTS**	**03.4-1**
03.4.1	Summary of SSI and SSSI Effects on the R/B Complex	03.4-1
03.4.1.1	First Peak SSI Frequency	03.4-1
03.4.1.2	Effect of Soil Profiles on the ARS	03.4-2
03.4.1.3	SSSI Effects	03.4-2
03.4.2	In-Structure Response Spectra (ISRS)	03.4-3
03.4.3	Seismic Loads	03.4-3
03.4.4	Maximum Relative Displacements	03.4-3
03.5.0	**CONCLUSION**	**03.5-1**
03.6.0	**REFERENCES**	**03.6-1**
APPENDIX 3-A	**R/B Complex Node Numbering and Grouping for ISRS Plots**	**3-A-i**
APPENDIX 3-B	**ISRS Plots for the R/B Complex**	**3-B-i**
APPENDIX 3-C	**Transfer Function Plots**	**3-C-i**

APPENDIX 3-D Parametric Study of Soil Model Depth 3-D-i

LIST OF FIGURES

Figure **Title** **Page No.**

Figure 03.2.0-1 Schematic of Foundation Layout 03.2-2
Figure 03.2.0-2 T/B - ESWPC Elevation View 03.2-3
Figure 03.3.1-1 Shear Wave Velocity Profile V_S - Soil 03.3-28
Figure 03.3.1-2 Shear Wave Velocity Profile V_S - Rock 03.3-29
Figure 03.3.1-3 Compression Wave Velocity Profile V_P – Soil 03.3-30
Figure 03.3.1-4 Compression Wave Velocity Profile V_P – Rock 03.3-31
Figure 03.3.1-5 Shear Wave Damping Ratio Profile - Soil 03.3-32
Figure 03.3.1-6 Shear Wave Damping Ratio Profile - Rock 03.3-33
Figure 03.3.2-1 5% Damped Enveloped H1 (NS) Inlayer Response vs. Horizontal CSDRS 03.3-34
Figure 03.3.2-2 5% Damped Enveloped H2 (EW) Inlayer Response vs. Horizontal CSDRS 03.3-34
Figure 03.3.2-3 5% Damped Enveloped Vertical Inlayer Response vs. Vertical CSDRS....03.3-35
Figure 03.3.2-4 5% Damped Enveloped H1 (NS) Surface Response vs. Horizontal CSDRS 03.3-35
Figure 03.3.2-5 5% Damped Enveloped H2 (EW) Surface Response vs. Horizontal CSDRS 03.3-36
Figure 03.3.2-6 5% Damped Enveloped V Surface Response vs. Vertical CSDRS....03.3-36
Figure 03.3.4.1-1 R/B Complex Structural Elements 03.3-37
Figure 03.3.4.1-2 R/B Complex with Excavated Soil Volume Elements 03.3-37
Figure 03.3.4.1-3 Excavated Soil Volume Elements 03.3-38
Figure 03.3.4.1-4 R/B Complex with Backfill Soil Elements 03.3-38
Figure 03.3.4.1-5 Backfill Soil Elements 03.3-39
Figure 03.3.4.1-6 R/B Complex with Backfill and Free Field Soils (Looking South) 03.3-39
Figure 03.3.4.1-7 R/B Complex with Backfill and Free Field Soils (Looking West) 03.3-40
Figure 03.3.4.2-1 R/B Complex – T/B SSSI Structural Model and Backfill Elements 03.3-40
Figure 03.3.4.2-2 R/B Complex – T/B SSSI Excavated Volume Elements 03.3-41
Figure 03.3.4.2-3 SSSI Model with Backfill and Free Field Soils (Looking East)....03.3-41
Figure 03.3.5-1 ACS SASSI Analysis Flow Chart....03.3-42
Figure 03.3.6-1 Example of ISRS Location Enveloping....03.3-43
Figure 03.3.6-2 Example of ISRS Soil Case Enveloping....03.3-43
Figure 03.3.6-3 Example of ISRS Stiffness Enveloping 03.3-44
Figure 03.3.6-4 Example of Combining SSI and SSSI ISRS....03.3-44
Figure 03.3.6-5 Example of ISRS Broadening....03.3-45
Figure 03.3.6-6 Example of Valley-Filling for Design Basis ISRS 03.3-45
Figure 03.4.1.1-1 First Peak Frequencies at Bottom of Basemat - NS Response (X)....03.4-10
Figure 03.4.1.1-2 First Peak Frequencies at Bottom of Basemat - EW Response (Y)....03.4-10
Figure 03.4.1.1-3 First Peak Frequencies at Bottom of Basemat - Vertical Response (Z)....03.4-11
Figure 03.4.1.1-4 Shear Wave Column Frequencies - Below Foundation 03.4-12

Figure 03.4.1.2-1 Top of Reactor Cavity - Uncracked 3% Damped ARS - NS Response (X) 03.4-13
Figure 03.4.1.2-2 Top of Reactor Cavity - Uncracked 3% Damped ARS - EW Response (Y) 03.4-14
Figure 03.4.1.2-3 Top of Reactor Cavity- Uncracked 3% Damped ARS - Vertical Response (Z) 03.4-15
Figure 03.4.1.2-4 Top of Reactor Cavity - Cracked 3% Damped ARS - NS Response (X) 03.4-16
Figure 03.4.1.2-5 Top of Reactor Cavity - Cracked 3% Damped ARS - EW Response (Y) 03.4-17
Figure 03.4.1.2-6 Top of Reactor Cavity - Cracked 3% Damped ARS - Vertical Response (Z) 03.4-18
Figure 03.4.1.3-1 Top of Reactor Cavity 5% Damped ARS Comparison- 270-200 - NS Response (X) 03.4-19
Figure 03.4.1.3-2 Top of Reactor Cavity 5% Damped ARS Comparison- Enveloped - NS Response (X) 03.4-20
Figure 03.4.1.3-3 Top of Reactor Cavity 5% Damped ARS Comparison- 270-200 - EW Response (Y) 03.4-21
Figure 03.4.1.3-4 Top of Reactor Cavity 5% Damped ARS Comparison- Enveloped - EW Response (Y) 03.4-22
Figure 03.4.1.3-5 Top of Reactor Cavity 5% Damped ARS Comparison- 270-200 - Vertical Response (Z) 03.4-23
Figure 03.4.1.3-6 Top of Reactor Cavity 5% Damped ARS Comparison- Enveloped - Vertical Response (Z) 03.4-24
Figure 03.4.1.3-7 R/B South Wall 5% Damped ARS Comparison- 270-200 - NS Response (X) 03.4-25
Figure 03.4.1.3-8 R/B South Wall 5% Damped ARS Comparison- Enveloped - NS Response (X) 03.4-26
Figure 03.4.1.3-9 R/B South Wall 5% Damped ARS Comparison- 270-200 - EW Response (Y) 03.4-27
Figure 03.4.1.3-10 R/B South Wall 5% Damped ARS Comparison- Enveloped - EW Response (Y) 03.4-28
Figure 03.4.1.3-11 R/B South Wall 5% Damped ARS Comparison- 270-200 - Vertical Response (Z) 03.4-29
Figure 03.4.1.3-12 R/B South Wall 5% Damped ARS Comparison- Enveloped - Vertical Response (Z) 03.4-30
Figure 03.4.2-1 Design Basis ISRS at Top of Reactor Cavity – 3% Damped Response in NS Direction (X) 03.4-31
Figure 03.4.2-2 Design Basis ISRS at Top of Reactor Cavity – 3% Damped Response in EW Direction (Y) 03.4-32
Figure 03.4.2-3 Design Basis ISRS at Top of Reactor Cavity – 3% Damped Response in Vertical Direction (Z) 03.4-33
Figure 03.4.3-1 PCCV SSI Shear Diagram - Envelope of Soil Cases - NS Response (X) 03.4-34
Figure 03.4.3-2 PCCV SSI Shear Diagram - Envelope of Soil Cases - EW Response (Y) 03.4-35

Figure 03.4.3-3 CIS SSI Shear Diagram - Envelope of Soil Cases - NS Response (X) 03.4-36
Figure 03.4.3-4 CIS SSI Shear Diagram - Envelope of Soil Cases - EW Response (Y) 03.4-37
Figure 03.4.3-5 R/B SSI Shear Diagram - Envelope of Soil Cases - NS Response (X) 03.4-38
Figure 03.4.3-6 R/B SSI Shear Diagram - Envelope of Soil Cases - EW Response (Y) 03.4-39
Figure 03.4.3-7 A/B SSI Shear Diagram - Envelope of Soil Cases - NS Response (X) 03.4-40
Figure 03.4.3-8 A/B SSI Shear Diagram - Envelope of Soil Cases - EW Response (Y) 03.4-41
Figure 03.4.3-9 East PS/B SSI Shear Diagram - Envelope of Soil Cases - NS Response (X) 03.4-42
Figure 03.4.3-10 East PS/B SSI Shear Diagram - Envelope of Soil Cases - EW Response (Y).....03.4-43
Figure 03.4.3-11 West PS/B SSI Shear Diagram - Envelope of Soil Cases - NS Response (X).....03.4-44
Figure 03.4.3-12 West PS/B SSI Shear Diagram - Envelope of Soil Cases - EW Response (Y).....03.4-45
Figure 03.4.3-13 R/B Peak Acceleration - Ground Floor Elevation - NS Direction (X) 03.4-46
Figure 03.4.3-14 R/B Peak Acceleration - Ground Floor Elevation - EW Direction (Y) 03.4-47
Figure 03.4.3-15 R/B Peak Acceleration - Ground Floor Elevation - Vertical Direction (Z).....03.4-48

LIST OF TABLES

Table	Title	Page No.
Table 03.3.1-1	Input 270-200 Soil Properties	03.3-12
Table 03.3.1-2	Input 270-500 Soil Properties	03.3-14
Table 03.3.1-3	Input 560-500 Soil Properties	03.3-17
Table 03.3.1-4	Input 900-100 Soil Properties	03.3-19
Table 03.3.1-5	Input 900-200 Soil Properties	03.3-20
Table 03.3.1-6	Input 2032-100 Soil Properties	03.3-21
Table 03.3.1-7	Site Model Depths	03.3-22
Table 03.3.1-8	Backfill Small-Strain Properties for Profiles 270-200, 270-500 and 560-500	03.3-23
Table 03.3.1-9	Backfill Small-Strain Properties for Profiles 900-100, 900-200 and 2032-100	03.3-23
Table 03.3.1-10	Backfill Element Material Properties for 270-200	03.3-24
Table 03.3.1-11	Backfill Element Material Properties for 270-500	03.3-24
Table 03.3.1-12	Backfill Element Material Properties for 560-500	03.3-24
Table 03.3.1-13	Backfill Element Material Properties for 900-100	03.3-24
Table 03.3.1-14	Backfill Element Material Properties for 900-200	03.3-25
Table 03.3.1-15	Backfill Element Material Properties for 2032-100	03.3-25
Table 03.3.4-1	S-Wave Vertical Mesh Passage Frequencies of the Excavated Volume Element	03.3-26
Table 03.3.4-2	NS Wave Passage Frequencies of the Excavated Volume Element	03.3-26
Table 03.3.4-3	EW Wave Passage Frequencies of the Excavated Volume Element	03.3-26
Table 03.3.5-1	Matrix of ACS SASSI Runs	03.3-27
Table 03.3.5-2	Wave Passage Frequencies of the Model Below Foundation	03.3-27
Table 03.4.1.1-1	Summary of First Peak Frequencies for R/B Complex Basemat Response - SSI Model	03.4-5
Table 03.4.1.1-2	Summary of First Peak Frequencies for R/B Complex Basemat Response – SSSI Model	03.4-5
Table 03.4.3-1	Weighted Average Floor Accelerations - PCCV	03.4-6
Table 03.4.3-2	Weighted Average Floor Accelerations - CIS	03.4-6
Table 03.4.3-3	Weighted Average Floor Accelerations - R/B	03.4-7
Table 03.4.3-4	Weighted Average Floor Accelerations - East PS/B	03.4-7
Table 03.4.3-5	Weighted Average Floor Accelerations - West PS/B	03.4-7
Table 03.4.3-6	Weighted Average Floor Accelerations - A/B	03.4-8
Table 03.4.3-7	Base Shears	03.4-8
Table 03.4.4-1	PCCV - R/B Maximum Relative Displacements - Basemat	03.4-8
Table 03.4.4-2	PCCV - CIS Maximum Relative Displacements - Basemat	03.4-9

03.1.0 INTRODUCTION

This Technical Report (TeR) documents the site-independent Soil-Structure Interaction (SSI) and Structure-Soil-Structure Interaction (SSSI) analyses of the R/B complex structures. The R/B complex structures include the R/B with the Fuel Handling Area (FH/A), the Pre-stressed Concrete Containment Vessel (PCCV), Containment Internal Structure (CIS), the East and West Power Source Buildings (East PS/B & West PS/B), the Auxiliary Building (A/B), and the Essential Service Water Pipe Chase (ESWPC). The R/B, PCCV, CIS, East PS/B & West PS/B, A/B, and the ESWPC are supported on a common basemat as shown in Part 2 of this TeR. The SSSI analysis is for the R/B complex with the Turbine Building (T/B). Section 03.2.0 provides a brief description of the R/B complex structures.

In accordance with Standard Review Plan (SRP) 3.7.2 (Reference 03-1), SSI effects are considered in the seismic response analyses of all Seismic Category I structures that are part of the R/B complex. Two sets of analyses are performed for the R/B complex to obtain seismic responses for design. These seismic responses are the In Structure Response Spectra (ISRS) at various locations in the R/B complex, seismic loads indicated by maximum nodal accelerations, resulting floor shear loads and displacements of various locations relative to center of the basemat. The first set of analyses, referred to as the SSI analyses herein is performed for the R/B complex. In these analyses, the R/B complex Finite Element (FE) models are employed. As discussed in Part 2 of this TeR, two models are geometrically the same. They are different in that the two bounding cases of the structural stiffness and associated damping ratio are considered to represent the effects of the concrete cracking on the seismic response of the structures. These two bounding cases of the stiffness represent a full (uncracked concrete) stiffness with Operating-Basis Earthquake (OBE) lower level damping and a reduced (cracked concrete) stiffness with Safe-Shutdown Earthquake (SSE) higher level damping. The models are assigned two stiffness levels that are referred to as the uncracked model and cracked model, respectively.

Figure 03.2.0-1 presents a schematic foundation layout of the R/B complex and T/B. Figure 03.2.0-2 presents an elevation view of the foundation layout between the R/B complex and the T/B. The T/B is located on the south side of the R/B complex and the clear distance between two foundations is approximately 20 ft. The distance between the two foundations and the comparable stiffness and masses of the two buildings necessitate the investigation of effects of the presence of the T/B on the seismic response of the R/B complex. The effects on the response of the R/B complex structures due to SSSI with much smaller and lighter buildings and foundations are considered negligible. Therefore, the second set of analyses, referred to as SSSI analysis herein is performed on the combined models of the R/B complex and T/B to investigate the dynamic coupling effects. Similar to the R/B complex SSI analyses, the SSSI analyses consider models with two levels of structural stiffness (i.e., R/B complex uncracked combined with the T/B uncracked model).

The SSI analysis is performed for the six generic layered soil profiles: 270-200, 270-500, 560-500, 900-100, 900-200 and 2032-100 and the SSSI analysis is performed for four selected generic layered soil profiles: 270-200, 560-500, 900-100 and 900-200. See Section 03.3.5 for discussion of the soil profiles selected for the SSSI analysis. Part 1 of this TeR provides the profile development information.

A total of twelve cases combining two stiffness levels and six soil profiles are performed in the SSI analysis. A total of eight cases combining two stiffness levels with the selected four soil profiles are analyzed to consider SSSI effects in the seismic design of the R/B complex.

To summarize, the SSI analyses of the R/B complex structures considers the following effects:

- Concrete cracking and associated stiffness variation through the consideration of two bounding stiffness levels for the structures;
- Flexibility of the foundation and basement by using FE models;
- Layering of the subgrade by using layered generic soil profiles;
- Embedment by directly analyzing the structures as embedded structures;
- SSSI effects by performing the seismic coupling analysis of the structure soil structure system.

As discussed in Part 2 of this TeR, the out-of-plane high frequency vibration of the local slabs is also considered. The floor slabs are capable of capturing high frequency responses up to 50 Hz.

The analyses are performed using SASSI (Reference 03-2). Therefore, the frequency dependent impedance of foundation soils is considered as well. In the analyses, the Certified Seismic Design Response Spectra (CSDRS) is identified as an outcrop motion in the free field of the R/B complex foundation level for the generic soil profiles and the corresponding within (inlayer) motions at the foundation level are used as input control motion for the analyses. A set of three statistically independent artificial time histories representing the input ground motion for the three orthogonal directions is used to derive the within motions. These artificial time histories are compatible with the broad frequency band CSDRS, as described in Part 1.

The results of the SSI and SSSI and analyses presented in Section 03.4.0 are used for development of the following seismic basis parameters for the structural design of the R/B complex:

- ISRS are presented in Section 03.4.2 that are the input for design and seismic evaluation of SSCs and equipment in the R/B complex. The ISRS are developed by enveloping and broadening the results of the SSI and SSSI analyses.
- Maximum nodal accelerations and average floor accelerations that are presented in Section 03.4.3. The information provided is used to develop seismic loads for equivalent-static analysis and design of the structures and then provide seismic demands for design of the R/B complex structures. The results from R/B complex SSI analyses are considered for this purpose.
- Maximum relative displacements that are provided in Section 03.4.4 are used as input for evaluation of the adequacy of the gaps between the CIS and PCCV, PCCV and R/B, as well as the R/B complex and the T/B. The results from R/B complex SSI analyses are considered for this purpose.

The R/B complex SSI analyses also provide artificial time histories of the seismic response of the R/B complex structure at each nodal point. These are used as input for the evaluation of sliding, overturning, and bearing pressure of the R/B complex.

The SSI and SSSI analyses are performed for the generic soil profiles that consider full saturated soil conditions. MUAP-11007 (Reference 03-3) presents the evaluation of the significance of water table effects for seismic standard plant design basis.

03.2.0 DESCRIPTION OF US-APWR STANDARD PLANT STRUCTURES

03.2.1 R/B Complex

Part 2 of this TeR provides a detailed description of the R/B complex. In summary, a common R/B complex basemat supports the R/B, as well as the PCCV, CIS, A/B, East PS/B, West PS/B and ESWPC. The complex of structures includes the following functional areas:

- PCCV and CIS, including the internals coupled with the Reactor Coolant Loop (RCL);
- Safety system pumps and heat exchangers area;
- FH/A;
- Main steam and feed water area;
- Safety related electrical areas;
- Gas Turbine Generator (GTG) areas.

Table 02.3.1-1 provides a summary of the R/B complex main dimensions.

03.2.2 T/B for SSSI Analyses

The description of the T/B model is presented in MUAP-11002 (Reference 03-4). The model is analyzed in conjunction with the R/B complex model for the SSSI analyses. Refer to Section 03.3.4.2 of this TeR for discussion of the T/B model.

Figure 03.2.0-1 Schematic of Foundation Layout

Security-Related Information – Withheld Under 10 CFR 2.390

Figure 03.2.0-2 T/B - ESWPC Elevation View

03.3.0 US-APWR SEISMIC DESIGN BASIS

03.3.1 Input Dynamic Soil Properties

Section 01.5.2 of this TeR provides input soil/rock properties for the SSI and SSSI analyses. The properties are compatible with the strains generated by the input ground motion and reflect the effects of geological, geotechnical, and hydrological site parameters for representative nuclear power plant sites within the Central and Eastern United States (CEUS).

A total of six generic layered profiles (referred to as free field soils) developed in Section 01.5.2 of this TeR are used for the SSI and SSSI analyses. The profiles are denoted as 270-200, 270-500, 560-500, 900-100, 900-200 and 2032-100. The associated median strain-compatible properties, total unit weight (γ), shear wave (V_s) and compression wave (V_p) velocities and corresponding hysteretic damping values (D_s, D_p) as provided in Section 01.5.2 are refined to form the input for SSI and SSSI analyses. The refinements are as follows:

- Different damping values for the shear waves and the compression waves are provided for the free field soils in Section 01.5.2. However, as a general practice and also supported by correlation study (Reference 03-5) and literature (Reference 03-6), the strain compatible shear wave median damping values are used for both shear and compression wave damping. Section 01.5.2 of this TeR presents a detailed discussion.
- The thick layer of the free field soils below the foundation is divided into multiple sub-layers, as necessary, to ensure that each sub-layer can transmit shear and compression waves with maximum frequency analyzed for the soil and structural system. The thickness of each sub-layer is determined such that it is not greater than 20% of the minimum wave length corresponding to the selected maximum frequency of analysis. For further details, refer to Section 03.3.3.5.
- The layering of the free field soils above the foundation (i.e., embedment soils) is adjusted to match the geometry of FE model mesh of the soil structure system. The following equations are utilized to refine the soil properties for the purpose of matching the meshes, assuming the adjusted layer with thickness H, shear/compression wave velocities V, unit weight γ and damping ratio D_s; and the layer consists of n layers of free field soils with thickness d_i, total unit weight γ_i, shear/compression wave velocities V, and damping Ds_i.

$$V = \frac{H}{\sum_{i=1}^{n} \frac{d_i}{V_i}} \qquad \text{Equation 03.3.1-1}$$

$$Ds = \frac{\sum_{i=1}^{n} Ds_i d_i}{H} \qquad \text{Equation 03.3.1-2}$$

$$\gamma = \frac{\sum_{i=1}^{n} \gamma_i d_i}{H} \qquad \text{Equation 03.3.1-3}$$

Figure 03.3.1-1 through Figure 03.3.1-6 present the dynamic soil properties of the six generic soil profiles from the ground surface to a depth of approximately 500 ft. In the Figures, the solid lines represent the refined properties and the dashed lines represent the properties provided in Section 01.5.2 of this TeR. Two lines representing the same soil profile overlap each other at depths below the foundation bottom level and discrepancy is show the depth

above the foundation level. This is because the layering and properties of the soil are refined for the structural meshes. The layering below the foundation is refined, but the properties remain the same.

The soil structure system models of SSI and SSSI have the same vertical mesh sizes for the soil structure interfaces and therefore they use the same SASSI site model for each soil profile. The site models in the SASSI (Reference 03-2) analyses use infinite horizontal layers (referred to as fixed layers whose depths vary with the soil profiles) to represent the approximately 1000 ft of the top soils. An additional 10 layers, referred to as variable layer, represents a half space of visco-elastic medium. For the same soil profile, the total thickness of variable depth layer varies with the frequency analyzed and is determined as $1.5V_s/f$, where V_s is shear wave velocity of the half space and f, in Hz, is the frequency of analysis. Table 03.3.1-1 through Table 03.3.1-6 present the input soil properties (site model). The last column in the tables lists the wave passage frequency of each layer that is defined as the shear wave velocity divided by five times the layer thickness.

Table 03.3.1-7 presents the site model depths used in the SSI analyses for the six generic soil profiles. The minimum site model depths analyzed as the sum of the variable layer depth at maximum frequency (cut-off frequency) and the fixed layer depth are greater than twice the R/B complex base dimension, which is approximately 410 ft. The table indicates that the half space S-wave velocities for all the soil cases but 270-500 represent very hard rock. A sensitivity study, as presented in Appendix 3-D, is performed for the 270-500 soil case for the R/B complex by including an additional rock layer and extending the site model depth down to hard rock level (i.e., making the half space in or below the hard rock stratum). The fixed layer depth of soil modeled is increased by approximately 36% from 951 ft to 1295 ft. The Acceleration Response Spectra (ARS) of several representative nodes are obtained to compare the response for different soil site model depths. The ARS plots demonstrate that the seismic response of the structure is closely matched to each other for the two site models that have different fixed layer depths. Therefore, the soil site models as described in Table 03.3.1-1 through Table 03.3.1-6 have adequate depth modeled for the SSI and SSSI analyses.

The foundation is modeled in SASSI as embedded SSI and SSSI models of the soil structural system. Solid elements connecting free field soils and the basement structural elements are used in the models to directly include the near field backfills (see Figure 03.3.1-1 and Figure 03.3.4.2-3). In addition, backfills at the top of the ESWPC and in the space between the basements of the R/B complex and T/B are also modeled in the SSI and SSSI models as solid elements. Elastic properties defined by strain compatible S-wave and P-wave velocities and damping values are assigned to the near field backfill elements that are representative of strain compatible properties of typical backfill materials. Two layers of soil are modeled as solid elements below the T/B foundation in order to match the bottom of the R/B complex foundation.

Two sets of granular backfill properties are used to develop the elastic properties and damping values for the backfill elements. In order to cover a wide range of soil-structure frequencies, a backfill with relatively soft properties, represented by lower V_s values, is used in conjunction with the softer soil cases (270-200, 270-500 and 560-500). A backfill with relatively stiff properties is used in conjunction with the harder rock cases (900-100, 900-200, and 2032-100). Table 03.3.1-8 through Table 03.3.1-9 provide average (mean) small strain S-wave and P-wave velocities of the two sets of near field backfills. To determine the strain compatible properties of the near field backfills that are assigned to the backfill elements, the free field soil effective shear strain generated by excitation with CSDRS compatible time histories are calculated first by performing soil column analysis using ACS SASSI soil module. Then, the backfills have the same shear strain as that of the free field soils at the same depth. The

Electric Power Research Institute (EPRI) shear modulus degradation curves and damping curves as shown in Figure 01.4.2-2 of this TeR are used to determine the strain compatible S-wave velocities and damping values for the backfill. For the P-wave property, linearity is assumed, therefore no degradation is considered. Table 03.3.1-10 through Table 03.3.1-15 provides resulting strain compatible properties for the aforementioned six profiles that are assigned to the backfill elements. The strain compatible S-wave damping values also are used for the P-wave.

03.3.2 Input Motions- Within Motions

Section 01.4.1 provides a set of three regulatory compliant acceleration time histories (H1, H2, and V). In the SSI and SSSI analyses, the H1, H2, and V acceleration time histories are used to derive the input control motions in Standard Plant North-South (NS), East-West (EW) and Vertical direction, respectively.

The CSDRS is developed as a free field outcrop motions at the bottom level of the R/B complex foundation basemat. In this case, the CSDRS can be directly compared to site specific Foundation Input Response Spectra that are computed as full soil column outcrop motions (See Nuclear Energy Institute (NEI) White Paper Reference 03-7 and Reference 03-8). However, for the SSI and SSSI analyses of the embedded model, “within” (inlayer) motions at the base of the foundation are needed as input control motions for each of the soil profiles that are analyzed. Therefore, in accordance with the description in Section 3.2.3, item 3 of the NEI White Paper (Reference 03-7 and Reference 03-8), site response analyses are performed, using outcrop time histories H1, H2 and V as input, to develop the within motions for SSI and SSSI analyses.

The soil column analyses or site response analyses use the strain compatible properties as shown in Section 01.5.2.2, Table 01.5.2.2-1 through Table 01.5.2.2-6 for the six generic soil profiles. Three analyses, two for horizontal and one for vertical, are performed for each soil profile. The horizontal time histories H1 and H2 are applied using the strain compatible S-wave velocities and the vertical time history V is applied using corresponding strain compatible P-wave velocities. The strain compatible S-wave damping is used for both horizontal and vertical analyses. The site profile properties are strain compatible and therefore, the analyses are carried out linearly without further degradation of the strain compatible shear modulus and damping profiles. The Soil module of SASSI (Reference 03-2) is used to perform the analysis.

The Soil module performs one dimensional site response analysis under vertically propagated S-waves based on SHAKE methodology, which employs equivalent-linear approach to consider nonlinear material behavior of the soils (Reference 03-9).

The within motion at foundation level, at depth of 42.25 ft, is obtained in terms of acceleration time histories and 5% damped acceleration response spectrum for each analysis. The resulting time histories of within motions are used as input control motions for the SSI and SSSI analyses performed for corresponding soil profile and earthquake excitation for each corresponding direction. A total of six sets of within motions are generated for the six soil profiles, one set for each profile. Each set of within motion includes two horizontal and one vertical motion. Figure 03.3.2-1 through Figure 03.3.2-3 present the enveloped (all six soil cases), 5% damped ARS, denoted as H1-Within Envelope, H2-Within Envelope and V-Within Envelope, of the within motion at the bottom of the foundation compared to the corresponding CSDRS. The within motion usually is deficient in components of the frequency of the soil

column above, however, as shown in Figure 03.3.2-1 through Figure 03.3.2-3, there are no deep valleys in the envelopes of response spectra obtained for the six soil cases due to the wide range of soil properties used in the analyses.

The 5% damped ARS at ground surface is also developed from the analysis and envelope of the ARS from the six soil profiles are shown in Figure 03.3.2-4 through Figure 03.3.2-6. The envelope of the horizontal ARS at ground surface is 30-35% higher than the horizontal CSDRS, while the envelope of the vertical ground surface ARS is approximately 20% higher than the vertical CSDRS.

03.3.3 SSI & SSSI Analyses Approach

This section discusses the approach that is utilized to perform SSI and SSSI analyses. The approach described applies for both SSI and SSSI analyses unless noted.

The SASSI computer program (Reference 03-2) is used for the SSI and SSSI analyses. The program employs the complex response method and FE technique to solve for the seismic response of the soil structure(s) system in the frequency domain. The response is calculated at selected frequencies and then interpolated for the range of frequencies of interest. The Fast Fourier Transformation (FFT) and inverse FFT technique are used to transform the input motion and the nodal responses of the system between frequency and time domains. The following are the guidelines regarding the application of SASSI in the SSI and SSSI analyses.

03.3.3.1 Number of Points in FFT

The number of FFT points is set to 8,192 (or 2^{13}) for the R/B complex model. This number is acceptable since the input excitation duration is about 22 seconds (4,417 time steps of 0.005 seconds) in addition to a quiet zone for free vibration of 20 seconds. This quiet zone ensures that the structure will be at rest after the entire 42 second duration.

03.3.3.2 Adequacy of Frequency Analyzed and Accuracy of the ATF

The selection of the initial frequency points of the SASSI model analyzed for the frequency range from 0 to 20 Hz, the spacing of the analysis frequency points is approximately 0.25 Hz, i.e., four frequency points in each 1.0 Hz frequency interval are selected; for the frequency range from 20 Hz to 33 Hz three frequency points per 1.0 Hz interval are selected; and for 33 Hz to 50 Hz frequency range, two frequency points per 1.0 Hz interval are selected. The plots of Acceleration Transfer Function (ATF) amplitudes for the response at various locations including major equipment support nodes and other locations of interest for building design serve as a check of the adequacy of the selected analysis frequencies and the accuracy of the transfer function interpolation. Based on an examination of the ATF results, additional calculation frequencies may be added to or removed from the SSI analysis as necessary, so that the final, interpolated ATFs are accurate, i.e., the interpolated ATF values match as closely as possible to the computed ATF amplitude values for all SSI frequencies. Appendix 3-C provides Transfer Function Plots for various locations throughout the R/B complex that are obtained from the SSI and SSSI analyses. The plots show the calculated ATF as dots, and interpolated ATF as solid lines. Review of these plots indicates that the number of frequencies selected provides a sufficiently dense grid of calculated points that capture all the significant spectral peaks that define the ATF shapes. Furthermore, the reconstruction of the ATF peaks at all Fourier frequencies up to the cut off frequency of analysis are accurate.

03.3.3.3 Three Directional Seismic Excitations

The three components of the earthquake are applied to the model separately and the solutions are superimposed to provide the solution for combined S- and P-wave excitations later to all nodes. The vertically propagating S-waves represent the two horizontal components of the design earthquake motion H1 and H2 that are applied in NS and EW direction, respectively. The vertical component of the design earthquake (V) is represented by vertically propagating P-waves. Seismic input motions are considered in both the SSI and SSSI analyses. The SSI and SSSI analyses use within motions at the bottom of the R/B complex as control motions. Refer to Section 03.3.2 for details.

03.3.3.4 Modified Subtraction Method

There are several modeling approaches that can be used with SASSI, the Flexible Volume Method (also known as the Direct Method (DM)), the Subtraction Method (SM), and the Modified Subtraction Method (MSM). Each method has different computational demands. The R/B complex SSI and SSSI uses MSM. A brief discussion of the different methods follows:

SASSI Flexible Volume substructure method partitions the soil structure system as superstructure plus basement minus the excavated soils, and the original soils (free field soils). It requires only the free-field motions and the free-field soil impedances to compute the seismic excitations on the foundation of structure. The numerical Green's function method is used to obtain the soil impedance to take full advantage of the axisymmetric condition of the free field soils. The soils to be excavated are retained with the foundation in the flexible volume system. Therefore, interaction between the structure and the foundation occurs at all excavated soil nodes. In the SASSI analysis, the DM treats all translational degrees of freedoms of the excavated soil as SSI interaction nodes. This corresponds to a theoretical exact SSI model for the excavated soil dynamics. DM is not used for the SSI and SSSI analyses.

The Subtraction Method (SM) is also not used for the R/B complex SSI and SSSI analyses. To reduce computational time, a simplified method, termed as SM was developed. The SM assumes only the nodes at interface of the excavated soil volume and surrounding free field soils as interaction nodes. In mathematical implementation, only those specified interaction nodes are described by correct equations of motion. The seismic load component and free field soil impedance are neglected for the non-interaction nodes within the excavated soil volume. Therefore the excavated soil motion will include a number of spurious vibration modes. These spurious modes will be more excited by the short wavelength components in the mid and high frequency ranges. As noted by The Department of Energy (DOE) study (Reference 03-10), this simplification results in anomalies in ATFs, usually represented by spurious spikes for soft free field soils at relative high frequency ranges. The DOE study recommends using SM with a cautious review of the resulting ATF for evidence of anomalous response to ensure the quality of the output.

The R/B complex SSI and SSSI analysis use an improved subtraction method, the MSM. In addition to the interaction nodes at the interface of the excavated soil volume and surrounding free field soil interface defined in the SM, MSM includes the nodes at the ground surface of the excavated soil as interaction nodes. By adding interaction nodes at the ground surface. The scattered surface waves that occur at the ground surface in the mid and high frequency range are captured much more accurately than in the SM method. In addition, the inclusion of the ground surface nodes as interaction nodes provides significantly improved boundary conditions for simulating the excavated soil dynamic behavior. The scattered waves manifest

primarily by Rayleigh and Love surface waves. It is very important to have a SSI modeling to appropriately describe the motion of the excavated soil nodes situated at the ground surface nodes. The vibration of these nodes at the ground surface is primarily controlled by surface wave components. Including surface nodes as interaction nodes greatly improves the excavation soil response accuracy.

A review of ATFs at various locations throughout the R/B complex indicates that the MSM model reasonably captures the seismic responses for the analyzed frequency (See Appendix 3-C). MSM is an accurate and robust method for the R/B complex, which has a large footprint shallow embedded foundation for the frequency range analyzed.

03.3.3.5 Cut-off Frequency of the Analyses

The cut-off frequency is the highest frequency used in the dynamic analysis of the soil structure(s) system. It sets an upper limit on the number of frequencies to be analyzed, and controls the maximum allowable element size which in turn controls the size of the problem to be solved. The maximum frequency of analysis is determined from the wave passage frequency (f_{pass}) of the soil layer and soil element size. The wave passage frequency is the maximum wave frequency that the soil layer can accurately transmit. It is determined using Equation 03.3.3.5-1 below (Reference 03-2) and provided that the soil element mass matrix is constructed from the combination of consistent and lump mass matrices (50% each), which is built in to the SASSI mass matrix computation that:

$$f_{pass} = \frac{V_s}{5 \cdot d} \qquad \text{Equation 03.3.3.5-1}$$

- where V_s is the shear wave velocity of the soil and d is either the thickness of the soil layer or the maximum size of the FE mesh of the structural model at the SSI interface or the excavated soil volume mesh size.

The maximum frequency in the analyses could be slightly greater than the wave passage frequency. The ATFs are reviewed to ensure that the maximum frequency of the analysis yields smooth curves with no anomalies. A list of the wave passage frequencies for the R/B complex SSI model including both soil layering and excavated volume is presented in Section 03.3.4.

The maximum frequencies in the analyses are determined to be 40 Hz for 270-200, 270-500 soil profiles, and 50 Hz for 560-500, 900-100, 900-200 and 2032-100 soil profiles. Refer to Section 03.3.5 for detailed discussion. Based on the maximum frequencies and intervals of frequency points as discussed in Section 03.3.3.2, for both SSI and SSSI analysis, a total number of 132 frequencies is analyzed for soil profiles 270-500 and 270-200, and a total number of 152 frequencies is analyzed for soil profiles 560-500, 900-100, 900-200 and 2032-100. For a graphical representation of the selected frequencies of analyses, see ATFs in Appendix 3-C.

03.3.4 SSI and SSSI Analyses – ACS SASSI Model Description

The R/B complex SSI analysis and R/B complex combined with T/B SSSI analysis address foundation embedment effects by directly analyzing the soil structure or structure soil structure system using embedded models. The corresponding SSI and SSSI embedded models are the design basis models for seismic analysis of the R/B complex.

The embedded model of the soil structure(s) system that is analyzed using SASSI consists of three portions based on SASSI sub-structuring framework (Reference 03-2):

- the structural model that simulates the superstructure, the basement and the foundation and near field backfill elements
- the excavated volume that models the free field soils that are replaced by basement and foundation, and the near field backfill
- the free field soil model, referred to as site model, that models the soils that exist before the structure is built

The same site model is used for both the SSI and SSSI analysis for the same soil profiles. The site models for the six soil profiles are discussed in Section 03.3.1 of this TeR. This section discusses the first two portions of the embedded model. The term “embedded model” will refer only to the first two portions herein for convenience of description.

03.3.4.1 R/B Complex Embedded Model (SSI Model)

Part 2 of this TeR documents the development and validation of the SASSI dynamic FE model of the R/B complex that represents the dynamic properties of the R/B complex structures for SSI analyses to provide nodal accelerations, which are in the form of maximum accelerations, acceleration time histories, floor ISRS, and displacements for seismic design of the R/B complex and equipment. In order to consider the effect of concrete cracking on the seismic response of the structures, two structural models with bounding stiffness, i.e., full stiffness associated with uncracked concrete (uncracked model) and reduced stiffness associated with cracked concrete (cracked model) are developed.

The R/B complex dynamic structural FE model consists of BEAM, SHELL, SOLID and SPRING elements. The use of finite elements ensures an accurate representation of the dynamic characteristics of the structures and the foundation that enables an accurate simulation of dynamic interaction with the flexible foundation and the surrounding soil. SHELL elements are used to model the reinforced concrete shear walls and slabs, and Three-Dimensional (3-D) BEAM elements model the reinforced concrete and steel columns and beams. SOLID elements are used to model the basemat foundation and the massive structural members of the CIS. SPRING and BEAM elements are used to model the supports and connection of the RCL model with the CIS FE mesh. The details of the dynamic FE model of the R/B complex are documented in Part 2 of this TeR.

The dynamic FE model of the R/B complex used for SSI analyses consists of the structural model (Figure 03.3.4.1-1) and an excavated volume that is based on ACS SASSI sub-structuring method (Reference 03-2), as shown in Figure 03.3.4.1-2. The excavated soil volume, presented in Figure 03.3.4.1-3, represents the free field soil component that is replaced by the basement structures and surrounding backfills. The backfill is modeled as two rows of structural elements having a total width of 14 ft surrounding the R/B complex. This width is chosen to satisfy the limitations on the size of the SASSI model. Also, backfill is modeled, using solid elements, in the areas above the ESWPC below plant grade, as shown in Figure 03.3.4.1-4 and Figure 03.3.4.1-5. Therefore, the excavated volume, in plan view, is approximately 14 ft larger than the basement/foundation of the R/B complex.

At the bottom and lateral surfaces of the excavated soil volume, the excavated soil and R/B complex structure/backfill share the same nodes. These nodes, along with the nodes at the top (ground) surface of the excavated soil volume are identified as interaction nodes in SSI and SSSI analyses as required by the MSM. As a result, the excavated volume soil elements

share the same mesh size as the structural elements below plant grade. At the bottom of the foundation level, the mesh size in the horizontal direction ranges from 6.0 to 9.0 ft, with an average of 6.62 ft in the NS direction and 7.32 ft in the EW direction. In the vertical direction, excavated soil volume mesh sizes are consistent with the soil layering as shown in Table 03.3.1-1 through Table 03.3.1-6. The wave passage frequencies of excavated soil volume elements, calculated as shear wave velocity divided by five times the mesh size, are presented in Table 03.3.4.1-1 through Table 03.3.4.1-3.

Figure 03.3.4.1-6 and Figure 03.3.4.1-7 schematically show the R/B complex embedded SSI model including structural elements, backfill elements and free field soils simulated in the site model.

03.3.4.2 R/B Complex –T/B Embedded Model (SSSI Model)

To perform site-independent SSSI analyses, the dynamic FE model of the R/B complex used for SSI analyses is combined with the T/B FE model to create a single dynamic FE model. The relative locations of the two structures within the SSSI model are shown in Figure 03.2.0-1 and Figure 03.2.0-2. Backfill is modeled in the surrounding areas of each building and in the gap between the two buildings below plant grade, as shown in Figure 03.3.4.2-1.

The T/B FE model accounts for two steel structures, namely the T/B and the Electrical Room. The two structures are supported by a common basemat. The steel columns and beams are modeled using BEAM elements. The foundation walls and base slabs are modeled with SHELL elements. The filled concrete parts are modeled with SOLID elements. The T/B foundation basemat has a large rectangular portion around the center that is filled by the Pedestal foundation, which is also modeled with SHELL elements.

In order to create an integrated R/B complex-T/B SSSI model, the foundation part of the T/B FE model is meshed so that the excavated soil layer interfaces for the R/B complex and T/B have the same nodal Z-coordinates, i.e., the T/B FE model basement and excavated volume meshes match the top five embedded layers of the R/B complex FE model, as shown in Figure 03.3.4.2-2. The bottom foundation level of the T/B is set at elevation -26.33 ft. Compared to the actual foundation bottom elevation of -24.58 ft the geometry adjustments have negligible effects on the T/B dynamic behavior.

Two layers of solid elements are added in the model below the T/B foundation to simulate the free field soils in order to create an excavated volume for the SSSI model with a level bottom. The corresponding free field soil strain compatible properties are assigned to the two layers of soil elements.

The excavated volume vertical meshes of the T/B portion match the R/B portion. In the T/B portion, the excavated volume has a nominal horizontal mesh size of 13 ft. The purpose of SSSI analysis is to investigate the effect of the presence of the T/B on the R/B complex. The larger horizontal mesh size in T/B portion is acceptable.

Figure 03.3.4.2-3 schematically shows the R/B complex and T/B embedded SSSI model including structural elements, soil elements below the T/B foundation, backfill elements and free field soils simulated in the site model.

03.3.5 Analysis Matrix

Figure 03.3.5-1 schematically presents the general procedure for the SSI and SSSI analyses using SASSI. The left portion of the figure describes the analyses step by step and the right portion depicts the procedure in the form of a flowchart.

Table 03.3.5-1 presents the matrix for SSI and SSSI production runs. Listed in the table are the analysis cases, cut-off Frequency, number of frequencies analyzed, and location of input control motion. A total of twenty cases are analyzed, twelve for SSI and eight for SSSI. The determination of cut-off frequency (maximum frequency calculated) is based on evaluation of Table 03.3.4.1-1 through Table 03.3.4.1-3, and Table 03.3.5-2. As the three tables show, the maximum wave passage frequencies as calculated using the rule of five points in one wave length are mainly controlled by the excavated soil volume element size in the horizontal direction. Because the earthquake excitations are modeled as vertically propagated waves, the wave passage frequencies of the vertical mesh size of the excavated volume are used to determine the maximum frequency to be analyzed. The cut-off frequencies as shown in Table 03.3.5-1 are slightly greater than the corresponding minimum numbers shown in Table 03.3.4.1-1 through Table 03.3.4.1-3. A review of the resulting ATFs at frequencies beyond the minimum frequencies is conducted to determine the accuracy of the results. The number of frequencies to be analyzed is determined by the cut-off frequencies and frequency point spacing as described in Section 03.3.3.2.

As Table 03.3.5-1 shows, the maximum frequencies analyzed are 40 Hz for soil profiles 270-500 and 270-200 and 50 Hz for soil profiles 560-500, 900-200, 900-100 and 2032-100. For soil profiles 270-500 and 270-200, the maximum frequencies analyzed or the maximum passage frequencies of the model meshes are smaller than 50 Hz. This is acceptable because a) it is recognized that for the soil sites, the relative soft soil will filter out high frequency content of the earthquake input motion propagated from the hard rock horizon (Reference 03-11); and b) as shown in Section 3.4.1, the 270-500 and 270-200 soil profiles control the seismic responses of the structures in terms of the ISRS at various locations for the frequencies far below 30 Hz.

Both cracked and uncracked SSI models are analyzed for the six generic soil profiles. This results in a total of twelve analyses for the R/B complex. The R/B-T/B combined models are analyzed for both cracked and uncracked stiffness and selected four selected generic soil profiles. A total of eight cases are analyzed for the SSSI effects. The four soil profiles are 270-200, 560-500, 900-200, and 900-100. Since the 2032-100 soil profile is a hard rock soil profile, the SSSI effects are minimal compared to the softer soil profiles; the responses for 270-500 soil profiles are on the same order as the ones from 270-200 soil profile and because of higher radiation damping, generally are lower. Therefore soil profiles 270-500 and 2032-100 are not analyzed for the SSSI effects.

03.3.6 Computation of In-Structure Response Spectra (ISRS)

ISRS are generated for various areas of the R/B complex in accordance with RG 1.122 (Reference 03-12) to serve as the seismic design basis for the design of pipe and equipment. The SASSI analyses provide results for the response of the PCCV, CIS, R/B, A/B, and PS/B structures due to the three directional design input ground motion for each of the six soil profiles. At representative node locations, ARS in the three orthogonal directions are calculated for each of the three orthogonal directions of the input ground motion from time histories generated by SASSI. The ARS are calculated at 301 frequency points equally distributed on the logarithmic scale at the range of frequency from 0.1 Hz to 100 Hz. The ARS for particular damping value obtained for the three directions of the input ground motion are then combined using the Square Root Sum of the Squares (SRSS) method as follows:

$$ARS_X = \sqrt{ARS_{XX}^2 + ARS_{YX}^2 + ARS_{ZX}^2} \qquad \text{Equation 03.3.6-1}$$

$$ARS_Y = \sqrt{ARS_{XY}^2 + ARS_{YY}^2 + ARS_{ZY}^2} \qquad \text{Equation 03.3.6-2}$$

$$ARS_Z = \sqrt{ARS_{XZ}^2 + ARS_{YZ}^2 + ARS_{ZZ}^2}$$ Equation 03.3.6-3

where:

- $ARS_{(m)(n)}$ are the SASSI ARS results for the response in "n" direction due to earthquake in "m," direction;
- ARS_X, ARS_Y, and ARS_Z are the combined ARS of the structural response in NS (x), EW (y), and vertical (z) direction, respectively.

Once the results of each of the generic soil cases are combined through SRSS at the nodes, the results are grouped for the nodes within the footprint/support of the equipment or floor areas for which the ISRS is developed. The grouped nodal results are then enveloped for each of the soil cases and both structural stiffness levels, as shown in Figure 03.3.6-1 through Figure 03.3.6-3. Enveloping the responses at the grouped nodes is to provides an ISRS for the equipment design and qualification that considers the potential non-uniform input at their support locations including the rocking and torsional effects. The grouped locations are presented in Appendix 3-A. Table 3-A.1.1-1 presents node grouping for the critical equipment and Table 3-A.1.2-1 provides locations on the building for which the ISRS are developed to indicate the level of the seismic load on the locations. The spectra from each analysis (SSI and SSSI) are then enveloped, as seen in Figure 03.3.6-4. The resulting spectra are broadened by 15% in spectral frequency to account for uncertainties in the analysis parameters, as seen in Figure 03.3.6-5. Further, the valleys in the enveloped ISRS between adjacent peaks are filled to capture potential frequency shifts within the range of the SSI and SSSI responses obtained from the generic soil profiles. To fill in the valleys in the SSI and SSSI responses caused by soil profiles, the lower peak is extended diagonally until it intersects with the side slope of the adjacent higher peak, as seen in Figure 03.3.6-6. No valley filling for the ISRS for the nodes shown on Table 3-A.1.2-1 is performed.

To generate additional ISRS at other damping values as necessary for design of SSCs, the same process described above is repeated by converting the same time histories output by SASSI at the same representative node locations to generate enveloped broadened ISRS for the various required damping values.

03.3.7 Computation of Equivalent-Static Seismic Loads

SASSI uses ANSYS-output files, with the three-directional design input ground motions to post-processes the maximum nodal accelerations; also known as Zero Period Acceleration (ZPA), which serve as basis for development of the seismic loads. These seismic loads are developed in the form of equivalent static accelerations as follows:

1. Calculate maximum accelerations in each of the three response directions due to each of the three direction input motions from the site-independent SSI analyses.
2. Apply the SRSS rule to combine the nodal maximum accelerations due to the three directions of the earthquake calculated in Step 1. Envelope the results of the SRSS combined maximum acceleration responses from the SSI analyses of the six generic soil conditions and the two structural stiffness levels
3. For each floor elevation, create contour plots of the enveloped maximum accelerations in three directions calculated in Step 2 that represent the enveloped response due to the three components of the earthquake.

4. Calculate weighted average accelerations at floor elevation “f” as follows:

$$A_i^f = \frac{\sum a_i^k \cdot w_k}{W_f}$$ Equation 03.3.7-1

where W_f is the total weight of the floor “f,” w_k is the weight participating to node “k,” A_i^f is the weighted average acceleration of floor “f” in “i’ direction, and a_i^k is the enveloped and SRSS combined maximum acceleration at node “k” in “i’ direction as calculated in Step 3 above.

5. Determine equivalent seismic equivalent-static load in each of the three directions at each floor elevation based on the maximum acceleration contour plots created in Step 3 or the weighted average accelerations calculated in Step 4.
6. Determine the out-of-plane seismic demands on slabs and walls with large unsupported areas based on the maximum acceleration plots created in Step 3.
7. Calculate story shear diagrams for the structures. The total shear at each floor elevation is obtained as the sum of the all nodal inertial forces at and above that elevation. The nodal inertial forces are the product of the nodal mass and the equivalent equivalent-static acceleration acting on the node calculated in Step 5 above. These values are representative design values, but will be confirmed during the design process.

03.3.8 Computation of Maximum Displacement

The results obtained from the SSI analyses of the R/B complex model with reduced (cracked concrete) stiffness properties and full stiffness properties (uncracked concrete) are used to compute the maximum relative displacements. These results serve as the basis for evaluation of gaps between CIS, PCCV and R/B. These maximum relative displacements are developed as follows:

1. Calculate maximum displacements relative to the basemat in each of the three response directions due to each of the 3-directional input motions from the SSI analyses of the R/B complex.
2. Apply the SRSS rule to combine the nodal maximum displacements due to the three directions of the earthquake calculated in Step 1.
3. Envelope the results of the SRSS combined maximum displacements from the SSI analyses of the six generic soil cases and the two structural stiffness levels
4. Compare maximum relative displacements at the perimeters of the buildings at elevations close to other structures to obtain contribution of elastic seismic displacements that serve for assessment of adequacy of gaps between buildings.

Table 03.3.1-1 Input 270-200 Soil Properties (Sheet 1 of 2)

Layer #	Thickness (ft)	Unit Weight (kcf)	Vs (ft/sec)	Vp (ft/sec)	Damping %	Shear Wave Passage Frequency (Hz)
1	5.58	0.125	1296	5284	1.52	46.4
2	5.58	0.125	1292	5363	1.91	46.3
3	7.00	0.125	1266	5328	2.25	36.2
4	5.38	0.125	1224	5153	2.37	45.5
5	5.38	0.125	1197	5128	2.69	44.6
6	6.67	0.125	1218	5244	2.80	36.5
7	6.67	0.125	1226	5308	2.92	36.8
8	3.41	0.125	1188	5213	3.20	69.7
9	3.41	0.125	1188	5213	3.20	69.7
10	4.29	0.125	1204	5318	3.30	56.1
11	4.29	0.125	1204	5318	3.30	56.1
12	4.29	0.125	1262	5555	3.29	58.8
13	4.29	0.125	1262	5555	3.29	58.8
14	4.29	0.125	1281	5653	3.38	59.7
15	4.29	0.125	1281	5653	3.38	59.7
16	4.29	0.125	1315	5808	3.40	61.3
17	4.29	0.125	1315	5808	3.40	61.3
18	4.69	0.125	1308	5788	2.63	55.8
19	4.69	0.125	1308	5788	2.63	55.8
20	4.69	0.125	1382	6093	2.58	59.0
21	4.69	0.125	1382	6093	2.58	59.0
22	4.69	0.125	1394	6159	2.62	59.5
23	4.69	0.125	1394	6159	2.62	59.5
24	4.69	0.125	1441	6343	2.60	61.5
25	4.69	0.125	1441	6343	2.60	61.5
26	4.69	0.125	1389	6160	2.76	59.2
27	4.69	0.125	1389	6160	2.76	59.2
28	4.69	0.125	1449	6406	2.70	61.8
29	4.69	0.125	1449	6406	2.70	61.8
30	5.00	0.131	1481	6533	2.61	59.2
31	5.00	0.131	1481	6533	2.61	59.2
32	5.00	0.131	1496	6617	2.63	59.8
33	5.00	0.131	1496	6617	2.63	59.8
34	5.00	0.131	1519	6729	2.63	60.8
35	5.00	0.131	1519	6729	2.63	60.8
36	5.00	0.131	1547	6843	2.63	61.9
37	5.00	0.131	1547	6843	2.63	61.9
38	5.00	0.131	1535	6809	2.70	61.4
39	5.00	0.131	1535	6809	2.70	61.4
40	5.00	0.131	1576	6988	2.67	63.0
41	5.00	0.131	1576	6988	2.67	63.0
42	8.20	0.131	2509	8230	0.50	61.2
43	8.20	0.131	2509	8230	0.50	61.2
44	8.20	0.131	2509	8230	0.50	61.2
45	8.20	0.131	2509	8230	0.50	61.2
46	8.20	0.131	2509	8230	0.50	61.2
47	8.20	0.131	2509	8230	0.50	61.2
48	8.20	0.131	2509	8230	0.50	61.2
49	8.20	0.131	2509	8230	0.50	61.2
50	8.20	0.131	2509	8230	0.50	61.2
51	8.20	0.131	2509	8230	0.50	61.2
52	8.20	0.131	2509	8230	0.50	61.2
53	8.20	0.131	2509	8230	0.50	61.2

Table 03.3.1-1 Input 270-200 Soil Properties (Sheet 2 of 2)

Layer #	Thickness (ft)	Unit Weight (kcf)	Vs (ft/sec)	Vp (ft/sec)	Damping %	Shear Wave Passage Frequency (Hz)
54	8.20	0.131	2509	8230	0.50	61.2
55	8.20	0.131	2509	8230	0.50	61.2
56	8.20	0.131	2509	8230	0.50	61.2
57	8.20	0.131	2509	8230	0.50	61.2
58	8.20	0.131	2509	8230	0.50	61.2
59	8.20	0.131	2509	8230	0.50	61.2
60	8.20	0.131	2509	8230	0.50	61.2
61	8.20	0.131	2509	8230	0.50	61.2
62	10.94	0.134	3281	8924	0.50	60.0
63	10.94	0.134	3281	8924	0.50	60.0
64	10.94	0.134	3281	8924	0.50	60.0
65	10.94	0.134	3281	8924	0.50	60.0
66	10.94	0.134	3281	8924	0.50	60.0
67	10.94	0.134	3281	8924	0.50	60.0
68	10.94	0.134	3281	8924	0.50	60.0
69	10.94	0.134	3281	8924	0.50	60.0
70	10.94	0.134	3281	8924	0.50	60.0
71	10.94	0.134	3281	8924	0.50	60.0
72	10.94	0.134	3281	8924	0.50	60.0
73	10.94	0.134	3281	8924	0.50	60.0
74	10.94	0.134	3281	8924	0.50	60.0
75	10.94	0.134	3281	8924	0.50	60.0
76	10.94	0.134	3281	8924	0.50	60.0
77	16.41	0.14	4921	11240	0.50	60.0
78	16.41	0.14	4921	11240	0.50	60.0
79	16.41	0.14	4921	11240	0.50	60.0
80	16.41	0.14	4921	11240	0.50	60.0
81	16.41	0.14	4921	11240	0.50	60.0
82	16.41	0.14	4921	11240	0.50	60.0
83	16.41	0.14	4921	11240	0.50	60.0
84	16.41	0.14	4921	11240	0.50	60.0
85	16.41	0.14	4921	11240	0.50	60.0
86	16.41	0.14	4921	11240	0.50	60.0
87	20.51	0.144	6562	14270	0.50	64.0
88	20.51	0.144	6562	14270	0.50	64.0
89	20.51	0.144	6562	14270	0.50	64.0
90	20.51	0.144	6562	14270	0.50	64.0
91	20.51	0.144	6562	14270	0.50	64.0
92	20.51	0.144	6562	14270	0.50	64.0
93	20.51	0.144	6562	14270	0.50	64.0
94	20.51	0.144	6562	14270	0.50	64.0
95	27.34	0.15	8203	15420	0.25	60.0
96	27.34	0.15	8203	15420	0.25	60.0
97	27.34	0.15	8203	15420	0.25	60.0
98	27.34	0.15	8203	15420	0.25	60.0
99	27.34	0.15	8203	15420	0.25	60.0
100	27.34	0.15	8203	15420	0.25	60.0
101	30.00	0.157	9285	16080	0.10	61.9
Half-space		0.157	9285	16080	0.10	--

Table 03.3.1-2 Input 270-500 Soil Properties (Sheet 1 of 3)

Layer #	Thickness (ft)	Unit Weight (kcf)	Vs (ft/sec)	Vp (ft/sec)	Damping %	Shear Wave Passage Frequency (Hz)
1	5.58	0.125	1178	5106	1.65	42.2
2	5.58	0.125	1175	5198	2.10	42.1
3	7.00	0.125	1175	5214	2.44	33.6
4	5.38	0.125	1180	5115	2.49	43.9
5	5.38	0.125	1167	5141	2.81	43.4
6	6.67	0.125	1202	5233	2.89	36.1
7	6.67	0.125	1232	5323	2.97	37.0
8	3.41	0.125	1256	5457	3.10	73.6
9	3.41	0.125	1256	5457	3.10	73.6
10	4.29	0.125	1301	5658	3.14	60.6
11	4.29	0.125	1301	5658	3.14	60.6
12	4.29	0.125	1277	5618	3.36	59.5
13	4.29	0.125	1277	5618	3.36	59.5
14	4.29	0.125	1271	5625	3.52	59.3
15	4.29	0.125	1271	5625	3.52	59.3
16	4.29	0.125	1327	5872	3.48	61.9
17	4.29	0.125	1327	5872	3.48	61.9
18	4.69	0.125	1309	5806	2.71	55.8
19	4.69	0.125	1309	5806	2.71	55.8
20	4.69	0.125	1352	5992	2.70	57.7
21	4.69	0.125	1352	5992	2.70	57.7
22	4.69	0.125	1350	6001	2.76	57.6
23	4.69	0.125	1350	6001	2.76	57.6
24	4.69	0.125	1332	5956	2.86	56.8
25	4.69	0.125	1332	5956	2.86	56.8
26	4.69	0.125	1419	6309	2.76	60.5
27	4.69	0.125	1419	6309	2.76	60.5
28	4.69	0.125	1448	6427	2.76	61.8
29	4.69	0.125	1448	6427	2.76	61.8
30	5.00	0.131	1504	6632	2.63	60.2
31	5.00	0.131	1504	6632	2.63	60.2
32	5.00	0.131	1541	6790	2.62	61.6
33	5.00	0.131	1541	6790	2.62	61.6
34	5.00	0.131	1578	6956	2.60	63.1
35	5.00	0.131	1578	6956	2.60	63.1
36	5.00	0.131	1575	6958	2.65	63.0
37	5.00	0.131	1575	6958	2.65	63.0
38	5.00	0.131	1589	7029	2.66	63.6
39	5.00	0.131	1589	7029	2.66	63.6
40	5.00	0.131	1592	7052	2.70	63.7
41	5.00	0.131	1592	7052	2.70	63.7
42	5.30	0.131	1616	7160	2.70	61.0
43	5.30	0.131	1616	7160	2.70	61.0
44	5.30	0.131	1710	7317	2.30	64.6
45	5.30	0.131	1710	7317	2.30	64.6
46	5.75	0.131	1771	7563	2.26	61.6
47	5.75	0.131	1771	7563	2.26	61.6
48	5.75	0.131	1684	7245	2.42	58.6
49	5.75	0.131	1684	7245	2.42	58.6
50	5.89	0.131	1691	7291	2.44	57.4
51	5.89	0.131	1691	7291	2.44	57.4
52	5.89	0.131	1691	7291	2.44	57.4
53	5.89	0.131	1705	7358	2.47	57.9

Table 03.3.1-2 Input 270-500 Soil Properties (Sheet 2 of 3)

Layer #	Thickness (ft)	Unit Weight (kcf)	Vs (ft/sec)	Vp (ft/sec)	Damping %	Shear Wave Passage Frequency (Hz)
54	5.89	0.131	1705	7358	2.47	57.9
55	5.89	0.131	1705	7358	2.47	57.9
56	5.89	0.131	1759	7574	2.43	59.7
57	5.89	0.131	1759	7574	2.43	59.7
58	5.89	0.131	1759	7574	2.43	59.7
59	6.08	0.131	1795	7723	2.42	59.0
60	6.08	0.131	1795	7723	2.42	59.0
61	6.08	0.131	1795	7723	2.42	59.0
62	6.08	0.131	1776	7665	2.50	58.4
63	6.08	0.131	1776	7665	2.50	58.4
64	6.08	0.131	1776	7665	2.50	58.4
65	6.08	0.131	1752	7591	2.57	57.6
66	6.08	0.131	1752	7591	2.57	57.6
67	6.08	0.131	1752	7591	2.57	57.6
68	6.08	0.131	1749	7585	2.62	57.5
69	6.08	0.131	1749	7585	2.62	57.5
70	6.08	0.131	1749	7585	2.62	57.5
71	6.67	0.131	1768	7659	2.62	53.0
72	6.67	0.131	1768	7659	2.62	53.0
73	6.67	0.131	1768	7659	2.62	53.0
74	6.67	0.131	1747	7600	2.69	52.4
75	6.67	0.131	1747	7600	2.69	52.4
76	6.67	0.131	1747	7600	2.69	52.4
77	6.67	0.131	1788	7767	2.66	53.6
78	6.67	0.131	1788	7767	2.66	53.6
79	6.67	0.131	1788	7767	2.66	53.6
80	6.67	0.131	1791	7791	2.69	53.7
81	6.67	0.131	1791	7791	2.69	53.7
82	6.67	0.131	1791	7791	2.69	53.7
83	6.67	0.131	1817	7903	2.68	54.5
84	6.67	0.131	1817	7903	2.68	54.5
85	6.67	0.131	1817	7903	2.68	54.5
86	6.67	0.131	1780	7770	2.77	53.4
87	6.67	0.131	1780	7770	2.77	53.4
88	6.67	0.131	1780	7770	2.77	53.4
89	5.20	0.131	1783	7791	2.78	68.5
90	5.20	0.131	1783	7791	2.78	68.5
91	10.25	0.131	2376	7795	0.50	46.3
92	10.25	0.131	2376	7795	0.50	46.3
93	10.25	0.131	2376	7795	0.50	46.3
94	10.25	0.131	2376	7795	0.50	46.3
95	10.25	0.131	2376	7795	0.50	46.3
96	10.25	0.131	2376	7795	0.50	46.3
97	10.25	0.131	2376	7795	0.50	46.3
98	10.25	0.131	2376	7795	0.50	46.3
99	10.25	0.131	2376	7795	0.50	46.3
100	10.25	0.131	2376	7795	0.50	46.3
101	10.25	0.131	2376	7795	0.50	46.3
102	10.25	0.131	2376	7795	0.50	46.3
103	10.25	0.131	2376	7795	0.50	46.3
104	10.25	0.131	2376	7795	0.50	46.3
105	10.25	0.131	2376	7795	0.50	46.3
106	10.25	0.131	2376	7795	0.50	46.3

Table 03.3.1-2 Input 270-500 Soil Properties (Sheet 3 of 3)

Layer	Thickness	Unit Weight	Vs	Vp	Damping	S-Wave Passage
#	(ft)	(kcf)	(ft/sec)	(ft/sec)	%	Frequency (Hz)
107	13.67	0.134	3281	8924	0.50	48.0
108	13.67	0.134	3281	8924	0.50	48.0
109	13.67	0.134	3281	8924	0.50	48.0
110	13.67	0.134	3281	8924	0.50	48.0
111	13.67	0.134	3281	8924	0.50	48.0
112	13.67	0.134	3281	8924	0.50	48.0
113	13.67	0.134	3281	8924	0.50	48.0
114	13.67	0.134	3281	8924	0.50	48.0
115	13.67	0.134	3281	8924	0.50	48.0
116	13.67	0.134	3281	8924	0.50	48.0
117	13.67	0.134	3281	8924	0.50	48.0
118	13.67	0.134	3281	8924	0.50	48.0
119	20.51	0.140	4922	11240	0.50	48.0
120	20.51	0.140	4922	11240	0.50	48.0
121	20.51	0.140	4922	11240	0.50	48.0
122	20.51	0.140	4922	11240	0.50	48.0
123	20.51	0.140	4922	11240	0.50	48.0
124	20.51	0.140	4922	11240	0.50	48.0
Half-space		0.140	4922	11240	0.50	--

Table 03.3.1-3 Input 560-500 Soil Properties (Sheet 1 of 2)

Layer	Thickness	Unit Weight	Vs	Vp	Damping	Shear Wave Passage Frequency (Hz)
#	(ft)	(kcf)	(ft/sec)	(ft/sec)	%	
1	5.58	0.125	1066	4647	2.16	38.2
2	5.58	0.125	1378	5147	2.58	49.4
3	7.00	0.125	1377	5279	3.10	39.3
4	5.38	0.125	1429	4998	2.71	53.2
5	5.38	0.125	1440	4946	2.62	53.6
6	6.67	0.130	1611	5150	2.56	48.3
7	6.67	0.131	1645	5208	2.60	49.3
8	4.00	0.131	1627	5240	2.81	81.3
9	4.00	0.131	1627	5240	2.81	81.3
10	6.00	0.131	1906	5515	2.25	63.5
11	6.00	0.131	1906	5515	2.25	63.5
12	6.00	0.131	1906	5515	2.25	63.5
13	7.25	0.131	2262	6146	2.08	62.4
14	7.25	0.131	2262	6146	2.08	62.4
15	7.25	0.131	2249	6357	2.19	62.0
16	7.25	0.131	2249	6357	2.19	62.0
17	6.67	0.131	2230	6010	2.30	66.9
18	6.67	0.131	2230	6010	2.30	66.9
19	6.67	0.131	2230	6010	2.30	66.9
20	6.67	0.131	2218	6206	1.80	66.5
21	6.67	0.131	2218	6206	1.80	66.5
22	6.67	0.131	2218	6206	1.80	66.5
23	7.56	0.131	2452	6557	1.72	64.9
24	7.56	0.131	2452	6557	1.72	64.9
25	7.56	0.131	2452	6557	1.72	64.9
26	7.56	0.131	2440	6774	1.78	64.6
27	7.56	0.131	2440	6774	1.78	64.6
28	7.56	0.131	2440	6774	1.78	64.6
29	7.56	0.131	2430	6970	1.84	64.3
30	7.56	0.131	2430	6970	1.84	64.3
31	7.56	0.131	2430	6970	1.84	64.3
32	10.00	0.131	2747	7485	1.71	54.9
33	10.00	0.131	2747	7485	1.71	54.9
34	10.50	0.131	2739	7567	1.75	52.2
35	10.50	0.131	2739	7567	1.75	52.2
36	6.25	0.131	2798	7457	1.55	89.5
37	6.25	0.131	2798	7457	1.55	89.5
38	6.25	0.131	2795	7444	1.57	89.4
39	6.25	0.131	2795	7444	1.57	89.4
40	6.25	0.131	2793	7422	1.58	89.4
41	6.25	0.131	2793	7422	1.58	89.4
42	6.25	0.131	2790	7409	1.59	89.3
43	6.25	0.131	2790	7409	1.59	89.3
44	6.25	0.131	2787	7393	1.61	89.2
45	6.25	0.131	2787	7393	1.61	89.2
46	6.25	0.131	2785	7535	1.62	89.1
47	6.25	0.131	2785	7535	1.62	89.1
48	6.25	0.131	2783	7574	1.63	89.0
49	6.25	0.131	2783	7574	1.63	89.0
50	6.25	0.131	2781	7561	1.65	89.0
51	6.25	0.131	2781	7561	1.65	89.0
52	6.25	0.131	2779	7539	1.66	88.9
53	6.25	0.131	2779	7539	1.66	88.9
54	6.25	0.131	2777	7518	1.67	88.9

Table 03.3.1-3 Input 560-500 Soil Properties (Sheet 2 of 2)

Layer #	Thickness (ft)	Unit Weight (kcf)	Vs (ft/sec)	Vp (ft/sec)	Damping %	Shear Wave Passage Frequency (Hz)
55	6.25	0.131	2777	7518	1.67	88.9
56	6.25	0.131	2775	7525	1.68	88.8
57	6.25	0.131	2775	7525	1.68	88.8
58	6.25	0.131	2773	7650	1.69	88.7
59	6.25	0.131	2773	7650	1.69	88.7
60	6.25	0.131	2771	7688	1.71	88.7
61	6.25	0.131	2771	7688	1.71	88.7
62	6.25	0.131	2769	7666	1.72	88.6
63	6.25	0.131	2769	7666	1.72	88.6
64	6.25	0.131	2767	7645	1.73	88.5
65	6.25	0.131	2767	7645	1.73	88.5
66	6.25	0.131	2766	7624	1.74	88.5
67	6.25	0.131	2766	7624	1.74	88.5
68	6.25	0.131	2764	7602	1.75	88.4
69	6.25	0.131	2764	7602	1.75	88.4
70	6.25	0.131	2762	7714	1.76	88.4
71	6.25	0.131	2762	7714	1.76	88.4
72	6.56	0.131	2760	7826	1.78	84.1
73	6.56	0.131	2760	7826	1.78	84.1
74	7.43	0.131	2759	7804	1.79	74.3
75	7.43	0.131	2759	7804	1.79	74.3
76	11.72	0.134	3461	9415	0.50	59.1
77	11.72	0.134	3461	9415	0.50	59.1
78	11.72	0.134	3461	9415	0.50	59.1
79	11.72	0.134	3461	9415	0.50	59.1
80	11.72	0.134	3461	9415	0.50	59.1
81	11.72	0.134	3461	9415	0.50	59.1
82	11.72	0.134	3461	9415	0.50	59.1
83	11.72	0.134	3461	9415	0.50	59.1
84	11.72	0.134	3461	9415	0.50	59.1
85	11.72	0.134	3461	9415	0.50	59.1
86	11.72	0.134	3461	9415	0.50	59.1
87	11.72	0.134	3461	9415	0.50	59.1
88	11.72	0.134	3461	9415	0.50	59.1
89	11.72	0.134	3461	9415	0.50	59.1
90	16.41	0.140	4921	11240	0.50	60.0
91	16.41	0.140	4921	11240	0.50	60.0
92	16.41	0.140	4921	11240	0.50	60.0
93	16.41	0.140	4921	11240	0.50	60.0
94	16.41	0.140	4921	11240	0.50	60.0
95	16.41	0.140	4921	11240	0.50	60.0
96	16.41	0.140	4921	11240	0.50	60.0
97	16.41	0.140	4921	11240	0.50	60.0
98	16.41	0.140	4921	11240	0.50	60.0
99	16.41	0.140	4921	11240	0.50	60.0
100	23.44	0.144	6562	14270	0.50	56.0
101	23.44	0.144	6562	14270	0.50	56.0
102	23.44	0.144	6562	14270	0.50	56.0
103	23.44	0.144	6562	14270	0.50	56.0
104	23.44	0.144	6562	14270	0.50	56.0
105	23.44	0.144	6562	14270	0.50	56.0
106	23.44	0.144	6562	14270	0.50	56.0
107	25.00	0.150	8203	15420	0.25	65.6
108	25.00	0.150	8203	15420	0.25	65.6
Half-space		0.150	8203	15420	0.25	--

Table 03.3.1-4 Input 900-100 Soil Properties

Layer #	Thickness (ft)	Unit Weight (kcf)	Vs (ft/sec)	Vp (ft/sec)	Damping %	Shear Wave Passage Frequency (Hz)
1	5.58	0.126	1514	4756	1.68	54.2
2	5.58	0.131	1925	5272	1.90	69.0
3	7.00	0.131	2078	5054	2.10	59.4
4	5.38	0.131	2457	5913	1.71	91.4
5	5.38	0.131	2694	6506	1.50	100.2
6	6.67	0.131	2997	7639	1.50	89.9
7	6.67	0.132	3069	7786	1.49	92.1
8	5.50	0.134	3249	8160	1.51	118.2
9	5.50	0.134	3249	8160	1.51	118.2
10	10.00	0.134	4103	9920	1.28	82.0
11	10.00	0.134	4103	9920	1.28	82.0
12	11.50	0.140	5315	12172	1.18	92.4
13	11.50	0.140	5315	12172	1.18	92.4
14	4.00	0.142	5634	12325	1.17	281.6
15	23.44	0.150	8623	16210	0.25	73.6
16	23.44	0.150	8623	16210	0.25	73.6
17	23.44	0.150	8623	16210	0.25	73.6
18	23.44	0.150	8623	16210	0.25	73.6
19	23.44	0.150	8623	16210	0.25	73.6
20	23.44	0.150	8623	16210	0.25	73.6
21	23.44	0.150	8623	16210	0.25	73.6
22	25.00	0.157	9285	16080	0.10	74.3
23	25.00	0.157	9285	16080	0.10	74.3
24	25.00	0.157	9285	16080	0.10	74.3
25	25.00	0.157	9285	16080	0.10	74.3
26	25.00	0.157	9285	16080	0.10	74.3
27	25.00	0.157	9285	16080	0.10	74.3
28	25.00	0.157	9285	16080	0.10	74.3
29	25.00	0.157	9285	16080	0.10	74.3
30	25.00	0.157	9285	16080	0.10	74.3
31	25.00	0.157	9285	16080	0.10	74.3
32	25.00	0.157	9285	16080	0.10	74.3
33	25.00	0.157	9285	16080	0.10	74.3
34	25.00	0.157	9285	16080	0.10	74.3
35	25.00	0.157	9285	16080	0.10	74.3
36	25.00	0.157	9285	16080	0.10	74.3
37	25.00	0.157	9285	16080	0.10	74.3
38	25.00	0.157	9285	16080	0.10	74.3
39	25.00	0.157	9285	16080	0.10	74.3
40	25.00	0.157	9285	16080	0.10	74.3
41	25.00	0.157	9285	16080	0.10	74.3
42	25.00	0.157	9285	16080	0.10	74.3
43	25.00	0.157	9285	16080	0.10	74.3
44	25.00	0.157	9285	16080	0.10	74.3
45	25.00	0.157	9285	16080	0.10	74.3
46	25.00	0.157	9285	16080	0.10	74.3
47	25.00	0.157	9285	16080	0.10	74.3
48	25.00	0.157	9285	16080	0.10	74.3
49	25.00	0.157	9285	16080	0.10	74.3
50	25.00	0.157	9285	16080	0.10	74.3
Half-space		0.157	9285	16080	0.10	--

Table 03.3.1-5 Input 900-200 Soil Properties

Layer #	Thickness (ft)	Unit Weight (kcf)	Vs (ft/sec)	Vp (ft/sec)	Damping %	Shear Wave Passage Frequency (Hz)
1	5.58	0.126	1561	4917	1.70	55.9
2	5.58	0.131	2003	5478	1.85	71.8
3	7.00	0.131	2171	5266	2.04	62.0
4	5.38	0.131	2450	5909	1.73	91.2
5	5.38	0.131	2606	6327	1.55	97.0
6	6.67	0.131	2949	7538	1.54	88.5
7	6.67	0.132	3029	7705	1.53	90.9
8	5.50	0.134	3431	8608	1.48	124.8
9	5.50	0.134	3431	8608	1.48	124.8
10	10.00	0.134	3749	9101	1.35	75.0
11	10.00	0.134	3749	9101	1.35	75.0
12	11.50	0.140	4731	10856	1.25	82.3
13	11.50	0.140	4731	10856	1.25	82.3
14	12.50	0.142	5660	12397	1.20	90.6
15	12.50	0.142	5660	12397	1.20	90.6
16	17.00	0.144	6589	13884	0.93	77.5
17	17.00	0.144	6589	13884	0.93	77.5
18	15.00	0.147	6576	13407	0.95	87.7
19	15.00	0.147	6576	13407	0.95	87.7
20	15.00	0.147	6576	13407	0.95	87.7
21	20.51	0.150	7958	14961	0.25	77.6
22	20.51	0.150	7958	14961	0.25	77.6
23	20.51	0.150	7958	14961	0.25	77.6
24	20.51	0.150	7958	14961	0.25	77.6
25	20.51	0.150	7958	14961	0.25	77.6
26	20.51	0.150	7958	14961	0.25	77.6
27	20.51	0.150	7958	14961	0.25	77.6
28	20.51	0.150	7958	14961	0.25	77.6
29	25.00	0.157	9285	16080	0.10	74.3
30	25.00	0.157	9285	16080	0.10	74.3
31	25.00	0.157	9285	16080	0.10	74.3
32	25.00	0.157	9285	16080	0.10	74.3
33	25.00	0.157	9285	16080	0.10	74.3
34	25.00	0.157	9285	16080	0.10	74.3
35	25.00	0.157	9285	16080	0.10	74.3
36	25.00	0.157	9285	16080	0.10	74.3
37	25.00	0.157	9285	16080	0.10	74.3
38	25.00	0.157	9285	16080	0.10	74.3
39	25.00	0.157	9285	16080	0.10	74.3
40	25.00	0.157	9285	16080	0.10	74.3
41	25.00	0.157	9285	16080	0.10	74.3
42	25.00	0.157	9285	16080	0.10	74.3
43	25.00	0.157	9285	16080	0.10	74.3
44	25.00	0.157	9285	16080	0.10	74.3
45	25.00	0.157	9285	16080	0.10	74.3
46	25.00	0.157	9285	16080	0.10	74.3
47	25.00	0.157	9285	16080	0.10	74.3
48	25.00	0.157	9285	16080	0.10	74.3
49	25.00	0.157	9285	16080	0.10	74.3
50	25.00	0.157	9285	16080	0.10	74.3
51	25.00	0.157	9285	16080	0.10	74.3
52	25.00	0.157	9285	16080	0.10	74.3
53	25.00	0.157	9285	16080	0.10	74.3
Half-space		0.157	9285	16080	0.10	--

Table 03.3.1-6 Input 2032-100 Soil Properties (Sheet 1 of 2)

Layer #	Thickness (ft)	Unit Weight (kcf)	Vs (ft/sec)	Vp (ft/sec)	Damping %	Shear Wave Passage Frequency (Hz)
1	5.58	0.140	5202	9711	2.82	186.3
2	5.58	0.140	5541	10189	2.83	198.5
3	7.00	0.140	5814	10534	2.84	166.1
4	5.38	0.140	5889	10461	2.85	219.1
5	5.38	0.140	6034	10599	2.86	224.5
6	6.67	0.140	6240	10880	2.87	187.2
7	6.67	0.140	6556	11356	2.90	196.7
8	8.00	0.140	6968	12069	2.98	174.2
9	16.67	0.140	7258	12572	2.98	87.1
10	16.67	0.140	7571	13113	2.98	90.9
11	16.66	0.140	8017	13886	2.98	96.2
12	22.00	0.157	8890	15397	0.10	80.8
13	22.00	0.157	8890	15397	0.10	80.8
14	22.00	0.157	8890	15397	0.10	80.8
15	22.00	0.157	8890	15397	0.10	80.8
16	22.00	0.157	8890	15397	0.10	80.8
17	22.00	0.157	8890	15397	0.10	80.8
18	22.00	0.157	8890	15397	0.10	80.8
19	22.00	0.157	8890	15397	0.10	80.8
20	22.00	0.157	8890	15397	0.10	80.8
21	22.00	0.157	8890	15397	0.10	80.8
22	22.00	0.157	8890	15397	0.10	80.8
23	22.00	0.157	8890	15397	0.10	80.8
24	22.00	0.157	8890	15397	0.10	80.8
25	22.00	0.157	8890	15397	0.10	80.8
26	22.00	0.157	8890	15397	0.10	80.8
27	22.00	0.157	8890	15397	0.10	80.8
28	22.00	0.157	8890	15397	0.10	80.8
29	22.00	0.157	8890	15397	0.10	80.8
30	22.00	0.157	8890	15397	0.10	80.8
31	22.00	0.157	8890	15397	0.10	80.8
32	22.00	0.157	8890	15397	0.10	80.8
33	22.00	0.157	8890	15397	0.10	80.8
34	22.00	0.157	8890	15397	0.10	80.8
35	22.00	0.157	8890	15397	0.10	80.8
36	22.00	0.157	8890	15397	0.10	80.8
37	22.00	0.157	8890	15397	0.10	80.8
38	22.00	0.157	8890	15397	0.10	80.8
39	22.00	0.157	8890	15397	0.10	80.8
40	22.00	0.157	8890	15397	0.10	80.8
41	22.00	0.157	8890	15397	0.10	80.8
42	22.00	0.157	8890	15397	0.10	80.8
43	22.00	0.157	8890	15397	0.10	80.8
44	22.00	0.157	8890	15397	0.10	80.8
45	22.00	0.157	8890	15397	0.10	80.8
46	22.00	0.157	8890	15397	0.10	80.8
47	22.00	0.157	8890	15397	0.10	80.8
48	22.00	0.157	8890	15397	0.10	80.8
49	22.00	0.157	8890	15397	0.10	80.8
50	22.00	0.157	8890	15397	0.10	80.8
51	22.00	0.157	8890	15397	0.10	80.8
52	22.00	0.157	8890	15397	0.10	80.8
53	22.00	0.157	8890	15397	0.10	80.8

Table 03.3.1-6 Input 2032-100 Soil Properties (Sheet 2 of 2)

Layer	Thickness	Unit Weight	Vs	Vp	Damping	Shear Wave Passage Frequency (Hz)
#	(ft)	(kcf)	(ft/sec)	(ft/sec)	%	
54	22.00	0.157	8890	15397	0.10	80.8
55	22.00	0.157	8890	15397	0.10	80.8
56	22.00	0.157	8890	15397	0.10	80.8
57	22.00	0.157	8890	15397	0.10	80.8
58	22.00	0.157	8890	15397	0.10	80.8
Half-space		0.157	8890	15397	0.10	--

Table 03.3.1-7 Site Model Depths

Soil Case	Depth of Fixed Layers (ft)	Half Space Vs (ft/s)	Cut-off Frequency (Hz)	Min. Variable Layer Depth (ft)	Min. Depth of Site Model (ft)
270-200	1050	9285	40	348	1398
270-500	951	4922	40	185	1136
560-500	1041	8203	50	246	1288
900-100	989	9285	50	279	1268
900-200	989	9285	50	279	1268
2032-100	1134	8890	50	267	1401

Notes: The Min. Variable Layer Depth is taken as 1.5*Vs/f where f is the Cut-off Frequency

The Min. Depth of Site Model is taken as the Depth of the Fixed Layers plus the Min. Variable Layer Depth

Table 03.3.1-8 Backfill Small-Strain Properties for Profiles 270-200, 270-500 and 560-500

Depth (ft)	Unit Weight (kcf)	Vs (ft/sec)	Vp (ft/sec)	Poisson's Ratio
0 - 3	0.125	650	1353	0.35
3 - 20	0.125	750	1561	0.35
20 - 40	0.125	900	1873	0.35

Table 03.3.1-9 Backfill Small-Strain Properties for Profiles 900-100, 900-200 and 2032-100

Depths (ft)	Unit Weight (kcf)	Vs (ft/sec)	Vp (ft/sec)	Poisson's Ratio
0 - 5	0.13	784	1467	0.3
5 - 10	0.13	959	1794	0.3
10 - 15	0.13	1038	1942	0.3
15 - 20	0.13	1088	2035	0.3
20 - 25	0.13	1160	2170	0.3
25 - 30	0.13	1193	2232	0.3
30 - 35	0.13	1231	2303	0.3
35 - 40	0.13	1265	2367	0.3
40 - 45	0.13	1295	2423	0.3
45 - 50	0.13	1324	2477	0.3
50 - 55	0.13	1351	2527	0.3

Table 03.3.1-10 Backfill Element Material Properties for 270-200

Bottom Depth (ft)	Unit Weight (kcf)	Vs (ft/sec)	Vp (ft/sec)	Damping	Poisson's Ratio
5.58	0.125	687.8	1453.7	0.020	0.36
11.16	0.125	712.1	1562.5	0.030	0.37
18.16	0.125	679.7	1562.5	0.040	0.38
23.54	0.125	770.7	1771.7	0.036	0.38
28.92	0.125	793.9	1871.2	0.041	0.39
35.59	0.125	783.6	1871.2	0.045	0.39
42.25	0.125	768.0	1871.2	0.050	0.40

Table 03.3.1-11 Backfill Element Material Properties for 270-500

Bottom Depth (ft)	Unit Weight (kcf)	Vs (ft/sec)	Vp (ft/sec)	Damping	Poisson's Ratio
5.58	0.125	684.2	1453.7	0.020	0.36
11.16	0.125	704.1	1562.5	0.035	0.37
18.16	0.125	662.9	1562.5	0.046	0.39
23.54	0.125	770.7	1771.7	0.037	0.38
28.92	0.125	788.8	1871.2	0.043	0.39
35.59	0.125	783.6	1871.2	0.046	0.39
42.25	0.125	768.0	1871.2	0.050	0.40

Table 03.3.1-12 Backfill Element Material Properties for 560-500

Bottom Depth (ft)	Unit Weight (kcf)	Vs (ft/sec)	Vp (ft/sec)	Damping	Poisson's Ratio
5.58	0.125	680.6	1453.7	0.023	0.36
11.16	0.125	716.0	1562.5	0.030	0.37
18.16	0.125	687.9	1562.5	0.037	0.38
23.54	0.125	784.7	1771.7	0.032	0.38
28.92	0.125	818.9	1871.2	0.035	0.38
35.59	0.125	823.8	1871.2	0.034	0.38
42.25	0.125	814.0	1871.2	0.036	0.38

Table 03.3.1-13 Backfill Element Material Properties for 900-100

Bottom Depth (ft)	Unit Weight (kcf)	Vs (ft/sec)	Vp (ft/sec)	Damping	Poisson's Ratio
5.58	0.130	795.3	1502.9	0.018	0.31
11.16	0.130	956.1	1825.6	0.022	0.31
18.16	0.130	1028.0	1994.3	0.025	0.32
23.54	0.130	1103.8	2118.6	0.020	0.31
28.92	0.130	1157.5	2210.1	0.021	0.31
35.59	0.130	1196.9	2297.4	0.020	0.31
42.25	0.130	1236.5	2386.0	0.021	0.32

Table 03.3.1-14 Backfill Element Material Properties for 900-200

Bottom Depth (ft)	Unit Weight (kcf)	Vs (ft/sec)	Vp (ft/sec)	Damping	Poisson's Ratio
5.58	0.130	795.3	1502.9	0.018	0.36
11.16	0.130	956.1	1825.6	0.022	0.37
18.16	0.130	1028.0	1994.3	0.025	0.38
23.54	0.130	1109.6	2118.6	0.020	0.38
28.92	0.130	1151.5	2210.1	0.021	0.39
35.59	0.130	1196.9	2297.4	0.021	0.39
42.25	0.130	1236.5	2386.0	0.022	0.40

Table 03.3.1-15 Backfill Element Material Properties for 2032-100

Bottom Depth (ft)	Unit Weight (kcf)	Vs (ft/sec)	Vp (ft/sec)	Damping	Poisson's Ratio
5.58	0.130	803.3	1502.9	0.014	0.30
11.16	0.130	975.8	1825.6	0.014	0.30
18.16	0.130	1066.0	1994.3	0.015	0.30
23.54	0.130	1132.4	2118.6	0.012	0.30
28.92	0.130	1181.4	2210.1	0.012	0.30
35.59	0.130	1228.0	2297.4	0.013	0.30
42.25	0.130	1275.4	2386.0	0.013	0.30

Table 03.3.4.1-1 S-Wave Vertical Mesh Passage Frequencies of the Excavated Volume Element

Layer	Thickness (ft)	Wave Passage Frequency (Hz)					
		270-200	270-500	560-500	900-100	900-200	2032-100
1	5.58	46.4	42.2	38.2	54.2	55.9	186.3
2	5.58	46.3	42.1	49.4	69.0	71.8	198.5
3	7.00	36.2	33.6	39.3	59.4	62.0	166.1
4	5.38	45.5	43.9	53.2	91.4	91.2	219.1
5	5.38	44.6	43.4	53.6	100.2	97.0	224.5
6	6.67	36.5	36.1	48.3	89.9	88.5	187.2
7	6.67	36.8	37.0	49.3	92.1	90.9	196.7

Table 03.3.4.1-2 NS Wave Passage Frequencies of the Excavated Volume Element

Layer	Average Mesh Size (ft)	Wave Passage Frequency (Hz)					
		270-200	270-500	560-500	900-100	900-200	2032-100
1	6.62	39.2	35.6	32.2	45.8	47.2	157.3
2	6.62	39.1	35.5	41.7	58.2	60.6	167.5
3	6.62	38.3	35.5	41.6	62.8	65.6	175.8
4	6.62	37.0	35.7	43.2	74.3	74.1	178.0
5	6.62	36.2	35.3	43.5	81.4	78.8	182.4
6	6.62	36.8	36.3	48.7	90.6	89.2	188.7
7	6.62	37.1	37.3	49.7	92.8	91.6	198.2

Table 03.3.4.1-3 EW Wave Passage Frequencies of the Excavated Volume Element

Layer	Average Mesh Size (ft)	Wave Passage Frequency (Hz)					
		270-200	270-500	560-500	900-100	900-200	2032-100
1	7.32	35.4	32.2	29.1	41.4	42.7	142.2
2	7.32	35.3	32.1	37.7	52.6	54.8	151.5
3	7.32	34.6	32.1	37.7	56.8	59.3	158.9
4	7.32	33.5	32.3	39.1	67.2	67.0	161.0
5	7.32	32.7	31.9	39.4	73.6	71.2	165.0
6	7.32	33.3	32.9	44.0	81.9	80.6	170.6
7	7.32	33.5	33.7	45.0	83.9	82.8	179.2

Table 03.3.5-1 Matrix of ACS SASSI Runs

Soil Case	Model	Cut-off Frequency (HZ)	Number of Frequencies Analyzed	Control Motion
270-200	SSI Uncracked	40	132	Foundation Bottom Level
	SSI Cracked			
	SSSI Uncracked			
	SSSI Cracked			
270-500	SSI Uncracked	40	132	Foundation Bottom Level
	SSI Cracked			
560-500	SSI Uncracked	50	152	Foundation Bottom Level
	SSI Cracked			
	SSSI Uncracked			
	SSSI Cracked			
900-100	SSI Uncracked	50	152	Foundation Bottom Level
	SSI Cracked			
	SSSI Uncracked			
	SSSI Cracked			
900-200	SSI Uncracked	50	152	Foundation Bottom Level
	SSI Cracked			
	SSSI Uncracked			
	SSSI Cracked			
2032-100	SSI Uncracked	50	152	Foundation Bottom Level
	SSI Cracked			

Table 03.3.5-2 Wave Passage Frequencies of the Model Below Foundation

Soil Case	Vertical Layer (Hz)	Horizontal Mesh (Hz)
270-200	55.8	32.5
270-500	46.3	34.3
560-500	52.2	44.5
900-100	73.6	88.8
900-200	74.3	93.7
2032-100	80.8	190.4

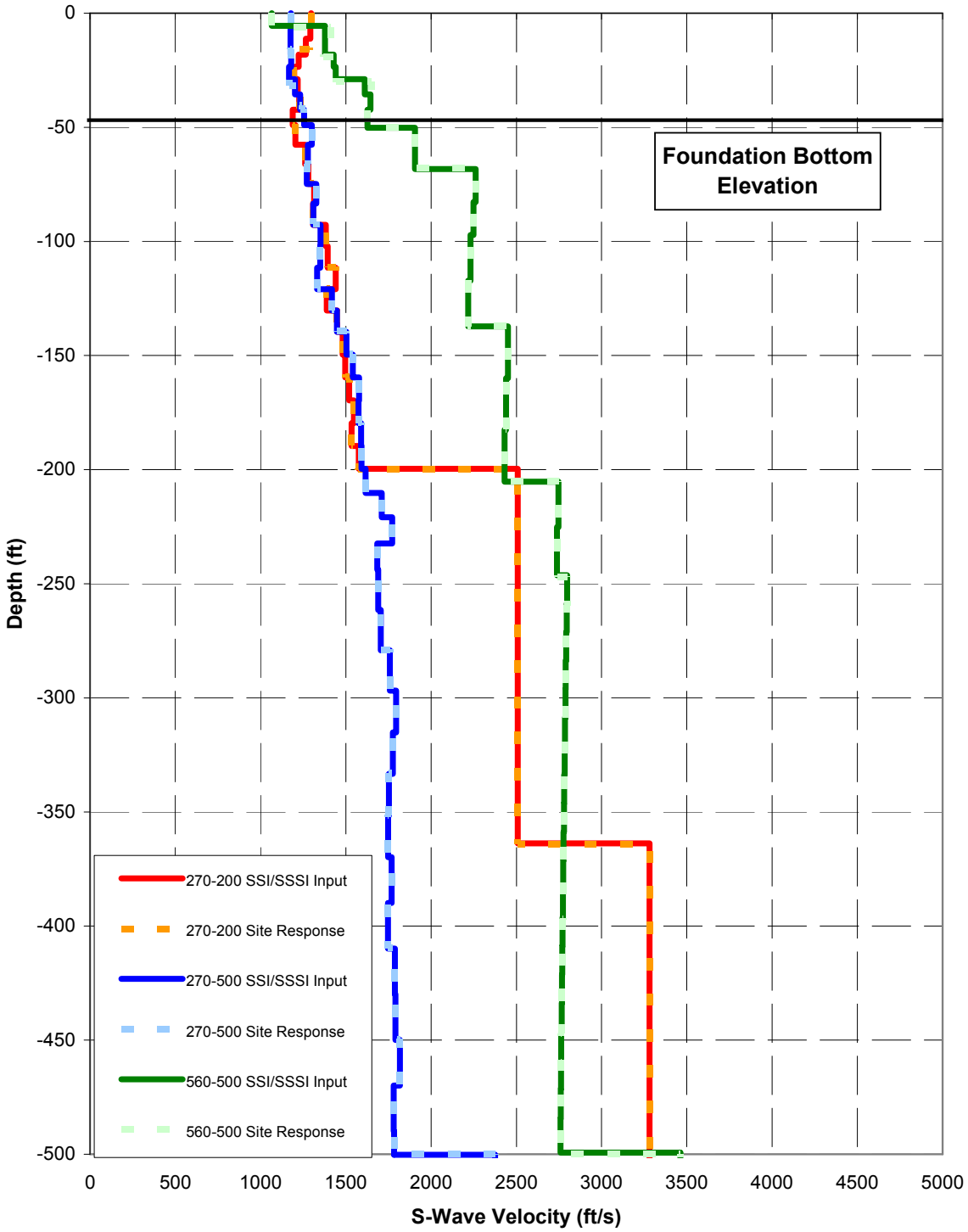

Figure 03.3.1-1 Shear Wave Velocity Profile V_S - Soil

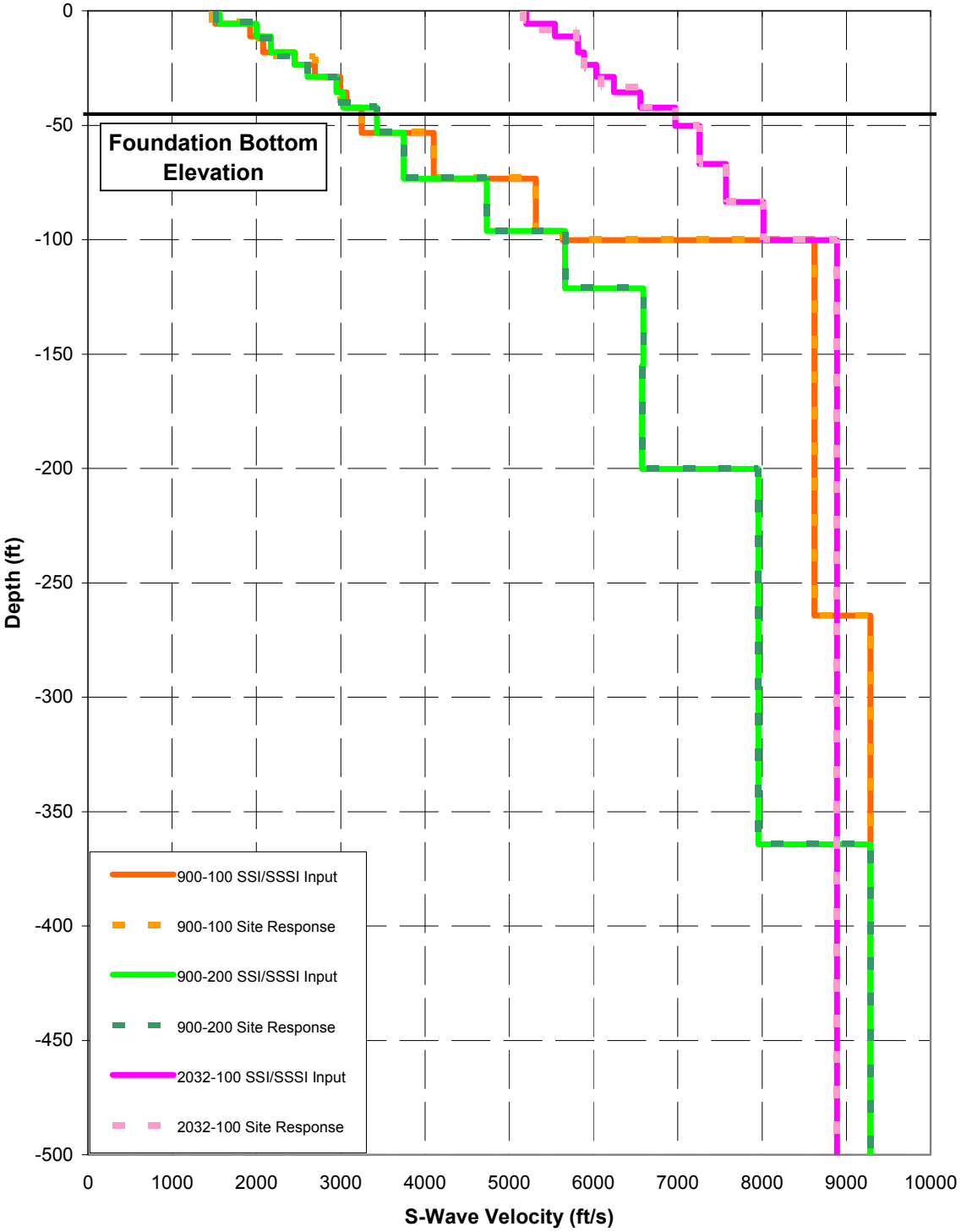

Figure 03.3.1-2 Shear Wave Velocity Profile V_S - Rock

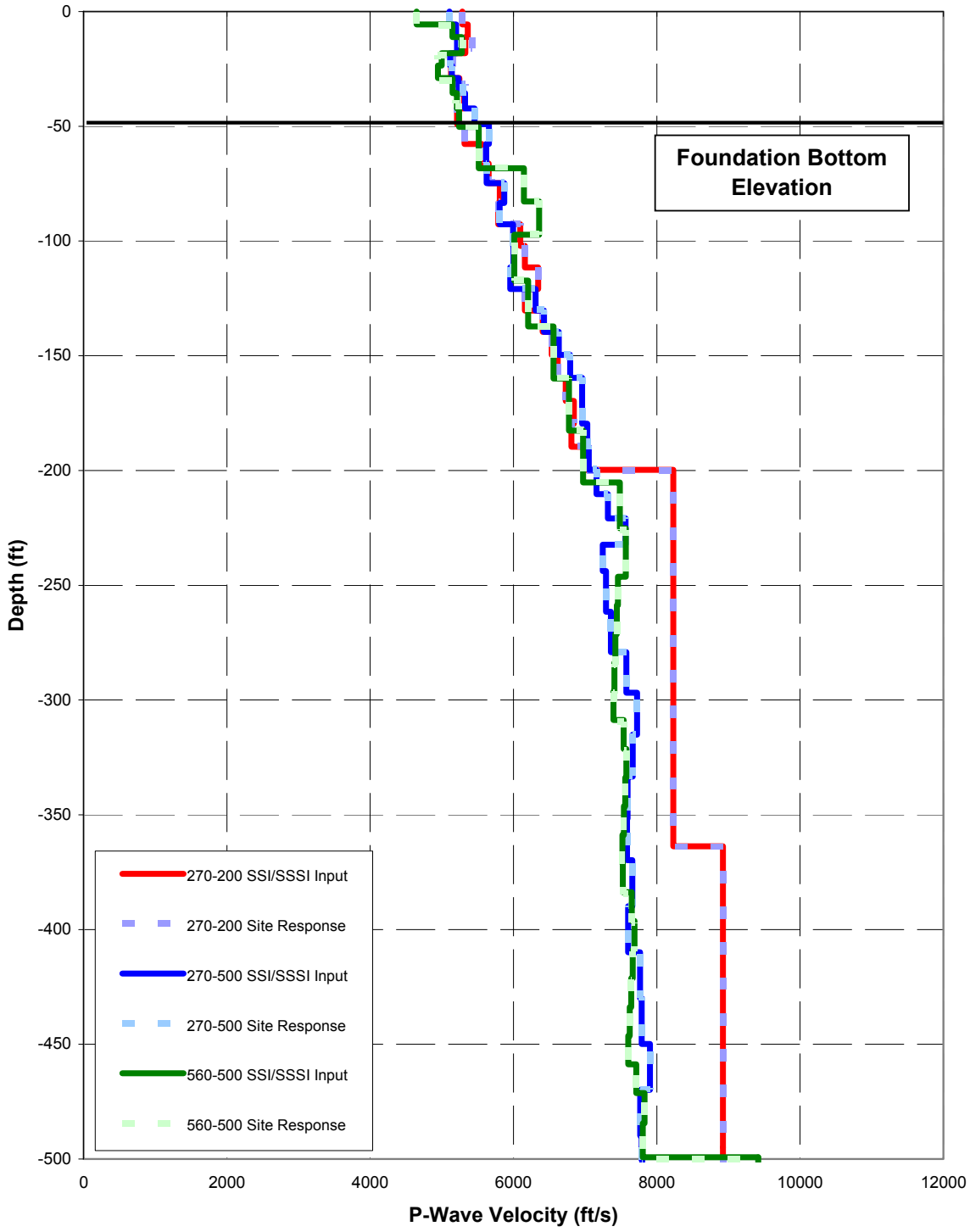

Figure 03.3.1-3 Compression Wave Velocity Profile V_P – Soil

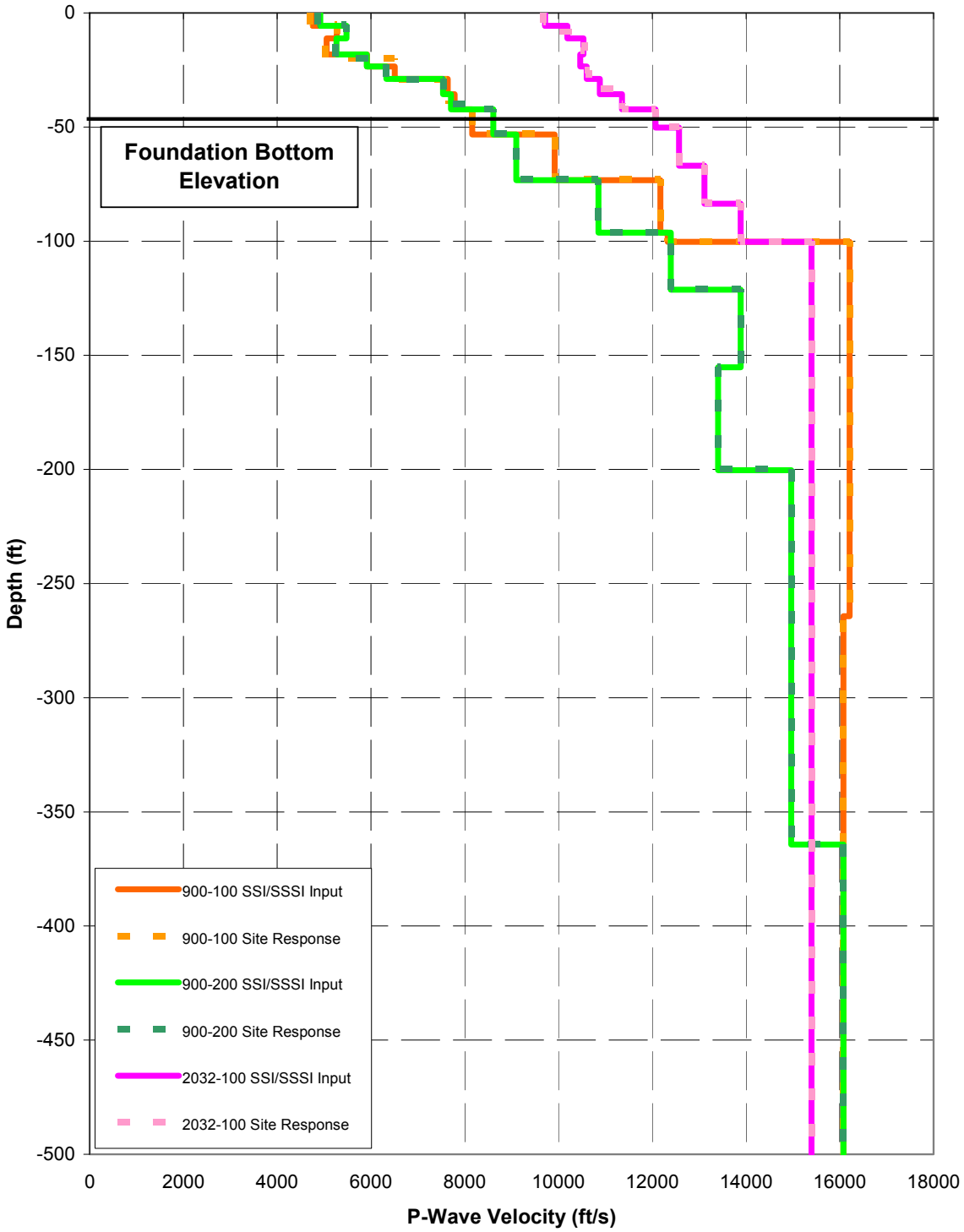

Figure 03.3.1-4 Compression Wave Velocity Profile V_P – Rock

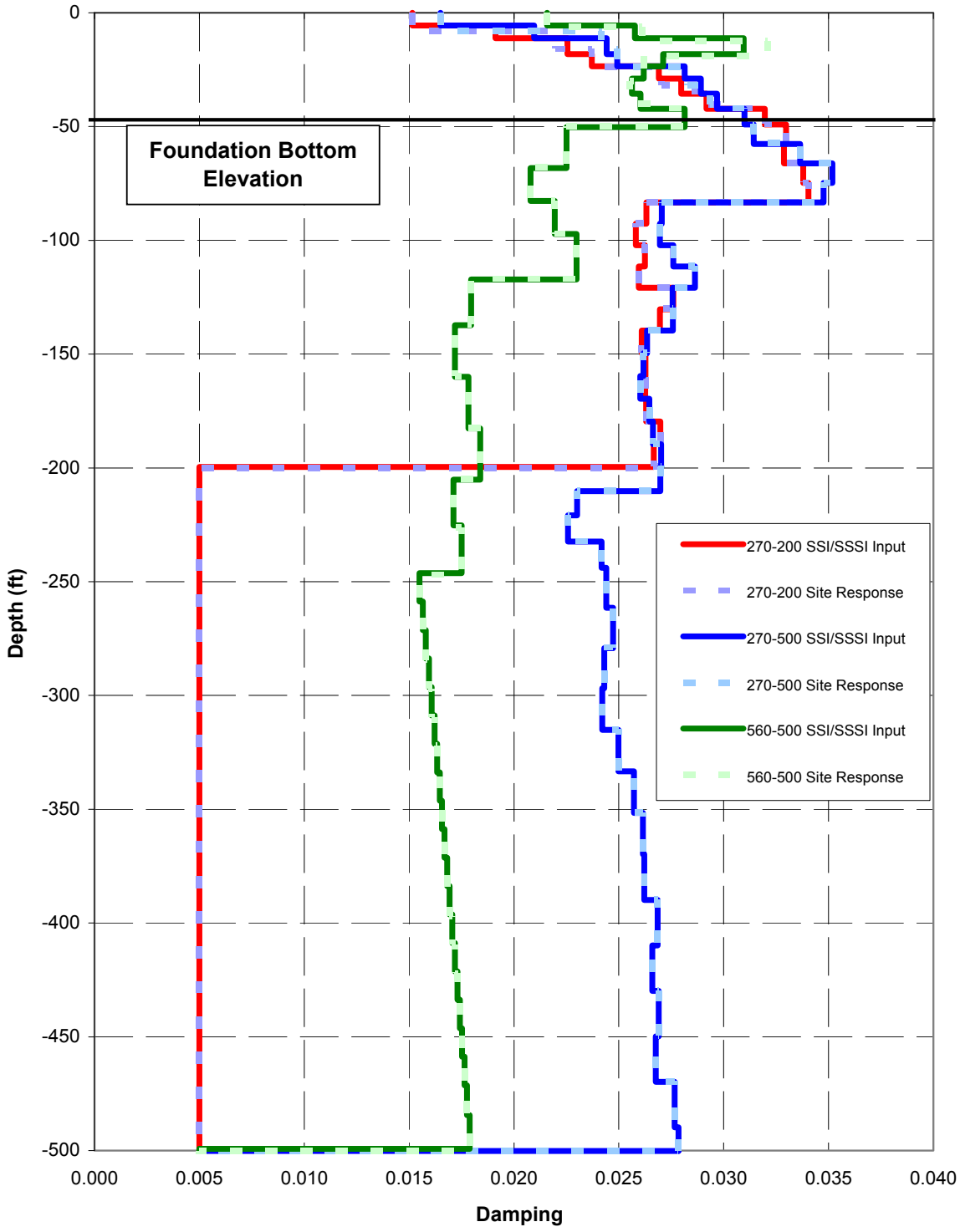

Figure 03.3.1-5 Shear Wave Damping Ratio Profile - Soil

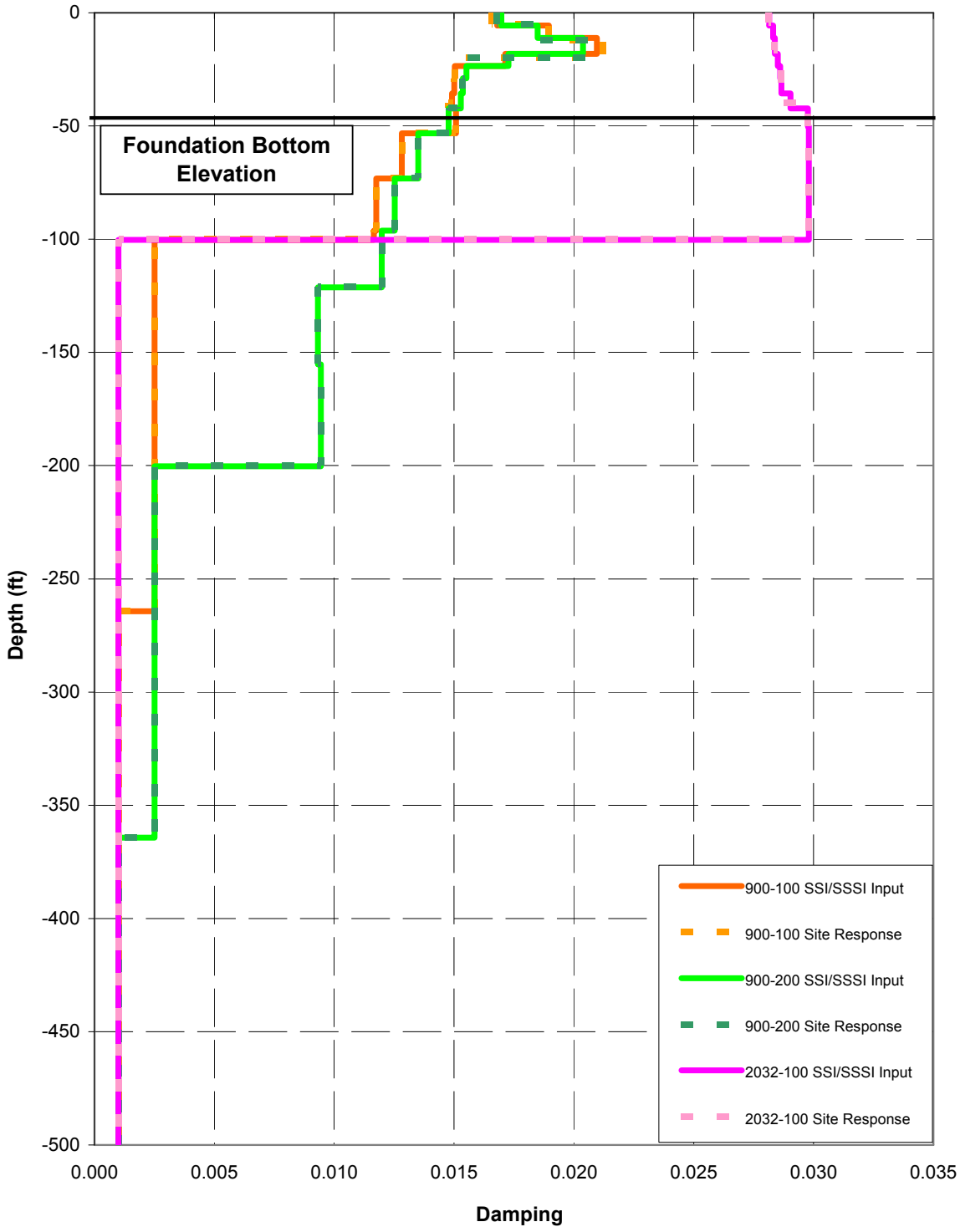

Figure 03.3.1-6 Shear Wave Damping Ratio Profile - Rock

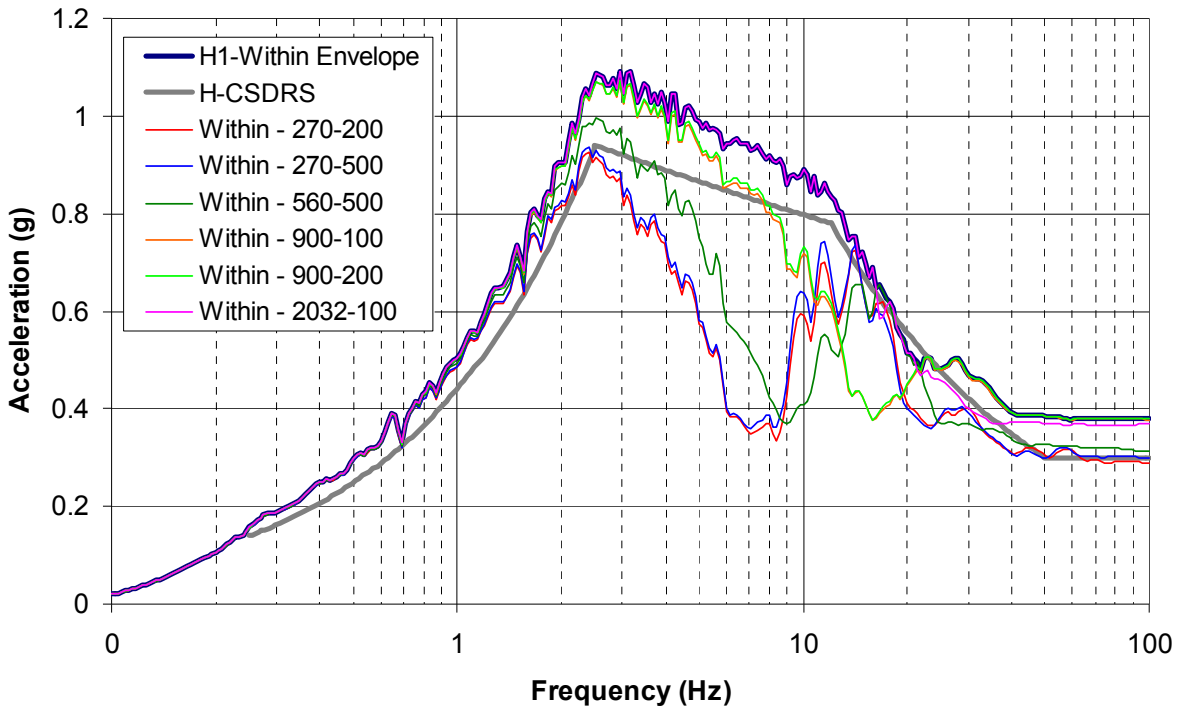

Figure 03.3.2-1 5% Damped Enveloped H1 (NS) Inlayer Response vs. Horizontal CSDRS

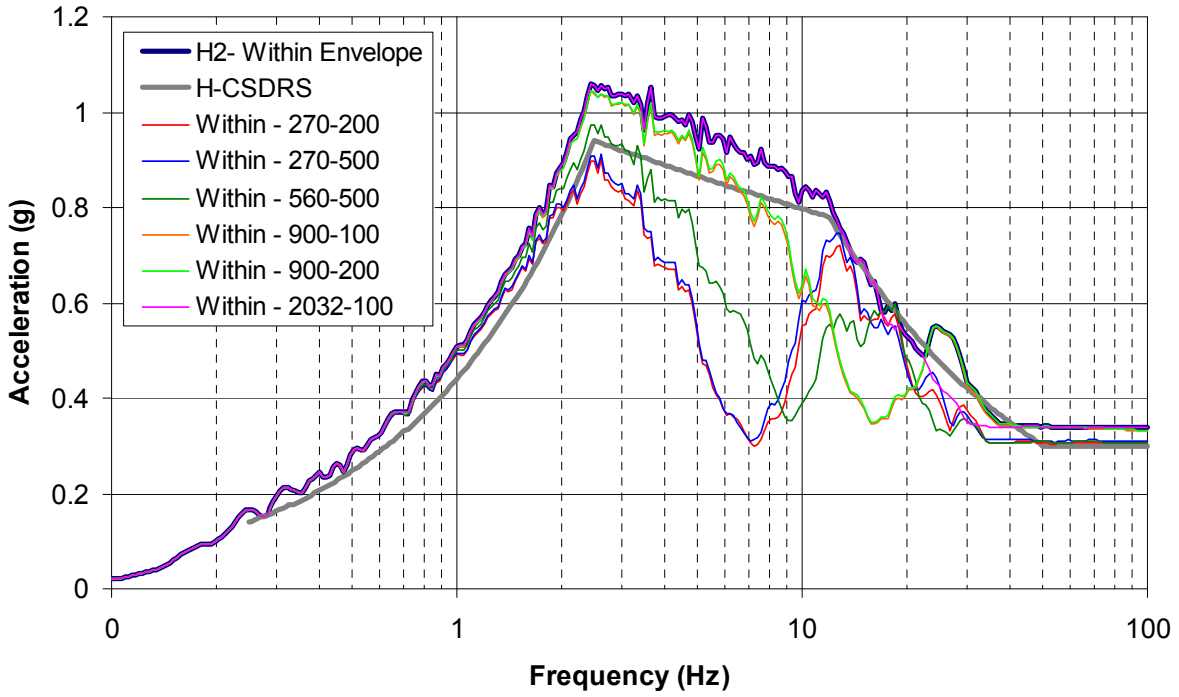

Figure 03.3.2-2 5% Damped Enveloped H2 (EW) Inlayer Response vs. Horizontal CSDRS

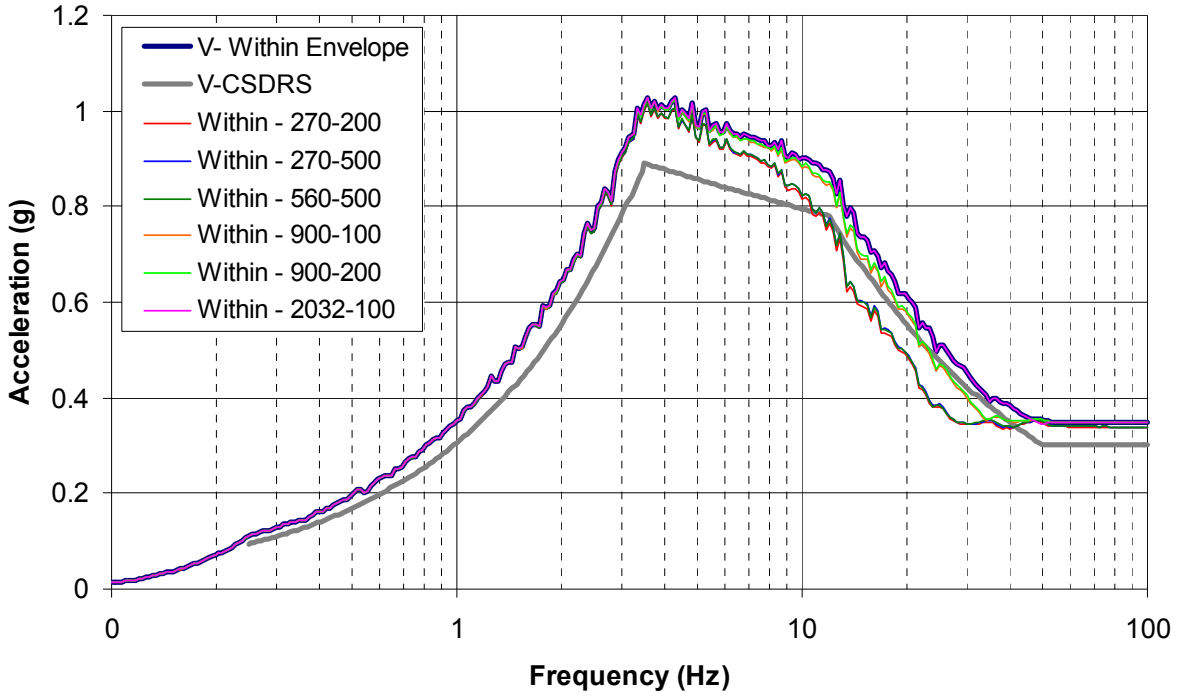

Figure 03.3.2-3 5% Damped Enveloped Vertical Inlayer Response vs. Vertical CSDRS

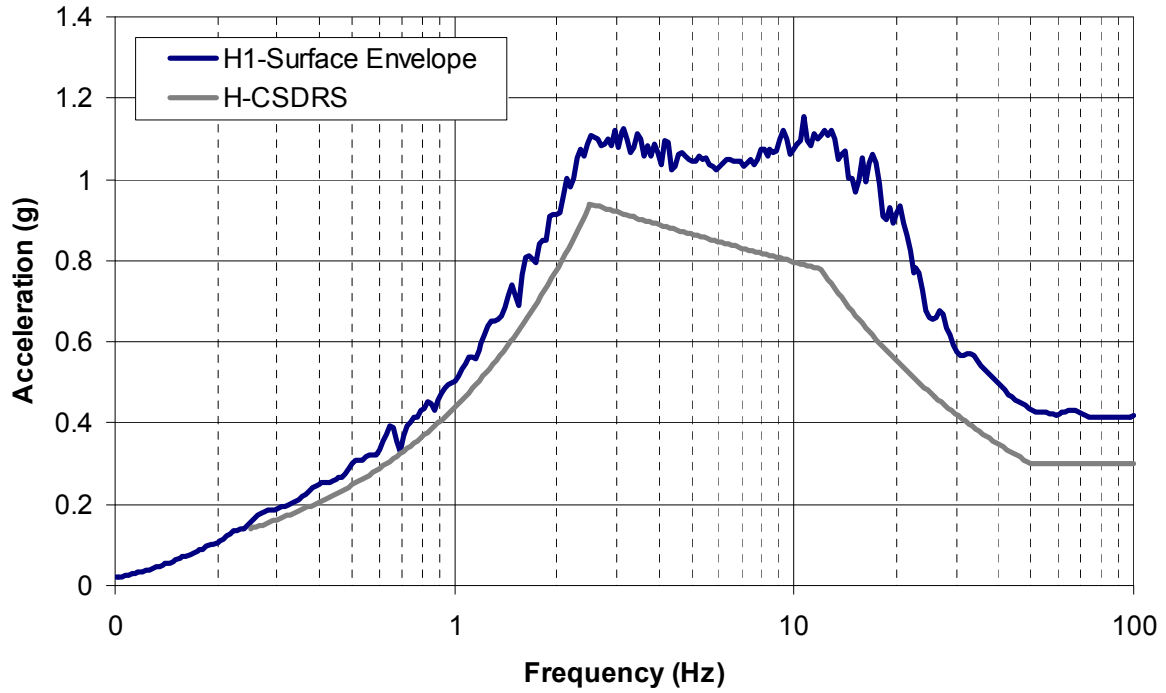

Figure 03.3.2-4 5% Damped Enveloped H1 (NS) Surface Response vs. Horizontal CSDRS

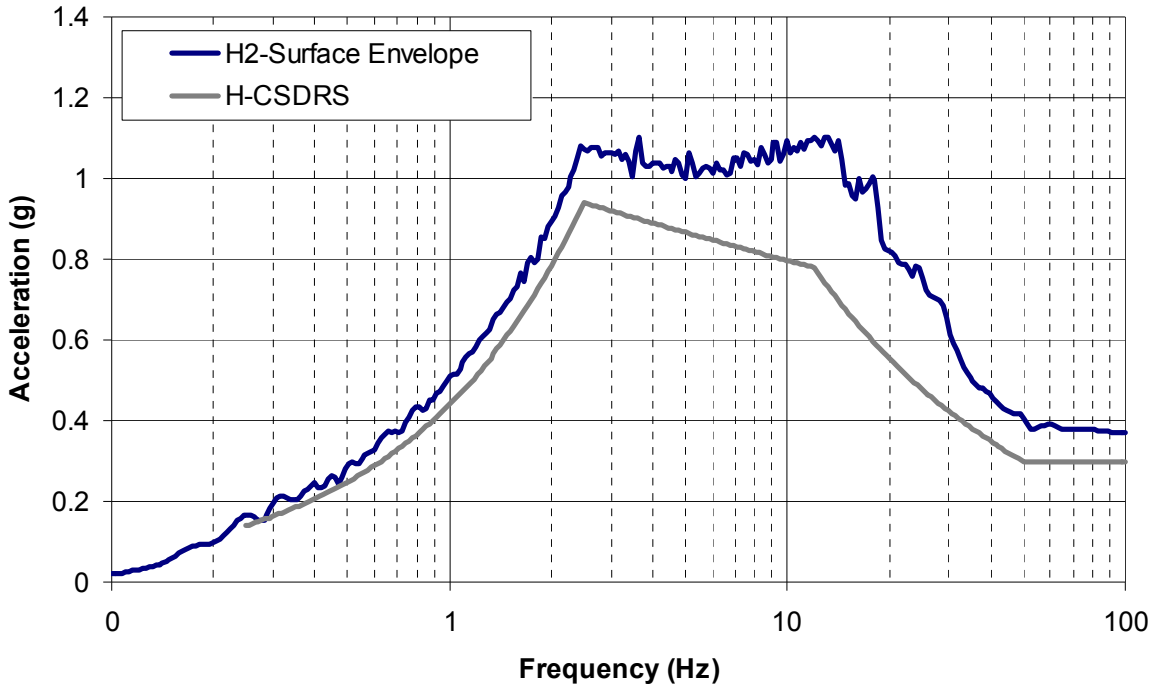

Figure 03.3.2-5 5% Damped Enveloped H2 (EW) Surface Response vs. Horizontal CSDRS

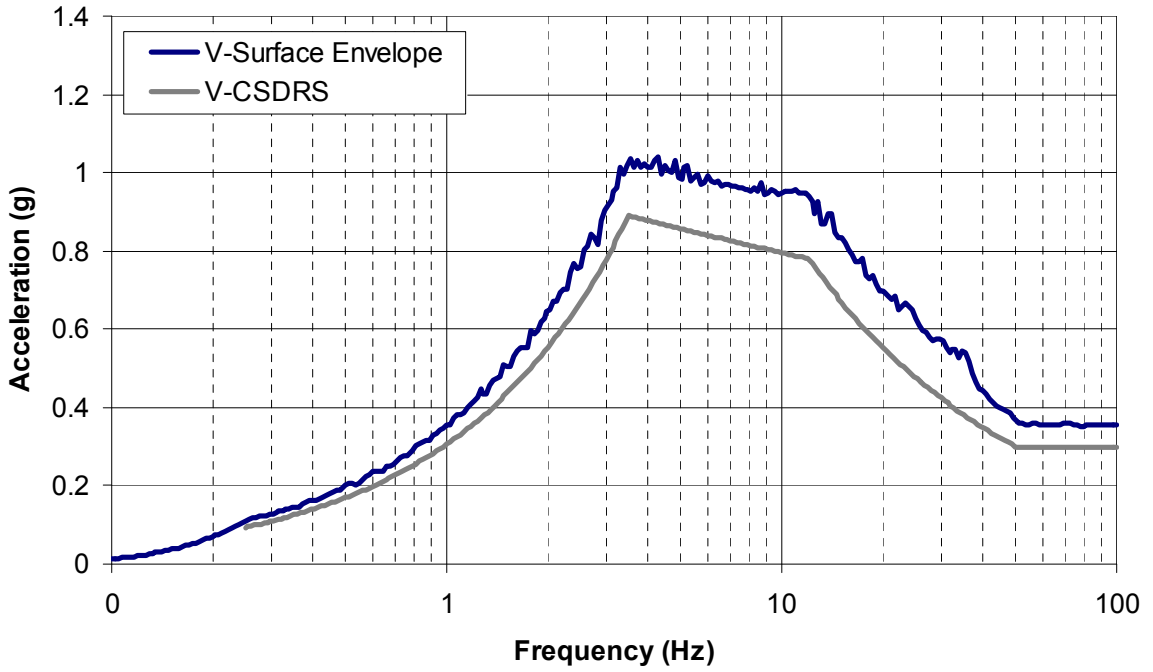

Figure 03.3.2-6 5% Damped Enveloped V Surface Response vs. Vertical CSDRS

Figure 03.3.4.1-1 R/B Complex Structural Elements

Figure 03.3.4.1-2 R/B Complex with Excavated Soil Volume Elements

Figure 03.3.4.1-3 Excavated Soil Volume Elements

Figure 03.3.4.1-4 R/B Complex with Backfill Soil Elements

Figure 03.3.4.1-5 Backfill Soil Elements

Figure 03.3.4.1-6 R/B Complex with Backfill and Free Field Soils (Looking South)

Figure 03.3.4.1-7 R/B Complex with Backfill and Free Field Soils (Looking West)

Figure 03.3.4.2-1 R/B Complex – T/B SSSI Structural Model and Backfill Elements

Figure 03.3.4.2-2 R/B Complex – T/B SSSI Excavated Volume Elements

Figure 03.3.4.2-3 SSSI Model with Backfill and Free Field Soils (Looking East)

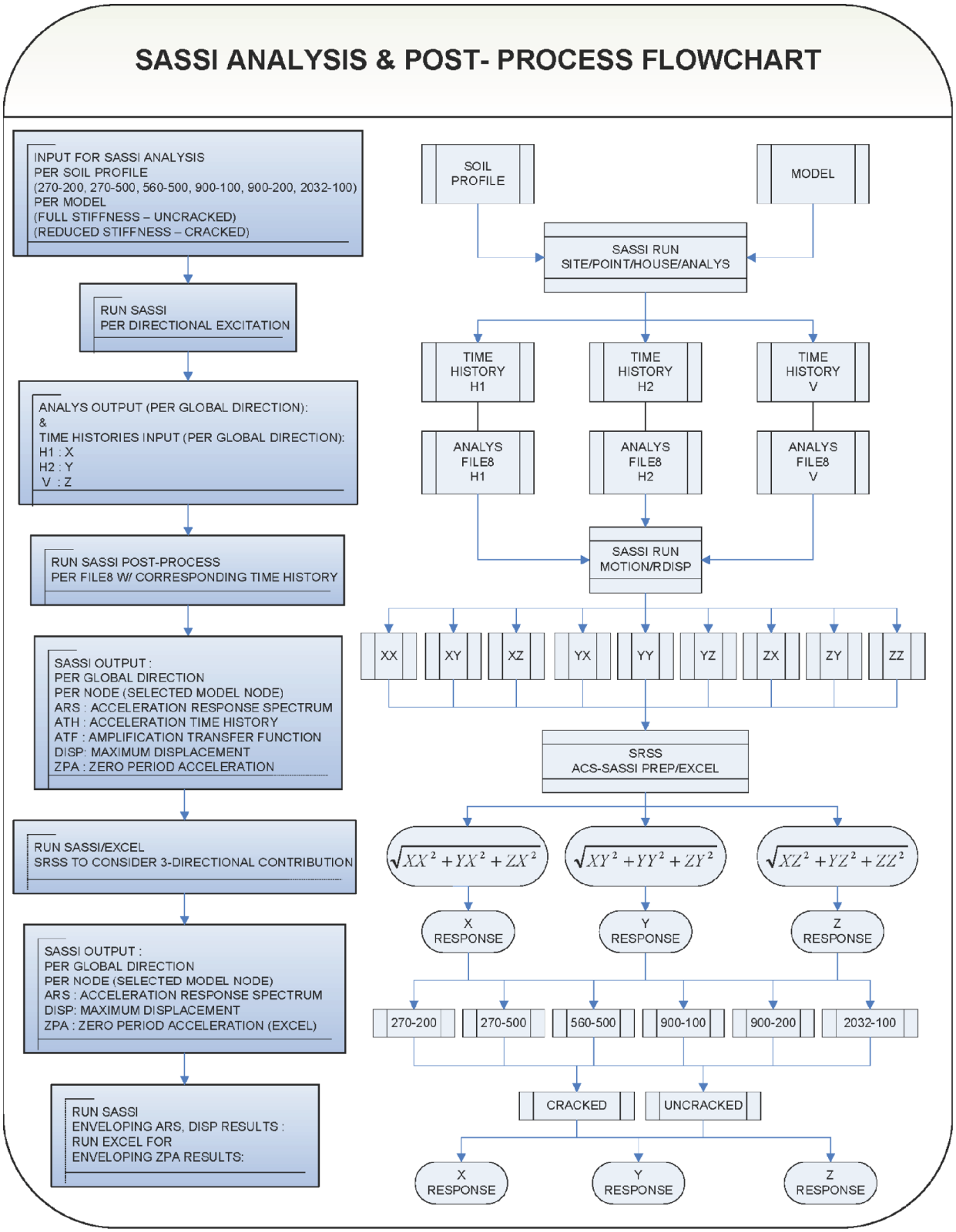

Figure 03.3.5-1 ACS SASSI Analysis Flow Chart

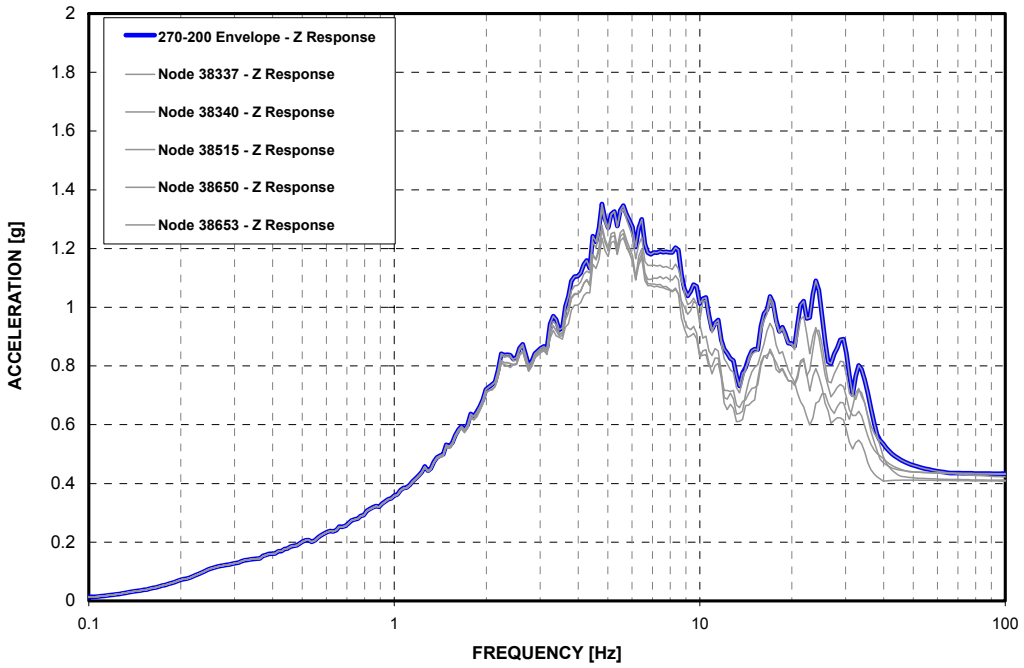

Figure 03.3.6-1 Example of ISRS Location Enveloping

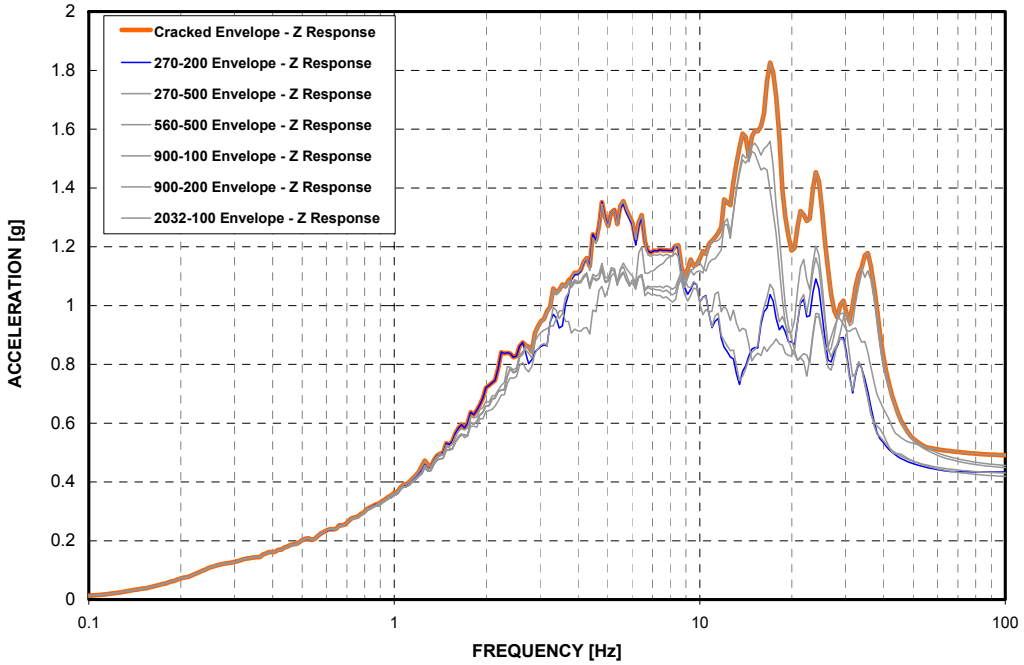

Figure 03.3.6-2 Example of ISRS Soil Case Enveloping

(The Location Envelope developed in Figure 03.3.6-1 is combined with similar envelopes developed for the other soil cases)

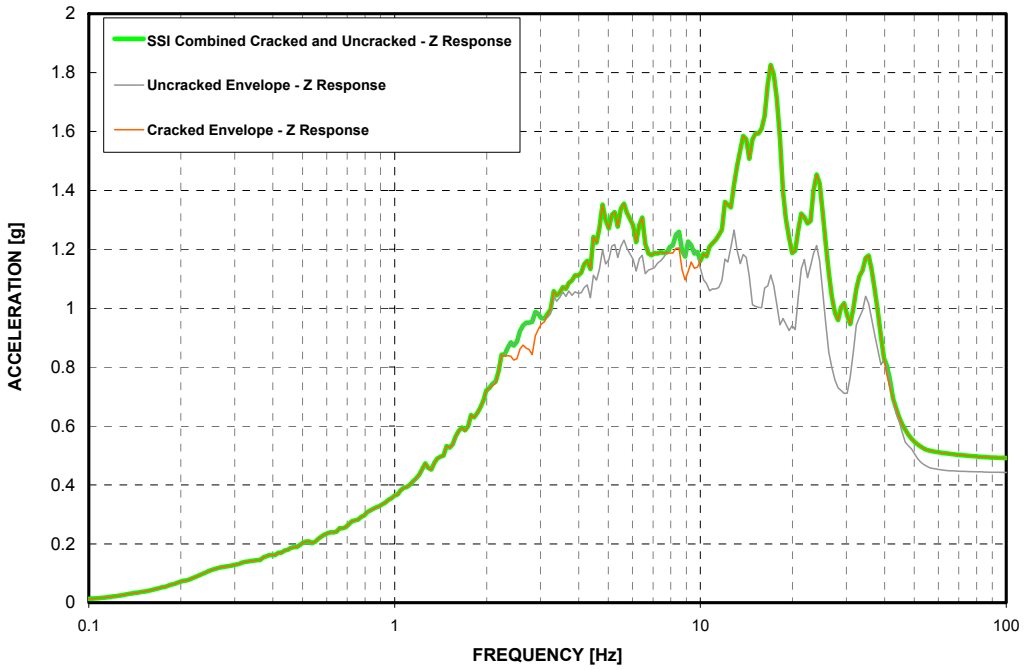

Figure 03.3.6-3 Example of ISRS Stiffness Enveloping

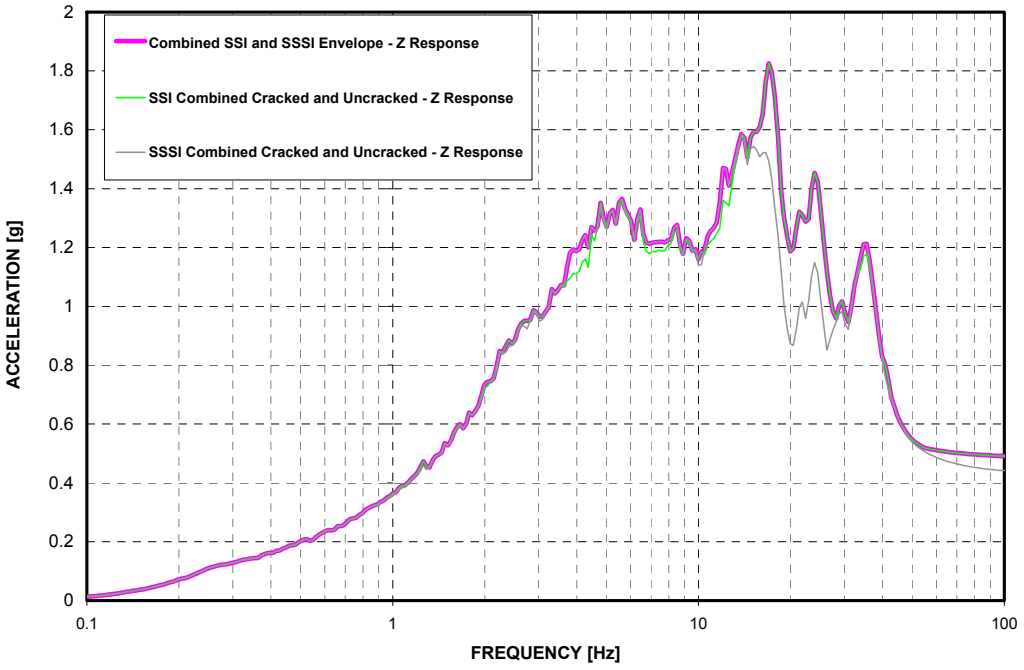

Figure 03.3.6-4 Example of Combining SSI and SSSI ISRS

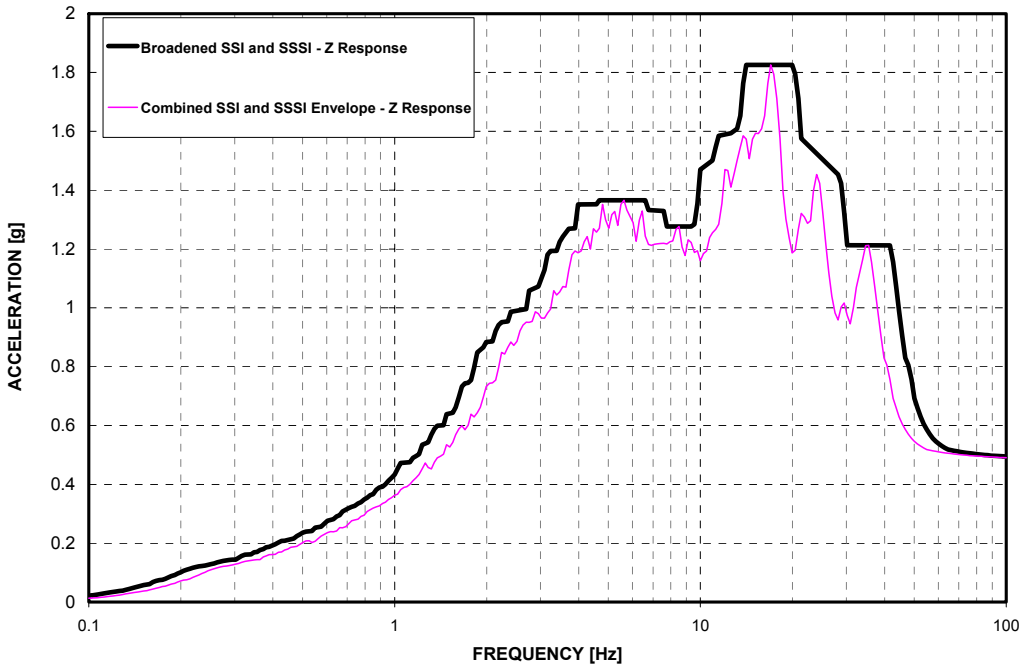

Figure 03.3.6-5 Example of ISRS Broadening

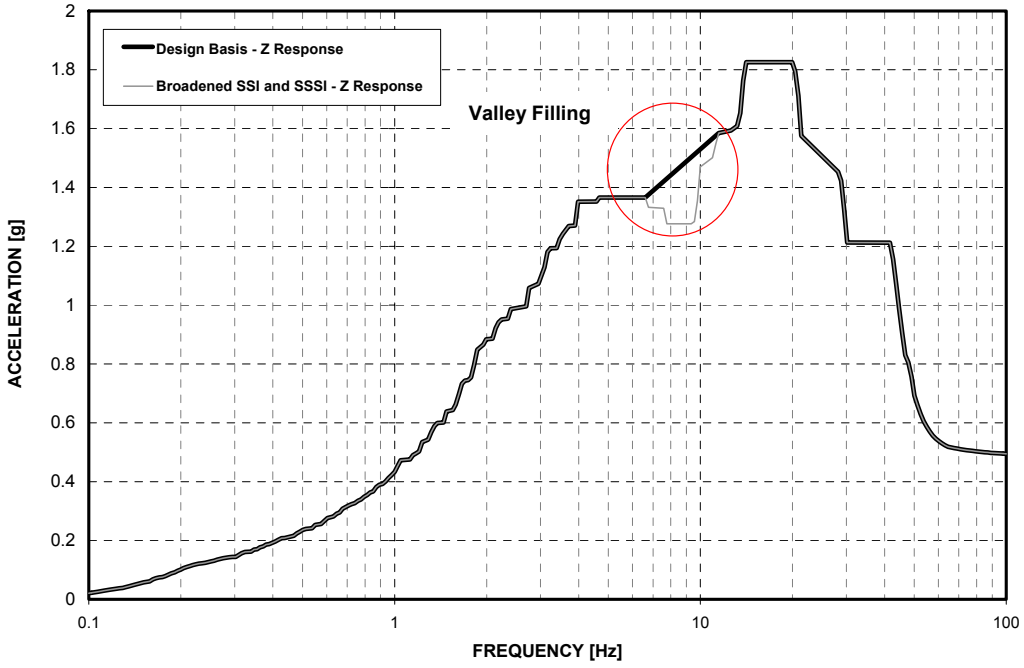

Figure 03.3.6-6 Example of Valley-Filling for Design Basis ISRS

03.4.0 ANALYSIS RESULTS

A total of twelve cases are analyzed for the R/B complex (SSI) and eight cases for the combined model of R/B complex and T/B (SSSI). The analysis cases are tabulated in Table 03.3.5-1. The Table also provides lists of the number of frequencies and cut-off frequencies of analyses. Appendix 3-D provides ATF plots from the SSI and SSSI analyses at various locations throughout the R/B complex. The ATF plots shown are generally smooth with no observed anomalies, and the plots reasonably capture the response peaks. This indicates that both the frequencies that were chosen to analyze and the coordination of the ATF interpolations are adequate. For development of design basis ISRS, the results from the twenty SSI and SSSI analyses are enveloped. Appendix 3-A provides node grouping information for major equipment and floor areas for which the ISRS are developed. The ISRS is the envelope of the responses from the nodes listed in the group. Appendix 3-B provides the resulting enveloped, broadened ISRS for a selection of equipment and structural locations throughout the R/B complex.

Comparison of the results from SSI and SSSI indicates that the presence of the T/B has minimal effects on the seismic responses of the R/B complex structures. The development of seismic loads in terms of the nodal maximum accelerations and resulting shear diagrams for the R/B complex structures are therefore based on SSI analysis results only. The nodal maximum accelerations and shear diagrams are the envelopes of the results from the analyses of the six generic soil profiles, and developed and presented for cracked and uncracked models separately. The nodal maximum accelerations and resulting shear diagrams serve as an indication of the seismic loads for equivalent-static analysis to determine the seismic demands to the structural members.

Seismic displacements, relative to the basemat, for various locations of CIS, PCCV and R/B are obtained from the SSI analysis. The results are provided for evaluation of the gap clearance between PCCV and CIS, PCCV and R/B during the design basis earthquake.

03.4.1 Summary of SSI and SSSI Effects on the R/B Complex

This section summarizes SSI effects on the R/B complex. The analysis presents information on first peak SSI frequencies, effects of soil profiles, embedment effects and effects of T/B on R/B complex.

03.4.1.1 First Peak SSI Frequency

For each model, the ATFs at the center of PCCV foundation bottom are calculated to evaluate the SSI effect by identifying the SSI frequencies as the first peak frequency of the ATF for each model. Table 03.4.1.1-1 summarizes the first peak frequencies for the twelve SSI runs and presents the information for the eight SSSI runs. The last column of the Table shows column frequencies of the side soil, i.e., embedment free field soils above foundation level that are identified from the ATF plots by reviewing the peaks. The structures have resonance responses at these frequencies for the case where the control motion is specified at foundation bottom level and SSI input as within time histories. Figure 03.4.1.1-1 through Figure 03.4.1.1-3 present the first peak frequencies in bar chart format for the cases analyzed for NS, EW and vertical responses, respectively. Figure 03.4.1.1-4 shows the shear column frequencies of the soils beneath the foundation for the six generic soil cases that are calculated using Equation 01.5.2.1 and Equation 01.5.2.2 of Part 1 of this TeR. The wide distributions of the first peak SSI frequencies and shear column frequencies of the subgrade soils demonstrate that the site-independent SSI analyses provide a range of SSI responses of

the R/B complex that envelope the possible response of the building at a vast number of candidate sites. For the soil profiles 270-200, 270-500, 560-500, the cracked and uncracked models have approximately the same first peak frequencies. However, for the harder soil profiles 900-200, 900-100 and 2032-100, the first peak frequencies are different between cracked and uncracked models. These indicate that the structural dynamic characteristic of the model dominates the response for the hard soil profiles while the soil dynamic characteristic dominates the response for softer soil profiles. These findings are consistent with generally accepted knowledge of SSI effects, i.e., SSI effects are more predominant for the softer subgrades than for the harder supporting soils/rocks.

03.4.1.2 Effect of Soil Profiles on the ARS

Figure 03.4.1.2-1 through Figure 03.4.1.2-6 present typical ARS plots to demonstrate the effects of soil profiles on the seismic response of the structure. The 3% damped ARS at the Reactor Vessel (RV) support location are plotted and compiled based on soil profiles for cracked and uncracked models. In the figures, thicker color lines represent ARS for soil profiles 270-500, 270-200 and 560-500 and thinner color lines for soil profiles 900-200, 900-100 and 2032-100. The plots indicate that for all the three directional (NS, EW and Vertical) responses, soil profiles 270-500, 270-200 and 560-500 control the response up to frequency of approximately 5 Hz. And the amplitudes of the responses from soil profiles 900-200, 900-100 and 2032-100 at higher frequency range are much greater than the ones from soil profiles 270-500, 270-200 and 560-500.

03.4.1.3 SSSI Effects

SSSI analyses are performed for soil profiles 270-200, 560-500, 900-200, and 900-100. The results indicate that for the same soil profiles, the presence of the T/B has negligible effects on the seismic response of the R/B complex. Generally, for the locations in R/B complex remote from the T/B, SSSI effect tends to slightly reduce the amplitude of the response to input from NS direction which is parallel to the direction that is defined by the two foundations, as indicated in Figure 03.4.1.3-1 and Figure 03.4.1.3-2. The responses to the EW direction input are practically the same for the SSI and SSSI analyses. Negligible differences are observed as shown in Figure 03.4.1.3-3 and Figure 03.4.1.3-4. This observation also applies to the vertical response as shown in Figure 03.4.1.3-5 and Figure 03.4.1.3-6. Figure 03.4.1.3-1, Figure 03.4.1.3-3, and Figure 03.4.1.3-5 show the ARS comparison of the SSI and SSSI analyses for the soil profile 270-200 uncracked at the reactor support (Top of Reactor Cavity). Figure 03.4.1.3-2, Figure 03.4.1.3-4, and Figure 03.4.1.3-6 show the ARS comparison of the SSI and SSSI analyses for the envelope of uncracked four selected soil profiles at reactor support (Top of Reactor Cavity).

Figure 03.4.1.3-7 through Figure 03.4.1.3-12 show the comparison of ARS at a point that is located at the ground floor south wall and the PCCV center line. Compared to the responses at the reactor support, minor SSSI amplifications are observed at frequencies higher than 7 Hz. The results of the SSSI analyses indicate that SSSI effects are small and have only modest impact on the design ISRS for SSCs located closer to the T/B. SSSI between the R/B complex and T/B for saturated site conditions either reduces the seismic response of the R/B complex structures at lower frequencies or has a negligible effect.

Based on the findings, it can be concluded that the standard design will not be affected by possible effects of SSSI between the R/B complex and Access Building (AC/B), or between the R/B complex and Tank House. Unlike the T/B, with size and weight comparable to the R/B

complex, these two buildings are too small and light to have any significant effect on the response of the much heavier and larger R/B complex.

The SSSI effects on ISRS are considered in the Standard Plant design by enveloping all twenty cases, twelve cases for SSI and eight cases for SSSI, as discussed at beginning of this section.

03.4.2 In-Structure Response Spectra (ISRS)

ISRS are generated at specific locations in the R/B complex following the methodology described in Section 03.3.6. Appendix 3-A provides figures showing the location within the R/B complex where the ISRS are developed. The 15% broadened envelope of the results obtained from the six generic soil profiles, cracked and uncracked , and both SSI and SSSI models, provide broad frequency ISRS. Appendix 3-B provides the design basis ISRS for a selection of equipment and structural locations throughout the R/B complex.

As an example, Figure 03.4.2-1 through Figure 03.3.4.2-3 present the design basis ISRS at the top of the Reactor Cavity for the NS, EW and Vertical directions, respectively. The top of the Reactor Cavity is comprised of eight structural nodes, presented in Table 3-A.1.1-1 and schematically in Figure 3-A.1.0-1. The design basis ISRS is developed with these eight structural nodes, using the process described in Section 03.3.6 and corresponding figures, Figure 03.3.6-1 through Figure 03.3.6-6.

03.4.3 Seismic Loads

The loads used for seismic design of R/B complex are developed following the methodology described in Section 03.3.7. The summary of weighted average floor accelerations of the PCCV, CIS, R/B, A/B, East PS/B and West PS/B are provided in Table 03.4.3-1 through Table 03.4.3-6. These Tables provide the cracked and uncracked results for the envelope of the six soil cases in all three directions. Figure 03.4.3-1 through Figure 03.4.3-12 present the story shear diagrams for these locations. The story shear diagrams present the comparison of the cracked (presented in dark blue) and uncracked (presented in pink) cases of the SSI model. The presented results (in kips) are the enveloped results of all six soil profiles. These values are representative design values, but will be confirmed during the design process. Table 03.4.3-7 provides the base shear forces at the bottom of the basemat. The table shows that 2032-100 is the governing soil case for all directional responses for both cracked and uncracked except for the cracked vertical response which is governed by the 900-200 soil case.

Figure 03.4.3-13 through Figure 03.4.3-15 present contour plots of the enveloped ZPA values at the R/B ground floor elevation. The plots for vertical acceleration contour are used to determine the out of plane accelerations for the slab design. The plots are created using ANSYS post-processing module (Reference 03-13).

03.4.4 Maximum Relative Displacements

Based on the methodology described in Section 03.3.8, the maximum displacements relative to the free field motion and basemat were determined from the SSI analysis of the R/B complex. The SRSS method was implemented to combine the motion inputs for determination of the nodal maximum displacements. The maximum displacement results envelope the maximum displacements of the soil cases analyzed. These results are tabulated in Table 03.4.4-1 and

Table 03.4.4-2.

The angular orientations are approximate locations. Based on the available model nodes, angular orientations were selected based on the available nodes between adjacent structures. The orientation of the PCCV - R/B and PCCV - CIS interfaces is based on North as 0 degrees with positive being Clockwise (CW).

The results were reviewed to determine the maximum coincident displacements which would result in the smallest gap between the structures. A conservative approach was taken where the maximum displacement across all elevations at a location in a structure was determined. This maximum was then compared with the maximum determined from the adjacent structure at the similar angular location. Adding to the conservative approach, the displacements compared are not radial results that occur along the same vector, but are the maximum scalar value found through the SRSS.

Following this approach, the minimum clearance, based on an initial minimum 4-inch gap between structures, was determined from the displacement results relative to center of the basemat to occur at the following locations:

- R/B-PCCV Interface - Table 03.4.4-1 shows that the largest coupled displacement of all the locations analyzed is 3.165 inches (1.728-inch displacement of R/B plus a 1.437-inch displacement of the PCCV) at 0 degrees CW of North for the cracked case. This results in a clearance of 0.835 inches (3.165 inches subtracted from the 4-inch gap).
- PCCV-CIS Interface – shows that the largest coupled displacement of all the locations analyzed is 1.599 inches (1.030-inch displacement of the PCCV plus a 0.569-inch displacement of the CIS) at 300 degrees CW of North for the cracked case. This results in a clearance of 2.401 inches (1.599 inches subtracted from the 4-inch gap).

Table 03.4.1.1-1 Summary of First Peak Frequencies for R/B Complex Basemat Response - SSI Model

Model	First Peak Frequency (Hz)			Soil Column Frequency - Horizontal (Hz)
	NS-Dir	EW-Dir	Vertical	
Cracked 270-200	1.50	1.50	2.25	7.25
Uncracked 270-200	1.50	1.50	2.25	
Cracked 270-500	1.50	1.50	2.00	7.00
Uncracked 270-500	1.50	1.50	2.00	
Cracked 560-500	2.25	2.25	3.25	9.25
Uncracked 560-500	2.50	2.25	3.50	
Cracked 900-100	3.00	3.00	7.75	16.00
Uncracked 900-100	4.00	4.00	9.75	
Cracked 900-200	2.90	2.95	7.25	16.00
Uncracked 900-200	3.90	3.75	8.50	
Cracked 2032-100	3.00	3.00	7.50	35.50
Uncracked 2032-100	4.00	4.00	9.75	

Table 03.4.1.1-2 Summary of First Peak Frequencies for R/B Complex Basemat Response – SSSI Model

Model	First Peak Frequency (Hz)			Soil Column Frequency - Horizontal (Hz)
	NS-Dir	EW-Dir	Vertical	
Cracked 270-200	1.50	1.50	2.25	7.25
Uncracked 270-200	1.50	1.50	2.25	
Cracked 560-500	2.25	2.25	3.25	9.25
Uncracked 560-500	2.50	2.25	3.50	
Cracked 900-100	3.00	3.00	7.75	16.00
Uncracked 900-100	4.00	4.00	9.75	
Cracked 900-200	2.90	2.95	7.25	16.00
Uncracked 900-200	3.90	3.75	8.50	

Table 03.4.3-1 Weighted Average Floor Accelerations - PCCV

Elevation	Cracked			Uncracked		
(ft)	AX(g)	AY(g)	AZ(g)	AX(g)	AY(g)	AZ(g)
2.583	0.432	0.403	0.503	0.468	0.418	0.413
32.146	0.543	0.562	0.612	0.617	0.555	0.490
50.181	0.628	0.737	0.693	0.766	0.656	0.555
68.215	0.728	0.846	0.759	0.890	0.755	0.607
86.250	0.838	0.923	0.820	1.014	0.831	0.658
99.812	0.923	0.969	0.861	1.105	0.873	0.693
113.375	1.042	1.045	0.908	1.225	1.007	0.739
131.375	1.160	1.138	0.953	1.347	1.140	0.802
145.583	1.264	1.279	1.030	1.465	1.579	0.910
165	1.450	1.315	1.020	1.582	1.347	0.900
187	1.639	1.450	1.115	1.801	1.503	1.010
204.092	1.877	1.573	1.285	2.063	1.655	1.303
232	2.000	1.635	1.417	2.193	1.734	1.555

Table 03.4.3-2 Weighted Average Floor Accelerations - CIS

Elevation	Cracked			Uncracked		
(ft)	AX(g)	AY(g)	AZ(g)	AX(g)	AY(g)	AZ(g)
2.583	0.408	0.401	0.460	0.433	0.390	0.394
9.500	0.423	0.409	0.466	0.441	0.413	0.402
16.000	0.451	0.423	0.471	0.457	0.453	0.406
23.583	0.450	0.421	0.489	0.458	0.461	0.425
32.222	0.484	0.441	0.503	0.471	0.521	0.447
40.394	0.553	0.524	0.600	0.538	0.618	0.683
49.5	0.612	0.592	0.565	0.607	0.702	0.530
59.083	0.677	0.685	0.584	0.661	0.792	0.564
67.25	0.681	0.719	0.563	0.689	0.832	0.534
75.417	0.794	0.846	0.773	0.755	0.943	0.697
87.722	1.116	1.068	0.685	0.948	1.191	0.657
106.181	1.884	1.427	0.753	1.492	1.756	0.793
112	1.658	1.386	0.721	1.317	1.471	0.656
127.833	2.598	1.597	0.759	1.840	1.567	0.673
138.583	2.881	1.791	0.794	1.969	1.694	0.690

Table 03.4.3-3 Weighted Average Floor Accelerations - R/B

Elevation	Cracked			Uncracked		
(ft)	AX(g)	AY(g)	AZ(g)	AX(g)	AY(g)	AZ(g)
-39.667	0.370	0.360	0.410	0.387	0.349	0.374
-26.333	0.377	0.367	0.420	0.395	0.353	0.377
-15.583	0.402	0.386	0.445	0.414	0.368	0.386
-8.583	0.406	0.398	0.453	0.425	0.381	0.390
2.583	0.445	0.422	0.482	0.452	0.428	0.417
25.250	0.578	0.512	0.544	0.575	0.558	0.508
35.170	0.627	0.558	0.554	0.620	0.610	0.510
48.500	0.744	0.682	0.606	0.743	0.733	0.572
74.830	0.867	0.860	0.664	0.872	0.922	0.629
99.750	1.013	1.039	0.705	1.057	1.157	0.650
113.830	1.371	1.156	0.888	1.468	1.353	0.812
130.500	1.873	1.362	0.934	2.079	1.660	0.892
156.000	2.727	1.440	1.045	2.951	1.811	1.126

Table 03.4.3-4 Weighted Average Floor Accelerations - East PS/B

Elevation	Cracked			Uncracked		
(ft)	AX(g)	AY(g)	AZ(g)	AX(g)	AY(g)	AZ(g)
-39.667	0.383	0.345	0.381	0.395	0.347	0.368
-26.333	0.384	0.349	0.389	0.399	0.350	0.371
-15.583	0.439	0.371	0.419	0.430	0.371	0.384
-8.583	0.459	0.386	0.427	0.458	0.397	0.384
2.583	0.464	0.401	0.454	0.508	0.443	0.397
25.250	0.605	0.507	0.483	0.649	0.548	0.420
35.170	0.653	0.531	0.569	0.682	0.574	0.486
48.500	0.847	0.626	0.769	0.786	0.632	0.657

Table 03.4.3-5 Weighted Average Floor Accelerations - West PS/B

Elevation	Cracked			Uncracked		
(ft)	AX(g)	AY(g)	AZ(g)	AX(g)	AY(g)	AZ(g)
-39.667	0.371	0.345	0.359	0.378	0.350	0.366
-26.333	0.376	0.350	0.365	0.380	0.354	0.370
-15.583	0.446	0.381	0.389	0.419	0.376	0.384
-8.583	0.489	0.414	0.411	0.454	0.395	0.385
2.583	0.481	0.425	0.425	0.466	0.435	0.396
25.250	0.560	0.494	0.494	0.536	0.511	0.442
35.170	0.574	0.540	0.583	0.535	0.546	0.518
48.500	0.579	0.588	0.724	0.547	0.578	0.657

Table 03.4.3-6 Weighted Average Floor Accelerations - A/B

Elevation (ft)	Cracked			Uncracked		
	AX(g)	AY(g)	AZ(g)	AX(g)	AY(g)	AZ(g)
-39.667	0.371	0.348	0.359	0.379	0.343	0.372
-26.333	0.374	0.354	0.364	0.385	0.345	0.376
-15.583	0.403	0.388	0.385	0.426	0.362	0.384
-8.583	0.423	0.412	0.399	0.452	0.381	0.392
2.583	0.467	0.456	0.433	0.495	0.425	0.405
25.250	0.512	0.543	0.499	0.514	0.524	0.447
35.170	0.579	0.600	0.533	0.543	0.592	0.468
48.500	0.622	0.647	0.644	0.579	0.654	0.568
74.830	0.743	0.796	0.831	0.664	0.827	0.730
99.750	0.771	0.973	0.891	0.700	1.055	0.724

Table 03.4.3-7 Base Shears

Soil Case	Cracked			Uncracked		
	FX (kips)	FY (kips)	FZ (kips)	FX (kips)	FY (kips)	FZ (kips)
270-200	463963	463662	513398	451022	461617	484817
270-500	446351	450915	501537	434770	448426	471531
560-500	548306	562874	512709	518408	524451	476755
900-100	750712	707025	682919	725043	677189	592056
900-200	749046	701996	683963	730436	664411	582786
2032-100	767171	719901	674955	777802	746807	632561

Table 03.4.4-1 PCCV - R/B Maximum Relative Displacements - Basemat

Degrees CW North	Elevation (ft)	Cracked		Uncracked	
		Displacement (in)		Displacement (in)	
		R/B	PCCV	R/B	PCCV
0	114	1.728	1.437	1.015	0.881
35	100	0.787	1.208	0.455	0.733
74	100	0.725	1.247	0.386	0.727
107	100	0.657	1.249	0.334	0.719
142	100	0.694	1.237	0.332	0.756
180	114	0.867	1.454	0.425	0.897
218	131	0.976	1.612	0.493	0.971
253	100	0.949	1.253	0.517	0.720
286	114	1.550	1.481	0.949	0.864
323	114	1.487	1.474	0.875	0.900

Table 03.4.4-2 PCCV - CIS Maximum Relative Displacements - Basemat

Degrees CW North	Elevation (ft)	Cracked		Uncracked	
		Difference (in)		Difference (in)	
		PCCV	CIS	PCCV	CIS
0	75	0.992	0.549	0.610	0.406
60	75	0.930	0.557	0.556	0.407
120	75	0.950	0.558	0.544	0.401
180	75	0.990	0.568	0.603	0.403
245	75	0.953	0.572	0.550	0.410
300	75	1.030	0.569	0.607	0.415

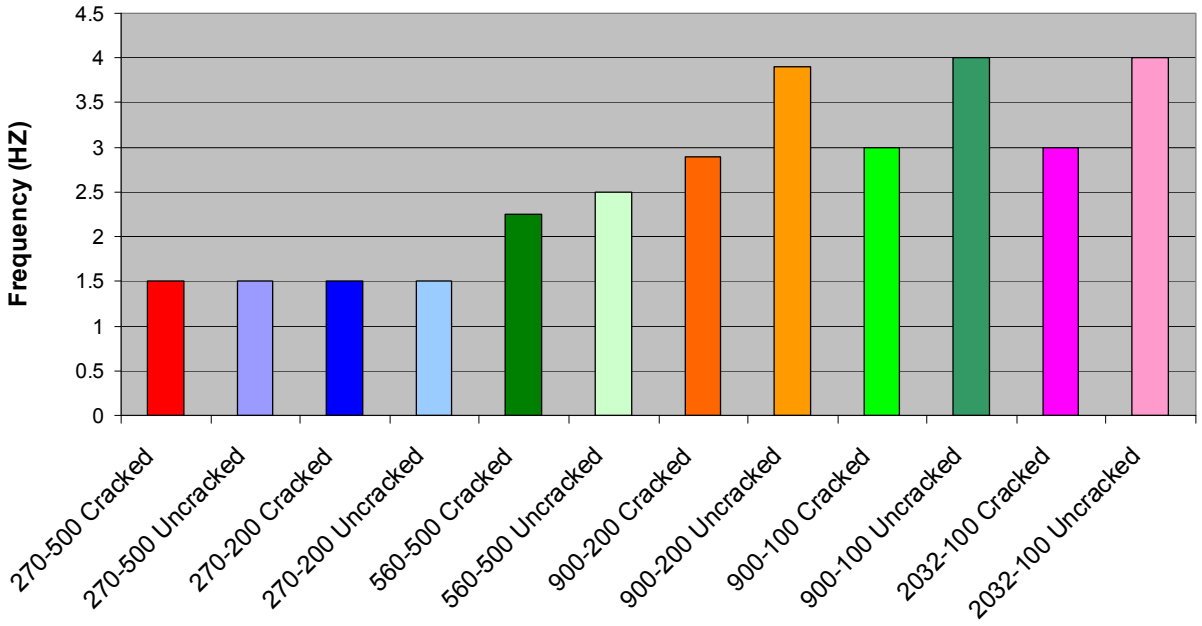

Figure 03.4.1.1-1 First Peak Frequencies at Bottom of Basemat - NS Response (X)

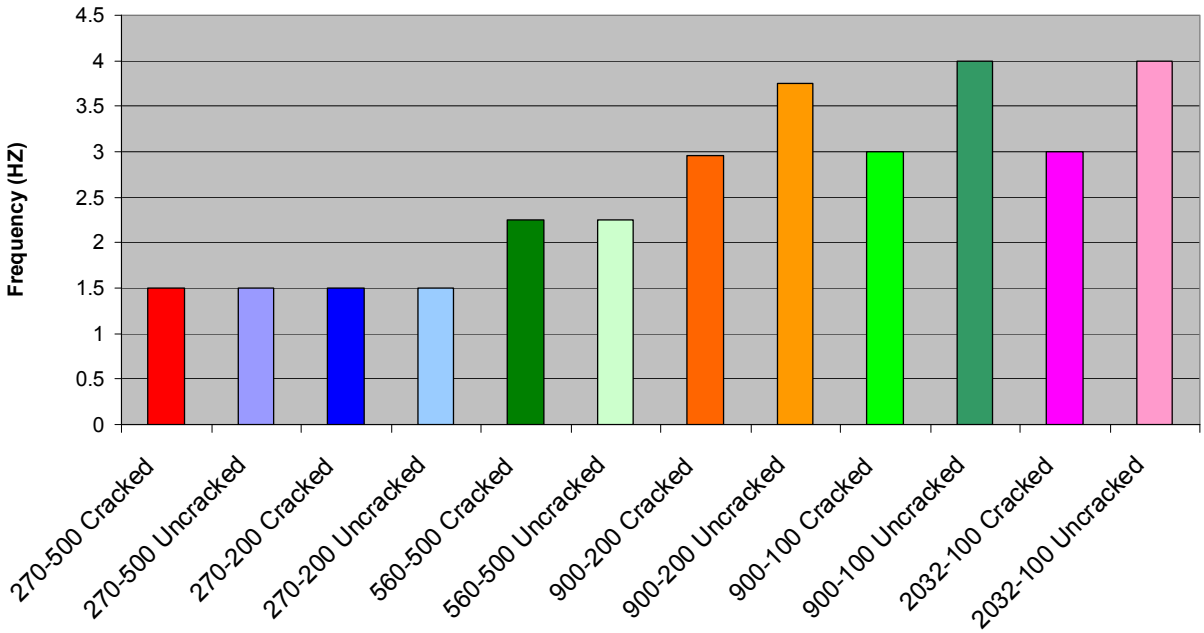

Figure 03.4.1.1-2 First Peak Frequencies at Bottom of Basemat - EW Response (Y)

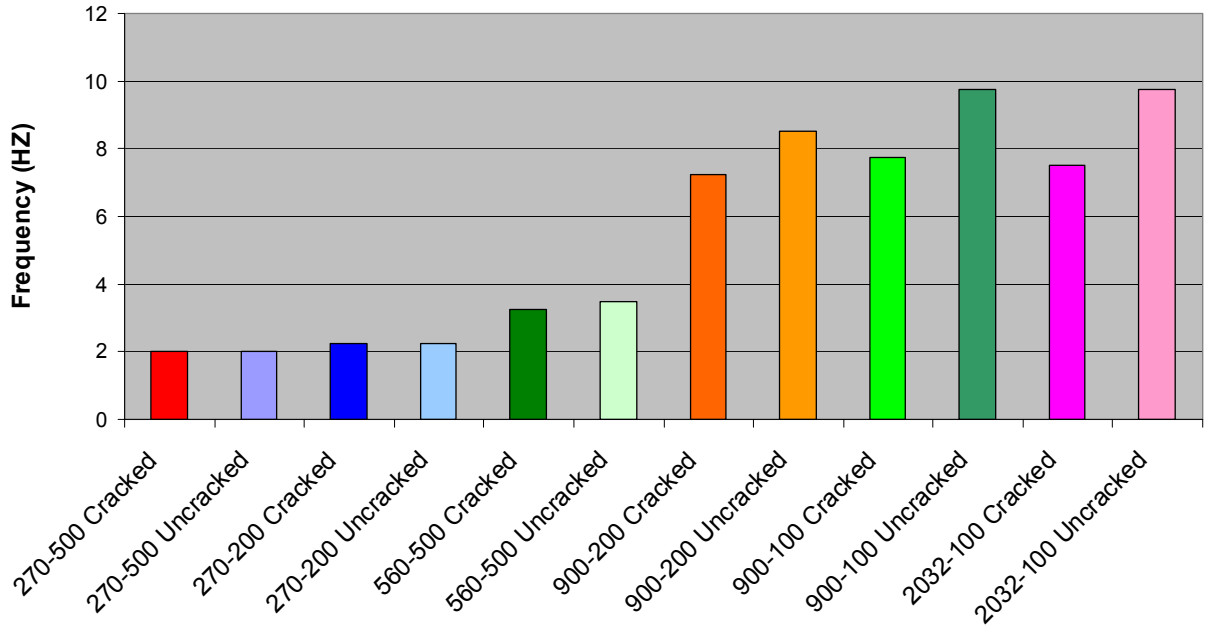

Figure 03.4.1.1-3 First Peak Frequencies at Bottom of Basemat - Vertical Response (Z)

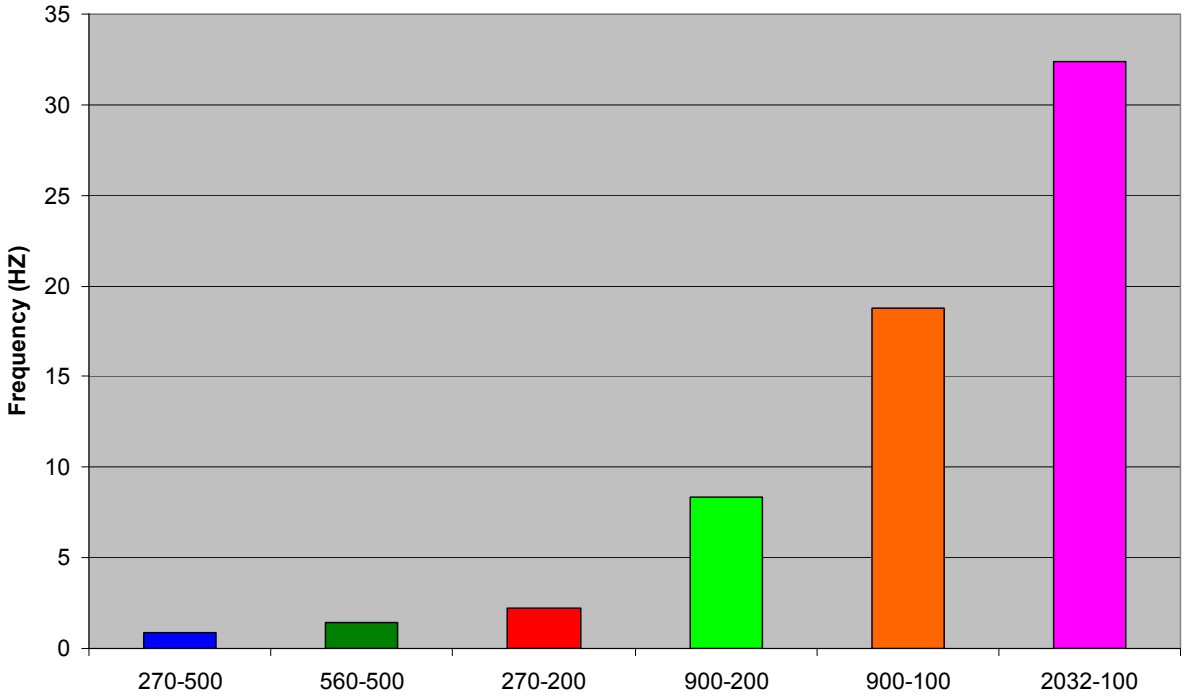

Figure 03.4.1.1-4 Shear Wave Column Frequencies - Below Foundation

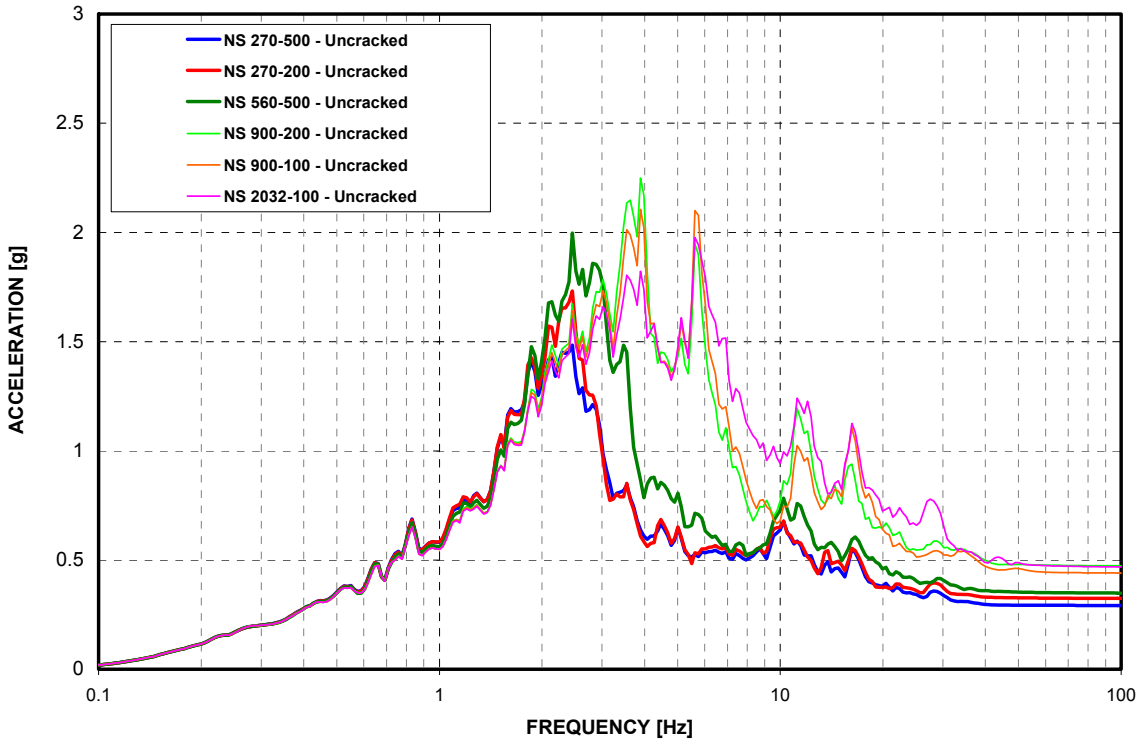

Figure 03.4.1.2-1 Top of Reactor Cavity - Uncracked 3% Damped ARS - NS Response (X)

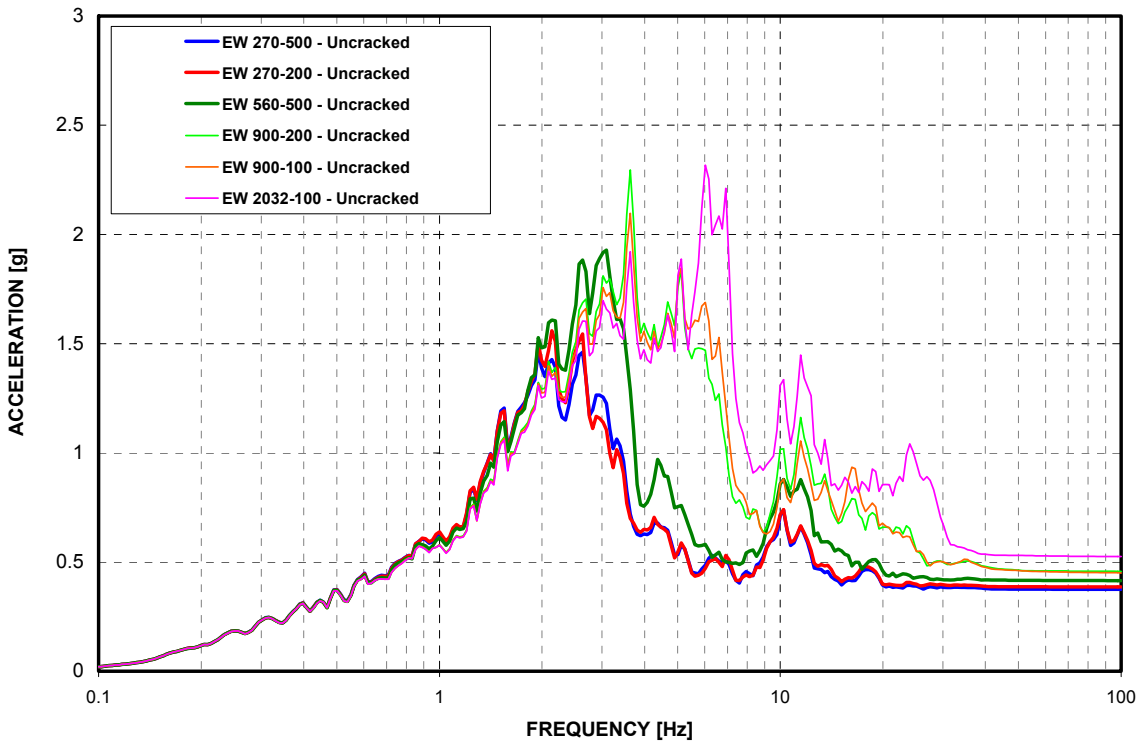

Figure 03.4.1.2-2 Top of Reactor Cavity - Uncracked 3% Damped ARS - EW Response (Y)

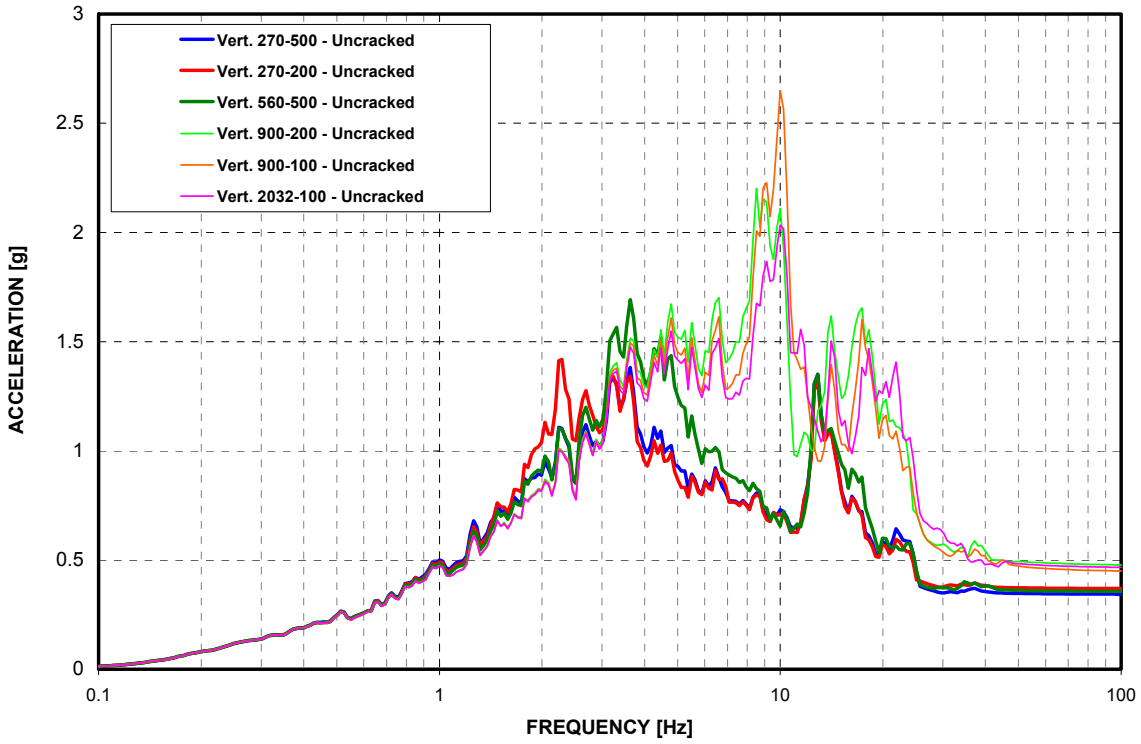

Figure 03.4.1.2-3 Top of Reactor Cavity- Uncracked 3% Damped ARS - Vertical Response (Z)

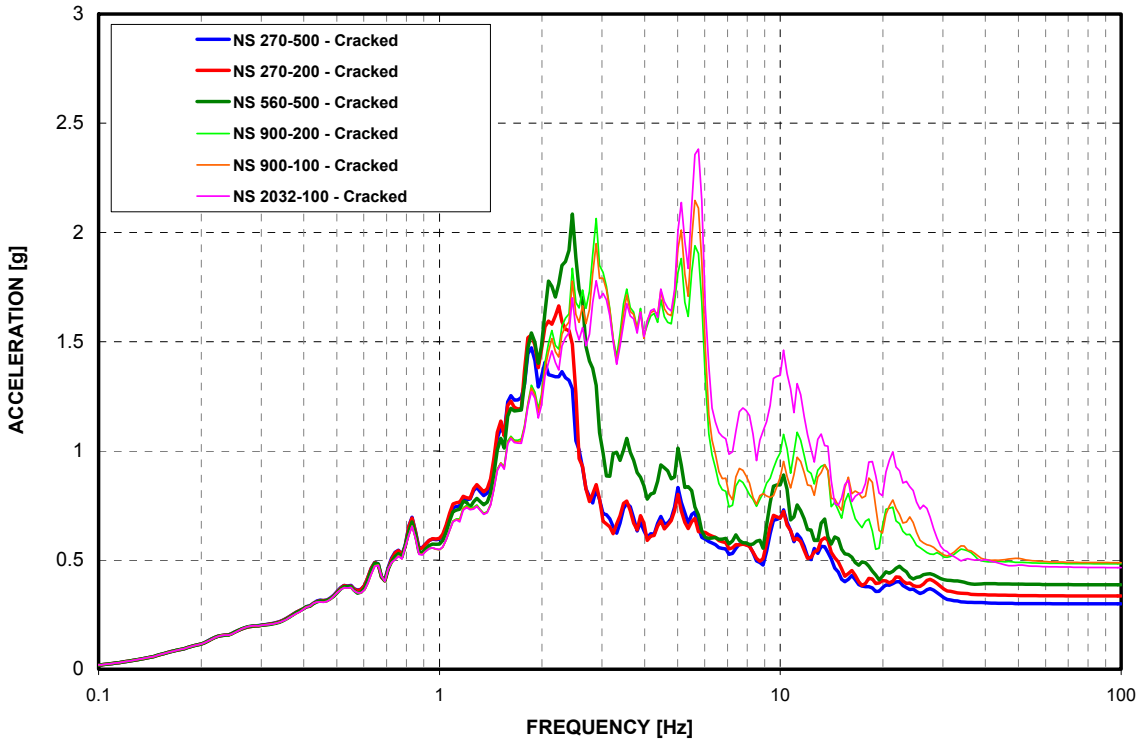

Figure 03.4.1.2-4 Top of Reactor Cavity - Cracked 3% Damped ARS - NS Response (X)

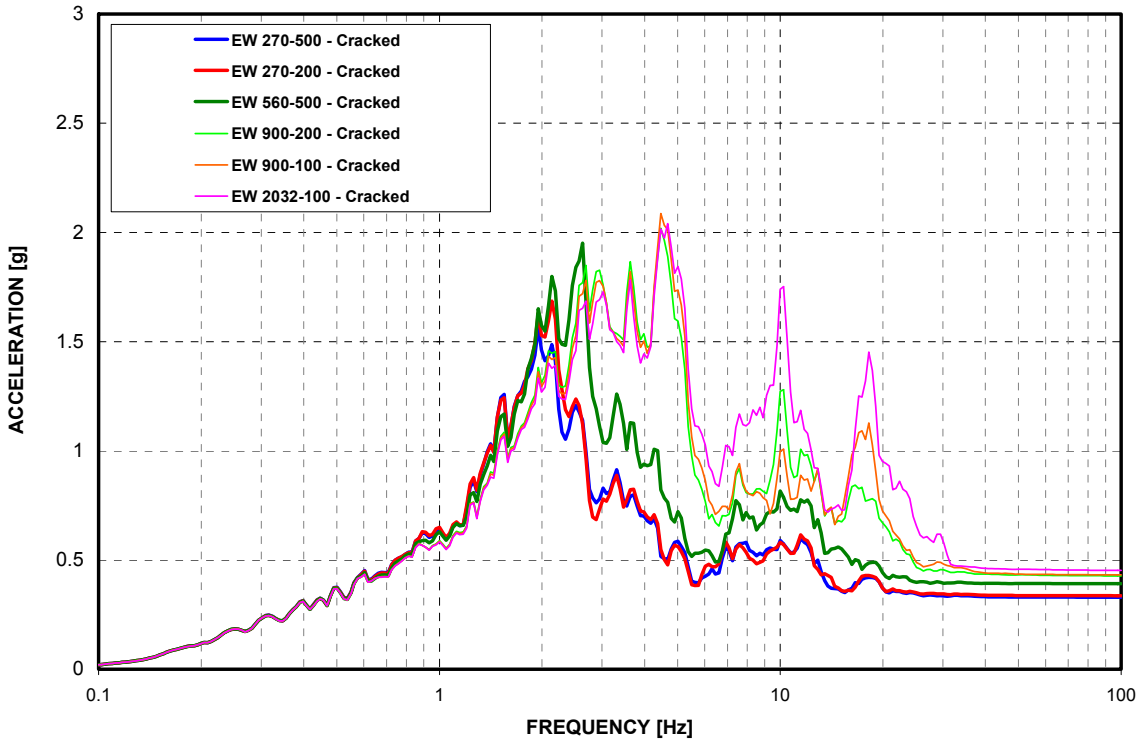

Figure 03.4.1.2-5 Top of Reactor Cavity - Cracked 3% Damped ARS - EW Response (Y)

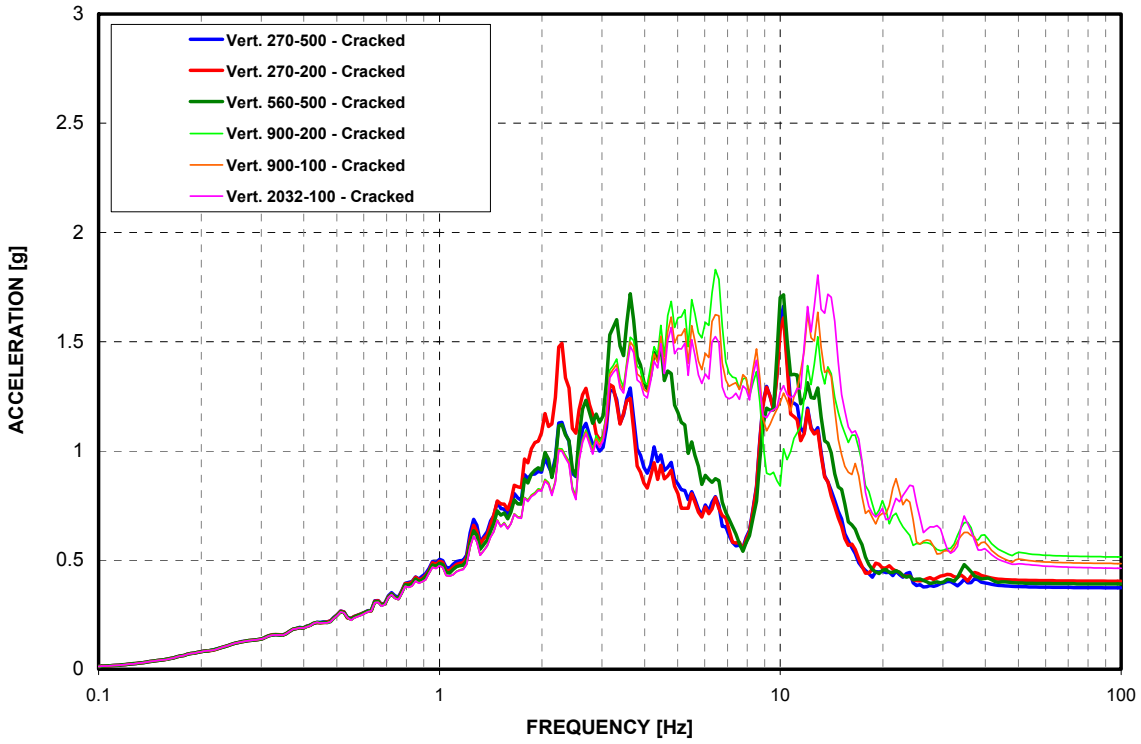

Figure 03.4.1.2-6 Top of Reactor Cavity - Cracked 3% Damped ARS - Vertical Response (Z)

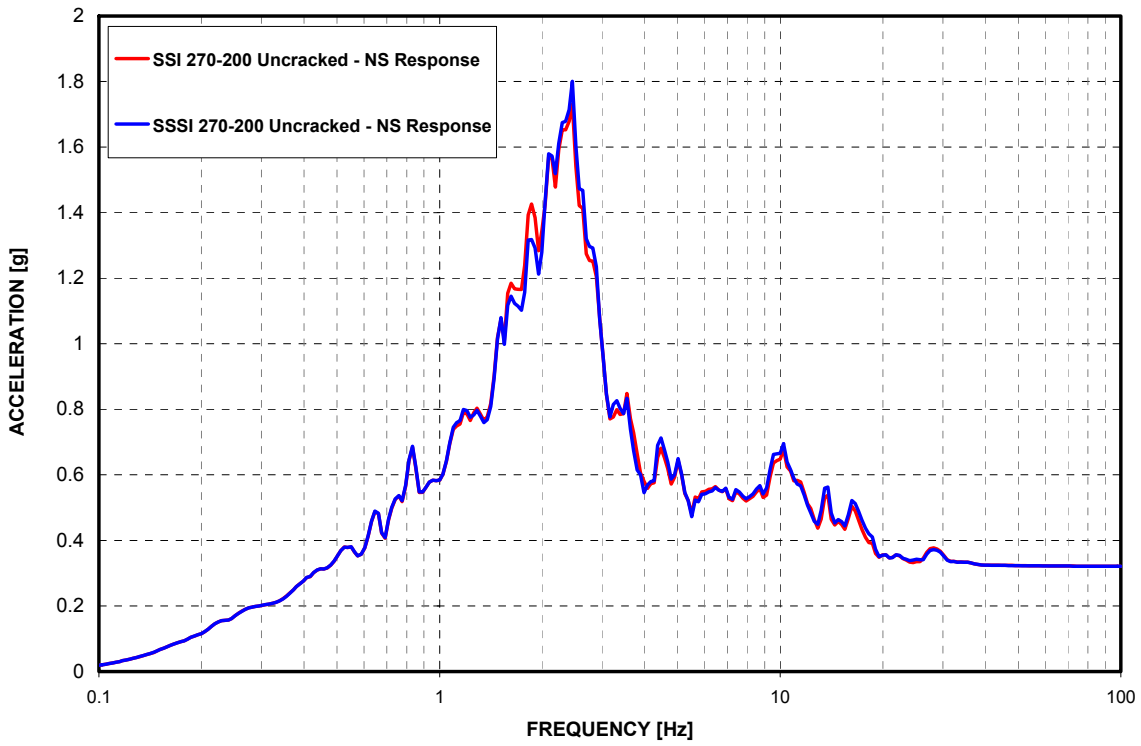

Figure 03.4.1.3-1 Top of Reactor Cavity 5% Damped ARS Comparison- 270-200 - NS Response (X)

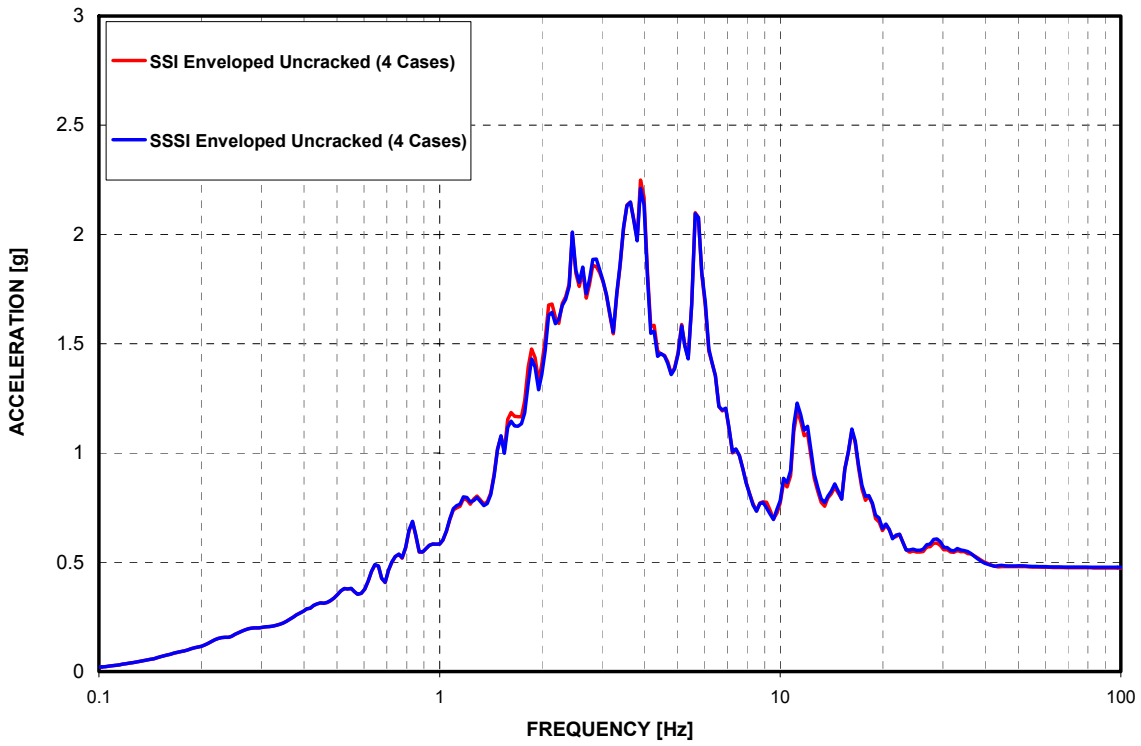

Figure 03.4.1.3-2 Top of Reactor Cavity 5% Damped ARS Comparison- Enveloped - NS Response (X)

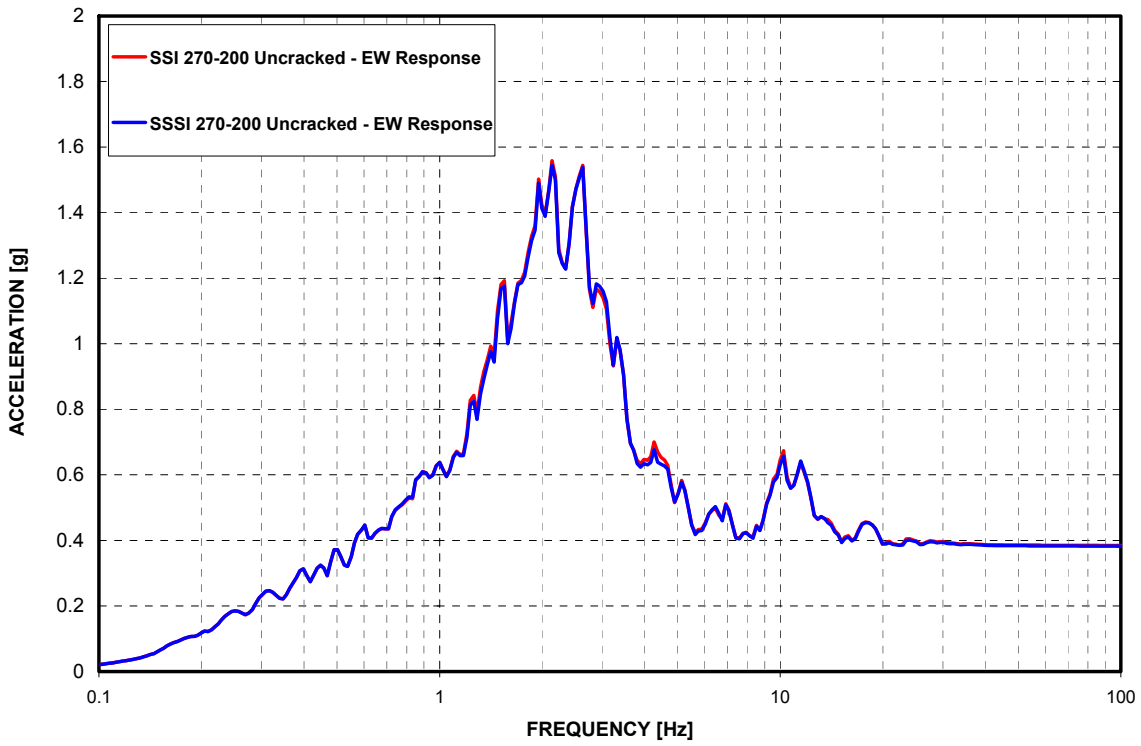

Figure 03.4.1.3-3 Top of Reactor Cavity 5% Damped ARS Comparison- 270-200 - EW Response (Y)

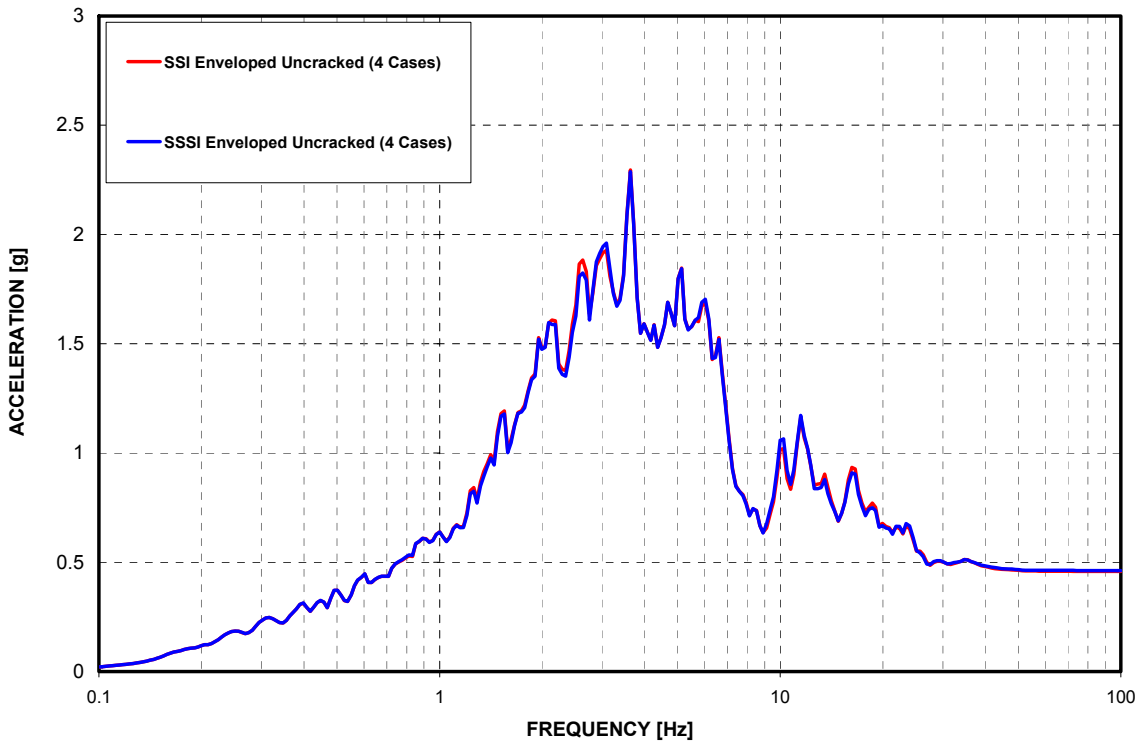

Figure 03.4.1.3-4 Top of Reactor Cavity 5% Damped ARS Comparison- Enveloped - EW Response (Y)

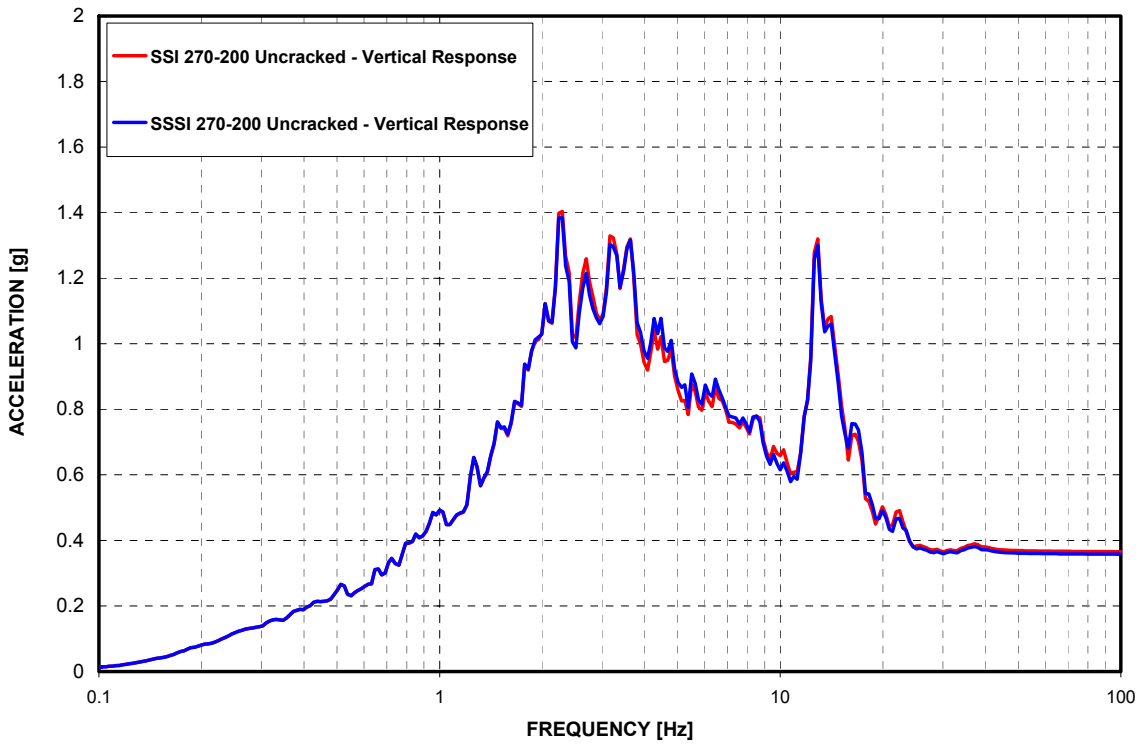

Figure 03.4.1.3-5 Top of Reactor Cavity 5% Damped ARS Comparison- 270-200 - Vertical Response (Z)

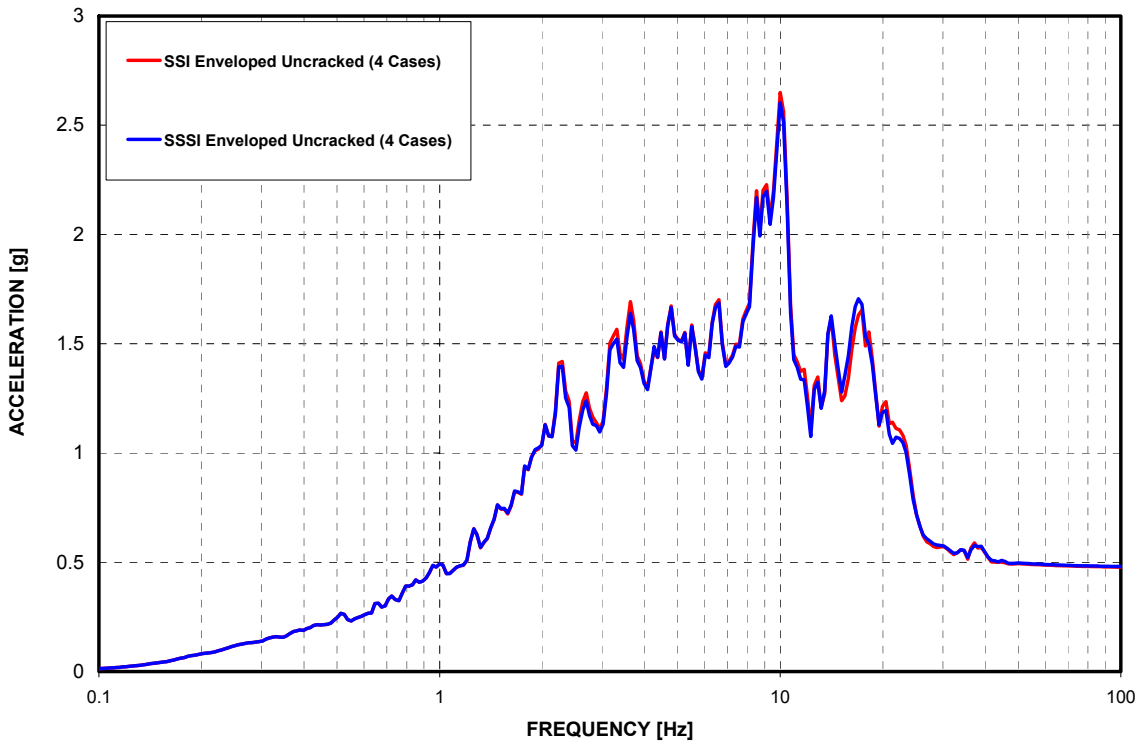

Figure 03.4.1.3-6 Top of Reactor Cavity 5% Damped ARS Comparison- Enveloped - Vertical Response (Z)

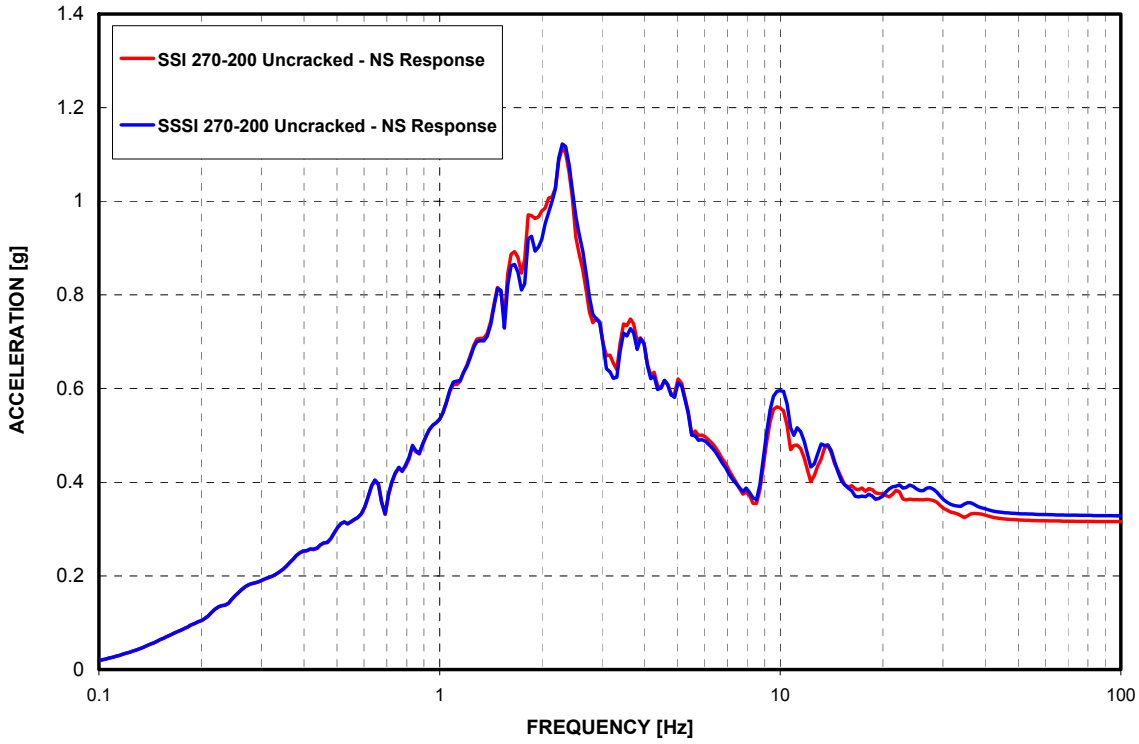

Figure 03.4.1.3-7 R/B South Wall 5% Damped ARS Comparison- 270-200 - NS Response (X)

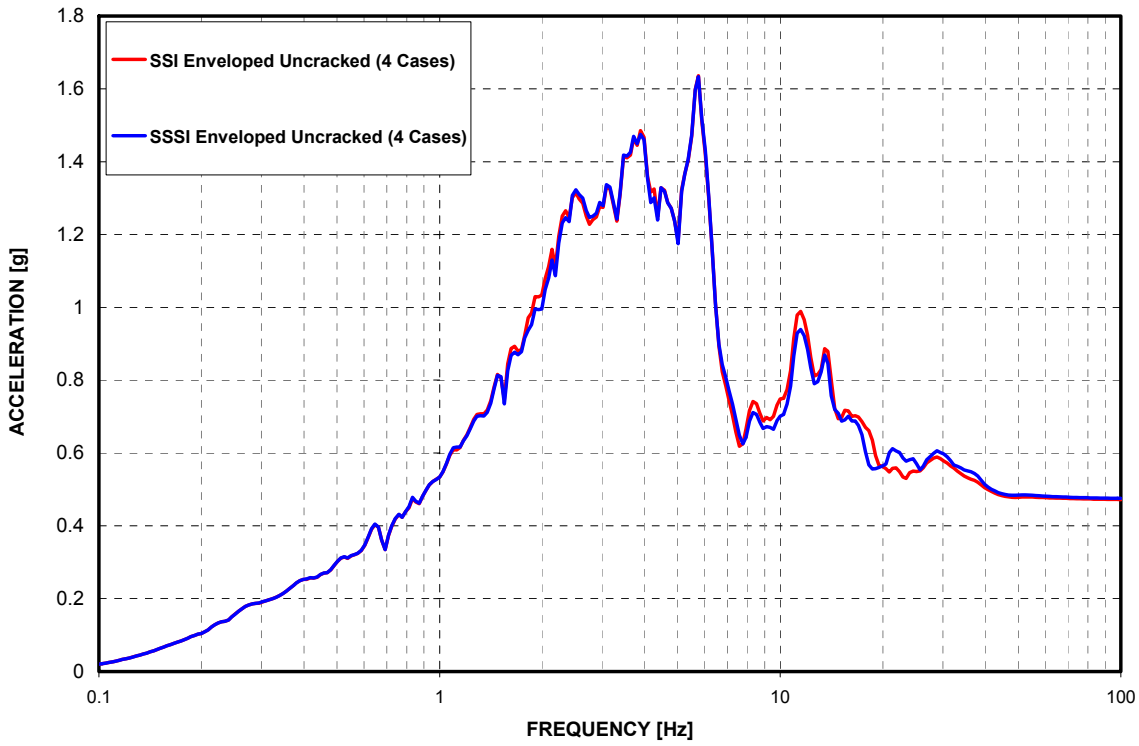

Figure 03.4.1.3-8 R/B South Wall 5% Damped ARS Comparison- Enveloped - NS Response (X)

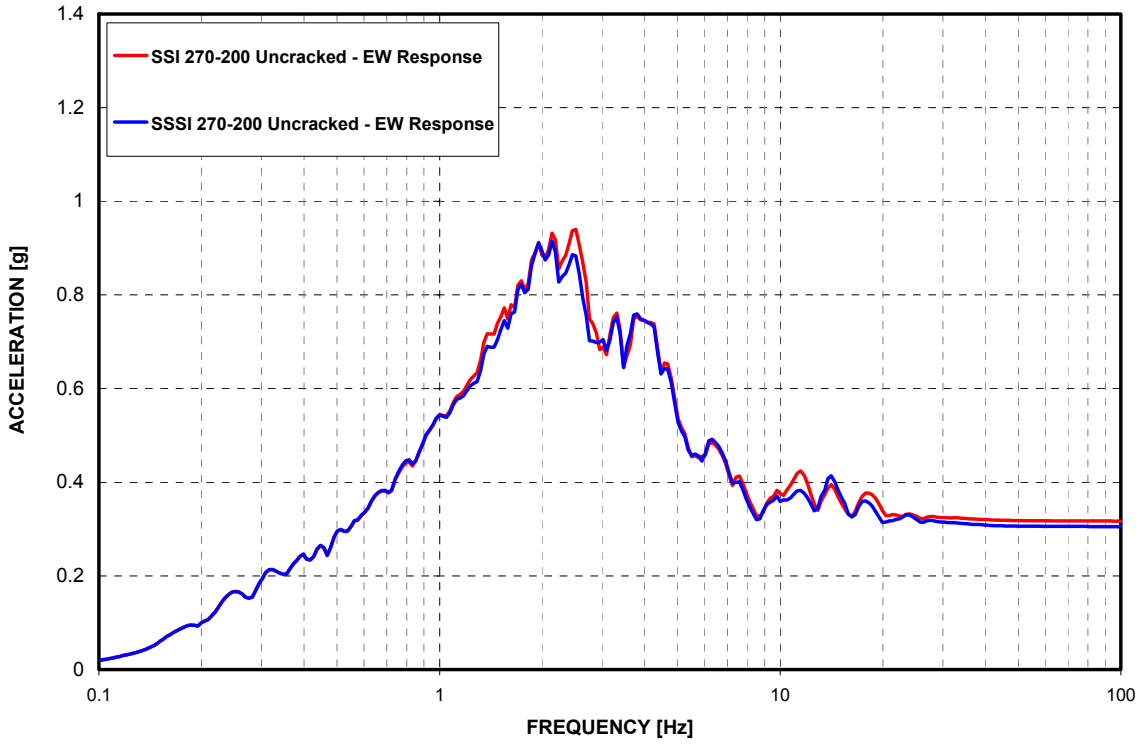

Figure 03.4.1.3-9 R/B South Wall 5% Damped ARS Comparison- 270-200 - EW Response (Y)

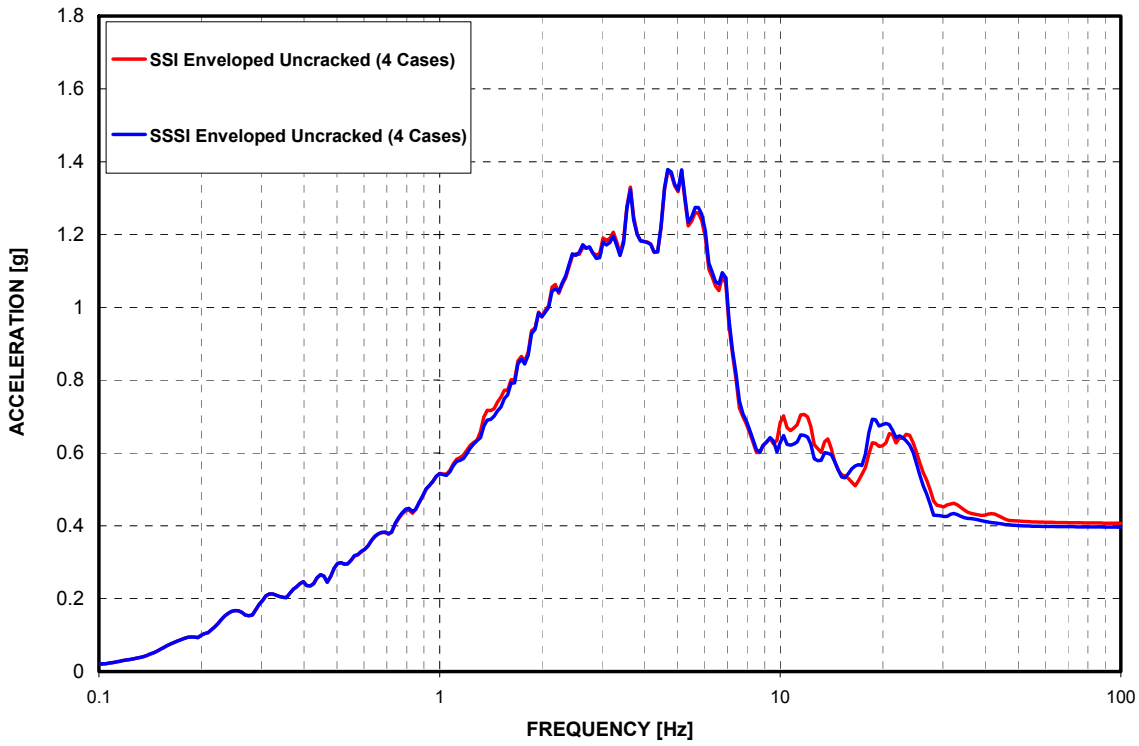

Figure 03.4.1.3-10 R/B South Wall 5% Damped ARS Comparison- Enveloped - EW Response (Y)

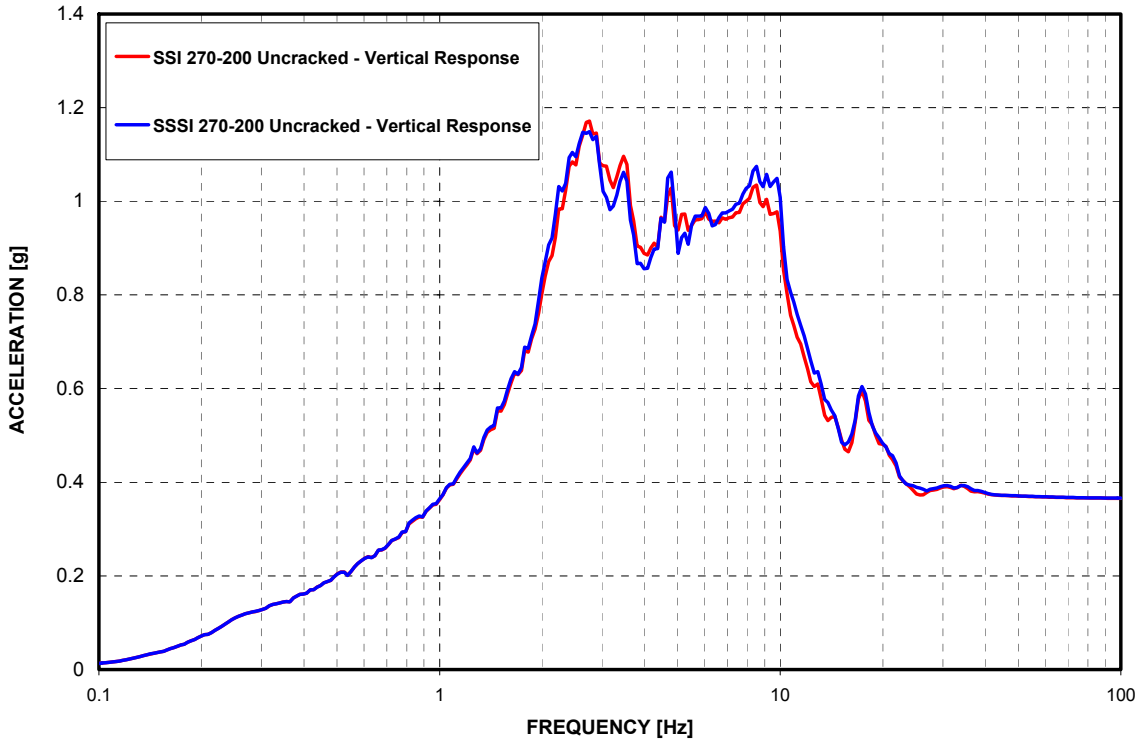

Figure 03.4.1.3-11 R/B South Wall 5% Damped ARS Comparison- 270-200 - Vertical Response (Z)

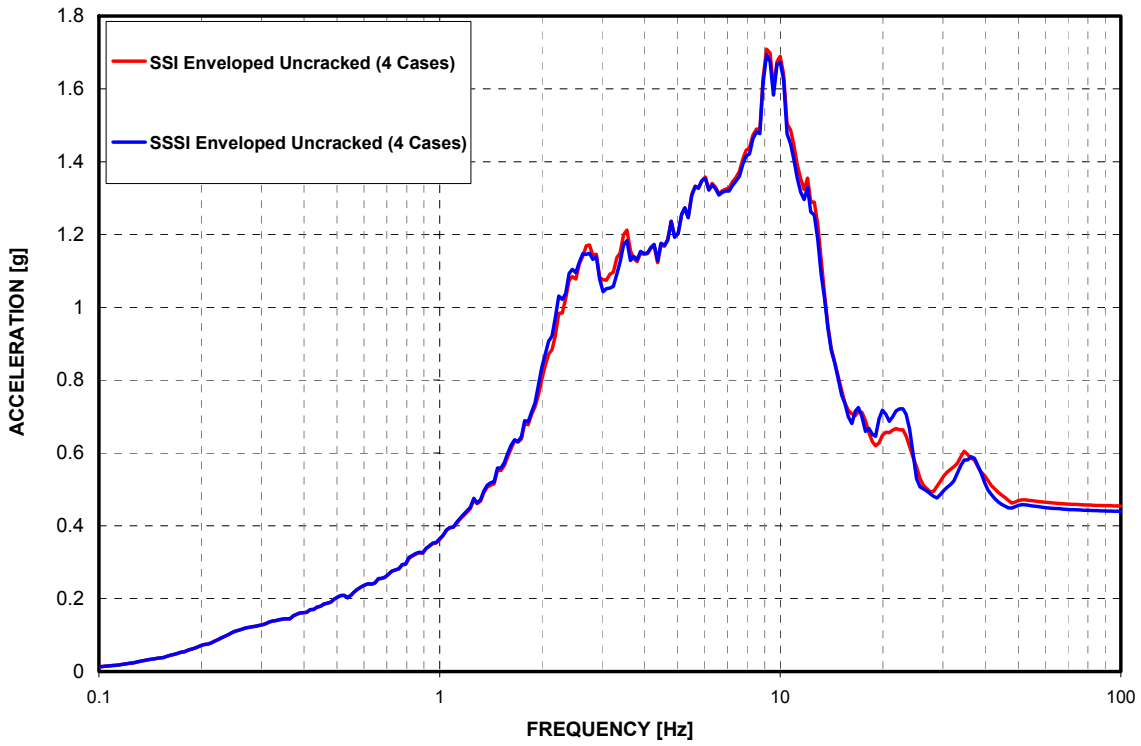

Figure 03.4.1.3-12 R/B South Wall 5% Damped ARS Comparison- Enveloped - Vertical Response (Z)

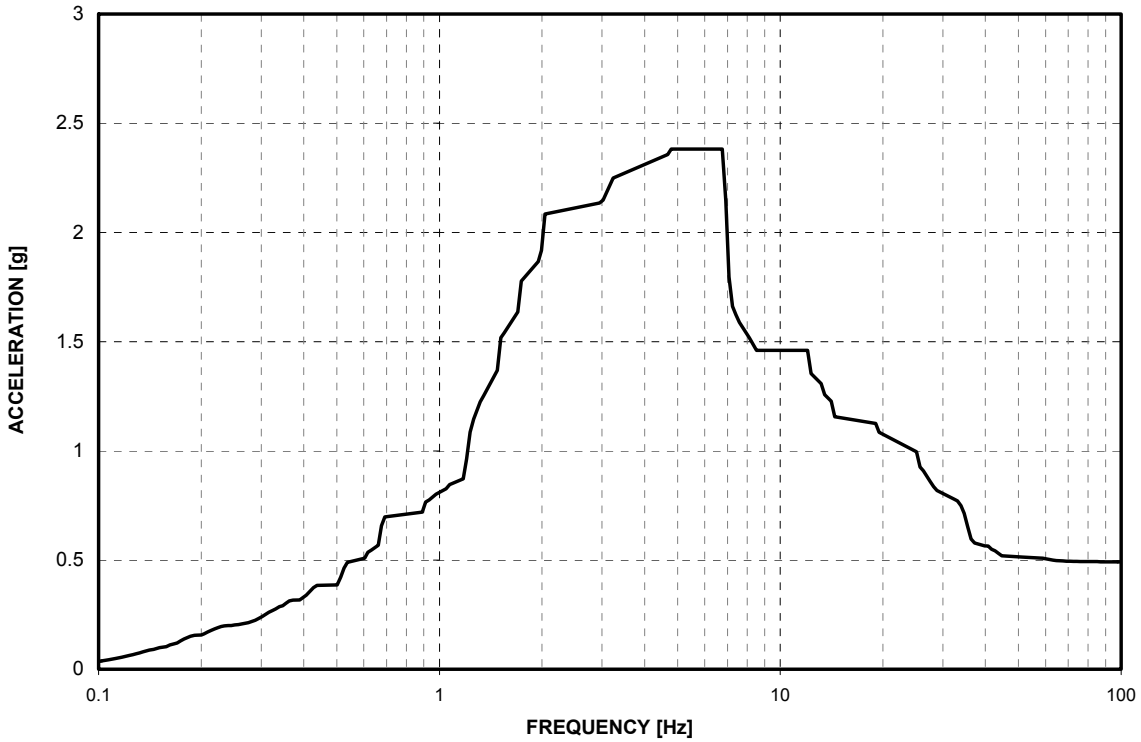

Figure 03.4.2-1 Design Basis ISRS at Top of Reactor Cavity – 3% Damped Response in NS Direction (X)

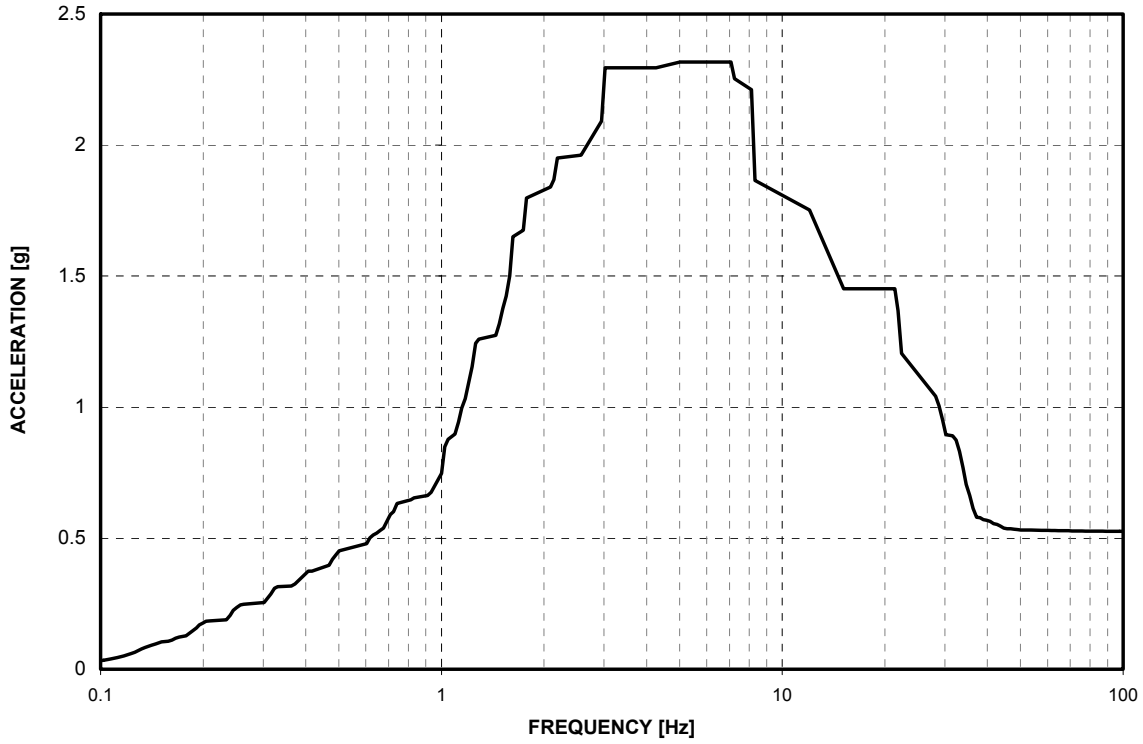

Figure 03.4.2-2 Design Basis ISRS at Top of Reactor Cavity – 3% Damped Response in EW Direction (Y)

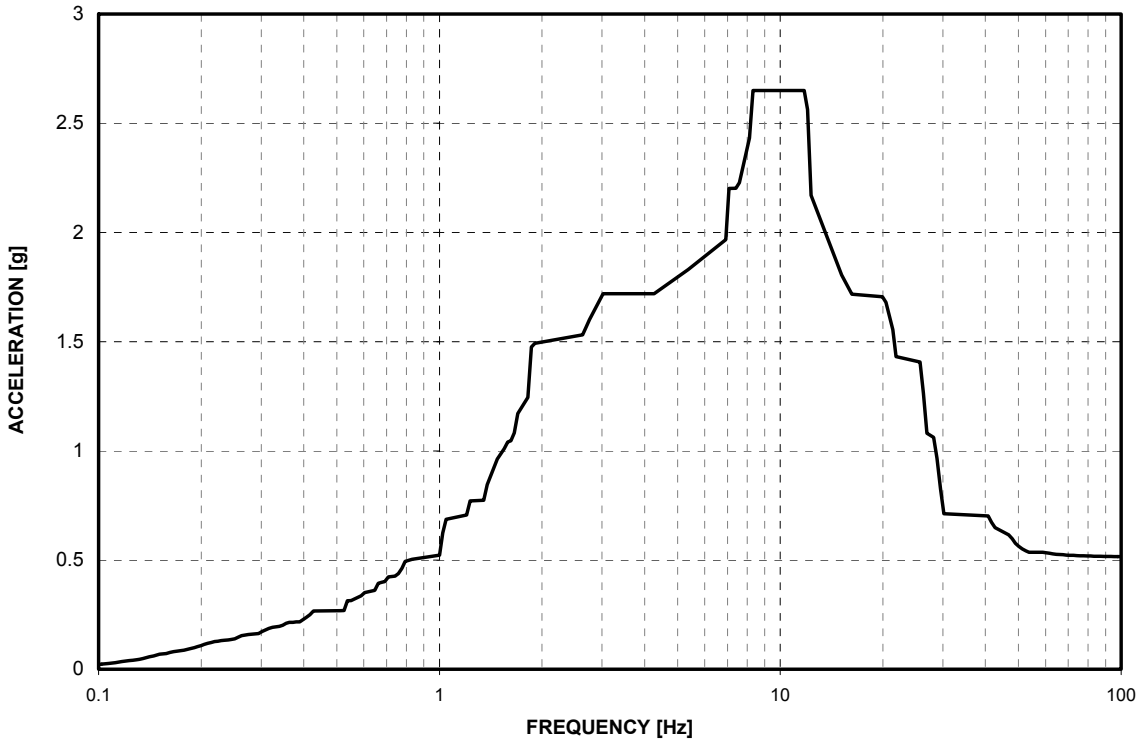

Figure 03.4.2-3 Design Basis ISRS at Top of Reactor Cavity – 3% Damped Response in Vertical Direction (Z)

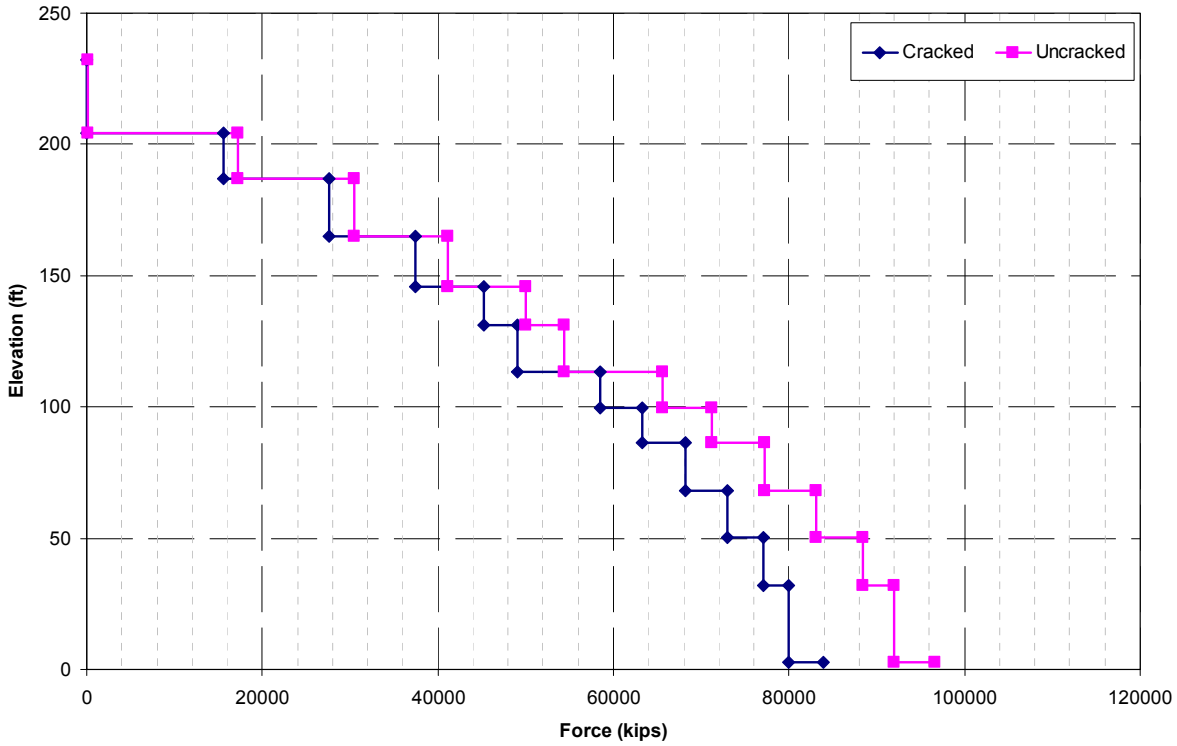

Figure 03.4.3-1 PCCV SSI Shear Diagram - Envelope of Soil Cases - NS Response (X)

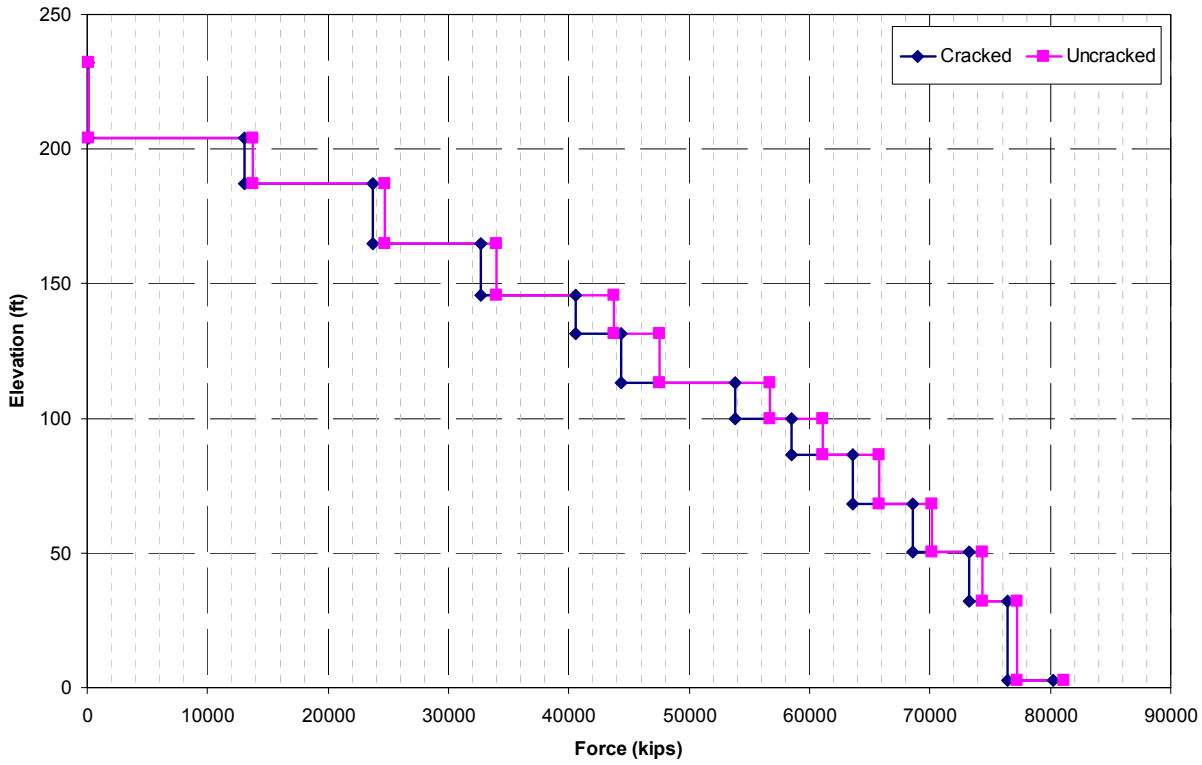

Figure 03.4.3-2 PCCV SSI Shear Diagram - Envelope of Soil Cases - EW Response (Y)

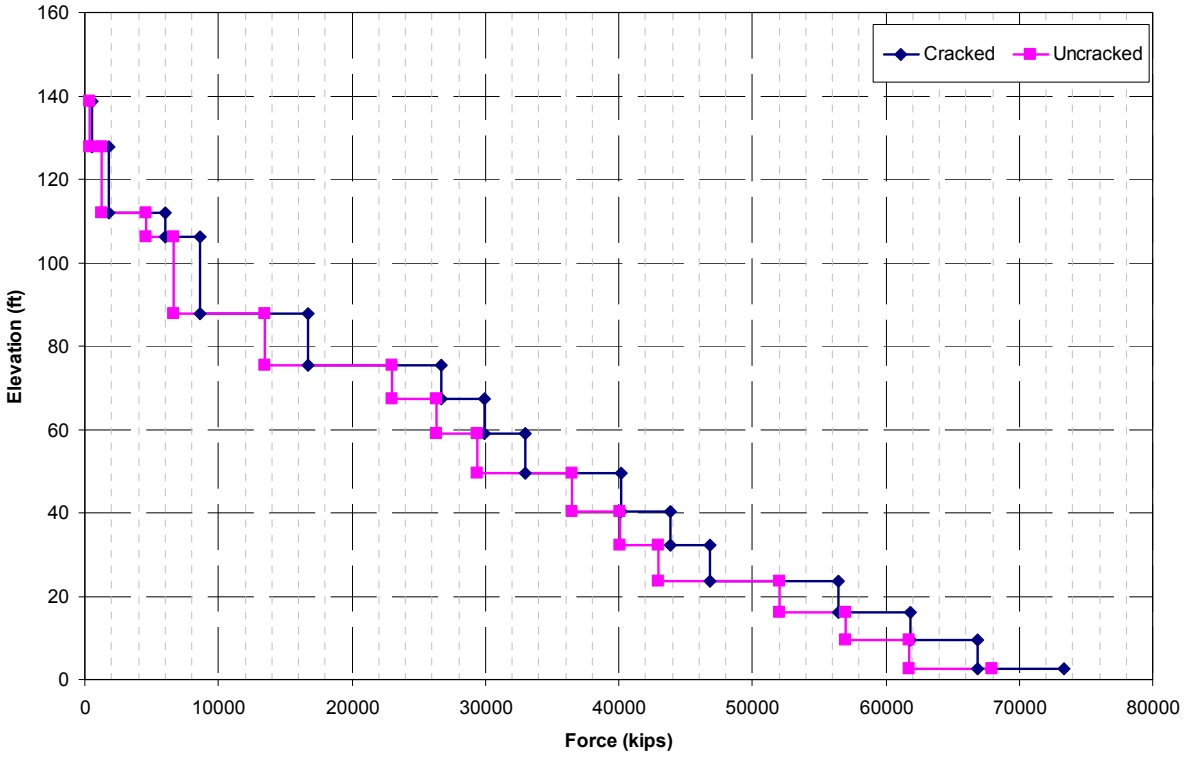

Figure 03.4.3-3 CIS SSI Shear Diagram - Envelope of Soil Cases - NS Response (X)

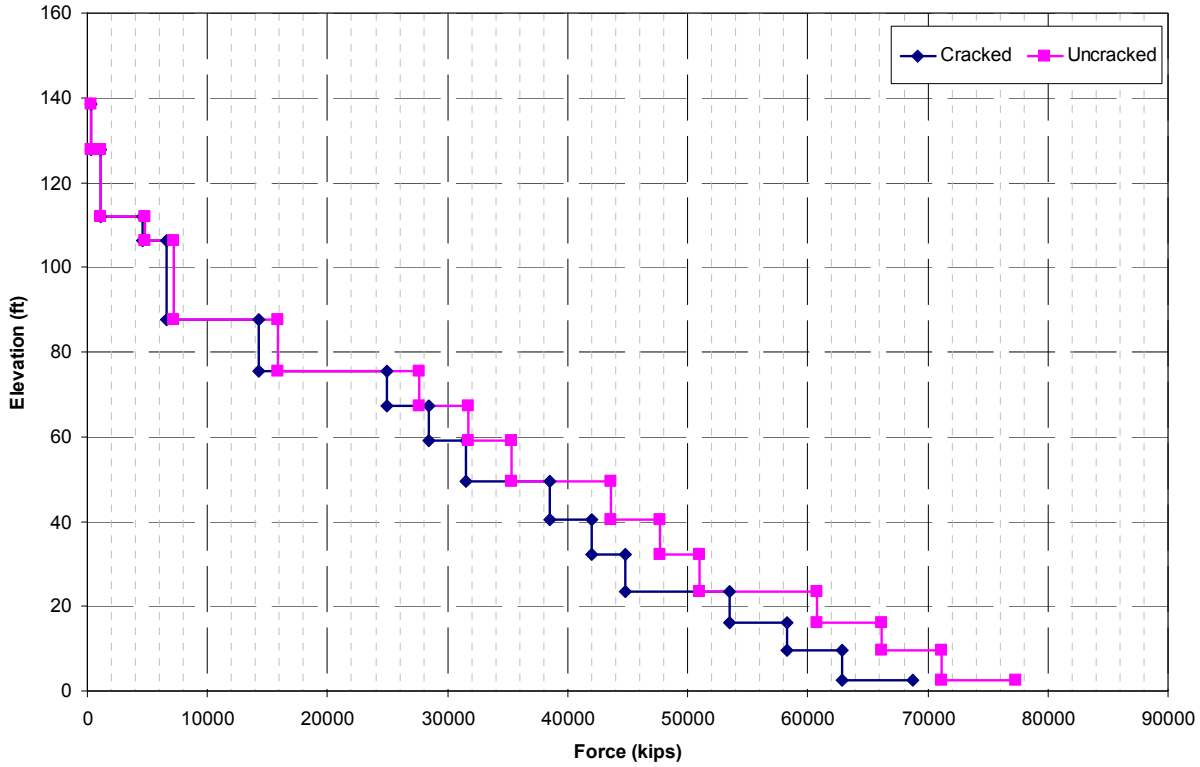

Figure 03.4.3-4 CIS SSI Shear Diagram - Envelope of Soil Cases - EW Response (Y)

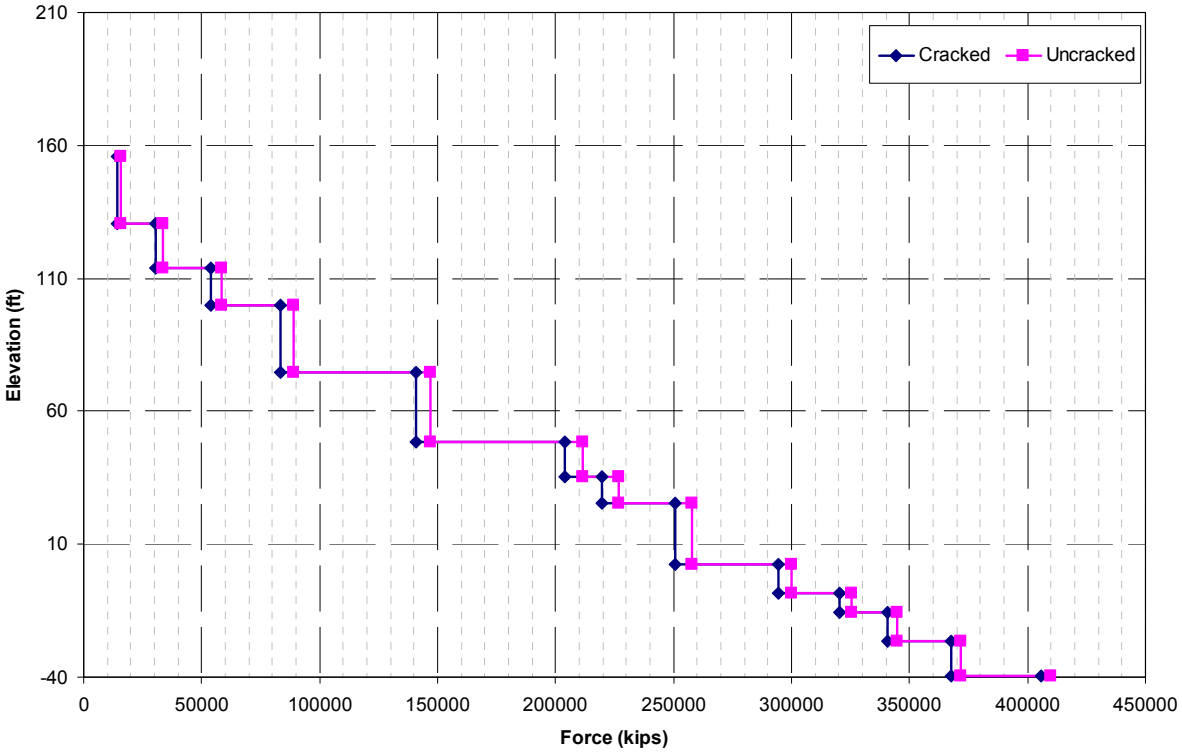

Figure 03.4.3-5 R/B SSI Shear Diagram - Envelope of Soil Cases - NS Response (X)

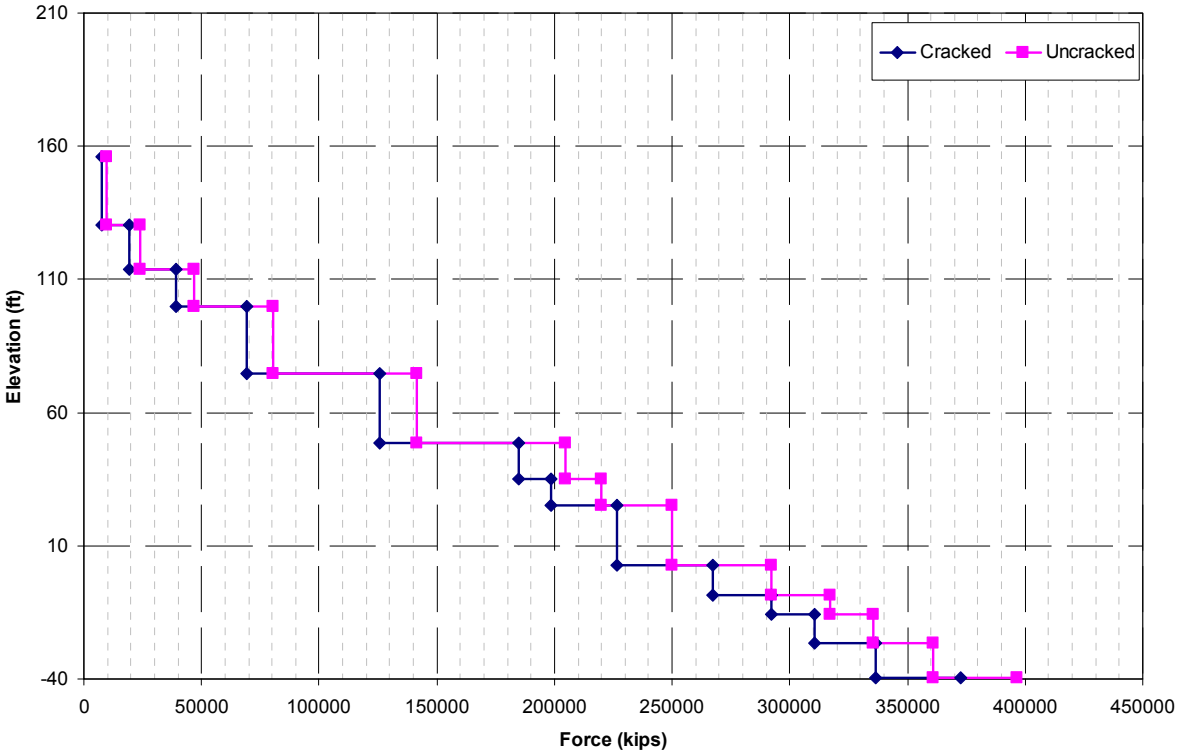

Figure 03.4.3-6 R/B SSI Shear Diagram - Envelope of Soil Cases - EW Response (Y)

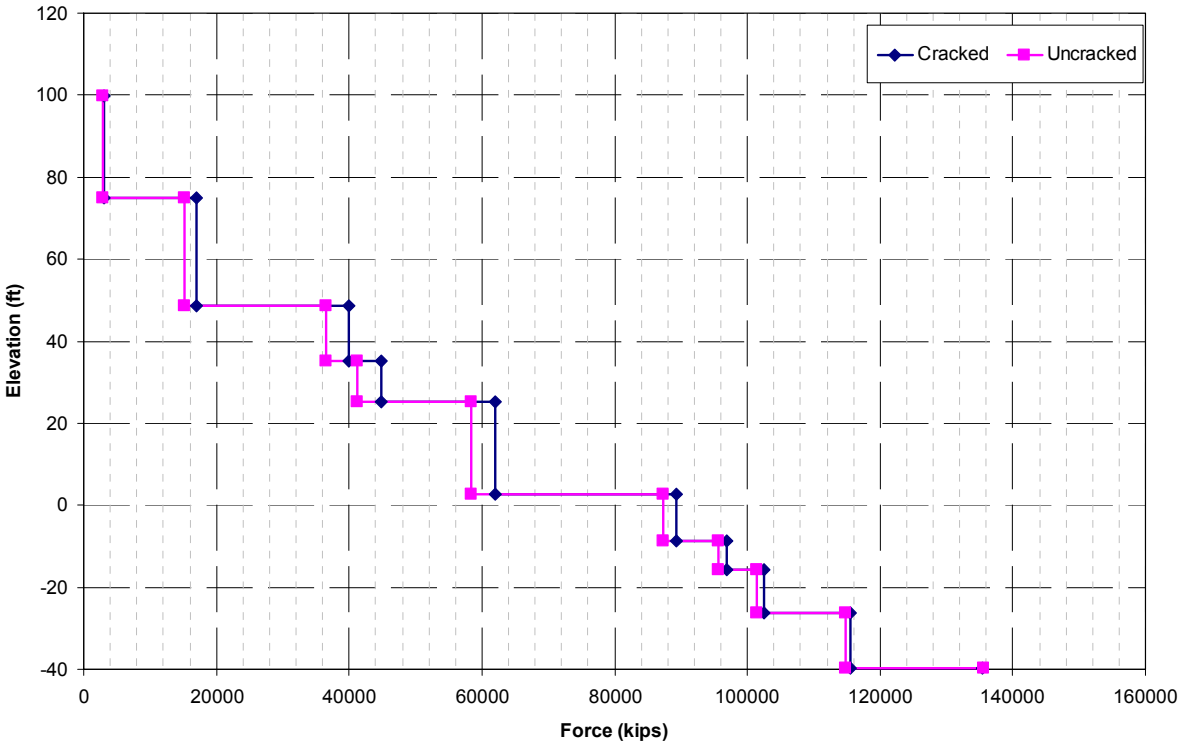

Figure 03.4.3-7 A/B SSI Shear Diagram - Envelope of Soil Cases - NS Response (X)

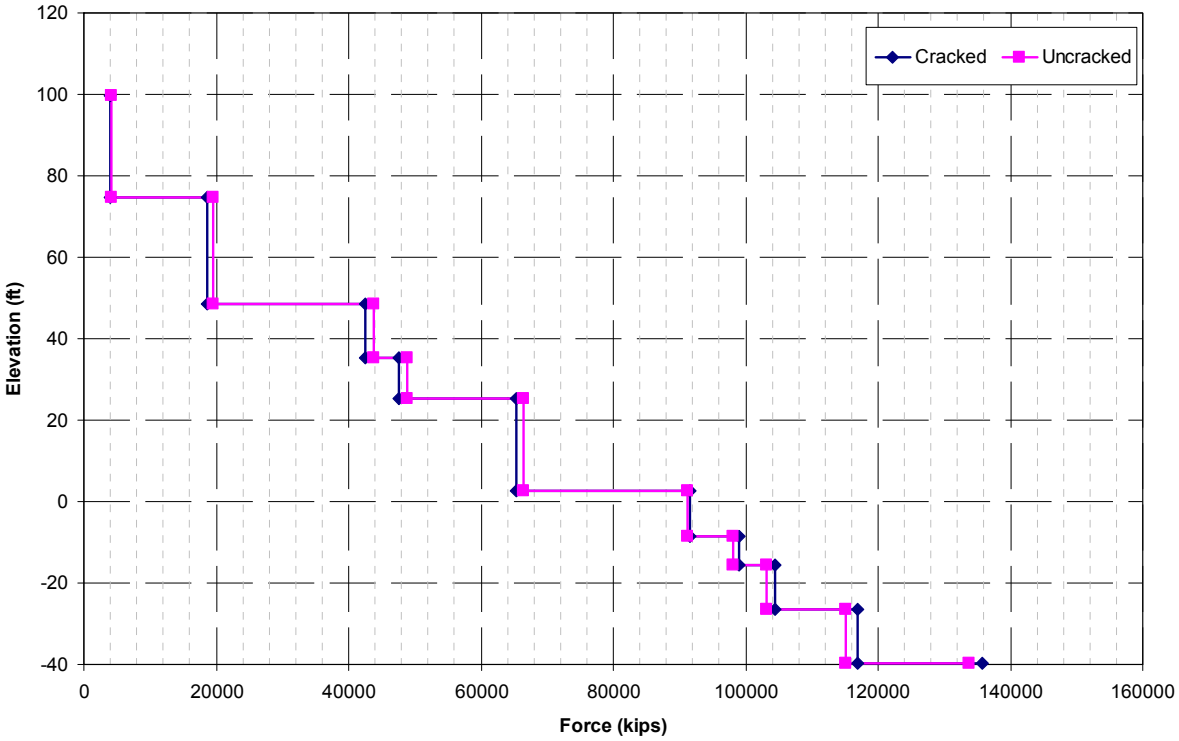

Figure 03.4.3-8 A/B SSI Shear Diagram - Envelope of Soil Cases - EW Response (Y)

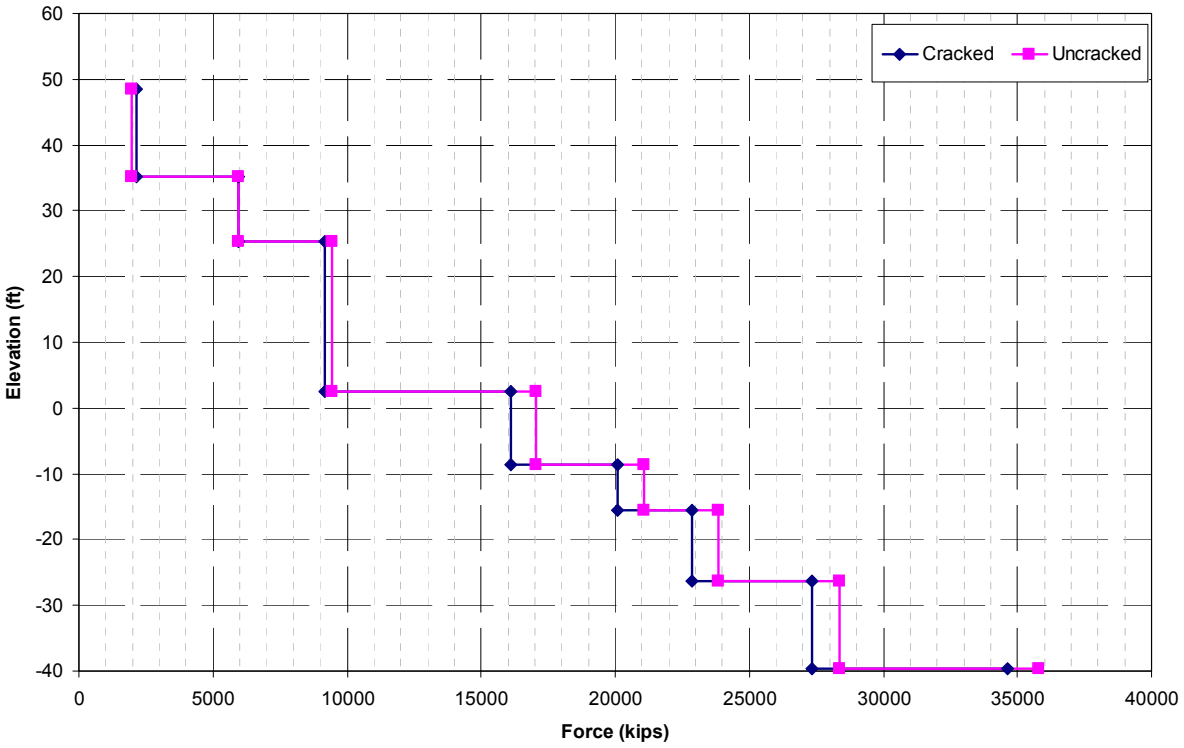

Figure 03.4.3-9 East PS/B SSI Shear Diagram - Envelope of Soil Cases - NS Response (X)

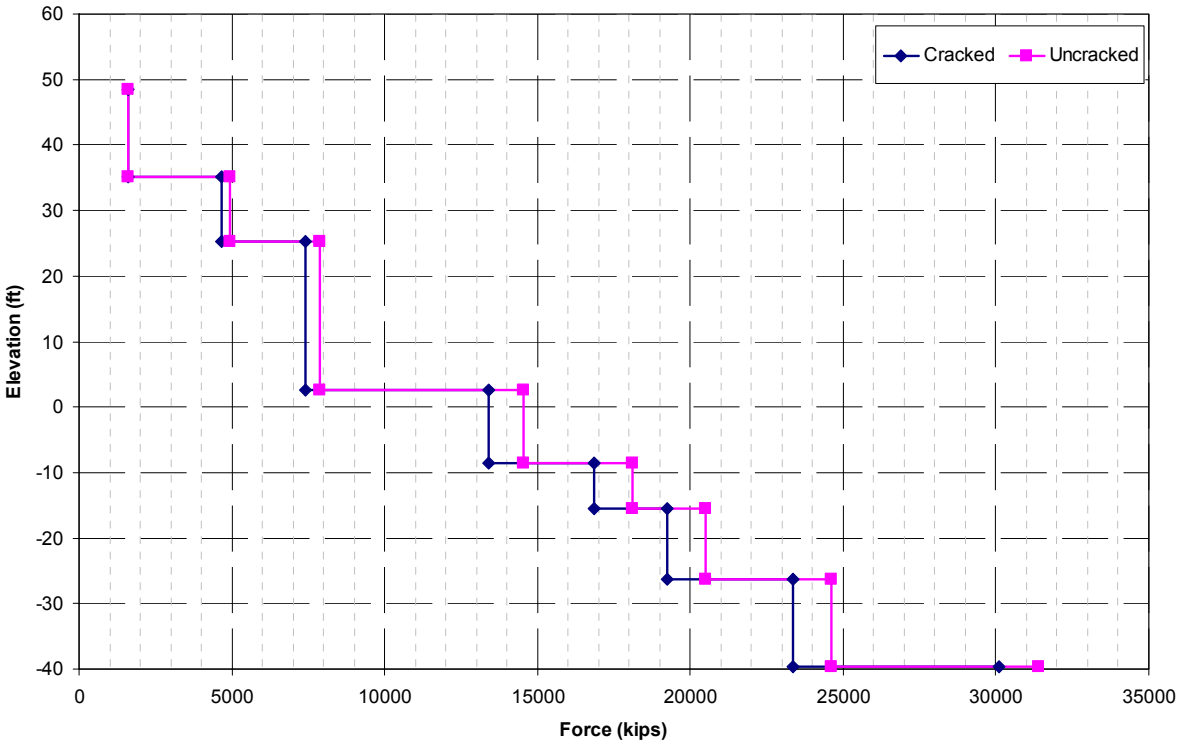

Figure 03.4.3-10 East PS/B SSI Shear Diagram - Envelope of Soil Cases - EW Response (Y)

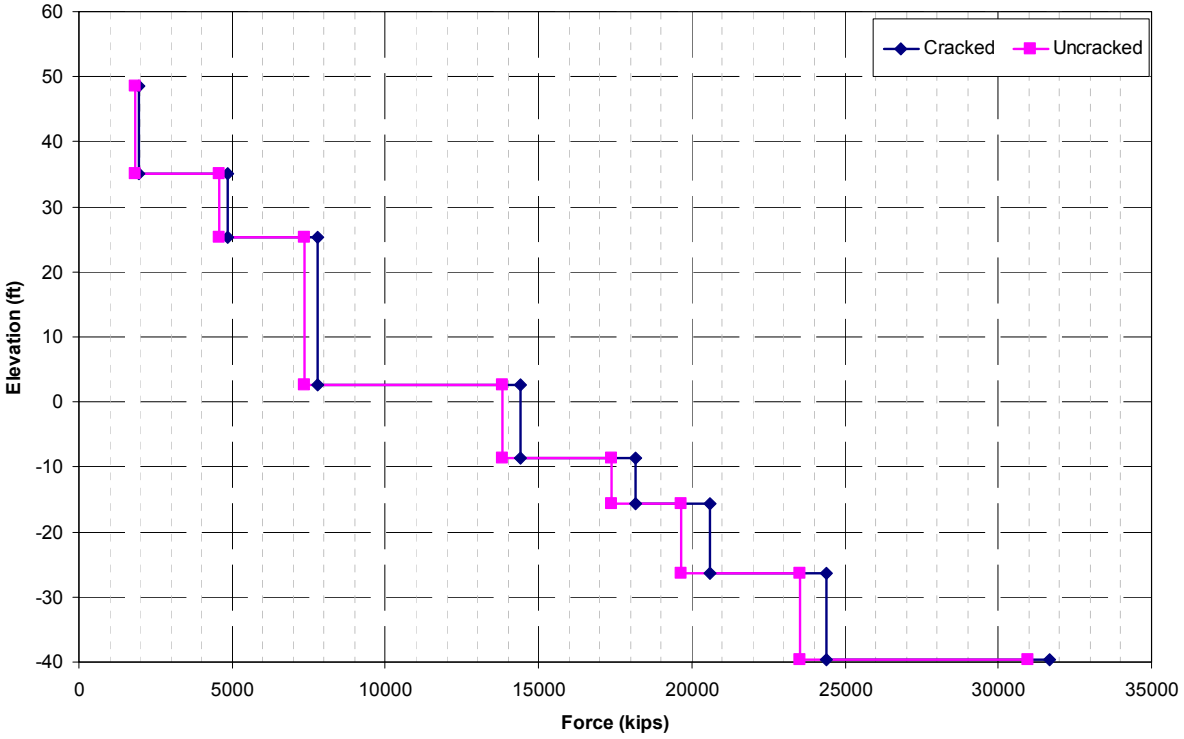

Figure 03.4.3-11 West PS/B SSI Shear Diagram - Envelope of Soil Cases - NS Response (X)

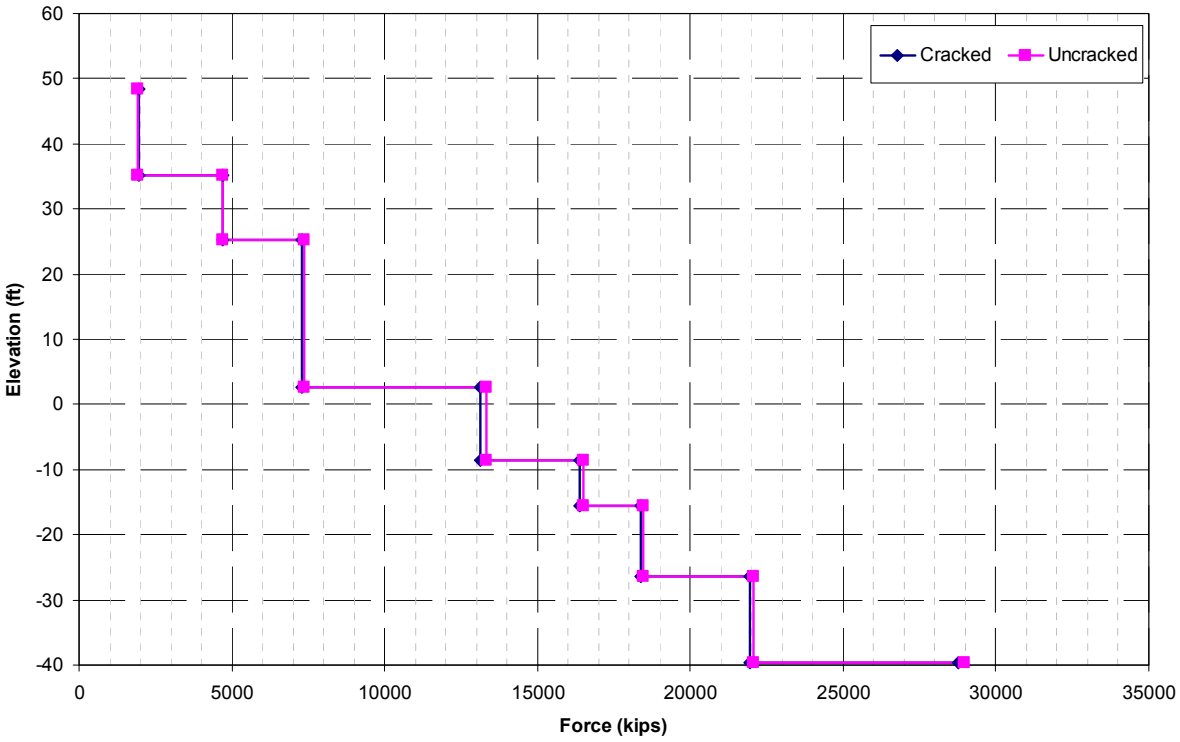

Figure 03.4.3-12 West PS/B SSI Shear Diagram - Envelope of Soil Cases - EW Response (Y)

Figure 03.4.3-13 R/B Peak Acceleration - Ground Floor Elevation - NS Direction (X)

Figure 03.4.3-14 R/B Peak Acceleration - Ground Floor Elevation - EW Direction (Y)

Figure 03.4.3-15 R/B Peak Acceleration - Ground Floor Elevation - Vertical Direction (Z)

03.5.0 CONCLUSION

This report has presented the SSI analyses of the R/B complex with six generic site profiles and SSSI analyses of the R/B complex combined with T/B using four selected generic site profiles. The soil profiles envelope the conditions at a variety of sites within the CEUS. The SSI analyses using finite element models consider a variety of SSI effects such as layering of the subgrade, the frequency dependence of the soil, the embedment effect and the SSSI effect. The results of SSI and SSSI analyses serve as basis for development of seismic design parameters used for the design of the R/B complex. This report presents the seismic design loads used for the standard design of the structural members of the R/B complex The ISRS with appropriate damping values are presented that define the seismic loads at different locations within the buildings for the design of pipe and equipment.

03.6.0 REFERENCES

03-1. Seismic System Analysis, NUREG-0800 Section 3.7.2, Revision 3, U.S. Nuclear Regulatory Commission, Washington, DC, March 2007.

03-2. ACS SASSI, Version 2.3.0 including “Option A” & NQA “Option FS,” “An Advanced Computational Software for 3-D Dynamic Analysis Including Soil Structure Interaction,” User Manuals Revision 7.0, Ghiocel Predictive Technologies, Inc., September 26, 2012.

03-3. Ground Water Effects on SSI, Mitsubishi Heavy Industries, Technical Report MUAP-11007, Revision 2, November, 2012.

03-4. T/B Model Properties, SSI Analyses, and Structural Integrity Evaluation, MUAP-11002, Revision 2, Mitsubishi Heavy Industries, Ltd., February, 2013.

03-5. Site Response Analyses of Vertical Excitation, Proceedings of the Third Specialty Conference on Geotechnical Earthquake Engineering and Soil Dynamics, Mok, Chin Man, Chang, C.-Y., and Lagapsi, Dante E., Seattle, Washington, Geotechnical Special Publication No. 75, ASCE, August 3 – 6, 1998.

03-6. Lysmer, J., et al, SASSI 2000 Theoretical Manual, Revision 1, Geotechnical Engineering Division, Civil department, University of California, Berkeley.

03-7. Interim Staff Guidance 17 (DC/COL-ISG-17) on Ensuring Hazard-Consistent Seismic Input for Site Response and Soil-Structure Interaction Analyses, U. S. Nuclear Regulatory Commission (NRC), July 2009

03-8. NEI White Paper, Consistent Site-Response/Soil-Structure Interaction Analysis and Evaluation, NEI, June 12, 2009 (ADAMS Accession No. ML091680715).

03-9. Schnable, P.B., Lysmer,J., and Seed, H.B. “SHAKE, A computer program for earthquake response analysis of horizontally layered sites” Earthquake Engineering Research Center, University of California at Berkeley, UBC/EERC 72-12.

03-10. U.S. Department of Energy, Soil-Structure Interaction report, July 2011

03-11. Seed H.B., Ugas, C., and Lysmer, J. “Site-dependent spectra for earthquake-resistant design,” Bulletin of the Seismological Society of America, Vol. 66, pp. 221-243.

03-12. Development of Floor Design Response Spectra for Seismic Design of Floor-Supported Equipment or Components, Regulatory Guide 1.122, Rev. 1, U.S. Nuclear Regulatory Commission, Washington, DC, February 1978.

03-13. ANSYS, Release 13.0, SAS IP, Inc., 2010.

Appendix 3-A

R/B Complex Node Numbering and Grouping for ISRS Plots

APPENDIX 3-A TABLE OF CONTENTS

Section **Title** **Page No.**

3-A.1.0 R/B COMPLEX MODEL NODE NUMBERING 3-A.1-1
3-A.1.1 R/B Complex Critical Locations – Equipment 3-A.1-1
3-A.1.2 R/B Complex Critical Locations – Structural 3-A.1-3

3-A.2.0 ARS GROUPING 3-A.2-1

LIST OF FIGURES

Figure **Title** **Page No.**

Figure 3-A.2.0-1 R/B Complex – Top of Reactor Cavity – Elevation 35.9 ft 2-2
Figure 3-A.2.0-2 R/B Complex – Sump Strainer – Elevation 2.58 ft 2-3
Figure 3-A.2.0-3 R/B Complex – SG Lower Supports – Elevation 45.64 ft 2-4
Figure 3-A.2.0-4 R/B Complex – SG Upper Supports – Elevation 96.58 ft 2-5
Figure 3-A.2.0-5 R/B Complex – SFP – Elevation 25.25 ft 2-6
Figure 3-A.2.0-6 R/B Complex – NFSP – Elevation 63.33 ft 2-7
Figure 3-A.2.0-7 R/B Complex – A-AAC GTG – Elevation 2.58 ft 2-8
Figure 3-A.2.0-8 R/B Complex – B-AAC GTG – Elevation 2.58 ft 2-9
Figure 3-A.2.0-9 R/B Complex – Looking East 2-10
Figure 3-A.2.0-10 R/B Complex – Looking West 2-11

LIST OF TABLES

Table **Title** **Page No.**

Table 3-A.1.1-1 Reactor Building Node Numbering and Locations for Critical Equipment Locations (Sheet 1 of 2) 3-A.1-1
Table 3-A.1.2-1 Reactor Building Node Numbering and Locations for Critical Structural Locations 3-A.1-3

3-A.1.0 R/B COMPLEX MODEL NODE NUMBERING

The nodes selected for the ARS are presented in the following tables. The specific nodes enveloped for each piece of equipment are located in Table 3-A.1.1-1. The critical structural node locations are in Table 3-A.1.2-1. The nodes numbers listed in Table 3-A.1.1-1 and Table 3-A.1.2-1 correspond with the node numbers shown in Figure 3-A.2.0-1 through Figure 3-A.2.0-10.

3-A.1.1 R/B Complex Critical Locations – Equipment

Table 3-A.1.1-1 Reactor Building Node Numbering and Locations for Critical Equipment Locations (Sheet 1 of 2)

Table 3-A.1.1-1 Reactor Building Node Numbering and Locations for Critical Equipment Locations (Sheet 2 of 2)

3-A.1.2 R/B Complex Critical Locations – Structural

Table 3-A.1.2-1 Reactor Building Node Numbering and Locations for Critical Structural Locations

3-A.2.0 ARS GROUPING

Figures of the ARS grouping for the R/B complex structures are shown in Figure 3-A.2.0-1 through Figure 3-A.2.0-10. Nodes are enveloped together to present responses at the selected equipment and structural locations.

Figure 3-A.2.0-1 R/B Complex – Top of Reactor Cavity – Elevation 35.9 ft

Figure 3-A.2.0-2 R/B Complex – Sump Strainer – Elevation 2.58 ft

Figure 3-A.2.0-3 R/B Complex – SG Lower Supports – Elevation 45.64 ft

Figure 3-A.2.0-4 R/B Complex – SG Upper Supports – Elevation 96.58 ft

Figure 3-A.2.0-5 R/B Complex – SFP – Elevation 25.25 ft

Figure 3-A.2.0-6 R/B Complex – NFSP – Elevation 63.33 ft

Figure 3-A.2.0-7 R/B Complex – A-AAC GTG – Elevation 2.58 ft

Figure 3-A.2.0-8 R/B Complex – B-AAC GTG – Elevation 2.58 ft

Figure 3-A.2.0-9 R/B Complex – Looking East

Figure 3-A.2.0-10 R/B Complex – Looking West

Appendix 3-B

ISRS Plots for the R/B Complex

APPENDIX 3-B TABLE OF CONTENTS

Section	Title	Page No.
3-B.1.0	**DESIGN BASIS ISRS**	**3-B.1-1**

LIST OF FIGURES

Figure	Title	Page No.
Figure 3-B.1.0-1	Design Basis ISRS at Top of Reactor Cavity – 3% DampedResponse in NS Direction (X)	3-B.1-1
Figure 3-B.1.0-2	Design Basis ISRS at Top of Reactor Cavity – 3% Damped Response in EW Direction (Y)	3-B.1-2
Figure 3-B.1.0-3	Design Basis ISRS at Top of Reactor Cavity – 3% Damped Response in Vertical Direction (Z)	3-B.1-3
Figure 3-B.1.0-4	Design Basis ISRS at Sump Strainer – 3% Damped Response in NS Direction (X)	3-B.1-4
Figure 3-B.1.0-5	Design Basis ISRS at Sump Strainer – 3% Damped Response in EW Direction (Y)	3-B.1-5
Figure 3-B.1.0-6	Design Basis ISRS at Sump Strainer - 3% Damped Response in Vertical Direction (Z)	3-B.1-6
Figure 3-B.1.0-7	Design Basis ISRS at SG Lower Supports - 3% Damped Response in NS Direction (X)	3-B.1-7
Figure 3-B.1.0-8	Design Basis ISRS at SG Lower Supports - 3% Damped Response in EW Direction (Y)	3-B.1-8
Figure 3-B.1.0-9	Design Basis ISRS at SG Lower Supports - 3% Damped Response in Vertical Direction (Z)	3-B.1-9
Figure 3-B.1.0-10	Design Basis ISRS at SG Upper Supports - 3% Damped Response in NS Direction (X)	3-B.1-10
Figure 3-B.1.0-11	Design Basis ISRS at SG Upper Supports - 3% Damped Response in EW Direction (Y)	3-B.1-11
Figure 3-B.1.0-12	Design Basis ISRS at SG Upper Supports - 3% Damped Response in Vertical Direction (Z)	3-B.1-12
Figure 3-B.1.0-13	Design Basis ISRS at SFP - 3% Damped Response in NS Direction (X)	3-B.1-13
Figure 3-B.1.0-14	Design Basis ISRS at SFP - 3% Damped Response in EW Direction (Y)	3-B.1-14
Figure 3-B.1.0-15	Design Basis ISRS at SFP - 3% Damped Response in Vertical Direction (Z)	3-B.1-15
Figure 3-B.1.0-16	Design Basis ISRS at NFSP - 4% Damped Response in NS Direction (X)	3-B.1-16

Figure 3-B.1.0-17 Design Basis ISRS at NFSP - 4% Damped Response in EW Direction (Y) 3-B.1-17
Figure 3-B.1.0-18 Design Basis ISRS at NFSP - 4% Damped Response in Vertical Direction (Z) 3-B.1-18
Figure 3-B.1.0-19 Design Basis ISRS at A-AAC GTG - 5% Damped Response in NS Direction (X) 3-B.1-19
Figure 3-B.1.0-20 Design Basis ISRS at A-AAC GTG - 5% Damped Response in EW Direction (Y) 3-B.1-20
Figure 3-B.1.0-21 Design Basis ISRS at A-AAC GTG - 5% Damped Response in Vertical Direction (Z) 3-B.1-21
Figure 3-B.1.0-22 Design Basis ISRS at B-AAC GTG - 5% Damped Response in NS Direction (X) 3-B.1-22
Figure 3-B.1.0-23 Design Basis ISRS at B-AAC GTG - 5% Damped Response in EW Direction (Y) 3-B.1-23
Figure 3-B.1.0-24 Design Basis ISRS at B-AAC GTG - 5% Damped Response in Vertical Direction (Z) 3-B.1-24
Figure 3-B.1.0-25 Design Basis ISRS at A/B NW Corner Basemat - 5% Damped Response in NS Direction (X) at Model Elevation -26’-4” 3-B.1-25
Figure 3-B.1.0-26 Design Basis ISRS at A/B NW Corner Basemat - 5% Damped Response in EW Direction (Y) at Model Elevation -26’-4” 3-B.1-26
Figure 3-B.1.0-27 Design Basis ISRS at A/B NW Corner Basemat - 5% Damped Response in Vertical Direction (Z) at Model Elevation -26’-4” 3-B.1-27
Figure 3-B.1.0-28 Design Basis ISRS at A/B NW Corner Roof - 5% Damped Response in NS Direction (X) at Model Elevation 74’-10” 3-B.1-28
Figure 3-B.1.0-29 Design Basis ISRS at A/B NW Corner Roof - 5% Damped Response in EW Direction (Y) at Model Elevation 74’-10”..... 3-B.1-29
Figure 3-B.1.0-30 Design Basis ISRS at A/B NW Corner Roof - 5% Damped Response in Vertical Direction (Z) at Model Elevation 74’-10”..... 3-B.1-30
Figure 3-B.1.0-31 Design Basis ISRS at West PS/B SW Corner Basemat - 5% Damped Response in NS Direction (X) at Model Elevation -26’-4” 3-B.1-31
Figure 3-B.1.0-32 Design Basis ISRS at West PS/B SW Corner Basemat - 5% Damped Response in EW Direction (Y) at Model Elevation -26’-4” 3-B.1-32
Figure 3-B.1.0-33 Design Basis ISRS at West PS/B SW Corner Basemat - 5% Damped Response in Vertical Direction (Z) at Model Elevation -26’-4” 3-B.1-33
Figure 3-B.1.0-34 Design Basis ISRS at West PS/B SW Corner Roof - 5% Damped Response in NS Direction (X) at Model Elevation 48’-6” 3-B.1-34
Figure 3-B.1.0-35 Design Basis ISRS at West PS/B SW Corner Roof - 5% Damped Response in EW Direction (Y) at Model Elevation 48’-6” 3-B.1-35

Figure 3-B.1.0-36 Design Basis ISRS at West PS/B SW Corner Roof - 5% Damped Response in Vertical Direction (Z) at Model Elevation 48’-6” 3-B.1-36
Figure 3-B.1.0-37 Design Basis ISRS at East PS/B SE Corner Basemat - 5% Damped Response in NS Direction (X) at Model Elevation -26’-4” 3-B.1-37
Figure 3-B.1.0-38 Design Basis ISRS at East PS/B SE Corner Basemat - 5% Damped Response in EW Direction (Y) at Model Elevation -26’-4” 3-B.1-38
Figure 3-B.1.0-39 Design Basis ISRS at East PS/B SE Corner Basemat - 5% Damped Response in Vertical Direction (Z) at Model Elevation -26’-4” 3-B.1-39
Figure 3-B.1.0-40 Design Basis ISRS at East PS/B SE Corner Roof - 5% Damped Response in NS Direction (X) at Model Elevation 48’-6” 3-B.1-40
Figure 3-B.1.0-41 Design Basis ISRS at East PS/B SE Corner Roof - 5% Damped Response in EW Direction (Y) at Model Elevation 48’-6” 3-B.1-41
Figure 3-B.1.0-42 Design Basis ISRS at East PS/B SE Corner Roof - 5% Damped Response in Vertical Direction (Z) at Model Elevation 48’-6” 3-B.1-42
Figure 3-B.1.0-43 Design Basis ISRS at R/B NE Corner Basemat - 5% Damped Response in NS Direction (X) at Model Elevation -26’-4” 3-B.1-43
Figure 3-B.1.0-44 Design Basis ISRS at R/B NE Corner Basemat - 5% Damped Response in EW Direction (Y) at Model Elevation -26’-4” 3-B.1-44
Figure 3-B.1.0-45 Design Basis ISRS at R/B NE Corner Basemat - 5% Damped Response in Vertical Direction (Z) at Model Elevation -26’-4” 3-B.1-45
Figure 3-B.1.0-46 Design Basis ISRS at FH/A NE Corner Roof - 5% Damped Response in NS Direction (X) at Model Elevation 156’-0” 3-B.1-46
Figure 3-B.1.0-47 Design Basis ISRS at FH/A NE Corner Roof - 5% Damped Response in EW Direction (Y) at Model Elevation 156’-0” 3-B.1-47
Figure 3-B.1.0-48 Design Basis ISRS at FH/A NE Corner Roof - 5% Damped Response in Vertical Direction (Z) at Model Elevation 156’-0” 3-B.1-48
Figure 3-B.1.0-49 Design Basis ISRS at Top of PCCV - 5% Damped Response in NS Direction (X) at Model Elevation 232’-0” 3-B.1-49
Figure 3-B.1.0-50 Design Basis ISRS at Top of PCCV - 5% Damped Response in EW Direction (Y) at Model Elevation 232’-0” 3-B.1-50
Figure 3-B.1.0-51 Design Basis ISRS at Top of PCCV - 5% Damped Response in Vertical Direction (Z) at Model Elevation 232’-0” 3-B.1-51

3-B.1.0 DESIGN BASIS ISRS

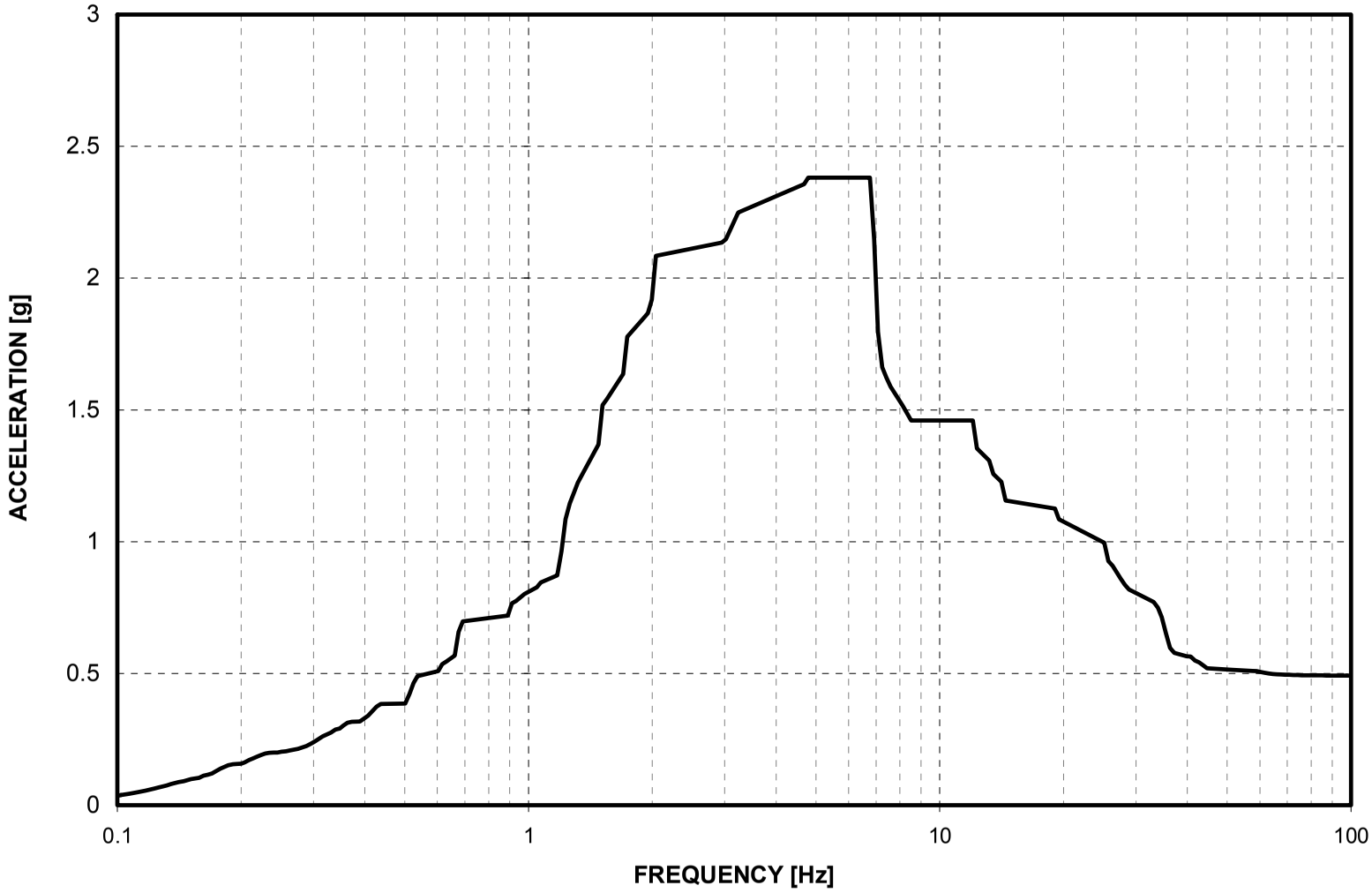

Figure 3-B.1.0-1 Design Basis ISRS at Top of Reactor Cavity – 3% Damped Response in NS Direction (X)

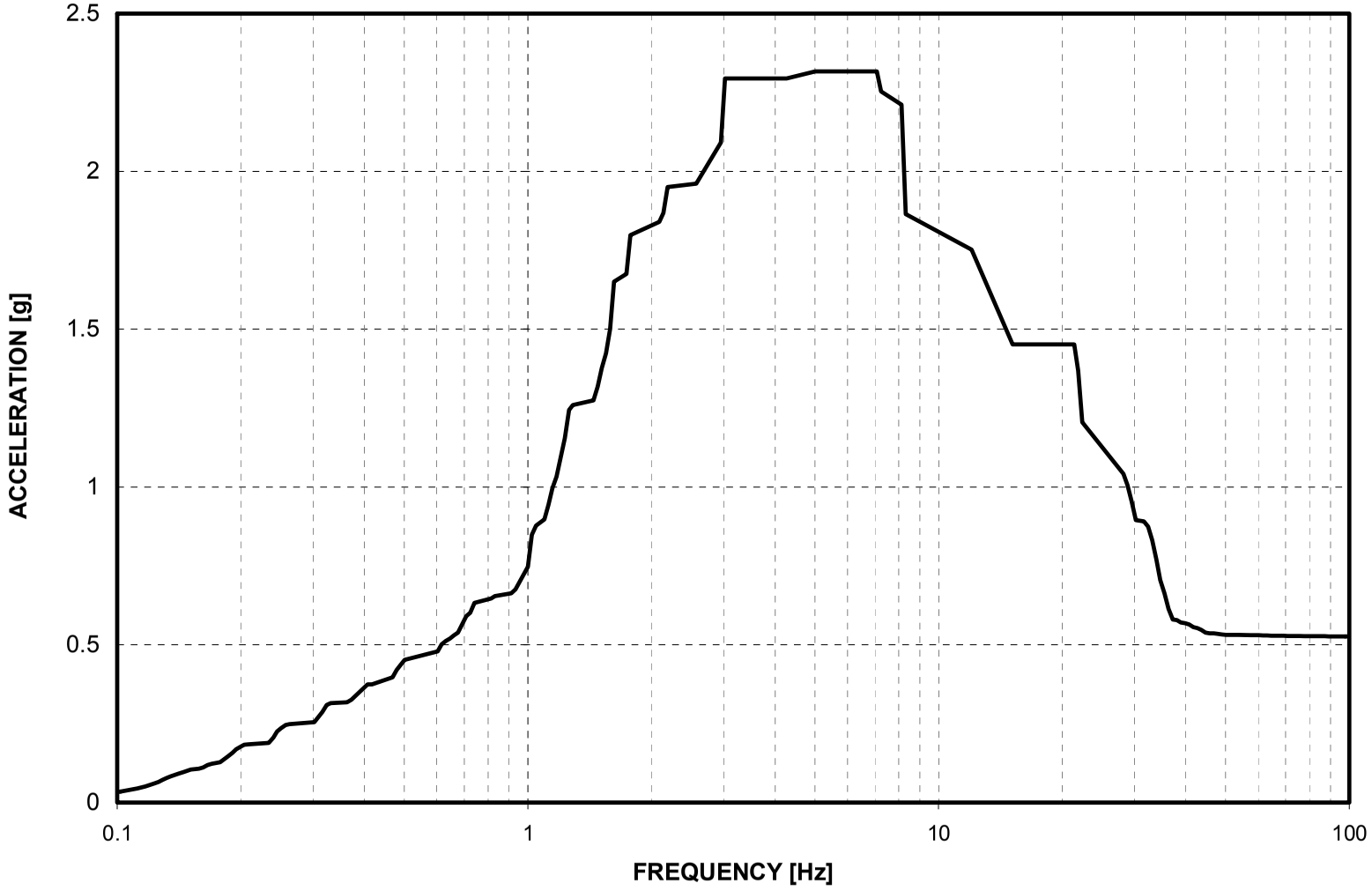

Figure 3-B.1.0-2 Design Basis ISRS at Top of Reactor Cavity – 3% Damped Response in EW Direction (Y)

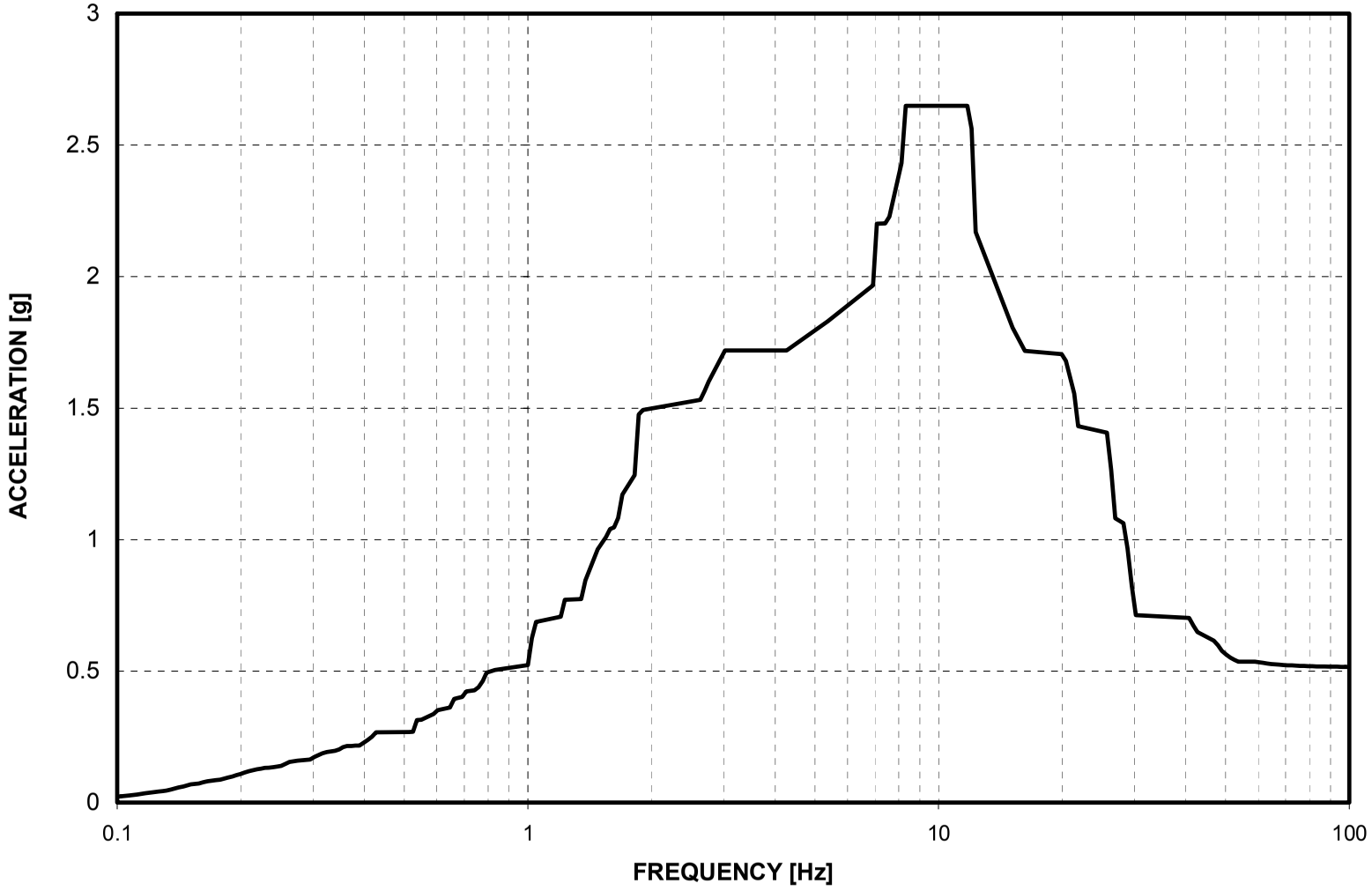

Figure 3-B.1.0-3 Design Basis ISRS at Top of Reactor Cavity – 3% Damped Response in Vertical Direction (Z)

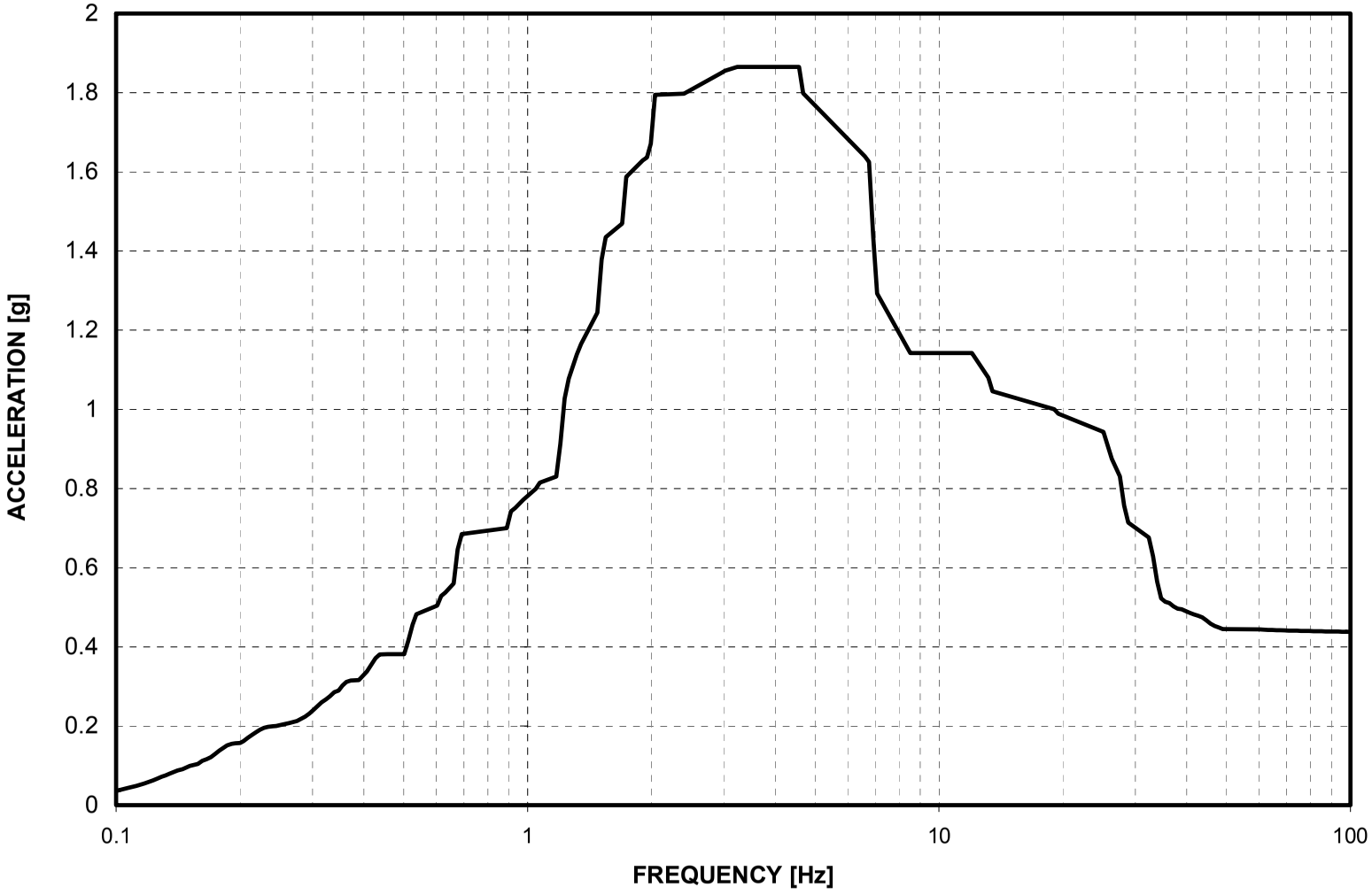

Figure 3-B.1.0-4 Design Basis ISRS at Sump Strainer – 3% Damped Response in NS Direction (X)

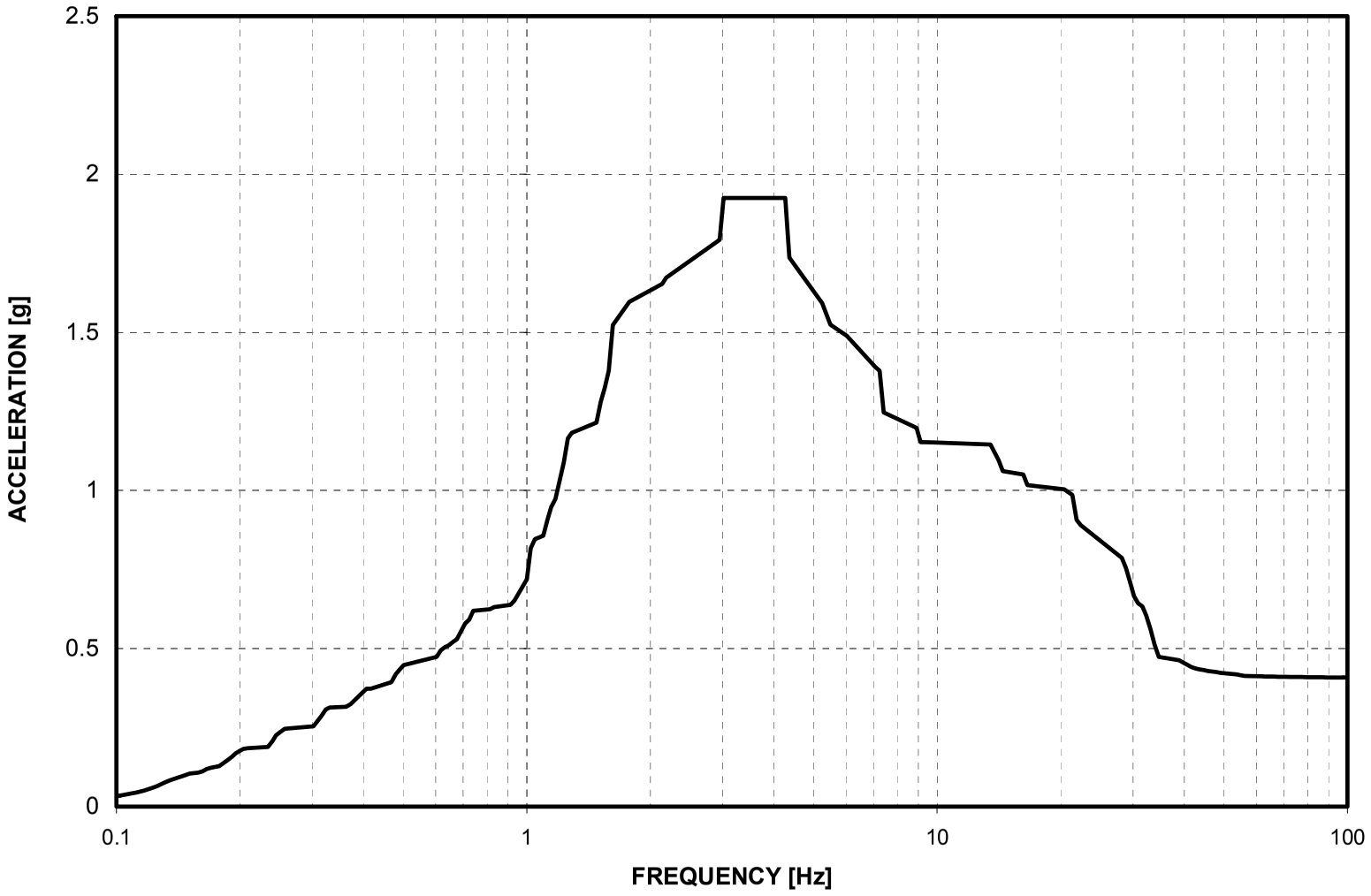

Figure 3-B.1.0-5 Design Basis ISRS at Sump Strainer – 3% Damped Response in EW Direction (Y)

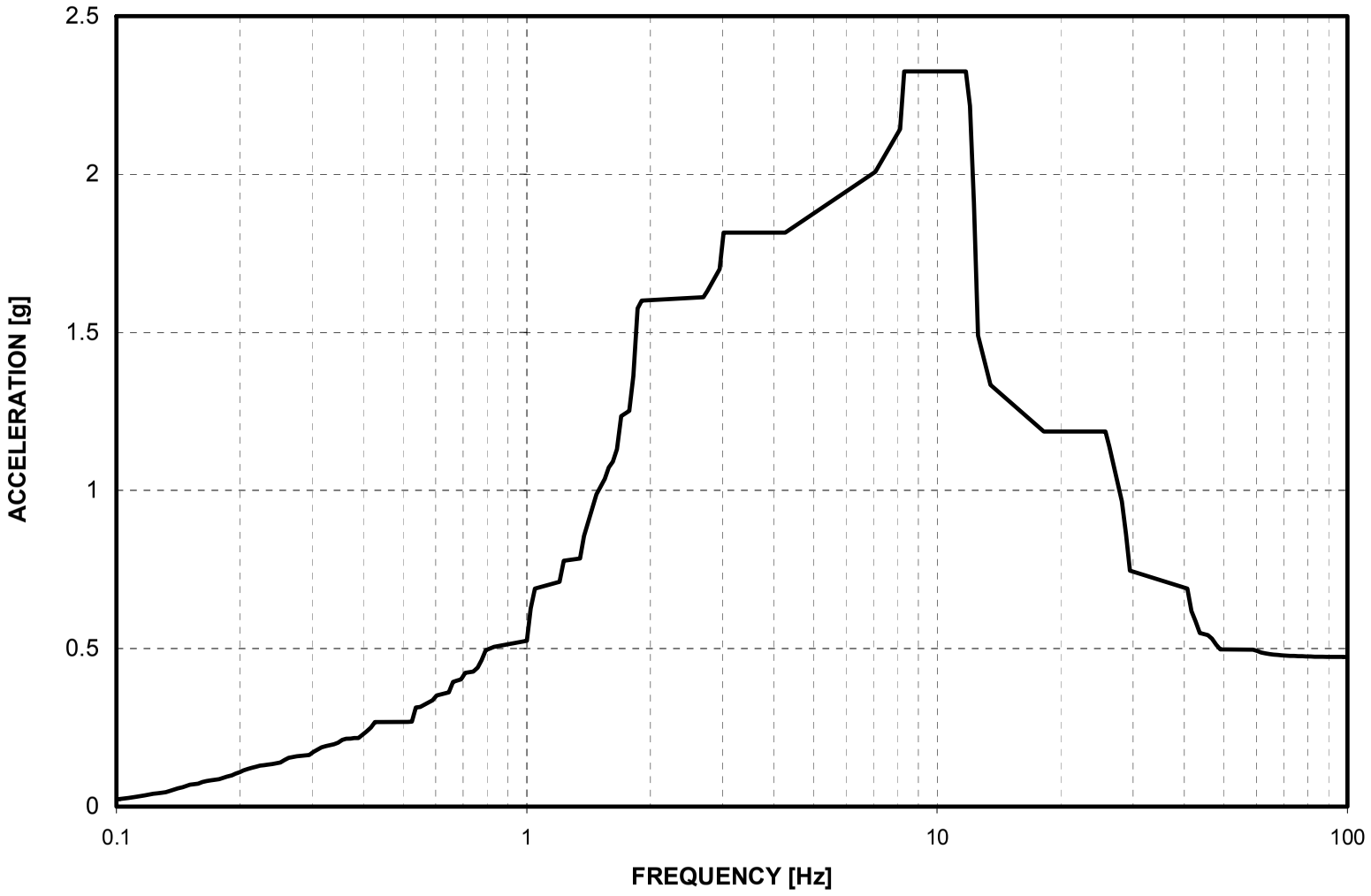

Figure 3-B.1.0-6 Design Basis ISRS at Sump Strainer - 3% Damped Response in Vertical Direction (Z)

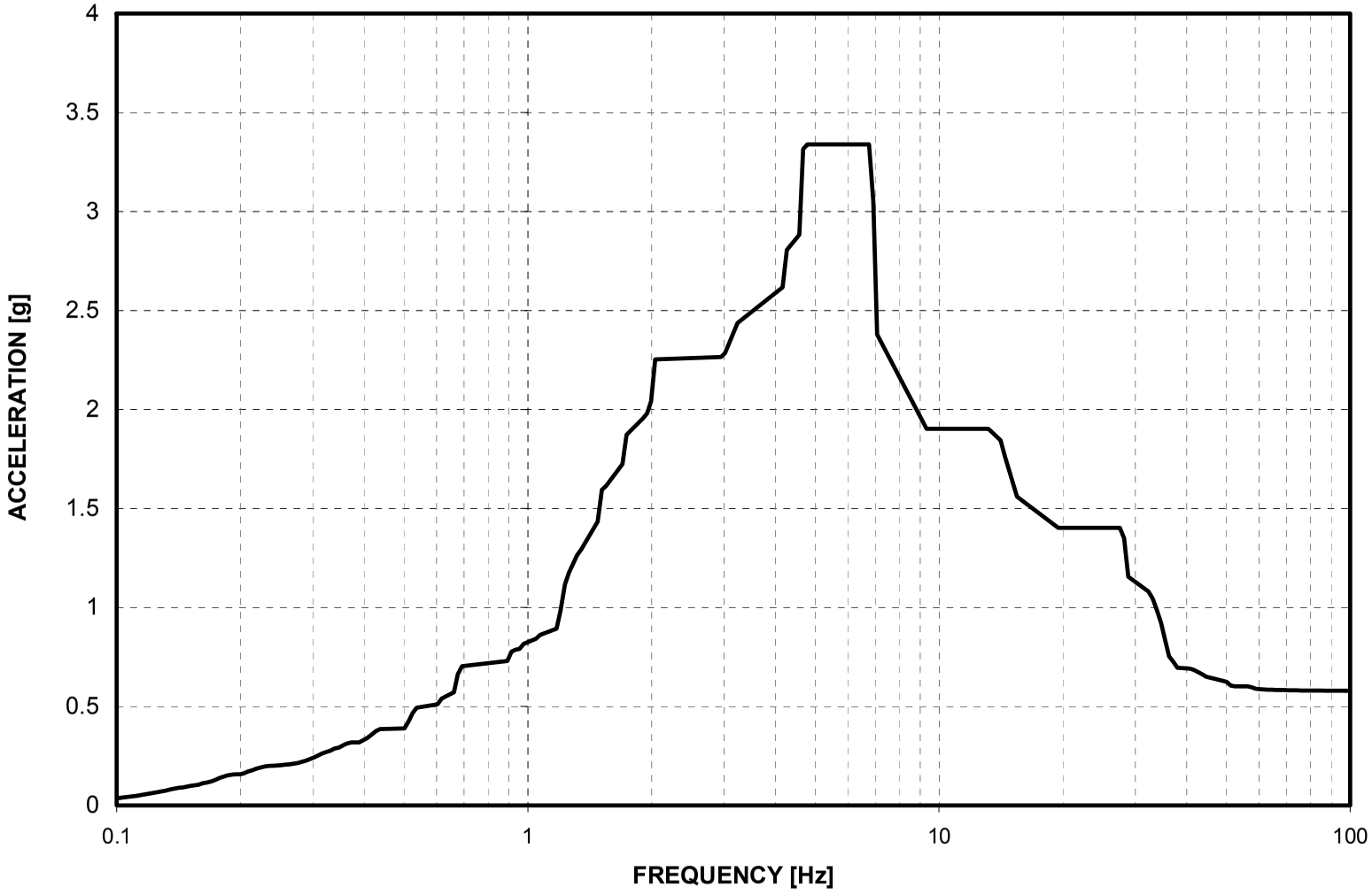

Figure 3-B.1.0-7 Design Basis ISRS at SG Lower Supports - 3% Damped Response in NS Direction (X)

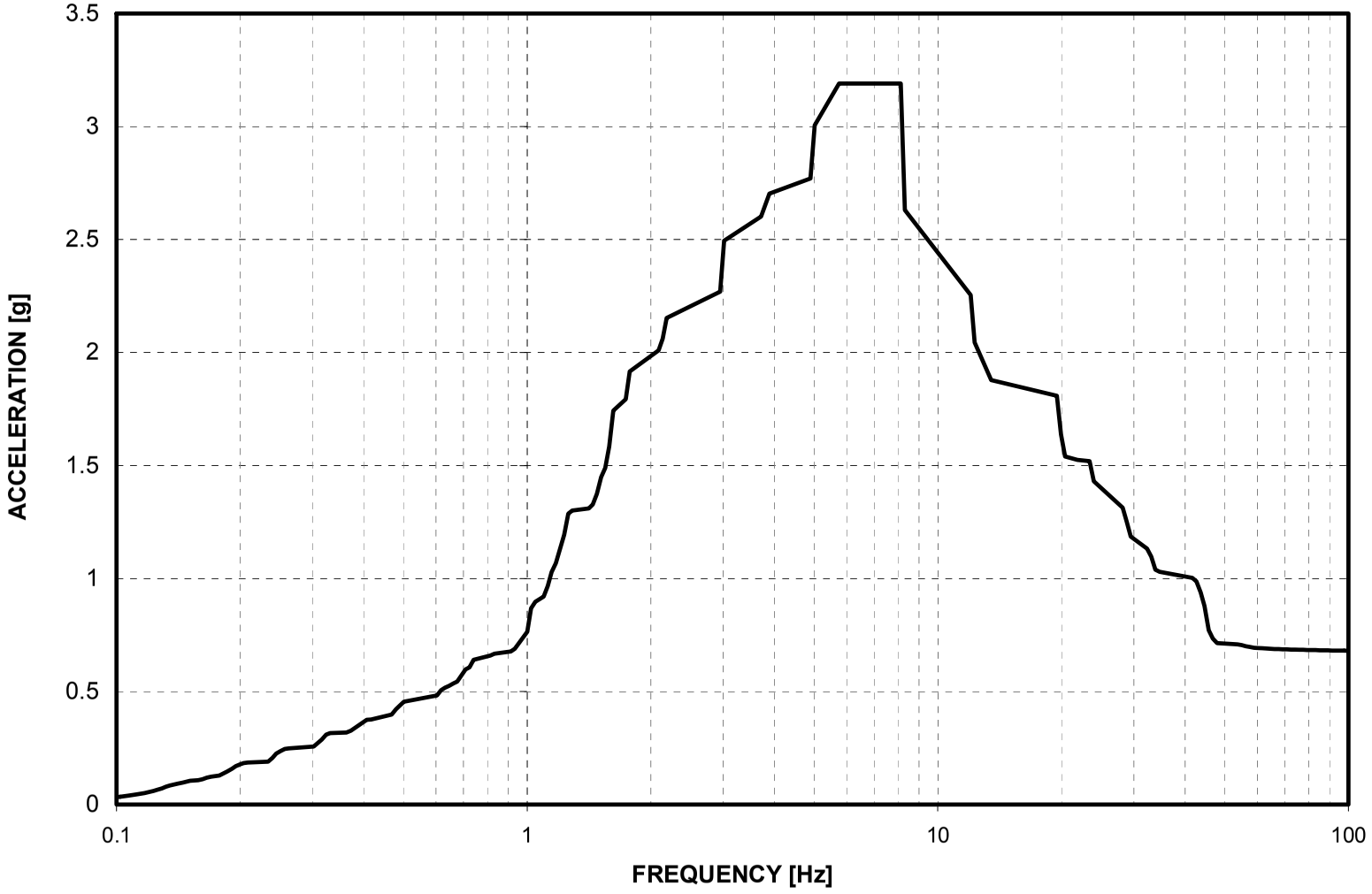

Figure 3-B.1.0-8 Design Basis ISRS at SG Lower Supports - 3% Damped Response in EW Direction (Y)

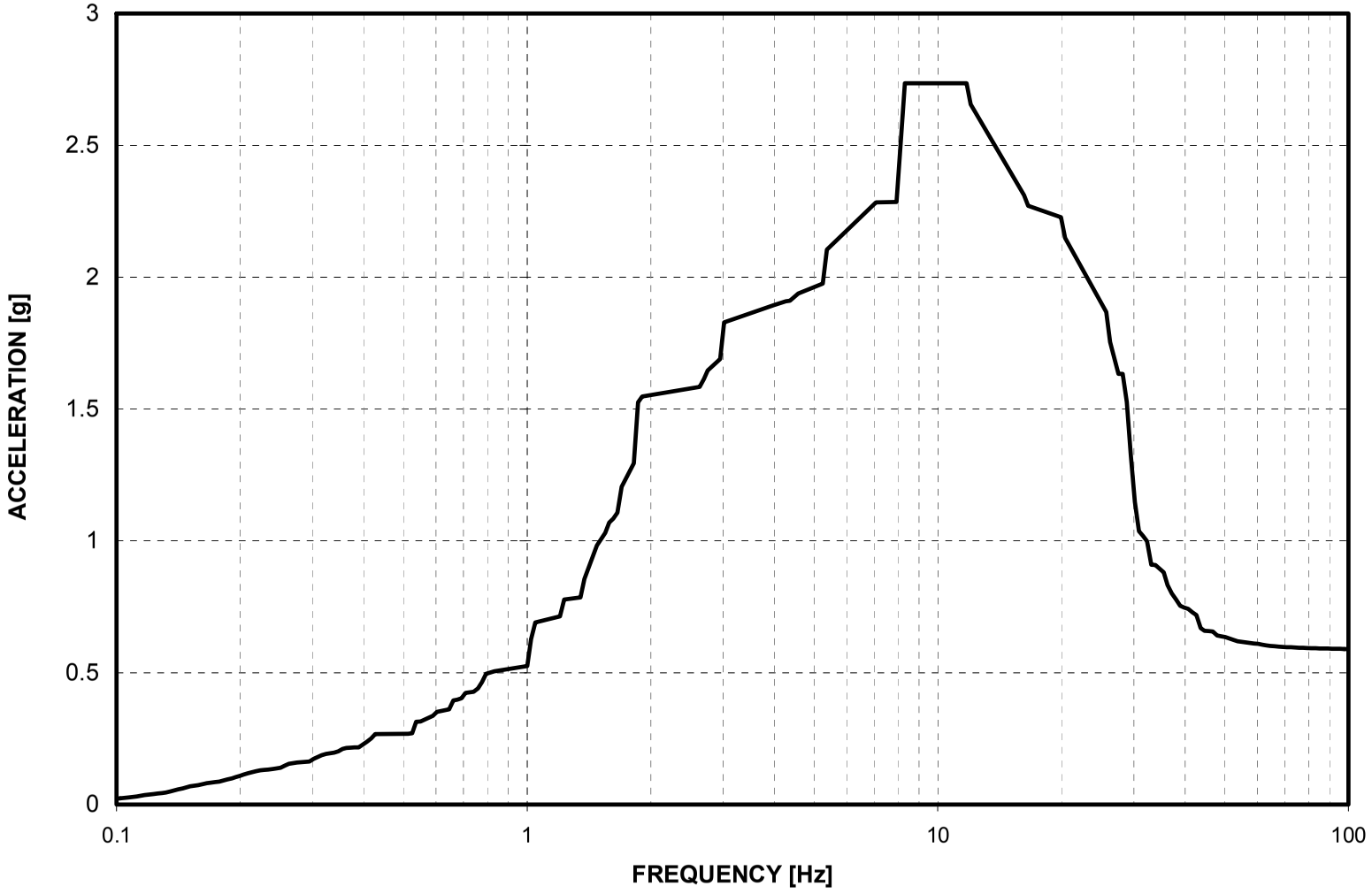

Figure 3-B.1.0-9 Design Basis ISRS at SG Lower Supports - 3% Damped Response in Vertical Direction (Z)

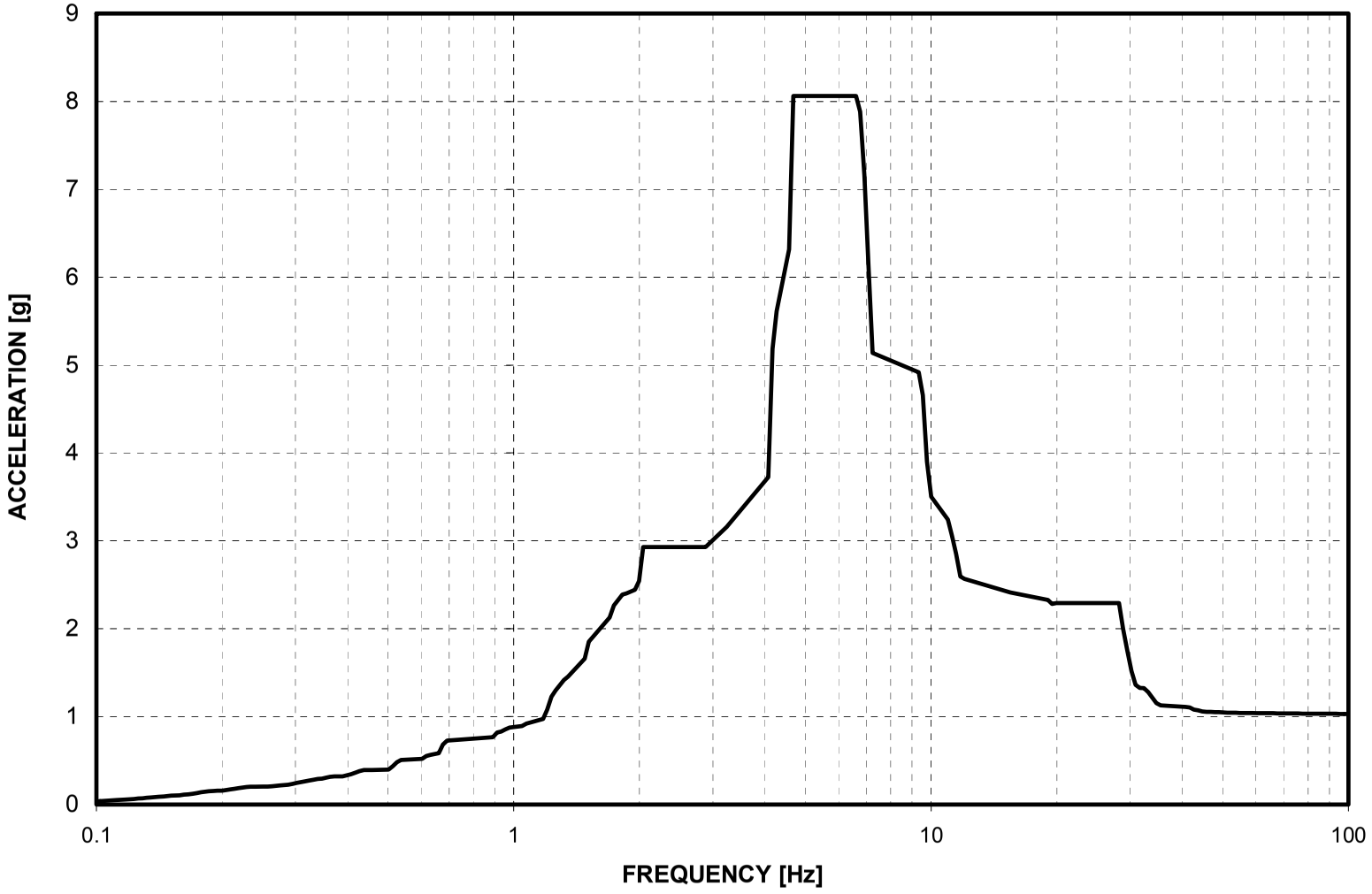

Figure 3-B.1.0-10 Design Basis ISRS at SG Upper Supports - 3% Damped Response in NS Direction (X)

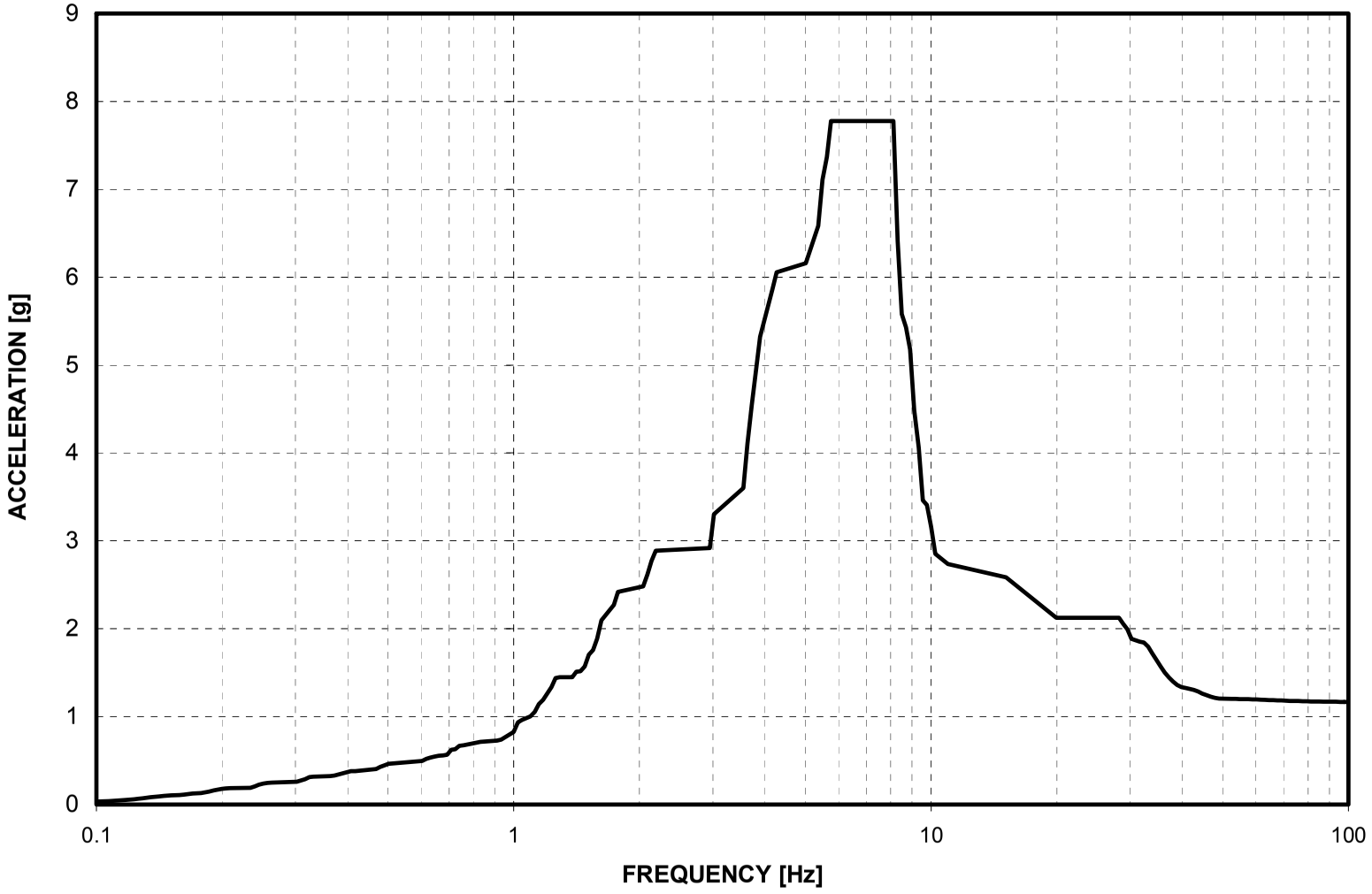

Figure 3-B.1.0-11 Design Basis ISRS at SG Upper Supports - 3% Damped Response in EW Direction (Y)

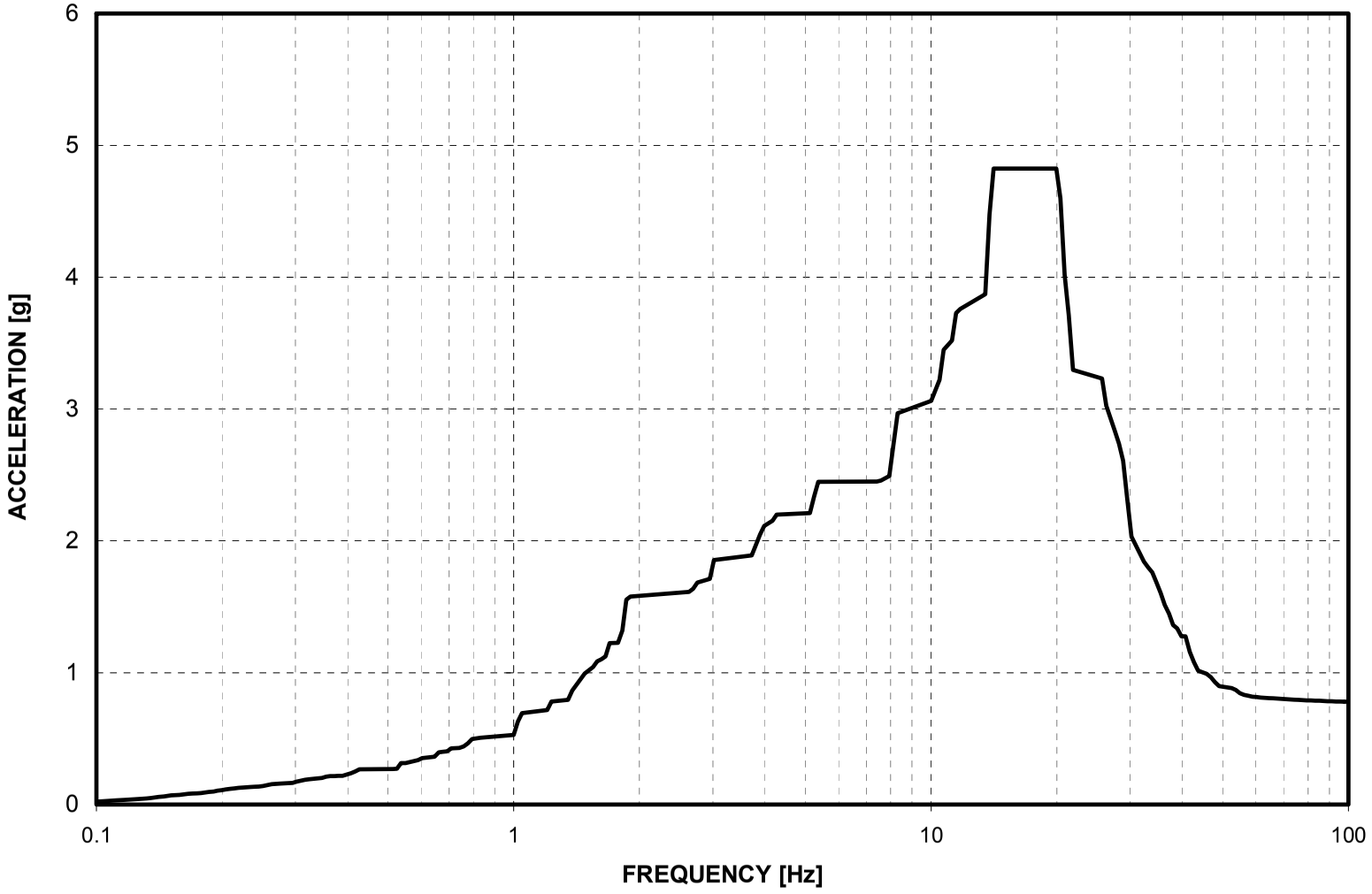

Figure 3-B.1.0-12 Design Basis ISRS at SG Upper Supports - 3% Damped Response in Vertical Direction (Z)

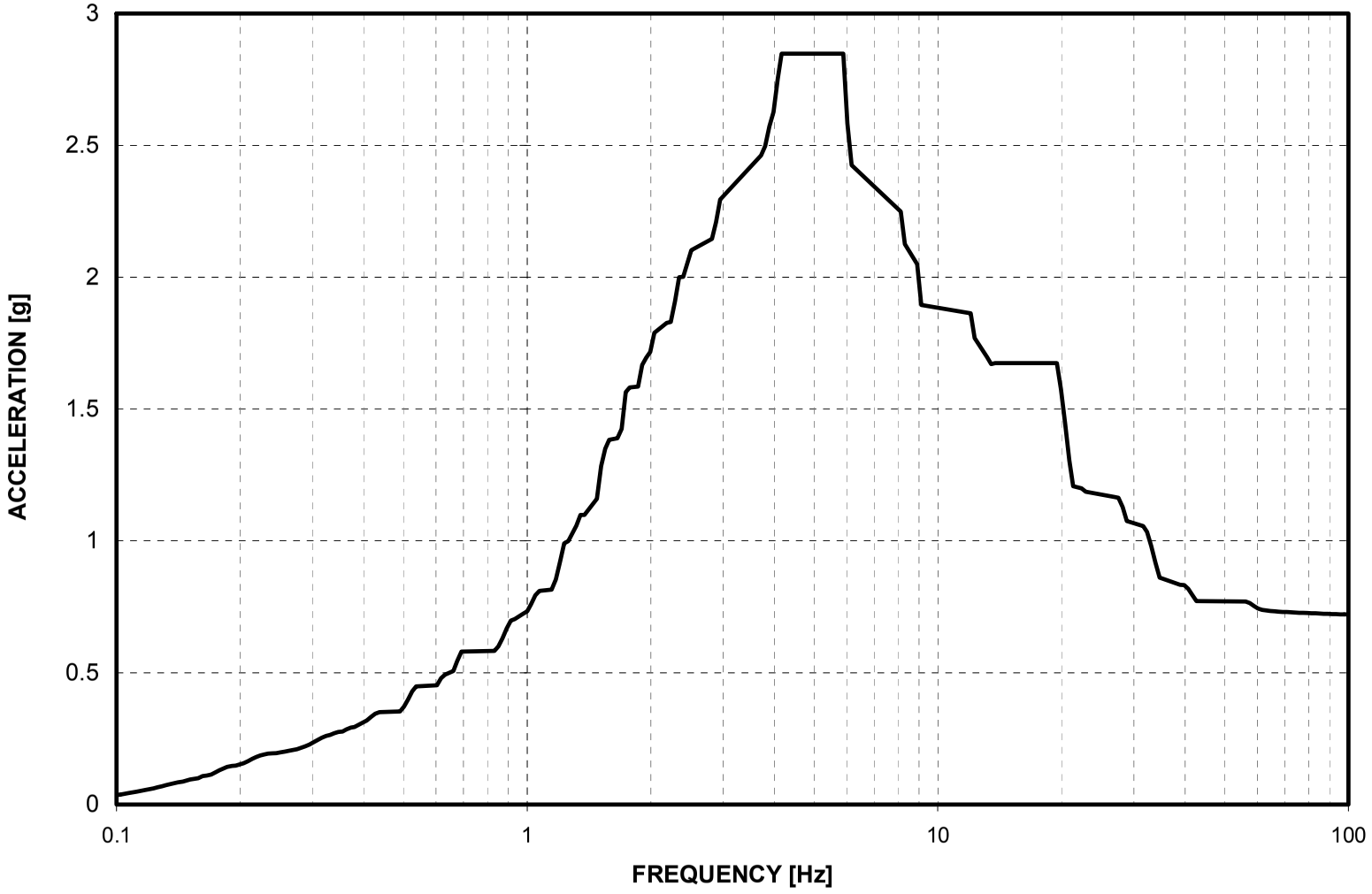

Figure 3-B.1.0-13 Design Basis ISRS at SFP - 3% Damped Response in NS Direction (X)

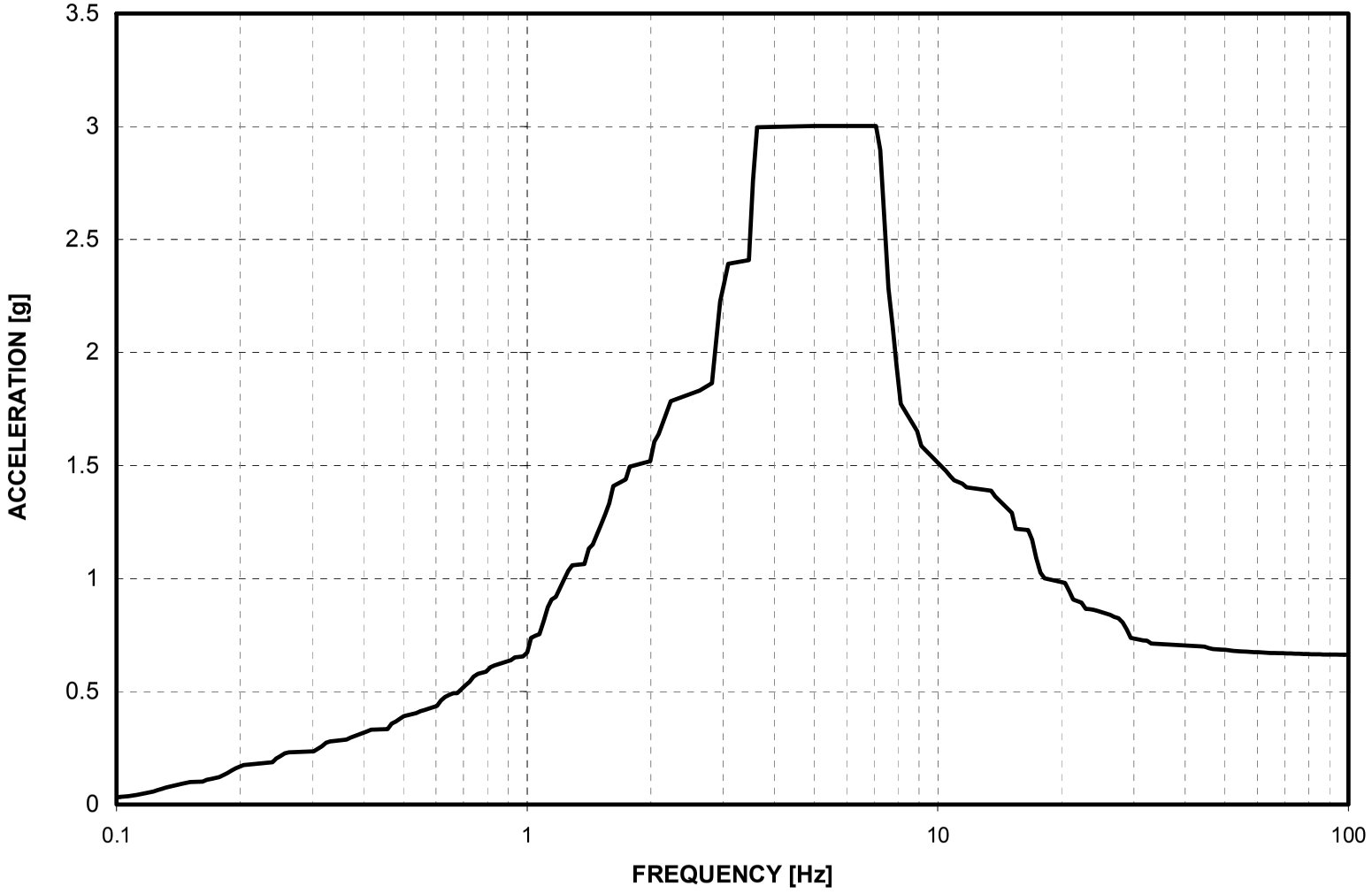

Figure 3-B.1.0-14 Design Basis ISRS at SFP - 3% Damped Response in EW Direction (Y)

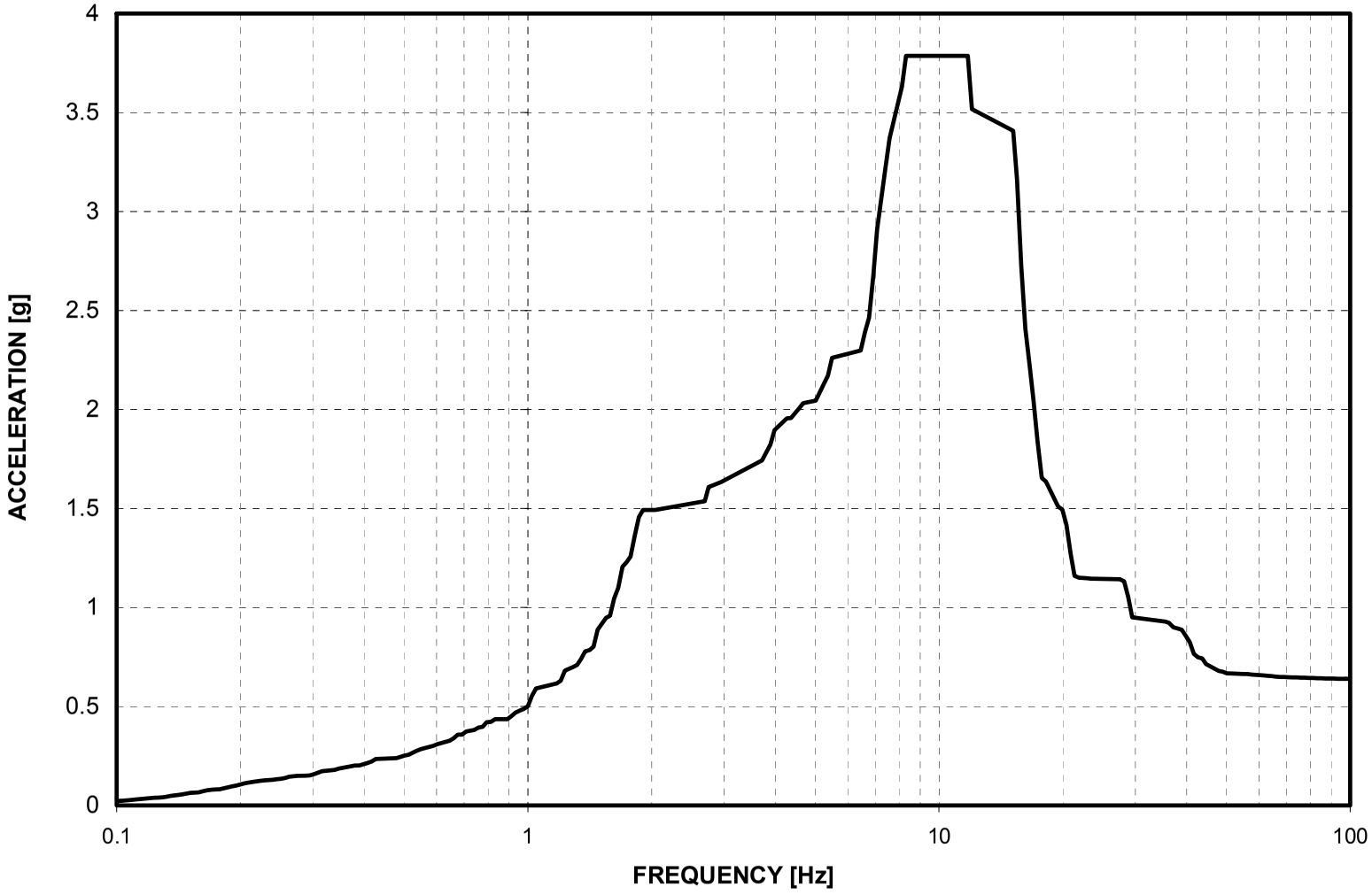

Figure 3-B.1.0-15 Design Basis ISRS at SFP - 3% Damped Response in Vertical Direction (Z)

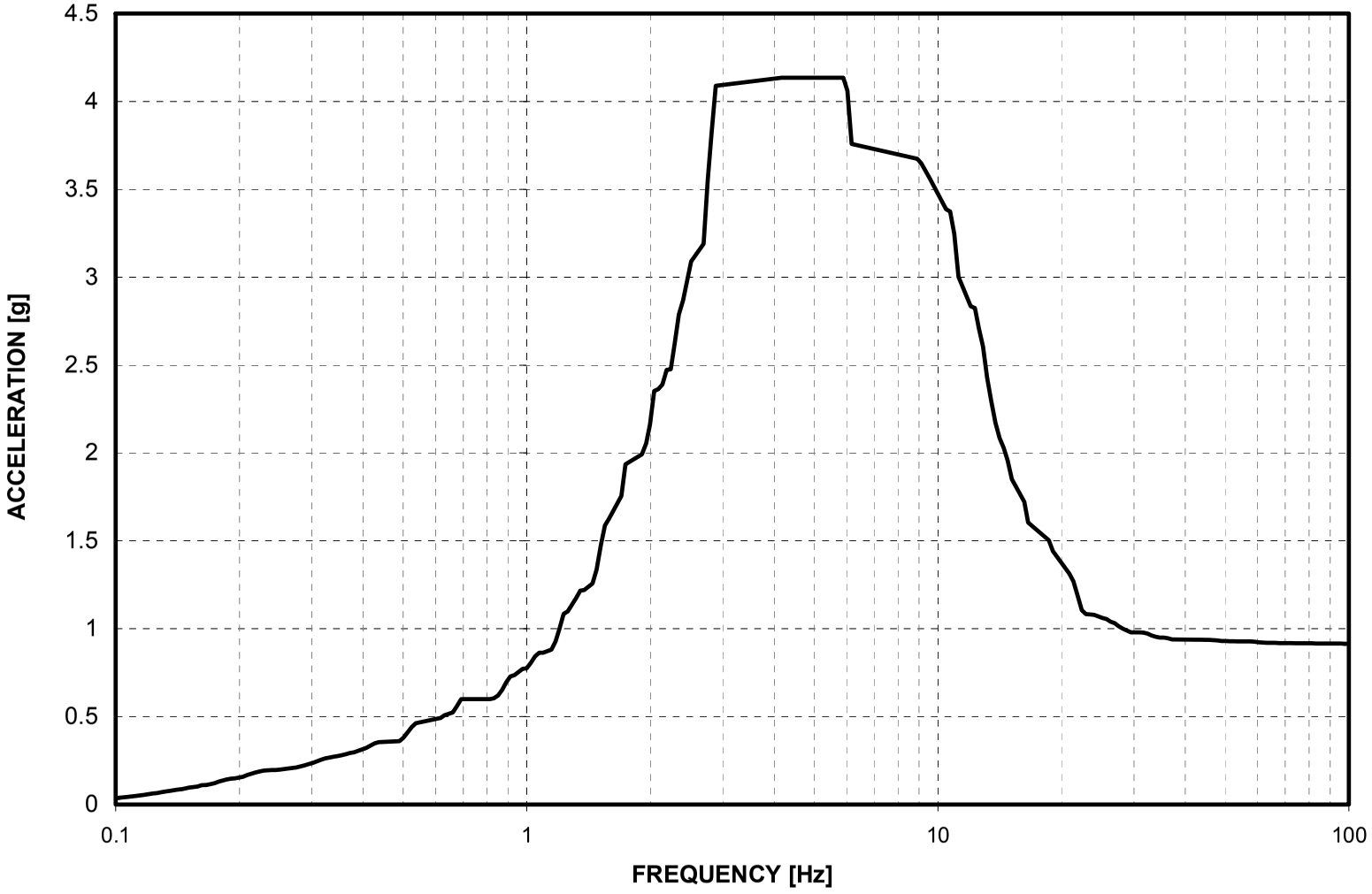

Figure 3-B.1.0-16 Design Basis ISRS at NFSP - 4% Damped Response in NS Direction (X)

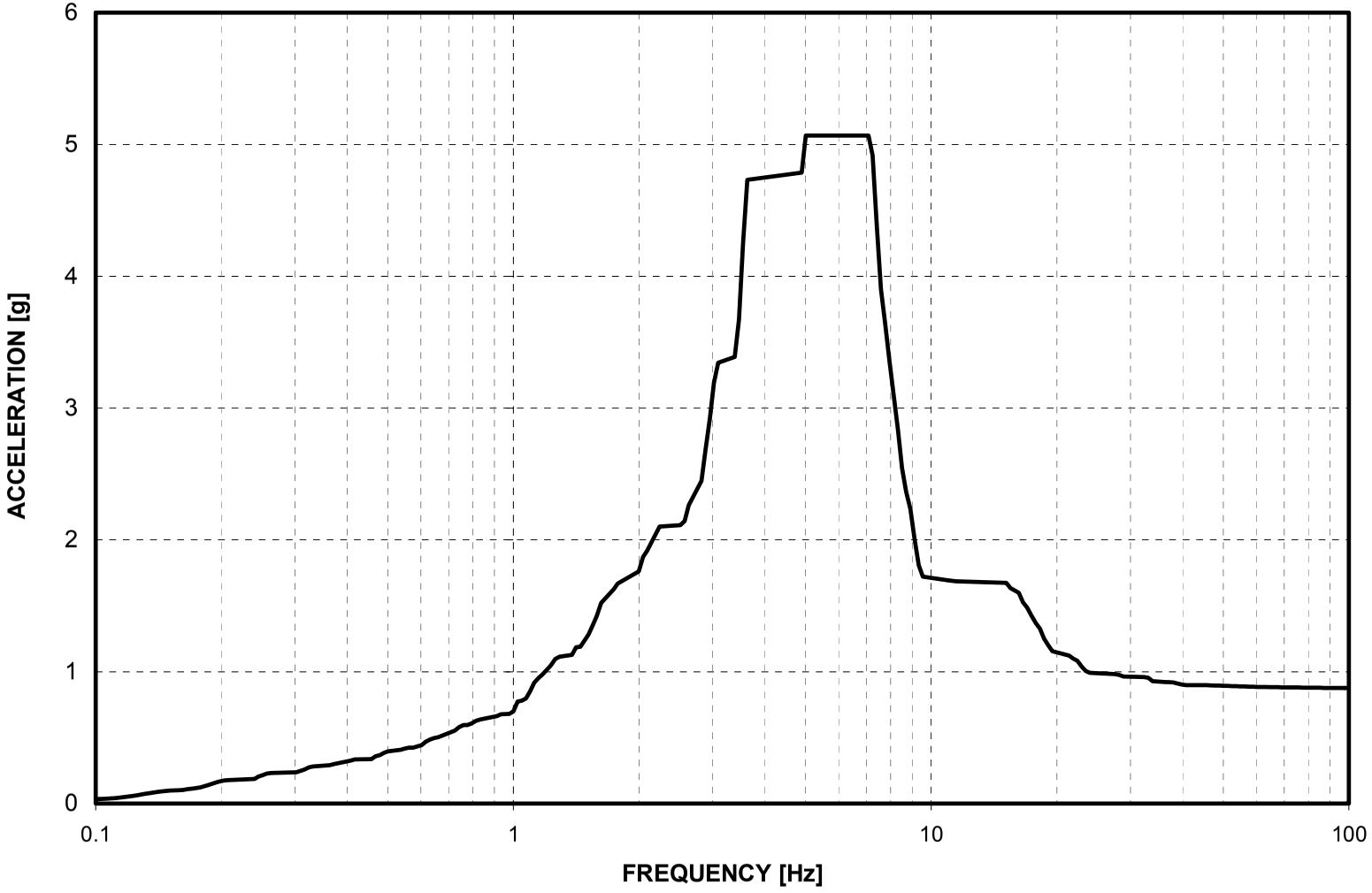

Figure 3-B.1.0-17 Design Basis ISRS at NFSP - 4% Damped Response in EW Direction (Y)

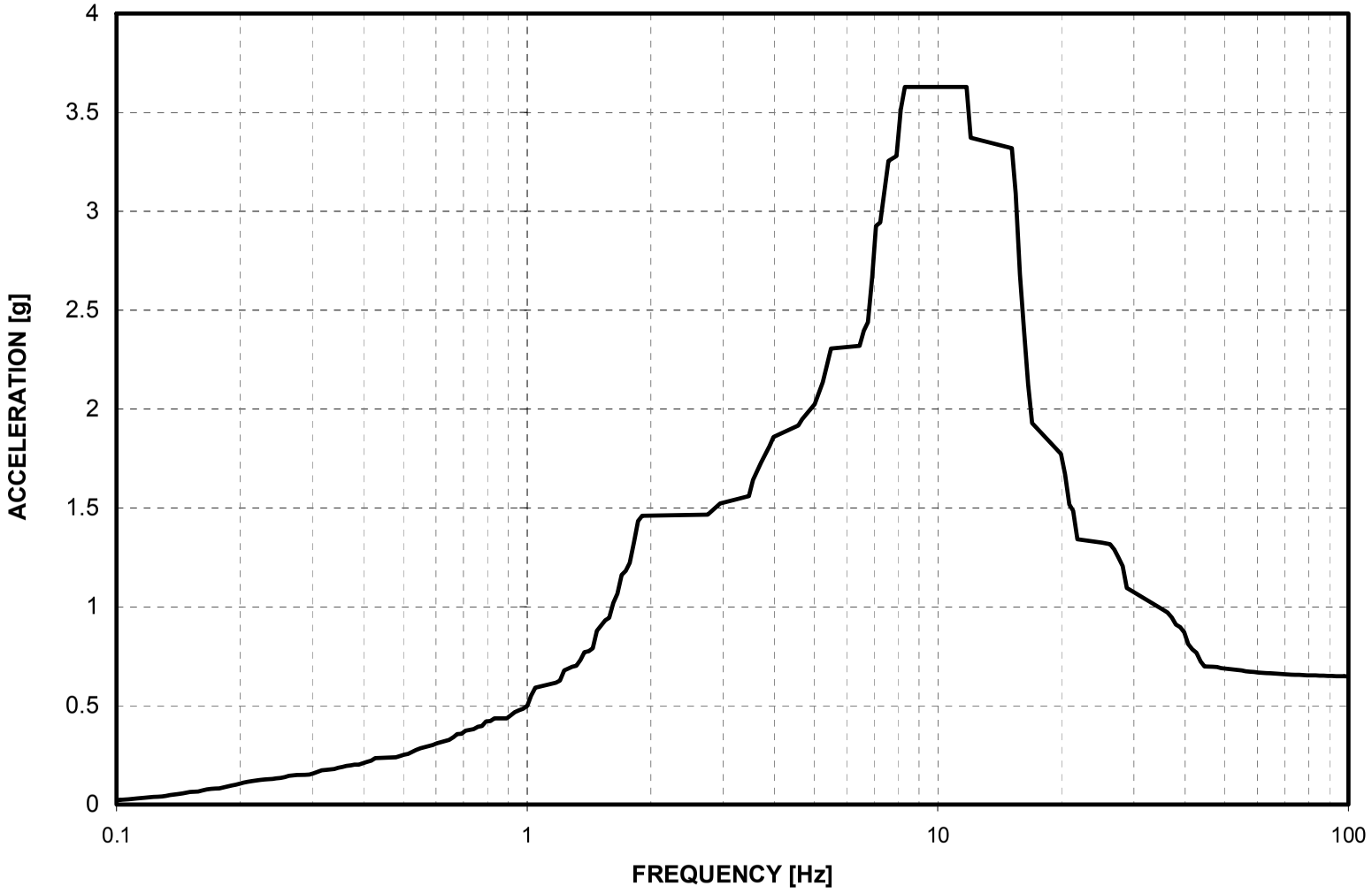

Figure 3-B.1.0-18 Design Basis ISRS at NFSP - 4% Damped Response in Vertical Direction (Z)

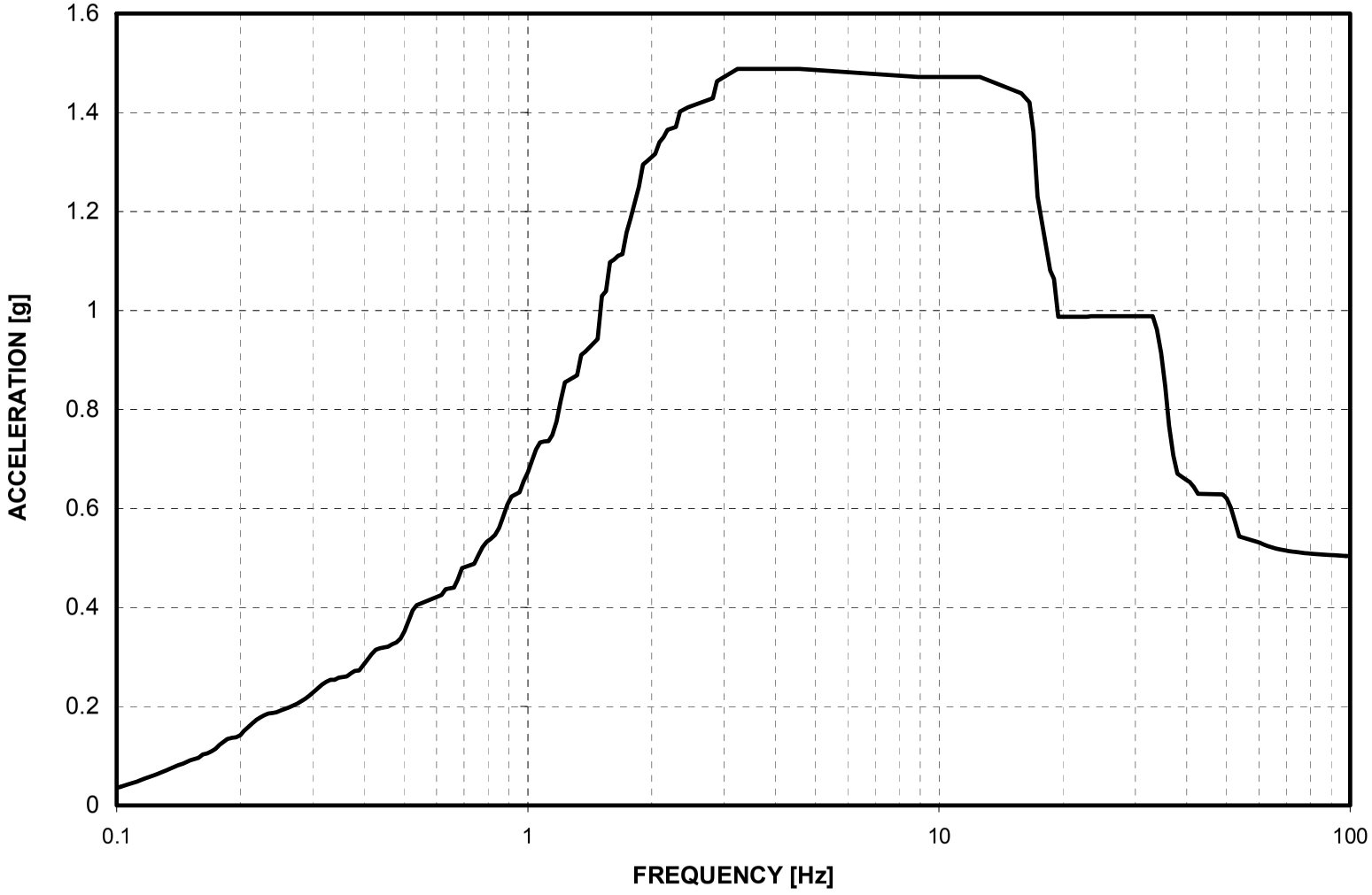

Figure 3-B.1.0-19 Design Basis ISRS at A-AAC GTG - 5% Damped Response in NS Direction (X)

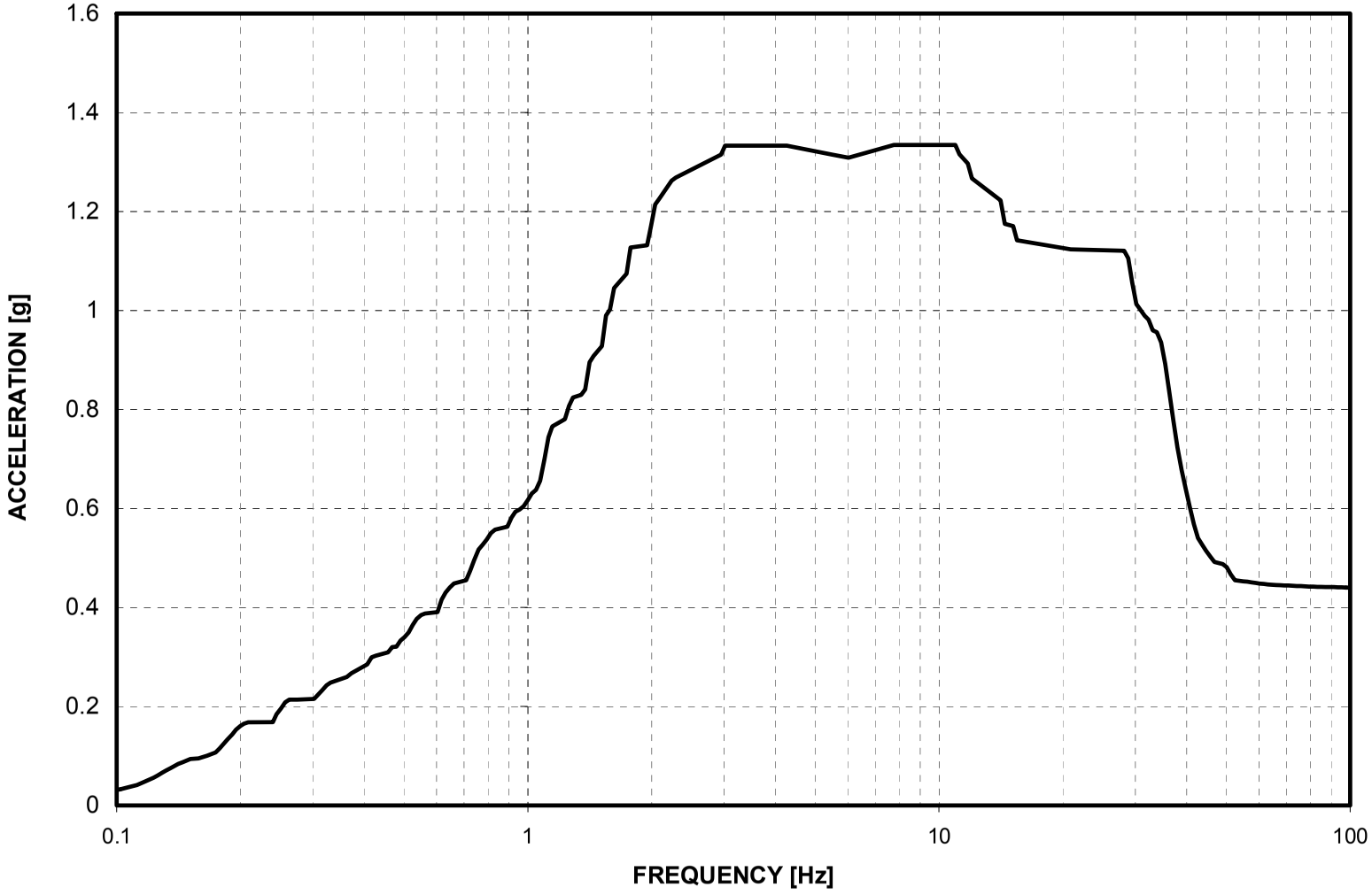

Figure 3-B.1.0-20 Design Basis ISRS at A-AAC GTG - 5% Damped Response in EW Direction (Y)

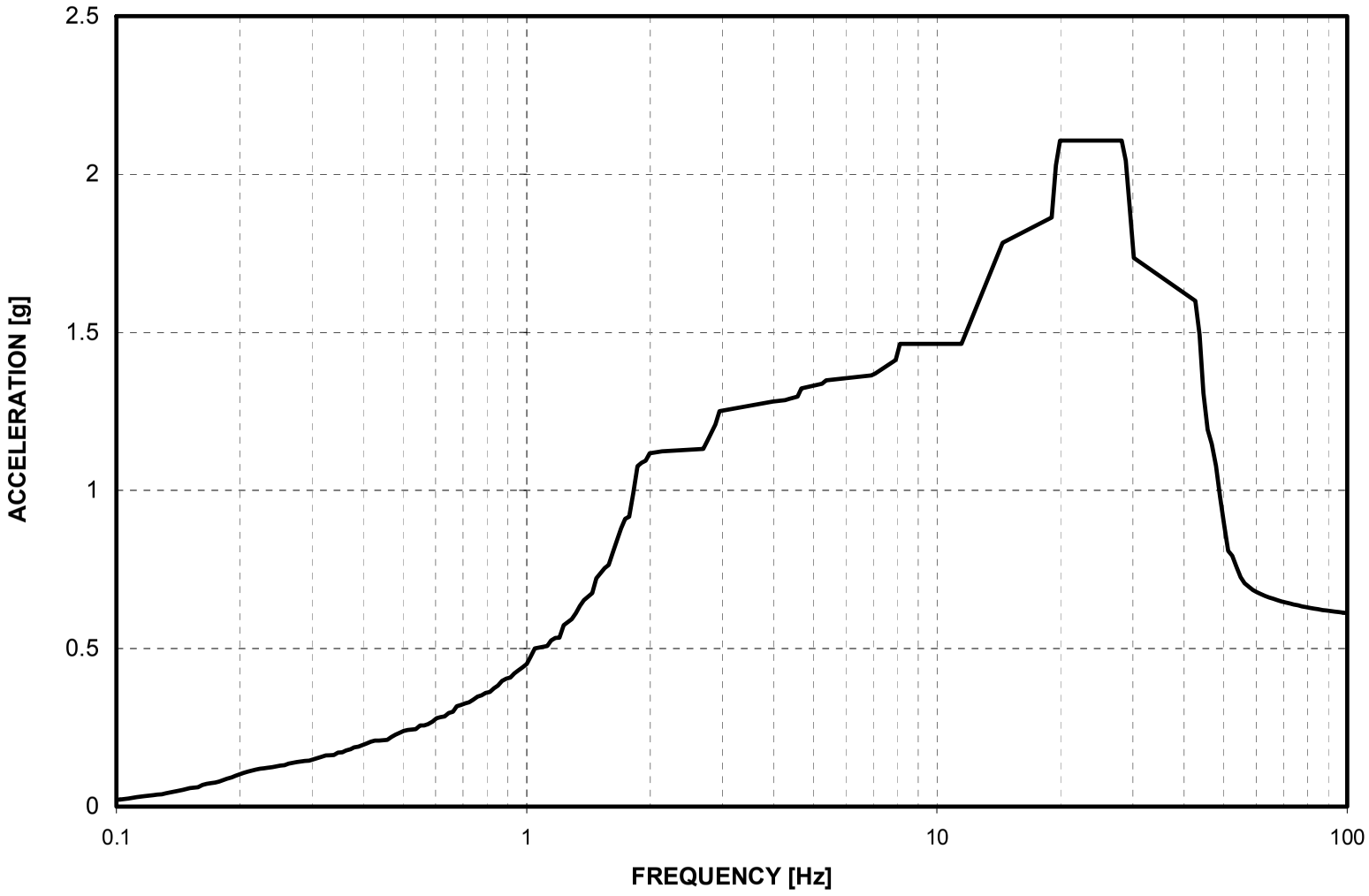

Figure 3-B.1.0-21 Design Basis ISRS at A-AAC GTG - 5% Damped Response in Vertical Direction (Z)

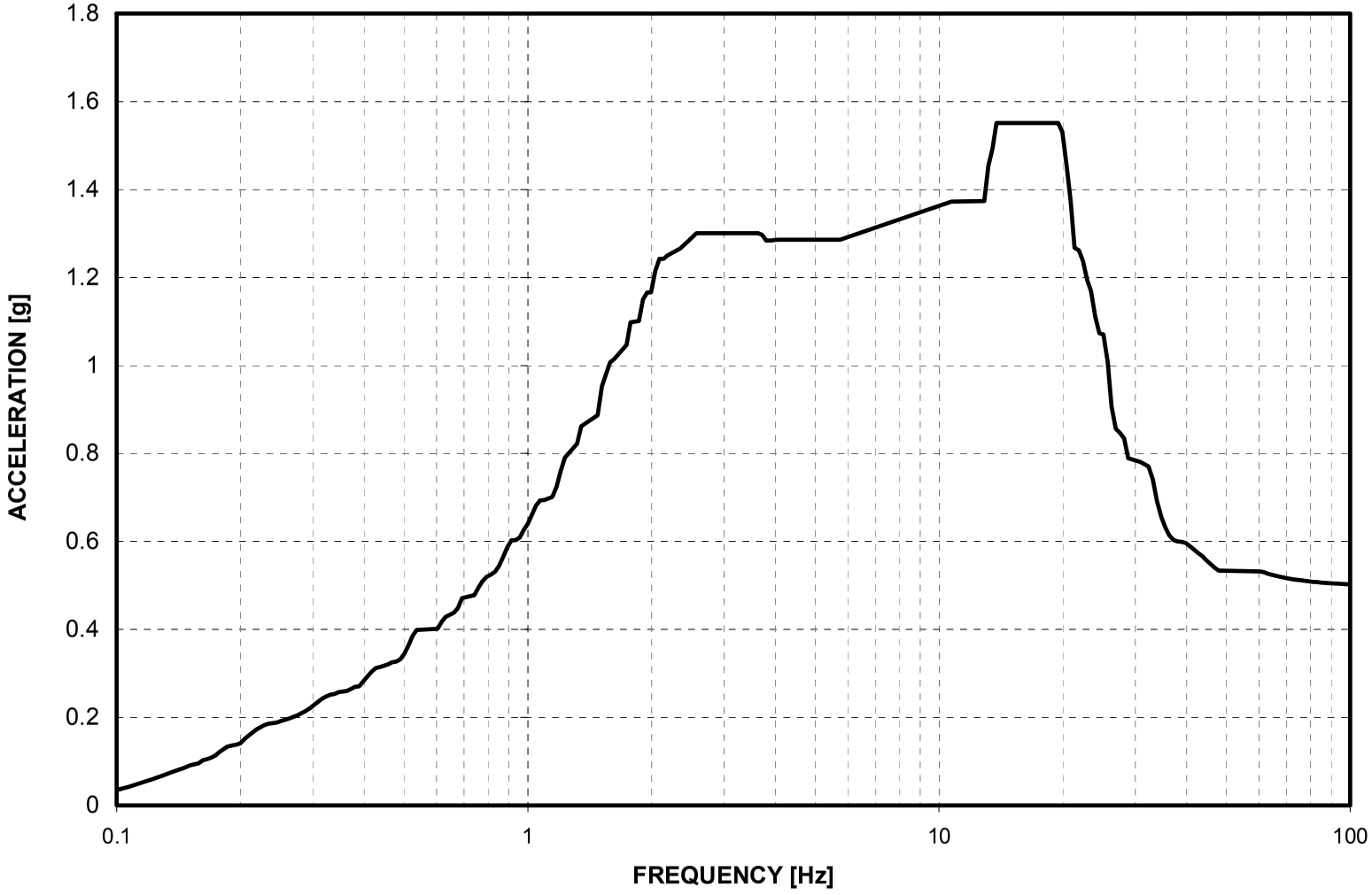

Figure 3-B.1.0-22 Design Basis ISRS at B-AAC GTG - 5% Damped Response in NS Direction (X)

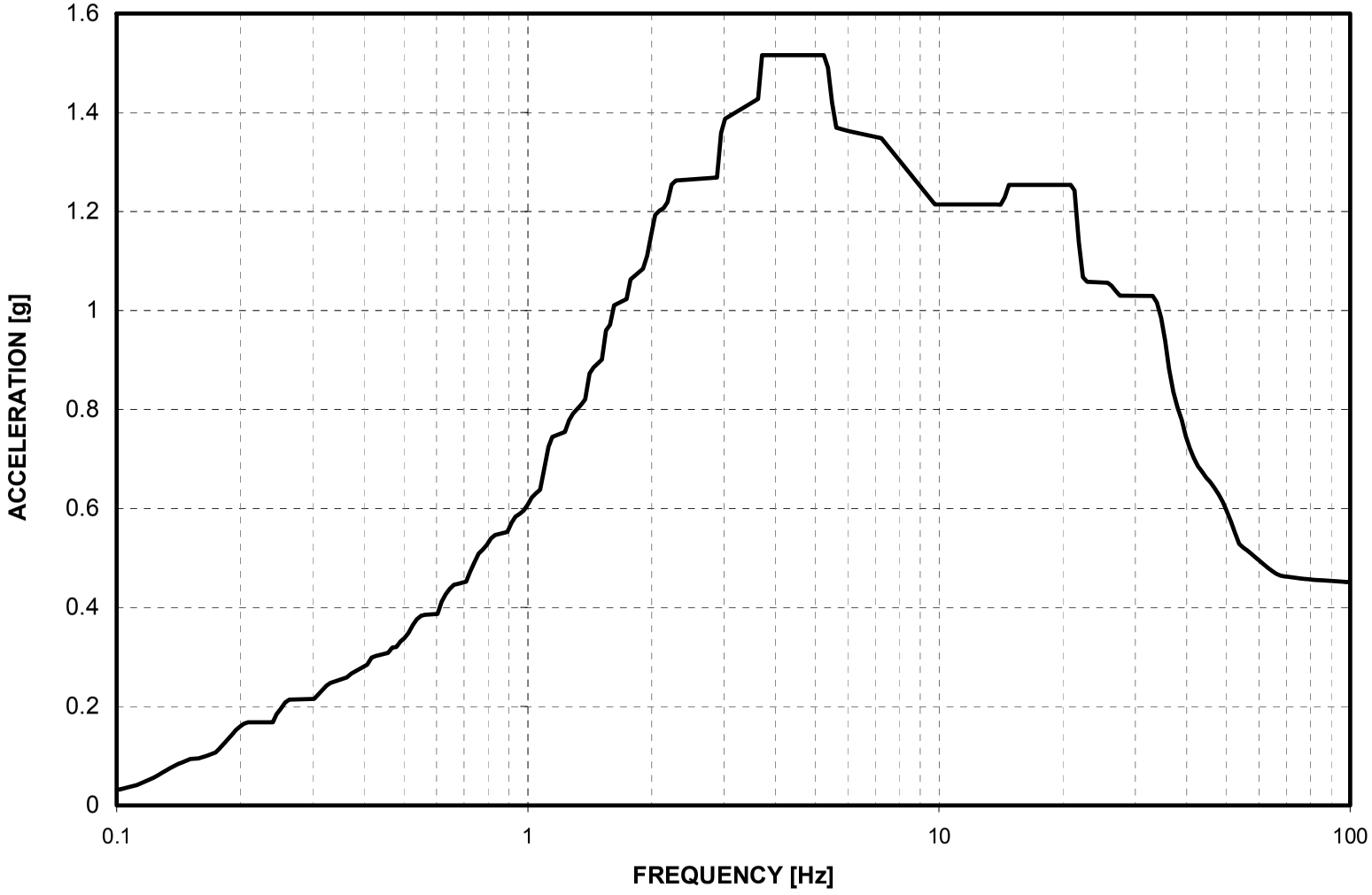

Figure 3-B.1.0-23 Design Basis ISRS at B-AAC GTG - 5% Damped Response in EW Direction (Y)

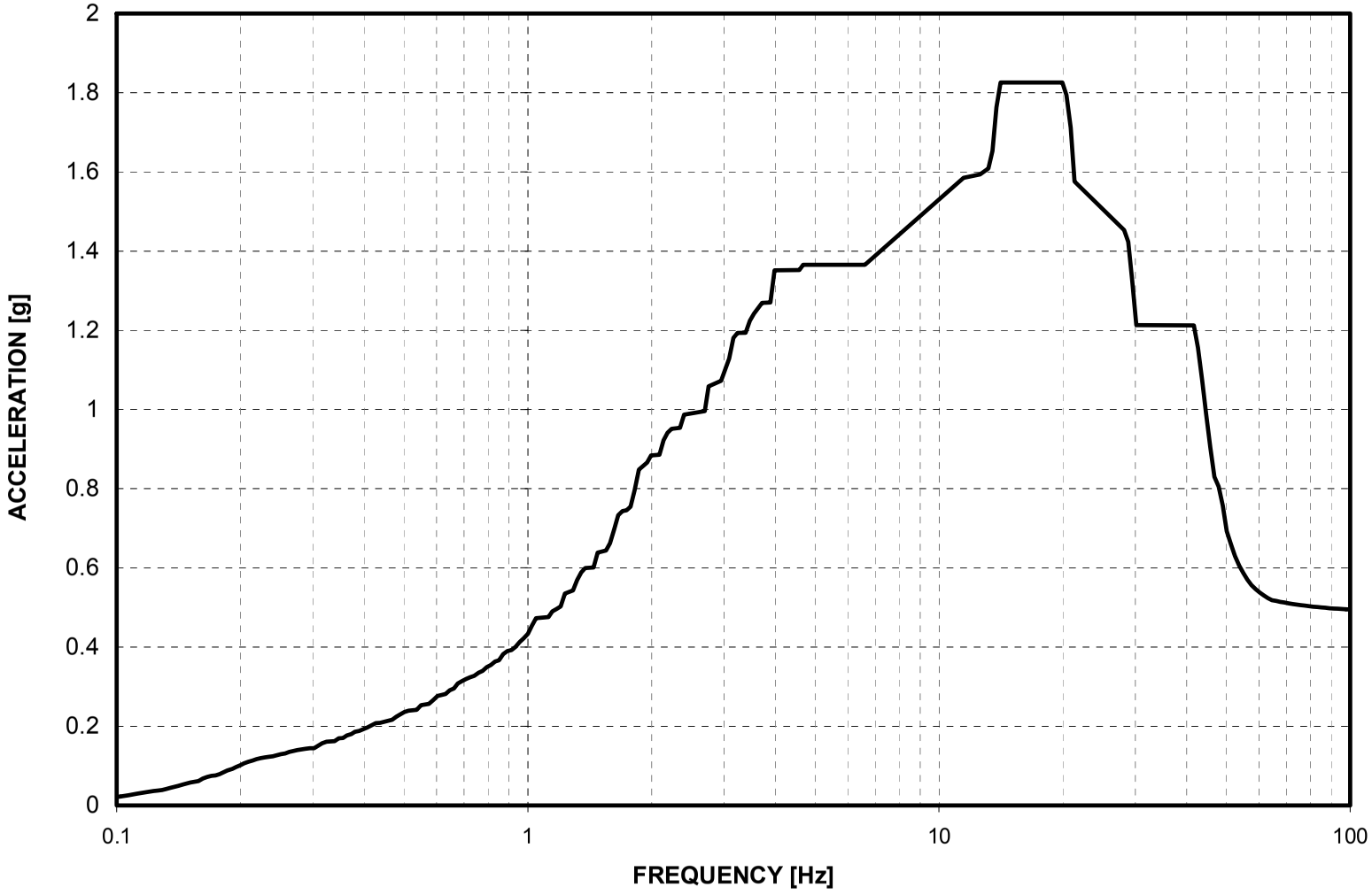

Figure 3-B.1.0-24 Design Basis ISRS at B-AAC GTG - 5% Damped Response in Vertical Direction (Z)

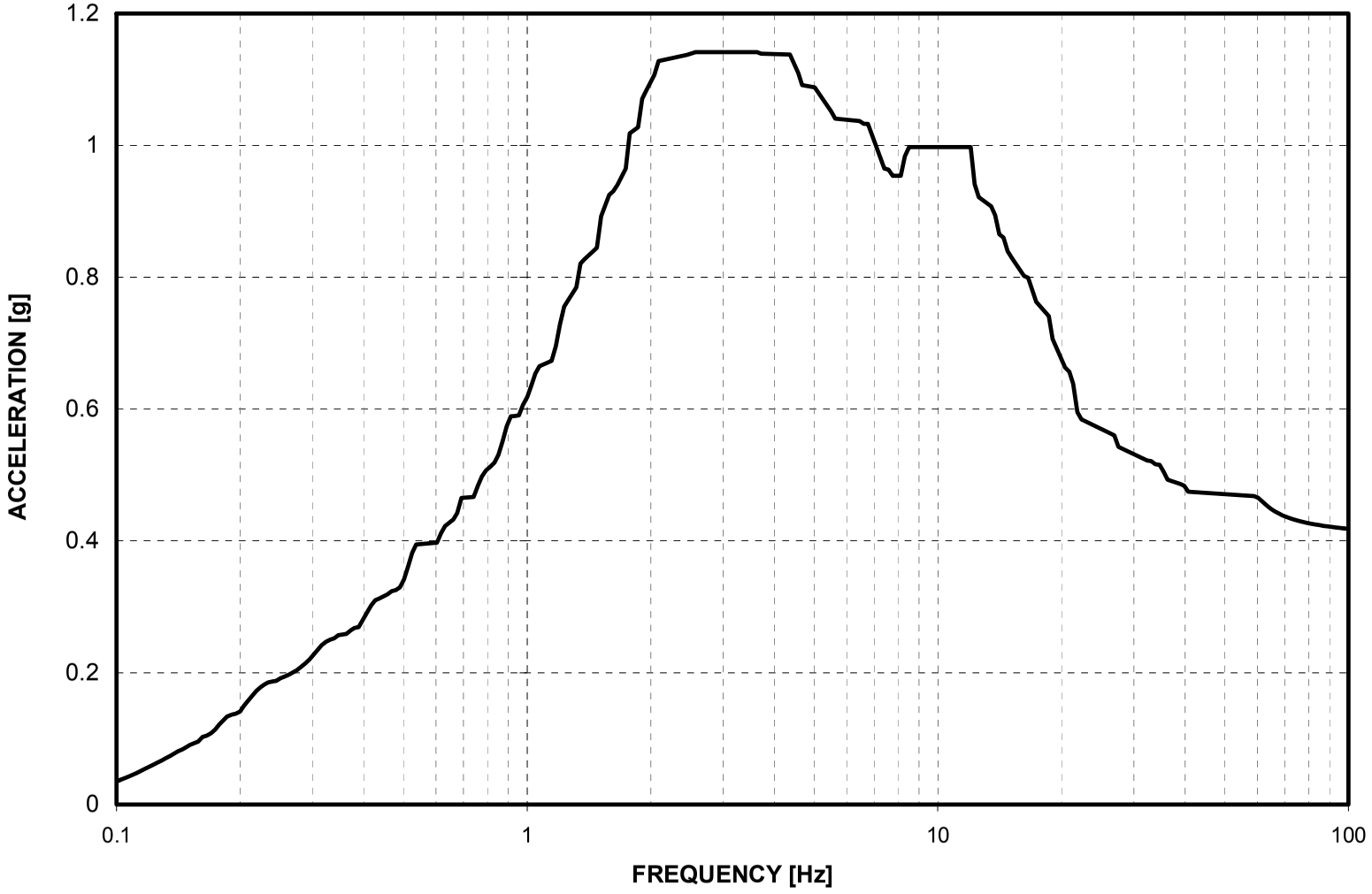

Figure 3-B.1.0-25 Design Basis ISRS at A/B NW Corner Basemat - 5% Damped Response in NS Direction (X) at Model Elevation -26'-4"

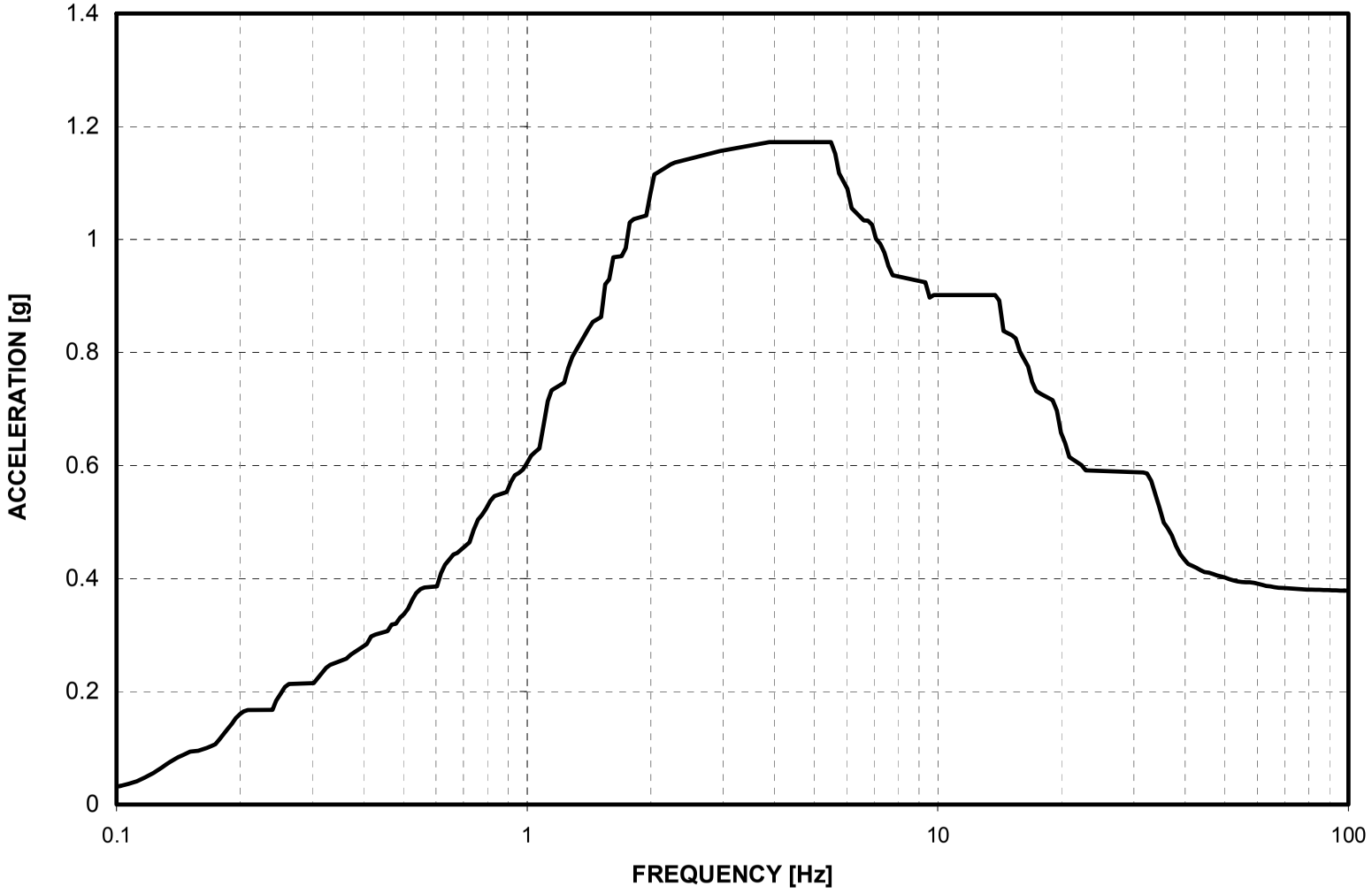

Figure 3-B.1.0-26 Design Basis ISRS at A/B NW Corner Basemat - 5% Damped Response in EW Direction (Y) at Model Elevation -26'-4"

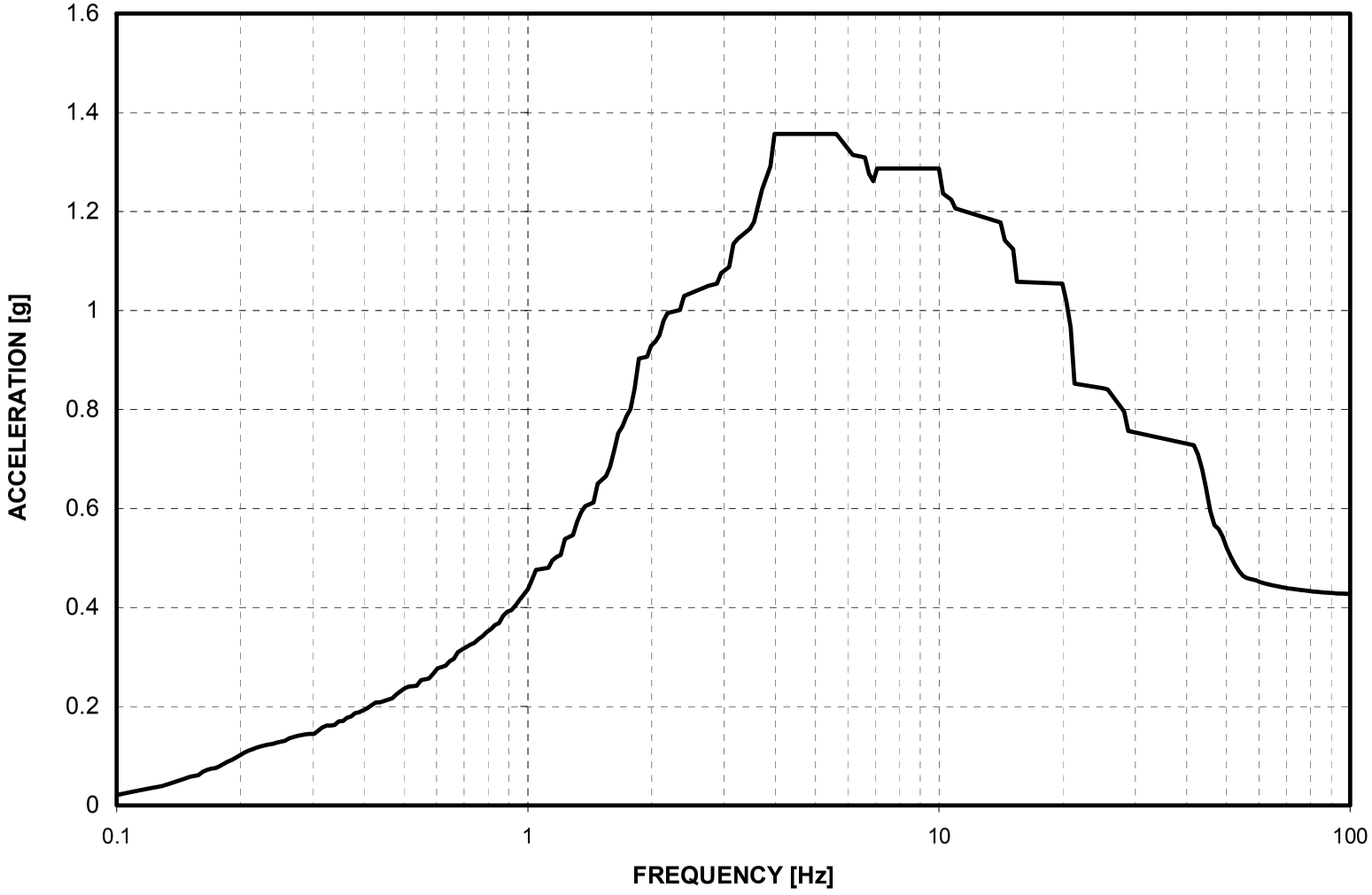

Figure 3-B.1.0-27 Design Basis ISRS at A/B NW Corner Basemat - 5% Damped Response in Vertical Direction (Z) at Model Elevation -26'-4"

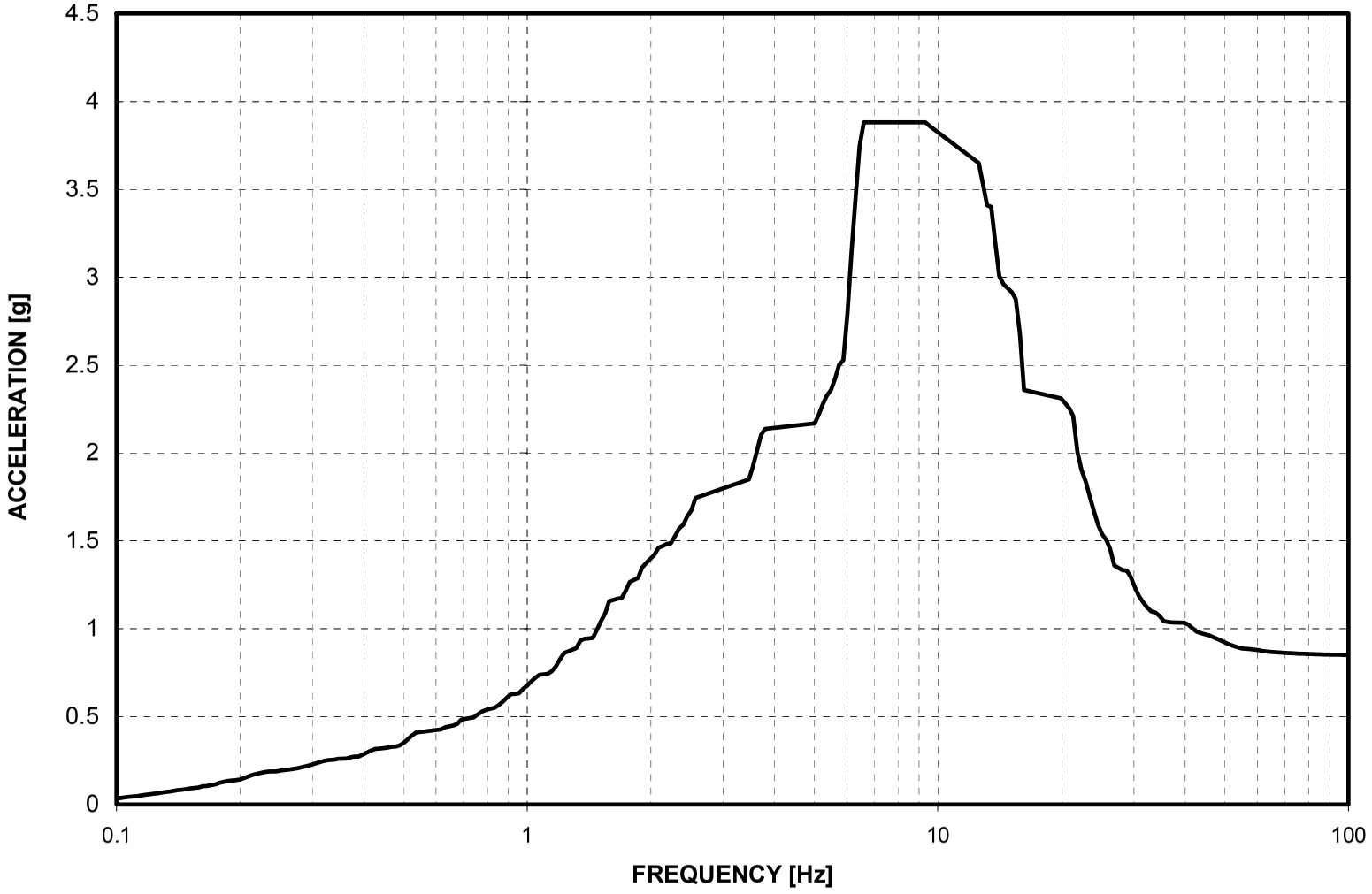

Figure 3-B.1.0-28 Design Basis ISRS at A/B NW Corner Roof - 5% Damped Response in NS Direction (X) at Model Elevation 74'-10"

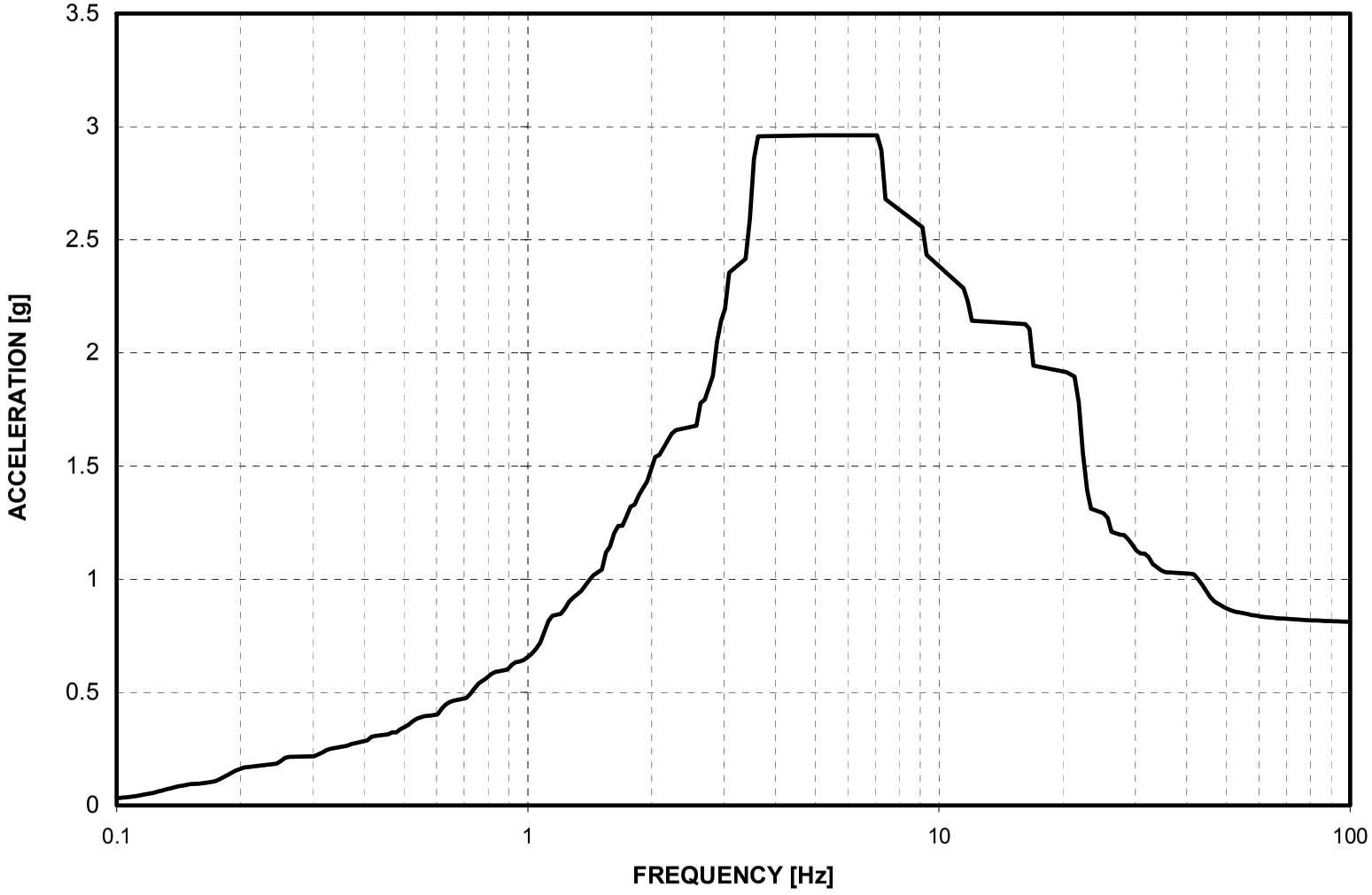

Figure 3-B.1.0-29 Design Basis ISRS at A/B NW Corner Roof - 5% Damped Response in EW Direction (Y) at Model Elevation 74'-10"

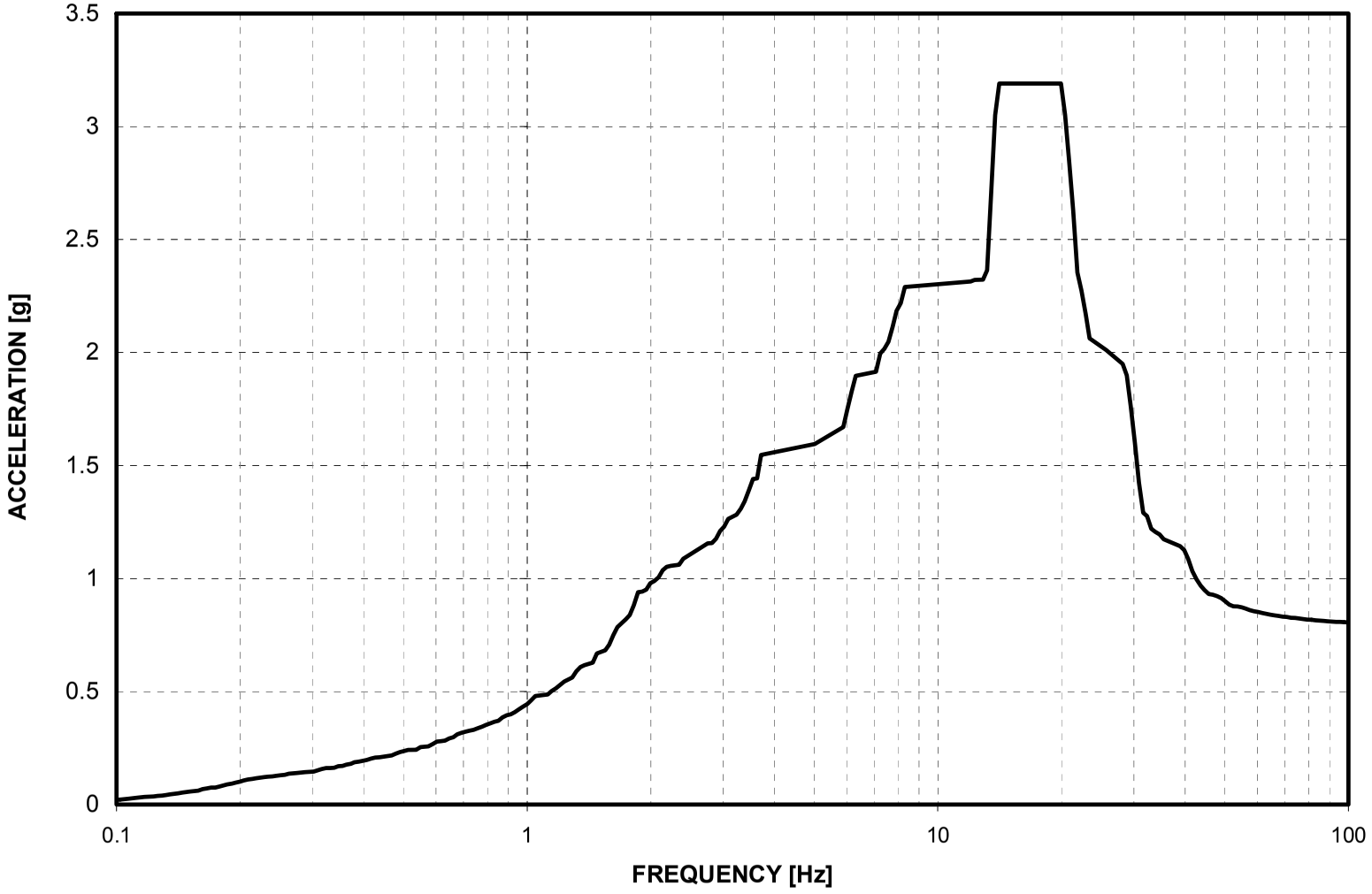

Figure 3-B.1.0-30 Design Basis ISRS at A/B NW Corner Roof - 5% Damped Response in Vertical Direction (Z) at Model Elevation 74'-10"

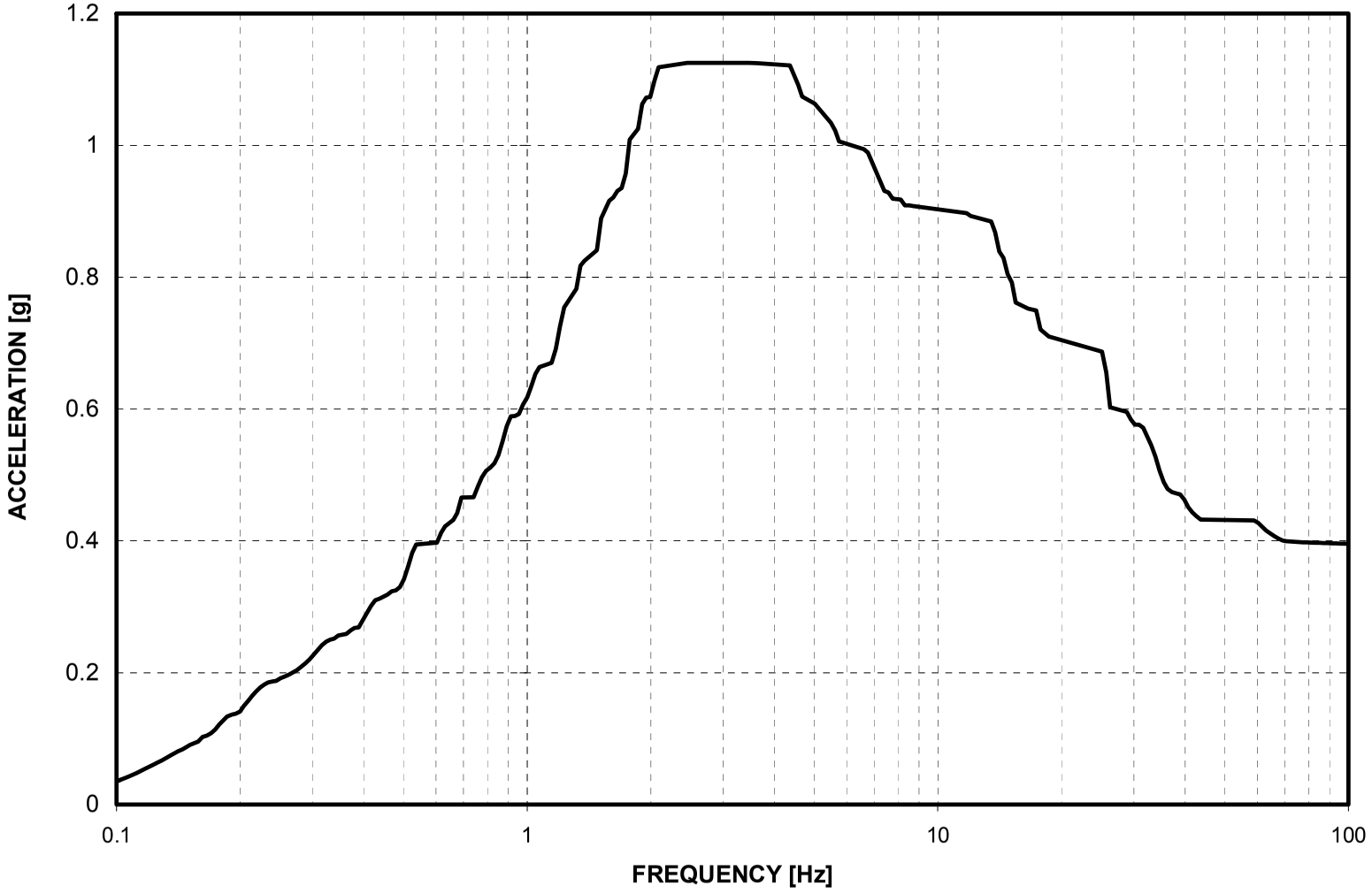

Figure 3-B.1.0-31 Design Basis ISRS at West PS/B SW Corner Basemat - 5% Damped Response in NS Direction (X) at Model Elevation -26'-4"

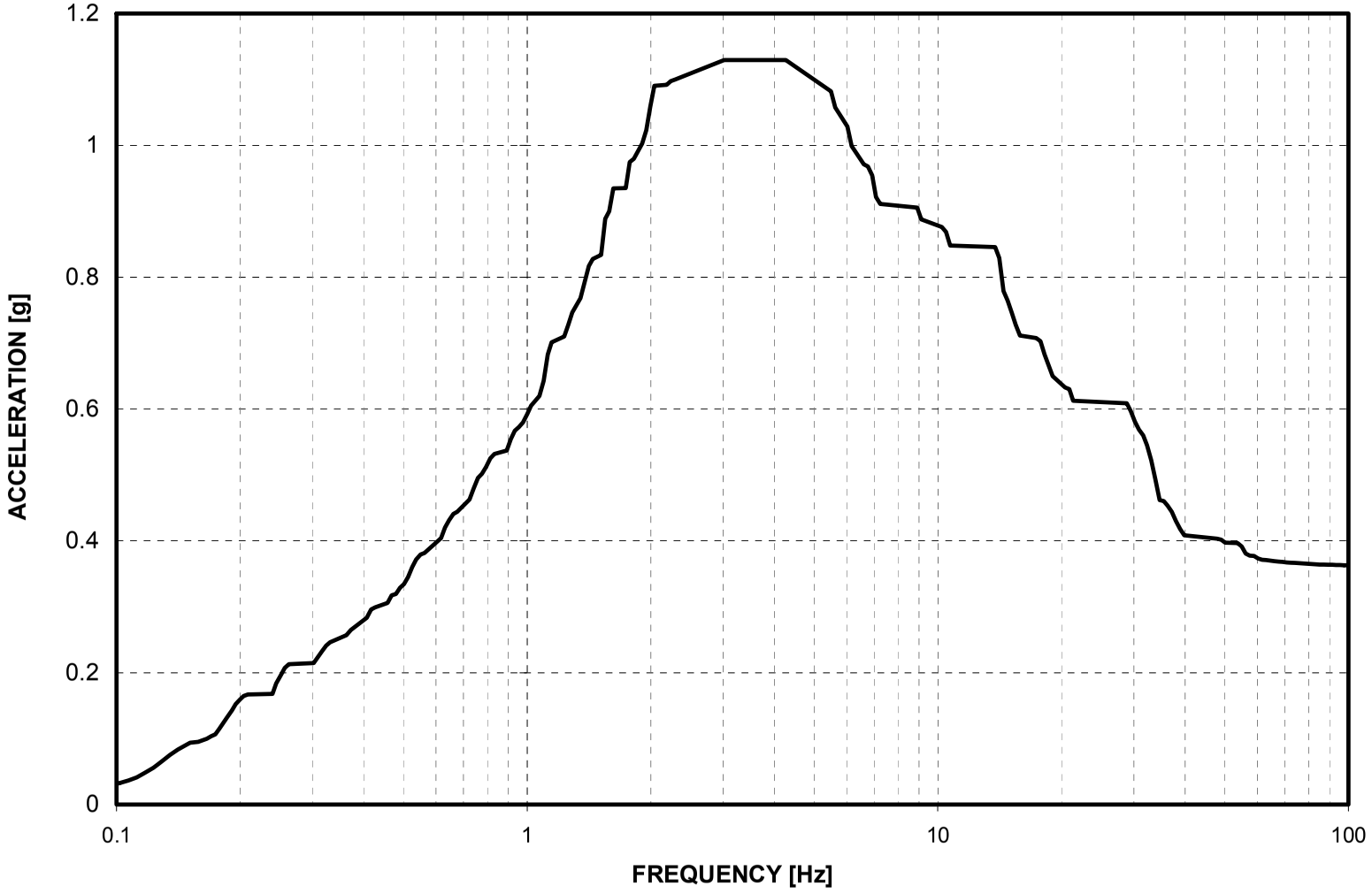

Figure 3-B.1.0-32 Design Basis ISRS at West PS/B SW Corner Basemat - 5% Damped Response in EW Direction (Y) at Model Elevation -26'-4"

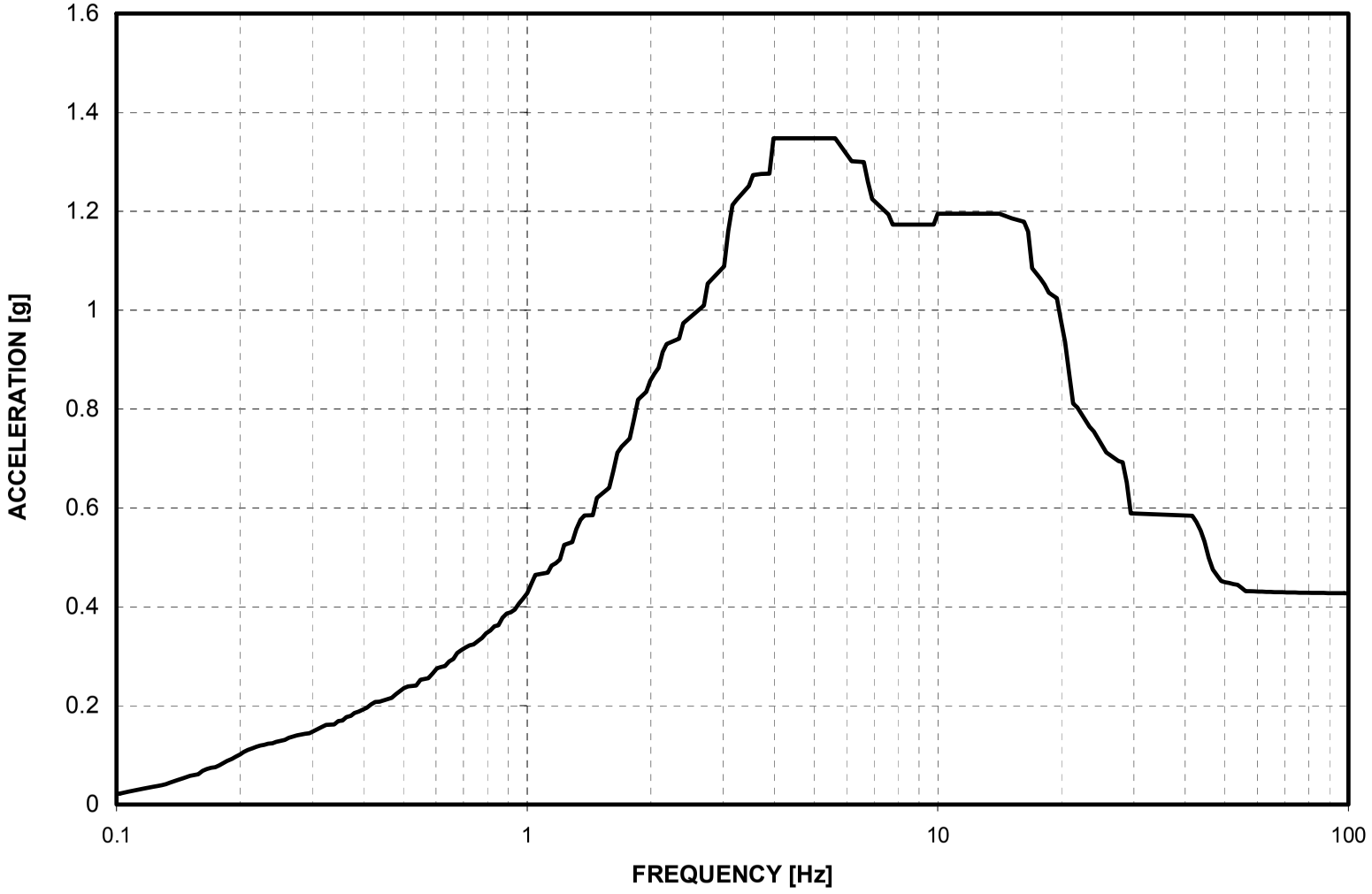

Figure 3-B.1.0-33 Design Basis ISRS at West PS/B SW Corner Basemat - 5% Damped Response in Vertical Direction (Z) at Model Elevation -26'-4"

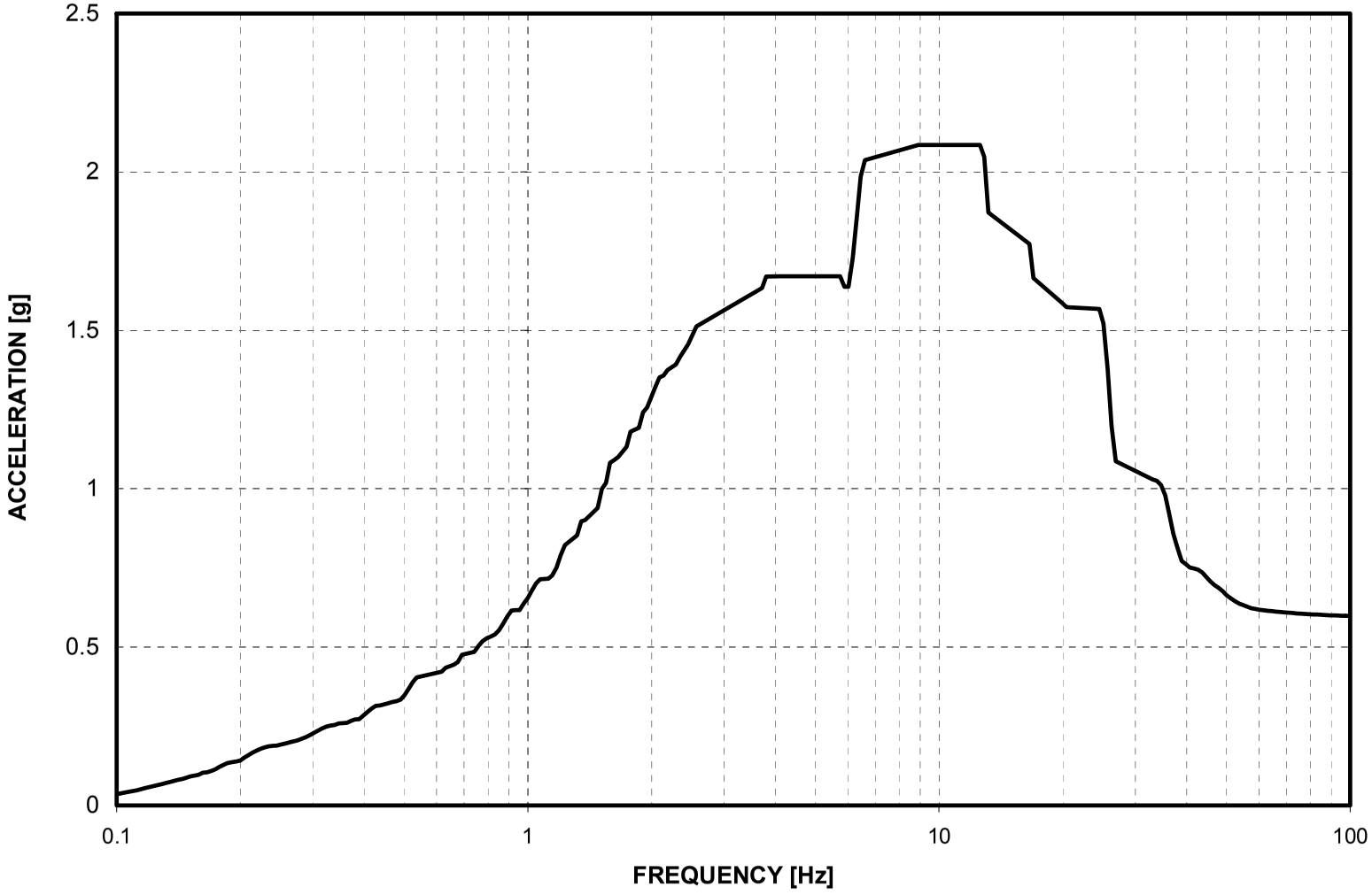

Figure 3-B.1.0-34 Design Basis ISRS at West PS/B SW Corner Roof - 5% Damped Response in NS Direction (X) at Model Elevation 48'-6"

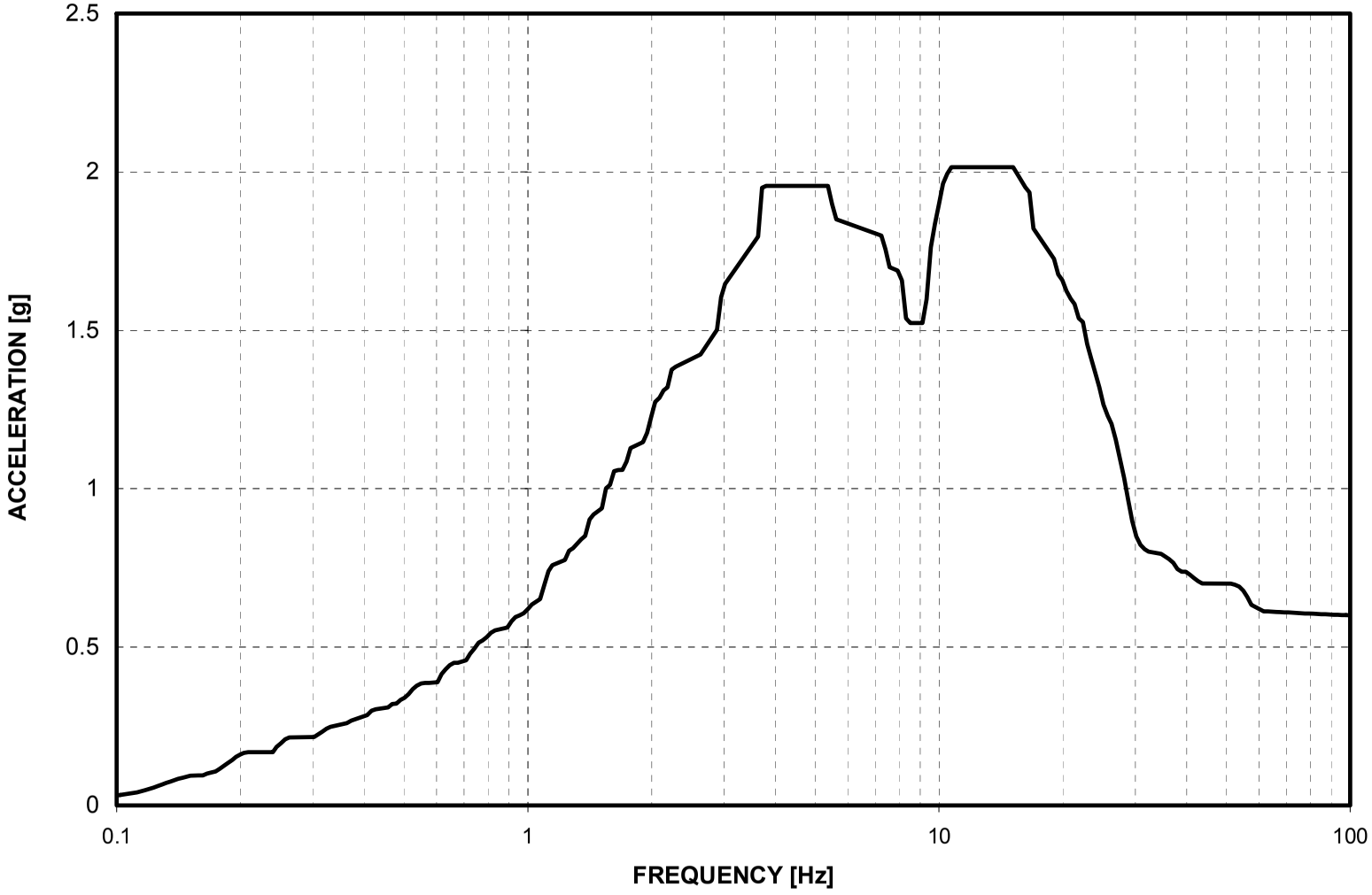

Figure 3-B.1.0-35 Design Basis ISRS at West PS/B SW Corner Roof - 5% Damped Response in EW Direction (Y) at Model Elevation 48'-6"

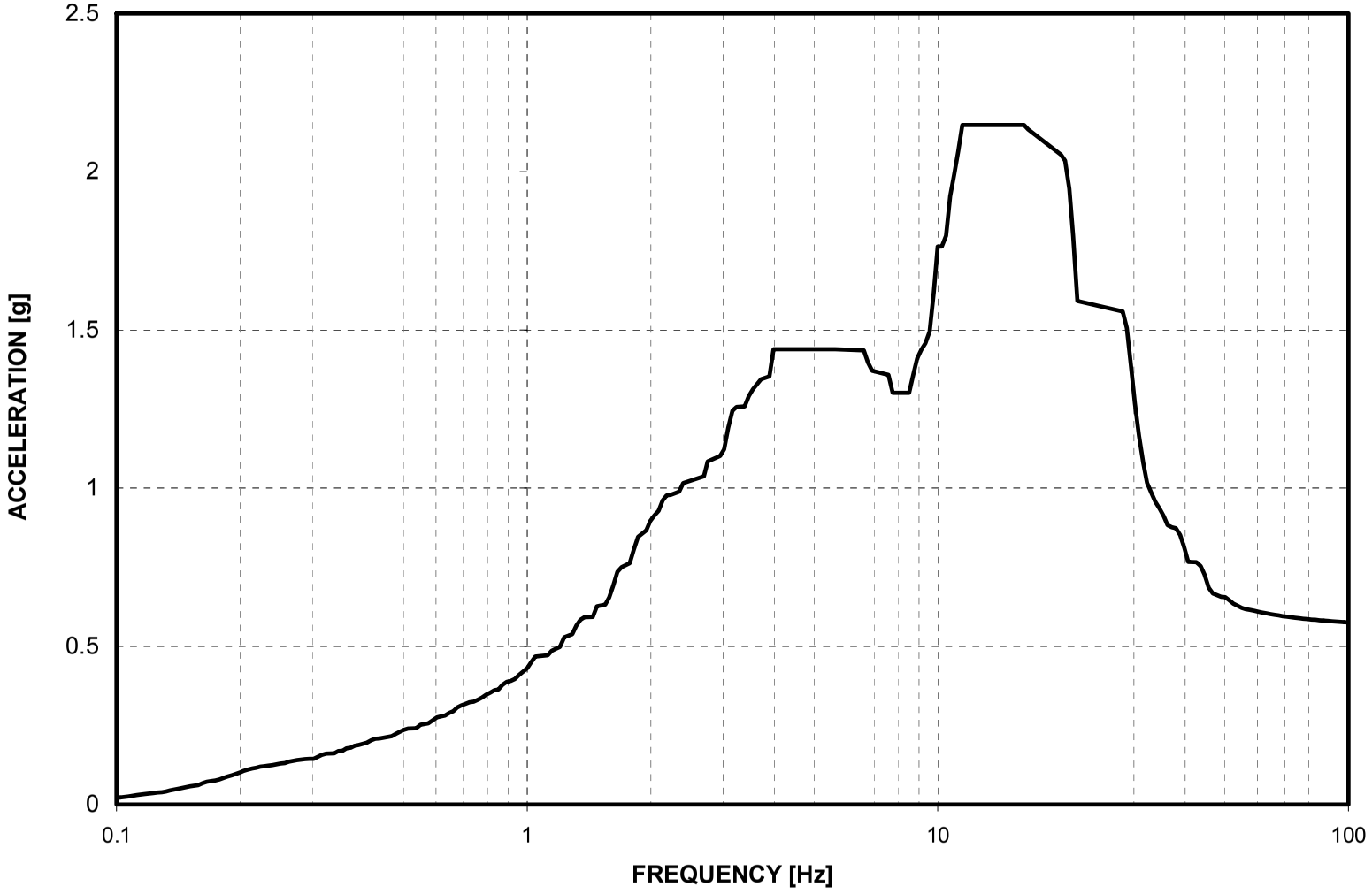

Figure 3-B.1.0-36 Design Basis ISRS at West PS/B SW Corner Roof - 5% Damped Response in Vertical Direction (Z) at Model Elevation 48'-6"

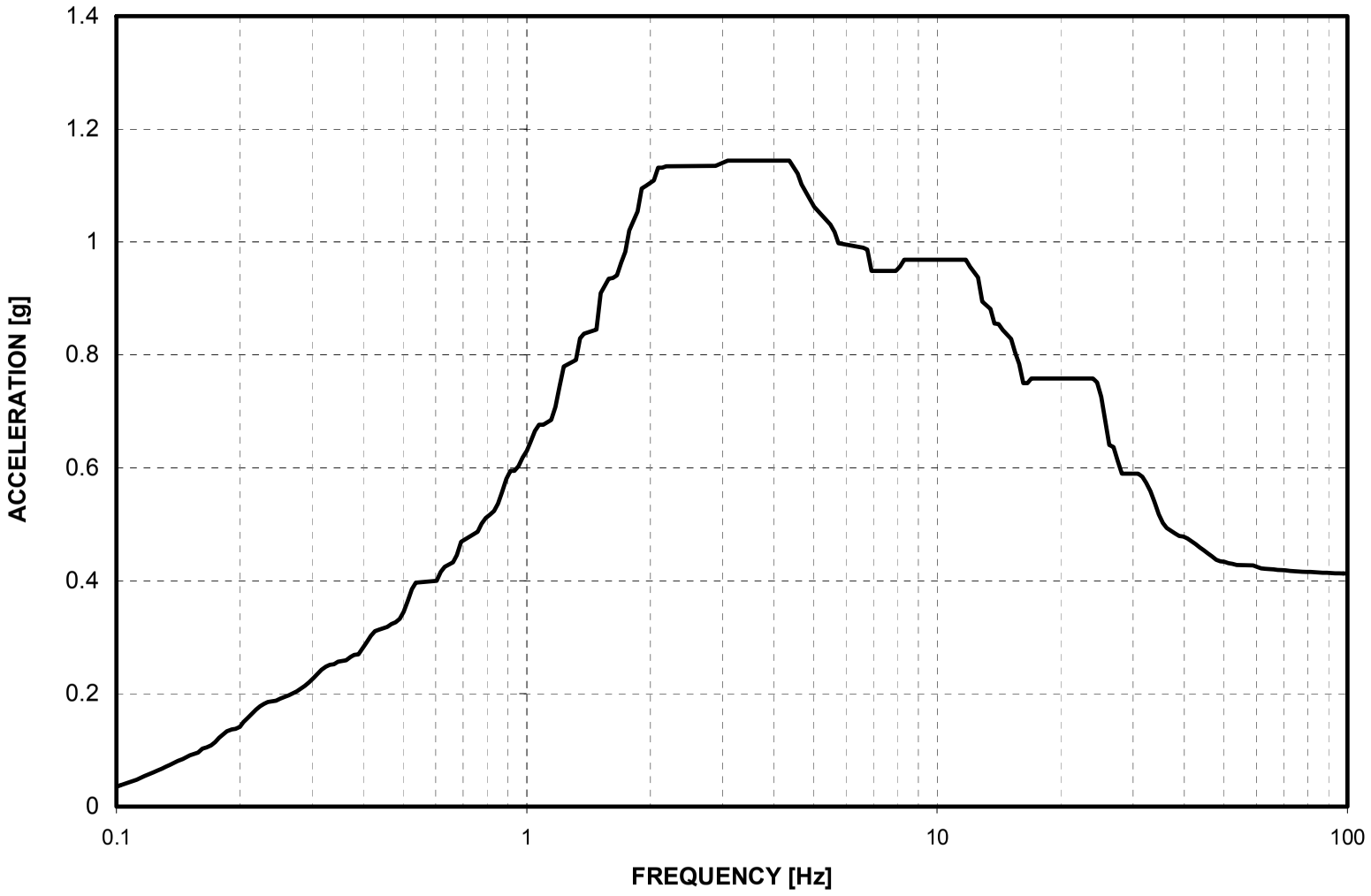

Figure 3-B.1.0-37 Design Basis ISRS at East PS/B SE Corner Basemat - 5% Damped Response in NS Direction (X) at Model Elevation -26'-4"

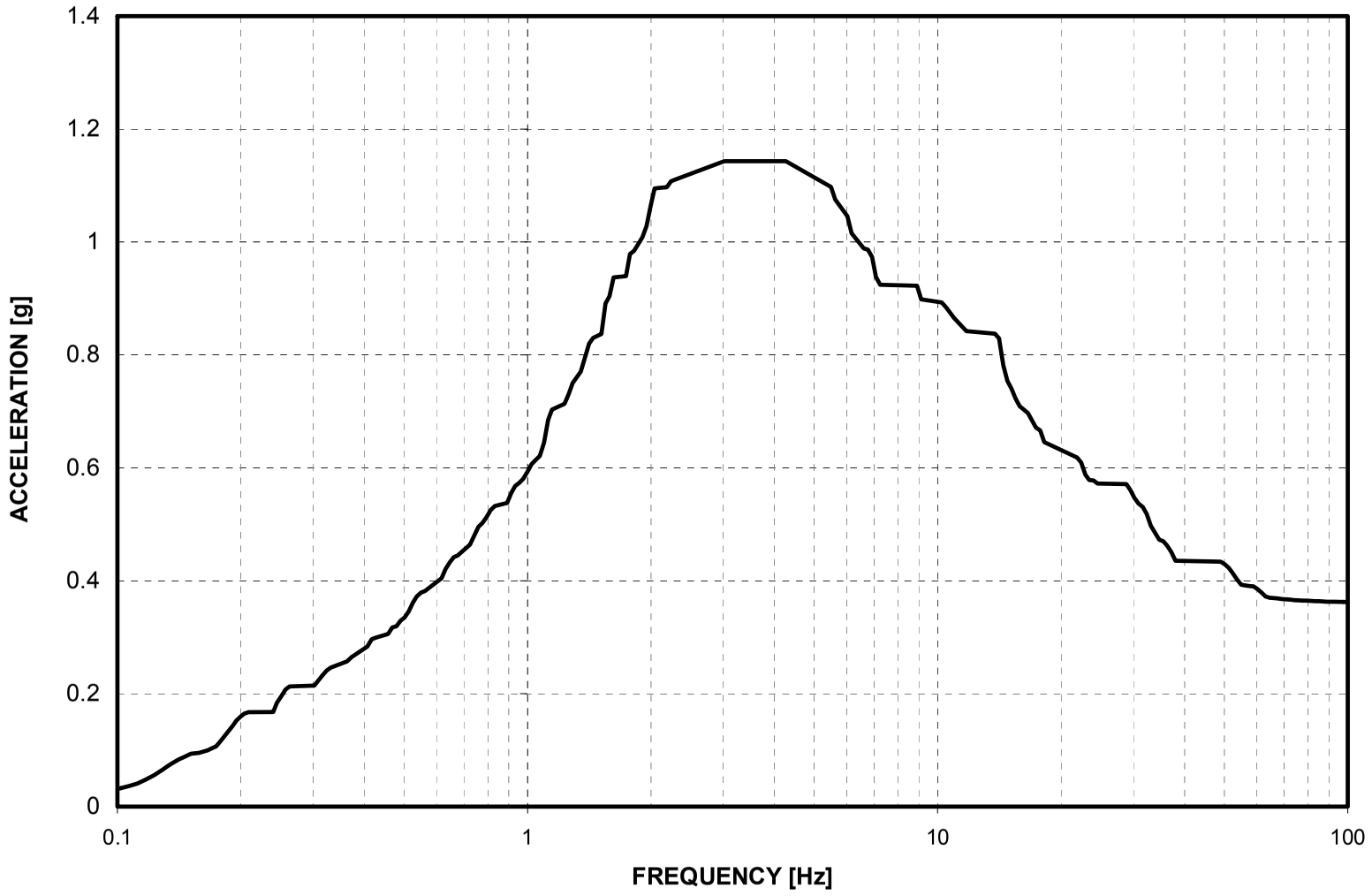

Figure 3-B.1.0-38 Design Basis ISRS at East PS/B SE Corner Basemat - 5% Damped Response in EW Direction (Y) at Model Elevation -26'-4"

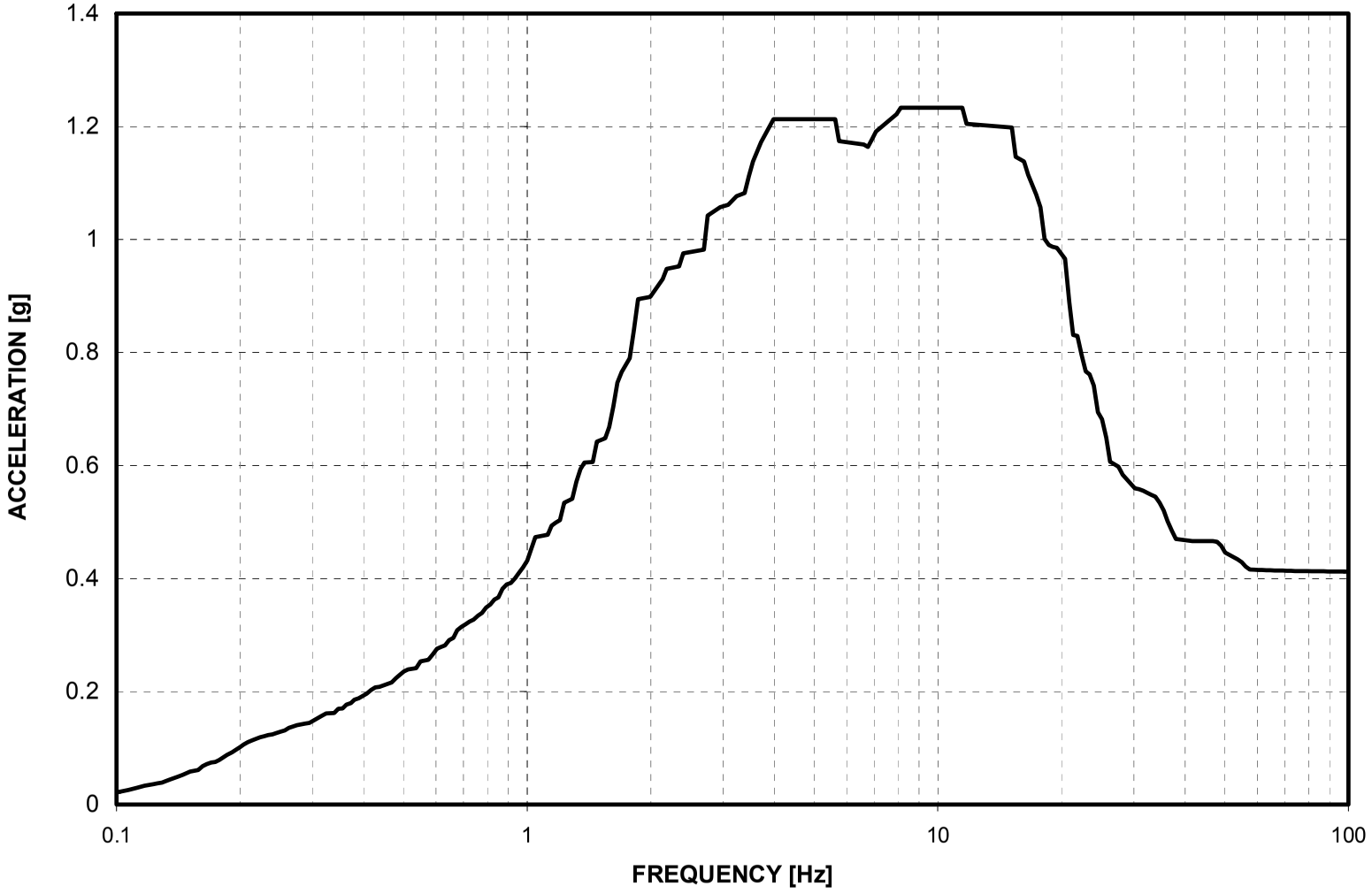

Figure 3-B.1.0-39 Design Basis ISRS at East PS/B SE Corner Basemat - 5% Damped Response in Vertical Direction (Z) at Model Elevation -26'-4"

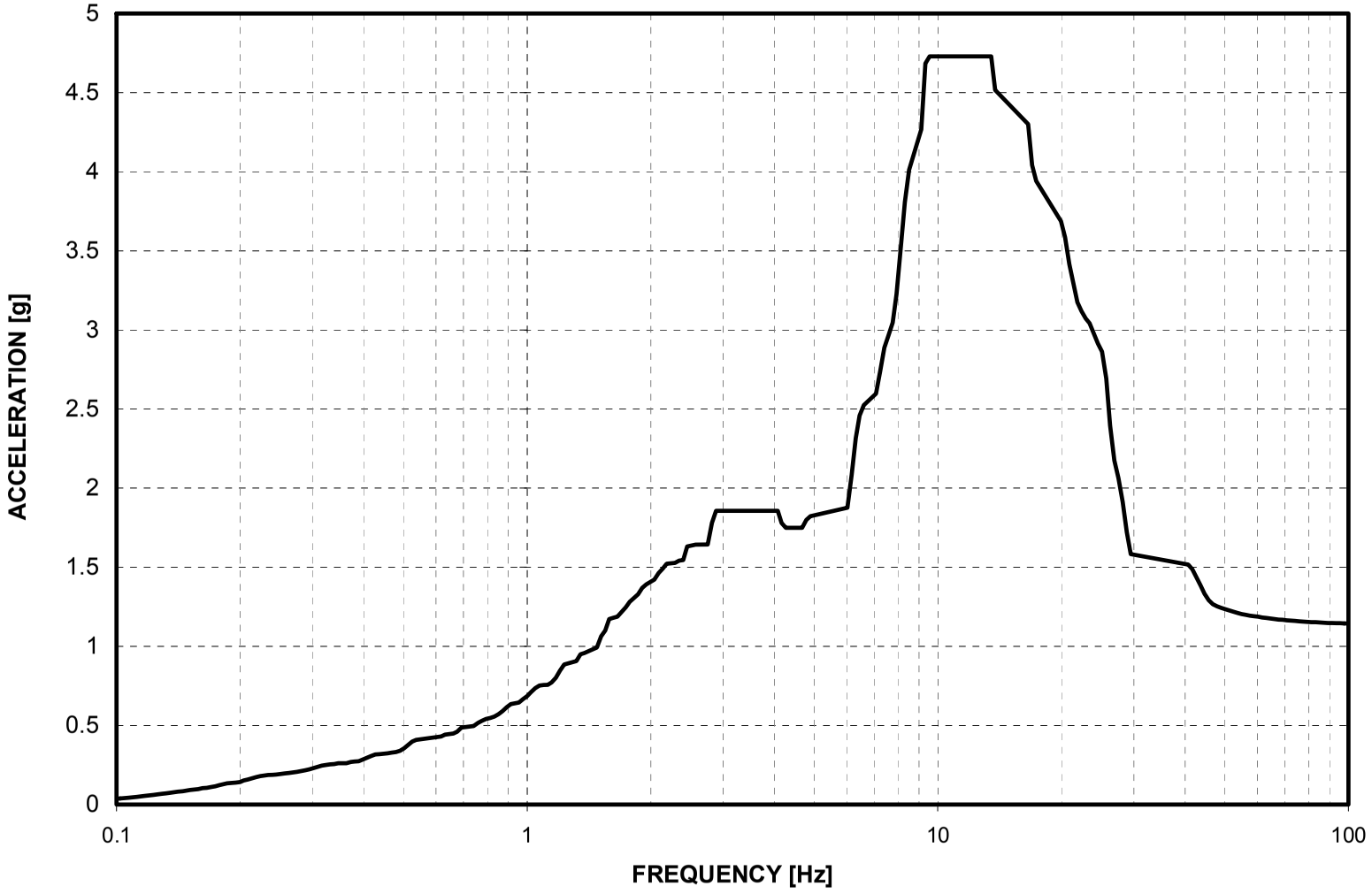

Figure 3-B.1.0-40 Design Basis ISRS at East PS/B SE Corner Roof - 5% Damped Response in NS Direction (X) at Model Elevation 48'-6"

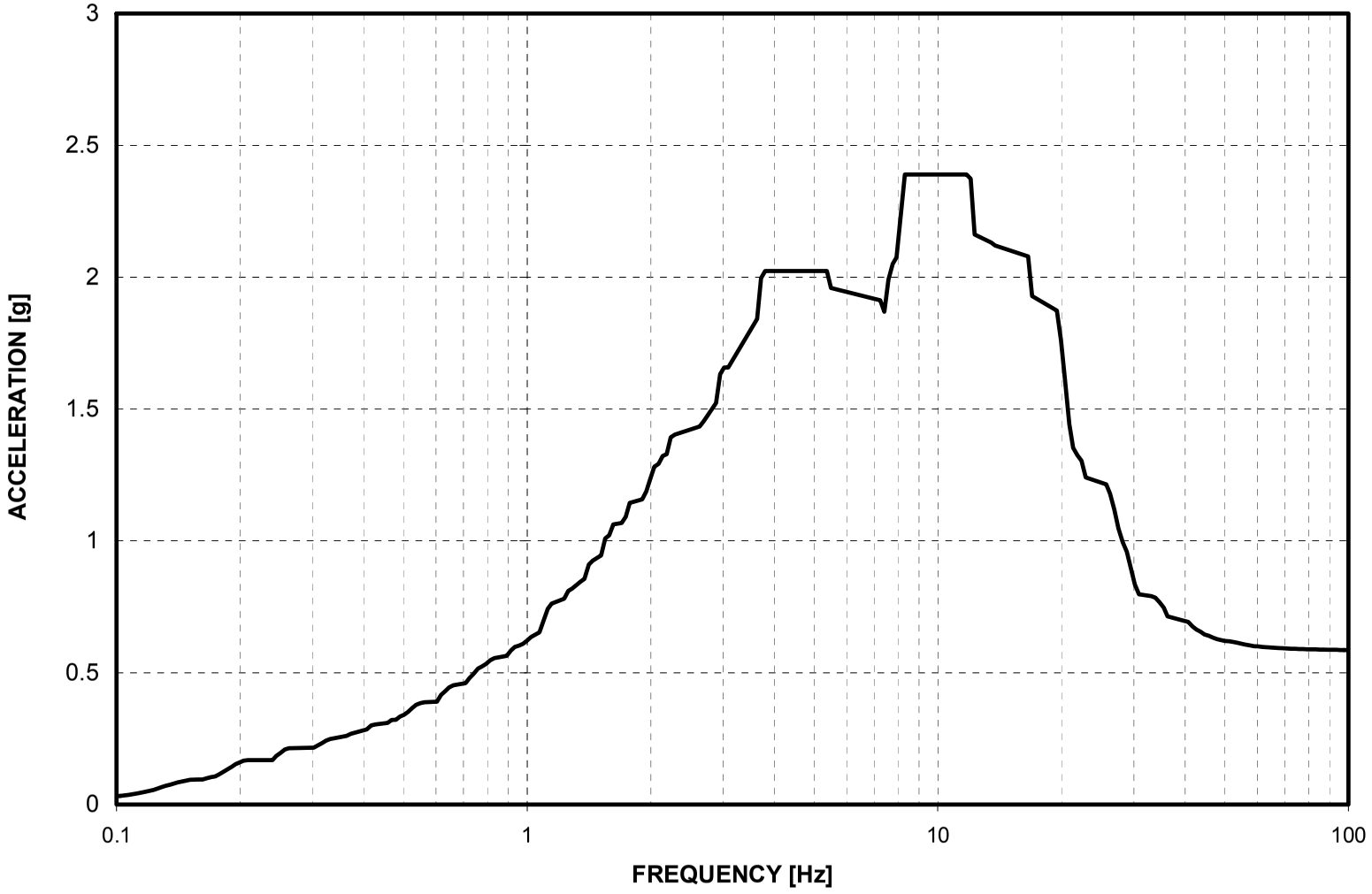

Figure 3-B.1.0-41 Design Basis ISRS at East PS/B SE Corner Roof - 5% Damped Response in EW Direction (Y) at Model Elevation 48'-6"

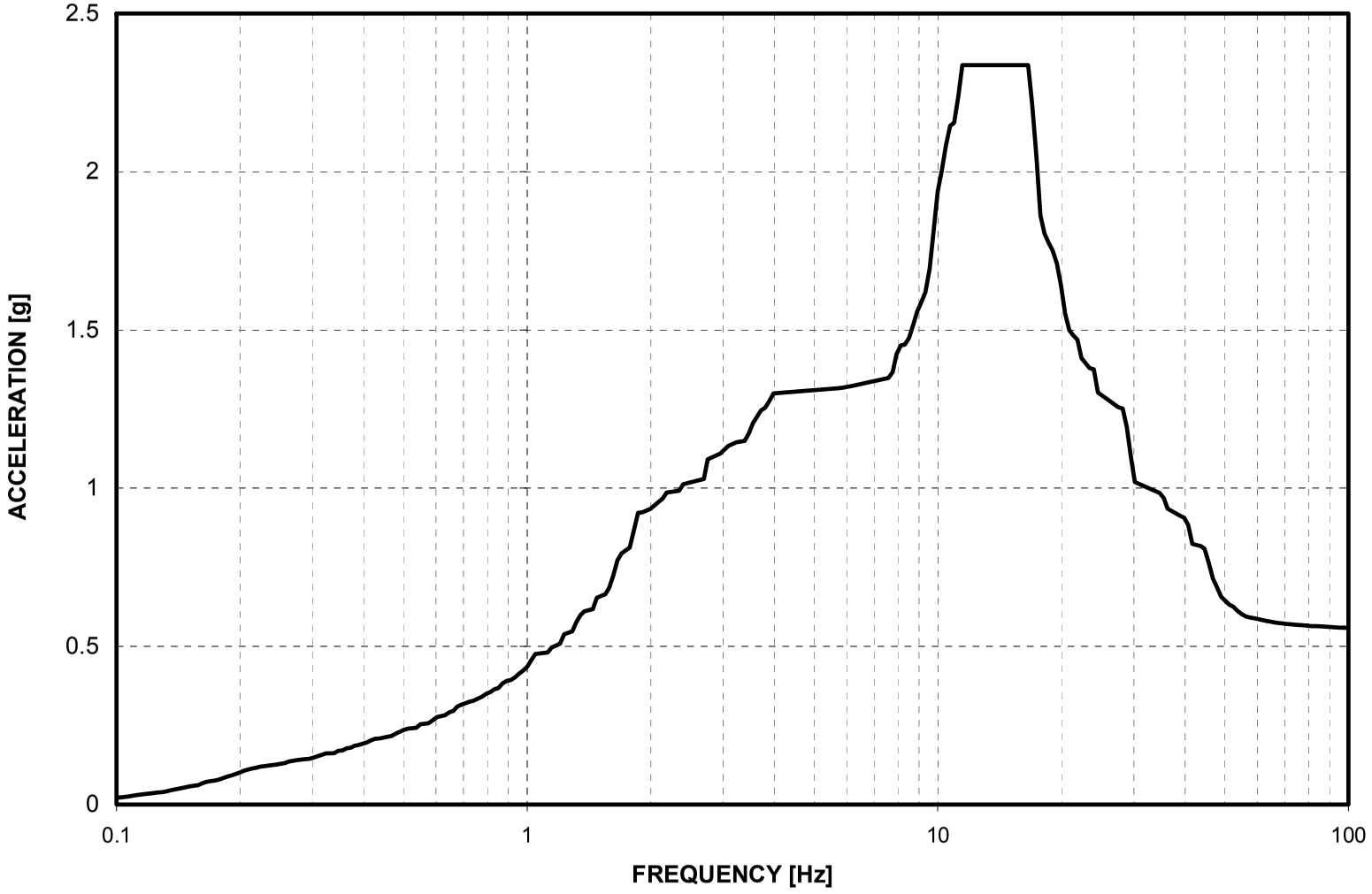

Figure 3-B.1.0-42 Design Basis ISRS at East PS/B SE Corner Roof - 5% Damped Response in Vertical Direction (Z) at Model Elevation 48'-6"

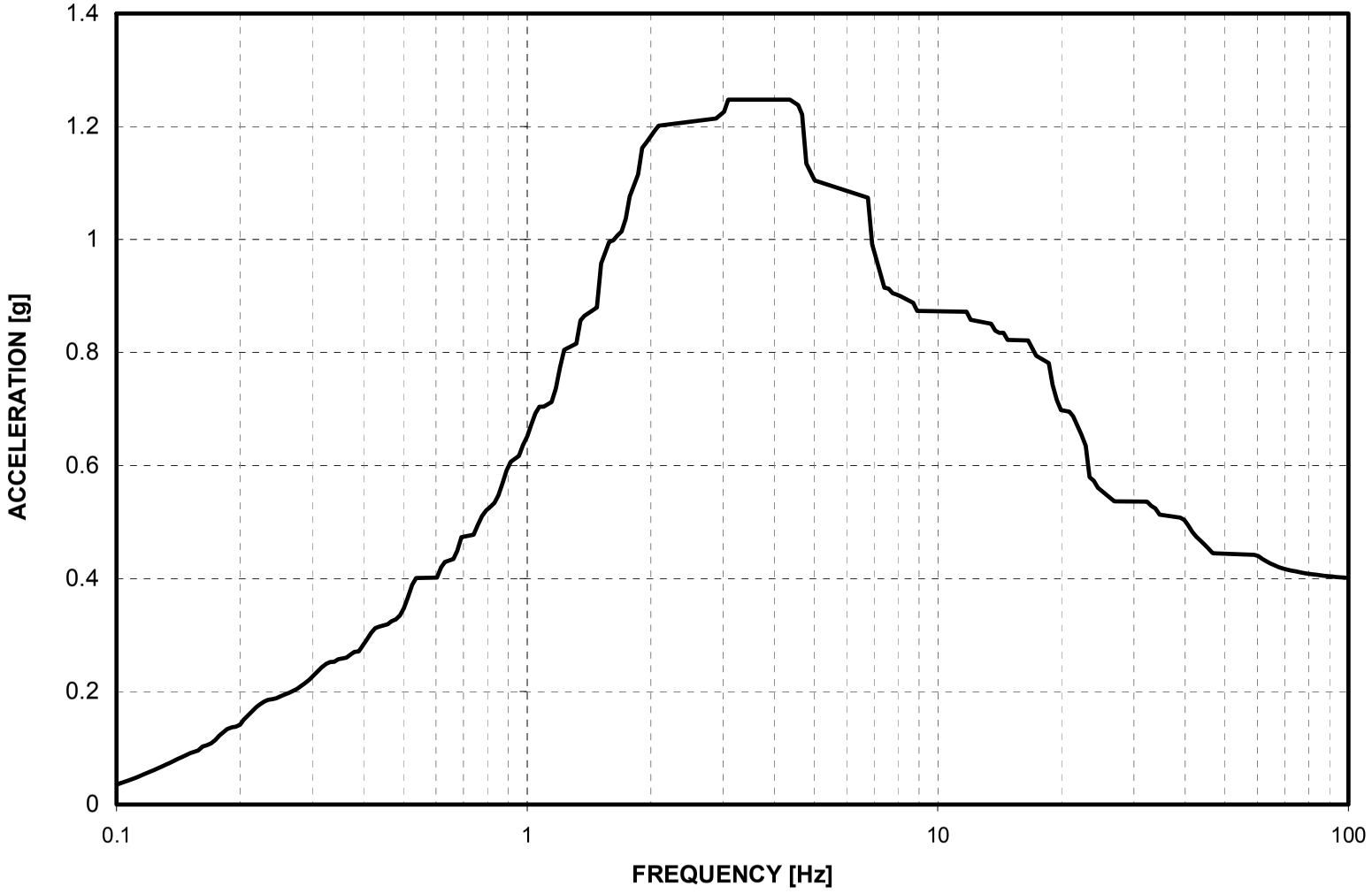

Figure 3-B.1.0-43 Design Basis ISRS at R/B NE Corner Basemat - 5% Damped Response in NS Direction (X) at Model Elevation -26'-4"

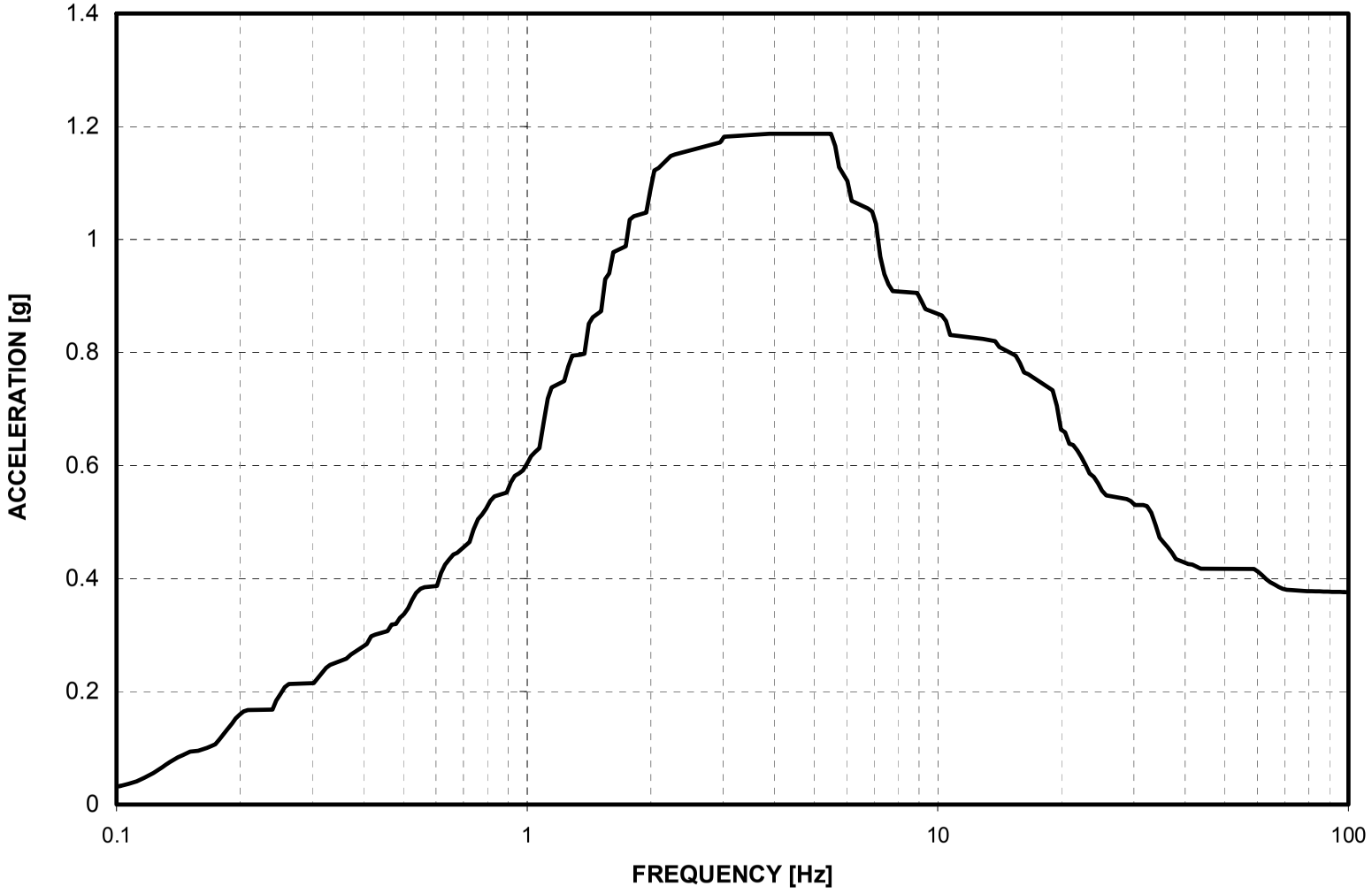

Figure 3-B.1.0-44 Design Basis ISRS at R/B NE Corner Basemat - 5% Damped Response in EW Direction (Y) at Model Elevation -26'-4"

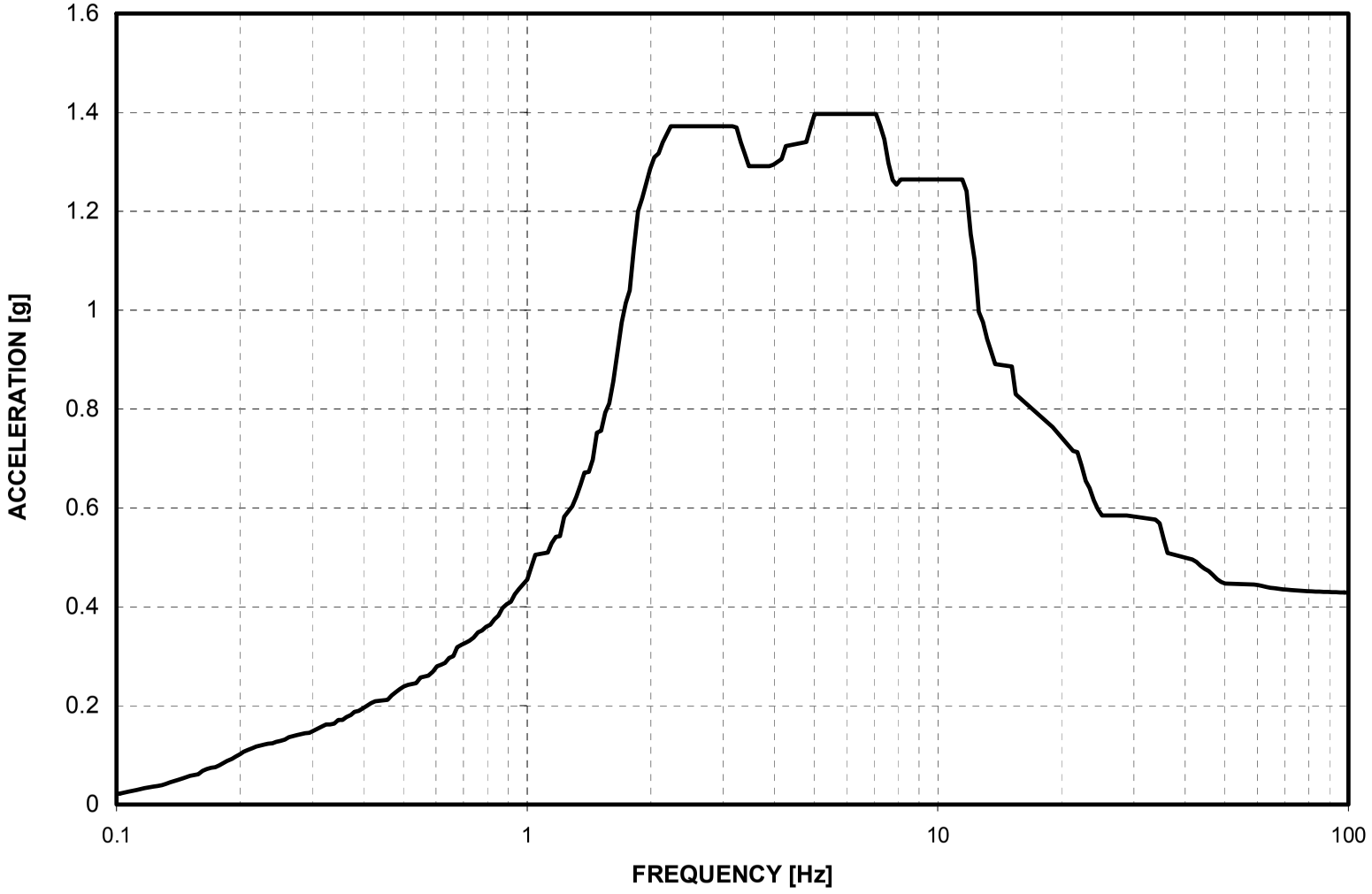

Figure 3-B.1.0-45 Design Basis ISRS at R/B NE Corner Basemat - 5% Damped Response in Vertical Direction (Z) at Model Elevation -26'-4"

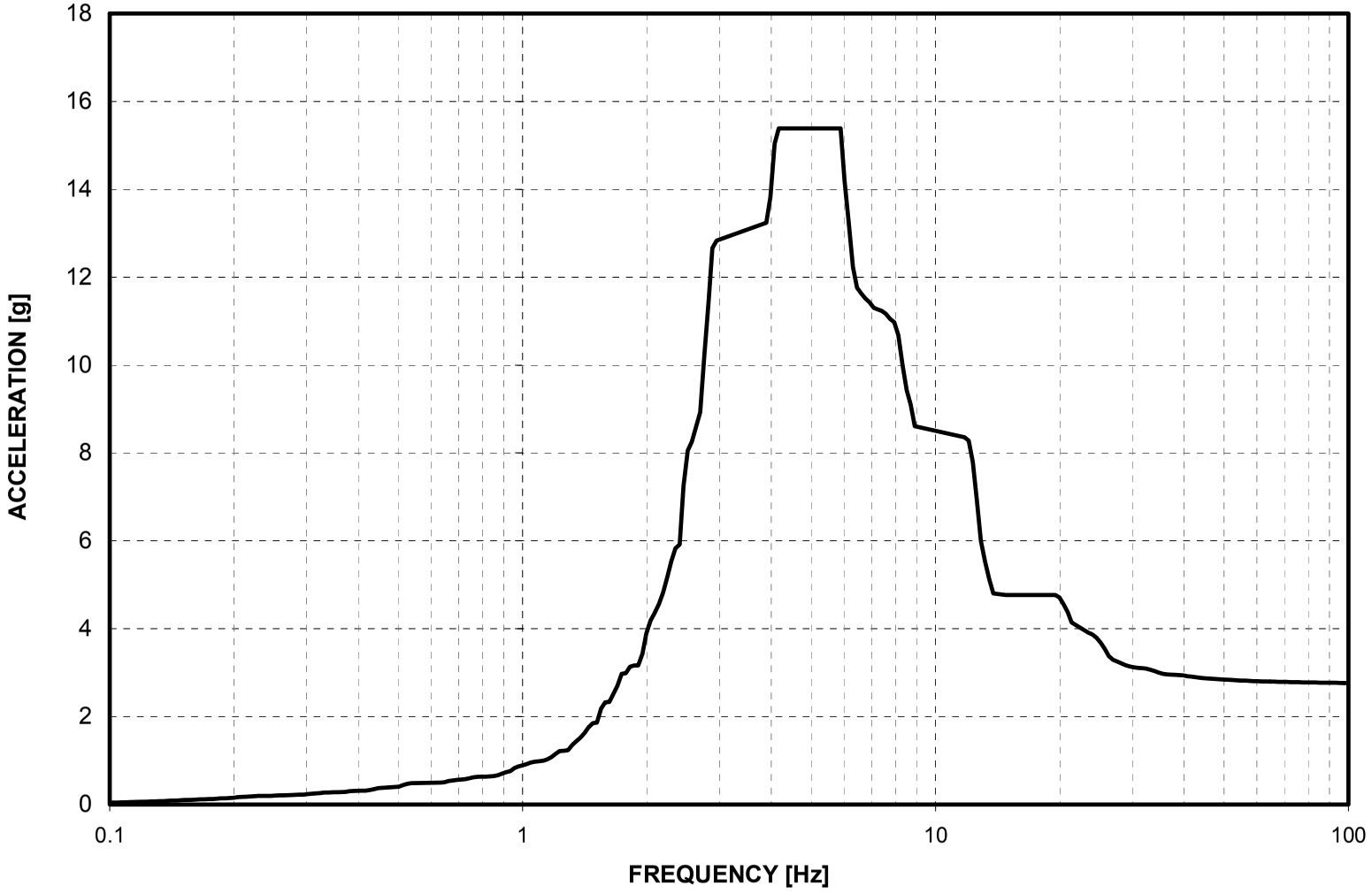

Figure 3-B.1.0-46 Design Basis ISRS at FH/A NE Corner Roof - 5% Damped Response in NS Direction (X) at Model Elevation 156'-0"

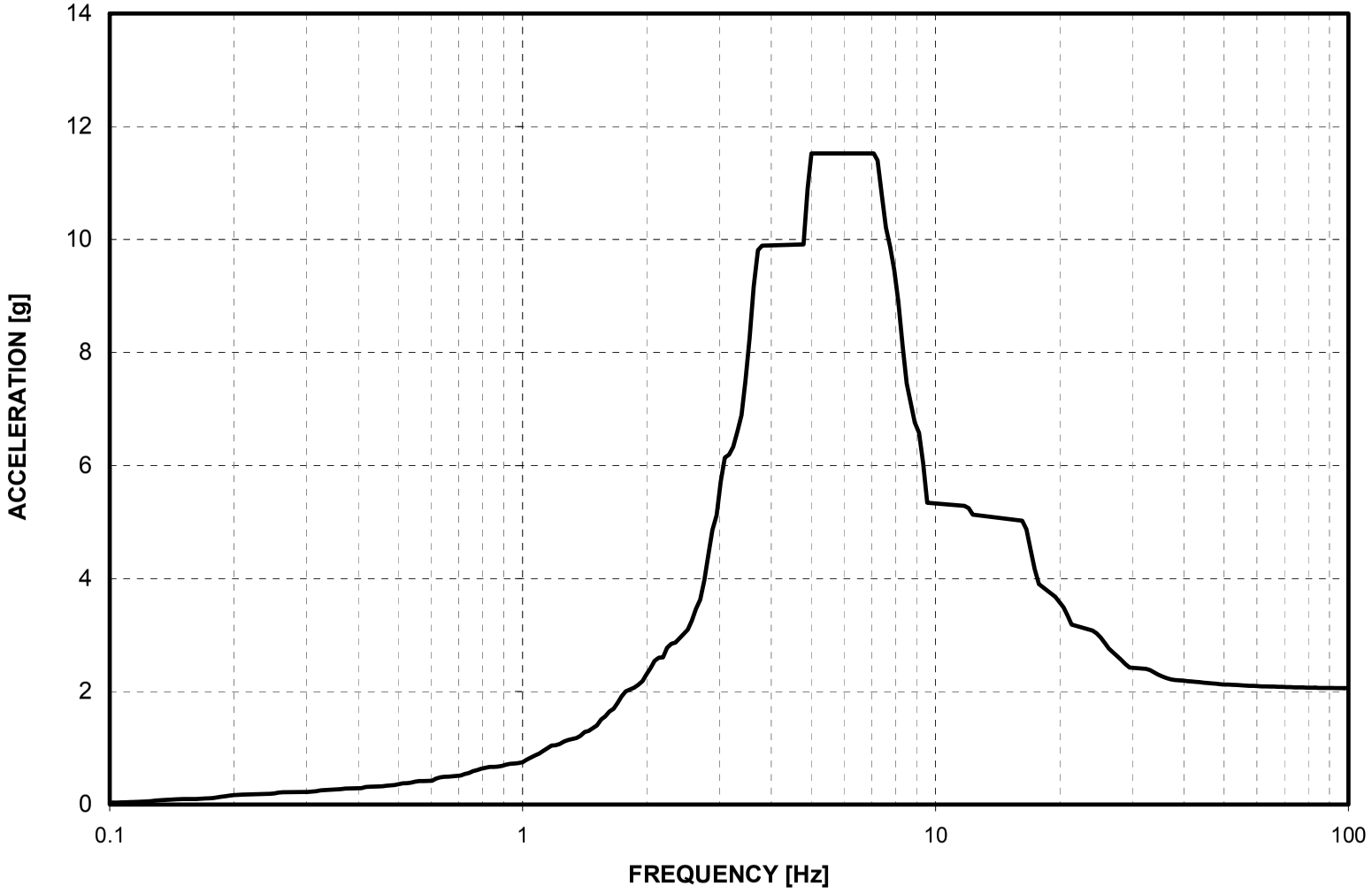

Figure 3-B.1.0-47 Design Basis ISRS at FH/A NE Corner Roof - 5% Damped Response in EW Direction (Y) at Model Elevation 156'-0"

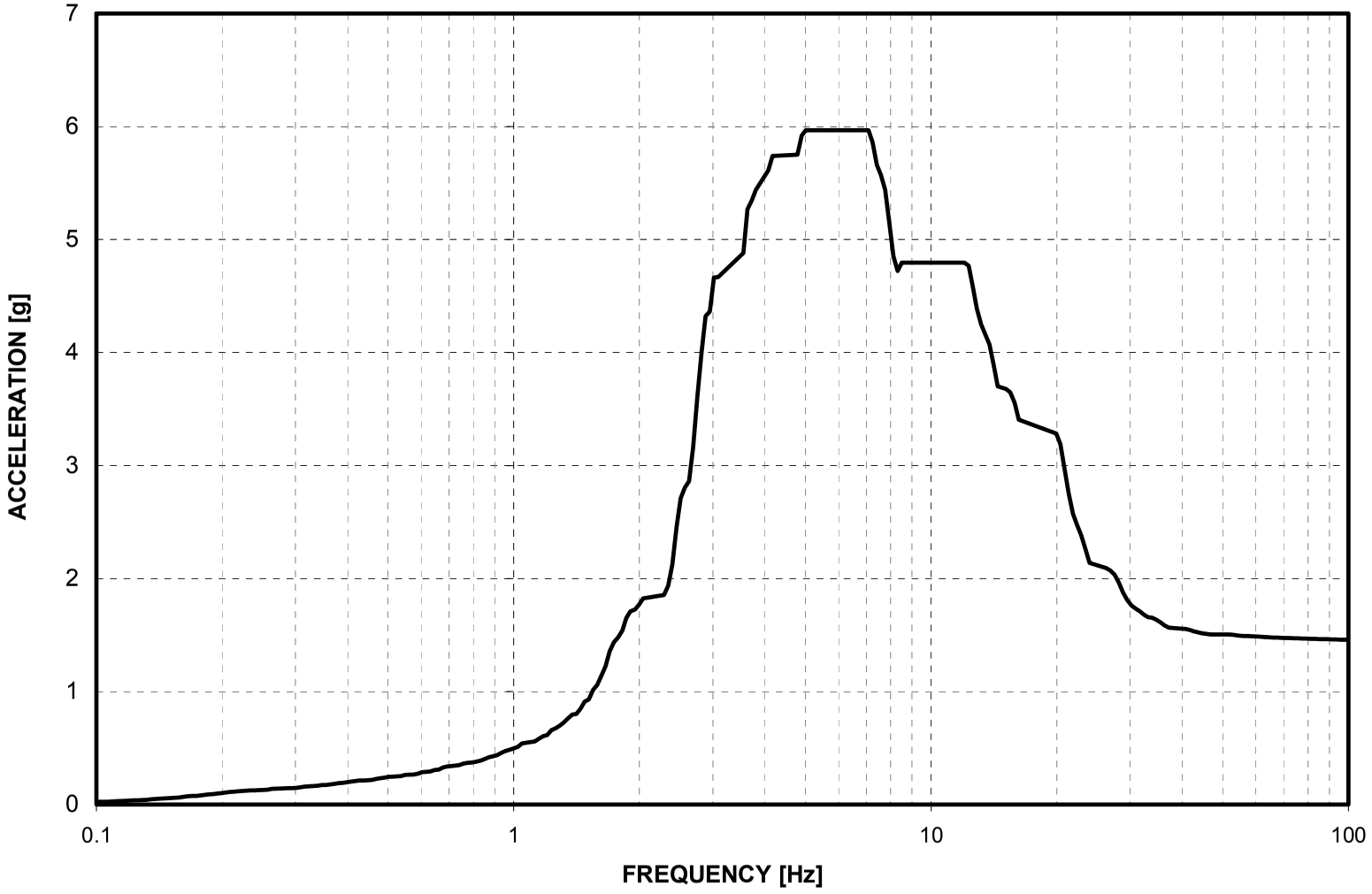

Figure 3-B.1.0-48 Design Basis ISRS at FH/A NE Corner Roof - 5% Damped Response in Vertical Direction (Z) at Model Elevation 156'-0"

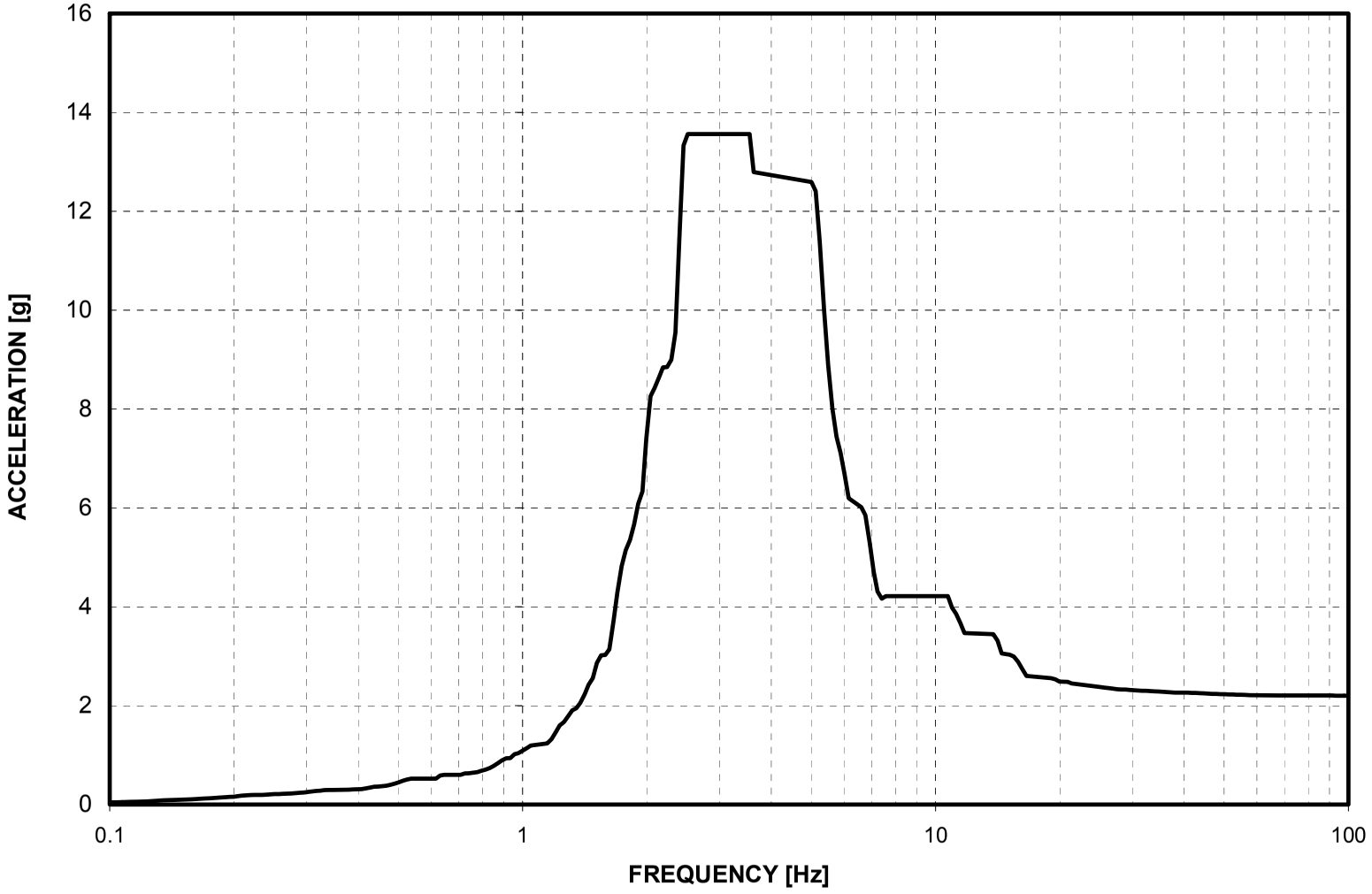

Figure 3-B.1.0-49 Design Basis ISRS at Top of PCCV - 5% Damped Response in NS Direction (X) at Model Elevation 232'-0"

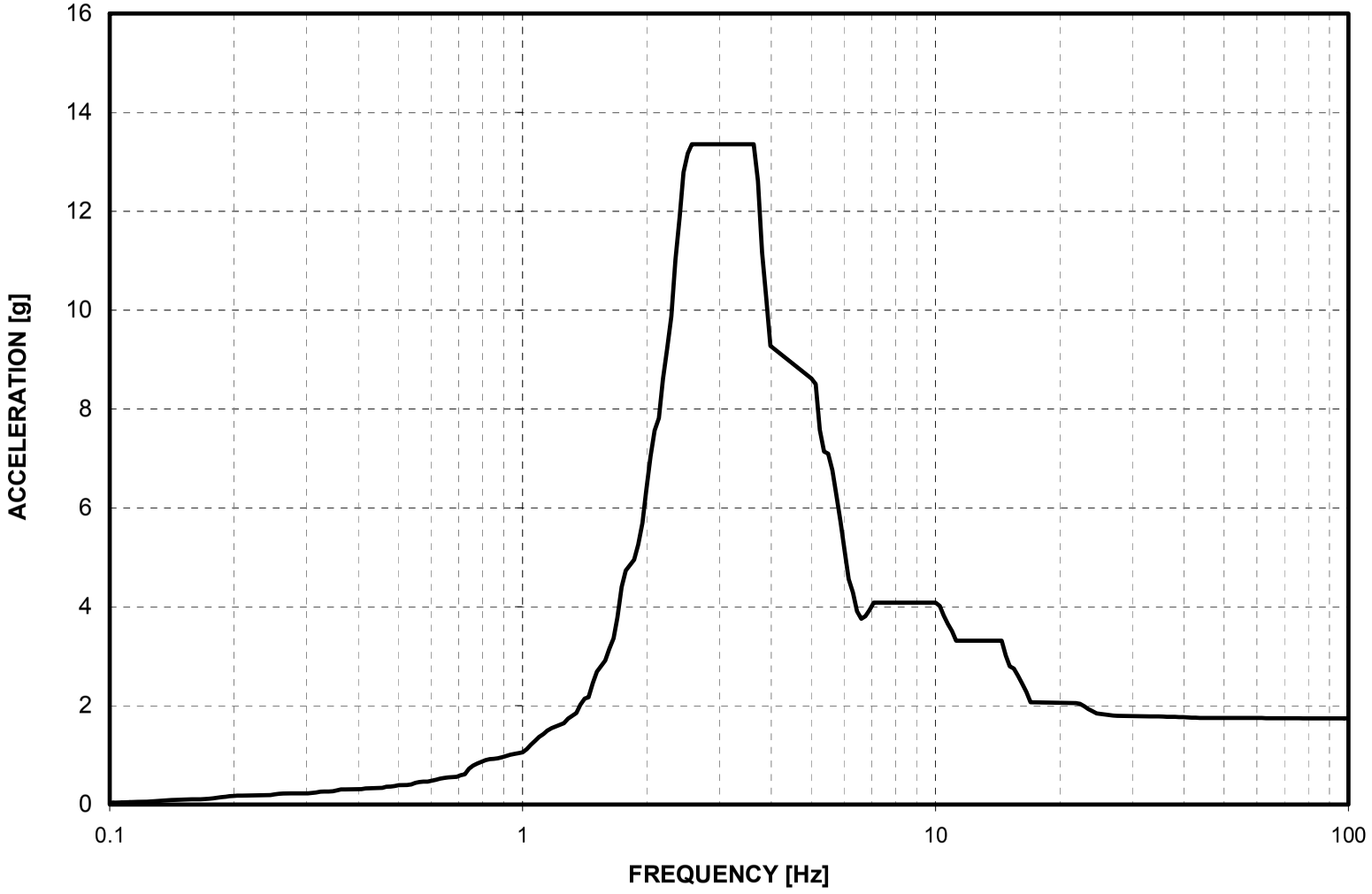

Figure 3-B.1.0-50 Design Basis ISRS at Top of PCCV - 5% Damped Response in EW Direction (Y) at Model Elevation 232'-0"

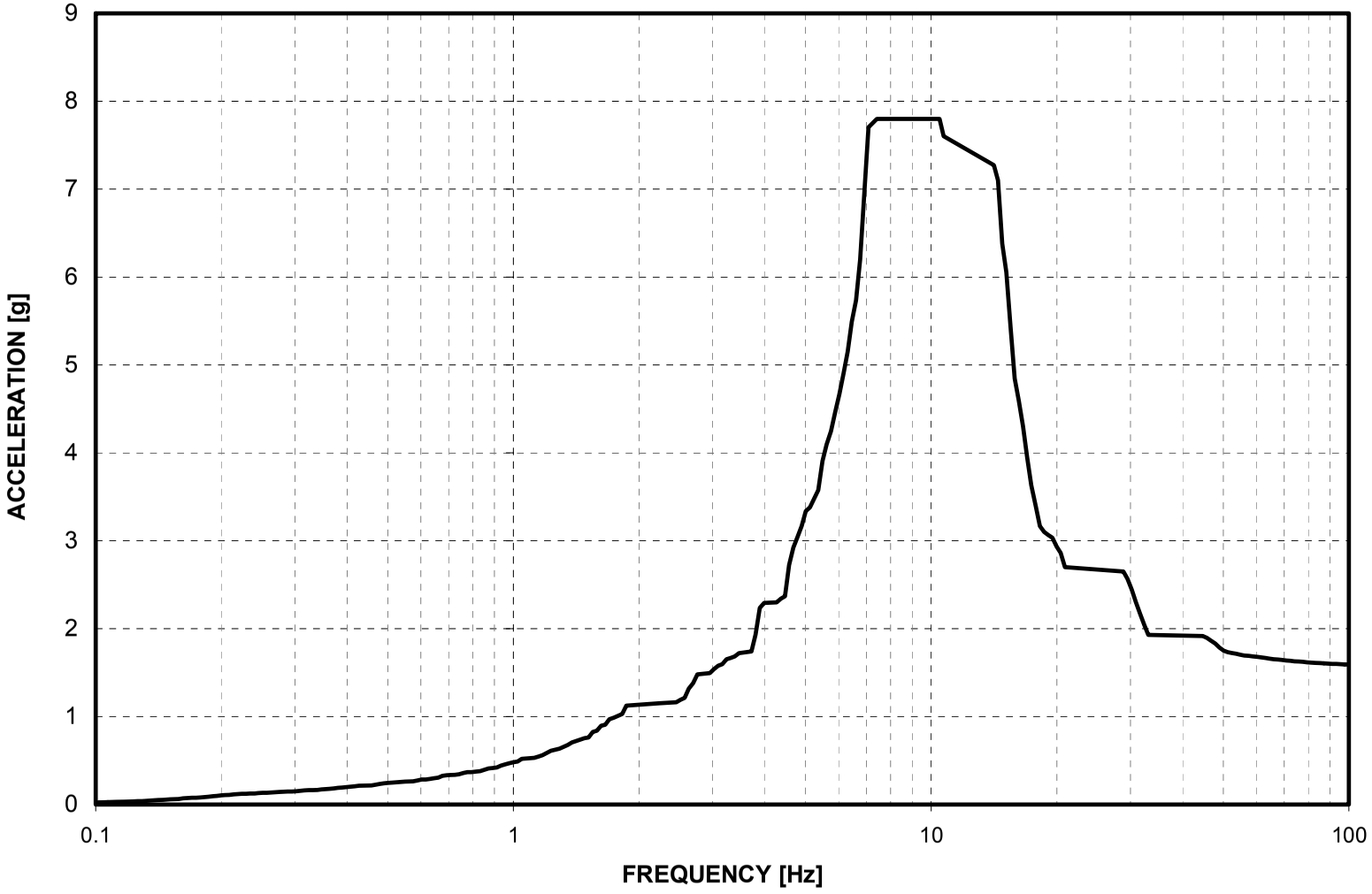

Figure 3-B.1.0-51 Design Basis ISRS at Top of PCCV - 5% Damped Response in Vertical Direction (Z) at Model Elevation 232'-0"

Appendix 3-C

Transfer Function Plots

APPENDIX 3-C TABLE OF CONTENTS

Section	Title	Page No.
3-C.1.0	SSI TRANSFER FUNCTION PLOTS	3-C.1-1
3-C.2.0	SSSI TRANSFER FUNCTION PLOTS	3-C.2-1

LIST OF FIGURES

Figure	Title	Page No.
Figure 3-C.1.0-1	Top of Reactor Cavity - Cracked - NS Direction (X)	3-C.1-1
Figure 3-C.1.0-2	Top of Reactor Cavity - Cracked - EW Direction (Y)	3-C.1-1
Figure 3-C.1.0-3	Top of Reactor Cavity - Cracked - Vertical Direction (Z)	3-C.1-2
Figure 3-C.1.0-4	Top of Reactor Cavity - Uncracked - NS Direction (X)	3-C.1-2
Figure 3-C.1.0-5	Top of Reactor Cavity - Uncracked - EW Direction (Y)	3-C.1-3
Figure 3-C.1.0-6	Top of Reactor Cavity - Uncracked - Vertical Direction (Z)	3-C.1-3
Figure 3-C.1.0-7	Sump Strainer Supports - Cracked - NS Direction (X)	3-C.1-4
Figure 3-C.1.0-8	Sump Strainer Supports - Cracked - EW Direction (Y)	3-C.1-4
Figure 3-C.1.0-9	Sump Strainer Supports - Cracked - Vertical Direction (Z)	3-C.1-5
Figure 3-C.1.0-10	Sump Strainer Supports - Uncracked - NS Direction (X)	3-C.1-5
Figure 3-C.1.0-11	Sump Strainer Supports - Uncracked - EW Direction (Y)	3-C.1-6
Figure 3-C.1.0-12	Sump Strainer Supports - Uncracked - Vertical Direction (Z)	3-C.1-6
Figure 3-C.1.0-13	SG Lower Supports - Cracked - NS Direction (X)	3-C.1-7
Figure 3-C.1.0-14	SG Lower Supports - Cracked - EW Direction (Y)	3-C.1-7
Figure 3-C.1.0-15	SG Lower Supports - Cracked - Vertical Direction (Z)	3-C.1-8
Figure 3-C.1.0-16	SG Lower Supports - Uncracked - NS Direction (X)	3-C.1-8
Figure 3-C.1.0-17	SG Lower Supports - Uncracked - EW Direction (Y)	3-C.1-9
Figure 3-C.1.0-18	SG Lower Supports - Uncracked - Vertical Direction (Z)	3-C.1-9
Figure 3-C.1.0-19	SG Upper Supports - Cracked - NS Direction (X)	3-C.1-10
Figure 3-C.1.0-20	SG Upper Supports - Cracked - EW Direction (Y)	3-C.1-10
Figure 3-C.1.0-21	SG Upper Supports - Cracked - Vertical Direction (Z)	3-C.1-11
Figure 3-C.1.0-22	SG Upper Supports - Uncracked - NS Direction (X)	3-C.1-11
Figure 3-C.1.0-23	SG Upper Supports - Uncracked - EW Direction (Y)	3-C.1-12
Figure 3-C.1.0-24	SG Upper Supports - Uncracked - Vertical Direction (Z)	3-C.1-12
Figure 3-C.1.0-25	SFP - Cracked - NS Direction (X)	3-C.1-13
Figure 3-C.1.0-26	SFP - Cracked - EW Direction (Y)	3-C.1-13
Figure 3-C.1.0-27	SFP - Cracked - Vertical Direction (Z)	3-C.1-14

Figure 3-C.1.0-28 SFP - Uncracked - NS Direction (X) 3-C.1-14
Figure 3-C.1.0-29 SFP - Uncracked - EW Direction (Y) 3-C.1-15
Figure 3-C.1.0-30 SFP - Uncracked - Vertical Direction (Z) 3-C.1-15
Figure 3-C.1.0-31 NFSP - Cracked - NS Direction (X) 3-C.1-16
Figure 3-C.1.0-32 NFSP - Cracked - EW Direction (Y) 3-C.1-16
Figure 3-C.1.0-33 NFSP - Cracked - Vertical Direction (Z) 3-C.1-17
Figure 3-C.1.0-34 NFSP - Uncracked - NS Direction (X) 3-C.1-17
Figure 3-C.1.0-35 NFSP - Uncracked - EW Direction (Y) 3-C.1-18
Figure 3-C.1.0-36 NFSP - Uncracked - Vertical Direction (Z) 3-C.1-18
Figure 3-C.1.0-37 East PS/B A-AAC GTG - Cracked - NS Direction (X) 3-C.1-19
Figure 3-C.1.0-38 East PS/B A-AAC GTG - Cracked - EW Direction (Y) 3-C.1-19
Figure 3-C.1.0-39 East PS/B A-AAC GTG - Cracked - Vertical Direction (Z) 3-C.1-20
Figure 3-C.1.0-40 East PS/B A-AAC GTG - Uncracked - NS Direction (X) 3-C.1-20
Figure 3-C.1.0-41 East PS/B A-AAC GTG - Uncracked - EW Direction (Y) 3-C.1-21
Figure 3-C.1.0-42 East PS/B A-AAC GTG - Uncracked - Vertical Direction (Z) 3-C.1-21
Figure 3-C.1.0-43 West PS/B B-AAC GTG - Cracked - NS Direction (X) 3-C.1-22
Figure 3-C.1.0-44 West PS/B B-AAC GTG - Cracked - EW Direction (Y) 3-C.1-22
Figure 3-C.1.0-45 West PS/B B-AAC GTG - Cracked - Vertical Direction (Z) 3-C.1-23
Figure 3-C.1.0-46 West PS/B B-AAC GTG - Uncracked - NS Direction (X) 3-C.1-23
Figure 3-C.1.0-47 West PS/B B-AAC GTG - Uncracked - EW Direction (Y) 3-C.1-24
Figure 3-C.1.0-48 West PS/B B-AAC GTG - Uncracked - Vertical Direction (Z) 3-C.1-24
Figure 3-C.1.0-49 A/B Northwest Corner at Basemat - Cracked - NS Direction (X) 3-C.1-25
Figure 3-C.1.0-50 A/B Northwest Corner at Basemat - Cracked - EW Direction (Y) 3-C.1-25
Figure 3-C.1.0-51 A/B Northwest Corner at Basemat - Cracked - Vertical Direction (Z) 3-C.1-26
Figure 3-C.1.0-52 A/B Northwest Corner at Basemat - Uncracked - NS Direction (X) 3-C.1-26
Figure 3-C.1.0-53 A/B Northwest Corner at Basemat - Uncracked - EW Direction (Y) 3-C.1-27
Figure 3-C.1.0-54 A/B Northwest Corner at Basemat - Uncracked - Vertical Direction (Z) 3-C.1-27
Figure 3-C.1.0-55 A/B Northwest Corner at Roof - Cracked - NS Direction (X) 3-C.1-28
Figure 3-C.1.0-56 A/B Northwest Corner at Roof - Cracked - EW Direction (Y) 3-C.1-28
Figure 3-C.1.0-57 A/B Northwest Corner at Roof - Cracked - Vertical Direction (Z) 3-C.1-29
Figure 3-C.1.0-58 A/B Northwest Corner at Roof - Uncracked - NS Direction (X) 3-C.1-29
Figure 3-C.1.0-59 A/B Northwest Corner at Roof - Uncracked - EW Direction (Y) 3-C.1-30
Figure 3-C.1.0-60 A/B Northwest Corner at Roof - Uncracked - Vertical Direction (Z) 3-C.1-30

Figure 3-C.1.0-61 West PS/B Southwest Corner at Basemat - Cracked - NS Direction (X) 3-C.1-31
Figure 3-C.1.0-62 West PS/B Southwest Corner at Basemat - Cracked - EW Direction (Y) 3-C.1-31
Figure 3-C.1.0-63 West PS/B Southwest Corner at Basemat - Cracked - Vertical Direction (Z) 3-C.1-32
Figure 3-C.1.0-64 West PS/B Southwest Corner at Basemat - Uncracked - NS Direction (X) 3-C.1-32
Figure 3-C.1.0-65 West PS/B Southwest Corner at Basemat - Uncracked - EW Direction (Y) 3-C.1-33
Figure 3-C.1.0-66 West PS/B Southwest Corner at Basemat - Uncracked - Vertical Direction (Z) 3-C.1-33
Figure 3-C.1.0-67 West PS/B Southwest Corner at Roof - Cracked - NS Direction (X) 3-C.1-34
Figure 3-C.1.0-68 West PS/B Southwest Corner at Roof - Cracked - EW Direction (Y) 3-C.1-34
Figure 3-C.1.0-69 West PS/B Southwest Corner at Roof - Cracked - Vertical Direction (Z) 3-C.1-35
Figure 3-C.1.0-70 West PS/B Southwest Corner at Roof - Uncracked - NS Direction (X) 3-C.1-35
Figure 3-C.1.0-71 West PS/B Southwest Corner at Roof - Uncracked - EW Direction (Y) 3-C.1-36
Figure 3-C.1.0-72 West PS/B Southwest Corner at Roof - Uncracked - Vertical Direction (Z) 3-C.1-36
Figure 3-C.1.0-73 East PS/B Southeast Corner at Basemat - Cracked - NS Direction (X) 3-C.1-37
Figure 3-C.1.0-74 East PS/B Southeast Corner at Basemat - Cracked - EW Direction (Y) 3-C.1-37
Figure 3-C.1.0-75 East PS/B Southeast Corner at Basemat - Cracked - Vertical Direction (Z) 3-C.1-38
Figure 3-C.1.0-76 East PS/B Southeast Corner at Basemat - Uncracked - NS Direction (X) 3-C.1-38
Figure 3-C.1.0-77 East PS/B Southeast Corner at Basemat - Uncracked - EW Direction (Y) 3-C.1-39
Figure 3-C.1.0-78 East PS/B Southeast Corner at Basemat - Uncracked - Vertical Direction (Z) 3-C.1-39
Figure 3-C.1.0-79 East PS/B Southeast Corner at Roof - Cracked - NS Direction (X) . 3-C.1-40
Figure 3-C.1.0-80 East PS/B Southeast Corner at Roof - Cracked - EW Direction (Y) 3-C.1-40
Figure 3-C.1.0-81 East PS/B Southeast Corner at Roof - Cracked - Vertical Direction (Z)..... 3-C.1-41

Figure 3-C.1.0-82 East PS/B Southeast Corner at Roof - Uncracked - NS Direction (X) 3-C.1-41
Figure 3-C.1.0-83 East PS/B Southeast Corner at Roof - Uncracked - EW Direction (Y) 3-C.1-42
Figure 3-C.1.0-84 East PS/B Southeast Corner at Roof - Uncracked - Vertical Direction (Z) 3-C.1-42
Figure 3-C.1.0-85 R/B Northeast Corner at Basemat - Cracked - NS Direction (X)..... 3-C.1-43
Figure 3-C.1.0-86 R/B Northeast Corner at Basemat - Cracked - EW Direction (Y)..... 3-C.1-43
Figure 3-C.1.0-87 R/B Northeast Corner at Basemat - Cracked - Vertical Direction (Z)..... 3-C.1-44
Figure 3-C.1.0-88 R/B Northeast Corner at Basemat - Uncracked - NS Direction (X).. 3-C.1-44
Figure 3-C.1.0-89 R/B Northeast Corner at Basemat - Uncracked - EW Direction (Y). 3-C.1-45
Figure 3-C.1.0-90 R/B Northeast Corner at Basemat - Uncracked - Vertical Direction (Z)..... 3-C.1-45
Figure 3-C.1.0-91 R/B Northeast Corner at Roof - Cracked - NS Direction (X) 3-C.1-46
Figure 3-C.1.0-92 R/B Northeast Corner at Roof - Cracked - EW Direction (Y) 3-C.1-46
Figure 3-C.1.0-93 R/B Northeast Corner at Roof - Cracked - Vertical Direction (Z) 3-C.1-47
Figure 3-C.1.0-94 R/B Northeast Corner at Roof - Uncracked - NS Direction (X) 3-C.1-47
Figure 3-C.1.0-95 R/B Northeast Corner at Roof - Uncracked - EW Direction (Y)..... 3-C.1-48
Figure 3-C.1.0-96 R/B Northeast Corner at Roof - Uncracked - Vertical Direction (Z).. 3-C.1-48
Figure 3-C.1.0-97 Top of PCCV - Cracked - NS Direction (X) 3-C.1-49
Figure 3-C.1.0-98 Top of PCCV - Cracked - EW Direction (Y) 3-C.1-49
Figure 3-C.1.0-99 Top of PCCV - Cracked - Vertical Direction (Z) 3-C.1-50
Figure 3-C.1.0-100 Top of PCCV - Uncracked - NS Direction (X) 3-C.1-50
Figure 3-C.1.0-101 Top of PCCV - Uncracked - EW Direction (Y)..... 3-C.1-51
Figure 3-C.1.0-102 Top of PCCV - Uncracked - Vertical Direction (Z)..... 3-C.1-51
Figure 3-C.2.0-1 Top of Reactor Cavity - Cracked – NS Direction (X)..... 3-C.2-1
Figure 3-C.2.0-2 Top of Reactor Cavity - Cracked - EW Direction (Y)..... 3-C.2-1
Figure 3-C.2.0-3 Top of Reactor Cavity - Cracked - Vertical Direction (Z)..... 3-C.2-2
Figure 3-C.2.0-4 Top of Reactor Cavity - Uncracked - NS Direction (X)..... 3-C.2-2
Figure 3-C.2.0-5 Top of Reactor Cavity - Uncracked - EW Direction (Y) 3-C.2-3
Figure 3-C.2.0-6 Top of Reactor Cavity - Uncracked - Vertical Direction (Z) 3-C.2-3
Figure 3-C.2.0-7 Sump Strainer Supports - Cracked - NS Direction (X) 3-C.2-4
Figure 3-C.2.0-8 Sump Strainer Supports - Cracked - EW Direction (Y) 3-C.2-4
Figure 3-C.2.0-9 Sump Strainer Supports - Cracked - Vertical Direction (Z) 3-C.2-5
Figure 3-C.2.0-10 Sump Strainer Supports - Uncracked - NS Direction (X) 3-C.2-5
Figure 3-C.2.0-11 Sump Strainer Supports - Uncracked - EW Direction (Y) 3-C.2-6

Figure 3-C.2.0-12 Sump Strainer Supports - Uncracked - Vertical Direction (Z) 3-C.2-6
Figure 3-C.2.0-13 SG Lower Supports - Cracked - NS Direction (X).....3-C.2-7
Figure 3-C.2.0-14 SG Lower Supports - Cracked - EW Direction (Y) 3-C.2-7
Figure 3-C.2.0-15 SG Lower Supports - Cracked - Vertical Direction (Z) 3-C.2-8
Figure 3-C.2.0-16 SG Lower Supports - Uncracked - NS Direction (X) 3-C.2-8
Figure 3-C.2.0-17 SG Lower Supports - Uncracked - EW Direction (Y) 3-C.2-9
Figure 3-C.2.0-18 SG Lower Supports - Uncracked - Vertical Direction (Z) 3-C.2-9
Figure 3-C.2.0-19 SG Upper Supports - Cracked - NS Direction (X).....3-C.2-10
Figure 3-C.2.0-20 SG Upper Supports - Cracked - EW Direction (Y) 3-C.2-10
Figure 3-C.2.0-21 SG Upper Supports - Cracked - Vertical Direction (Z) 3-C.2-11
Figure 3-C.2.0-22 SG Upper Supports - Uncracked - NS Direction (X) 3-C.2-11
Figure 3-C.2.0-23 SG Upper Supports - Uncracked - EW Direction (Y) 3-C.2-12
Figure 3-C.2.0-24 SG Upper Supports - Uncracked - Vertical Direction (Z) 3-C.2-12
Figure 3-C.2.0-25 SFP - Cracked - NS Direction (X) 3-C.2-13
Figure 3-C.2.0-26 SFP - Cracked - EW Direction (Y).....3-C.2-13
Figure 3-C.2.0-27 SFP - Cracked - Vertical Direction (Z).....3-C.2-14
Figure 3-C.2.0-28 SFP - Uncracked - NS Direction (X).....3-C.2-14
Figure 3-C.2.0-29 SFP - Uncracked - EW Direction (Y).....3-C.2-15
Figure 3-C.2.0-30 SFP - Uncracked - Vertical Direction (Z).....3-C.2-15
Figure 3-C.2.0-31 NFSP - Cracked - NS Direction (X).....3-C.2-16
Figure 3-C.2.0-32 NFSP - Cracked - EW Direction (Y).....3-C.2-16
Figure 3-C.2.0-33 NFSP - Cracked - Vertical Direction (Z).....3-C.2-17
Figure 3-C.2.0-34 NFSP - Uncracked - NS Direction (X).....3-C.2-17
Figure 3-C.2.0-35 NFSP - Uncracked - EW Direction (Y) 3-C.2-18
Figure 3-C.2.0-36 NFSP - Uncracked - Vertical Direction (Z) 3-C.2-18
Figure 3-C.2.0-37 East PS/B A-AAC GTG - Cracked - NS Direction (X) 3-C.2-19
Figure 3-C.2.0-38 East PS/B A-AAC GTG - Cracked - EW Direction (Y) 3-C.2-19
Figure 3-C.2.0-39 East PS/B A-AAC GTG - Cracked - Vertical Direction (Z) 3-C.2-20
Figure 3-C.2.0-40 East PS/B A-AAC GTG - Uncracked - NS Direction (X) 3-C.2-20
Figure 3-C.2.0-41 East PS/B A-AAC GTG - Uncracked - EW Direction (Y).....3-C.2-21
Figure 3-C.2.0-42 East PS/B A-AAC GTG - Uncracked - Vertical Direction (Z).....3-C.2-21
Figure 3-C.2.0-43 West PS/B B-AAC GTG - Cracked - NS Direction (X) 3-C.2-22
Figure 3-C.2.0-44 West PS/B B-AAC GTG - Cracked - EW Direction (Y) 3-C.2-22
Figure 3-C.2.0-45 West PS/B B-AAC GTG - Cracked - Vertical Direction (Z) 3-C.2-23
Figure 3-C.2.0-46 West PS/B B-AAC GTG - Uncracked - NS Direction (X) 3-C.2-23

Figure 3-C.2.0-47 West PS/B B-AAC GTG - Uncracked - EW Direction (Y)..... 3-C.2-24
Figure 3-C.2.0-48 West PS/B B-AAC GTG - Uncracked - Vertical Direction (Z)..... 3-C.2-24
Figure 3-C.2.0-49 A/B Northwest Corner at Basemat - Cracked - NS Direction (X) 3-C.2-25
Figure 3-C.2.0-50 A/B Northwest Corner at Basemat - Cracked - EW Direction (Y) 3-C.2-25
Figure 3-C.2.0-51 A/B Northwest Corner at Basemat - Cracked - Vertical Direction (Z)..... 3-C.2-26
Figure 3-C.2.0-52 A/B Northwest Corner at Basemat - Uncracked - NS Direction (X) . 3-C.2-26
Figure 3-C.2.0-53 A/B Northwest Corner at Basemat - Uncracked - EW Direction (Y). 3-C.2-27
Figure 3-C.2.0-54 A/B Northwest Corner at Basemat - Uncracked - Vertical Direction (Z)..... 3-C.2-27
Figure 3-C.2.0-55 A/B Northwest Corner at Roof - Cracked - NS Direction (X)..... 3-C.2-28
Figure 3-C.2.0-56 A/B Northwest Corner at Roof - Cracked - EW Direction (Y)..... 3-C.2-28
Figure 3-C.2.0-57 A/B Northwest Corner at Roof - Cracked - Vertical Direction (Z)..... 3-C.2-29
Figure 3-C.2.0-58 A/B Northwest Corner at Roof - Uncracked - NS Direction (X)..... 3-C.2-29
Figure 3-C.2.0-59 A/B Northwest Corner at Roof - Uncracked - EW Direction (Y) 3-C.2-30
Figure 3-C.2.0-60 A/B Northwest Corner at Roof - Uncracked - Vertical Direction (Z) . 3-C.2-30
Figure 3-C.2.0-61 West PS/B Southwest Corner at Basemat - Cracked - NS Direction (X) 3-C.2-31
Figure 3-C.2.0-62 West PS/B Southwest Corner at Basemat - Cracked - EW Direction (Y) 3-C.2-31
Figure 3-C.2.0-63 West PS/B Southwest Corner at Basemat - Cracked - Vertical Direction (Z) 3-C.2-32
Figure 3-C.2.0-64 West PS/B Southwest Corner at Basemat - Uncracked - NS Direction (X) 3-C.2-32
Figure 3-C.2.0-65 West PS/B Southwest Corner at Basemat - Uncracked - EW Direction (Y) 3-C.2-33
Figure 3-C.2.0-66 West PS/B Southwest Corner at Basemat - Uncracked - Vertical Direction (Z) 3-C.2-33
Figure 3-C.2.0-67 West PS/B Southwest Corner at Roof - Cracked - NS Direction (X) 3-C.2-34
Figure 3-C.2.0-68 West PS/B Southwest Corner at Roof - Cracked - EW Direction (Y) 3-C.2-34
Figure 3-C.2.0-69 West PS/B Southwest Corner at Roof - Cracked - Vertical Direction (Z) 3-C.2-35
Figure 3-C.2.0-70 West PS/B Southwest Corner at Roof - Uncracked - NS Direction (X) 3-C.2-35
Figure 3-C.2.0-71 West PS/B Southwest Corner at Roof - Uncracked - EW Direction (Y) 3-C.2-36

Figure 3-C.2.0-72 West PS/B Southwest Corner at Roof - Uncracked - Vertical Direction (Z) 3-C.2-36
Figure 3-C.2.0-73 East PS/B Southeast Corner at Basemat - Cracked - NS Direction (X) 3-C.2-37
Figure 3-C.2.0-74 East PS/B Southeast Corner at Basemat - Cracked - EW Direction (Y) 3-C.2-37
Figure 3-C.2.0-75 East PS/B Southeast Corner at Basemat - Cracked - Vertical Direction (Z) 3-C.2-38
Figure 3-C.2.0-76 East PS/B Southeast Corner at Basemat - Uncracked - NS Direction (X) 3-C.2-38
Figure 3-C.2.0-77 East PS/B Southeast Corner at Basemat - Uncracked - EW Direction (Y) 3-C.2-39
Figure 3-C.2.0-78 East PS/B Southeast Corner at Basemat - Uncracked - Vertical Direction (Z) 3-C.2-39
Figure 3-C.2.0-79 East PS/B Southeast Corner at Roof - Cracked - NS Direction (X) . 3-C.2-40
Figure 3-C.2.0-80 East PS/B Southeast Corner at Roof - Cracked - EW Direction (Y) 3-C.2-40
Figure 3-C.2.0-81 East PS/B Southeast Corner at Roof - Cracked - Vertical Direction (Z)..... 3-C.2-41
Figure 3-C.2.0-82 East PS/B Southeast Corner at Roof - Uncracked - NS Direction (X) 3-C.2-41
Figure 3-C.2.0-83 East PS/B Southeast Corner at Roof - Uncracked - EW Direction (Y) 3-C.2-42
Figure 3-C.2.0-84 East PS/B Southeast Corner at Roof - Uncracked - Vertical Direction (Z) 3-C.2-42
Figure 3-C.2.0-85 R/B Northeast Corner at Basemat - Cracked - NS Direction (X)..... 3-C.2-43
Figure 3-C.2.0-86 R/B Northeast Corner at Basemat - Cracked - EW Direction (Y)..... 3-C.2-43
Figure 3-C.2.0-87 R/B Northeast Corner at Basemat - Cracked - Vertical Direction (Z)..... 3-C.2-44
Figure 3-C.2.0-88 R/B Northeast Corner at Basemat - Uncracked - NS Direction (X).. 3-C.2-44
Figure 3-C.2.0-89 R/B Northeast Corner at Basemat - Uncracked - EW Direction (Y) . 3-C.2-45
Figure 3-C.2.0-90 R/B Northeast Corner at Basemat - Uncracked - Vertical Direction (Z)..... 3-C.2-45
Figure 3-C.2.0-91 R/B Northeast Corner at Roof - Cracked - NS Direction (X) 3-C.2-46
Figure 3-C.2.0-92 R/B Northeast Corner at Roof - Cracked - EW Direction (Y) 3-C.2-46
Figure 3-C.2.0-93 R/B Northeast Corner at Roof - Cracked - Vertical Direction (Z) 3-C.2-47
Figure 3-C.2.0-94 R/B Northeast Corner at Roof - Uncracked - NS Direction (X) 3-C.2-47
Figure 3-C.2.0-95 R/B Northeast Corner at Roof - Uncracked - EW Direction (Y)..... 3-C.2-48
Figure 3-C.2.0-96 R/B Northeast Corner at Roof - Uncracked - Vertical Direction (Z).. 3-C.2-48
Figure 3-C.2.0-97 Top of PCCV - Cracked - NS Direction (X) 3-C.2-49

Figure 3-C.2.0-98 Top of PCCV - Cracked - EW Direction (Y) 3-C.2-49
Figure 3-C.2.0-99 Top of PCCV - Cracked - Vertical Direction (Z) 3-C.2-50
Figure 3-C.2.0-100 Top of PCCV - Uncracked - NS Direction (X) 3-C.2-50
Figure 3-C.2.0-101 Top of PCCV - Uncracked - EW Direction (Y).....3-C.2-51
Figure 3-C.2.0-102 Top of PCCV - Uncracked - Vertical Direction (Z).....3-C.2-51

3-C.1.0 SSI TRANSFER FUNCTION PLOTS

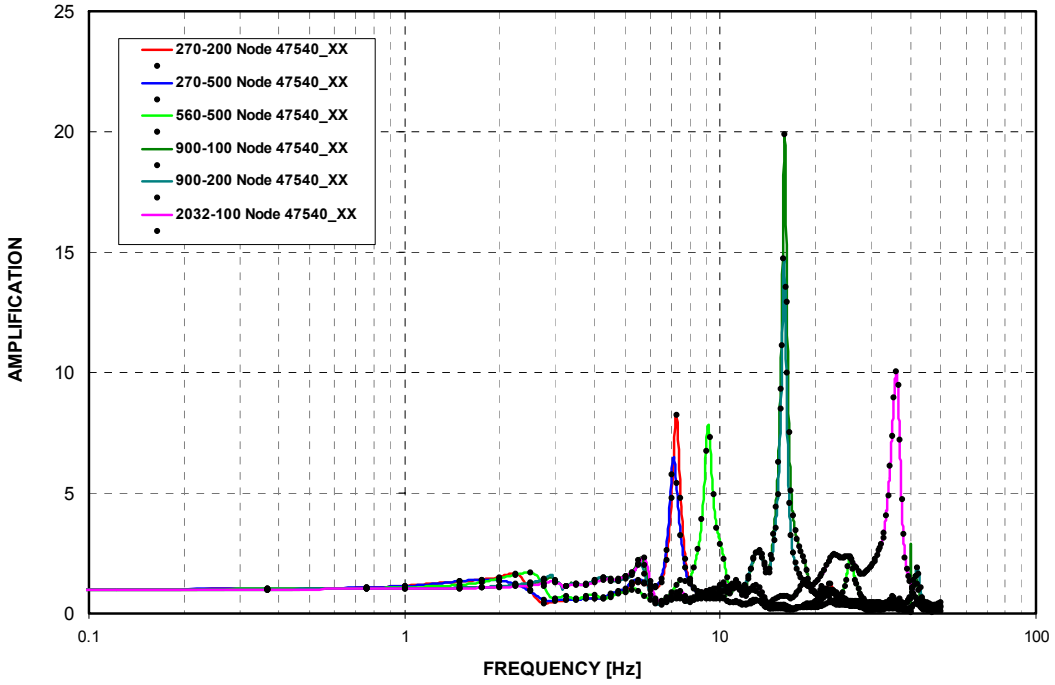

Figure 3-C.1.0-1 Top of Reactor Cavity - Cracked - NS Direction (X)

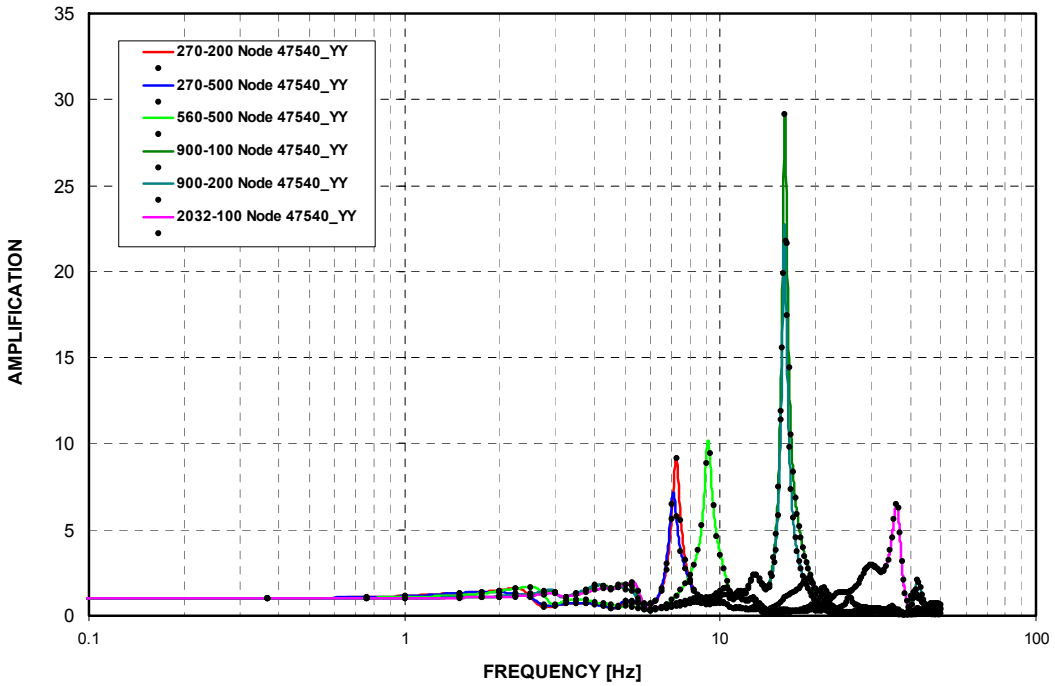

Figure 3-C.1.0-2 Top of Reactor Cavity - Cracked - EW Direction (Y)

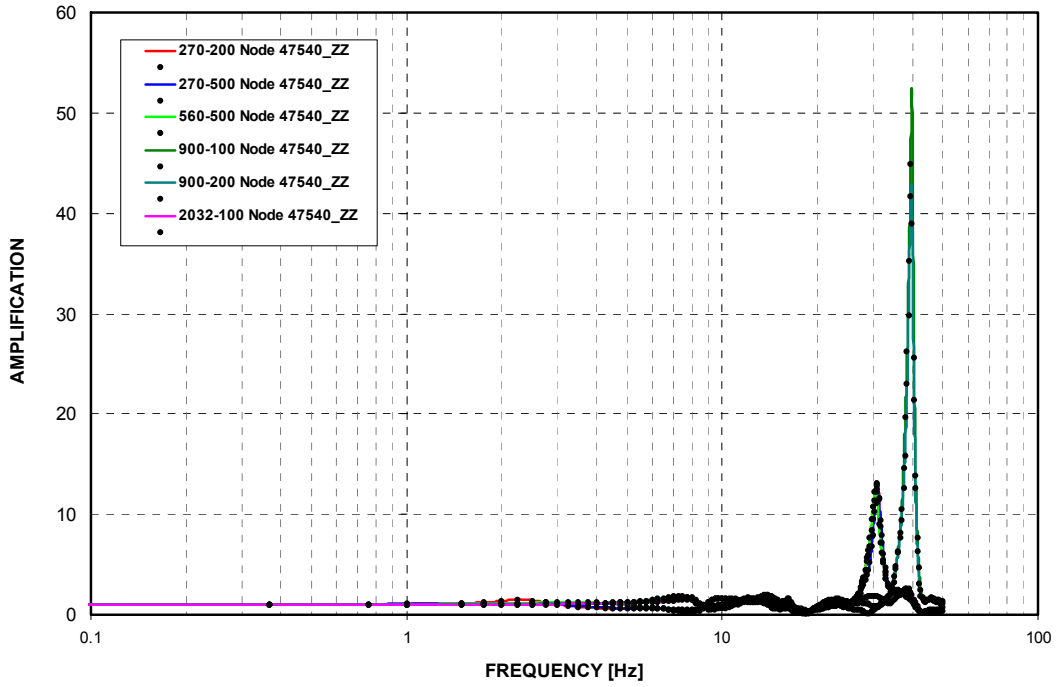

Figure 3-C.1.0-3 Top of Reactor Cavity - Cracked - Vertical Direction (Z)

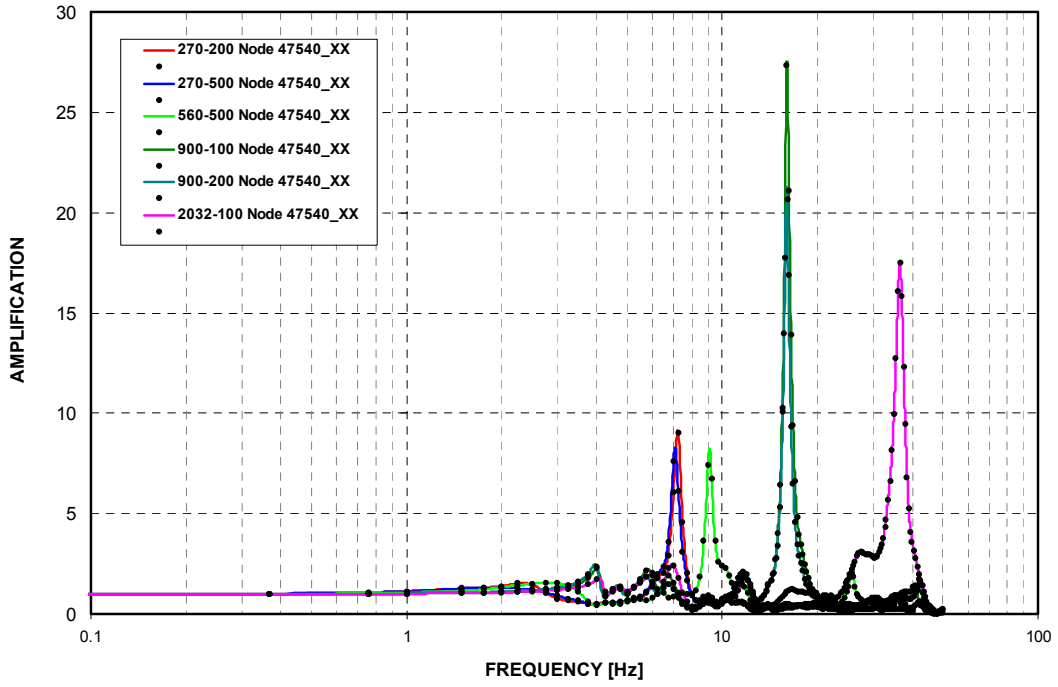

Figure 3-C.1.0-4 Top of Reactor Cavity - Uncracked - NS Direction (X)

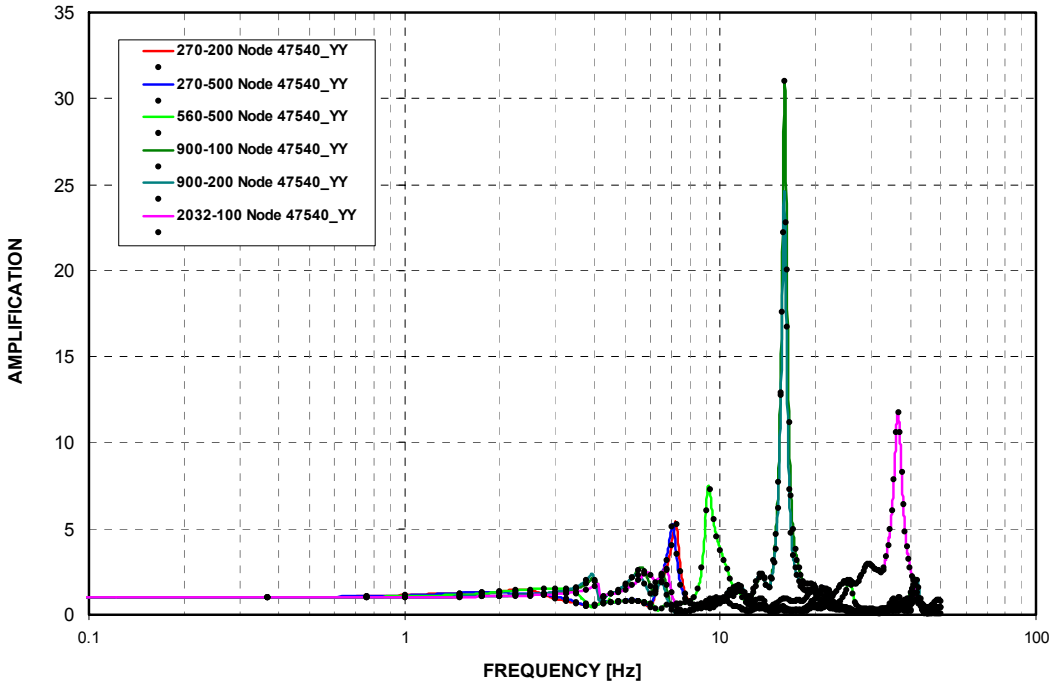

Figure 3-C.1.0-5 Top of Reactor Cavity - Uncracked - EW Direction (Y)

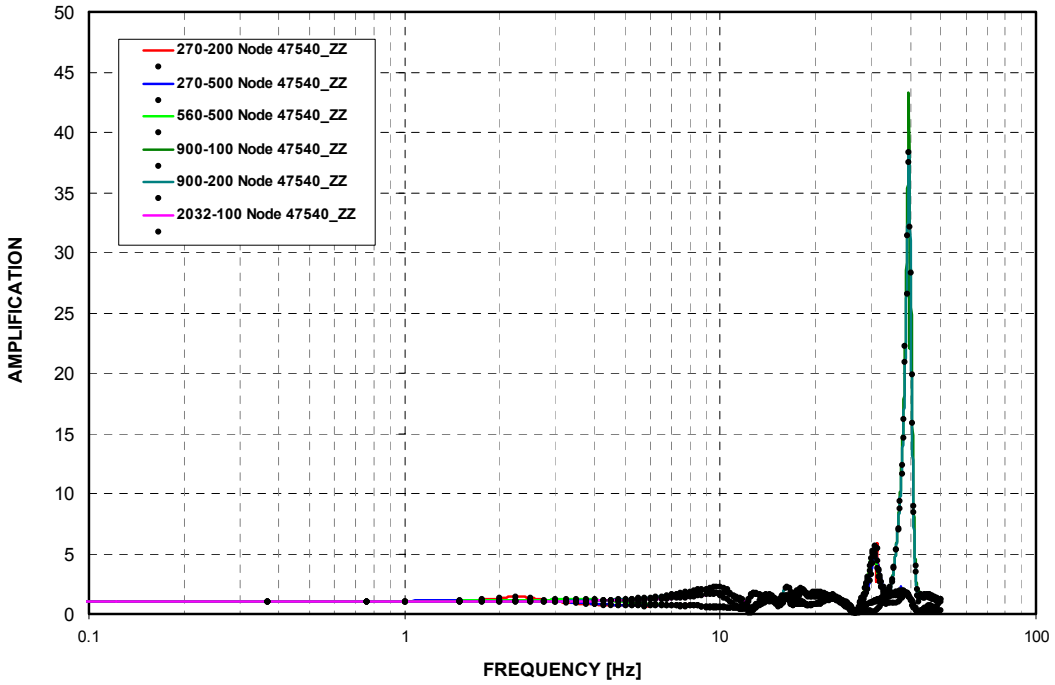

Figure 3-C.1.0-6 Top of Reactor Cavity - Uncracked - Vertical Direction (Z)

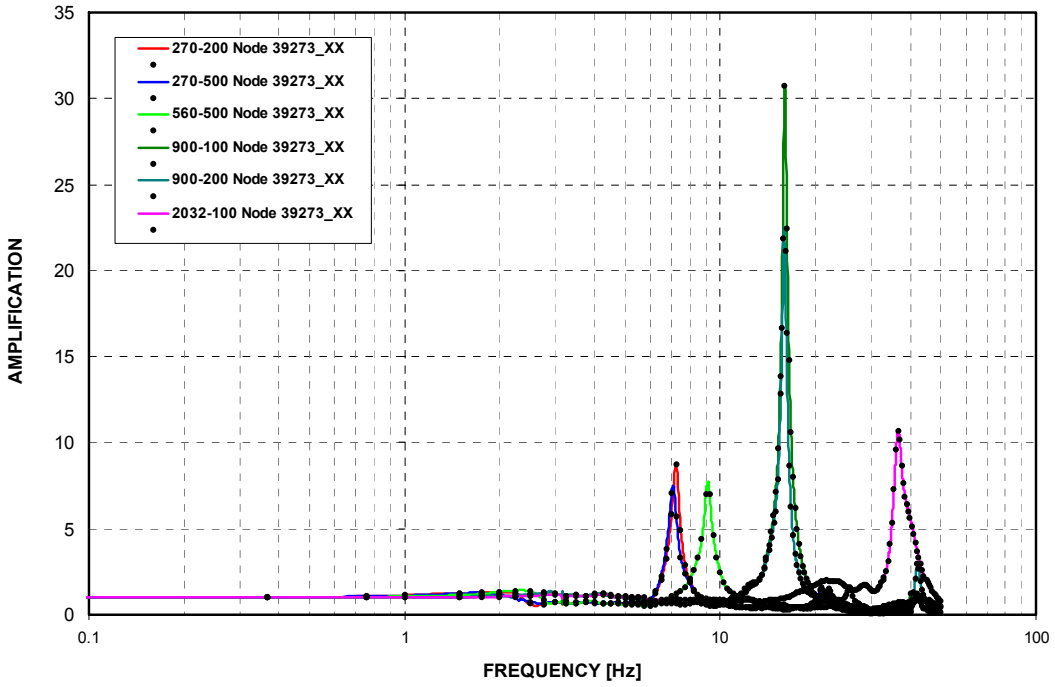

Figure 3-C.1.0-7 Sump Strainer Supports - Cracked - NS Direction (X)

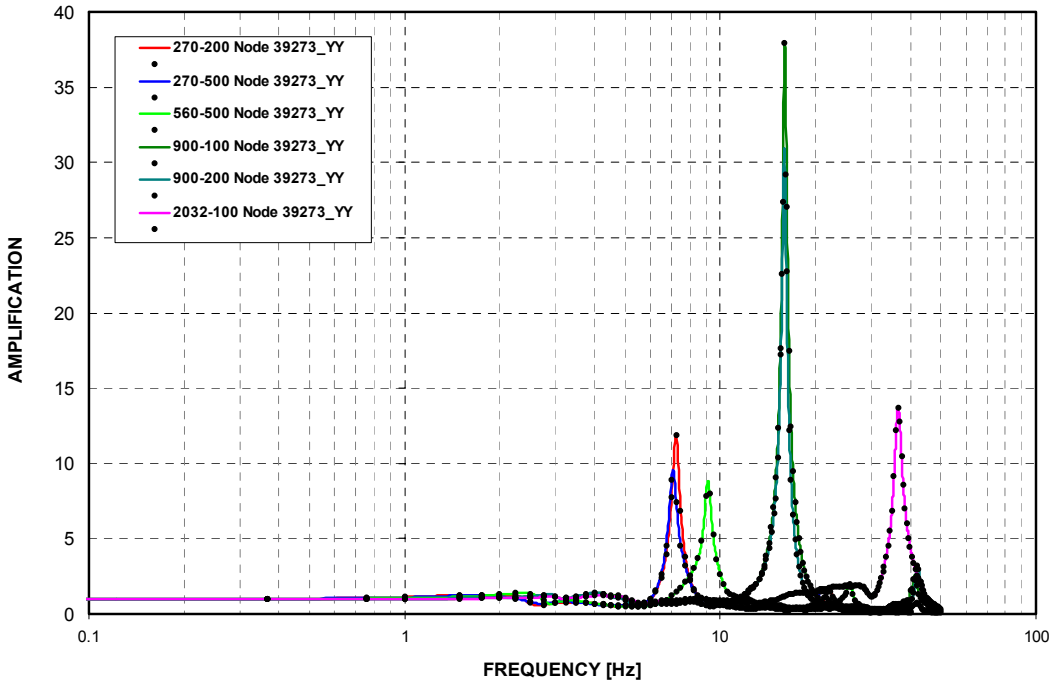

Figure 3-C.1.0-8 Sump Strainer Supports - Cracked - EW Direction (Y)

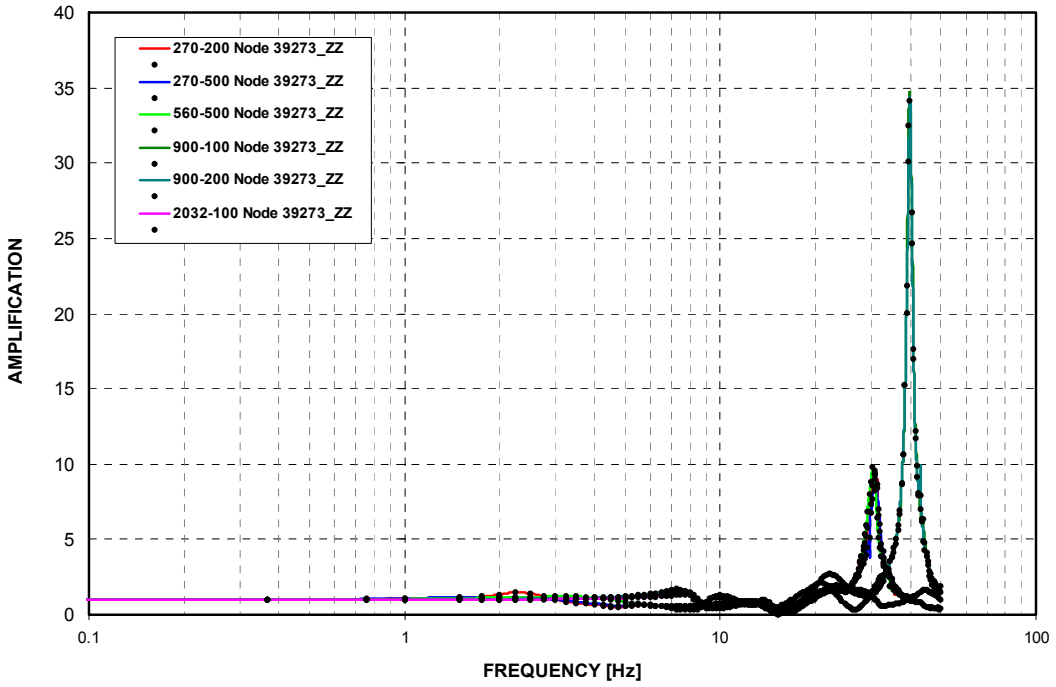

Figure 3-C.1.0-9 Sump Strainer Supports - Cracked - Vertical Direction (Z)

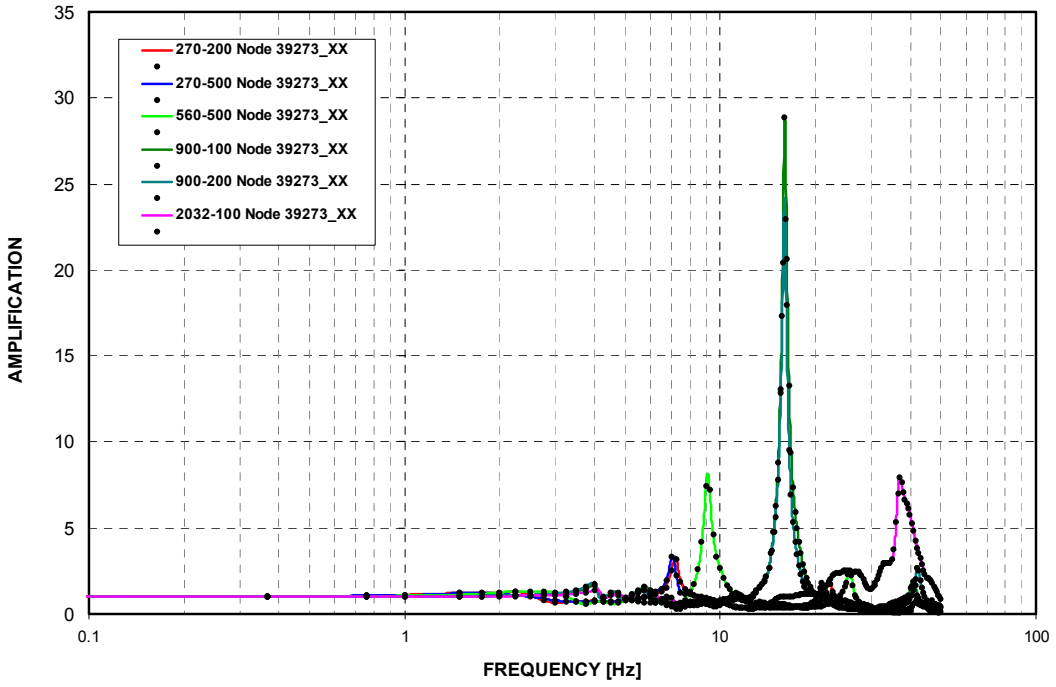

Figure 3-C.1.0-10 Sump Strainer Supports - Uncracked - NS Direction (X)

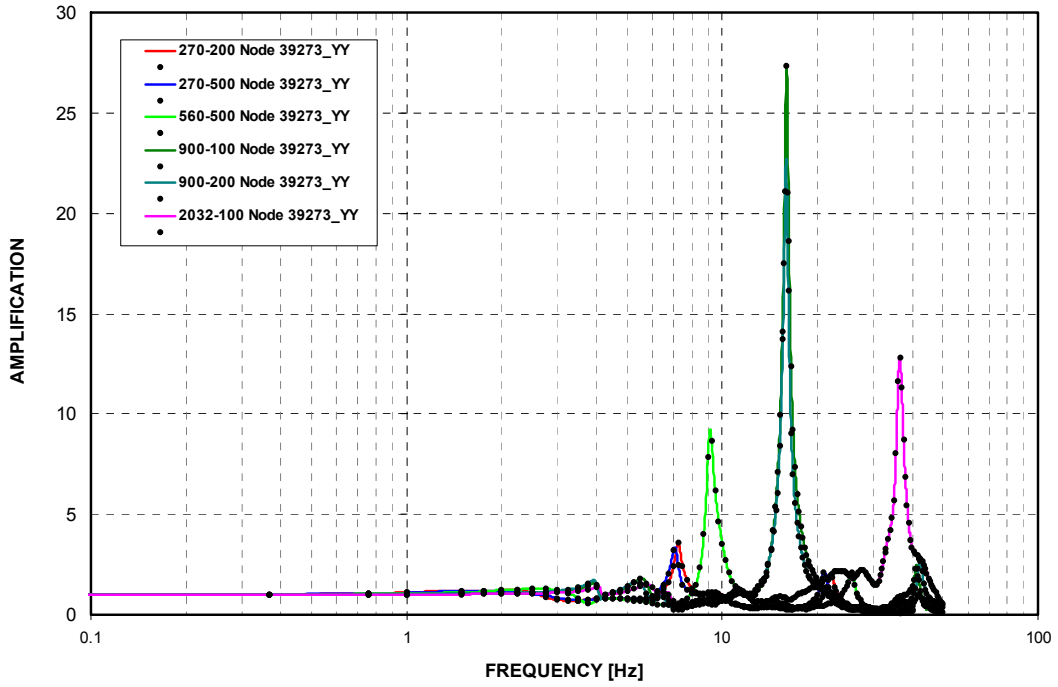

Figure 3-C.1.0-11 Sump Strainer Supports - Uncracked - EW Direction (Y)

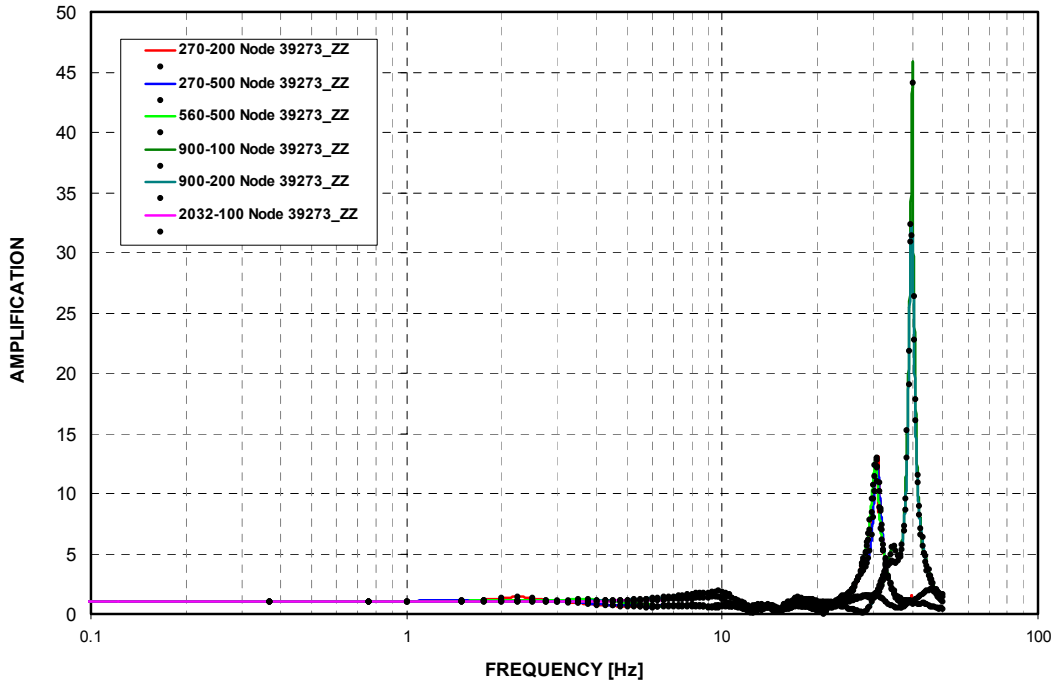

Figure 3-C.1.0-12 Sump Strainer Supports - Uncracked - Vertical Direction (Z)

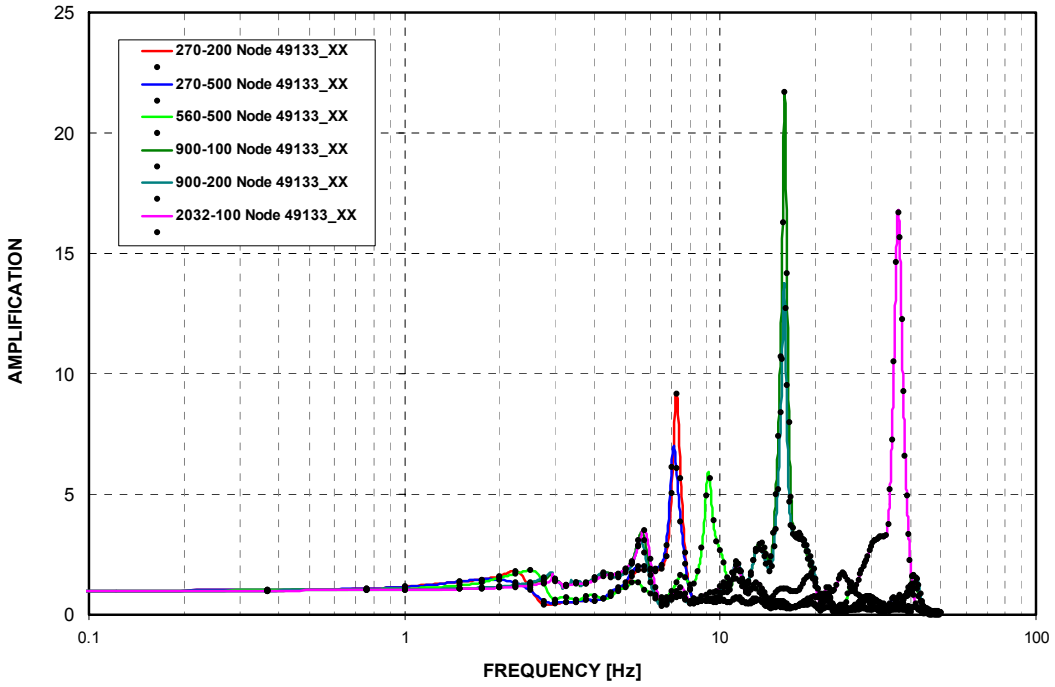

Figure 3-C.1.0-13 SG Lower Supports - Cracked - NS Direction (X)

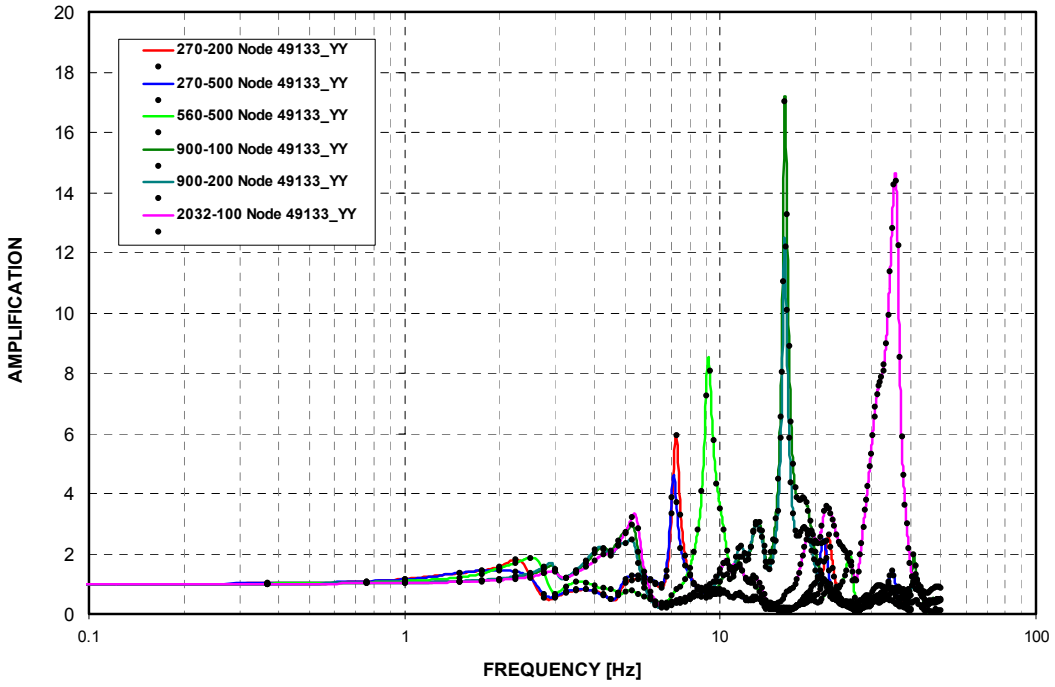

Figure 3-C.1.0-14 SG Lower Supports - Cracked - EW Direction (Y)

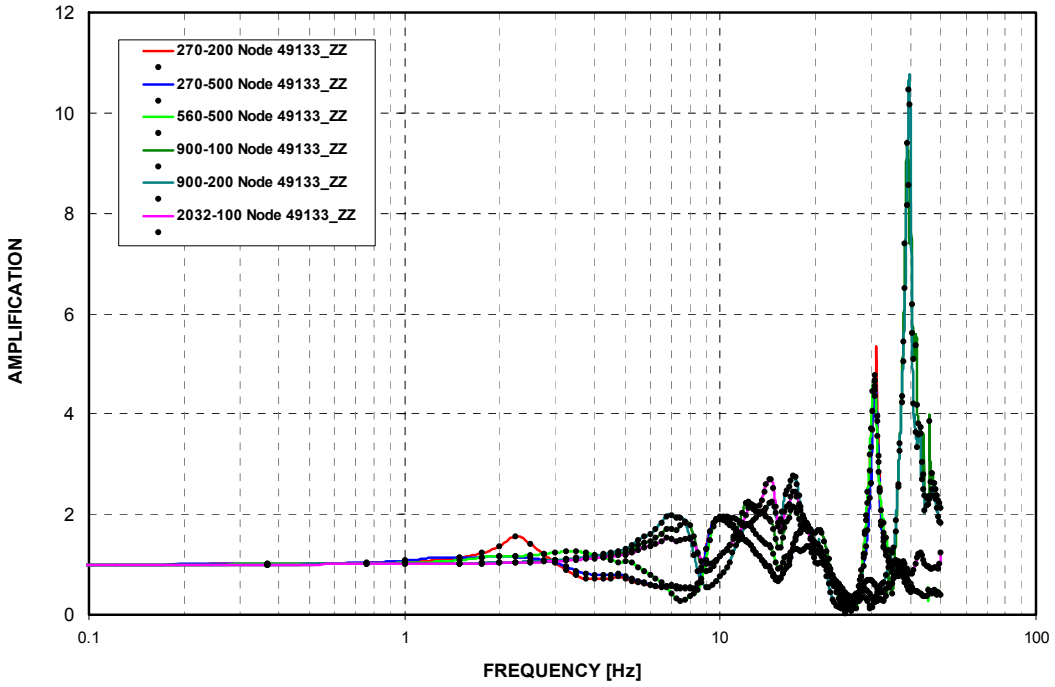

Figure 3-C.1.0-15 SG Lower Supports - Cracked - Vertical Direction (Z)

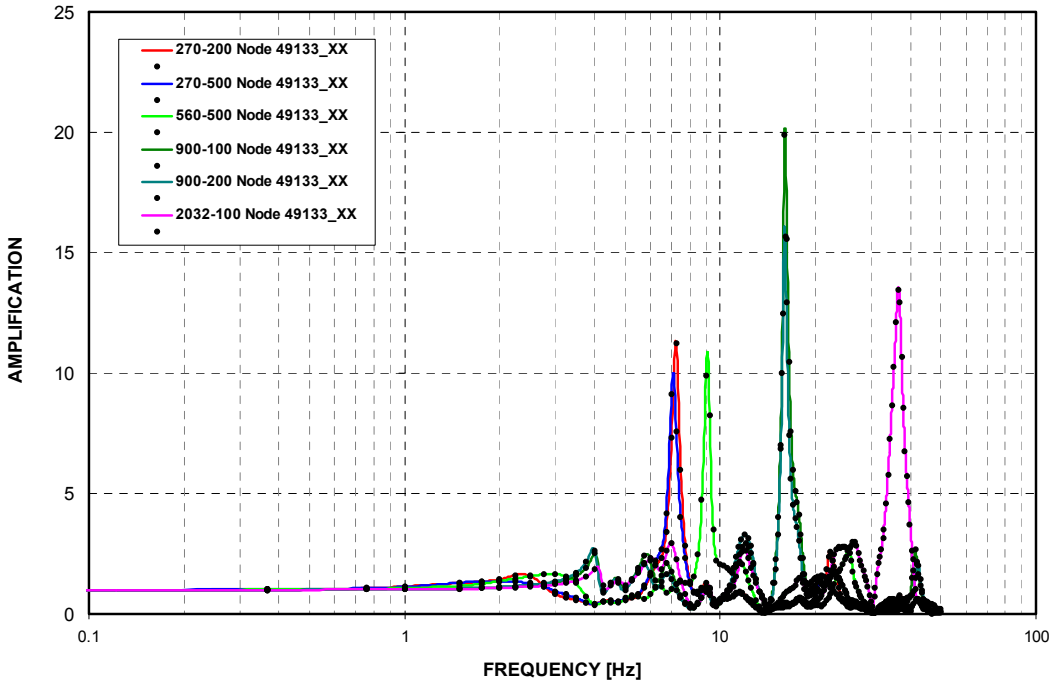

Figure 3-C.1.0-16 SG Lower Supports - Uncracked - NS Direction (X)

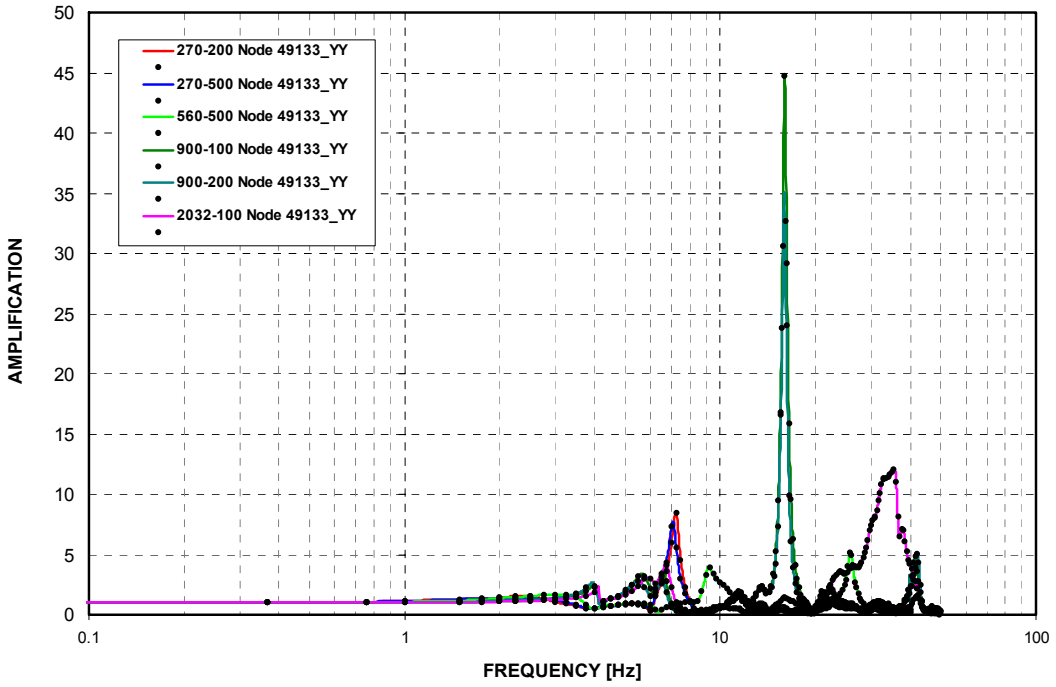

Figure 3-C.1.0-17 SG Lower Supports - Uncracked - EW Direction (Y)

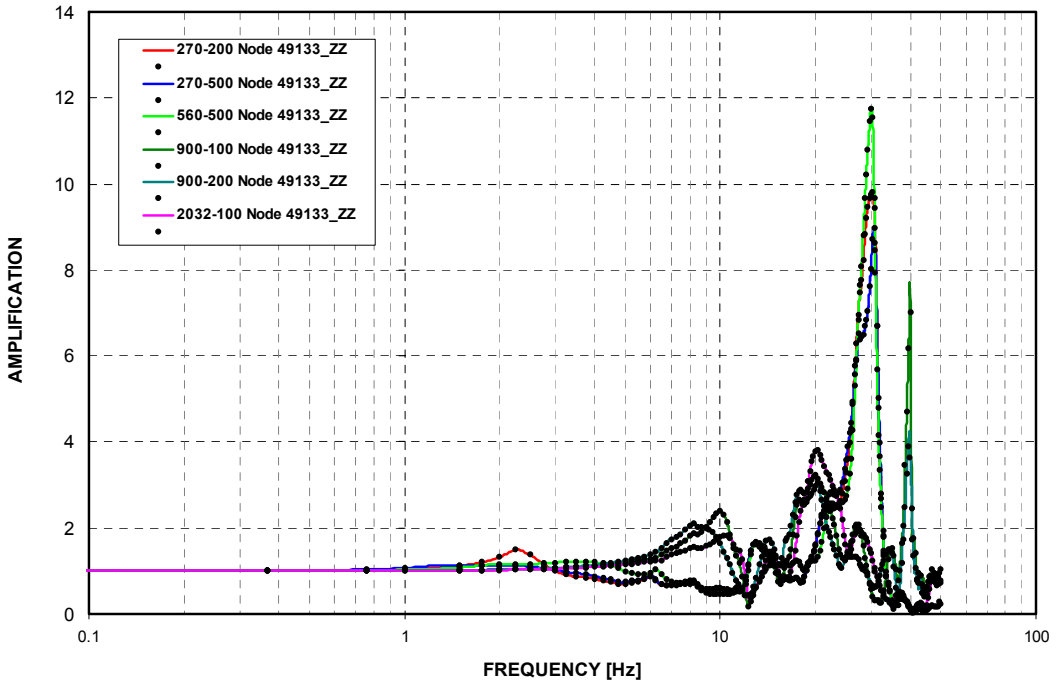

Figure 3-C.1.0-18 SG Lower Supports - Uncracked - Vertical Direction (Z)

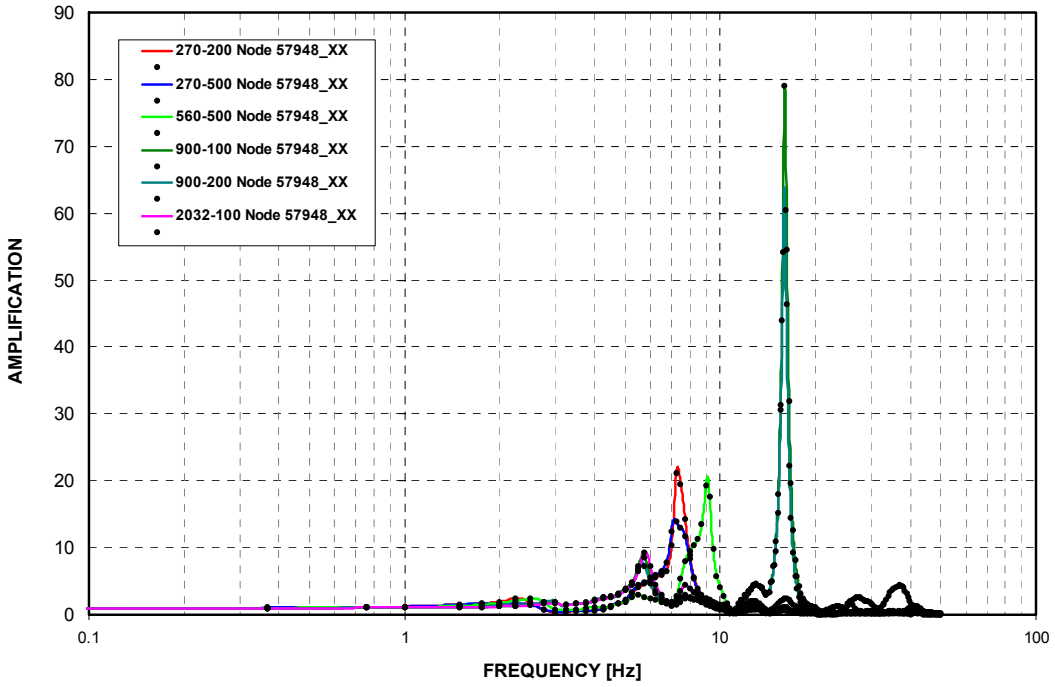

Figure 3-C.1.0-19 SG Upper Supports - Cracked - NS Direction (X)

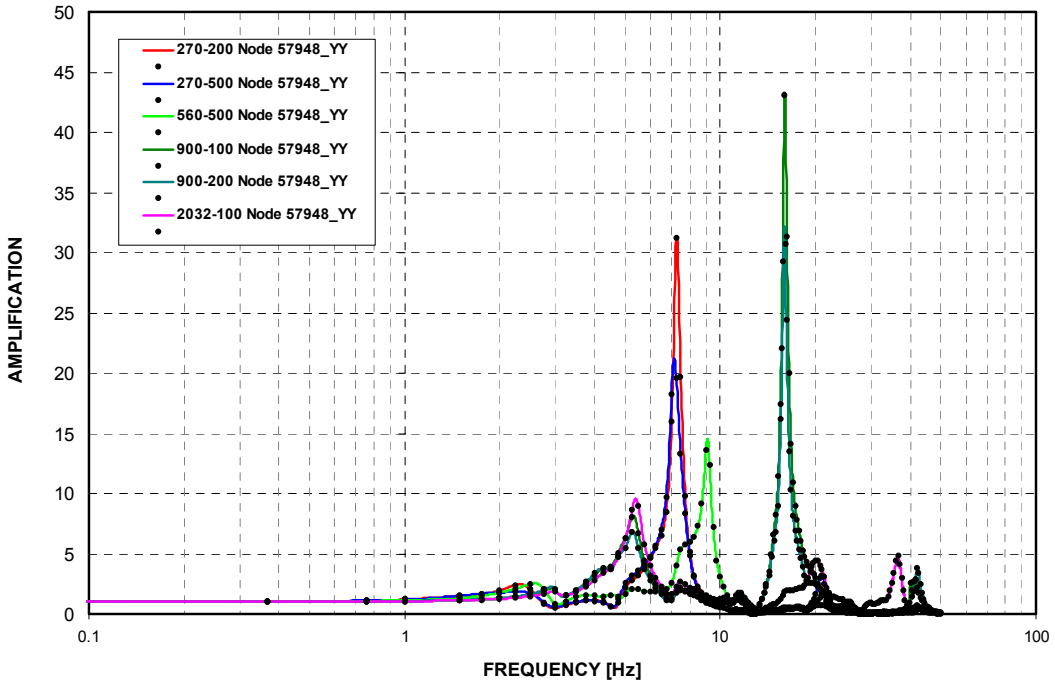

Figure 3-C.1.0-20 SG Upper Supports - Cracked - EW Direction (Y)

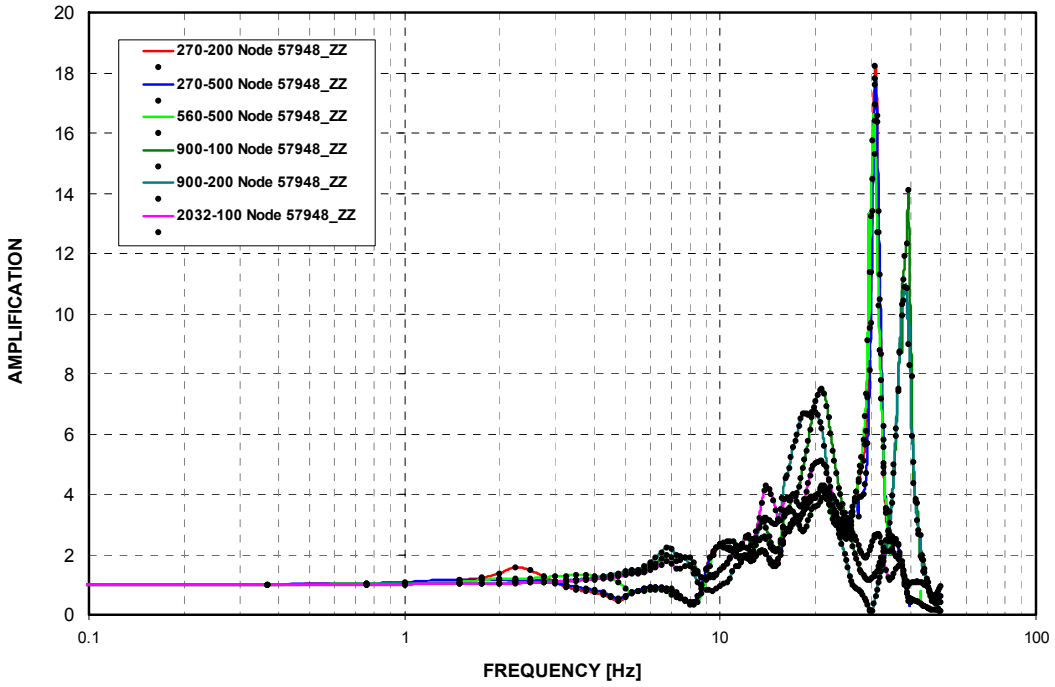

Figure 3-C.1.0-21 SG Upper Supports - Cracked - Vertical Direction (Z)

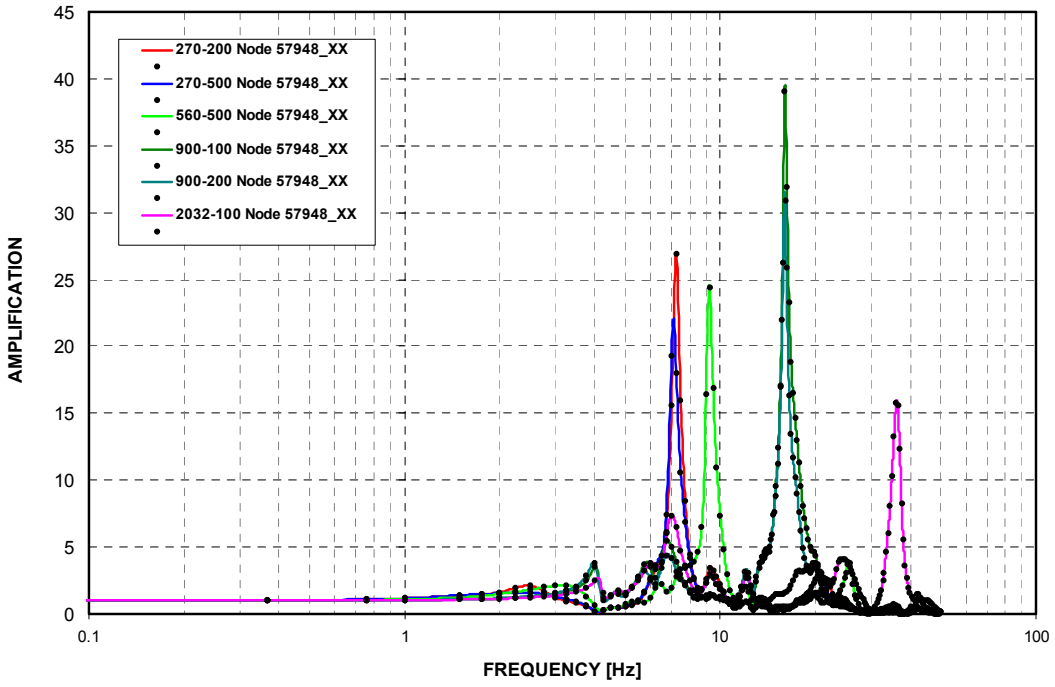

Figure 3-C.1.0-22 SG Upper Supports - Uncracked - NS Direction (X)

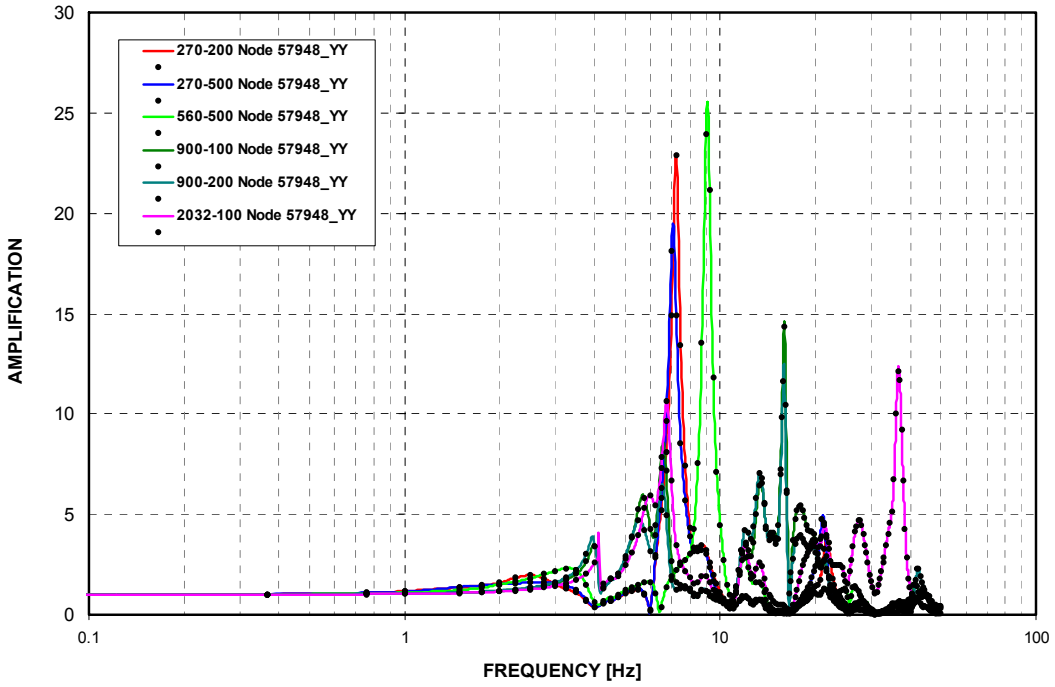

Figure 3-C.1.0-23 SG Upper Supports - Uncracked - EW Direction (Y)

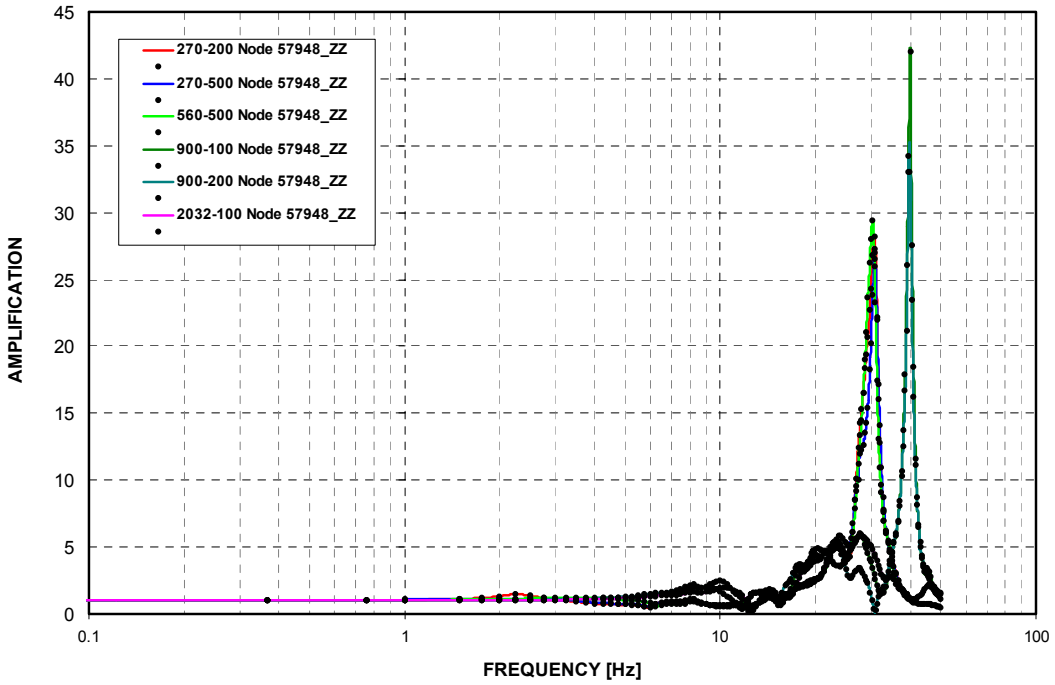

Figure 3-C.1.0-24 SG Upper Supports - Uncracked - Vertical Direction (Z)

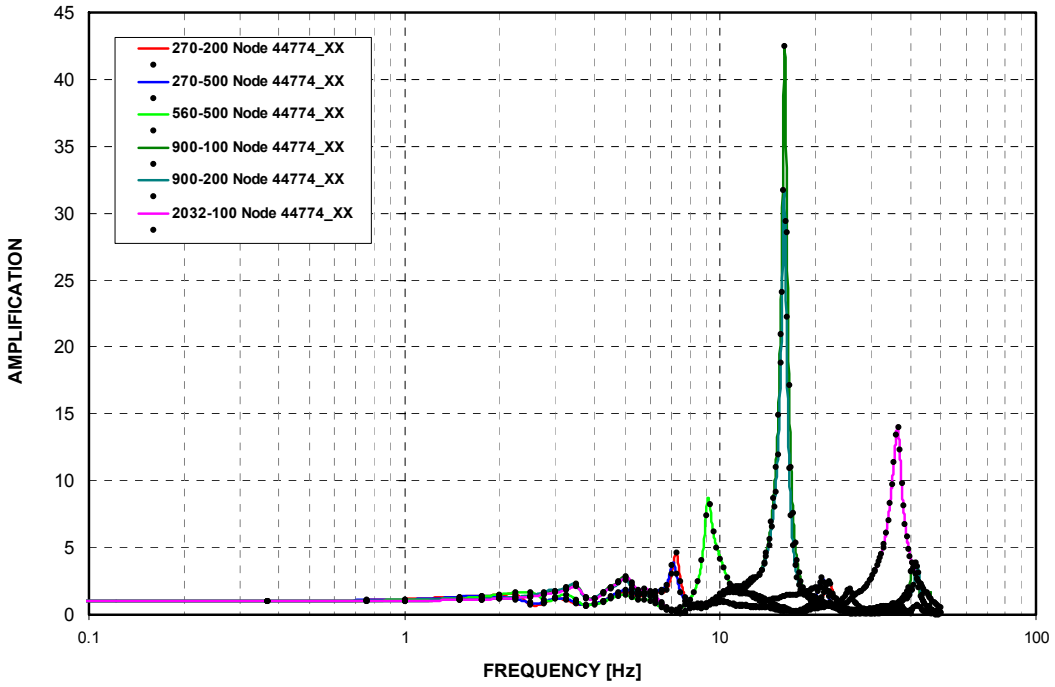

Figure 3-C.1.0-25 SFP - Cracked - NS Direction (X)

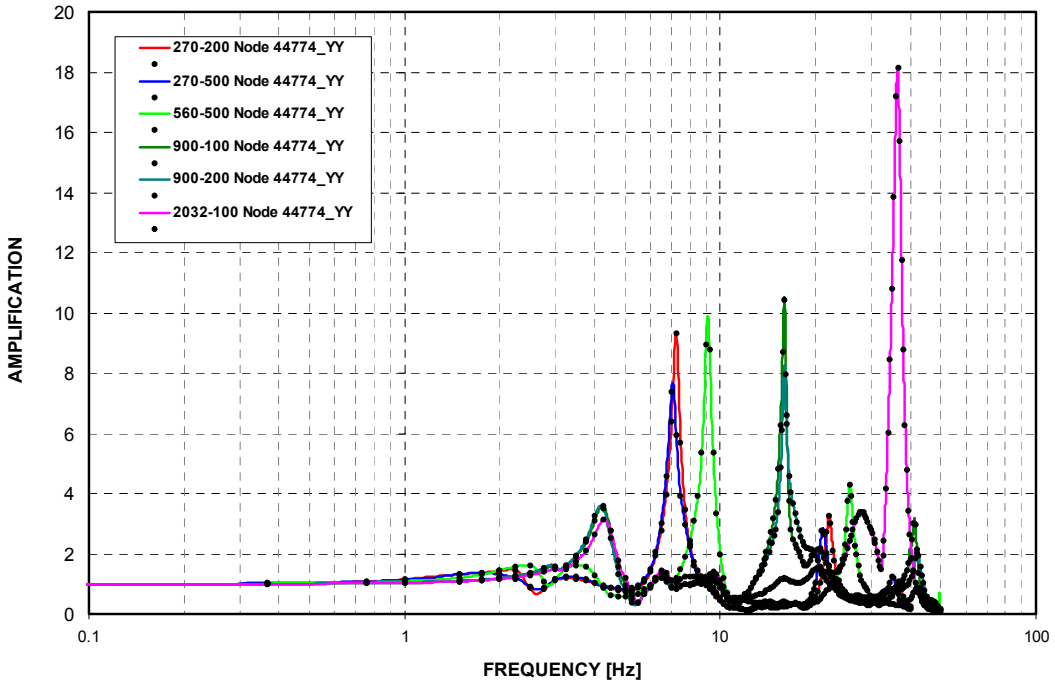

Figure 3-C.1.0-26 SFP - Cracked - EW Direction (Y)

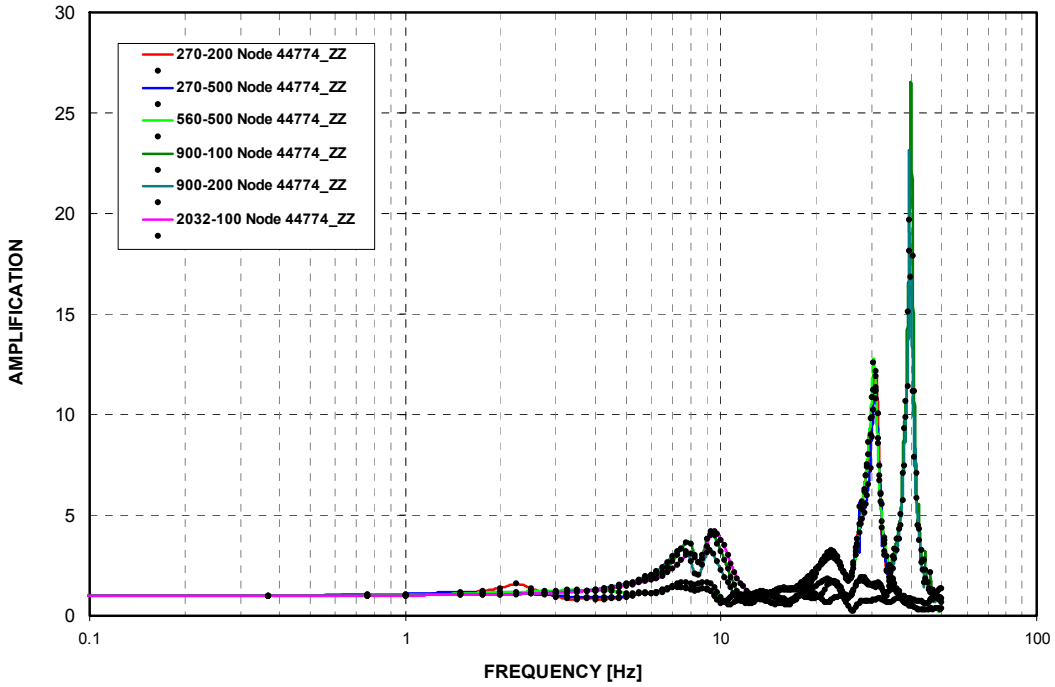

Figure 3-C.1.0-27 SFP - Cracked - Vertical Direction (Z)

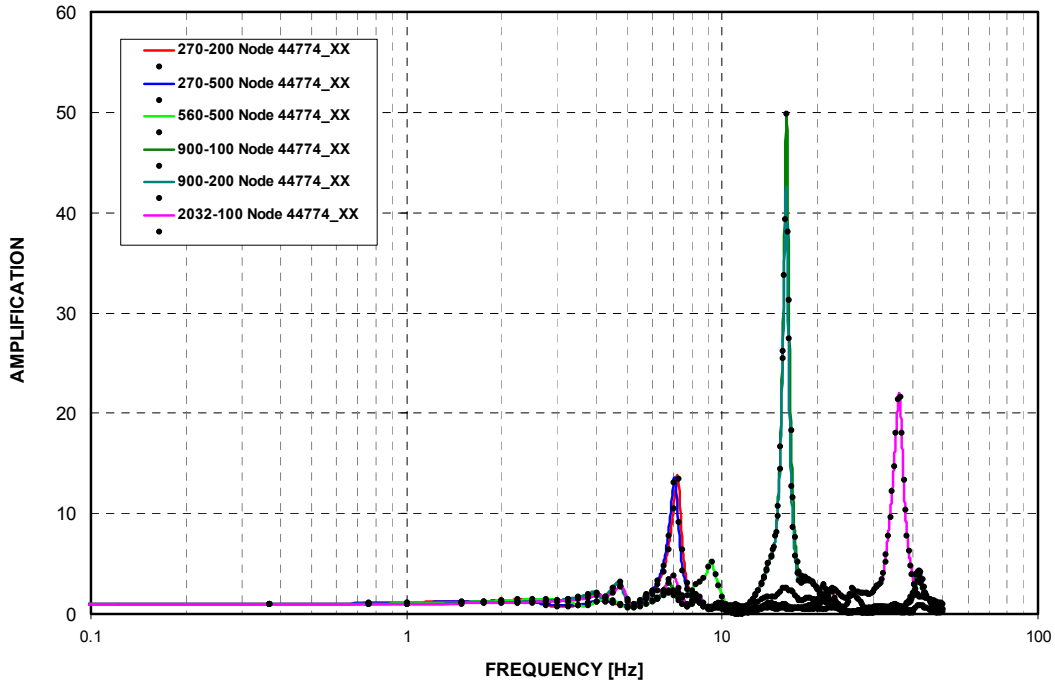

Figure 3-C.1.0-28 SFP - Uncracked - NS Direction (X)

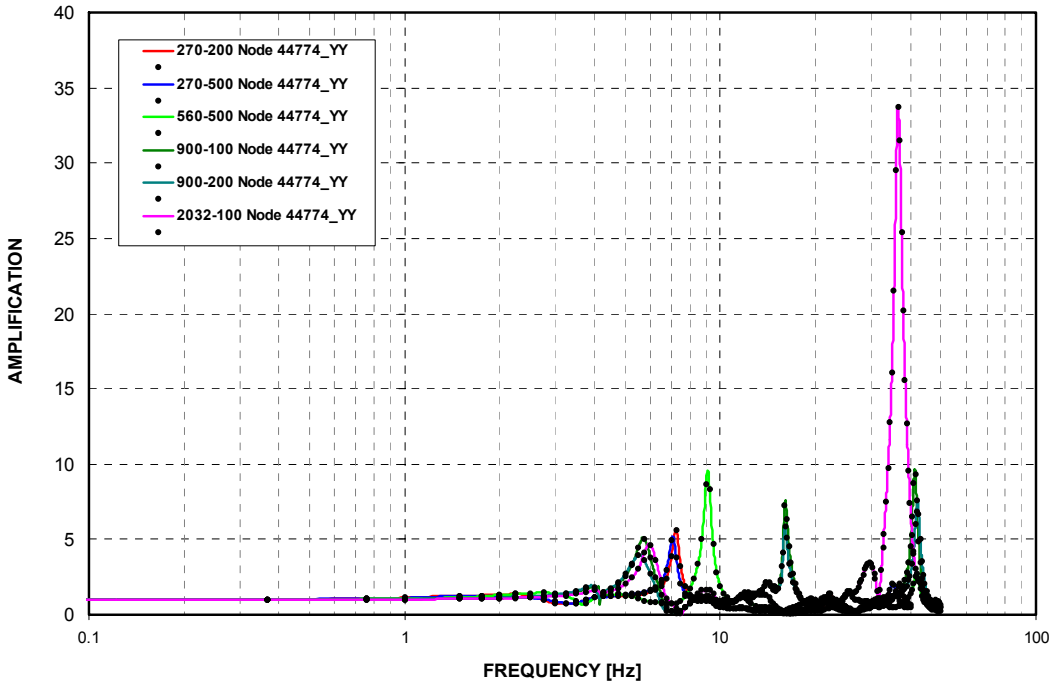

Figure 3-C.1.0-29 SFP - Uncracked - EW Direction (Y)

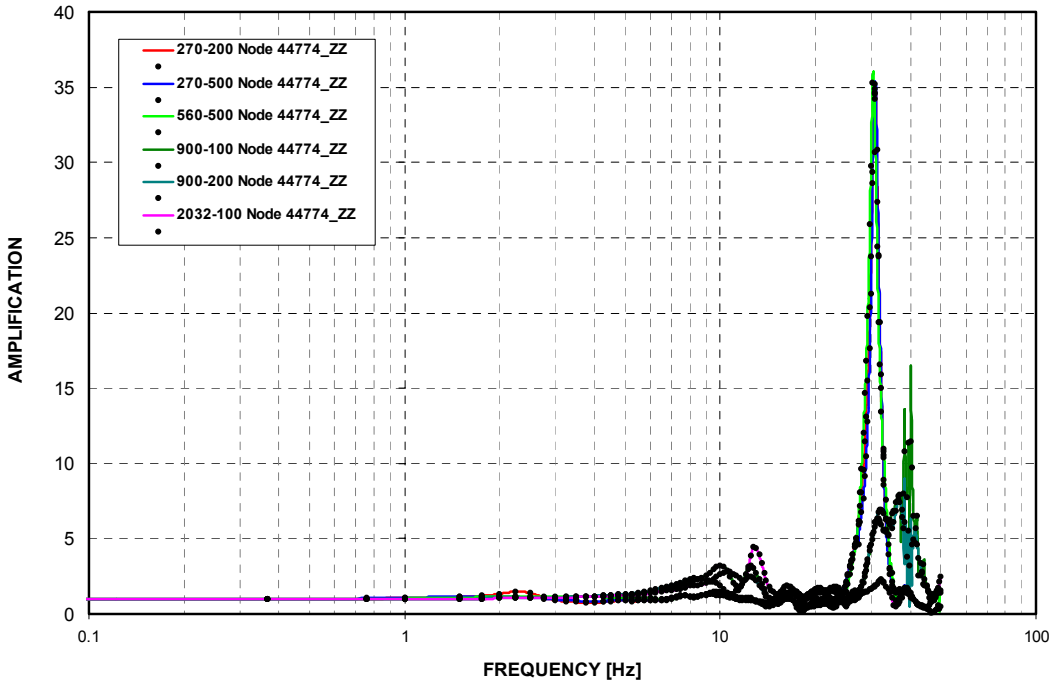

Figure 3-C.1.0-30 SFP - Uncracked - Vertical Direction (Z)

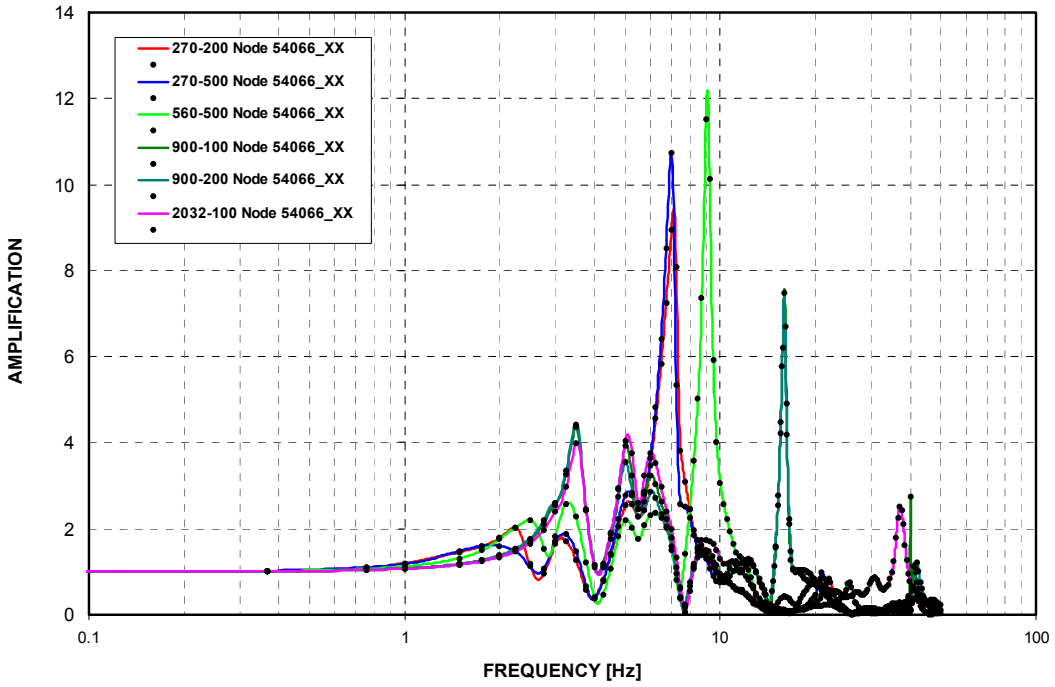

Figure 3-C.1.0-31 NFSP - Cracked - NS Direction (X)

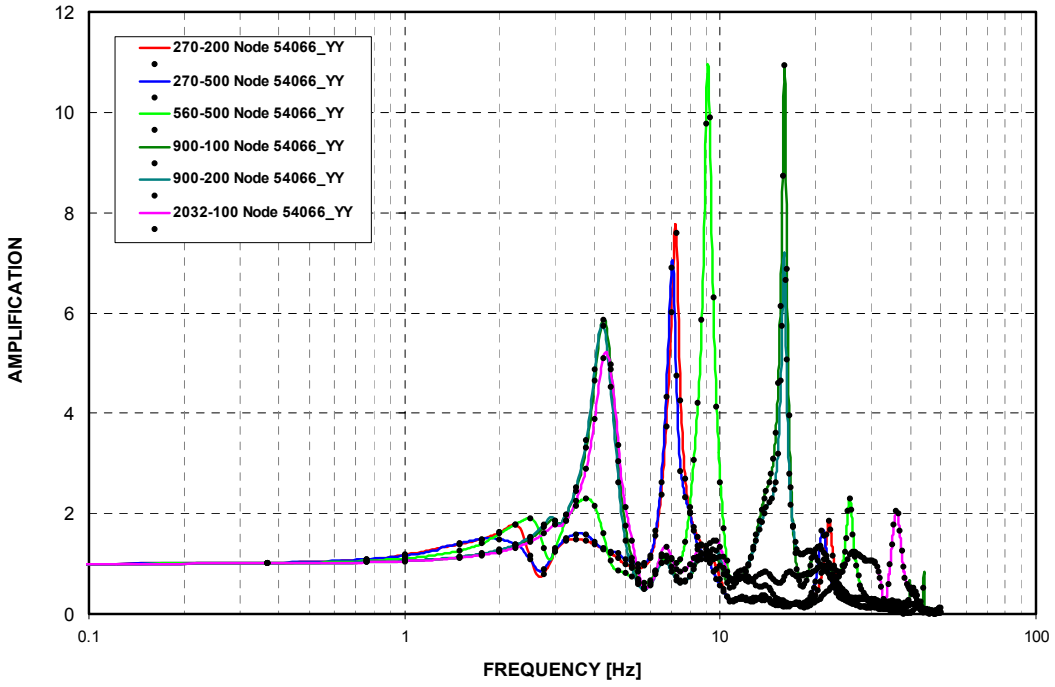

Figure 3-C.1.0-32 NFSP - Cracked - EW Direction (Y)

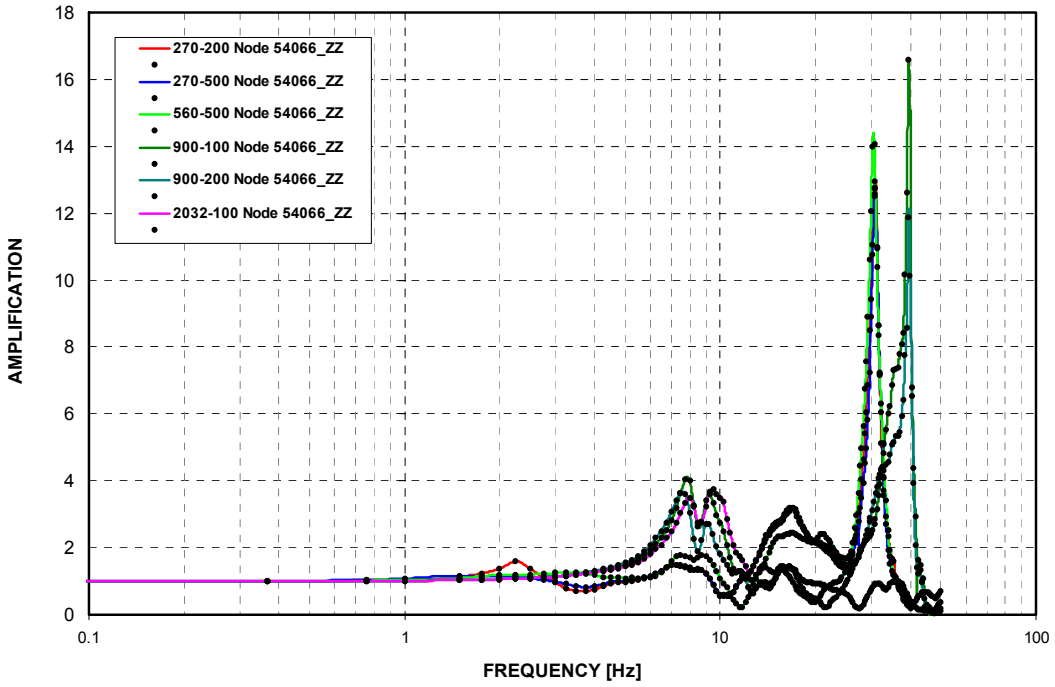

Figure 3-C.1.0-33 NFSP - Cracked - Vertical Direction (Z)

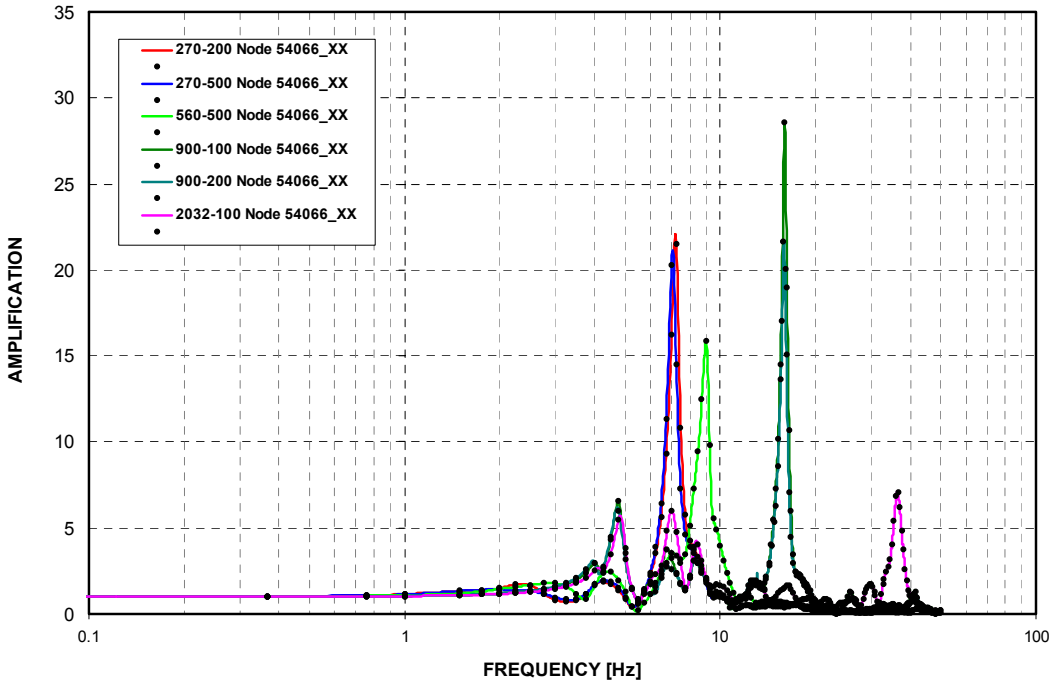

Figure 3-C.1.0-34 NFSP - Uncracked - NS Direction (X)

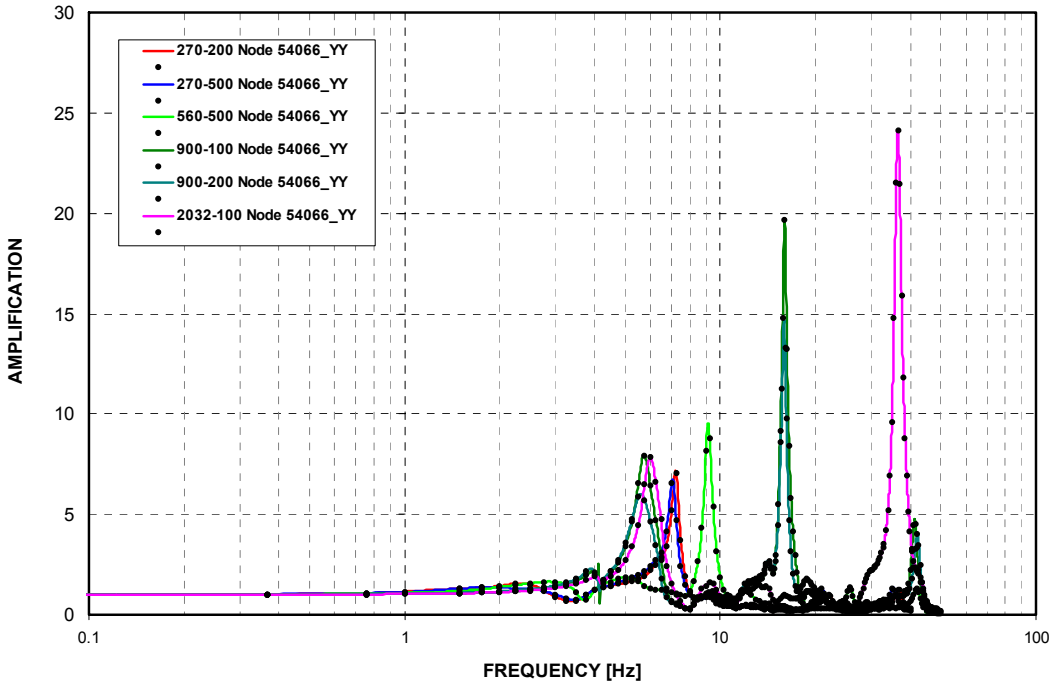

Figure 3-C.1.0-35 NFSP - Uncracked - EW Direction (Y)

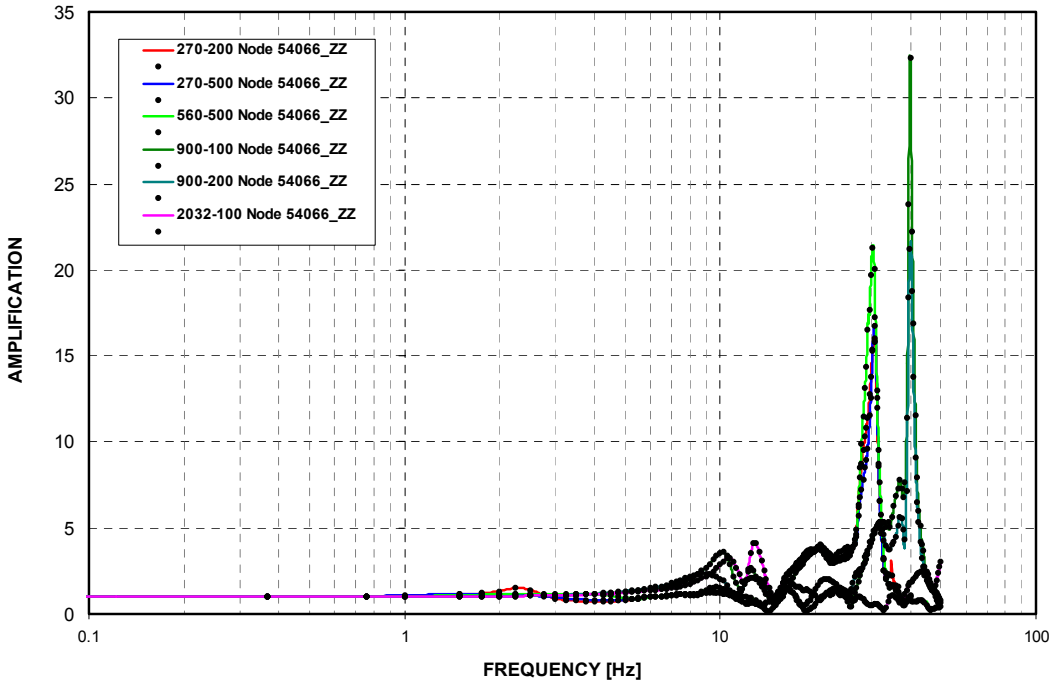

Figure 3-C.1.0-36 NFSP - Uncracked - Vertical Direction (Z)

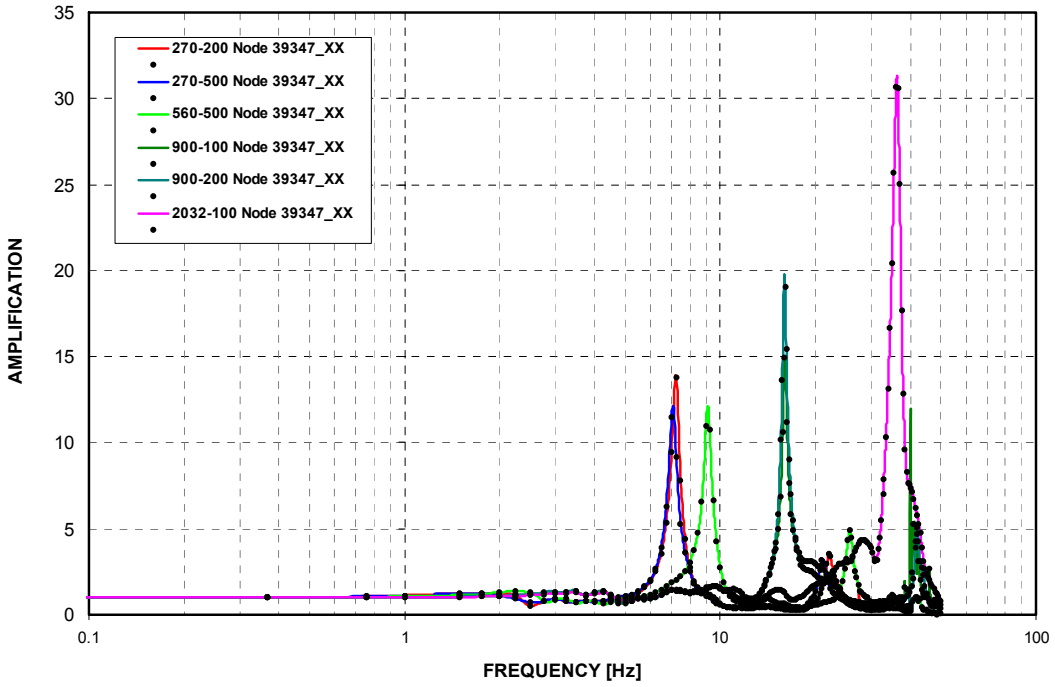

Figure 3-C.1.0-37 East PS/B A-AAC GTG - Cracked - NS Direction (X)

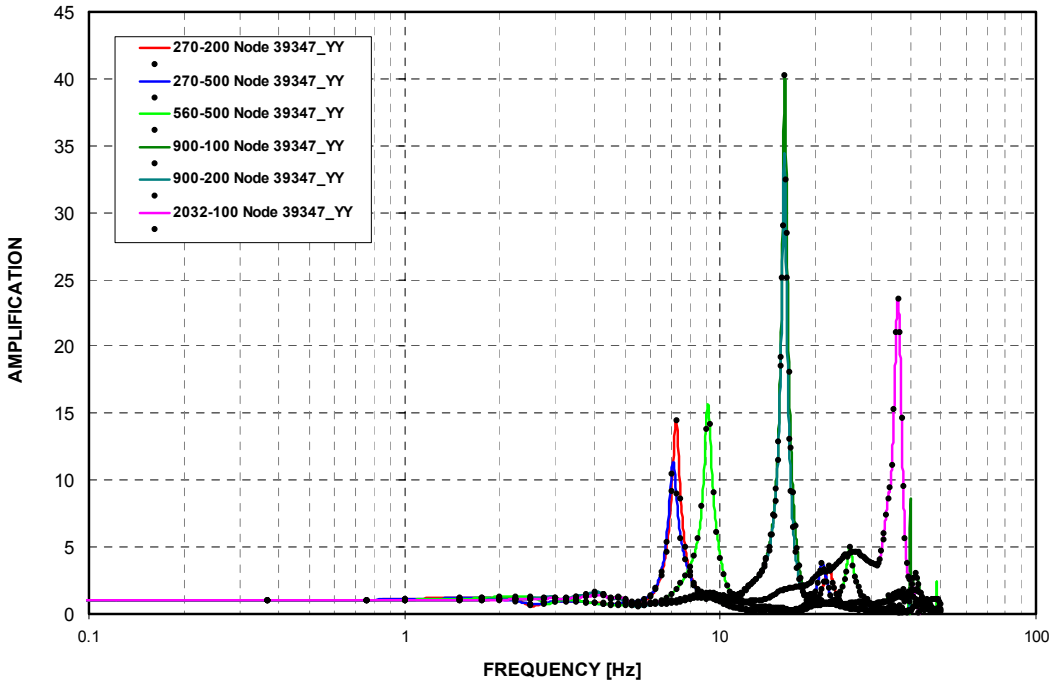

Figure 3-C.1.0-38 East PS/B A-AAC GTG - Cracked - EW Direction (Y)

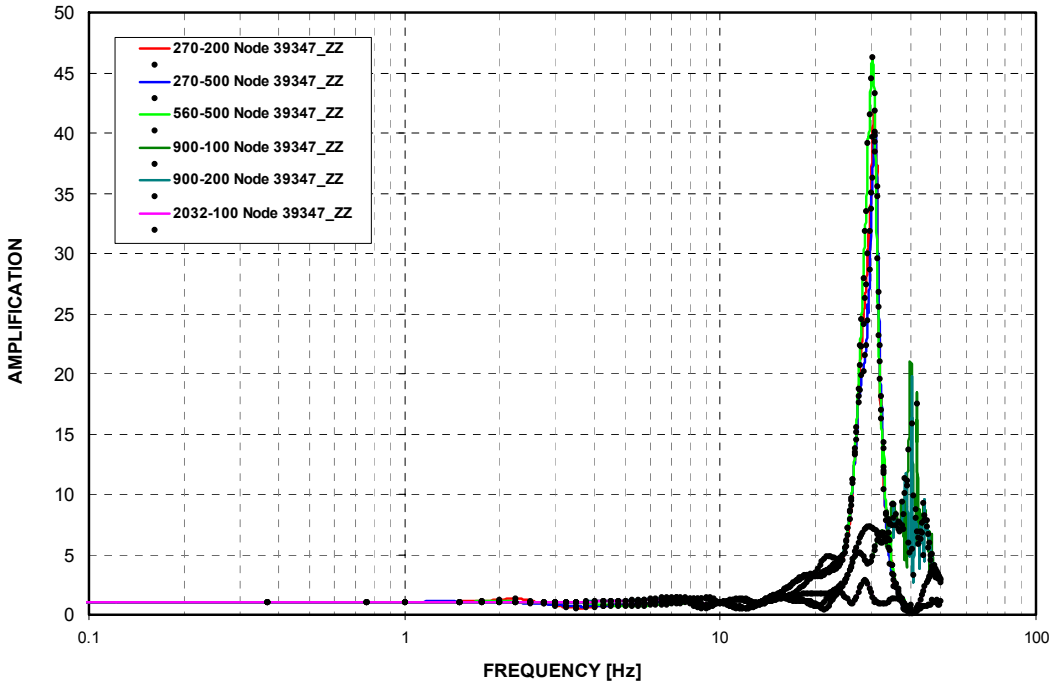

Figure 3-C.1.0-39 East PS/B A-AAC GTG - Cracked - Vertical Direction (Z)

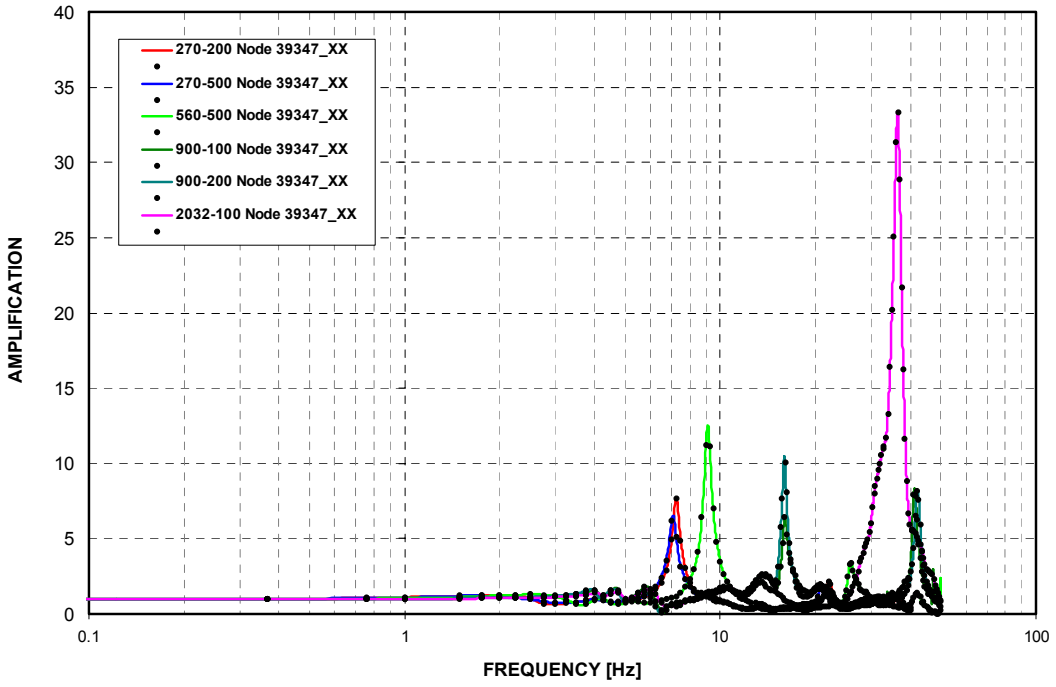

Figure 3-C.1.0-40 East PS/B A-AAC GTG - Uncracked - NS Direction (X)

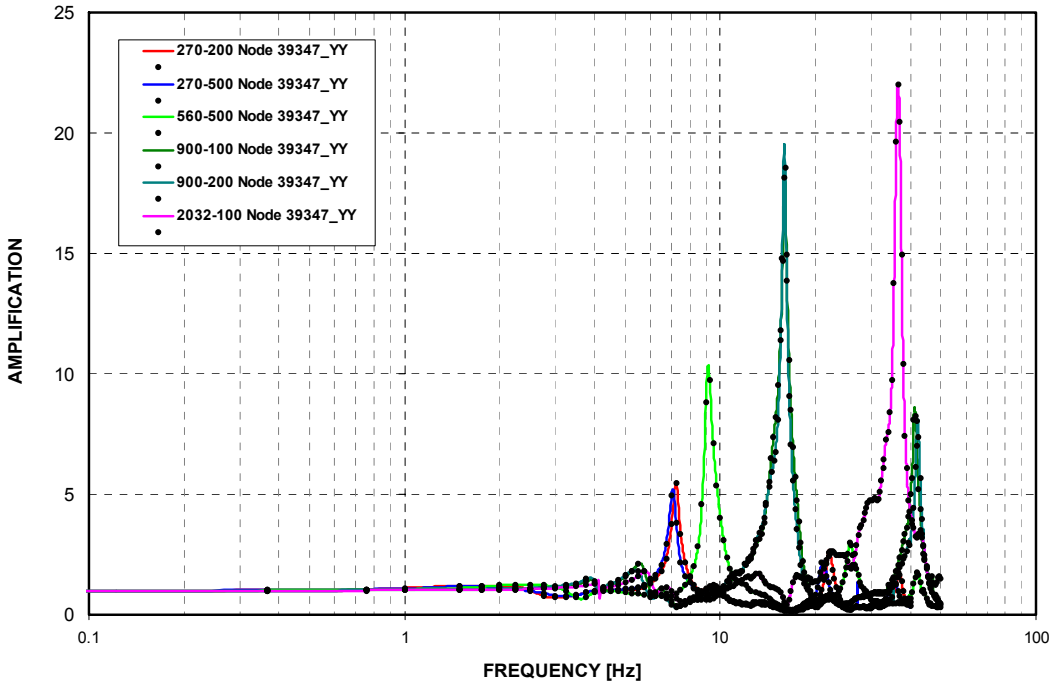

Figure 3-C.1.0-41 East PS/B A-AAC GTG - Uncracked - EW Direction (Y)

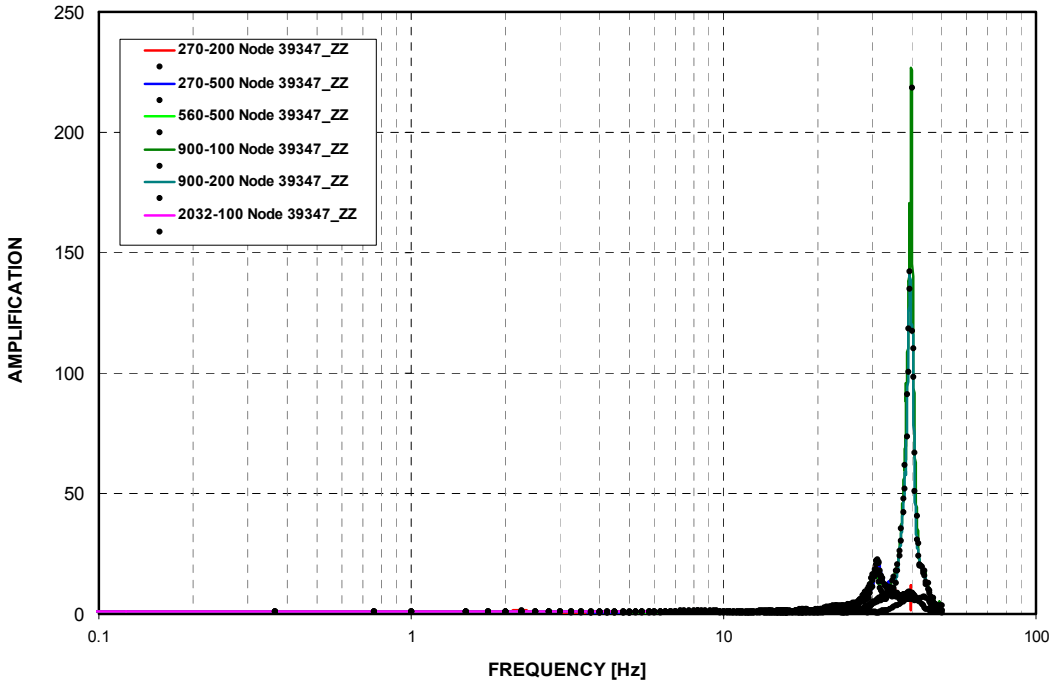

Figure 3-C.1.0-42 East PS/B A-AAC GTG - Uncracked - Vertical Direction (Z)

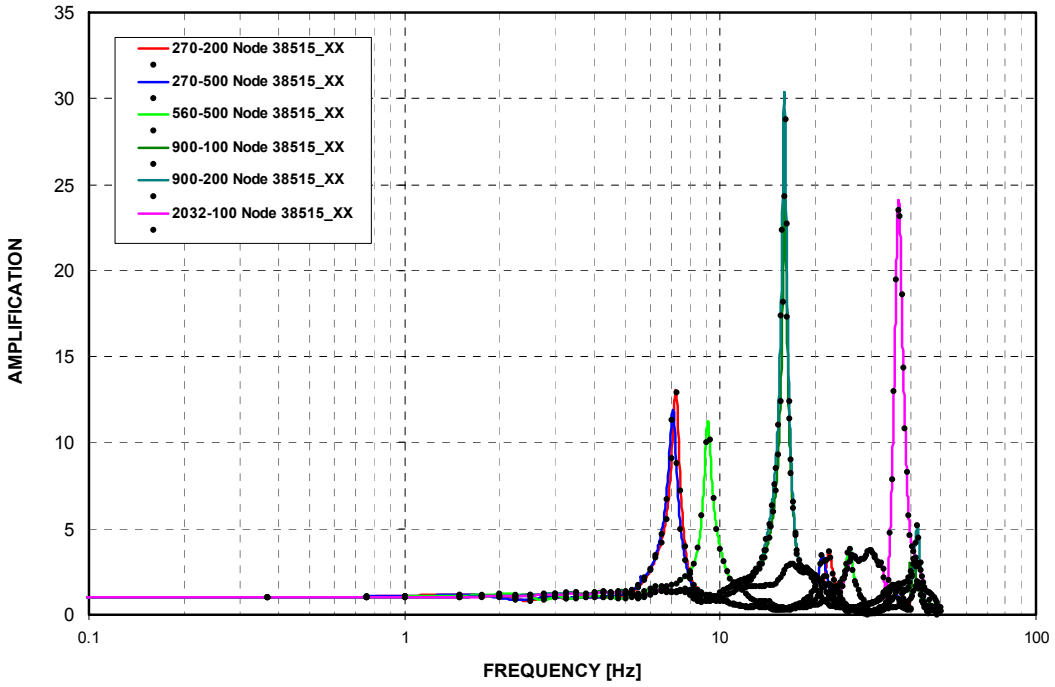

Figure 3-C.1.0-43 West PS/B B-AAC GTG - Cracked - NS Direction (X)

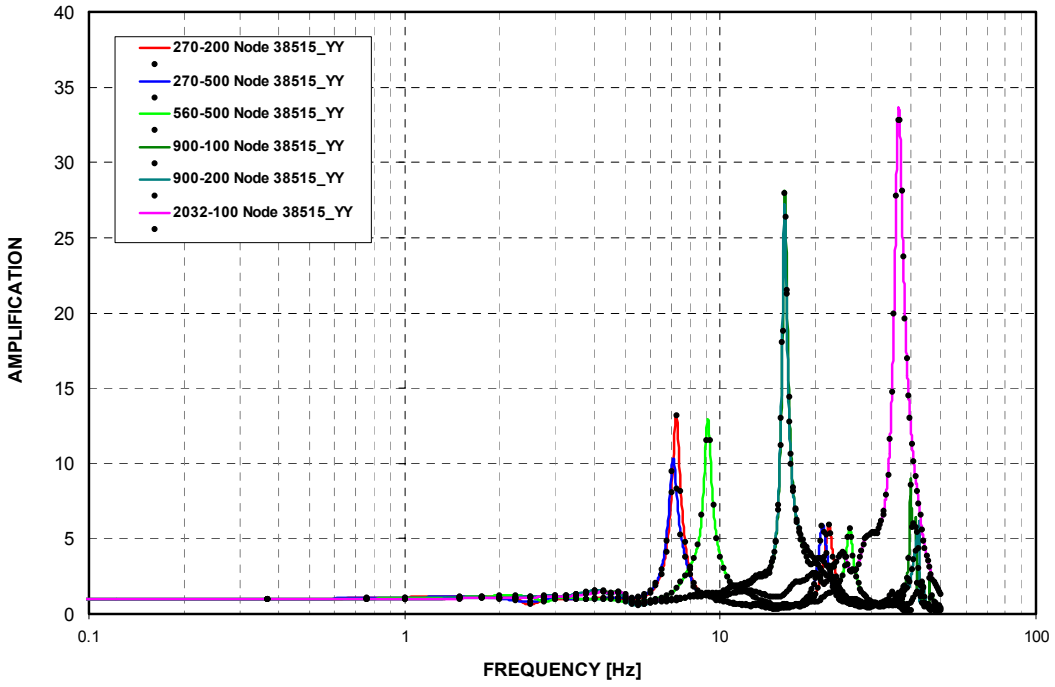

Figure 3-C.1.0-44 West PS/B B-AAC GTG - Cracked - EW Direction (Y)

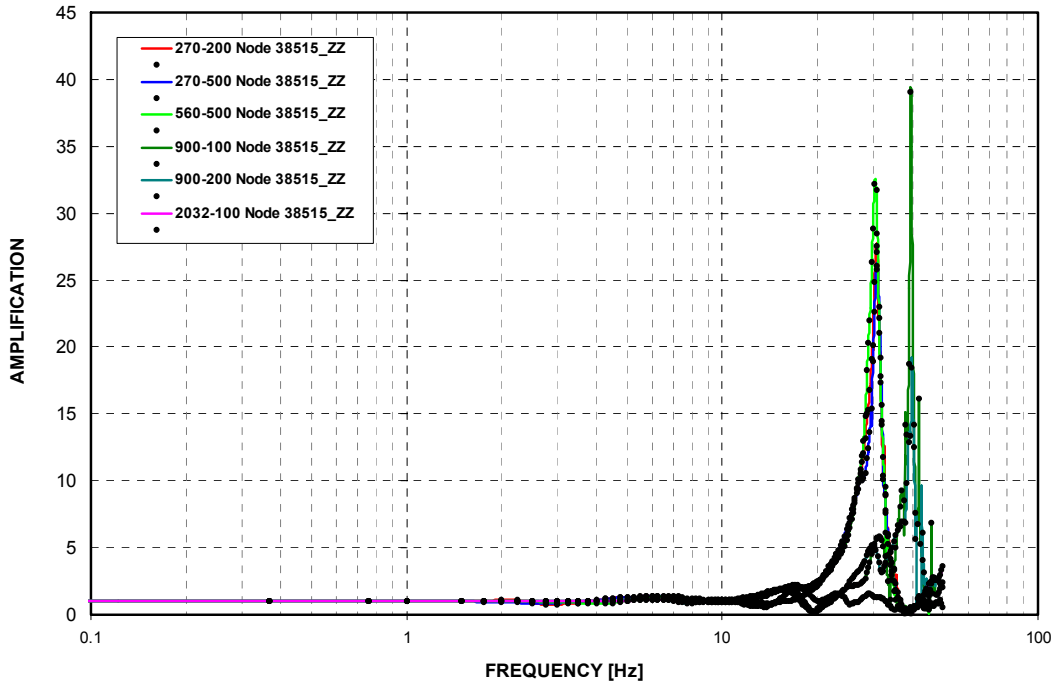

Figure 3-C.1.0-45 West PS/B B-AAC GTG - Cracked - Vertical Direction (Z)

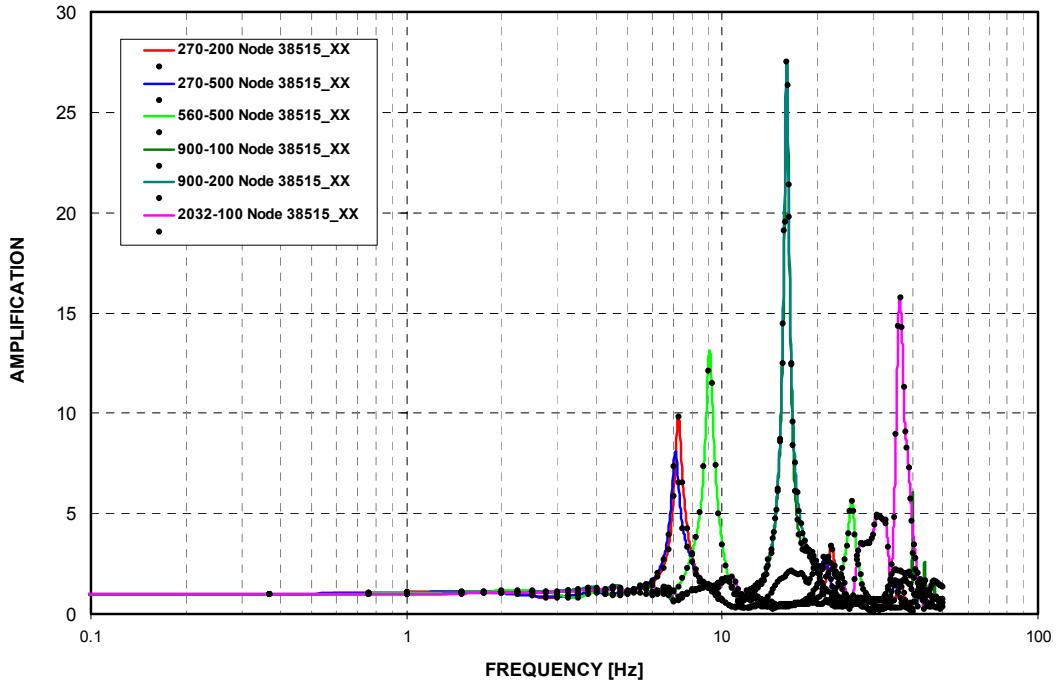

Figure 3-C.1.0-46 West PS/B B-AAC GTG - Uncracked - NS Direction (X)

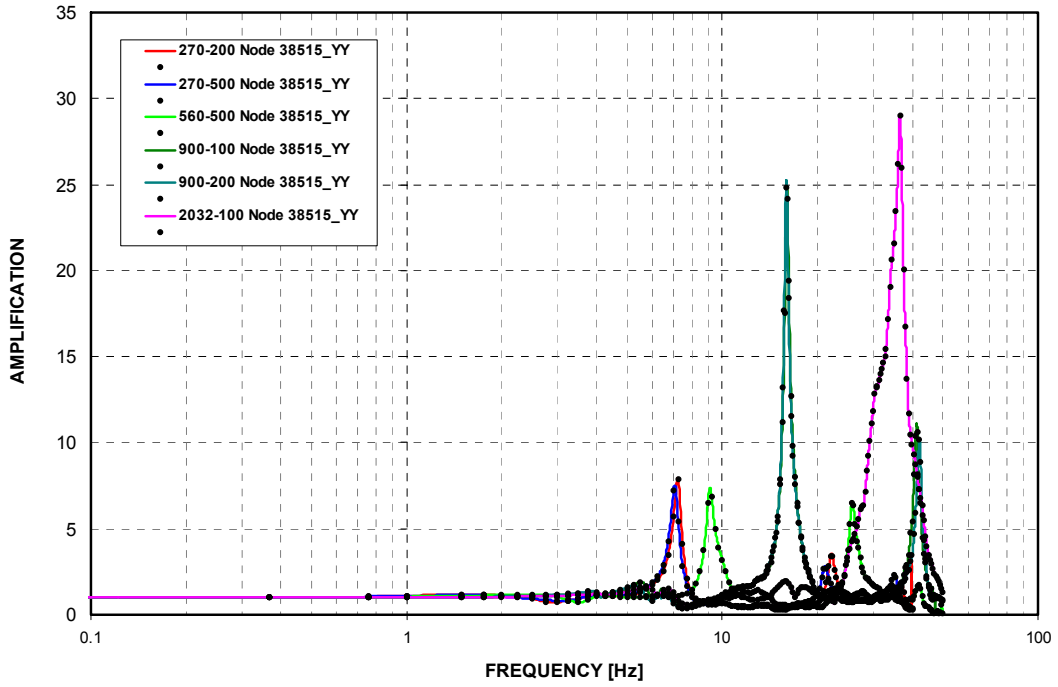

Figure 3-C.1.0-47 West PS/B B-AAC GTG - Uncracked - EW Direction (Y)

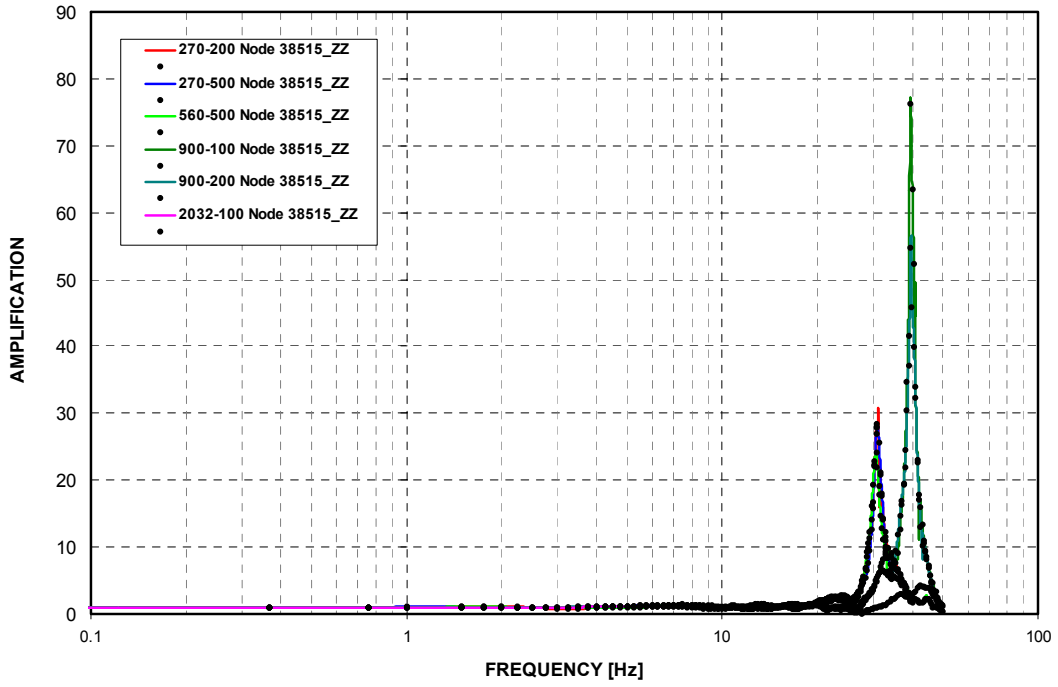

Figure 3-C.1.0-48 West PS/B B-AAC GTG - Uncracked - Vertical Direction (Z)

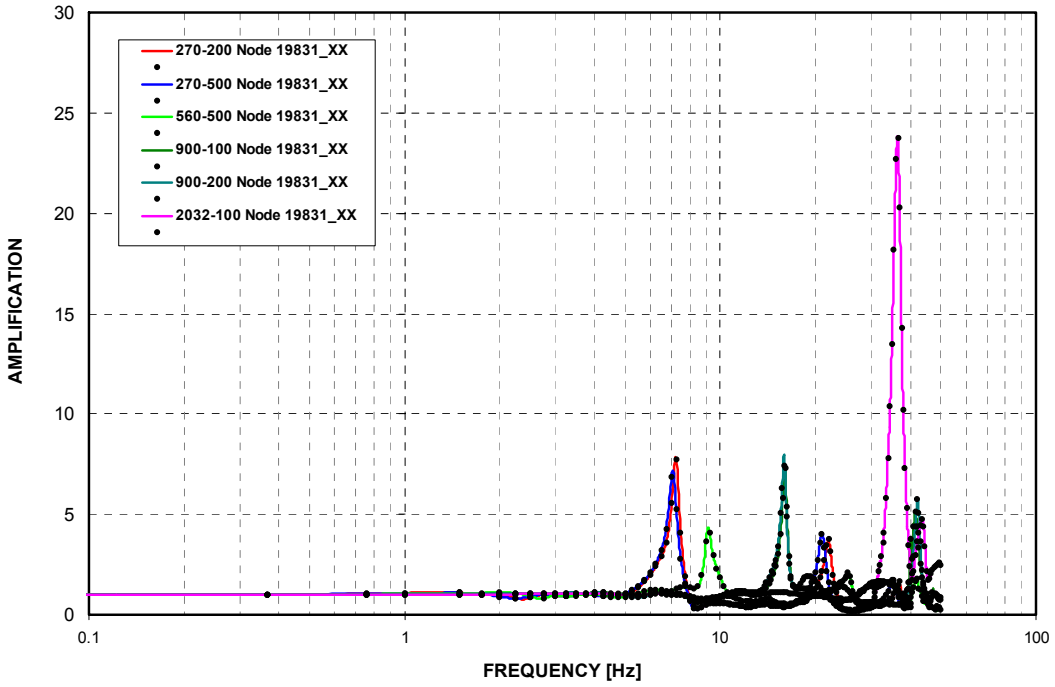

Figure 3-C.1.0-49 A/B Northwest Corner at Basemat - Cracked - NS Direction (X)

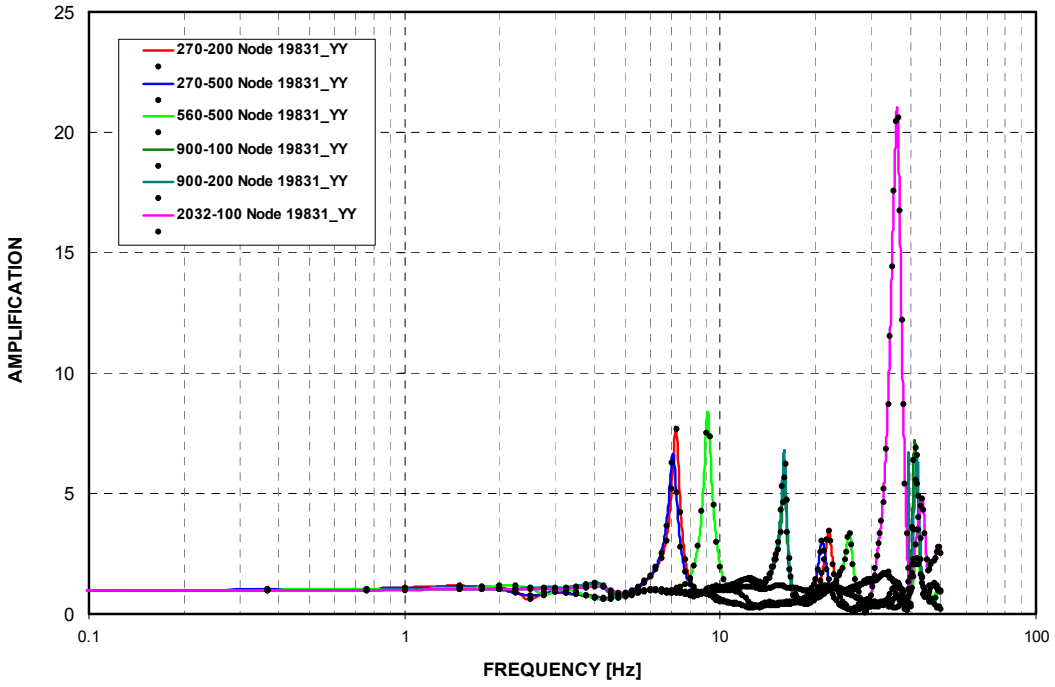

Figure 3-C.1.0-50 A/B Northwest Corner at Basemat - Cracked - EW Direction (Y)

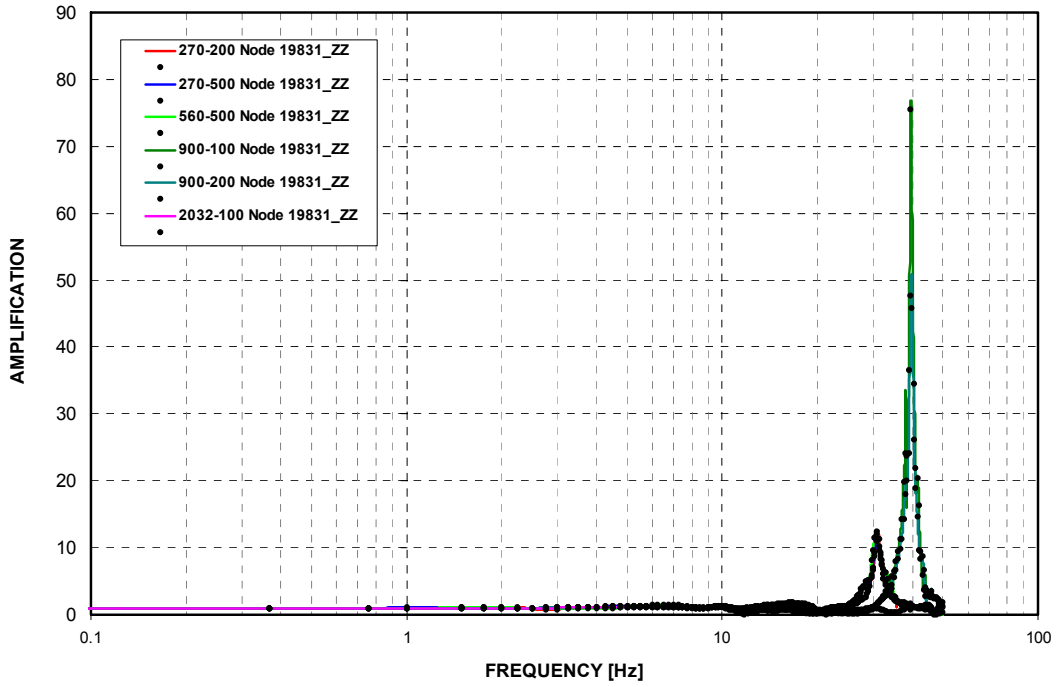

Figure 3-C.1.0-51 A/B Northwest Corner at Basemat - Cracked - Vertical Direction (Z)

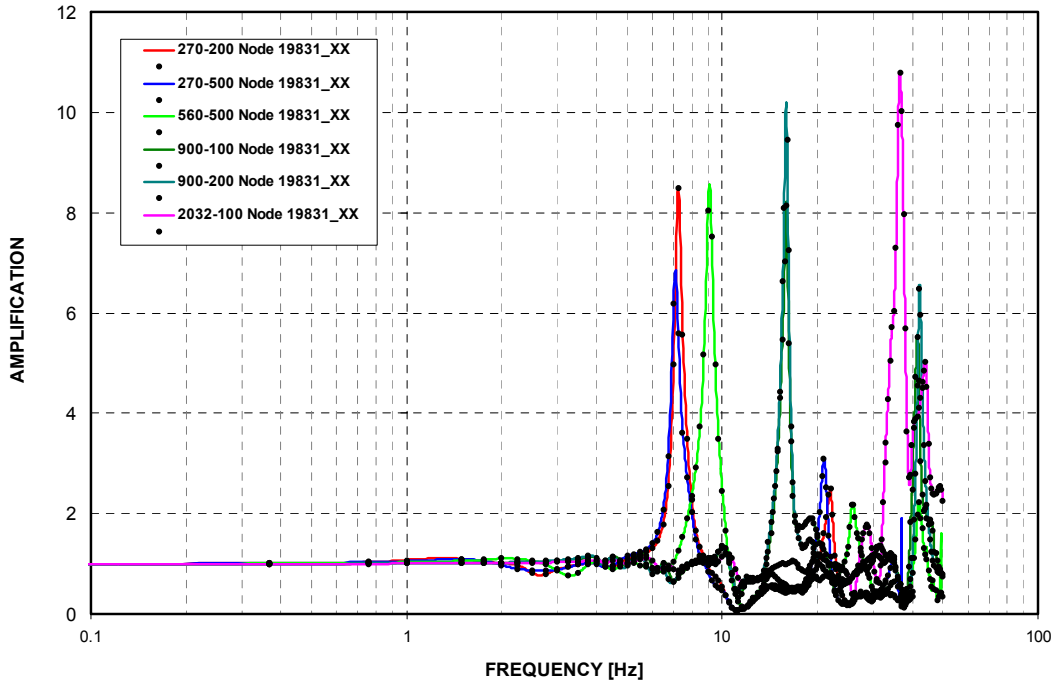

Figure 3-C.1.0-52 A/B Northwest Corner at Basemat - Uncracked - NS Direction (X)

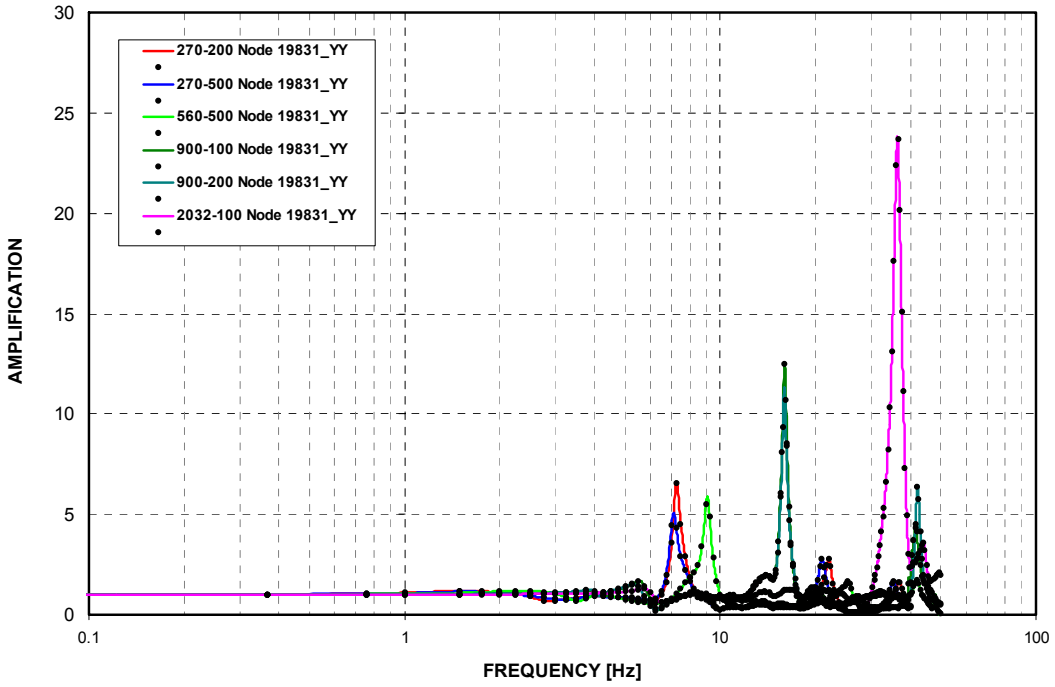

Figure 3-C.1.0-53 A/B Northwest Corner at Basemat - Uncracked - EW Direction (Y)

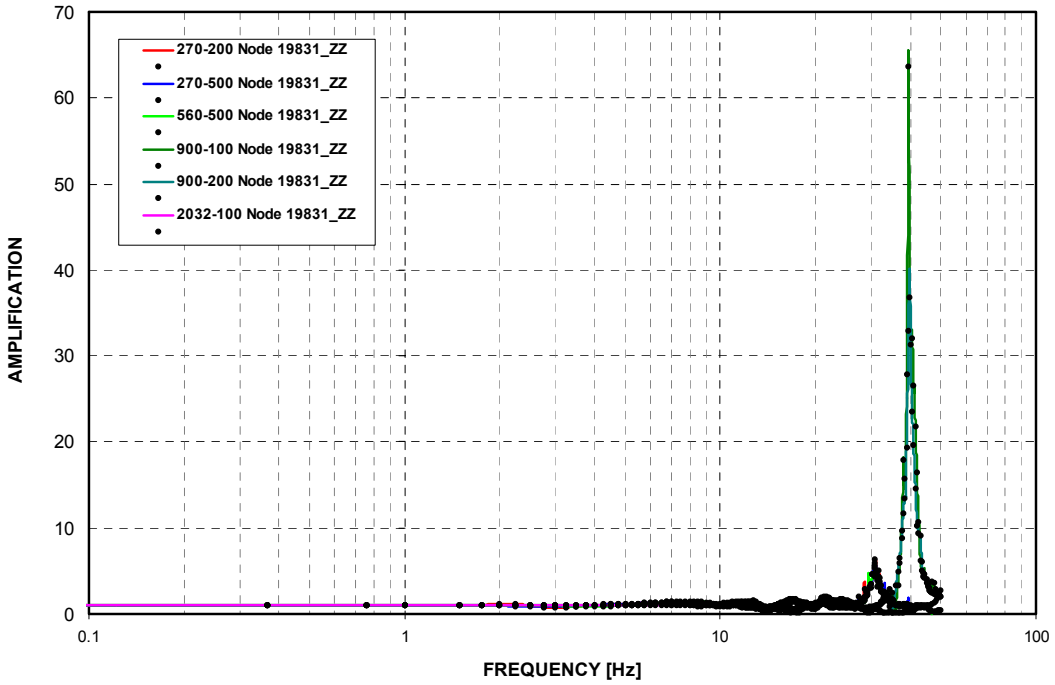

Figure 3-C.1.0-54 A/B Northwest Corner at Basemat - Uncracked - Vertical Direction (Z)

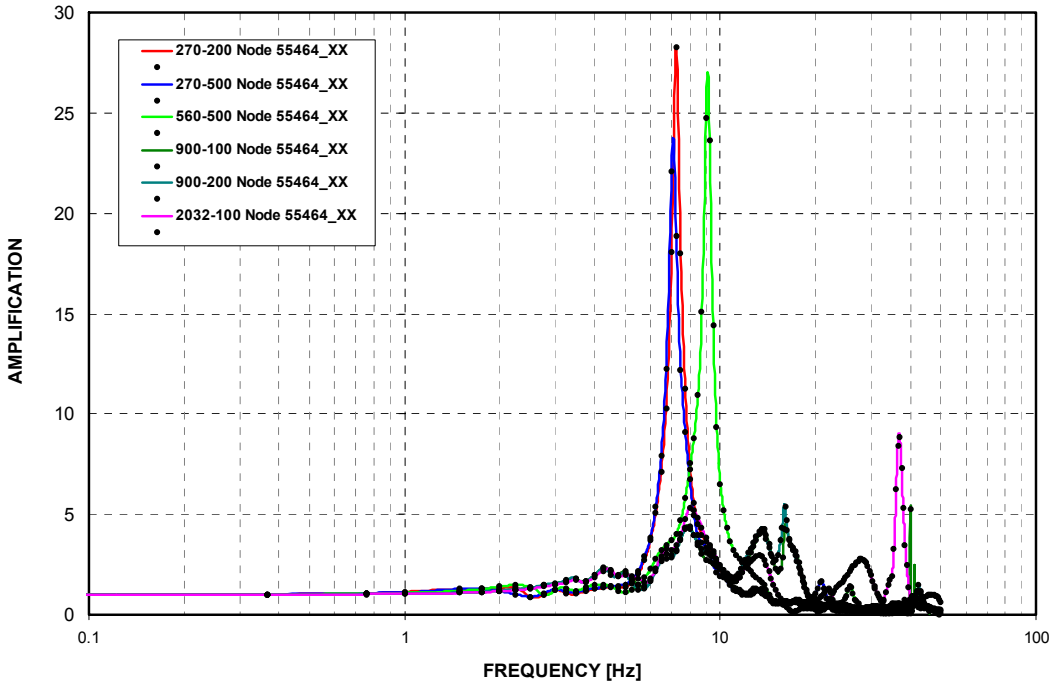

Figure 3-C.1.0-55 A/B Northwest Corner at Roof - Cracked - NS Direction (X)

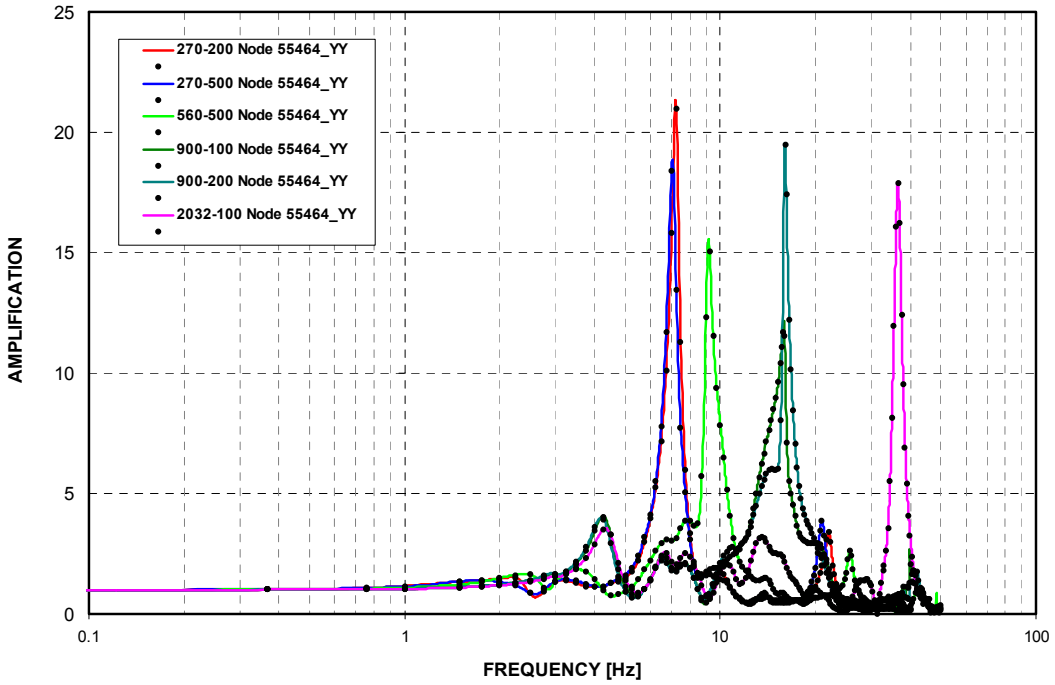

Figure 3-C.1.0-56 A/B Northwest Corner at Roof - Cracked - EW Direction (Y)

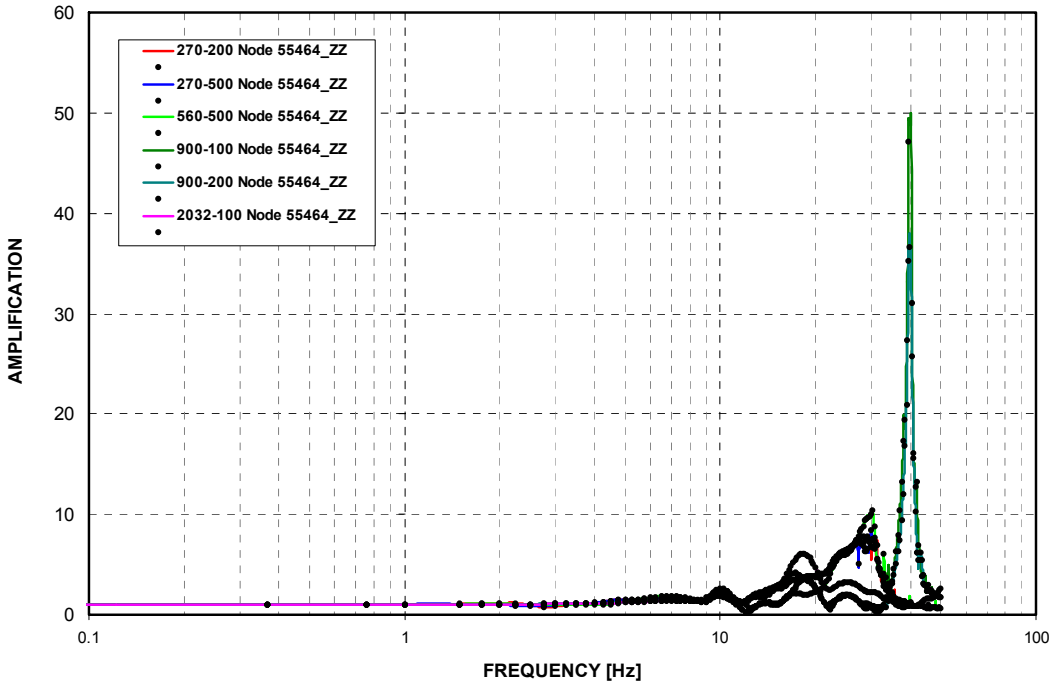

Figure 3-C.1.0-57 A/B Northwest Corner at Roof - Cracked - Vertical Direction (Z)

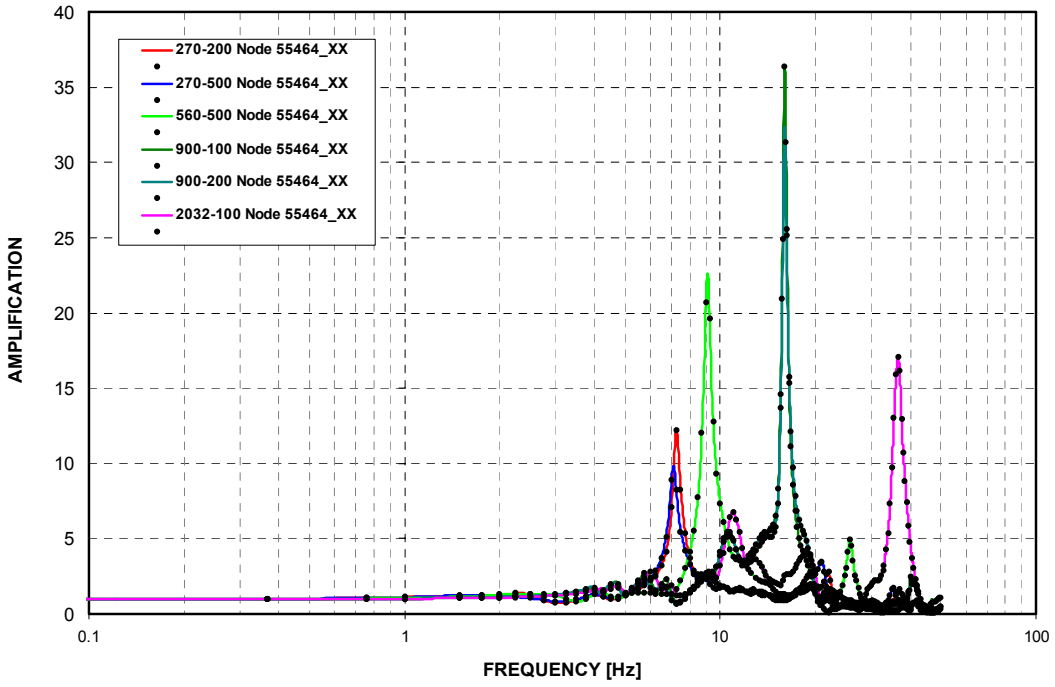

Figure 3-C.1.0-58 A/B Northwest Corner at Roof - Uncracked - NS Direction (X)

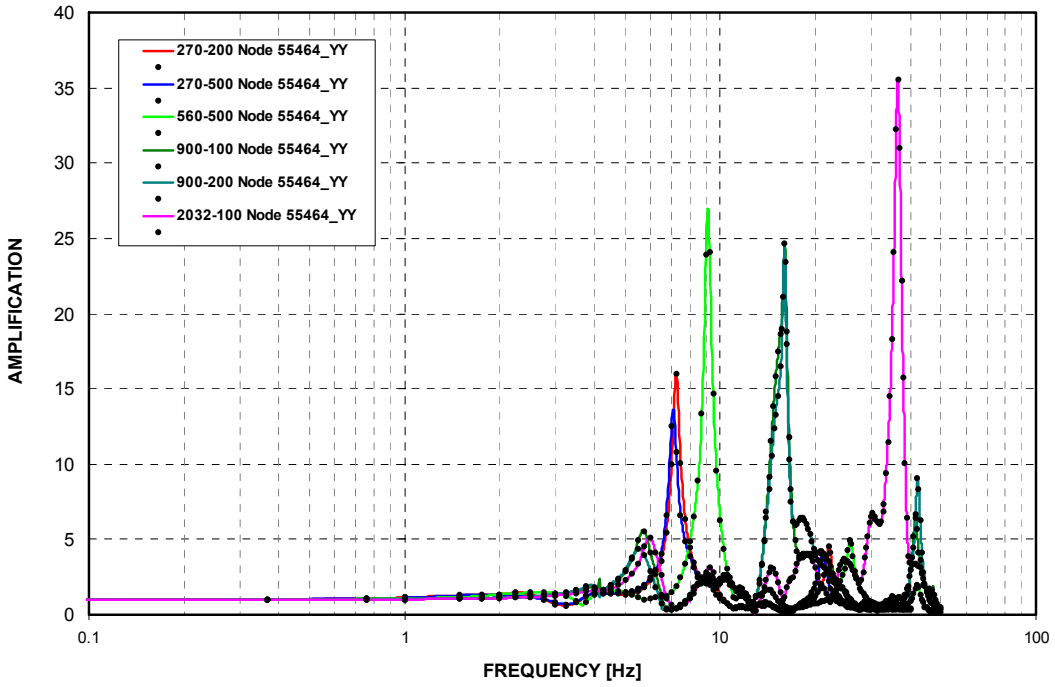

Figure 3-C.1.0-59 A/B Northwest Corner at Roof - Uncracked - EW Direction (Y)

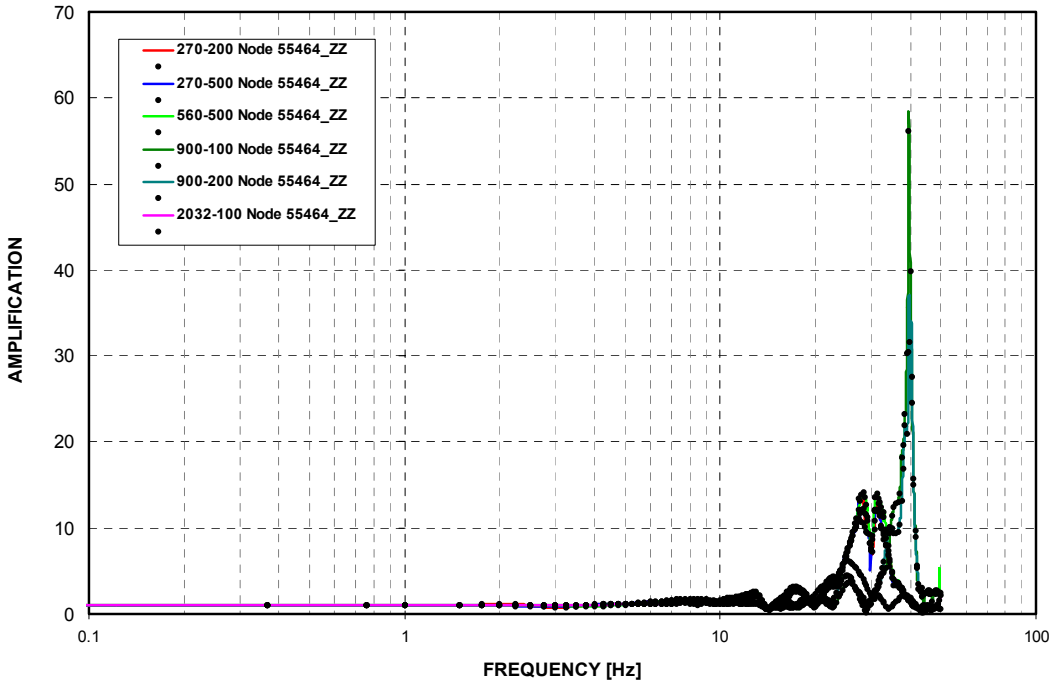

Figure 3-C.1.0-60 A/B Northwest Corner at Roof - Uncracked - Vertical Direction (Z)

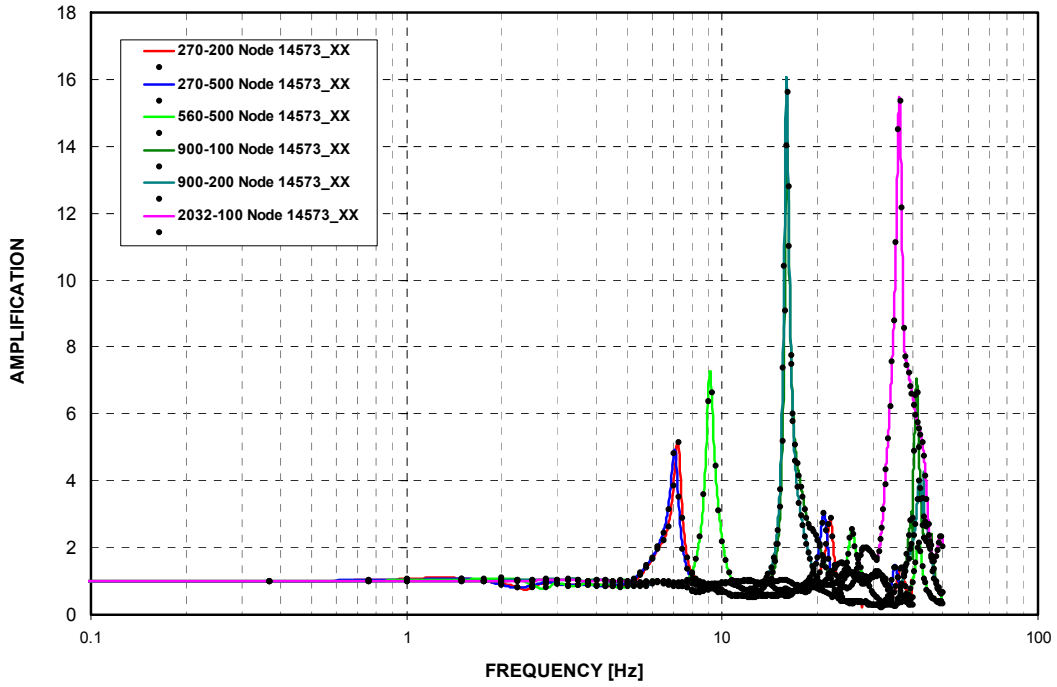

Figure 3-C.1.0-61 West PS/B Southwest Corner at Basemat - Cracked - NS Direction (X)

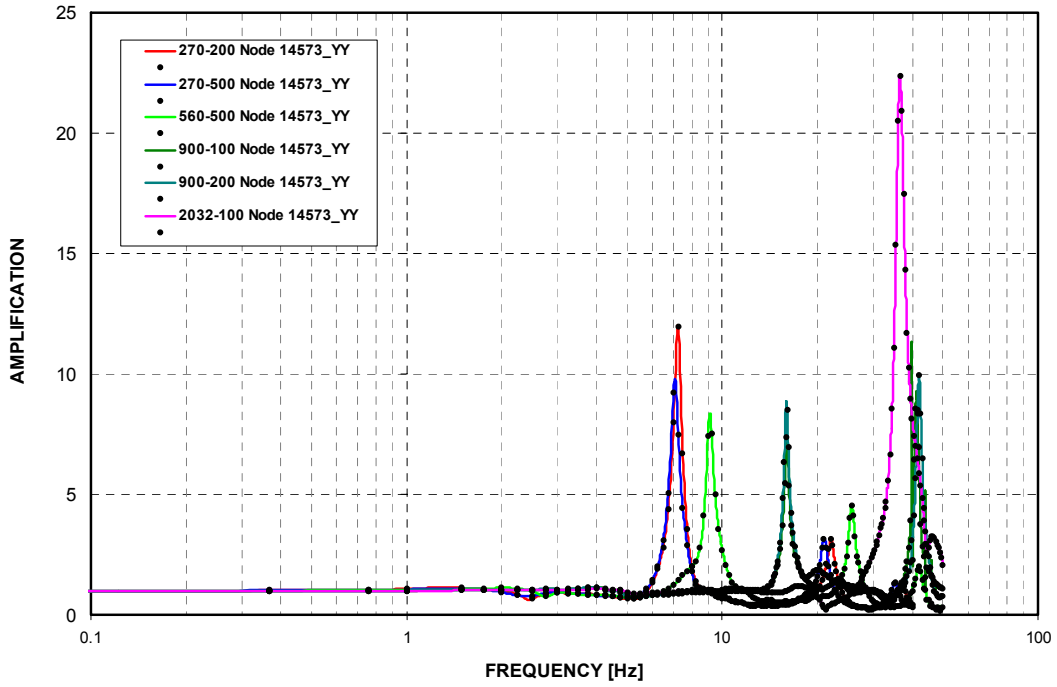

Figure 3-C.1.0-62 West PS/B Southwest Corner at Basemat - Cracked - EW Direction (Y)

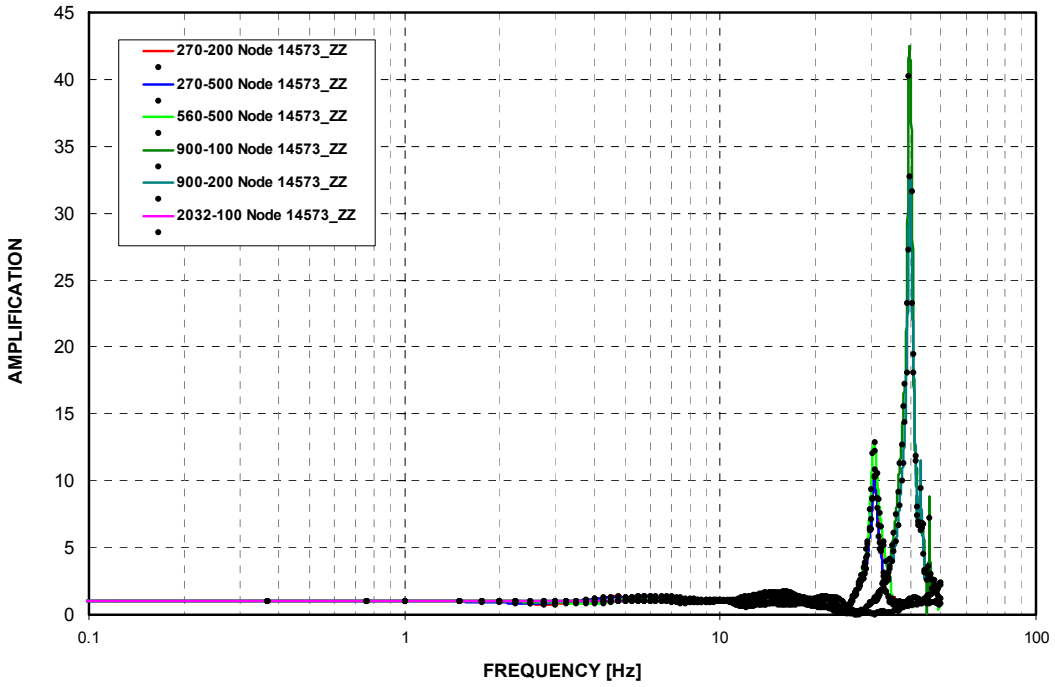

Figure 3-C.1.0-63 West PS/B Southwest Corner at Basemat - Cracked - Vertical Direction (Z)

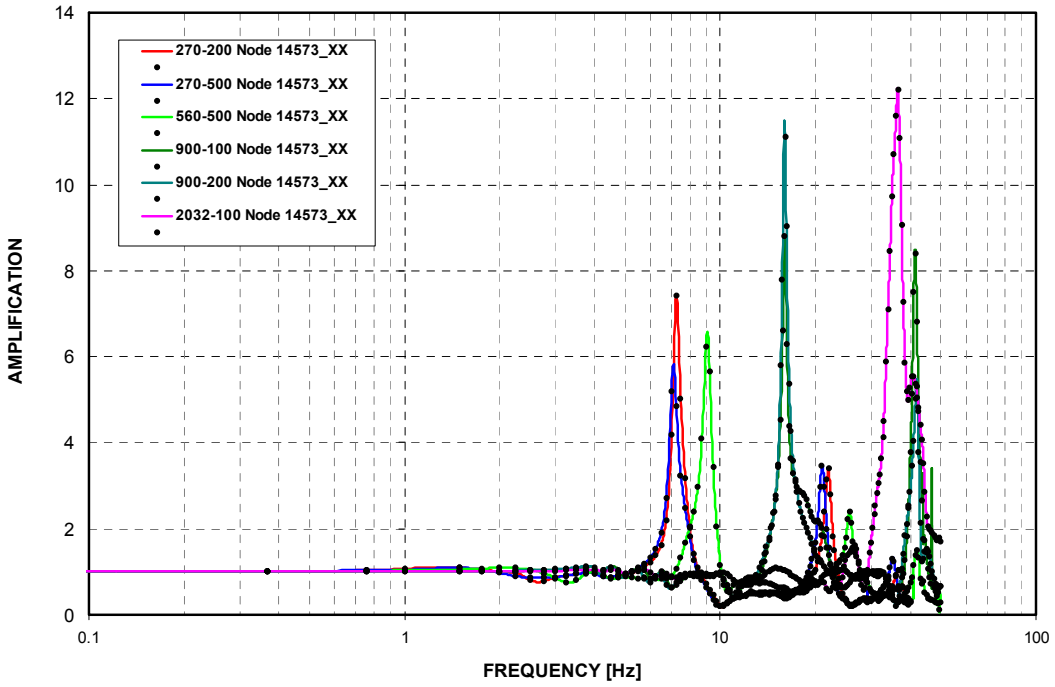

Figure 3-C.1.0-64 West PS/B Southwest Corner at Basemat - Uncracked - NS Direction (X)

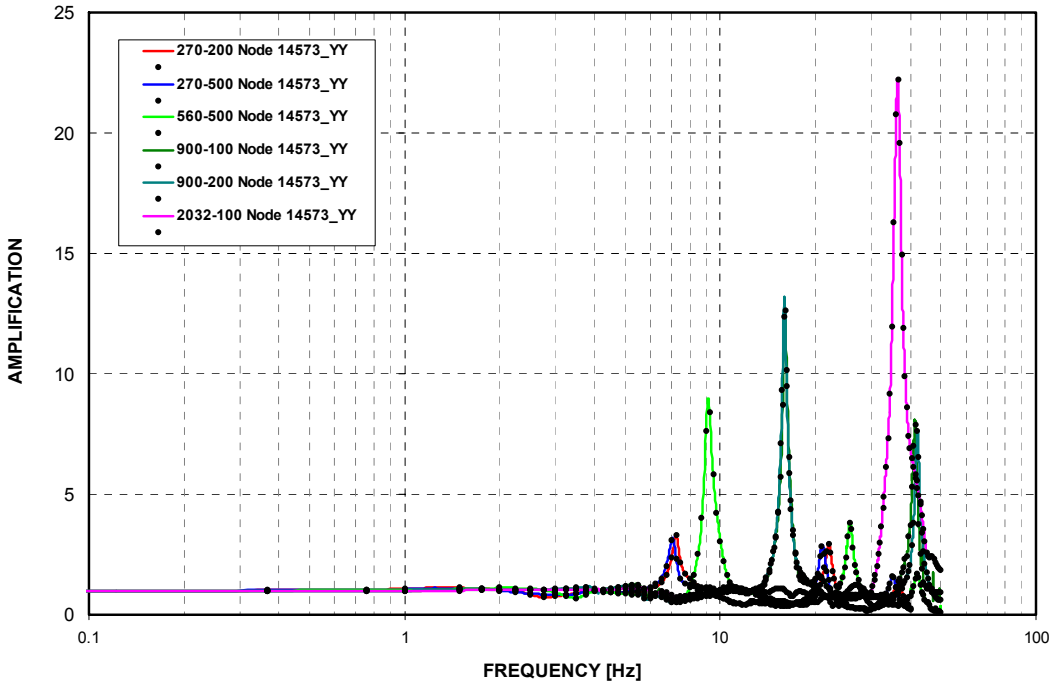

Figure 3-C.1.0-65 West PS/B Southwest Corner at Basemat - Uncracked - EW Direction (Y)

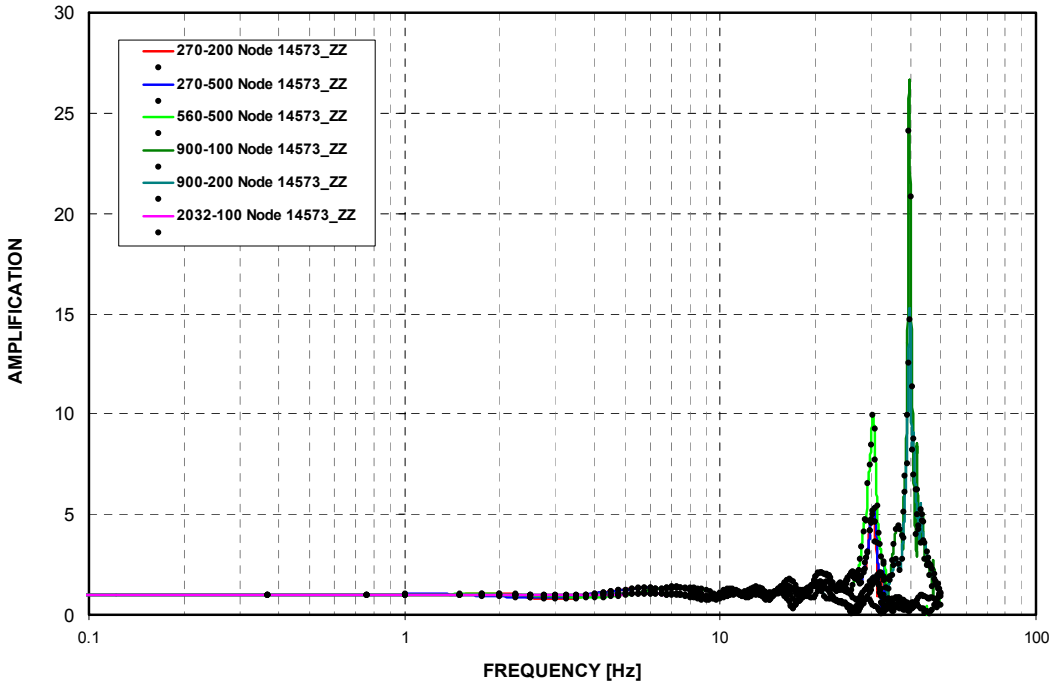

Figure 3-C.1.0-66 West PS/B Southwest Corner at Basemat - Uncracked - Vertical Direction (Z)

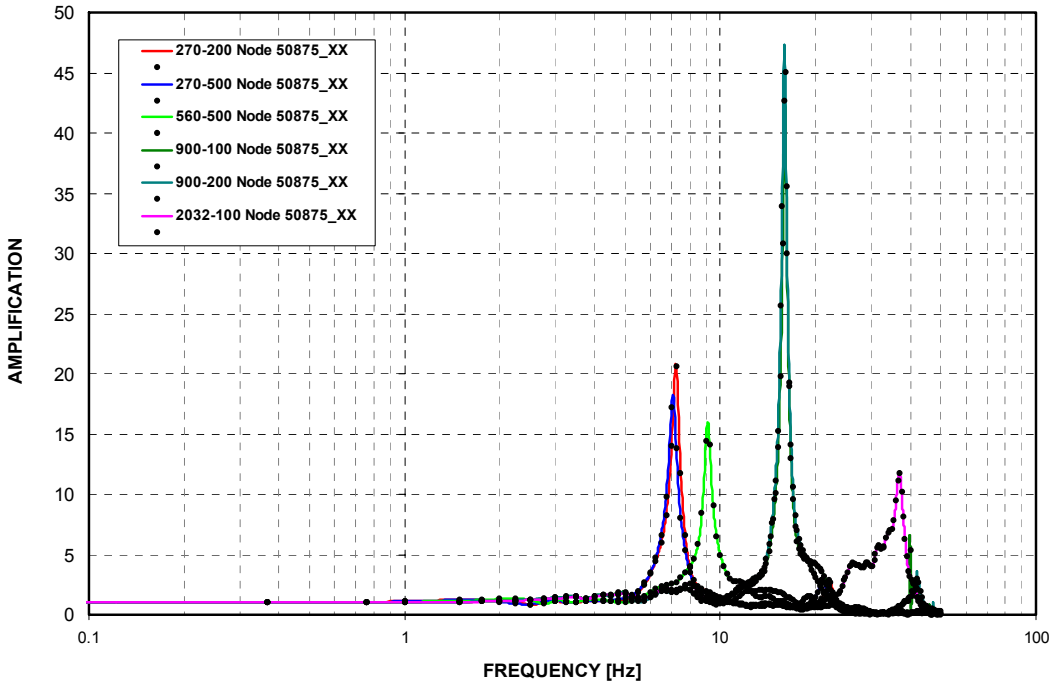

Figure 3-C.1.0-67 West PS/B Southwest Corner at Roof - Cracked - NS Direction (X)

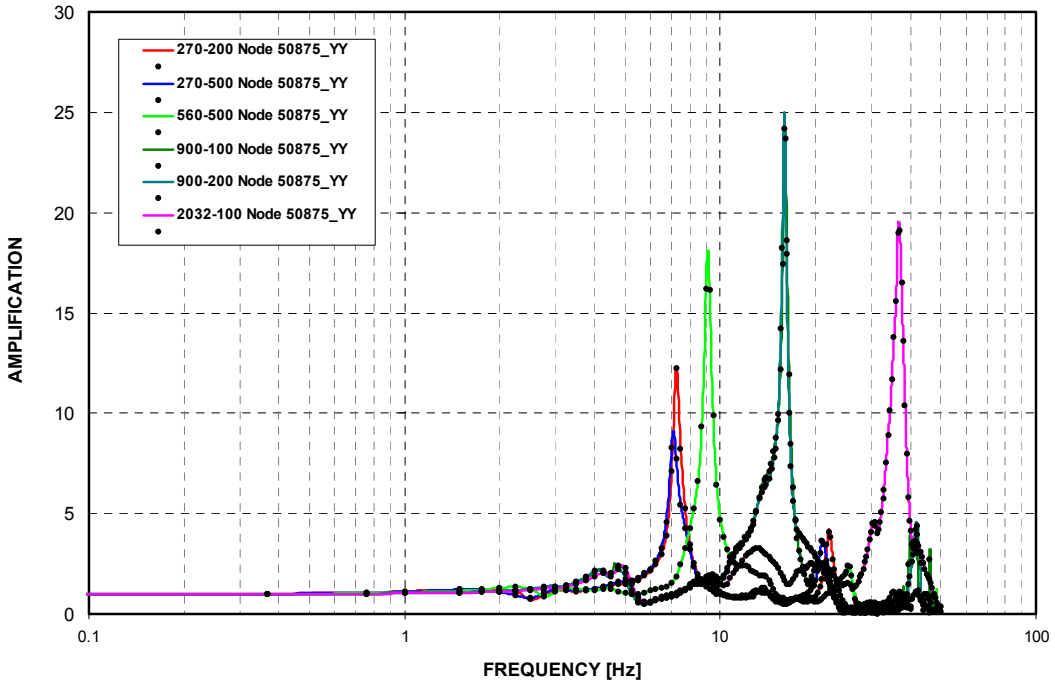

Figure 3-C.1.0-68 West PS/B Southwest Corner at Roof - Cracked - EW Direction (Y)

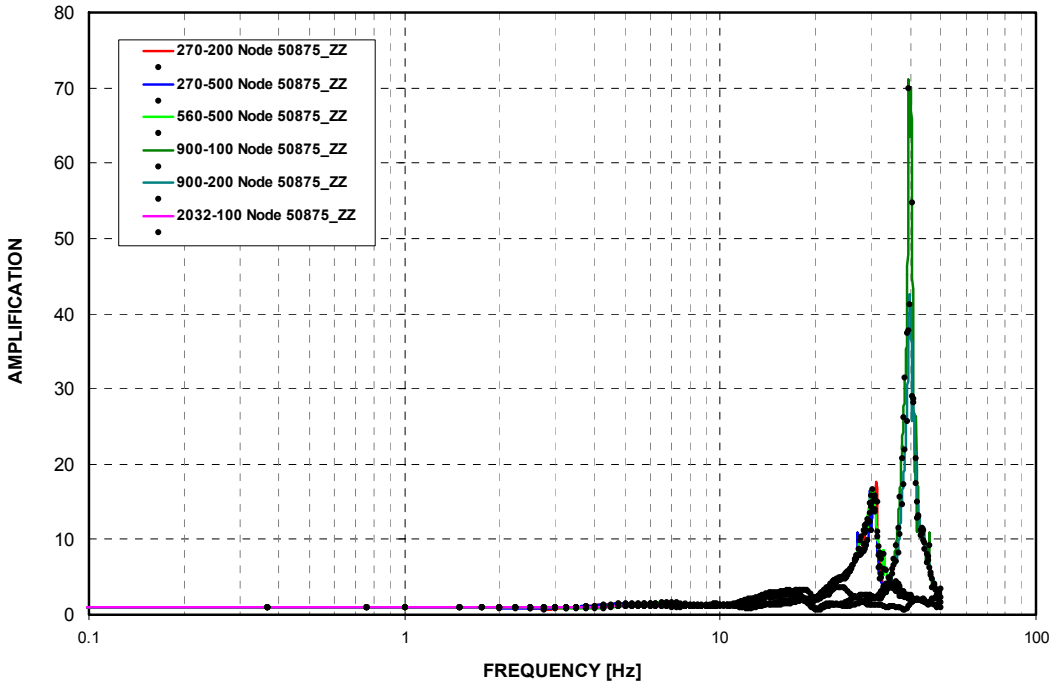

Figure 3-C.1.0-69 West PS/B Southwest Corner at Roof - Cracked - Vertical Direction (Z)

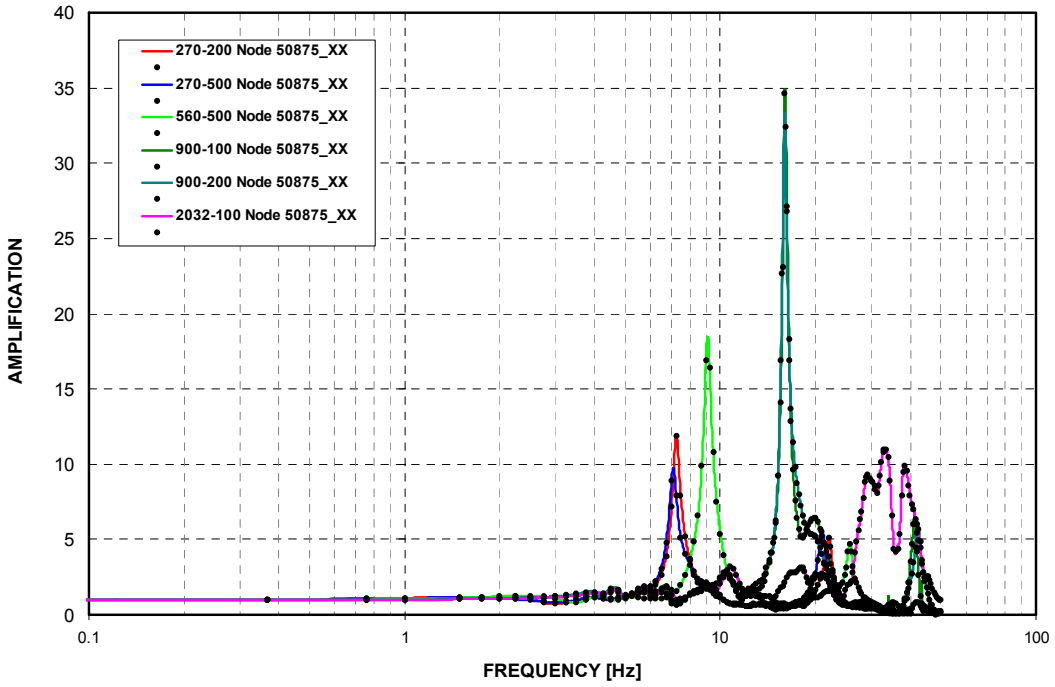

Figure 3-C.1.0-70 West PS/B Southwest Corner at Roof - Uncracked - NS Direction (X)

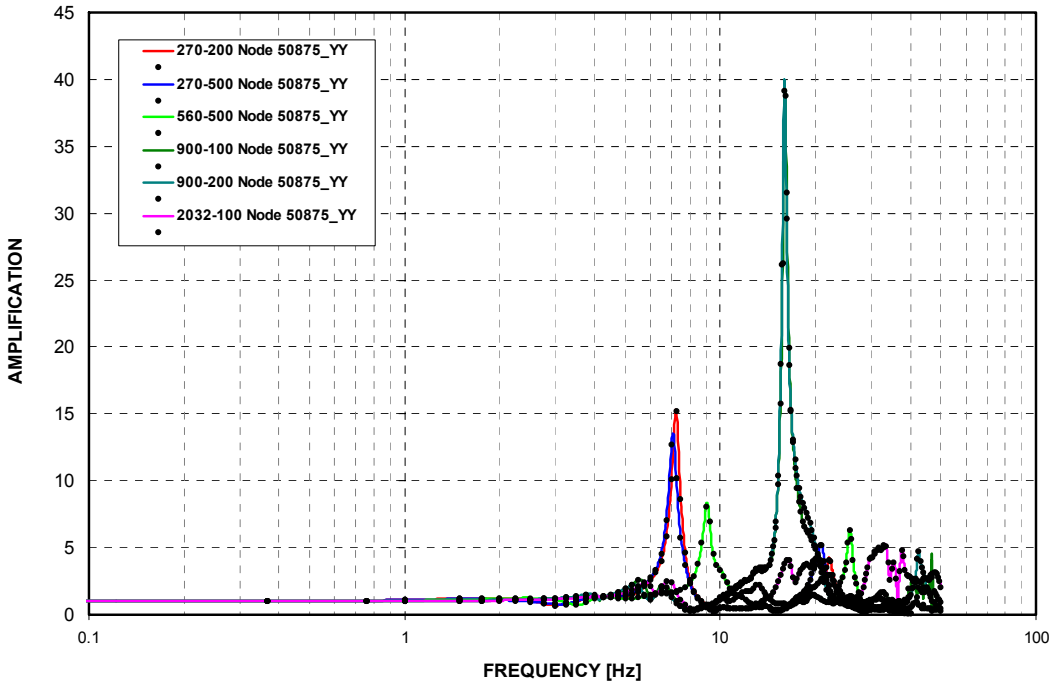

Figure 3-C.1.0-71 West PS/B Southwest Corner at Roof - Uncracked - EW Direction (Y)

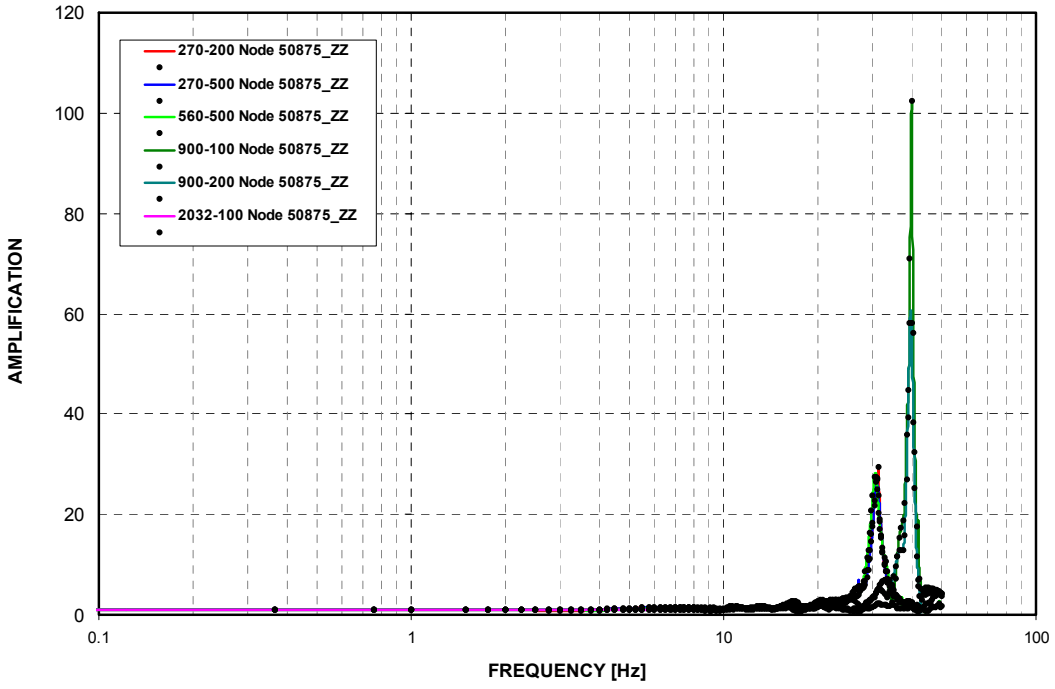

Figure 3-C.1.0-72 West PS/B Southwest Corner at Roof - Uncracked - Vertical Direction (Z)

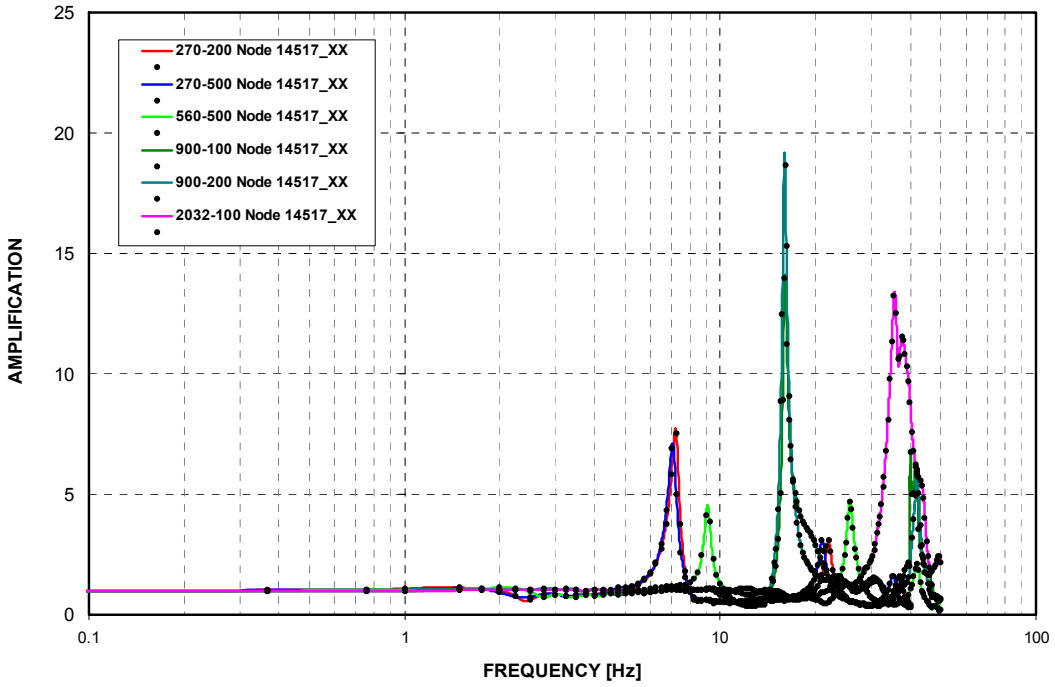

Figure 3-C.1.0-73 East PS/B Southeast Corner at Basemat - Cracked - NS Direction (X)

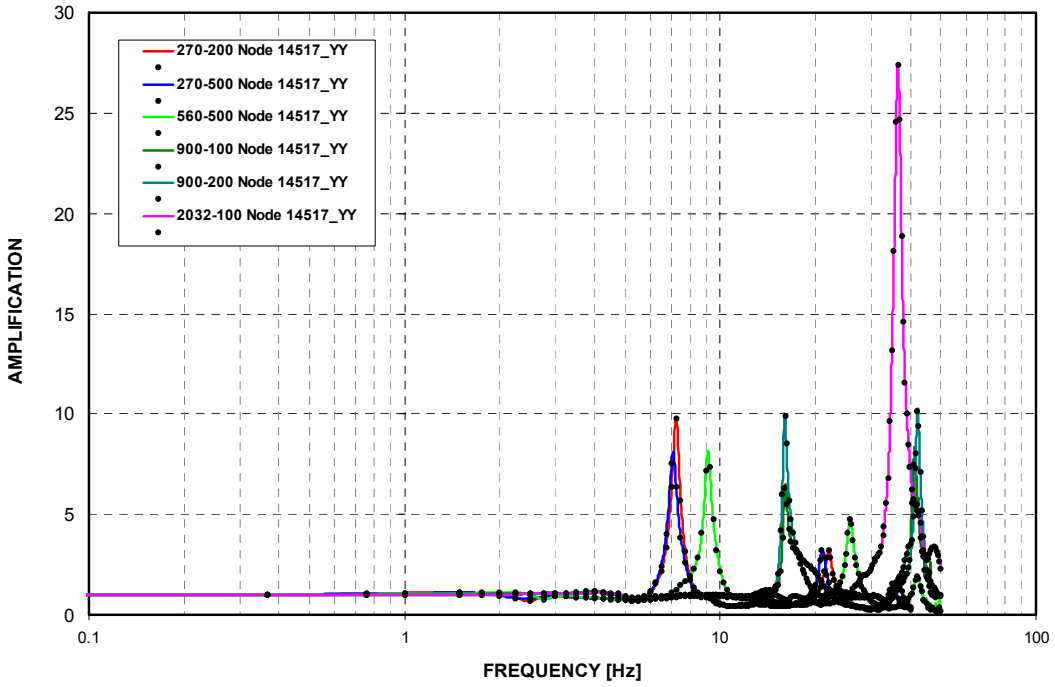

Figure 3-C.1.0-74 East PS/B Southeast Corner at Basemat - Cracked - EW Direction (Y)

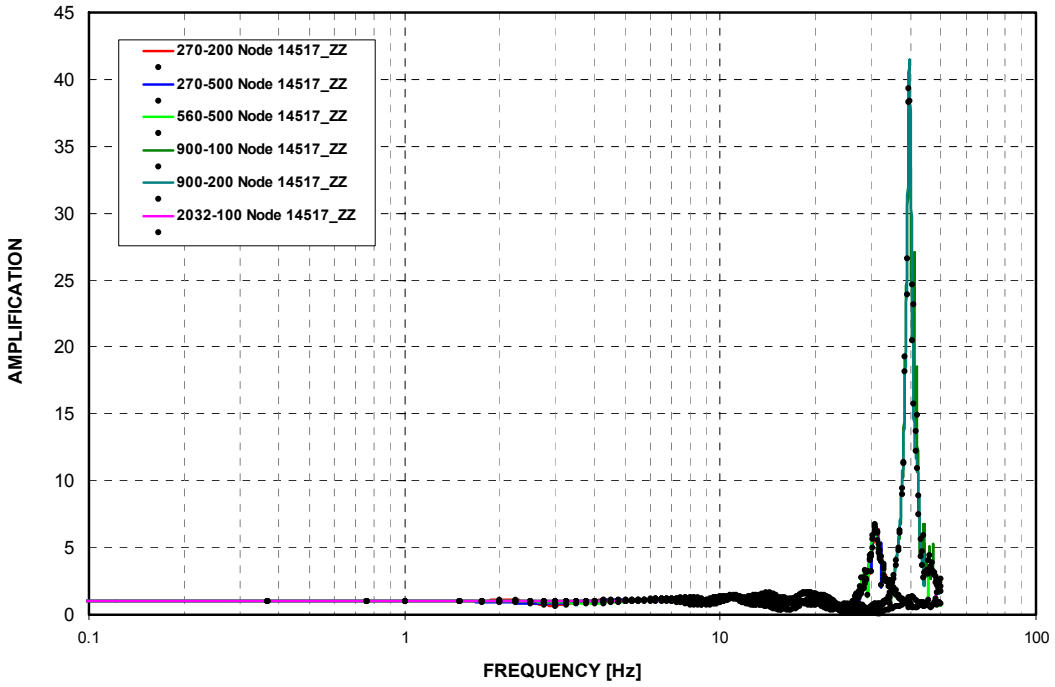

Figure 3-C.1.0-75 East PS/B Southeast Corner at Basemat - Cracked - Vertical Direction (Z)

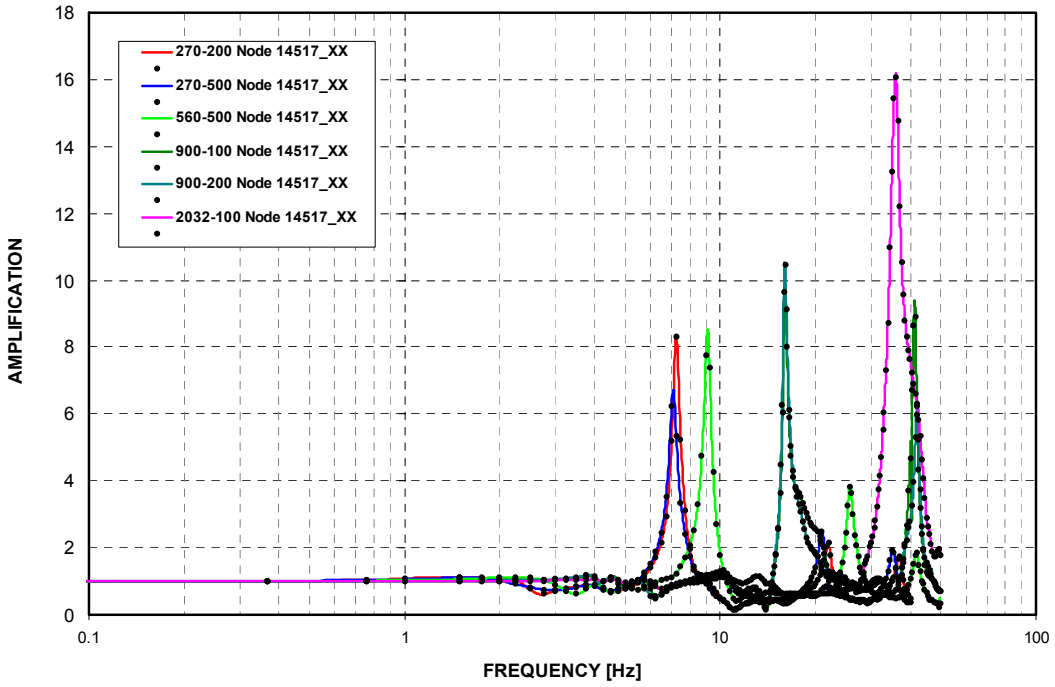

Figure 3-C.1.0-76 East PS/B Southeast Corner at Basemat - Uncracked - NS Direction (X)

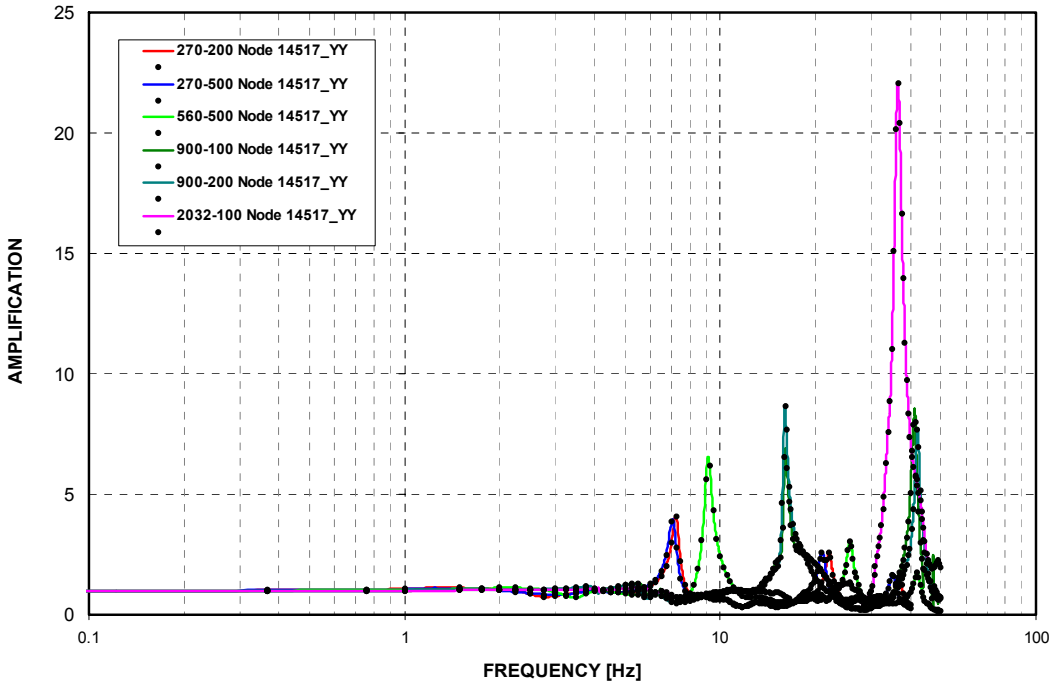

Figure 3-C.1.0-77 East PS/B Southeast Corner at Basemat - Uncracked - EW Direction (Y)

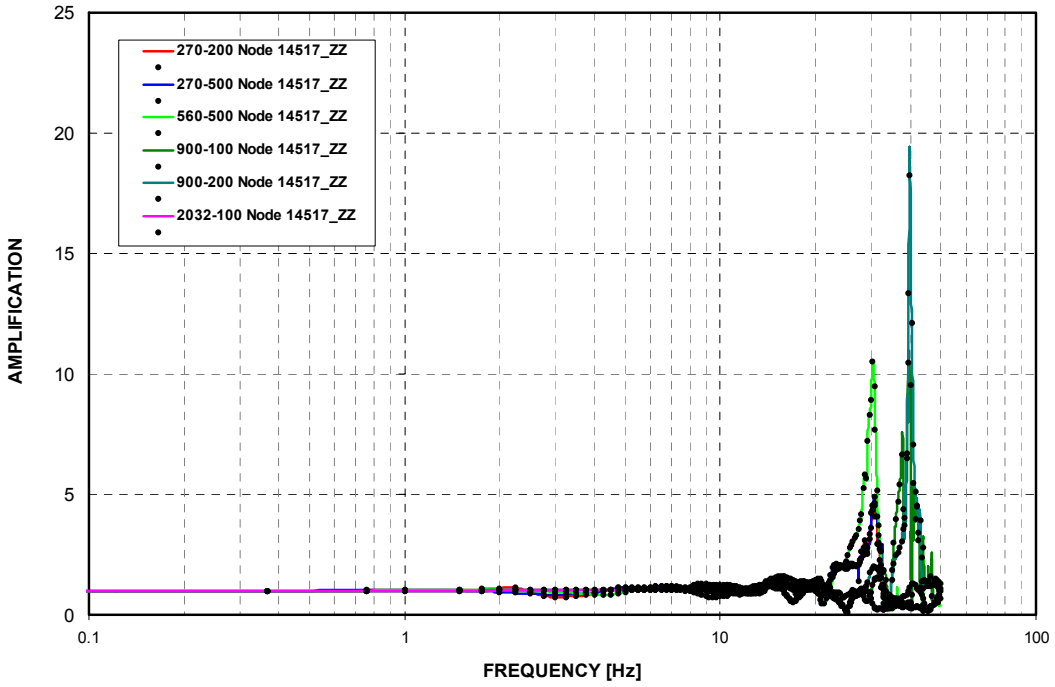

Figure 3-C.1.0-78 East PS/B Southeast Corner at Basemat - Uncracked - Vertical Direction (Z)

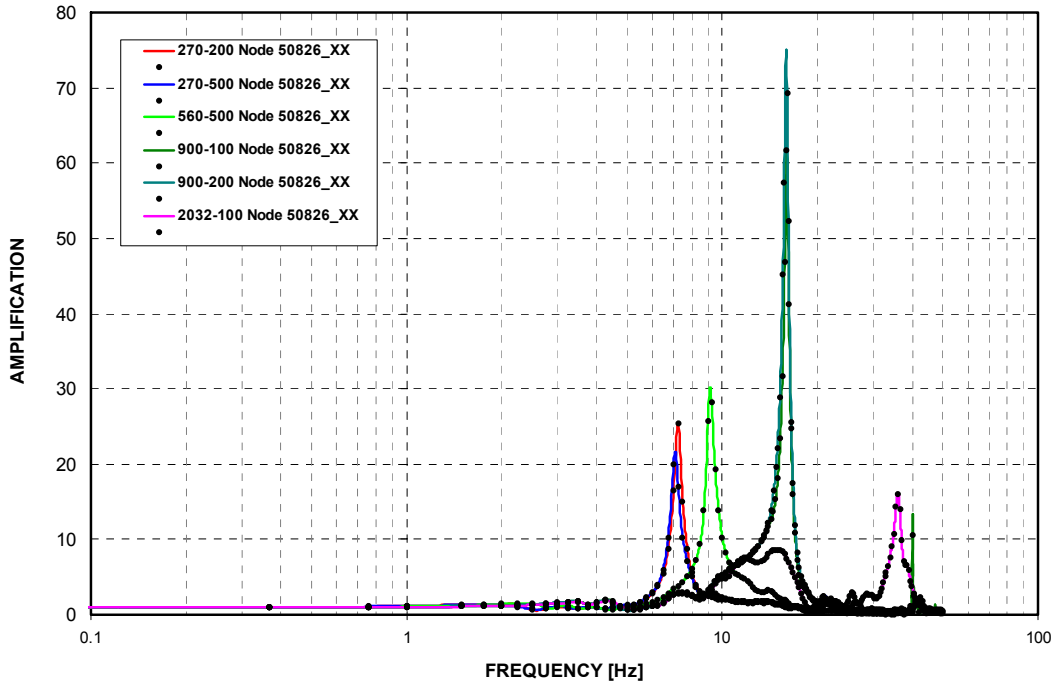

Figure 3-C.1.0-79 East PS/B Southeast Corner at Roof - Cracked - NS Direction (X)

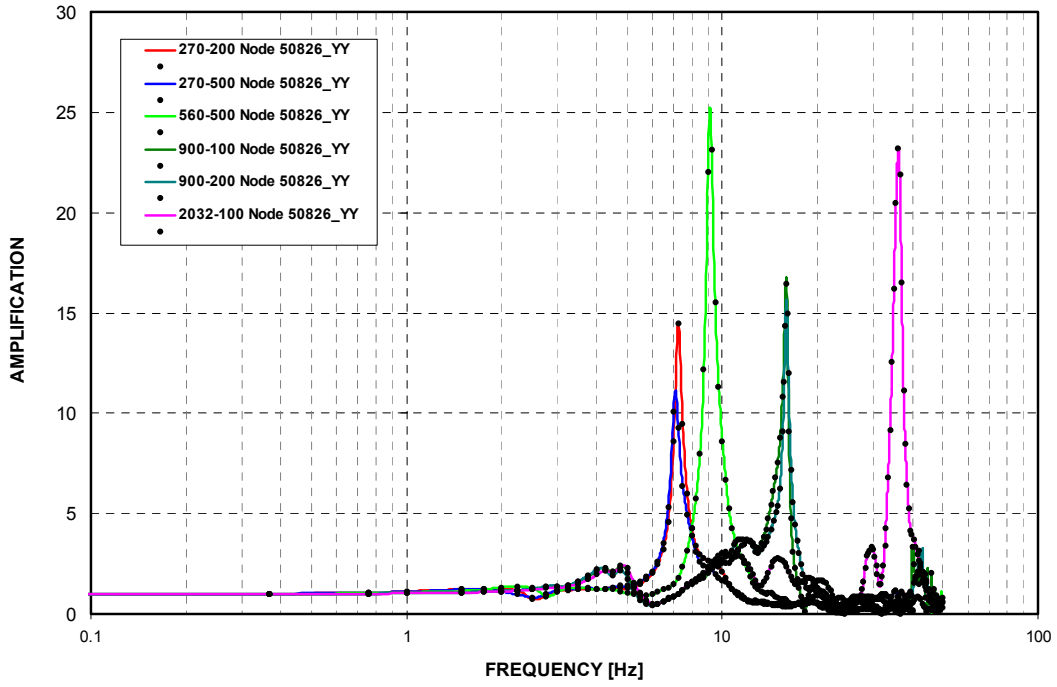

Figure 3-C.1.0-80 East PS/B Southeast Corner at Roof - Cracked - EW Direction (Y)

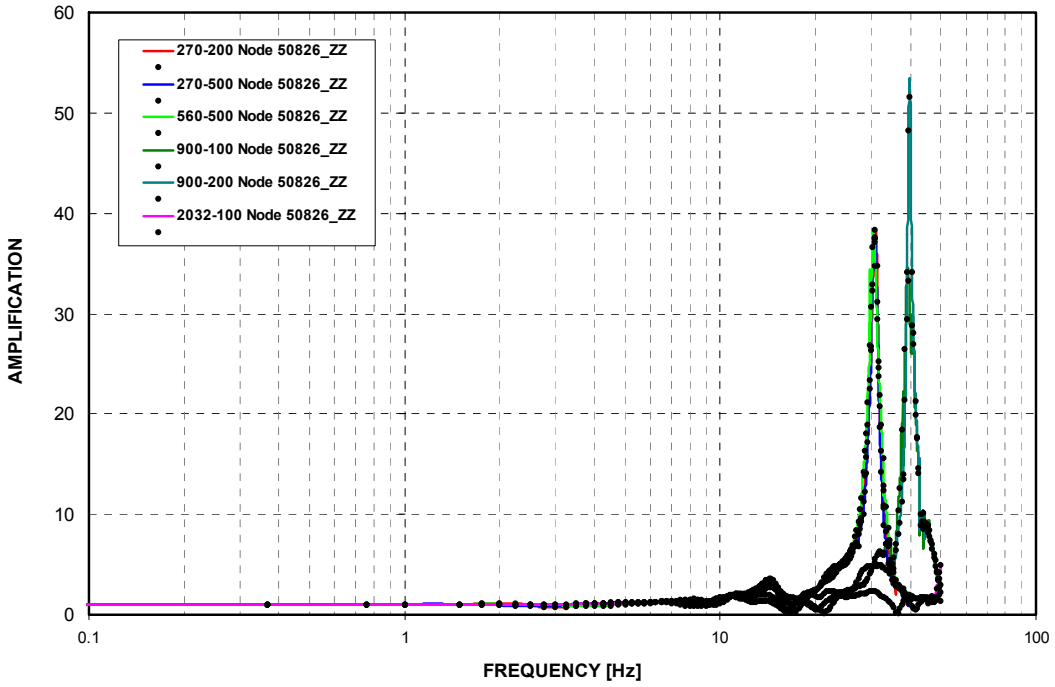

Figure 3-C.1.0-81 East PS/B Southeast Corner at Roof - Cracked - Vertical Direction (Z)

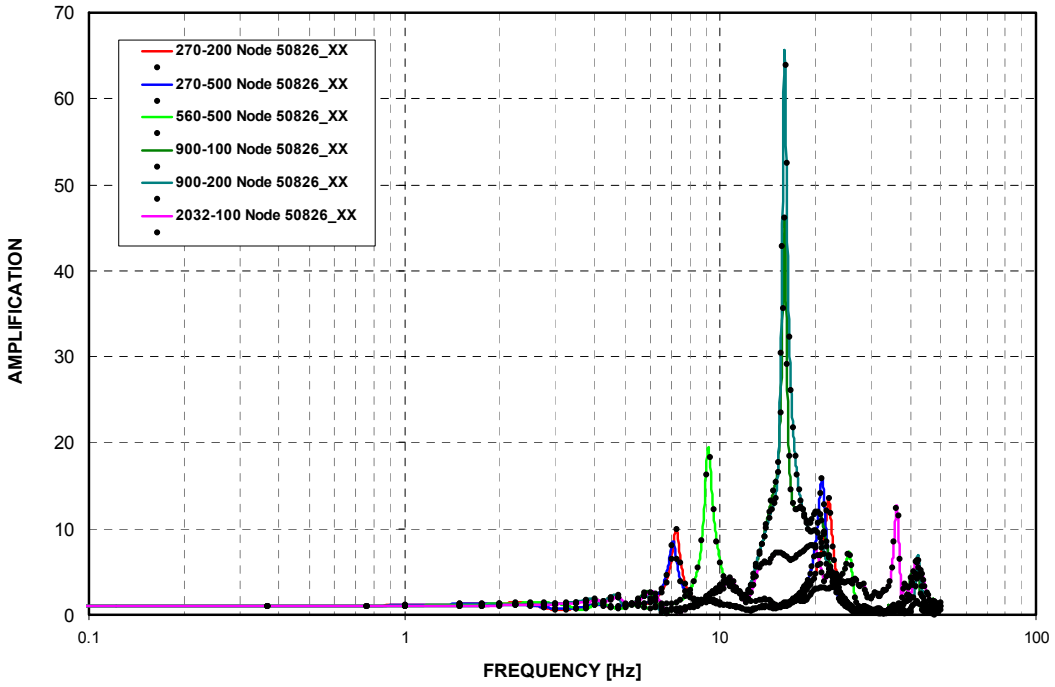

Figure 3-C.1.0-82 East PS/B Southeast Corner at Roof - Uncracked - NS Direction (X)

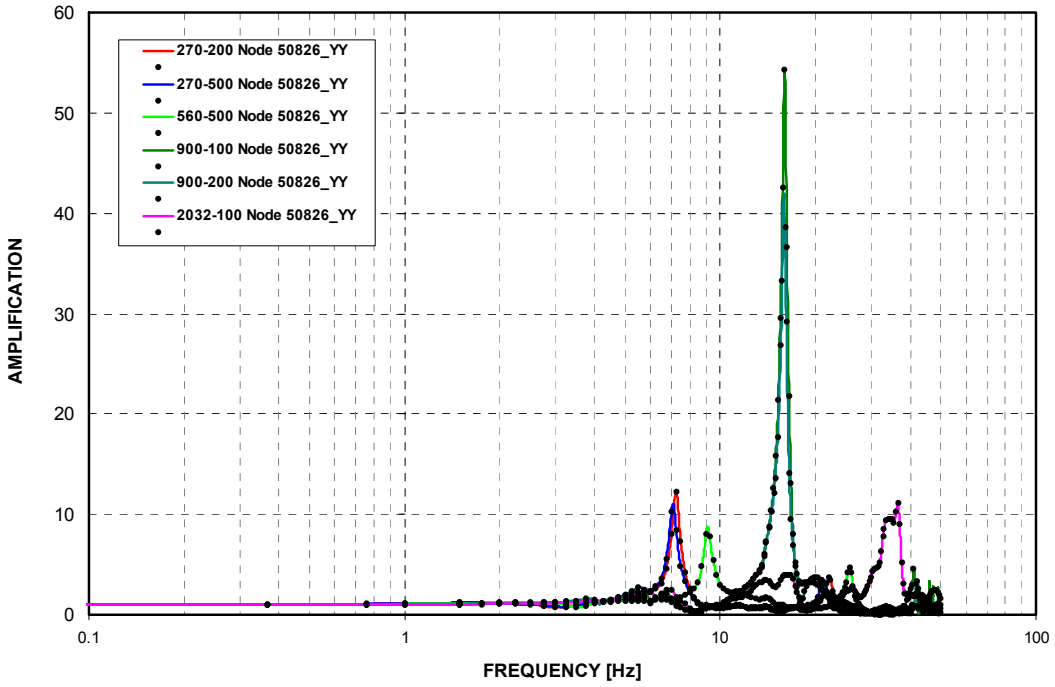

Figure 3-C.1.0-83 East PS/B Southeast Corner at Roof - Uncracked - EW Direction (Y)

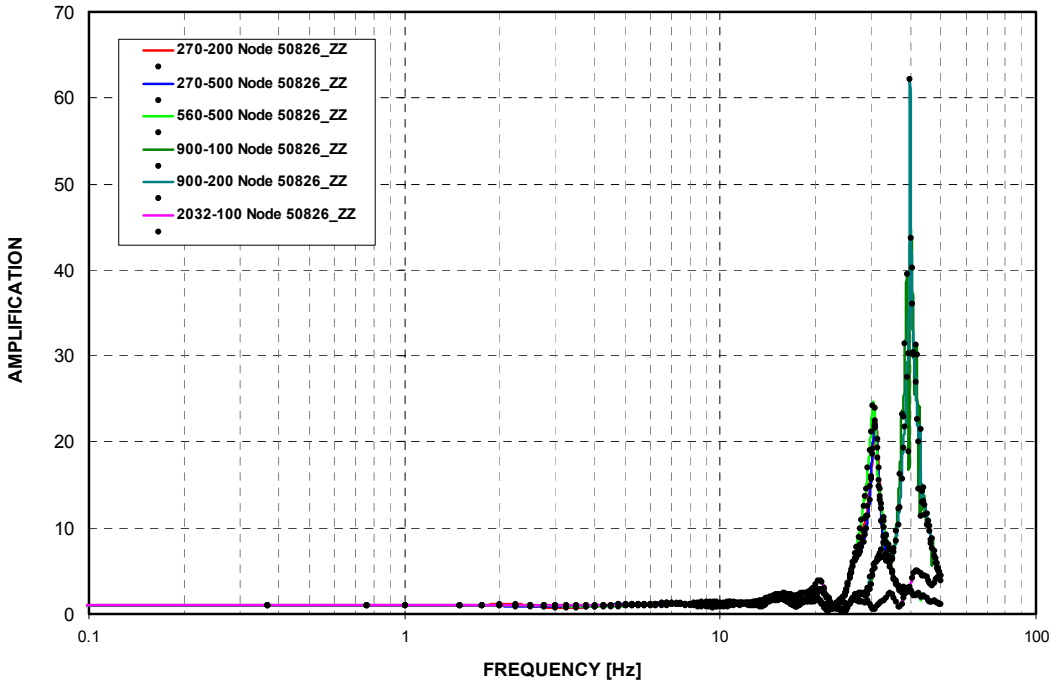

Figure 3-C.1.0-84 East PS/B Southeast Corner at Roof - Uncracked - Vertical Direction (Z)

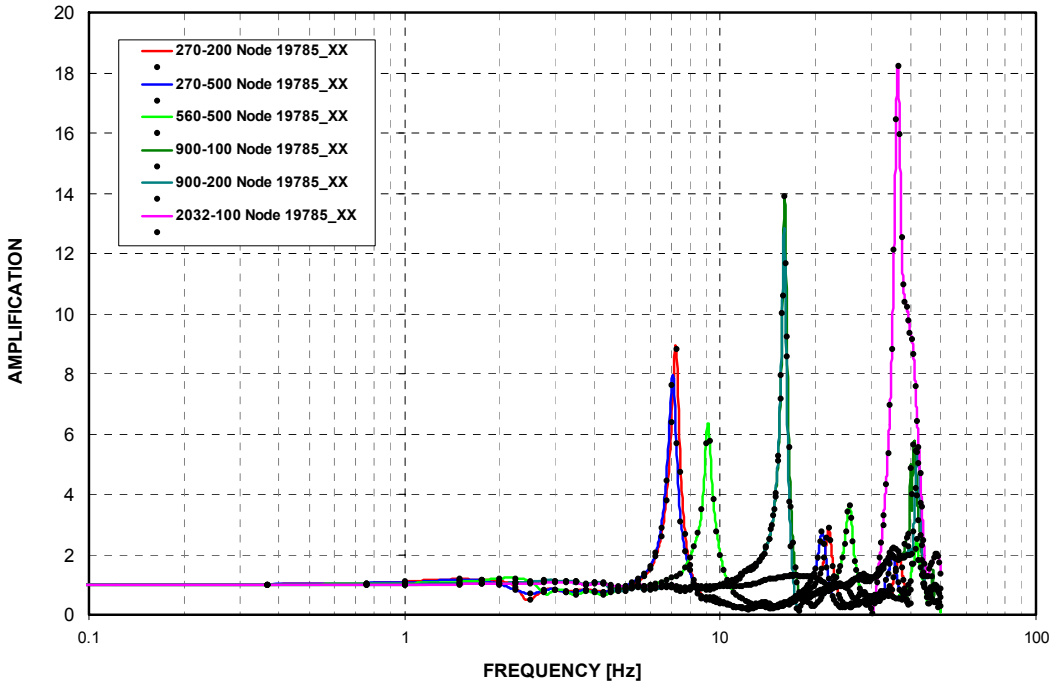

Figure 3-C.1.0-85 R/B Northeast Corner at Basemat - Cracked - NS Direction (X)

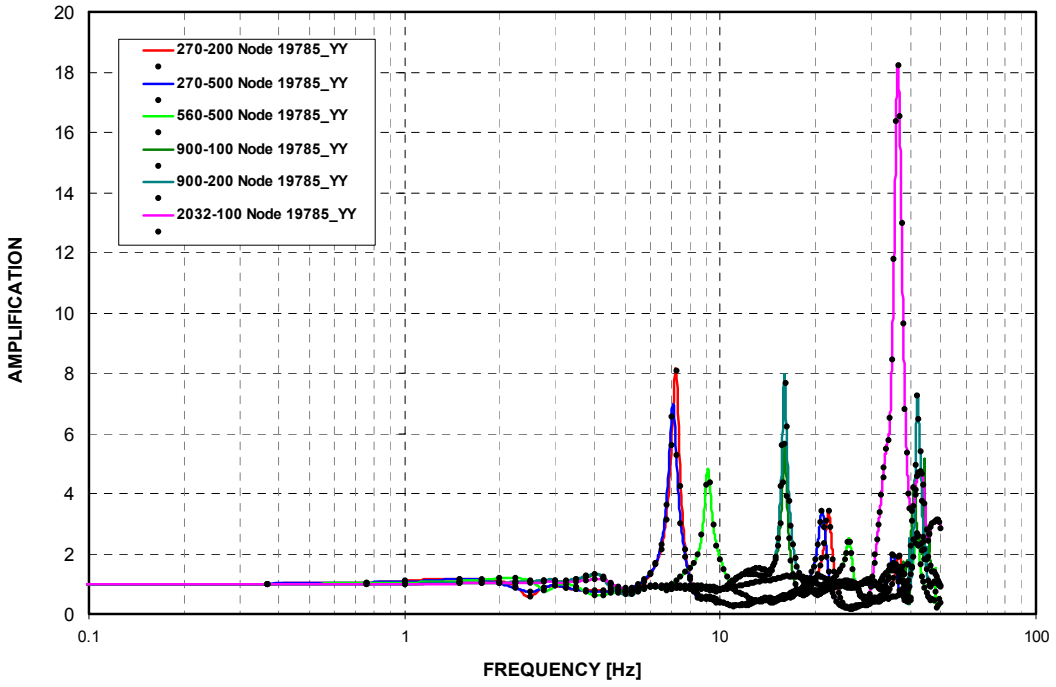

Figure 3-C.1.0-86 R/B Northeast Corner at Basemat - Cracked - EW Direction (Y)

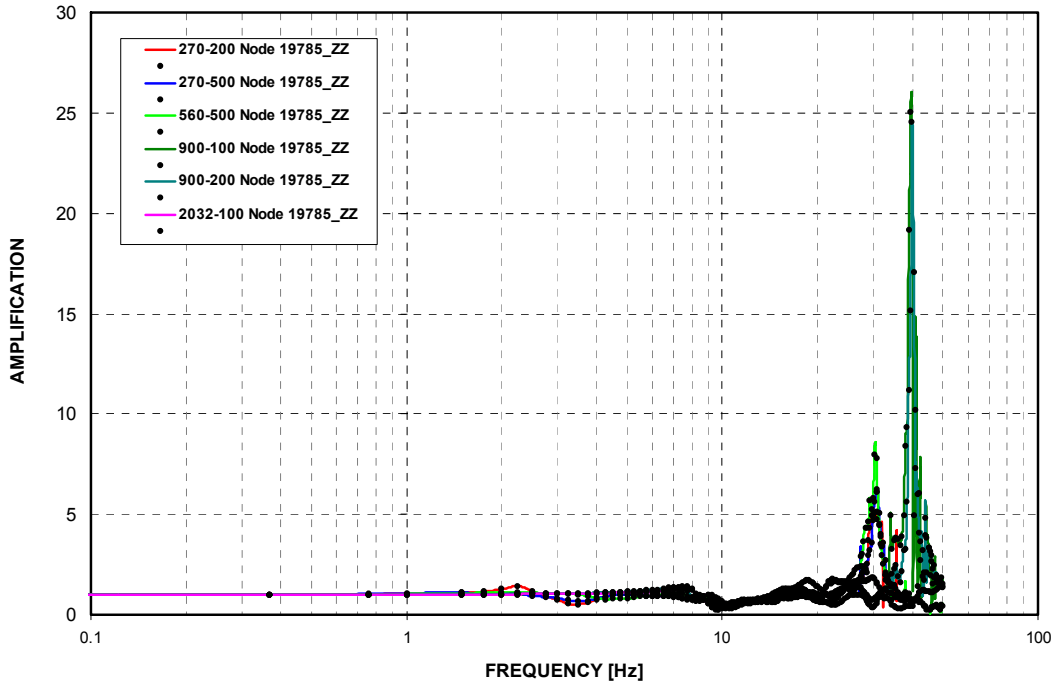

Figure 3-C.1.0-87 R/B Northeast Corner at Basemat - Cracked - Vertical Direction (Z)

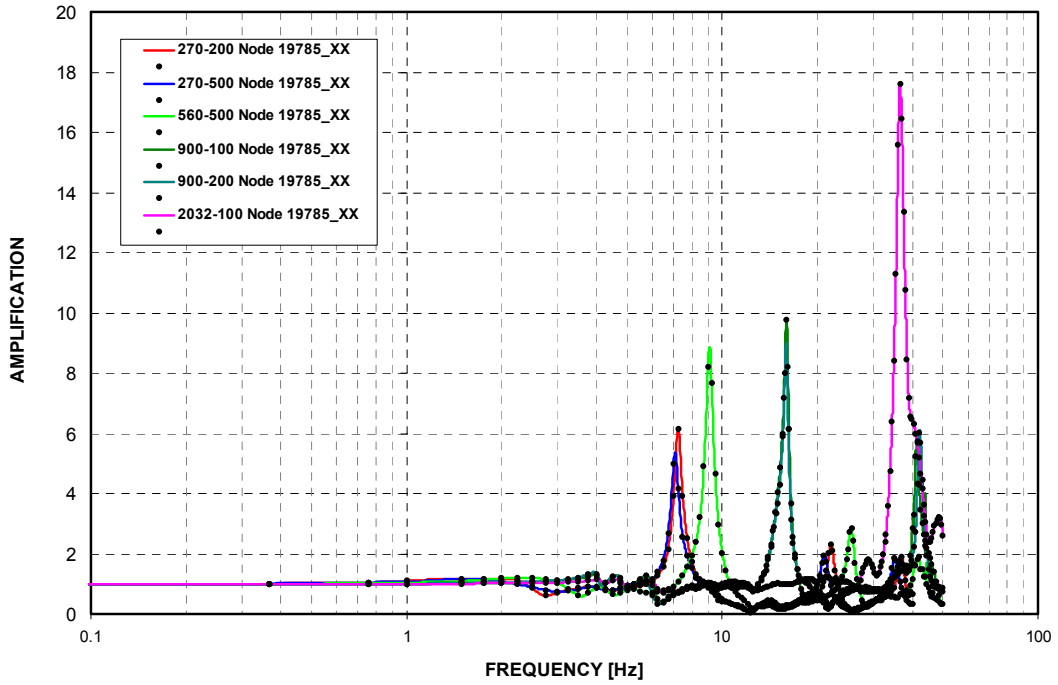

Figure 3-C.1.0-88 R/B Northeast Corner at Basemat - Uncracked - NS Direction (X)

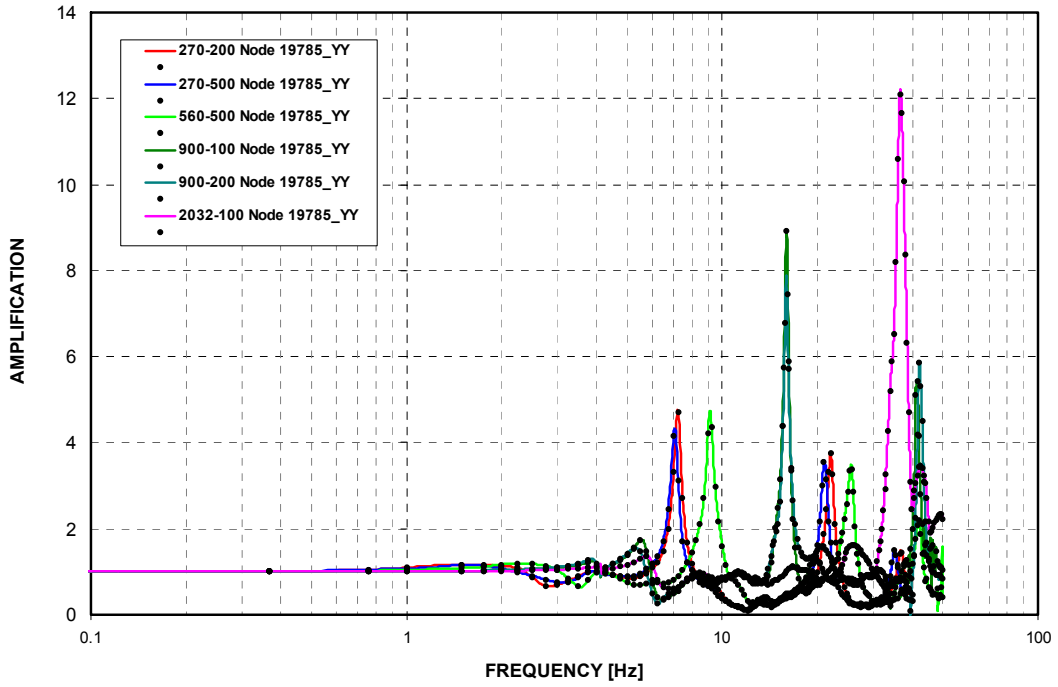

Figure 3-C.1.0-89 R/B Northeast Corner at Basemat - Uncracked - EW Direction (Y)

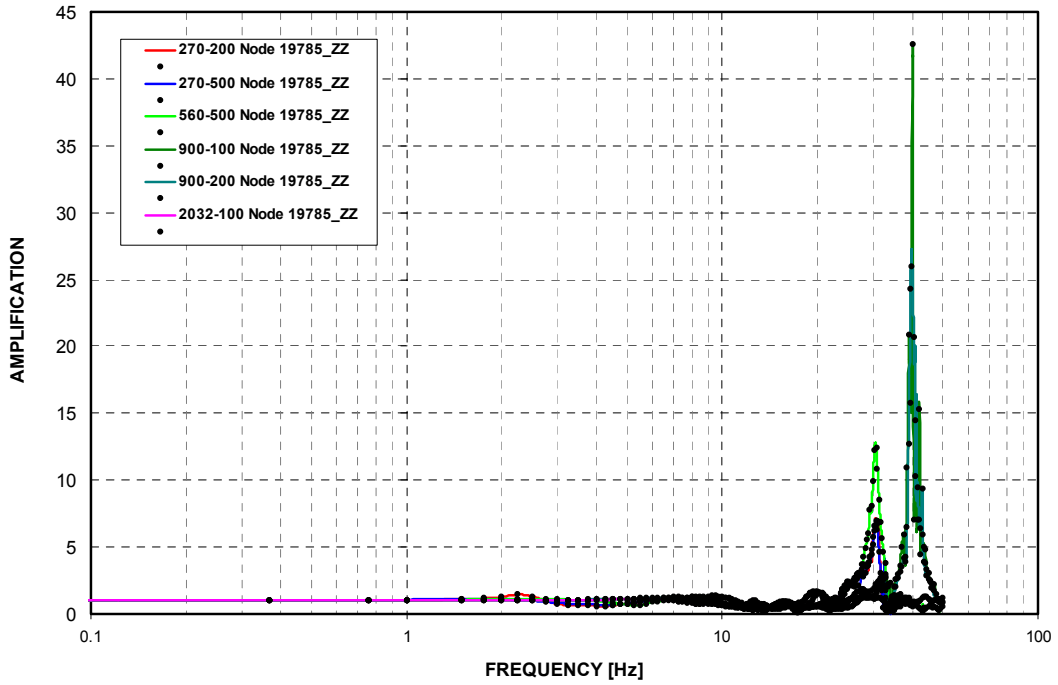

Figure 3-C.1.0-90 R/B Northeast Corner at Basemat - Uncracked - Vertical Direction (Z)

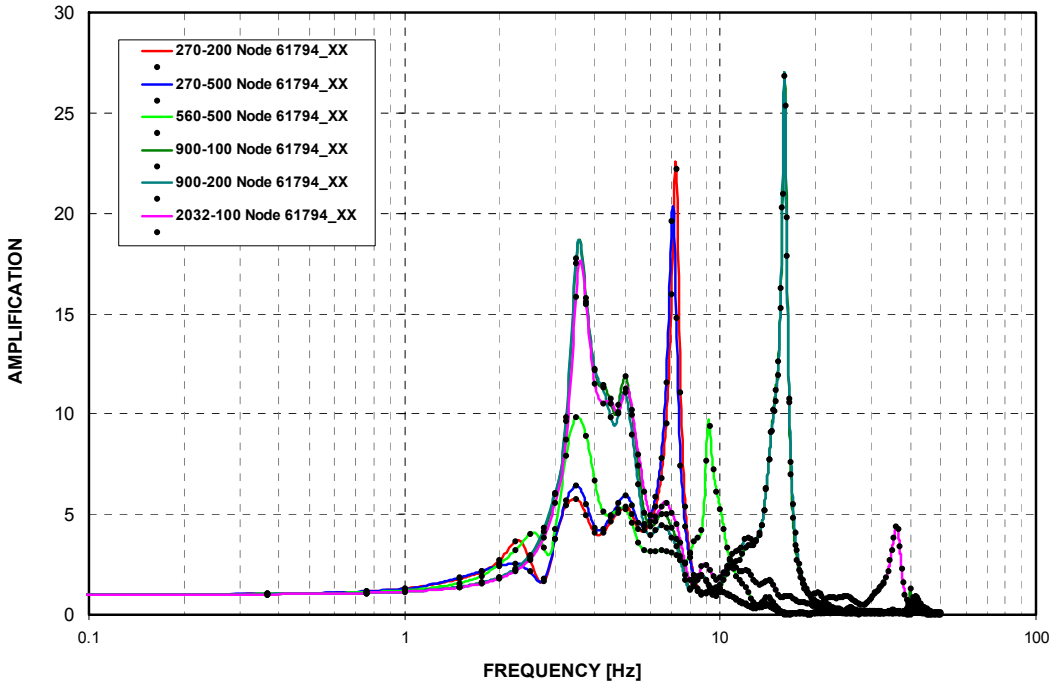

Figure 3-C.1.0-91 R/B Northeast Corner at Roof - Cracked - NS Direction (X)

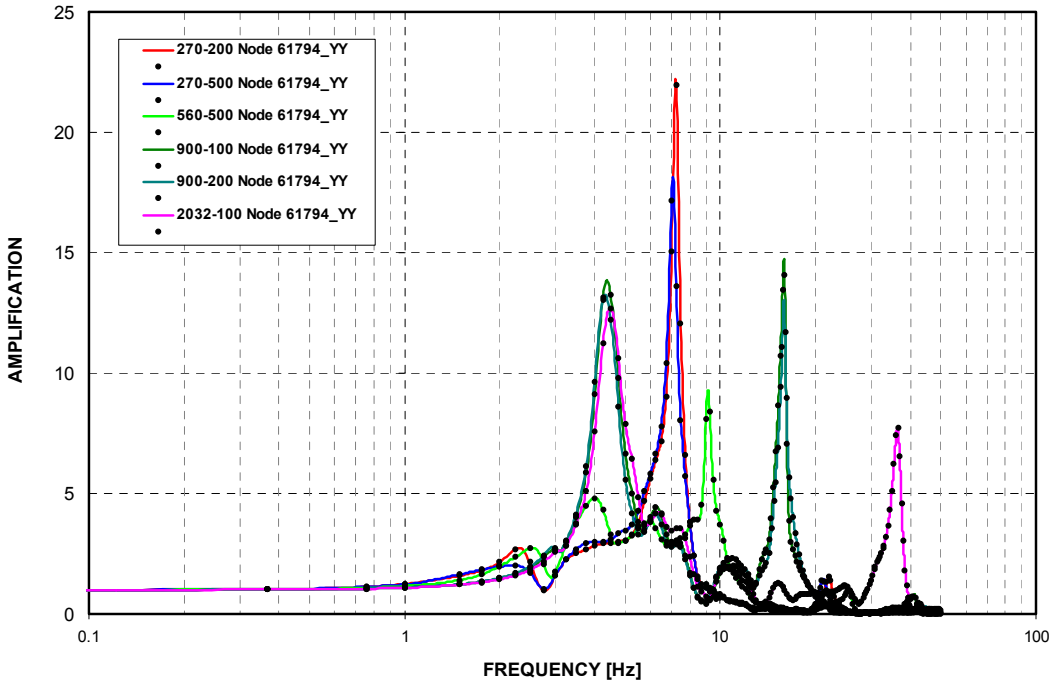

Figure 3-C.1.0-92 R/B Northeast Corner at Roof - Cracked - EW Direction (Y)

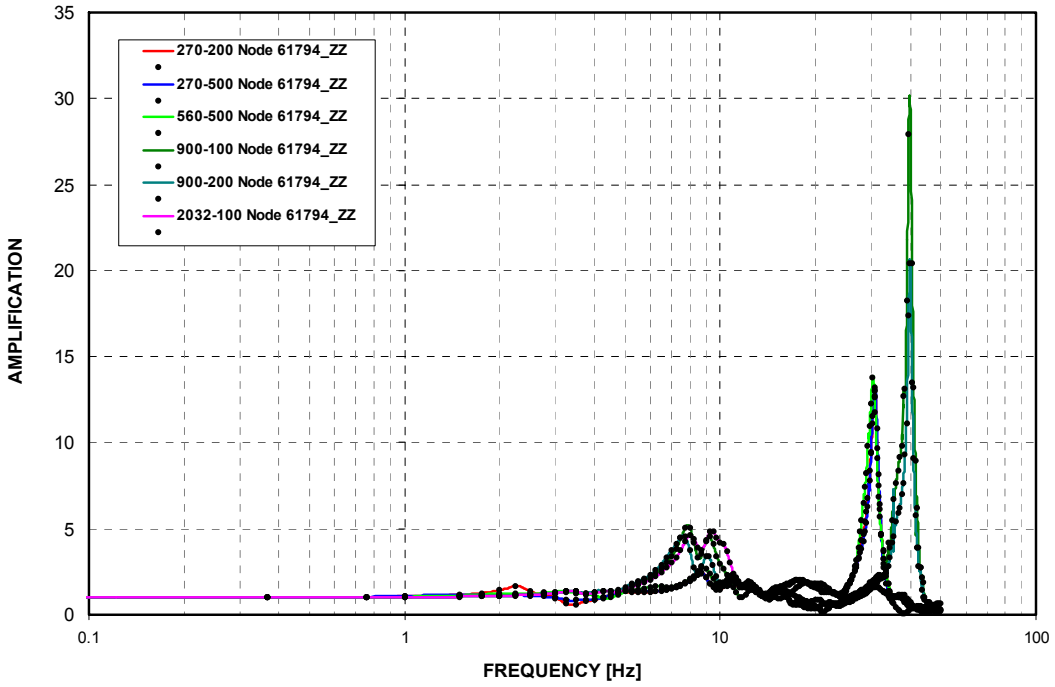

Figure 3-C.1.0-93 R/B Northeast Corner at Roof - Cracked - Vertical Direction (Z)

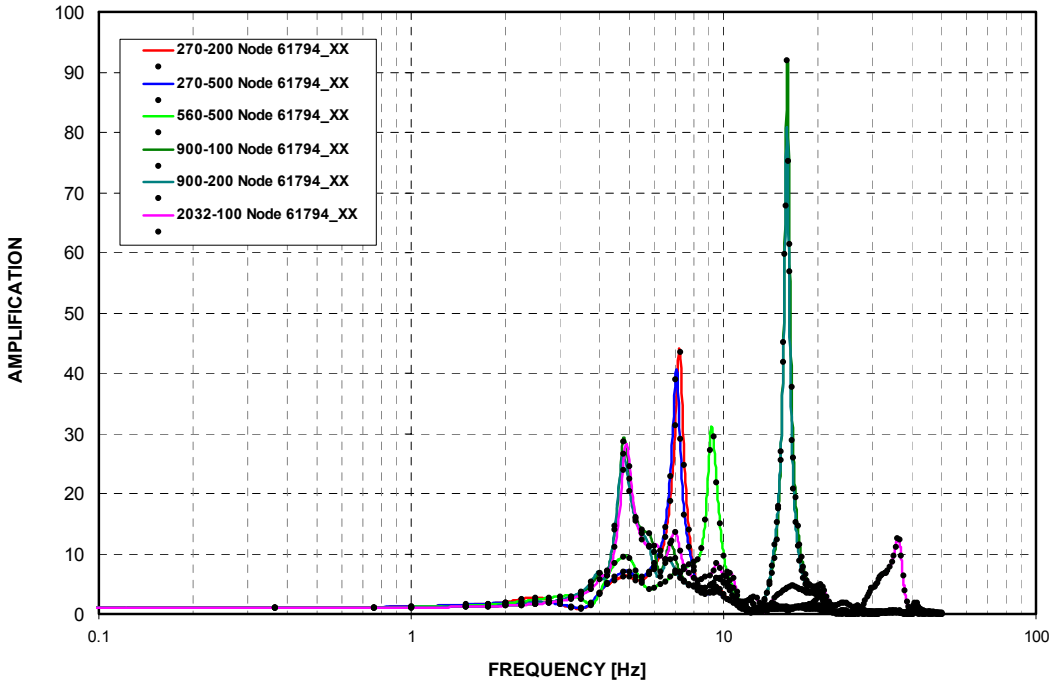

Figure 3-C.1.0-94 R/B Northeast Corner at Roof - Uncracked - NS Direction (X)

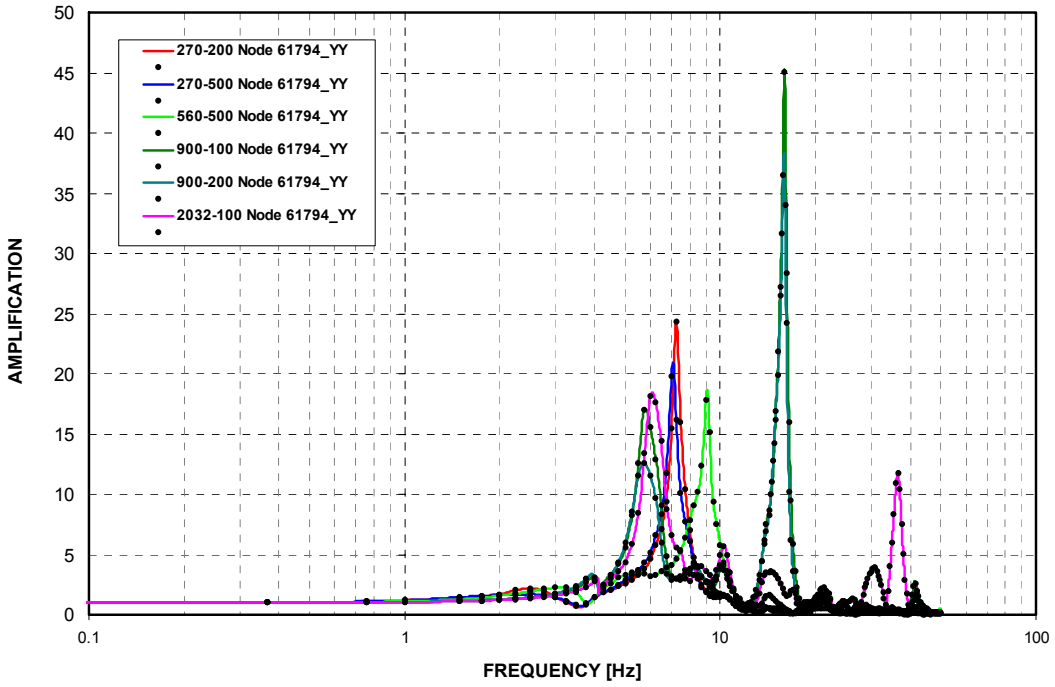

Figure 3-C.1.0-95 R/B Northeast Corner at Roof - Uncracked - EW Direction (Y)

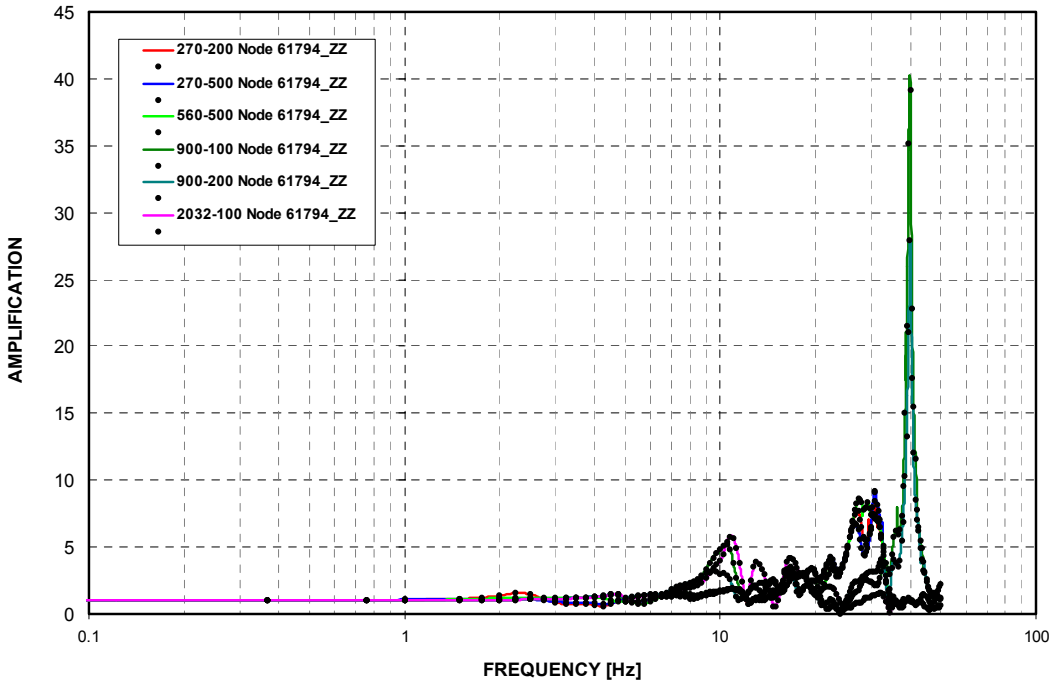

Figure 3-C.1.0-96 R/B Northeast Corner at Roof - Uncracked - Vertical Direction (Z)

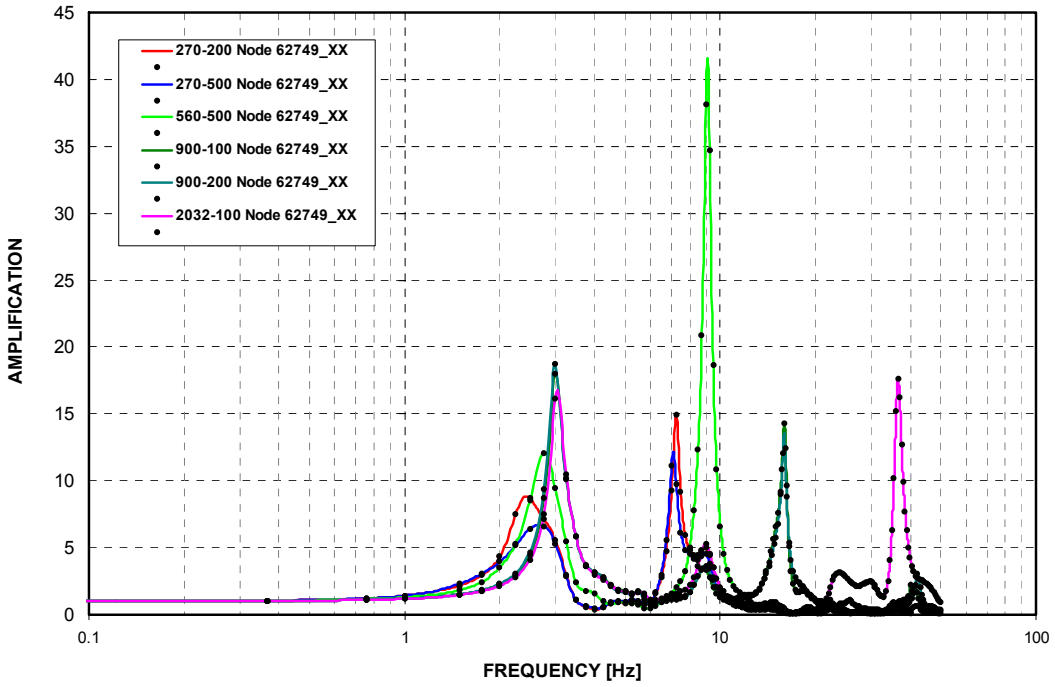

Figure 3-C.1.0-97 Top of PCCV - Cracked - NS Direction (X)

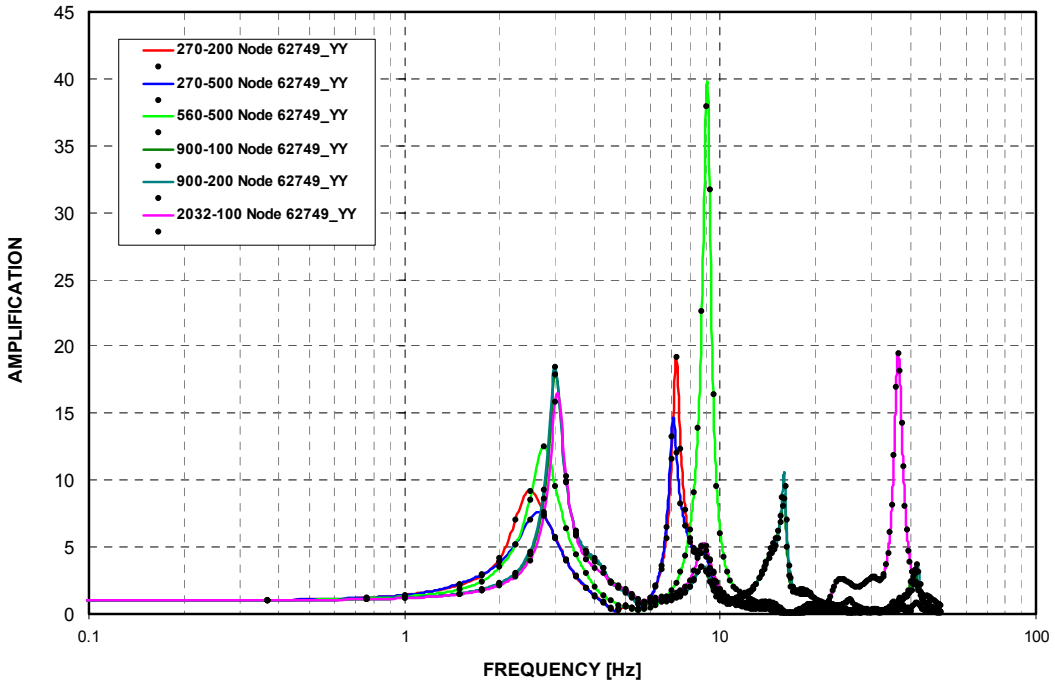

Figure 3-C.1.0-98 Top of PCCV - Cracked - EW Direction (Y)

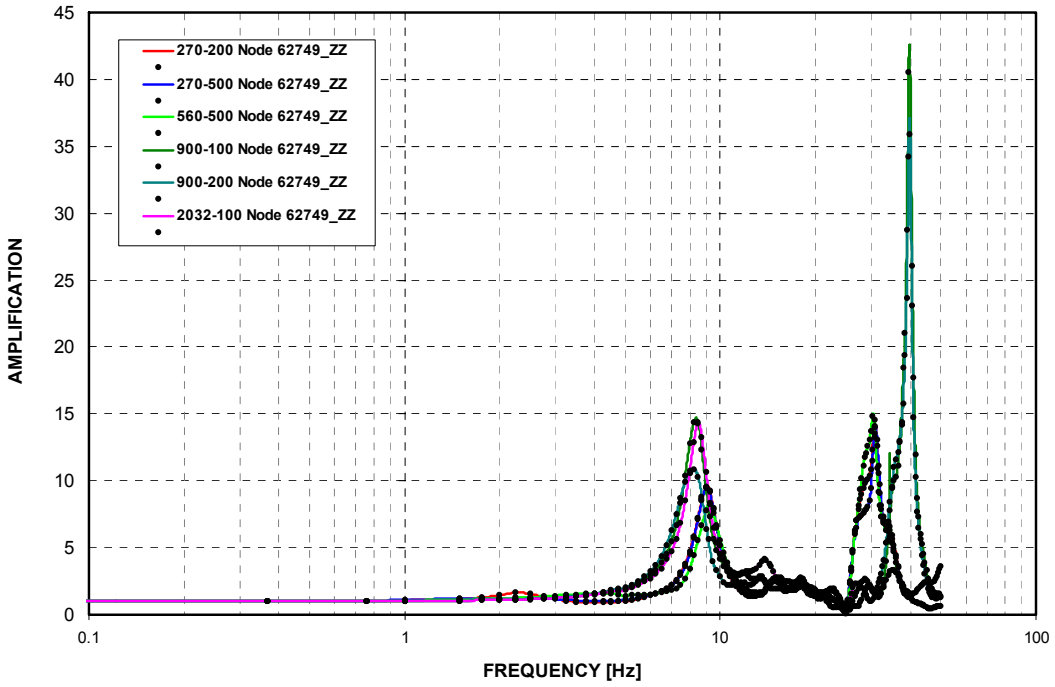

Figure 3-C.1.0-99 Top of PCCV - Cracked - Vertical Direction (Z)

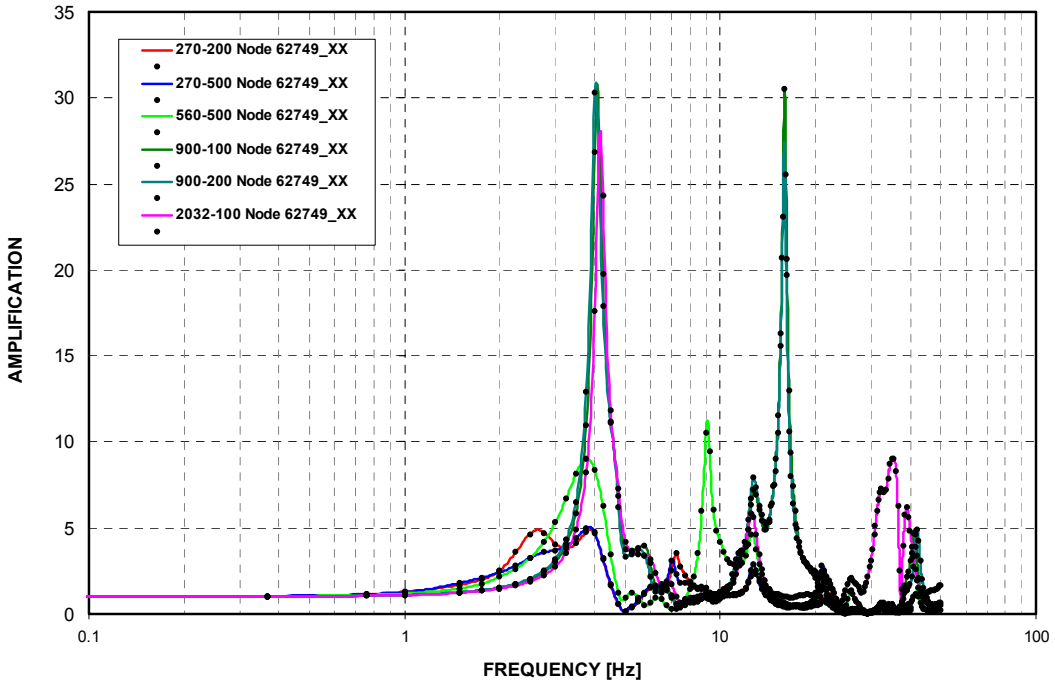

Figure 3-C.1.0-100 Top of PCCV - Uncracked - NS Direction (X)

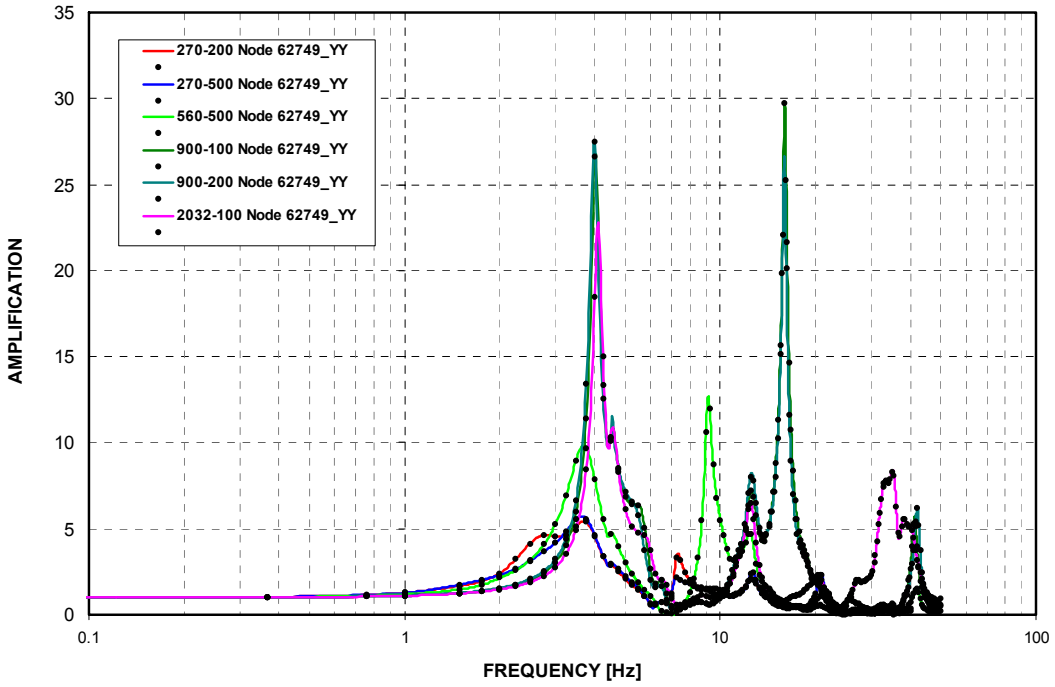

Figure 3-C.1.0-101 Top of PCCV - Uncracked - EW Direction (Y)

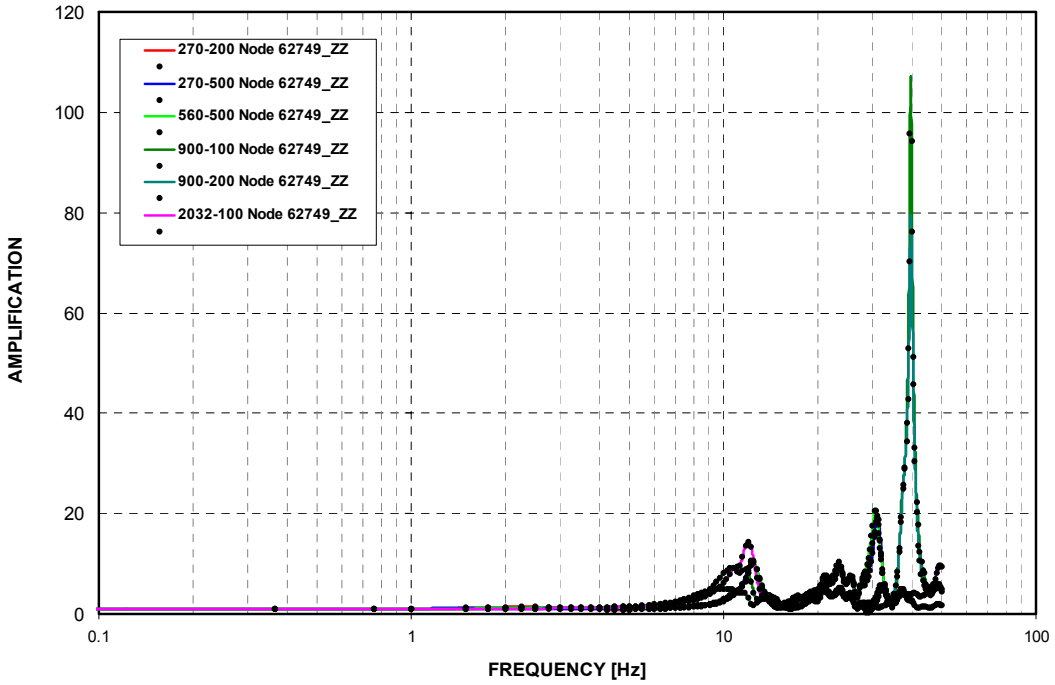

Figure 3-C.1.0-102 Top of PCCV - Uncracked - Vertical Direction (Z)

3-C.2.0 SSSI TRANSFER FUNCTION PLOTS

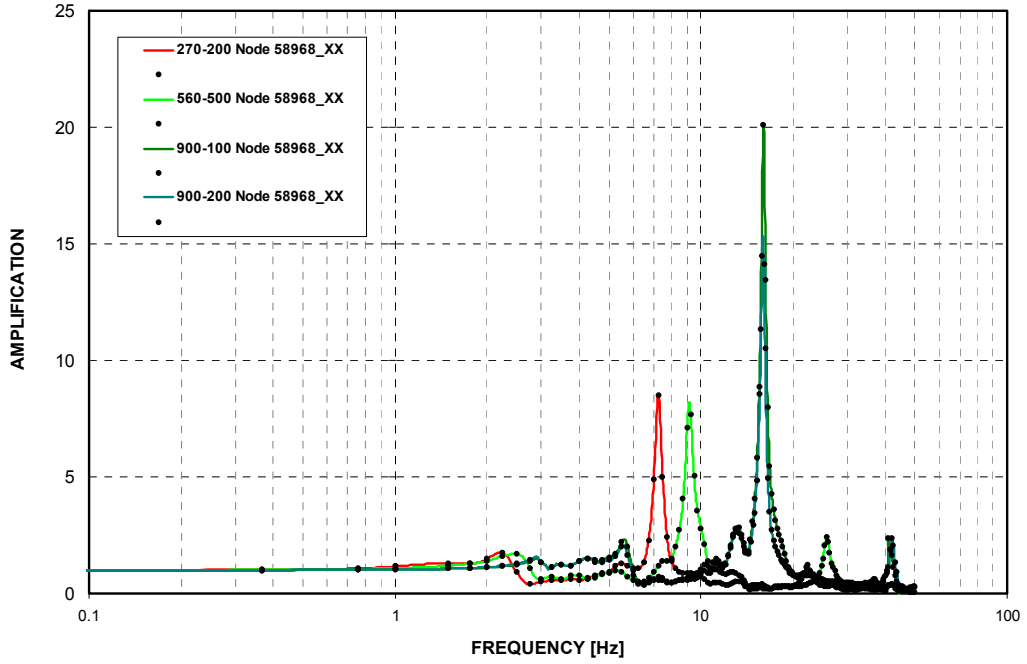

Figure 3-C.2.0-1 Top of Reactor Cavity - Cracked – NS Direction (X)

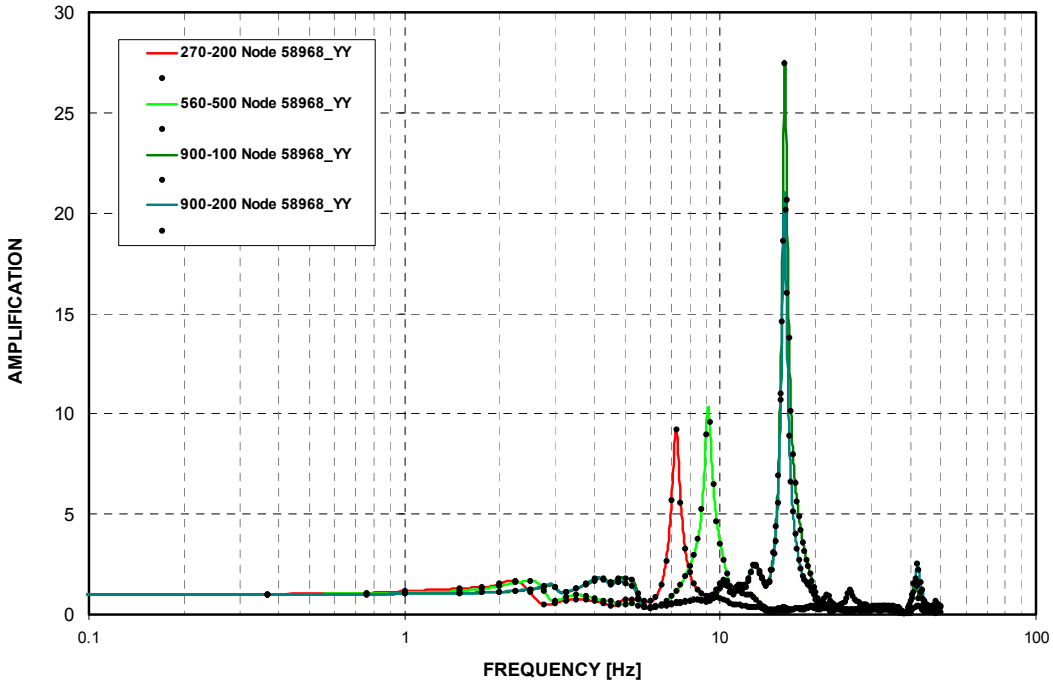

Figure 3-C.2.0-2 Top of Reactor Cavity - Cracked - EW Direction (Y)

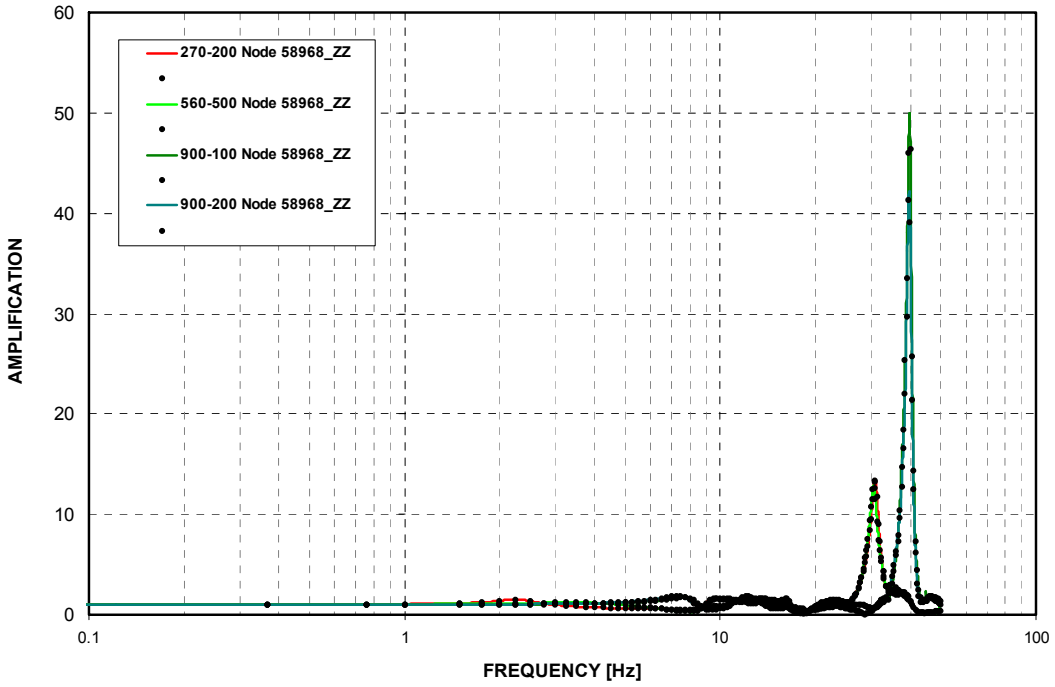

Figure 3-C.2.0-3 Top of Reactor Cavity - Cracked - Vertical Direction (Z)

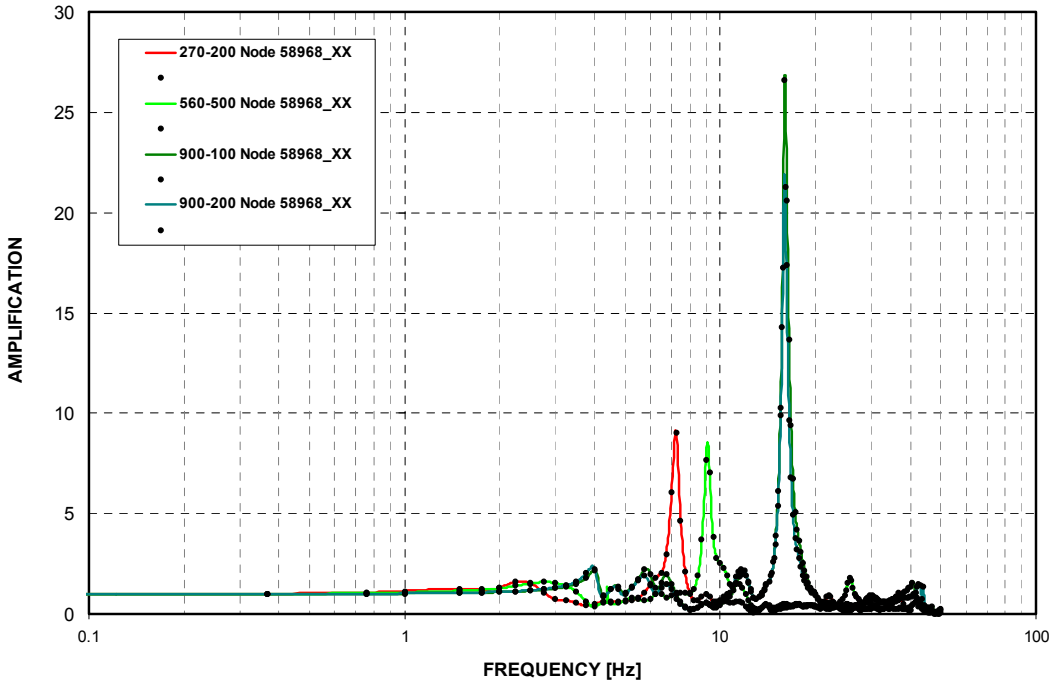

Figure 3-C.2.0-4 Top of Reactor Cavity - Uncracked - NS Direction (X)

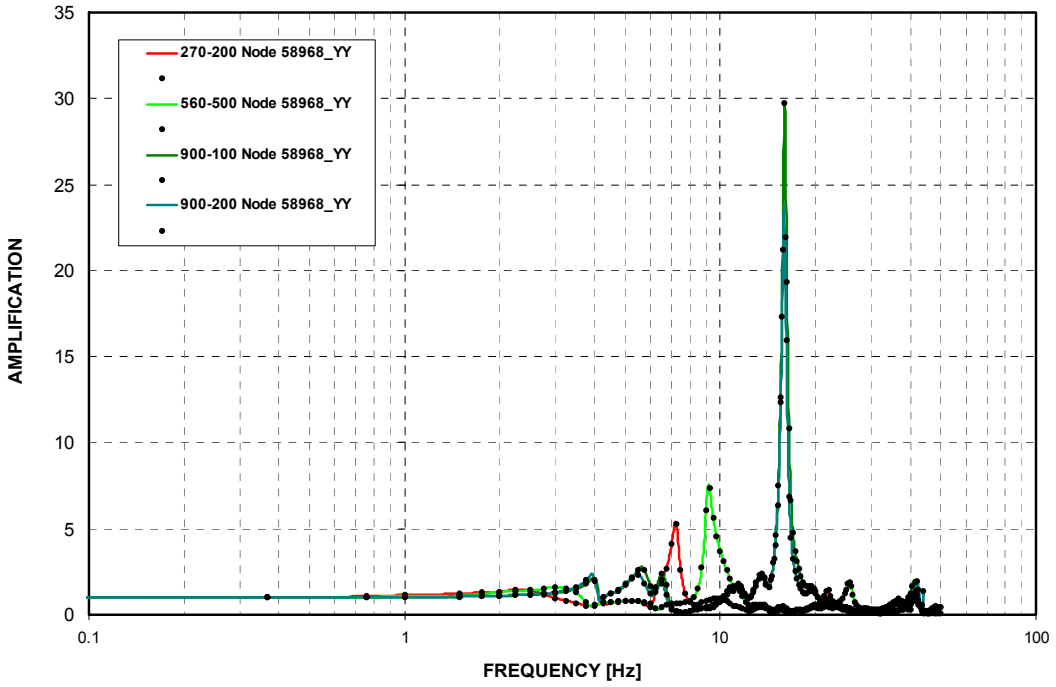

Figure 3-C.2.0-5 Top of Reactor Cavity - Uncracked - EW Direction (Y)

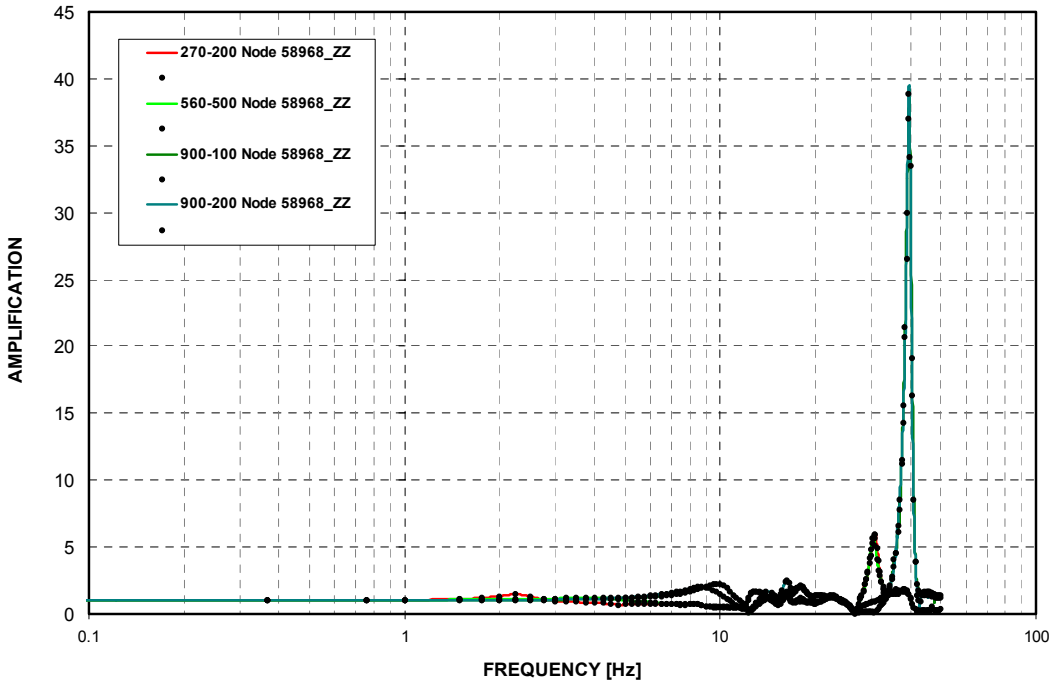

Figure 3-C.2.0-6 Top of Reactor Cavity - Uncracked - Vertical Direction (Z)

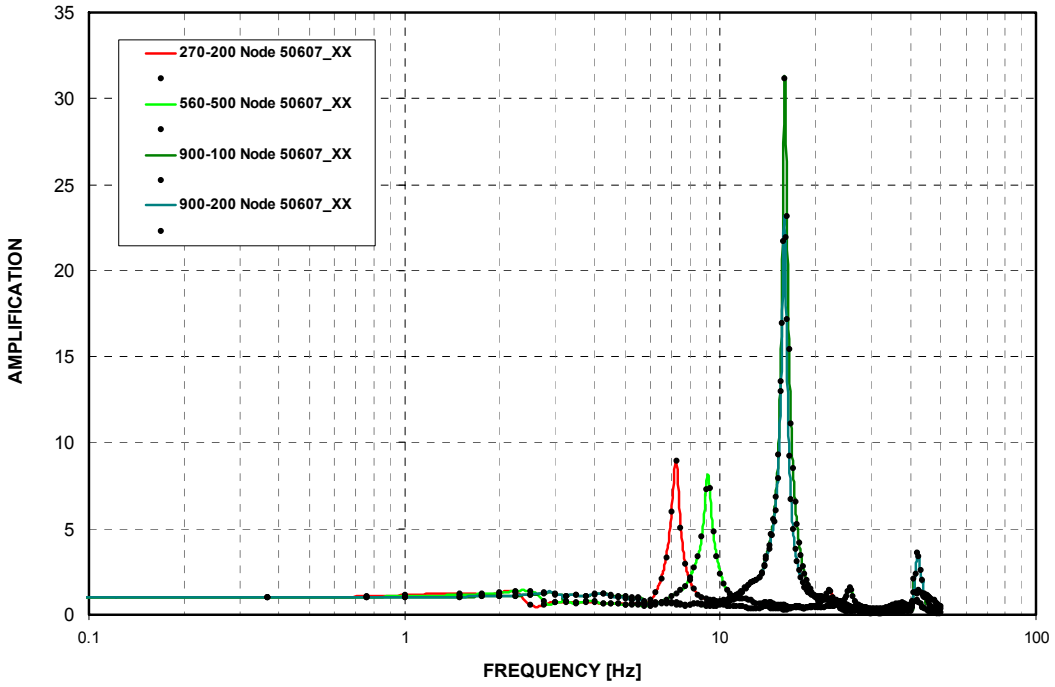

Figure 3-C.2.0-7 Sump Strainer Supports - Cracked - NS Direction (X)

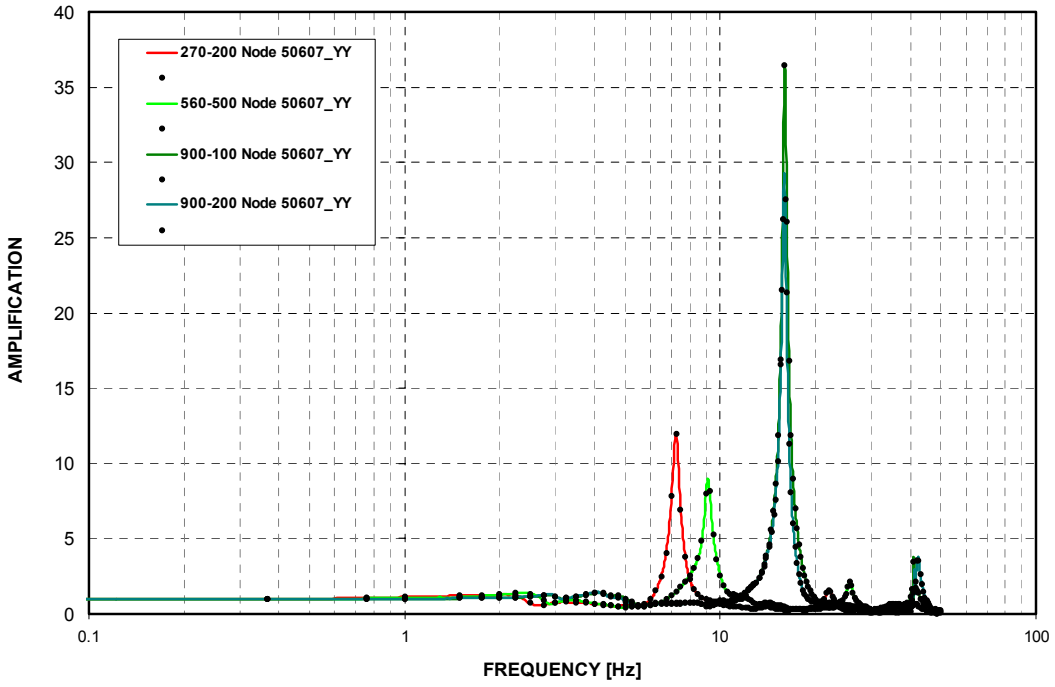

Figure 3-C.2.0-8 Sump Strainer Supports - Cracked - EW Direction (Y)

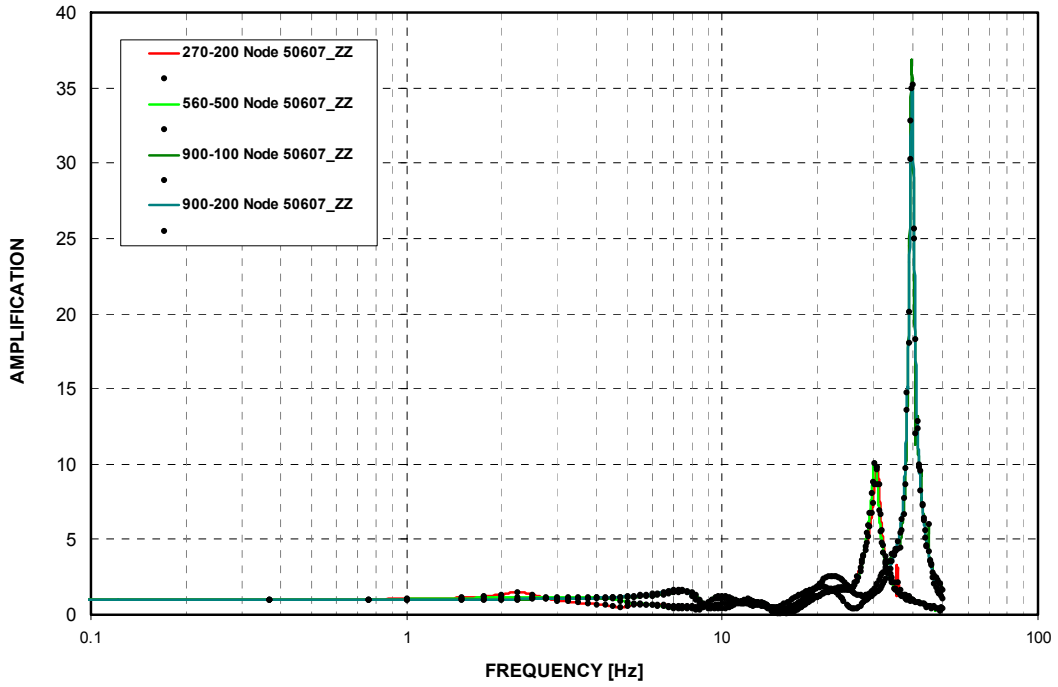

Figure 3-C.2.0-9 Sump Strainer Supports - Cracked - Vertical Direction (Z)

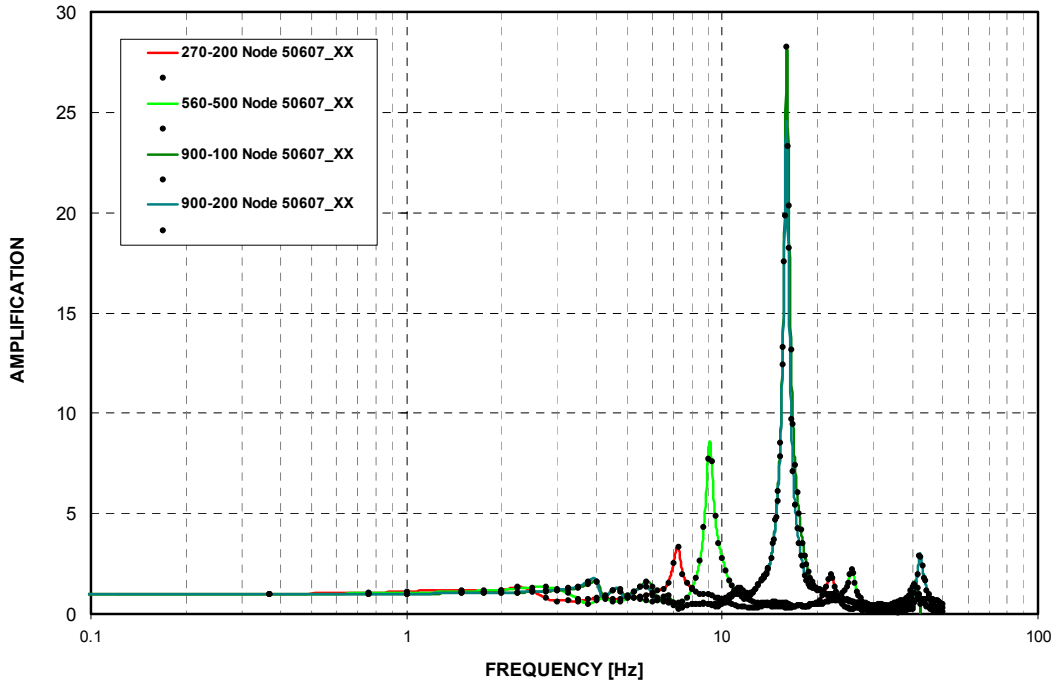

Figure 3-C.2.0-10 Sump Strainer Supports - Uncracked - NS Direction (X)

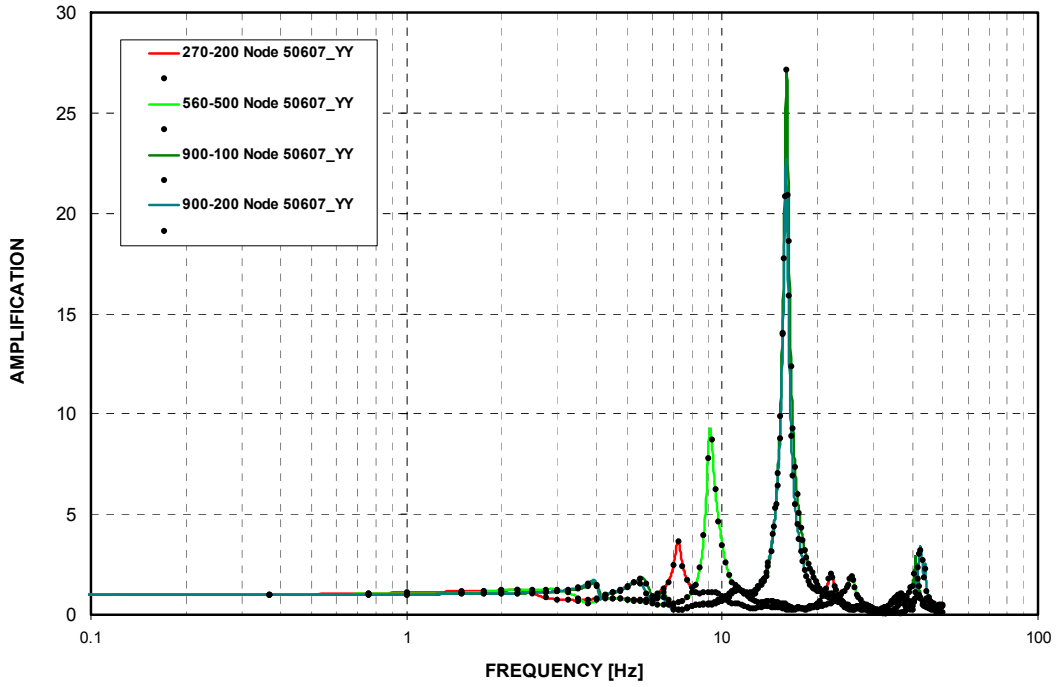

Figure 3-C.2.0-11 Sump Strainer Supports - Uncracked - EW Direction (Y)

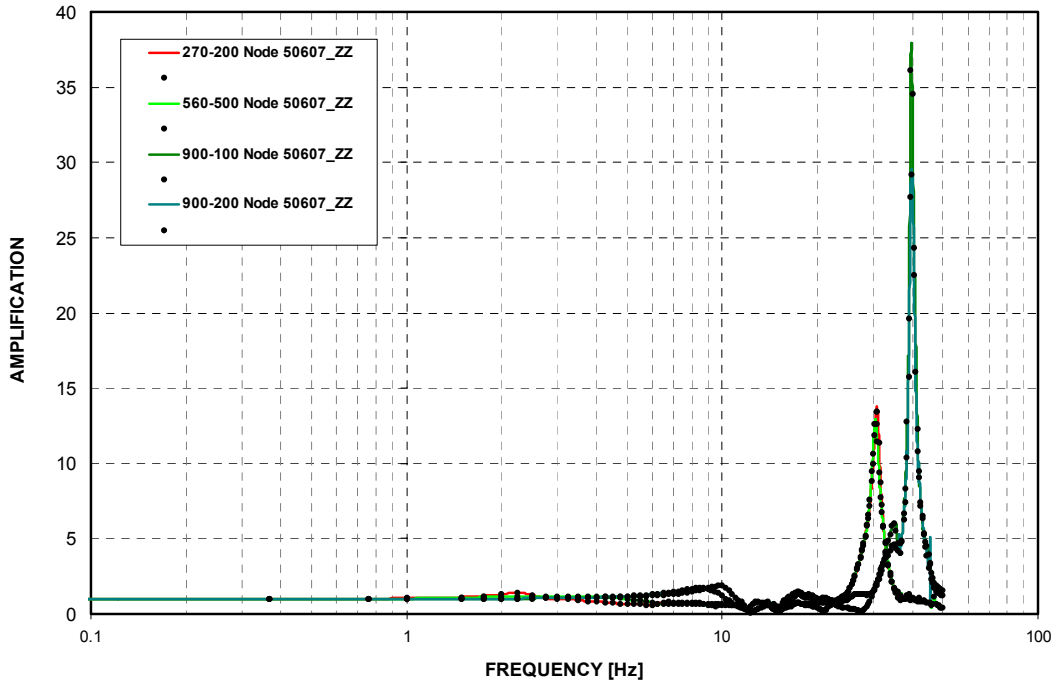

Figure 3-C.2.0-12 Sump Strainer Supports - Uncracked - Vertical Direction (Z)

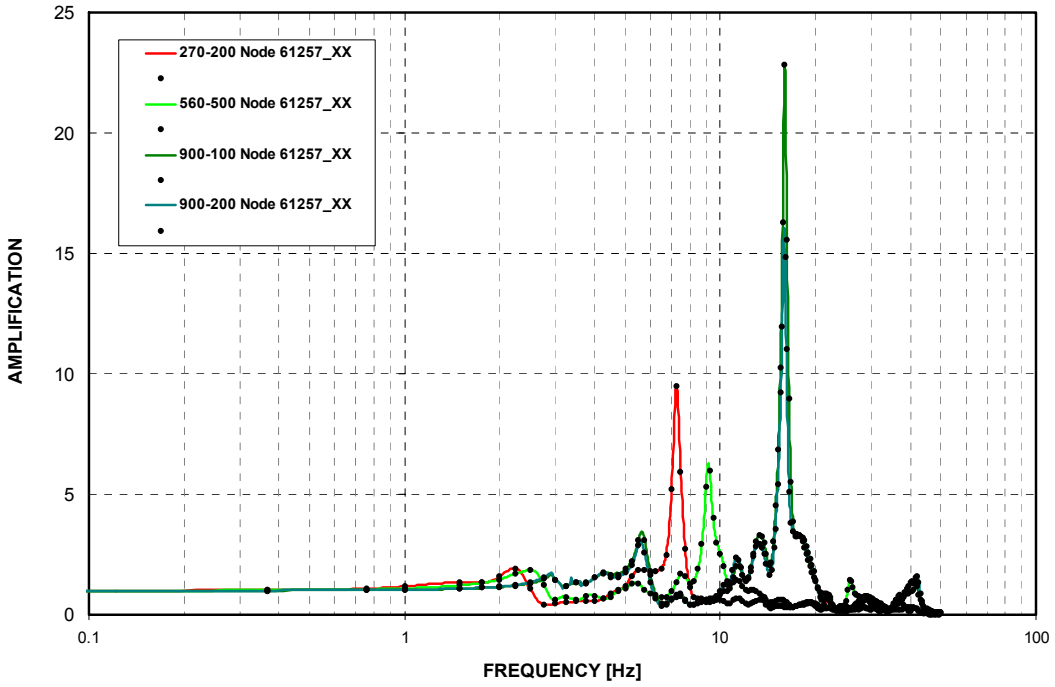

Figure 3-C.2.0-13 SG Lower Supports - Cracked - NS Direction (X)

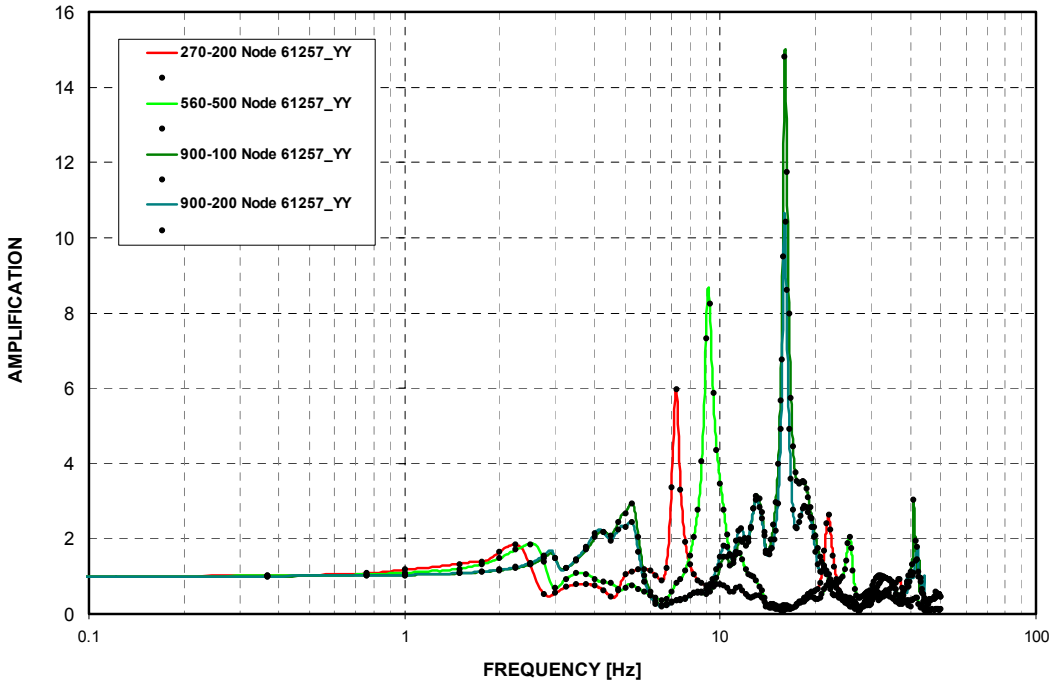

Figure 3-C.2.0-14 SG Lower Supports - Cracked - EW Direction (Y)

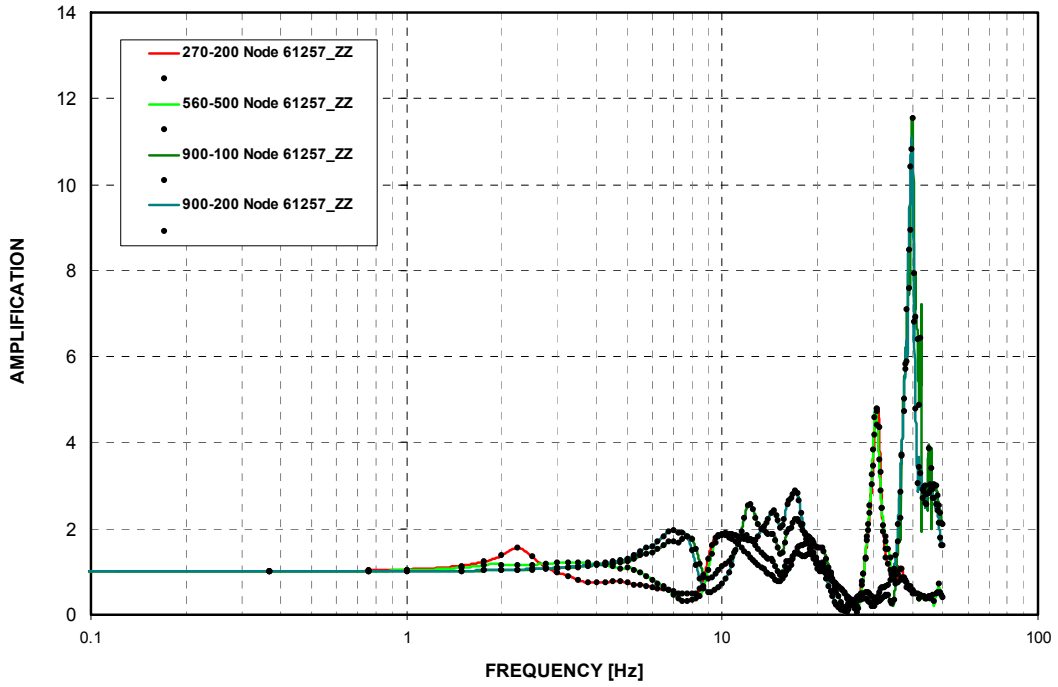

Figure 3-C.2.0-15 SG Lower Supports - Cracked - Vertical Direction (Z)

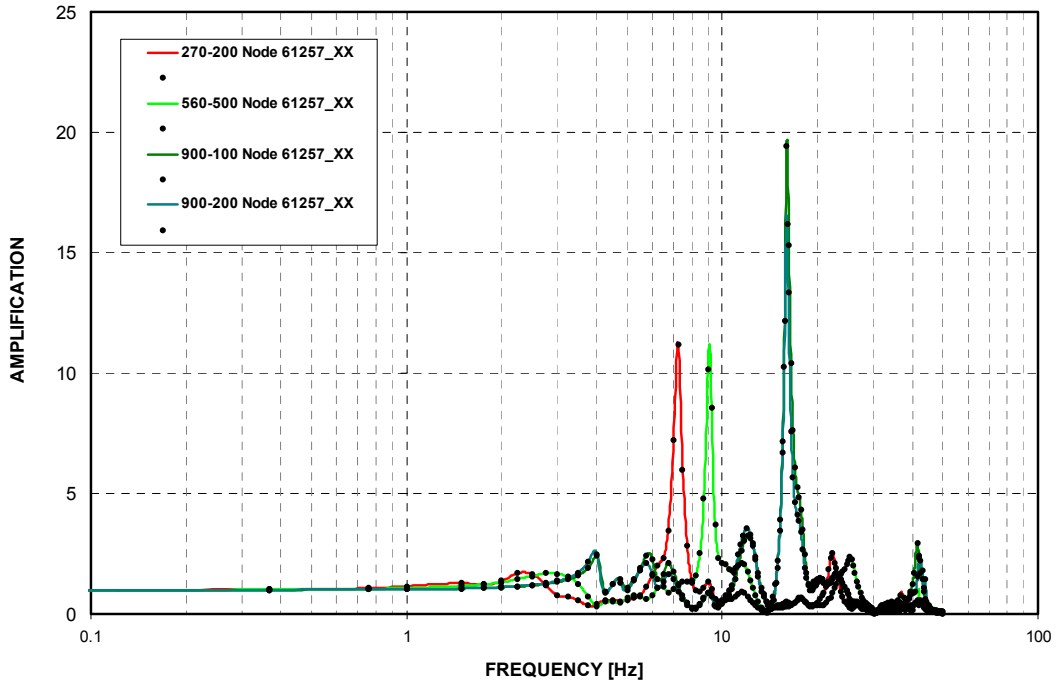

Figure 3-C.2.0-16 SG Lower Supports - Uncracked - NS Direction (X)

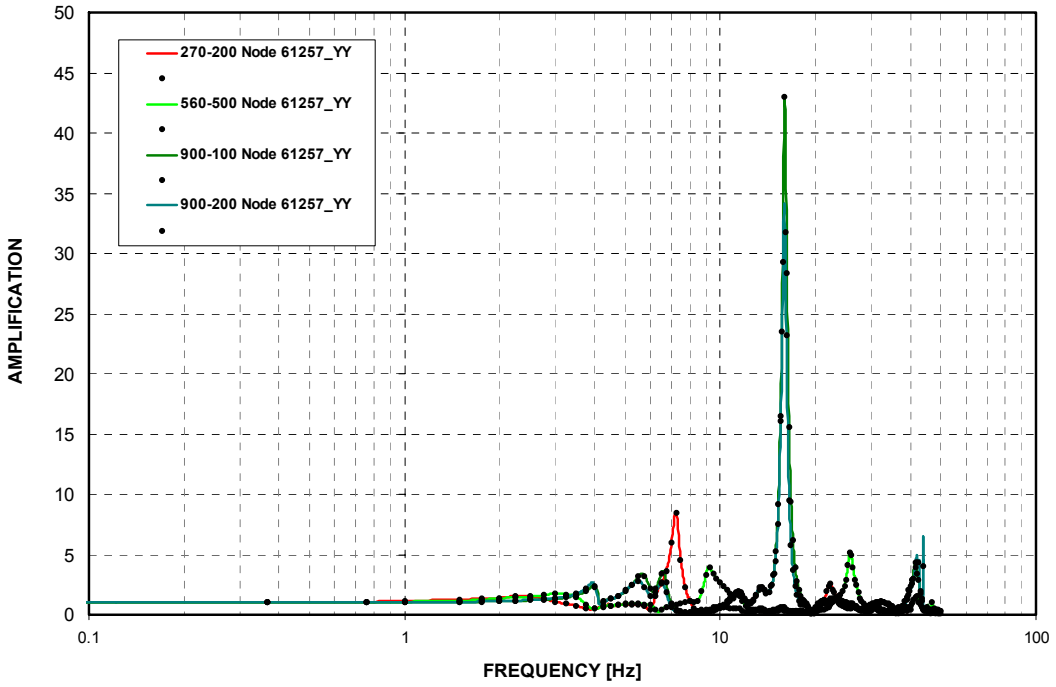

Figure 3-C.2.0-17 SG Lower Supports - Uncracked - EW Direction (Y)

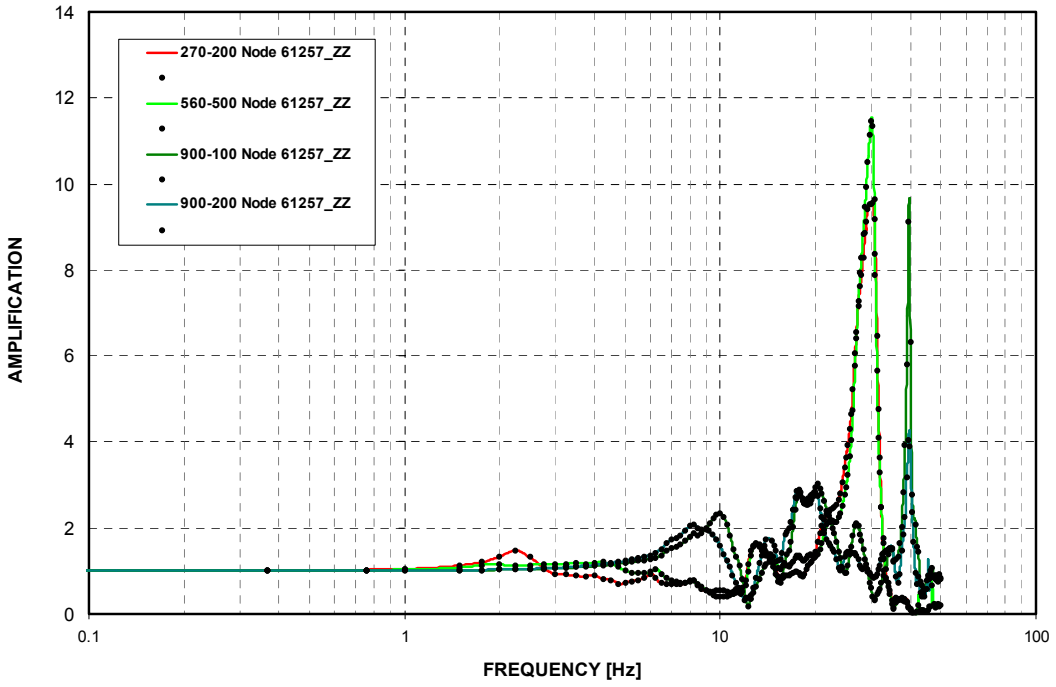

Figure 3-C.2.0-18 SG Lower Supports - Uncracked - Vertical Direction (Z)

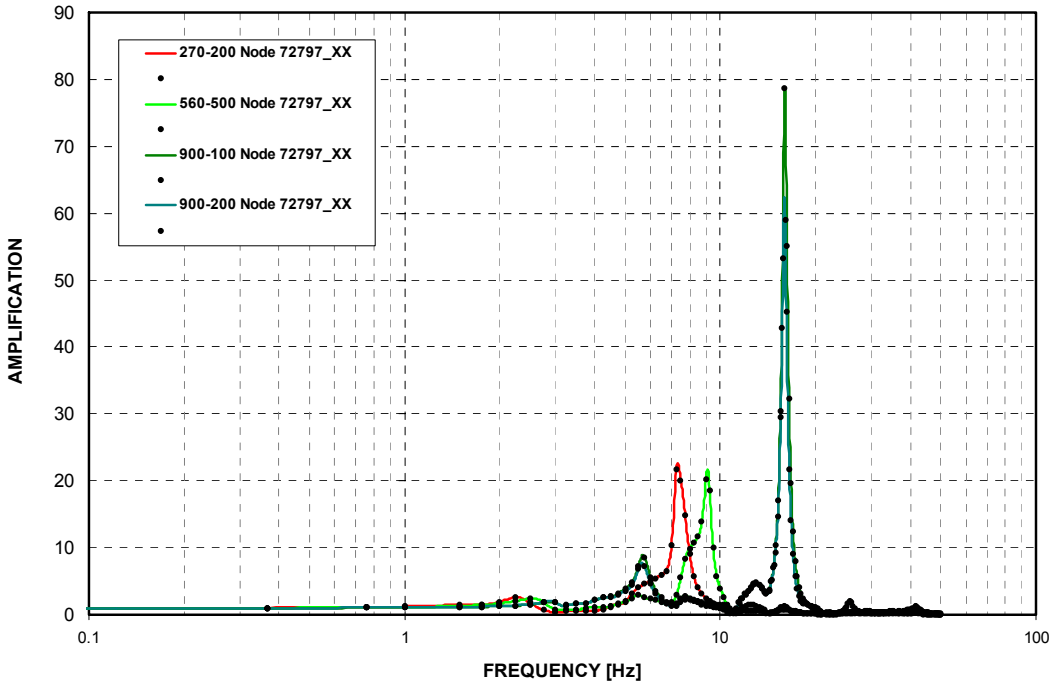

Figure 3-C.2.0-19 SG Upper Supports - Cracked - NS Direction (X)

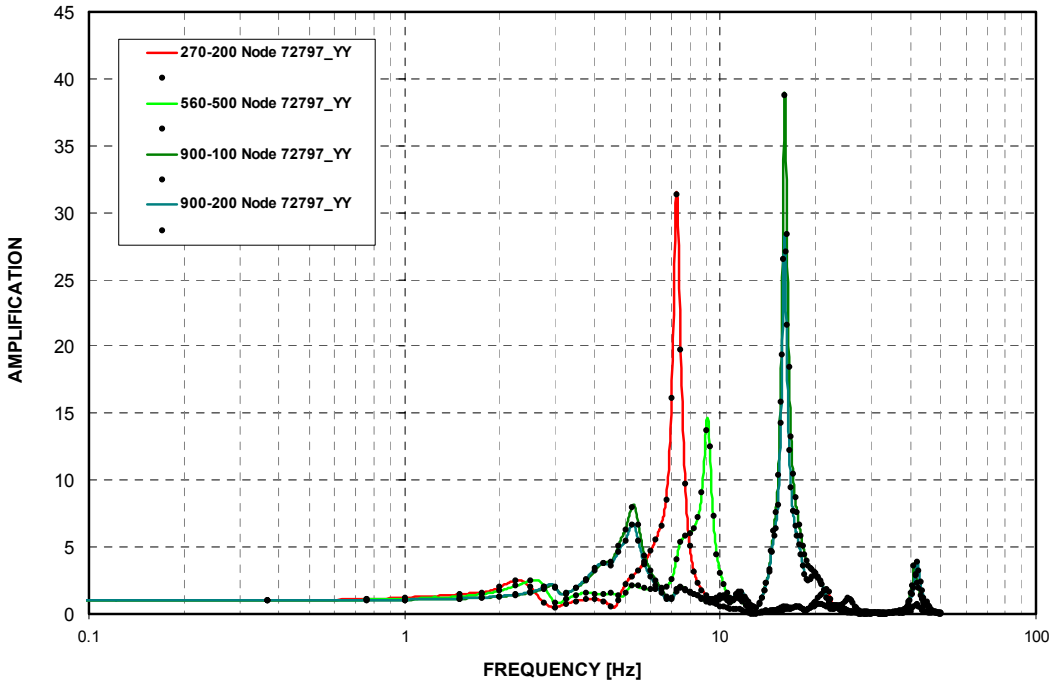

Figure 3-C.2.0-20 SG Upper Supports - Cracked - EW Direction (Y)

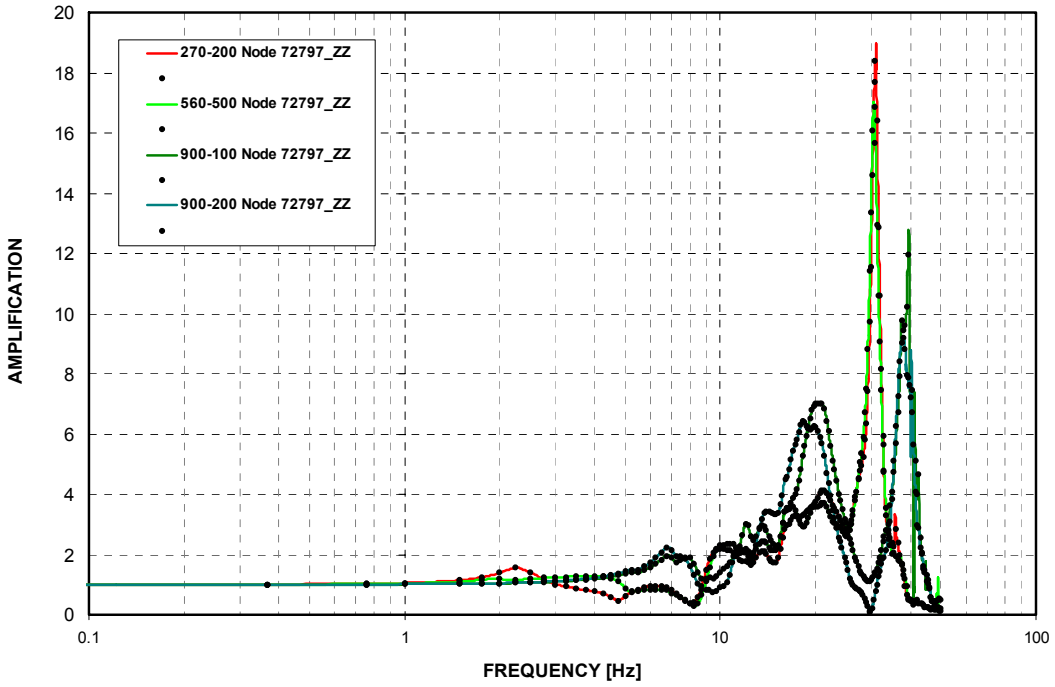

Figure 3-C.2.0-21 SG Upper Supports - Cracked - Vertical Direction (Z)

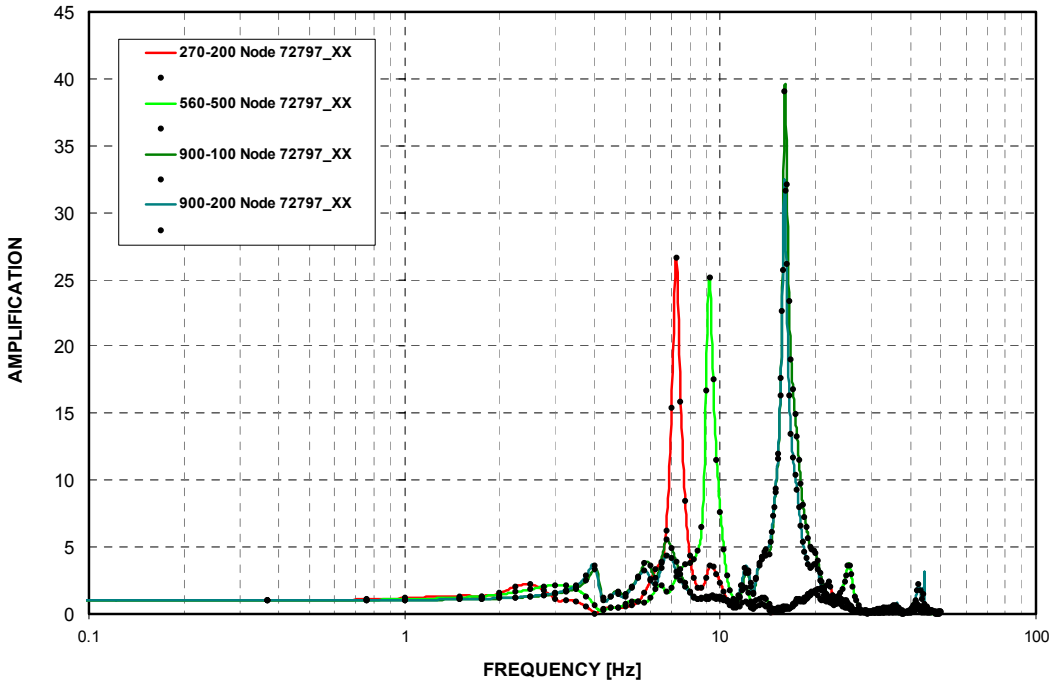

Figure 3-C.2.0-22 SG Upper Supports - Uncracked - NS Direction (X)

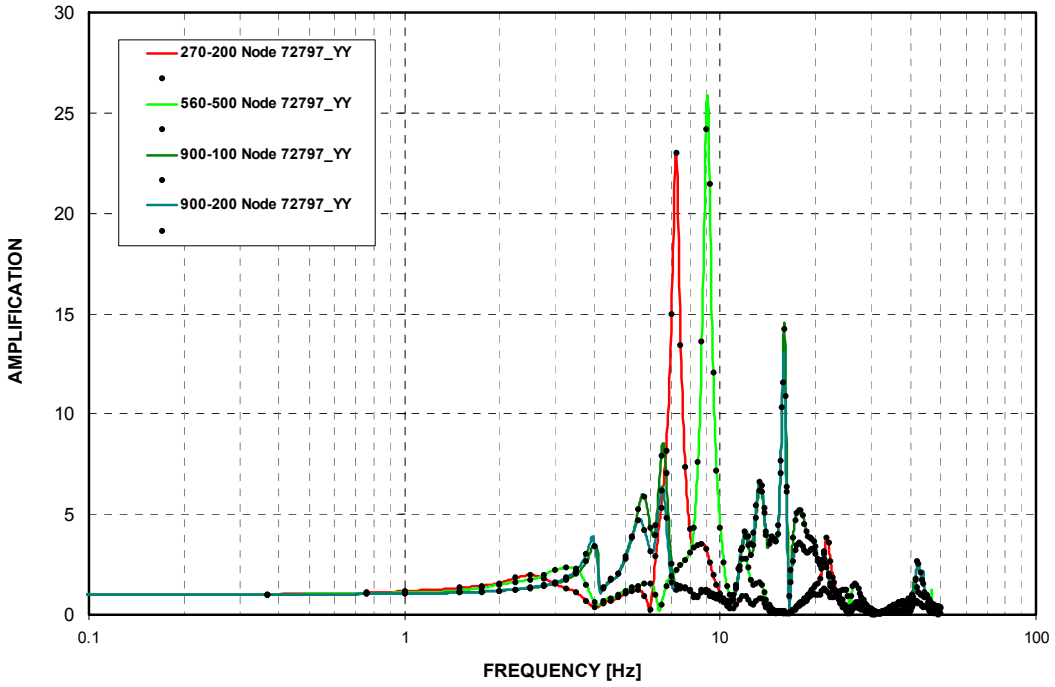

Figure 3-C.2.0-23 SG Upper Supports - Uncracked - EW Direction (Y)

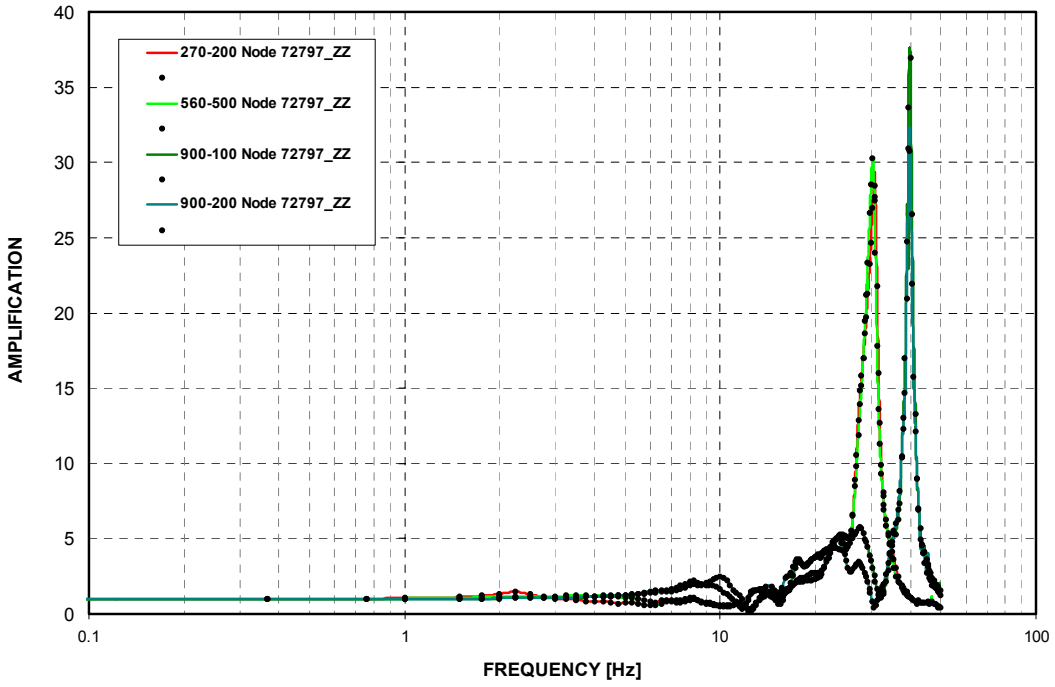

Figure 3-C.2.0-24 SG Upper Supports - Uncracked - Vertical Direction (Z)

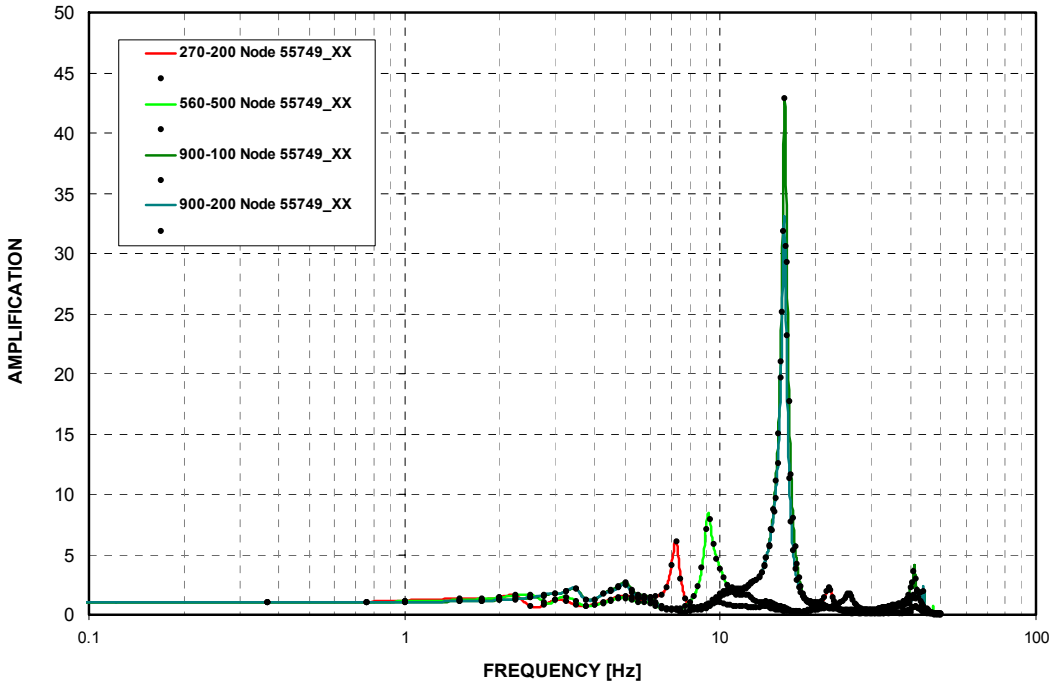

Figure 3-C.2.0-25 SFP - Cracked - NS Direction (X)

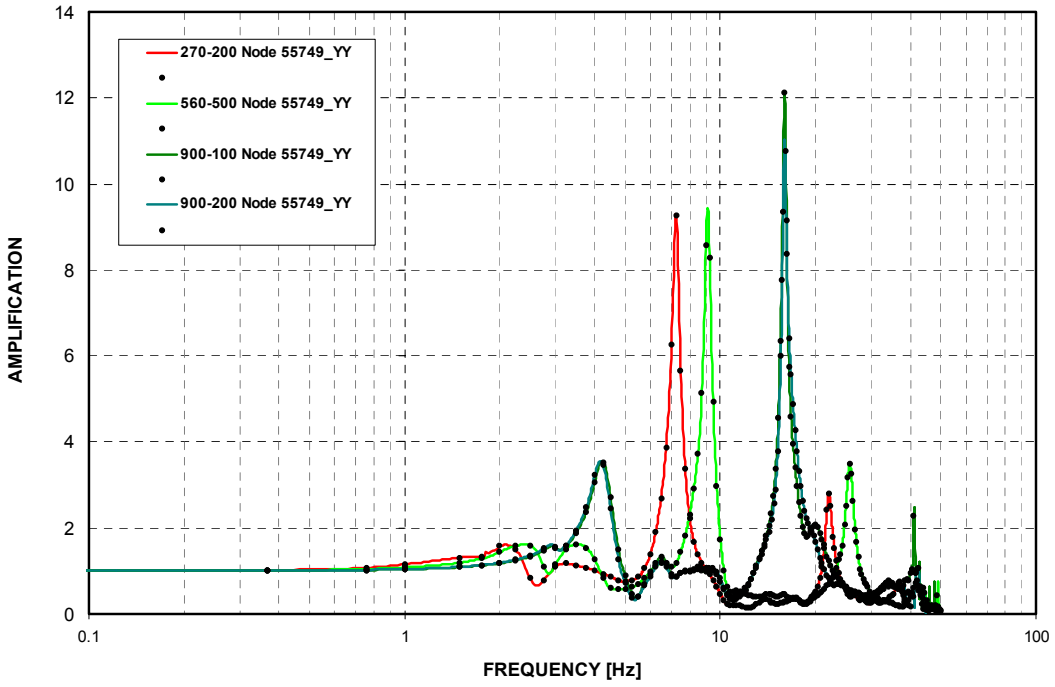

Figure 3-C.2.0-26 SFP - Cracked - EW Direction (Y)

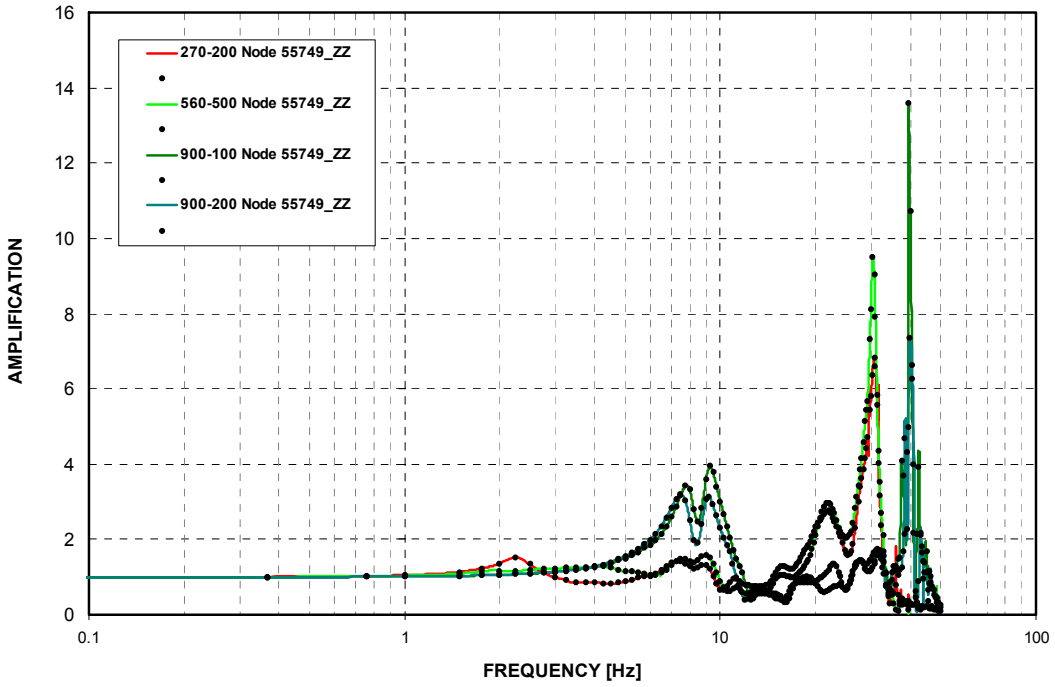

Figure 3-C.2.0-27 SFP - Cracked - Vertical Direction (Z)

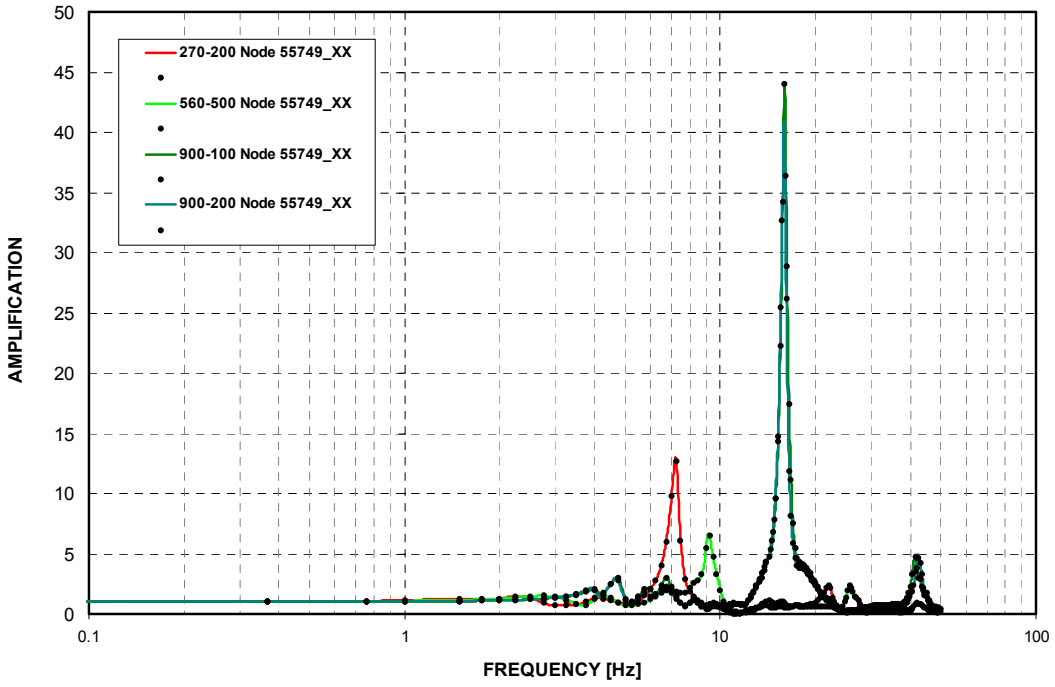

Figure 3-C.2.0-28 SFP - Uncracked - NS Direction (X)

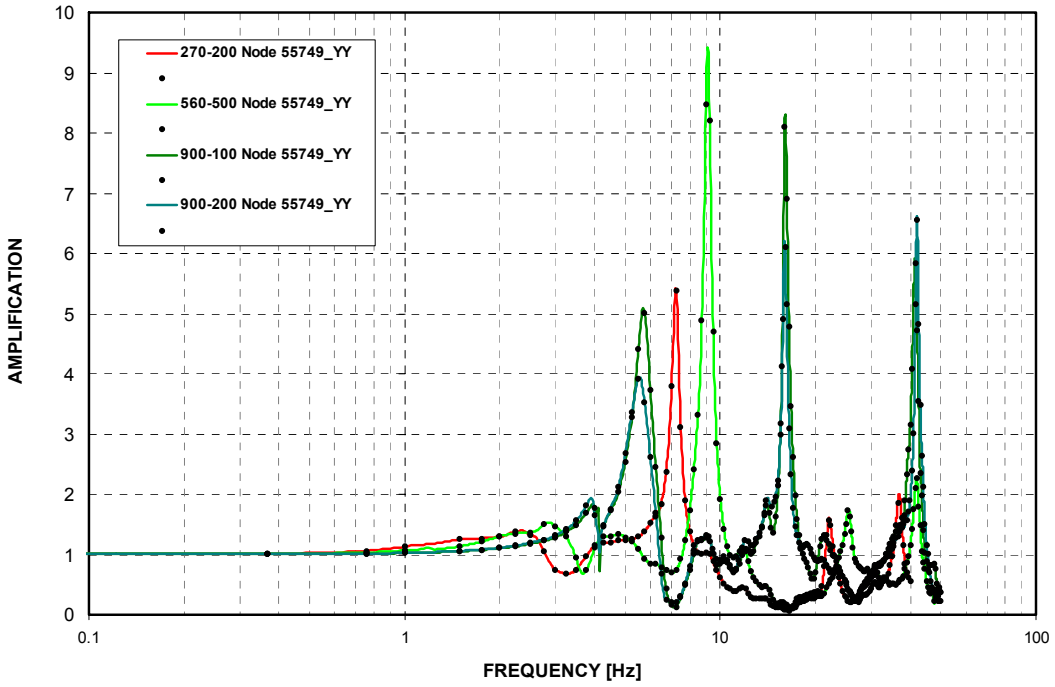

Figure 3-C.2.0-29 SFP - Uncracked - EW Direction (Y)

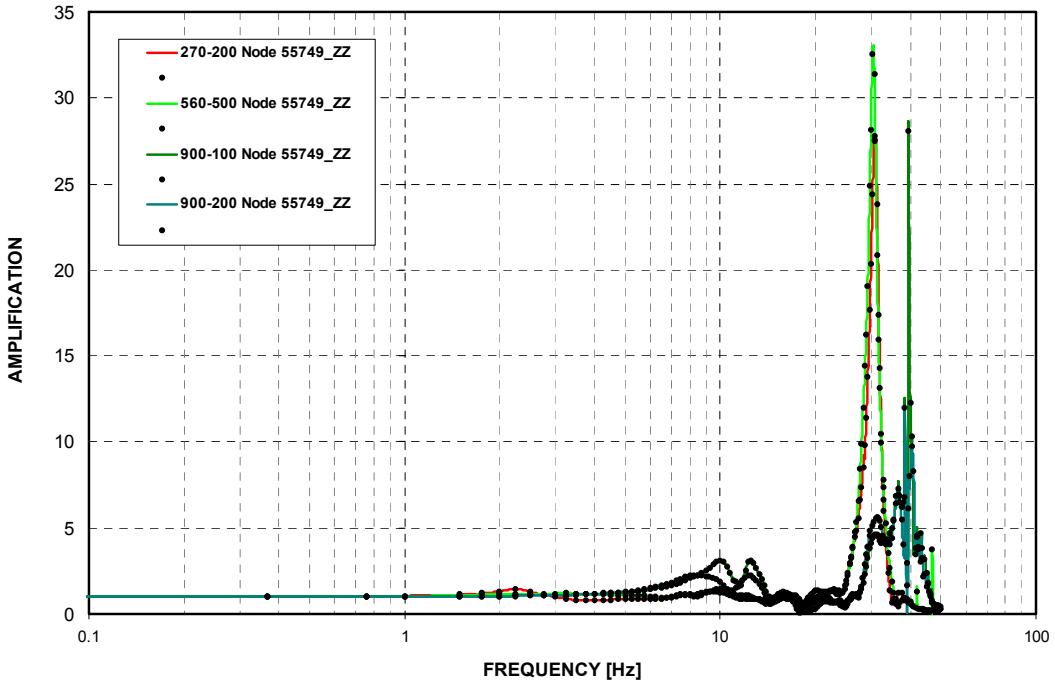

Figure 3-C.2.0-30 SFP - Uncracked - Vertical Direction (Z)

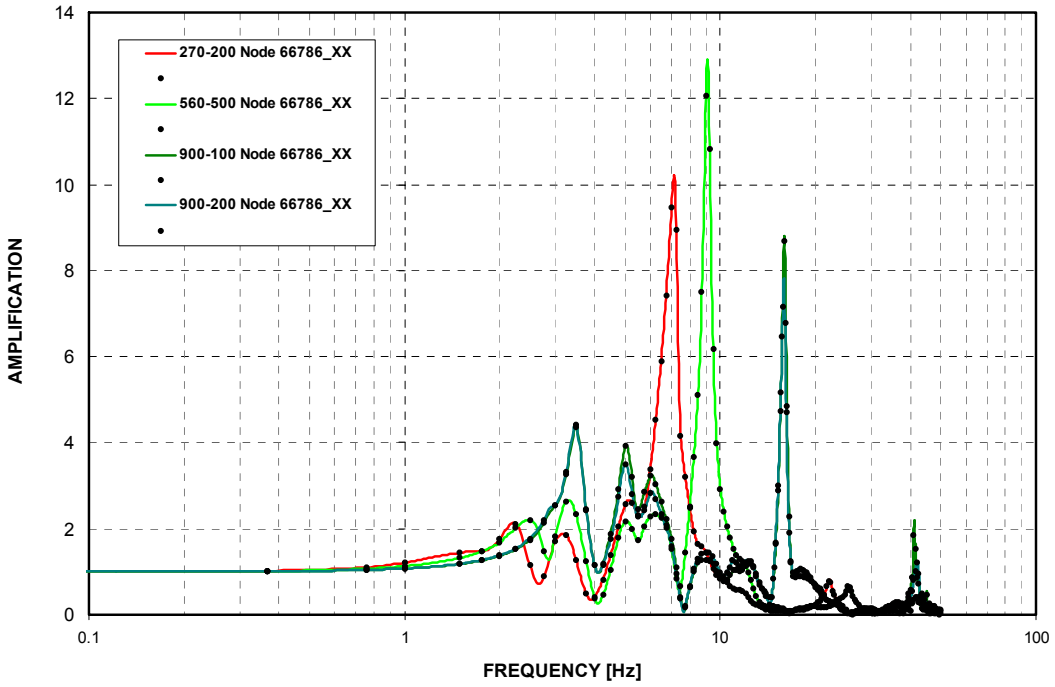

Figure 3-C.2.0-31 NFSP - Cracked - NS Direction (X)

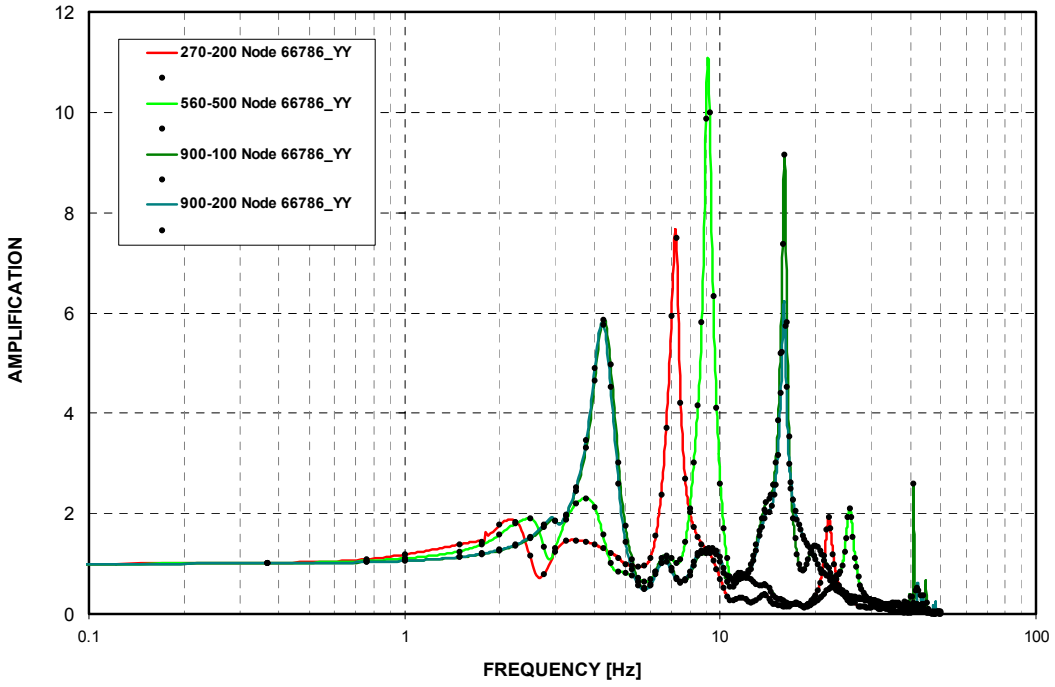

Figure 3-C.2.0-32 NFSP - Cracked - EW Direction (Y)

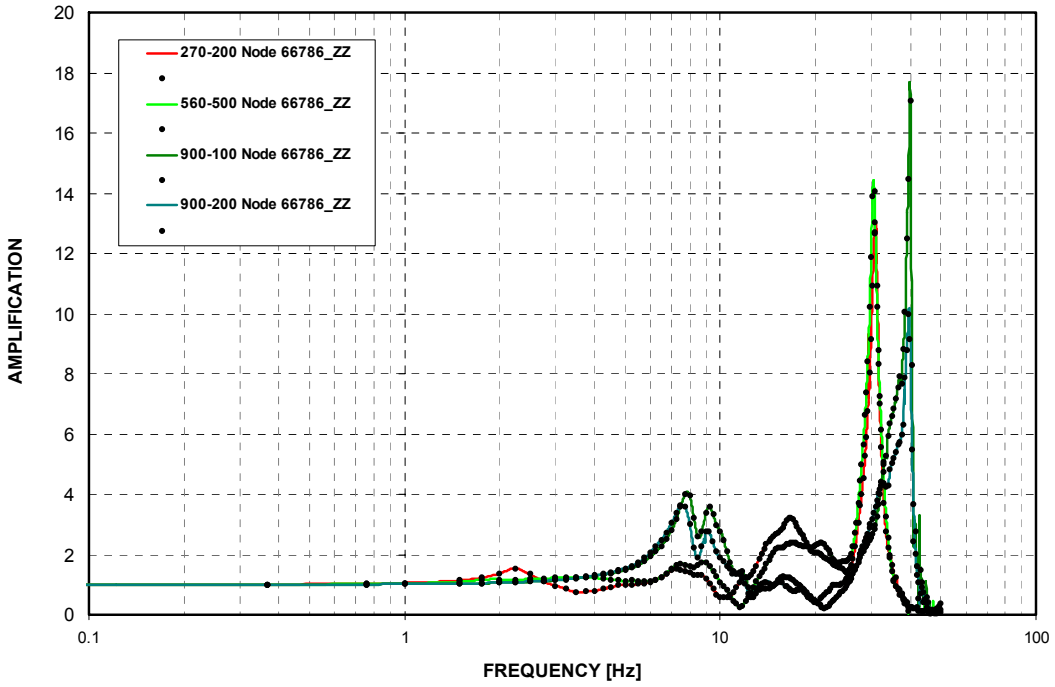

Figure 3-C.2.0-33 NFSP - Cracked - Vertical Direction (Z)

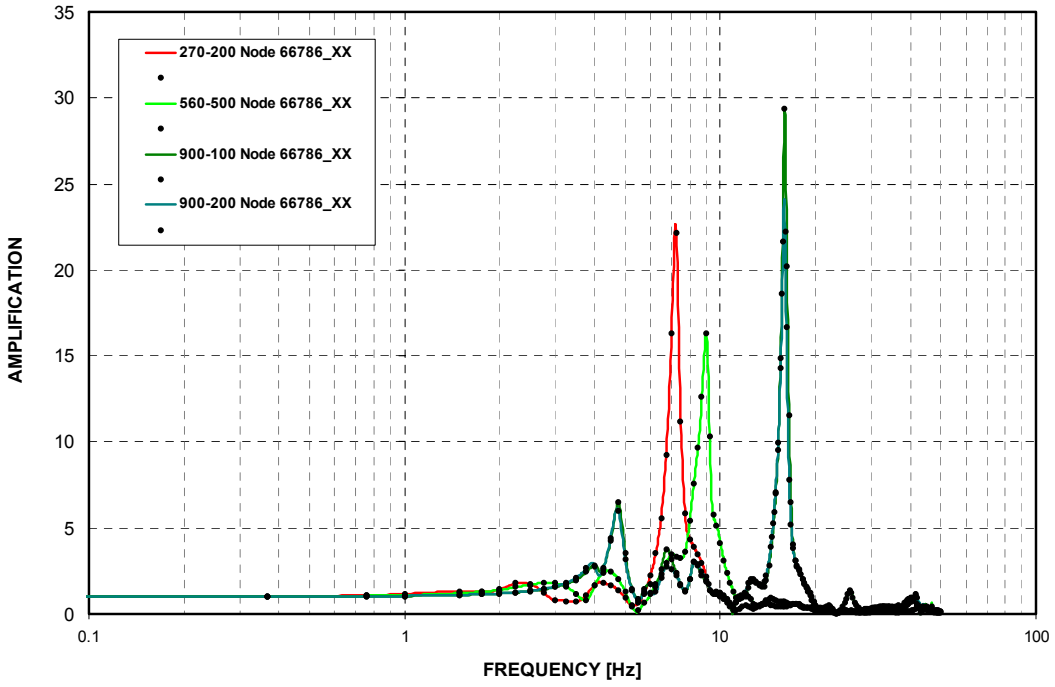

Figure 3-C.2.0-34 NFSP - Uncracked - NS Direction (X)

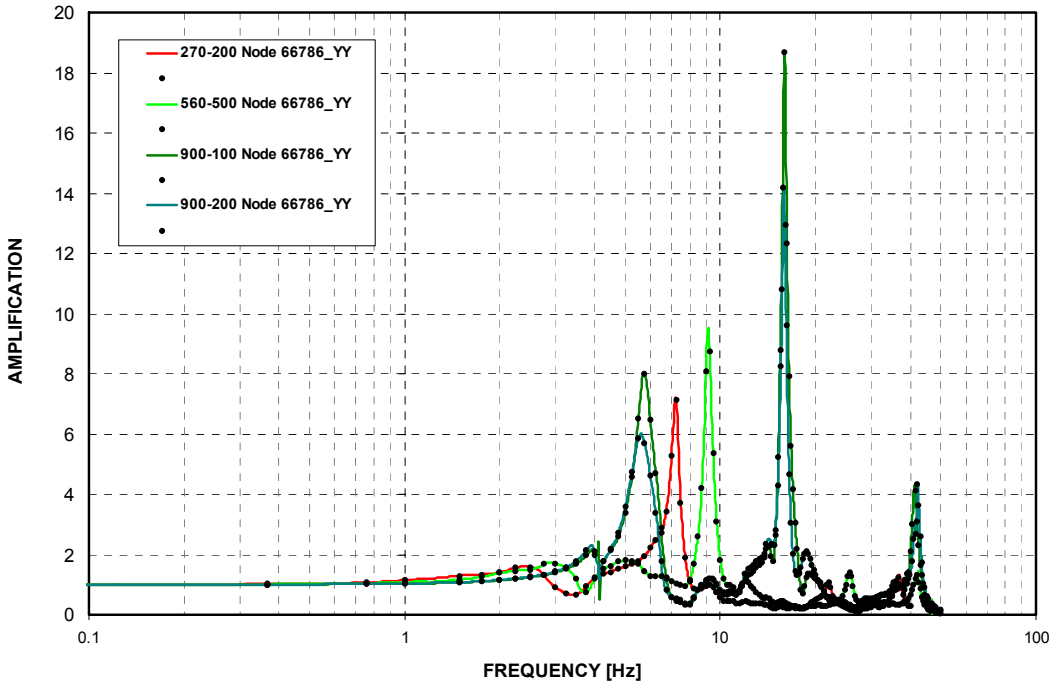

Figure 3-C.2.0-35 NFSP - Uncracked - EW Direction (Y)

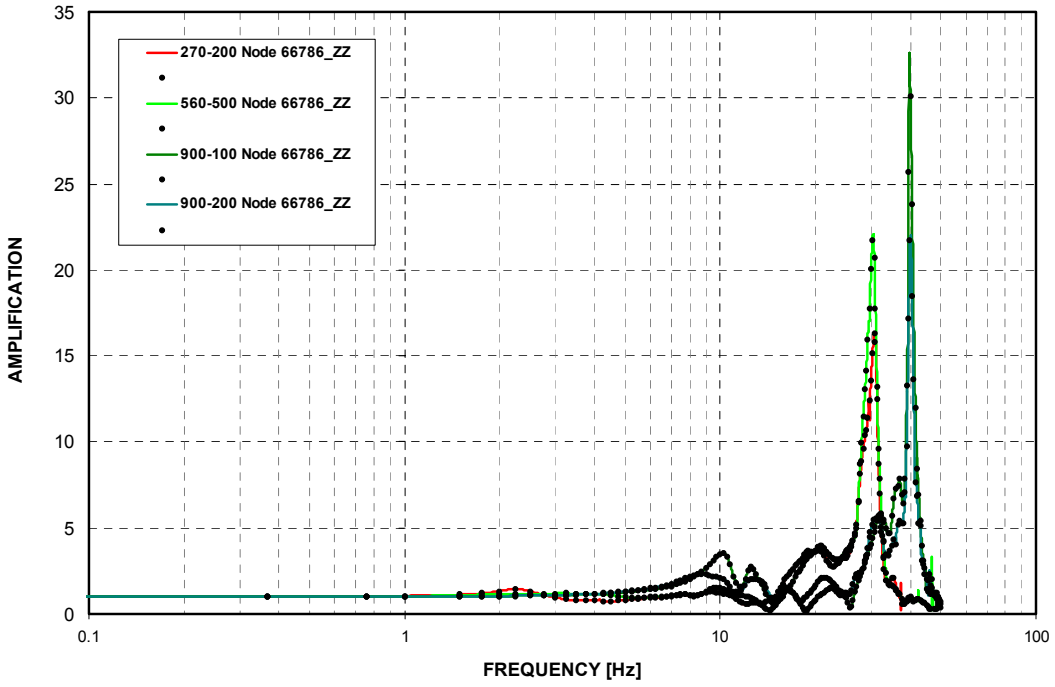

Figure 3-C.2.0-36 NFSP - Uncracked - Vertical Direction (Z)

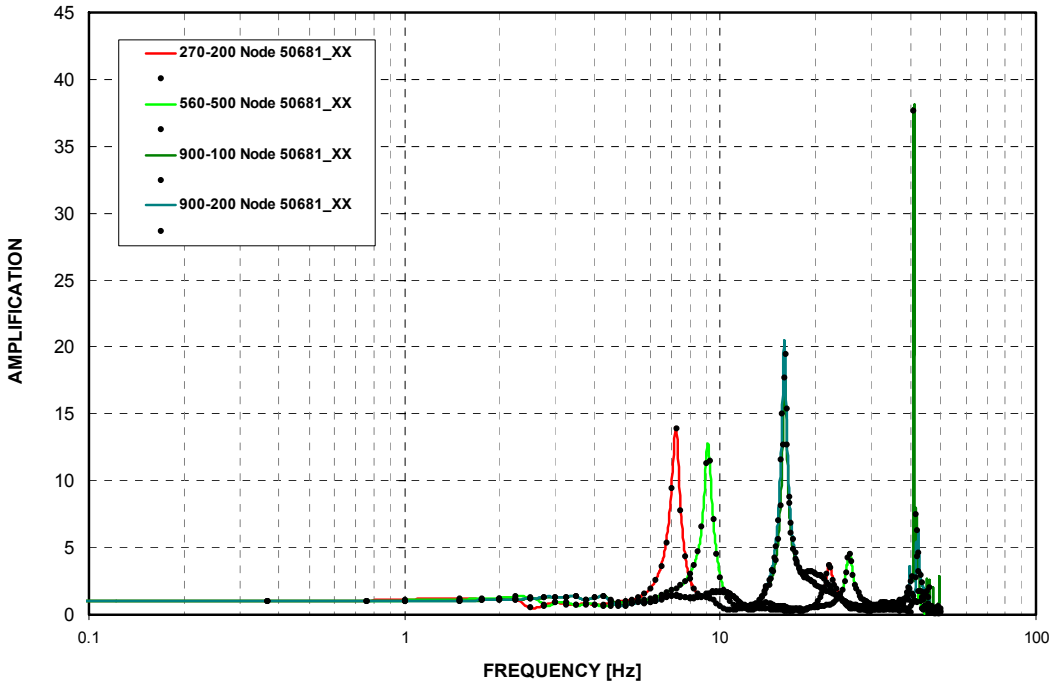

Figure 3-C.2.0-37 East PS/B A-AAC GTG - Cracked - NS Direction (X)

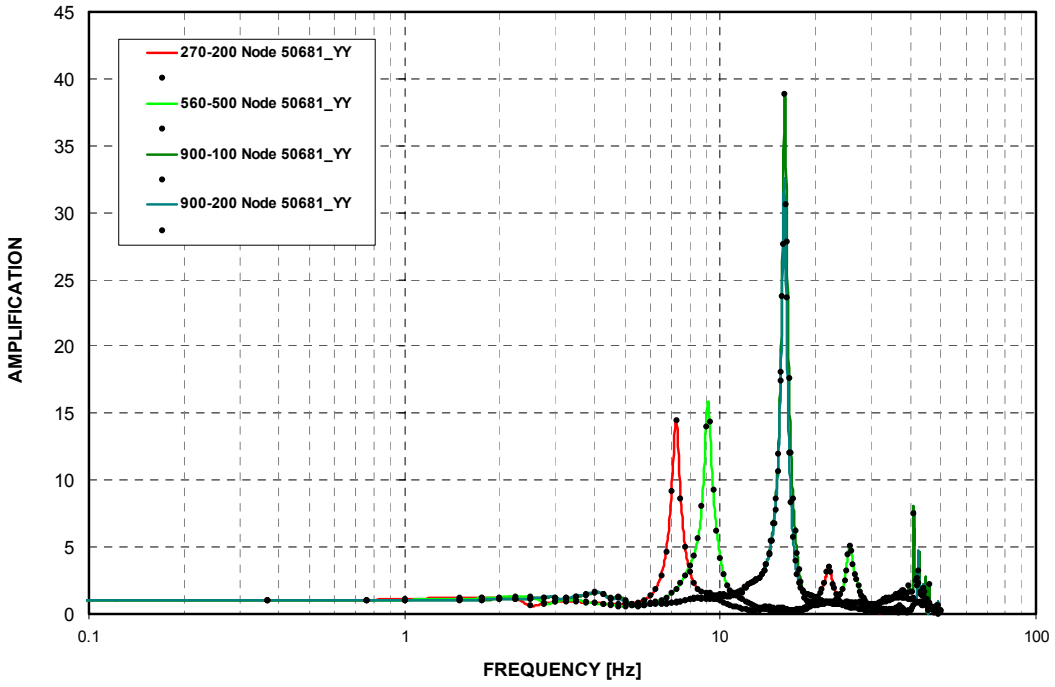

Figure 3-C.2.0-38 East PS/B A-AAC GTG - Cracked - EW Direction (Y)

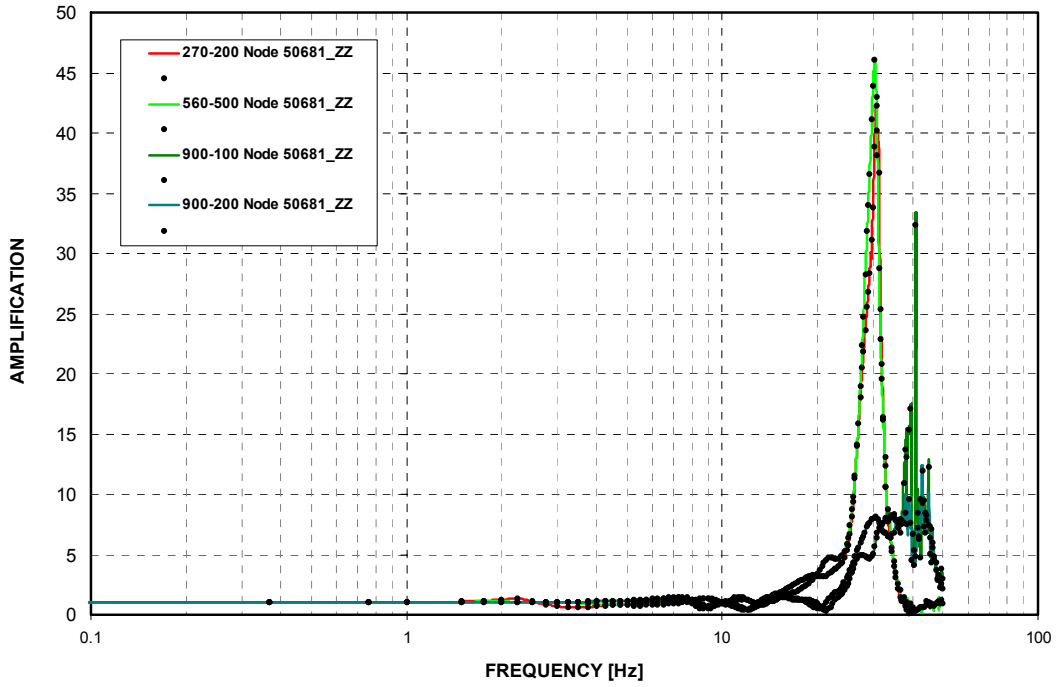

Figure 3-C.2.0-39 East PS/B A-AAC GTG - Cracked - Vertical Direction (Z)

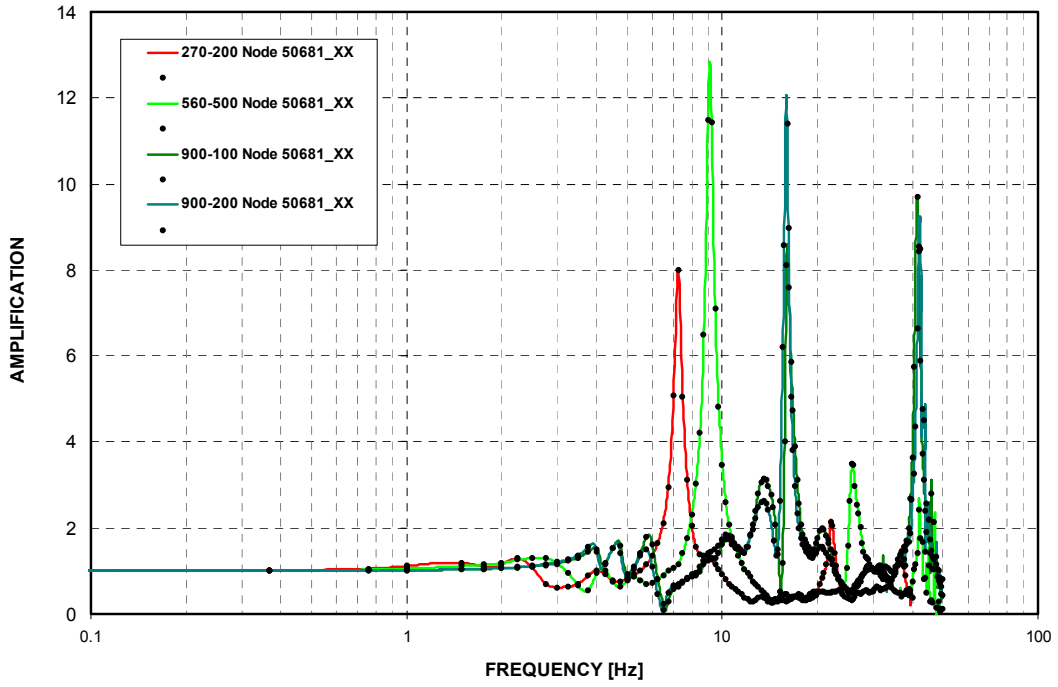

Figure 3-C.2.0-40 East PS/B A-AAC GTG - Uncracked - NS Direction (X)

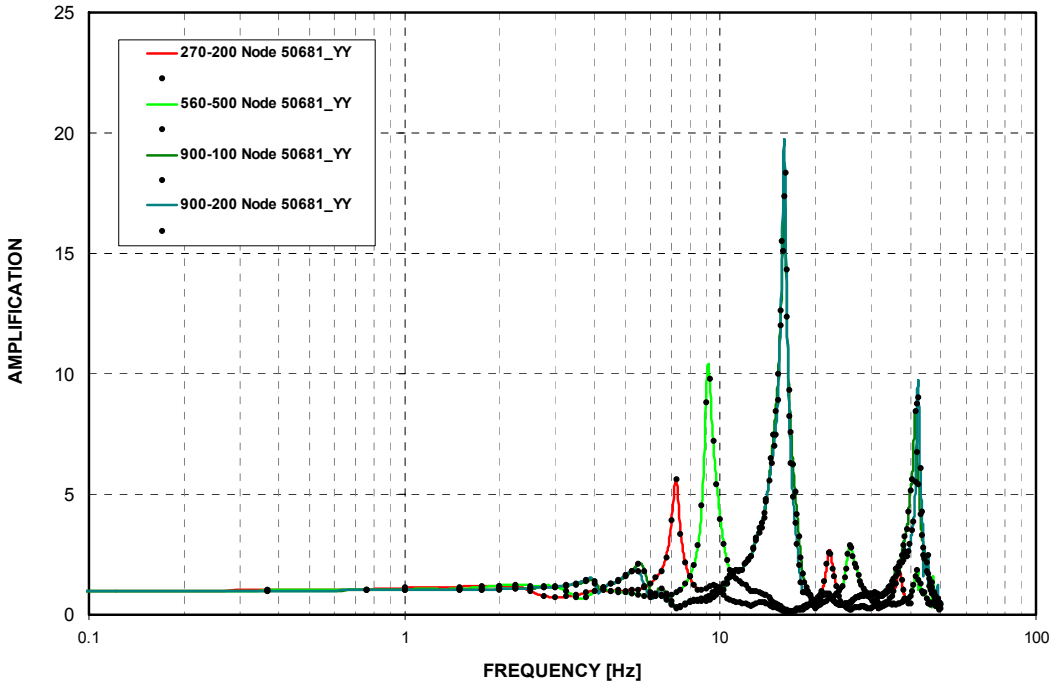

Figure 3-C.2.0-41 East PS/B A-AAC GTG - Uncracked - EW Direction (Y)

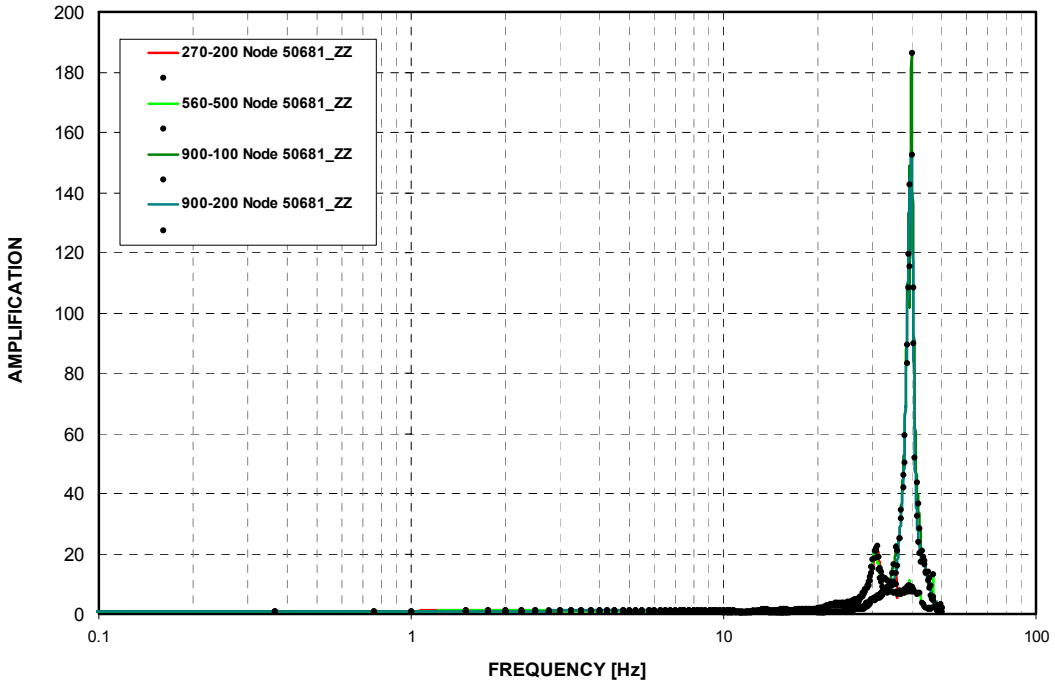

Figure 3-C.2.0-42 East PS/B A-AAC GTG - Uncracked - Vertical Direction (Z)

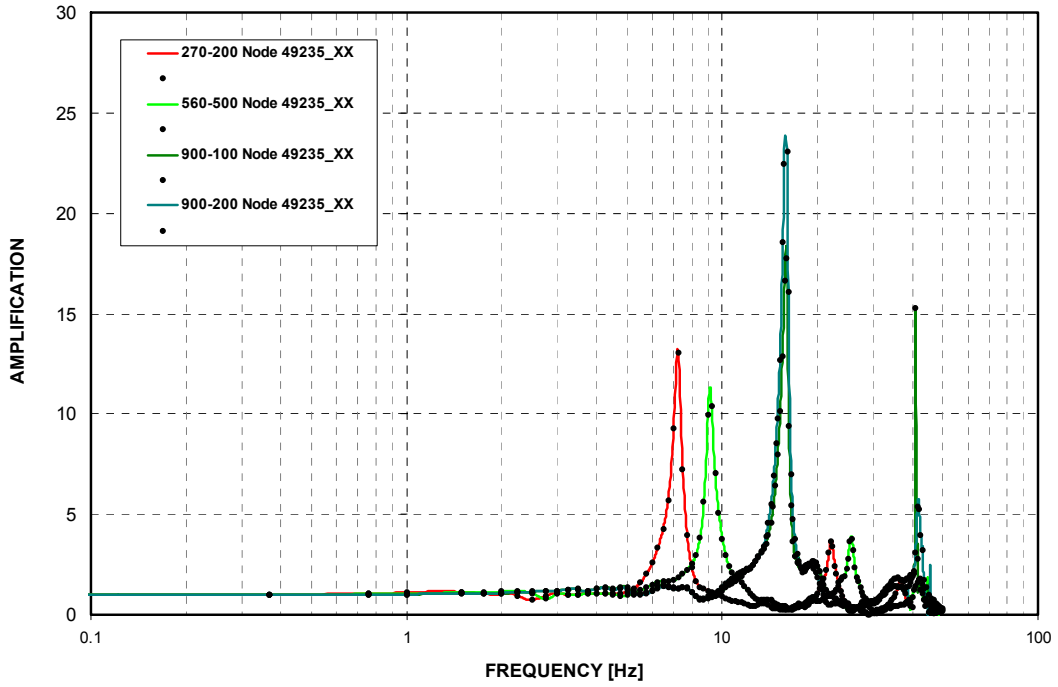

Figure 3-C.2.0-43 West PS/B B-AAC GTG - Cracked - NS Direction (X)

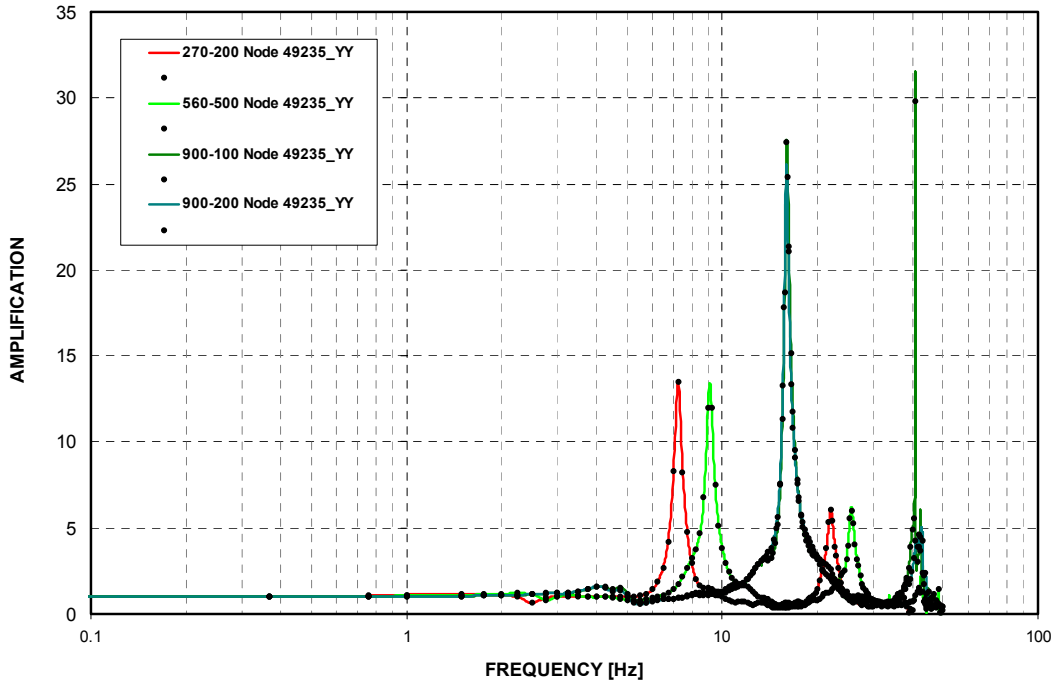

Figure 3-C.2.0-44 West PS/B B-AAC GTG - Cracked - EW Direction (Y)

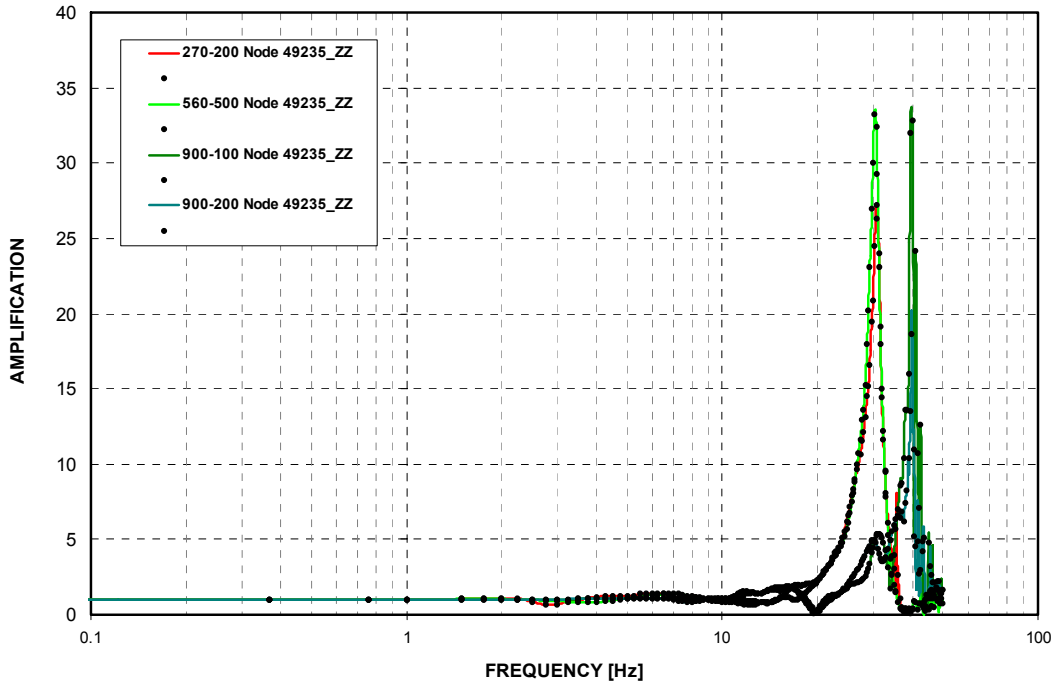

Figure 3-C.2.0-45 West PS/B B-AAC GTG - Cracked - Vertical Direction (Z)

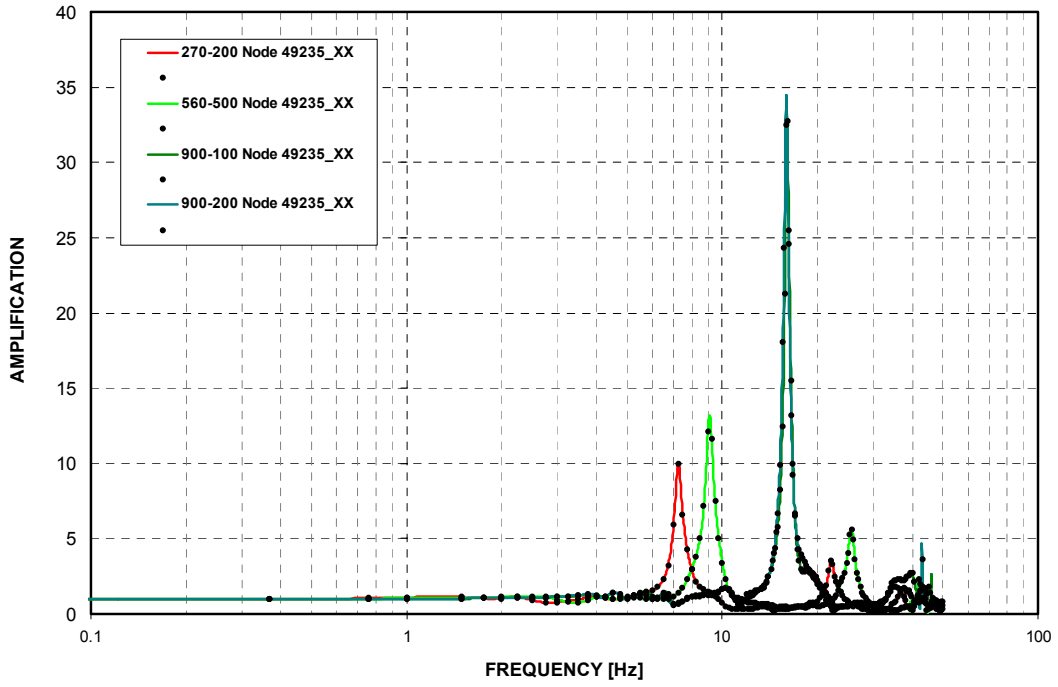

Figure 3-C.2.0-46 West PS/B B-AAC GTG - Uncracked - NS Direction (X)

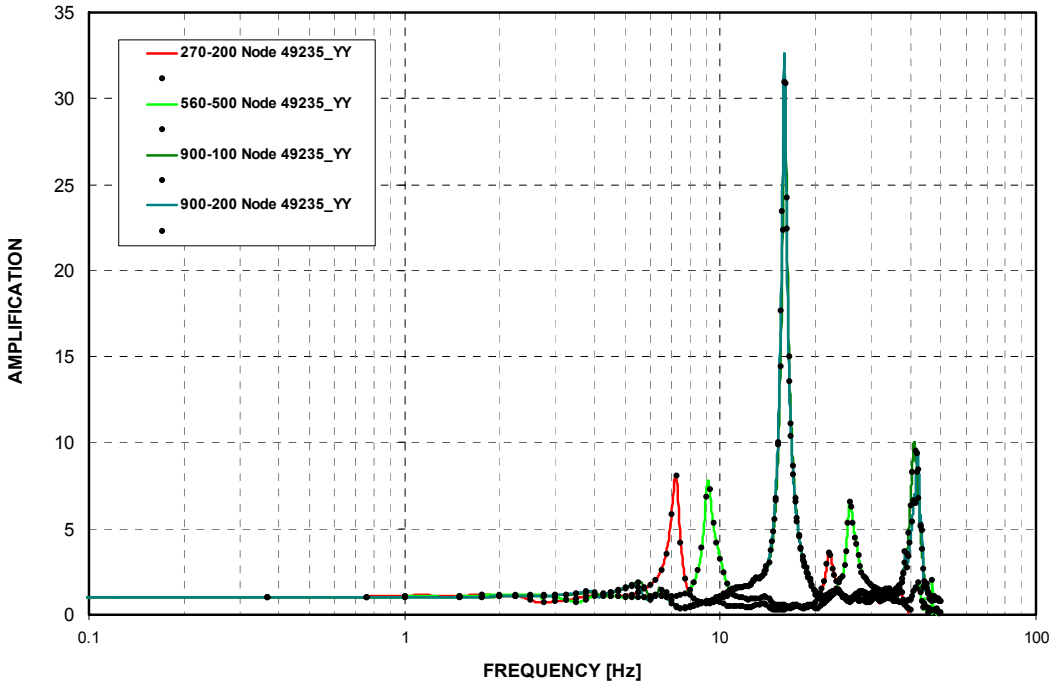

Figure 3-C.2.0-47 West PS/B B-AAC GTG - Uncracked - EW Direction (Y)

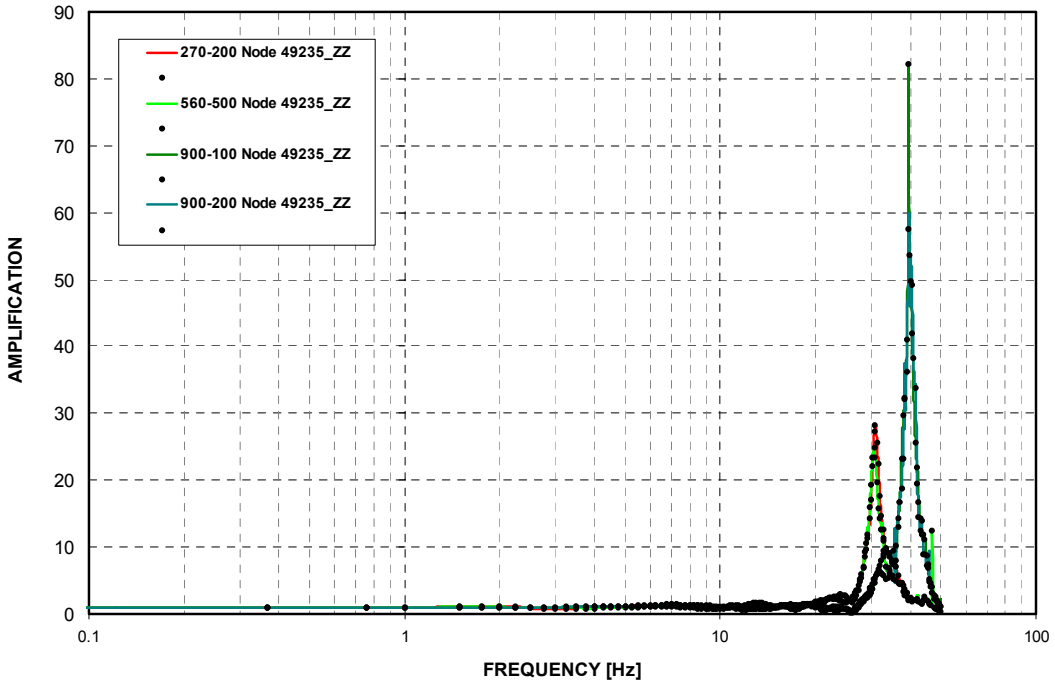

Figure 3-C.2.0-48 West PS/B B-AAC GTG - Uncracked - Vertical Direction (Z)

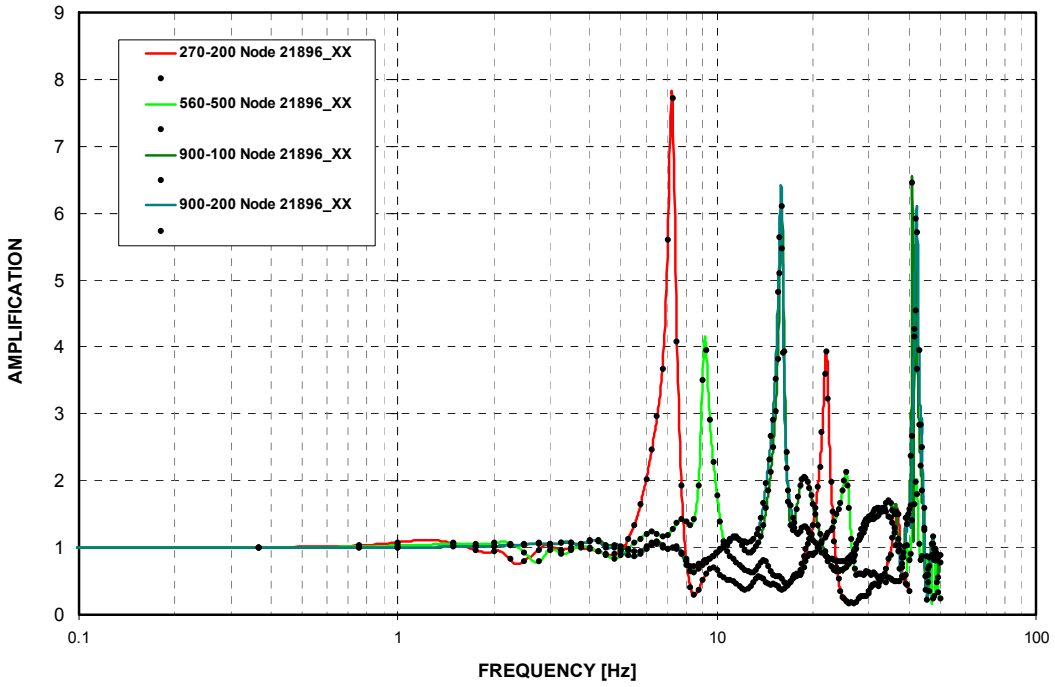

Figure 3-C.2.0-49 A/B Northwest Corner at Basemat - Cracked - NS Direction (X)

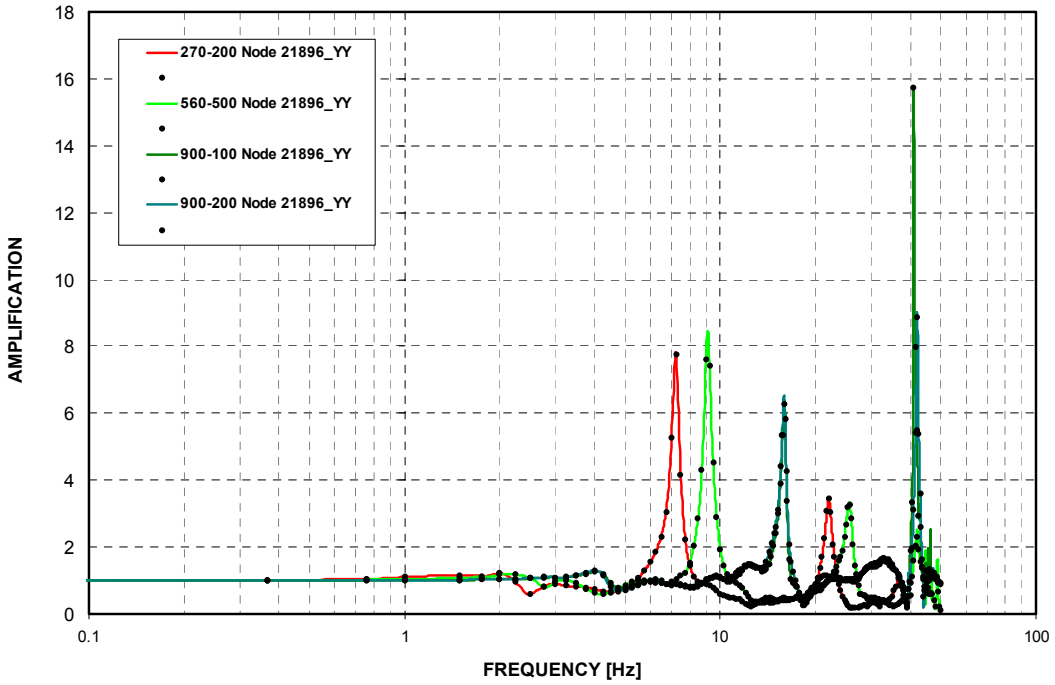

Figure 3-C.2.0-50 A/B Northwest Corner at Basemat - Cracked - EW Direction (Y)

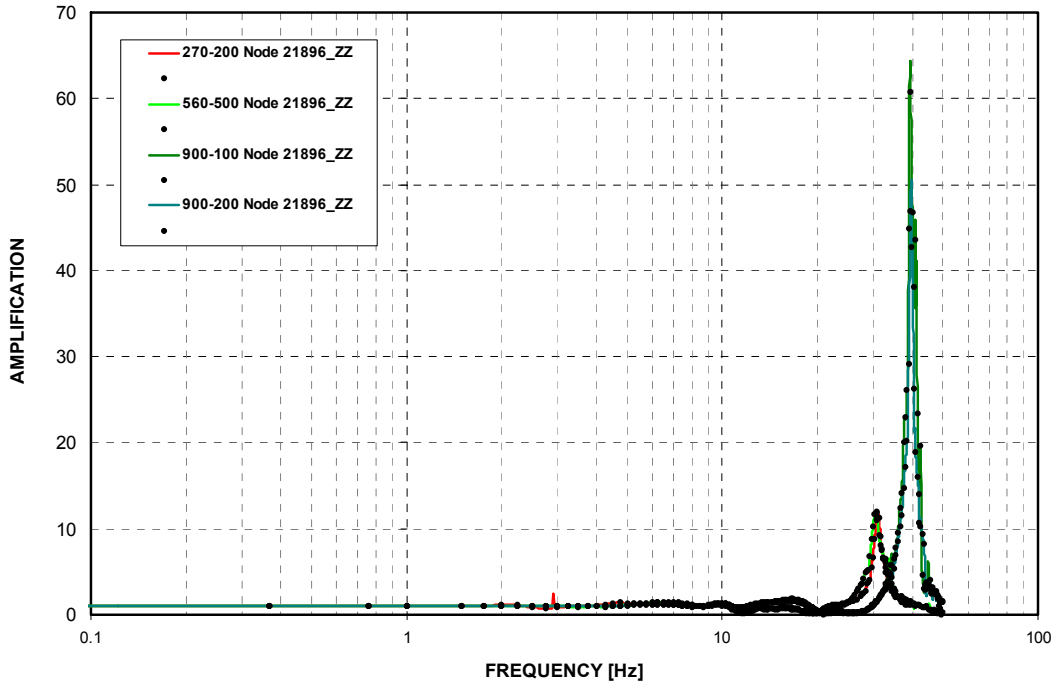

Figure 3-C.2.0-51 A/B Northwest Corner at Basemat - Cracked - Vertical Direction (Z)

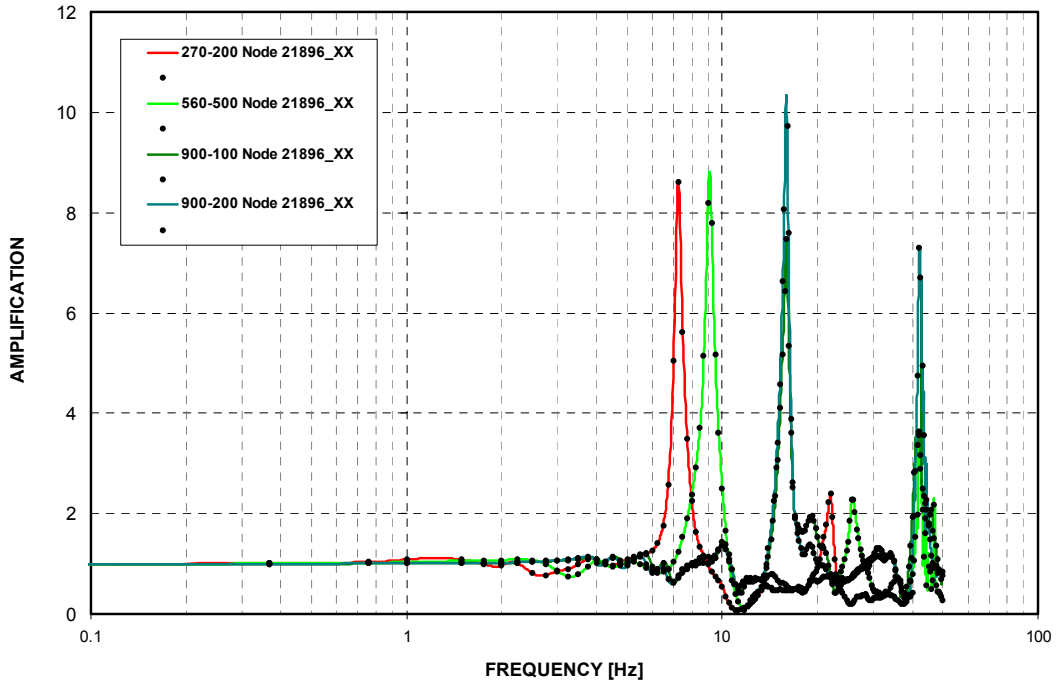

Figure 3-C.2.0-52 A/B Northwest Corner at Basemat - Uncracked - NS Direction (X)

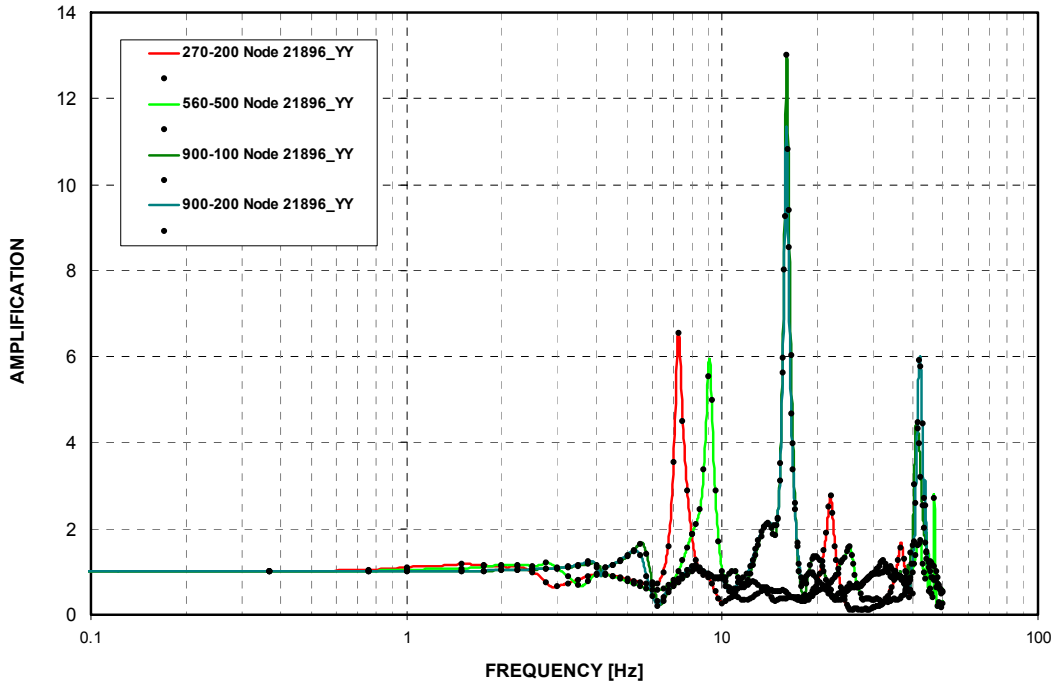

Figure 3-C.2.0-53 A/B Northwest Corner at Basemat - Uncracked - EW Direction (Y)

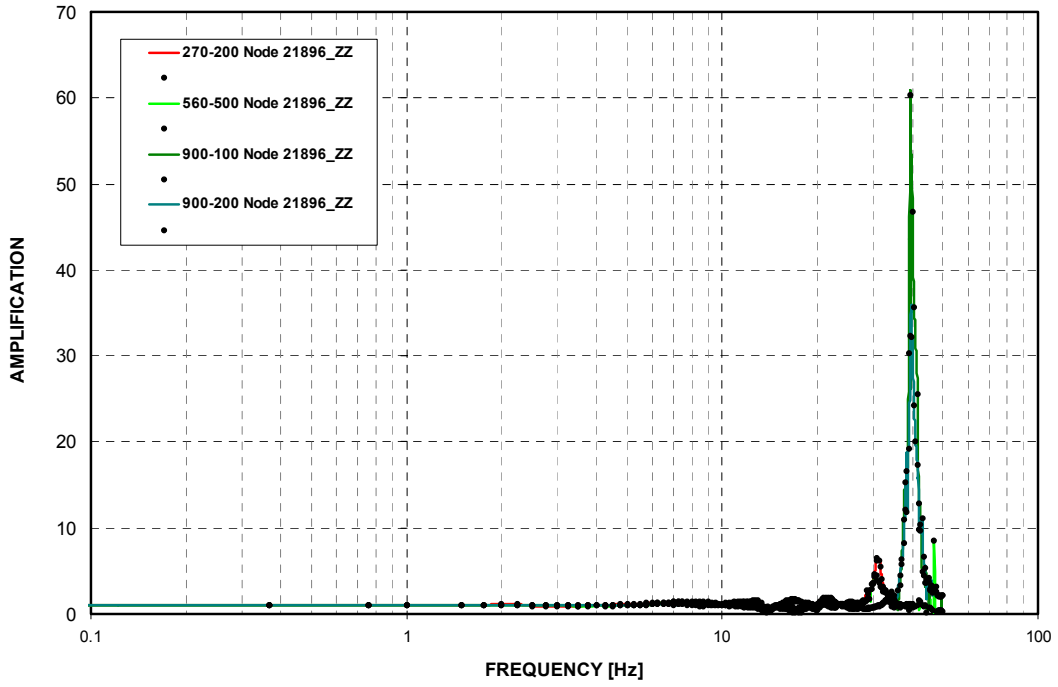

Figure 3-C.2.0-54 A/B Northwest Corner at Basemat - Uncracked - Vertical Direction (Z)

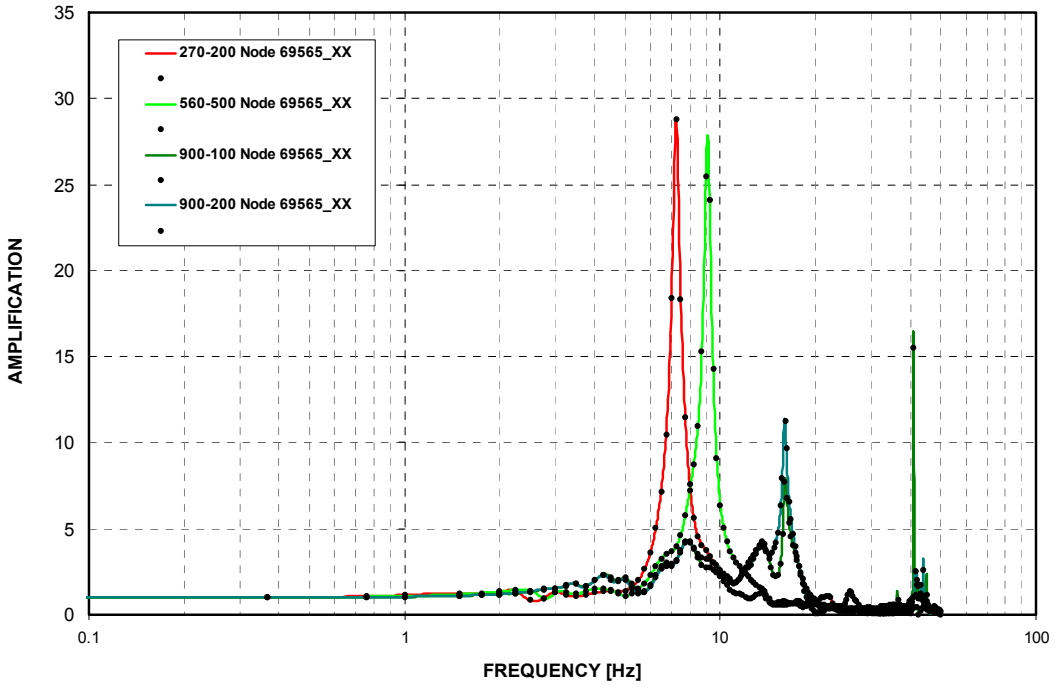

Figure 3-C.2.0-55 A/B Northwest Corner at Roof - Cracked - NS Direction (X)

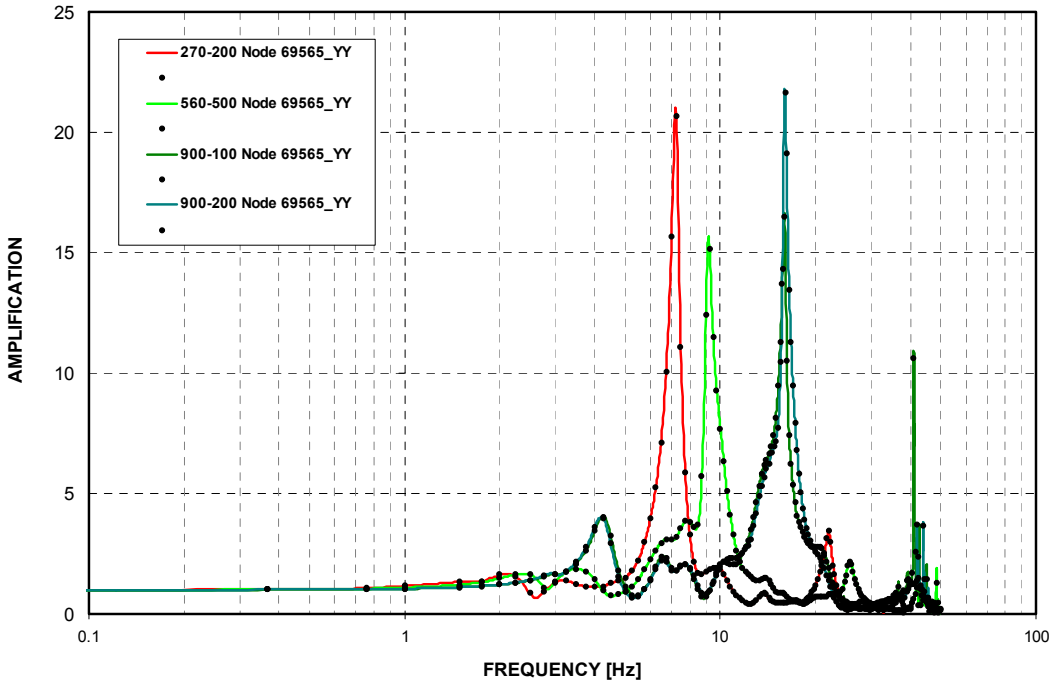

Figure 3-C.2.0-56 A/B Northwest Corner at Roof - Cracked - EW Direction (Y)

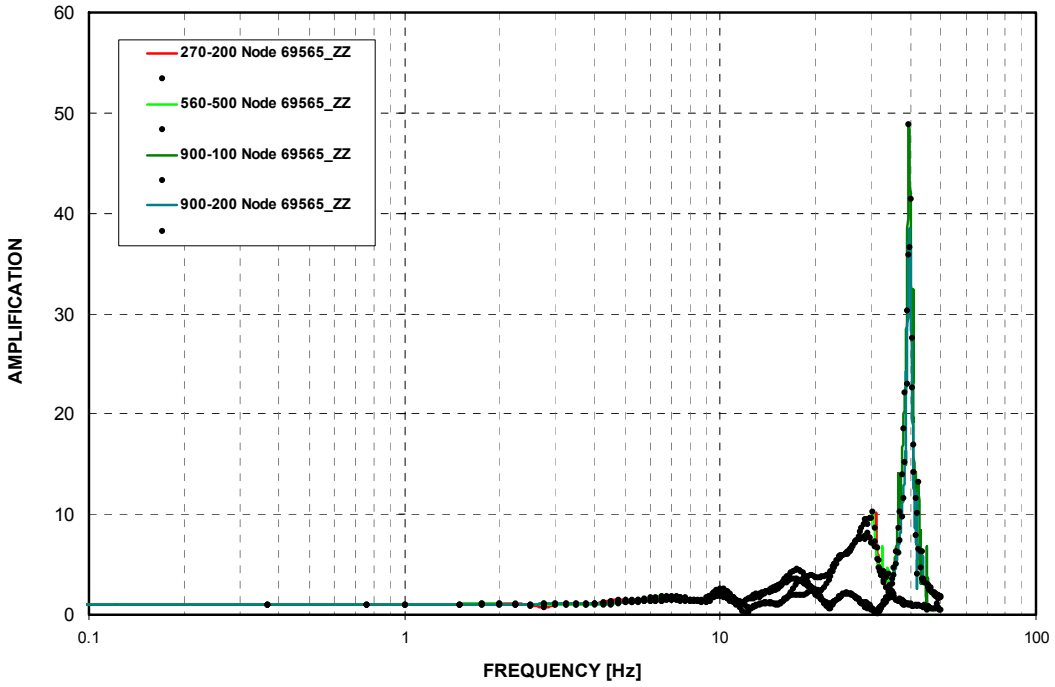

Figure 3-C.2.0-57 A/B Northwest Corner at Roof - Cracked - Vertical Direction (Z)

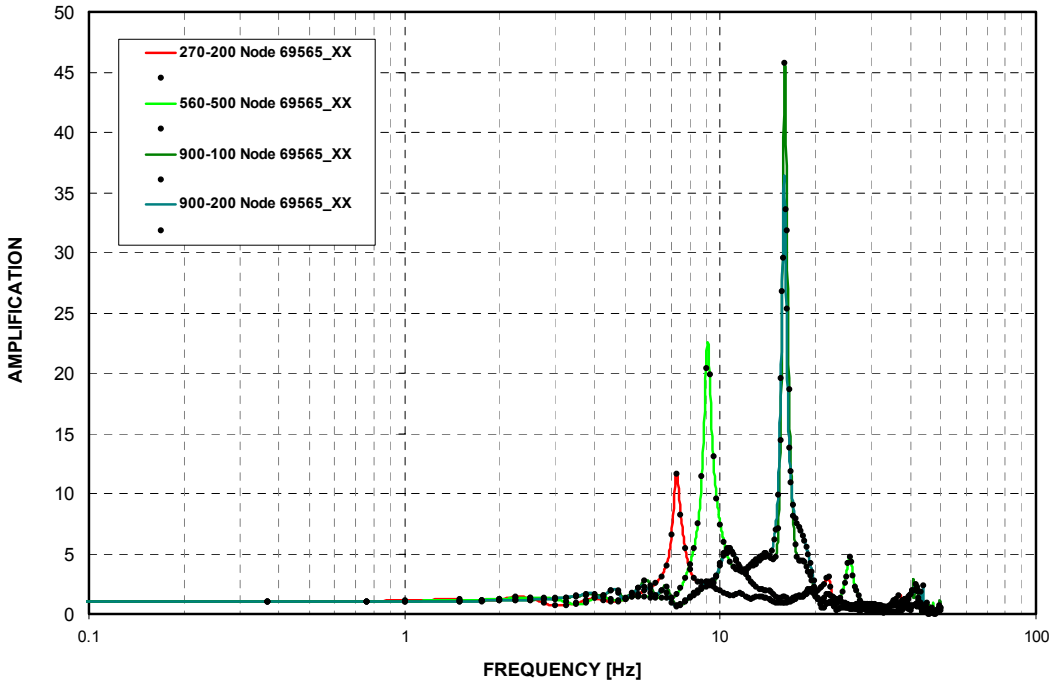

Figure 3-C.2.0-58 A/B Northwest Corner at Roof - Uncracked - NS Direction (X)

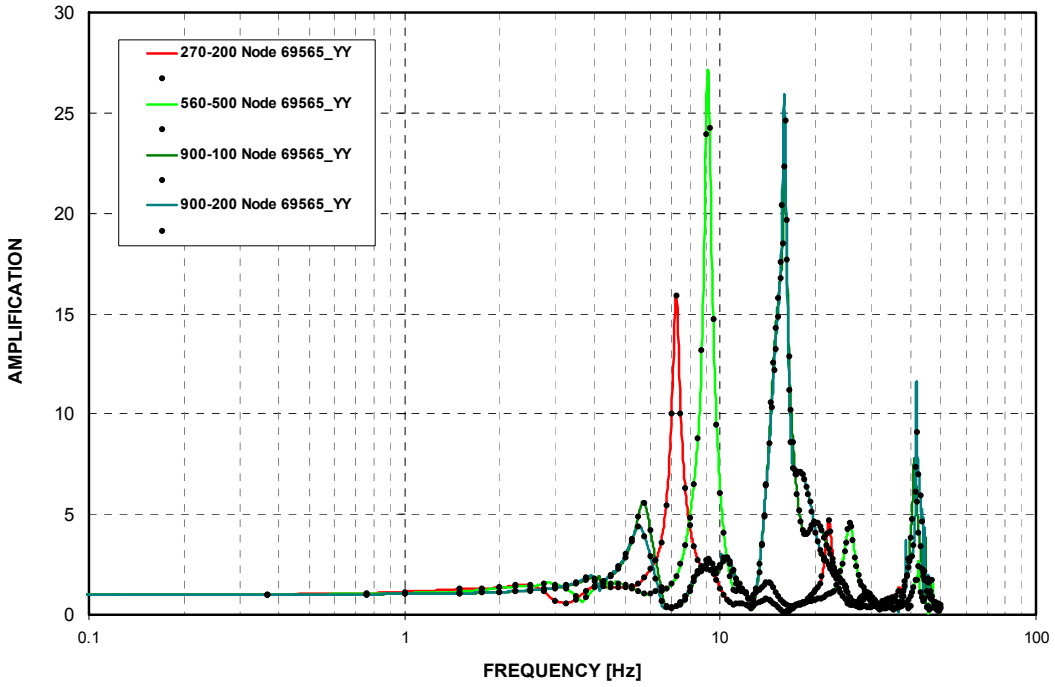

Figure 3-C.2.0-59 A/B Northwest Corner at Roof - Uncracked - EW Direction (Y)

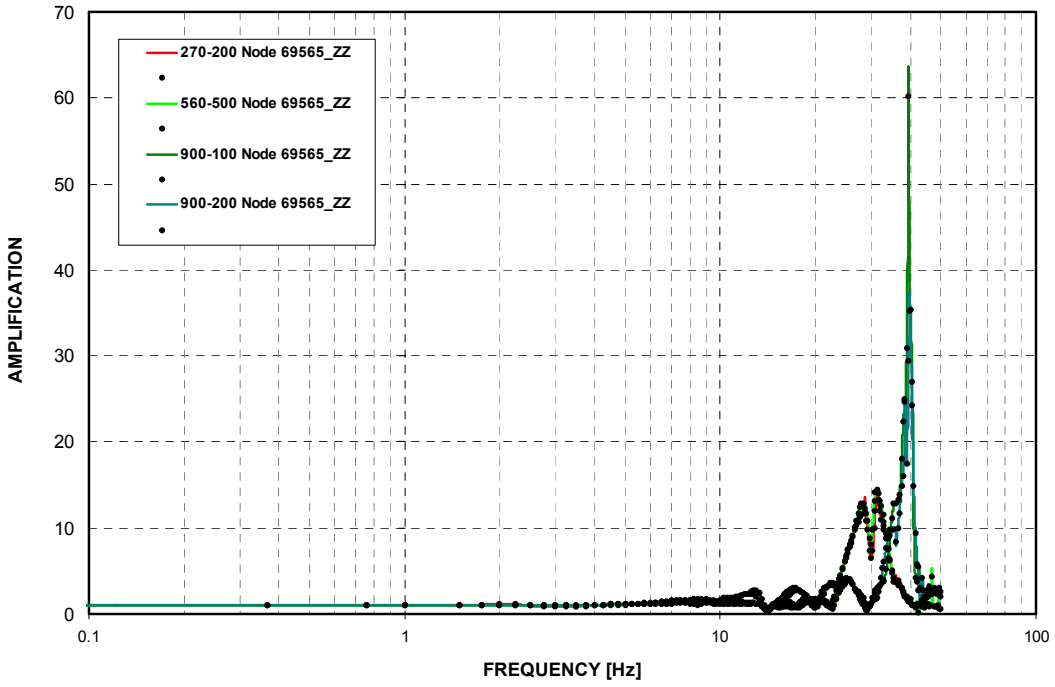

Figure 3-C.2.0-60 A/B Northwest Corner at Roof - Uncracked - Vertical Direction (Z)

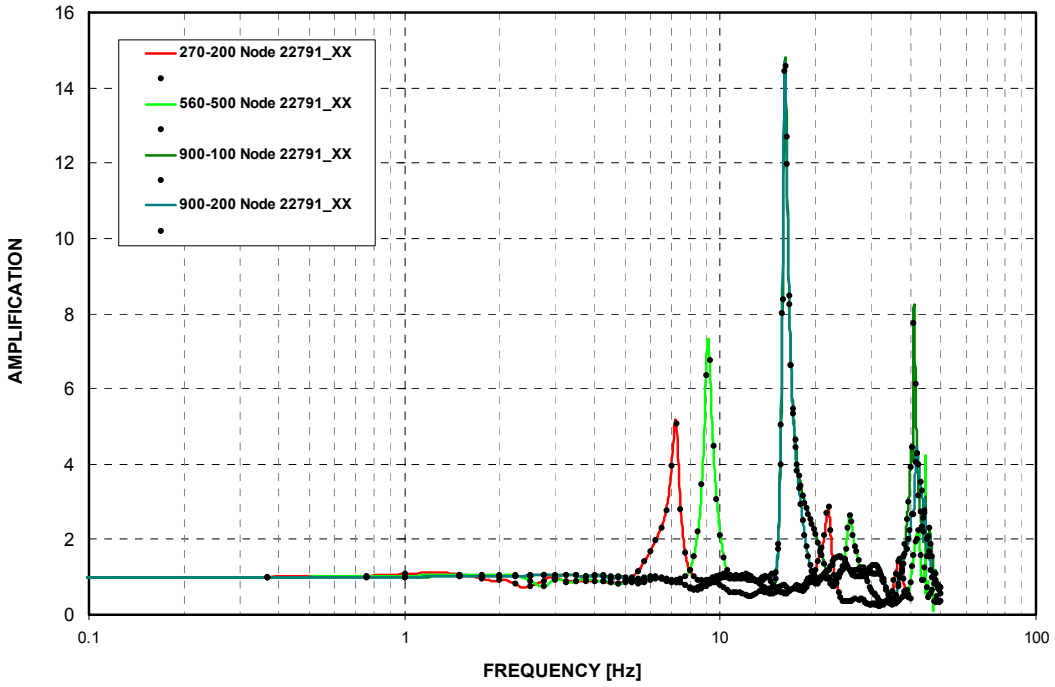

Figure 3-C.2.0-61 West PS/B Southwest Corner at Basemat - Cracked - NS Direction (X)

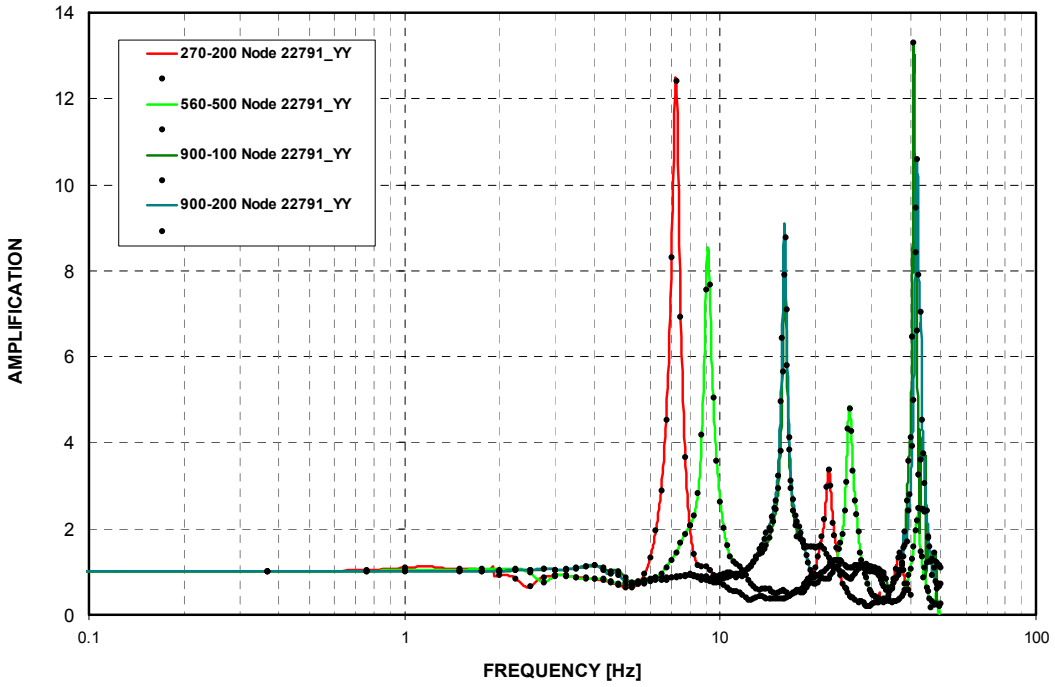

Figure 3-C.2.0-62 West PS/B Southwest Corner at Basemat - Cracked - EW Direction (Y)

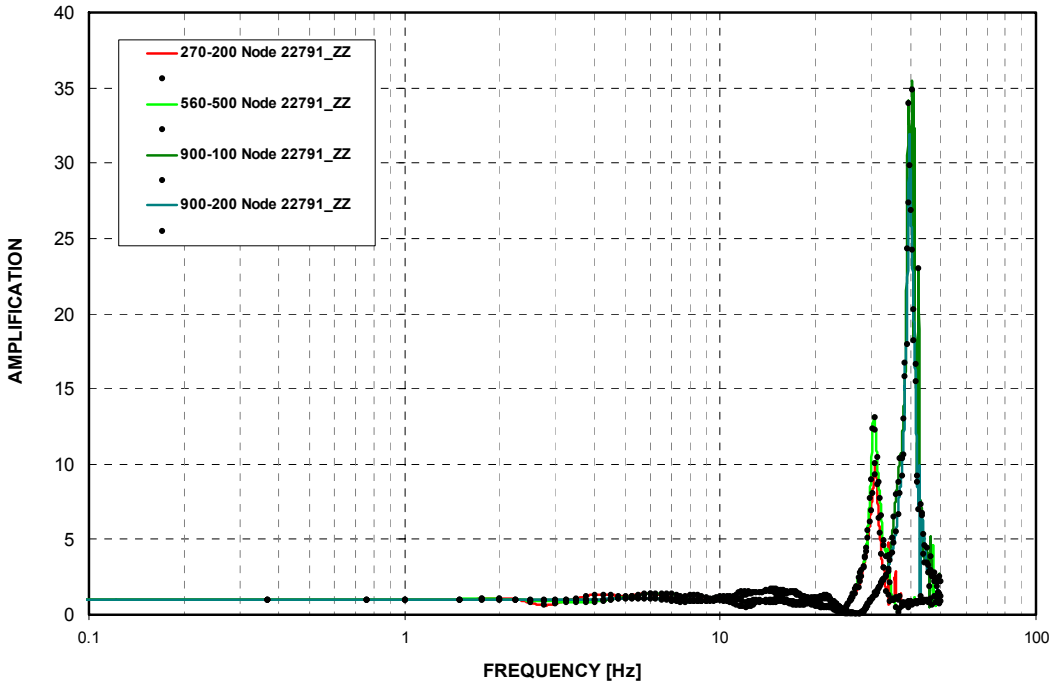

Figure 3-C.2.0-63 West PS/B Southwest Corner at Basemat - Cracked - Vertical Direction (Z)

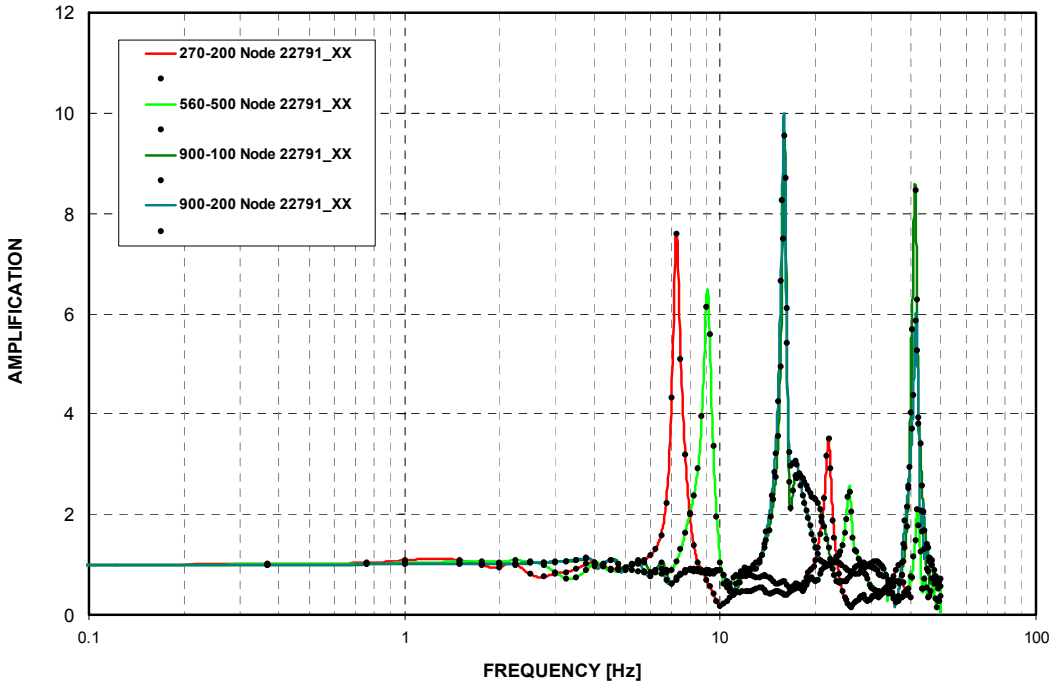

Figure 3-C.2.0-64 West PS/B Southwest Corner at Basemat - Uncracked - NS Direction (X)

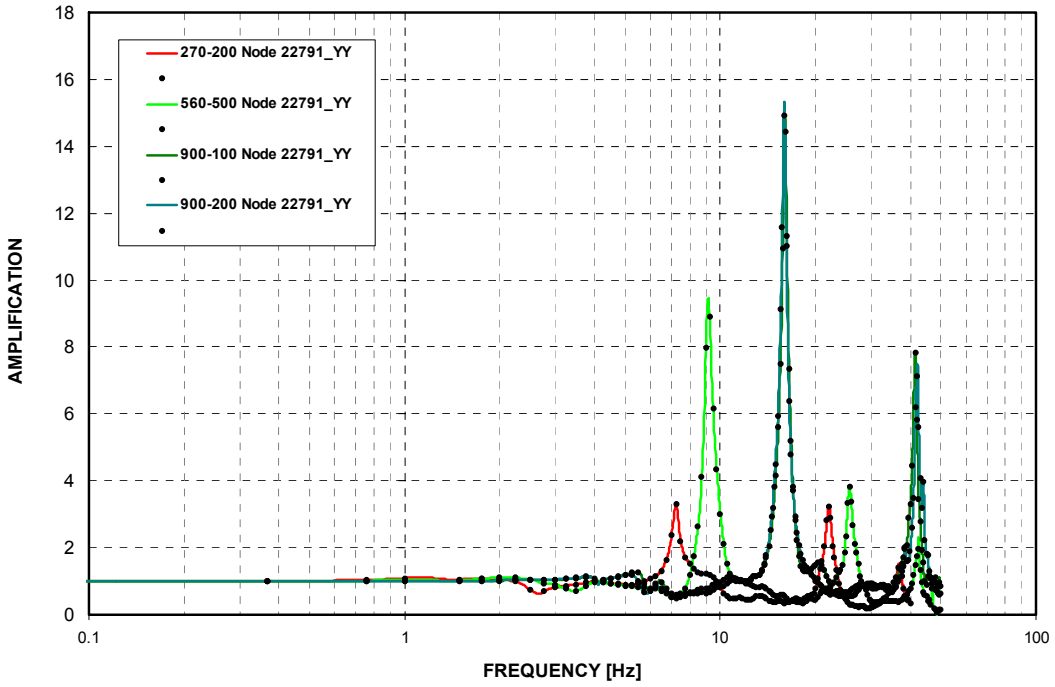

Figure 3-C.2.0-65 West PS/B Southwest Corner at Basemat - Uncracked - EW Direction (Y)

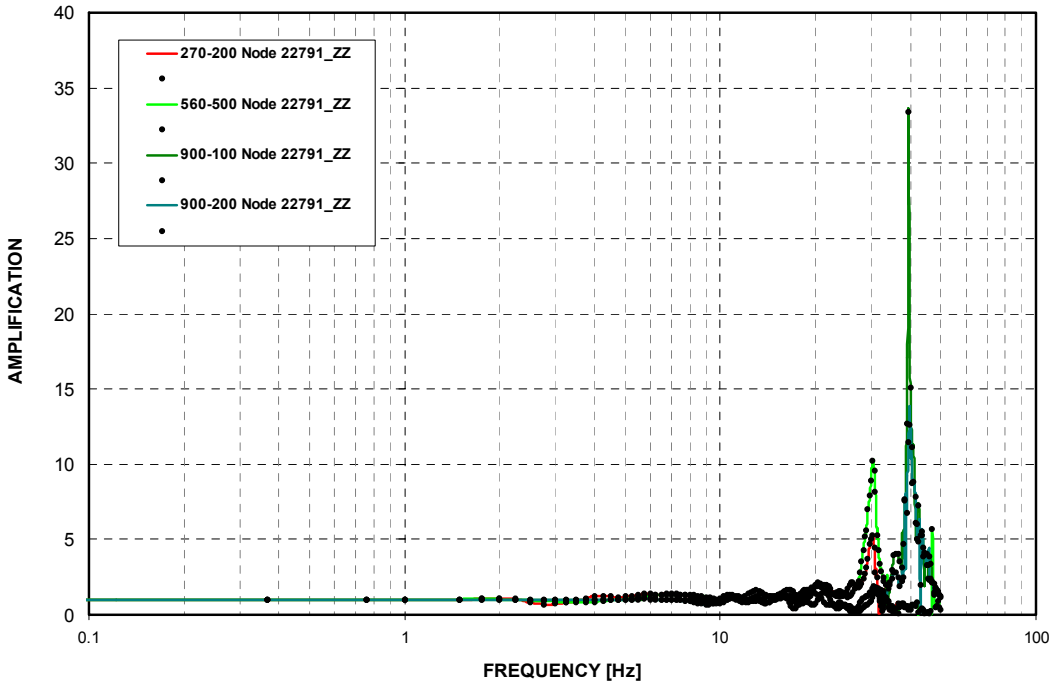

Figure 3-C.2.0-66 West PS/B Southwest Corner at Basemat - Uncracked - Vertical Direction (Z)

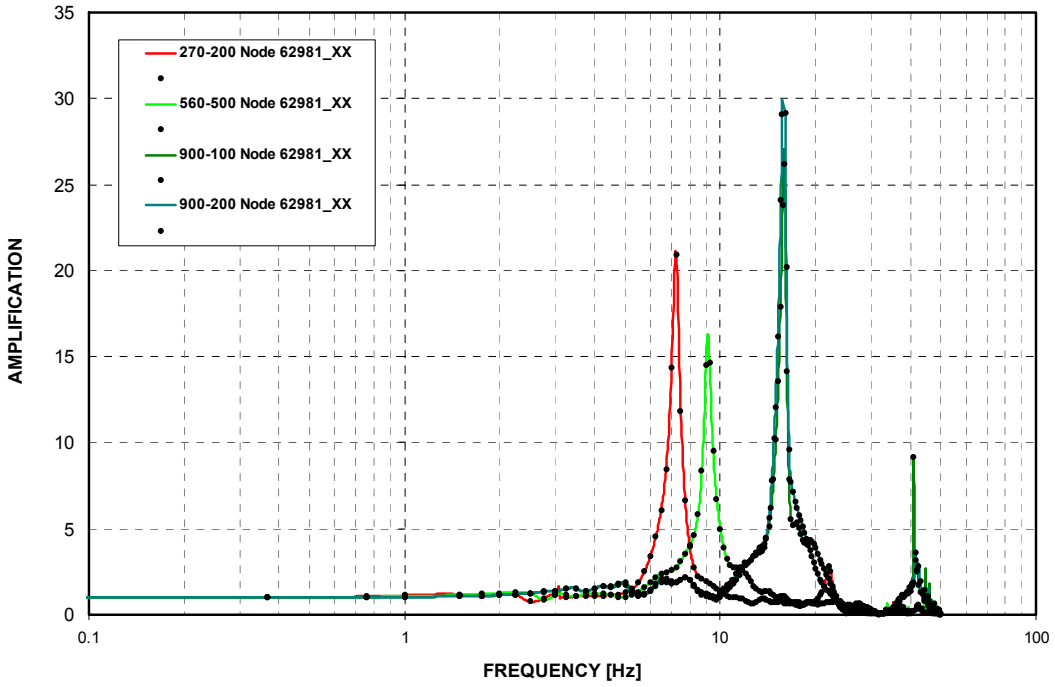

Figure 3-C.2.0-67 West PS/B Southwest Corner at Roof - Cracked - NS Direction (X)

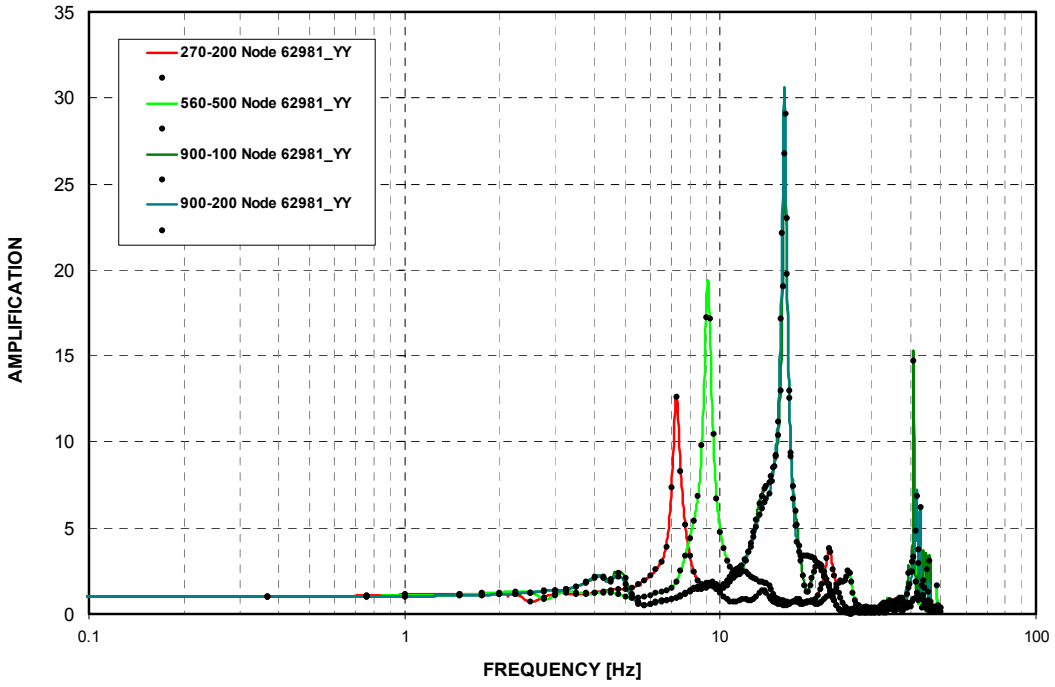

Figure 3-C.2.0-68 West PS/B Southwest Corner at Roof - Cracked - EW Direction (Y)

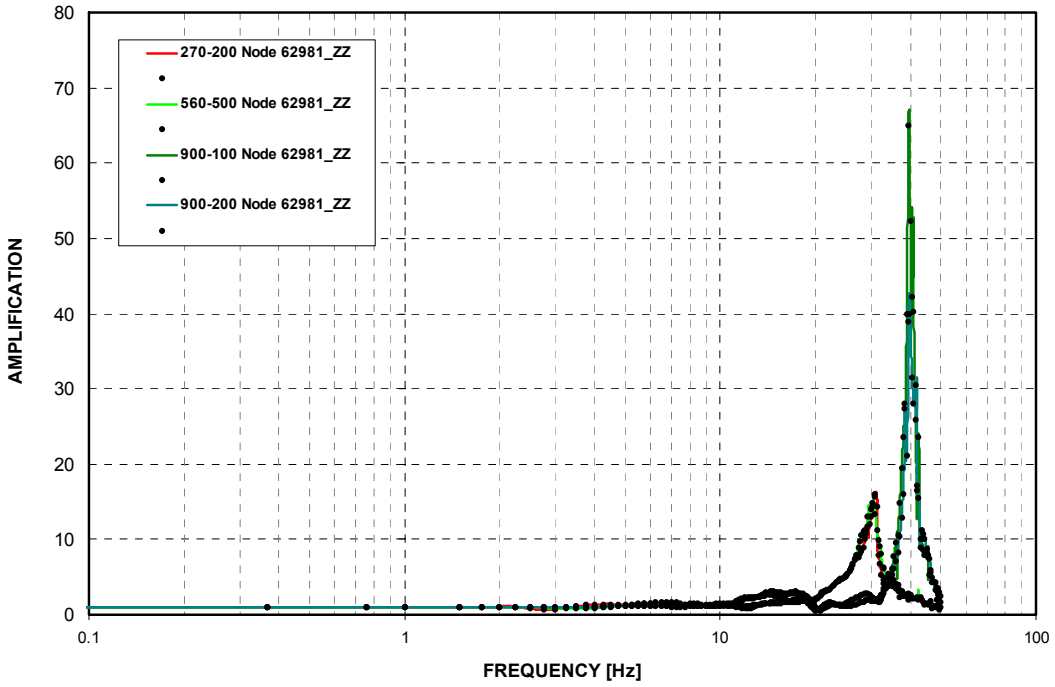

Figure 3-C.2.0-69 West PS/B Southwest Corner at Roof - Cracked - Vertical Direction (Z)

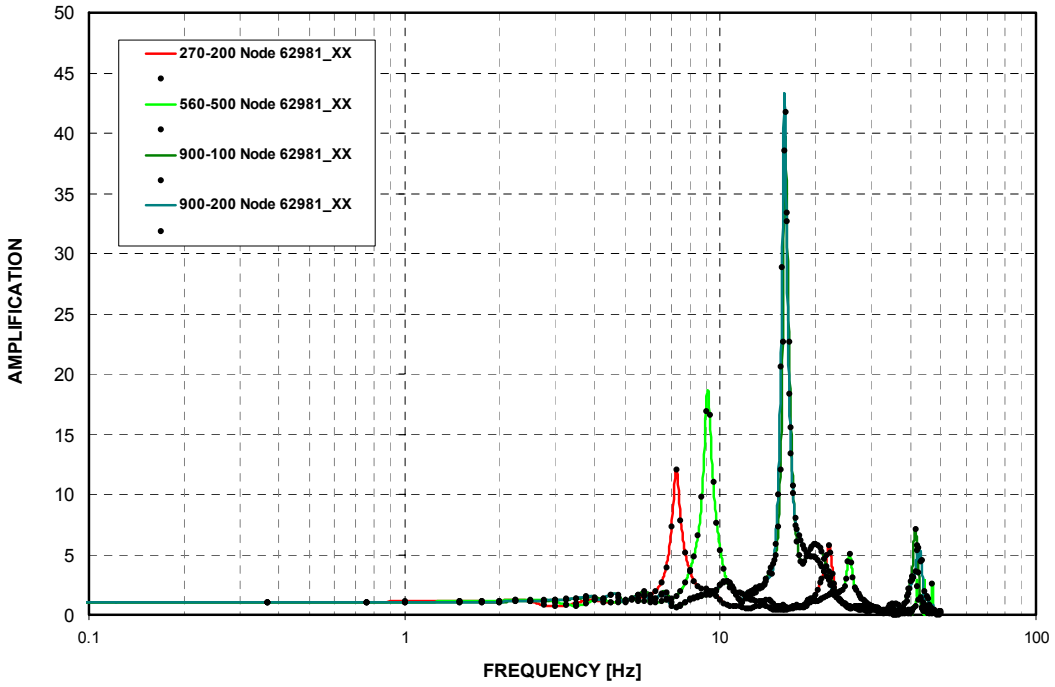

Figure 3-C.2.0-70 West PS/B Southwest Corner at Roof - Uncracked - NS Direction (X)

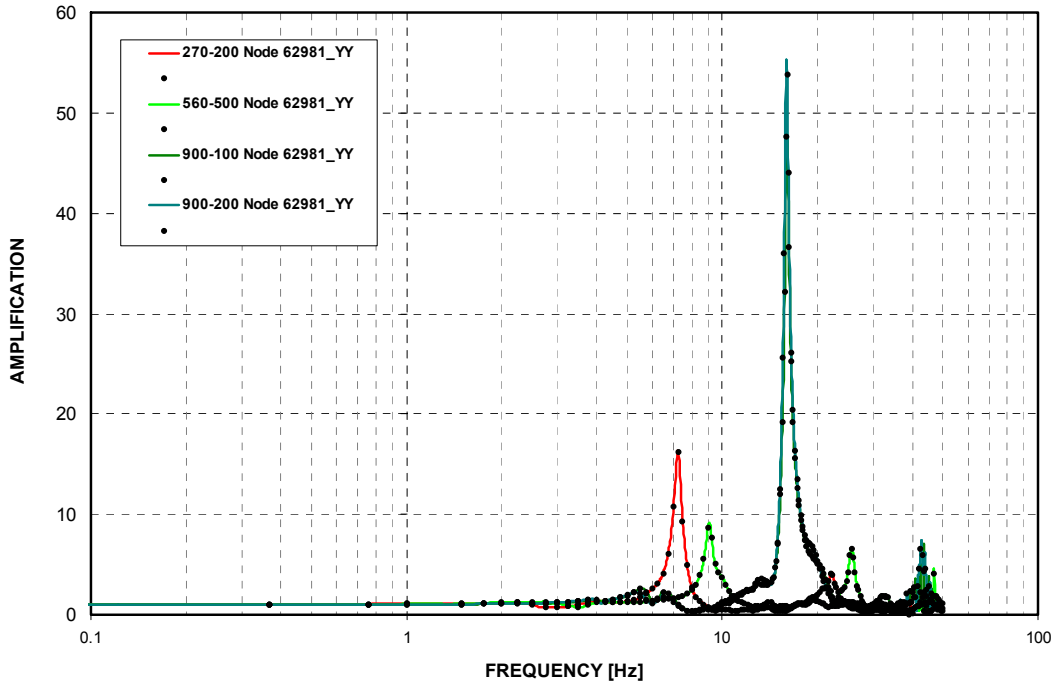

Figure 3-C.2.0-71 West PS/B Southwest Corner at Roof - Uncracked - EW Direction (Y)

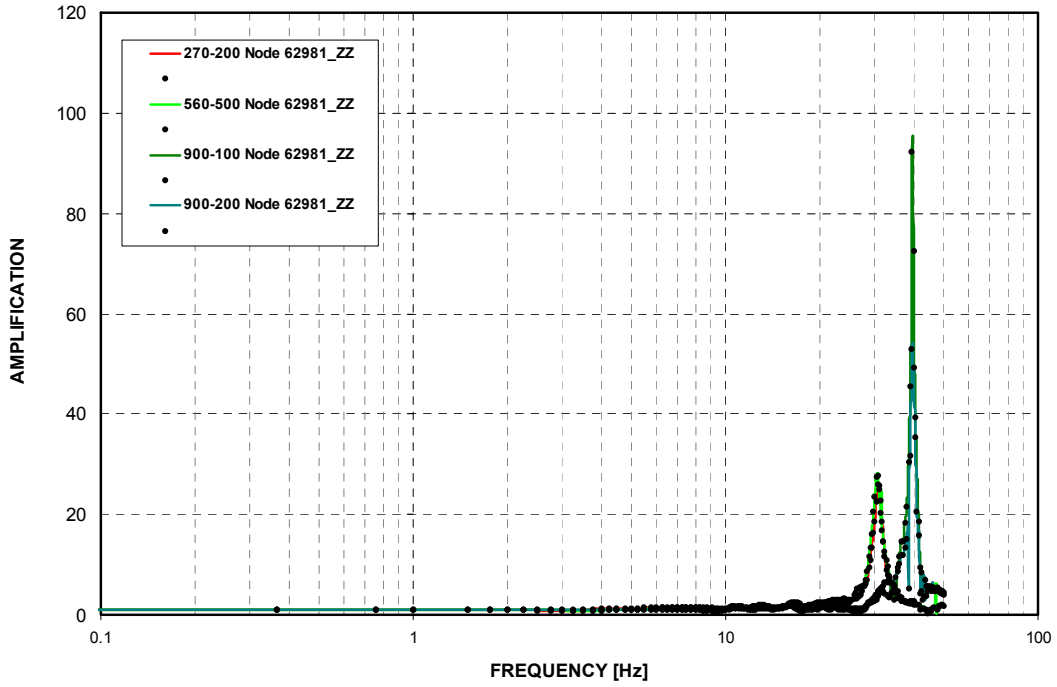

Figure 3-C.2.0-72 West PS/B Southwest Corner at Roof - Uncracked - Vertical Direction (Z)

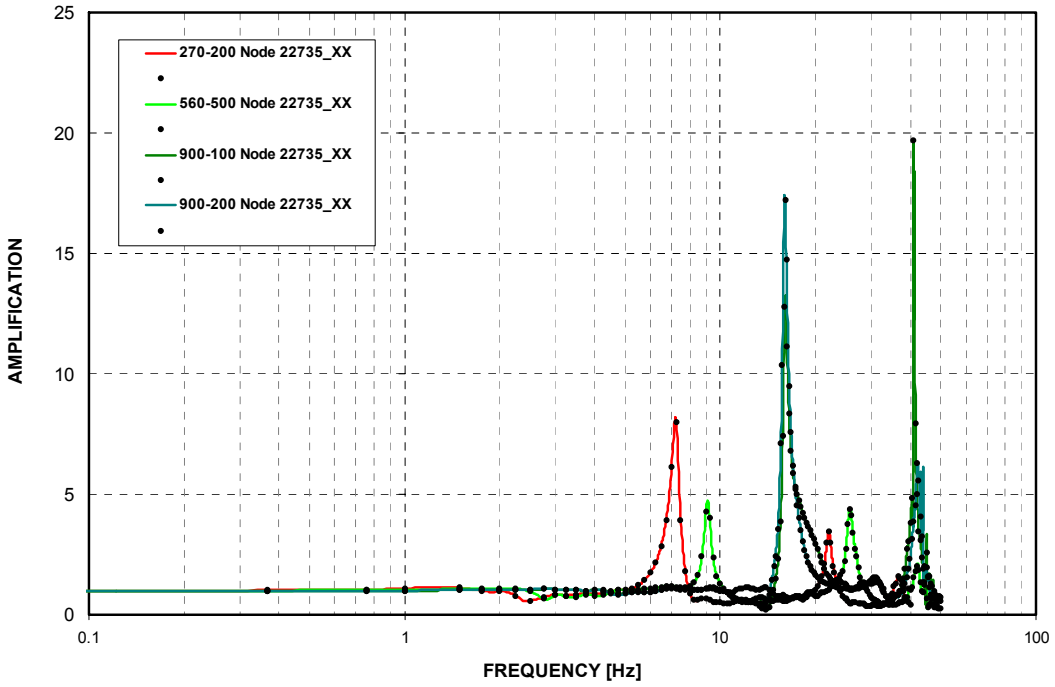

Figure 3-C.2.0-73 East PS/B Southeast Corner at Basemat - Cracked - NS Direction (X)

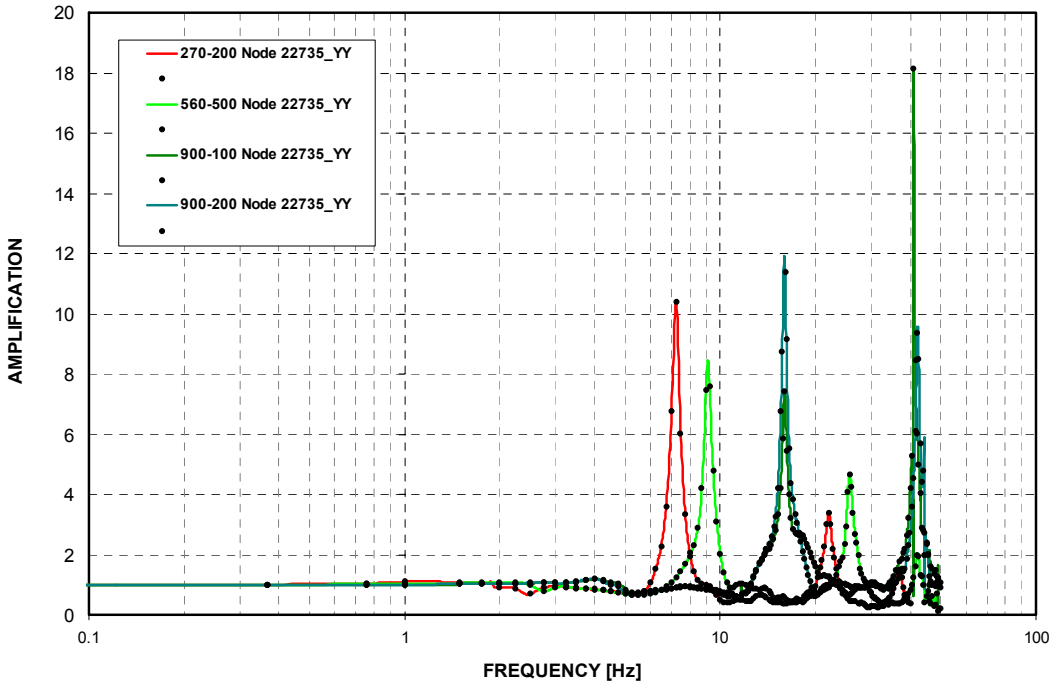

Figure 3-C.2.0-74 East PS/B Southeast Corner at Basemat - Cracked - EW Direction (Y)

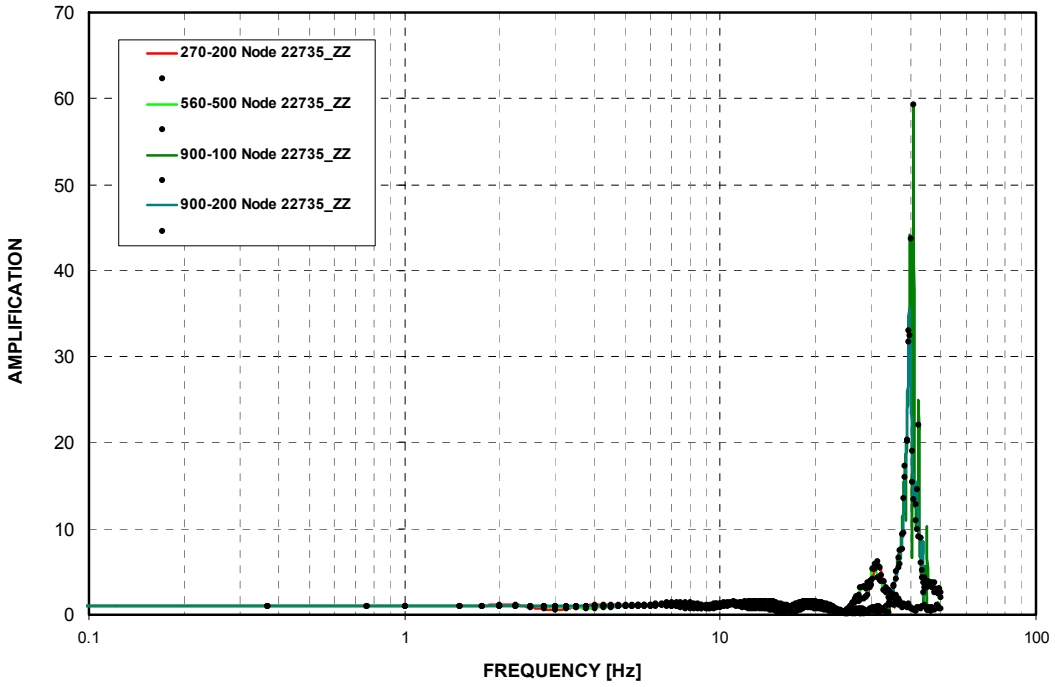

Figure 3-C.2.0-75 East PS/B Southeast Corner at Basemat - Cracked - Vertical Direction (Z)

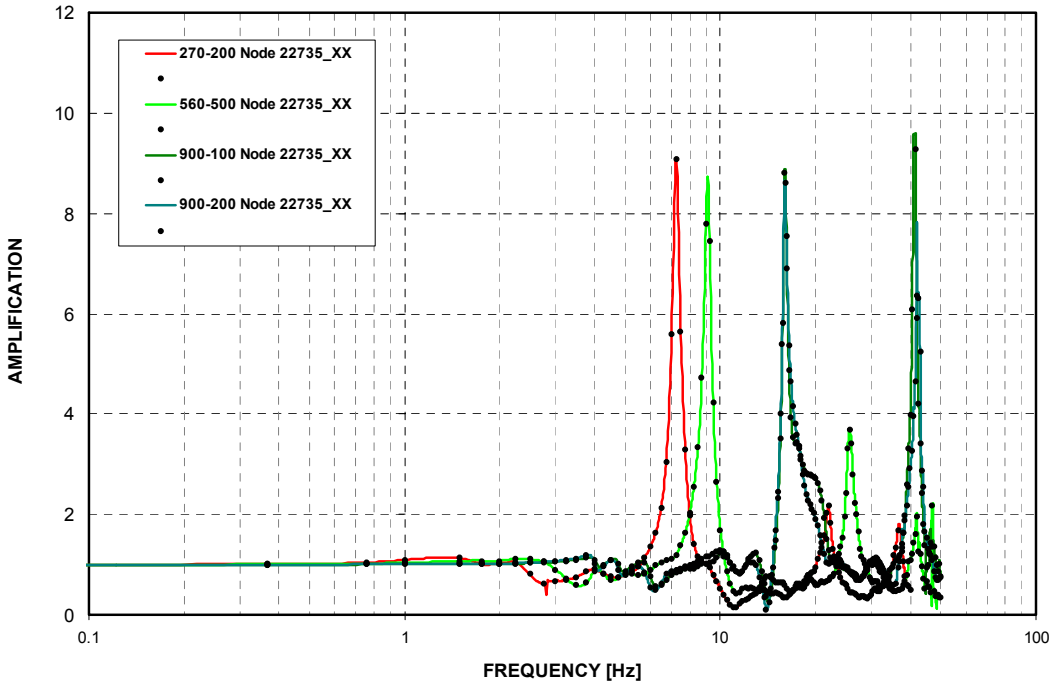

Figure 3-C.2.0-76 East PS/B Southeast Corner at Basemat - Uncracked - NS Direction (X)

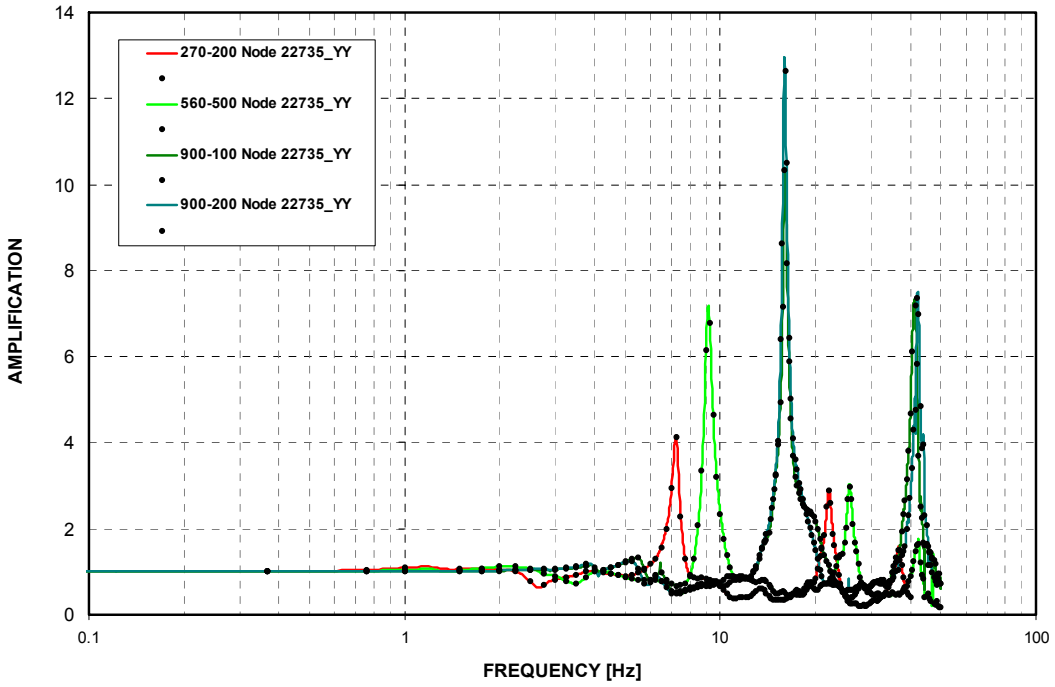

Figure 3-C.2.0-77 East PS/B Southeast Corner at Basemat - Uncracked - EW Direction (Y)

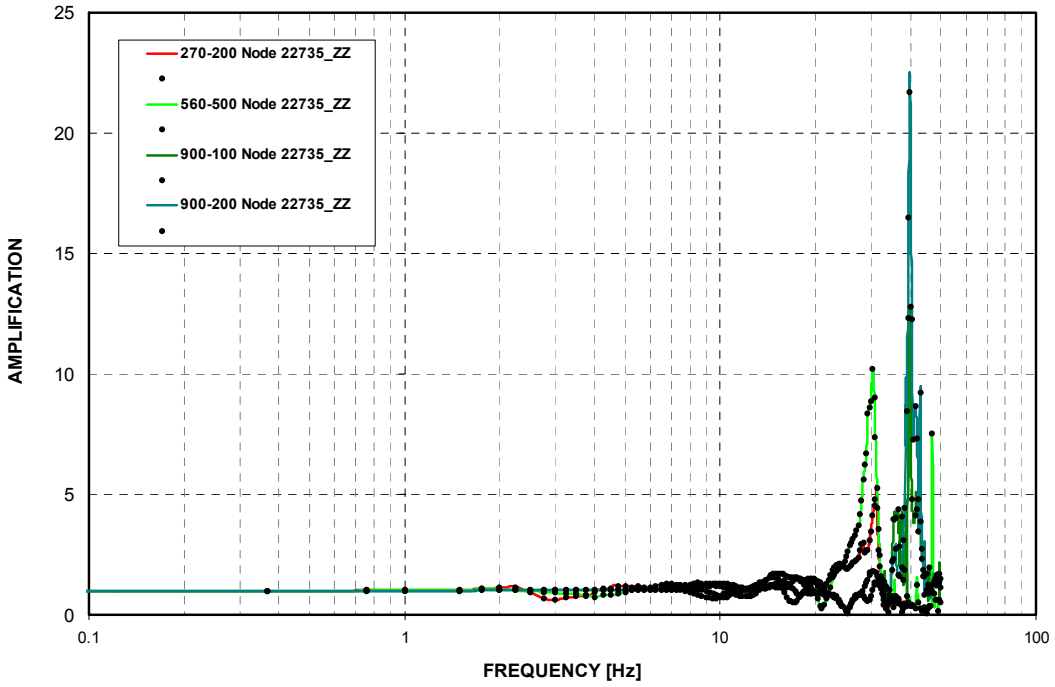

Figure 3-C.2.0-78 East PS/B Southeast Corner at Basemat - Uncracked - Vertical Direction (Z)

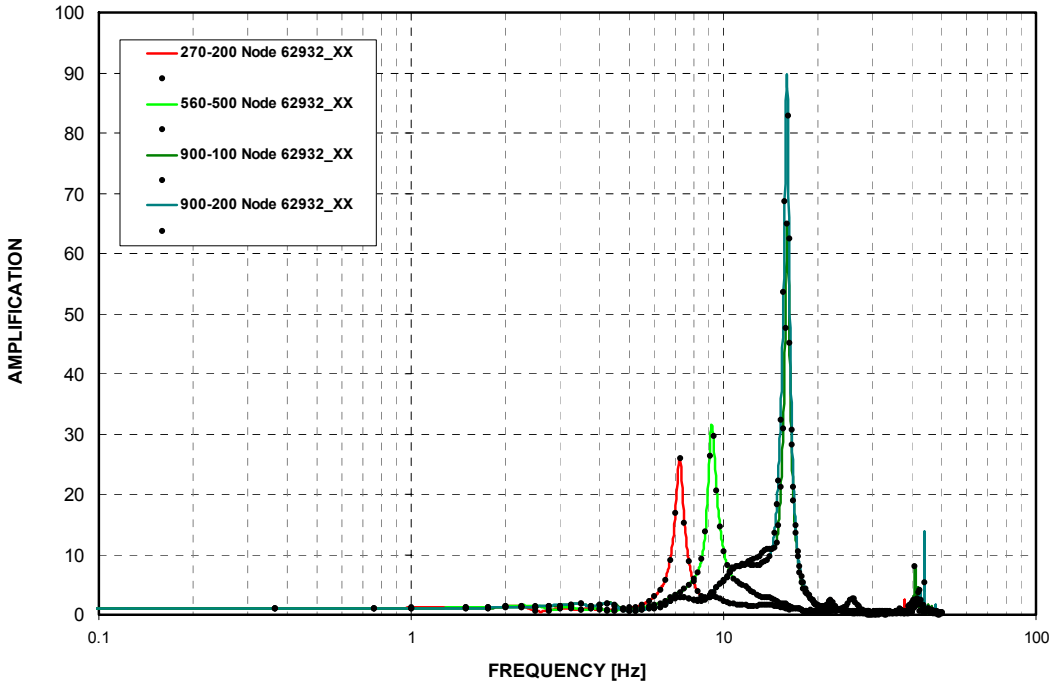

Figure 3-C.2.0-79 East PS/B Southeast Corner at Roof - Cracked - NS Direction (X)

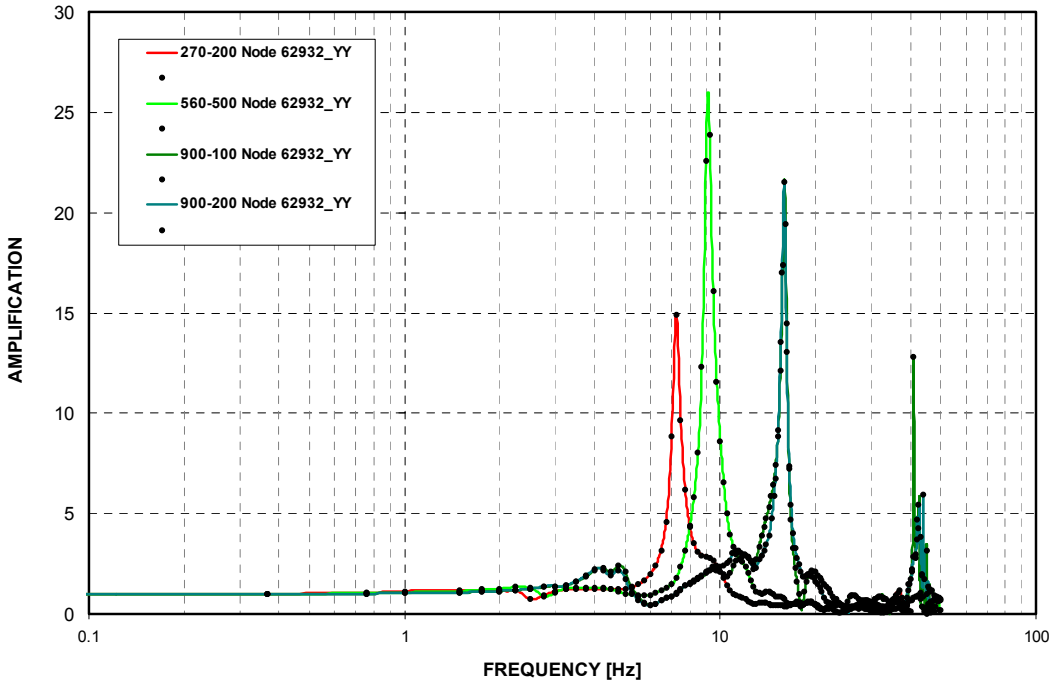

Figure 3-C.2.0-80 East PS/B Southeast Corner at Roof - Cracked - EW Direction (Y)

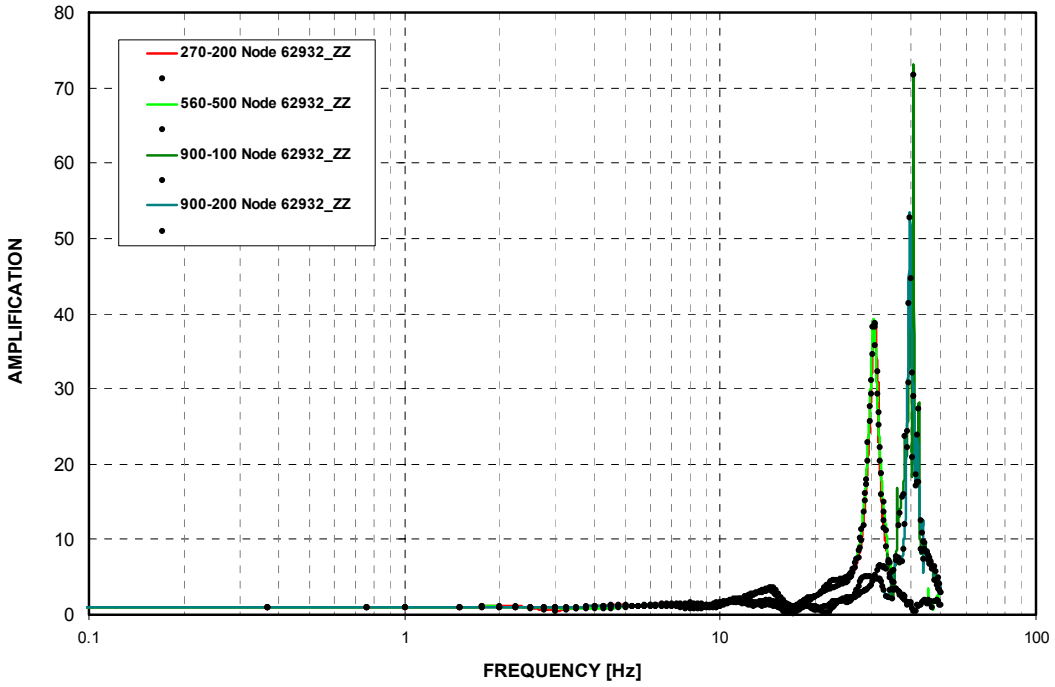

Figure 3-C.2.0-81 East PS/B Southeast Corner at Roof - Cracked - Vertical Direction (Z)

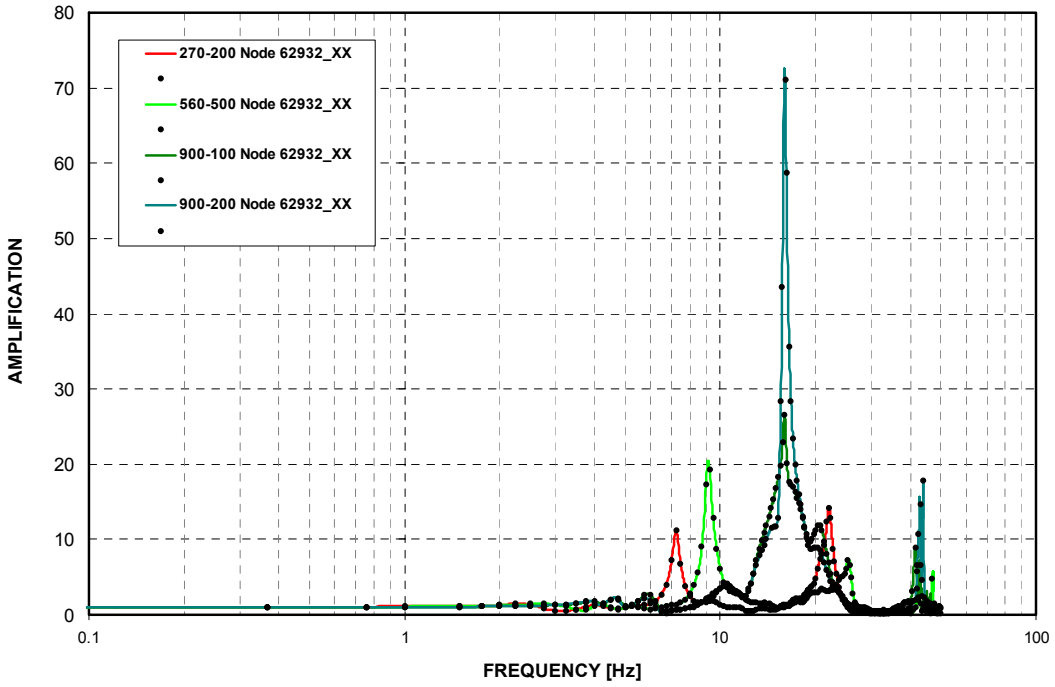

Figure 3-C.2.0-82 East PS/B Southeast Corner at Roof - Uncracked - NS Direction (X)

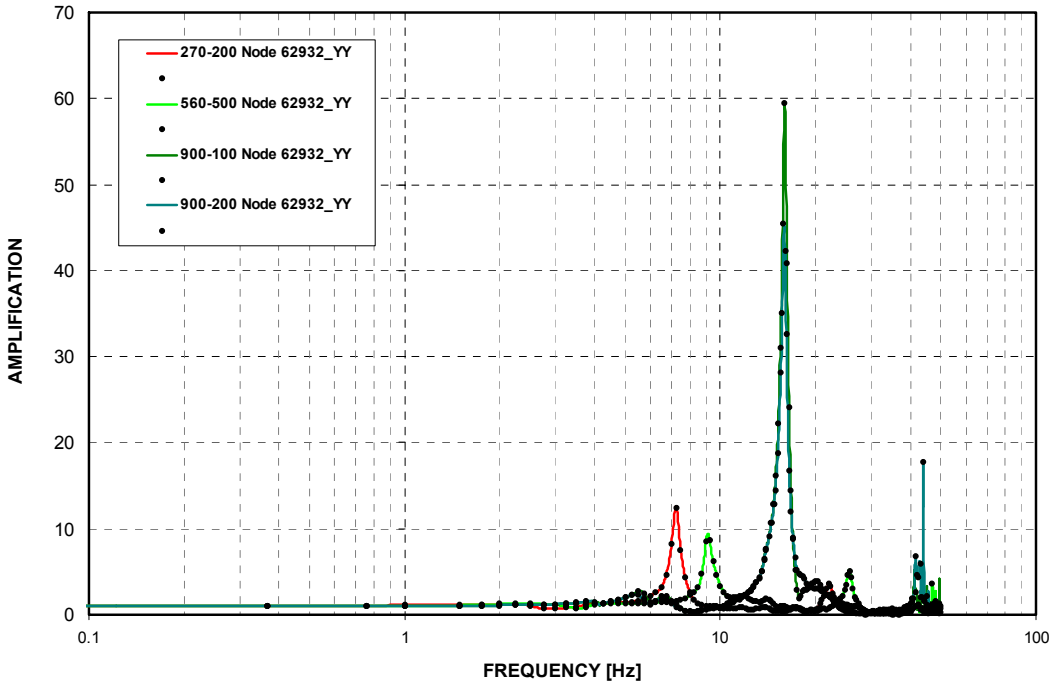

Figure 3-C.2.0-83 East PS/B Southeast Corner at Roof - Uncracked - EW Direction (Y)

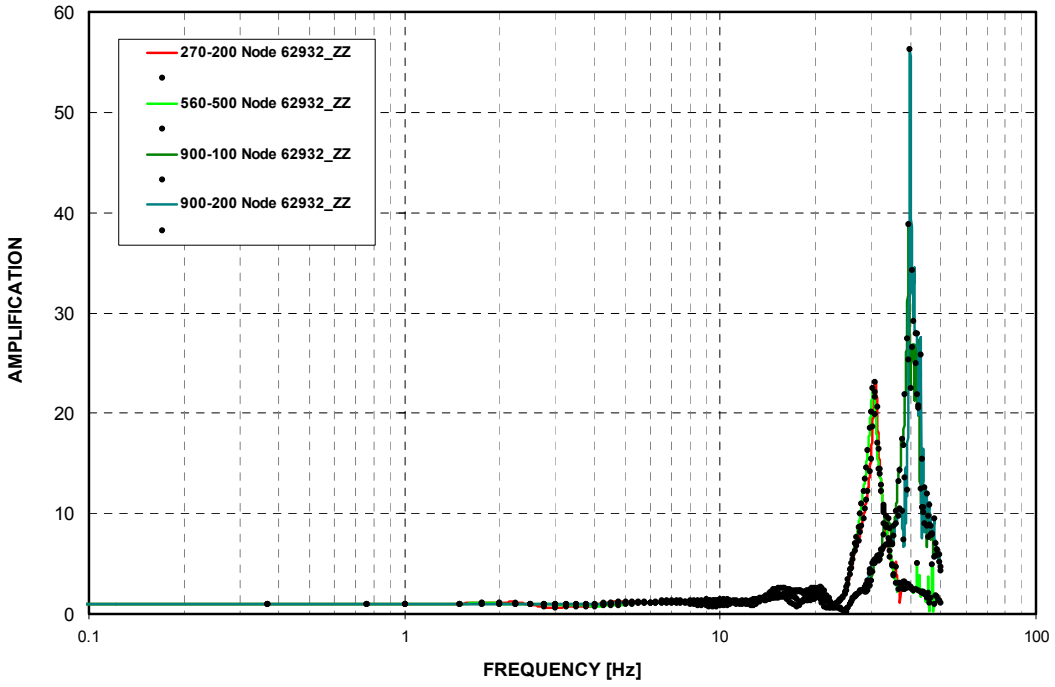

Figure 3-C.2.0-84 East PS/B Southeast Corner at Roof - Uncracked - Vertical Direction (Z)

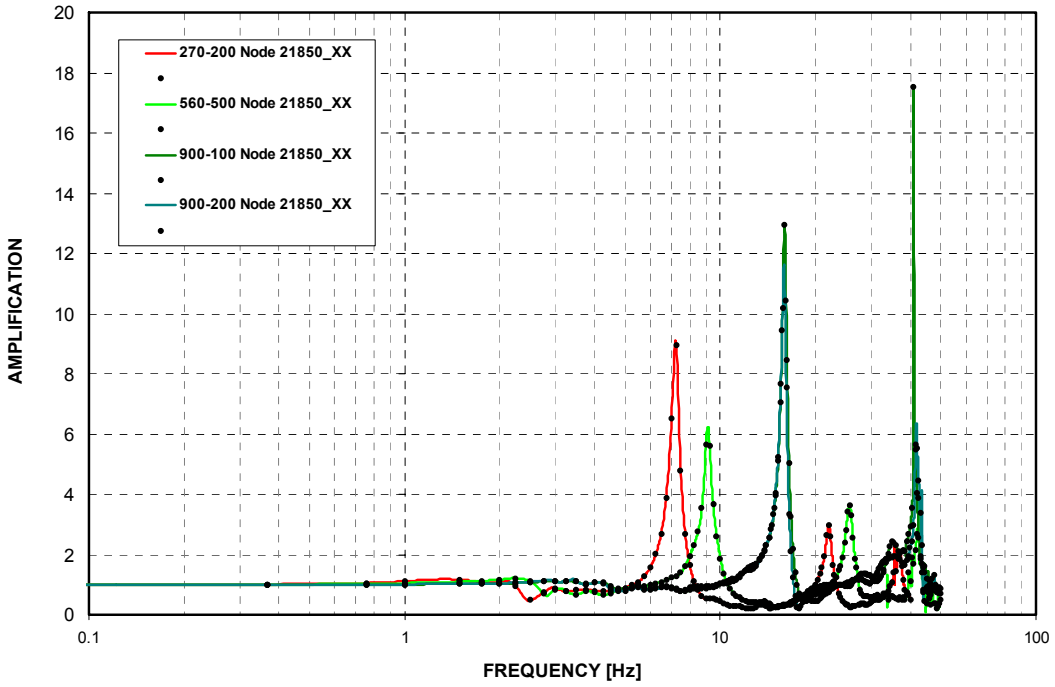

Figure 3-C.2.0-85 R/B Northeast Corner at Basemat - Cracked - NS Direction (X)

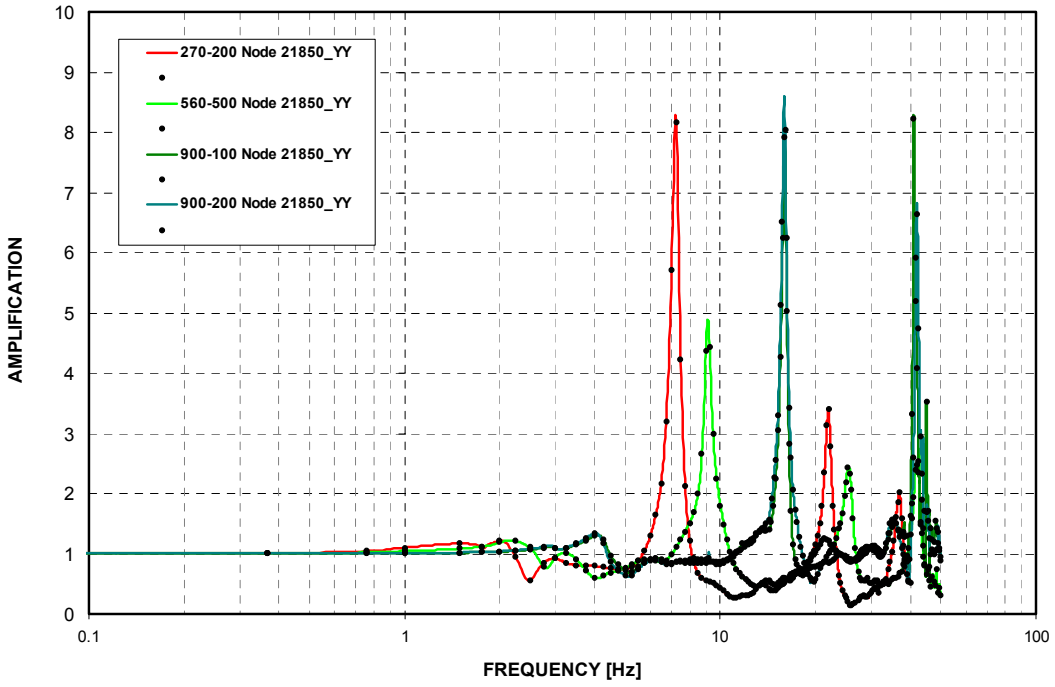

Figure 3-C.2.0-86 R/B Northeast Corner at Basemat - Cracked - EW Direction (Y)

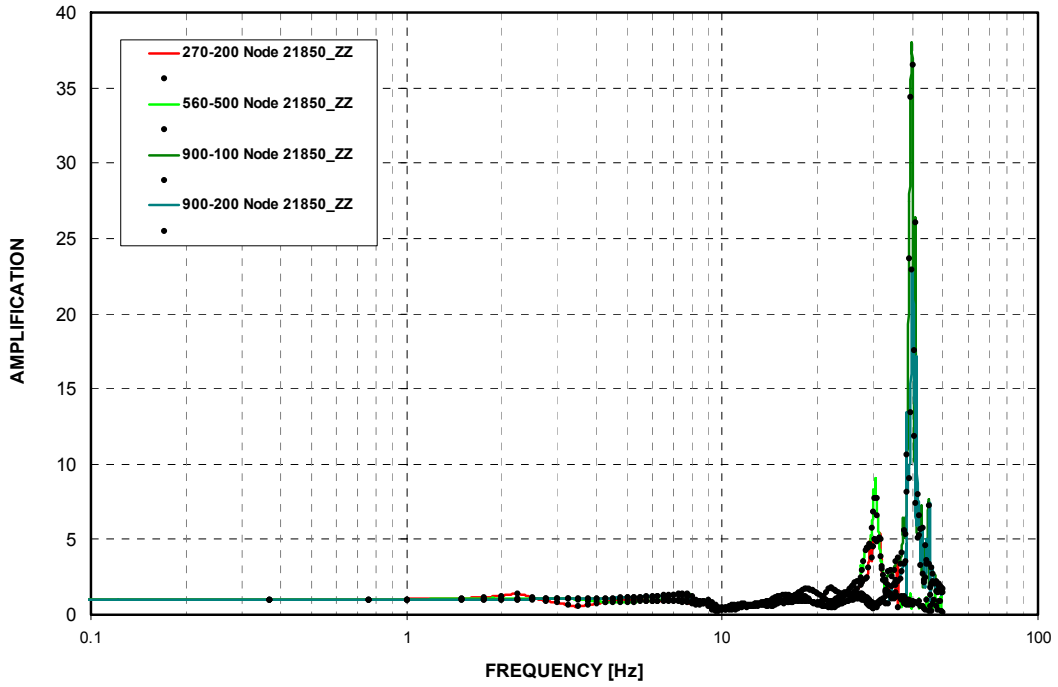

Figure 3-C.2.0-87 R/B Northeast Corner at Basemat - Cracked - Vertical Direction (Z)

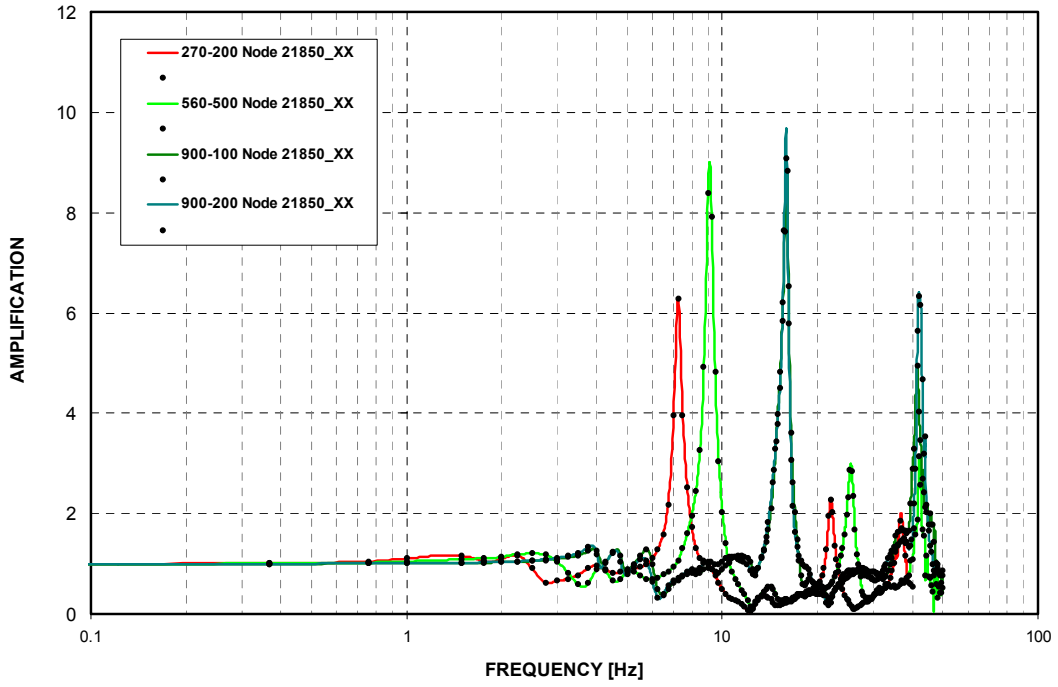

Figure 3-C.2.0-88 R/B Northeast Corner at Basemat - Uncracked - NS Direction (X)

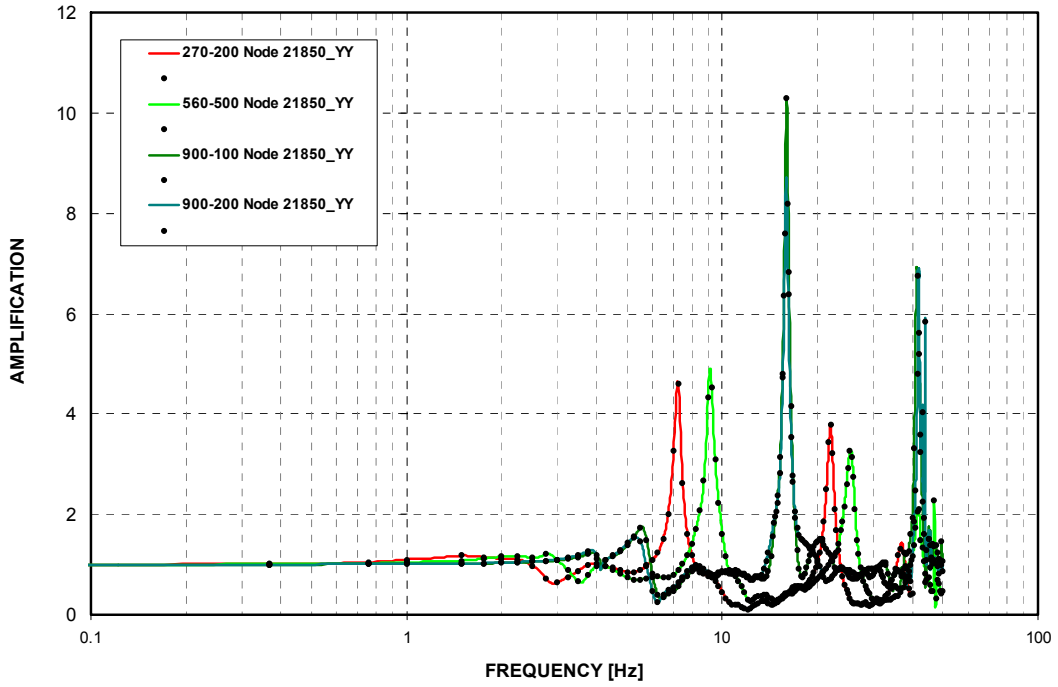

Figure 3-C.2.0-89 R/B Northeast Corner at Basemat - Uncracked - EW Direction (Y)

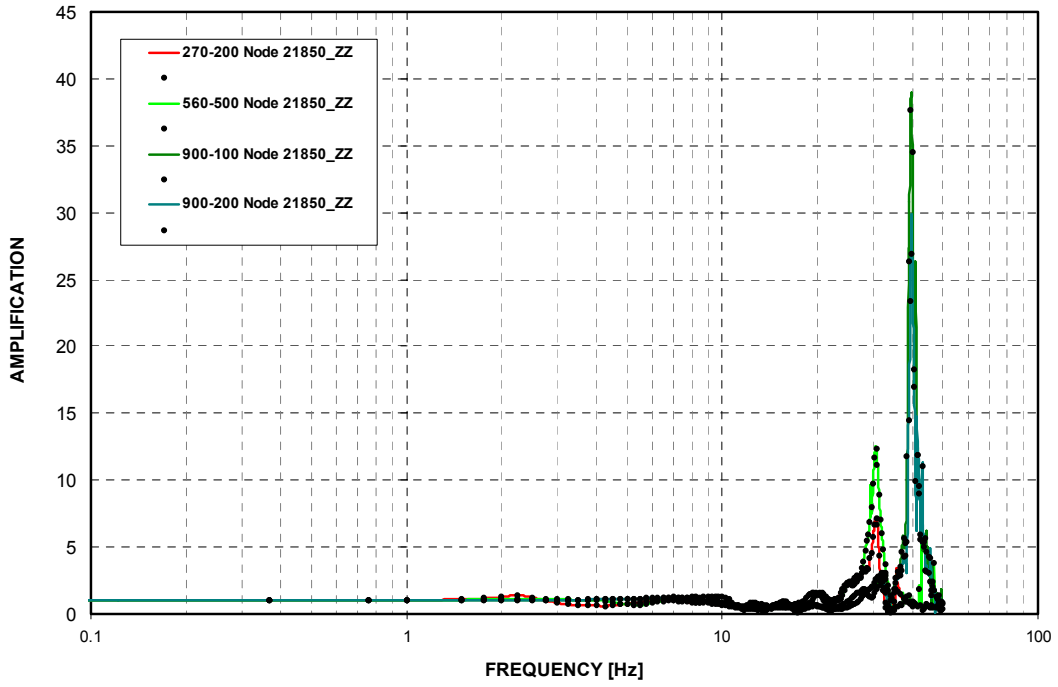

Figure 3-C.2.0-90 R/B Northeast Corner at Basemat - Uncracked - Vertical Direction (Z)

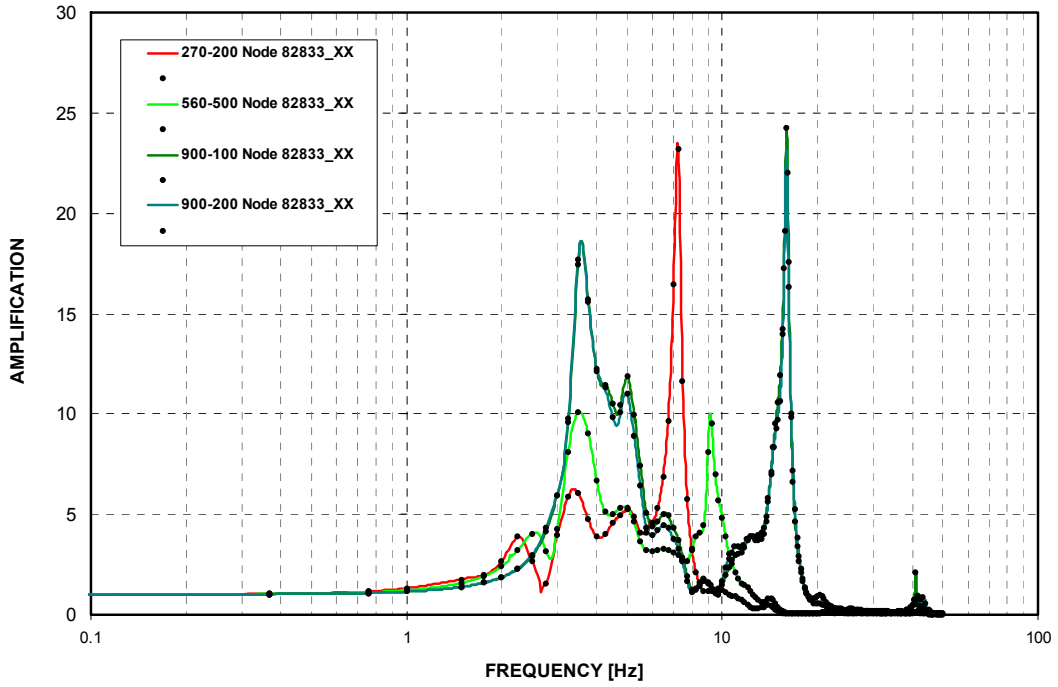

Figure 3-C.2.0-91 R/B Northeast Corner at Roof - Cracked - NS Direction (X)

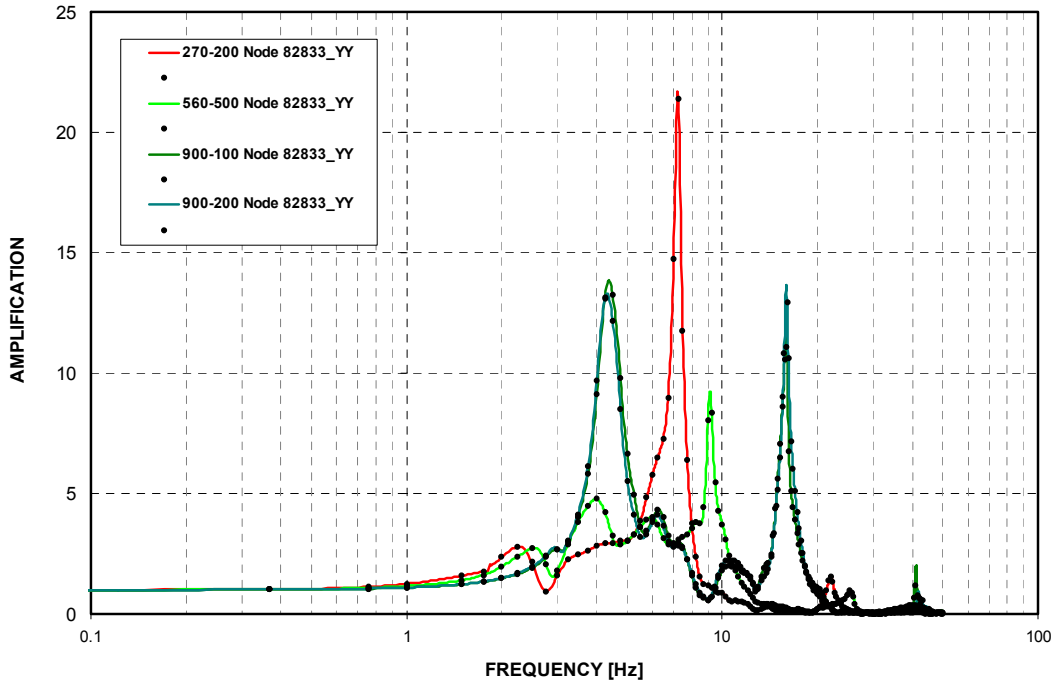

Figure 3-C.2.0-92 R/B Northeast Corner at Roof - Cracked - EW Direction (Y)

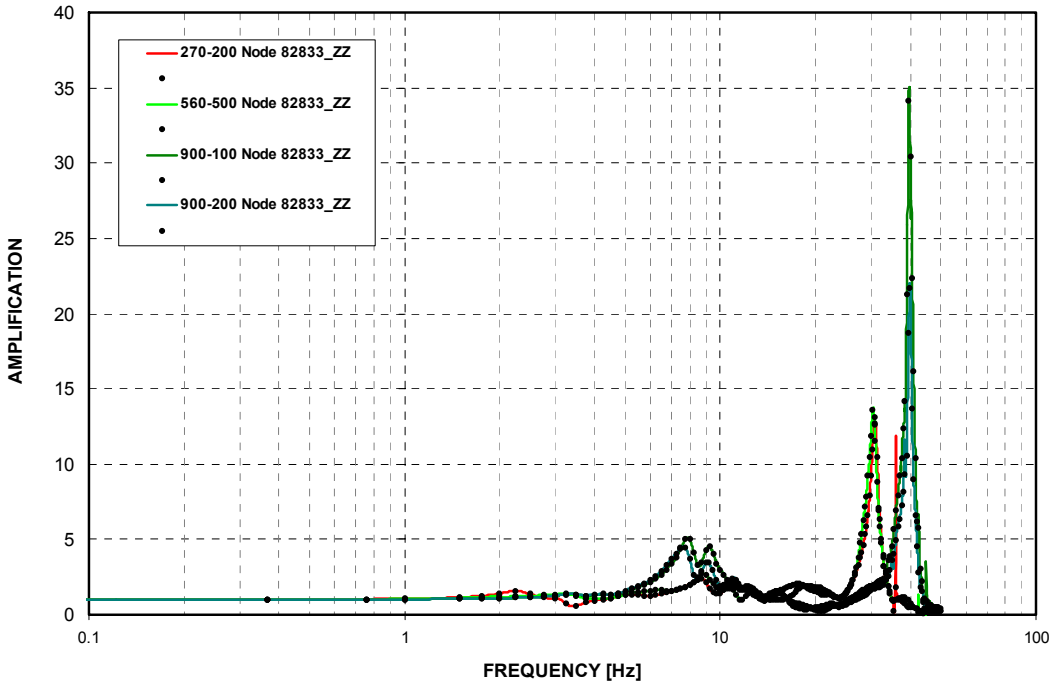

Figure 3-C.2.0-93 R/B Northeast Corner at Roof - Cracked - Vertical Direction (Z)

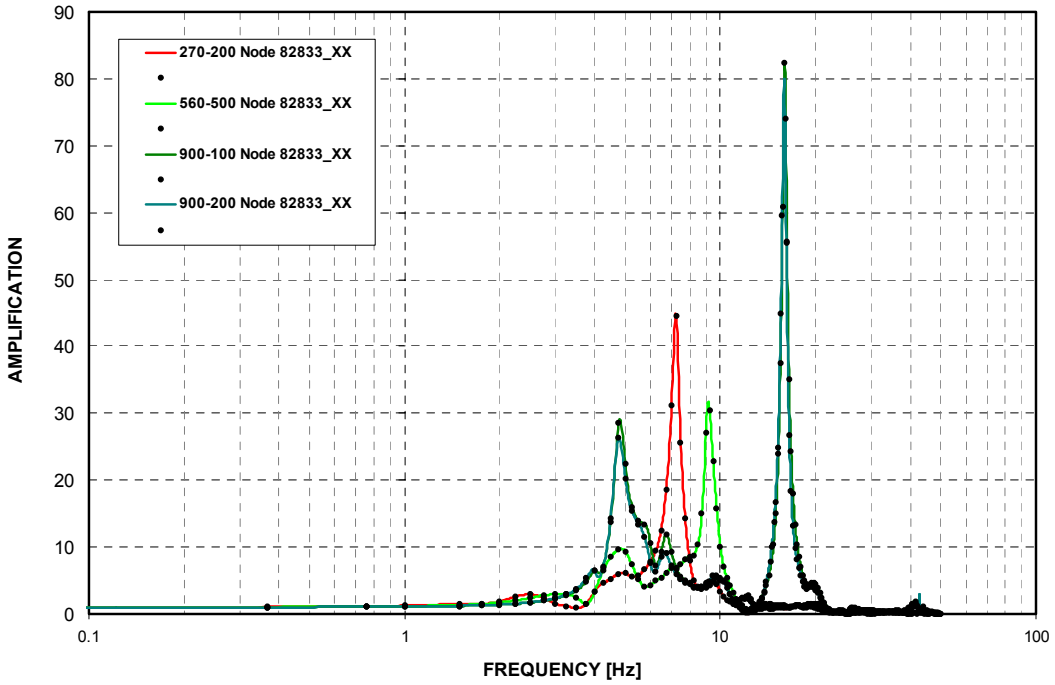

Figure 3-C.2.0-94 R/B Northeast Corner at Roof - Uncracked - NS Direction (X)

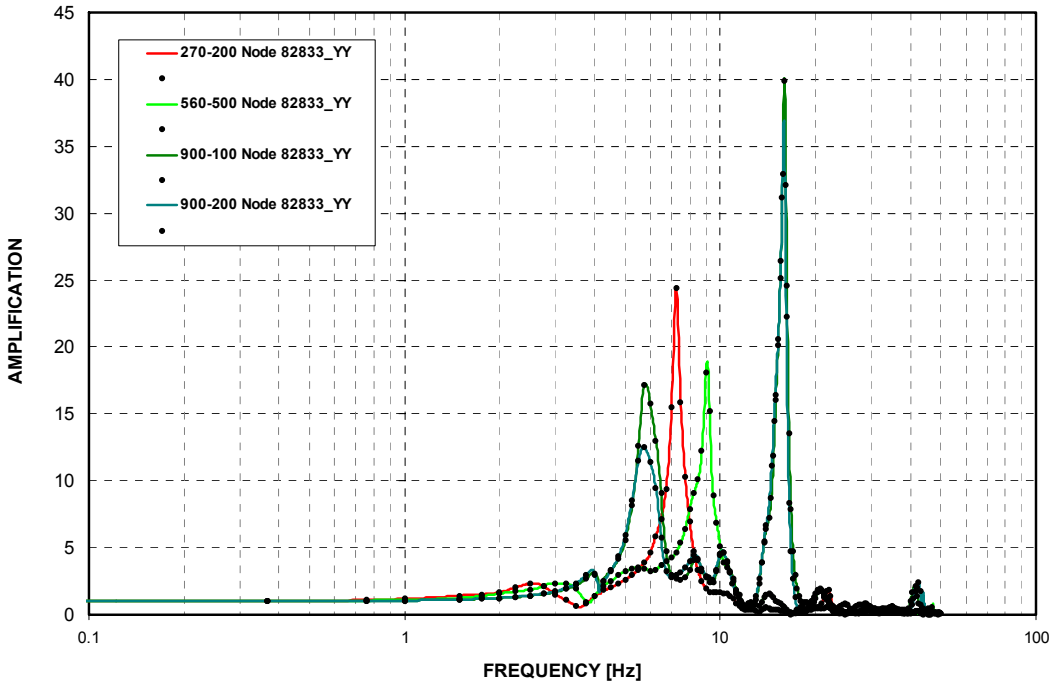

Figure 3-C.2.0-95 R/B Northeast Corner at Roof - Uncracked - EW Direction (Y)

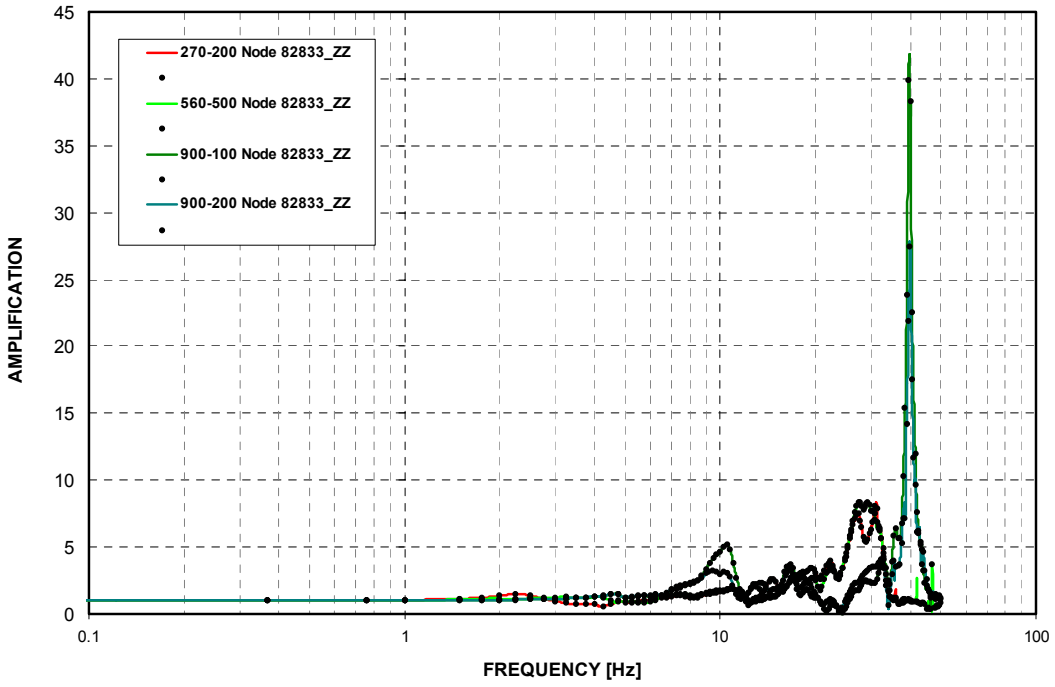

Figure 3-C.2.0-96 R/B Northeast Corner at Roof - Uncracked - Vertical Direction (Z)

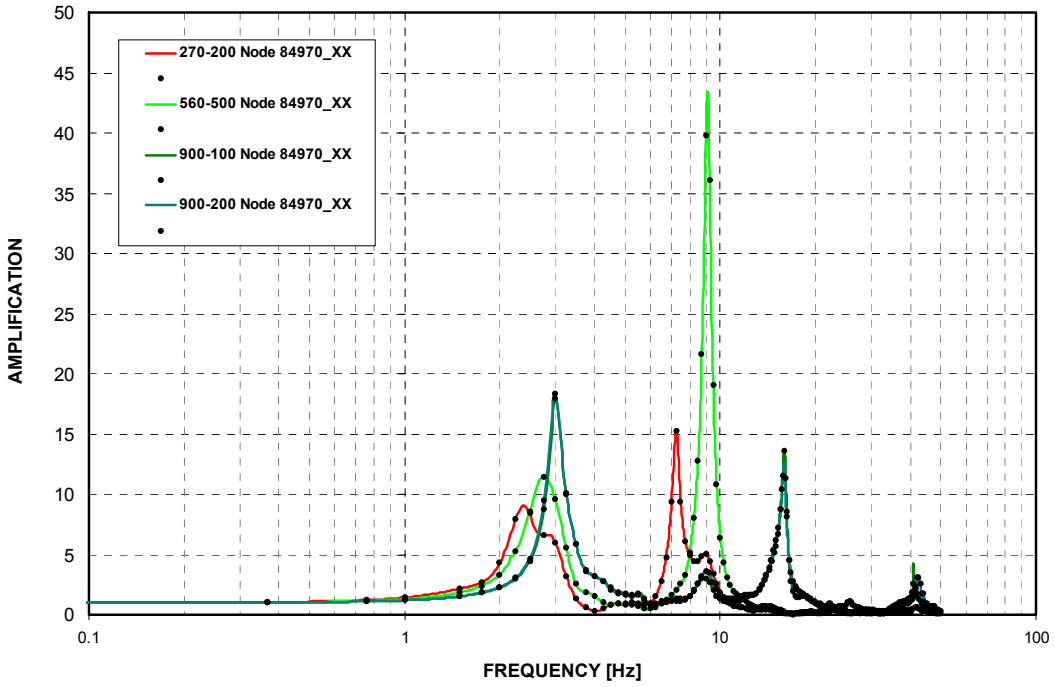

Figure 3-C.2.0-97 Top of PCCV - Cracked - NS Direction (X)

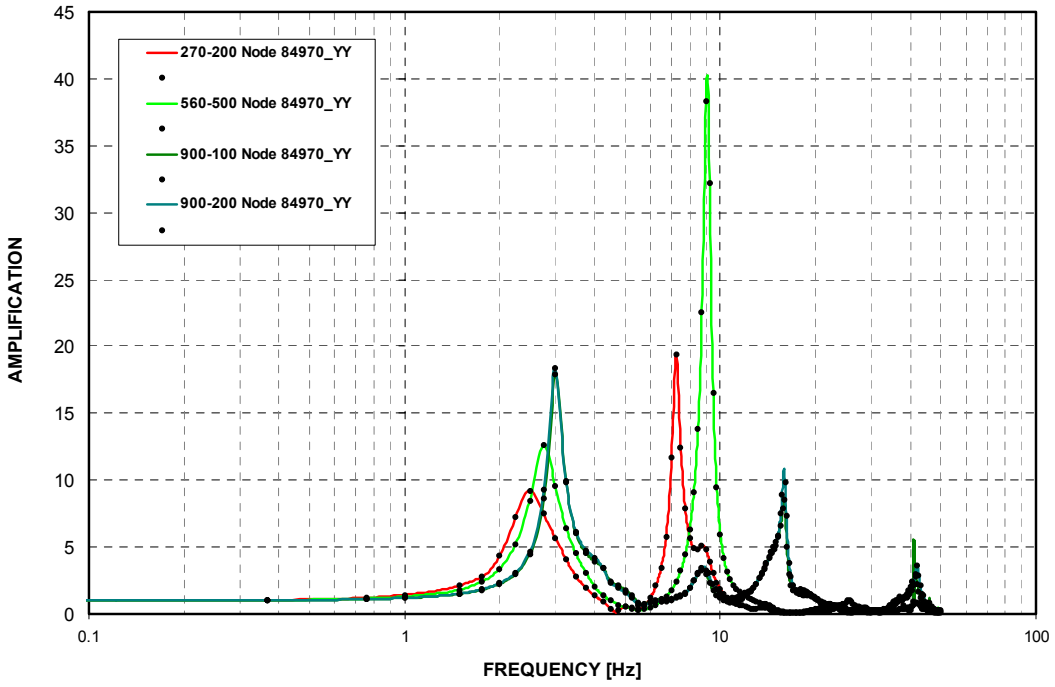

Figure 3-C.2.0-98 Top of PCCV - Cracked - EW Direction (Y)

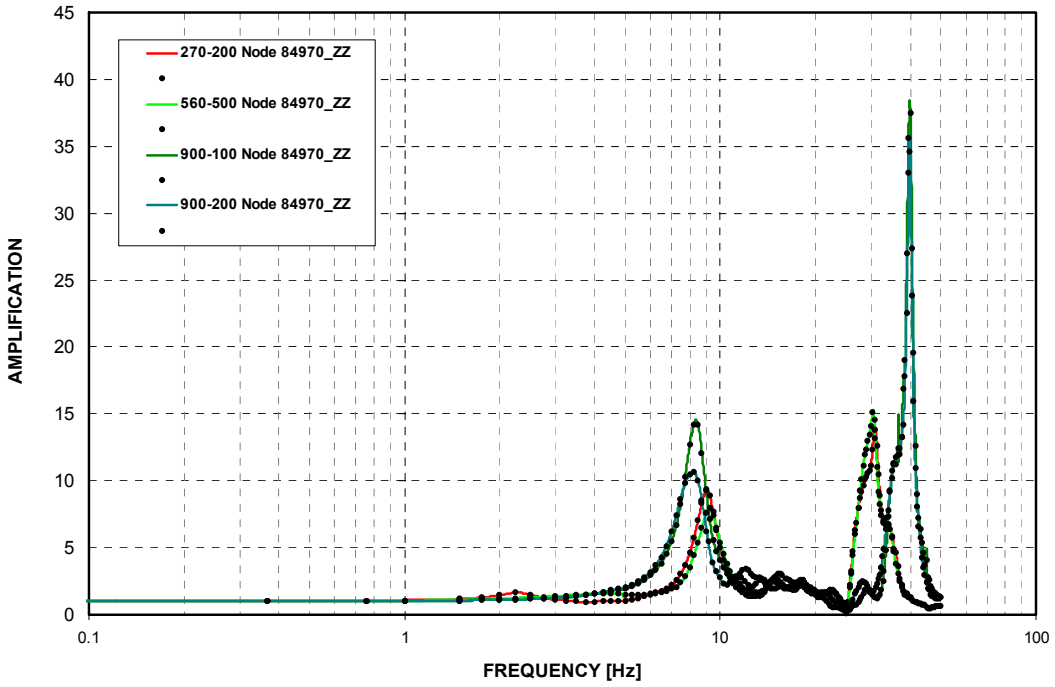

Figure 3-C.2.0-99 Top of PCCV - Cracked - Vertical Direction (Z)

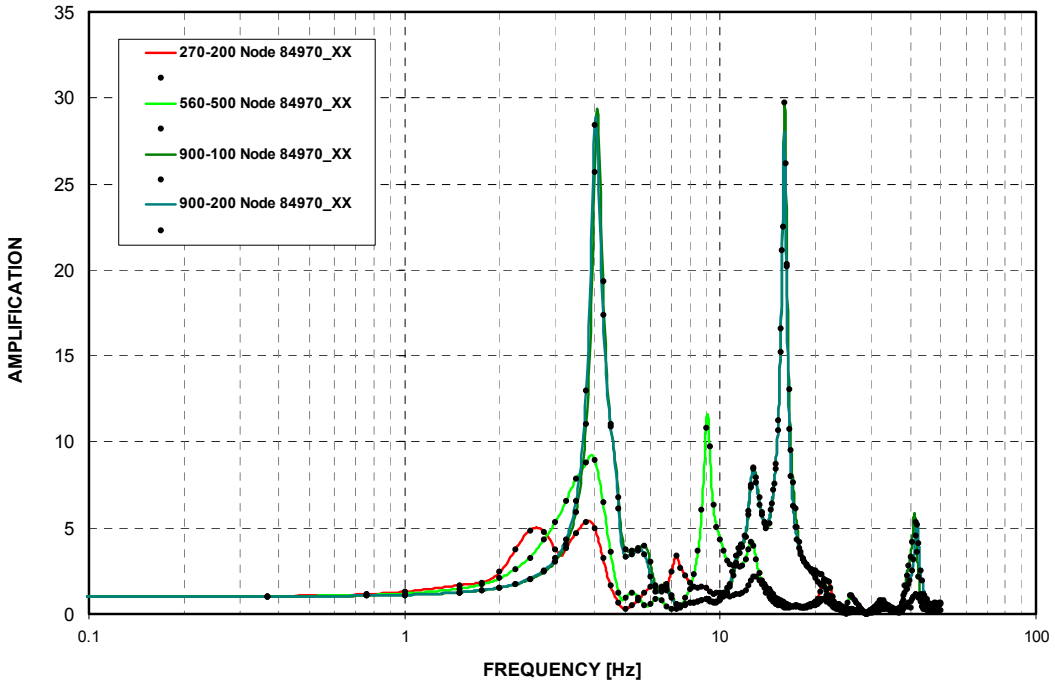

Figure 3-C.2.0-100 Top of PCCV - Uncracked - NS Direction (X)

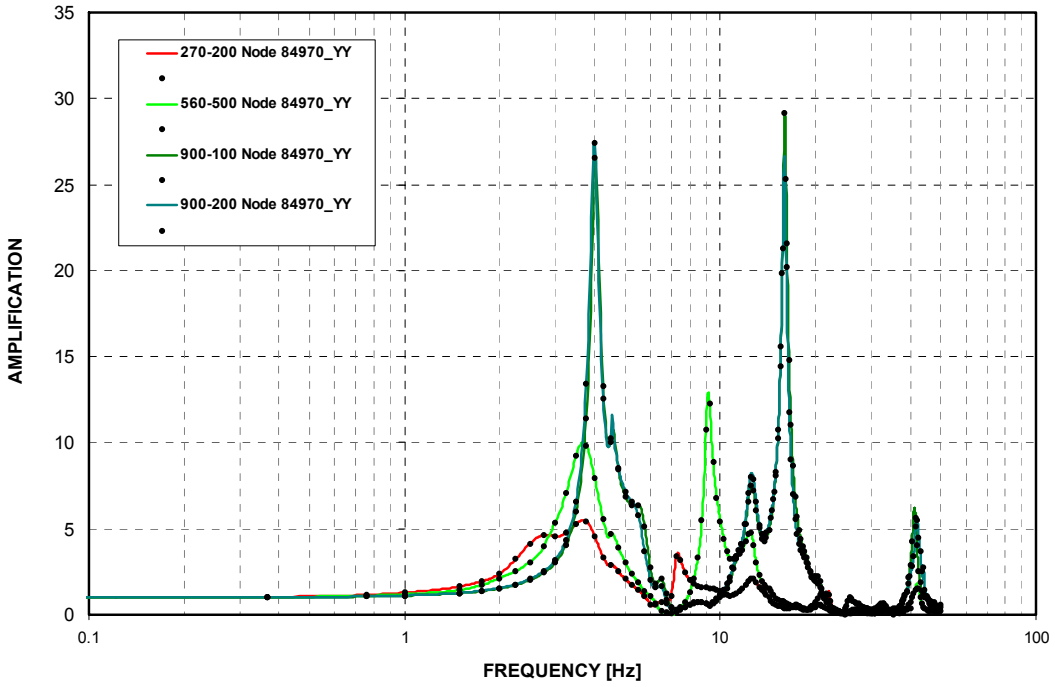

Figure 3-C.2.0-101 Top of PCCV - Uncracked - EW Direction (Y)

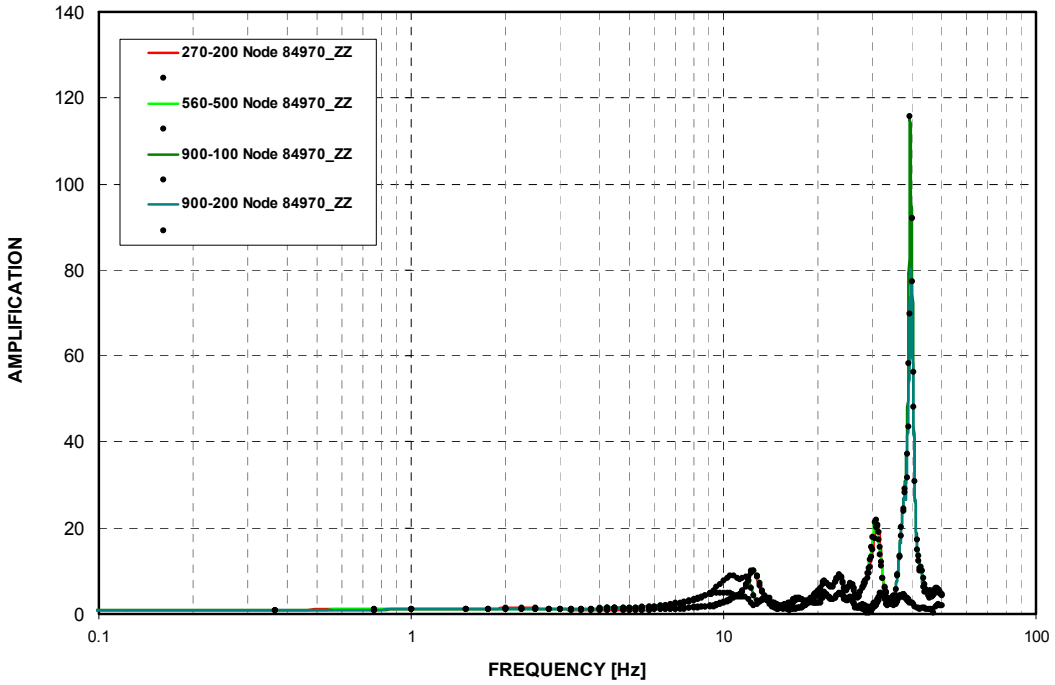

Figure 3-C.2.0-102 Top of PCCV - Uncracked - Vertical Direction (Z)

Appendix 3-D

Parametric Study of Soil Model Depth

APPENDIX 3-D TABLE OF CONTENTS

Section	Title	Page No.
3-D.1.0	OBJECTIVE	3-D.1-1
3-D.2.0	METHODOLOGY	3-D.2-1
3-D.3.0	COMPUTATION	3-D.3-1
3-D.4.0	RESULTS AND CONCLUSION	3-D.4-1

LIST OF FIGURES

Figure	Title	Page No.
Figure 3-D.4.0-1	Top of Reactor Cavity - Response Spectra - NS Direction (X)	3-D.4-2
Figure 3-D.4.0-2	Top of Reactor Cavity - Response Spectra - EW Direction (Y)	3-D.4-3
Figure 3-D.4.0-3	Top of Reactor Cavity - Response Spectra - Vertical Direction (Z)	3-D.4-4
Figure 3-D.4.0-4	Sump Strainer Supports - Response Spectra - NS Direction (X)	3-D.4-5
Figure 3-D.4.0-5	Sump Strainer Supports - Response Spectra - EW Direction (Y)	3-D.4-6
Figure 3-D.4.0-6	Sump Strainer Supports - Response Spectra - Vertical Direction (Z)	3-D.4-7
Figure 3-D.4.0-7	SG Lower Supports - Response Spectra - NS Direction (X)	3-D.4-8
Figure 3-D.4.0-8	SG Lower Supports - Response Spectra - EW Direction (Y)	3-D.4-9
Figure 3-D.4.0-9	SG Lower Supports - Response Spectra - Vertical Direction (Z)	3-D.4-10
Figure 3-D.4.0-10	SG Upper Supports - Response Spectra - NS Direction (X)	3-D.4-11
Figure 3-D.4.0-11	SG Upper Supports - Response Spectra - EW Direction (Y)	3-D.4-12
Figure 3-D.4.0-12	SG Upper Supports - Response Spectra - Vertical Direction (Z)	3-D.4-13
Figure 3-D.4.0-13	SFP - Response Spectra - NS Direction (X)	3-D.4-14
Figure 3-D.4.0-14	SFP - Response Spectra - EW Direction (Y)	3-D.4-15
Figure 3-D.4.0-15	SFP - Response Spectra - Vertical Direction (Z)	3-D.4-16
Figure 3-D.4.0-16	NFSP - Response Spectra - NS Direction (X)	3-D.4-17
Figure 3-D.4.0-17	NFSP - Response Spectra - EW Direction (Y)	3-D.4-18
Figure 3-D.4.0-18	NFSP - Response Spectra - Vertical Direction (Z)	3-D.4-19
Figure 3-D.4.0-19	A-AAC GTG - Response Spectra - NS Direction (X)	3-D.4-20
Figure 3-D.4.0-20	A-AAC GTG - Response Spectra - EW Direction (Y)	3-D.4-21
Figure 3-D.4.0-21	A-AAC GTG - Response Spectra - Vertical Direction (Z)	3-D.4-22
Figure 3-D.4.0-22	B-AAC GTG - Response Spectra - NS Direction (X)	3-D.4-23
Figure 3-D.4.0-23	B-AAC GTG - Response Spectra - EW Direction (Y)	3-D.4-24
Figure 3-D.4.0-24	B-AAC GTG - Response Spectra - Vertical Direction (Z)	3-D.4-25

Figure 3-D.4.0-25 A/B Northwest Corner at Basemat - Response Spectra - NS Direction (X) 3-D.4-26
Figure 3-D.4.0-26 A/B Northwest Corner at Basemat - Response Spectra - EW Direction (Y) 3-D.4-27
Figure 3-D.4.0-27 A/B Northwest Corner at Basemat - Response Spectra - Vertical Direction (Z) 3-D.4-28
Figure 3-D.4.0-28 A/B Northwest Corner at Roof - Response Spectra - NS Direction (X) 3-D.4-29
Figure 3-D.4.0-29 A/B Northwest Corner at Roof - Response Spectra - EW Direction (Y) 3-D.4-30
Figure 3-D.4.0-30 A/B Northwest Corner at Roof - Response Spectra - Vertical Direction (Z) 3-D.4-31
Figure 3-D.4.0-31 West PS/B Southwest Corner at Basemat - Response Spectra - NS Direction (X) 3-D.4-32
Figure 3-D.4.0-32 West PS/B Southwest Corner at Basemat - Response Spectra EW Direction (Y) 3-D.4-33
Figure 3-D.4.0-33 West PS/B Southwest Corner at Basemat - Response Spectra - Vertical Direction (Z) 3-D.4-34
Figure 3-D.4.0-34 West PS/B Southwest Corner at Roof - Response Spectra - NS Direction (X) 3-D.4-35
Figure 3-D.4.0-35 West PS/B Southwest Corner at Roof - Response Spectra - EW Direction (Y) 3-D.4-36
Figure 3-D.4.0-36 West PS/B Southwest Corner at Roof - Response Spectra - Vertical Direction (Z) 3-D.4-37
Figure 3-D.4.0-37 East PS/B Southeast Corner at Basemat - Response Spectra - NS Direction (X) 3-D.4-38
Figure 3-D.4.0-38 East PS/B Southeast Corner at Basemat - Response Spectra - EW Direction (Y) 3-D.4-39
Figure 3-D.4.0-39 East PS/B Southeast Corner at Basemat - Response Spectra - Vertical Direction (Z) 3-D.4-40
Figure 3-D.4.0-40 East PS/B Southeast Corner at Roof - Response Spectra - NS Direction (X) 3-D.4-41
Figure 3-D.4.0-41 East PS/B Southeast Corner at Roof - Response Spectra - EW Direction (Y) 3-D.4-42
Figure 3-D.4.0-42 East PS/B Southeast Corner at Roof - Response Spectra - Vertical Direction (Z) 3-D.4-43
Figure 3-D.4.0-43 R/B Northeast Corner at Basemat - Response Spectra - NS Direction (X) 3-D.4-44
Figure 3-D.4.0-44 R/B Northeast Corner at Basemat - Response Spectra - EW Direction (Y) 3-D.4-45
Figure 3-D.4.0-45 R/B Northeast Corner at Basemat - Response Spectra - Vertical Direction (Z) 3-D.4-46

Figure 3-D.4.0-46 R/B Northeast Corner at Roof - Response Spectra - NS Direction (X) 3-D.4-47
Figure 3-D.4.0-47 R/B Northeast Corner at Roof - Response Spectra - EW Direction (Y) 3-D.4-48
Figure 3-D.4.0-48 R/B Northeast Corner at Roof - Response Spectra - Vertical Direction (Z) 3-D.4-49
Figure 3-D.4.0-49 Top of PCCV - Response Spectra - NS Direction (X) 3-D.4-50
Figure 3-D.4.0-50 Top of PCCV - Response Spectra - EW Direction (Y) 3-D.4-51
Figure 3-D.4.0-51 Top of PCCV - Response Spectra - Vertical Direction (Z) 3-D.4-52

LIST OF TABLES

Table **Title** **Page No.**
Table 3-D.3.0-1 SSI Soil Input for 270-500-Extended Site Model 3-D.3-1
Table 3-D.3.0-2 Matrix of SASSI Runs 3-D.3-4
Table 3-D.3.0-3 Frequencies of Analysis 3-D.3-4
Table 3-D.4.0-1 Nodes of Response Spectra 3-D.4-1

3-D.1.0 OBJECTIVE

The objective of this appendix is to demonstrate that the depth of the site models of the soil profiles summarized in Section 3.3.1 of this report are established at an adequate depth in accordance with Acceptance Criteria 4 of SRP 3.7.2 (Reference 03-1). A sensitivity study therefore is performed for the 270-500 soil case by including an additional rock layer and extending the site model depth down to hardrock level (i.e., making the half space in or below the hard rock stratum). The results presented herein demonstrate that the site model depths used in the SSI analysis are adequate. Further extending the half space into or below hard rock layer has an insignificant impact on the accuracy of the computed SSI response of the R/B complex.

3-D.2.0 METHODOLOGY

Representative nodes are selected for comparison of ARS. The nodes included represent the support of the RV, the SFP, NFSP, Sump Strainer, the top of the PCCV, one A-AAC GTG of the East PS/B and one B-AAC GTG of the West PS/B, and four corner of the R/B at the basemat and roof elevations.

ARS plots are generated for the in-line response of each input seismic motion showing the two site models; 270-500, which represents the site model used in production run with fixed layer depth of 951 ft, and 270-500-extended with a deeper depth of 1295 ft. The shallower soil model shall be considered adequate if its seismic response is comparable to the deeper model's seismic response.

3-D.3.0 COMPUTATION

The 270-500 soil profile model used in the SSI and SSSI analyses is shown in Table 03.3.1-2. The properties for the deeper soil profile (270-500 Extended) used for this parametric study is shown in Table 3-D.3.0-1.

Table 3-D.3.0-2 presents the matrix of the ACS SASSI analyses performed for the parametric study. Note that the first analysis shown is the SSI analysis and the second shown is performed for the extended depth site model. The frequencies of analysis are listed in Table 3-D.3.0-3. The comparative analysis is performed on the R/B complex model with full structural stiffness and associated damping ratios.

Table 3-D.3.0-1 SSI Soil Input for 270-500-Extended Site Model (Sheet 1 of 3)

Layer	Thickness	Depth	Unit Weight	Vs	Vp	Damp.
#	[ft]	[ft]	[kcf]	[ft/sec]	[ft/sec]	%
1	5.583	0.0	0.125	1178	5106	1.65
2	5.583	5.6	0.125	1175	5198	2.10
3	7.000	11.2	0.125	1175	5214	2.44
4	5.375	18.2	0.125	1180	5115	2.49
5	5.375	23.5	0.125	1167	5141	2.81
6	6.667	28.9	0.125	1202	5233	2.89
7	6.667	35.6	0.125	1232	5323	2.97
8	3.411	42.3	0.125	1256	5457	3.10
9	3.411	45.7	0.125	1256	5457	3.10
10	4.290	49.1	0.125	1301	5658	3.14
11	4.290	53.4	0.125	1301	5658	3.14
12	4.290	57.7	0.125	1277	5618	3.36
13	4.290	61.9	0.125	1277	5618	3.36
14	4.290	66.2	0.125	1271	5625	3.52
15	4.290	70.5	0.125	1271	5625	3.52
16	4.290	74.8	0.125	1327	5872	3.48
17	4.290	79.1	0.125	1327	5872	3.48
18	4.689	83.4	0.125	1309	5806	2.71
19	4.689	88.1	0.125	1309	5806	2.71
20	4.687	92.8	0.125	1352	5992	2.70
21	4.687	97.5	0.125	1352	5992	2.70
22	4.689	102.1	0.125	1350	6001	2.76
23	4.689	106.8	0.125	1350	6001	2.76
24	4.687	111.5	0.125	1332	5956	2.86
25	4.687	116.2	0.125	1332	5956	2.86
26	4.689	120.9	0.125	1419	6309	2.76
27	4.689	125.6	0.125	1419	6309	2.76
28	4.687	130.3	0.125	1448	6427	2.76
29	4.687	135.0	0.125	1448	6427	2.76
30	5.000	139.6	0.131	1504	6632	2.63
31	5.000	144.6	0.131	1504	6632	2.63
32	5.000	149.6	0.131	1541	6790	2.62
33	5.000	154.6	0.131	1541	6790	2.62

Table 3-D.3.0-1 SSI Soil Input for 270-500-Extend Site Model (Sheet 2 of 3)

Layer	Thickness	Depth	Unit Weight	Vs	Vp	Damp.
#	[ft]	[ft]	[kcf]	[ft/sec]	[ft/sec]	%
34	5.000	159.6	0.131	1578	6956	2.60
35	5.000	164.6	0.131	1578	6956	2.60
36	5.000	169.6	0.131	1575	6958	2.65
37	5.000	174.6	0.131	1575	6958	2.65
38	5.000	179.6	0.131	1589	7029	2.66
39	5.000	184.6	0.131	1589	7029	2.66
40	5.000	189.6	0.131	1592	7052	2.70
41	5.000	194.6	0.131	1592	7052	2.70
42	5.299	199.6	0.131	1616	7160	2.70
43	5.299	204.9	0.131	1616	7160	2.70
44	5.299	210.2	0.131	1710	7317	2.30
45	5.299	215.5	0.131	1710	7317	2.30
46	5.750	220.8	0.131	1771	7563	2.26
47	5.750	226.6	0.131	1771	7563	2.26
48	5.750	232.3	0.131	1684	7245	2.42
49	5.750	238.1	0.131	1684	7245	2.42
50	5.889	243.8	0.131	1691	7291	2.44
51	5.889	249.7	0.131	1691	7291	2.44
52	5.889	255.6	0.131	1691	7291	2.44
53	5.889	261.5	0.131	1705	7358	2.47
54	5.889	267.4	0.131	1705	7358	2.47
55	5.889	273.3	0.131	1705	7358	2.47
56	5.889	279.2	0.131	1759	7574	2.43
57	5.889	285.1	0.131	1759	7574	2.43
58	5.889	291.0	0.131	1759	7574	2.43
59	6.083	296.8	0.131	1795	7723	2.42
60	6.083	302.9	0.131	1795	7723	2.42
61	6.083	309.0	0.131	1795	7723	2.42
62	6.083	315.1	0.131	1776	7665	2.50
63	6.083	321.2	0.131	1776	7665	2.50
64	6.083	327.3	0.131	1776	7665	2.50
65	6.083	333.3	0.131	1752	7591	2.57
66	6.083	339.4	0.131	1752	7591	2.57
67	6.083	345.5	0.131	1752	7591	2.57
68	6.083	351.6	0.131	1749	7585	2.62
69	6.083	357.7	0.131	1749	7585	2.62
70	6.083	363.8	0.131	1749	7585	2.62
71	6.667	369.8	0.131	1768	7659	2.62
72	6.667	376.5	0.131	1768	7659	2.62
73	6.667	383.2	0.131	1768	7659	2.62
74	6.667	389.8	0.131	1747	7600	2.69
75	6.667	396.5	0.131	1747	7600	2.69
76	6.667	403.2	0.131	1747	7600	2.69
77	6.667	409.8	0.131	1788	7767	2.66
78	6.667	416.5	0.131	1788	7767	2.66
79	6.667	423.2	0.131	1788	7767	2.66

Table 3-D.3.0-1 SSI Soil Input for 270-500-Extend Site Model (Sheet 3 of 3)

Layer	Thickness	Depth	Unit Weight	Vs	Vp	Damp.
#	[ft]	[ft]	[kcf]	[ft/sec]	[ft/sec]	%
80	6.667	429.8	0.131	1791	7791	2.69
81	6.667	436.5	0.131	1791	7791	2.69
82	6.667	443.2	0.131	1791	7791	2.69
83	6.667	449.8	0.131	1817	7903	2.68
84	6.667	456.5	0.131	1817	7903	2.68
85	6.667	463.2	0.131	1817	7903	2.68
86	6.667	469.8	0.131	1780	7770	2.77
87	6.667	476.5	0.131	1780	7770	2.77
88	6.667	483.2	0.131	1780	7770	2.77
89	5.202	489.8	0.131	1783	7791	2.78
90	5.202	495.0	0.131	1783	7791	2.78
91	13.671	500.3	0.131	2376	7795	0.50
92	13.671	513.9	0.131	2376	7795	0.50
93	13.671	527.6	0.131	2376	7795	0.50
94	13.671	541.3	0.131	2376	7795	0.50
95	13.671	554.9	0.131	2376	7795	0.50
96	13.671	568.6	0.131	2376	7795	0.50
97	13.671	582.3	0.131	2376	7795	0.50
98	13.671	595.9	0.131	2376	7795	0.50
99	13.671	609.6	0.131	2376	7795	0.50
100	13.671	623.3	0.131	2376	7795	0.50
101	13.671	637.0	0.131	2376	7795	0.50
102	13.671	650.6	0.131	2376	7795	0.50
103	18.228	664.3	0.134	3281	8924	0.50
104	18.228	682.5	0.134	3281	8924	0.50
105	18.228	700.8	0.134	3281	8924	0.50
106	18.228	719.0	0.134	3281	8924	0.50
107	18.228	737.2	0.134	3281	8924	0.50
108	18.228	755.4	0.134	3281	8924	0.50
109	18.228	773.7	0.134	3281	8924	0.50
110	18.228	791.9	0.134	3281	8924	0.50
111	18.228	810.1	0.134	3281	8924	0.50
112	27.342	828.4	0.140	4922	11240	0.50
113	27.342	855.7	0.140	4922	11240	0.50
114	27.342	883.0	0.140	4922	11240	0.50
115	27.342	910.4	0.140	4922	11240	0.50
116	27.342	937.7	0.140	4922	11240	0.50
117	27.342	965.1	0.140	4922	11240	0.50
118	41.013	992.4	0.144	6562	14270	0.50
119	41.013	1033.4	0.144	6562	14270	0.50
120	41.013	1074.4	0.144	6562	14270	0.50
121	41.013	1115.4	0.144	6562	14270	0.50
122	46.000	1156.5	0.150	8203	15420	0.25
123	46.000	1202.5	0.150	8203	15420	0.25
124	46.000	1248.5	0.150	8203	15420	0.25
Half Space		1294.5	0.150	8203	15420	0.25

Table 3-D.3.0-2 Matrix of SASSI Runs

SASSI Run	Soil Case	Depth (ft)	No. of Frequencies of Analysis	Cut-off Frequency (Hz)
1. 270-500	270-500	951	132	40
2. 270-500 Extended	270-500	1295	132	40

Table 3-D.3.0-3 Frequencies of Analysis

SASSI Run	Frequency of Analysis (Hz)	SASSI Run	Frequency of Analysis (Hz)	SASSI Run	Frequency of Analysis (Hz)	SASSI Run	Frequency of Analysis (Hz)
1	0.02	34	8.74	67	16.99	100	27.00
2	0.37	35	9.01	68	17.26	101	27.37
3	0.76	36	9.25	69	17.50	102	27.76
4	1.00	37	9.50	70	17.75	103	28.00
5	1.49	38	9.74	71	17.99	104	28.34
6	1.76	39	10.01	72	18.26	105	28.76
7	2.00	40	10.25	73	18.51	106	29.00
8	2.25	41	10.50	74	18.75	107	29.32
9	2.49	42	10.74	75	18.99	108	29.76
10	2.76	43	11.01	76	19.24	109	30.00
11	3.00	44	11.25	77	19.51	110	30.37
12	3.25	45	11.50	78	19.75	111	30.76
13	3.49	46	11.74	79	20.00	112	31.01
14	3.76	47	12.01	80	20.34	113	31.37
15	4.00	48	12.26	81	20.70	114	31.74
16	4.25	49	12.50	82	21.00	115	32.01
17	4.49	50	12.74	83	21.36	116	32.35
18	4.76	51	12.99	84	21.75	117	32.74
19	5.01	52	13.26	85	22.00	118	33.01
20	5.25	53	13.50	86	22.34	119	33.50
21	5.49	54	13.75	87	22.75	120	34.01
22	5.76	55	13.99	88	23.00	121	34.50
23	6.01	56	14.26	89	23.34	122	35.01
24	6.25	57	14.50	90	23.75	123	35.50
25	6.49	58	14.75	91	24.00	124	36.01
26	6.74	59	14.99	92	24.34	125	36.50
27	7.01	60	15.26	93	24.76	126	37.01
28	7.25	61	15.50	94	25.00	127	37.50
29	7.50	62	15.75	95	25.37	128	37.99
30	7.74	63	15.99	96	25.76	129	38.50
31	8.01	64	16.26	97	26.00	130	38.99
32	8.25	65	16.50	98	26.34	131	39.50
33	8.50	66	16.75	99	26.76	132	39.99

3-D.4.0 RESULTS AND CONCLUSION

Seventeen representative nodes are selected for the generation of ARS as shown in Table 3-D.4.0-1. The ARS plots are presented in Figure 3-D.4.0-1 through Figure 3-D.4.0-51. The figures demonstrate that the seismic response of the structure is similar regardless of the depth of soil modeled.

Table 3-D.4.0-1 Nodes of Response Spectra

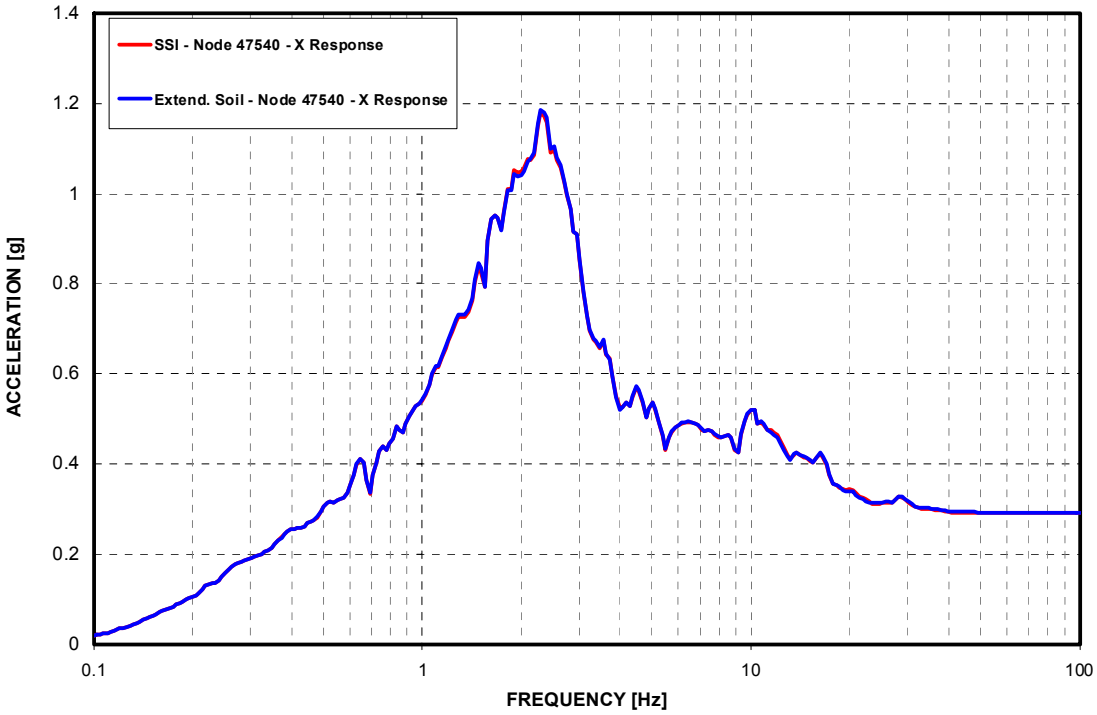

Figure 3-D.4.0-1 Top of Reactor Cavity - Response Spectra - NS Direction (X)

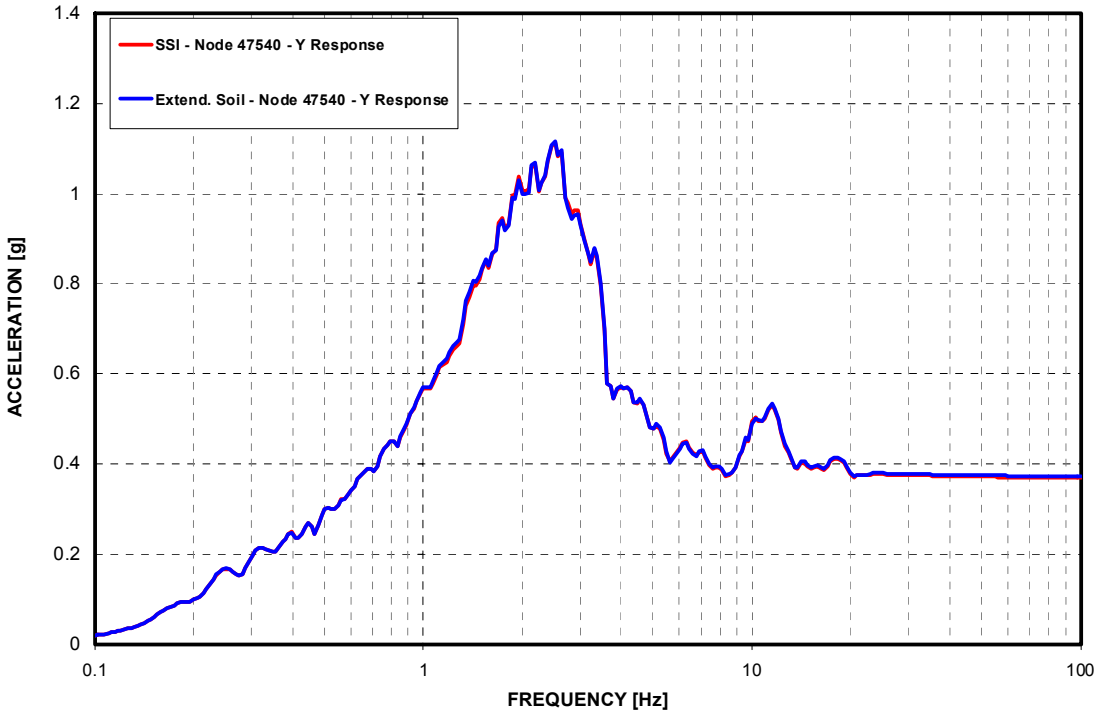

Figure 3-D.4.0-2 Top of Reactor Cavity - Response Spectra - EW Direction (Y)

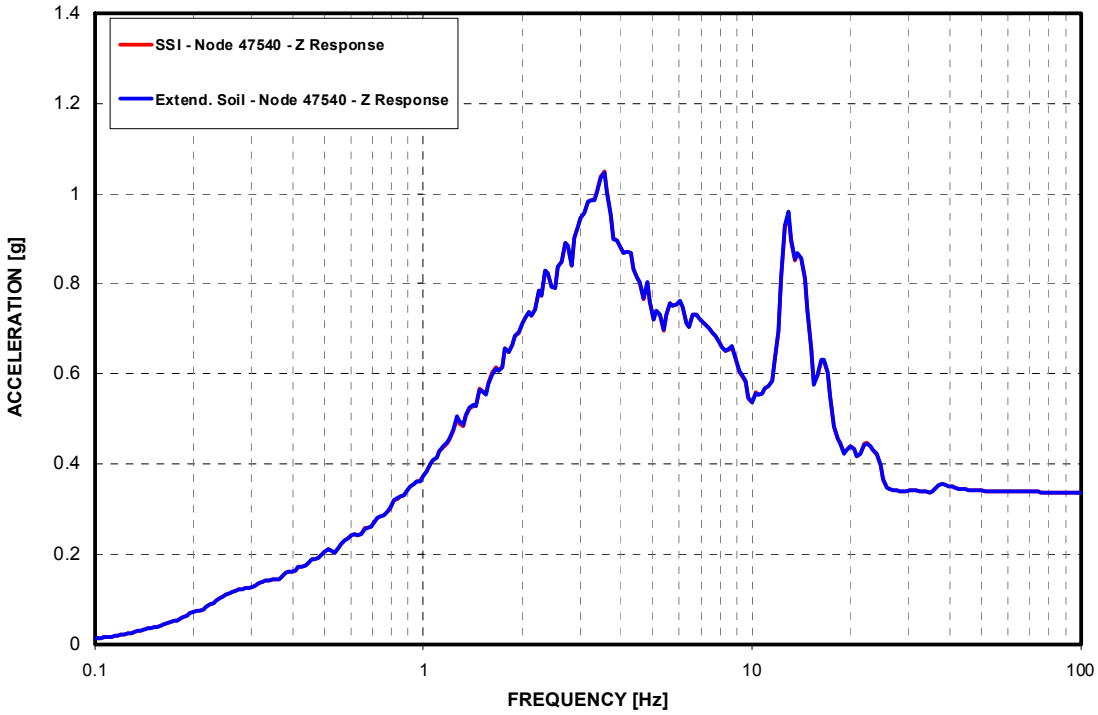

Figure 3-D.4.0-3 Top of Reactor Cavity - Response Spectra - Vertical Direction (Z)

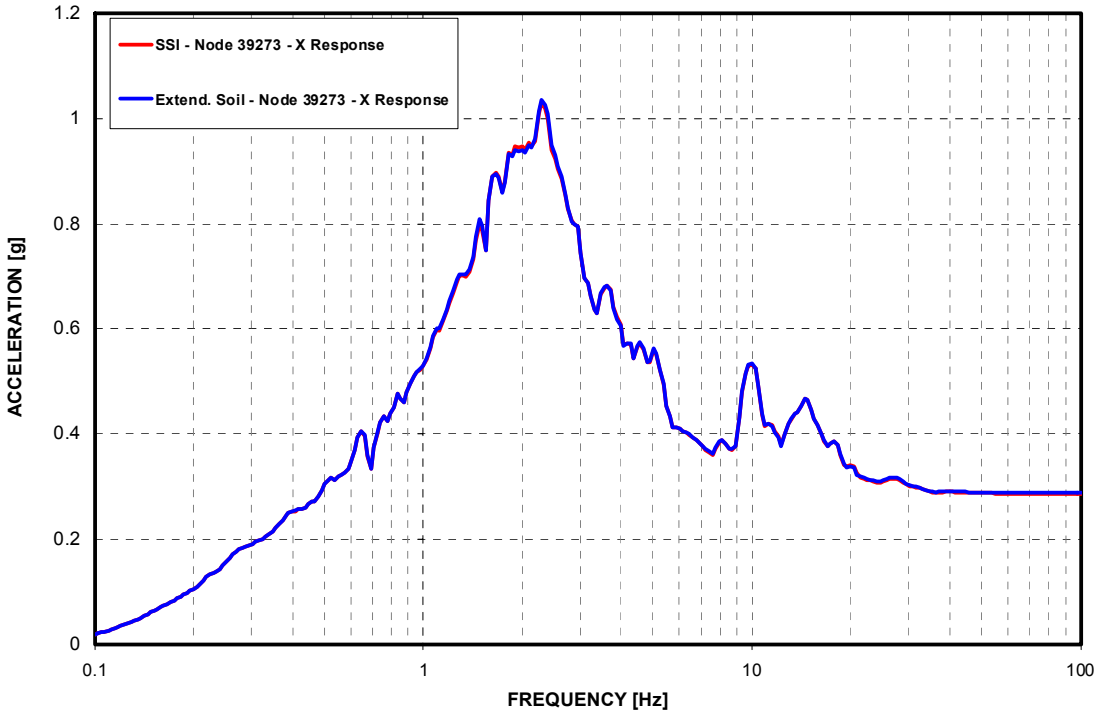

Figure 3-D.4.0-4 Sump Strainer Supports - Response Spectra - NS Direction (X)

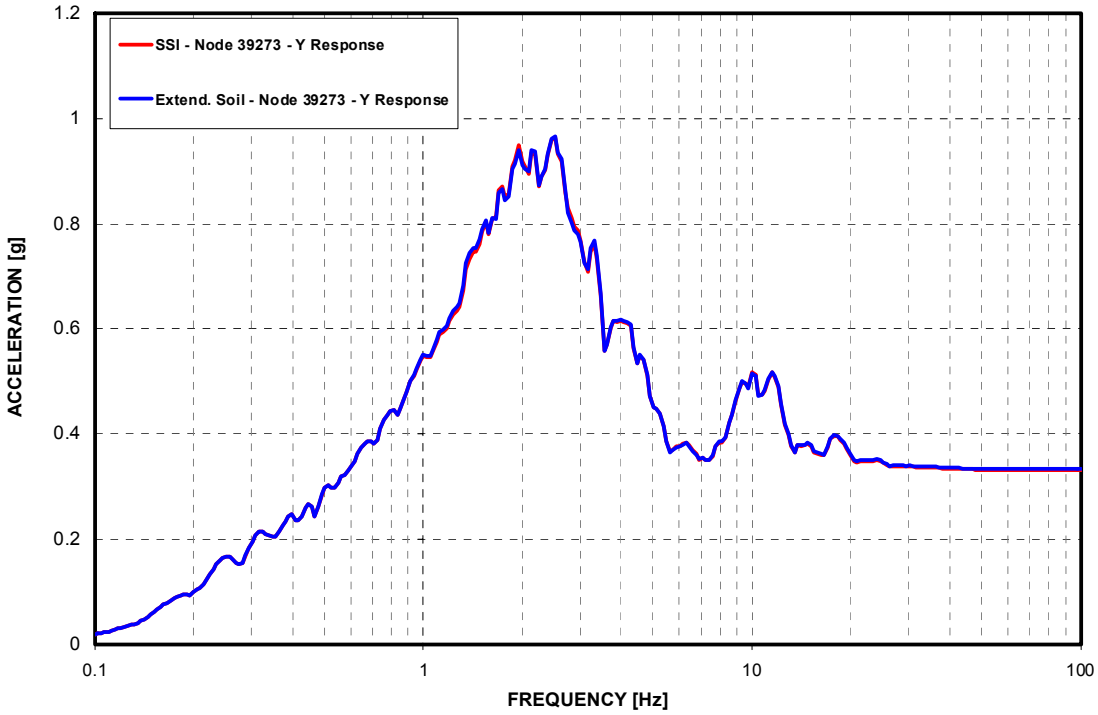

Figure 3-D.4.0-5 Sump Strainer Supports - Response Spectra - EW Direction (Y)

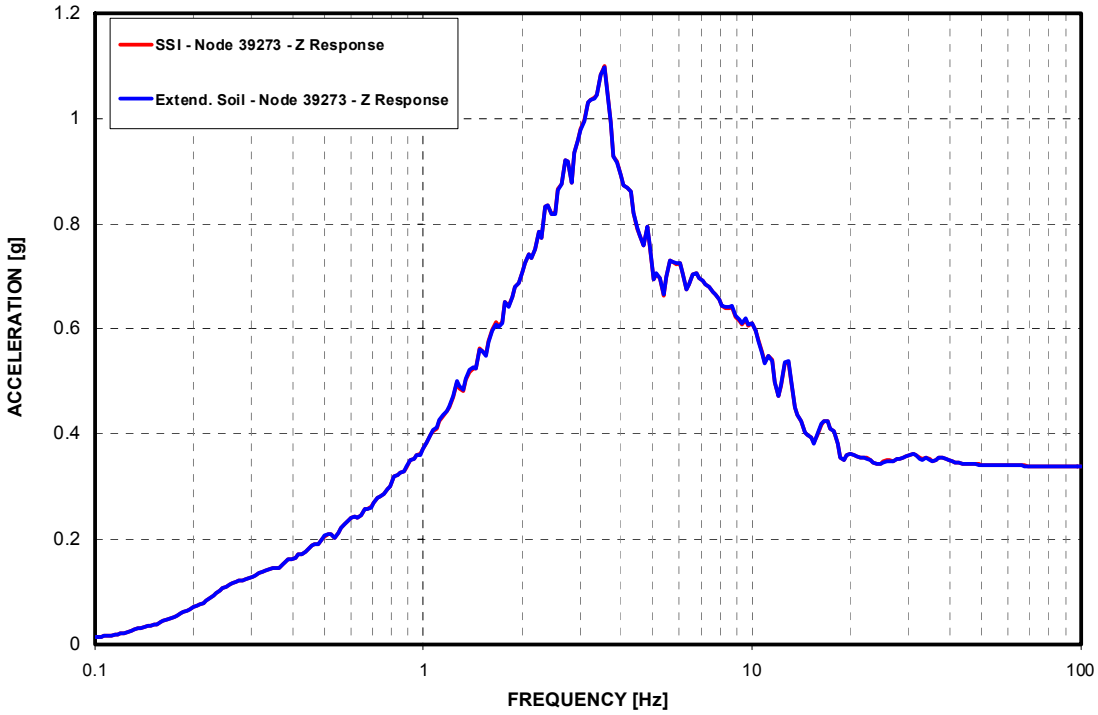

Figure 3-D.4.0-6 Sump Strainer Supports - Response Spectra - Vertical Direction (Z)

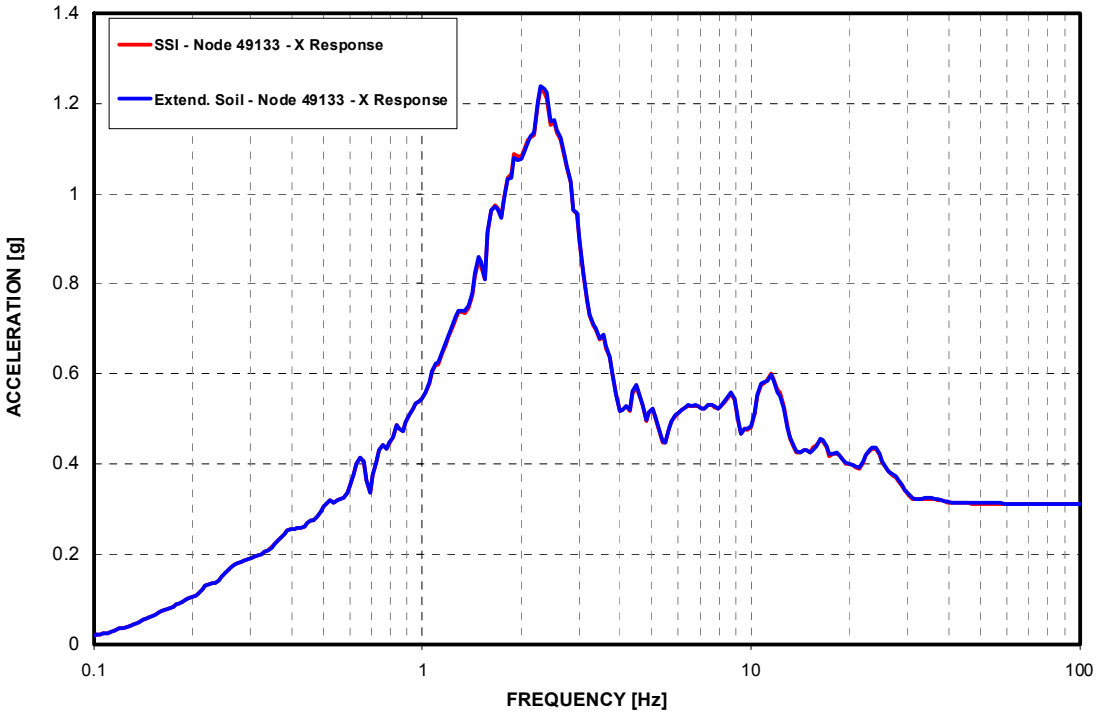

Figure 3-D.4.0-7 SG Lower Supports - Response Spectra - NS Direction (X)

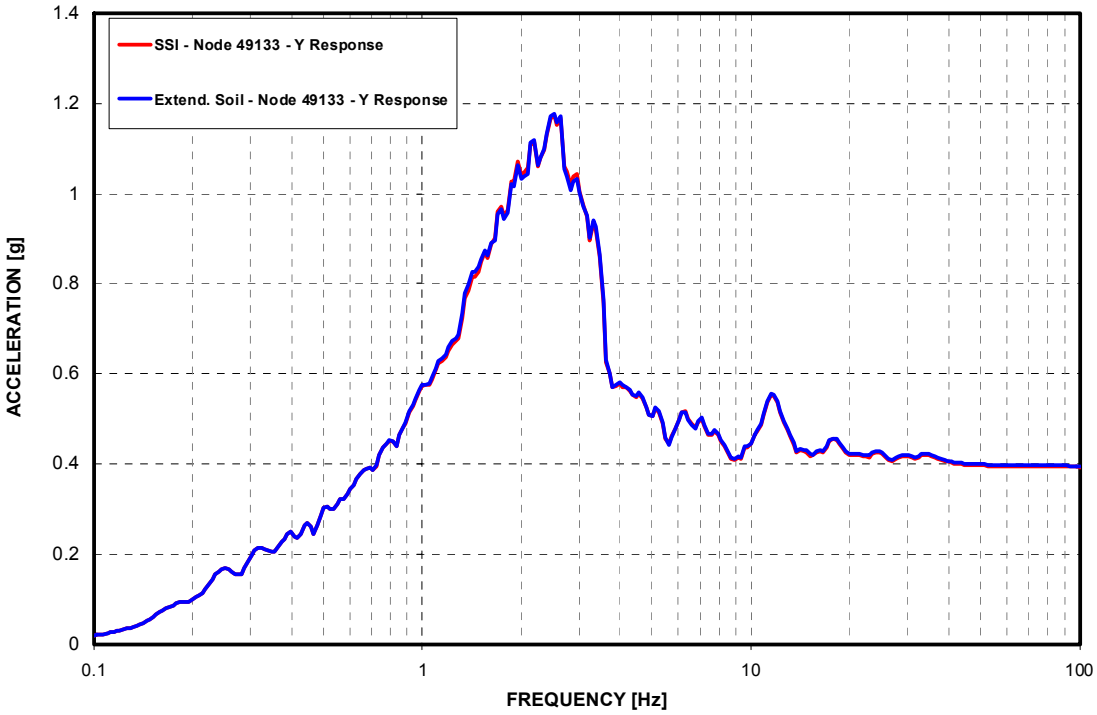

Figure 3-D.4.0-8 SG Lower Supports - Response Spectra - EW Direction (Y)

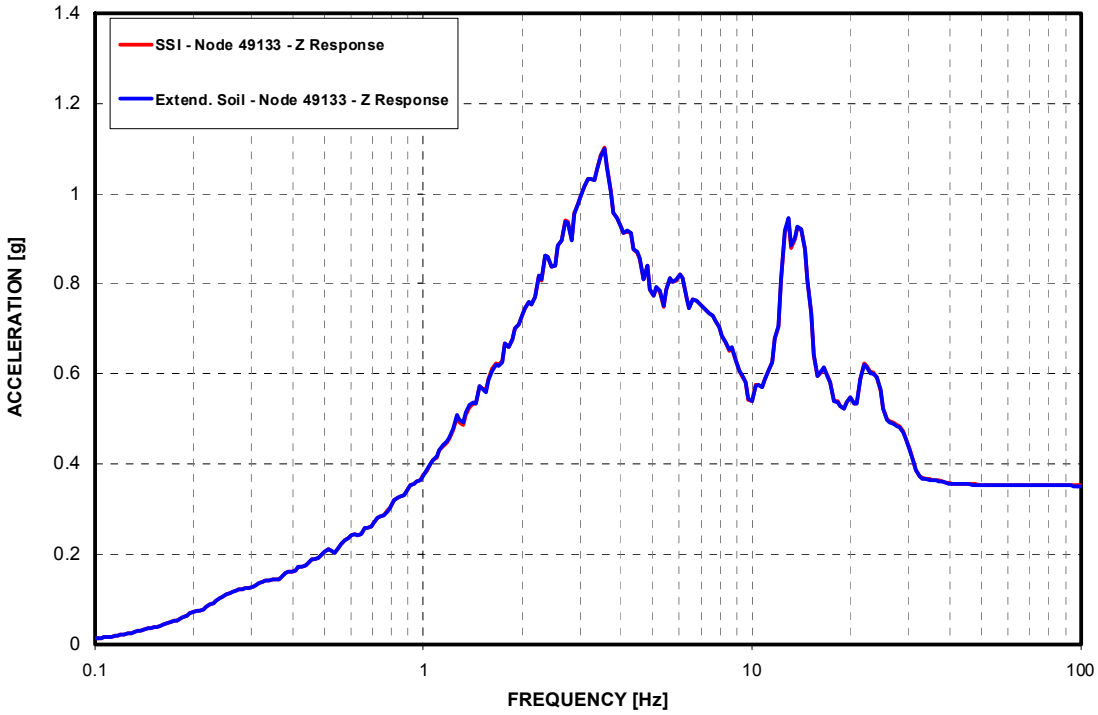

Figure 3-D.4.0-9 SG Lower Supports - Response Spectra - Vertical Direction (Z)

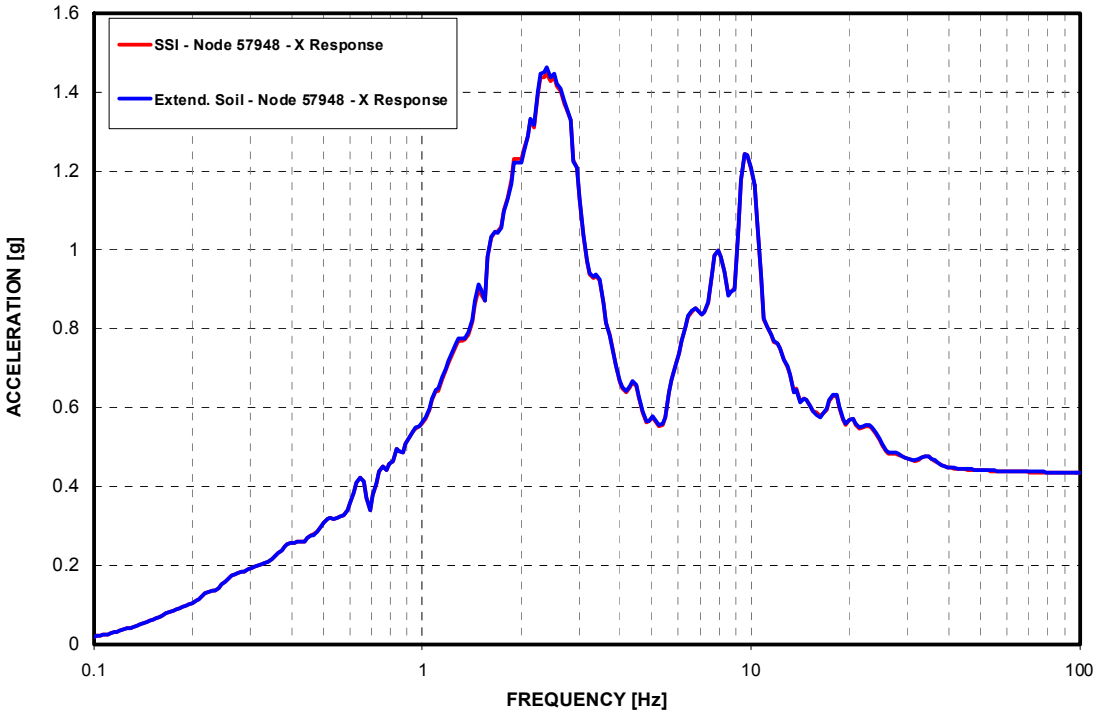

Figure 3-D.4.0-10 SG Upper Supports - Response Spectra - NS Direction (X)

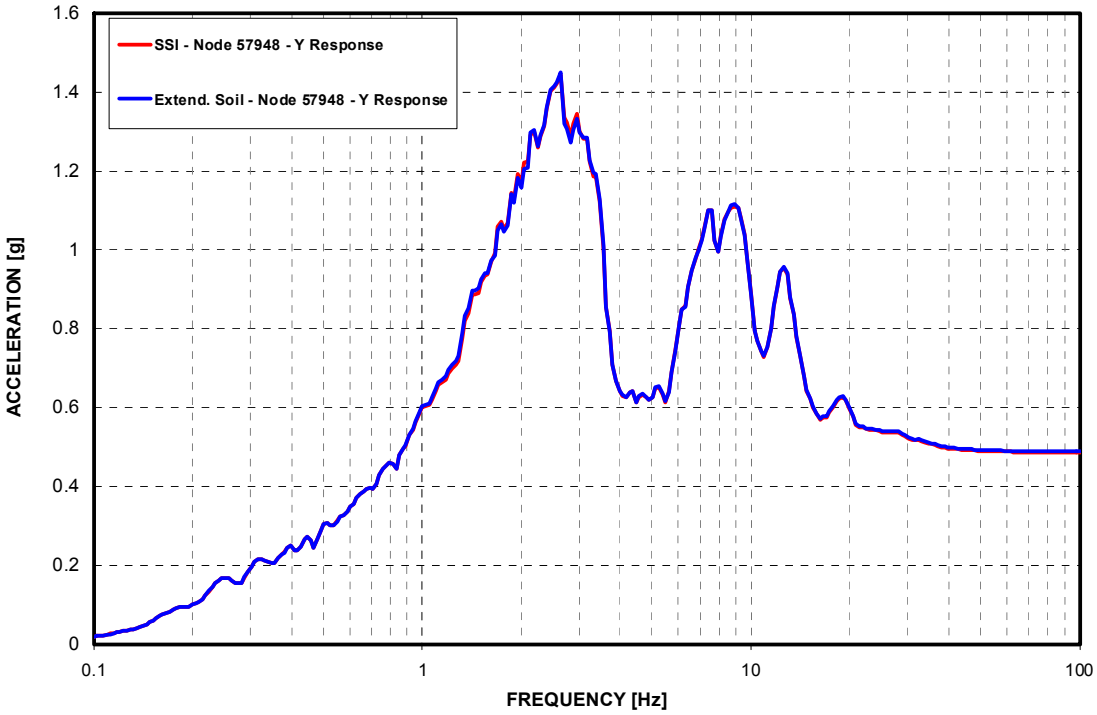

Figure 3-D.4.0-11 SG Upper Supports - Response Spectra - EW Direction (Y)

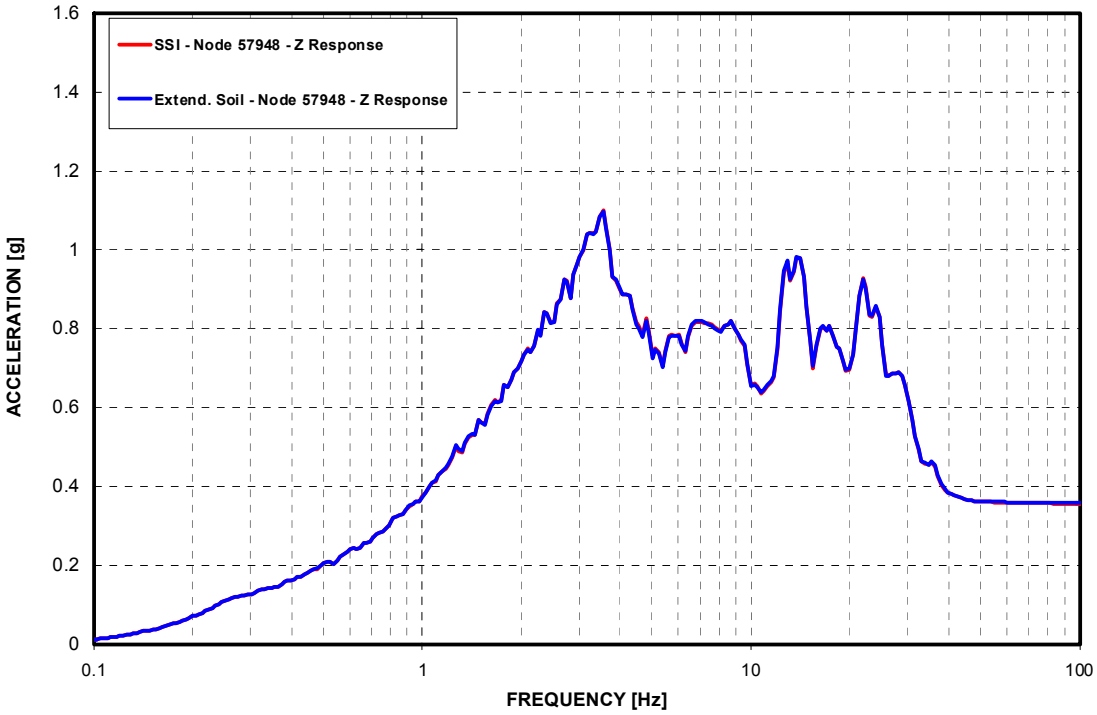

Figure 3-D.4.0-12 SG Upper Supports - Response Spectra - Vertical Direction (Z)

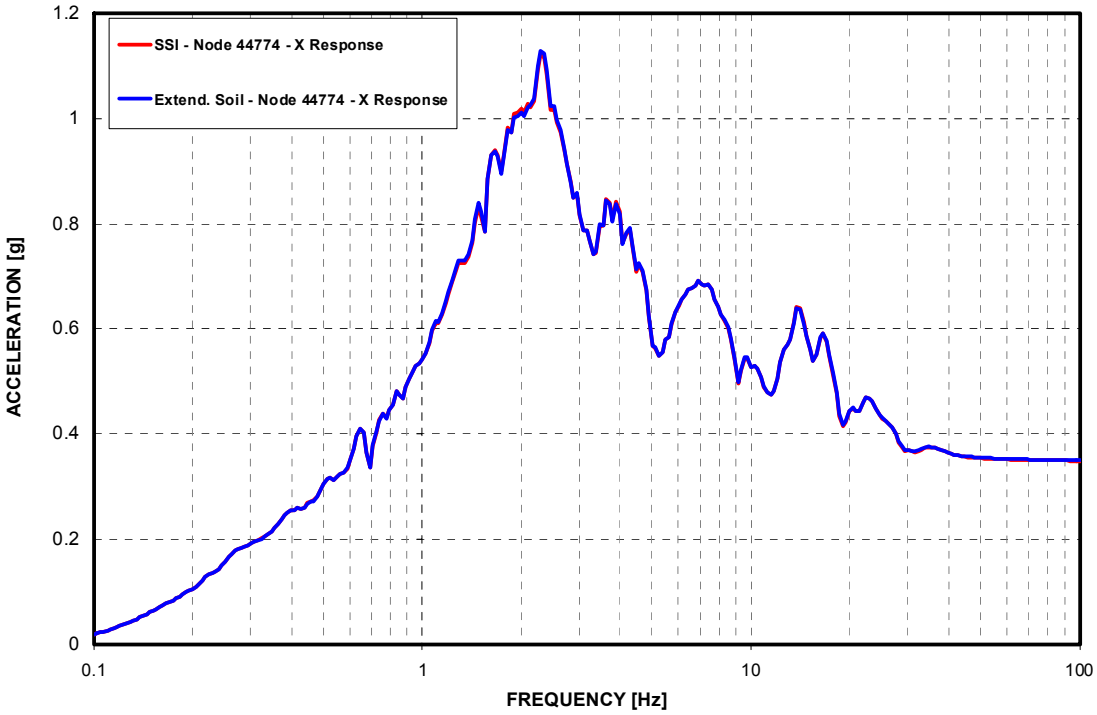

Figure 3-D.4.0-13 SFP - Response Spectra - NS Direction (X)

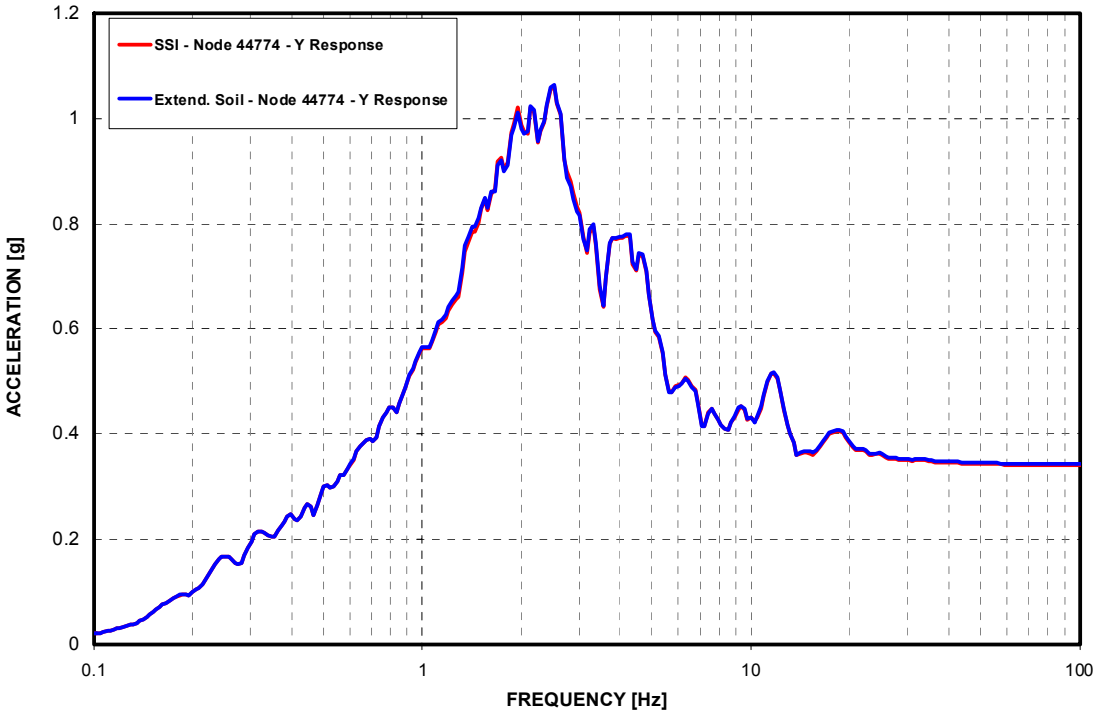

Figure 3-D.4.0-14 SFP - Response Spectra - EW Direction (Y)

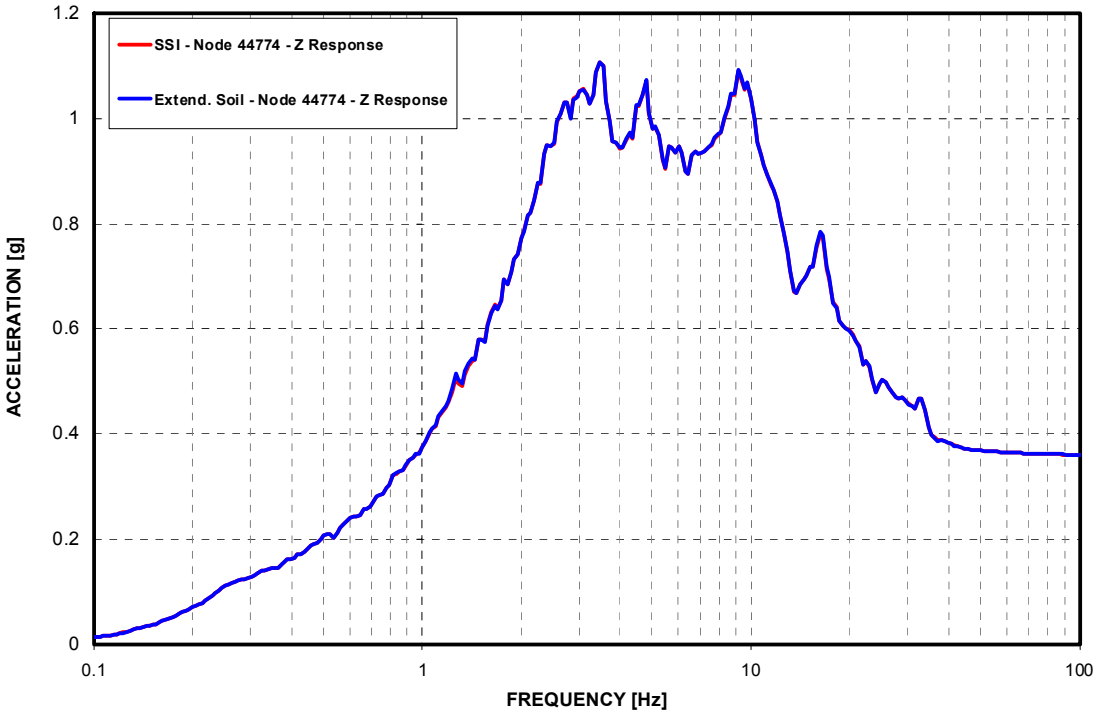

Figure 3-D.4.0-15 SFP - Response Spectra - Vertical Direction (Z)

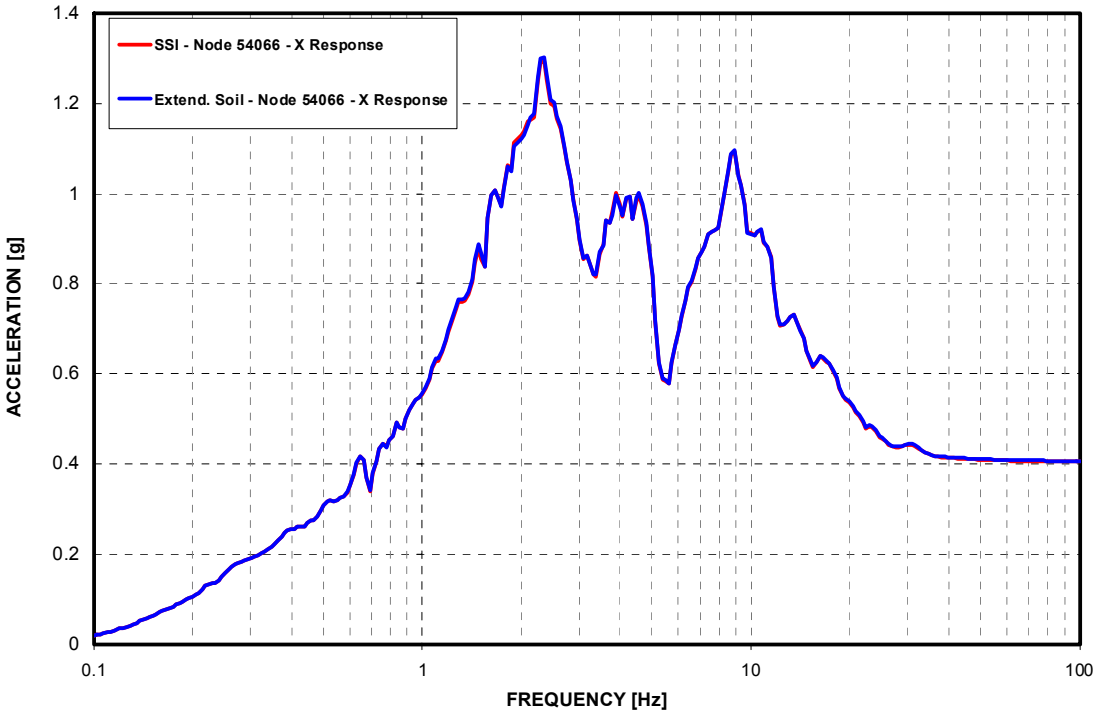

Figure 3-D.4.0-16 NFSP - Response Spectra - NS Direction (X)

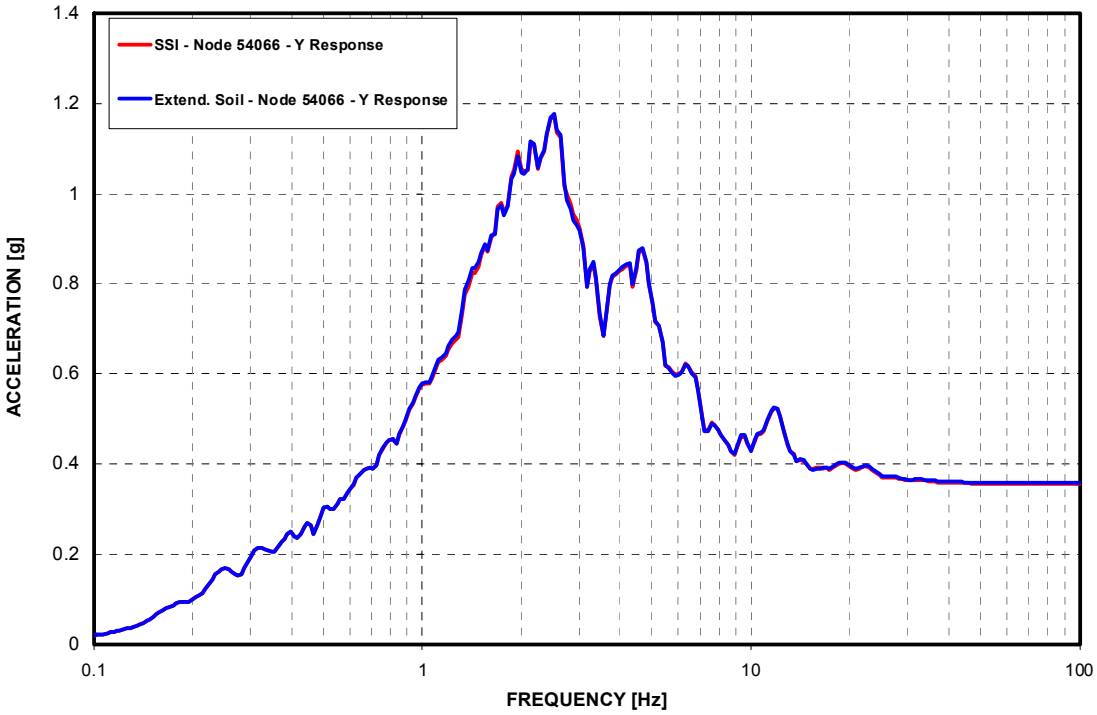

Figure 3-D.4.0-17 NFSP - Response Spectra - EW Direction (Y)

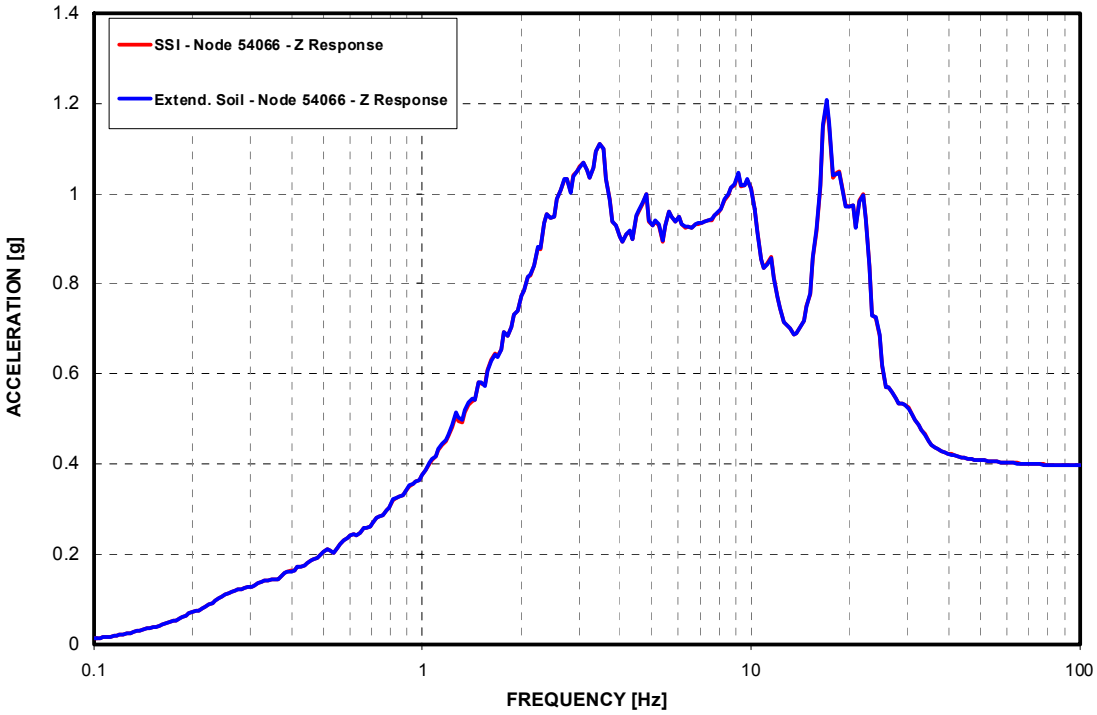

Figure 3-D.4.0-18 NFSP - Response Spectra - Vertical Direction (Z)

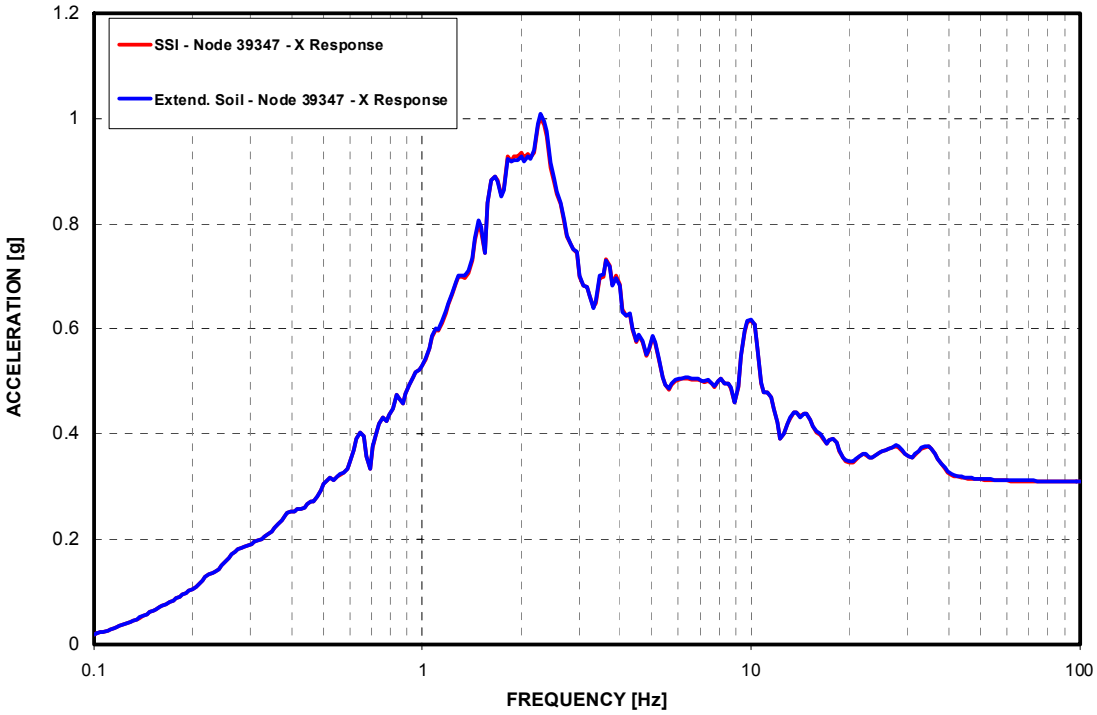

Figure 3-D.4.0-19 A-AAC GTG - Response Spectra - NS Direction (X)

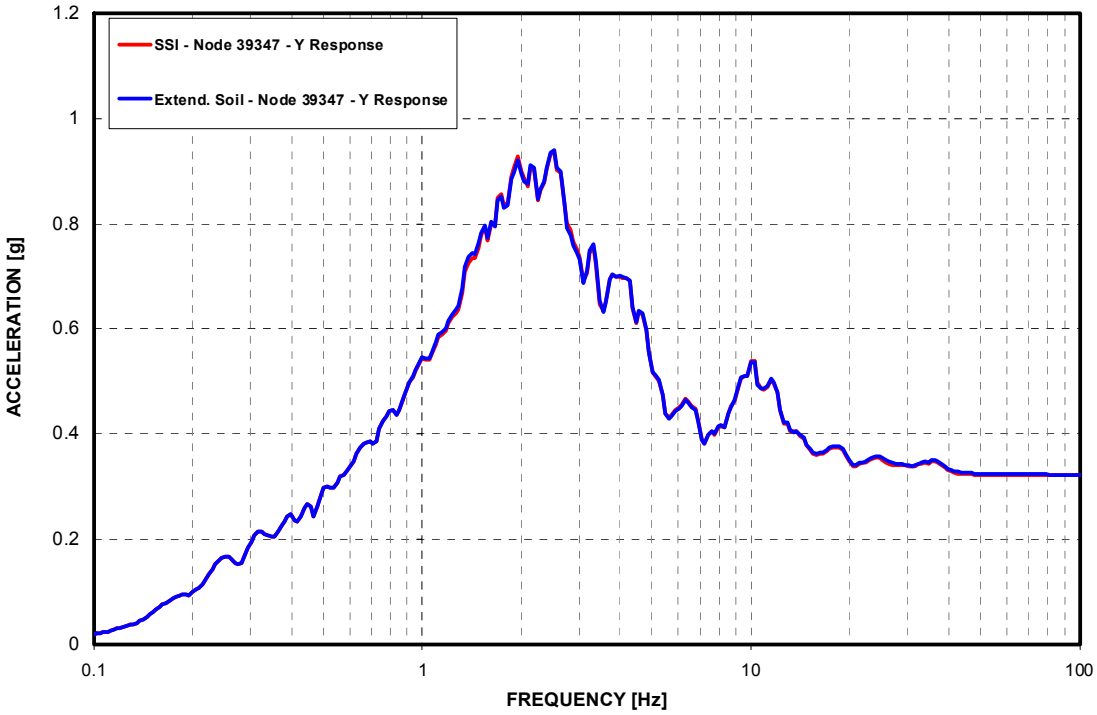

Figure 3-D.4.0-20 A-AAC GTG - Response Spectra - EW Direction (Y)

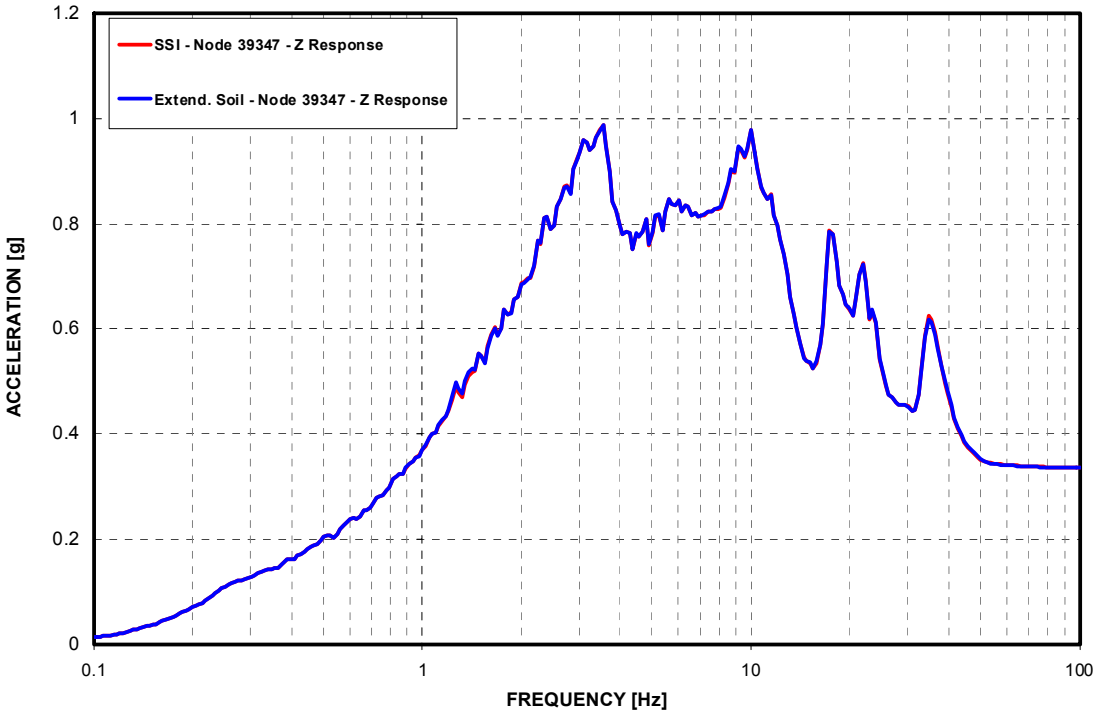

Figure 3-D.4.0-21 A-AAC GTG - Response Spectra - Vertical Direction (Z)

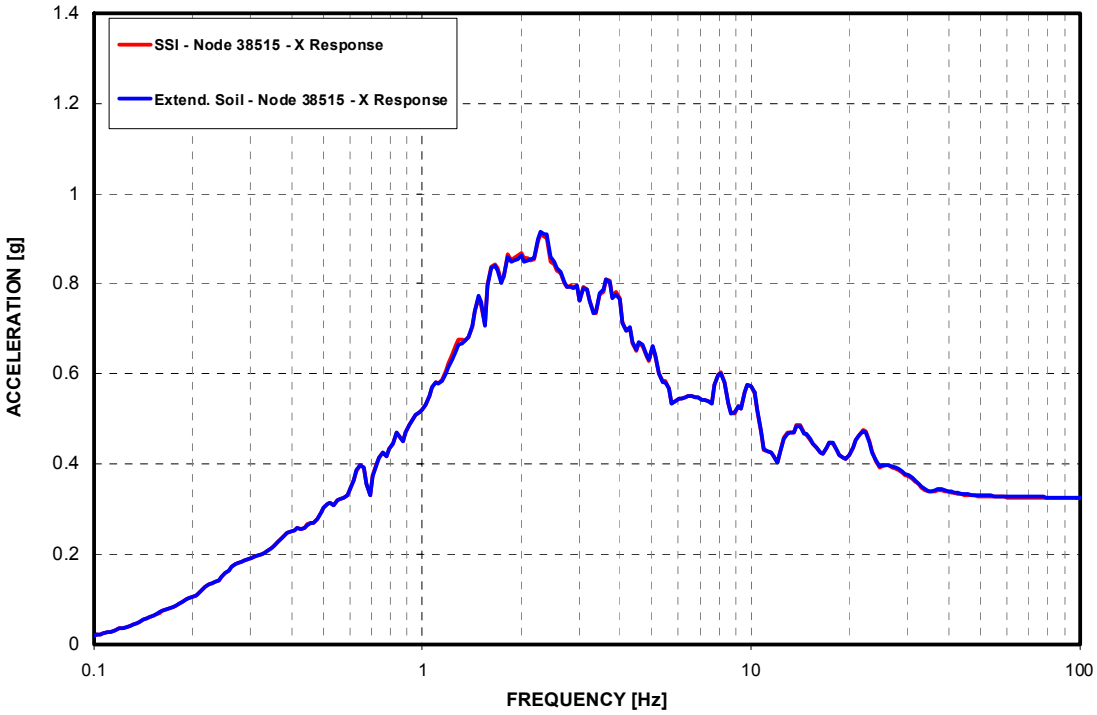

Figure 3-D.4.0-22 B-AAC GTG - Response Spectra - NS Direction (X)

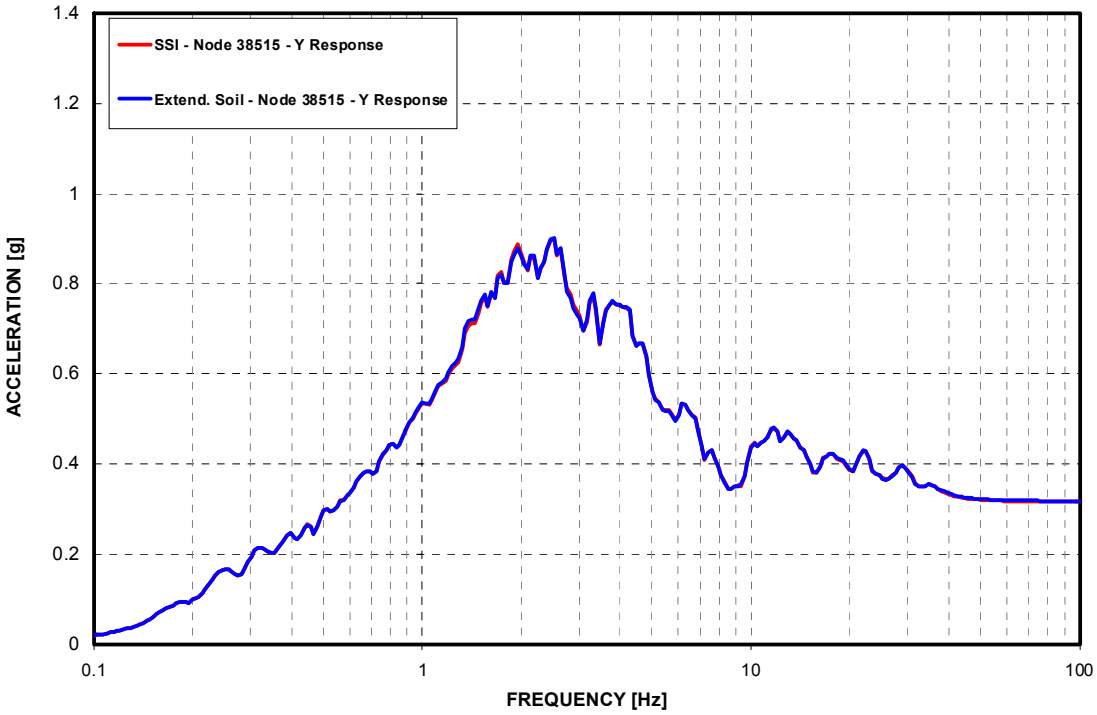

Figure 3-D.4.0-23 B-AAC GTG - Response Spectra - EW Direction (Y)

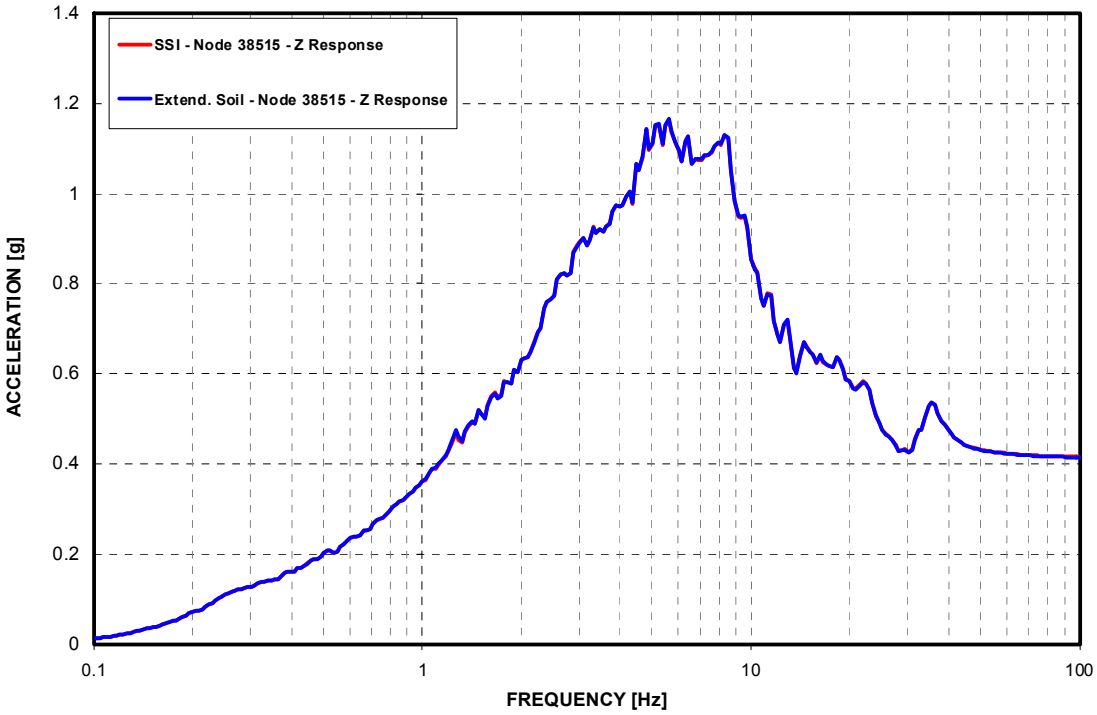

Figure 3-D.4.0-24 B-AAC GTG - Response Spectra - Vertical Direction (Z)

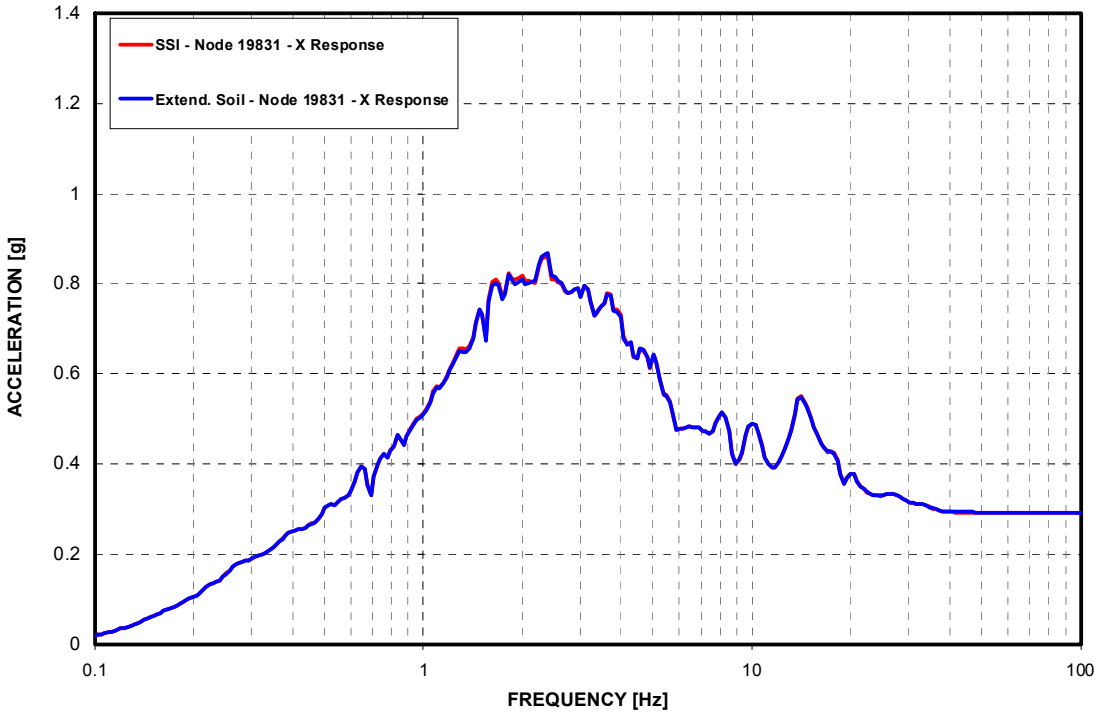

Figure 3-D.4.0-25 A/B Northwest Corner at Basemat - Response Spectra - NS Direction (X)

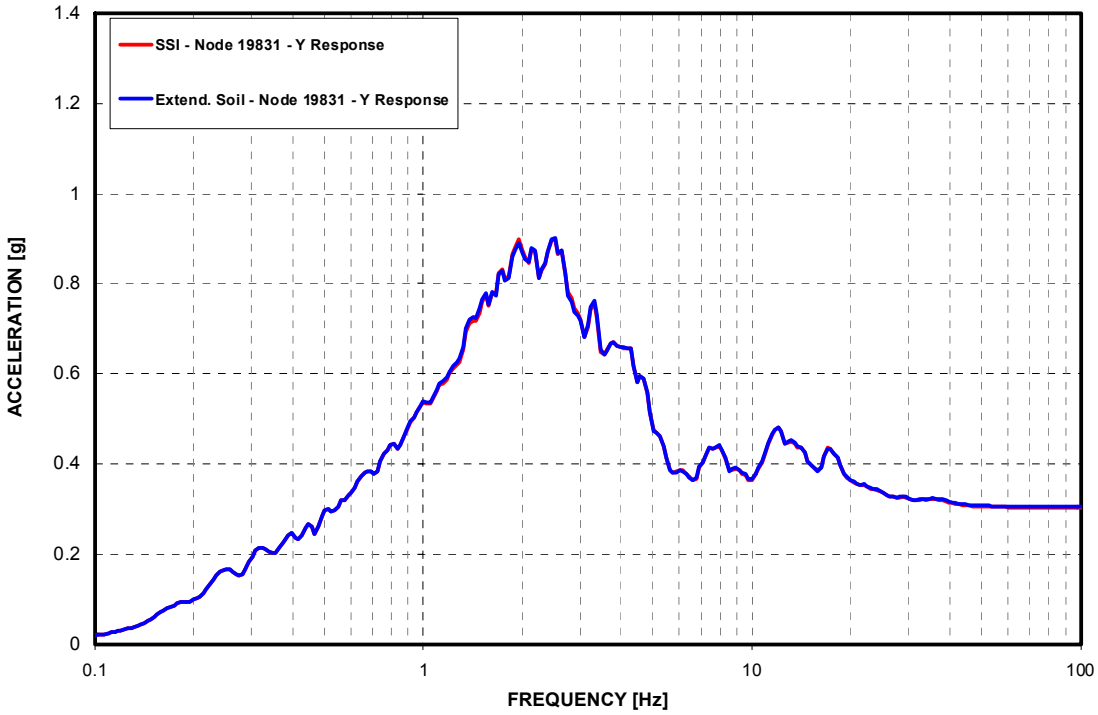

Figure 3-D.4.0-26 A/B Northwest Corner at Basemat - Response Spectra - EW Direction (Y)

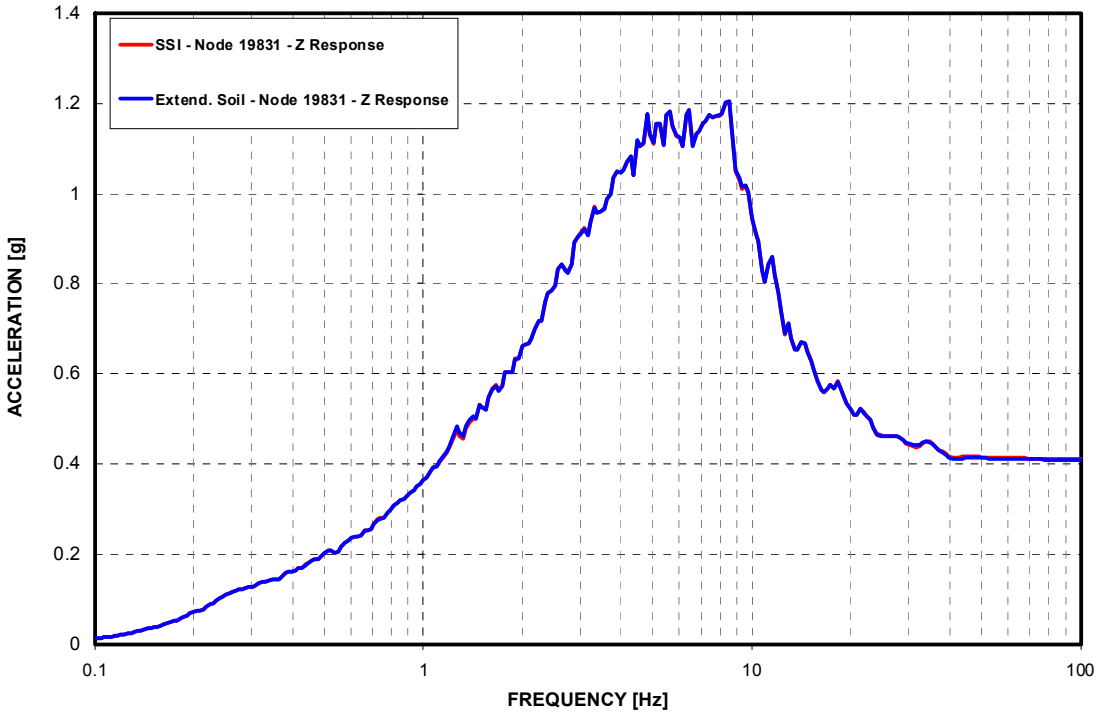

Figure 3-D.4.0-27 A/B Northwest Corner at Basemat - Response Spectra - Vertical Direction (Z)

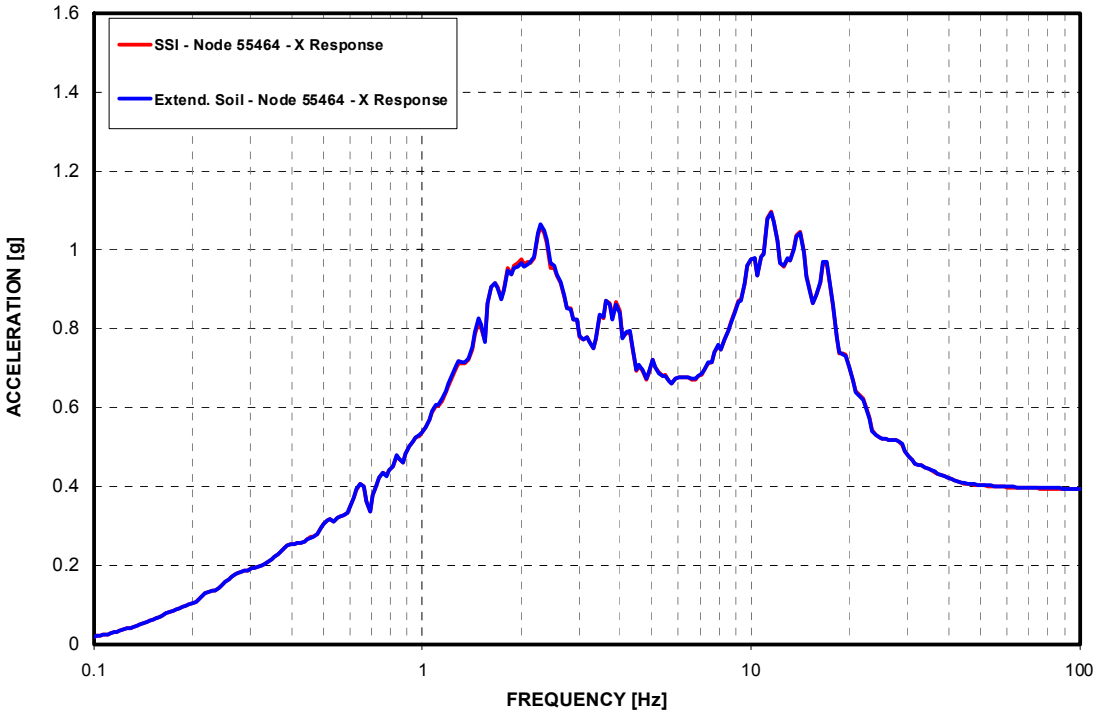

Figure 3-D.4.0-28 A/B Northwest Corner at Roof - Response Spectra - NS Direction (X)

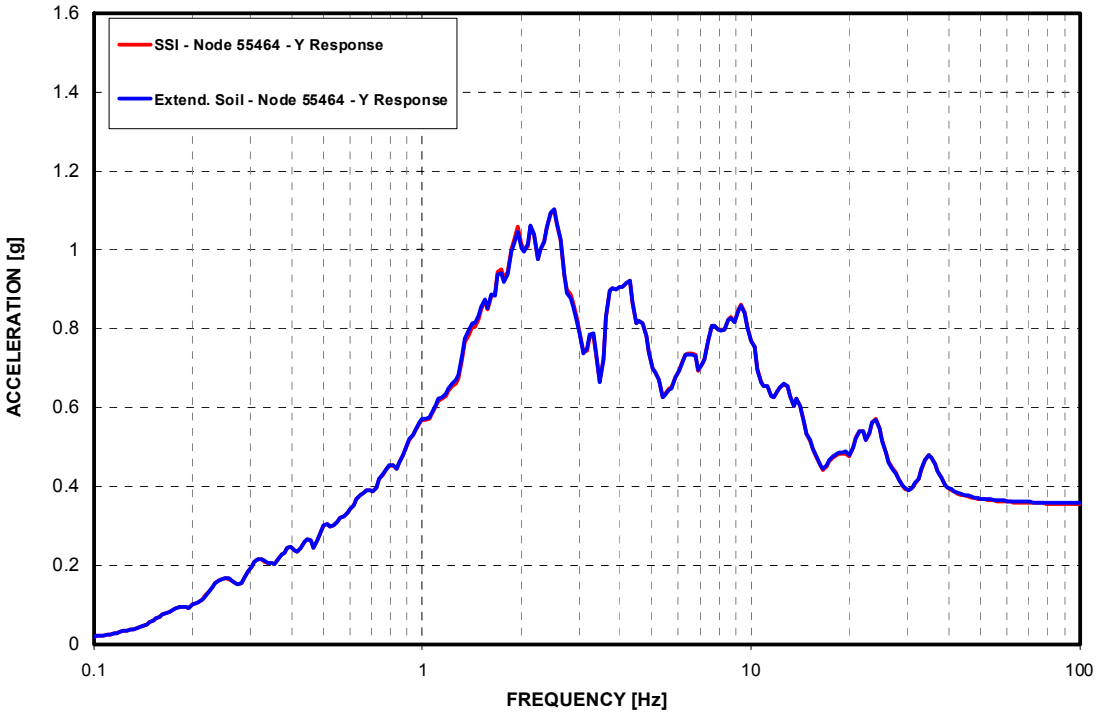

Figure 3-D.4.0-29 A/B Northwest Corner at Roof - Response Spectra - EW Direction (Y)

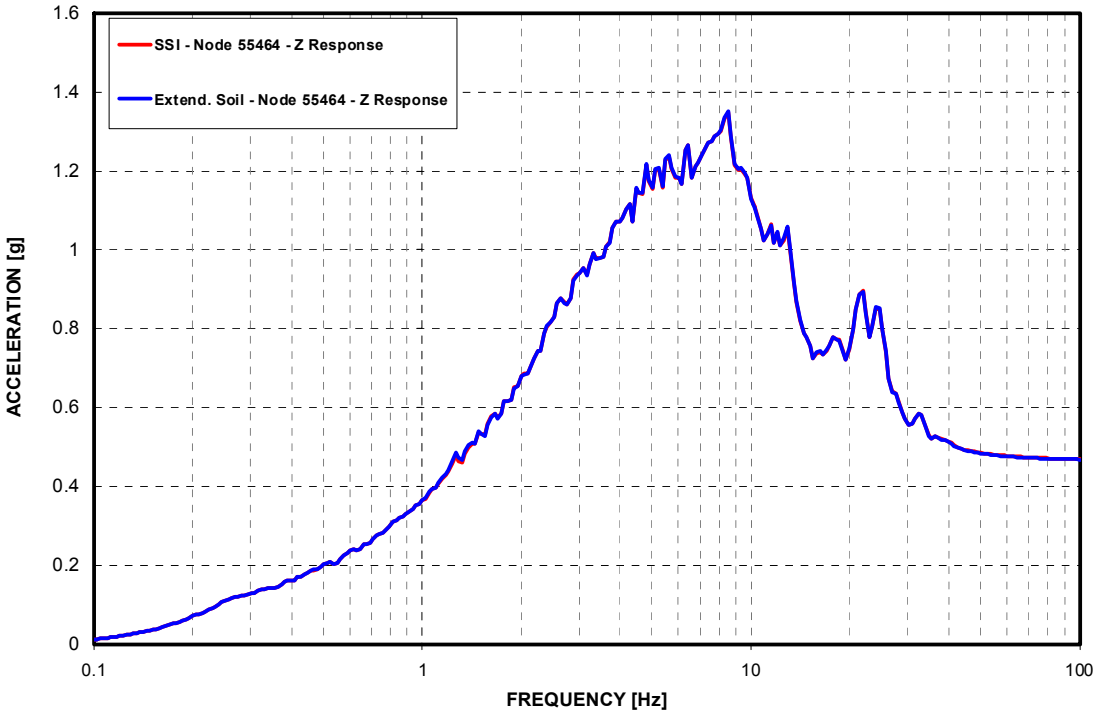

Figure 3-D.4.0-30 A/B Northwest Corner at Roof - Response Spectra - Vertical Direction (Z)

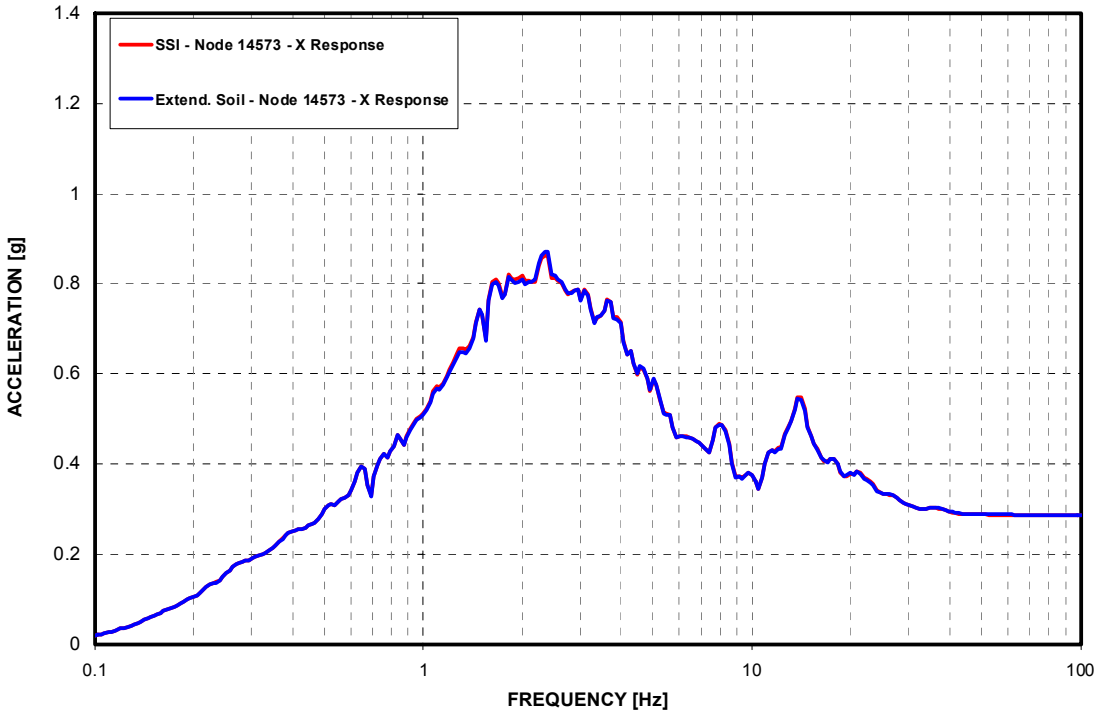

Figure 3-D.4.0-31 West PS/B Southwest Corner at Basemat - Response Spectra - NS Direction (X)

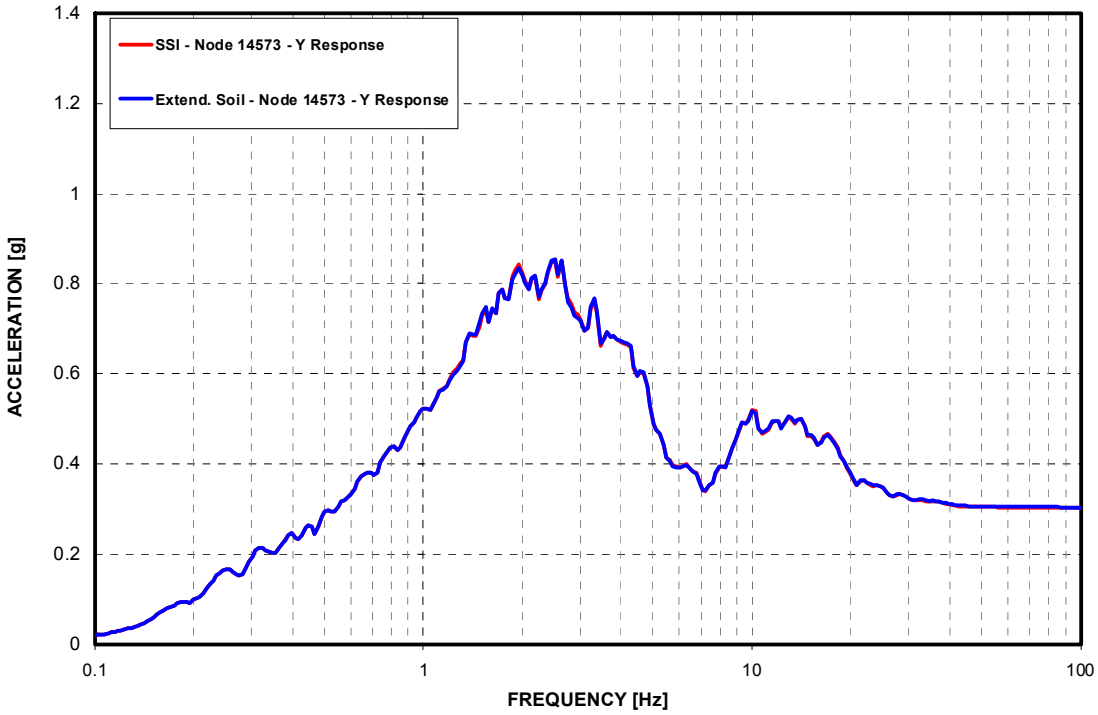

Figure 3-D.4.0-32 West PS/B Southwest Corner at Basemat - Response Spectra - EW Direction (Y)

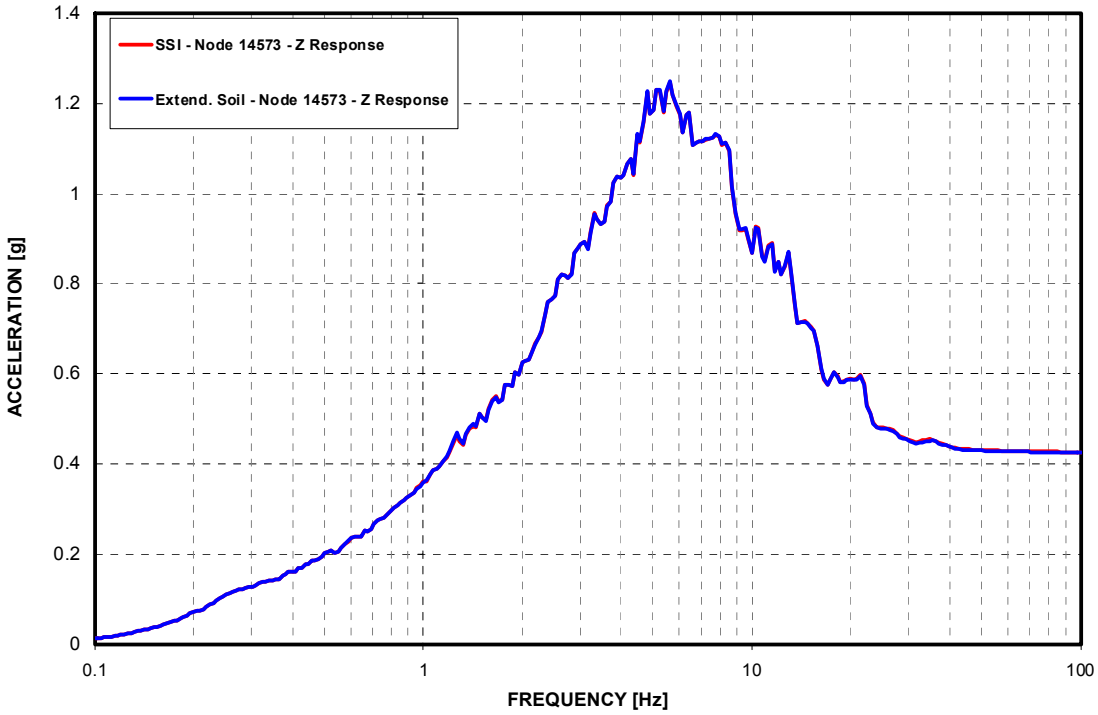

Figure 3-D.4.0-33 West PS/B Southwest Corner at Basemat - Response Spectra - Vertical Direction (Z)

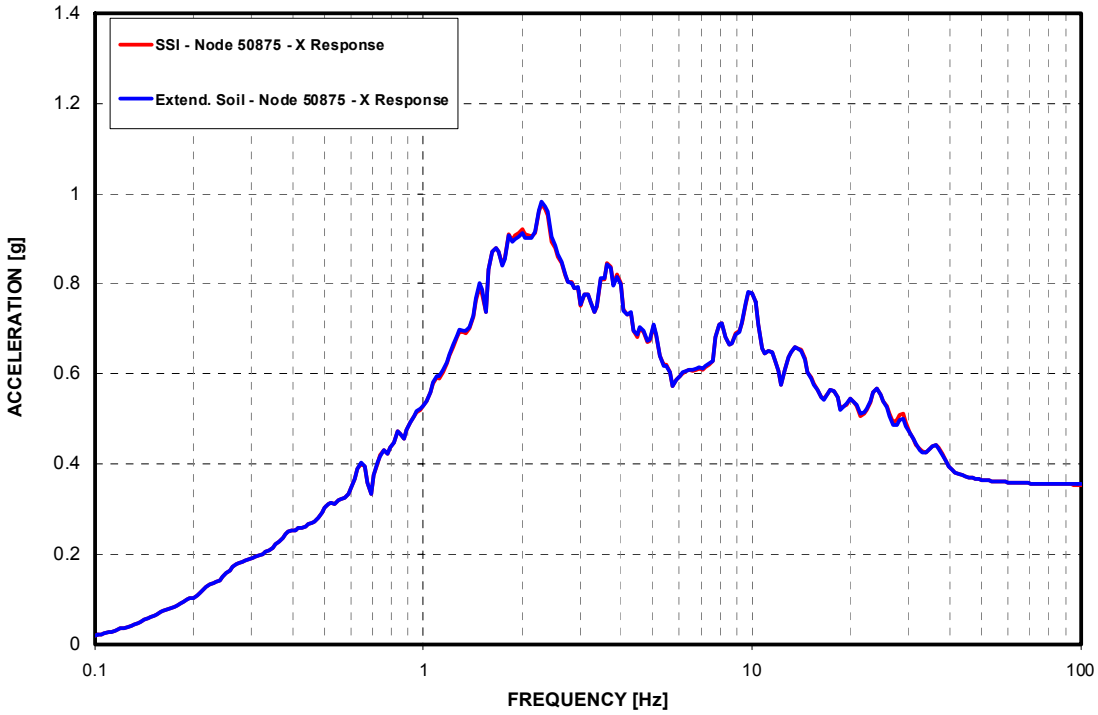

Figure 3-D.4.0-34 West PS/B Southwest Corner at Roof - Response Spectra - NS Direction (X)

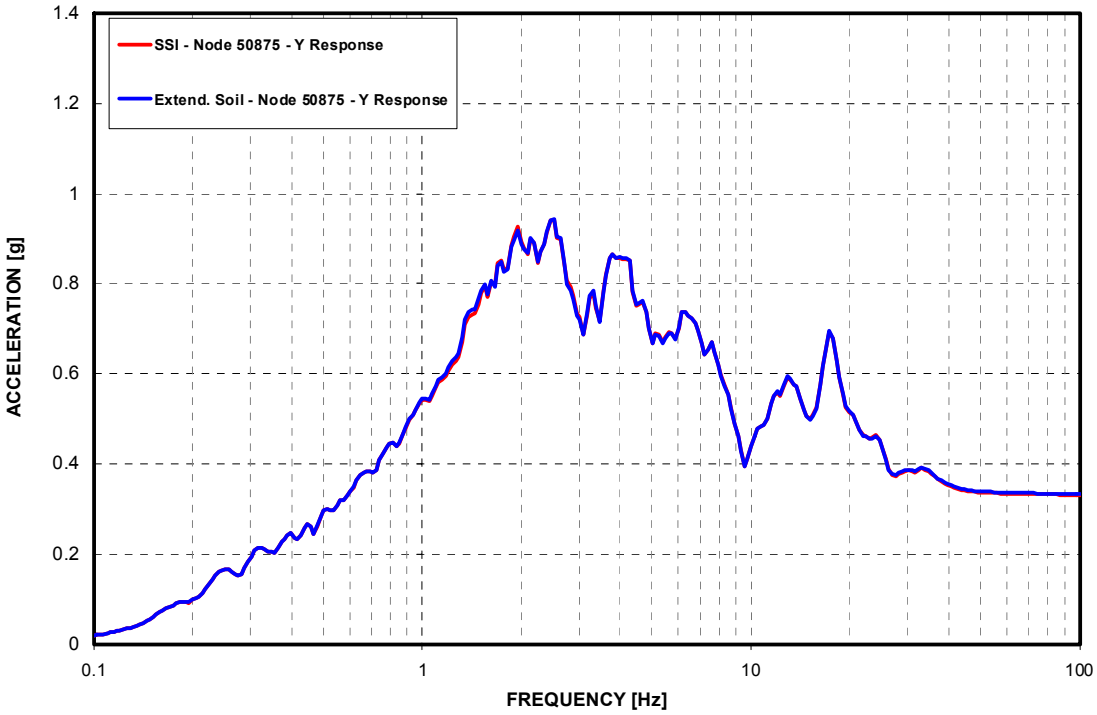

Figure 3-D.4.0-35 West PS/B Southwest Corner at Roof - Response Spectra - EW Direction (Y)

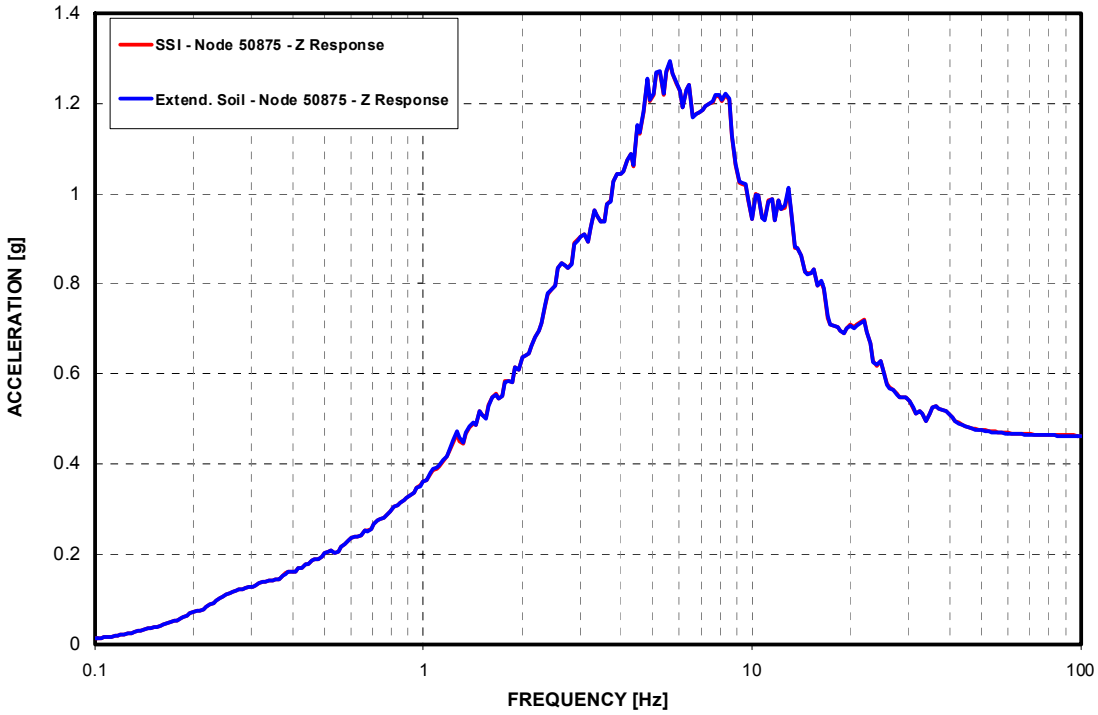

Figure 3-D.4.0-36 West PS/B Southwest Corner at Roof - Response Spectra - Vertical Direction (Z)

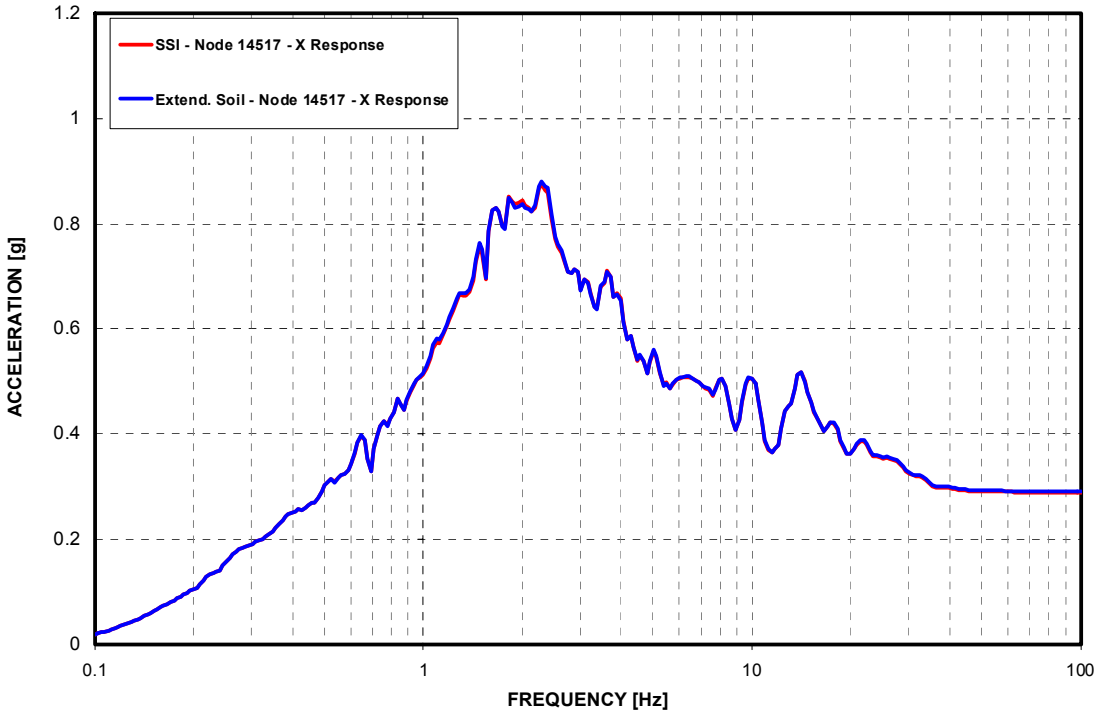

Figure 3-D.4.0-37 East PS/B Southeast Corner at Basemat - Response Spectra - NS Direction (X)

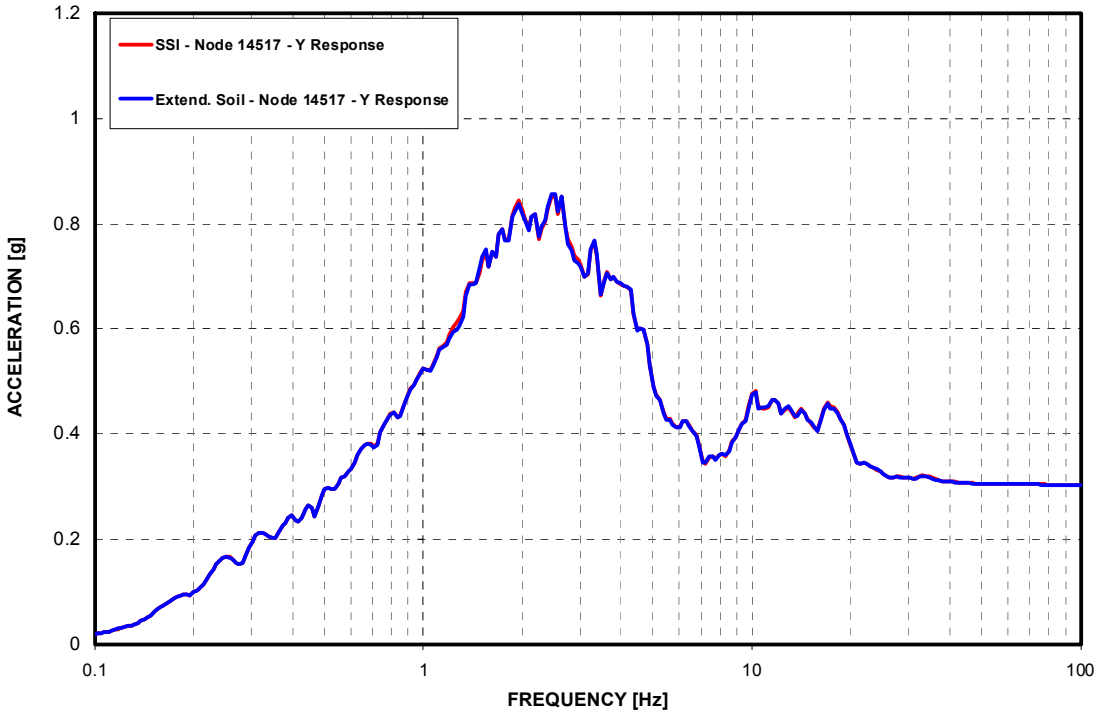

Figure 3-D.4.0-38 East PS/B Southeast Corner at Basemat - Response Spectra - EW Direction (Y)

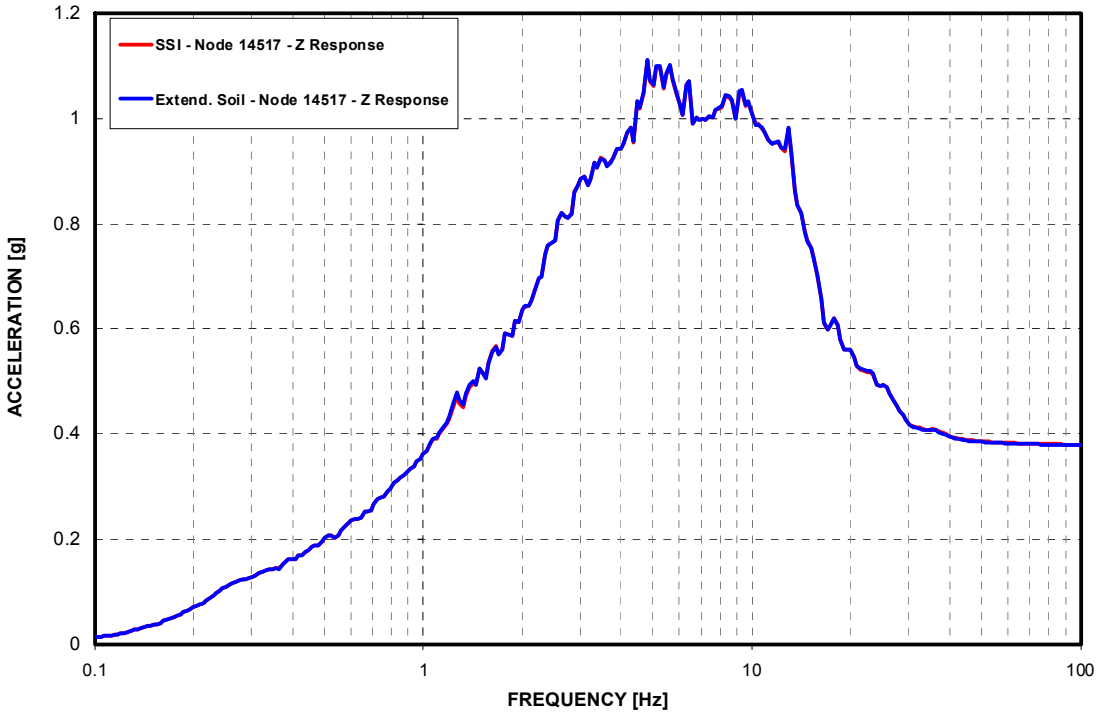

Figure 3-D.4.0-39 East PS/B Southeast Corner at Basemat - Response Spectra - Vertical Direction (Z)

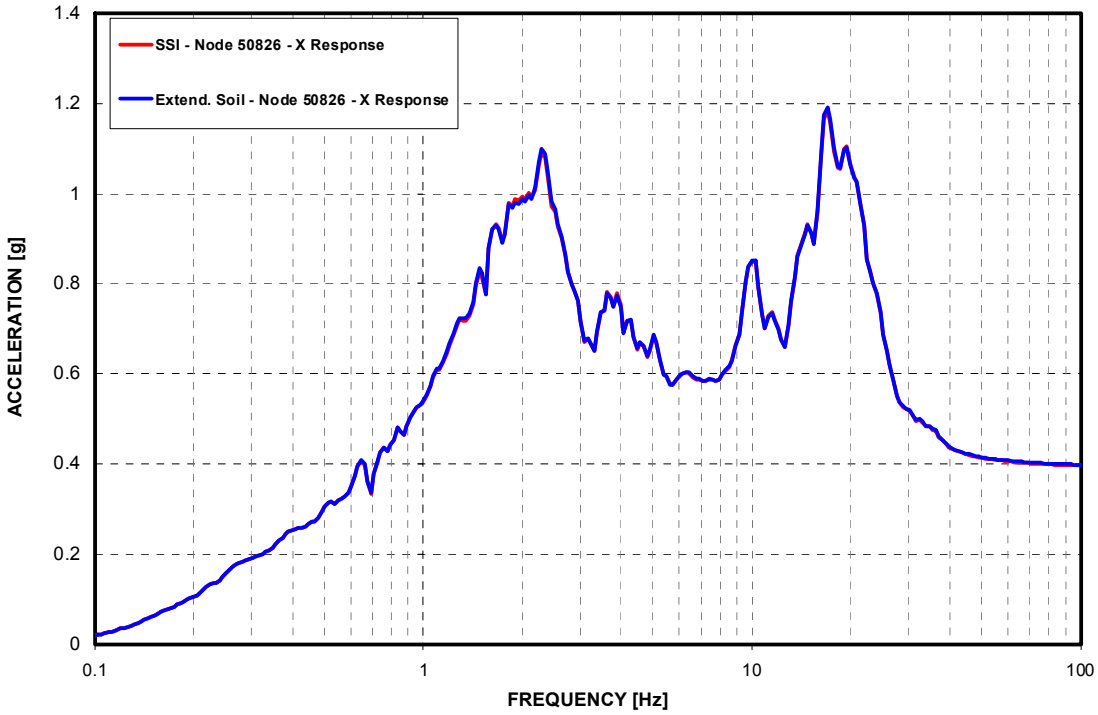

Figure 3-D.4.0-40 East PS/B Southeast Corner at Roof - Response Spectra - NS Direction (X)

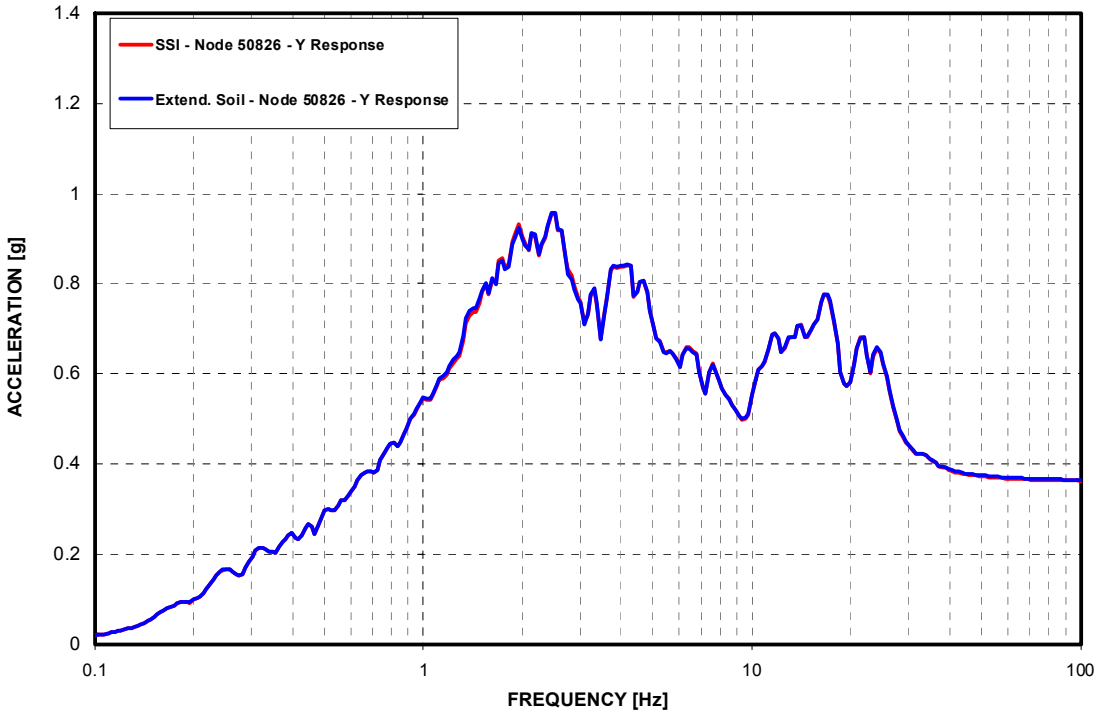

Figure 3-D.4.0-41 East PS/B Southeast Corner at Roof - Response Spectra - EW Direction (Y)

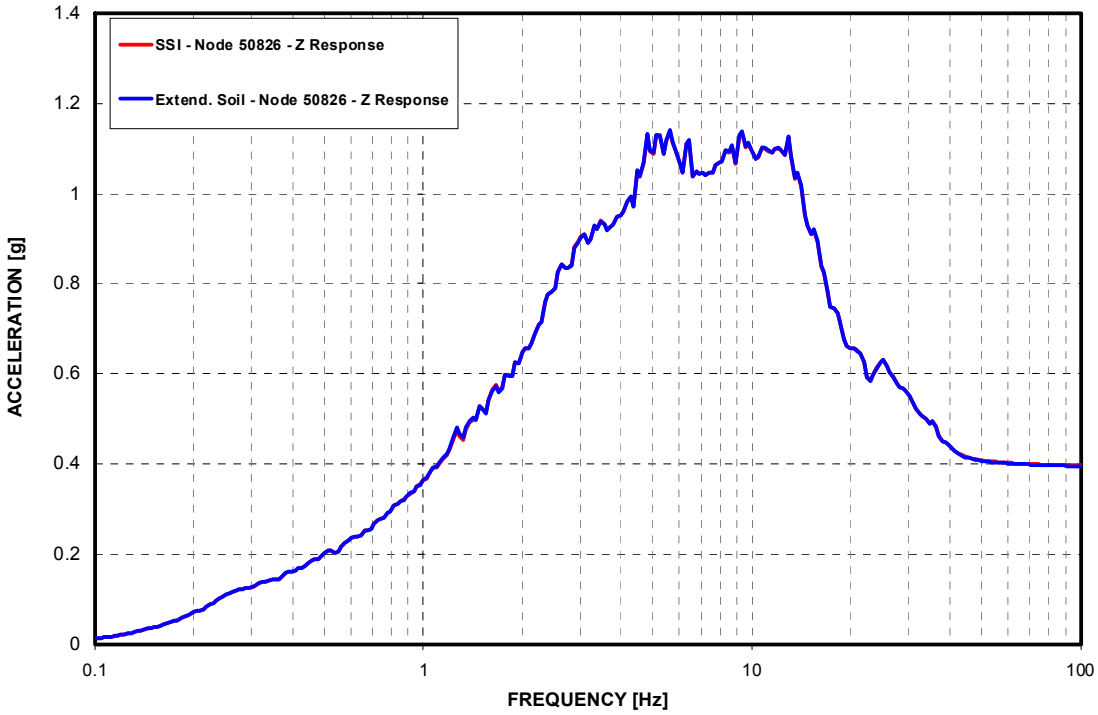

Figure 3-D.4.0-42 East PS/B Southeast Corner at Roof - Response Spectra - Vertical Direction (Z)

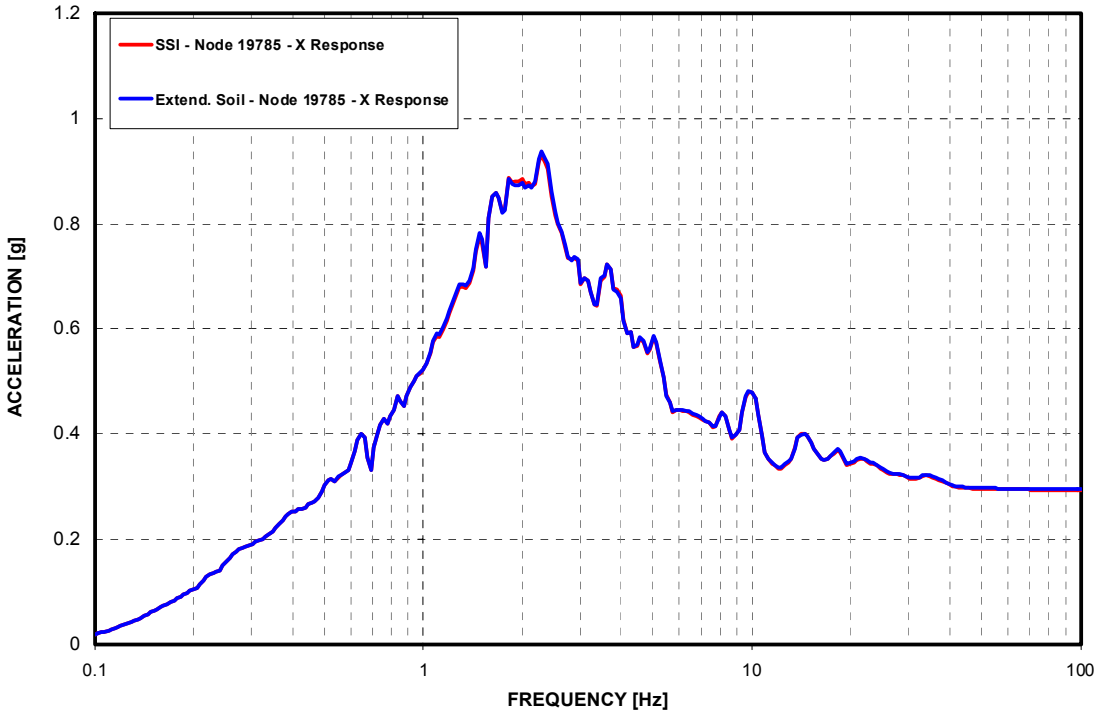

Figure 3-D.4.0-43 R/B Northeast Corner at Basemat - Response Spectra - NS Direction (X)

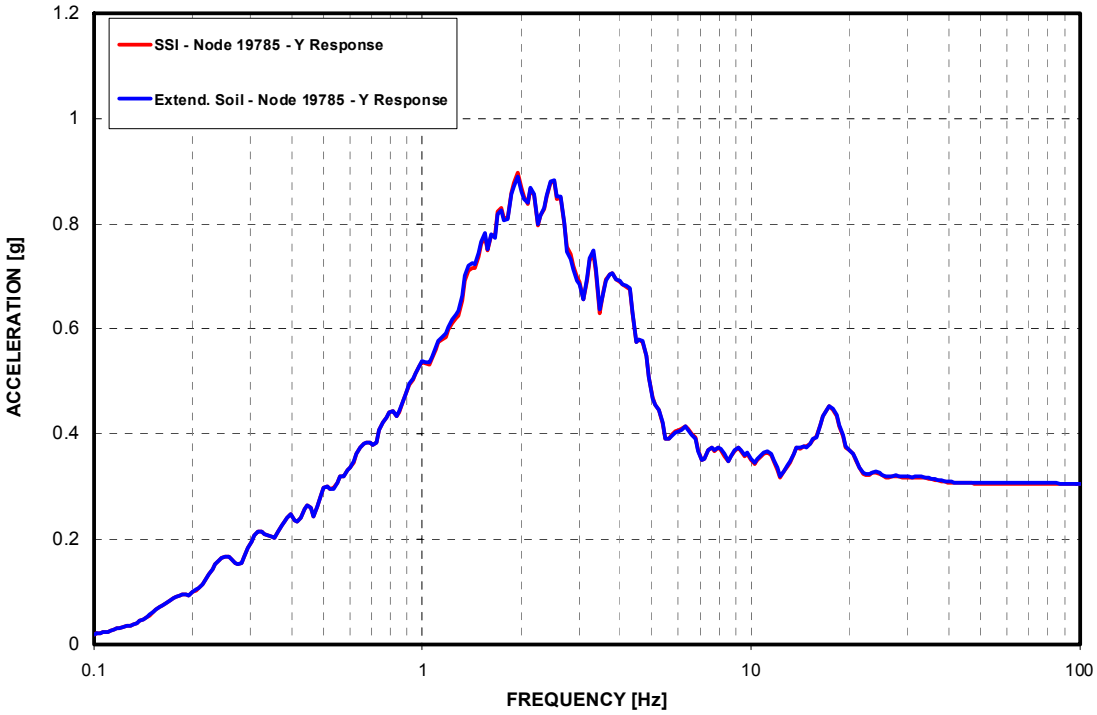

Figure 3-D.4.0-44 R/B Northeast Corner at Basemat - Response Spectra - EW Direction (Y)

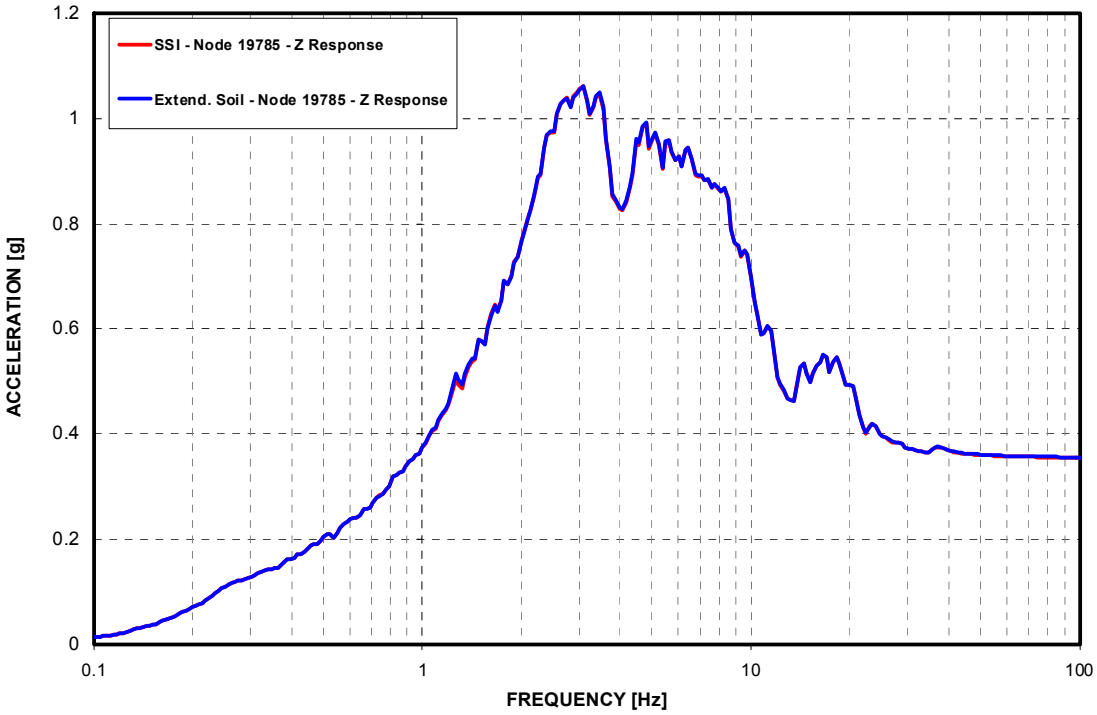

Figure 3-D.4.0-45 R/B Northeast Corner at Basemat - Response Spectra - Vertical Direction (Z)

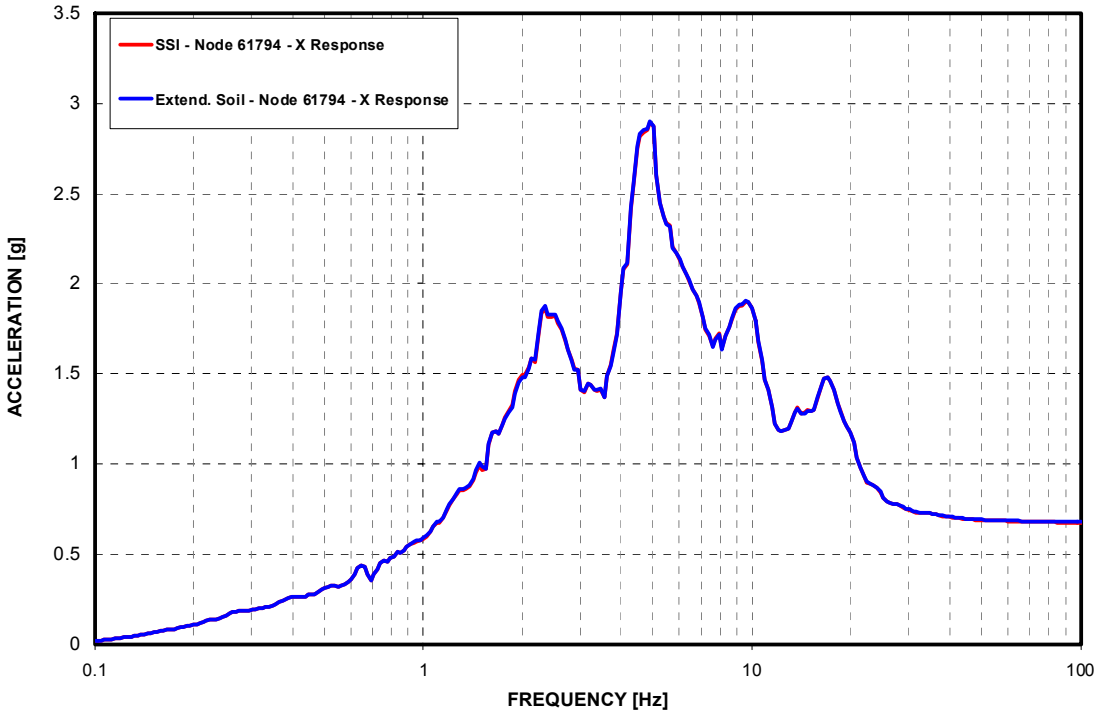

Figure 3-D.4.0-46 R/B Northeast Corner at Roof - Response Spectra - NS Direction (X)

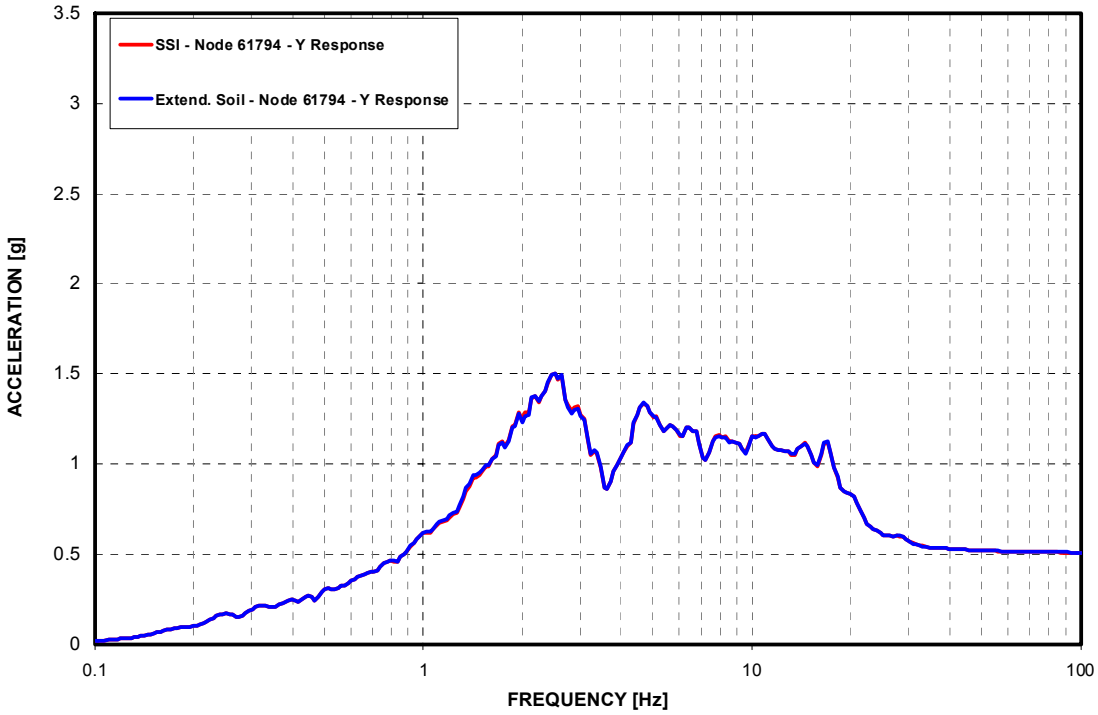

Figure 3-D.4.0-47 R/B Northeast Corner at Roof - Response Spectra - EW Direction (Y)

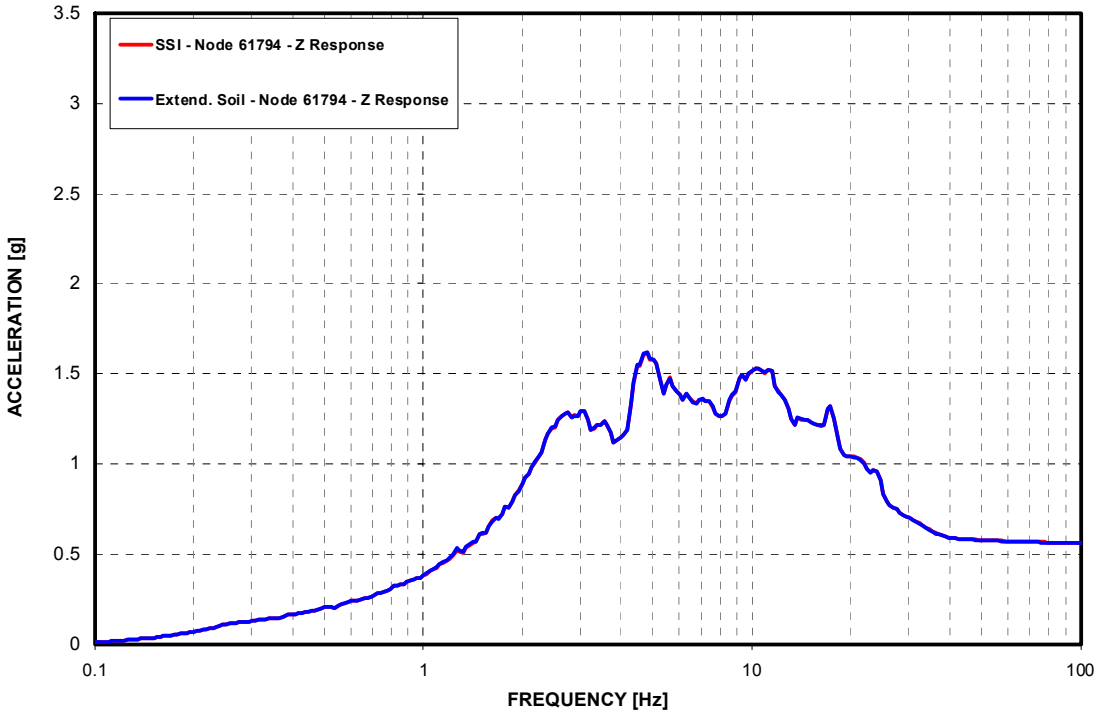

Figure 3-D.4.0-48 R/B Northeast Corner at Roof - Response Spectra - Vertical Direction (Z)

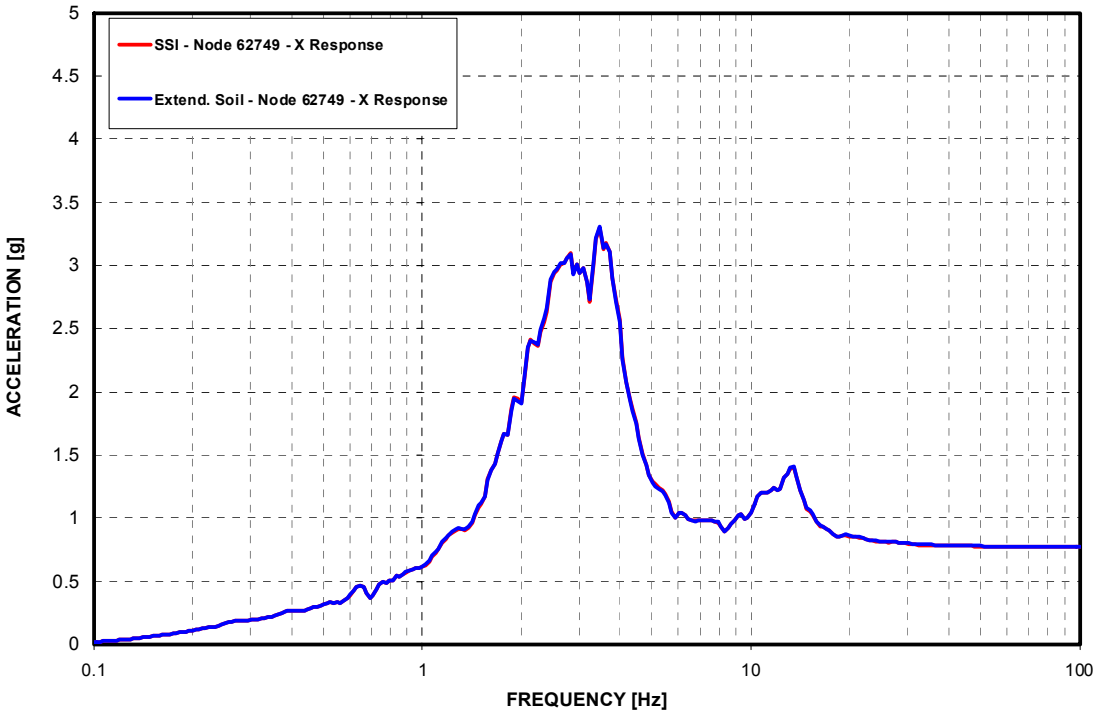

Figure 3-D.4.0-49 Top of PCCV - Response Spectra - NS Direction (X)

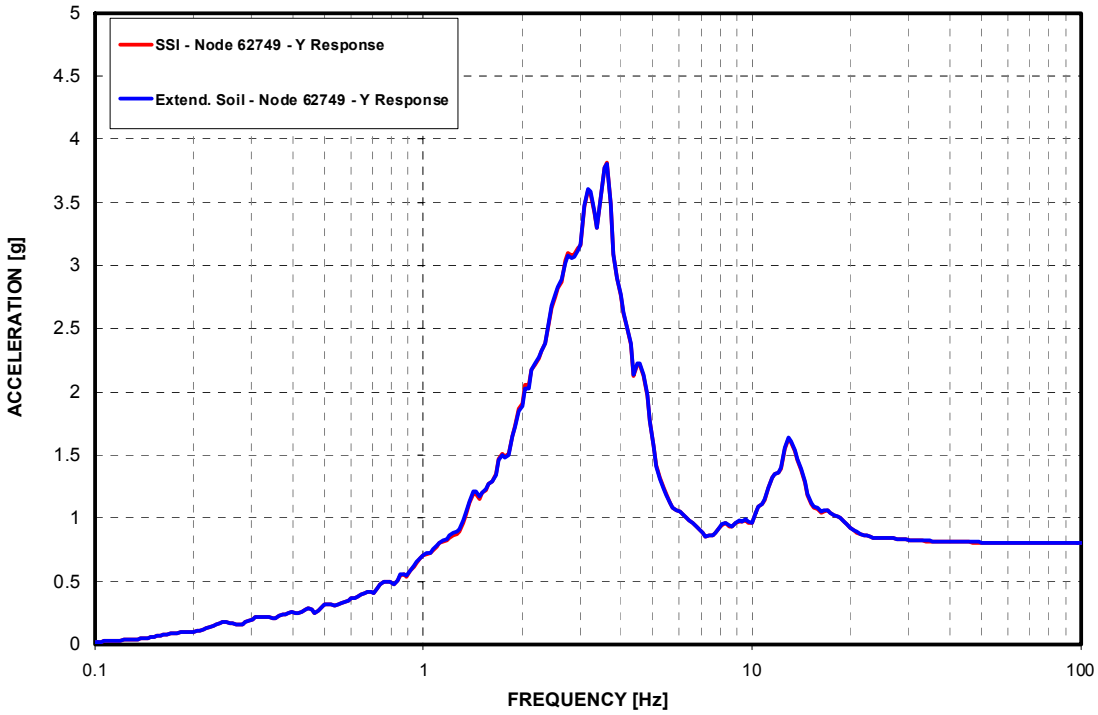

Figure 3-D.4.0-50 Top of PCCV - Response Spectra - EW Direction (Y)

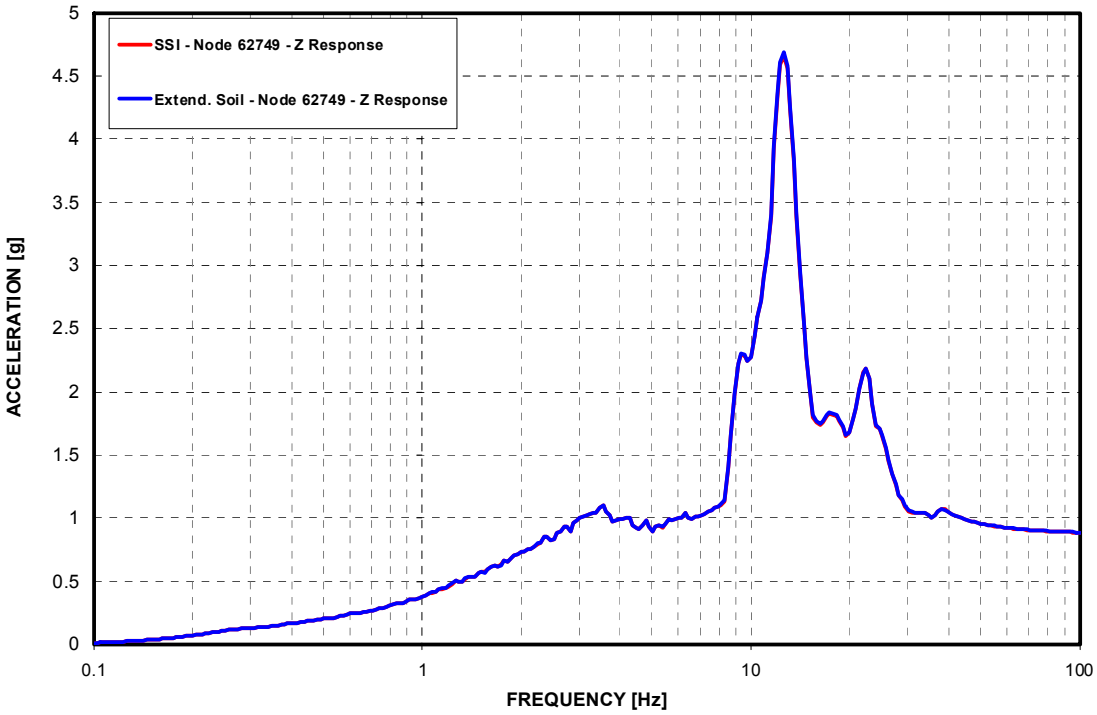

Figure 3-D.4.0-51 Top of PCCV - Response Spectra - Vertical Direction (Z)